

Synthesis, Comparison and Application of Oxazoline Ligands for Homogeneous Catalysis

DISSERTATION

vorgelegt von
M.Sc. Chemie

Swantje Wiebalck

aus Stade

zur Erlangung des akademischen Grades

Doktor der Naturwissenschaften

-Dr. rer. nat.-

März 2015

eingereicht im Fachbereich Biologie, Chemie und Pharmazie
der Freien Universität Berlin

Die vorliegende Arbeit wurde im Zeitraum vom Oktober 2010 bis September 2014 unter Anleitung von Prof. Dr. C. C. Tzschucke am Institut für Chemie und Biochemie der Freien Universität Berlin angefertigt.

Erstgutachter: Prof. Dr. C. Christoph Tzschucke

Zweitgutachter: Prof. Dr. Ulrich Abram

Disputation am 10. Juni 2015

För mien Öllern

Meinen Eltern Uta und Jürgen

Abstract

For the first time, a collection of different oxazoline ligands with the core structures 2,2'-bioxazoline (box), 2-(pyridine-2-yl)-oxazoline (pyrox), 2-(2-methylpyridine-2-yl)-oxazoline (mepyro) and 2-(quinolin-2-yl)-oxazoline (quinox) was prepared and studied regarding their sterical and electrical properties as well as the catalytic activity of their Ir(I) complexes. For the investigation of electrical and sterical properties with IR spectroscopy, Ir(I) carbonyl complexes of the oxazoline ligands were prepared. The application of the same Ir(I) metal center guaranteed a high comparability of the carbonyl complexes and the pre-catalysts for C-H activation and hydrogenation. Furthermore, the oxazolines were applied as ligands in heteroleptic Ru(II) complexes for surface immobilisation.

For the **synthesis of box structures**, a three-step procedure and for pyrox, mepyro and quinox a two-step procedure was developed. Both procedures were optimized to obtain high conversions and to allow easy workup of the single steps. In the first step, commercially available chiral aminols were coupled with carboxylic acids. Since a large variety of substituted starting materials is commercially available, a comprehensive variation of the target structures is possible. Good to excellent total yields were achieved for 20 structurally related compounds which were prepared in half-gram-scale.

For the evaluation of the electronic properties of the oxazoline ligands, square planar **Ir(I) dicarbonyl complexes** were prepared and their corresponding ν_{CO} absorption frequencies were measured by IR spectroscopy. To prepare the complexes, $[\text{Ir}(\text{cis,cis-1,5-cyclooctadiene})\text{Cl}]_2$ was initially treated with different silver salts (AgPF_6 , AgBF_4 , $\text{Ag}[\text{tetrakis}(3,5\text{-bis}(\text{trifluoromethyl})\text{phenyl})\text{borate}]$), to exchange the chloride for a non-coordinating counterion. Subsequently, the ligand was added to give complexes of the general composition $[\text{Ir}(\text{ligand})(\text{cod})]\text{X}$. These complexes were converted into dicarbonyl complexes by addition of stoichiometric amounts of CO gas at atmospheric pressure. The CO complexes were studied by ATR-IR measurements of the solid compound or as solution in tetrahydrofuran. The interpretation of the IR measurements was supported by DFT calculations. The carbonyl stretching frequencies of the square planar dicarbonyl complexes $[\text{Ir}(\text{ligand})(\text{CO})_2]\text{PF}_6$ turned out to be mainly influenced by the steric properties of the oxazoline ligands, while trigonal bipyramidal monocarbonyl complexes $[\text{Ir}(\text{ligand})(\text{cis,cis-1,5-cyclooctadiene})(\text{CO})]\text{PF}_6$ reflected more the electrical properties of the ligands.

The formation of **heteroleptic Ru(II) complexes** of the general composition $[\text{Ru}(\text{oxazoline})(\text{bipyridine})\text{X}_2]$ was investigated. The complexes were designed to contain an oxazoline ligand carrying the chiral information and a substituted bipyridine ligand, suitable for further functionalisation and immobilisation on an electrode surface. The complex synthesis started with $[\text{Ru}(p\text{-cymene})\text{Cl}_2]_2$ or $[\text{Ru}(\text{S}(\text{CH}_3)_2\text{O})_4(\text{Cl})_2]$ and the oxazoline ligand was introduced as first or second ligand. If the oxazoline was introduced as first ligand, the addition of a bipyridine led to bisheteroleptic bipyridine complexes. If the oxazoline was introduced as second ligand, an inseparable mixture, probably isomers, was obtained.

The prepared oxazolines were tested as ligands in direct **aromatic and aliphatic borylation**. As catalytic system $[\text{Ir}(\text{cis},\text{cis}\text{-}1,5\text{-cyclooctadiene})(\text{OCH}_3)_2]$ was used in combination with the respective ligand and bis(picanolato)diboron served as boron source. Aromatic borylations were carried out in the neat monosubstituted arenes such as toluene, tert-butylbenzene, anisole, cyclohexylbenzene, trifluorotoluene and ethyl benzoate. The *meta:para* ratios of the products were investigated by $^1\text{H-NMR}$ spectroscopy, showing a purely substrate induced effect on the regioselectivity. Aliphatic borylations of *n*-octane and *n*-hexane were unsuccessful under the applied conditions.

Hydridosilylether directed γ -C-H activation was carried out with a catalytic system of $[\text{Ir}(\text{cis},\text{cis}\text{-}1,5\text{-cyclooctadiene})(\text{OCH}_3)_2]$ and an oxazoline ligand instead of the usually applied 3,4,7,8-tetramethylphenanthroline ligand. Initially ketones or alcohols were transformed into their (hydrido)silyl ether derivatives, followed by a γ -C-H activation which led to the formation of an oxasilolane. Norbornene was added stoichiometrically as hydrogen acceptor. The (hydrido)silyl ether formation was optimized and the stereochemical influence of the chiral ligands in the C-H activation step was investigated. A racemic mixture of ((3,7-dimethyloctan-3-yl)oxy)diethylsilane served for this purpose as substrate regarding its kinetic resolution. The products were obtained in enantiomeric excess up to 44% ee.

Precatalysts for homogeneous **hydrogenation** had the general composition $[\text{Ir}(\text{ligand})(\text{cod})]$ [tetrakis(3,5-bis(trifluoromethyl)phenyl)borate)] and were prepared by initial mixing of $[\text{Ir}(\text{cis},\text{cis}\text{-}1,5\text{-cyclooctadiene})(\text{Cl})_2]$ with $\text{Ag}[\text{tetrakis}(3,5\text{-bis}(\text{trifluoromethyl})\text{phenyl})\text{borate}]$ and subsequent addition of the oxazoline ligand. The hydrogenations were carried out in neat substrate or in dichloromethane at 40 bar hydrogen pressure. The products were analyzed by $^1\text{H-NMR}$ spectroscopy and/or GC-FID measurements. The oxazoline containing complexes led to yields up to 99% and showed a high chemoselectivity for C-C double bonds when they were applied for the hydrogenation of α,β -unsaturated ketones, but no stereoselectivity was observed.

Zusammenfassung

Erstmalig wurde eine Sammlung verschiedener Oxazolinliganden mit den Strukturtypen 2,2'-Bioxazolin (box), 2-(Pyridine-2-yl)-oxazolin (pyrox), 2-(2-Methylpyridine-2-yl)-oxazolin (mepyro) und 2-(Chinolin-2-yl)-oxazolin (quinox), angelegt und deren sterische sowie elektronische Eigenschaften, sowie die katalytische Aktivität ihrer Ir(I) Komplexe, untersucht. Zur Analyse der elektronischen und sterischen Eigenschaften mit Hilfe der IR Spektroskopie wurden Ir(I) Carbonylkomplexe der Oxazoline synthetisiert. Die konsistente Verwendung des Ir(I) Metallzentrums gewährleistet eine gute Vergleichbarkeit zwischen den Carbonylkomplexen und den Präkatalysatoren für C-H Aktivierung und Hydrierung. Des Weiteren wurden die dargestellten Oxazolinstrukturen als Liganden in heteroleptischen Ru(II) Komplexen zur zukünftigen Oberflächenimmobilisierung verwendet.

Für die **Darstellung der box Strukturen** wurde eine zwei-stufige und für die pyrox, mepyro und quinox Strukturen eine drei-stufige Syntheseroute entwickelt. In beiden Syntheserouten wurde der Schwerpunkt auf möglichst vollständige Umsätze gelegt, um zeitintensive Aufreinigungsschritte zu vermeiden. Als Reaktionspartner für die chiralen Aminole wurden kommerziell erhältliche Carbonsäuren gewählt. Durch die Vielfalt der kommerziell erhältlichen Ausgangsstoffe besteht die Möglichkeit zur umfangreichen Variation der Zielstrukturen. Mit den entwickelten Syntheserouten wurden gute bis hervorragende Gesamtausbeuten erreicht und insgesamt 20 strukturell verwandte Verbindungen im halb-Gramm-Maßstab dargestellt.

Für die Evaluierung der elektronischen Eigenschaften der Oxazolinliganden wurden quadratisch planare **Ir(I) Dicarboxylkomplexe** dargestellt und deren ν_{CO} Schwingungsfrequenzen mit Hilfe der Infrarotspektroskopie (IR) gemessen. Die Komplexe wurden ausgehend von $[\text{Ir}(\text{cis,cis-1,5-cyclooctadiene})\text{Cl}]_2$ durch eine neuentwickelte Syntheseroute dargestellt. Das $[\text{Ir}(\text{cis,cis-1,5-cyclooctadiene})\text{Cl}]_2$ wurde zunächst mit einem Silbersalz (AgPF_6 , AgBF_4 , $\text{Ag}[\text{tetrakis}(3,5\text{-bis(trifluoromethyl)phenyl)borat}]$) zur Reaktion gebracht, um das Chlorid gegen ein nicht-koordinierendes Gegenion auszutauschen. Darauf folgend wurde der Ligand zugegeben, um so Komplexe der allgemeinen Zusammensetzung $[\text{Ir}(\text{Ligand})(\text{cis,cis-1,5-cyclooctadiene})]\text{X}$ zu erhalten. Diese Komplexe wurden durch die stöchiometrische Zugabe von CO Gas bei Atmosphärendruck in ihre Dicarboxylkomplexe überführt. Die Analyse der Carbonylkomplexe erfolgte per ATR-IR Spektroskopie der festen Substanzen sowie durch Messungen ihrer Lösungen in Tetrahydrofuran. Die Interpretation der IR Daten wurde durch DFT-Rechnungen unterstützt. Die Carbonylschwingungsabsorptionen der Dicarboxylkomplexe $[\text{Ir}(\text{ligand})(\text{CO})_2]\text{PF}_6$ wurden überwiegend von den sterischen Eigenschaften der Oxazolinliganden beeinflusst, während die der Monocarboxylkomplexe $[\text{Ir}(\text{ligand})(\text{cis,cis-1,5-cyclooctadiene})(\text{CO})]\text{PF}_6$ hauptsächlich die elektronischen Eigenschaften der Liganden widerspiegeln.

Die Synthese von **heteroleptischen Ru(II) Komplexen** der allgemeinen Zusammensetzung $[\text{Ru}(\text{Oxazolin})(\text{Bipyridin})\text{X}_2]$ wurde ebenfalls untersucht. Die Komplexe sollten einen chiralen Oxazolinliganden sowie einen substituierten Bipyridin Liganden tragen. Der Bipyridinligand sollte zur Immobilisierung auf einer Elektrodenoberfläche geeignet sein, da in zukünftigen Projekten die Redoxeeigenschaften der Komplexe auf einer solchen Elektrodenoberfläche studiert werden sollen. Die Komplexsynthese wurde entweder ausgehend von $[\text{Ru}(p\text{-cymene})\text{Cl}_2]_2$ oder $[\text{Ru}(\text{S}(\text{CH}_3)_2\text{O})_4(\text{Cl})_2]$ durchgeführt, wobei der Oxazolinligand als erster oder zweiter Ligand eingeführt wurde. Allerdings konnte ein Bipyridin Ligand den zuerst eingeführten Oxazolinliganden vollständig aus dem Komplex verdrängen, sodass fast ausschließlich bisheteroleptische Bipyridinkomplexe gebildet wurden. Wurde der Oxazolin Ligand als zweiter eingeführt, bildeten sich die Produktkomplexe als untrennbare Mischungen, vermutlich aus verschiedenen Isomeren. Die gewünschten heteroleptischen Rutheniumkomplexen konnten nicht als isolierte Strukturen dargestellt werden.

Die dargestellten Oxazoline wurden als Liganden in direkter **aromatischer und aliphatischer Borylierung** verwendet. Als katalytisches System wurde eine Kombination aus $[\text{Ir}(\text{cis},\text{cis}\text{-}1,5\text{-cyclooctadiene})(\text{OCH}_3)]_2$ und dem entsprechenden Liganden verwendet, wobei Bis(picanolato)diboran als Borquelle fungierte und die Reaktionen in reinem Substrat durchgeführt wurden. In der aromatischen Borylierung fanden monosubstituierte Aromaten wie Toluol, *tert*-Butylbenzol, Anisol, Cyclohexylbenzol, Trifluortoluol und Ethylbenzoat als Substrate Verwendung. Gegenstand der Analyse war die Bestimmung des *meta:para* Verhältnisses der Produkte durch $^1\text{H-NMR}$ Spektroskopie, wobei ein reiner substratinduzierter Effekt auf die Regioselektivität festgestellt werden konnte. Die aliphatische Borylierung von *n*-Oktan und *n*-Hexan gelang unter den angewendeten Bedingungen nicht.

Die **hydridosilylether dirigierte γ -C-H Aktivierung** wurden mit einem katalytischen System aus $[\text{Ir}(\text{cis},\text{cis}\text{-}1,5\text{-cyclooctadiene})(\text{OCH}_3)]_2$ und einem Oxazolinliganden, der den üblicherweise verwendeten 3,4,7,8-tetramethylphenanthrolin Liganden ersetzte, durchgeführt. Zunächst wurden Ketone oder Alkohole in ihre (Hyrido)silylether umgesetzt, woraufhin eine γ -C-H Aktivierung unter Ausbildung eines Oxasilolans stattfand. Norbornen wurde als stöchiometrisch eingesetzter Wasserstoffakzeptor den Reaktionsmischungen zugefügt. Die Bildung der Hydridosilylether wurde optimiert und der stereochemische Einfluss der chiralen Liganden in der C-H Aktivierung untersucht. Als Substrat diente für diesen Zweck ((3,7-Dimethyloctan-3-yl)oxy)diethylsilan, dessen kinetische Racemattrennung analysiert wurde. Die Produkte wurden mit enantiomeren Überschüssen bis zu 44% ee erhalten.

Präkatalysatoren für die homogene **Hydrierung** waren von der generellen Zusammensetzung $[\text{Ir}(\text{ligand})(\text{cis},\text{cis}\text{-}1,5\text{-cyclooctadiene})][\text{tetrakis}(3,5\text{-bis}(\text{trifluoromethyl})\text{phenyl})\text{borat}]$ und wurden durch vorangehendes Mischen von $[\text{Ir}(\text{cis},\text{cis}\text{-}1,5\text{-cyclooctadiene})\text{Cl}]_2$ mit $\text{Ag}[\text{tetrakis}(3,5\text{-bis}(\text{trifluoromethyl})\text{phenyl})\text{borat}]$ und anschließender Zugabe des entsprechenden Oxazolin Liganden

dargestellt. Die Hydrierungen wurden in reinem Substrat oder in Dichlormethan bei einem Wasserstoffdruck von 40 bar durchgeführt und die Produkte anhand von $^1\text{H-NMR}$ Spektroskopie und/oder GC-FID analysiert. Die oxazolinhaltigen Komplexe erzielten Ausbeuten bis zu 99% und zeigten eine hohe Chemoselektivität für C-C Doppelbindungen bei der Verwendung von α,β -ungesättigten Ketonen als Substrate. Eine Stereoselektivität konnte nicht beobachtet werden.

Danksagung

Ich bedanke mich bei Prof. Dr. C. Christoph Tzschucke für die Betreuung und Durchsicht meiner Doktorarbeit sowie für die Bereitstellung des interessanten sowie vielfältigen Projekts. Ich habe während der letzten Jahre sehr viel gelernt.

Bei Prof. Dr. Ulrich Abram bedanke ich mich für die Übernahme des Zweitgutachtens.

Für die Durchsicht meiner Arbeit bedanke ich mich bei Dr. Daniela Ponader, Dr. Fanni Sypaseuth und Dr. Jacek Kozuch.

Des Weiteren möchte ich mich bei Prof. Dr. Dieter Lentz und Dr. Jelena Wiecko für die Durchführung von Kristallstrukturanalysen und bei Dr. Jacek Kozuch für eine hervorragende wissenschaftliche Kooperation in verschiedenen Projekten bedanken. Ebenso gilt mein Dank den Serviceabteilungen der chemischen Fakultät für deren Arbeit sowie für die kompetente Hilfe, die ich bei Problemen erfahren habe.

Mein besonderer Dank gilt allen meinen Studenten, die ich in Bachelor- oder Masterarbeiten sowie Forschungsprojekten betreuen durfte. Diese Studenten waren Gisa Meißner (B.Sc. und FP), Cindy Glor (FP und M.Sc.), Patrick Kuhrt (FP), Silke Plachetta (FP und M.Sc.) und Alexander Erhardt (FP). Gisa, es war eine tolle Zeit mit Dir. Du hast die Laborwelt ein wenig fröhlicher und vor allem bunter gemacht. Deine Begeisterung für die Chemie sucht ihresgleichen. Cindy, wenn ich an Dich denke, dann assoziiere ich sofort die Farbe Lila. Vielen Dank für Deine unglaublich motivierte und zuverlässige Mitarbeit und die unzählbaren Versuche die Rutheniumkomplexe aufzutrennen. Silke, vielen Dank für die absolut zuverlässige Arbeit. Auch wenn Vieles nicht funktioniert hat (so ist chemische Forschung nun einmal leider häufig). Auch diese Ergebnisse lieferten einen sehr wertvollen Teil zu meiner Arbeit. Du genießt mein uneingeschränktes Vertrauen. Patrick, Du hast durch eine einzigartige Eigeninitiative und ein „dickes Fell“ gegläntzt. Vielen Dank für Deine Mitarbeit! Zu Guter Letzt Alex. Du bist ein besonderer Mensch, von dem ich viel lernen durfte. Vielen Dank für gute Gespräche und natürlich dafür, dass Du dich für eine Mitarbeit an meinem Projekt entschieden hast. Ich wünsche Dir von ganzem Herzen nur das Beste!

Den Mitgliedern der AG Tzschucke danke ich für eine sehr angenehme Arbeitsatmosphäre, wissenschaftliche Hilfe und auch für spannende Treffen und Feiern nach der Laborarbeit. Besonders Bedanken möchte ich mich dabei bei Dr. Sasa Duric, Dr. Michal Andrä, Dr. Ralf Albrecht, Dr. Fanni Sypaseuth, Anja Sokolowski, Emma Svensson und Shanshan Liu. Sasa, du warst immer ein wissenschaftliches und menschliches Vorbild für mich. Michal, auch wenn wir manchmal Differenzen hatten sitzen wir dennoch im gleichen Boot und können gegenseitig unsere Erfahrungen austauschen und darüber bin ich sehr froh. Ich wünsche dir, dass Deine Vorstellungen von der Zukunft in Erfüllung gehen. Ralf, du bist einer der nettesten Kollegen, den man sich nur wünschen kann. Ich bin nach wie

vor fasziniert von Deiner Disziplin. Fanni, wir sind zusammen durch so viele Höhen und Tiefen während der Doktorarbeit gegangen. Ohne Dich wäre alles schwieriger gewesen und ich bin sehr froh, dass Du dich damals für unsere Arbeitsgruppe entschieden hast. Anja und Emma, ihr habt definitiv dazu beigetragen dass es im Labor ein bisschen lustiger war. Vielen Dank für eine schöne Zeit. Ich wünsche Euch alles Gute für Eure eigenen Doktorarbeiten. Shanshan, du bist ein unglaublich lieber Mensch. Ich freue mich, dass ich Dich kennenlernen durfte und bedanke mich für die netten Gespräche. Auch Dir wünsche ich nichts mehr, als ein gutes Ende deiner Doktorarbeit. Außerdem hoffe ich, dass Dein Deutsch inzwischen gut genug ist, um das hier zu verstehen. ;)

Während meiner Doktorarbeit hatte ich das Privileg, Mitglied der Graduiertenschule „Berlin International Graduate School for Natural Sciences and Engineering“ zu sein. Von dort konnte ich viele positive Erfahrungen mitnehmen und bekam viel Hilfe, sei es wissenschaftlicher oder organisatorischer Natur. Auch die Zusammenarbeit mit anderen Studenten bei Veranstaltungen wie z.B. die „Lange Nacht der Wissenschaften“ oder auch die Teilnahme an der Summer School 2013 in Tarragona (Spanien) habe ich sehr geschätzt. Mein besonderer Dank gilt unserem Koordinator, Dr. Jean-Philippe Lonjaret, der mir stets bei meinen Anliegen mit Rat und Tat zur Seite stand und mir immer eine wichtige Stütze war. Bedanken möchte ich mich bei allen weiteren Studenten der Graduiertenschule, mit denen ich viele schöne Momente erlebt habe und die mein Leben bereichert haben.

Ebenfalls bedanken möchte ich mich bei meinem ehemaligen Chemielehrer Herrn Buck, der durch seinen interessanten, begeisterten und anspruchsvollen Unterricht mein Interesse an der Chemie bedeutend unterstützt hat.

Zu Guter Letzt gilt mein Dank denjenigen, die mich schon lange mein Leben lang bedingungslos unterstützt und immer an mich geglaubt haben; meinen Eltern Uta und Jürgen, meiner Schwester Mareike sowie dem Rest meiner Familie, Oma Traute, Oma Kathie, Uschi, Nadja, Ilhan und natürlich Jil. Es war unglaublich wichtig für mich, immer Menschen in meiner Nähe zu wissen, die zu mir halten. Ich weiß, dass so etwas nicht immer selbstverständlich ist und deshalb möchte ich jetzt die Gelegenheit nutzen, Euch zu sagen, wie wichtig mir das war und ist und wie dankbar ich euch dafür bin. Außerdem möchte ich mich bei Mariola und Jan für ihre ständige Hilfe und Unterstützung bedanken. Mein ganz besonderer und allerletzter Dank gilt natürlich meinem Jacek. Jacek, Du bist ein so aufrichtiger und begeisterungsfähiger Mensch, dass mir nichts anderes übrig bleibt als Dich zu lieben. Ich wünsche mir für uns beide, dass das niemals aufhören wird.

Table of Contents

ABSTRACT	VII
ZUSAMMENFASSUNG	IX
DANKSAGUNG	XIII
ABBREVIATIONS	XXIX
TABLE OF LIGANDS	XXXIV

1 INTRODUCTION AND MOTIVATION	37
--------------------------------------	-----------

I. SCIENTIFIC BACKGROUND

2 OXAZOLINE BASED STRUCTURES	45
-------------------------------------	-----------

2.1 Preparation of Bisoxazolines and Pyridyloxazolines	45
--	----

2.2 Structural Diversity of Oxazoline Ligands	48
---	----

2.3 Catalytic Application of Oxazoline-Ligands	51
--	----

3 IRIDIUM AND RUTHENIUM COMPLEXES	57
--	-----------

3.1 Transition Metal Carbonyl Complexes	57
---	----

3.1.1 CO as Ligand in Transition Metal Complexes	57
--	----

3.1.2 Evaluation of Monodentate Ligands in Carbonyl Complexes	59
---	----

3.1.3 Evaluation of bidentate Ligands in Carbonyl Complexes	61
---	----

3.1.4 Preparation of Square Planar Ir(I) Bipyridine Carbonyl Complexes	64
--	----

3.2 Heteroleptic Ruthenium(II) Complexes	67
--	----

3.2.1 Preparation	68
-------------------	----

3.2.2 Application in Redox-Reactions	72
--------------------------------------	----

4 CATALYSIS	75
--------------------	-----------

4.1 Borylation	75
----------------	----

4.1.1 Aromatic Borylation	76
---------------------------	----

4.1.2 Aliphatic Borylation	81
----------------------------	----

4.2 (Hydrido)silyl Ether Directed γ -C-H Activation	83
--	----

4.3	Hydrogenation	88
-----	---------------	----

II. RESULTS AND DISCUSSION

5	LIGAND SYNTHESIS	99
5.1	Bisoxazolines	99
5.2	Pyridyloxazolines	101
6	IRIDIUM AND RUTHENIUM COMPLEXES	109
6.1	Iridium(I) Carbonyl Complexes	109
6.1.1	Cyclooctadiene Iridium(I) Cl^- and PF_6^- Complexes	110
6.1.2	Cyclooctadiene Iridium(I) BAr^{F^-} Complexes	115
6.1.3	Synthesis of Carbonyl Complexes	119
6.1.4	Evaluation of IR Data of the Carbonyl Complexes	127
6.2	Heteroleptic Ruthenium(II) Complexes	140
6.2.1	$[\text{Ru}(p\text{-cymene})\text{Cl}]_2$ Precursor: Introduction of the First Ligand	141
6.2.2	$[\text{Ru}(\text{cymene})\text{Cl}]_2$ Precursor: Introduction of the Second Ligand	143
6.2.3	$[\text{Ru}(\text{dmsO})_4\text{Cl}_2]$ Precursor: Introduction of the First Ligand	144
6.2.4	$[\text{Ru}(\text{dmsO})_4\text{Cl}_2]$ Precursor: Introduction of the Second Ligand	148
6.2.5	Initial Catalysis Experiments: Transferhydrogenation	152
7	CATALYSIS	155
7.1	Aromatic Borylation	155
7.1.1	Independent Synthesis of the Borylation Products	155
7.1.2	Borylation Experiments	156
7.2	Aliphatic Borylation	170
7.3	Silylether Directed γ -C-H Activation	175
7.4	Hydrogenation	183

III. SUMMARY & CONCLUSION

8	SUMMARY	195
8.1	Synthesis of Ligands	195
8.2	Synthesis of Transition Metal Complexes	196
8.3	Catalysis	198
8.4	Evaluation of the Ligands in Carbonyl Complexes	200

IV. EXPERIMENTAL SECTION

10	GENERAL METHODS	207
11	LIGANDS	209
	11.1 Box-structures	209
	11.1.1 Bioxalamides	209
	11.1.1.1 <i>N,N'</i> -Bi((<i>S</i>)-1-hydroxypropan-2-yl)oxalamid (3a)	209
	11.1.1.2 <i>N,N'</i> -Bi((<i>S</i>)-1-hydroxy-3-methylbutan-2-yl)oxalamide (3b)	209
	11.1.1.3 <i>N,N'</i> -Bi((<i>S</i>)-1-hydroxy-3,3-dimethylbutan-2-yl)oxalamide (3c)	210
	11.1.1.4 <i>N,N'</i> -Bi((2 <i>S</i> ,3 <i>S</i>)-1-hydroxy-3-methylpentan-2-yl)oxalamide (3d)	211
	11.1.1.5 <i>N,N'</i> -Bi((<i>S</i>)-1-hydroxy-4-methylpentan-2-yl)oxalamide (3e)	211
	11.1.1.6 <i>N,N'</i> -Bi((<i>S</i>)-1-hydroxyhexan-2-yl)oxalamide (3f)	212
	11.1.1.7 <i>N,N'</i> -Bi((<i>S</i>)-2-hydroxy-1-phenylethyl)oxalamide (3g)	212
	11.1.1.8 <i>N,N'</i> -Bi((<i>S</i>)-1-hydroxy-3-phenylpropan-2-yl)oxalamide (3h)	213
	11.1.2 Bi- β -chlorooxalamide	214
	11.1.2.1 <i>N,N'</i> -Bi((<i>S</i>)-1-chloropropan-2-yl)oxalamid (4a)	214
	11.1.2.2 <i>N,N'</i> -Bi((<i>S</i>)-1-chloro-3-methylbutan-2-yl)oxalamide (4b)	214
	11.1.2.3 <i>N,N'</i> -Bi((<i>S</i>)-1-chloro-3,3-dimethylbutan-2-yl)oxalamide (4c)	215
	11.1.2.4 <i>N,N'</i> -Bi((2 <i>S</i> , 3 <i>S</i>)-1-chloro-3-methylpentan-2-yl)oxalamide (4d)	215
	11.1.2.5 <i>N,N'</i> -Bi((<i>S</i>)-2-chloro-4-methylpentan-2-yl)oxalamid (4e)	216
	11.1.2.6 <i>N,N'</i> -Bi((<i>S</i>)-1-chlorohexan-2-yl)oxalamid (4f)	216
	11.1.2.7 <i>N,N'</i> -Bi((<i>S</i>)-2-Chloro-1-phenylethyl)oxalamid (4g)	217
	11.1.2.8 <i>N,N'</i> -Bi((<i>S</i>)-1-chloro-3-phenylpropan-2-yl)oxalamid (4h)	217
	11.1.3 Bisoxazolines	218
	11.1.3.1 2,2'-Bi((4 <i>S</i> , 4' <i>S</i>)-4,4'-dimethyl)-oxazolin (5a)	218
	11.1.3.2 2,2'-Bi((4 <i>S</i> ,4' <i>S</i>)-4,4'-diisopropyl)-oxazolin (5b)	219
	11.1.3.3 2,2'-Bi((4 <i>S</i> ,4' <i>S</i>)-4,4'-di- <i>tert</i> -butyl)-oxazolin (5c)	219
	11.1.3.4 2,2'-Bi((4 <i>S</i> , 4' <i>S</i>)-4,4'-di((<i>S</i>)- <i>sec</i> -butyl)-oxazolin (5d)	220
	11.1.3.5 2,2'-Bi((4 <i>S</i> , 4' <i>S</i>) -4,4'-diisobutyl)-oxazolin (5e)	221
	11.1.3.6 2,2'-Bi((4 <i>S</i> , 4' <i>S</i>) -4,4'-dibutyl)-oxazolin (5f)	221
	11.1.3.7 2,2'-Bi((4 <i>R</i> , 4' <i>R</i>)-4,4'-diphenyl)-oxazolin (5g)	222
	11.1.3.8 2,2'-Bi((4 <i>R</i> , 4' <i>R</i>)-4,4'-dibenzyl)-oxazolin (5h)	223
	11.1.3.9 (<i>S</i>)-4,4'-diisopropyl-2,2'-bithiazolin (7b)	224
	11.2 Pyrox, meprox and quinox structures	224
	11.2.1 β -Hydroxyamides	224
	11.2.1.1 General Procedure A for β -hydroxyamides	224

11.2.1.2	(<i>S</i>)- <i>N</i> -(1-Hydroxy-3-methylbutan-2-yl)picolinamide (9b)	225
11.2.1.3	(<i>S</i>)- <i>N</i> -(1-Hydroxyhexan-2-yl)picolinamide (9f)	228
11.2.1.4	(<i>R</i>)- <i>N</i> -(4-Hydroxy-1-phenylbutan-2-yl)picolinamide (9h)	228
11.2.1.5	(<i>S</i>)- <i>N</i> -(2-Hydroxy-1-phenylethyl)picolinamide (9g)	228
11.2.1.6	(<i>S</i>)- <i>N</i> -(1-hydroxy-3,3-dimethylbutan-2-yl)picolinamide (9c)	229
11.2.1.7	(<i>S</i>)- <i>N</i> -(2-Hydroxy-1-phenylethyl)-6-methylpicolinamide (17b)	229
11.2.1.8	(<i>S</i>)- <i>N</i> -(1-Hydroxyhexan-2-yl)-6-methylpicolinamide (17f)	229
11.2.1.9	(<i>R</i>)- <i>N</i> -(2-Hydroxy-1-phenylethyl)-6-methylpicolinamide (17h)	230
11.2.1.10	(<i>R</i>)- <i>N</i> -(1-Hydroxy-3-phenylpropan-2-yl)-6-methylpicolinamide (17g)	230
11.2.1.11	(<i>S</i>)- <i>N</i> -(1-Hydroxy-3-methylbutan-2-yl)quinoline-2-carboxamide (18b)	230
11.2.1.12	(<i>S</i>)- <i>N</i> -(1-Hydroxyhexan-2-yl)-6-quinoline-2-carboxamide (18f)	231
11.2.1.13	(<i>S</i>)- <i>N</i> -(2-Hydroxy-1-phenylethyl)quinoline-2-carboxamide (18g)	231
11.2.2	Oxazolines	231
11.2.2.1	General Procedure B for pyridyloxazolines	231
11.2.2.2	(<i>S</i>)-4-Isopropyl-2-(pyridine-2-yl)-oxazolin (10b)	232
11.2.2.3	(<i>S</i>)-4-Butyl-2-(pyridine-2-yl)-oxazolin (10f)	233
11.2.2.4	(<i>R</i>)-4-Benzyl-2-(pyridine-2-yl)-oxazolin (10h)	233
11.2.2.5	(<i>R</i>)-4-Phenyl-2-(pyridine-2-yl)-oxazolin (10g)	234
11.2.2.6	(<i>S</i>)-4-(<i>tert</i> -butyl)-2-(pyridine-2-yl)-oxazolin (10c)	235
11.2.2.7	(<i>S</i>)-4-Isopropyl-2-(6-methylpyridin-2-yl)-oxazolin (19b)	235
11.2.2.8	(<i>S</i>)-4-Butyl-2-(6-methylpyridin-2-yl)-oxazolin (19f)	236
11.2.2.9	(<i>R</i>)-2-(6-Methylpyridin-2-yl)-oxazolin (19g)	237
11.2.2.10	(<i>R</i>)-4-Benzyl-2-(6-methylpyridin-2-yl)-oxazolin (19h)	237
11.2.2.11	(<i>S</i>)-4-Isopropyl-2-(quinolin-2-yl)-oxazolin (20b)	238
11.2.2.12	(<i>S</i>)-4-Butyl-2-(quinolin-2-yl)-oxazolin (20f)	239
11.2.2.13	(<i>R</i>)-4-Phenyl-2-(quinolin-2-yl)-oxazolin (20g)	240
12	COMPLEXES	241
	12.1 Starting Materials	241
12.1.1	<i>bis</i> -(1,5-Cyclooctadien)-di-iridium(I)chloride, [Ir(cod)Cl] ₂ (23)	241
12.1.2	Silver (<i>tetrakis</i> -3,5-bis(trifluoromethyl)phenyl)borate; AgBAR ^F (34)	241
12.1.3	[RuCl ₂ (η ⁶ - <i>p</i> -cymol)] ₂ , Di-μ-chloro-bis-[(η ⁶ - <i>p</i> -cymol)-chloro-ruthenium(II)] (46)	242
12.1.4	Dichlorotetrakis(dimethyl-sulfoxid)ruthenium(II); [Ru(DMSO) ₄ Cl ₂] (47)	242
	12.2 Iridium(I)-cod Cl⁻ Complexes	243

12.2.1	General Procedure C for [Ir(N [^] N)(cod)]Cl Complexes 24	243
12.2.2	1,5-Cyclooctadiene[(4,4'-di- <i>tert</i> -butyl-2,2'-bipyridine)]iridium(I) chlorid, [Ir(dtbpv)(cod)]Cl (24a)	244
12.2.3	1,5-Cyclooctadiene[((<i>S</i>)-4-Isopropyl-2-(quinolin-2-yl)-oxazolin)]iridium(I) chlorid, [Ir(ⁱ Pr-quinox)(cod)]Cl (24b)	244
12.2.4	1,5-Cyclooctadien[(<i>S</i>)-4-isopropyl-2-(pyridin-yl)-oxazolin]iridium(I) chlorid, [Ir(ⁱ Pr-pyrox)(cod)]Cl (24c)	245
12.2.5	1,5-Cyclooctadien[2,2'-bioxazolin]iridium(I) chlorid, [Ir(H-box)(cod)]Cl (24d)	246
	12.3 Iridium(I)-cod PF₆⁻ Complexes 25	246
12.3.1	General procedure D for the formation of [Ir(N [^] N)(cod)]PF ₆ complexes 25	246
12.3.2	1,5-Cyclooctadiene[(2,2'-bioxazole)]iridium(I) hexaflourophosphate, [Ir(H-box)(cod)]PF ₆ (25a)	247
12.3.3	1,5-Cyclooctadiene[(2,2'-Bis((4 <i>S</i> , 4' <i>S</i>)-4,4'-dimethyl)-oxazolin)]iridium(I) hexaflourophosphate, [Ir(Me-box)(cod)]PF ₆ (25b)	248
12.3.4	1,5-Cyclooctadiene[(2,2'-Bis((4 <i>S</i> ,4' <i>S</i>)-4,4'-diisopropyl)-oxazolin)]iridium(I) hexaflourophosphate, [Ir(ⁱ Pr-box)(cod)]PF ₆ (25c)	248
12.3.5	1,5-Cyclooctadiene[(2,2'-Bis((4 <i>S</i> ,4' <i>S</i>)-4,4'-di- <i>tert</i> -butyl)-oxazolin)]iridium(I) hexaflourophosphate, [Ir(^t Bu-box)(cod)]PF ₆ (25d)	249
12.3.6	1,5-Cyclooctadiene[(2,2'-Bis((4 <i>S</i> , 4' <i>S</i>) -4,4'-dibutyl)-oxazolin)]iridium(I) hexaflourophosphate, [Ir(ⁿ Bu-box)(cod)]PF ₆ (25e)	250
12.3.7	1,5-Cyclooctadiene[(2,2'-Bis((4 <i>R</i> , 4' <i>R</i>)-4,4'-diphenyl)-oxazolin)]iridium(I) hexaflourophosphate, [Ir(Ph-box)(cod)]PF ₆ (25f)	250
12.3.8	1,5-Cyclooctadiene[((4 <i>S</i> ,4' <i>S</i>)-4,4'-diisopropyl-2,2'-bithiazolin)]iridium(I) hexaflourophosphate, [Ir(ⁱ Pr-bta)(cod)]PF ₆ (25g)	251
12.3.9	1,5-Cyclooctadiene[(<i>S</i>)-4-isopropyl-2-(pyridin-yl)-oxazolin]iridium(I) hexaflourophosphate, [Ir(ⁱ Pr-pyrox)(cod)]PF ₆ (25h)	252
12.3.10	1,5-Cyclooctadiene[((<i>S</i>)-4-(<i>tert</i> -butyl)-2-(pyridine-2-yl)-oxazolin)]iridium(I) hexaflourophosphate, [Ir(^t Bu-pyrox)(cod)]PF ₆ (25i)	252
12.3.11	1,5-Cyclooctadiene[((<i>S</i>)-4-Isopropyl-2-(6-methylpyridin-2-yl)-oxazolin)]iridium(I) hexaflourophosphate, [Ir(ⁱ Pr-mepyrox)(cod)]PF ₆ (25j)	253
12.3.12	1,5-Cyclooctadiene[((<i>S</i>)-4-butyl-2-(6-methylpyridin-2-yl)-oxazolin)]iridium(I) hexaflourophosphate, [Ir(ⁿ Bu-mepyrox)(cod)]PF ₆ (25k)	254
12.3.13	1,5-Cyclooctadiene[((<i>R</i>)-2-(6-methylpyridin-2-yl)-4-phenyl-oxazolin)]iridium(I) hexaflourophosphate, [Ir(Ph-mepyrox)(cod)]PF ₆ (25l)	255
12.3.14	1,5-Cyclooctadiene[((<i>S</i>)-4-isopropyl-2-(quinolin-2-yl)-oxazole)]iridium(I) hexaflourophosphate, [Ir(ⁱ Pr-quinox)(cod)]PF ₆ (25m)	256

12.3.15	1,5-Cyclooctadiene[((<i>R</i>)-4-Phenyl-2-(quinolin-2-yl)-oxazolin)]iridium(I) hexafluorophosphate, [Ir(Ph-quinox)(cod)]PF ₆ (25o)	257
12.3.16	1,5-Cyclooctadiene[((<i>S</i>)-4-Butyl-2-(quinolin-2-yl)-oxazolin)]iridium(I) hexafluorophosphate, [Ir(^t Bu-quinox)(cod)]PF ₆ (25n)	258
12.3.17	1,5-Cyclooctadiene[(2,6-bis((<i>R</i>)-4- <i>iso</i> -propyl-oxazolin)pyridine)]iridium(I) hexafluorophosphate, [Ir(ⁱ Pr-pybox)(cod)]PF ₆ (25p)	258
12.3.18	1,5-Cyclooctadiene[(2,2'-bipyridine)]iridium(I) hexafluorophosphate, [Ir(bpy)(cod)]PF ₆ (25q)	259
12.3.19	1,5-Cyclooctadiene[(4,4'-di- <i>tert</i> -butyl-2,2'-bipyridine)]iridium(I) hexafluorophosphate, [Ir(dtbpy)(cod)]PF ₆ (25r)	260
12.3.20	1,5-Cyclooctadiene[(1,10-phenanthroline)]iridium(I) hexafluorophosphate, [Ir(phen)(cod)]PF ₆ (25s)	261
12.3.21	1,5-Cyclooctadiene[(3,4,7,8-tetramethyl-1,10-phenanthroline)]iridium(I) hexafluorophosphate, [Ir(TMphen)(cod)]PF ₆ (25t)	261
12.3.22	1,5-Cyclooctadiene[((<i>S</i>)-2-(2-(diphenylphosphanyl)phenyl)-4-phenyl-oxazolin)]iridium(I) hexafluorophosphate, [Ir(Ph-phox)(cod)]PF ₆ (25u)	262
12.3.23	1,5-Cyclooctadiene[(2-(3,5-dimethyl-1 <i>H</i> -pyrazol-1-yl)pyridine)]iridium(I) hexafluorophosphate, [Ir(pypyraz)(cod)]PF ₆ (25v)	263
12.3.24	1,5-Cyclooctadiene[2-(pyridine-2-yl)-1 <i>H</i> -benzo[<i>d</i>]imidazole]iridium(I) hexafluorophosphate, [Ir(pybenzim)(cod)]PF ₆ (25w)	264
12.4	Iridium(I)-cod BAr^{F-} complexes 30	264
12.4.1	General Procedure E for [Ir(N [^] N)(cod)]BAr ^F complexes 30	264
12.4.2	General Procedure F for [Ir(N [^] N)(cod)]BAr ^F complexes 30	265
12.4.3	1,5-cyclooctadiene[(4 <i>S</i>)-2-(diphenylphosphino- <i>P</i>)phenyl]-oxazolin]iridium(I) tetrakis-[3,5- <i>bis</i> (trifluoromethyl)phenyl]borate (30a)	265
12.4.4	1,5-Cyclooctadiene[(2,2'-Bis((4 <i>S</i> ,4' <i>S</i>)-4,4'-methyl)-oxazolin)]iridium(I) tetrakis[3,5- <i>bis</i> (trifluoromethyl)phenyl]borate (30b)	265
12.4.5	1,5-Cyclooctadiene[(2,2'-Bis((4 <i>S</i> ,4' <i>S</i>)-4,4'-diisopropyl)-oxazolin)]iridium(I) tetrakis[3,5- <i>bis</i> (trifluoromethyl)phenyl]borate (30c)	266
12.4.6	1,5-Cyclooctadiene[(2,2'-Bis((4 <i>S</i> ,4' <i>S</i>)-4,4'-di((<i>S</i>)- <i>sec</i> -butyl)-oxazolin)]iridium(I) tetrakis[3,5- <i>bis</i> (trifluoromethyl)phenyl]borate (30f)	267
12.4.7	1,5-Cyclooctadiene[(2,2'-Bis((4 <i>S</i> ,4' <i>S</i>)-4,4'-diisobutyl)-oxazolin)]iridium(I) tetrakis[3,5- <i>bis</i> (trifluoromethyl)phenyl]borate (30g)	268
12.4.8	1,5-Cyclooctadiene[(2,2'-Bis((4 <i>R</i> ,4' <i>R</i>)-4,4'-diphenyl)-oxazolin)]iridium(I) tetrakis[3,5- <i>bis</i> (trifluoromethyl)phenyl]borate (30h)	269

12.4.9	1,5-Cyclooctadiene[(((<i>S</i>)-4-Isopropyl-2-(pyridine-2-yl)-oxazolin)]iridium(I) tetrakis[3,5-bis(trifluoromethyl)phenyl]borate (30i)	270
12.4.10	1,5-Cyclooctadiene[(((<i>S</i>)-4-Butyl-2-(pyridine-2-yl)-oxazolin)]iridium(I) tetrakis[3,5-bis(trifluoromethyl)phenyl]borate (30j)	271
12.4.11	1,5-Cyclooctadiene[(((<i>S</i>)-4-Isopropyl-2-(6-methylpyridin-2-yl)-oxazolin)]iridium(I) tetrakis[3,5-bis(trifluoromethyl)phenyl]borate (30e)	272
12.4.12	1,5-Cyclooctadiene[(((<i>R</i>)-4-phenyl-2-(6-Methylpyridin-2-yl)-oxazolin)]iridium(I) tetrakis[3,5-bis(trifluoromethyl)phenyl]borate (30k)	273
12.4.13	1,5-Cyclooctadiene[(((<i>S</i>)-4-Isopropyl-2-(quinolin-2-yl)-oxazolin)]iridium(I) tetrakis[3,5-bis(trifluoromethyl)phenyl]borate (30d)	273
12.4.14	1,5-Cyclooctadiene[(((<i>S</i>)-4-Butyl-2-(quinolin-2-yl)-oxazolin)]iridium(I) tetrakis[3,5-bis(trifluoromethyl)phenyl]borate (30l)	274
	12.5 Carbonyl complexes	276
12.5.1	General procedure G for the formation of [Ir(N ^N)(CO) ₂]PF ₆ complexes 28	276
12.5.2	Bi-carbonyl[(2,2'-bioxazole)]iridium(I) hexafluorophosphate, [Ir(H-box)(CO) ₂]PF ₆ (28a)	277
12.5.3	Carbonyl(1,5-cyclooctadiene)(2,2'-bioxazole)iridium(I) hexafluorophosphate, [Ir(H-box)(cod)(CO)]PF ₆ (26a)	277
12.5.4	Bi-carbonyl[(2,2'-Bis((4 <i>S</i> , 4' <i>S</i>)-4,4'-dimethyl)-oxazolin)]iridium(I) hexafluorophosphate, [Ir(Me-box)(CO) ₂]PF ₆ (28b)	278
12.5.5	Bi-carbonyl [(2,2'-Bis((4 <i>S</i> ,4' <i>S</i>)-4,4'-diisopropyl)-oxazolin)]iridium(I) hexafluorophosphate, [Ir(ⁱ Pr-box)(CO) ₂]PF ₆ (28c)	278
12.5.6	Bi-carbonyl [(2,2'-Bis((4 <i>S</i> ,4' <i>S</i>)-4,4'-di- <i>tert</i> -butyl)-oxazolin)]iridium(I) hexafluorophosphate, [Ir(^t Bu-box)(CO) ₂]PF ₆ (28d)	279
12.5.7	Bi-carbonyl [(2,2'-Bis((4 <i>S</i> , 4' <i>S</i>)-4,4'-dibutyl)-oxazolin)]iridium(I) hexafluorophosphate, [Ir(ⁿ Bu-box)(CO) ₂]PF ₆ (28e)	279
12.5.8	Bi-carbonyl [(2,2'-Bis((4 <i>R</i> , 4' <i>R</i>)-4,4'-diphenyl)-oxazolin)]iridium(I) hexafluorophosphate, [Ir(Ph-box)(CO) ₂]PF ₆ (28f)	280
12.5.9	1,5-Cyclooctadiene[(((4 <i>S</i> ,4' <i>S</i>)-4,4'-diisopropyl-2,2'-bithiazolin)]iridium(I) hexafluorophosphate, [Ir(ⁱ Pr-bta)(CO) ₂]PF ₆ (28g)	280
12.5.10	Bi-carbonyl [(<i>S</i>)-4-isopropyl-2-(pyridin-yl)-oxazolin]iridium(I) hexafluorophosphate, [Ir(ⁱ Pr-pyrox)(CO) ₂]PF ₆ (28h)	281
12.5.11	Bi-carbonyl [(((<i>S</i>)-4-(<i>tert</i> -butyl)-2-(pyridine-2-yl)-oxazolin)]iridium(I) hexafluorophosphate, [Ir(^t Bu-pyrox)(CO) ₂]PF ₆ (28i)	281
12.5.12	Bis-(¹³ C-carbonyl)[(((<i>S</i>)-4-(<i>tert</i> -butyl)-2-(pyridine-2-yl)-oxazolin)]iridium(I) hexafluorophosphate, [Ir(^t Bu-pyrox)(¹³ CO) ₂]PF ₆ (¹³ C-28i) 282	

12.5.13	Bi-carbonyl [((<i>S</i>)-4-Isopropyl-2-(6-methylpyridin-2-yl)-oxazolin)]iridium(I) hexaflourophosphate, [Ir(ⁱ Pr-mepyrox)(CO) ₂]PF ₆ (28j)	283
12.5.14	Carbonyl(1,5-cyclooctadiene) [((<i>S</i>)-4-Isopropyl-2-(6-methylpyridin-2-yl)-oxazolin)]iridium(I) hexaflourophosphate, [Ir(ⁱ Pr-mepyrox)(cod)(CO)]PF ₆ (26j)	284
12.5.15	Bi-carbonyl[(((<i>S</i>)-4-butyl-2-(6-methylpyridin-2-yl)-oxazolin)]iridium(I) hexaflourophosphate, [Ir(ⁿ Bu-mepyrox)(CO) ₂]PF ₆ (28k)	284
12.5.16	Bi-carbonyl [((<i>R</i>)-2-(6-methylpyridin-2-yl)-4-phenyl-oxazolin)]iridium(I) hexaflourophosphate, [Ir(Ph-mepyrox)(CO) ₂]PF ₆ (28l)	284
12.5.17	Bi-carbonyl [((<i>S</i>)-4-isopropyl-2-(quinolin-2-yl)-oxazole)]iridium(I) hexaflourophosphate, [Ir(ⁱ Pr-quinox)(CO) ₂]PF ₆ (28m)	285
12.5.18	Carbonyl(1,5-cyclooctadiene[(((<i>S</i>)-4-isopropyl-2-(quinolin-2-yl)-oxazole)] iridium(i) hexaflourophosphate, [Ir(iPr-quinox)(cod)(CO)]PF ₆ (26m)	286
12.5.19	Bi-carbonyl [((<i>S</i>)-4-Butyl-2-(quinolin-2-yl)-oxazolin)]iridium(I) hexaflourophosphate, [Ir(ⁿ Bu-quinox)(CO) ₂]PF ₆ (28n)	286
12.5.20	Bi-carbonyl [(2,6-bis((<i>S</i>)-4- <i>iso</i> -propyl-oxazolin)pyridine)]iridium(I) hexaflourophosphate, [Ir(ⁱ Pr-pybox)(CO) ₂]PF ₆ (28o)	287
12.5.21	Bi-carbonyl [((<i>S</i>)-2-(2-(diphenylphosphanyl)phenyl)-4-phenyl-oxazolin)]iridium(I) hexaflourophosphate, [Ir(Ph-phox)(CO) ₂]PF ₆ (28u)	287
12.5.22	Bi-carbonyl [(2-(3,5-dimethyl-1 <i>H</i> -pyrazol-1-yl)pyridine)]iridium(I) hexaflourophosphate, [Ir(pypyraz)(CO) ₂]PF ₆ (28v)	288
12.5.23	Bi-carbonyl[2-(pyridine-2-yl)-1 <i>H</i> -benzo[<i>d</i>]imidazole]iridium(I) hexaflourophosphate, [Ir(TMphen)(CO) ₂]PF ₆ (28w)	288
12.5.24	Bi-carbonyl [(4,4'-di-tert-butyl-2,2'-bipyridine)]iridium(I) hexaflourophosphate, [Ir(dtbp)(CO) ₂]PF ₆ (28r)	289
12.5.25	Carbonyl(1,5-cyclooctadiene[(4,4'-di-tert-butyl-2,2'-bipyridine)] iridium(I) hexaflourophosphate, [Ir(dtbp)(cod)(CO)]PF ₆ (26r)	289
12.5.26	Carbonyl(1,5-cyclooctadiene)(2,2'-bipyridine) iridium(I) hexaflourophosphate, [Ir(bpy)(cod)(CO)]PF ₆ (26q)	290
12.5.27	Carbonyl(1,5-cyclooctadiene)(1,10-phenanthroline) iridium(I) hexaflourophosphate, [Ir(^{phen})(cod)(CO)]PF ₆ (26s)	290
12.5.28	Carbonyl(1,5-cyclooctadiene)(3,4,7,8-tetramethyl-1,10-phenanthroline) iridium(I) hexaflourophosphate, [Ir(TMphen)(cod)(CO)]PF ₆ (26t)	290
	12.6 Ruthenium Complexes	291
12.6.1	Reactions based on [Ru(cymene)Cl ₂] ₂	291

12.6.1.1	General procedure H for complexation of box ligands 5 with [Ru(cymene)Cl] ₂ (46)	291
12.6.1.2	[chloro-[(2,2'-Bis((4 <i>S</i> ,4' <i>S</i>)-4,4'-diisopropyl)-oxazolin)]-(η ⁶ - <i>p</i> -cymol)-ruthenium(II)] chloride; [Ru(ⁱ Pr-box)(cymene)Cl]Cl (48a)	292
12.6.1.3	[chloro-[(2,2'-Bis((4 <i>R</i> ,4' <i>R</i>)-4,4'-diphenyl)-oxazolin)]-(η ⁶ - <i>p</i> -cymol)-ruthenium(II)]chloride; [Ru(Ph-box)(cymene)Cl]Cl (48b)	292
12.6.1.4	[chloro-[2,2'-Bis((4 <i>S</i> ,4' <i>S</i>)-4,4'-diisobutyl)-oxazolin)]-(η ⁶ - <i>p</i> -cymol)-ruthenium(II)]chloride; [Ru(ⁱ Bu-box)(cymene)Cl]Cl (48c)	293
12.6.1.5	[chloro-[2,2'-Bis((4 <i>R</i> ,4' <i>R</i>)-4,4'-dibenzyl)-oxazolin)]-(η ⁶ - <i>p</i> -cymol)-ruthenium(II)]chloride; [Ru(Bn-box)(cymene)Cl]Cl (48d)	293
12.6.1.6	[dichloro-[(2,2'-Bis((4 <i>S</i> ,4' <i>S</i>)-4,4'-diisopropyl)-oxazolin)]-[2,2':6',2''-Terpyridin]-ruthenium(II)]; [Ru(ⁱ Pr-box)(tpy)Cl ₂] (54a)	294
12.6.1.7	Reaction of [Ru(ⁱ Pr-box)(cymene)Cl]Cl (48a) with bipyridine 37	294
12.6.2	Reactions based on [Ru(dmsO) ₄ Cl ₂]	295
12.6.2.1	Dichloro(2,2'-bipyridyl)-bis((<i>s</i>)-dimethylsulfoxid)ruthenium(II);[Ru(bpy)(dmsO) ₂ Cl ₂] (56)	295
12.6.2.2	Dichloro(2,2':6',2''-terpyridyl)((<i>s</i>)-dimethylsulfoxid)ruthenium(II);[Ru(tpy)(dmsO)Cl ₂] (57)	296
12.6.2.3	Dichloro(2,2'-bis[oxazolin-2-yl])bis(dimethylsulfoxid)ruthenium(II);[Ru(H-box)(dmsO) ₂ Cl ₂] (49a)	296
12.6.2.4	Dichloro(4,4'-diisopropyl-2,2'-bis[oxazolin-2-yl])bis((<i>s</i>)-dimethylsulfoxid)ruthenium(II);[Ru(ⁱ Pr-box)(dmsO) ₂ Cl ₂] (49b)	297
12.6.2.5	Dichloro(4,4'-diphenyl-2,2'-bis[oxazolin-2-yl])bis(dimethylsulfoxid)ruthenium(II);[Ru(Ph-box)(dmsO) ₂ Cl ₂] (49c)	298
12.6.2.6	Dichloro(2-[4'-isopropyl-oxazolin-2-yl]pyridyl)bis((<i>s</i>)-dimethylsulfoxid)ruthenium(II); [Ru(ⁱ Pr-pyrox)(dmsO) ₂ Cl ₂] (49d)	299
12.6.2.7	Dichloro(2,6-bis[4'-isopropyl-oxazolin-2-yl]pyridyl)((<i>s</i>)-dimethylsulfoxid)ruthenium(II),[Ru(ⁱ Pr-pybox)(dmsO)Cl ₂] (58)	299
12.6.2.8	[chloro(2,2'-bis[oxazolin-2-yl])(2,2'-bipyridyl)(dimethylsulfoxid)ruthenium(II)] chlorid; [Ru(H-box)(bpy)((<i>s</i>)-dmsO)Cl] ⁺ Cl ⁻ (61)	300
12.6.2.9	[chloro(4,4'-diisopropyl-2,2'-bis[oxazolin-2-yl])(2,2'-bipyridyl)((<i>s</i>)-dimethylsulfoxid)ruthenium(II)] chlorid; [Ru(ⁱ Pr-box)(bpy)(dmsO)Cl] ⁺ Cl ⁻ (61b)	301
12.6.2.10	[chloro(4,4'-diphenyl-2,2'-bis[oxazolin-2-yl])(2,2'-bipyridyl)(dimethylsulfoxid)ruthenium(II)] chlorid; [Ru(Ph-box)(bpy)(dmsO)Cl] ⁺ Cl ⁻ (61c)	302
12.6.2.11	[chloro(2,2'-bis[oxazolin-2-yl])(2,2':6',2''-terpyridyl)ruthenium(II)] chlorid; [Ru(H-box)(tpy)Cl] ⁺ Cl ⁻ (54b)	302

12.6.2.12	[chloro(4,4'-diisopropyl-2,2'-bis[oxazolin-2-yl])(2,2':6',2''-terpyridyl)ruthenium(II)] chlorid; [Ru(ⁱ Pr-box)(tpy)Cl ⁺]Cl ⁻ (54a)	303
12.6.2.13	[chloro(4,4'-diphenyl-2,2'-bis[oxazolin-2-yl])(2,2':6,2''-terpyridyl)ruthenium(II)] chlorid; [Ru(Ph-box)(tpy)Cl ⁺]Cl ⁻ (54c)	304
12.6.2.14	[chloro(2,6-bis[(<i>S</i>)-4'-isopropyl-oxazolin-2-yl]pyridyl)(2,2'-bipyridyl)-ruthenium(II)] chlorid; [Ru(ⁱ Pr-pybox)(bpy)Cl ⁺]Cl ⁻ (64)	304
12.6.2.15	Transferhydrogenation	305
13	CATALYSIS	306
13.1	Aromatic Borylation	306
13.1.1	Independent Preparation of Borylationproducts	306
13.1.1.1	2-(4-(<i>tert</i> -butyl)phenyl)-4,4,5,5-tetramethyl-1,3,2-dioxaborolane (68a)	307
13.1.1.2	2-(3-(<i>tert</i> -butyl)phenyl)-4,4,5,5-tetramethyl-1,3,2-dioxaborolane (67a)	307
13.1.1.3	4,4,5,5-tetramethyl-2-(4-(trifluoromethyl)phenyl)-1,3,2-dioxaborolane (68b)	308
13.1.1.4	4,4,5,5-tetramethyl-2-(3-(trifluoromethyl)phenyl)-1,3,2-dioxaborolane (67b)	308
13.1.1.5	ethyl 4-(4,4,5,5-tetramethyl-1,3,2-dioxaborolan-2-yl)benzoate (68c)	309
13.1.1.6	ethyl 3-(4,4,5,5-tetramethyl-1,3,2-dioxaborolan-2-yl)benzoate (67c)	309
13.1.1.7	4,4,5,5-tetramethyl-2-(<i>p</i> -tolyl)-1,3,2-dioxaborolane (68d)	310
13.1.1.8	4,4,5,5-tetramethyl-2-(<i>m</i> -tolyl)-1,3,2-dioxaborolane (67d)	310
13.1.1.9	2-(4-cyclohexylphenyl)-4,4,5,5-tetramethyl-1,3,2-dioxaborolane (68e)	310
13.1.1.10	2-(4-methoxyphenyl)-4,4,5,5-tetramethyl-1,3,2-dioxaborolane (68f)	311
13.1.1.11	2-(3-methoxyphenyl)-4,4,5,5-tetramethyl-1,3,2-dioxaborolane (67f)	311
13.1.2	2-(4-chlorophenyl)-4,4,5,5-tetramethyl-1,3,2-dioxaborolane (68g)	312
13.1.2.1	2-(3-chlorophenyl)-4,4,5,5-tetramethyl-1,3,2-dioxaborolane (67g)	312
13.1.3	Borylation Experiments	313
13.1.3.1	Borylation of C ₆ D ₆	313
13.1.3.2	Borylation of Monosubstituted Arenes Using [Ir(cod)Cl] (23) as Iridium Source	314
13.1.3.3	Optimization of the Catalytic System	315

13.1.3.4	Borylation of PhCF ₃ (65b) at 80 °C	316
13.1.3.5	Borylation of PhCF ₃ (65b) at 70 °C	319
13.1.3.6	Borylation of PhCF ₃ (65b) at Room Temperature	320
13.1.3.7	Borylation of <i>tert</i> -butyl-benzene (65a)	321
13.1.3.8	Borylation of cyclohexylbenzene (65e)	325
13.1.3.9	Borylation of anisol (65f) at Room Temperature	326
13.1.3.10	Borylation of ethylbenzoate (65c) at Room Temperature	328
	13.2 Aliphatic Borylation	329
13.2.1	Borylation of <i>n</i> -Octane (98)	329
13.2.1.1	Preparation of Reference Compound <i>n</i> -Octyl picanolato borane (97)	330
13.2.1.2	Borylation of <i>n</i> -Octane	330
13.2.1.3	Borylation of <i>n</i> -Decane (100)	331
13.2.1.4	Control experiments for the borylation of <i>n</i> -decane (100)	332
	13.3 (Hydrido)silyl Ether Directed γ-C-H Activation	335
13.3.1	(Hydrido)silyl ethers	335
13.3.1.1	General procedure J for the formation of (hydrido)silyl ethers 103 and 107 from ketones 102 or alcohols 106	335
13.3.1.2	diethyl(<i>tert</i> -pentyloxy)silane (103c)	336
13.3.1.3	((3,7-dimethyloctan-3-yl)oxy)diethylsilane (103b)	336
13.3.1.4	diethyl((2-methylheptan-3-yl)oxy)silane (103b)	337
13.3.1.5	diethyl(pentan-3-yloxy)silane (107b)	338
13.3.1.6	((2,4-dimethylpentan-3-yl)oxy)diethylsilane (107d)	339
13.3.1.7	(benzhydroxy)diethylsilane (107e)	339
13.3.2	Oxasilolanes	340
13.3.2.1	General procedure K for the formation of oxasilolanes 104 and 108	340
13.3.2.2	2,2-diethyl-5-methyl-5-(4-methylpentyl)-1,2-oxasilolane (104b)	341
13.3.2.3	2,2-diethyl-5,5-dimethyl-1,2-oxasilolane (104c)	342
13.3.2.4	1,1-diethyl-3-phenyl-1,3-dihydrobenzo[<i>c</i>][1,2]oxasilole (108e)	342
13.3.2.5	5-butyl-2,2-diethyl-4-methyl-1,2-oxasilolane (108c)	343
13.3.2.6	2,2,5-triethyl-1,2-oxasilolane (108c)	344
13.3.2.7	2,2-diethyl-5-isopropyl-4-methyl-1,2-oxasilolane (108d)	345
	2,2-diethyl-5-methyl-5-(4-methylpentyl)-1,2-oxasilolane (104b)	346
	13.4 Hydrogenation	348
13.4.1	General Procedure La and Lb for Hydrogenations.	348
13.4.2	(<i>E</i>)-1,2-Diphenylethene (113)	349
13.4.3	(<i>Z</i>)-1,2-Diphenylethene (115)	350

13.4.4	Cyclooctene (116)	350
13.4.5	Cyclohex-2-enol (118)	350
13.4.6	Cyclohexanone (120)	351
13.4.7	4-(<i>tert</i> -Butyl)cyclohexanone (121)	351
13.4.8	Acetophenone (123)	352
13.4.9	Ethyl cinnamate (125)	352
13.4.10	(<i>E</i>)-4-Phenylbut-3-en-2-one (129)	353
13.4.11	(<i>E</i>)-2-Methyl-3-phenylacrylaldehyde (133)	353
13.4.12	(<i>E</i>)-Hex-4-en-3-one (137)	354
13.4.13	Cyclohex-2-enone (141)	354
13.4.14	3,5,5-Trimethylcyclohex-2-enone (142)	355
BIBLIOGRAPHY		357
CURRICULUM VITAE		365
SCIENTIFIC CONTRIBUTIONS		366

V. APPENDIX

APPENDIX A: CRYSTALLOGRAPHIC DATA	A3
APPENDIX B: NMR SPECTRA	A23
APPENDIX C: IR SPECTRA OF CARBONYL COMPLEXES	A109

Abbreviations

Ac	acetyl
Ad	adamantyl
annilinox	2-(oxazoline-2-yl)aniline
approx.	approximately
Ar	aryl
asymm	asymmetric
ATR-IR	attenuated total reflection infrared
B ₂ pin ₂	bis(pinacolato)diboron
BAr ^F	(tetrakis[3,5-bis(trifluoromethyl)phenyl]borate
BINAP	2,2'-bis(diphenylphosphino)1,1'-binaphthyl
bipyrox	6,6'-bis(oxazolin-2-yl)-2,2'-bipyridine
Bn	benzoyl
box	2,2'-bioxazoline
bpy	2,2'-bipyridine
BSA	<i>N,O</i> -bis(trimethylsilyl)acetamide
bta	4,4'-diisopropyl-2,2'-bithiazolin
btp	2,2'-bithiophen
calc.	calculated
cat	catechol (benzene-1,2-diol)
cat*	4-methylcatechol (4-methylbenzene-1,2-diol)
cat.	catalytic
cf.	confer
CHex	cyclohexane
cod	<i>cis,cis</i> -1,5-cyclooctadiene
coe	<i>cis</i> -cyclooctene
cond.	conditions
config.	configuration
conv.	conversion
cot	1,3,5,7-cyclooctatetraene
Cp	Cyclopentadien anion
Cp*	1,2,3,4,5-pentamethylcyclopentadien anion
CSD	Cambridge Structural Database
Cy	cyclohexyl

cybox	1,2-bis(oxazolin-2-yl)cyclohexane
d (NMR)	doublet
DAST	<i>N,N</i> -Diethylaminosulfur trifluoride
DCE	1,2-dichloroethane
DCM	dichloromethane
DFT	density functional theory
DIOP	<i>O</i> -isopropylidene-2,3-dihydroxy-1,4-bis(diphenylphosphino)butane
DIPAMP	ethane-1,2-diylbis[(2-methoxyphenyl)phenylphosphane]
DMF	<i>N,N</i> -dimethylformamide
DM-mebox	2-bis(oxalin-2-yl)propane
DPEN	1,2-diphenyl-1,2-ethylenediamine
dppp	1,3-bis(dimethylphosphino)propane
dr	diastereomeric ratio
dtbpy	4,4'-di- <i>tert</i> -butyl-2,2'-bipyridin
EDCI	3-(ethyliminomethylidenamino)- <i>N,N</i> -dimethyl-propan-1-amine
ee	enantiomeric excess
EI	electron ionisation
equiv.	equivalent
er	enantiomeric ratio
ESI	electrospray ionisation
Et	ethyl
FWHM	full width at half maximum
HMphen	3,4,5,6,7,8-hexamethylphenanthrolin
HOBt	<i>N</i> -hydroxybenzotriazol
HRMS	high resolution mass spectrometry
i.a.	inter alia
iBCF	isobutyl chloroformate
ⁱ Bu	<i>iso</i> -butyl
int.	integral
ⁱ Pr	<i>iso</i> -propyl
IR	infrared spectroscopy
L	any monodentate ligand
L ^Λ L	any bidentate ligand
L ^Λ L ^Λ L	any tridentate ligand
<i>m</i> -	<i>meta</i> -

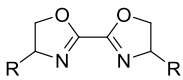
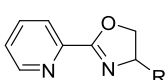
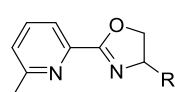
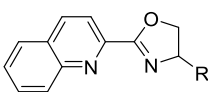
m (IR)	medium
m (NMR)	multiplet
m.p.	melting point
Me	methyl
mebox	bis(oxazolin-2-yl)methane
meprox	2-(6-methylpyridine-2-yl)-oxazoline
Mes	mesitylen (2,4,6-trimethylphenyl)
MO	molecular orbital
MOM	methoxymethyl
MS	mass spectrometry
n.d.	not determined
nbe	norbornene
NHC	<i>N</i> -heterocyclic carbene
NMM	<i>N</i> -methylmorpholin
NMR	nuclear magnetic resonance spectroscopy
<i>o</i> -	<i>ortho</i> -
opbox	<i>ortho</i> -bis(oxazolin-2-yl)benzene
<i>p</i> -	<i>para</i> -
<i>p</i> -cymene	4-(<i>iso</i> -propyl)-toluene
Ph	phenyl
phebox	1,3-bis(oxazolin-2-yl)benzene
phen	phenanthroline
phenbox	2-(1,10-phenanthrolin-2-yl)oxazolin
phox	2-(2-phosphanyl)phenyl-oxazolin
pin	pinacol (2,3-dimethyl-2,3-butanediol)
Piv	pivalyl
pox	2-(pyrrolidin-2-yl)oxazolin
ppm	parts per million
Pr	2,6-diisopropylphenyl
py	pyridine
pybenzim	2-(pyridin-2-yl)-1 <i>H</i> -benzo[<i>d</i>]imidazole
pybox	2,6-bis(oxazolin-2-yl)pyridine
ppyraz	2-(3,5-dimethyl-1 <i>H</i> -pyrazol-1-yl)pyridine
pyrox	2-(pyridine-2-yl)-oxazoline
q (NMR)	quartet

uant.	quantitative
quin (NMR)	quintet
quinox	2-(quinolin-2-yl)-oxazoline
r. t.	room temperature
rac.	racemate
R _f	retention factor
rfx.	reflux
S	solvent molecule (coordinated as ligand to a metal)
s (IR)	strong
s (NMR)	singlet
saox	<i>N</i> -((oxazolin-2-yl)methyl)-4-methylbenzenesulfonamide
sat.	saturated
^{sec} Bu	<i>sec</i> -butyl
sep (NMR)	septet
symm	symmetric
t (NMR)	triplet
tartbox	2,2'-(2,2-dimethyl-1,3-dioxolane-4,5-diyl)bis(oxazoline)
TBAF	tetrabutylammonium fluoride
TBHP	<i>tert</i> -butylhydroperoxide
^t Bu	<i>tert</i> -butyl
Temp.	temperature
TEP	Tolman's electronic parameter
THF	tetrahydrofuran
thiox	2-(thiophen-2-yl)oxazoline
TLC	thin layer chromatography
TMB	1,3,5-trimethoxybenzene
TMEDA	<i>N,N,N,N</i> -tetramethylethane-1,2-diamine
TMphen	3,4,7,8-tetramethylphenanthrolin
TOF	turn over frequency
TON	turn over number
tpy	2,2':6',2''-terpyridine
t _R	retention time
TsDPEN	<i>N</i> -tosyl-1,2-diphenyl-1,2-ethylendiamin
w (IR)	weak

XyliPHOS

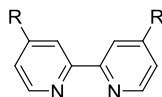
(*R*)-1-[(*S*)-2-diphenylphosphino]-ferrocenyl]-ethyl-bis-(3,5-dimethylphenyl)phosphine

Table of Ligands

box			pyrox		
2,2'-bioxazoline			2-(pyridine-2-yl)-oxazoline		
					
5a	Me-box	R=(<i>S</i>)-CH ₃	10b	ⁱ Pr-pyrox	R=(<i>S</i>)-CH(CH ₃) ₂
5b	ⁱ Pr-box	R=(<i>S</i>)-CH(CH ₃) ₂	10c	^t Bu-pyrox	R=(<i>S</i>)-C(CH ₃) ₃
5c	^t Bu-box	R=(<i>S</i>)-C(CH ₃) ₃	10f	ⁿ Bu-pyrox	R=(<i>S</i>)-C ₄ H ₉
5d	^{sec} Bu-box	R=(<i>S</i>)-((<i>R</i>)-CH(CH ₃)(C ₂ H ₅))	10g	Ph-pyrox	R=(<i>R</i>)-C ₆ H ₅
5e	ⁱ Bu-box	R=(<i>S</i>)-CH ₂ CH(CH ₃) ₂	10h	Bn-pyrox	R=(<i>R</i>)-CH ₂ -C ₆ H ₅
5f	ⁿ Bu-box	R=(<i>S</i>)-C ₄ H ₉			
5g	Ph-box	R=(<i>R</i>)-C ₆ H ₅			
5h	Bn-box	R=(<i>R</i>)-CH ₂ -C ₆ H ₅			
5i	H-box	R=H			
mepyrox			quinox		
2-(2-methylpyridine-2-yl)-oxazoline			2-(quinolin-2-yl)-oxazoline		
					
19b	ⁱ Pr-mepyrox	R=(<i>S</i>)-CH(CH ₃) ₂	20b	ⁱ Pr-quinox	R=(<i>S</i>)-CH(CH ₃) ₂
19f	ⁿ Bu-mepyrox	R=(<i>S</i>)-C ₄ H ₉	20f	ⁿ Bu-quinox	R=(<i>S</i>)-C ₄ H ₉
19g	Ph-mepyrox	R=(<i>R</i>)-C ₆ H ₅	20g	Ph-mepyrox	R=(<i>R</i>)-C ₆ H ₅
19h	Bn-mepyrox	R=(<i>R</i>)-CH ₂ -C ₆ H ₅			

bpy

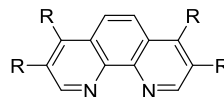
2,2'-bipyridine



- 37 Bpy R=H
32 dtbpy R=C(CH₃)₃

phen

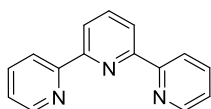
phenanthroline



- 38 phen R=H
39 TMphen R=CH₃

tpy

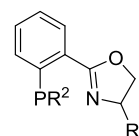
(2,2';6,2'')-terpyridine



- 51 tpy

phox

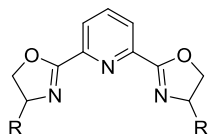
2-(2-phosphanil)phenyl-oxazolin



- 31 ⁱPr-phox R¹=(*R*)-CH(CH₃)₂, R²=Ph
40 Ph-phox R¹=(*S*)-C₆H₅, R²=Ph

pybox

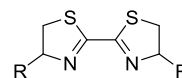
2,6-bis(oxazolin-2-yl)pyridine



- 36 ⁱPr-pybox R=(*R*)-CH(CH₃)₂

bta

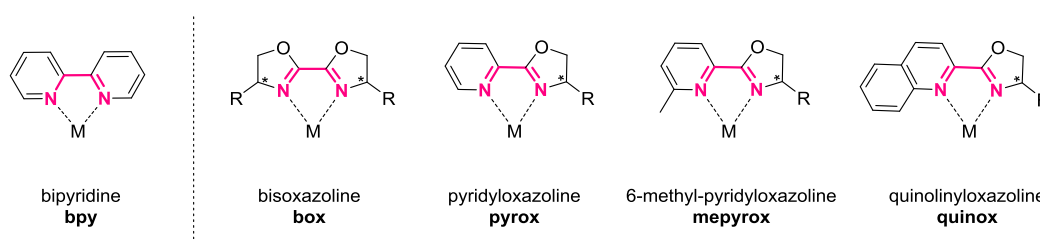
4,4'-diisopropyl-2,2'-bithiazolin



- 7 ⁱPr-bta R=(*S*)-CH(CH₃)₂

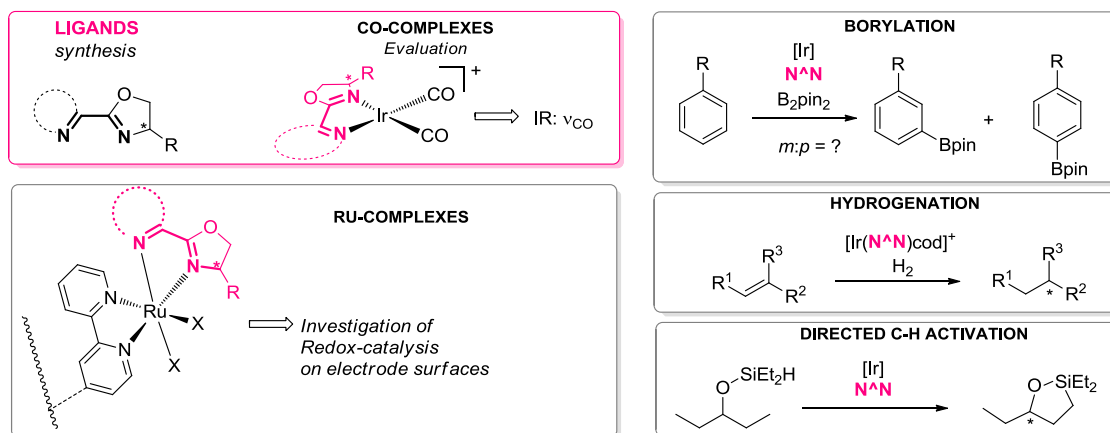
1 Introduction and Motivation

Bipyridines are an important class of ligands applied in homogeneous catalysis, *e.g.* in aromatic borylation, amination or in catalytic water oxidation.^[1-4] The development of asymmetric versions of such catalytic reactions offers a large impact on areas where stereoselective synthesis is of high interest, for example on the pharmaceutical industry. Since it is difficult to introduce chiral information into bipyridines, here structures containing a chiral oxazoline motif, such as bisoxazolines (box), pyridyloxazolines (pyrox), 6-methylpyridyloxazolines (mepyrox) and quinolyloxazolines (quinox), were chosen as ligands. As depicted in Scheme 1-1, the mentioned oxazoline structures show a high structural similarity and therefore could be suitable replacements for bipyridines.



Scheme 1-1. Comparison of bipyridine and different bidentate oxazolines. The structures show the same bite angle upon coordination to a metal center (M) and the donor atoms are similarly hybridized.

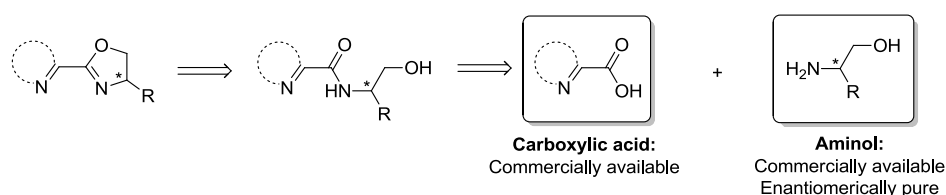
In this project, differently substituted box, pyrox and related structures were prepared and their electrical and steric properties were investigated by IR analysis of their Ir(I) carbonyl complexes (Scheme 1-2). In addition, the oxazolines were applied as ligands on Ir(I) catalyst-precursors in three different homogeneous catalytic reactions; aromatic borylation, hydrogenation and (hydrido)silyl ether directed γ -C-H activation. Besides, the preparation of heteroleptic ruthenium(II) complexes, suitable for surface immobilization, were investigated. The future aim for these complexes is to obtain redox active catalysts suitable for electrode immobilization, to study the catalysts directly on electrodes.



Scheme 1-2. The preparation of bidentate oxazoline ligands and the evaluation of their electrical and sterical properties in Ir(I) carbonyl complexes builds the basis of this work. The ligands were further applied sub-projects concerning the catalytic activity of their Ir(I) complexes (borylation, hydrogenation and directed C-H activation and the formation of heteroleptic Ru(II) complexes for the future application as redox catalysts on gold surfaces.

Oxazolines

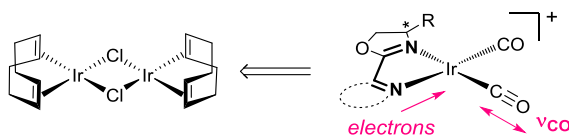
Oxazoline structures can be derived in enantiopure form from the chiral pool of natural amino acids (Scheme 1-3). Furthermore, a large variety of amino acids is available, allowing the preparation of collections of the corresponding oxazoline ligands. As direct reaction partner for the aminols, carboxylic acids are suitable. These compounds are commercially available in a large variety, which also contributes to a time efficient preparation of oxazoline ligand collections.



Scheme 1-3. Oxazolines can be prepared from commercially available carboxylic acids and aminols. The aminols are derived from the (natural) pool of amino acids.

Carbonyl Complexes

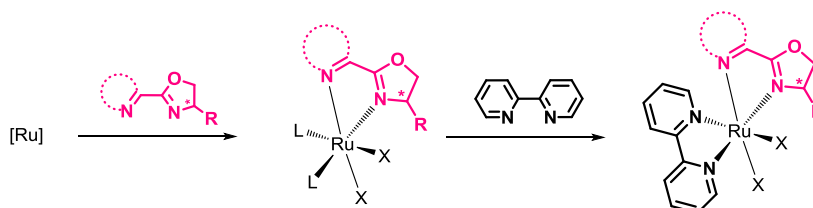
Many steps in a catalytic cycle can be influenced by the electron density donated by the ligand toward the central metal, *e.g.* oxidative addition or reductive elimination. Therefore, the prepared oxazoline ligands were evaluated towards their electronic and steric properties by measuring the stretching frequencies of their corresponding dicarbonyl complexes (Scheme 1-4). The stretching frequencies of CO ligands are dependent on the C-O bonding order, which in turn is influenced by the electron density of the central metal. This makes the CO stretching frequencies a good representative for the electronic properties of the oxazoline ligands and was also used extensively before in the determination of the electronic properties of *e.g.* phosphorous ligands.^[5-6] The stretching frequencies of CO appear in the IR spectrum around 2000 cm^{-1} , where typically no other absorptions bands occur. This allows an easy identification of these bands. The carbonyl complexes can be prepared from $[\text{Ir}(\text{cod})(\text{Cl})_2]$.^[7-8]



Scheme 1-4. The electronic properties of the oxazoline ligands can be evaluated by measuring the IR absorption frequencies of the carbonyl ligands. The carbonyl complexes can be synthesized from $[\text{Ir}(\text{cod})(\text{Cl})_2]$.

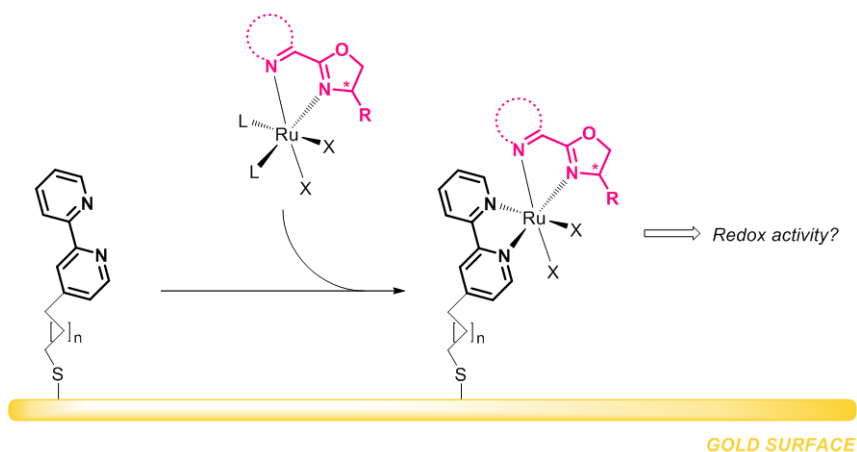
Ruthenium Complexes

The first target of this subproject was to study the stepwise introduction of an oxazoline and a bipyridine ligand to a ruthenium center (Scheme 1-5). As complex precursor $[\text{Ru}(p\text{-cymene})(\text{Cl})_2]_2$ or $[\text{Ru}(\text{dmsO})_4(\text{Cl})_2]$ are suitable. The right precursor for the planned stepwise complex synthesis was investigated and the products were analyzed by standard methods. The heteroleptic target complexes were tested towards their ability to act as redox catalyst in transfer hydrogenation.



Scheme 1-5. Stepwise introduction of an oxazoline and a bipyridine.

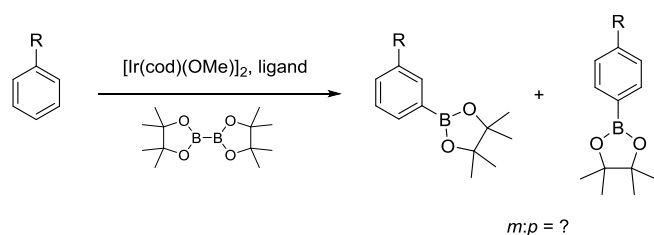
In future applications, the immobilization of redox complexes on electrode surfaces is envisaged to study their redox properties (Scheme 1-6). Substituted bipyridines can serve as potential ligands for surface immobilization, because these bidentate ligands are known to coordinate as strong ligands to a metal. Oxazolines could add chiral information to such a complex and redox catalysis, such as alcohol oxidation, could be performed stereoselectively. The catalyst formation on an electrode surface would happen on a bipyridine functionalized surface, reacting with an oxazoline containing complex, which is added in solution.



Scheme 1-6. Formation of a chiral catalyst on a gold surface which was functionalized with bipyridine before.

Borylation

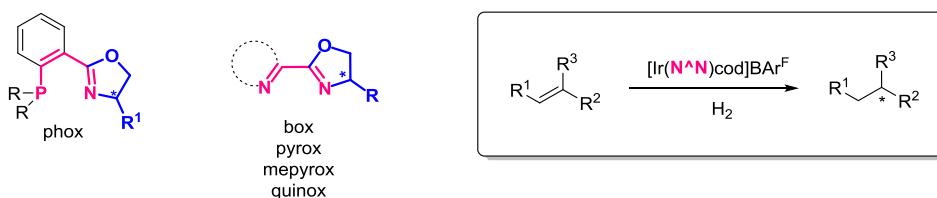
Aromatic borylation is a well working reaction with electron rich bipyridines as ligands, in the presence of $[\text{Ir}(\text{cod})(\text{OMe})_2]$ as iridium source.^[1] Up to date, aromatic borylation is depending on the steric hindrance of residues on the arene. For example is the sterically hindered *ortho* position usually not borylated unless a directing group is present. In this project, the bipyridine ligand was replaced by oxazolines and the catalytic system was applied on monosubstituted arenes, analyzing the *meta:para* ratio of the formed products by $^1\text{H-NMR}$ and/or GC-FID (Scheme 1-7).



Scheme 1-7. Aromatic borylation of monosubstituted arenes leads to *meta* and *para* substitution. Due to steric hindrance, *ortho* borylation is not occurring.

Hydrogenation

For asymmetric homogeneous hydrogenation usually phosphinooxazolines (phox) are applied as ligands. The ligand containing complex is synthesized prior to catalysis and has the general structure $[\text{Ir}(\text{ligand})(\text{cod})]\text{BAr}^{\text{F}}$ (Scheme 1-8).^[9] Since these complexes were obtained as intermediates in the preparation of carbonyl complexes, they were conveniently probed towards their reactivity in hydrogenation. Compared to the usually applied phox ligands, the oxazoline ligands have different bite angles and instead of coordination via P,N-donor atoms, they coordinate via N,N-donors. However, the origin of chirality is the same for both ligand classes and their comparison in hydrogenation can offer interesting results.



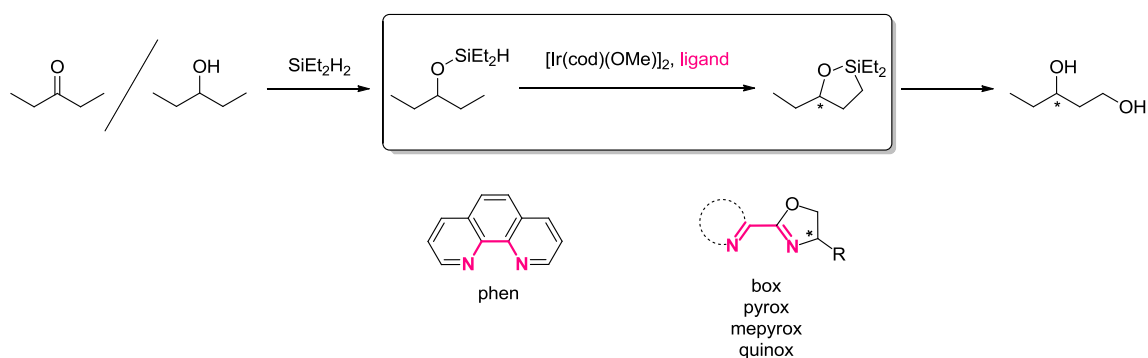
Scheme 1-8. Structural comparison of phox and bidentate oxazoline structures and general reaction scheme for catalytic hydrogenation.

Hydrosilyl ether directed γ -C-H activation

Recently, an elegant method for hydrosilyl ether directed γ -C-H activation was developed by the group of Hartwig (Scheme 1-9).^[10] The C-H activation is catalyzed by a system of $[\text{Ir}(\text{cod})(\text{OMe})]_2$ and phenanthroline as ligand. Since the non-chiral phenanthrolines are structurally closely related to bidentate oxazolines, the replacement of phenanthrolines by oxazolines was possible.

The reaction sequence uses ketones or alcohols that are transformed into their hydrosilyl ethers. The C-H activation is occurring with the formation of a cyclic oxasilolane in γ -position to the hydrosilyl ether. Oxidative cleavage of the oxasilolane leads to the formation of an 1,3-diol.

In this project, the influence of the chiral ligand in the stereoselective C-H activation step was investigated.

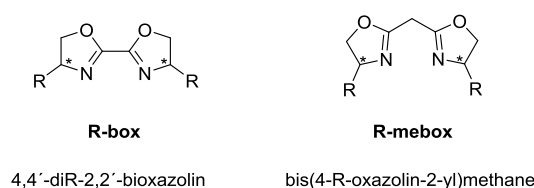


Scheme 1-9. Reaction sequence for the formation of a hydrosilyl ether, C-H activation and oxidative cleavage.

I. Scientific Background

2 Oxazoline Based Structures

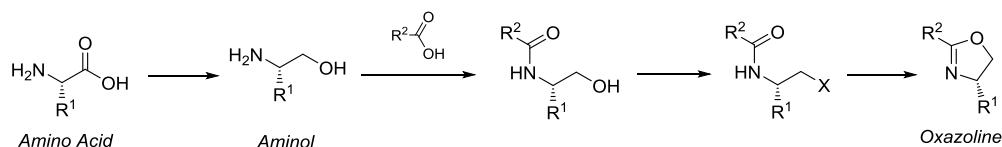
Oxazoline structures were widely used and are at least known since 1989, when Brunner and Obermann reported a synthesis for these structures.^[11] since then, a lot of different synthesis routes for a large variety of oxazoline containing structures were reported by various research groups and will be presented briefly in the following chapter. Since 2,2'-bioxazolines were less often applied as bis(oxalin-2-yl)methanes, often no distinction in their naming was made and both were referred to as "bioxazolines" or "box".^[12-17] For this work, it was decided to denote 2,2'-bioxazolines with "box" and the methylene bridged bis(oxalin-2-yl)methanes with "mebox" (Scheme 2-1). For convenience, all structures containing two oxazoline moieties will collectively be called "bioxazolines".



Scheme 2-1. Denomination of bisoxazolines in this work.

2.1 Preparation of Bisoxazolines and Pyridyloxazolines

The oxazoline structure is prepared from chiral aminols that are derived from the naturally available pool of amino acids. The oxazoline formation itself requires two key steps; firstly the condensation of the aminol with a carboxylic acid and secondly the base-induced ring closure of the resulting β -hydroxy-amide. The latter step may require the introduction of a suitable leaving group beforehand (Scheme 2-2). Therefore, the wide range of typical oxazoline syntheses is comprised of two or three step procedures. However, also protocols for single step procedures are known that realize amide formation as well as oxazoline ring closure in one working step.^[18]

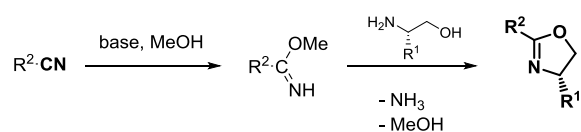


Scheme 2-2. General oxazoline formation.

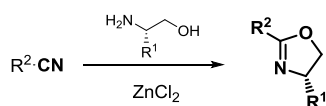
Regarding the activation of the carboxylic acid for the amide formation with the aminol, several traditional methods, such as the transformation to an acid chloride^[19-21], an anhydride^[22-23] or the use of

a nitrile^[24-27] as carboxylic acid analogue, were described. The first example for the synthesis of a 2-(pyridine-2-yl)-oxazoline (pyrox) was described by Brunner and Obermann in 1989.^[11] In this work, a nitrile group was chosen as carboxylic acid analogue and after its transformation into the methyl imidate, the oxazoline was formed under release of ammonia and methanol in the final step (Scheme 2-3a). A slight variation of this method is presently known as the “Witte-Seeliger-method”^[28] which was applied *i.a.* by Bolm *et al.* in 1991.^[29] This zinc chloride-catalyzed method allows for the condensation of an aminol with a nitrile and the subsequent oxazoline ring closure in one step (Scheme 2-3b).

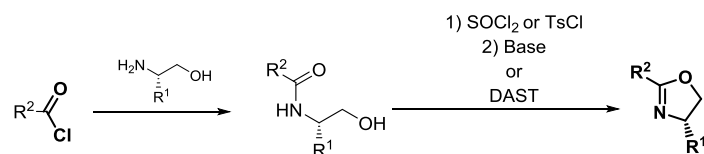
a) Nitrile method (Brunner, Obermann)



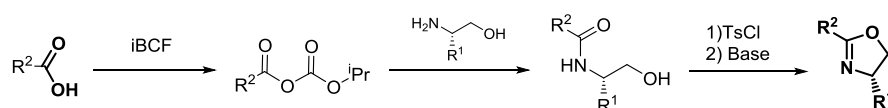
b) Nitrile method (Witte Seeliger)



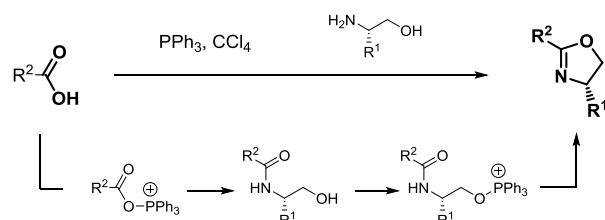
c) Acid chloride method



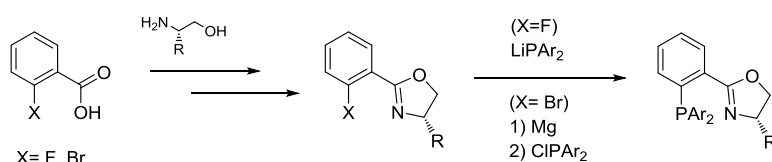
d) Mixed-anhydride method



e) Appel conditions


Scheme 2-3. Overview of established methods for carboxylic acid activation in oxazoline synthesis.

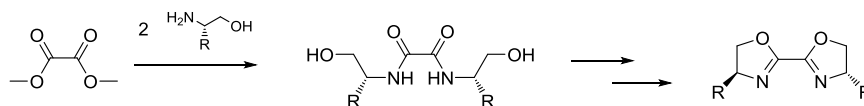
The activation of the carboxylic acid as an acid chloride was described by Nishiyama *et al.* in 1993, who used this approach for the synthesis of 2,2'-oxazoline substituted bipyridines (Scheme 2-3c).^[19] Furthermore, examples using the mixed-anhydride *iso*-butyrylchloroformate (iBCF) as amide coupling reagent, were reported by the groups of Sigman and Stahl (Scheme 2-3d).^[22, 30] McManus and Guiry discovered an approach for the amide coupling using the isatoic anhydride as mixed-anhydride.^[31] In 1993, Vorbrüggen and Krolkiewicz reported a method using Appel conditions in order to avoid the harsh conditions when SOCl_2 is used as chlorinating agent (Scheme 2-3e). Using this method, a number of differently substituted as well as unsubstituted (oxazoline-2-yl)arenes, (oxazoline-2-yl)pyridines (pyrox) and thiazolines were prepared.^[32] The group of Helmchen used this method *i.a.* for the formation of 2-halogen substituted (oxazoline-2-yl)arenes that were subsequently transformed into their phosphorus, sulfur and selenium containing derivatives. In the case of the substitution with phosphorus the thereby resulting phosphines, known as phosphinoxazolines (phox) or "Pfaltz-Helmchen" ligands, appeared to be highly effective for example in iridium catalyzed asymmetric hydrogenations (Scheme 2-4).



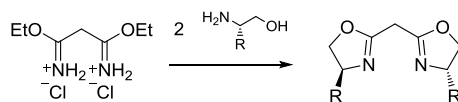
Scheme 2-4. Formation of phox compounds by Helmchen.^[33]

Bisamidates from which box or mebox are subsequently prepared, are mostly often accessed from their methoxy or ethoxy esters by simple condensation with the aminol in an unpolar solvent such as toluene (Scheme 2-5a). Alternatively, a one-step procedure using an ethyl imidate was described by the same authors (Scheme 2-5b).^[20-21]

a) box formation from a methyl ester



b) mebox formation from an ethyl imidate



Scheme 2-5. Formation of bisoxazoline compounds.

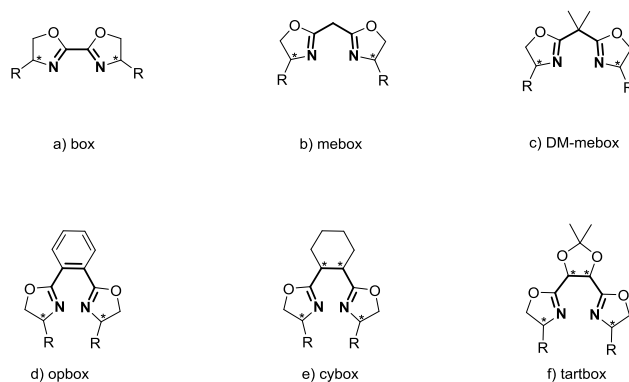
Except for the few one-step examples, such as the Witte-Seeliger method or the Vorbrüggen and Krolkiewicz method using Appel conditions (Scheme 2-3) and the bisamidate method (Scheme 2-5b), the β -hydroxy-amide has to be activated in a separate step prior to the amide formation. In general, for the formation of bisoxazolines, the hydroxyl group is transformed into a chloride^[20-21, 34] or mesylate^[35], followed by the ring closure induced by a base such as KOH, NaOH or NEt₃. For this step, the use of different polar solvents as tetrahydrofurene (THF), methanol, ethanol, but also the weakly polar solvent 1,2-dichloroethane (DCE) was described. In these examples, the ring closure proceeded always under increased temperature.^[20-21] To obtain pyrox structures, also, a chloride leaving group or alternatively a tosylate was introduced. In few examples also the use of the mild reagent diethylaminosulfur trifluoride (DAST)^[36-38] was described (Scheme 2-3 c).

2.2 Structural Diversity of Oxazoline-Ligands

Oxazoline-containing ligands were prepared in an immense variety. In this chapter, selected examples of different ligand classes will be shown. However, this collection makes no claim to be complete since a lot more variations of oxazoline derived structures are known and the corresponding ligands were prepared and used in many more reported studies. The abbreviations of some ligand were made particularly for this project for practical reasons.

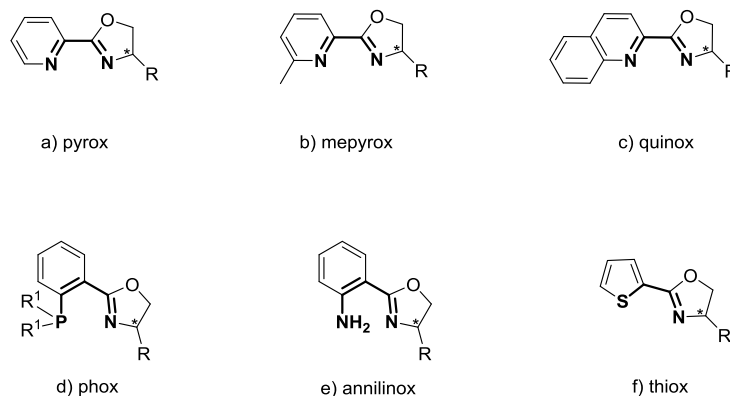
C₂-symmetric bisoxazolines (Scheme 2-6) differ primarily in their rigidity as well as in their bite angle due to different backbone structures. The simplest of among them is the bisoxazoline (box) (a) which is the most rigid one since the two C-N double bonds are in conjugation with each other. Compared to box (a), the methylene bridged bisoxazolines mebox (b) and 2-bis(oxalin-2-yl)propane (DMmebox) (c) are much more flexible and they bear a larger bite angle. Therefore their residues obtain a closer proximity towards a metal center. The last three ligands of this collection bear an even higher flexibility: *ortho*-bis(oxazolin-2-yl)benzene (opbox) (d), 1,2-bis(oxazolin-2-yl)cyclohexane (cybox) (e) and the tartaric acid derived 2,2'-(2,2-dimethyl-1,3-dioxolane-4,5-diyl)bis(oxazoline) (tartbox) (f). In all of them, the oxazolines are connected *via* a C₂-bridge which leads to a seven-membered metallacycle upon coordination. The two last examples cybox (e) and tartbox (f) also contain two additional stereocenters in their backbone, which offers more possibilities for tuning these ligands in asymmetric catalysis.

Scheme 2-7 displays examples of bidentate oxazolines including an aromatic moiety. The upper row illustrates three closely related pyrox-type structures with different steric influences in the 6-position of the pyridine moiety. While pyrox (a) bears solely a hydrogen atom in this position, the 2-(6-methylpyridine-2-yl)-oxazoline (mepyrox) (b) carries a free rotatable methyl group, presumably with a high steric influence. In the quinolinic acid derived structure, 2-(quinolin-2-yl)-oxazoline (quinox) (c), occurs steric hindrance strictly in the plane of the ligand due to the annulated aromatic system.



Scheme 2-6. Bisoxazolines a^[20-21, 34], b^[20], c^[39], d^[40-41], e^[42], f^[43].

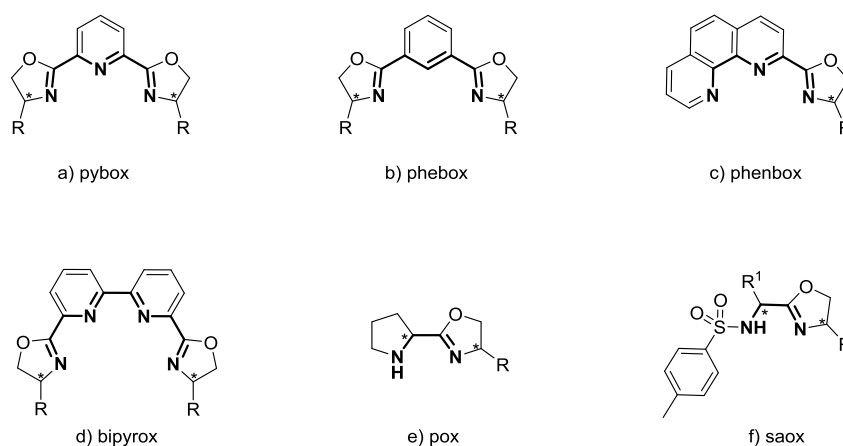
In the bottom row of Scheme 2-7, 2-(2-(phosphanyl)phenyl)oxazoline (phox) (d) may be one of the most well known oxazoline-containing ligands, since ligands of this type are very effective in asymmetric hydrogenation.^[44] The introduction of phosphorous as donor atom, leads to a bidentate P,N ligand with very different *trans*-effects of both coordination sites. Also the sulfur containing S,N ligand 2-(thiophen-2-yl)oxazoline (thiox) (f) has different *trans*-effects of both donor atoms. The aniline derived 2-(oxazoline-2-yl)aniline (annilinox) (e) bears a larger bite angle, compared to pyrox, with one of the N-donors being a primary amine instead of an aromatic nitrogen.



Scheme 2-7. “Monooxazolines” connected to an aromatic moiety a^[19, 22], b^[22, 24], c^[22], d^[44], e^[31], f^[27].

Besides the bidentate examples of oxazoline ligands, also tridentate or even tetradentate versions exist. In Scheme 2-8, examples of this kind are depicted as well as some structures that act as monoanionic ligands. The most commonly used ones are 2,6-bis(oxazolin-2-yl)pyridine (pybox) (a) and 1,3-bis(oxazolin-2-yl)benzene (phebox) (b). 2-(1,10-phenanthroline-2-yl)oxazolin (phenbox) (c) is structurally related to pybox (a), but with only one asymmetric center. Also related to pyrox (a), but acting as tetradentate ligand, is 6,6'-bis(oxazolin-2-yl)-2,2'-bipyridine (bipyrox) (d). The last two structures from this scheme are 2-(pyrrolidin-2-yl)oxazolin (pox) (e) and *N*-((oxazolin-

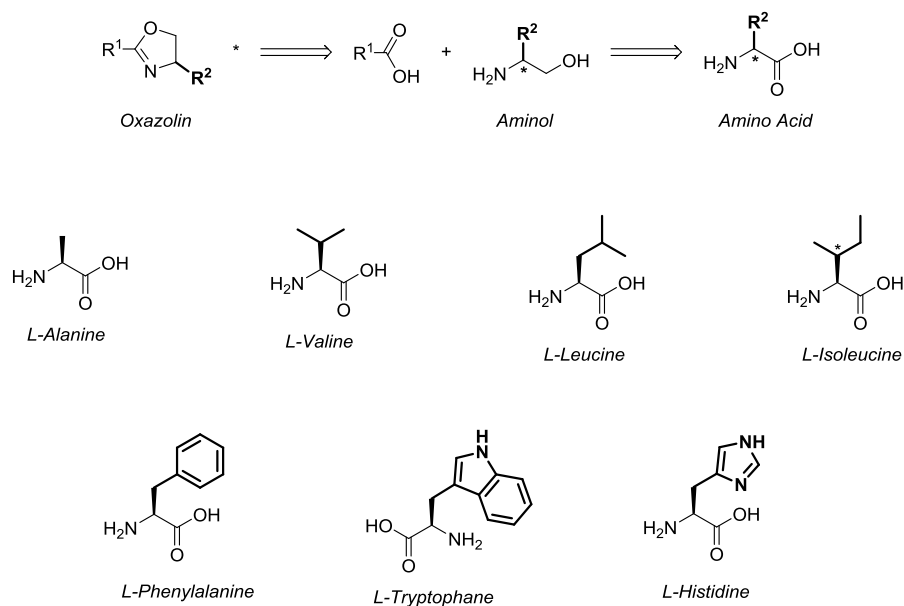
2-yl)methyl)-4-methylbenzenesulfonamide (saox) (f), which both act as monoanionic ligands. The latter one, saox (f), bears also an additional stereocenter in α -position to the nitrogen of the sulfonamide moiety.



Scheme 2-8. Polydentate neutral examples a^[19], c^[19], d^[19] and monoanionic examples b^[45], e^[37], f^[46-49] of oxazoline ligands.

These examples illustrate that the structural variety of oxazoline ligands is immense. The same is true for the residue at the chiral position. Conveniently, the 20 proteinogenic amino acids and a plethora of non-natural variants are available as starting materials. In particular, those structures without a functional group in the side chain are privileged for the use in oxazolines, since no protecting groups are necessary for the reduction step to the aminol. Among the natural amino acids, these are alanine, valine, leucine, isoleucine, phenylalanine and, with restrictions, tryptophane and histidine (Scheme 2-9). Their *S*-enantiomer is naturally abundant and can be isolated from natural sources in large amounts. If their *R*-enantiomer is desired, it can be obtained by chemical synthesis like in the Strecker reaction, which leads to a racemic mixture in the first place. This racemic mixture can be separated using different methods such as the enzymatic separation of enantiomers or the crystallization with a chiral counterion.^[50-51]

Also non-proteinogenic amino acids are convenient starting materials for oxazolines, if they are commercially available. Two examples for such non-proteinogenic amino acids are *tert*-leucine and phenylglycine (Scheme 2-10). Both are prepared industrially in appropriate amounts, since they are of economical interest as antibiotal and pharmacological agents.^[52-53]



Scheme 2-9. Suitable proteinogenic amino acids for application in oxazoline ligands.



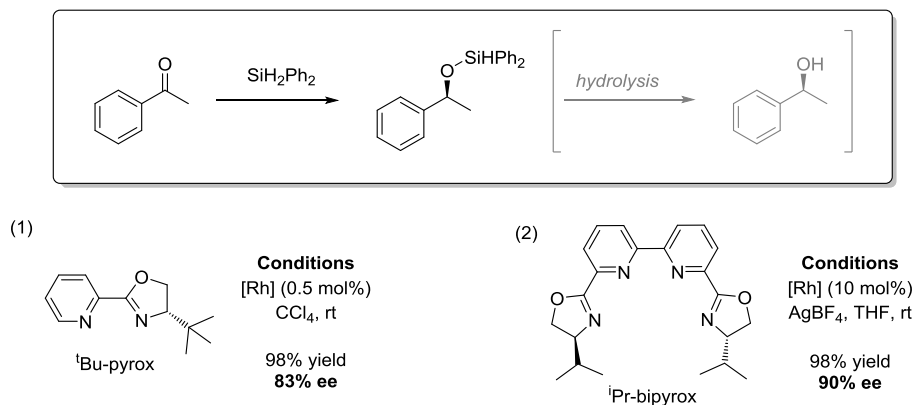
Scheme 2-10. Two examples of commercially available non-proteinogenic amino acids.

2.3 Catalytic Application of Oxazoline-Ligands

In general, a wide range of different catalytic reactions were successfully performed with oxazoline ligands such as hydrosilylation,^[11, 19, 43, 54-55] transferhydrogenation,^[20, 23, 37, 56] hydroarylation,^[54] cyclopropanation,^[20, 38, 57-58] allylic substitution,^[24, 26-27, 41, 59-61] allylic amination,^[39] decarboxylative allylic etherification,^[62] allylic oxidative amidation,^[22] alkene difunctionalization,^[63-65] Heck-type reactions^[45, 66-67] and Wacker-type reactions^[30, 68-71]. Some of these reactions will be presented briefly in the following text with a focus on the structures of oxazoline ligands which were applied.

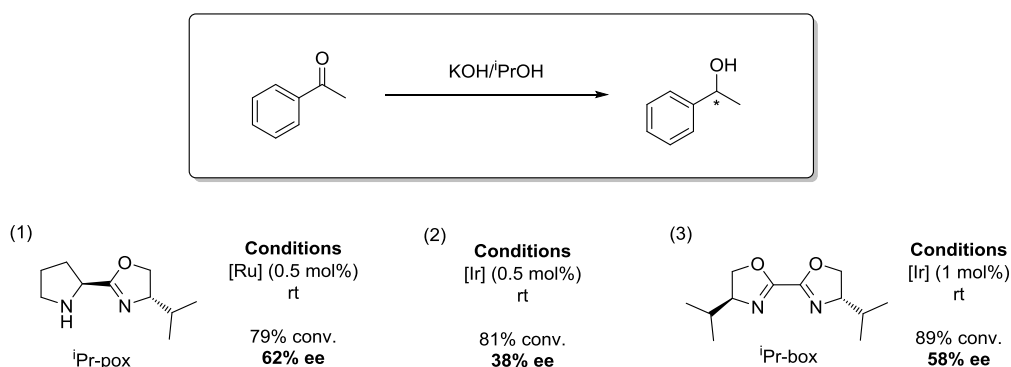
One of the first examples for the use of oxazolines in homogeneous catalysis was published by Brunner and Obermann in 1989.^[11] They applied several pyrox ligands in square planar Rh(I)cod complexes in asymmetric hydrosilylation of acetophenone (Scheme 2-11). The achieved enantioselectivities were

moderate to good while the best results were obtained with ^tBu-pyrox. Also the C_2 -symmetric ⁱPr-bipybox ligand, described by Nishiyama et al. in 1992, led to very good results although the catalyst loading was very high in this example (example 2).^[19]



Scheme 2-11. Hydrosilylation of acetophenone with oxazoline ligands. (1)^[11] [Rh]=1/2 [Rh(cod)Cl]₂; (2)^[19] [Rh]=1/2 [Rh(coe)₂Cl]₂.

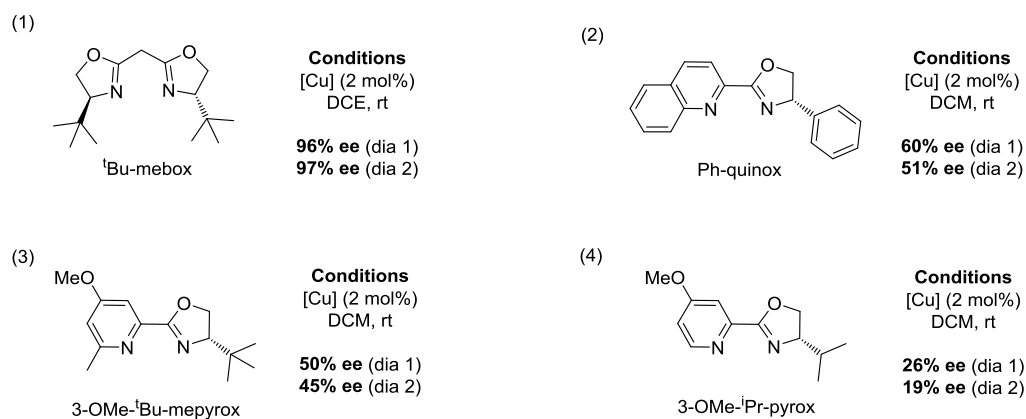
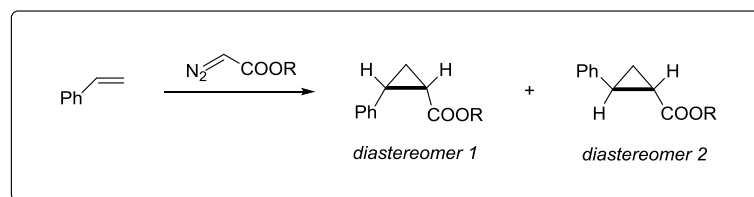
Since transferhydrogenation is closely related to hydrosilylation, oxazolines were also successfully applied in this reaction. As depicted in Scheme 2-12, different kinds of oxazoline ligands successfully applied as ligands for the asymmetric transferhydrogenation of acetophenone (Scheme 2-12). A moderate enantioselectivity of 60% ee was achieved by the use of the C_2 -symmetrical ⁱPr-box as well as by the non-symmetrical ⁱPr-pyrox. This example of asymmetric transferhydrogenation is one of the very rare examples for a successful application of a box ligand that led to an enantioselectivity larger than 50% ee.



Scheme 2-12. Asymmetric transfer hydrogenation of acetophenone catalyzed by oxazoline complexes. (1)^[37] [Ru]=1/2 [Ru(p-cymene)(Cl)₂]₂; (2)^[37] [Ir]=1/2 [Ir(cod)(Cl)]₂; (3)^[20] [Ir]=1/2 [Ir(cod)(Cl)]₂.

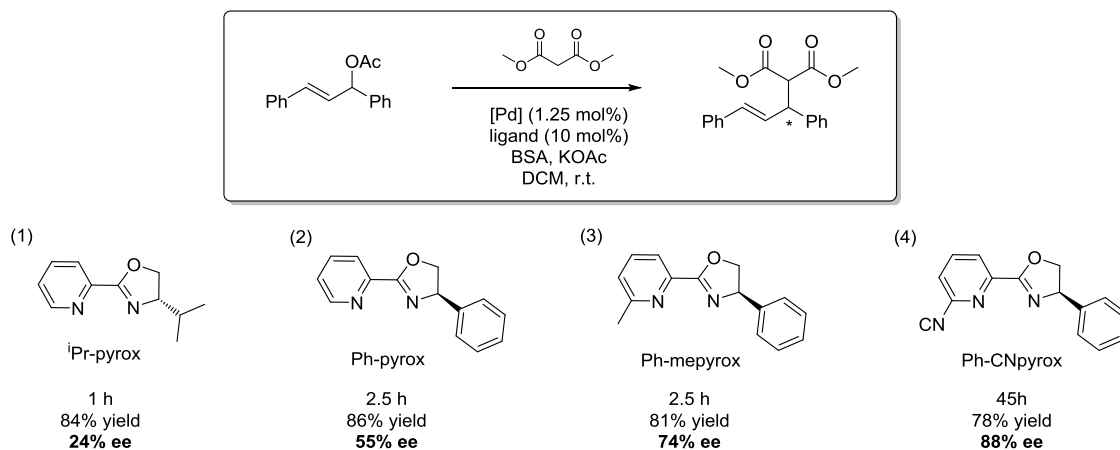
Cyclopropanation of styrene was also used as a model reaction in order to investigate oxazoline ligands. Also in this reaction complexes with C_2 -symmetrical as well as with non-symmetrical ligands were reactive and resulted in good yields with moderate to high enantiomeric excesses of the

diastereomeric products. The best enantioselectivities were observed when the C_2 -symmetrical ^tBu-mebox was applied as ligand, while the non-symmetrical pyrox-type ligands (examples 2-4) resulted in moderate enantioselectivities. Comparing the mepyrox (example 3) and the pyrox (example 4), which differ only in one methyl group in the 6-position of the pyridine moiety, the strongly decreased enantioselectivity caused by the pyrox ligand attracts attention. These two examples show how important a small change in the ligand structure can be for the reaction outcome.

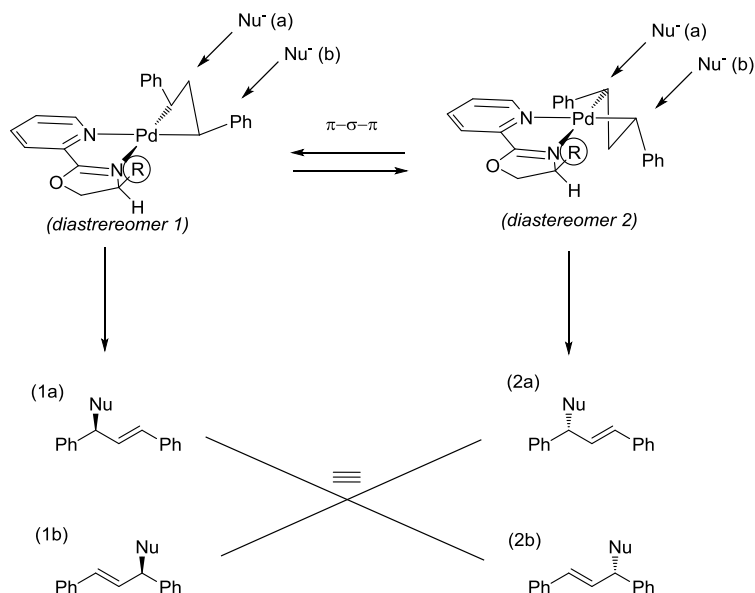


Scheme 2-13. Cyclopropanation of styrene catalyzed by oxazoline complexes. (1)^[20] [Cu]=[Cu(ligand)₂], R=(1*R*,3*R*,4*S*)-menthyl; (2), (3) and (4)^[58] [Cu]=[CuOTf], R=Et.

Another successful application of oxazolines was found in the allylic substitution (Scheme 2-14). The comparison of different pyrox-type ligands exhibits an increasing enantioselectivity from 24-74% ee with increasing steric demand of the respective ligand (examples 1-3). The highest enantioselectivity of nearly 90% ee was achieved by the application of a nitrile substituted pyrox (example 4). This result can be understood on the basis of the steric properties of the nitrile group of Ph-CN-pyrox, which is thinner but also longer than the methyl group in Ph-mepyrox. Also, an electronic effect of the nitrile substituted ligand can be responsible. Since this ligand is much more electron withdrawing, it might influence the stereoselectivity determining step of the catalytic cycle differently than the other ligands.



Scheme 2-14. Allylic substitution catalyzed by oxazoline complexes. (1), (2) and (3)^[59]; (4)^[59] [Pd]=[Pd(η^3 -C₃H₅)Cl]₂.

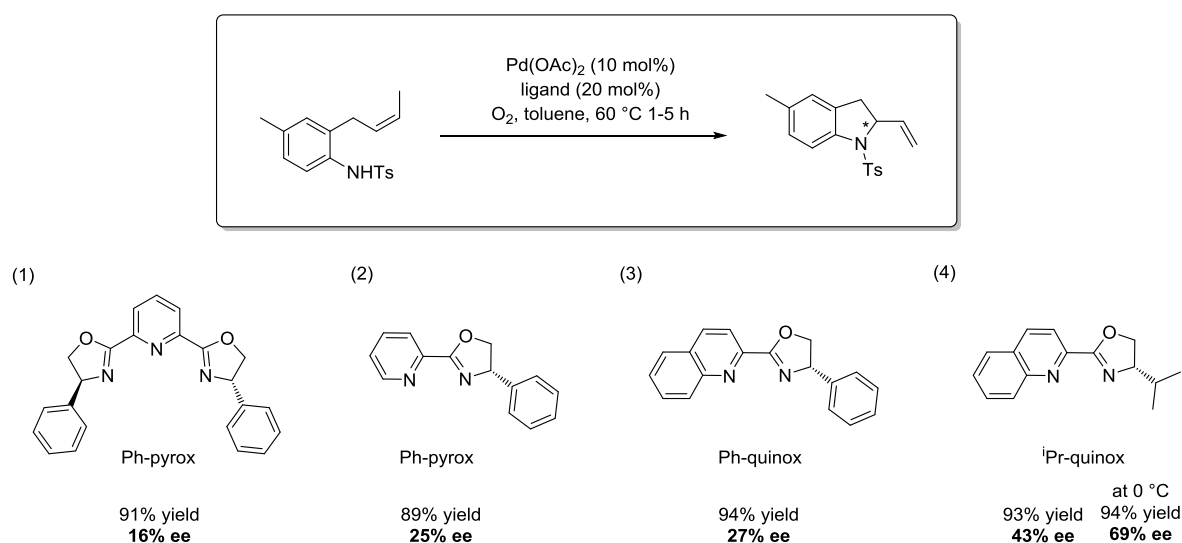


Scheme 2-15. Origin of enantioselectivity in allylic substitution reactions.

C₂-symmetric box ligands do not lead to enantioselectivity in this reaction. As illustrated in Scheme 2-15, the ligand has to be able to stabilize one of two possible diastereomeric structures and to favor the nucleophilic attack from just one side (a) or (b). Assuming that the ligand would just stabilize one diastereomer without favoring the nucleophilic attack at a special site, the product would be racemic. Therefore, the box ligands could not have caused stereoselectivity.

One last example is given in the asymmetric aza-Wacker-type cyclisation of olefinic tosylamides (Scheme 2-16). Here, a C₂-symmetrical pybox ligand (example 1) and three pyrox-type ligands (examples 2-4) were tested among other chiral ligands. The application of the C₂-symmetrical and

sterically very demanding Ph-pyrox led to a very high yield but only low enantioselectivity. Similar yields but higher enantioselectivities were achieved by application of the pyrox-type ligands, while the *iso*-propyl substituted ⁱPr-quinox (example 4) caused the highest enantioselectivities of 43% ee. Comparison with the phenyl substituted analogues Ph-quinox (example 3), which only led to 27% ee, demonstrates again how important small structural changes in the ligand can be. After identifying ⁱPr-quinox as the best ligand, the catalytic reaction was repeated with this ligand at decreased temperatures by which the enantioselectivity was increased to 69% ee.



Scheme 2-16. Aza-Wacker-type cyclization catalyzed by oxazoline complexes. (1)-(4)^[69]

In conclusion, oxazoline ligands were successfully applied in different catalytic reactions. Only very few examples were reported, in which the C_2 -symmetrical box ligands were applied, in contrary to their methylene bridged mebox analogues. The non-symmetrical pyrox type ligands were applied much more often and their stereochemical influence was dependent on small structural changes of the ligands.

3 Iridium and Ruthenium Complexes

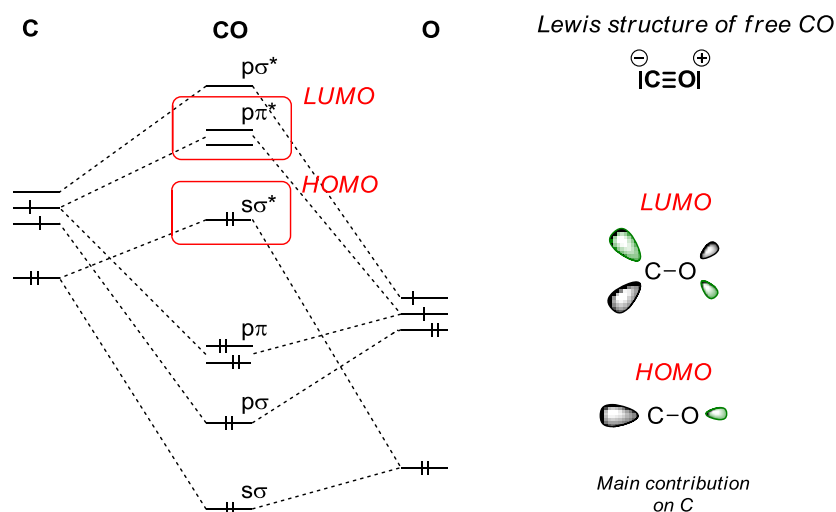
3.1 Transition Metal Carbonyl Complexes

Transition metal complexes with carbon monoxide ligands are known since 1884, when Ludwig Mond converted nickel powder to the volatile $\text{Ni}(\text{CO})_4$ complex by heating it in a CO stream.^[72] The simple heating of a pure metal under CO atmosphere is still one of three convenient methods to obtain carbonyl complexes and works well for low valent metal species. Another method is the reaction of CO gas with a high oxidation state metal salt in combination with a reducing agent. Consequently, this reaction type is called reductive carbonylation. The third synthesis route does not use elementary CO but organic, molecular CO-donors such as aldehydes, alcohols or CO_2 as carbonylation agents.^[72-73]

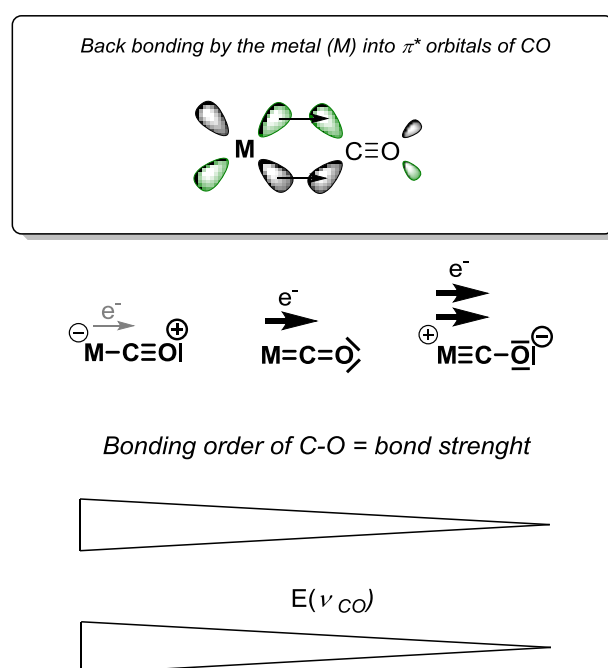
Upon coordination, carbon monoxide becomes activated on the oxygen atom towards electrophilic and, in turn, the carbon towards nucleophilic attack. This increased CO reactivity of carbonyl complexes is used in numerous reactions such as methanol synthesis, synthesis of alkanes or alkenes, alcohols (Fischer Tropsch Synthesis), synthesis of carbene complexes or in many different carbonylation reactions *e.g.* hydroformylation, hydroxycarboxylation, hydroesterification and carbonylation of an alcohol to give the corresponding carboxylic acid. In case of acetic acid production, the reaction is also known as “Monsanto acetic acid process”.^[74-75]

3.1.1 CO as Ligand in Transition Metal Complexes

Carbon monoxide acts as a neutral ligand and binds often monodentate *via* the carbon atom, but also many complexes with bridging CO ligands are known. In free CO, the atoms are connected *via* a triple bond, which gives rise to a negative polarization on the carbon and a positive polarization on the oxygen. However, the negative charge at the carbon is nearly compensated by the high electronegativity of the oxygen, which polarizes the bonding orbitals towards itself. These counteracting effects result in a small dipole moment of nearly zero. The MO scheme of CO is depicted in Scheme 3-1, highlighting the HOMO and LUMO, showing that the highest coefficient of both orbitals is located at the carbon. Therefore this atom is the best the bonding partner for a metal because it can donate two electrons from the HOMO into an empty d_σ orbital of the metal while the two degenerate LUMOs can accept electrons from filled d_π orbitals. Upon coordination to a metal, the back donation of d-electrons from the metal into a π^* -orbital of the ligand weakens the π -bonds resulting in a decreased C-O bonding order (Scheme 3-2). Consequently, the strengths of the back bonding is reflected in the bond strength of the C-O bond.^[76]



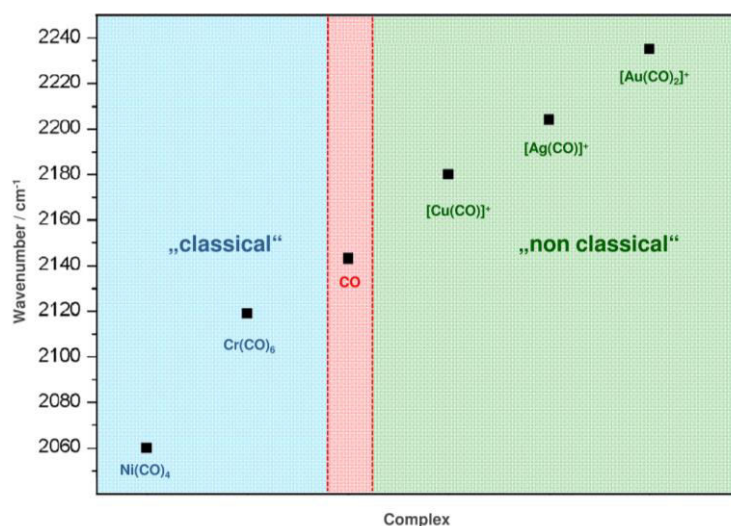
Scheme 3-1. MO scheme of free CO.^[73]



Scheme 3-2. Back bonding in carbonyl complexes and consequences for IR absorption energies.^[73]

The change in bond strength can be analyzed by measuring the IR absorption frequency of the CO stretching vibration. The IR absorption of the CO molecule occurs in the range of 1820 cm^{-1} to 2150 cm^{-1} and normally does not overlap with other vibrational bands which facilitates the interpretation of the corresponding spectra.^[72] Comparison of IR spectra of carbonyl complexes with the one of free carbon monoxide leads to the observation, that in some complexes the CO bond becomes weaker upon coordination, while in other complexes it becomes stronger. The latter ones are commonly classified as “non classical” carbonyl complexes. In turn, these complexes that weaken the

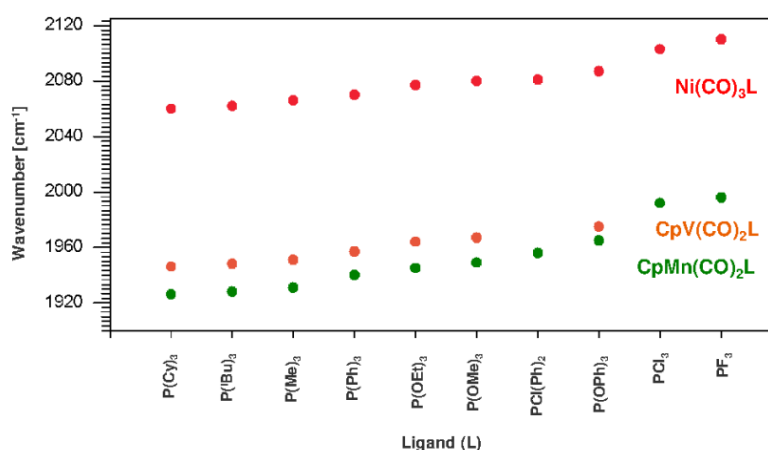
CO bond, are classified as “classical” carbonyl complexes (Scheme 3-3). In heteroleptic carbonyl complexes, the CO bond strength is also influenced by the electronic properties of other ligands, therefore the C-O stretching frequencies can serve as tool for the comparison of the electronic properties of these ligands. Because of their simplicity of recording, IR measurements of carbonyl complexes have become a standard tool for the comparison of electronic properties of diverse ligands.



Scheme 3-3. Classification of carbonyl complexes on basis of their CO stretching frequencies.^[73]

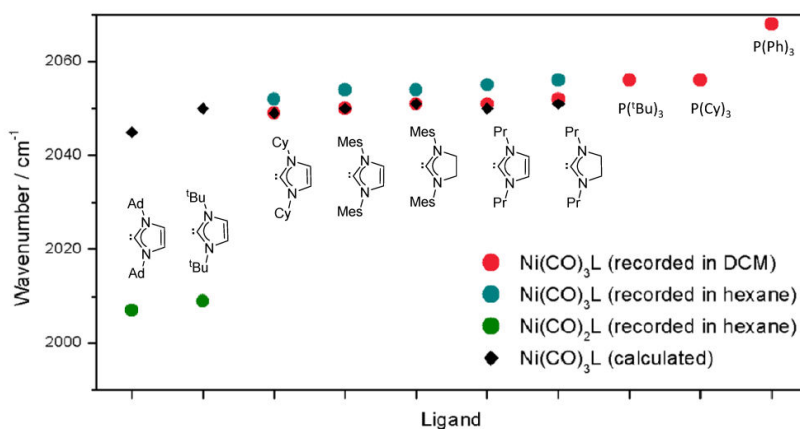
3.1.2 Evaluation of Monodentate Ligands in Carbonyl Complexes

Monodentate phosphorus ligands and *N*-heterocyclic carbenes (NHC) are often used ligands in homogeneous catalysis. Therefore their electronic properties were investigated intensively by measuring the ν_{CO} absorption energies of the corresponding carbonyl complexes. For monodentate phosphorus ligands, Tolman established tetrahedral Ni(CO)₃L complexes as standard complexes for such measurements in a well known review from 1977.^[5] The complexes were easily obtained from Ni(CO)₄ and today “Tolman’s electronic parameter” (TEP) refers to these carbonyl complexes.^[6, 77] Tolman’s review is based on work of Strohmeier and Müller from 1967, which describes the comparison of different CpMn(CO)₂L complexes but also others such as CpV(CO)₃L, Fe(CO)₄L, Ni(CO)₃L, Cr(CO)₅L and W(CO)₅L.^[78-79] The work of Strohmeier and Müller demonstrates that large differences in the ν_{CO} stretching frequencies exist when one ligand is attached to different metals, but the relative ν_{CO} stretching frequencies within a series of ligands attached to the same metal, stayed always the same (Scheme 3-4). Therefore, the ν_{CO} stretching frequencies of different ligands attached to the same type of complex are comparable.



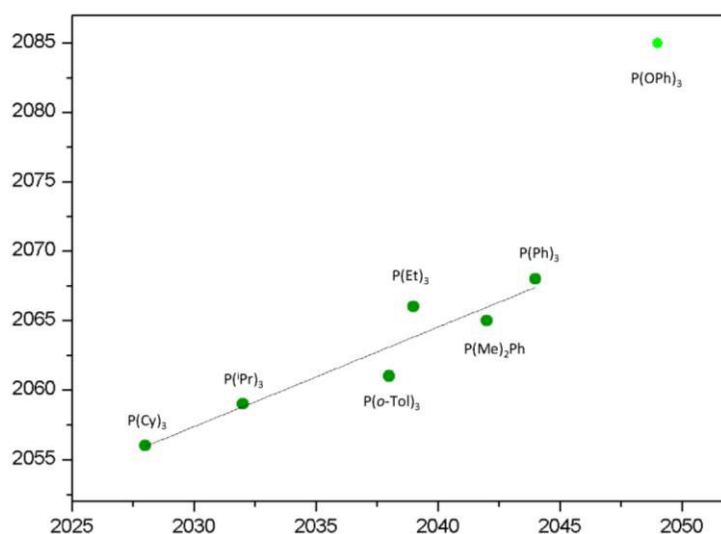
Scheme 3-4. IR Stretching frequencies of different phosphine and phosphite carbonyl complexes.^[78]

In analogy to the phosphine carbonyl complexes, CO stretching frequencies of NHC carbonyl complexes were evaluated as their $\text{Ni}(\text{CO})_3\text{L}$ complexes (Scheme 3-5). In these complexes NHCs cause ν_{CO} stretching frequencies lower, or in the range, of trisalkylphosphines.^[80] With the sterically very demanding adamantyl and *tert*-butyl substituted imidazole-NHC ligands instead of the usually formed tri complexes only dicarbonyl complexes were obtained. Comparison of the tris- and dicarbonyl complexes shows a large difference between their ν_{CO} stretching frequencies (Scheme 3-5). In order to overcome the experimental problems with sterically demanding ligands, Gusev investigated the comparability of calculated IR stretching frequencies with the experimental ones (Scheme 3-5).^[77] ^{81]} The author found a strong correlation between calculated and measured ν_{CO} stretching frequencies. In addition, the electronic properties of the sterically demanding ligands are in line with the other ligands. These results indicate that electronic properties of ligands can be predicted by calculating the corresponding ν_{CO} stretching frequencies of experimentally inaccessible carbonyl complexes. Gusev listed a collection of 76 NHC ligands and their calculated electronic properties. Some of them have not been experimentally described but can now be prepared on demand if their special electronic behavior were required for a certain application.



Scheme 3-5. IR stretching frequencies of different NHC complexes and comparison with calculated values.^[80-81]

Since the precursor for the tetrahedral nickel carbonyls, $\text{Ni}(\text{CO})_4$, is highly toxic and the handling extremely dangerous because of its volatility, nowadays carbonyl complexes are preferably prepared from other metal complexes.^[82-86] For example, Schmedake reported the use of octahedral *trans*- $\text{M}(\text{CO})_4(\text{L})_2$ ($\text{M} = \text{Cr}, \text{Mo}, \text{W}$) for the evaluation of *N*-heterocyclic silylene ligands.^[87] Another large group of carbonyl complexes for the evaluation of NHC ligands are the square planar, homologues Rh(I) and Ir(I) complexes.^[82-86] The complexes are typically prepared from the corresponding cod dimers $[\text{M}(\text{cod})\text{Cl}]_2$ ($\text{M} = \text{Rh}, \text{Ir}$), leading to the cod complexes $[\text{MCl}(\text{cod})\text{L}]$, which yield under atmospheric pressure of gaseous CO the corresponding dicarbonyl complexes. The Crabtree group published the ν_{CO} stretching frequencies of $[\text{IrCl}(\text{CO})_2\text{L}]$ for the evaluation of two new carbene ligands and compared them with the data obtained for various phosphine ligands, for which the corresponding $[\text{IrCl}(\text{CO})_2\text{L}]$ complexes were prepared as well.^[86] However, the application of other metalcarbonyls than $\text{Ni}(\text{CO})_3\text{L}$ bears the general problem that the obtained data are not comparable with the previously reported TEP values. Therefore, the Crabtree group tried to find a method which allows for the comparison of TEP values with the data obtained from the described iridium complexes. The plot of the average ν_{CO} stretching frequencies of the iridium complexes over corresponding TEP values led to a linear correlation (Scheme 3-6). However, this correlation seems to be limited to poor π -acceptors such as trisalkyl phosphines.

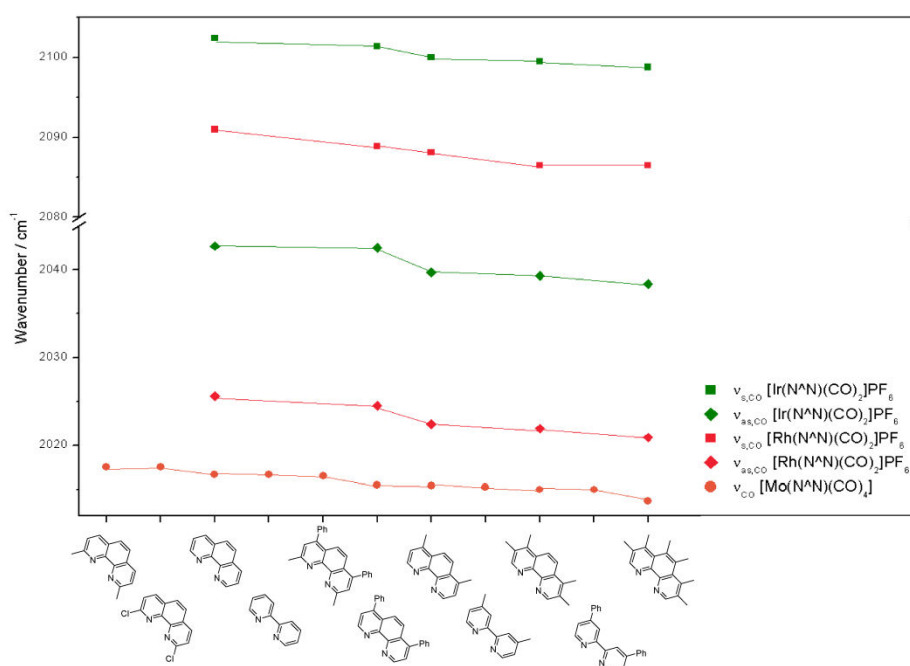


Scheme 3-6. Plot of TEP-values over average IR absorption of $[\text{Ir}(\text{CO})_2\text{LCl}]$. For the poor π -acceptor phosphine a linear correlation between these two values exists.

3.1.3 Evaluation of bidentate Ligands in Carbonyl Complexes

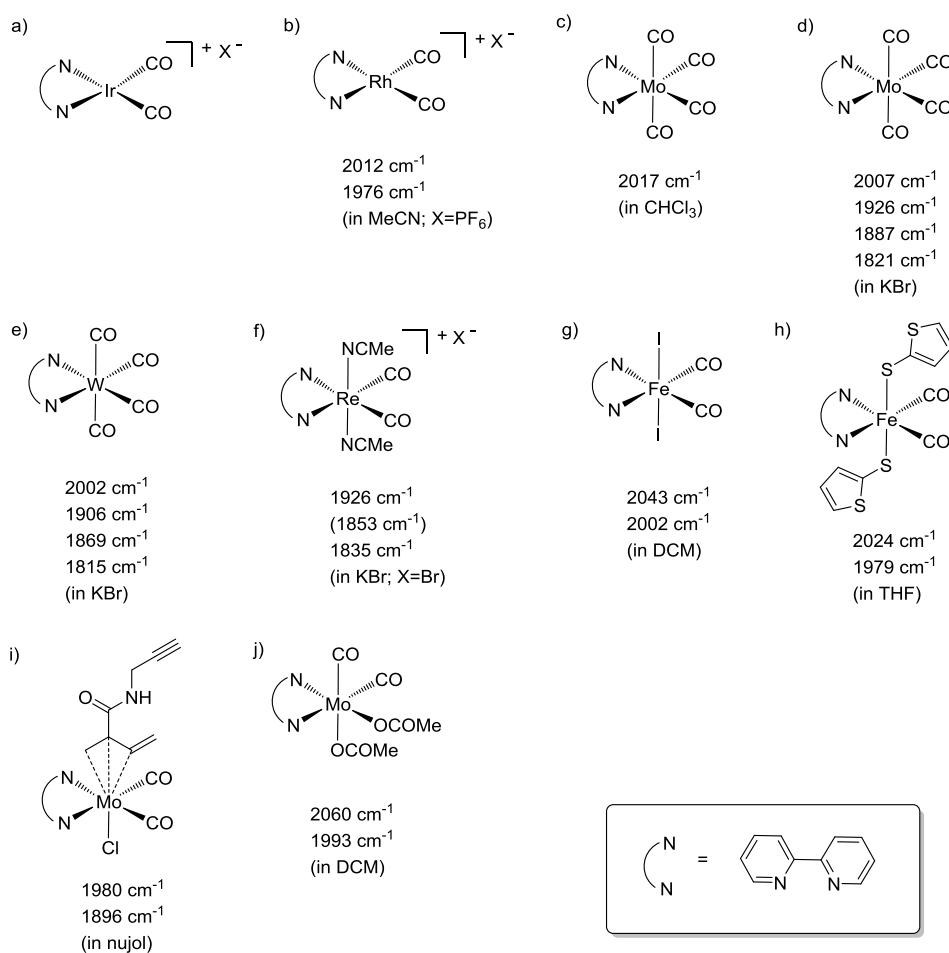
Bidentate ligands as bipyridines (bpy) and phenanthrolines (phen) were much less investigated than phosphorous ligands and NHCs. Some important research was reported by Mestroni, Camus, Cocevar, Zassinovch and Clauti in 1972 and 1985.^[7, 88-90] Their research interest was first motivated by the investigation of new complexes and their applicability as catalysts. The authors prepared and

investigated *i.a.* complexes of the type $[\text{Rh}(\text{N}^{\wedge}\text{N})(\text{cod})]\text{X}$ and $[\text{Ir}(\text{N}^{\wedge}\text{N})(\text{cod})]\text{X}$ as well as their reaction products with carbon monoxide $[\text{M}(\text{N}^{\wedge}\text{N})(\text{CO})_3]\text{X}$ and $[\text{M}(\text{N}^{\wedge}\text{N})(\text{CO})_2]\text{X}$. As bidentate N,N-coordinating ligands bipyridines and phenanthrolines were chosen.^[7, 88] Few years later, a work about chelating N[^]N ligands in agreement to the work of Tolman about electronic properties of phosphorous ligands was reported.^[6, 90] Here, the authors applied besides the rhodium and iridium complexes $[\text{M}(\text{N}^{\wedge}\text{N})(\text{CO})_2]\text{X}$ also the molybdenum complexes $[\text{Mo}(\text{N}^{\wedge}\text{N})(\text{CO})_4]$. The latter ones were chosen for their clearly predictable octahedral geometry and very good solubility in non-coordinating solvents. The resulting IR absorption energies were compared with reactivity of the ligands in reduction reactions and led to a correlation between electron density on the metal and reactivity. The reported ν_{CO} stretching frequencies (Scheme 3-7) are still cited by scientists today. The obtained ν_{CO} stretching frequencies show clearly, that the lowest absorption energies were caused by electron rich bipyridine and phenanthroline ligands, leading to a comparable high electron density at the central metal. The trends obtained by Rh(I), Ir(I) or Mo(0) are consistent.



Scheme 3-7. Reported ν_{CO} stretching frequencies of different N[^]N-chelated carbonyl complexes. For the dicarbonyl complexes, the asymmetric and symmetric ν_{CO} absorption bands are both reported. For molybdenum complexes the highest wavenumber is reported.^[90]

Even though they were not prepared particularly for the evaluation of their electronic properties, a huge variation of bipyridine carbonyl complexes was prepared and isolated by different research groups. To give a brief overview, some of these complexes are presented in Scheme 3-8. If reported, the IR stretching frequencies of the carbonyl ligands are listed as well.

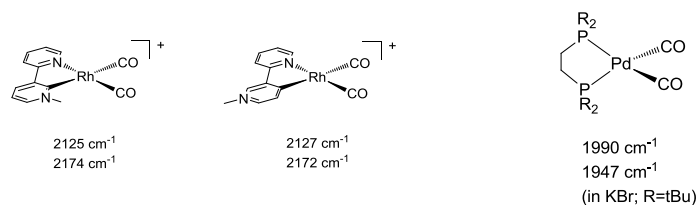


Scheme 3-8. a)+c)^[90] b)^[88] d)+e)^[91] f)^[92] g)^[93] h)^[94] i)^[95] j)^[96] For complex a), no spectroscopical data was reported in the publications of the Mestroni group. For complex c) only the highest ν_{CO} stretching frequency is reported.

The comparison of the molybdenum complexes c) and d) shows how different the absorption frequencies can be for different media. The highest CO stretching frequency obtained in chloroform differs from that measured in KBr about 10 cm^{-1} .

Scheme 3-9 shows the IR data for some monoanionic, pyridine related ligands. In the corresponding publication by the Li group, the carbonyl complexes were prepared in order to compare the electronic properties of the ligands.^[97] However, the reported data were still not obtained experimentally but by calculation. The authors used the average absorption energies for the comparison of the ligands.

The group of Pörschke investigated palladium dicarbonyl complexes with symmetrical bisphosphines (Scheme 3-9). These complexes have a tetrahedral coordination sphere, as it was also the case for the nickel complexes which were used for the determination of TEP values.^[98]

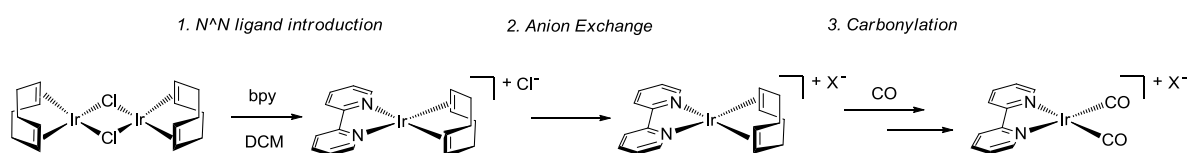


Scheme 3-9. Rhodium dicarbonyl complexes with N,C-ligands and tetrahedral palladium dicarbonyl complexes.^[97-98]

3.1.4 Preparation of Square Planar Ir(I) Bipyridine Carbonyl Complexes

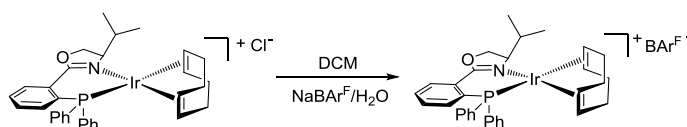
The focus of this work is the replacement of non-chiral bipyridines by chiral bisoxazolines in homogeneous catalysis. Since the reactions of interest for this work are mainly catalyzed by iridium complexes, the comparison of the used ligands in iridium dicarbonyl complexes is desired. Thus, the synthesis Ir(I) and Rh(I) carbonyl complexes reported by the Mestroni group formed the basis for the carbonyl complex synthesis during this project.^[7-8, 88-90]

The synthesis of the carbonyl complexes starts with the dimeric cod complexes $[M(\text{cod})\text{Cl}_2]_2$ ($M = \text{Ir}, \text{Rh}$). These complexes are mixed in a 1:1 ratio of metal and $N^{\wedge}N$ -ligand in a suitable solvent such as methanol or DCM at room temperature. The resulting complex of the type $[M(N^{\wedge}N)(\text{cod})]\text{Cl}$ forms immediately and quantitatively (Scheme 3-10). Subsequently, the Cl^- anion is exchanged for less strongly coordinating ions such as PF_6^- or BF_4^- . In the last step, square planar dicarbonyl complexes are formed by substitution of the cod ligand.^[8]



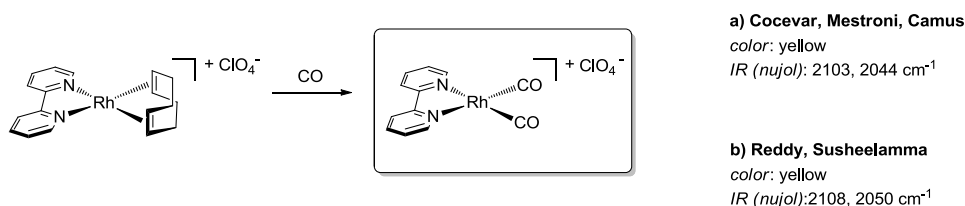
Scheme 3-10. Synthesis of square planar iridium carbonyl complexes.^[8]

The anion exchange to a non-coordinating counteranion in the second step is of certain importance in order to obtain a square planar complex instead of a pentacoordinated trigonal bipyramidal. The anion exchange to $X = \text{PF}_6^-$ was for example realized for rhodium complexes by treatment of the methanolic complex solution with saturated aqueous NH_4PF_6 solution.^[89] Since the analogous phox complexes with $\text{BAR}^{\text{F}-}$ as counteranion play an important role in asymmetric hydrogenation reactions (cf. chapter 4.3), some similar protocols also exist for these complexes. For such complexes, the precursor was dissolved in DCM and treated with an aqueous solution of the sodium salt of the new anion in a biphasic mixture.^[99]



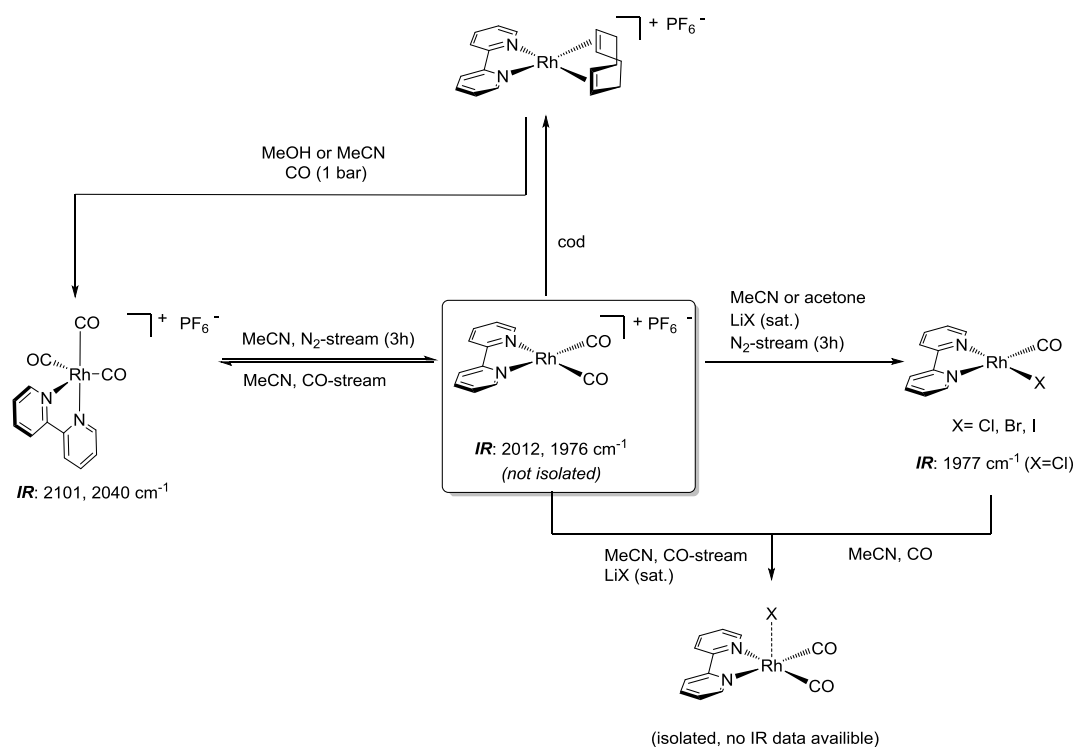
Scheme 3-11. Anion exchange at phox complex.^[99]

The third step, the carbonylation, was described by the group of Mestroni for rhodium complexes as well as for iridium complexes. However, the formation of rhodium carbonyl complexes was described more detailed. Mestroni described the preparation of Rh(I) dicarbonyl complexes from $[\text{Rh}(\text{bpy})(\text{cod})]\text{ClO}_4$ or $[\text{Rh}(\text{bpy})(\text{cot})]\text{ClO}_4$ (cot = 1,3,5,7-cyclooctatetraene) in 1971^[88]. The identity of the complexes was confirmed by comparison with previously reported ν_{CO} stretching frequencies (Scheme 3-12).^[100-102]



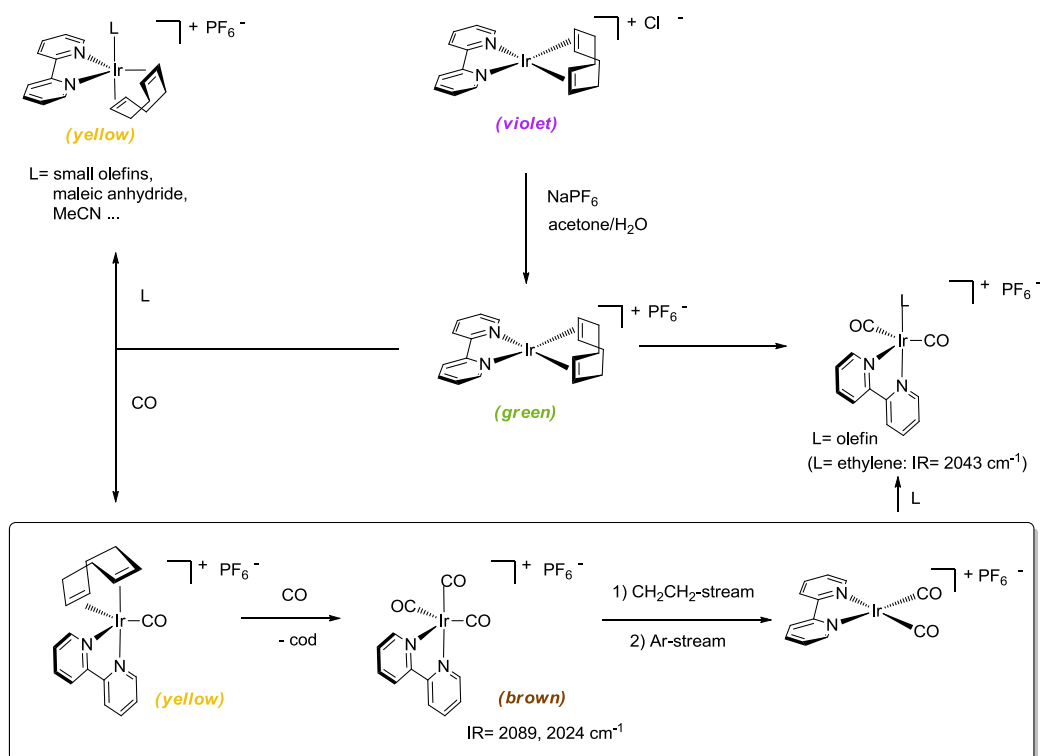
Scheme 3-12. Comparison of IR data a)^[88] and b)^[100] for $[\text{Rh}(\text{bpy})(\text{CO})_2]\text{ClO}_4$.

The results obtained by Mestroni and co-workers were corrected by the same authors in a following publication in 1974, when they identified the prepared carbonyl complexes as tricarbonyl complexes.^[89] The correction was triggered by the observation of a set of two ν_{CO} stretching frequencies shifted towards lower wavenumbers, subsequent to purging nitrogen through a solution of bipyridine carbonyl complex (Scheme 3-13). This process was observed to be reversible when CO gas was led through the corresponding complex solution. The authors assumed that the nitrogen gas replaced one of three carbonyl ligand to result the pentacoordinated dicarbonyl complex $[\text{Rh}(\text{bpy})(\text{CO})_2(\text{N}_2)]^+$, which formed back the tricarbonyl complex $[\text{Rh}(\text{bpy})(\text{CO})_3]^+$ upon purging with CO gas. In this publication, no further information, for example about the shape and broadness of the absorption bands are included.



Scheme 3-13. Formation and reactivity of rhodium carbonyl complexes.^[89]

The publications about analogous iridium complexes appeared first in 1972 and in 1974 on the basis of the investigations about rhodium complexes.^[7-8] As it was also described for rhodium complexes, the synthesis started with $[\text{Ir}(\text{bpy})(\text{cod})]\text{X}$ ($\text{X}=\text{PF}_6, \text{ClO}_4$) and reactivity studies showed that the cod ligand was replaceable by a variety of small molecules such as CO, ethylene or maleic anhydride to form the corresponding yellow pentacoordinated complexes $[\text{Ir}(\text{bpy})(\text{cod})\text{L}]^+$ (Scheme 3-14). The pentacoordinated monocarbonyl complex $[\text{Ir}(\text{bpy})(\text{cod})(\text{CO})]^+$ released the cod ligand upon the further addition of CO and the product was assumed to be the tri complex $[\text{Ir}(\text{bpy})(\text{CO})_3]^+$, similarity to the corresponding rhodium complexes. Purging a solution of the tricarbonyl complex with ethylene resulted a shift of the two ν_{CO} stretching bands and the formed complex was assumed to be identical with $[\text{Ir}(\text{bpy})(\text{CO})_2(\text{CH}_2\text{CH}_2)]^+$. Referring to the authors, purging the solution of the complex with argon removed the ethylene from the pentacoordinated dicarbonyl complex to form its corresponding square planar dicarbonyl complex $[\text{Ir}(\text{bpy})(\text{CO})_2]^+$. However, for the dicarbonyl complex $[\text{Ir}(\text{bpy})(\text{CO})_2]^+$ no spectroscopical data were reported.



Scheme 3-14. Formation and reactivity of iridium carbonyl complexes.^[7-8]

3.2 Heteroleptic Ruthenium(II) Complexes

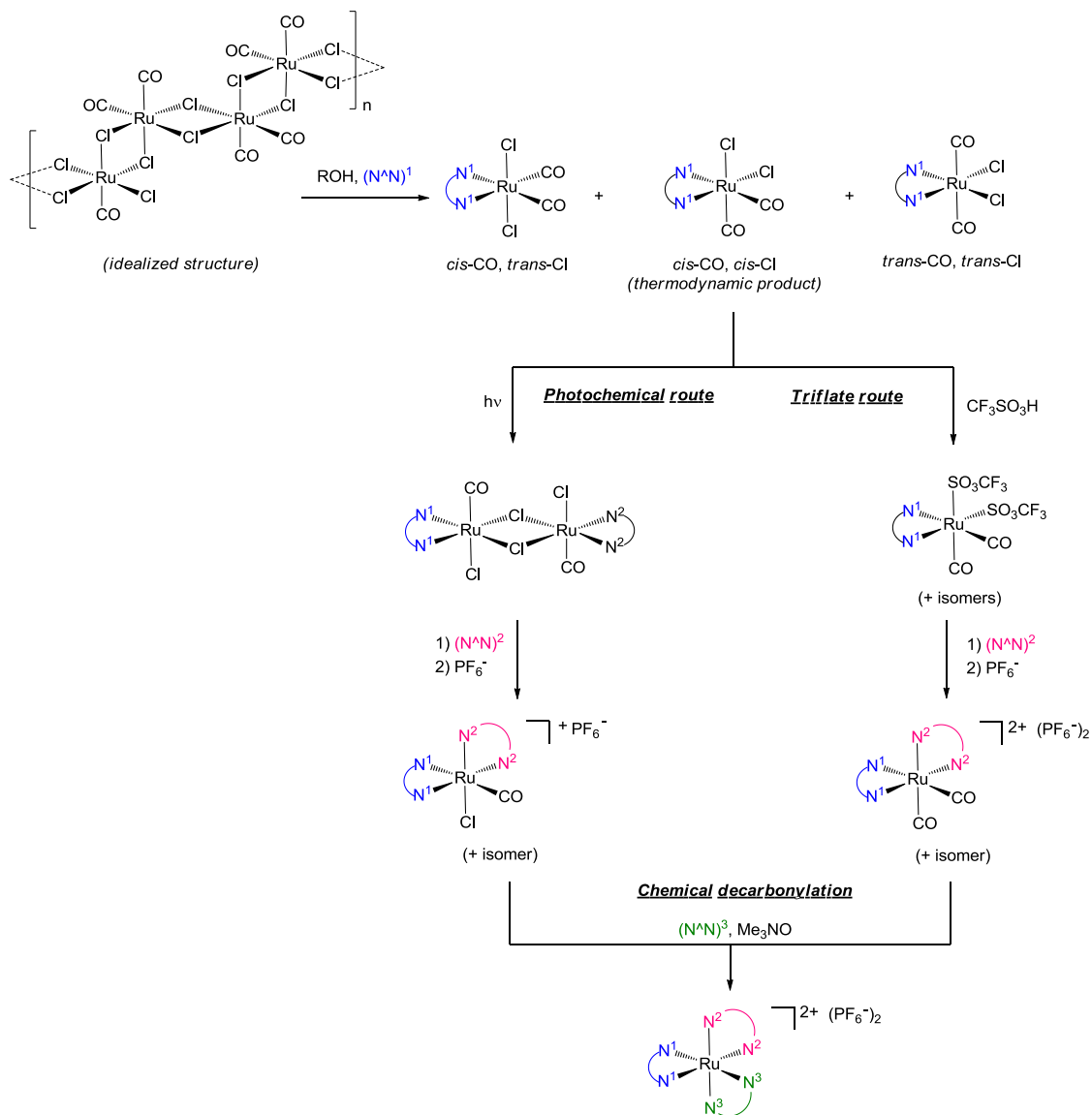
Many different variations of heteroleptic ruthenium complexes, containing at least two dissimilar ligands, are known. One of the simplest examples of such a complex is [Ru(bpy)₂Cl₂] which was first described by Meyer and co-workers.^[103] Due to their remarkable photochemical properties, bisheteroleptic and trisheteroleptic ruthenium complexes [Ru(N[^]N)¹₂(N[^]N)²]²⁺ and [Ru(N[^]N)¹(N[^]N)²(N[^]N)³]²⁺ are well investigated.^[104] In this work, the stepwise introduction of two dissimilar bidentate ligands, one bipyridine (bpy) and one bisoxazoline (box), was attempted. The resulting complexes would have the general composition [Ru(bpy)(box)L₂]²⁺, while L is equal a labile ligand such as a solvent molecule. Alternatively, one of the chelate ligands can also be a tridentate terpyridine (tpy) or pyridylbisoxazoline (pybox) giving the general composition [Ru(tpy)(box)L]²⁺ or [Ru(bpy)(pybox)L]²⁺. Analogous protocols for the stepwise introduction of dissimilar bipyridines or terpyridines serve for the preparation of these complexes.

3.2.1 Preparation

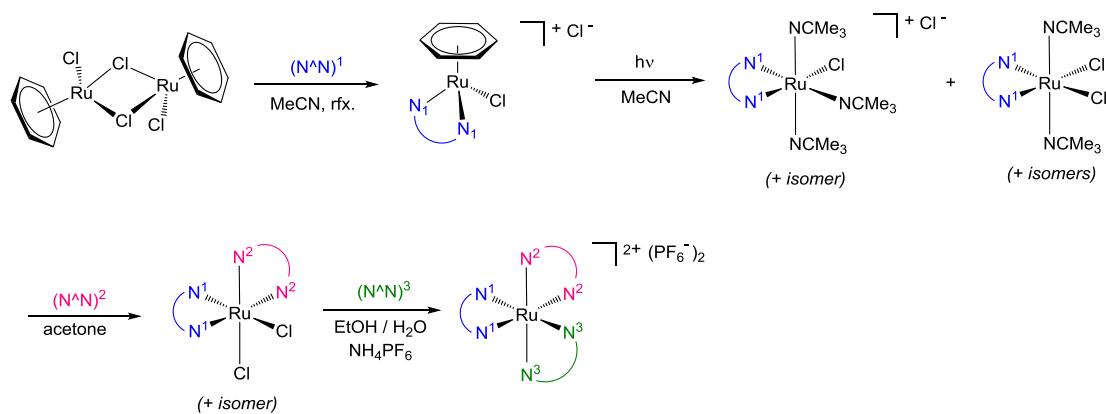
The major challenge in the preparation of heteroleptic complexes with the general constitution $[\text{Ru}(\text{N}^{\wedge}\text{N})^1(\text{N}^{\wedge}\text{N})^2\text{L}_n]^{2+}$ is the controlled, stepwise introduction of two different ligands. First investigations concerning heteroleptic Ru(II) complexes were performed with complexes of the type $[\text{Ru}(\text{N}^{\wedge}\text{N})^1_2(\text{N}^{\wedge}\text{N})^2]^{2+}$, in which first two ligands of the same kind were introduced, leading to a stable $[\text{Ru}(\text{N}^{\wedge}\text{N})^1_2\text{L}_2]^{2+}$ complex which labile ligands L could more or less easily be replaced with a third ligand.^[104] Until today, up to four fundamentally different synthetic approaches starting with different Ru(II) precursors have been established. These approaches were subsequently varied and optimized for the formation of trisheteroleptic Ru(II) complexes. One, often applied method for the formation of $[\text{Ru}(\text{N}^{\wedge}\text{N})^1_2(\text{N}^{\wedge}\text{N})^2]^{2+}$ includes the reaction of a bidentate ligand with $\text{RuCl}_3 \cdot \text{H}_2\text{O}$ in DMF, in which the solvent also acts as reductant converting Ru(III) into Ru(II).^[103, 105-108]

The stepwise introduction of two different bidentate ligands was first realized starting from polymeric $[\text{Ru}(\text{CO})_2\text{Cl}_2]_n$, which forms with a bidentate $(\text{N}^{\wedge}\text{N})^1$ ligand the monomeric dicarbonyl complexes $(\text{Ru}(\text{N}^{\wedge}\text{N})^1(\text{CO})_2\text{Cl}_2)$ in three different isomeric structures (Scheme 3-15).^[109-111] Alternatively, $[\text{Ru}(\text{CO})_3\text{Cl}_2]$ instead of the polymeric precursor compound can be applied.^[112-116] For the introduction of a second ligand $(\text{N}^{\wedge}\text{N})^2$ two different pathways are possible. In the “triflate route” the two chloro ligands are displaced by triflate ligands, which can subsequently be exchanged by a bidentate ligand $(\text{N}^{\wedge}\text{N})^2$.^[109, 117] In the “photochemical route”, one of the carbonyl ligands is removed photochemically resulting in the binuclear complex $[\text{Ru}(\text{N}^{\wedge}\text{N})^1(\text{CO})\text{Cl}_2]_2$ which is then available for the coordination to a second bidentate ligand $(\text{N}^{\wedge}\text{N})^2$.^[110-111, 118-119] However, the “photochemical route” was only suitable for the bipyridine and phenanthroline complexes because the excited state needs to be stabilized by the delocalized system of the ligand.^[104] Finally both routes finish with chemical decarbonylation of the remaining carbonyl ligands in the presence of a third ligand $(\text{N}^{\wedge}\text{N})^3$ resulting in the trisheteroleptic target complex $[\text{Ru}(\text{N}^{\wedge}\text{N})^1(\text{N}^{\wedge}\text{N})^2(\text{N}^{\wedge}\text{N})^3]^{2+}$. If $(\text{N}^{\wedge}\text{N})^3$ is not compatible with the decarbonylating agent Me_3NO , the carbonyl ligands can first be replaced by suitable solvent molecules such as MeCN, which can be replaced by the bidentate ligand afterwards.^[120-121] However, both routes were not suitable when the incorporated ligands carried anionic functional groups.^[104]

One mild synthesis strategy tolerating a variety of functional groups on the ligand was found in the application of arene complexes and was established by Mann and co-workers (Scheme 3-16).^[122-123] The first ligand $(\text{N}^{\wedge}\text{N})^1$ was introduced into the chloro-bridged dimer $[\text{Ru}(\text{arene})\text{Cl}_2]_2$ (arene = benzene or cymene) resulting in a coordinatively saturated monomeric complex $[\text{Ru}(\text{N}^{\wedge}\text{N})^1(\text{arene})\text{Cl}]\text{Cl}$. Subsequent photolysis in a MeCN solution exchanged the arene ligand with two or three equivalents of solvent molecules which, in turn, were substituted by another bidentate ligand $(\text{N}^{\wedge}\text{N})^2$ to give $[\text{Ru}(\text{N}^{\wedge}\text{N})^1(\text{N}^{\wedge}\text{N})^2\text{Cl}]\text{Cl}$. Finally, the third ligand $(\text{N}^{\wedge}\text{N})^3$ was introduced in refluxing aqueous ethanol exchanging the remaining chloro ligands. This route was successfully applied for the introduction of different terpyridines and bipyridines,^[124] bisoxazolines,^[125] and pyridylbisoxazolines^[126]. Bisoxazolines were always introduced as second ligand.

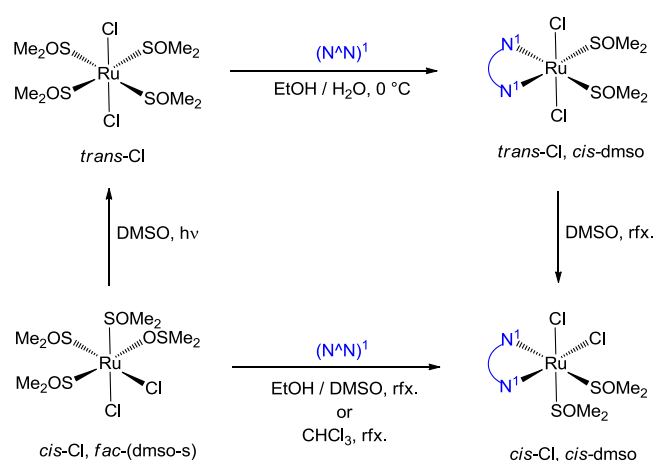


Scheme 3-15. Preparation of trisheteroleptic Ru(II) complexes from polymeric $[\text{Ru}(\text{CO})_2\text{Cl}_2]_n$.^[104]



Scheme 3-16. Preparation of trisheteroleptic Ru(II) complexes from dimeric $[\text{Ru}(\text{arene})\text{Cl}_2]_2$.^[104, 122]

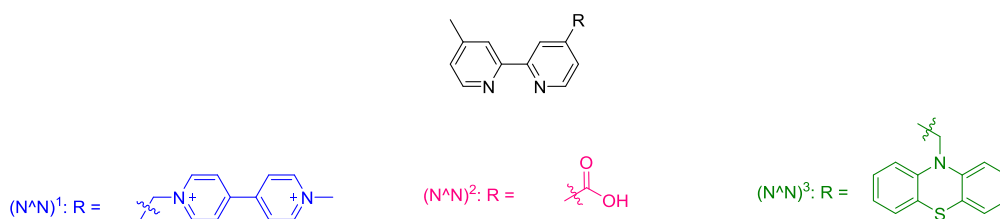
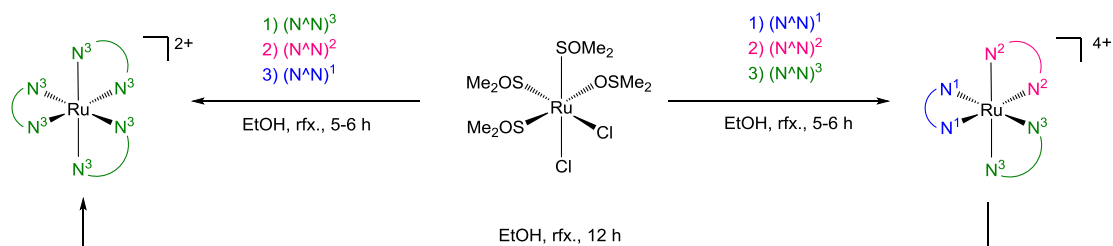
Another mild method utilizes $[\text{Ru}(\text{dmsO})_4\text{Cl}_2]$ as precursor for the selective introduction of bidentate ligands.^[106, 124, 127-136] The Ru(II) precursor complex itself can conveniently be prepared from Ru(III) trichloride in neat DMSO.^[127, 137] The product of the monosubstitution is, solvent dependent, obtained in different isomers (Scheme 3-17).^[133-134, 137] For example leads direct reaction of the ruthenium precursor with the ligand $(\text{N}^{\wedge}\text{N})^1$ in an ethanol-DMSO mixture or in chloroform as solvent to the monosubstituted, thermodynamic product *cis*-Cl, *cis*-dmsO- $[\text{Ru}(\text{N}^{\wedge}\text{N})^1(\text{dmsO-S})_2\text{Cl}_2]$ (Scheme 3-17).^[134]



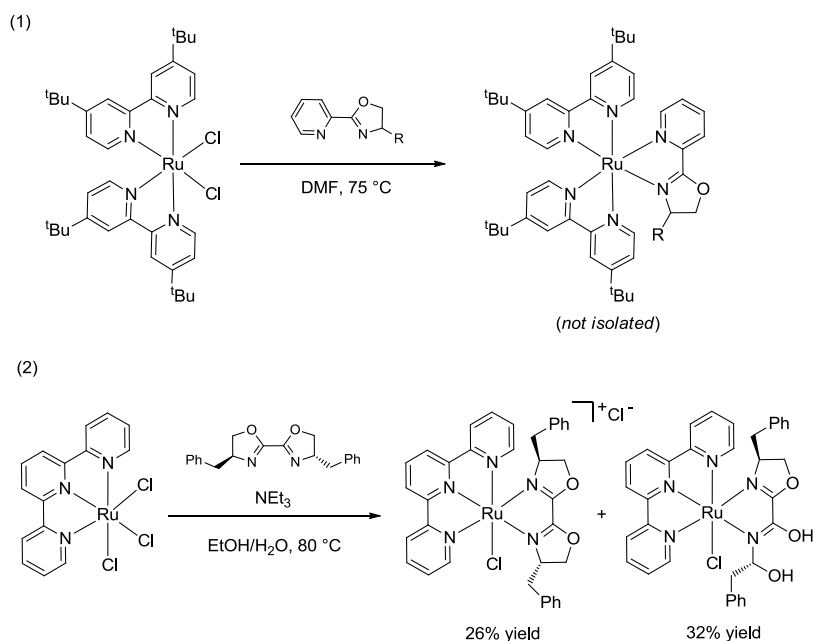
Scheme 3-17. Monoligation of $[\text{Ru}(\text{dmsO})_4\text{Cl}_2]$.^[133-134, 137]

The second ligand $(\text{N}^{\wedge}\text{N})^2$ was introduced under similar conditions^[106, 131] as the first one, but also procedures applying much harsher conditions with *e.g.* DMF^[133, 136] as solvent at reaction temperatures above 100 °C are known. As variation to the existing multi-step procedures, also one-pot procedures for the introduction of two dissimilar ligands were developed, applying ethanol as sole solvent.^[130, 135] Meyer and co-workers found out that for the on-pot procedure the right order of ligand addition was crucial. If the first ligand was too basic, the tris-ligated homoleptic complex $[\text{Ru}(\text{N}^{\wedge}\text{N})_3]^{2+}$ was formed immediately (Scheme 3-18).

With oxazoline ligands, relevant for this work, only few examples were reported. In these examples bisoxazolines or pyridyloxazolines were introduced as second ligand subsequent to bipyridine or terpyridine (Scheme 3-19).^[125, 138-139] As solvents aqueous ethanolic solutions or DMF at reaction temperatures of approximately 80 °C were applied. When $[\text{Ru}(\text{tpy})\text{Cl}_3]$ was used as precursor complex (Scheme 3-19, example 2), triethylamine served as reducing agent and was applied together with the oxazoline ligand. However, the purification appeared difficult since the oxazoline ligand was partially hydrolyzed upon column chromatography over basic alox.



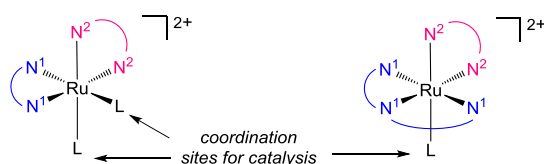
Scheme 3-18. One-pot procedure for tris-heteroleptic Ru(II) complexes developed by Meyer and co-workers.^[130]



Scheme 3-19. Introduction of oxazolines for the formation of heteroleptic Ru(II) complexes. In example (2), the box ligand partially hydrolyzed upon column chromatography over basic alox. (1)^[139] (2)^[138]

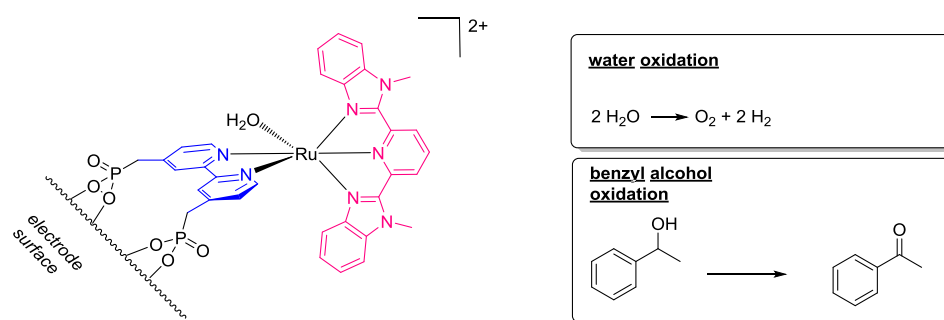
3.2.2 Application in Redox-Reactions

Since the ruthenium complexes prepared in this project were supposed to act as redox catalysts in artificial photosystems, the redox catalysis of related complexes is of certain interest (Scheme 3-20). Such complexes need to bear one or two labile ligands providing open coordination sites for suitable substrates. However, not many examples for redox catalysts fulfilling these requirements were reported. Two examples matching the complex on the right of Scheme 3-20 will be presented.



Scheme 3-20. Bisheteroleptic Ru(II)-complexes. L presents labile ligands that provide open coordination sites upon catalysis.

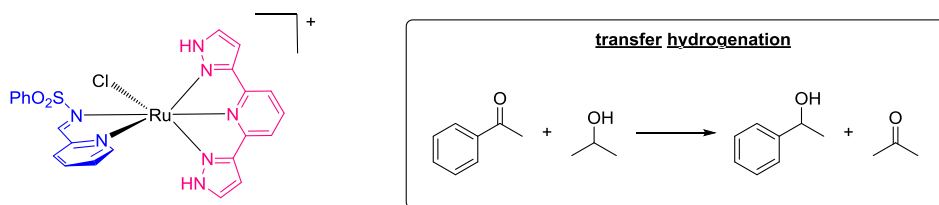
The most well known example for redox catalysis performed by bisheteroleptic ruthenium complexes with one coordination site for substrate binding might be the Ru(II)-aqua complex $[\text{Ru}(\text{bpy})(\text{tpy})\text{H}_2\text{O}]^{2+}$ for water oxidation, which was intensively studied by the group of Meyer.^[4, 140-143] As extension to their work on homogeneous water oxidation with such a complex, an improved version was successfully immobilized on an electrode surface and used for water oxidation in aqueous as well as in non-aqueous media.^[140-141] Later, this immobilized catalyst was also found to be active in the oxidation of benzyl alcohol (Scheme 3-21).^[142] A structurally closely related, but dinuclear Ru(II) complex was active in the same reaction as reported by the group of Rocha.^[144] This dinuclear complex consisted of a Ru(II)-Ru(II) chromophore-catalyst dyad and was operating in solution.



Scheme 3-21. Bisheteroleptic, surface bound, Ru(II) complex suitable for water and alcohol oxidation.^[141-142]

Recently, Ru(II) complexes containing bipyridine and tris-pyridylamine ligands were photochemically activated to perform benzylic and allylic oxidation of different substrates.^[145] Further complexes

offering the (N[^]N[^]N), (N[^]N) ligands motive combined with one labile ligand were tested in transfer hydrogenation with great success. Ligand combinations of a pyridylimine with different tridentate ligands such as bis-pyrazolylpyridine were probed on substituted acetaldehydes and resulted good to excellent conversions (Scheme 3-22).

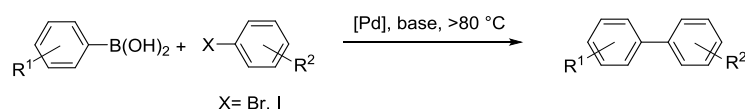


Scheme 3-22. Ru(II) complex with one open coordination site for transfer hydrogenation.^[145]

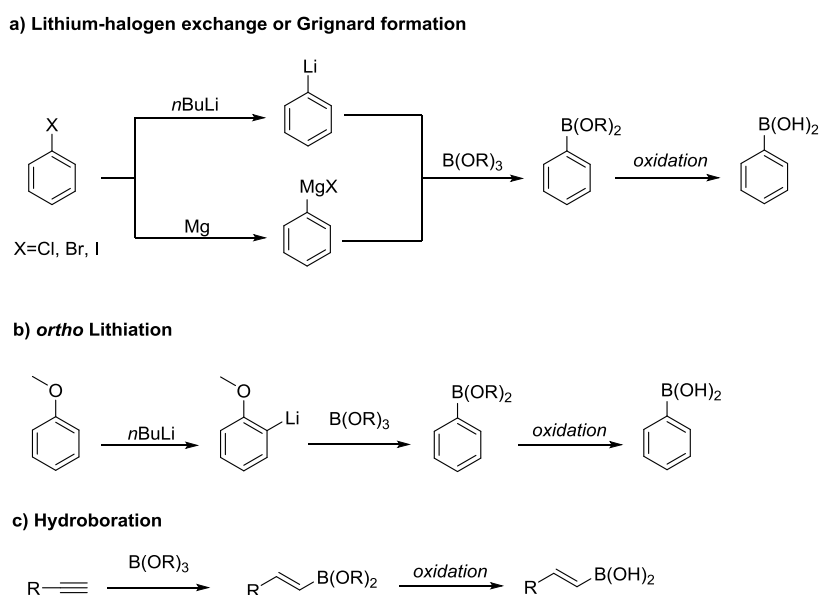
4 Catalysis

4.1 Borylation

Organoboron compounds are of major interest in synthetic chemistry because they are widely used in Suzuki cross-coupling reactions (Scheme 4-1).^[73] The use of boronic acids is advantageous for different reasons. For example they are moisture stable which makes them easy to handle and they are thermally stable which allows reactions under elevated temperatures. The arylboron compounds are traditionally prepared *via* lithium-halogen exchange of aryl halides or directed *ortho* metallation of arenes carrying functional groups, such as ethers or amides, followed by borylation of the obtained lithium compounds. Alternatively, arylboronates can be obtained from Grignard reagents and alkenylboronates can be synthesized by hydroboration of triple bonds (Scheme 4-2).^[146-147]



Scheme 4-1. General reaction scheme for Suzuki cross coupling.

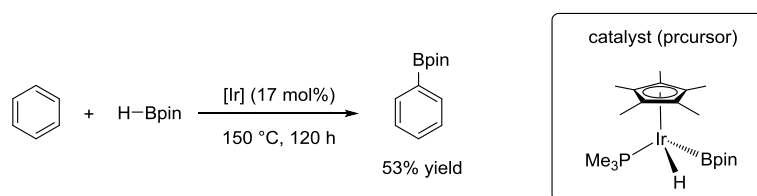


Scheme 4-2. Preparation of boron substrates suitable for Suzuki cross coupling.

However, the preparation of the boronates requires pre-functionalized starting materials and is also strongly limited to substances containing no functional groups that are sensitive towards lithium or magnesium reagents. To make the total reaction sequence shorter, several protocols for the tandem borylation–Suzuki cross coupling or related couplings were reported.^[148-153] A more attractive and elegant method would be direct C-H functionalization, because it allows to obtain the corresponding boron compounds in one step, without the need for pre-installed functional groups.^[147, 154] Based on aromatic borylation, further functionalizations introducing fluorinated groups^[155-157] or nitrogen functionalities^[158-159] were reported and a “one-pot” protocol for aromatic borylation followed by 1,4-conjugate addition^[160] was developed.

4.1.1 Aromatic Borylation

The first example of catalytic direct borylation was reported by the group of Smith in 1999. The authors borylated neat benzene at high temperatures with a high catalyst loading of 17 mol% [Ir(cp*)(PMe₃)(Bpin)(H)] complex and achieved yields of approximately 50%. However, these results were very valuable because they paved the way for efficient conversion of C-H bonds into C-B bonds.^[161] Following borylations were performed with a rhodium catalyst^[162-163] and cyclohexene as solvent or as one-pot procedures^[164] of borylation accelerated by iridium arene trisboryl complexes and palladium catalyzed cross coupling.

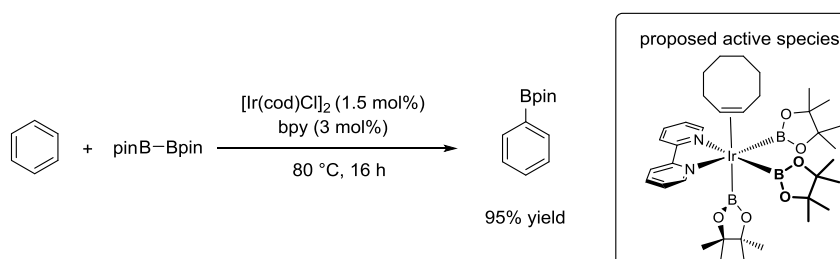


Scheme 4-3. First example of direct, catalytic aromatic borylation.^[161]

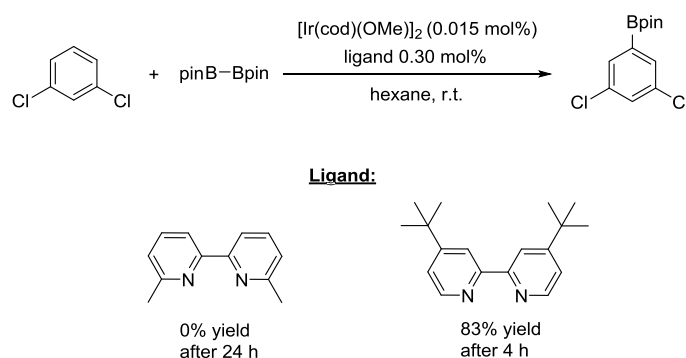
A new catalytic system, which was developed by Miyaura and Hartwig in 2002, allowed much milder conditions than before. The new system was not based on iridium arene complexes, but on the dimeric chloro bridged *cis,cis*-cyclooctadiene (cod) precursor [Ir(cod)Cl]₂ (Scheme 4-4).^[1] The new catalytic system was running at only 80 °C and with a catalyst loading of 1.5 mol%. Using bipyridine or phenanthroline as ligand led to nearly full conversion. As for the iridium arene system reported, the cod complexes also showed the same stereoselectivity for the *meta* and *para* position when using substituted benzenes as substrates. A cod trisboryl complex was identified to be chemically and kinetically competent as an intermediate in the catalytic cycle.

Further investigation showed a high dependence of the yield on the electronic nature of the bidentate ligand. Bipyridine ligands which donate electron density towards the iridium turned out to be most efficient. It was also important to avoid substituents in the 2,2'-positions due to steric hindrance. Also the application of coordinating solvents such as DMF were beneficial. Improvement of the reaction

parameters made the reaction possible even at room temperature (Scheme 4-5).^[2, 165] A large improvement of the reaction outcome was achieved when instead of the chloro bridged dimeric catalyst precursor its methanolato bridged equivalent $[\text{Ir}(\text{cod})(\text{OMe})_2]$ was used. It was also found, that -Bpin reacts much faster than -Bcat*, presumably also due to its stronger electron donating ability.^[166]



Scheme 4-4. Effective catalytic system with $[\text{Ir}(\text{cod})\text{Cl}]_2$ as precatalyst.^[1]



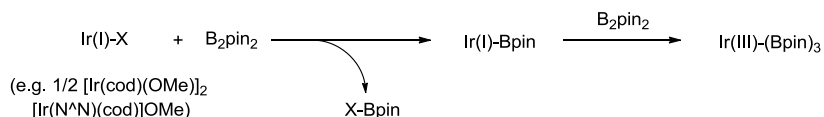
Scheme 4-5. Optimized reaction conditions for aromatic borylation at room temperature.^[1]

To date, a mechanistic proposal based on the formation of a catalytically active Ir(III) trisboryl complex is commonly accepted. Several theoretical and experimental studies support this mechanism.^[1, 167-171]

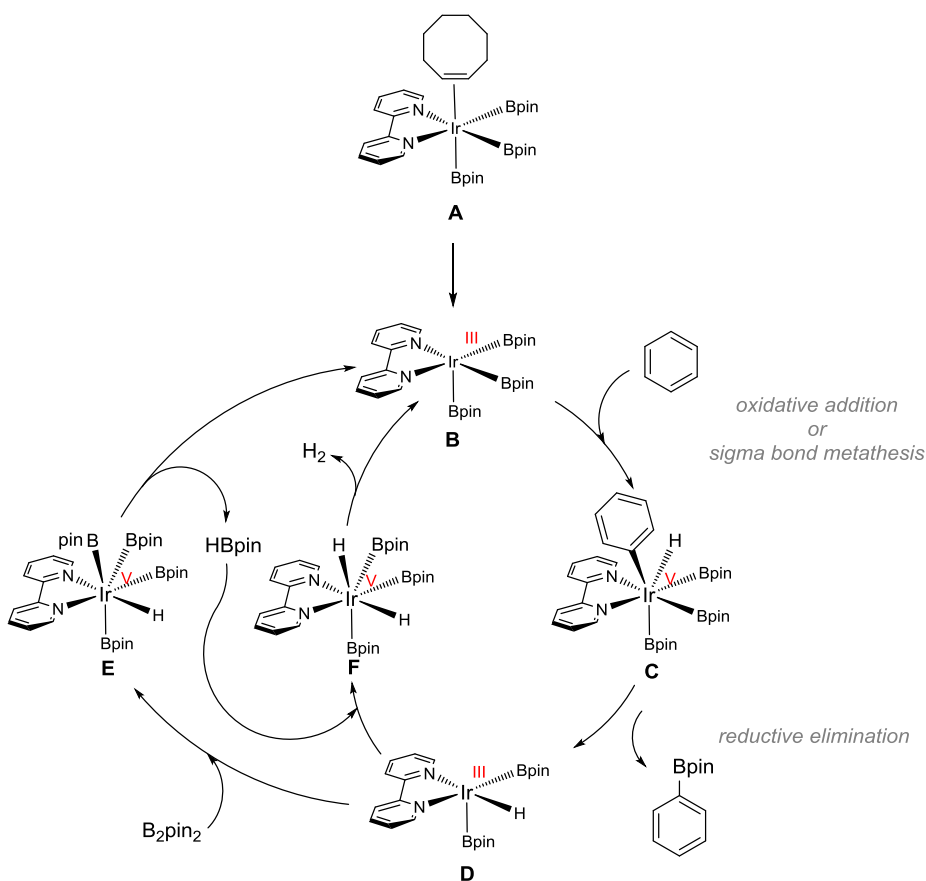
However, the formation of such a trisboryl complex is not completely understood. The commonly presented mechanism, here depicted in Scheme 4-6, might be a strong simplification since the combination of B_2pin_2 with several iridium precursor of the type $[\text{Ir}(\text{L}^{\wedge}\text{L})\text{X}]_2$ ($\text{L}^{\wedge}\text{L} = \text{cod}, \text{coe}; \text{X} = \text{Cl}, \text{OMe}$) did not lead to the formation of the desired trisboryl complex within 30 min.^[170] In addition, the significantly long induction period in catalytic reactions shows, that the catalytically active species is not formed instantly from B_2pin_2 and a dimeric iridium precursor. This induction period was overcome by adding small amounts of HBpin to the reaction mixture. The Hartwig group was also able to show that the reduction of cod to coe might play an important role for catalyst generation.^[1]

However, since the trisboryl complexes were proven to be kinetically competent with the catalytic cycle, a mechanism based on their formation was proposed (Scheme 4-7). Once formed, the trisboryl complex **A** can liberate the coe ligand to give the coordinatively unsaturated catalytically active species

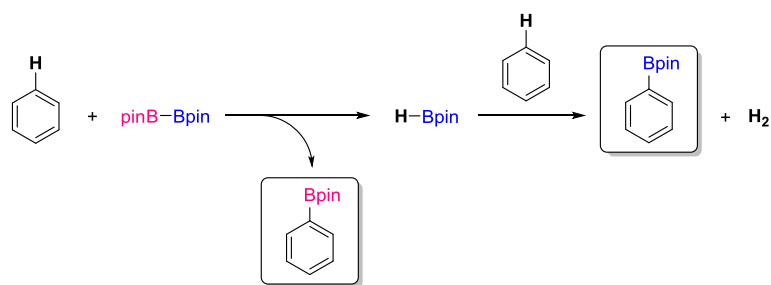
B. Rate limiting oxidative addition of an C-H bond of an aromatic compound yields in the Ir(V) complex **C**, which releases the product by reductive elimination. The resulting hydrido complex **D** can now oxidatively add B_2pin_2 or $HBpin$ to form complex **E** or **F**, respectively. Reductive elimination of $HBpin$ from **E**, or H_2 from **F** regenerates the trisboryl complex **B**. The fact, that both equivalents of B_2pin_2 are transferred into the product (Scheme 4-8) demonstrates, that both reaction pathways for the regeneration of **B** via complex **E** or **F** are suitable.



Scheme 4-6. Formation of iridium trisboryl complex.^[147]



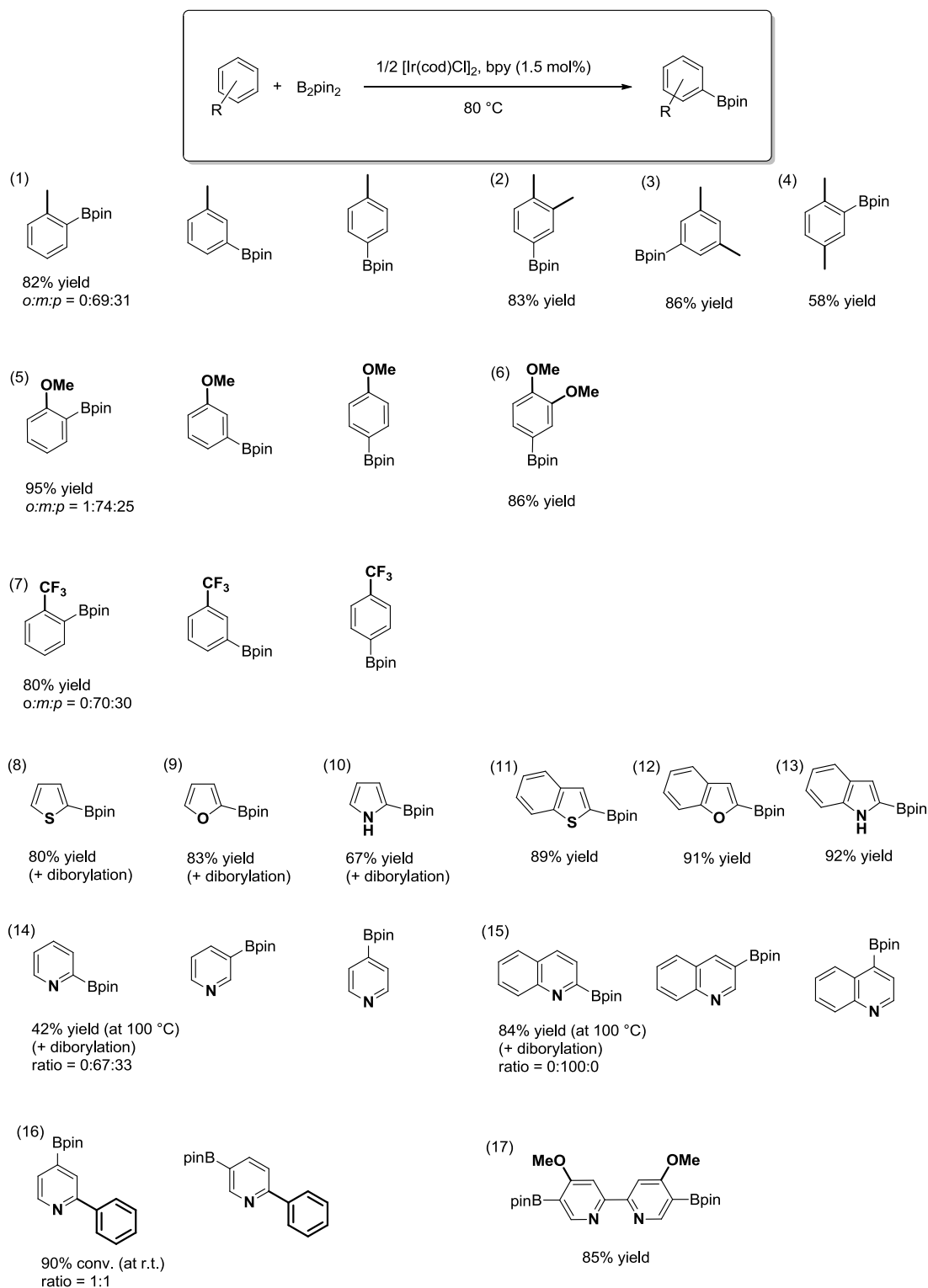
Scheme 4-7. Mechanistic proposal for aromatic borylation.^[147, 170]



Scheme 4-8. Formal aromatic borylation with B_2pin_2 .

In Scheme 4-9 some examples of aromatic borylations are depicted. For monosubstituted arenes, typically a *meta* and *para* selectivity was observed (entries 1, 5 and 7). Only from anisole, a small amount of the *ortho* borylated product was formed, in contrast to toluene. If the arene is disubstituted, C-H functionalization occurs in the *meta* position due to the lack of a free *para* position (entries 2,3 and 6). However, if there are only *ortho* CH bonds available, borylation can even be observed in this sterically hindered position as it was the case for *p*-xylene (entry 4). However, the yield was relatively low. Interestingly, borylation in heteroarenes takes place next to the heteroatom, if this atom is part of a five-membered aromatic compound (entries 8-13). In case of pyridine, substitution of the 3-position was preferred (entry 14 and 15). This behavior was not changed in case an additional arene was annulated (entries 11,12,13 and 15). Phenyl substituted pyridine was only on the pyridine ring borylated, but not in the 4-position to the nitrogen and to the phenyl substituent in a 1:1 ratio (entry 16). In case, a 4,4'-methoxy substituent in a 2,2'-bipyridine was present, borylation even occurred in the 4-position to the methoxyl group (entry 17).^[163, 172-174]

The lack of borylation in *ortho* position in aromatic borylation is usually explained by the steric hindrance present in this position. For pyridines, the preferred selectivity for the 3-position can also be explained by steric reasons, but this argument fails for pyrroles, which were preferably substituted in the 2-position. Here, the electronic structure of the substrate might play a selectivity determining role as well. Also, the selectivities observed for substituted pyridine derivatives cannot be explained by sterics.^[167, 175-176]

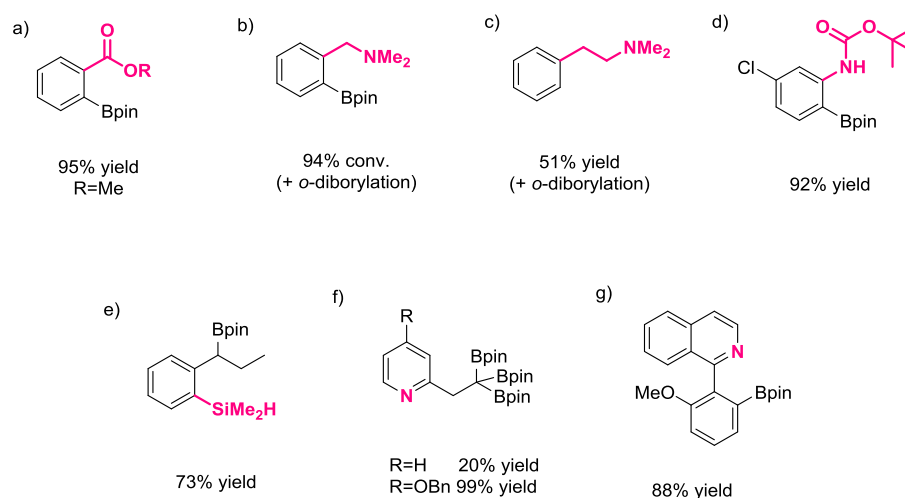


Scheme 4-9. Substitution patterns and yields typical for aromatic borylation. Diborylation products were observed in 12-17% yield. References (1)-(7),^[1] (8)-(15),^[174] (16), (17)^[175].

Directed borylation by application of additional functional groups is a convenient tool for enforcing the stereoselectivity of borylation. For example, esters, amines and methylamines direct into the challenging *ortho*-position (Scheme 4-10 a, b, c and d).^[171, 177-178] In order to optimize the selectivity as

well as yields, in some cases the commonly used bipyridine ligand was replaced by a bisphosphine or bisamine ligand.

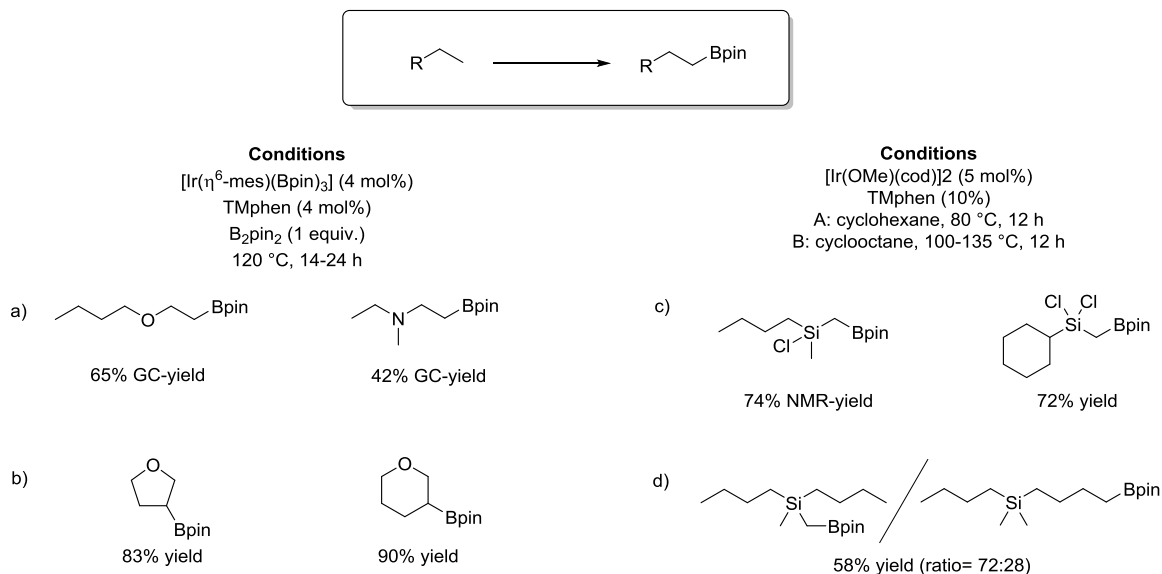
Directed borylation of sp^3 -C-H bonds was also described for *ortho*-alkyl substituent hydrosilylenylarenes, which directed the borylation into the corresponding γ -position on the side chain (Scheme 4-10f).^[179-180] A similar reactivity was achieved with a 2-ethylpyridine, which was trisborylated on the CH_3 group, presumably due to coordinating effect of the pyridine nitrogen (Scheme 4-10). In other substrates, coordination of the pyridine nitrogen was also reported to have a directing effect on the borylation of benzene substituents (Scheme 4-10 h).^[181-182]



Scheme 4-10. Directing groups in borylation reactions. References a),^[178] b), c),^[177] d),^[171]; e),^[179] f),^[181] g)^[182].

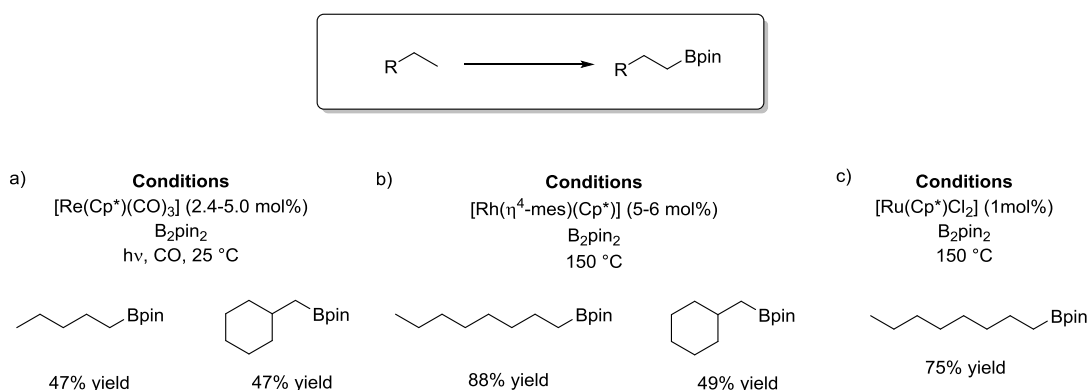
4.1.2 Aliphatic Borylation

As mentioned in chapter 4.1.1, borylation of methyl C-H bonds by directing heteroatoms or other suitable functional groups is a well working method which works also in the presence of aromatic methylene C-H bonds (cf. Scheme 4-10). Methylsilanes were selectively borylated at the α -methyl C-H bond to the silicon which was attributed to the ability of silicon to stabilize negative charges.^[183-184] In alkylamines and alkylethers, the β -position to the heteroatom was borylated.^[185-186] In the early examples a trisboryl iridium arene complex instead of the dimeric cod complex was used as catalyst precursor but later catalytic systems with $[Ir(cod)(OMe)]_2$ /ligand were used. Also, the temperature required for methyl C-H activation was with 120 °C higher than that for aromatic borylation which runs at room temperature or at elevated temperatures of 80 °C (Scheme 4-11).



Scheme 4-11. Aliphatic borylation directed by heteroatoms. References a);^[185] b);^[186] c);^[184] d)^[183].

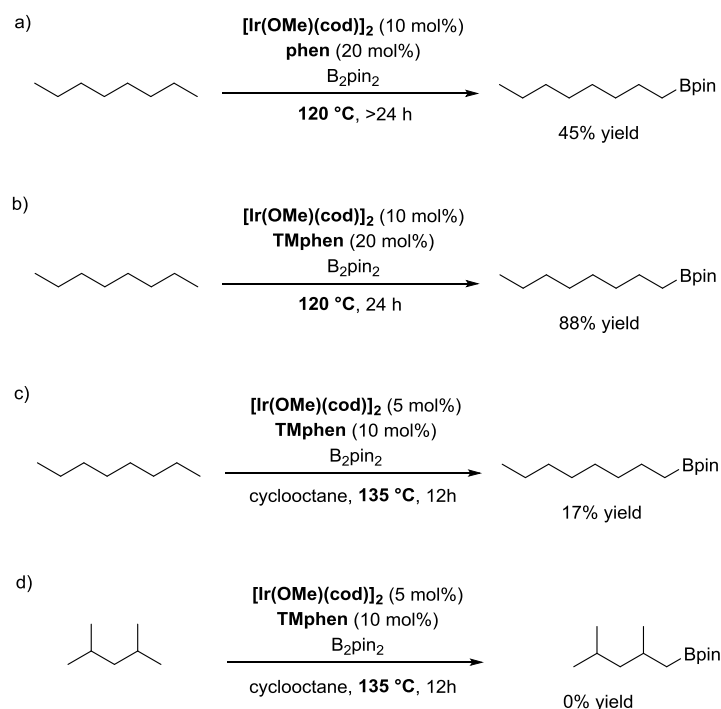
Borylation of unfunctionalized alkanes was first described by Chen and Hartwig in 1999.^[187] The authors were able to borylate hexane quantitatively (in respect of one boron equivalent of B₂pin₂) by application of the tri rhenium arene complex [Re(Cp)(CO)₃] in combination with B₂pin₂ under irradiation. Comparable results were achieved using a related tungsten complex.^[188] Octane was borylated with [Ru(Cp*)Cl₂]₂ at 150 °C or with [Ir(Cp*)H₄], in each case with B₂pin₂ as boron source and without any additional ligand (Scheme 4-12).^[189-191]



Scheme 4-12. Borylation of unfunctionalized alkanes. References a);^[187] b);^[191] c)^[190].

When *n*-octane was borylated using the [Ir(OMe)(cod)]₂/N,N-ligand system, which was also successfully applied in aromatic borylation, contradictory results are reported. In some cases it was described as well working system^[186] and sometimes *n*-octane was described as inert solvent for such a

catalytic system^[147]. As depicted in Scheme 4-13, *n*-octane was borylated in 88% yield with a catalyst loading of 10mol% (a). Under the same condition, *n*-hexane was borylated in only 45% yield (b). With a lower catalyst loading of 5 mol, but under higher temperature as in the previous examples, the yield of the borylation of *n*-octane dropped down to 17% (c). For the sterically more hindered 2,4-dimethylpentane no borylated product was observed (d).

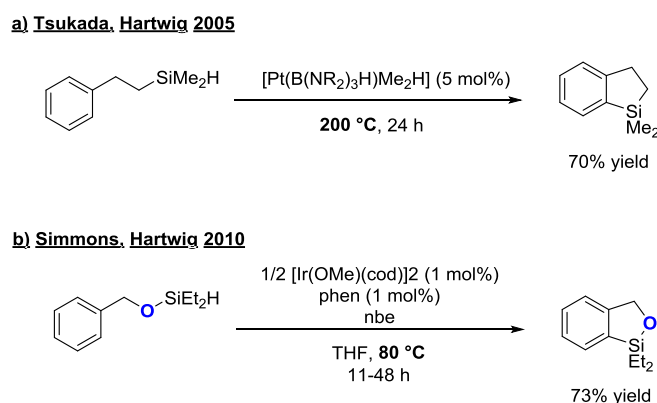


Scheme 4-13. Borylation of unactivated alkanes by an $[\text{Ir}(\text{OMe})(\text{cod})]/\text{TMphen}$ system. References a), b);^[186] c),d)^[183]

4.2 (Hydrido)silyl Ether Directed γ -C-H Activation

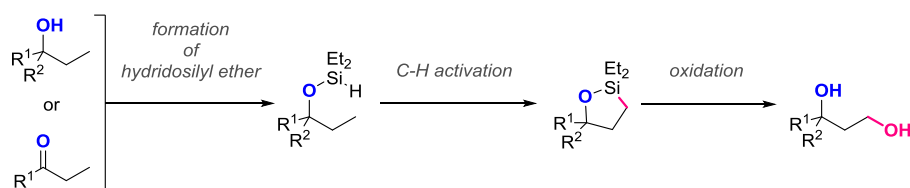
For the (hydrido)silyl ether directed γ -C-H activation, ketones or alcohols are used as starting materials for the formation of their (hydrido)silyl ether. Subsequently, the C-H bond is activated by the formation of an oxasilolane. The application of a silyl intermediate bears different advantages, for example they are not very expensive and easy storable. Furthermore, they tolerate the presence of halides, several protected alcohols and offer also the possibility for easy further functionalization *via* cross coupling (*e.g.* Hiyama-Denmark) or oxidation reactions (*e.g.* Tamao-Fleming).^[192]

The development of (hydrido)silyl ether directed C-H activation started a few years earlier in 2005, when a platinum catalyzed aromatic silylation with alkyl (hydrido)silanes was investigated by Hartwig and co-workers (Scheme 4-14). This procedure was a first step towards the elegant procedure known today, but it suffered from the harsh conditions necessary which strongly limited the applications.^[193] First success with silyl ethers was achieved in the aromatic silylation subsequent to the silyl ether generation from a ketone or an alcohol.^[194]



Scheme 4-14. Aromatic dehydrogenative silylation of a)^[193] alkyl (hydrido)silanes and b)^[194] (hydrido)silyl ethers.

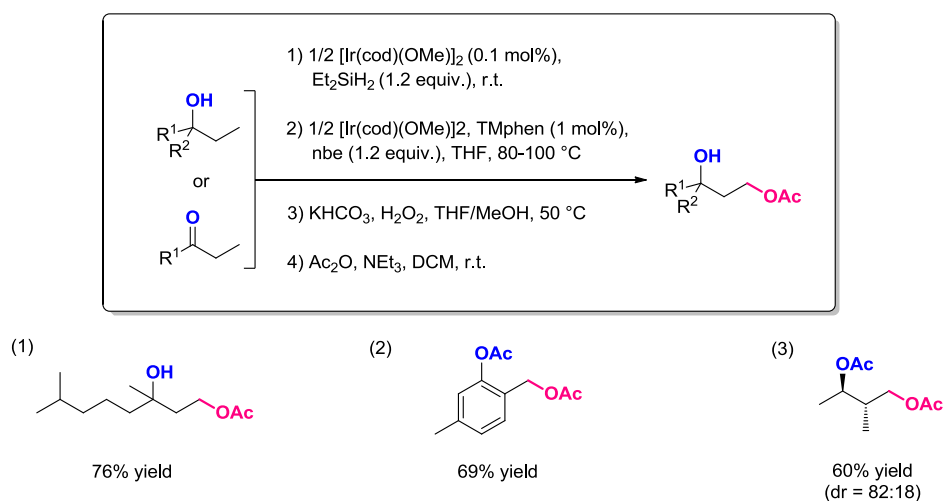
Silylation of less reactive aliphatic C-H bonds was achieved under conditions similar to these discovered for the aromatic C-H activation of (hydrido)silyl ethers.^[10] Both reactions, aromatic and aliphatic C-H activation of (hydrido)silyl ethers are based on the introduction of a Si-H bond that acts as directing group and functionalizing reagent at the same time. Conveniently, both ketones and alcohols can serve as starting materials to form (hydrido)silyl ethers by hydrosilylation or dehydrogenative silylation, respectively. The (hydrido)silyl ether undergoes iridium catalyzed site-selective γ -functionalisation resulting in a five membered oxasilolane that subsequently can be oxidized to a 1,3-diol (Scheme 4-15). The first two steps of the reaction sequence are both catalyzed by the same Ir(I) precursor. Therefore, it is not necessary to remove the catalyst after the (hydrido)silyl ether formation step. Since the final oxidation step is also possible from the crude reaction mixture, the whole procedure is very convenient.



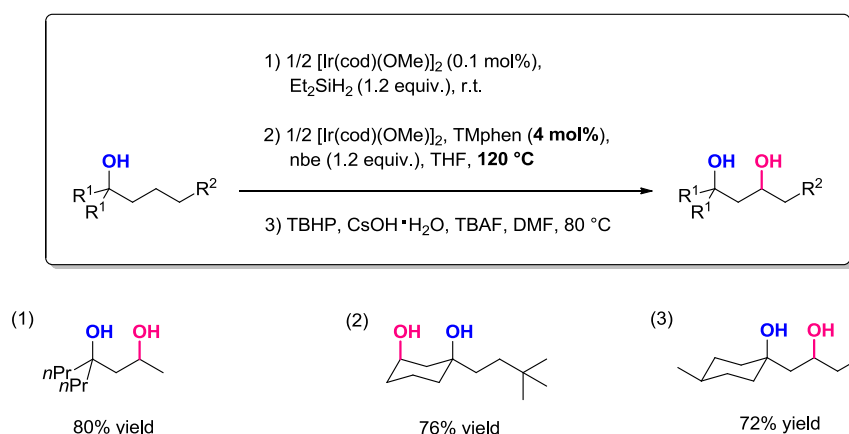
Scheme 4-15. General scheme for subsequent silylation, C-H activation and oxidative removal of the silyl group.^[10]

From a variety of bipyridines and phenanthrolines the most electron donating ligand, 3,4,7,8-tetramethylphenanthroline (TMphen) was identified as most effective. The whole reaction sequence was successfully tested on secondary, tertiary and aromatic (hydrido)silyl ethers while no competing reactions with more reactive aromatic C-H bonds or intermolecular side reactions were observed. In case of diastereotopic methyl groups present in the substrate, a preferred

trans-configuration of the product was observed which is attributed to the precedent formation of a less strained *trans*-disubstituted oxasilolane (Scheme 4-16, (3)).^[10]

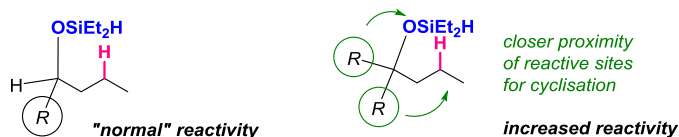


Scheme 4-16. Selected results of the silylation, C-H activation, oxidation and acylation sequence.^[10]



Scheme 4-17. Examples of activation of methylene C-H bonds by a silylation, C-H activation and oxidation sequence.^[195]

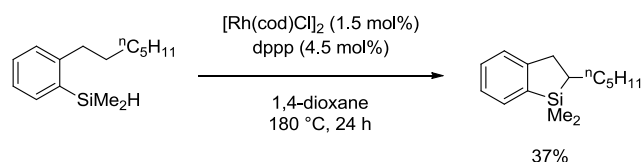
Thorpe-Ingold effect



Scheme 4-18. Illustration of the Thorpe-Ingold effect. Left side: "Normal" reactivity of a medium substituted substrate. Right side: Highly substituted position between to potential cyclisation points "pushes" these points into closer proximity and therefore simplifies the cyclisation.

As extension to the above described methyl C-H activation, the Hartwig group developed the methylene C-H activation under very similar conditions. For this purpose, only the temperature and catalyst loading had to be increased. Also the last oxidation step required harsher conditions (Scheme 4-17).^[195] However, this reaction is working only for tertiary alcohols or secondary analogues bearing large residues in both β -positions. The authors suggest this as “manifestation of the Thorpe-Ingold effect”.^[195] The Thorpe-Ingold effect describes an increased cyclisation rate for highly substituted substrates (Scheme 4-18).^[196-198]

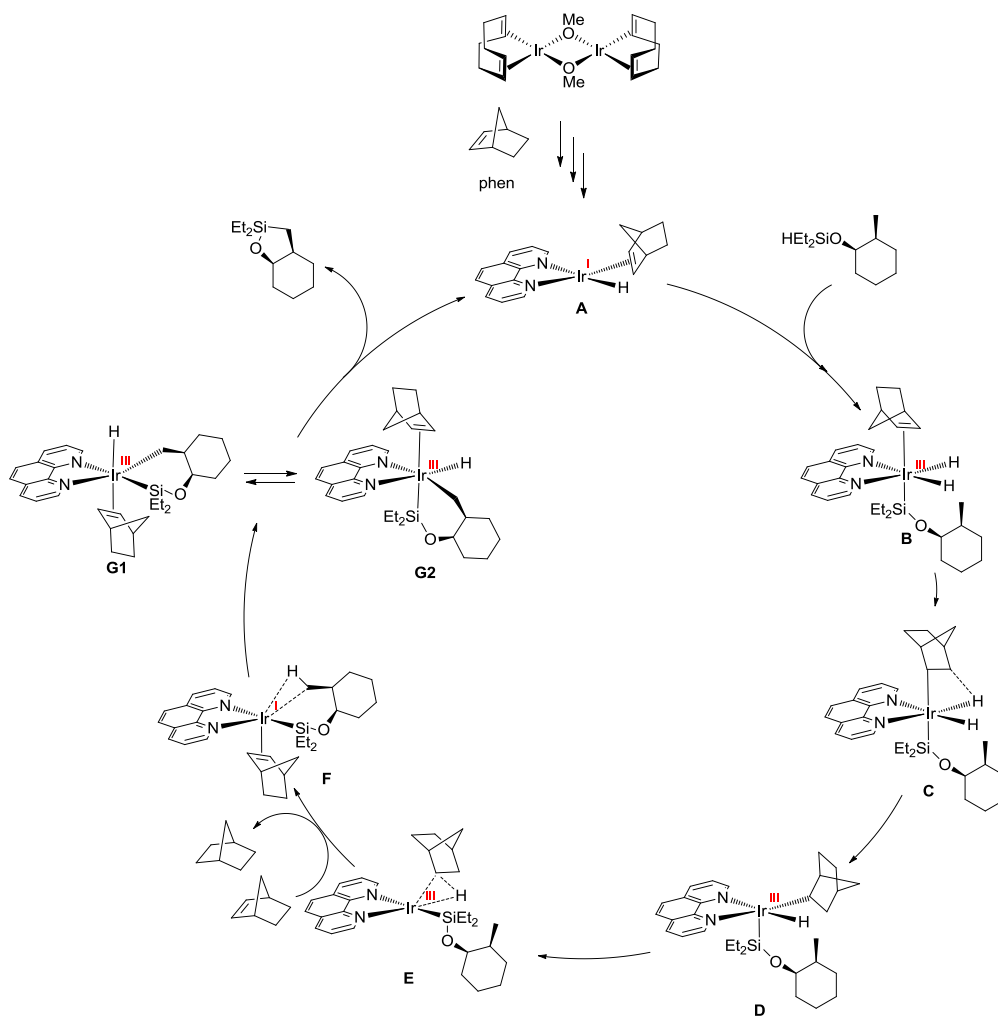
Another related strategy for methylene C-H activation was described by the group of Takai.^[199] The authors applied aromatic (hydrido)silanes for the δ -C-H activation of aliphatic side chains and used as catalytic system a Rh(I) precursor and a bisphosphine ligand. However, methylene C-H bonds were only activated in 37% yield.



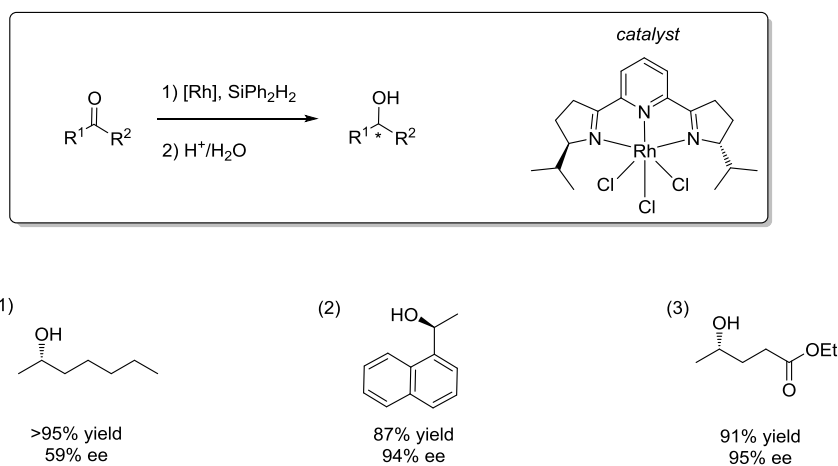
Scheme 4-19. Rhodium catalyzed methylene C-H activation.^[199]

Among the discussed examples, the conditions discovered by the Hartwig group formed the basis for the mild, site-selective (hydrido)silyl ether directed C-H activation applied in this work. Since this reaction was only discovered recently, not much mechanistical investigation has been undertaken up to today. The only suggestion for a mechanism was published by the group of Sunoj and is exclusively based on DFT calculations.^[200]

The authors assumed that the cod and methoxy ligands are initially replaced for the phenanthroline and the norbornene (nbe) to form the neutral hydrido complex **A**. Considered was also its monocationic equivalent without a hydrido ligand but the calculations revealed the neutral complex being much more likely. Oxidative addition of the silane to the catalytic active species **A** gives Ir(III) dihydride **B**, from which nbe is released as norbornane. The open coordination site is immediately occupied by a new molecule of nbe (structure **E** to **F**). On the hydride-free, 16-electron complex **F**, the C-H activation is initiated by agostic interaction of the γ -C-H bond, which undergoes oxidative addition leading to complex **G1**. **G1** isomerizes easily to the energetically favorable structure **G2**, from which the product is released by reductive elimination regenerating the active catalyst. The reductive elimination is facilitated by the crowded coordination environment on the iridium created by the norbornene ligand.



Scheme 4-20. Proposed mechanism for (hydrido)silyl ether directed γ -C-H activation.^[200]

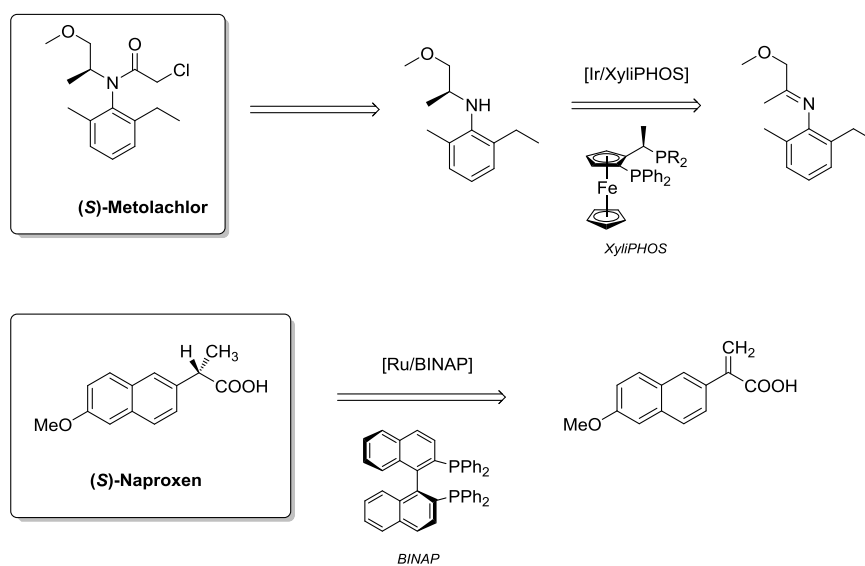


Scheme 4-21. Examples for enantioselective rhodium catalyzed hydrosilylation of selected prochiral ketones.^[201]

In this work, the (hydrido)silyl ether will be formed following the procedure of Hartwig and co-workers catalyzed by Ir(I) only, without any (chiral) ligand.^[10] Consequently, the (hydrido)silyl ether products will exist as racemic mixtures, if they are chiral. However, stereoselectivity controlling methods for hydrosilylation of ketones can be catalyzed by rhodium NHC complexes,^[202-203] rhodium pybox complexes,^[201] rhodium bisphosphene complexes,^[204] rhodium ferrocene complexes^[205] and copper NHC complexes^[206]. Aromatic substrates such as acetophenone and benzophenone are usually converted with high enantioselectivity. More challenging purely aliphatic substrates give moderate enantioselectivities of 50-70% ee (Scheme 4-21).

4.3 Hydrogenation

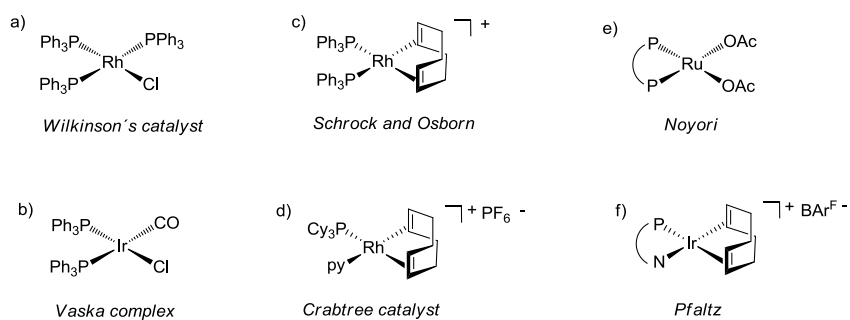
Hydrogenation catalysts were investigated intensively, because this type of homogeneous catalysis finds an exceptional wide application range in industry. It is applied often for key steps in the preparation of pharmaceuticals and fine-chemicals. Examples are the preparation of (*S*)-Metolachlor, a pesticide, or (*S*)-Naproxen, an anti-inflammation drug (Scheme 4-22).^[74] In the respective synthesis, the chiral catalysts reduce selectively an imine or the C-C double bond of a α,β -unsaturated ketone.



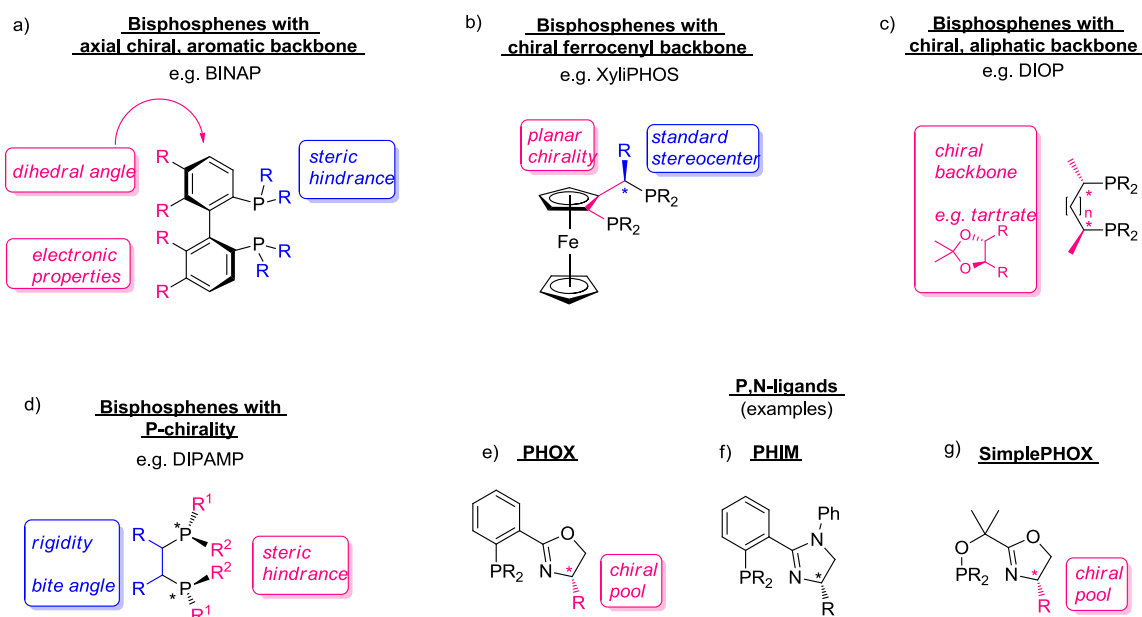
Scheme 4-22. Examples of homogeneous hydrogenation catalysis applied in industry.^[74]

Nowadays, a large number of hydrogenation catalyst classes are known and Scheme 4-23 shows a representative selection. Among them, there are neutral phosphine complexes such as the “Wilkinson-catalyst” or the “Vaska-complex” and ionic transition metal complexes such as the “Schrock-Osborn-catalyst” or the “Crabtree-catalyst”. Another important class is built by the “Noyori-type-catalysts” which are ruthenium complexes carrying chelate ligands.^[74, 207] The very

efficient “Pfaltz-catalysts” are based on the Crabtree-catalyst and are used for asymmetric hydrogenation. These complexes introduce chirality through their asymmetric P,N-coordinating phox ligands. A transfer hydrogenation catalyst such as the Noyori-catalyst [Ru(*p*-cymene)(TsDPEN)Cl] (TsDPEN=*N*-tosyl-1,2-diphenyl-1,2-ethylenediamin) should also be mentioned for the sake of completeness. Transfer hydrogenation is a special class of hydrogenation using molecular hydrogen donors.



Scheme 4-23. Common complex types used in classical homogeneous hydrogenation.^[74, 207]



Scheme 4-24. Chiral ligands used for homogeneous hydrogenation.^[207]

Not only the number of catalyst classes for hydrogenation is large, but also the variety of their ligands. For enantioselective hydrogenation, there are predominantly five ligand classes described (Scheme 4-24). The C_2 -symmetric bisphosphines containing an aromatic, axial chiral backbone such as 2,2'-bis(diphenylphosphino)1,1'-binaphthyl (binap), build one class and were first reported by

Noyori.^[208] Enantioselectivity caused by these ligands can be influenced by the dihedral angle of the aromatic backbone, by applying substituents of different steric extent on the phosphorus or by changing the electronic properties of the backbone (Scheme 4-24, a). Another class, the C_1 -symmetrical ferrocenyl ligands, possess two elements of chirality; the planar chirality on the ferrocene and stereocenter(s) on the substituents. These ligands exhibit very different bite angles, depending on the position of the phosphine (Scheme 4-24, b). Other chiral phosphine are *i.a.* C_2 -symmetrical bisphosphines with a chiral, aliphatic backbone that is often derived from the natural chiral pool (Scheme 4-24 c) and bisphosphines in which the phosphorous itself is stereogenic (Scheme 4-24, d). A further important class of asymmetric ligands for hydrogenation are the P,N-ligands, for example the 2-(2-phosphanyl)phenyl-oxazolines (phox) ligands developed by Pfalz and Helmchen.^[209] The chirality can be derived from the natural pool of amino acids, if the N-donor is part of an oxazoline ligand. An essential feature of these ligands is the different *trans*-effect of the dissimilar donor atoms, which also directs enantioselectivity (Scheme 4-24, e-g).

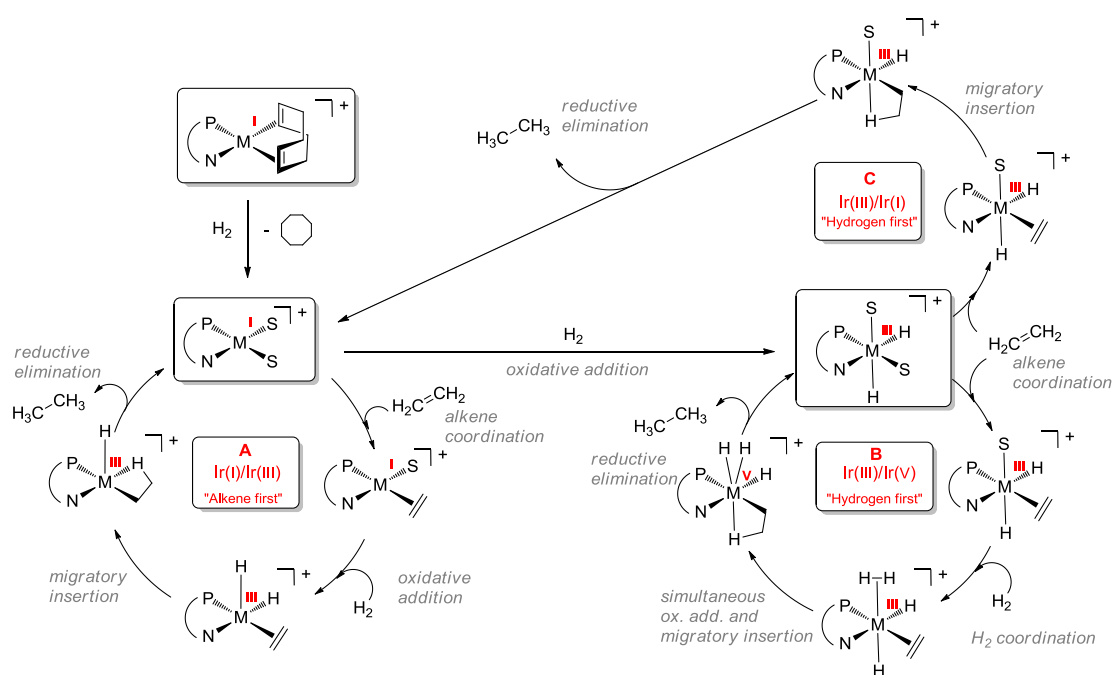
For the purpose of this project, the focus will lie on catalysts with chiral P,N-ligands of the general constitution $[M(P^{\wedge}N)(cod)]X$, which mimics their achiral predecessor, the Crabtree catalyst $[Ir(cod)(PCy_3)(py)]PF_6$.^[9, 44, 210-213]

The proposed mechanisms for the cationic pre-catalysts $[M(L^{\wedge}L)(cod)]X$ start with the same first step; the reduction of the olefinic ligand and its replacement by solvent molecules (Scheme 4-25).^[207] The main differences in the mechanistic proposals lie in the question when the reactants are coordinated to the complex. In the “alkene first” mechanism, initially the alkene coordinates to the catalytic active Ir(I) complex (Scheme 4-25 cycle A) followed by oxidative addition of hydrogen resulting in a pentacoordinated Ir(III) complex. The product is formed by migratory insertion and subsequent reductive elimination and released from the catalyst. During the last step, the catalytic active species is regenerated. The “alkene first” mechanism is especially favored by alkenes carrying a donor moiety, which is able to occupy an open coordination site on the coordinatively unsaturated complex during catalysis.

In the “hydrogen first” mechanism, the catalytic cycle starts with the oxidative addition of hydrogen (Scheme 4-25 cycle B and C). This mechanism is conceivable only in the case that the solvated, cationic Ir(I) complex $[Ir(P^{\wedge}N)S_2]^+$ is electron rich enough to facilitate an oxidative addition. In the I(III)/Ir(V) mechanism (cycle B), in a late stage another molecule of hydrogen has to add to the complex, generating an Ir(V) species. However, Pfalz and co workers proposed an Ir(I)/Ir(III) mechanism starting with the oxidized dihydrido complex (cycle C). Here, no second molecule of hydrogen adds to the complex and the coordinatively unsaturated intermediates in the catalytic cycle are supposed to be solvent stabilized.^[9, 214] Especially stabilization of the unsaturated complex after reductive elimination is in this mechanism important.

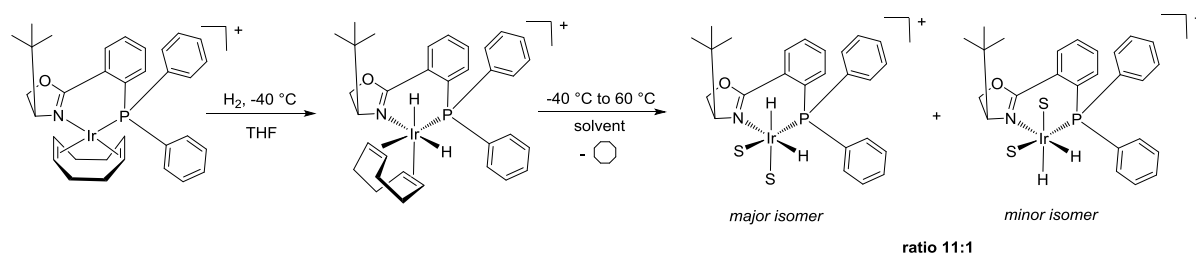
Despite the large effort, investigations have not led to a clear understanding about the mechanism for hydrogenation with $[M(P^{\wedge}N)(cod)]^+$ complexes. However, a “hydrogen first” mechanism is supported by several mechanistic investigations which will now be discussed in chronological order. Already in

1979, Crabtree undertook some mechanistic investigations when he originally intended to investigate catalysts of the Schrock and Osborn type. These rhodium phosphine complexes were known to be too reactive to study possible intermediates. This problem should be solved by using the equivalent iridium complexes, which were at this time thought to be nearly unreactive. Contrary to this expectations, Crabtree and co-workers discovered the remarkable high activity of the mixed phosphine pyridine complexes of iridium, which are known as “Crabtree-catalysts” today.^[215-216] In these early studies the authors could isolate the Ir(III) dihydride-olefin species $[\text{Ir}(\text{olefin})\text{H}_2\text{L}_n]^+$, which appears in all of the proposed mechanisms and was also detected in catalytic solutions. At this point, none of the two possible reaction pathways, “Alkene first” and “Hydrogen first”, could be excluded.



Scheme 4-25. Simplified mechanistic proposals for Iridium catalyzed hydrogenations (M equals iridium or rhodium).^[9, 207, 214]

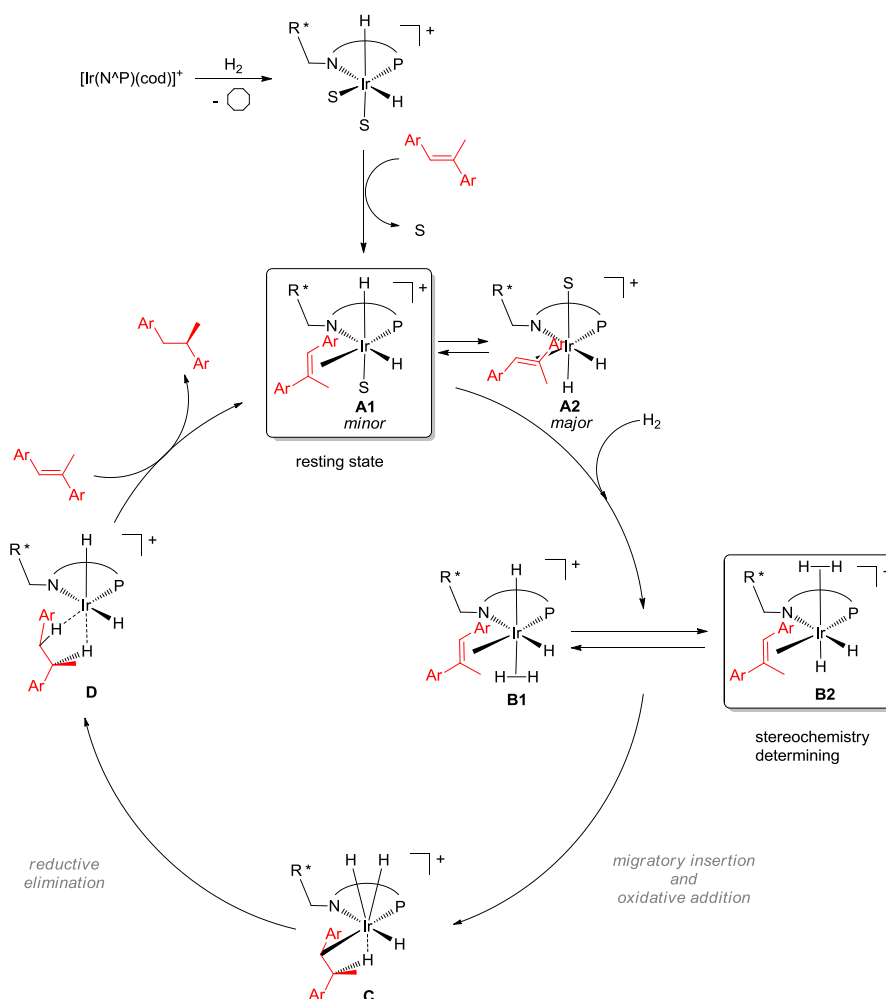
Pfaltz and co-workers were able to show experimentally an initial oxidative addition of hydrogen to the phox-cod catalyst precursor forming the *cis*-dihydrido isomer with one hydride occupying a position *trans* to the N-donor of the oxazoline moiety (Scheme 4-26).^[9] Upon warming above 0 °C, the complex released immediately cyclooctane and another hydrogen molecule added to form a new, solvent stabilized, *cis*-dihydrido complex. The Ir-H bond was again formed *trans* to the N-donor while the other hydride can now occupy two possible positions; above or below the N-Ir-P plane. This can be attributed to low steric hindrance of the solvate ligand, indicating that steric factors play a major role in this mechanism. These findings indicated that hydrogen was added first to the catalyst precursor, but did not solve the question if an Ir(I)/Ir(III) or Ir(III)/Ir(V) cycle was operating. Therefore, an “Alkene first” mechanism is nowadays rarely considered but numerous versions of the “Hydrogen first” mechanism are discussed.



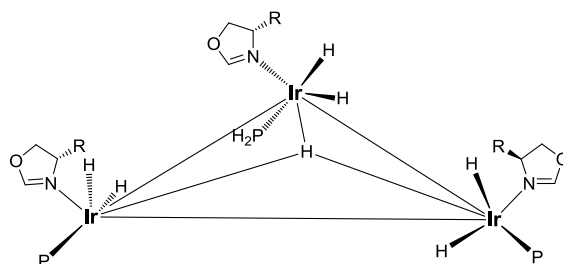
Scheme 4-26. Formation of the catalytically active dihydride species from the precursor complex.^[9]

Andersson and co-workers showed by means of DFT calculations on a strongly truncated model that the addition of hydrogen to an Ir(III) is thermodynamically feasible.^[217-218] This model was confirmed by Burgess, Hall and co-workers, who suggested as well an Ir(III)/Ir(V) mechanism on the basis of DFT calculations.^[219] Their calculations also confirmed the electronic factors directing the hydride *trans* to the oxazoline-N, but stated also steric effects being exclusively responsible for enantioselectivity. Chen and Dietiker undertook mechanistical experiments in the gas phase.^[220] The authors were not able to find evidence for an Ir(V) species taking part in the catalytic cycle, but strong indication supporting an Ir(I)/Ir(III) cycle were found, mainly through deuteration experiments in ESI-MS/MS. In 2014, additional experimental and computational evidence, supporting an Ir(III)/Ir(V) mechanism, were reported by the groups of Pfaltz, Hopmann and Sparta.^[221-223] Pfaltz and co-workers found a way to form iridium-dihydride species with coordinated substrate and initiate under hydrogen atmosphere the product release.^[224] The fact that product release from a dihydride Ir(III) complex was only possible under hydrogen atmosphere, strongly indicates a further oxidized Ir(V) species as intermediate. These results were computationally confirmed by the work of Hopmann, Frediani and Bayer who undertook this time calculations on a full model of an iridium-phox complex.^[222]

Based on the early and recent results, an Ir(III)/Ir(V) is the most likely mechanism (Scheme 4-27). The isomeric dihydrido-iridium complexes (Scheme 4-26), lead upon substrate coordination (Scheme 4-27) to the corresponding isomeric complexes A1 and A2. The minor isomer turned out to be more reactive and therefore hydrogen coordination occurred preferably to this structure. Comparisons of calculations and experimental results showed, that the right enantiomers of the product are either obtained *via* metathesis pathway from isomer B1 or *via* migratory insertion from isomer B2. The latter pathway was computationally predicted to be the preferred way and B1 is converted into B2 by isomerization.^[223] The theoretical results show that the isomerization barrier increases with decreased temperature in a way that it becomes larger than the C-H bond forming step under temperatures of $-40\text{ }^{\circ}\text{C}$.^[222] This explains the found low enantioselectivity of 72% at $-40\text{ }^{\circ}\text{C}$ compared to 98% at room temperature.^[221] Migratory insertion and simultaneous oxidative addition from B2 are resulting in the Ir(V) complex C, from which the product is generated by reductive elimination. The alkane product stays first weakly coordinated to the Ir(II) compound and is then exchanged for a new substrate molecule, which regenerates also the catalyst A1. This species was observed in large amounts in the reaction mixture, therefore it was proposed to be the resting state of the catalytic cycle.^[222]



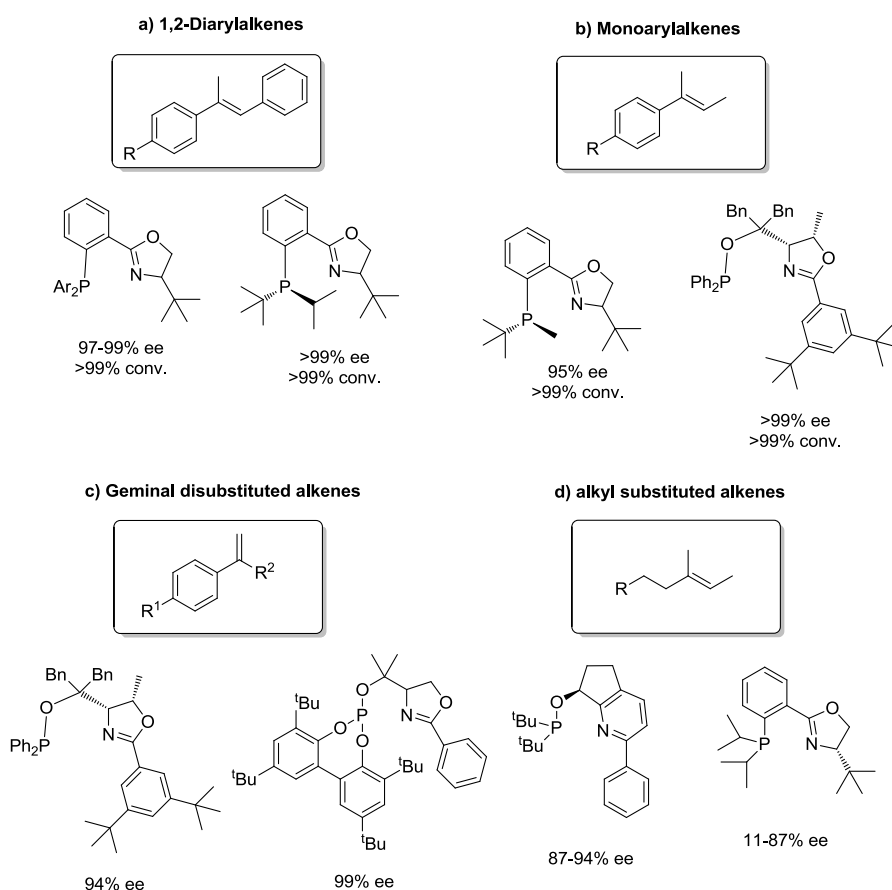
Scheme 4-27. Current mechanistic proposal for asymmetric hydrogenation by $[\text{Ir}(\text{N}^*\text{P})(\text{cod})]^+$ complexes.^[213, 221-223]



Scheme 4-28. Trinuclear, hydrogen-bridged iridium cluster.^[225]

Additionally, side reactions that inhibit the catalytic process need to be considered. Deactivation is probably the most important limiting factor for the catalyst efficiency. Investigations of Crabtree indicated that deactivation can be attributed to the irreversible formation of trinuclear and polynuclear hydride-bridged iridium-clusters.^[216] With phox containing catalysts, the Pfalz group similarly isolated a remarkably stable trinuclear iridium species (Scheme 4-28).^[225] This deactivation pathway was suppressed by lowering the hydrogen pressure from 50 to 7 bar and lowering the concentration of the

catalyst.^[214] However, the real breakthrough was achieved when instead of PF_6^- the bigger and even less coordinating (tetrakis[3,5-bis(trifluoromethyl)phenyl]borate (BAr^{F}) anion was used as counteranion for the phox complexes. The $[\text{Ir}(\text{phox})(\text{cod})]\text{BAr}^{\text{F}}$ complexes did not suffer from deactivation, therefore their loading could be reduced to 0.02 mol% instead of 4 mol%, which had been the limiting loading possible for PF_6^- complexes.^[99, 226] Kinetic studies showed that the catalysis with PF_6^- complexes is first order in the olefin substrate while for the corresponding BAr^{F} complexes it is zeroth order in olefin. This can be due to the higher availability of the complex with the less coordinating BAr^{F} anion for olefin coordination resulting in permanent olefin saturation on the catalyst. The PF_6^- anion might slow down the olefin coordination up to a point that this process becomes relevant for the reaction rate and in addition allowing for a competing cluster formation leading to catalyst deactivation. Therefore the use of BAr^{F} as counteranion for the phox catalysts turned out to be the method of choice. Also these complexes appeared to be less sensitive to moisture so they are much better to handle under air than their PF_6^- analogues.



Scheme 4-29. Substrates and Ligands described for a hydrogenations with $[\text{Ir}(\text{P}^{\wedge}\text{N})(\text{cod})]\text{BAr}^{\text{F}}$ complexes. a), b)^[210], c)^[44], d)^[227].

While the substrate scope of rhodium and ruthenium diphosphine complexes is limited to alkenes functionalized with a polar group, the phox complexes are capable of the reduction of unfunctionalized as well as functionalized olefins.^[44, 210-211] However, many substrates have an aromatic moiety directly

connected to the alkene. Trisubstituted olefins are most commonly investigated substrates. Especially for 1,2-diarylalkenes a large number of phox complexes is known that give good results.^[218, 228-229] Monoarylalkenes are more challenging substrates but until today some pyridinyl phosphinite complexes were identified to reduce these substrates effectively.^[214, 218, 230] Even for the purely alkyl trisubstituted alkenes these complexes have been successful.^[227] Further examples for substrates in asymmetric hydrogenations catalyzed by P,N-ligated complexes are for example Weinreb amides,^[231] α,β -unsaturated nitriles^[232] and α,β -unsaturated ester^[233]. A brief overview of some substrates and corresponding P,N-ligands which were used for their hydrogenation as ligands, is given in Scheme 4-29.

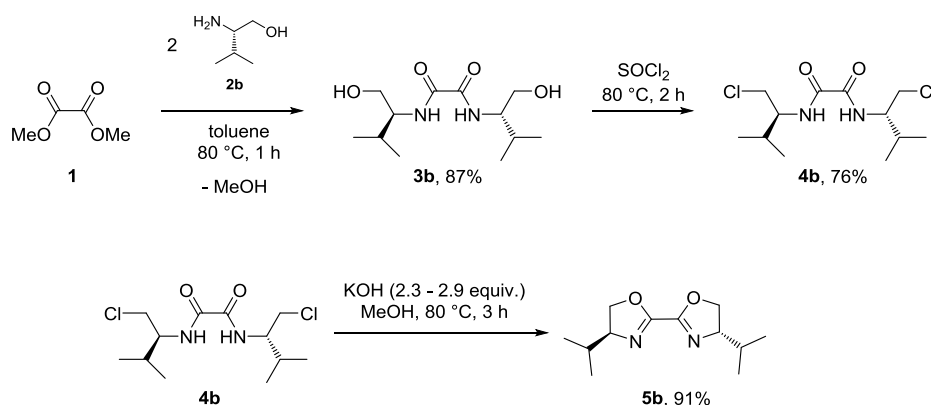
II. Results and Discussion

5 Ligand Synthesis

Contributions: Experimental help by Gisa Meissner under my supervision.

5.1 Bisoxazolines

In this work, bisoxazolines were prepared in three steps. The synthesis started with the condensation of an oxalic acid derivative with an aminol to the corresponding bisoxalamide, which was further transformed into its bischloride and subsequently transformed into the bisoxazoline (Scheme 5-1). The first two steps of the synthesis route, that was optimized for ⁱPr-box (**5b**), went on straightforward according to a procedure of the Butula group (Scheme 5-1).^[21] Firstly the amide formation with dimethyloxalate was easy to observe because the starting materials **1** and **2b** were very well soluble in the solvent while the product **3b** precipitated immediately upon formation. Therefore the end of the reaction was observed visually and the bisoxalamide product **3b** could be isolated by filtration and intensive washing with toluene. Secondly the substitution of the hydroxyl groups of the bis- β -hydroxyloxalamide **3b** by chloride was performed without any problems. The starting material **3b** was well soluble in a small amount of thionylchloride and the bis- β -chloroxalamide **4b** was obtained in pure form by recrystallization from ethylacetate at -20 °C.

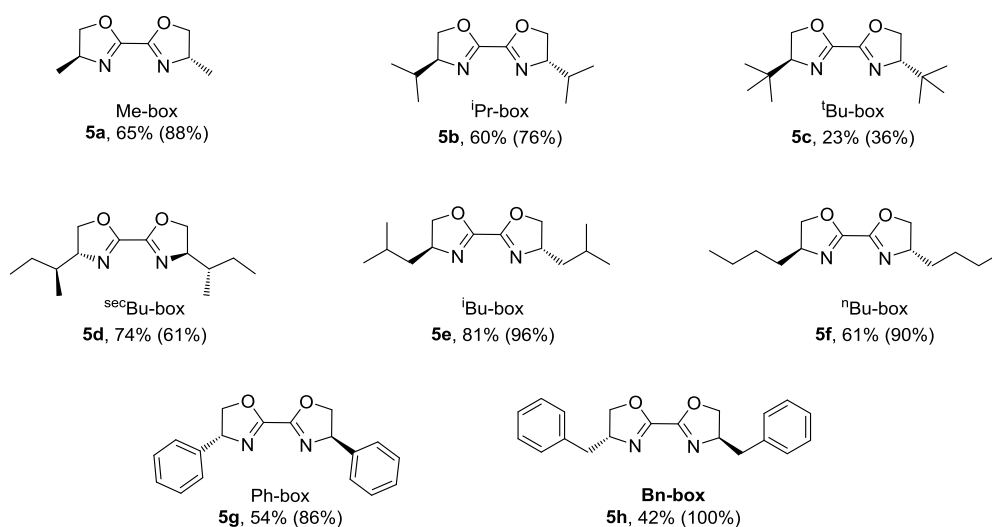


Scheme 5-1. Synthesis of ⁱPr-box **5b**.

Alternatively to the bis- β -chloroxalamide **4b** also the corresponding bis- β -mesyloxalamide was prepared successfully according to a procedure of the Denmark group.^[35] However, in the following oxazoline ring closure the products **5b** obtained from this substrate contained unidentified impurities. The oxazoline product obtained from the bis- β -chloroxalamide **4b** contained only little starting material as impurity. Therefore the synthetic route *via* the bis- β -mesyloxalamide was abandoned. For a successful oxazoline ring closure the right amount of strong base and the right choice of solvent was

very important. Different combinations of NaOH in pure methanol, methanol-water or ethanol-THF solvent mixtures were tried, but neither bis- β -chloroxalamide **4b** nor bis- β -mesyloxalamide dissolved very well. The results were not satisfying since in all cases the maximum yield was below 5%. At last, a procedure analogous to one published by the group of Sirbu, was chosen.^[34] Here, the bis- β -chloroxalamide **4b** was dissolved in a small amount of boiling methanol followed by dropwise addition of a slightly overstoichiometric amount (2.3 equiv.) of KOH in methanol. Heating to reflux for approx. 3 h led to nearly full conversion and the product was isolated by extraction with DCM. Since ¹Pr-box **5b** was not isolated in pure form after this procedure, subsequently a recrystallization from ethylacetate was undertaken. Through this treatment the pure bisoxazoline **5b** was isolated from the filtrate while the remaining white solid was identified as starting material.

The optimized procedure was successfully applied on the synthesis of seven further box-ligands (Scheme 5-2). Some adoptions had to be made during the synthesis due to different solubility, *e.g.* instead of crystallization from ethylacetate some ligands had to be precipitated with hexane from an ethylacetate solution. In later experiments accidentally 2.9 equiv. instead of 2.3 equiv. of KOH were applied. This led surprisingly to a much better quality of the crude box product **5b** without increasing the yield.

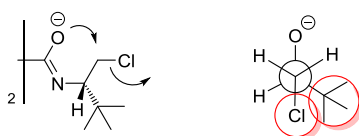


Yields over three steps (yields in brackets refer to the last step of the oxazoline synthesis).

Scheme 5-2. Product scope of prepared box-ligands.

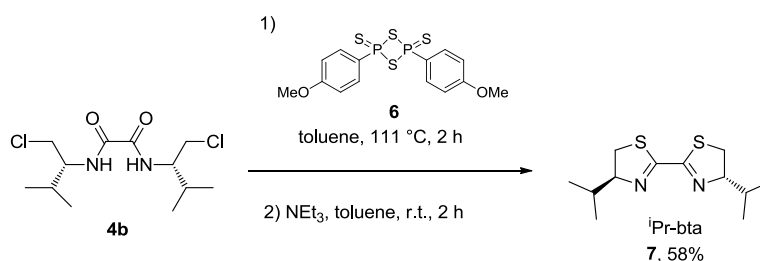
As depicted in Scheme 5-2, the total yields of the different box structures with values of 40% to 80% are relatively good. The only exception was found for ¹Bu-box (**5c**), which only gave a total yield of 23%. The yield in brackets refer to the oxazoline ring closure only and show that this low value is caused by this last step of the synthesis, which gave only a poor yield of 36%. This can be explained by

the unusual high steric hindrance of the *tert*-butyl group, which can be seen nicely in the corresponding Newman projection of the nucleophilic attack during the ring closure, as illustrated in Scheme 5-3. The carbonyl oxygen and the chlorine leaving group have to occupy an antiperiplanar positioning in order to go through an S_N2 mechanism. Consequently, the *tert*-butyl residue has to occupy a position gauche to the chlorine causing unfavorable steric interactions between these two substituents.



Scheme 5-3. Nucleophilic attack and corresponding Newman projection in the oxazoline ring closure of ^tBu-box **5c**.

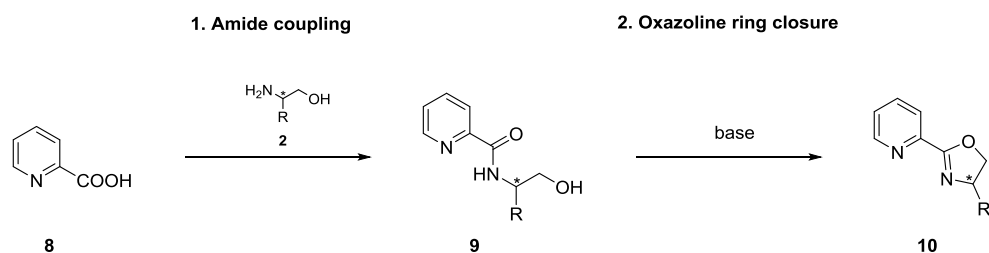
In addition to the box ligands also an analogous 2,2'-bithiazoline (bta) was prepared. In comparison to oxygen, sulfur is larger and less electronegative, which will have an effect on the electronic properties of the ligand. To date, several strategies for the preparation of thiazolines were reported.^[32, 49, 234-235] Most convenient for this project was a method, which allowed for the introduction of sulfur into the bis- β -chloroxalamide **4b**, reported by Nishio.^[49] As sulfinating reagent served Lawesson's reagent (**6**) which was simply mixed with the β -chloroamide **4b** in boiling toluene. Addition of base induced the ring closure as usual and the desired bta ligand **7** was obtained in 58% yield as pure substance.



Scheme 5-4. Preparation of ⁱPr-bta (**7b**) by use of Lawesson's reagent (**6**).

5.2 Pyridyloxazolines

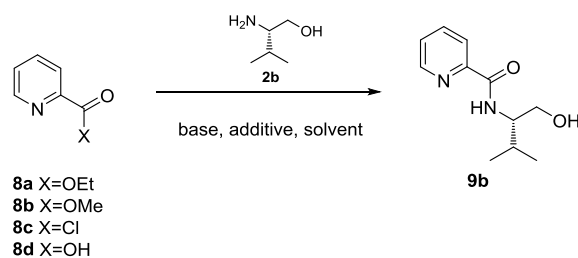
As introduced in chapter 2.1, the synthesis of pyrox and related ligands involves two general steps. Firstly the amide coupling of a picolinic acid or derivative **8** with the desired aminol **2** and secondly the oxazoline ring closure (Scheme 5-5).



Scheme 5-5. Synthesis of pyrox compounds.

The synthesis for pyrox and related ligands was optimized for one of their simplest representatives, ⁱPr-pyrox (**10b**). The optimized reaction conditions were later directly transferred to the other analogues.

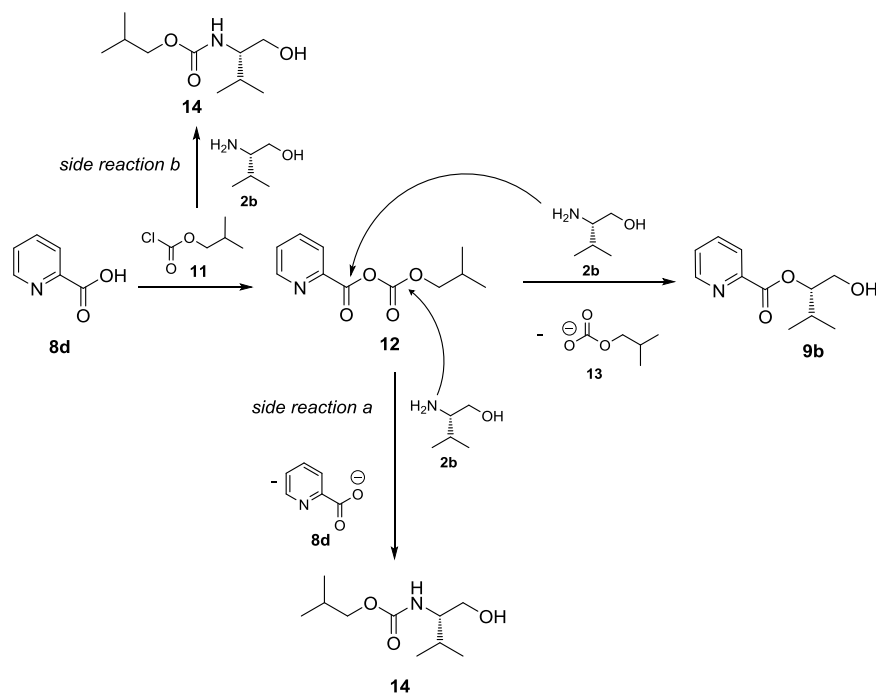
At the beginning, the amide coupling of picolinic acid (**8**) was investigated (Table 5-1). In first attempts, aminolysis of methyl and ethyl picolinate (**8a** and **8b**) (Table 5-1, entries 1 and 2) similar to the conditions used for the preparation of bisoxalamides **3** (cf. Scheme 5-1) was tried and TLC analysis during the reaction indicated incomplete product formation in both cases. However, the substitution of methanolate went on slightly more effectively. Unlike the bisoxalamides **3**, the product did not precipitate from the reaction mixture. Thus, the crude product had to be purified by column chromatography which went well in case of the ethyl picolinate (**8a**) but did not lead to success in case of its methyl analogue because the retention time of the product **9b** was nearly identical to that one of the starting material **8b**. The product from the reaction of ethylpicolinate (**8a**) was obtained very purely in a yield of 62%. However, a method using commercially available carboxylic acids and preferably without purification by column chromatography, would be the method of choice for the preparation of a whole ligand collection. Therefore the picolinic acid was also activated as acid chloride (Table 5-1, entry 3) as well as asymmetric anhydride^[22] **12** (Table 5-1, entry 4). The product obtained by the reaction of the acid chloride was strongly impure as analysis by ¹H-NMR spectroscopy showed. The product obtained by the reaction with the asymmetric anhydride **12** was isolated in 10% yield only. At last, the classical coupling reagents 3-(ethyliminomethylideneamino)-*N,N*-dimethyl-propan-1-amine (EDCI) and *N*-hydroxybenzotriazol (HOBt) were tested since results from other projects had shown that EDCI in combination with HOBt leads in some cases to more impure products than the use of EDCI alone does. Thus, one test reaction was carried out with EDCI only (Table 5-1, entry 6) and another one with the combination of both reagents (Table 5-1, entry 5). However, avoiding HOBt was not beneficial and many impurities were detected in the ¹H-NMR spectrum. Satisfyingly, the combination of EDCI and HOBt led after aqueous extraction to a satisfyingly pure compound as determined in the ¹H-NMR spectrum. Purification by column chromatography on silica gel was possible without high losses of product, but not necessary for the following ring closure as shown by subsequent experiments. Consequently, the conditions from Table 5-1 (entry 5) were chosen for further amide couplings.

Table 5-1. Optimization of amide coupling with picolinic acid derivatives.

Entry	Substrate	Base	Additive	Solvent	Result ^e
1 ^{a,c}	8a	-	-	toluene	62% ^f
2 ^{a,c}	8b	-	-	DCE	No isolation (¹ H-NMR impure, 9b detected on TLC besides 2 other substances)
3 ^{a,c}	8c	NEt ₃	-	DCE	No isolation (¹ H-NMR strongly impure, 9b detected on TLC besides 4 other substances)
4 ^{a,d}	8d	NMM	IBCF (11)	toluene	10% ^f
5 ^{b,d}	8d	NMM	EDCI, HOBT	DCM	100% ^g
6 ^{b,d}	8d	NMM	EDCI	DCM	No isolation (¹ H-NMR strongly impure, 9b detected on TLC)

^a**8** (1.0 equiv.), (*R*)-valinol (**2b**) (1.0 equiv.), base = NEt₃ (2.3 equiv.), NMM (1.4). ^b**8** (1.0 equiv.) EDCI (1.1 equiv.), HOBT (1.1 equiv.), NMM (1.3 equiv.), (*R*)-valinol (**2b**) (1.2 equiv.). ^c heated under reflux. ^d -5°C to r.t. ^e All results were also confirmed by HRMS. ^f Isolated yield after column chromatography (SiO₂) ^g Crude product.

However, the surprisingly low yield obtained by reaction of the asymmetric anhydride **12** was subject of further investigations. Since the formed asymmetric anhydride **12** (Scheme 5-6) bears two electrophilic carbonyl positions, both attacks are conceivable. The desired attack on the carbonyl position next to the pyridine ring is sterically and electronically favored and forms *iso*-butylcarbonate (**13**) as leaving group whereas the attack on the carbonate carbon results in the formation of the stable picolinate leaving group (**8d**) (*side reaction a*). In addition, also the possibility of a direct reaction of IBCF (**11**) with the primary amine of the aminol **2b** should be considered (*side reaction b*) and avoided giving the reaction between substrate **8d** and IBCF enough time to proceed quantitatively before adding the aminol **2**. Both side reactions are leading to the same, unreactive, carbamate **14**.



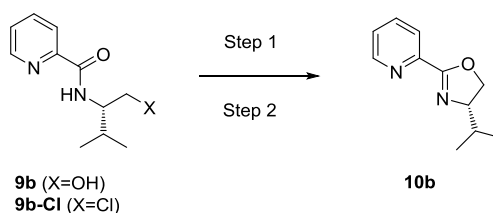
Scheme 5-6. Amide coupling with IBCF (**11**) as coupling reagent.

Having these side reactions in mind, the reaction was observed in detail by TLC analysis. Within one hour, the substrate was consumed completely and transferred into the asymmetric anhydride **12** quantitatively. Subsequently, the aminol **2b** was added slowly and allowed to react with the anhydride **12** in the melting ice bath over a time period of two hours. TLC analysis of the resulting reaction mixture showed no residue of the anhydride **12** and two new spots. In previous experiments, one of them was identified as the product **9b**. After a small scale column chromatography, the $^1\text{H-NMR}$ spectrum of the first fraction showed no aromatic signals but typical ones for IBCF (**11**). However a clear identification of the substance failed due to impurities and just a small isolated amount of the corresponding solid. As expected, the other fraction contained the product **9b** that was also identified in the corresponding $^1\text{H-NMR}$ spectrum. In conclusion, it was shown that this reaction did not lead to a quantitative yield of the coupling product but to a mixture of different compounds.

The next challenge was the oxazoline ring closure. Therefore, the hydroxyl group was activated as chloride or tosylate and a suitable base had to be found (Table 5-2). First, the conditions known from literature^[22] were applied on the β -hydroxylamide **9b**. As reported in the respective publication, the ring closure should be possible by simple heating of the NEt_3 containing reaction mixture. However, these conditions resulted in a strongly impure product (entry 1). Without heating, however, no product was formed (Table 5-2, entry 4). Application of the conditions developed for the bisoxazoline synthesis also led to a strongly impure product (Table 5-2, entry 5). Here, the hydroxyl group was transformed into a chloride first and then heated in the presence of KOH to induce the ring closure. The best result was achieved when both methods were combined (Table 5-2, entry 2). The tosyl group was introduced

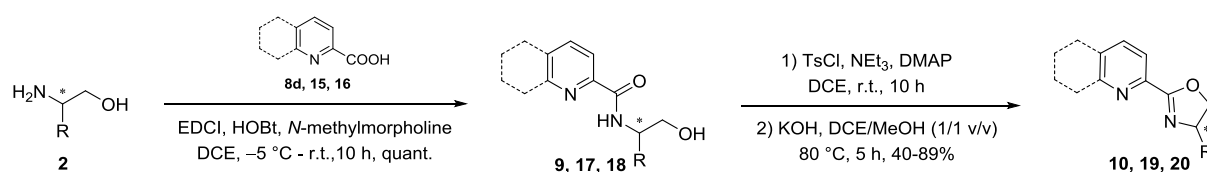
at room temperature in DCE with DMAP as catalyst and after a few hours a solution of KOH in methanol was added and the mixture heated under reflux for some hours. Comparison with entry 3, where THF was used as solvent for the ring closure, shows, that not only the strong base is crucial for this step, but also the presence of a protic polar solvent. The combined optimized reaction conditions for both steps of pyrox formation are illustrated in Scheme 5-7.

Table 5-2. Optimization of pyrox ring closure.



Entry	Substrate	Conditions Step 1	Conditions Step 2	Relative Quality of Product ^c
1 ^a	9b	TsCl, NEt ₃ , DMAP, DCE, rt (15 h), 80 °C(10 h)	-	Strongly impure
2 ^a	9b	TsCl, NEt ₃ , DMAP, DCE, rt (20 h)	KOH, MeOH 80 °C (21 h)	Good, with few impurities
3 ^a	9b	TsCl, NEt ₃ , DMAP, DCE, rt (20 h)	KOH, THF 80 °C (21 h)	Strongly impure
4 ^a	9b	TsCl, NEt ₃ , DMAP, DCE, rt (20 h)	-	No product
5	9b-Cl ^b	-	KOH, MeOH 80 °C (3 h)	Strongly impure
6	9b	TsCl, NEt ₃ , DMAP, DCM, rt (20 h)	KO ^t Bu, MeOH rt (48 h)	Strongly impure

^a Weak basic aqueous workup. ^b Prepared by treatment of the alcohol **9b** with SOCl₂ under reflux over 3 h. ^c Determined by ¹H-NMR analysis.



Scheme 5-7. Optimized reaction conditions for pyrox structure formation.

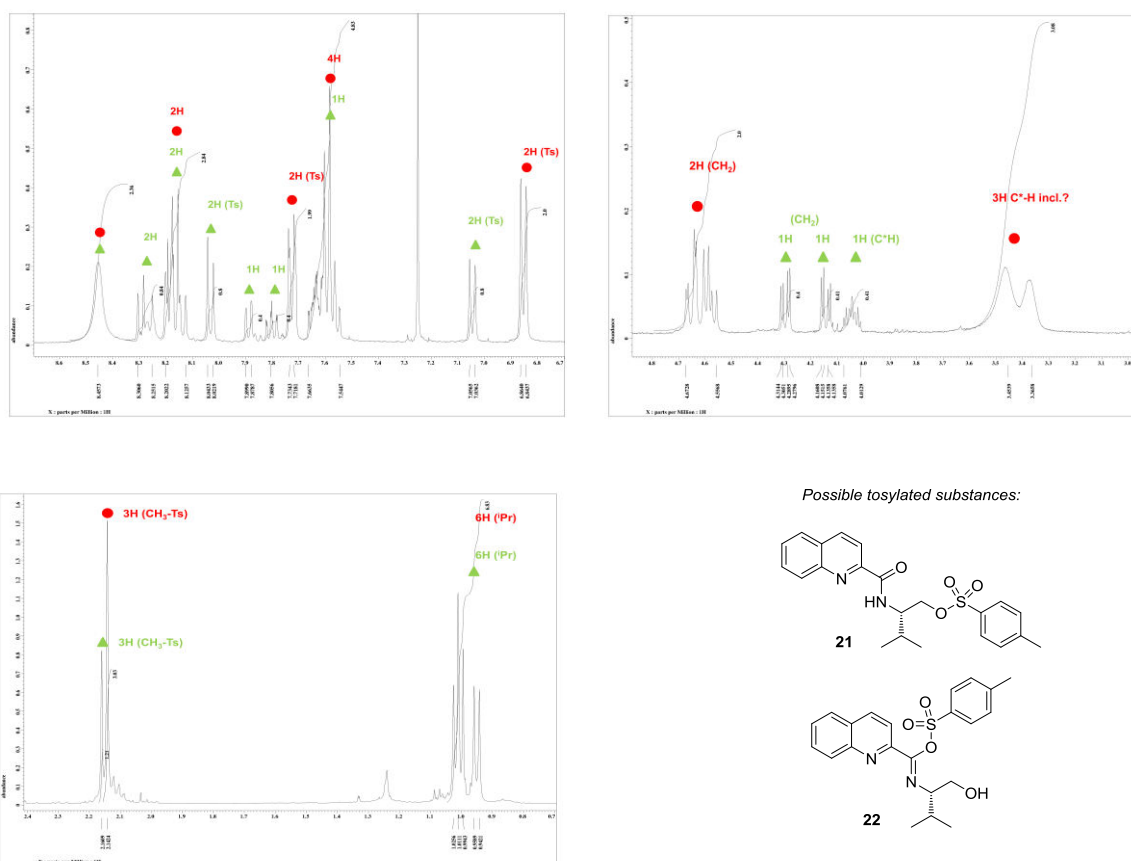
After successful oxazoline ring closure and aqueous workup, the crude product still contained too many impurities such as starting material and tosyl containing substances. Thus a column chromatography was necessary. However, this turned out to be challenging because previous experiments had shown that the box-type ligands were quantitatively hydrolyzed on silica gel, so only flash chromatography of max. 15 min over a short column of basic alox turned out to be suitable for the purification of box compounds. The best solvent combination for the mobile phase was hexane/ethylacetate while the combination of pentane/Et₂O led to less satisfying separation of fractions. The crude products were most efficiently brought onto the column as solution in a small amount of DCM and subsequent flushing with pure hexane. Prior absorption of the crude product on alox or sea sand led to decomposition of the product.

In order to get more insight into the mechanism of oxazoline ring closure by *in situ* tosylation, attempts to isolate and identify the tosylated structure were undertaken. Pure quinaldic acid valinol amide **18b** was treated under the optimized conditions of the first step of the oxazoline ring closure (Scheme 5-7) **for a few hours. After aqueous workup, the reaction mixture was purified by column chromatography to yield a mixture of two different tosylated compounds in one fraction, as indicated by TLC and confirmed by ¹H-NMR analysis.**

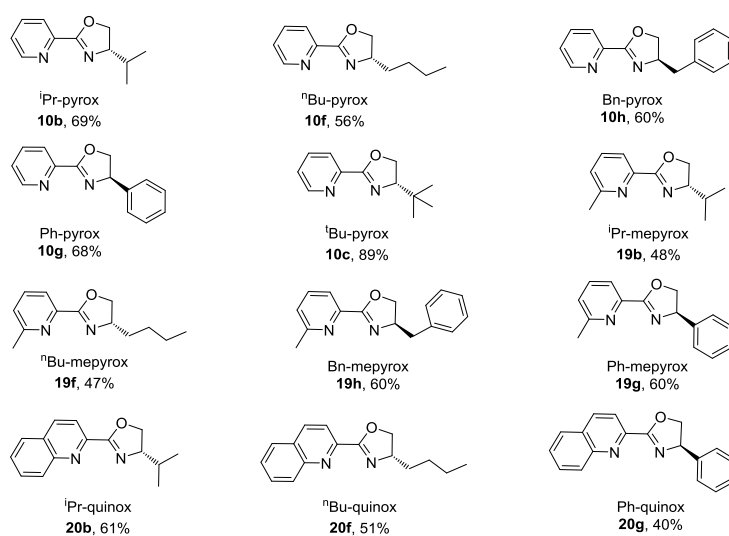
Scheme 5-8 shows a detailed view of the proton spectrum. It shows clearly two species of a tosylated substance for which a ratio of 7:3 was determined by integration of the two tosyl doublets at 6.85 ppm and 7.04 ppm. In the aromatic region, for both substances all proton signals can be identified plus a broad singlet at 8.46 ppm which might correspond to the exchangeable protons. The area between 3 ppm and 5 ppm shows a typical signal set for the asymmetric proton and the methylene group next to it for at least one of the two compounds. For the other compound, the methylene group was identified, but the methane C-H signal could not be assigned unambiguously. It is possibly located in the broad doublet at 3.37 ppm. Both *iso*-propyl groups were also identified in the aliphatic region and the methyl singlets corresponding to the tosyl groups were found. Also, their integrals are in nice agreement to their corresponding aromatic signals. Both protons on the tertiary carbons of the *iso*-propyl groups could not be identified.

In contrary to the bis- β -chloroxalamide **4b** from which the bisoxazolines **5** were prepared, the formation of an oxazoline by *in situ* formation of a tosylate on a β -hydroxyl-picolinylamide derivative might go *via* two different tosylated intermediates.

The optimized reaction conditions were successfully applied to eleven other structures (Scheme 5-9).



Scheme 5-8. Analysis of tosylated compounds after the first step of oxazoline formation.



Scheme 5-9. Prepared pyrox (**10**), mepyrox (**19**) and quinox (**20**) ligands. Yields over two steps.

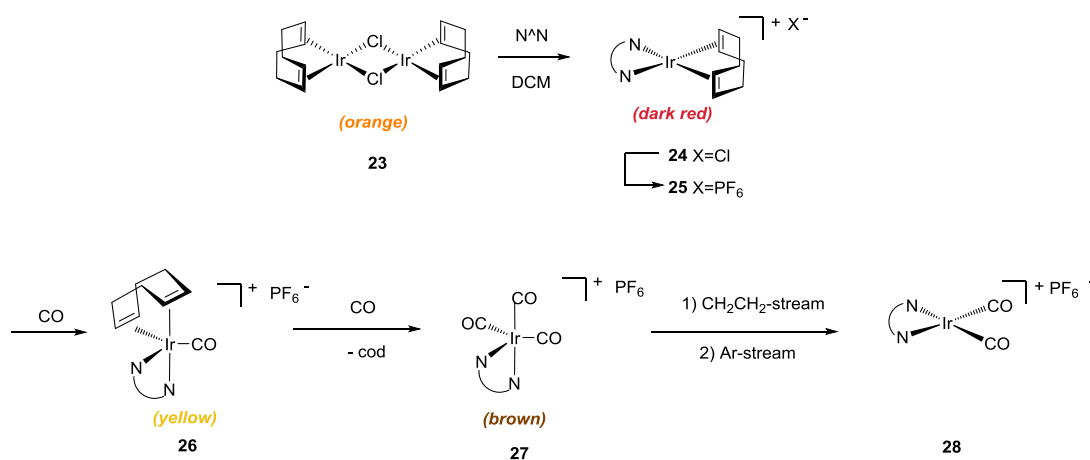
6 Iridium and Ruthenium Complexes

Contributions: Experimental help by Gisa Meissner, Patrick Kuhrt and Silke Plachetta (iridium complexes) and Cindy Glohr (ruthenium complexes) under my supervision.

DFT calculations and special IR-measurements (cryo IR and IR from solution) were performed by Dr. Jacek A. Kozuch (Technische Universität Berlin).

6.1 Iridium(I) Carbonyl Complexes

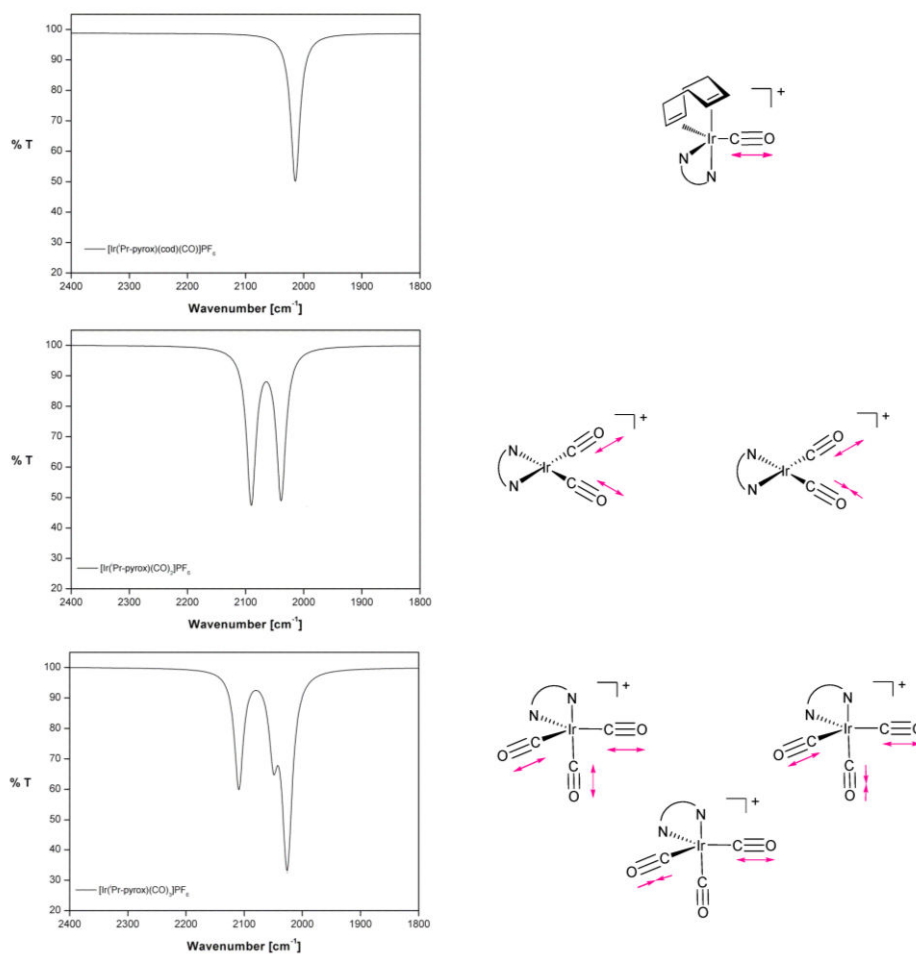
The synthesis of the iridium(I) carbonyl complexes was developed based on the synthesis reported by Mestroni (Scheme 6-1, cf. chapter 3.1.4), who prepared carbonyl complexes from the chloro bridged iridium dimer $[\text{Ir}(\text{cod})\text{Cl}]_2$ (**23**) which was brought to reaction with a bipyridine or phenanthroline ligand.^[7-8] In the procedure of Mestroni, the chloride anion of complex **24** was exchanged for the non-coordinating PF_6^- to give complex **25** and coordination of CO at atmospheric pressure led first to the pentacoordinated, not isolated complex **26**. From this complex, the tricarbonyl complex **27** was formed immediately by loss of the cod ligand and addition of two further CO molecules.



Scheme 6-1. Formation of iridium(I) carbonyl complexes as reported by the Mestroni group.^[7-8]

For a better understanding of the spectra of different carbonyl species, in this work theoretical IR spectra were predicted using density functional theory (DFT) calculations. Geometry optimization and vibrational analysis was performed on the BP86^[236-237] level of theory to avoid the use of scaling factors using Gaussian 09. For iridium, the LanL2DZ^[238] and for all other atoms the 6-31g* basis set was used.

The typical predicted spectra for mono-, di- and tricarbonyl complexes are depicted in Scheme 6-2. Due to the strong coupling of the C-O oscillators^[239] one does not observe single vibrations for each carbonyl ligand, but collective coupled vibrations of different symmetry. For a dicarbonyl complex, for instance, a symmetric and an asymmetric C-O vibration is obtained where the carbonyl ligands oscillate in-phase or out-of-phase, respectively. For the tricarbonyl complex two of three expected bands are very close to each other so that it is possible that they form one broad band in the experimental spectrum.

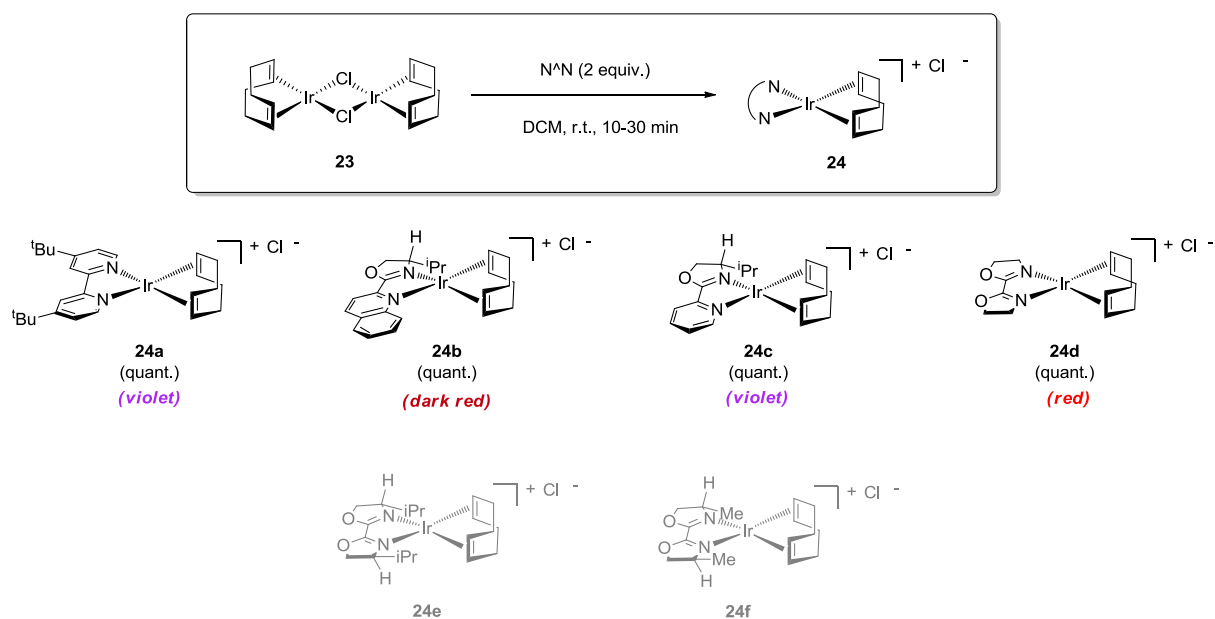


Scheme 6-2. Typical shapes of carbonyl complex IR spectra. The depicted spectra were calculated for the example of $[\text{Ir}(\text{Pr-pyrox})(\text{CO})_n]^+$.

6.1.1 Cyclooctadiene Iridium(I) Cl^- and PF_6^- Complexes

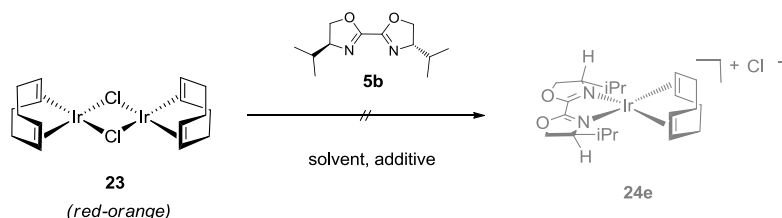
According to the synthesis of Mestroni and co-workers, in this work the dimeric iridium precursor **24** was mixed with two equivalents of the $\text{N}^{\wedge}\text{N}$ ligand in DCM at room temperature and resulted in the corresponding cod chloro complex $[\text{Ir}(\text{N}^{\wedge}\text{N})(\text{cod})]\text{Cl}$ (**24**).^[7-8] The reactions were conducted in

deuterated DCM and the purity of the reaction product was assessed by $^1\text{H-NMR}$ measurements directly from the reaction mixture.



Scheme 6-3. Prepared cod chloride complexes **24**. The preparation of the sterically more hindered complexes **24e** and **24f** failed.

Table 6-1. Screening of reaction condition for the formation of $[\text{Ir}(\text{iPr-box})(\text{cod})]\text{Cl}$ (**24e**).^a



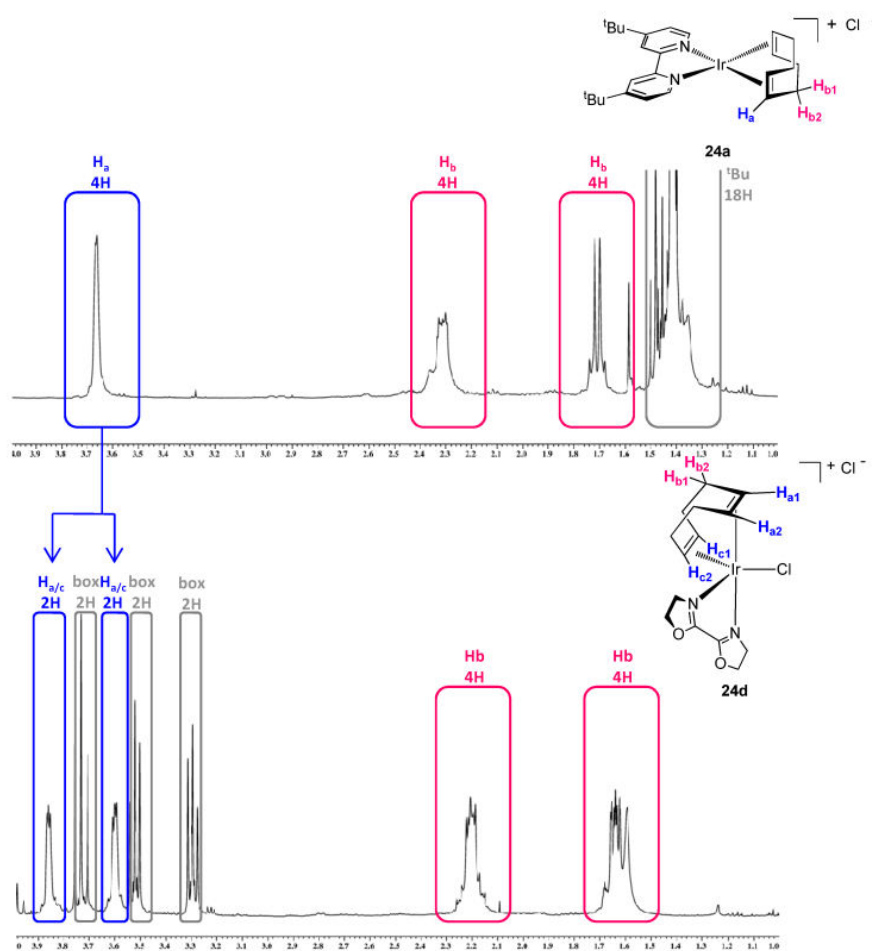
Entry	Solvent	Temp.	Additiv ^b	Time	Color	Color after additional 4 h (r.t.)
1	DCM-d ₂	r. t.	-	10 min	Orange	Orange
2	DCM-d ₂	r. t.	AgBF ₄	20 min	Orange	Orange (+ grey solid)
3	DCE	80 °C	-	5 h	Orange	Orange (in DCM-d ₂) ^c
4	Acetone-d ₆	r. t.	-	4 h	Orange	Orange
5	Acetone-d ₆	r. t.	AgBF ₄	2 d	Orange	Yellow-orange (+ grey solid)

^aReactions were carried out under an argon atmosphere using $[\text{Ir}(\text{cod})\text{Cl}]_2$ (**23**) (10 mg, 1 equiv.) and iPr-box (**5b**) (8.4 mg, 2.5 equiv.) in 5 mL solvent. The crude reaction mixtures were analyzed by $^1\text{H-NMR}$ spectroscopy, which resulted for each test reaction in a strongly impure reaction mixture. ^bAdded subsequently to ligand addition. ^cAfter 5 h the DCE was removed in vacuum and the solid residue was dissolved in DCM-d₂ to measure a $^1\text{H-NMR}$ spectrum.

The bipyridine, quinox, pyrox and H-box complexes **24a**, **24b**, **24c** and **24d** were formed straightforwardly. However, the preparation of the analogues complexes with the sterically more demanding ligands iPr-box (**5b**) and Me-box (**5a**) failed completely under the given reaction

conditions. As listed in Table 6-1, attempts to optimize the reaction conditions by variation of solvent, temperature, reaction time and the addition of a silver salt to precipitate the chloride as silver chloride, were not successful as analyzed by $^1\text{H-NMR}$ spectroscopy.

The successfully prepared chloride complexes **24** with oxazoline ligands (Scheme 6-3) exhibited in the $^1\text{H-NMR}$ spectrum a splitting of the olefinic protons of cod into two sets with different chemical shifts (Scheme 6-4). This observation was not made for the bipyridine complex **24a**, which $^1\text{H-NMR}$ spectrum showed only one signal for these protons. Upon coordination of the chloride to a bisoxazoline complex, this complex loses its C_{2v} symmetry resulting in a trigonal bipyramide (complex **24d**). Due to Berry pseudorotation of the trigonal bipyramidal structure, the atoms H_{a1} and H_{c2} or H_{a2} and H_{c1} , respectively, become equivalent. This results in two different signals for these protons in the $^1\text{H-NMR}$ spectrum.



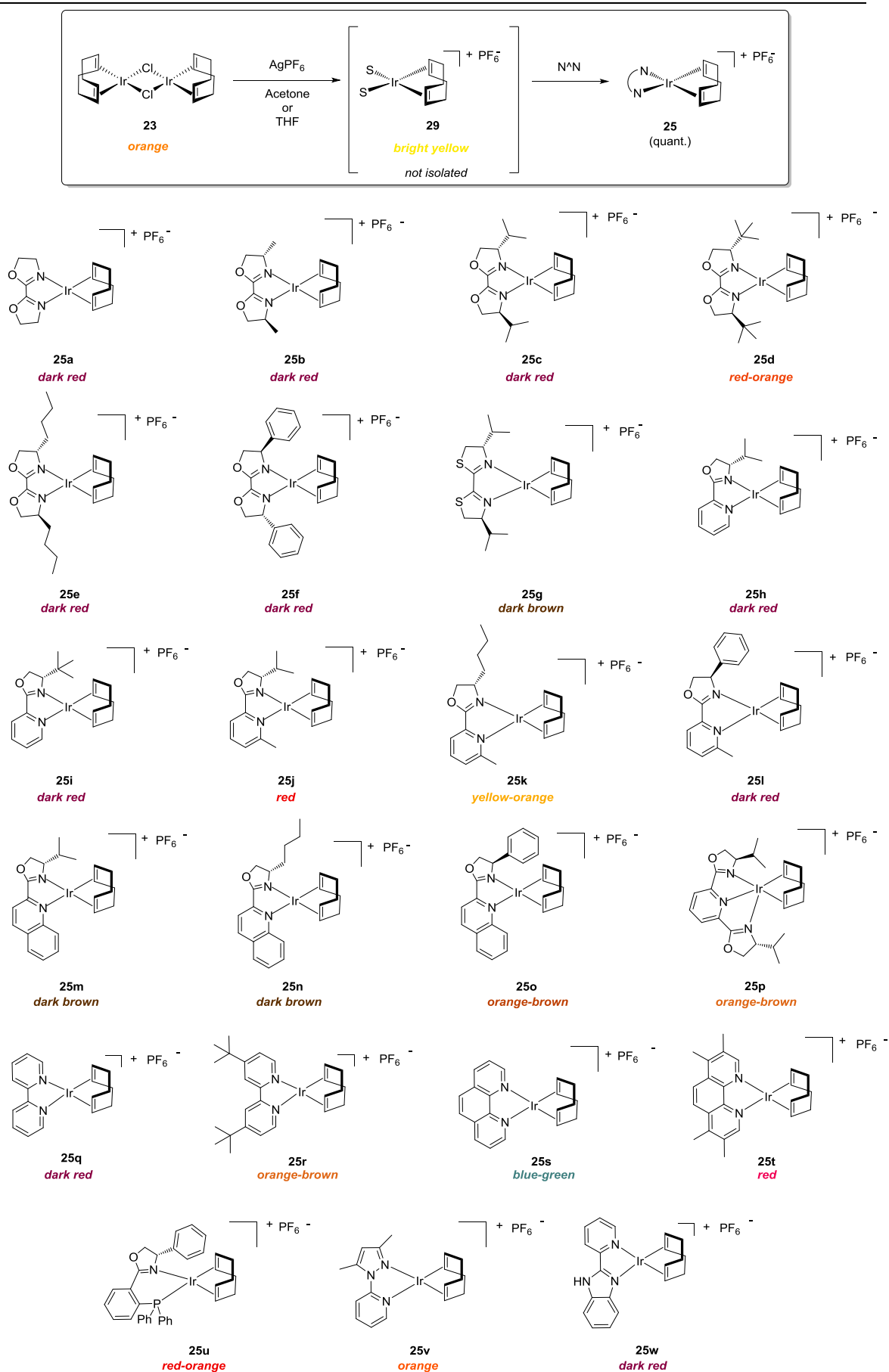
Scheme 6-4. $^1\text{H-NMR}$ spectra of complexes **24a** and **24d**, shown is the area from 1.0-4.0 ppm. The olefinic protons of cod in complex **24d** split up upon coordination of the chloride counteranion. The coordination geometry cannot be assigned by NMR spectroscopy and both possible structures are illustrated and assigned as complexes **24d(1)** and **24d(2)**. Depending on the true structure either both cod-double bonds (**24d(2)**) or their protons itself (**24d(1)**) become chemically inequivalent.

This observation might be attributed to a strong coordination of the bipyridine ligand, thus weakening the other ligands which results an ionic character of the chloride. In turn, the box ligand is less tightly bound resulting in longer ligand-metal bonds which leaves more space around the iridium for a

coordination of the chloride. However, this theory is not yet proven since no crystal structures of structurally related bisoxazoline and bipyridine complexes with iridium as central metal are reported. The only available data of comparable crystal structures was found for Rh(III) complexes of the type $[\text{Rh}(\text{N}^{\wedge}\text{N})_2(\text{Cl})_2]^+$ bearing either bipyridines^[240] or bisoxazolines^[17]. These complexes show Rh-N(bpy) bond lengths of 2.02 Å and Rh-N(box) bond lengths of 2.09 Å. Even though the difference is not very large, it supports the theory that box, as weaker ligand, has a longer bond length to iridium. In substituted box ligands such as Me-box (**5a**), two unfavorable effects for a successful coordination were combined; the weak coordinating character of the box structures and in addition steric hindrance from the substituent. Consequently, no chloride cod complexes **24** were formed with these ligands.

To facilitate the coordination of the box ligands, it was decided to replace the coordinating chloride by a less coordinating anion prior to oxazoline ligand introduction. PF_6^- was chosen as counter anion for the cationic complexes. The new synthesis strategy entailed the removal of the chlorides from the precursor complex $[\text{Ir}(\text{cod})\text{Cl}]_2$ (**23**) as insoluble silver chloride by addition of the silver salt of the new anion (Scheme 6-5). To stabilize the resulting, coordinatively unsaturated iridium complex **29**, the well coordinating solvent acetone was used. Later, also THF or acetonitrile were applied successfully as solvents in this reaction, in which the precursor complex showed even higher solubility.

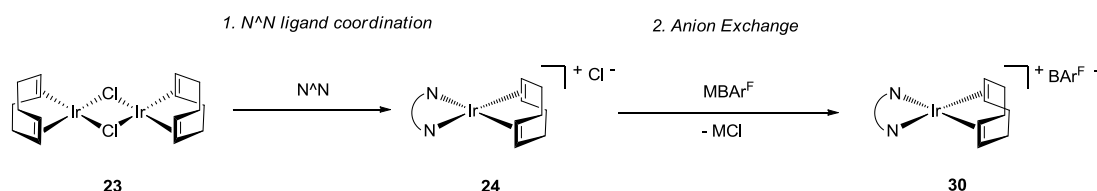
In first reactions, the silver chloride precipitate was not removed from the solution that contained the solvent stabilized complex **29** before the ligand was added. The resulting complex **25** remained in solution while the silver chloride was filtered of. A few complexes were successfully prepared by this strategy and analyzed by $^1\text{H-NMR}$ spectroscopy, but the results were not reproducible, presumably because of interference with the silver ions. Consequently, in following syntheses the silver salt was removed from the reaction mixture prior to coordination of the oxazoline or bipyridine ligand. Since the silver chloride precipitated as very fine powder, filtration was not sufficient. Therefore, the solutions were left standing without stirring for 1-2 hours, so that the solid collected at the bottom allowing decantation of the complex containing bright yellow-orange solution. The cod PF_6^- complexes were prepared as depicted in Scheme 6-5 and applied for the formation of carbonyl complexes (cf. chapter 6.1.3).


 Scheme 6-5. Prepared cod complexes 25 with PF₆⁻ as counteranion.

6.1.2 Cyclooctadiene Iridium(I) BAr^{F^-} Complexes

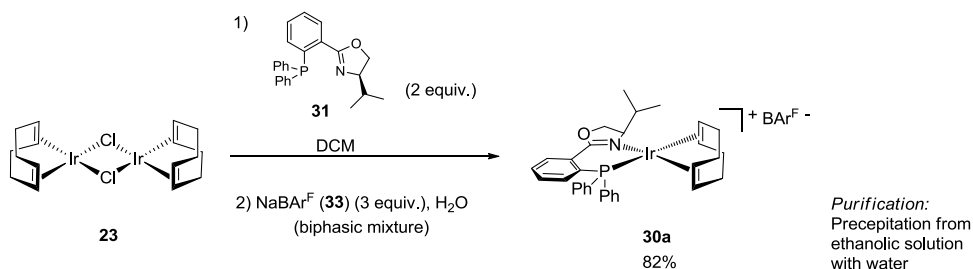
In order to assess the catalytic quality of the oxazoline-type $\text{N}^{\wedge}\text{N}$ ligands in homogeneous catalytic hydrogenations (cf. chapter 4.3), first the synthesis of cationic iridium cod complexes combined with a BAr^{F^-} counteranion was required. These $[\text{Ir}(\text{N}^{\wedge}\text{N})(\text{cod})]\text{BAr}^{\text{F}}$ (**30**) complexes were chosen as precatalysts for hydrogenation, because their phox analogues, in which the chiral information is conferred by the oxazoline moiety, are known to be very active in these reactions. Therefore comparisons to the established catalysts should be easily possible.

The synthesis of the cod complexes starts with the dimeric $[\text{Ir}(\text{cod})\text{Cl}]_2$ (**23**) precursor and a bidentate $\text{N}^{\wedge}\text{N}$ ligand, resulting in the corresponding chloro complex $[\text{Ir}(\text{N}^{\wedge}\text{N})(\text{cod})]\text{Cl}$ (**24**). For the desired BAr^{F^-} complex **30**, only one anion exchange is necessary (Scheme 6-6).



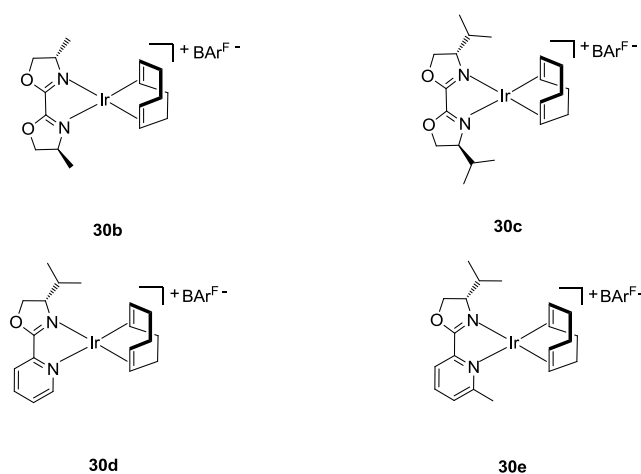
Scheme 6-6. Synthesis of target compound $[\text{Ir}(\text{N}^{\wedge}\text{N})(\text{cod})]\text{BAr}^{\text{F}}$ (**30**).

As already discussed in chapter 6.1.1, the first step of the synthesis, the introduction of the N,N -ligand, proceeded as expected. For the crucial anion exchange, a procedure of the Pfaltz group gave no satisfying results. In this procedure the anion exchange is described in a biphasic mixture of DCM and water with the sodium salt of BAr^{F^-} .^[99] The resulting NaCl dissolves in the aqueous phase, while the BAr^{F^-} complex **30** can be isolated from the organic phase. After evaporation of the organic solvent, the complex can be redissolved in ethanol and obtained as pure product by precipitation with water. In order to test the applicability of the procedure, the anion exchange was tested on one of the originally applied ligands from the Pfaltz group, the phox ligand ^iPr -phox (**31**) (Scheme 6-7). For this phox complex **30a** the procedure gave the pure complex in 82% yield



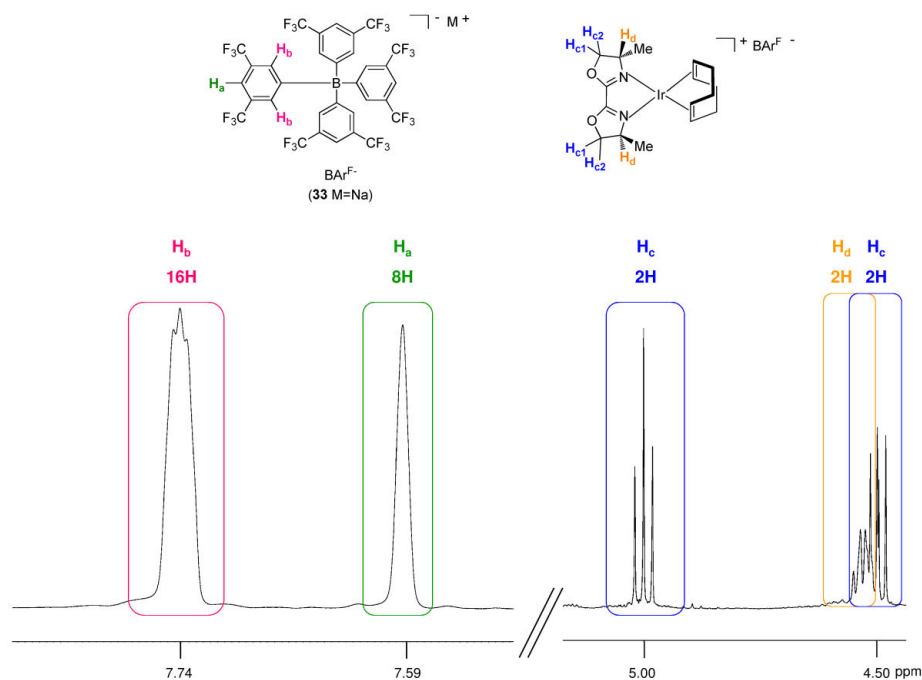
Scheme 6-7. Preparation of reference complex $[\text{Ir}(\text{phox})(\text{cod})]\text{BAr}^{\text{F}}$ (**30a**) by anion exchange from the corresponding chloro complex.

When the procedure was transferred to the anion exchange of $[\text{Ir}(\text{}^i\text{Pr-pyrox})(\text{cod})]\text{Cl}$ (**24b**), the purification step failed due to too high solubility of the complex. Therefore, next synthesis attempts were performed without purification, stopping after evaporation of the organic solvent. Consequently, NaBAR^{F} had to be added in stoichiometric amounts. Four complexes, **30b**, **30c**, **30d** and **30e** were obtained as red-brown or black solids by this method (Scheme 6-8). The $^1\text{H-NMR}$ spectra of each of them showed no free ligand anymore and the typical signals of the $\text{BAR}^{\text{F}-}$ anion in the aromatic region were present. However, the $\text{BAR}^{\text{F}-}$ signals integrated twice as high as expected. The methylene protons on the box moiety of the ligand and the $\text{BAR}^{\text{F}-}$ protons are supposed to have an integral ratio of 1:1 (H_{c1} , $\text{H}_{\text{c2}}:\text{H}_{\text{a}}$) and 1:2 (H_{c1} , $\text{H}_{\text{c2}}:\text{H}_{\text{b}}$) respectively (Scheme 6-9). Actually found for all of the prepared complexes were ratios of 1:2 and 1:4.

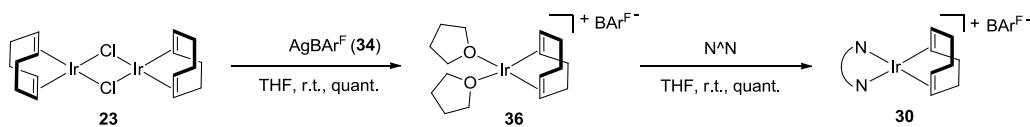


Scheme 6-8. Synthesized iridium cod $\text{BAR}^{\text{F}-}$ complexes **30**.

Since the analysis of the $\text{BAR}^{\text{F}-}$ complexes **30**, which were obtained by anion exchange of the corresponding chloro complexes, did not lead to satisfying results, AgBAR^{F} (**34**) was prepared from AgNO_3 (**35**) and NaBAR^{F} (**33**) following an optimized procedure by Buschmann and Miller^[241] and used in a similar approach as already developed for analogue PF_6^- complexes (cf. chapter 6.1.1). The optimized synthesis route is depicted in Scheme 6-10 and starts with the dimeric iridium precursor **23**, which was dissolved in the well coordinating solvent THF. Addition of the silver salt caused an immediate color change from red-orange to bright yellow while a colorless solid precipitated from the solution. The solid could not be removed by filtration because the particles formed were too small. Leaving the suspension standing over night resulted in a clear solution of the solvent stabilized complex **36** which would be decanted from the solid. Further extraction of the solid with more solvent enabled the preparation of a well-defined stock solution that was stable enough for one day. From such a stock solution, five to ten different $\text{BAR}^{\text{F}-}$ complexes **30** were prepared by addition of the respective ligand. Evaporation of the solvent led to the pure product complexes **30** that now showed expected integrals in the respective $^1\text{H-NMR}$ spectra. The complexes obtained by this method are shown in Scheme 6-11.

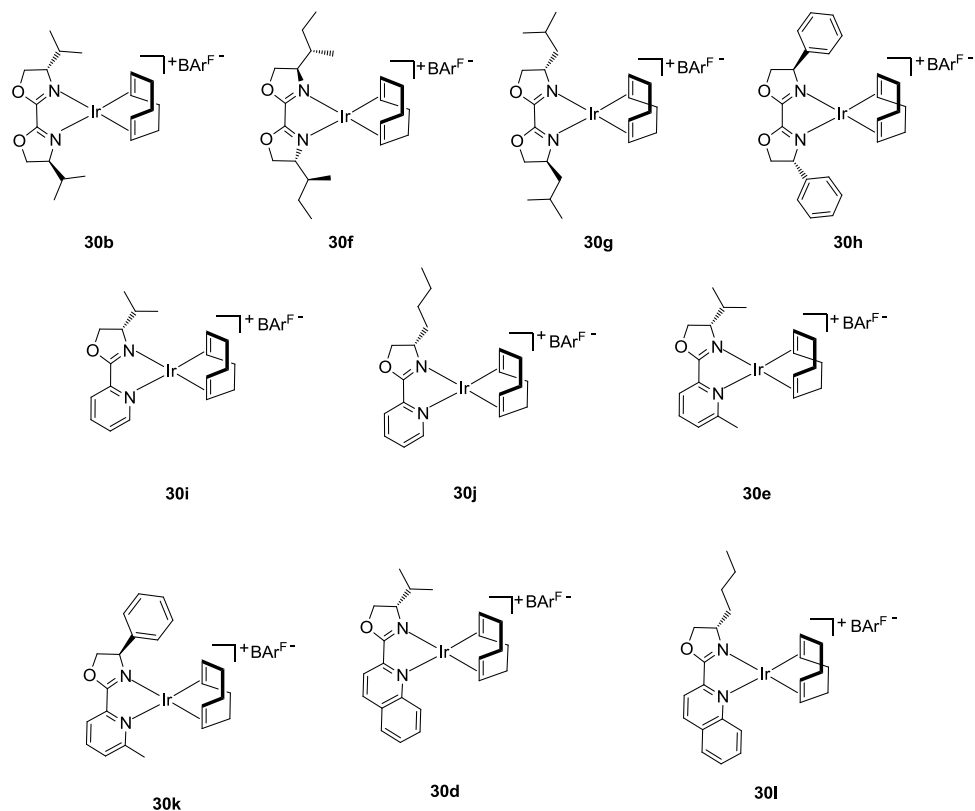


Scheme 6-9. Proton NMR of **30b**: Relevant areas of the aromatic and oxazoline proton-signals are shown. The expected relative intensity of H_{c1} , H_{c2} : H_a is 1:1. Here the ratio is 1:2, which was always observed for complexes prepared by subsequent anion exchange.

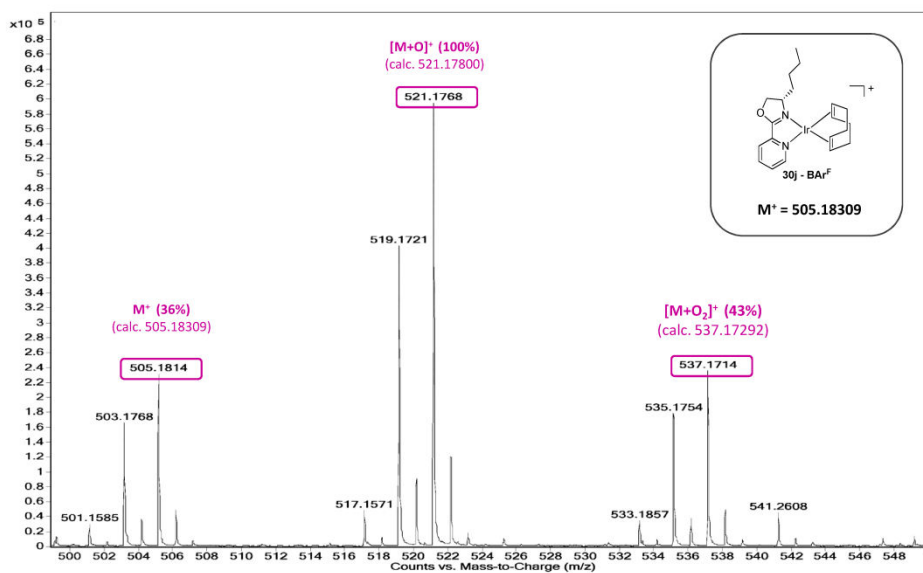


Scheme 6-10. Optimized synthesis of iridium cod $BArF^-$ complexes **30**.

The complexes behaved unexpectedly during ESI-MS analysis since they were usually detected as their $[M+O]^+$ adducts, showing a high tendency to oxidize under the given analysis conditions (Scheme 6-12). In most cases also a much smaller signal for the corresponding $[M+O_2]^+$ adduct was found, supporting an oxidation mechanism *via* dioxygen addition. The signal of the pure cation M^+ could only be detected in low intensity, if it was present at all. In the example Scheme 6-12, the signal of the pure cation M^+ is with a relative intensity of 36% unusually high.



Scheme 6-11. Synthesized iridium cod BArF^- complexes **30** for application as precatalysts in catalytic hydrogenation.



Scheme 6-12. Example of HRMS (ESI-MS) spectrum of the iridium cod BArF^- complex **30j** measured in DCM/MeCN at a fragmentor voltage of 200.0 V. Typical for these complexes is the main signal of the $[\text{M}+\text{O}]^+$ adduct and the corresponding $[\text{M}+\text{O}_2]^+$ adduct in lower intensity. In this example the signal of the pure cation M^+ is unusually high.

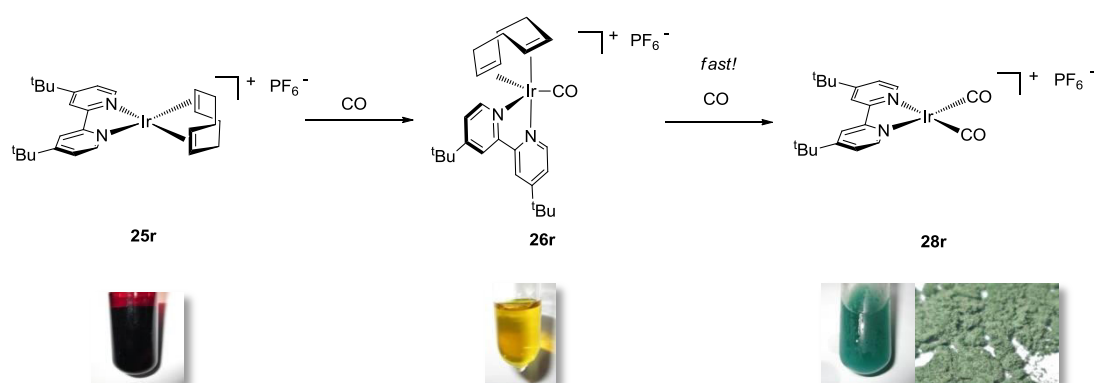
In summary, BAr^{F^-} oxazoline complexes **30** could not successfully be prepared by a late-stage anion exchange, as it was described for the analogue phox complexes. Comparison with the phox complex **30a** showed, that the box complexes were not suitable for the last purification step because they were too soluble. BAr^{F^-} oxazoline complexes **30** were quantitatively obtained after initial anion exchange by treating the dimeric iridium precursor $[\text{Ir}(\text{cod})\text{Cl}]_2$ (**23**) with $\text{AgBAr}^{\text{F}^-}$ (**34**) and subsequent oxazoline ligand introduction. Following this procedure, ten complexes were obtained as pure compounds, making the need for a purification step unnecessary. By ESI-MS spectrometry these complexes were usually detected as their $[\text{M}+\text{O}]^+$ adducts.

All complexes depicted in Scheme 6-11 were applied as precatalysts in catalytic hydrogenation which will be discussed in chapter 7.4.

6.1.3 Synthesis of Carbonyl Complexes

Carbonyl complexes were initially prepared as described by Mestroni and co-workers (cf. chapter 3.1.4). Therefore, the atmosphere in a reaction flask containing the cod precursor **25q** as solution in DCM, was fully exchanged for CO gas at atmospheric pressure. However, more convenient was the stoichiometric application of CO, which was developed as standard method. In this procedure, the CO gas was added *via* a syringe through a rubber septum into the argon atmosphere over the precursor solution. THF, acetone, acetonitrile and DMSO were tested for the carbonylation as well and proved to be suitable for this reaction. The complexes were best purified by precipitation from DCM or THF with hexane. The resulting solids or oils could be separated from the solution, which still contained free cod. Drying the solid residue in vacuum led to the pure carbonyl complexes. However, this procedure was not very well reproducible and led in many cases to unidentifiable compounds. The quality of the carbonyl complexes and their precursors appeared to be very sensitive to removal of solvent and exposure to air. Therefore the complexes prepared for the screening of their ν_{CO} absorption frequencies were kept in the same solvent from the beginning of the synthesis (Scheme 6-5) and the IR of the solid was measured directly by drying a drop of the reaction mixture on the ATR diamond.

As illustrated in Scheme 6-13 using the example of the bpy complex, the formation of the carbonyl complexes was easily observed by the change of color of the reaction mixture. The cod precursor **25** was always dark red or brown colored and addition of CO gas caused an immediate color change to bright yellow, which can be attributed to the formation of the penta-coordinated monocarbonyl complex **26**. After some minutes, when the dicarbonyl complex was formed, this bright yellow solution turned to dark orange, brown or green.



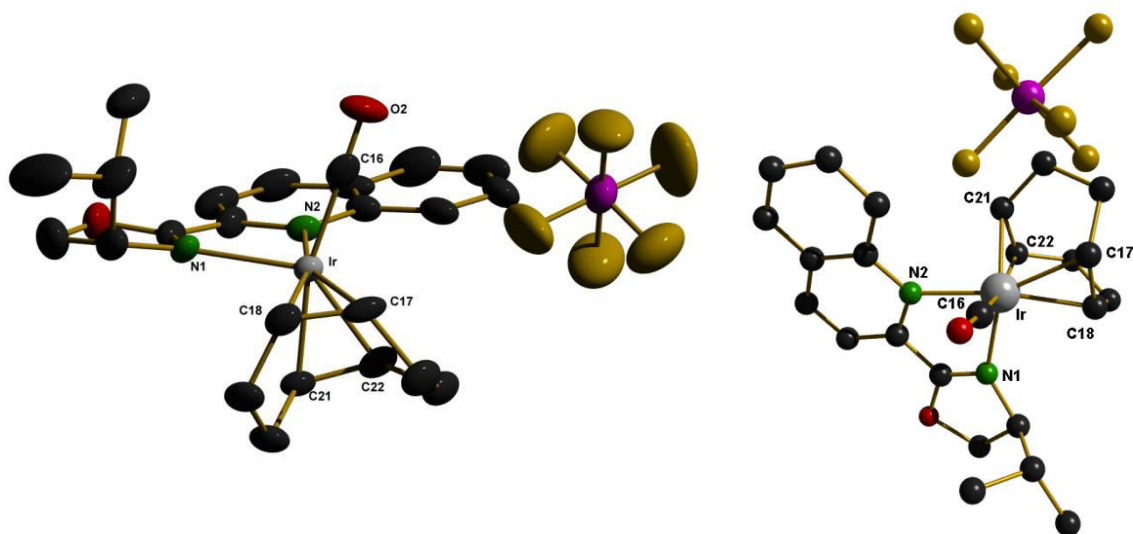
Scheme 6-13. Preparation of carbonyl complexes with typical color change.

In some cases, the monocarbonyl intermediate **26** could be isolated by interrupting the carbonylation at this stage. This was achieved by precipitation of the yellow complex with hexane. For the sterically demanding ⁱPr-quinox complex **26m** single crystals were obtained by vapor diffusion of hexane into a DCM/acetone mixture which contained the dissolved complex.

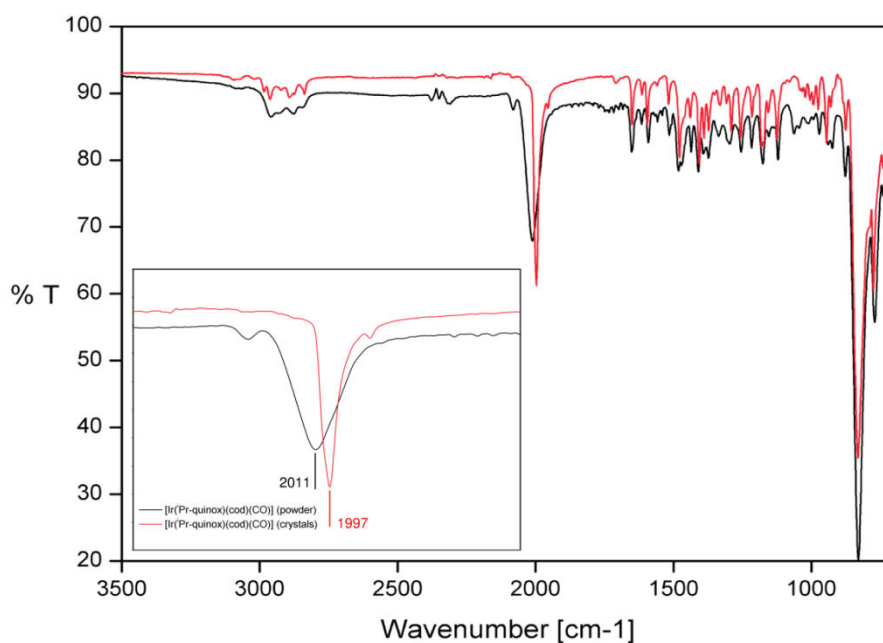
In the monocarbonyl complex $[\text{Ir}(\text{}^i\text{Pr-quinox})(\text{cod})(\text{CO})]\text{PF}_6$ **26m** (Scheme 6-14), Ir(I) is pentacoordinated in a distorted trigonal bipyramidal coordination sphere. The quinoline-N (N2) and one double bond of the cod ligand (C17, C18) form the axis and the trigonal plane is defined by the oxazoline-N (N1), a cod double bond (C21, C22) and the carbonyl Ligand (C16O). The carbonyl ligand is orientated towards the same side of the oxazoline ligand as the *iso*-propyl group, while the cod ligand occupies the sterically less hindered opposite side. The Ir-N(oxazoline) bond length is with 2.202 Å slightly longer than the Ir-N(pyridine) bond with a length of 2.121 Å.

As shown in Scheme 6-1, the ν_{CO} absorption band of the bulk powder is much broader than the one of the single crystal. This can be understood on the basis of heterogeneities in the precipitated powder, such as a distribution of the exact position of the counter anion. Due to the broadness of the absorption band from the powder, the maximum is shifted by ca. 4 cm^{-1} .

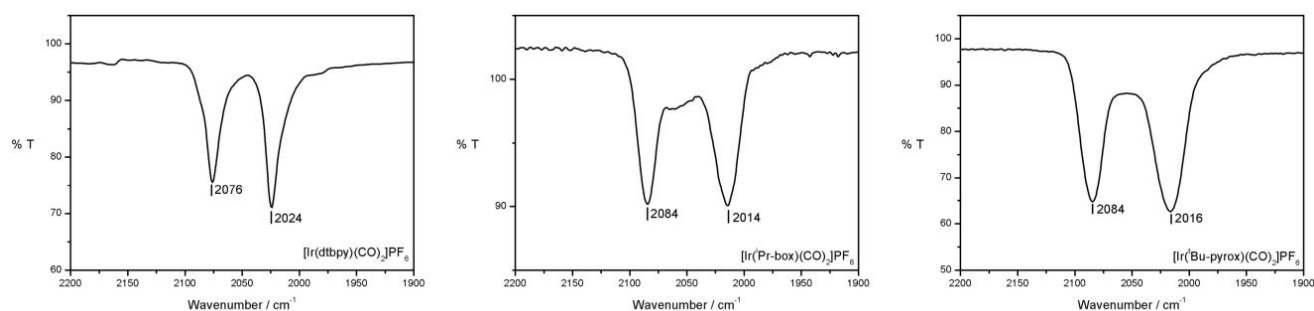
The same broadening of the ν_{CO} absorption bands was observed for dicarbonyl complexes (Scheme 6-16). Especially for those with pyrox-type ligands a broadening of the lower wavenumber band was observed (right spectrum), thus it was not clear if these spectra had to be assigned to bi- or tricarbonyl complexes.



Scheme 6-14. Solid state structure of $[\text{Ir}(\text{Pr-quinox})(\text{cod})(\text{CO})]\text{PF}_6$ (**26m**) with ellipsoids at 50% probability (left structure) and ball and stick model (right structure), omitting hydrogen atoms for clarity. Selected bond angles and distances: Ir-N1: 2.202(5) Å; Ir-N2: 2.121(7) Å; Ir-C16: 1.881(8) Å; Ir-C18: 2.144(8) Å; Ir-C17: 2.204(7) Å; Ir-C21: 2.126(8) Å; Ir-C22: 2.170(9) Å; C16-Ir-N1: 102.5(3) °; C16-Ir-N2: 88.9(3) °; centroid(C21, C22)-Ir-N2: 88.51 °; centroid(C21, C22)-Ir-C16: 146.60; centroid(C21, C22)-Ir-N1: 109.13 °; centroid(C17, C18)-Ir-N2: 173.33 °; centroid(C17, C18)-Ir-centroid(C12, C22): 86.18 °; N1-Ir-N2: 75.84 °.



Scheme 6-15. IR spectra from of $[\text{Ir}(\text{Pr-quinox})(\text{cod})(\text{CO})]\text{PF}_6$ (**26m**) as bulk powder (black) and as single crystal (red).

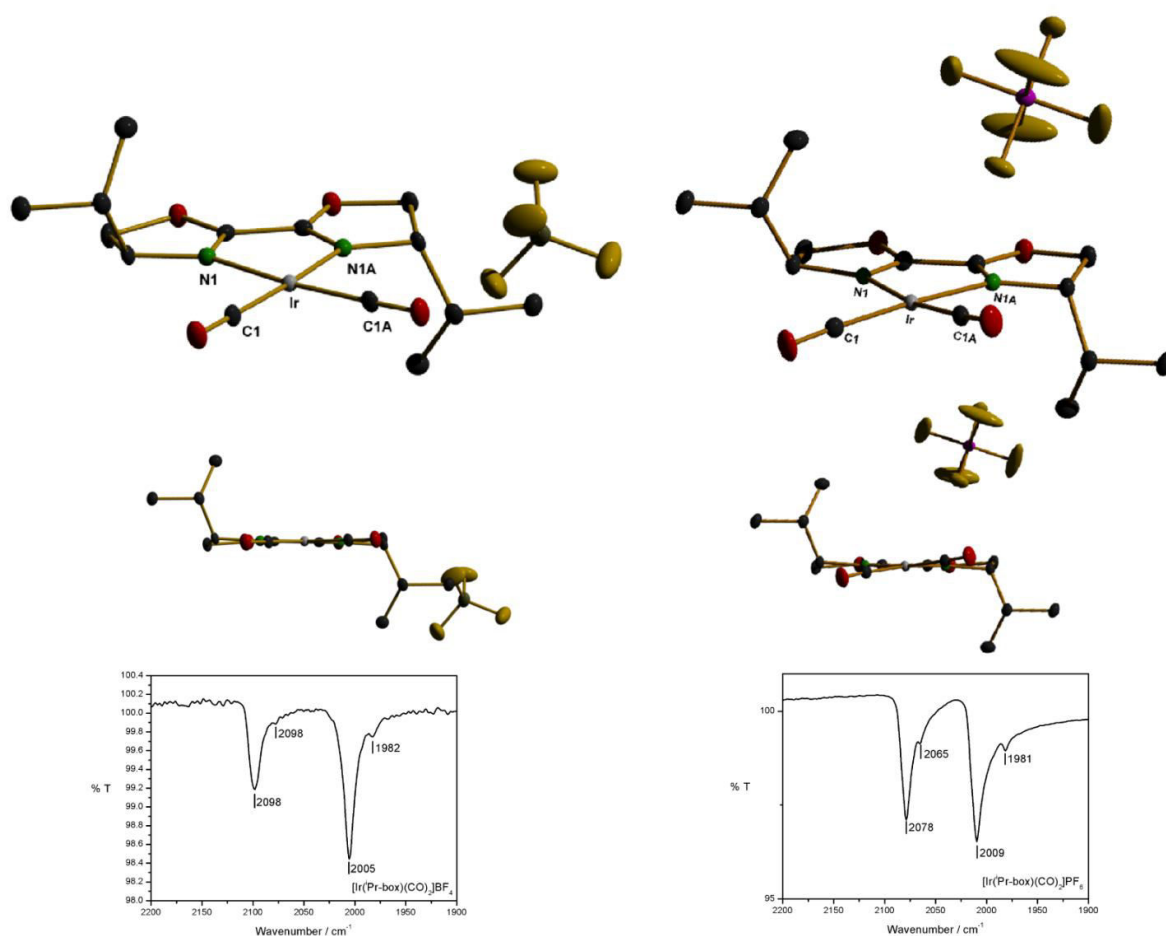


Scheme 6-16. Typical shape of IR spectra measured from solid carbonyl compounds.

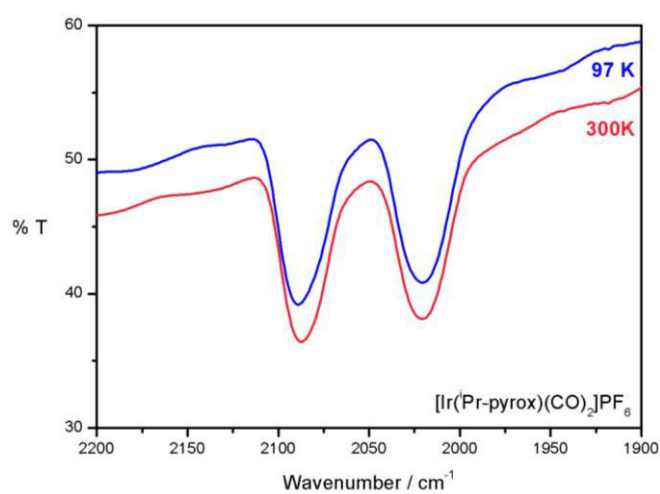
For ⁱPr-box (**5b**), two crystal structures of corresponding dicarbonyl complexes, one for the complex with a BF₄⁻ anion (complex **43**) and one with a PF₆⁻ anion (complex **28c**, Scheme 6-17) were obtained. The Ir(I) is in both complexes in a square planar coordination environment, as it is expected for a d⁸-metal. However, the carbonyl ligands of the PF₆⁻ complex are slightly twisted out of the N-Ir-N plane. Further, the Ir-N and Ir-C bond are shorter by 0.032 Å and 0.048 Å respectively than in the analogous BF₄⁻ complex. This difference can be attributed to the identity and relative position of the counteranions. The different Ir-C bond lengths are reflected in the positions of the corresponding ν_{CO} absorption bands, which were measured from the single crystals with an IR-microscope. While there is only a moderate difference between the asymmetric stretching frequencies of the carbonyls which appear at 2005 cm⁻¹ (**43**) and 2009 cm⁻¹ (**28c**), the symmetrical stretching differs by ca. 20 cm⁻¹. The higher stretching frequencies of the BF₄⁻ complex **43** correlate very well with the longer Ir-C bonds, which reflect a weaker π-back donation from the Ir to the CO ligands. Consequently, this leads to a stronger C-O bond observed as higher ν_{CO} absorption energies in the IR spectrum.

The IR measurement of the single crystals showed also absorption bands of a normal full width at half maximum (FWHM) of approximately 13 cm⁻¹. These experiments indicate, that the broadening of the spectra which were measured from the solid compounds is attributed to the heterogenic nature of the amorphous bulk powder.

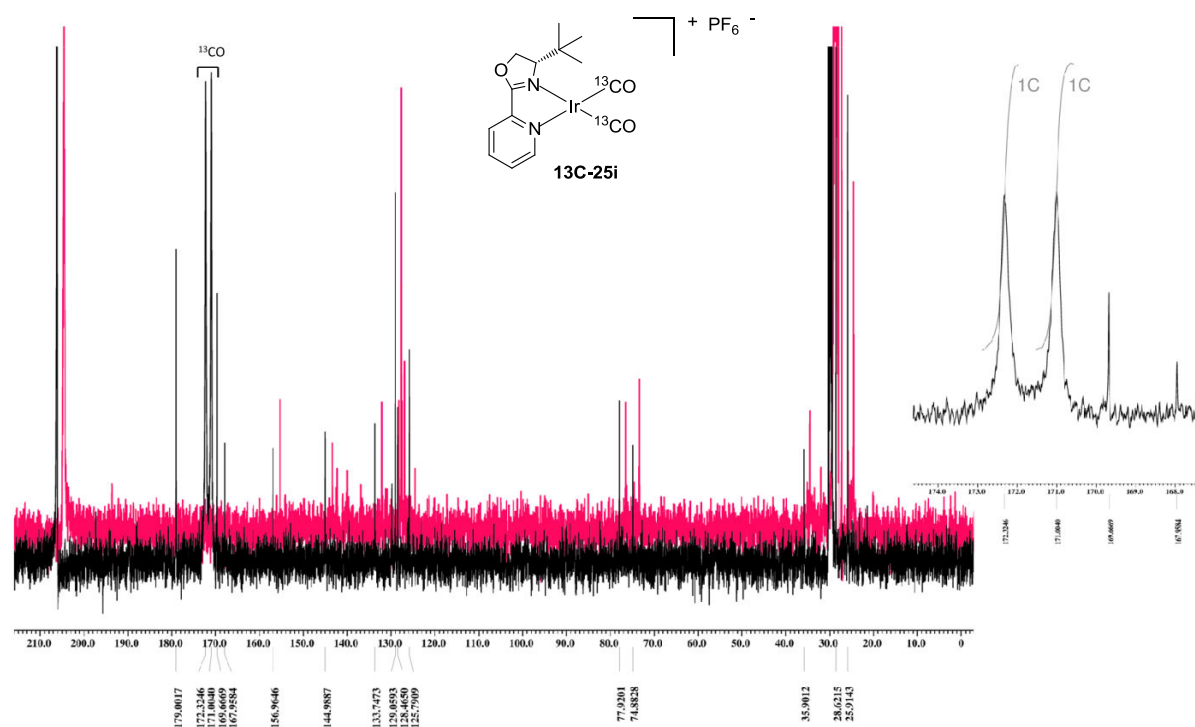
However, considering the broad bands of the powder spectra, one cannot exclude the formation of tricarbonyl complexes, in case of complexes with pyrox-type ligand, which showed always a more pronounced broadening of the asymmetric CO stretching band. Here, two of three bands might be so close to each other that they formed one single, very broad band, for example due to coalescence at room temperature. This coalescence was reported for square pyramidal [Fe(cod)(CO)₃] complexes, in which the carbonyl ligands underwent a fast exchange *via* the turnstile rotation mechanism at room temperature.^[242] To exclude a similar scenario for the iridium complexes, the IR spectra of one pyrox complex were measured at 300 K and at 97 K (Scheme 6-18). The obtained spectra showed no difference between the measurements at different temperatures, thus one can exclude coalescence between two bands of a tricarbonyl complex and assign those complexes to dicarbonyl species.



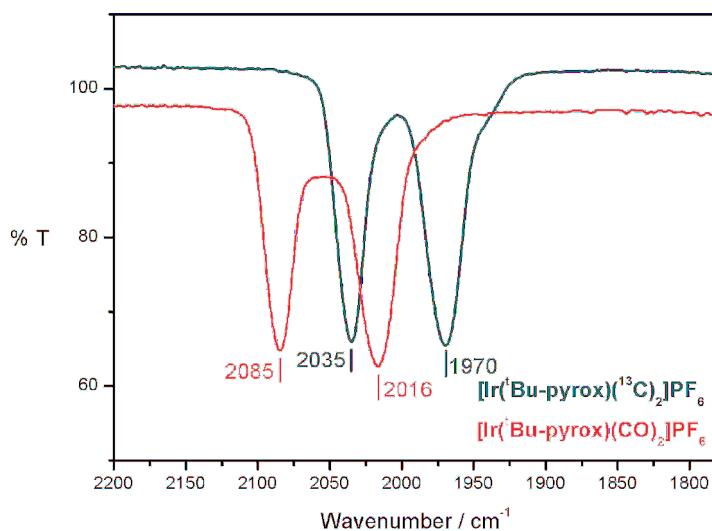
Scheme 6-17. Solid state structures of $[\text{Ir}(\text{Pr-box})(\text{CO})_2]\text{BF}_4$ (**43**) and $[\text{Ir}(\text{Pr-box})(\text{CO})_2]\text{PF}_6$ (**28c**) with ellipsoids at 50% probability, omitting hydrogen atoms for clarity. Selected bond angles and distances: $[\text{Ir}(\text{Pr-box})(\text{CO})_2]\text{BF}_4$ (**43**): Ir-N1=Ir-N1A: 2.117(3) Å; Ir-C1=Ir-C1A: 1.891(4) Å; C1A-Ir-N1=C1-Ir-N1A: 173.53(17) °; C1-Ir-C1A: 89.6(2); C1-Ir-N1=C1A-Ir-N1A: 69.74(11); $[\text{Ir}(\text{Pr-box})(\text{CO})_2]\text{PF}_6$ (**28c**): Ir-N1=Ir-N1A: 2.085(3) Å; Ir-C1=Ir-C1A: 1.842(4) Å; C1-Ir-N1=C1A-Ir-N1A: 97.23(13) °; C1-Ir-C1A: 88.7(2) °; C1-Ir-N1A=C1A-Ir-N1: 172.09(16) °. The IR spectra were measured with an IR-microscope from single crystals of the compounds.



Scheme 6-18. IR spectrum of $[\text{Ir}(\text{Pr-pyrox})(\text{CO})_2]\text{PF}_6$ (**28h**) at 300 K (red spectrum) and at 97 K (blue spectrum).



Scheme 6-19. ^{13}C -NMR spectrum of ^{13}C -marked dicarbonyl complex ^{13}C -**25i** (black spectrum) and unmarked analogue structure **25i** (red spectrum). The spectra were measured in acetone- d_6 .

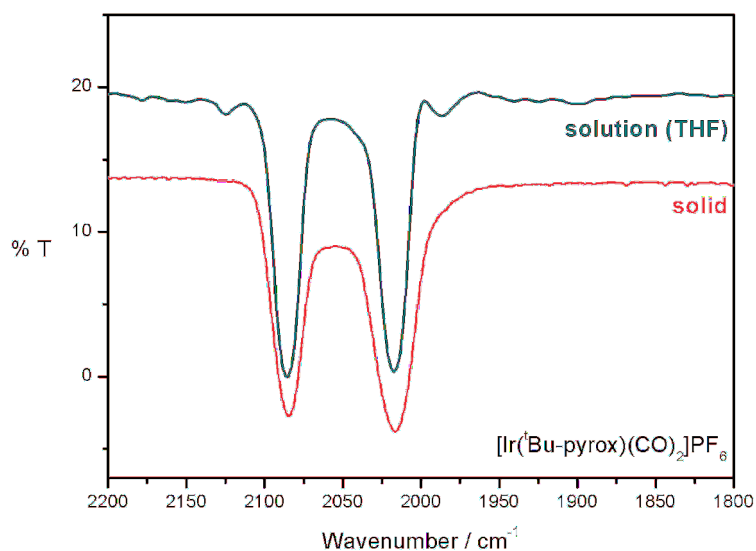


Scheme 6-20. IR spectra from solid compounds of dicarbonyl complex ^{13}C -**25i** (green spectrum) and unmarked analogue structure **25i** (red spectrum).

To support this interpretation and determine directly how many carbonyl ligands were coordinated to the pyrox-type complexes, a ^{13}C labeling experiment of the carbonyl ligands was undertaken. Labeled ^{13}CO gas was generated from 9-methyl-9H-fluorene-9-carbonyl- ^{13}C chloride by a Pd(0) catalyzed reaction and added to the cod ^tBu -pyrox precursor complex **25i**. Subsequently, the resulting carbonyl complex ^{13}C -**25i** was analyzed by ^{13}C -NMR (Scheme 6-19) and IR spectroscopy (Scheme 6-20). The

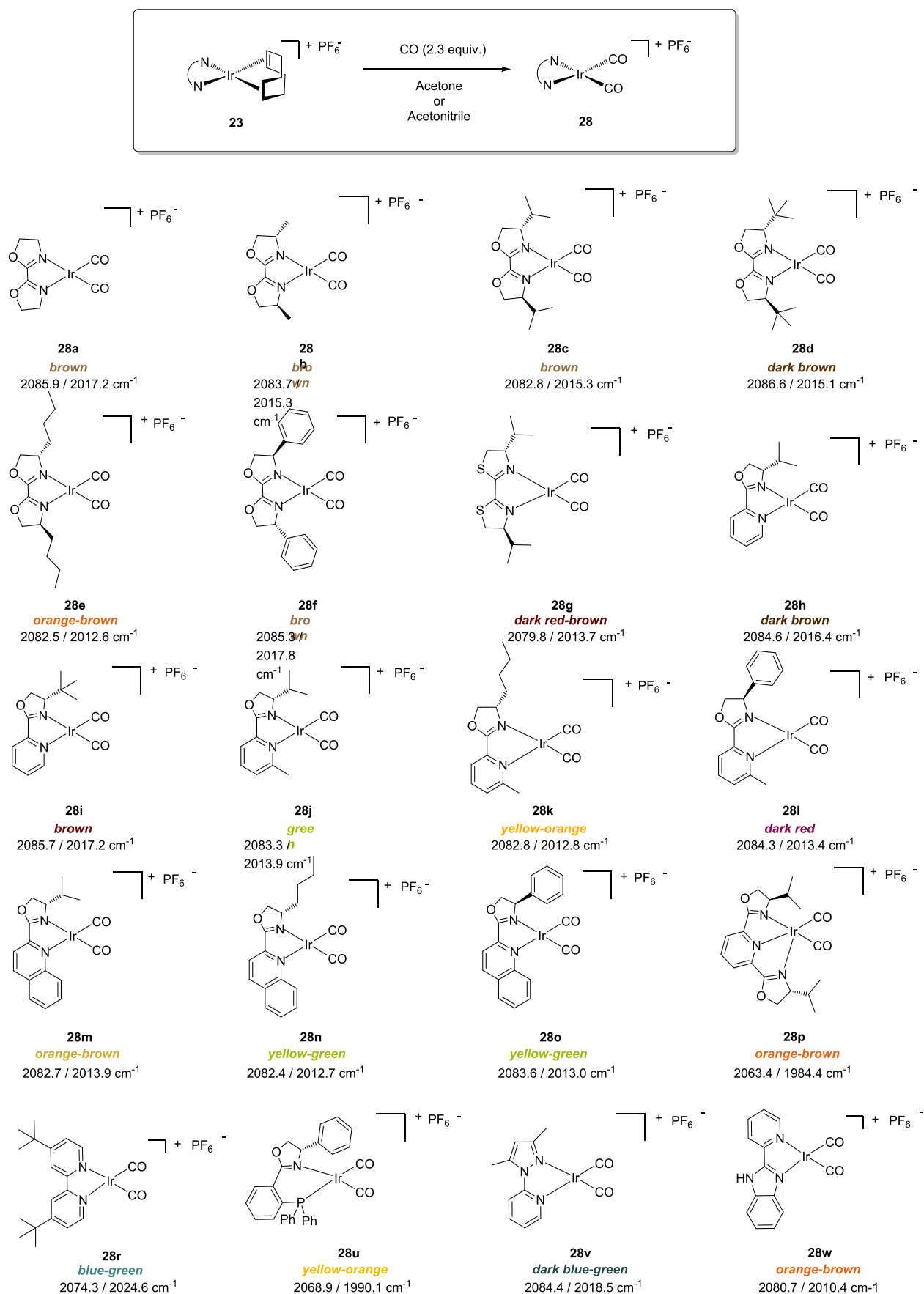
IR spectrum showed the same shape with two CO bands, only shifted by approximately 50 cm^{-1} because of the higher mass of the ^{13}C -isotope. In the ^{13}C -NMR, two singlets with an integral ratio of 1:1 were assigned to two chemically inequivalent ^{13}CO ligands, which proves that these complexes are dicarbonyl complexes.

Since the broadening and possible shifts of the band due to different counter anion positions would aggravate the determination of the exact position and thus the comparison between different ligands, measurements in solution were performed to overcome this problem. In solution the counter anions are solvated and therefore play a minor role for the cationic complex. The measurements were performed on an ATR-silicon crystal, because the usually used diamond crystal had a too strong self-absorption in the carbonyl range around 2000 cm^{-1} . For the solution ATR-IR spectra (Scheme 6-21) the complexes were dissolved in THF and centrifuged to remove all insoluble compounds which would precipitate onto the ATR crystal. The solution measurements resulted in sharp absorption bands, for which the absorption maxima could be identified more precisely.

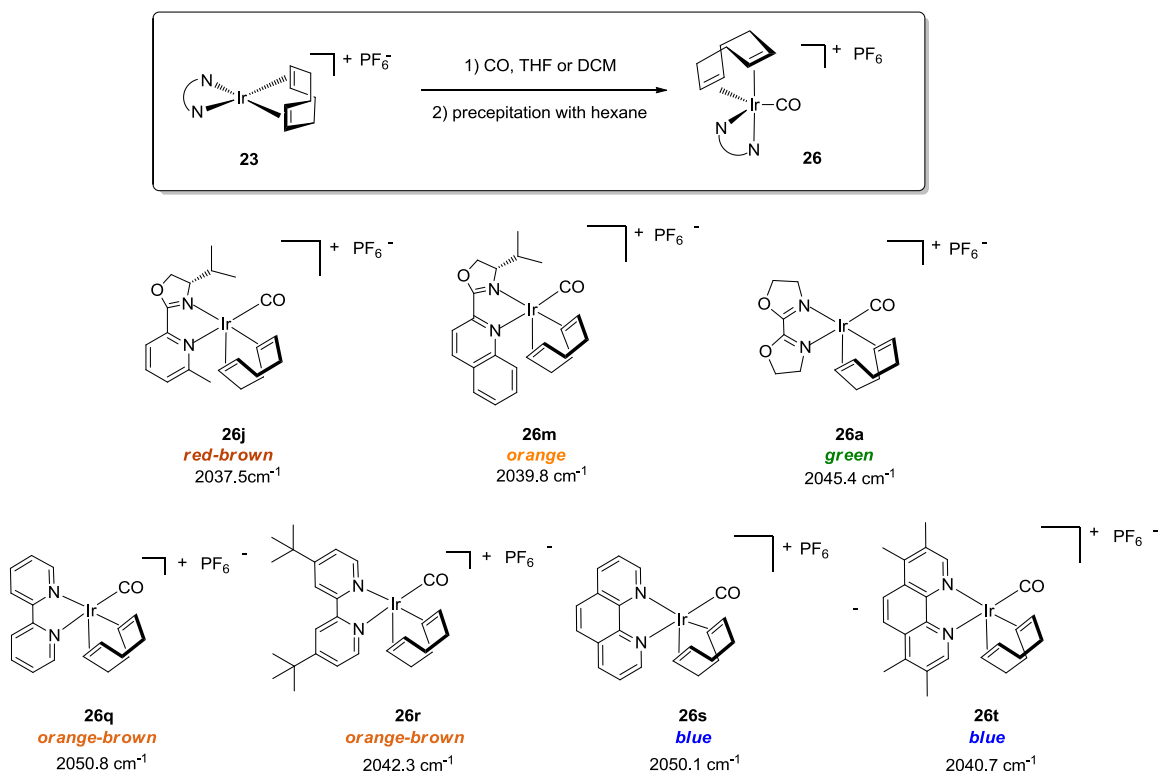


Scheme 6-21. Comparison of IR spectrum from the solid compound (red spectrum) and from solution in THF (green spectrum) on the example of $[\text{Ir}(\text{iBu-pyrox})(\text{CO})_2]\text{PF}_6$ (**28i**).

The prepared dicarbonyl complexes **28** are illustrated together with their ν_{CO} absorption energies in Scheme 6-22. For bpy (**37**) and the phenanthroline ligands **38** and **39**, only monocarbonyl complexes were obtained. For the potentially tridentate ligand iPr-pybox (**36**), a mixture of dicarbonyl and monocarbonyl complex was obtained, presumably as pentacoordinated $[\text{Ir}(\text{iPr-pybox})(\text{CO})_2]\text{PF}_6$ (**28p**) and tetracoordinated $[\text{Ir}(\text{iPr-pybox})(\text{CO})]\text{PF}_6$. (**44**) The collection of monocarbonyl complexes and their corresponding ν_{CO} absorption energies is depicted in Scheme 6-23.



Scheme 6-22. Prepared dicarbonyl complexes **28** with ν_{CO} absorption frequencies obtained by ATR-IR measurement from a solution of the corresponding complex in THF on a silicon ATR-crystal.



Scheme 6-23. Prepared monocarbonyl complexes **26** with ν_{CO} absorption frequencies obtained by ATR-IR measurement from a solution of the corresponding complex in THF on a silicon ATR-crystal.

6.1.4 Evaluation of IR Data of the Carbonyl Complexes

Dicarbonyl Complexes

The measured ν_{CO} absorption frequencies of the carbonyl complexes were plotted together with the predicted values from DFT calculations (Scheme 6-25 and Scheme 6-26). The ligands are ordered into groups of structurally related compounds (Scheme 6-24). This allows comparing the ligand groups with each other as well as the differently substituted ligands within one group. The data which were used for the plots are listed in Table 6-1.

Table 6-2. Overview of measured and calculated stretching frequencies for dicarbonyl complexes.

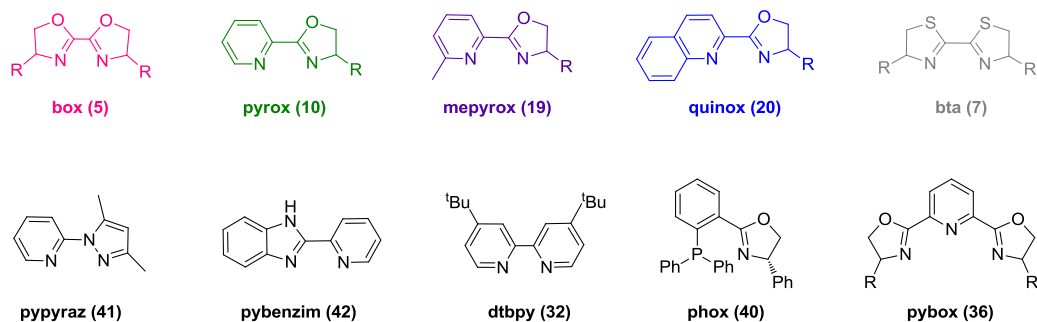
Entry	[Ir(N/P^N)(CO) ₂] ₂ PF ₆	Experiment in THF ^a [cm ⁻¹]		Calculation [cm ⁻¹]		Average [cm ⁻¹]	
		v (sym)	v (asym)	v (sym)	v (asym)	Experiment	Calculation
1	Ph-box (5g)	2085.3	2017.8	2069.5	2010.3	2051.6	2039.9
2	H-box (5i)	2085.9	2017.2	2070.0	2009.5	2051.6	2039.7
3	^t Bu-box (5c)	2086.6	2015.1	2067.5	2006.3	2050.9	2036.9
4	ⁱ Pr-box (5b)	2082.8	2015.3	2066.3	2005.3	2049.1	2036.5
5	Me-box (5a)	2083.7	2014.3	2067.0	2006.0	2049.0	2036.5
6	ⁿ Bu-box (5f)	2082.5	2012.6	2067.5	2006.8	2047.6	2036.4
7	ⁱ Pr-bta (7b)	2079.8	2013.7	2060.9	2003.8	2046.8	2032.3
8	^t Bu-pyrox (10c)	2085.7	2017.2	2065.1	2004.4	2051.5	2034.8
9	ⁱ Pr-pyrox (10b)	2084.6	2016.4	2064.9	2004.2	2050.5	2034.5
10	Ph-mepyrox (19g)	2084.3	2013.4	2066.5	2003.4	2048.9	2032.1
11	ⁱ Pr-mepyrox (19b)	2083.3	2013.9	2064.8	2002.2	2048.6	2032.8
12	ⁿ Bu-mepyrox (19f)	2082.8	2012.8	2065.1	2002.6	2047.8	2031.8
13	Ph-quinox (20g)	2083.6	2013.0	2063.9	2001.8	2048.3	2035.4
14	ⁱ Pr-quinox (20b)	2082.7	2013.9	2062.8	2000.9	2048.3	2034.8
15	ⁿ Bu-quinox (20f)	2082.4	2012.7	2062.1	2000.3	2047.6	2032.9
16	pypyraz (41)	2084.4	2018.5	2064.8	2006.1	2051.4	2028.5
17	dtbpy (32)	2074.3	2024.6	2065.1	2004.4	2049.5	2025.6
18	pybenzim (42)	2080.7	2010.4	2062.5	2003.4	2045.6	2032.1
19	phox (40)	2068.9	1990.1	2056.4	2000.5	2029.5	2032.9
20	ⁱ Pr-pybox (36)	2063.4	1984.4	2055.6	1995.7	2023.9	2031.8

^aExperiments were performed with a homogeneous complex solution in THF, measured on a ATR-silicon crystal. Reading error: ± 0.25 cm⁻¹.

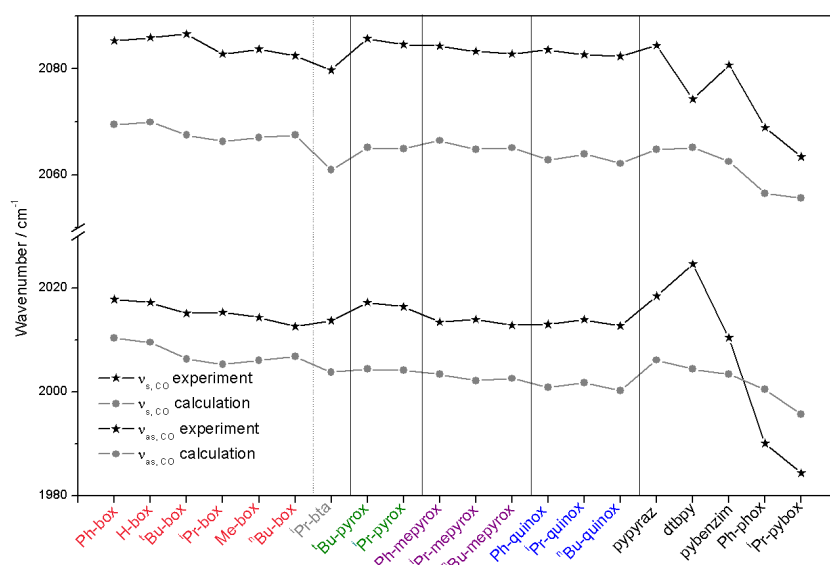
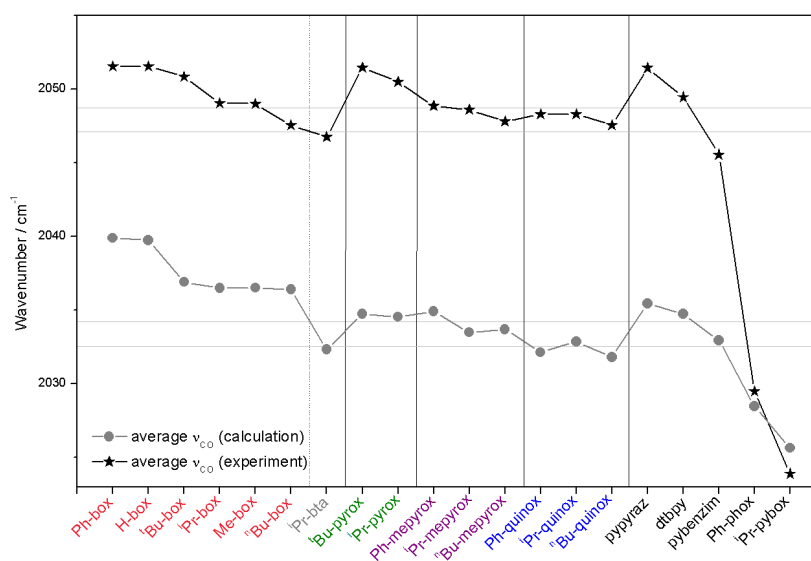
Comparing the experimental values shown in Scheme 6-25, it can be seen that the symmetrical and the asymmetrical stretching frequencies show an overall related trend. However, when evaluating the exact positions in more detail, subtle differences of these two bands can be perceived. For example, the splitting between the bands becomes smaller for ⁱPr-box (**5b**; 67.5 cm⁻¹) than it is the case for ^tBu-box (**5c**; 71.5 cm⁻¹) and results in opposed trends for the symmetrical and asymmetrical C-O stretches of these ligands, respectively. In general, the difference between both bands ranges from ca. 79 cm⁻¹ for phox (**40**) and ⁱPr-pybox (**36**) to 49.7 cm⁻¹ for dtbpy (**32**).

Because of the inconsistent distance between the symmetrical and the asymmetrical ν_{CO} absorption bands, it was decided to compare the average band positions of the different ligands (Scheme 6-26).

The first observation is that the average values of the ν_{CO} absorption energies of all box (**5**), pyrox (**10**), mepyrox (**19**), and quinox (**20**) ligands overlap between 2052 cm⁻¹ and 2047 cm⁻¹. Although these differences are relatively small, especially for box and pyrox ligands trends are identifiable in dependence of their oxazoline residues. Mepyrox and quinox ligands show nearly no differences in the ν_{CO} absorption energies between the differently substituted ligands. For the complex with the dtbpy (**32**) ligand, a ν_{CO} absorption energy of 2049.5 cm⁻¹ was obtained, which is similar to these obtained for the oxazoline ligands. For the complexes with the phox (**40**) and pybox (**36**) much lower ν_{CO} absorption energies of 2029.5 cm⁻¹ and 2023.9 cm⁻¹, respectively, were obtained.



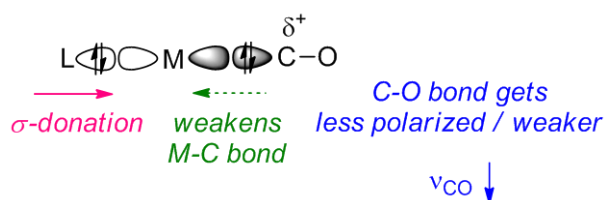
Scheme 6-24. Overview of ligands and ligand groups.

Scheme 6-25. Symmetrical and asymmetrical ν_{CO} absorption energies of dicarbonyl complexes $[\text{Ir}(\text{N}/\text{P}^{\wedge}\text{N})(\text{CO})_2]\text{PF}_6$ (**28**) in comparison with calculated values.Scheme 6-26. Average ν_{CO} absorption energies of dicarbonyl complexes $[\text{Ir}(\text{N}/\text{P}^{\wedge}\text{N})(\text{CO})_2]\text{PF}_6$ (**28**) in comparison with calculated values.

For the differences in the ν_{CO} absorption energies in theory three factors can play a role:

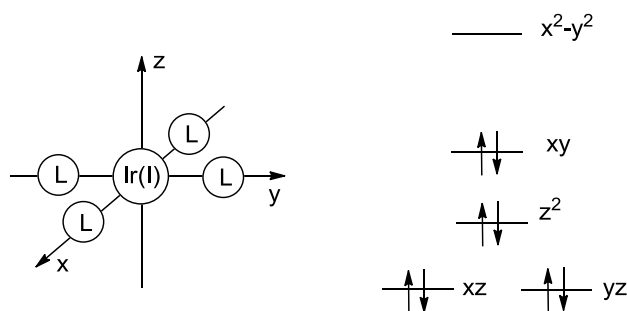
1. σ -donation from the ligand to the metal,
2. π -donation from the ligand to the metal,
3. π -back donation from the metal to the ligand.

The σ -donation ability correlates with the Lewis basicity of the donor atom, which donates a lone pair into an empty d-orbital of the metal thus forming a dative σ -bond. In a carbonyl complex, an electron donation of a ligand which is orientated *trans* to a carbonyl ligand, weakens the M-C σ -bond. Consequently, the C-O bond gets less polarized which results in a weaker C-O bond. The decreased C-O bond strengths is reflected in a decreasing ν_{CO} absorption energy (Scheme 6-27).^[73]



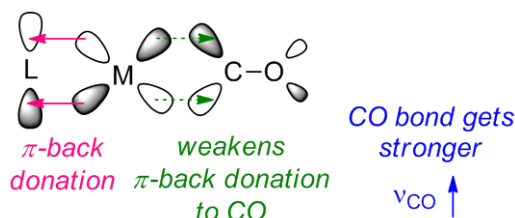
Scheme 6-27. Effect of σ -donation from a ligand, orientated *trans* to a CO ligand, on the CO stretching frequency.

For the π -donation, the ligand donates electrons from a filled π -orbital into an empty d-orbital from the metal. For this, an empty metal d-orbital of the appropriate symmetry is required. In a square planar complex in theory the d_{xy} , d_{xz} and d_{yz} orbitals provide this symmetry which allows acceptance of electrons from a filled π -orbital of the ligand. However, in a d^8 metal complex these orbitals are filled and therefore they are not suitable for accepting π -donation from a ligand (Scheme 6-28). Consequently, π -donation is not expected to be a relevant factor for the ν_{CO} absorption energies of $[\text{Ir}(\text{N/P}^{\wedge}\text{N})(\text{CO})_2]^+$ complexes.



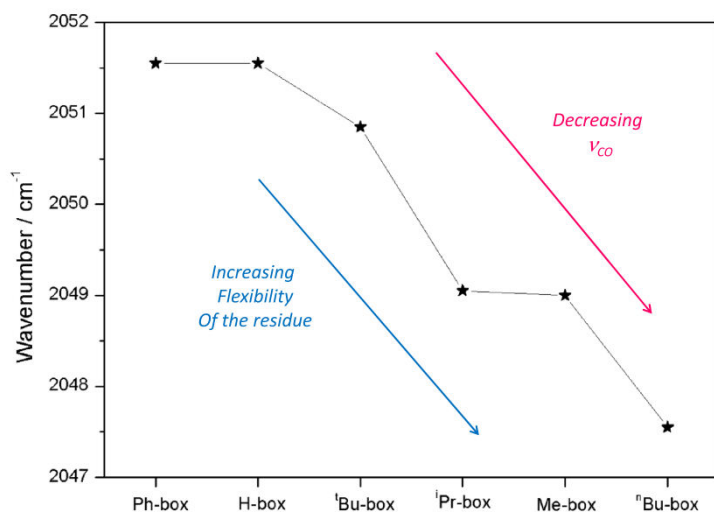
Scheme 6-28. Ligand field splitting of a square planar coordination geometry and electron configuration for a d^8 metal complex.

The π -back donation is occurring from a filled metal d-orbital into the lowest ligand π^* -orbital. Donation of electrons from the metal to the ligand lowers the electron density on the metal thus decreasing its π -donation ability to the CO ligand. If less electron density is donated into the π^* of the CO ligand, the C-O bond gets stronger, which is reflected in an increasing ν_{CO} absorption energy (Scheme 6-29).

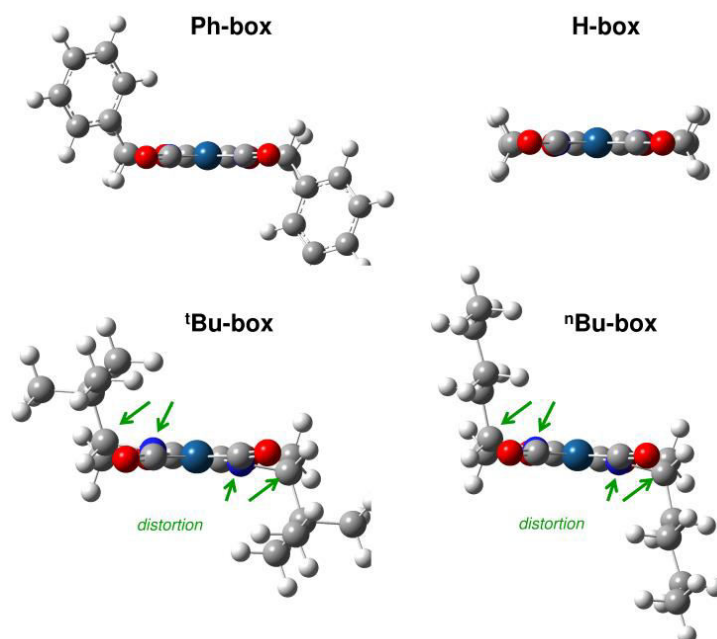


Scheme 6-29. Effect of π -back donation of a metal to a ligand on the CO stretching frequency.

Concentrating on the box ligands first, the following trend for the residues was identified: $-\text{Ph} / -\text{H} > -^i\text{Bu} > -^i\text{Pr} / -\text{Me} > {}^n\text{Bu}$ in decreasing order of ν_{CO} absorption energies (Scheme 6-30). The phenyl substituted Ph-box (**5g**) and the unsubstituted H-box (**5i**) have the same influence, which can be attributed to a similar steric influence of the hydrogen atom and the flat phenyl substituent. However, this trend is broken with ${}^t\text{Bu}$ -box (**5c**). This complex, found in the middle of this trend, bears the highest steric influence, which decreases over ${}^i\text{Pr}$ -box (**5b**) to ${}^n\text{Bu}$ -box (**5f**). Also the inductive electron donation ability decreases in this order. However, the inductive electron donation should affect the ν_{CO} absorption energies in the opposite direction. The higher electron donating effect of ${}^t\text{Bu}$ -box should cause a higher basicity of the ligand and therefore an increase of its σ -donor strength, resulting in a lower ν_{CO} absorption energy than observed for the other ligands. Since this does not resemble the observations, other effects must play a role. Possibly, the increasing flexibility of the residue from $-\text{Ph}$ to ${}^n\text{Bu}$ is leading to a higher distortion of the ligand. A twisting of the ligand backbone could result in two effects; firstly the conjugation of the donor atoms is weakened, which would result in a higher Lewis basicity, leading to a decreased ν_{CO} absorption energy (cf. Scheme 6-27). Secondly, a twisting of the ligand backbone itself and of the whole ligand out of the N-Ir-N plane, would lead to a worse overlap of the π -orbitals which are responsible for a π -back bonding (cf. Scheme 6-29). Both effects would lead to decreased ν_{CO} absorption energies, which is in accordance with the observations. Supporting this assumption, the geometry optimized models of the complexes show an increased twisting of the ligands with increased flexibility of the residues (Scheme 6-31). In these pictures it can also be seen that a phenyl and a hydrogen substituent both cause no twisting of the ligand, which is in accordance with the obtained same high ν_{CO} absorption energies of 2051.6 cm^{-1} which were observed for the complexes of these two ligands.



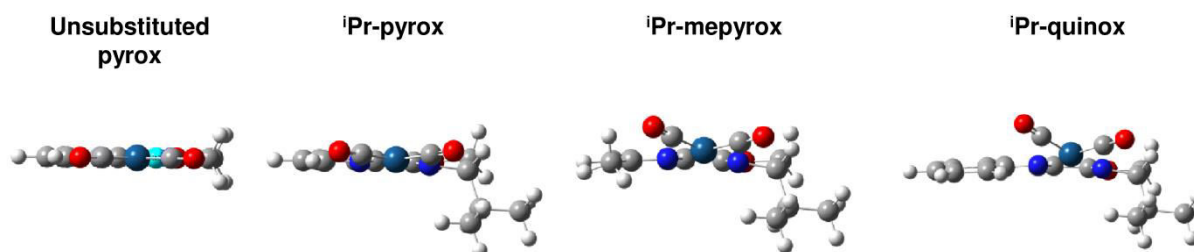
Scheme 6-30. Average ν_{CO} absorption energies of box-dicarbonyl complexes $[\text{Ir}(\text{Rbox})(\text{CO})_2]\text{PF}_6$ (**28**).



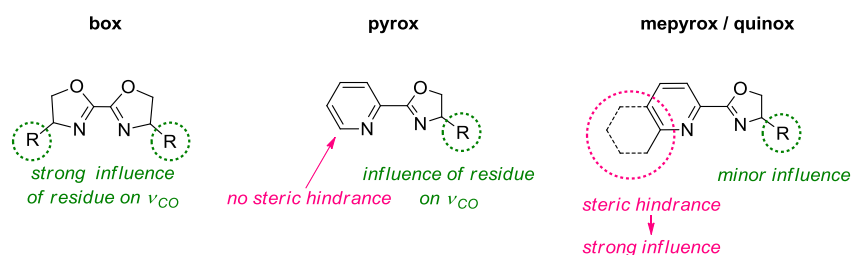
Scheme 6-31. Geometry optimized models of dicarbonyl complexes with different box ligands.

This concept can be extended to the pyrox ligands, which also show a relatively high dependence of the ν_{CO} absorption energy on the oxazoline residue, whereas mepyrox and quinox complexes show nearly no change of ν_{CO} absorption energies for different oxazoline residues. This can be attributed to the high steric hindrance of these ligands in the 6- or 9-position, respectively. Due to the high steric hindrance of the methyl group or the annulated benzene, the environment of the complex is strongly influenced and the ligand is again twisted within the oxazoline moiety and in addition out of the C-Ir-C plane

(Scheme 6-32). Thus, the changing residues on the oxazoline moiety have only minor influence on the geometry and therefore on the ν_{CO} absorption frequencies (Scheme 6-33).



Scheme 6-32. Geometry optimized models of dicarbonyl complexes with different pyrox-type ligands.



Scheme 6-33. Comparison of steric influences on box, pyrox and mepyrox and quinox in the complex geometry in $[\text{Ir}(\text{ligand})(\text{CO})_2]\text{PF}_6$ (**28**) resulting in different ν_{CO} absorption energies.

In comparison to its oxygen analogues, for the complex with the bithiazolin ligand $^i\text{Pr-bta}$ (**7**) the lowest ν_{CO} absorption frequency within the group of the C_2 -symmetrical box ligands was observed. This can be attributed to a higher basicity of the N-donor, which can be explained by a lower electronegativity of the sulfur in the thiazoline thus having a less electron withdrawing effect than an oxygen. Alternatively, it can be assumed that the larger sulfur causes a strong distortion of the thiazolin, which would result in a lower conjugation of the nitrogen, leading also to an increased basicity.

For the P,N-coordinating phox (**40**) and the N,N,N-coordinating pybox (**36**) ligands the lowest ν_{CO} absorption energies were observed. For phox (**40**), this is in accordance with the assumption that phosphorous atom is a strong σ -donor, resulting in allow ν_{CO} absorption frequency. Since phosphines are also known as good acceptors for π -back bonding,^[72, 207] the obtained results show that π -back bonding plays no major role in this square planar biscarbonyl complexes. Otherwise the C-O bond would become stronger (cf. Scheme 6-29) and the ν_{CO} absorption frequency would be expected to be much higher. Either, the π -back bonding is generally not very strong in the cationic complexes or the phosphine ligand is also distorted and therefore twisted out of the C-Ir-C plane making an overlap of

the corresponding orbitals for the back bonding less possible. For pybox (**36**), the explanation for such a large shift in the ν_{CO} absorption energies is not obvious. The most likely explanation is, that the complex with the tridentate ligand is pentacoordinated which leads to a different coordination sphere around the iridium. Consequently, the pybox complex is not comparable with the oxazoline complexes.

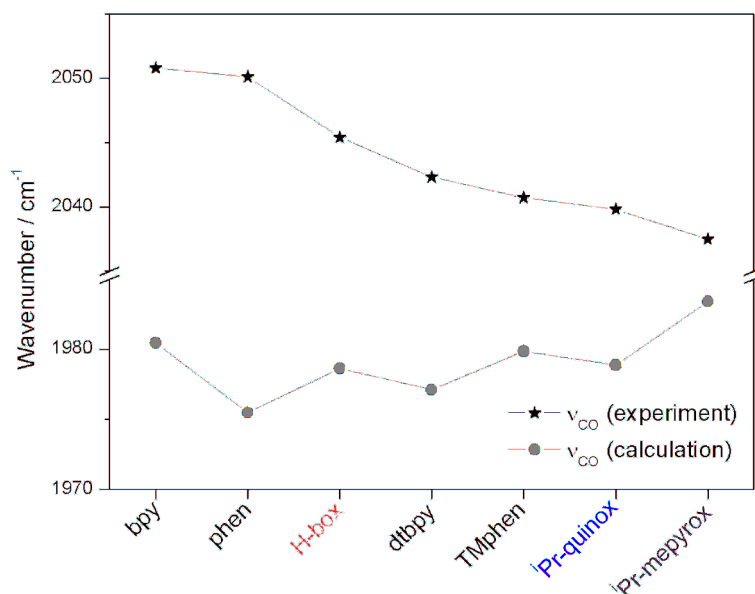
Monocarbonyl Complexes

The comparison of monocarbonyl complexes $[\text{Ir}(\text{N}^{\wedge}\text{N})(\text{cod})(\text{CO})]\text{PF}_6$ (**26**) (Scheme 6-34 and Table 6-3) shows, how the box and pyrox-type ligands can be compared with different bipyridines and phenanthrolines. For unsubstituted bipyridine and phenanthroline ligands the highest ν_{CO} absorption energies of approximately 2050 cm^{-1} were obtained. In comparison with their methyl-substituted analogues dtbpy (**32**) and TMphen (**39**), the ν_{CO} absorption frequencies are approximately 10 cm^{-1} higher. As it was also the case for the dicarbonyl complexes $[\text{Ir}(\text{N}^{\wedge}\text{N})(\text{CO})_2]\text{PF}_6$ (**28**), the unsubstituted H-box (**5i**) ligand causes a higher ν_{CO} absorption frequency, than the relatively electron rich bipyridine dtbpy (**32**) and TM-phen (**39**), with a ν_{CO} of approximately 2045 cm^{-1} . For ⁱPr-quinox (**20b**) and ⁱPr-mepyrox (**19b**) again very similar ν_{CO} absorption energies were obtained. However, for the monocarbonyl complexes of these two ligands, a difference of approximately 2.5 cm^{-1} was observed, while the values for the corresponding dicarbonyl complexes are the approximately same. Here, the 6-methyl substituted mepyrox ligand causes slightly higher electron density on the iridium which is in agreement with the assumption that the methyl substituent donates more electron density than an annulated benzene, resulting in a higher basicity of the N-donor as it is the case for the quinox ligand **20b**. Obviously, the electronic properties of the ligands play a greater role in the monocarbonyl complexes than it was observed for the dicarbonyl complexes.

Table 6-3. IR data for monocarbonyl complexes $[\text{Ir}(\text{N}^{\wedge}\text{N})(\text{cod})(\text{CO})]\text{PF}_6$ (**26**).

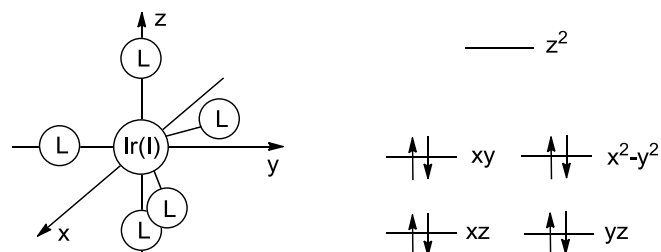
Entry	$[\text{Ir}(\text{N}^{\wedge}\text{N})(\text{cod})(\text{CO})]\text{PF}_6$ (26)	ν_{CO} (exp.) [cm^{-1}]	ν_{CO} (calc.) [cm^{-1}]
1	bpy (37)	2050.8	1980.5
2	Phen (38)	2050.1	1975.5
3	H-box (5i)	2045.4	1979.0
4	dtbpy (32)	2042.3	1977.1
5	TM-phen (39)	2040.7	1979.9
6	ⁱ Pr-quinox (20b)	2039.8	1979.0
7	ⁱ Pr-mepyrox (19b)	2037.5	1983.0

^aExperiments were performed of a homogeneous complex solution in THF, measured on a ATR-silicon crystal. Reading error: $\pm 0.25\text{ cm}^{-1}$.



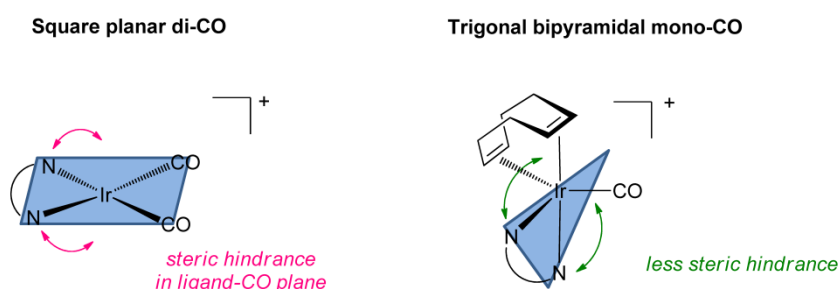
Scheme 6-34. Monocarbonyl ν_{CO} absorption energies of complexes $[\text{Ir}(\text{N}^{\wedge}\text{N})(\text{cod})(\text{CO})]\text{PF}_6$ (**26**) in comparison with calculated values.

The effects relevant for the position of the CO stretching band are here basically the same as discussed for dicarbonyl complexes. The σ -donation of the ligand as well as π -back donation from the metal influence the C-O bond strength, while π -donation is not expected to occur, because the only empty d-orbital in the trigonal bipyramidal coordination sphere of a Ir(I) complex is the d_{z^2} -orbital (Scheme 6-35) which does not have the appropriate geometry for the acceptance of π electrons.



Scheme 6-35. Ligand field splitting of a trigonal bipyramidal coordination geometry and an electron configuration for a d^8 metal complex.

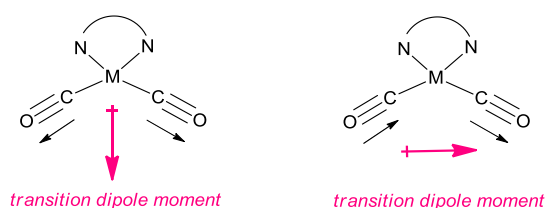
The reason for a larger effect of the electronic properties of the ligands in the monocarbonyl complexes can be found in the different coordination spheres present in monocarbonyl complexes in contrast to dicarbonyl complexes. The coordination sphere of the pentacoordinated monocarbonyl complexes is trigonal bipyramidal (cf. solid state structure of $[\text{Ir}(\text{iPr-quinox})(\text{cod})(\text{CO})]\text{PF}_6$; Scheme 6-5). Therefore less steric hindrance is occurring in the N-Ir-N plane and the steric properties of the side chains in the ligands cannot influence the geometry of the corresponding ligands in such a large extent as it was found for dicarbonyl complexes. Consequently, the ν_{CO} stretching frequencies of the monocarbonyl complexes reflect better the electronic properties of the ligands (Scheme 6-36).



Scheme 6-36. Comparison of the coordination spheres of dicarbonyl and monocarbonyl complexes and the resulting steric hindrance in the ligand-iridium plane.

Comparison of Experimental and Calculated CO Stretching Frequencies

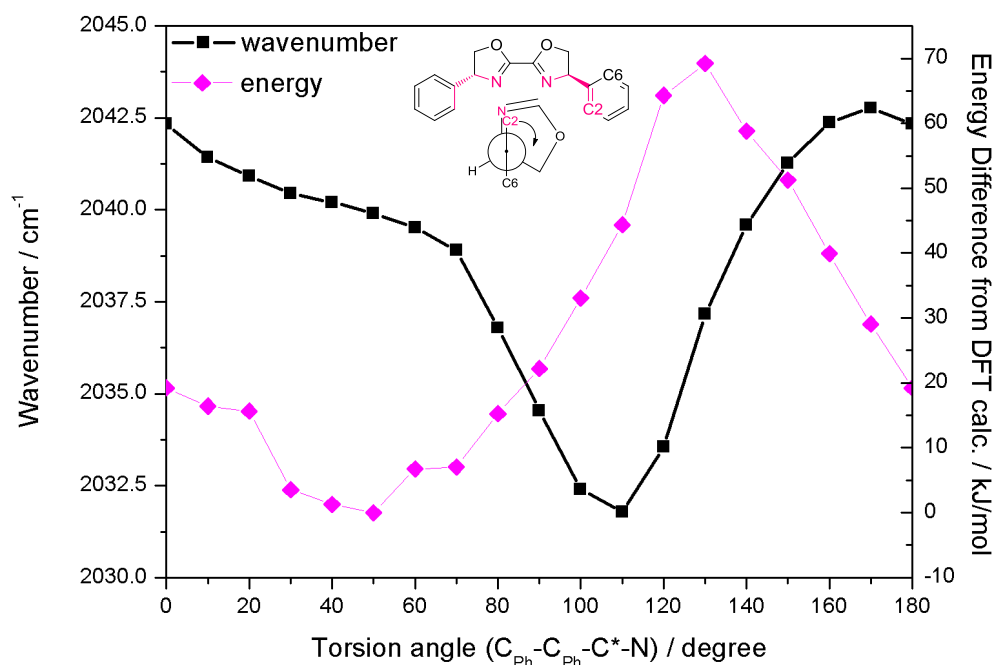
The comparison of the experimental results with the calculated values (Scheme 6-25) shows that the symmetric ν_{CO} stretching frequencies were much better predicted as the asymmetric ones. An explanation might be that the transition dipole moments of the different stretch couplings are perpendicularly orientated to each other (Scheme 6-38). The vector of the transition dipole moment of the symmetric ν_{CO} bisects the angle between the two carbonyl ligands. In the case of a C_2 symmetrical ligand, this vector is even equal with the C_2 axis. In case of the asymmetrical stretch, the transition dipole moment bisects the molecule between the bidentate ligand and the two carbonyls. It is possible, that both bands are differently influenced by several additional factors such as changes of the symmetry of the molecule.



Scheme 6-37. Transition dipole moments for symmetrical and asymmetrical stretches in a bended dicarbonyl complex.^[243]

From the comparison of the average ν_{CO} stretching frequencies (Scheme 6-26) it can also be seen that trends within a group of ligands can be predicted very well. However, comparing different ligand types, the calculated box complexes seem to yield too high average ν_{CO} values when compared with the experimental ones. This can be explained on the basis of the flexibility of the ligands. In DFT calculations, the vibrational frequencies are derived only from the optimized structure. However, in an IR experiment in solution at room temperature not only the thermodynamic stable structure is present,

but a wide range of conformations, with *e.g.* different rotamers of the residues, are present at the same time. Therefore, the theoretical calculations fail to predict the distribution of structures which can affect the ν_{CO} stretching frequencies. Since the box ligands have two rotating residues and more flexible core structure due to the lack of aromaticity, the measured IR frequencies are influenced much stronger than for example for pyrox, in which the pyridine provides a rather rigid structure. To illustrate how strong this flexibility can affect the IR spectra, the ν_{CO} absorption energies of the Ph-box dicarbonyl complex (**28f**) were calculated for different angles of the Ph residues with the C-N bond. In the energy optimized structure, this angle is 50° and corresponds to an average ν_{CO} stretching frequency of 2039.9 cm^{-1} . However, when rotating the phenyl residue, wavenumbers in a rather broad range of to 2042.5 to 2032.2 cm^{-1} are calculated. The experiment, in principle, yields the average value of all conformers, with the highest proportion of the thermodynamically most stable structure.

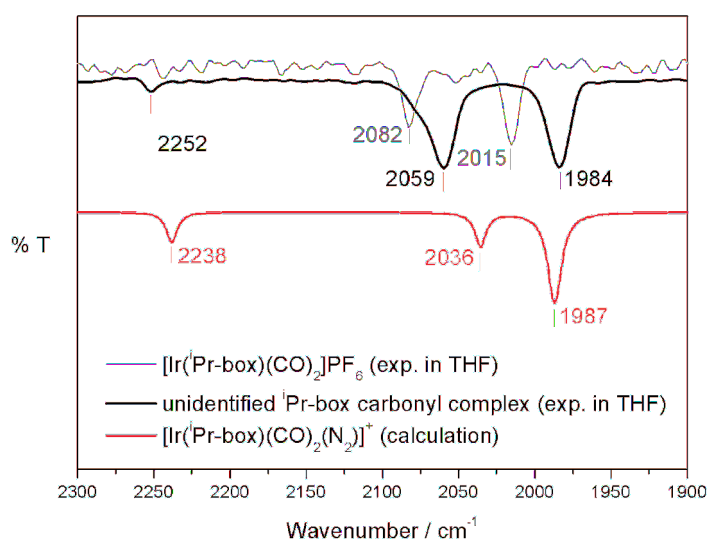


Scheme 6-38. Calculated average ν_{CO} absorption energies of Ph-box (**5g**) in dependence on the $\text{C}_{\text{Ph}}\text{-C}_{\text{Ph}}\text{-C}^*\text{-N}$ torsion angle. For simplicity both angles were set equal, maintaining C_2 -symmetry, for each point.

The prediction for the bipyridine ligand deviates most from the measurement. Here, the interpretation is not straight forward. From the ligands evaluated in this project, it can be seen that the prediction of a trend of ν_{CO} stretching frequencies does only work for structurally related ligands and fails for the comparison of different ligand classes. For monocarbonyls the calculation results even in different trends than observed by the experiments, presumably due to the very flexible structure of the complexes with cod ligands which actual geometry might be too hard to predict.

Dicarbonyl Adduct with Lower CO Stretching Frequencies

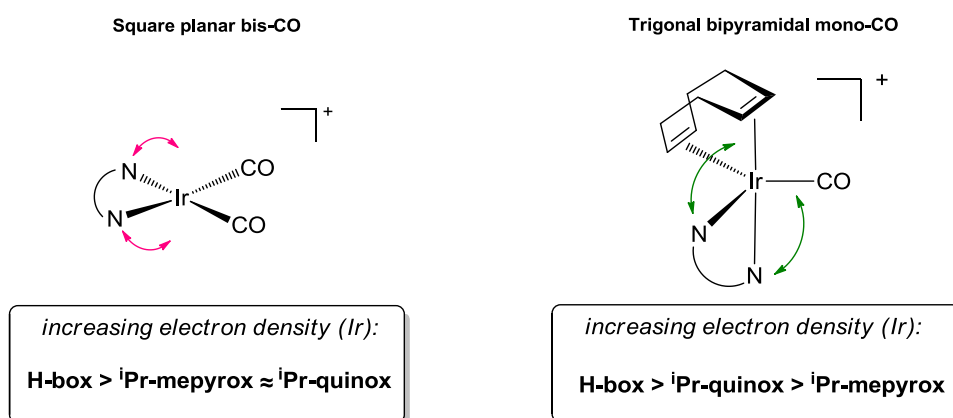
Besides the identified dicarbonyl complexes, in some spectra a second set of ν_{CO} bands, shifted approximately by 20 cm^{-1} to lower wavenumbers, was found (Scheme 6-39). This set of shifted wavenumbers might be assigned to the same complex which Mestroni observed upon purging solutions of carbonyl complexes with nitrogen (cf. chapter 3.1.4).^{18, 891} Mestroni assigned these signals to pentacoordinated $[\text{Ir}(\text{ligand})(\text{CO})_2(\text{N}_2)]\text{PF}_6$ (**45**) complexes, formed by the exchange of one carbonyl ligand of a pentacoordinated tricarbonyl complex $[\text{Ir}(\text{ligand})(\text{CO})_3]\text{PF}_6$ (**27**) for one N_2 -ligand. Since tricarbonyl complexes were not observed in this project and the bands at higher wavenumbers were clearly assigned to dicarbonyl complexes, a tricarbonyl-precursor complex can be excluded here. Calculations of pentacoordinated O_2 , cod or N_2 adducts of dicarbonyl complexes showed that the formation of such structures would be suitable explanations for the observed low frequency ν_{CO} absorption bands. A similar observation was also made for the pentacoordinated pybox complex, for which comparably low ν_{CO} absorption energies were observed. A hint for the identity of the additional ligand in the, presumably pentacoordinated, adducts was given by the very small band at 2252 cm^{-1} , which was observed in spectra with relatively strong ν_{CO} absorption bands of the unidentified species. Calculations for the nitrogen adduct $[\text{Ir}(\text{ligand})(\text{CO})_2(\text{N}_2)]\text{PF}_6$ (**45**) of the dicarbonyl complex showed a band of the $\nu_{\text{N-N}}$ absorption also in this area. Therefore, and because Mestroni obtained a similar IR spectrum after purging a carbonyl complex with nitrogen, the species with ν_{CO} absorption bands at approximately 2060 cm^{-1} and 1985 cm^{-1} can be most likely assigned as nitrogen adducts $[\text{Ir}(\text{ligand})(\text{CO})_2(\text{N}_2)]\text{PF}_6$ (**45**) of a dicarbonyl complex $[\text{Ir}(\text{ligand})(\text{CO})_2]\text{PF}_6$ (**28**). However, also coordination of other molecules such as O_2 , free cod or dissolved CO cannot be excluded.



Scheme 6-39. IR spectra of the unidentified ^iPr -box carbonyl complex (black line) in comparison with the IR spectra of the corresponding square planar dicarbonyl complex (grey line) and the calculated spectrum of the pentacoordinated nitrogen adduct (red line).

Summary

In summary, trends between the oxazoline ligand groups and trends within these groups were observed for dicarbonyl complexes $[\text{Ir}(\text{N}/\text{P}^{\wedge}\text{N})(\text{CO})_2]\text{PF}_6$ (**28**) concerning the resulting CO bond strength. In these square planar complexes, the steric properties of the ligands played a major role for the electron density on the iridium, because they strongly influence the geometry of the ligand which is reflected either in the σ -basicity of the ligand or in its π -acidity. Especially the result obtained for the complex with the P,N-coordinating phox ligand (**40**) indicated that the obtained ν_{CO} absorption energies were mainly influenced by the σ -basicity, because otherwise the ν_{CO} absorption energies for this complex would be expected to be much higher. For trigonal bipyramidal monocarbonyl complexes, the electronic properties of a ligand became more predominant, leading to a switched trend between the ligands ⁱPr-mepyrox (**19b**) and ⁱPr-quinox (**20b**) (Scheme 6-40). Therefore the square planar complexes unexpectedly turned out to be a tool for the evaluation of structural properties of the tested ligands while the trigonal bipyramidal monocarbonyl complexes exhibited information about the electrical properties.

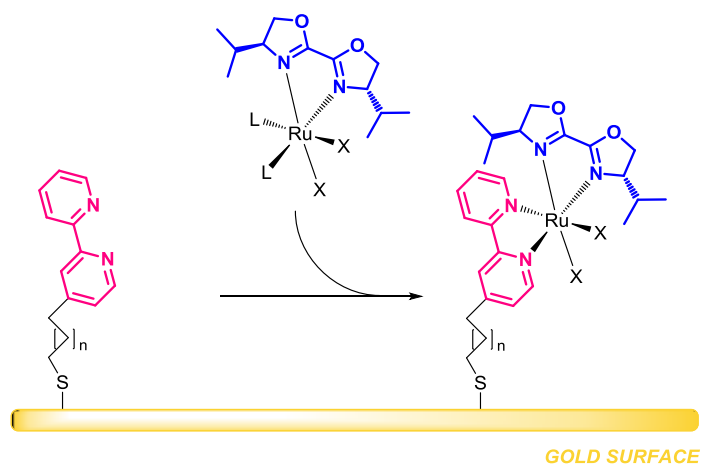


Scheme 6-40. Trends for box, mepyrox and quinox ligands observed for monocarbonyl and dicarbonyl complexes.

Prediction of the ν_{CO} stretching frequencies by DFT calculation gave the correct trends for structurally related ligands in dicarbonyl complexes but failed for the comparison of different types of ligands, due to an underestimation of the structural flexibility of the ligands.

6.2 Heteroleptic Ruthenium(II) Complexes

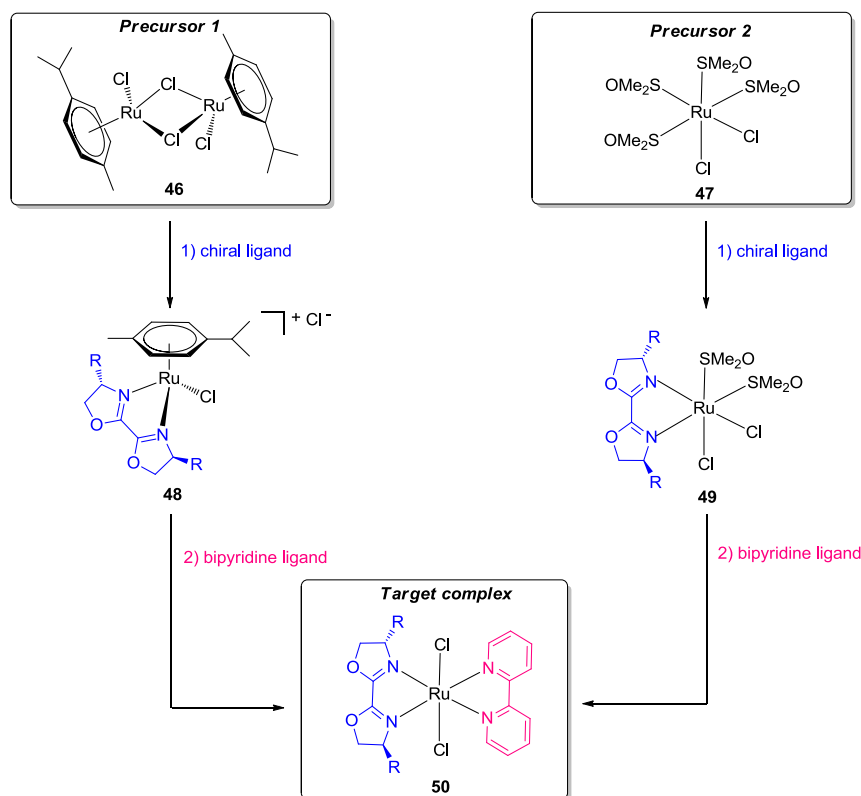
For future immobilization on electrode surfaces (cf. chapter 1) the stepwise introduction of bipyridine and oxazoline ligands on a ruthenium(II) precursor was investigated. As illustrated in Scheme 6-41 the chiral oxazoline ligand needs to be introduced first while the bipyridine ligand is already immobilized on a surface and therefore introduced as second ligand.



Scheme 6-41. Immobilization of a ruthenium(II) complex on a bipyridine functionalized gold surface. The ruthenium precursor carries already a chiral oxazoline ligand while the bipyridine serves as connection to the surface and is introduced as second ligand.

Following this strategy, two different approaches for the stepwise ligand introduction were adapted and investigated. As shown in Scheme 6-42, either the cymene ruthenium dimer **46** or the dmsu complex **47** was chosen as precursor complex. The use of the cymene complex **46** promises a straightforward introduction of only one ligand first, because the cymene ligand is not labile enough to dissociate easily. This, on the other hand, might become a problem when a second ligand should replace the cymene ligand. Therefore a second route starting with the dmsu-precursor **47** will be investigated as well. The dmsu and chloro ligands are far more labile than the cymene ligand from complex **46**, enabling ligand substitution processes at milder conditions. The challenge by applying this complex will be the controlled stepwise coordination of different ligands.

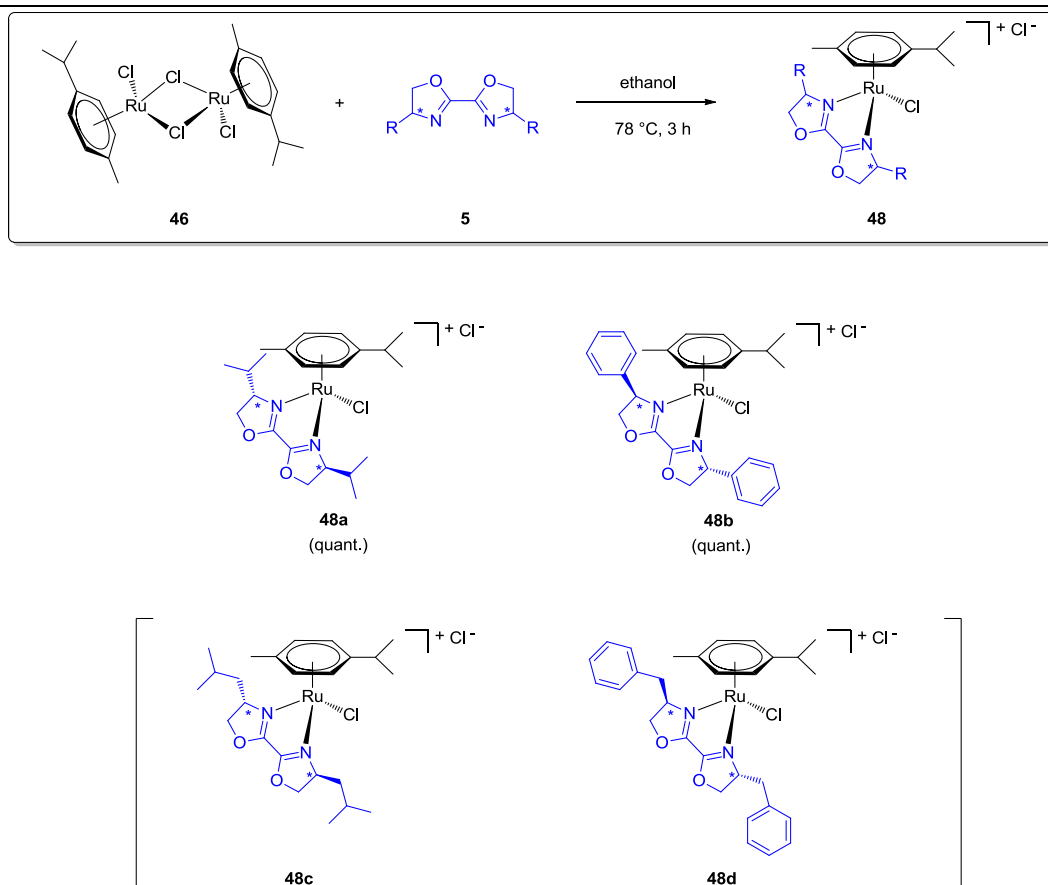
In this chapter, to facilitate the assignment of the discussed complexes, the terms “homoleptic” and “heteroleptic” will refer to the bidentate and tridentate ligands only. For example will a complex containing two identical bipyridine ligands, one dmsu ligand and one chloro ligand be referred to as “homoleptic”.



Scheme 6-42. Preparation of heteroleptic target complex **50** following the cymene-complex **46** route (precursor 1) or the dmsol-complex **47** route (precursor 2).

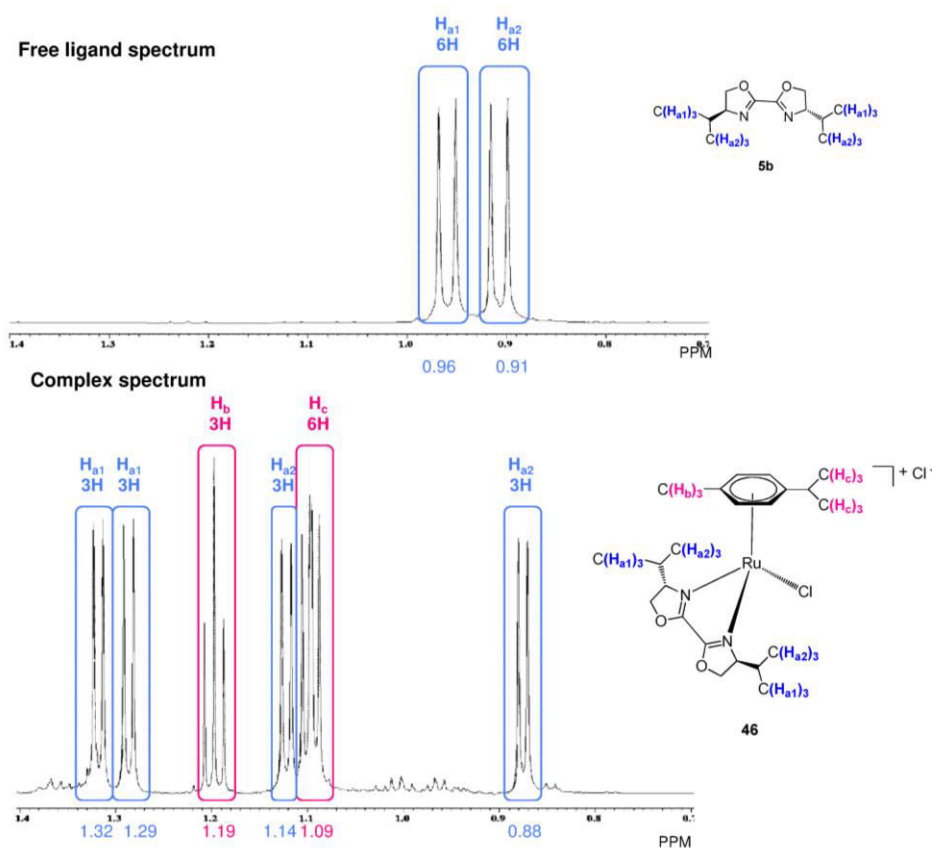
6.2.1 $[\text{Ru}(p\text{-cymene})\text{Cl}]_2$ Precursor: Introduction of the First Ligand

The introduction of a first ligand on the cymene precursor **46** proceeded straightforward as expected before. Complexations on this ruthenium precursor are usually performed in protic solvents such as *iso*-propanol at elevated temperatures.^[244] Here, ethanol was chosen because the box ligands **5** were well soluble in this solvent. Initial experiments were carried out with ^{*i*}Pr-box (**5b**) that was heated under reflux for 3 h together with the cymene precursor **46**. The pure product **48a** was obtained quantitatively by simple evaporation of the solvent, and the procedure was successfully transferred to the introduction of Ph-box (**5g**), which could also be obtained as pure product **48b**. However, when the conditions were applied to the analogous reaction with the more flexible ^{*i*}Bu-box (**5e**) and Bn-box (**5h**) ligands, only impure products were formed. The complexes **48c** and **48d** were detected by ESI-HRMS spectroscopy but the ¹H-NMR spectra showed too many impurities thus an identification of the individual signals failed. Purification attempts by precipitation failed because the complexes were oily compounds.



Scheme 6-43. Ligand introduction on cymol precursor **46**. The complexes **48a** and **48b** were obtained as pure substances while the complexes **48c** and **48d** could not be identified doubtlessly.

Coordination of the *iso*-propyl substituted ligands can be easily observed in the $^1\text{H-NMR}$ spectrum, as depicted in Scheme 6-44. In the C_2 -symmetrical free ligand the methyl groups of the *iso*-propyl groups are diastereotopic and therefore two doublets with an integration of 6 H-atoms each, can be observed close to each other between 0.9 and 1.0 ppm. After successful coordination, the *iso*-propyl groups are fixed in a different chemical surrounding and therefore become chemically inequivalent. Consequently, the spectrum of the complex shows four different doublets which can be assigned to these four methyl groups.

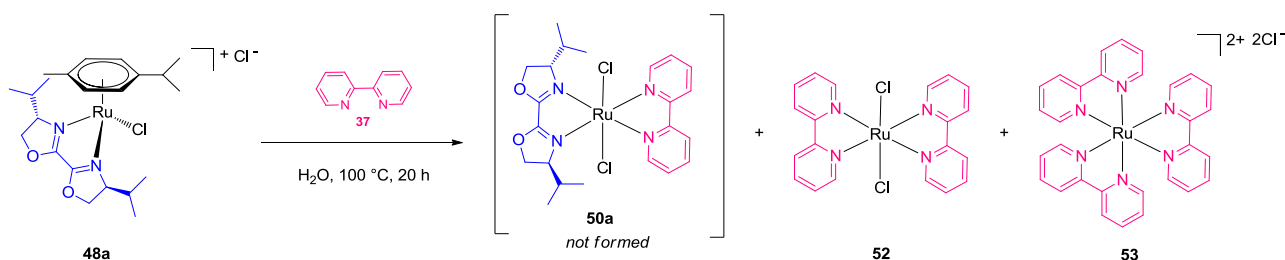


Scheme 6-44. Typical change of the chemical shift of the *iso*-propyl groups of ¹Pr-box **5b** upon coordination to [Ru(*p*-cymene)Cl]₂ **46** in ¹H-NMR spectrum (500 MHz, CDCl₃). The upper spectrum shows the two doublets of two chemically different methyl groups C(H_{a1})₃ and C(H_{a2})₃ of the *iso*-propyl groups respectively of the free ligand. Upon coordination all four methyl groups of the *iso*-propyl groups are fixed in a different chemical surrounding and become therefore chemically different, which is represented in the four different doublets corresponding to these groups.

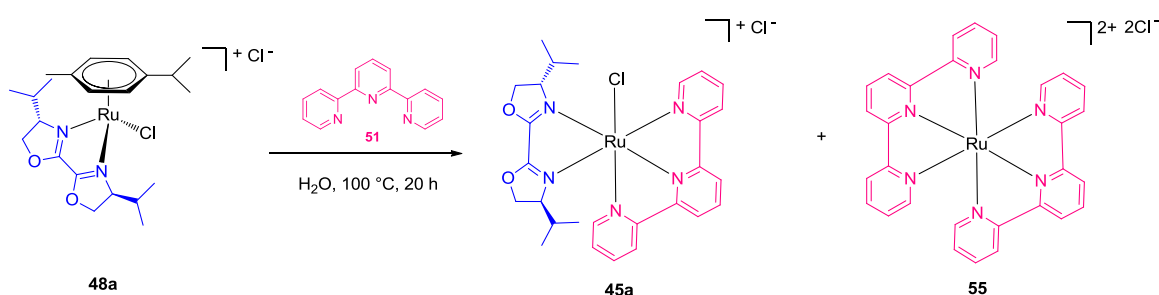
6.2.2 [Ru(cymene)Cl]₂ Precursor: Introduction of the Second Ligand

Since [Ru(ⁱPr-box)(*p*-cymene)Cl]Cl (**48a**) was prepared as pure compound, it was chosen as starting material for the introduction of a second ligand. Together with bipyridine **37** (Scheme 6-45) or terpyridine **51** (Scheme 6-46), it was heated at elevated temperatures of 100 °C in water as solvent for 20 h. These high temperatures and long reaction times were necessary, because the cymene ligand did not decoordinate under milder conditions. Upon coordination with bipyridine **37**, no heteroleptic product **50a** was found as assigned in the ¹H-NMR spectrum, which did not show the typical doublets of the *iso*-propyl groups of the box ligand. Therefore, it is very likely, that the box ligand decoordinates quantitatively and only a bipyridine containing complex was formed. Supporting this assumption, the homoleptic complexes **52** and **53** were detected by HRMS. Upon complexation with terpyridine **51**, the analysis of the ¹H-NMR spectrum failed due to too many overlapping signals.

However, after this reaction the heteroleptic complex **54a** as well as the homoleptic complex **55** were identified by HRMS, but a purification of the two cationic complexes by crystallization failed.



Scheme 6-45. Complexation of $[\text{Ru}(\text{Pr-box})(p\text{-cymene})\text{Cl}]\text{Cl}$ (**48a**) with bipyridine **37**. The desired heteroleptic complex **50a** was not formed as confirmed by $^1\text{H-NMR}$ spectroscopy. The homoleptic complexes **52** and **53** were identified by HRMS.

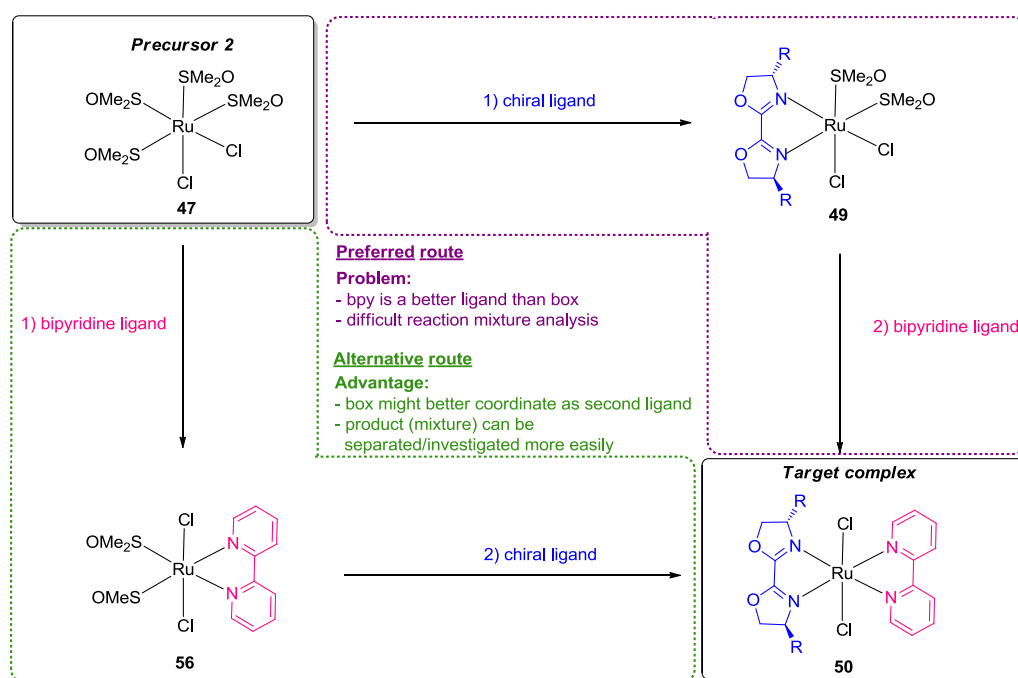


Scheme 6-46. Complexation of $[\text{Ru}(\text{Pr-box})(p\text{-cymene})\text{Cl}]\text{Cl}$ (**48a**) with terpyridine **51**. As side product the homoleptic complex **55** was identified by HRMS.

These two experiments showed that it is very difficult to introduce a second ligand to $[\text{Ru}(\text{Pr-box})(p\text{-cymene})\text{Cl}]\text{Cl}$ (**48a**) that is a bipyridine or terpyridine because these are much better ligands and tend to displace the box ligand on the complex. It is also possible, that the box ligand is hydrolyzed under the very harsh conditions.

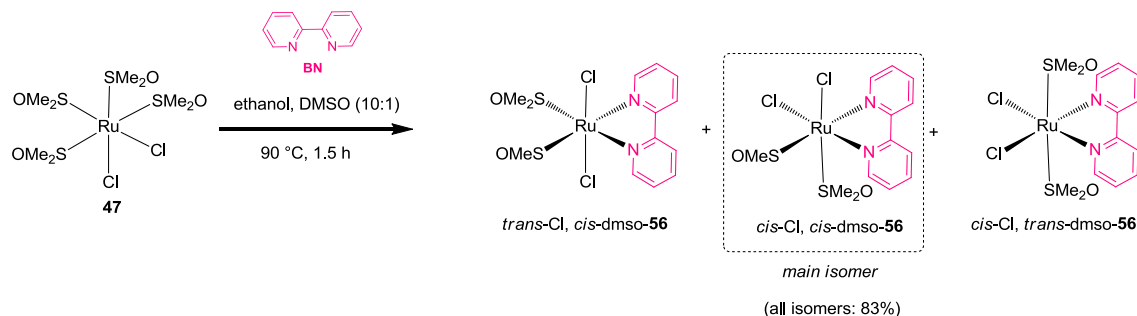
6.2.3 $[\text{Ru}(\text{dmsO})_4\text{Cl}_2]$ Precursor: Introduction of the First Ligand

After the failure of the first route, an alternative route starting with the dmsO-precursor complex **47**, was investigated. Even though it was intended to discover a method to introduce the oxazoline ligand as first ligand, in the following experiments a bipyridine ligand was applied as first ligand. This procedure promised to deliver results and knowledge about the heteroleptic complexes faster, since the first step was already described by the group of Toyama. After gaining experience in the synthesis as well as analytical data about the heteroleptic target complex **50**, the challenging stepwise synthesis beginning with oxazolines as first ligands, could be developed.



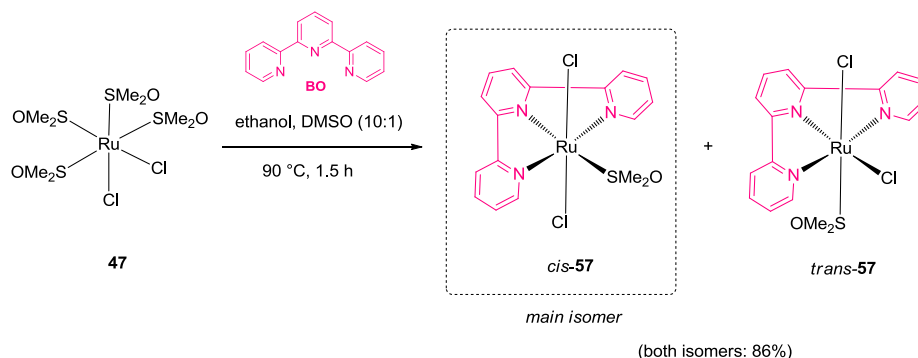
Scheme 6-47. Two ways to prepare the heteroleptic target complex **50**. In the preferred route the chiral ligand is introduced at first but the alternative route is more promising, since the first step was already described by the group of Toyama.^[134] Investigation of the product mixtures and analytical data of the target complex can be transferred onto the preferred route, after following the alternative route.

For the introduction of bipyridine **37** to the dmsocomplex **47** the same conditions as reported by Toyama's group, were chosen. Both complexes were heated in ethanol in the presence of DMSO for 1-2 hours. The thermodynamically most stable *cis*, *cis*-isomer of three possible isomers **50** was preferentially formed, in accordance to the reported results.^[134] However, the configuration of the complex is not relevant because the subsequent coordination to the coordinatively saturated complex **50** is supposed to proceed *via* a dissociative mechanism.



Scheme 6-48. Introduction of bipyridine **37** as first ligand on **47**.

Also the coordination of terpyridine **51** instead of bipyridine proceeded without any problems and resulted in a very good yield of 86% of **57**. This complex exists in two isomers in which the chloro ligands can occupy positions *trans* or *cis* to each other.



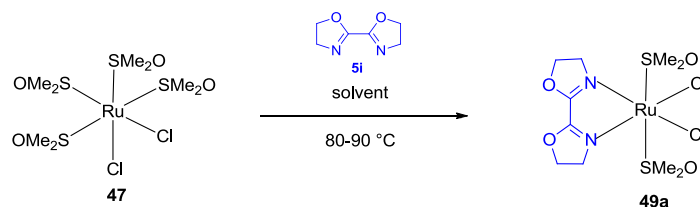
Scheme 6-49. Introduction of terpyridine **51** as first ligand on **47**.

The successful reaction conditions of the complexation of bipyridine and terpyridine were transferred to the coordination of a bisoxazoline ligand. Slightly varying conditions were screened to find suitable conditions resulting in full conversion and a pure product. The results of these test reactions are collected in Table 6-4. With 1 equivalent H-box ligand (**5i**), pure product was never obtained. In an ethanol/DMSO mixture, the starting material was found, too, after short reaction times up to 5 h (entries 1, 2 and 4). After a greatly extended reaction time of 24 h, only unidentified impurities were found in the reaction mixture (entry 5). With the amount of ligand being increased up to 1.5 equivalents, a very good result was obtained after a reaction time of 1 h (entry 6). The ¹H-NMR spectrum confirmed the clean formation of only one isomer. A reaction time extension about just half an hour led to the reformation of starting material (entry 7), which was supported by the results of the reaction after 2 h, in which also starting material was found. These results showed, how important a well adjusted reaction time is for the sensible box ligands. It seems likely, that the H-box (**5i**) ligand in these screening reactions was decomposed after successful coordination resulting in the reformation of the starting compound **47**.

The reaction conditions identified by the test screening (Table 6-4, entry 6) were applied on further coordinations of different oxazoline ligands (Scheme 6-50). One main problem appeared during these coordination experiments: It was not possible to identify most of the prepared complexes in their ¹H-NMR spectrum because of too many overlapping signals. Due to the high number of possible isomers it was also not clear if the crowded spectra were caused by many different product isomers or if they also showed impurities. The desired complexes were detected by ESI-HRMS, but this method allows no judgment concerning purity and quantity. Applying this method, an unexpected side product was detected. The complexes containing ¹Pr-pyrox (**10b**) and the tridentate ¹Pr-pybox (**36**) did not only

form their neutral bis-chloro complexes **49d** and **58** respectively, but also their cationic chloride complexes **57d** and **59**.

Table 6-4. Optimization of reaction conditions for the introduction of H-box (**5i**) to dmsoc complex **47**.^a

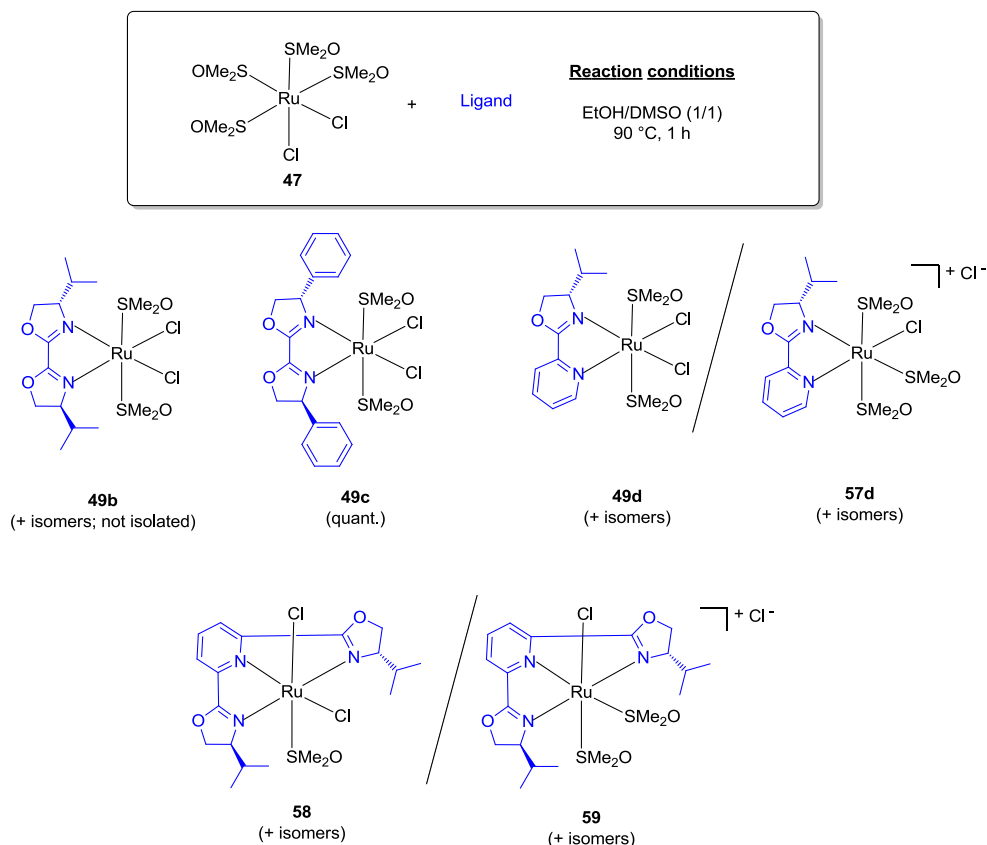


Entry	Equiv. 5i	Time [h]	Solvent	Result ^c		
				47	49a	Impurities
1	1.0	1.0	EtOH/DMSO ^b	×	×	
2	1.0	1.5	EtOH/DMSO ^b	×	×	
3	1.0	1.5	EtOH		×	×
4	1.0	1.5	EtOH/DMSO ^b	×	×	
5	1.0	24	EtOH/DMSO ^b			×
6	1.1	1.0	EtOH/DMSO ^b		× ^d	
7	1.1	1.5	EtOH/DMSO ^b	×	×	
8	1.1	2.0	EtOH/DMSO ^b	×	×	

^aReactions were carried out with [Ru(dmsoc)₂Cl₂] (**47**) (0.05 mmol) in 1 mL solvent. ^bEtOH/DMSO = 10/1 v/v. ^cDetermined by HRMS (ESI-TOF) and ¹H-NMR analysis. ^dThe product was obtained in 57% yield.

As already mentioned, ESI-HRMS is not suitable for quantification and the cationic complexes cause much stronger signals because they are already ionic compounds. Thus it is possible that they were only present in small amounts in the reaction mixtures. Among the prepared complexes, only the Ph-box complex **49c** was identified in its ¹H-NMR spectrum. A single isomer was formed, but the configuration could not be identified. It is possible that the relatively large residues of the applied ligand supports the preferred formation of only one isomer. Since it is known that the analogue complexes with bipyridine ligands can be separated by column chromatography using silica gel as stationary phase and water/MeCN mixtures with salt additives such as KNO₃, column chromatography was tested as suitable separation method for the different isomeric product mixtures. Different approaches using this method failed, until the attempt of preparative TLC analysis indicated decomposition of the complexes. It was already known from the ligand synthesis that the free oxazoline ligands decomposed very quickly after the elution from silica gel, it is possible that the same happened to them even though they were coordinated to a metal center. Also attempts to purify the

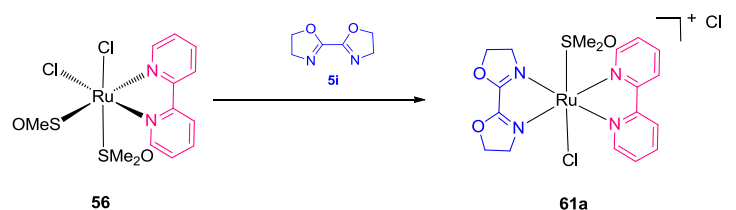
complexes by precipitation, failed because they were usually oily compounds. At least the neutral and monocationic complexes should have different solubility but this assumed behavior could not be used for purification.



Scheme 6-50. Results of the reaction of the dms complex **47** with different oxazoline ligands.

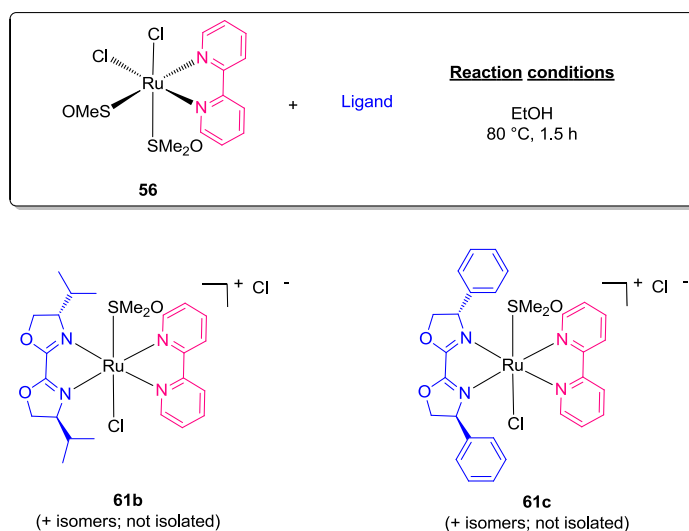
6.2.4 [Ru(dms)₄Cl₂] Precursor: Introduction of the Second Ligand

The reaction conditions for the introduction of a second ligand on the bipyridine complex **56** were evaluated using H-box (**5i**) as second ligand because it bears no stereocenter and therefore does not form enantiomeric structures. In addition, it has a minimum of steric hindrance. The results of the optimization are collected in Table 6-5. In chloroform and dichloromethane no product formation was observed (entries 1 and 2). In DMF and ethanol the reaction proceeded as expected, while the product mixture obtained from the reaction in ethanol after 1.5 h contained less impurities (entry 4). The product mixture could be purified by column chromatography over silica gel with a water/MeCN mixture as eluent. However, the product fraction still contained two inseparable isomers in a total yield of 48%. The products were always detected as the monocationic chloride complexes **61a**.

Table 6-5. Optimization of reaction conditions for the introduction of a second ligand.^a

Entry	Solvent	Time [h]	Result ^b
1	CHCl ₃	1.5	No product
2	DCM	1.5	No product
3	DMF	4	Product, many impurities
4	EtOH	1.5	Product, few impurities ^c

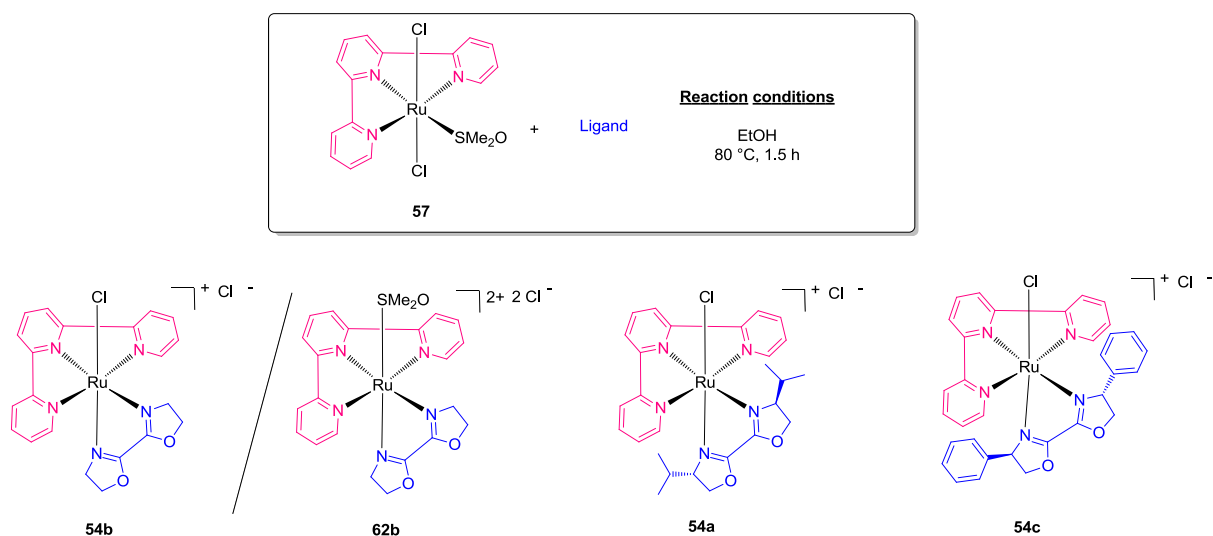
^aReactions were carried out under an argon atmosphere with [Ru(bpy)(dmsO)₂Cl₂] (**56**) (0.02 mmol) and H-box (**5i**) (0.02 mmol) in the respective solvent (5 mL). The reaction mixture was heated until the boiling point of the respective solvent. ^bAnalyzed by HRMS (ESI-TOF) and ¹H-NMR spectroscopy. ^cThe product **61a** was purified by column chromatography and obtained as isomer mixture of two isomers in 48% yield.

**Scheme 6-51.** Introduction of a box ligand as second ligand to the bipyridine complex **60**. The identities of the complexes were confirmed by HRMS. ¹H-NMR analysis failed due to too many overlapping signals in the corresponding spectra.

As depicted in Scheme 6-51, ¹Pr-box (**5b**) and Ph-box (**5h**) were also introduced as second ligand under the optimized reaction conditions. The resulting complexes **61b** and **61c** were also obtained as monocationic complexes as confirmed by HRMS. An interpretation of their ¹H-NMR spectra failed, because of too many overlapping signals. The complexes [Ru(box)(bpy)(dmsO)Cl]Cl (**49**) formed in maximum four different isomers which will lead to different signals in the proton NMR spectrum. The presence of the neutral [Ru(box)(bpy)Cl₂] (**50**) complex can also not be excluded, since it is harder to detect by ESI-MS. Signals originating from this complex can also complicate the ¹H-NMR spectrum.

Purification by column chromatography, as performed for complex **57**, was not successful because of inefficient separation of the different fractions. An anion exchange of the chloride of complex **61b** with PF_6^- (applied as KPF_6) in aqueous solution caused a spontaneous precipitation of an orange solid. The quality of the $^1\text{H-NMR}$ spectrum of this compound was slightly better than the one of the original complex, but still no interpretation was possible.

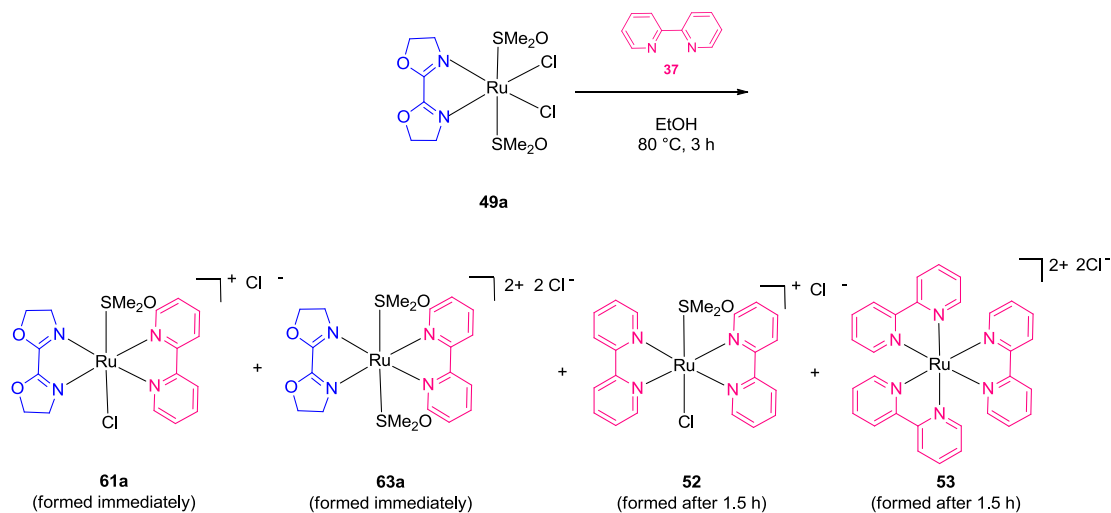
When the terpyridine complex **57** is applied as starting material for the coordination of a C_2 -symmetrical box ligand as second ligand, no structural isomer can be formed. However, complexations with three representative box ligands did not lead to the isolation of pure compounds (Scheme 6-52). In case of coordination with the H-box ligand (**5i**), remaining starting material was detected in the product mixture by $^1\text{H-NMR}$ spectroscopy. The product appeared as mixture of the monocationic complex **54b** and the dicationic complex **62b**. Both were precipitated from an aqueous solution by anion exchange for PF_6^- . The resulting PF_6^- complexes exhibited different retention times on silica gel with a water/MeCN mixture as eluent, but in the isolated fractions no product complex was left. It is possible that the ligand decomposed under the slightly acidic conditions on the silica gel. The other two complexes **54a** and **54c** were also detected by HRMS only. These two complexes did only form their monocationic versions but the proton NMR spectrum was still too crowded to identify the complexes. All further purification attempts failed.



Scheme 6-52. Introduction of a box ligand as second ligand to the terpyridine complex **57**. The identities of the complexes were confirmed by HRMS. $^1\text{H-NMR}$ analysis failed due to too many overlapping signals in the corresponding spectra.

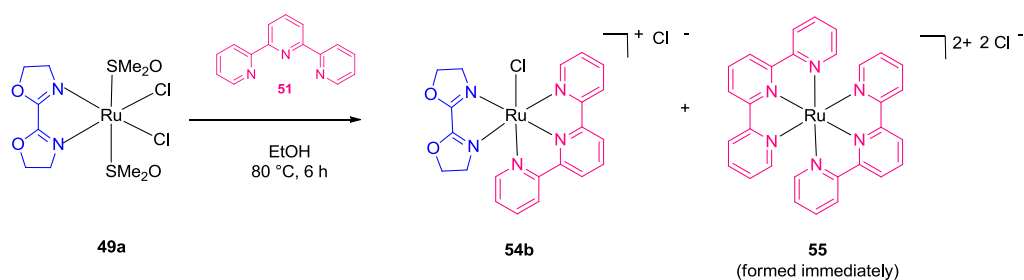
Despite the problematic work-up experienced during the last reactions, the H-box complex **49a** (Scheme 6-53 and Scheme 6-54) and the ^iPr -pybox complex **58** (Scheme 6-55) were reacted with a second ligand. As depicted in Scheme 6-53, several side products were identified in the reaction mixture of H-box complex **49a** and bipyridine **37**. The desired heteroleptic complex appeared as monocationic structure **61a** and dicationic structure **63a** which were formed a few minutes after the

reaction had started, as detected by ESI-HRMS. After approximately 1.5 h also the heteroleptic complexes **52** and **53** were formed. The starting material was not fully consumed during the whole reaction.



Scheme 6-53. Introduction of bipyridine (**37**) as second ligand to the H-box complex **49a**.

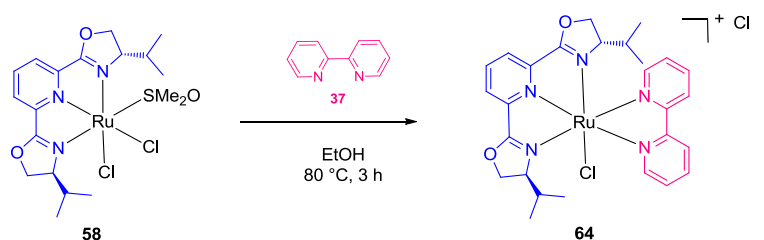
When terpyridine (**51**) was applied as second ligand, the homoleptic complex **55** was formed as well. In this case, it was detected from the beginning on. The desired heteroleptic complex **54b** appeared only in its monocationic form. As it was already investigated for the box-cymene complexes (cf. chapter 6.2.2), the box ligands appeared to be too weak to remain coordinated when bipyridine or terpyridine was present.



Scheme 6-54. Introduction of terpyridine (**51**) as second ligand to the H-box complex **49a**.

This behavior appeared to be different for the complexes **58** containing the tridentate ⁱPr-pybox ligand. As illustrated in Scheme 6-55, only one product was formed by its reaction with bipyridine **37**. The tridentate pybox ligand is obviously much stronger than the bidentate box ligands and therefore it was not substituted by bipyridine. However, the product complex **64** was still not pure enough to be

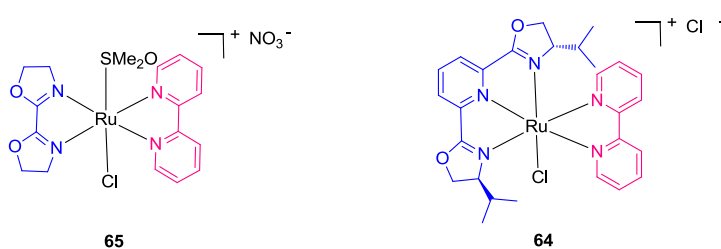
identified in the $^1\text{H-NMR}$ spectrum. The only evidence for this complex was obtained by HRMS analysis.



Scheme 6-55. Introduction of bipyridine (37) as second ligand to the ^iPr -pybox complex 58.

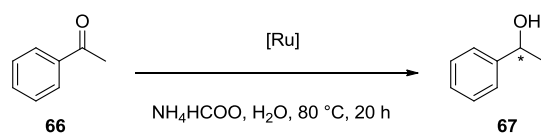
6.2.5 Initial Catalysis Experiments: Transferhydrogenation

Even though the complexation experiments (cf. chapter 6.2.1, 6.2.2, 6.2.3 and 6.2.4) turned out not to be very successful, two complexes were tested towards their catalytic activity in transfer hydrogenation. If catalytic activity of the new complexes was observed, further optimization of their preparation would be worthwhile. One of the most pure compounds that were tested is $[\text{Ru}(\text{H-box})(\text{bpy})(\text{dmsO})\text{Cl}]\text{Cl}$ **61a**. It was treated by an anion exchange during column chromatography with NO_3^- because KNO_3 was added to the eluent mixture and was therefore applied as $[\text{Ru}(\text{H-box})(\text{bpy})(\text{dmsO})\text{Cl}]\text{NO}_3$ **65**. The other one was the pybox complex $[\text{Ru}(^i\text{Pr-pybox})(\text{bpy})\text{Cl}]\text{Cl}$ **64** (Scheme 6-56).



Scheme 6-56. Complexes applied in test reactions for catalytic transferhydrogenation.

Acetophenone (**66**) was chosen as substrate, *iso*-propanol or ammoniumformate were chosen as hydrogen donors. The results were analyzed by GC-MS, which allows only for qualitative analysis. Catalytic activity for both complexes was found in an aqueous system with ammonium formate as donor while *iso*-propanol turned out to be an ineffective combination with the applied complexes. In the aqueous system, the complexes were applied in loadings from 0.5 to 3.0 mol% and reaction times of 20 h.



Scheme 6-57. Transfer hydrogenation on acetophenone using ammoniumformiate as donor. Complex **65** was applied in 0.5 and 3.0 mol% and **64** in 2.5 mol%. Product was observed in all three cases by GC-MS.

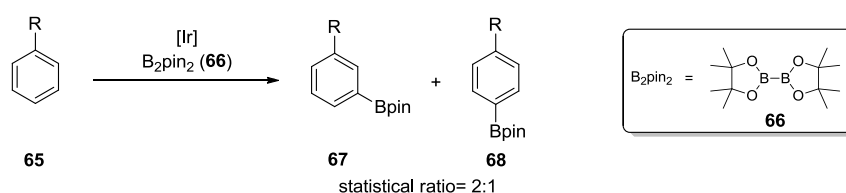
The obtained results are promising. For the tested complexes catalytic activity was observed and the next step should be the quantification of the catalytic results by a method such as GC-FID.

7 Catalysis

Contributions: Experimental help by Gisa Meissner (borylation), Silke Plachetta (borylation and (hydrido)silylether directed γ -C-H activation) and Alexander Erhard ((hydrido)silylether directed γ -C-H activation) under my supervision.

7.1 Aromatic Borylation

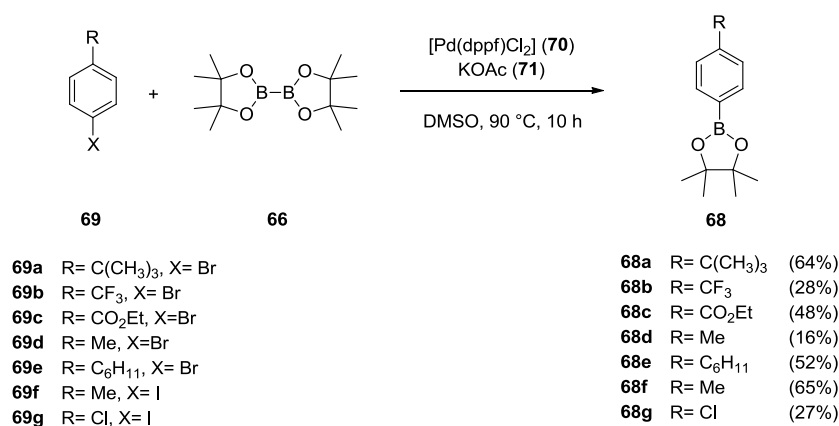
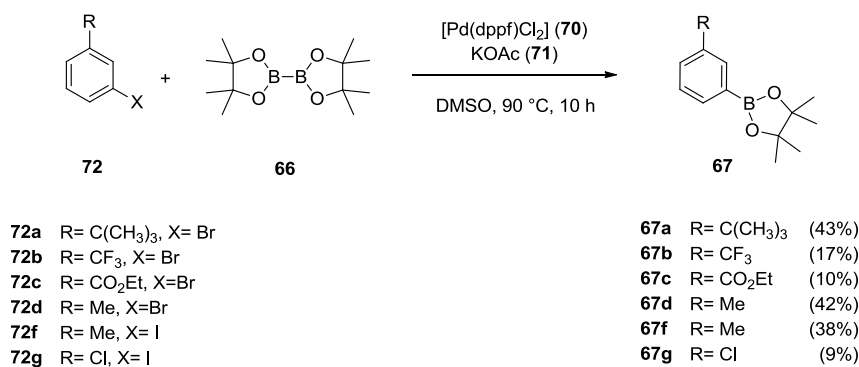
The aim of this project was to find out, how chiral ligands influence the regioselectivity of the borylation of monosubstituted arenes. Expected is a mono-borylation in the *meta* or *para* position, while *ortho* borylation is usually not occurring because the aromatic borylation is very sensitive towards steric influence (cf. chapter 4.1.1). Because two *meta* positions and only one *para* position are available, the statistical *meta:para* ratio is 2:1 (Scheme 7-1).



Scheme 7-1. Borylation of a monosubstituted arene **65**. The statistical ratio for *meta:para* substitution is 2:1. Due to steric hindrance, *ortho* borylation is not occurring.

7.1.1 Independent Synthesis of the Borylation Products

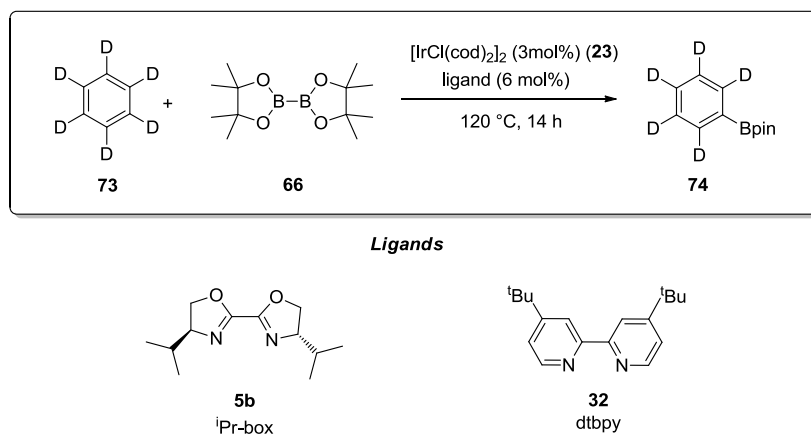
The expected borylation products were prepared independently for comparison of their analytical data with the catalytic reactions. The preparation was realized by a Pd(II) catalyzed coupling reaction of B_2pin_2 (**66**) with iodine or bromine substituted aromatic compounds, following a procedure reported by the Miyaura group.^[245] The reactions were carried out under elevated temperature for ten hours. In dependence of the residue, the yields in this reaction differed a lot, as depicted in Scheme 7-2 and Scheme 7-3. The applied halide seemed to play no role for the outcome of the reactions. Even though only small amounts of product could be isolated, reference $^1\text{H-NMR}$ spectra and GC-MS data of all prepared compounds were collected.

Scheme 7-2: Preparation of *para* substituted borylation products **68**.Scheme 7-3. Preparation of *meta* substituted borylation products **67**.

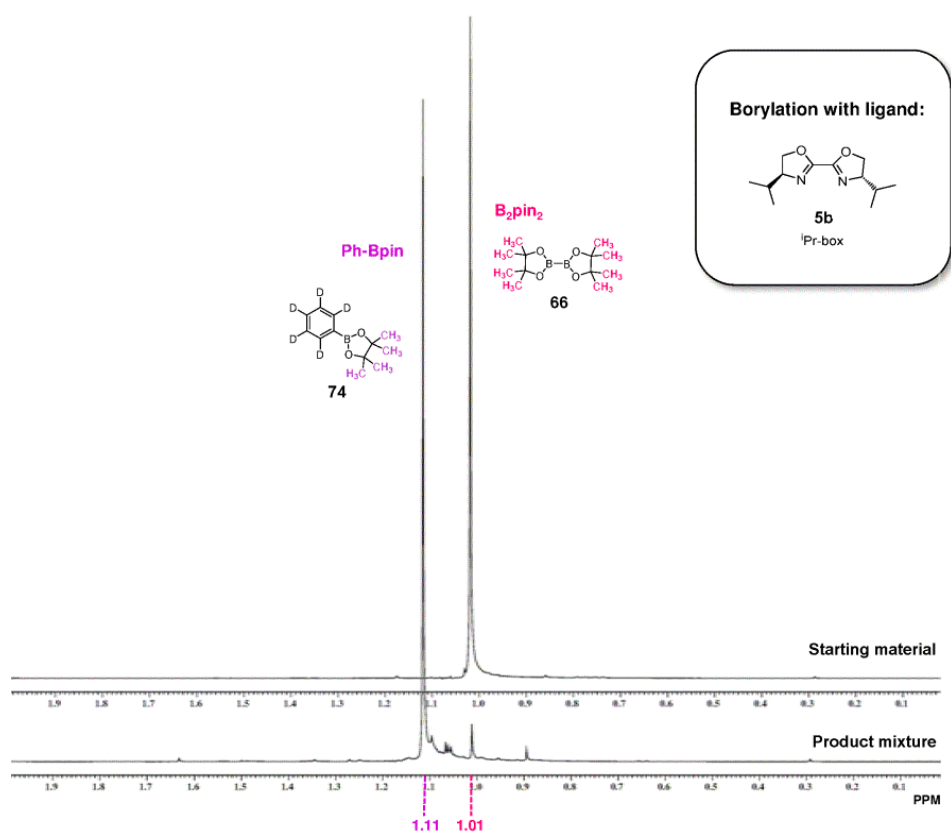
7.1.2 Borylation Experiments

Initially, the ⁱPr-box (**5b**)/[Ir(cod)(Cl)] (**23**) system was probed towards its reactivity in aromatic borylation. For the test reactions, deuterated benzene was used as substrate because it allowed an easy analysis of the crude reaction mixtures by ¹H-NMR spectroscopy. As reference ligand served 2,2'-(4,4'-di-*tert*-butyl)-bipyridine (dtbpy) (**32**) because it was described to be very active in such reactions (cf. chapter 4.1.1).

As illustrated in Scheme 7-5, the ¹H-NMR analysis revealed almost full conversion of B₂pin₂, when ⁱPr-box (**5b**) was applied as ligand. The NMR yield of the respective reaction using dtbpy (**32**) was comparable. Therefore, similar reactivity of both catalytic systems under the given conditions was assumed.



Scheme 7-4. Initial borylation experiments using ⁱPr-box (**5b**) as representative oxazoline ligand and dtbpy (**32**) as reference ligand. Both experiments led to product formation almost quantitatively.

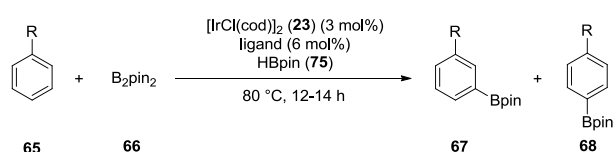


Scheme 7-5. ¹H-NMR spectra before and after the borylation reaction with ⁱPr-box (**5b**) as ligand. Nearly full conversion of B₂pin₂ (**66**) to Ph-Bpin (**74**) appeared. HBpin (**75**) has a chemical shift of 0.98 ppm and was not observed.

Because the general reactivity of ⁱPr-box (**5b**) was confirmed by the experiment with deuterated benzene, the substrate and ligand scope were investigated. Further box ligands bearing aliphatic

residues with different steric properties and one with a phenyl substituent were applied in the borylation of three different monosubstituted arenes. These reactions were carried out at 80 °C instead of 120 °, because test reactions showed that ⁱPr-box (**5b**) did not cause full conversion any more at temperatures of 80 °C and below. This was important, because the intention was to compare the different ligands toward their activity as well as selectivity. In addition, slower reactions can be more selective. The results are listed in Scheme 7-1.

Table 7-1. Borylation of different monosubstituted compounds with different box ligands.^a

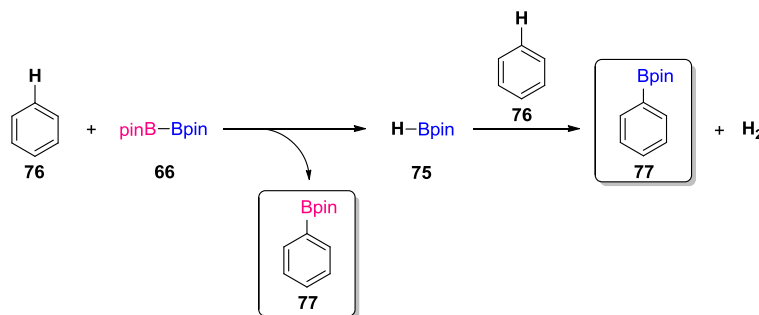


Entry	R	Ligand	m:p - ratio ^b	HBpin (66) ^c
1	Me	dtbpy (32)	2.0:1.0	yes
2	Me	ⁱ Pr-box (5b)	2.0:1.0	yes
3	Me	^t Bu-box (5c)	2.0:1.0	yes
4	Me	^{sec} Bu-box (5d)	2.0:1.0	yes
5	Me	Ph-box (5g)	2.0:1.0	yes
6	Cl	dtbpy(32)	3.3:1.0	yes
7	Cl	ⁱ Pr-box (5b)	3.3:1.0	yes
8	Cl	^t Bu-box (5c)	3.6:1.0	yes
9	Cl	^{sec} Bu-box (5d)	3.6:1.0	yes
10	Cl	Ph-box (5g)	3.0:1.0	yes
11	CF ₃	dtbpy(32)	2.6: 1.0	yes
12	CF ₃	ⁱ Pr-box (5b)	2.6: 1.0	yes
13	CF ₃	^t Bu-box (5c)	2.7: 1.0	yes
14	CF ₃	^{sec} Bu-box (5d)	3.4: 1.0	yes
15	CF ₃	Ph-box (5g)	2.2: 1.0	yes

^aReactions were carried out under argon atmosphere in flame-sealed NMR tubes with B₂pin₂ (**66**) (50 mg, 1 equiv.) in 1.0 mL of the respective substrate. ^bDetermined by ¹H-NMR spectroscopy. ^cIdentified in ¹¹B-NMR spectrum.

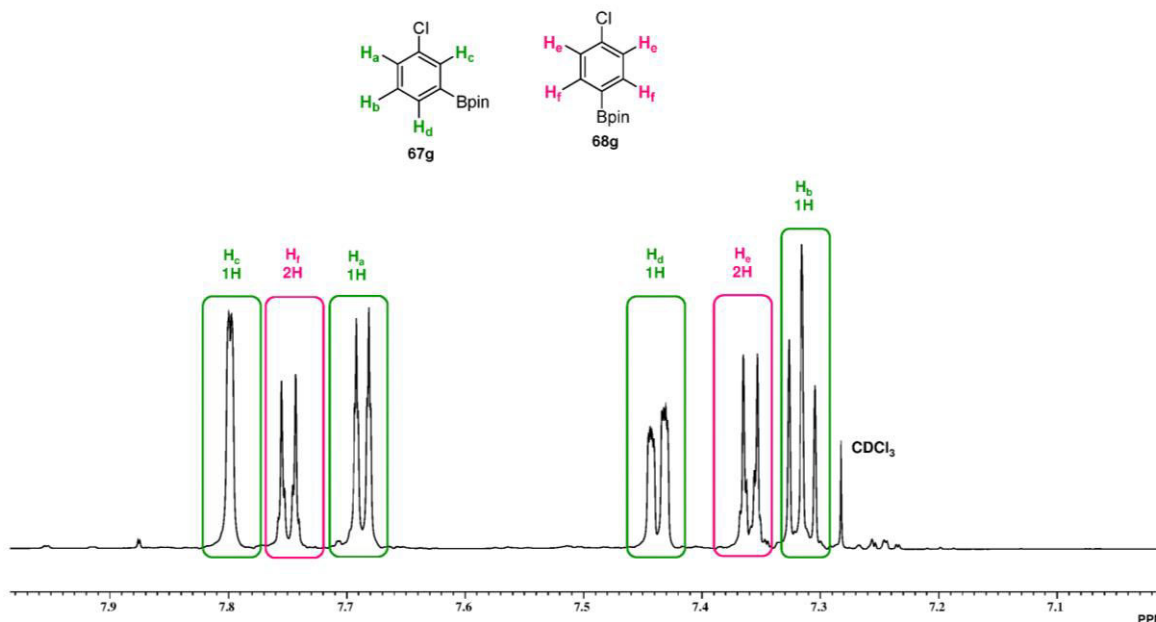
In case of toluene (**65d**) all ligands caused a statistical *meta:para* ratio of 2:1 (entries 1-5). For the chloro substituted substrate **65g** the non-chiral dtbpy (**32**) caused a ratio in which the *meta* position was slightly preferred (entry 6). This trend was maintained by the other ligands, while ^tBu-box (**5c**) showed with a ratio of 3.3:1.0 the highest preference for the *meta* position. Trifluorotoluene (**65b**) was also substituted with a preference for the *meta* position s, even though not as much as it was observed for

chlorobenzene (**65g**). For this substrate, the *sec*-butyl substituted box ligand **5d** showed with a 3.4:1.0 ratio the highest preference for the *meta* position (entry 14). In all reactions HBpin (**75**) was identified in the ^{11}B -NMR spectrum, indicating that not both equivalents of B_2pin_2 (**66**) were consumed (Scheme 7-6). It was not possible to identify the signal of B_2pin_2 (**66**) in the ^{11}B -NMR spectrum because its chemical shift is very similar to these of the borylated products **68** and **67**.



Scheme 7-6. Aromatic borylation with B_2pin_2 (**66**).

The determination of the *meta:para* ratio was performed by measuring the integrals of the corresponding ^1H -NMR signals in the aromatic region. As demonstrated on an example of borylated chlorotoluene **68g** and **67g**, these signals were usually well separated from each other and were therefore reliably integrated.



Scheme 7-7. ^1H -NMR-spectra of **68g** and **67g**. Shown is the aromatic region.

Because in some reactions only very small signals were found in the respective ^1H -NMR spectra, which made the determination of the *meta:para* ratio very difficult, some optimization with another iridium precursor and with the addition of an inert solvent were undertaken. The aim of these optimization reactions was to obtain a better conversion while keeping the temperature relatively low at

the same time. The results are listed in Table 7-2. Surprisingly, with dtbpy the best results were achieved with the chloro bridged iridium precursor **23** (entries 1 and 2). The addition of cyclohexane (**78**) as inert solvent led in one case to an increase (entry 2) and in another case to a decrease (entry 4) of the total yield. The *meta:para* ratios of all experiments with this ligand were the same. With application of the non-chiral H-box ligand (**5i**), this ratio was shifted with 2.5:1.0 a little bit more towards the statistical ratio (entries 5-6). For this ligand, the highest yield was achieved with the methoxy bridged precursor **79** (entry 6). In a similar reaction with the chloro bridged precursor **23**, the yield dropped from 72% to 49% (entry 7). For the application of the ⁿBu-box ligand (**5f**), similar results were observed (entries 8-10). The *meta:para* ratio caused by ⁿBu-box (**5f**) showed the same preference for the *meta* position as it was observed for dtbpy (**32**).

Table 7-2. Optimization of the catalytic system of aromatic borylation.^a



Entry	Ligand	X	Solvent ^b	Yield [%] ^c	meta [%] ^c	para [%] ^c	m:p - ratio ^c
1	dtbpy (32)	Cl	-	78	60	18	3.2:1.0
2	dtbpy (32)	Cl	CHex (78)	91	69	22	3.2:1.0
3	dtbpy (32)	OMe	-	76	57	19	3.2:1.0
4	dtbpy (32)	OMe	CHex (78)	47	36	11	3.3:1.0
5	H-box (5i)	Cl	CHex (78)	14	10	4	2.5:1.0
6	H-box (5i)	OMe	-	72	51	21	2.5:1.0
7	H-box (5i)	OMe	CHex (78)	49	35	14	2.4:1.0
8	ⁿ Bu-box (5f)	Cl	CHex (78)	30	24	6	4.0:1.0
9	ⁿ Bu-box (5f)	OMe	-	34	26	8	3.3:1.0
10	ⁿ Bu-box (5f)	OMe	CHex (78)	34	26	8	3.3:1.0

^aReactions were carried out under argon atmosphere in a flame-sealed NMR tube with B₂pin₂ (**66**) (50 mg, 1 equiv.). ^bReactions were carried out in 1.5 mL solvent (either the neat substrate or a 1:2 mixture substrate:CHex (**78**) (v/v)). ^cDetermined by ¹H-NMR relative to the internal standard TMB (**80**).

Even though the results obtained when using the chloro-bridged dimer **23** seemed to be promising, the ¹H-NMR spectra showed in some cases unidentified signals and the results of the reactions carried out using [Ir(cod)OMe]₂ (**79**) as iridium source were much better reproducible. Therefore, [Ir(cod)OMe]₂ (**79**) was chosen as precursor for the following experiments. For quantification, the internal NMR standard 1,2,3-trimethoxybenzene (TMB) (**80**) was not reliable enough, because the resulting solid,

which was obtained after the reaction work-up and that already contained the solid standard, did sometimes not dissolve completely in the deuterated solvent. Therefore it was not possible to judge if the standard was dissolved completely. As a better method, quantification by GC-FID was chosen for the following borylation experiments, because the analysis by this method was possible from the crude reaction mixture.

In Table 7-3, the catalysis results of the borylation of trifluorotoluene substrate (**65b**) in the presence of the different oxazoline ligands are listed, whereas in Table 7-4, the respective results using different bipyridine, phox, pybox and some more ligands are shown. The reactions were carried out in neat solvent. The reaction volume was with 0.8 mL chosen to be smaller than in previous experiments, aiming for a higher B₂pin₂ (**66**) concentration.

A blank sample without any added ligand led to only 17% conversion of B₂pin₂ (**66**), indicating the necessity of a ligand for the formation of an active catalyst (Table 7-4, entry 15). Consequently, it can be assumed that the observed differences in reactivities were brought about by the respective ligands. In the reported reactions, the symmetrical standard ligand dtbpy (**32**) led to a *meta:para* ratio of 3.0:1.0, which means that the *meta* position was slightly preferred in comparison with the expected statistical ratio of 2:1 (Table 7-4, entry 1). As expected, by application of this ligand full conversion of B₂pin₂ (**66**) was achieved. Other, unsymmetrically substituted bipyridines also resulted in full conversion and a *meta:para* ratio of approximately 3:1 (Table 7-4, entries 2-5). However, the preference for the *meta*-position was somewhat more pronounced for the bipyridines bearing activating amine and amide substituents **81** and **83** (Table 7-4, entries 2 and 4) than for the deactivating ester and nitrile substituents **82** and **84** (Table 7-4, entries 3 and 5). The conversions were quantitative for all bipyridines and no residual HBpin (**75**) was identified in the ¹¹B-NMR spectrum. The unsubstituted H-box ligand (**5i**) showed a result similar to that one obtained by dtbpy (**32**) (Table 7-3, entry 21). The application of all other box-ligands gave full conversions as well, except for three cases in which still high conversions of above 90% were obtained (Table 7-3, entries 15, 17 and 23). One of the less activating ligands is the *tert*-butyl substituted **5c**, which might be due to too high steric hindrance (Table 7-3, entry 17). The *meta:para* ratios are around 3.0:1.0 in nearly all cases, when box ligands were applied. Only the Ph-box (**5g**) caused with 2.1:1.0 a ratio close to the statistical ratio (Table 7-3, entry 16). The *iso*-butyl substituted box ligand (**5e**) shows a *meta:para* ratio of 3.5:1.0 under the box ligands to the highest preference for the *meta*-position (Table 7-3 entry 18). Applying the pyrox **10**, mepyrox **19** and quinox **20** ligands resulted in full conversions (Table 7-3, entries 1-13). Moreover, when the ⁱPr-quinox (**20b**) was applied with a catalyst loading of only 0.35 mol%, the reaction reached full conversion without any HBpin signals detected by ¹¹B-NMR (Table 7-3, entry 11). The pyrox-type ligands caused a somewhat stronger preference for borylation in the *meta* position. Especially ⁱPr-quinox (**20b**) and Bn-pyrox (**10h**) led to a relatively high *meta:para* ratios of 4.3:1.0 and 4.0:1.0, respectively (Table 7-3, entry 9 and 4). The phenyl substituted ligands **10g**, **19g**, **20g** and **5g** showed the lowest preference for the *meta* position (Table 7-3, entries 2, 6, 12 and 16). For this substitution pattern, *ortho*-metallation on the ligand should be taken into account as unwanted side-reaction.

Results and Discussion

Table 7-3. Ligand screening for borylation of trifluorotoluene (**65b**): Box (**5**), pyrox (**10**), mepyrox (**19**) and quinox (**20**) ligands.^a



Entry	Ligand	Cat.-loading [mol%] ^b	<i>m:p</i> .ratio ^c	Conv. [%] ^d	HBpin ^e
1	iPr-pyrox (10b)	3	3.0 : 1.0	100	no
2	Ph-pyrox (10g)	3	3.0 : 1.0	100	no
3	ⁿ Bu-pyrox (10f)	3	3.8 : 1.0	100	no
4	Bn-pyrox (10h)	3	4.0 : 1.0	100	no
5	iPr-mepyrox (19b)	3	2.7 : 1.0	100	no
6	Ph-mepyrox (19g)	3	2.8 : 1.0	100	no
7	ⁿ Bu-pyrox (19f)	3	3.8 : 1.0	100	no
8	Bn-pyrox (19h)	3	3.3 : 1.0	100	no
9	iPr-quinox (20b)	3	4.3 : 1.0	100	no
11	iPr-quinox (20b)	0.35	3.6 : 1.0	100	no
12	Ph-quinox(20g)	3	2.6 : 1.0	100	no
13	ⁿ Bu-quinox (20f)	3	3.3 : 1.0	100	no
14	iPr-box (5b)	3	3.7 : 1.0	100	-
15	iPr-box (5b)	0.35	3.8 : 1.0	87	yes
16	Ph-box (5g)	3	2.1 : 1.0	100	yes
17	^t Bu-box (5c)	3	3.1 : 1.0	94	yes
18	ⁱ Bu-box (5e)	3	3.5 : 1.0	100	no
19	ⁿ Bu-box (5f)	3	3.0 : 1.0	100	yes
20	Bn-box (5h)	3	3.2 : 1.0	100	no
21	H-box (5i)	3	2.9 : 1.0	100	no
22	Me-box (5a)	3	3.4 : 1.0	100	yes
23	^{sec} Bu-box (5d)	3	3.3 : 1.0	99	no

^aReactions were carried out in sealed NMR tubes with B₂pin₂ (**66**) (50.0 mg, 1 equiv.) and 1.0 mL of neat substrate. After the reaction was finished, 50 μL n-Dodecane was added as GC-standard. ^b[Ir(cod)(OMe)]₂ (**79**) (2.77 mg, 3 mol% or 0.46 mg 0.35 mol%) and ligand (6 mol% or 0.7 mol%). ^cDetermined by ¹H-NMR. ^dDetermined by GC-FID. ^eDetermined by ¹¹B-NMR.

Table 7-4. Ligand screening for borylation of trifluorotoluene (**65b**): Bipyridine and miscellaneous ligands.^a

Reaction scheme: **65b** (trifluorotoluene) reacts with $[\text{Ir}(\text{cod})\text{OMe}]_2$ (**79**) (3 mol%), ligand (6 mol%), and B_2pin_2 (**66**) at 80 °C, 14 h to yield **67b** (3-boryl-1-(trifluoromethyl)benzene) and **68b** (4-boryl-1-(trifluoromethyl)benzene).

Entry	Ligand	<i>m:p</i> ratio ^b	Conv. [%] ^c	HBpin ^d
1	Dtbpy (32)	3.0 : 1.0	100	no
2	NH_2 -bpy (81)	3.3 : 1.0	100	no
3	COOMe-bpy (82)	2.5 : 1.0	100	no
4	MeCONH-bpy (83)	3.2 : 1.0	100	no
5	NC-bpy (84)	2.7 : 1.0	100	no
6	<i>i</i> Pr-diamide (85)	-	52	yes
7	Ph-diamide (86)	2.3 : 1.0	59	yes
8	ⁿ Bu-diamide (87)	2.3 : 1.0	54	yes
9	Ph-phox (40)	2.0 : 1.0	76	yes
10	<i>i</i> Pr-pybox (36)	3.1 : 1.0	100	no
11	Pybenzim (42)	2.7 : 1.0	100	no
12	P-py (88)	2.7 : 1.0	32	yes
13	Me_2 -Ph-box (89)	2.4 : 1.0	90	yes
14	Pyrim (41)	3.2 : 1.0	100	no
15	-	- ^e	17	no

^aReactions were carried out in sealed NMR tubes with B_2pin_2 (**66**), (50.0 mg, 1 equiv.) $[\text{Ir}(\text{cod})\text{OMe}]_2$ (**79**) (2.77 mg) and 1.0 mL of neat substrate. After the reaction was finished, 50 μL *n*-Dodecane was added as GC-standard. ^bDetermined by ¹H-NMR. ^cDetermined by GC-FID. ^dDetermined by ¹¹B-NMR.

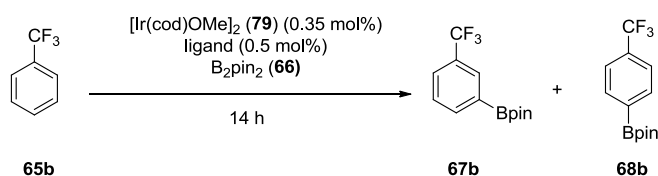
Using open chained box-precursors **85**, **86** and **87** resulted in conversions of around 50% and, if detectable, a nearly statistical *meta:para* ratio (Table 7-4, entries 6-8). Other bidentate N^N ligands did also cause full conversion and a *meta:para* ratios around 2.5:1.0 (Table 7-4, entries 12 and 13). In comparison to oxazolin ligands, the structurally related pybox and methylene-box ligands showed interesting results. While the tridentate pybox (**36**) (Table 7-4, entry 10) still led to full conversion without any traces of HBpin (**75**) and a *meta:para* - ratio similar to the dtbpy (**32**) (Table 7-4, entry 1) and H-box (**5i**) (Table 7-3, entry 21), the methylene bridged box ligand (**89**) did not lead to full conversion (Table 7-4, entry 13). It still gave a high conversion of 90%, but the lowest of all oxazolin type ligands. The *meta:para* ratio caused by this ligand was very close to the statistical distribution (Table 7-4, entry 13). This result might be interpreted such that the flexibility of the methylene bridged **89** leads to a larger bite angle causing too high steric hindrance of the complex which might make the formation of the catalytic active complex unfavorable. Since the box-type ligand systems caused in most cases full conversion, two experiments were repeated with 0.35 mol% instead of 3 mol% catalyst loading (Table 7-3, entry 11 and 15). In these reactions, differences caused by the box **5b** and the quinox **20b** ligands became detectable. Using the quinox ligand system full conversion was achieved, while the box ligand showed a limit of 87% conversion of B₂pin₂ (**66**). In case of the box ligand, the *meta:para* ratio remained the same as in the reaction with a higher catalyst loading, but in case of the quinox ligand a decrease from 4.3:1.0 to 3.6:1.0 was detected.

In summary, the catalytic systems with pyrox **10**, mepyrox **19** and quinox **20** ligands were the most promising ones. These ligands offered the best compromise between the good coordination ability of the aromatic pyridines and the chiral moiety of the bisoxazolines. It is remarkable, that the reaction was not inhibited by the substituents in the 6-position of the mepyrox and quinox ligands, as it was reported for symmetrical 6,6'-substituted bipyridines (cf. chapter 4.1.1).^[1] Besides, the promising results using tridentate pybox **36** ligands make further investigation of this catalytic system desirable. Therefore in following experiments the focus laid on pyrox **10**, mepyrox **19** quinox **20** and pybox **36**.

In the next reactions, the temperature was further decreased to possibly increase the selectivity of the applied ligands. Table 7-5 shows the results obtained from the borylation of trifluorotoluene (**65b**) at 70 °C and at room temperature (entries 13 and 14). Aromatic borylation with bipyridines and phenanthrolines as ligands was already reported to be proceeding at room temperature (cf. chapter 4.1.1)^[1]. Here, the two pyrox ligands **10f** and **10b** were investigated towards their reactivity at room temperature and in both cases conversions of 90% and higher were achieved, while the combined yields of product **68b** and **67b** were relatively low, 31% and 45%, respectively. These yields represent the conversion of approximately one equivalent of boron reagent **66** into the aromatic product. Considering the reactions carried out at 70 °C (entries 1-12), more than one boron equivalent was converted into product, except for when box ligands **5f** (entry 4), **5b** (entry 5), **5g** (entry7), **5d** (entry 8) and **5i** (entry 9) were applied. These results are in accordance with those listed in Table 7-3, where the application of box ligands also resulted in less active catalytic systems. The *meta:para* ratios were in

all experiments approximately 3.0:1.0, showing a slight preference for borylation in the *meta*-position. The highest *meta*-preference, 3.5:1.0, was obtained at room temperature for both applied ligands, indicating that lowering the temperature did lead to higher selectivity.

Table 7-5. Borylation of trifluorotoluene (**65b**) with different oxazoline ligands at 70 °C and room temperature.^a



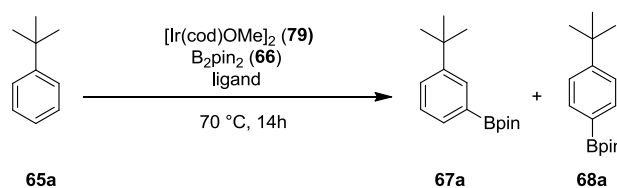
Entry	Ligand	Temp. [°C]	<i>m:p</i> ratio ^b	Conv. [%] ^c	Yield [%] ^c	HBpin ^d
1	ⁿ Bu-pyrox (10f)	70	3.3 : 1.0	100	87	no
2	ⁿ Bu-mepyrox (19f)	70	2.8 : 1.0	100	87	no
3	ⁿ Bu-quiniox (20f)	70	2.8 : 1.0	99	80	yes
4	ⁿ Bu-box (5f)	70	2.6 : 1.0	84	28	yes
5	ⁱ Pr-box (5b)	70	2.7 : 1.0	79	34	yes
6	ⁱ Pr-quiniox (20b)	70	2.7 : 1.0	100	86	no
7	Ph-box (5g)	70	2.0 : 1.0	90	42	yes
8	^{sec} Bu-box (5d)	70	2.9 : 1.0	96	52	yes
9	H-box (5i)	70	2.5 : 1.0	100	33	yes
10	ⁱ Pr-pyrox (10b)	70	3.0 : 1.0	100	84	no
11	ⁱ Pr-mepyrox (19b)	70	3.0 : 1.0	100	81	no
12	ⁱ Pr-pybox (36)	70	2.3 : 1.0	100	79	yes
13	ⁿ Bu-pyrox(10f)	r.t.	3.5 : 1.0	90	31	no
14	ⁱ Pr-pyrox (10b)	r.t.	3.5 : 1.0	99	45	no

^aReactions were carried out in sealed NMR tubes with B₂pin₂ (**66**), (50.0 mg, 1 equiv.)[Ir(cod)(OMe)]₂ (**79**) (0.46 mg) and 0.8 mL of neat substrate. After the reaction was finished, 50 μL *n*-Dodecane was added as GC-standard. ^bDetermined by ¹H-NMR. ^cCombined yield for **67b** and **68b** were determined by GC-FID. ^dDetermined by ¹¹B-NMR.

In Table 7-6 results for the borylation of *tert*-butylbenzene (**65a**) at different temperatures and different catalyst loadings are presented. In these experiments, no GC calibrations for the products **67a** and **68a** were prepared and only the conversions of B₂pin₂ (**66**) were determined. The reactions were carried out applying temperature/catalyst loadings as follows: (1) 70 °C/2.1 mol%, (2) 60 °C/2.1 mol% and (3) 70 °C/0.35 mol%. A clear trend considering selectivity and conversion in these reactions could not be observed. Except for four examples, in which the differences in conversions between 70 °C and 60 °C with the same catalyst loadings were only minimal, while the yield usually dropped when a lower catalyst loading was applied (entries 3-6, 8, 11 and 12). In the other five experiments, the conversions stayed quantitatively (entries 1, 2 and 10) or increased slightly, compared to the reaction carried out with higher catalyst loading (entry 7). Quantitative conversions were achieved when using dtbpy (**32**),

ⁿBu-pyrox (**10f**) and ⁱPr-pyrox (**10b**) ligands. A preference for the *para*-position was observed in most cases, except for when ⁿBu-pyrox (**10f**) and ⁱPr-pyrox (**10b**) ligands and low catalyst loadings were applied (entries 2 and 10). Using lower catalyst loadings, in six cases the preference for the *para*-position decreased slightly (entries 1-3, 8, 10 and 12), in four cases it stayed the same (entries 4, 6, 9 and 11) and in two cases it increased (entries 5 and 7) relative to reactions when higher catalyst loadings were used. However, these differences were usually only minimal and no influence of the type of ligand could be identified, the changes in selectivity were rather random.

Table 7-6. Borylation of *tert*-butylbenzene (**65a**) with oxazoline ligands.^a



Entry	Ligand	70 °C, 2.1 mol% [Ir]		60 °C, 2.1 mol% [Ir]		60 °C, 0.35 mol% [Ir]	
		<i>m:p</i> ^b	Conv. [%] ^c	<i>m:p</i> ^b	Conv. [%] ^c	<i>m:p</i> ^b	Conv. [%] ^c
1	dtbpy (32)	1.4 : 1.0	100	1.3 : 1.0	100	1.5 : 1.0	100
2	ⁿ Bu-pyrox (10f)	1.7 : 1.0	100	2.0 : 1.0	100	2.3 : 1.0	100
3	ⁿ Bu-mepyrox (19f)	0.6 : 1.0	55	0.3 : 1.0	65	1.2 : 1.0	40
4	ⁿ Bu-quiniox (20f)	1.7 : 1.0	78	0.7 : 1.0	85	1.7 : 1.0	47
5	ⁿ Bu-box (5f)	1.2 : 1.0	49	0.7 : 1.0	43	1.0 : 1.0	24
6	ⁱ Pr-box (5b)	1.0 : 1.0	47	0.5 : 1.0	51	1.0 : 1.0	30
7	ⁱ Pr-quiniox (20b)	2.0 : 1.0	83	0.8 : 1.0	80	0.2 : 1.0	95
8	Ph-box (5g)	1.0 : 1.0	64	1.6 : 1.0	40	1.5 : 1.0	32
9	H-box (5i)	0.5 : 1.0	40	0.4 : 1.0	37	0.6 : 1.0	45
10	ⁱ Pr-pyrox (10b)	1.5 : 1.0	100	1.6 : 1.0	100	3.3 : 1.0	100
11	ⁱ Pr-mepyrox (19b)	0.1 : 1.0	63	0.8 : 1.0	62	0.3 : 1.0	32
12	ⁱ Pr-pybox (36)	0.3 : 1.0	55	1.0 : 1.0	33	0.8 : 1.0	21

^aReactions were carried out in sealed NMR tubes with B₂pin₂ (**66**), (50.0 mg, 1 equiv.) [Ir(cod)(OMe)]₂ (**79**) (0.46 mg) and 0.8 mL of neat substrate. After the reaction was finished, 50 μL *n*-Dodecane was added as GC-standard. ^bDetermined by ¹H-NMR. ^cDetermined by GC-FID.

For the borylation of cyclohexylbenzene (**65e**), conversions and *meta:para* ratios were investigated as listed in Table 7-7. Similarly to the results obtained when using *tert*-butylbenzene as substrate (**65a**) (see Table 7-6), ⁿBu-pyrox (**10f**) and ⁱPr-pyrox (**10b**) were the only oxazoline ligands resulting in full conversion in the borylation of cyclohexylbenzene (entries 2 and 11). Regarding the other ligands, no trend was observed. For this substrate, a preference for *para* substitution was observed with *meta:para*

– ratios of 1.5:1.0. Only when applying ^{sec}Bu-box (**5d**) ligand in the catalytic system, *meta* preference with a *meta:para* ratio of 2:1 was observed (entry 9).

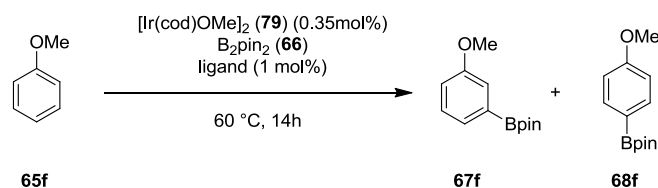
Table 7-7. Borylation of cyclohexylbenzene (**65e**) using oxazoline ligands.^a



Entry	Ligand	<i>m:p ratio</i> ^b	Conv.[%] ^c
1	dtbpy (32)	1.4 : 1.0	21
2	ⁿ Bu-pyrox (10f)	1.5 : 1.0	100
3	ⁿ Bu-mepyrox (19f)	1.4 : 1.0	30
4	ⁿ Bu-quiniox (20f)	1.2 : 1.0	37
5	ⁿ Bu-box (5f)	1.4 : 1.0	32
6	ⁱ Pr-box (5b)	1.4 : 1.0	36
7	ⁱ Pr-quiniox (20b)	0.8 : 1.0	45
8	Ph-box (5g)	1.8 : 1.0	17
9	^{sec} Bu-box (5d)	2.2 : 1.0	-
10	H-box (5i)	1.8 : 1.0	46
11	ⁱ Pr-pyrox (10b)	1.8 : 1.0	100
12	ⁱ Pr-mepyrox (19b)	1.3 : 1.0	18
13	ⁱ Pr-pybox (36)	1.6 : 1.0	10

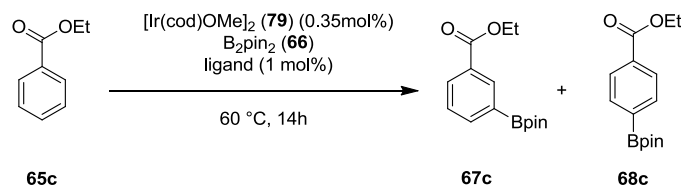
^aReactions were carried out in sealed NMR tubes with B₂pin₂ (**66**), (50.0 mg, 1 equiv.) [Ir(cod)(OMe)]₂ (**79**) (0.46 mg) and 0.8 mL of neat substrate. After the reaction was finished, 50 μL *n*-Dodecane was added as GC-standard. ^bDetermined by ¹H-NMR. ^cDetermined by GC-FID.

Since the previously discussed borylation already indicated a substrate induced selectivity without any influence of the applied ligand, for anisol (**65f**) and ethylbenzoate (**65c**) only very few experiments were conducted (Table 7-8 and Table 7-9). The observed *meta:para* selectivity indicates a substrate specific product distribution, since anisol (**65f**) was substituted with a high preference in the *meta* position while for ethylbenzoate (**65c**) the opposite was observed. For these two substrates the yields of the products as well as conversions were determined.

Table 7-8. Borylation of anisol (**65f**) using oxazoline ligands.^a

Entry	Ligand	<i>m:p</i> ratio ^b	Conv. [%] ^c	Yield [%] ^c
1	dtbpy (32)	4.0 : 1.0	100	15
2	ⁿ Bu-pyrox (10f)	4.0 : 1.0	100	8
3	ⁿ Bu-mepyrox (19f)	3.7 : 1.0	56	5
4	ⁿ Bu-quinox (20f)	4.0 : 1.0	77	11
5	ⁱ Pr-quinox (20b)	3.2 : 1.0	81	5
6	H-box (5i)	3.5 : 1.0	93	10

^aReactions were carried out in sealed NMR tubes with B₂pin₂ (**66**), (50.0 mg, 1 equiv.) [Ir(cod)(OMe)₂] (**79**) (0.46 mg) and 0.8 mL of neat substrate. After the reaction was finished, 50 μL *n*-Dodecane was added as GC-standard. ^bDetermined by ¹H-NMR. ^cDetermined by GC-FID.

Table 7-9. Borylation of ethylbenzoate (**65c**) using oxazoline ligands.^a

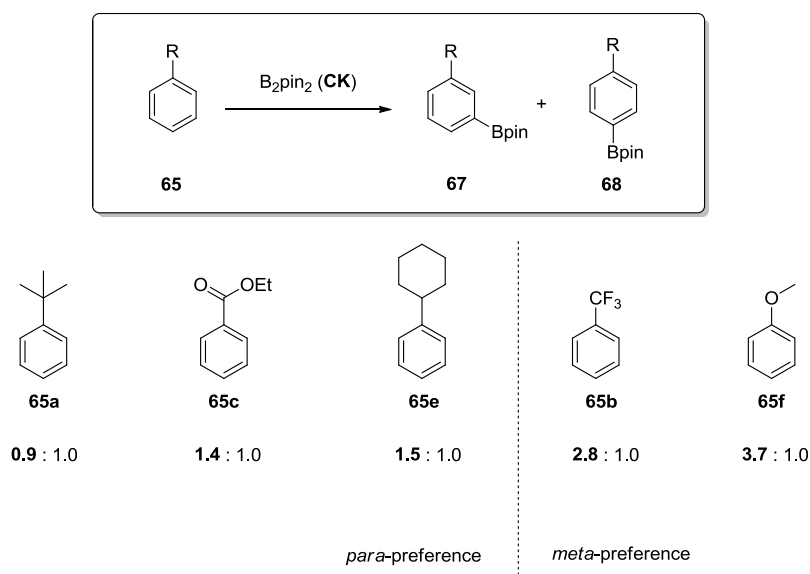
Entry	Ligand	<i>m:p</i> ratio	Conv. [%]	Yield [%]
1	dtbpy (32)	1.3 : 1.0	100	11
2	ⁿ Bu-pyrox (10f)	1.4 : 1.0	100	8
3	ⁿ Bu-mepyrox (19f)	1.3 : 1.0	83	6
4	ⁿ Bu-quinox (20f)	1.2 : 1.0	100	7
5	ⁱ Pr-quinox (20b)	1.6 : 1.0	100	6
6	H-box (5i)	1.3 : 1.0	100	10

^aReactions were carried out in sealed NMR tubes with B₂pin₂ (**66**), (50.0 mg, 1 equiv.) [Ir(cod)(OMe)₂] (**79**) (0.46 mg) and 0.8 mL of neat substrate. After the reaction was finished, 50 μL *n*-Dodecane was added as GC-standard. ^bDetermined by ¹H-NMR. ^cDetermined by GC-FID.

Despite the high conversions of about 90%, for both substrates only extremely low yields of about 10% were observed, indicating a consumption of B₂pin₂(**66**) for the formation to an unidentified product. It

might be possible that a polymeric, or at least insoluble, structure was formed that was removed upon filtration of the reaction mixture or that numerous different unidentified side products were produced in small amounts. Similar results were obtained in the aliphatic borylation (cf. chapter 7.2), when B_2pin_2 (**66**) was consumed with high conversions, while hardly any product was formed. Control reactions indicated the importance of the presence of catalytic amounts of iridium for the B_2pin_2 (**66**) consumption. Since the different ligands led to very different conversions, it can also be assumed that the presence of ligand is important for the unknown reaction as well.

In conclusion, for two substrates no yield could be determined and two substrates showed a very high difference between conversions and actual yields. Only for trifluorotoluene (**65b**) (Table 7-5), reasonable yields were obtained. Consequently, a discussion of the relative activity caused by the different ligands is not possible. However, the average selectivities for the different investigated substrates were quite consistent and are summarized in Scheme 7-8. For *tert*-butylbenzene (**65a**), ethylbenzoate (**65c**) and cyclohexylbenzene (**65e**) a preference for the *para* position was found and for trifluorotoluene (**65b**) as well as for anisol (**65f**) the opposite, a preference for a substitution of the *meta* position was observed. An electronic reason for this behavior, as it is known from electrophilic aromatic substitution, is very unlikely. The substrates for which a *meta* preference was observed, have both an electron withdrawing inductive effect, but the methoxy group of anisol (**65f**) can also donate electron mesomerically, which is supposed to be stronger than an inductive effect. The obvious difference for the identified preferences in *meta:para* selectivity can simply be found in the steric hindrance of the substituent on the respective arene. The highest steric hindrance is caused by the *tert*-butyl residue in *tert*-butylbenzene (**65a**), for which the highest *para* preference was observed, followed by the ethylester and cyclohexyl substituted benzene. For substrates with comparable small residues, such as trifluoromethyl and methoxyl, the *meta* position can be substituted with preference.

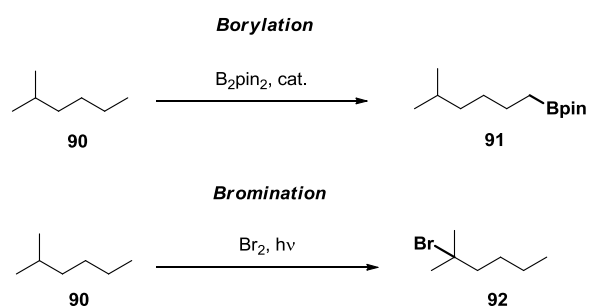


Scheme 7-8. Overview of average *meta:para* ratios in aromatic borylation of monosubstituted arenes (**65**).

Since the regioselectivity of borylation of monosubstituted arenes was found to be strictly substrate induced, these reactions were not investigated in further detail. In summary, using trifluorotoluene as substrate (**65b**), the box ligands caused lower conversions and yields than the pyrox-type ligands in each case and all oxazoline ligands were not as effective as the usually applied dtbpy (**32**). Interestingly, the substituents in the 6-position or 9-position in the mepyrox **19** and quinox **20** ligands and pybox **36** did not inhibit the reaction, while for the methylene bridged box **89** a decrease in reactivity was observed. 6,6'-substituted bipyridines were reported to be completely inadequate for aromatic borylation.^[1] These findings indicate, that only steric and ligand strengths is decisive for the success of the reaction while the selectivity is determined by the substrate only.

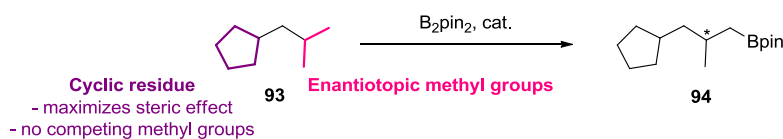
7.2 Aliphatic Borylation

Encouraged by results of the Hartwig group who reported successful aliphatic borylation of *n*-octane with the catalytic system^[186] developed for aromatic borylation consisting of [Ir(cod)Cl]₂/N,N-ligand, aliphatic borylation was as well investigated with the oxazoline ligands. Since borylation is due to steric reasons selectively occurring in terminal positions, the functionalization with boronic acid esters allows for the further functionalization of C-H bonds that are not activated. As example for such a procedure, halogenation by radical mechanism leads to the functionalization of C-H bonds on high substituted carbon atoms (Scheme 7-9).



Scheme 7-9. Borylation and radical bromination activate contrary kinds of C-H bonds.

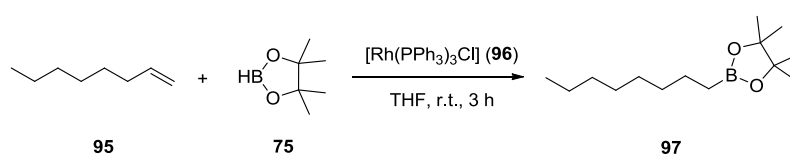
When aromatic borylation is performed with chiral ligands, the catalyst might be able to differentiate between two prochiral methyl groups. Such a substrate requires, besides these methylene groups, only methylene groups in other residues or strongly blocked methyl groups to ensure that no competing methyl groups present. A suitable substrate fulfilling these requirements is depicted in Scheme 7-10.



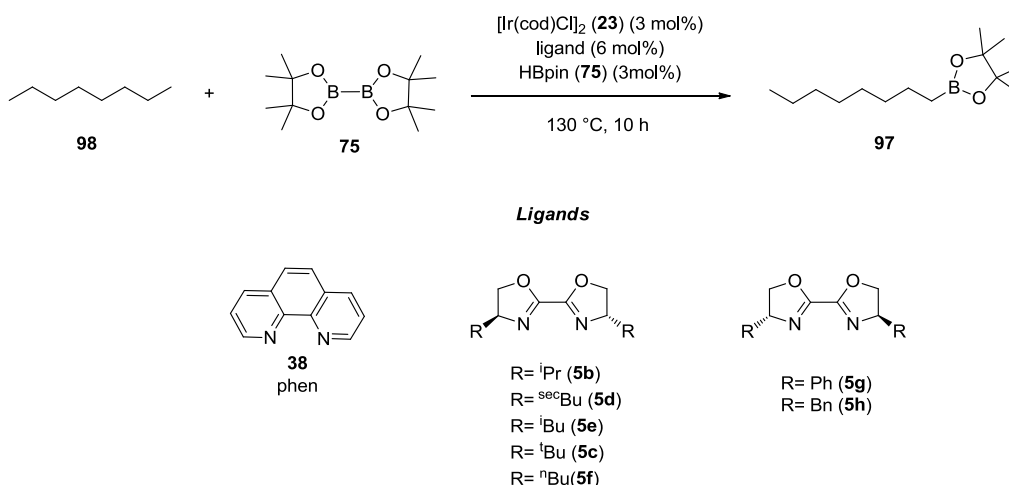
Scheme 7-10. Suitable substrate for enantioselective aliphatic borylation

The envisioned substrate bears, compared to *n*-octane, high steric hindrance. Therefore, commercially available substrates with comparable steric hindrance should be tested as substrates before. Initially the general activity of the oxazoline ligands was probed on *n*-octane.

Before the initial experiments with *n*-octane as substrate were started, the product was prepared separately via rhodium catalyzed hydroboration of *n*-octene, following a procedure of the Miyauchi group (Scheme 7-11).^[245] Substance **97** was identified by GC-MS and the data were used as reference for the following experiments.

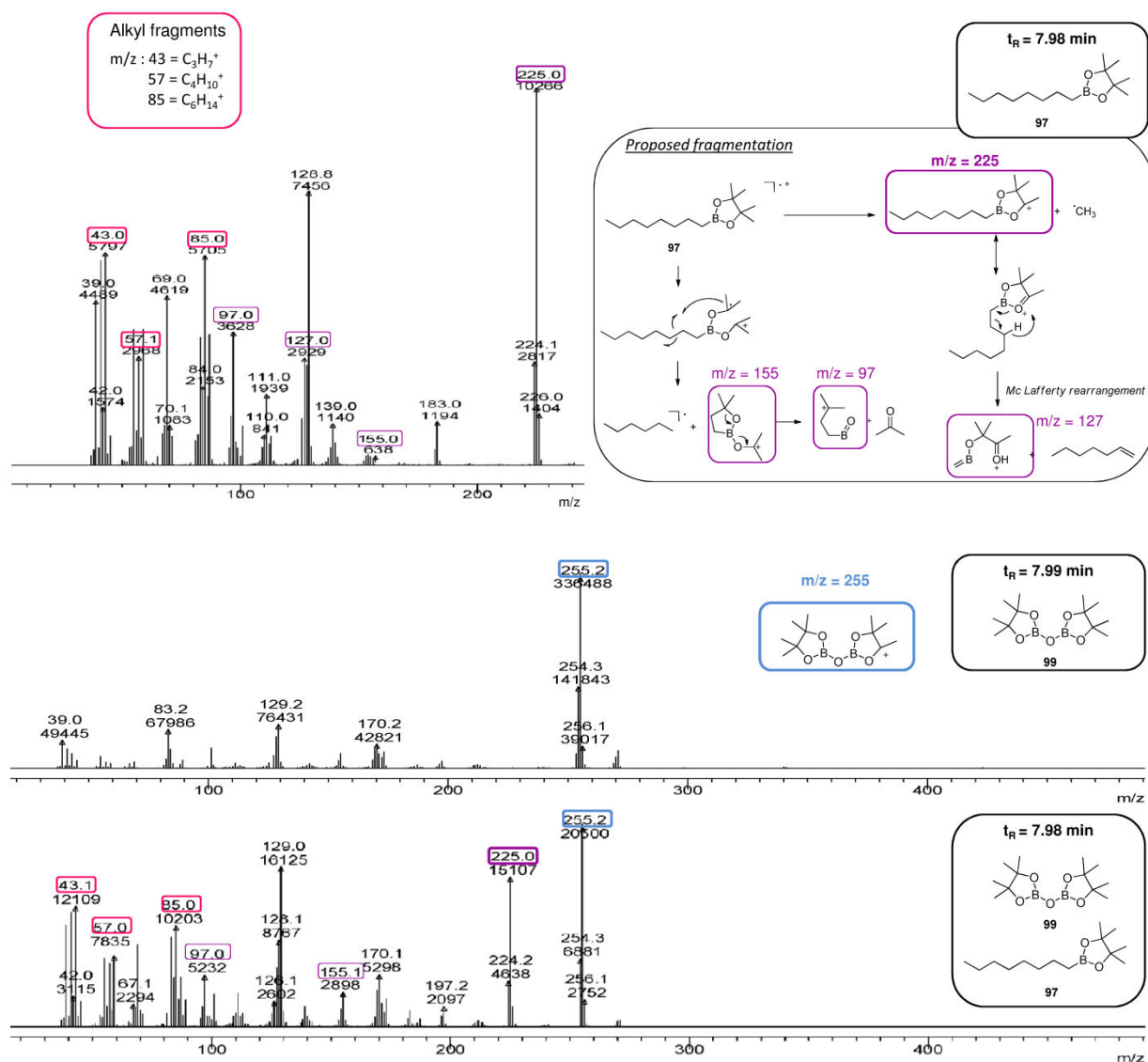


Scheme 7-11. Independent preparation of the borylation substrate **95** by hydroboration.



Scheme 7-12. Catalytic, aliphatic borylation. The reaction were carried out under argon with 50 mg B_2pin_2 (**66**) and 1 mL dry *n*-Octane (**98**) in sealed NMR tubes. The GC-MS results of all experiments indicated the presence of product **97** as well as oxidized B_2pin_2 ($\text{O}(\text{Bpin})_2$ (**99**)).

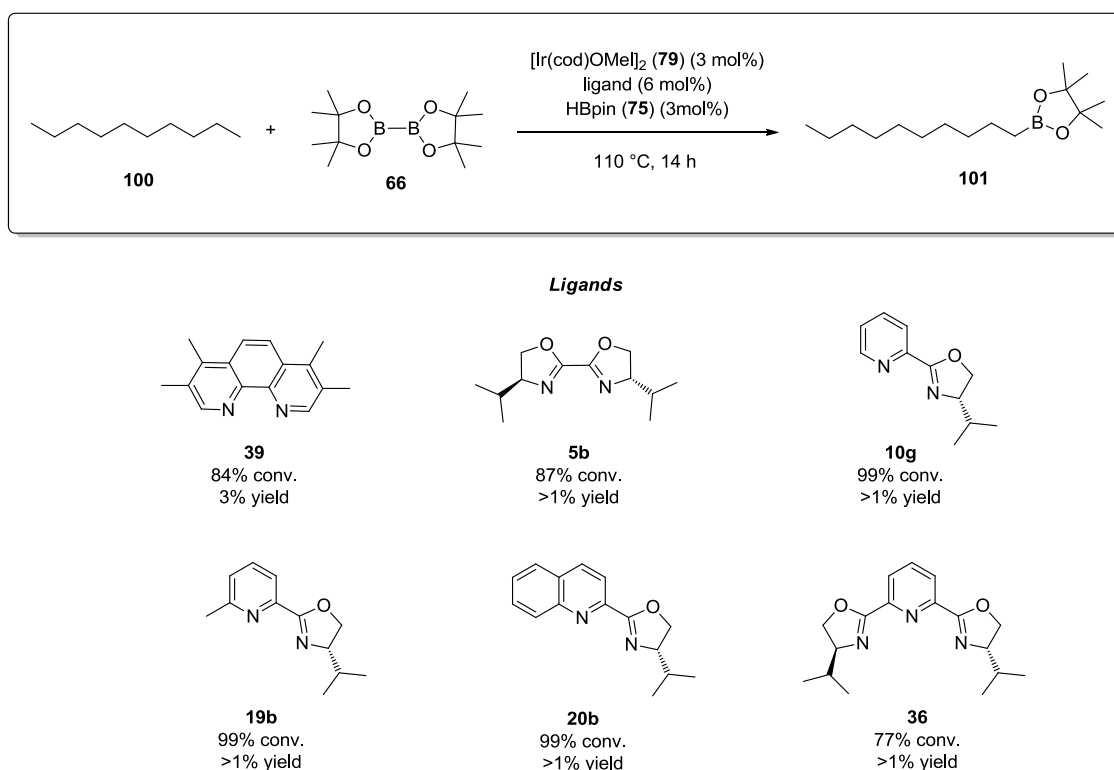
Aliphatic borylation of *n*-octane (**98**) was performed using the standard system for aromatic borylation with $[\text{Ir}(\text{cod})\text{Cl}]_2$, B_2pin_2 , and different $\text{N}^{\wedge}\text{N}$ chelating box ligands. As reference ligand phenanthroline (**38**) was chosen, because this very electron rich ligand was reported to be efficient in this reaction.^[186] HBpin (**75**) was added as well, to shorten the induction period in which the catalytically active species is formed (cf. chapter 4.1.1). Because aliphatic C-H bonds are much more challenging to activate than aromatic C-H bonds, the reactions were run at elevated temperatures of 130 °C. The analysis was performed by GC-MS, which allows only qualitative analysis. All applied ligand-iridium systems led to product formation and formation of the side product $(\text{O}(\text{Bpin})_2$ (**99**)), as determined by GC-MS (Scheme 7-12).



Scheme 7-13. GC-MS analysis of reference compound **97** (upper spectrum) and the catalysis mixture of the borylation of *n*-octane (**98**) with the phenanthroline ligand (middle and lower spectrum). The main GC-peak in the catalysis mixture contained two different substances that were mostly overlaying each other. One substance was identified at a retention time of 7.99 min as oxidized $\text{O}(\text{Bpin})_2$ (**99**) (middle spectrum) while the other substance at $t_R = 7.98$ min showed characteristic signals of the desired product **97** (lower spectrum).

An example of the interpretation of the GC-MS results is given in Scheme 7-13. The depicted spectra were all detected at the same retention time of 7.98-7.99 min and the upper one shows the spectrum of the independently prepared product **97** (cf. Scheme 7-11). In the EI-mass spectra the molar peak of pinacolboranes is in most cases not detected. As soon as the radical cation of the molecule is formed, the pinacol residue fragments into a methyl radical and a stable secondary cation that also benefits from its stabilizing α -position to oxygen. Therefore, this cation lacking a methyl group is characteristic for the corresponding pinacolborane. For the *n*-octyl borane **97** its characteristic m/z value is 225 while the corresponding cation originating from $O(\text{Bpin})_2$ (**99**) has a $m/z = 255$. Both masses were found in the spectrum of the catalytic reactions overlaying at the same retention time of 7.98/7.99 min. Supporting the presence of the product, additional characteristic peaks, *e.g.* the fragmentation masses of an alkyl chain, were also identified.

However, due to the overlap of the product and the $O(\text{Bpin})_2$ signals, the success of the reactions could not be determined unambiguously. Consequently, the reactions were repeated with *n*-decane because its product was expected to have a different retention time than the one obtained from *n*-octane and therefore should be suitable for analysis. For these experiments, GC-FID calibration curves for $B_2\text{pin}_2$ (**66**) and the commercially available borylation product of *n*-decane **100** were prepared.



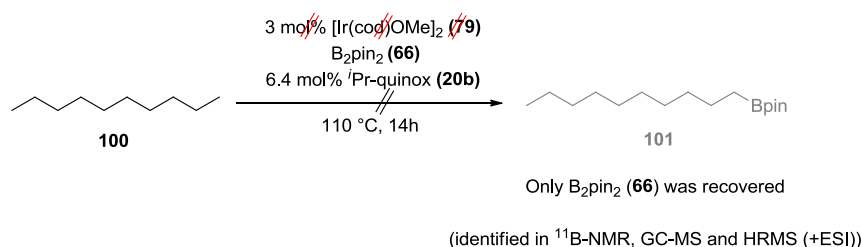
Scheme 7-14. Borylation of *n*-decane (**100**). Conversions and yields were determined by GC-FID.

The GC-FID measurements were performed in addition to GC-MS measurements, to obtain both qualitative and quantitative data. Catalyst precursor $[\text{Ir}(\text{cod})\text{Cl}]_2$ (**23**) was replaced by the more active $[\text{Ir}(\text{cod})(\text{OMe})]_2$ (**79**). The results of these experiments are depicted in Scheme 7-14, showing that the conversions of B_2pin_2 (**66**) were high, between 77-99%. Considering this, the yields were surprisingly low, in most experiments lower than 1%. Based on the obtained GC-MS data, only traces of product were formed, and this time no $\text{O}(\text{Bpin})_2$ (**99**) was observed.

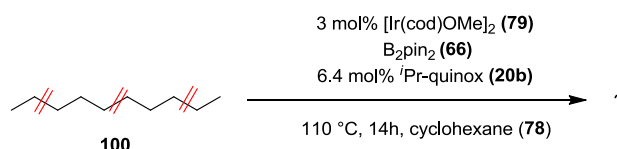
In order to determine what happened with the substrate B_2pin_2 (**66**) and which reaction pathways are responsible for its consumption, two control experiments were performed. One experiment was carried out without adding the iridium source **79** (Scheme 7-15) and another one without the substrate *n*-decane (**100**) (Scheme 7-16). In the latter one cyclohexane (**78**) was taken as solvent because it was expected to be inert in borylation, since it only bears methylene groups. When no iridium was present, no conversion of B_2pin_2 (**66**) was observed. The remaining substrate was identified by ^{11}B -NMR spectroscopy, GC-MS and HRMS.

When *n*-decane (**100**) was replaced by the inert cyclohexane (**78**), full conversion of B_2pin_2 was observed by ^{11}B -NMR spectroscopy and GC-MS. In the ^{11}B -NMR spectrum one or two unidentified (overlapping) signals appeared next to a small signal corresponding to HBpin (**75**). By HRMS, two masses corresponding to mono and bis borylated hexane were found. Their main peak was in both cases the $[\text{M}+\text{Na}]^+$ ion, but also the respective $[\text{M}+\text{H}]^+$ and $[\text{M}+\text{K}]^+$ ions were found. These structures are supported by the GC spectrum that showed two peaks at 8.27 and 13.73 min with corresponding mass spectra showing fragments of the proposed structures. The analysis was always performed after filtration of the reaction mixture. Thus, possibly polymeric or other, insoluble, structures formed in side-reactions might have been removed before.

Since no measurable product was formed and no satisfying answer for the conversion of B_2pin_2 (**66**) in cyclohexane (**78**) was found, the attempts to borylate aliphatic compounds by the same system as for aromatic borylation, were not continued. As mentioned in chapter 4.1.2, the group of Suginome also reported that aliphatic borylation with the $[\text{Ir}(\text{cod})(\text{OMe})]_2$ (**79**)/ TMphen (**39**) system was unsuccessful.^[183] These results were published towards the end of this project and are in agreement with the here described results.



Scheme 7-15. Control experiment: Borylation of *n*-decane (**100**) without adding the iridium source.

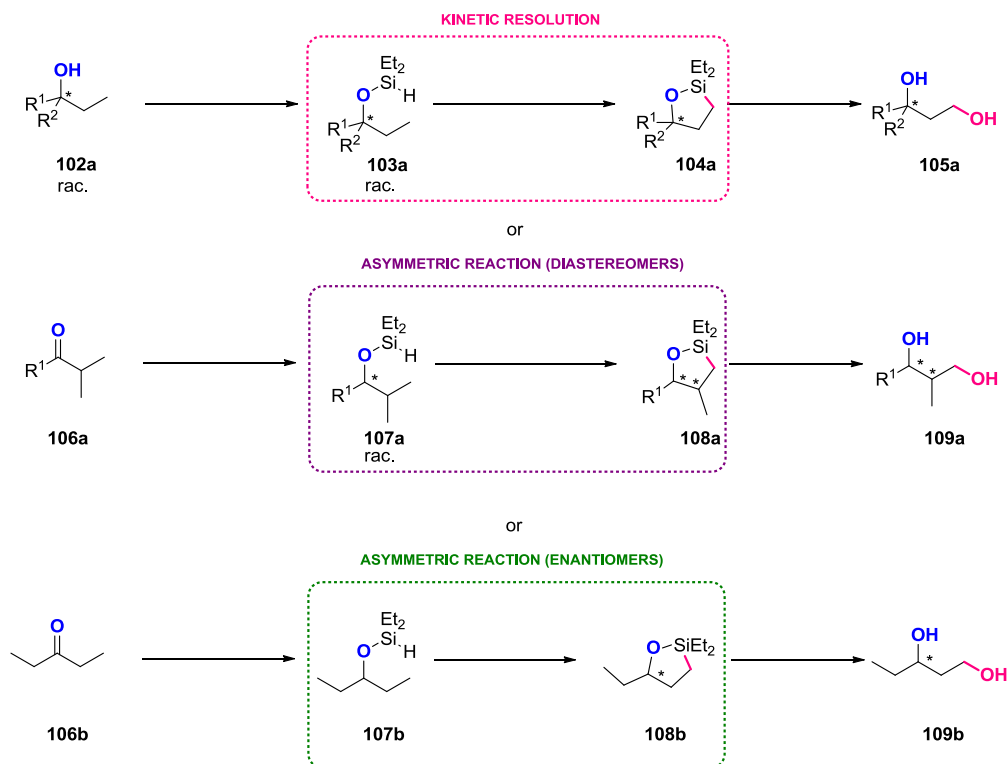


Scheme 7-16. Control experiment: Borylation without *n*-decane (**100**) in cyclohexane as inert solvent.

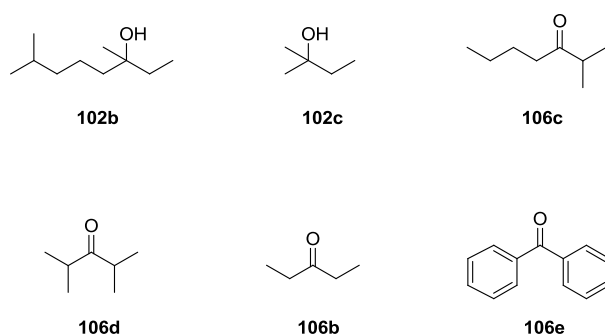
7.3 Silylether Directed γ -C-H Activation

As introduced in chapter 4.2, the Hartwig group has found an elegant three-step procedure for the utilization of a hydroxyl group, or alternatively, a ketone as indirect directing group for γ -C-H activation (Scheme 7-17). In the first step of this procedure, a small amount of [Ir(cod)(OMe)]₂ (**79**) catalyzes the formation of a (hydrido)silyl ether **103** or **107**. In the second ligand assisted step, the C-H activation occurs together with the formation of a five membered oxasilolane ring **104** or **108**. Usually TMphen is used as well suited ligand, but its replacement by a chiral ligand can open the possibility for stereocontrol. This stereocontrol can have different aspects, as illustrated in Scheme 7-17. A racemic tertiary alcohol **102a**, will give a racemic mixture of the corresponding (hydrido)silyl ether **103a** that can be transformed to an enantioenriched cyclic oxasilolan **104a** by kinetic resolution. The same principle can be applied to a prochiral ketone. If an *iso*-propyl group is attached to this molecule, for example as in **106a**, the methyl groups become diastereotopic. The example molecule **107a** forms upon cyclisation diastereomeric structures **108a**. If a symmetrical ketone **106b** is applied, the cyclisation reaction to **108b** desymmetrizes this molecule, resulting in a pair of enantiomers. Subsequently to the asymmetric reaction step, the cyclic oxasilolanes **104** and **108** can be oxidized to their corresponding 1,3-diols **105** and **109**.

For the silyl ether γ -C-H activation during this project, six different molecules were chosen as substrates. The tertiary alcohol **102b** that was also successfully applied by the Hartwig group, can be used to study kinetic resolution. The tertiary alcohol **102c** served as test substrate for small molecules and the ketone **106c** was supposed to result in a diastereomeric mixture. Also three symmetrical ketones **106d**, **106b** and **106e** were chosen as substrates. The di-*iso*-propyl substituted ketone **106d** was expected to give a diastereomeric product mixture while the simpler di-ethyl ketone **106b** and benzophenone (**106e**) would form enantiomeric product mixtures.



Scheme 7-17. (Hydrido)silyl ether directed γ -C-H activation of a tertiary alcohol **102a**, a symmetrical ketone **106b** and a ketone **106a** bearing a prochiral side chain.



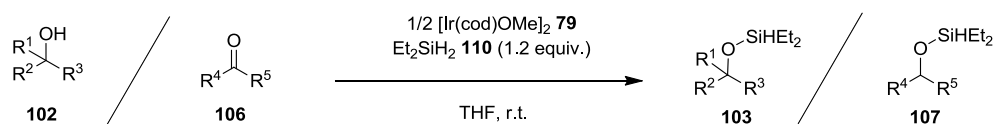
Scheme 7-18. Applied molecules in the first series of silyl ether directed γ -C-H activation.

The initial formation of the (hydrido)silyl ether **103** and **107** was performed with a catalyst loading of 0.08 mol% at room temperature inside a glove box. The conversion of substrate was checked by GC-MS and could be increased for the small alcohol **102b** up to full conversion by extension of reaction time (entries 1 and 2). However, the yields obtained for alcohol **102b** and ketone **106c** are not quantitatively in contrary to the previously reported results. The products **103** and **104** were isolated by

evaporating the volatile compounds, *e.g.* remaining silane **110** in vacuum. In case of the small alcohol **102e** it was important to cool the reaction mixture down to $-78\text{ }^{\circ}\text{C}$, otherwise the product was evaporated as well. The (hydrido)siloxanes **103** and **107** were identified by $^1\text{H-NMR}$ and $^{13}\text{C-NMR}$ analysis.

Because no full conversion was achieved in the first set of (hydrido)silyl ether formation (Table 7-10, entries 1-4, 6 and 7), another reaction with the alcohol **102d** was run with an increased catalyst loading of 1.0 mol% (Table 7-10, entry 5). Full conversion would have been beneficial, because the product isolation would be easier when no starting material was present any more. Three substrates were applied successfully under higher catalyst loading and did achieve full conversion under the modified reaction conditions (Table 7-10, entry 5, 8 and 9).

Table 7-10. Formation of (hydrido)silyl ether **103** and **107**.

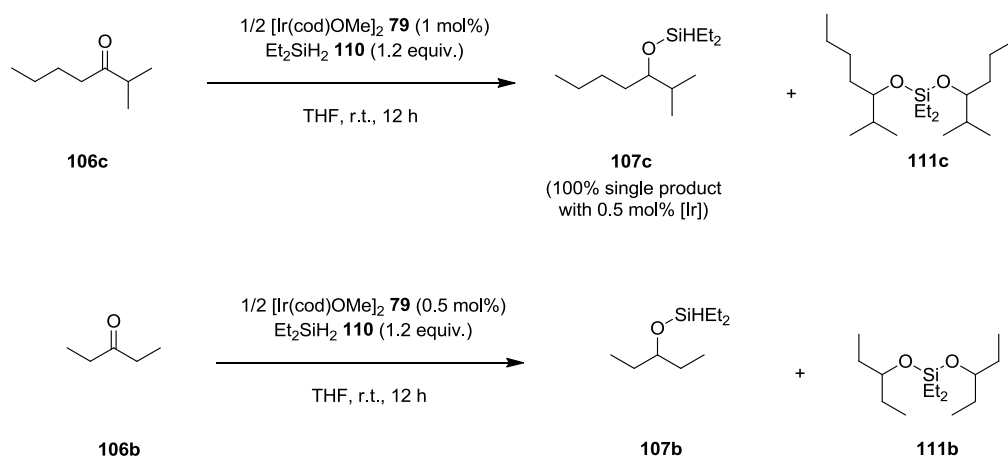


Entry	Substrate	[Ir][mol%]	Time [h]	Yield [%] ^b
1		0.08	17	73
2	102c	0.08	89	97
3		0.08	18	75
4	102b	0.08	89 + 20 ^c	77
5		1	12	100
6		0.08	19	40
7	106c	0.08	89 + 20 ^c	33
8		1	12	98
9		1	12	96

^aReactions were carried out under argon atmosphere using 5.0 mmol of the respective substrate in THF (5.0 mL). ^bIsolated yield. ^cAdditional reaction time at 40 $^{\circ}\text{C}$.

However, for sterically less demanding substrates the formation of di-alkoxysilanes **111** occurred as side reaction, as verified by $^1\text{H-NMR}$ spectroscopy and GC-MS (Scheme 7-19). In case of the larger

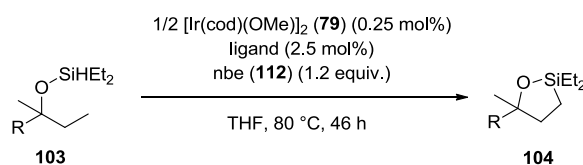
ketone **106c**, reduction of the catalyst loading to 0.5 mol% led to success. This attempt failed for the very small diethylketone (**102b**).



Scheme 7-19. Silylation of sterically less demanding molecules with formation of di-alkoxysilanes as side reaction.

The preparations of the oxasilolanes were performed following the procedure described by the Hartwig group. As depicted in Table 7-11, the iridium precursor **79** was applied with an iridium loading of 0.25 mol% and the ligand was added with ten equivalents in respect to iridium. Nbe (**112**) was added as hydrogen acceptor. The products were isolated by kugelrohrdistillation. The products of the small (hydrido)silyl ether **103c** were highly impure, consequently the true yield of the pure product would be even lower (entries 1 and 2). The isolated products of the larger (hydrido)silyl ether **103b** were isolated in much higher purity but still the yields were not larger than 29%, when the non-chiral H-box (**5i**) was applied as ligand. The application of the chiral ¹Pr-pyrox (**10b**) led to a yield of 14% (entry 4). However, also the application of TMphen (**39**) (entry 1) did not lead to success, even though this ligand had given good results in the experiments by Hartwig and co-workers.^[10] A reason for these contrary results might be a different quality of one or more reagents than the ones used by the Hartwig group. The products were not supposed to be very sensitive, since their work-up under normal atmosphere was reported. For the following experiments it was decided to apply 2 mol% of iridium in combination with 2 mol% ligand. The aim was to obtain pure material of each oxasilolane suitable as reference material for GC calibration. After the calibration, the suitable ligands for the oxasilolane formation would be screened by GC analysis of the reaction mixtures.

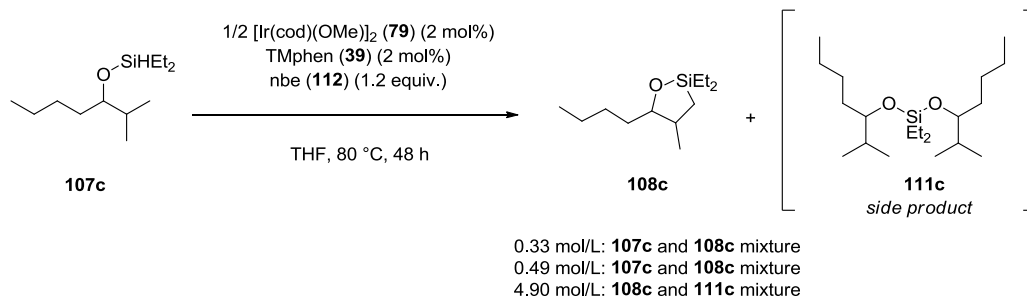
Simple increase of the catalyst loading did not lead to success for the substrate **107c**. As shown in Scheme 7-20, starting material was still detected by GC-MS in the first reaction. Lowering the concentration from 4.90 mol/L to 0.33 mol/L led to full conversion, but caused also decomposition to the di-alkoxysilane **111c**, which was also observed in some silylation reactions (cf. Scheme 7-19). Under the given conditions, this decomposition product can only be created by the incorporation of two molecules starting material **107c**.

Table 7-11. Formation of oxasilolanes from (hydrido)silyl ether **103**.^a

Entry	Substrate	Ligand	Yield [%] ^b
1		 TMphen (39)	(12) ^c
2		 H-box (5i)	(25) ^c
3		 H-box (5i)	29
4		 <i>i</i> Pr-pyrox (10b)	14

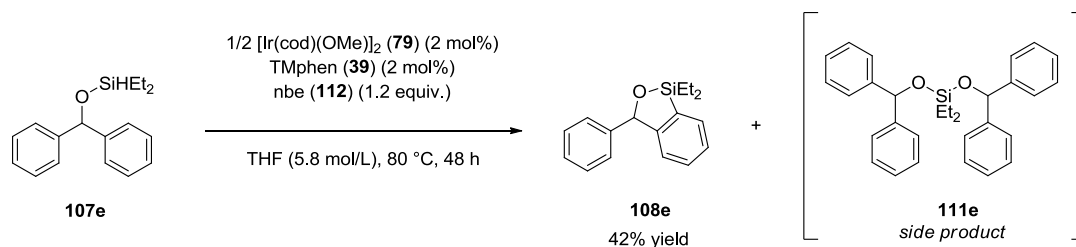
^aReactions were carried out under argon atmosphere with 1.0 mmol of substrate in THF (0.8 mL; 1.25 mol/L).

^bIsolated yield after purification by kugelrohrdistillation. ^cImpure product.

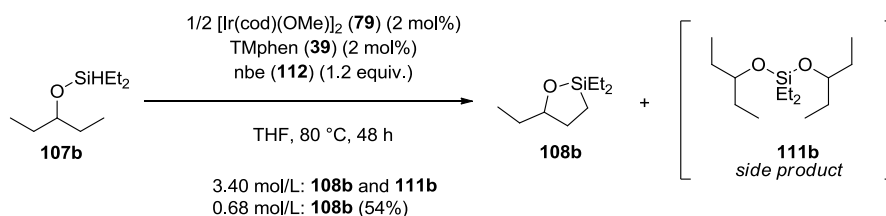
**Scheme 7-20.** Formation of oxasilolane **107c**. The product could not be isolated as pure compound.

When the benzophenone derived (hydrido)silyl ether **107e** was brought to reaction with a higher catalyst loading, the reaction mixture contained a large amount of decomposition product **111e**. When the reaction mixture was more diluted a higher yield of pure product resulted. The corresponding

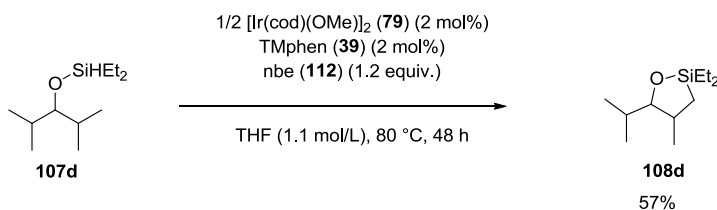
¹H-NMR spectrum still showed few unidentified impurities. Consequently, the obtained product was not suitable as reference material for a GC-FID calibration.



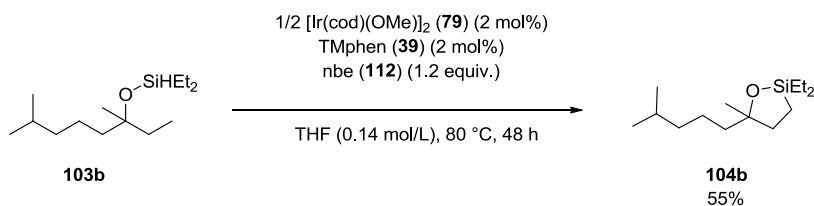
Scheme 7-21. Formation of oxasilolane **107e**. The ¹H-NMR spectrum shows few impurities and by GC-MS the decomposition product **111e** was identified.



Scheme 7-22. Formation of oxasilolane **108b**.



Scheme 7-23. Formation of oxasilolane **108d**.



Scheme 7-24. Formation of oxasilolane **104b**.

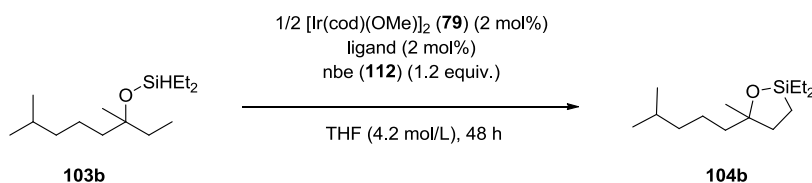
Cyclisation of the sterically unhindered (hydrido)silyl ether **107b** turned out to be very sensitive towards the formation of the decomposition product **111b**, when the concentration was too high (Scheme 7-22). In addition, the reaction turned out to be highly exothermic and therefore had to be cooled down when the reagents were added. A relatively low concentration of approximately 0.7 mol/L was beneficial for the cyclisation of **107b** and led to the isolation of pure product in 54%.

The formation of the oxasilolanes **108d** (Scheme 7-23) and **104b** (Scheme 7-24) was successful for different concentrations. Maybe these substrates are much more robust towards changes in the concentration. Both products were obtained by kugelrohrdistillation as pure substances suitable for a GC-FID calibration.

Table 7-12 shows the results of the ligand screening with substrate **103b**. For the racemic substrate the enantioenrichment of the product was obtained by kinetic resolution. Therefore it was important to identify the conditions that were going to lead to a maximum conversion of 50%. These test reactions are reported in entries 1-4. TMphen (**39**) as typical ligand and H-box (**5i**) as non-chiral representative of the box ligands were used in these test reactions. In order to decrease the conversion, the reactions were performed at lower temperature (Scheme 7-24). At 70 °C, with TMphen (**39**) still a GC yield of 68% was achieved (entry 1) while the result caused by H-box (**5i**) was already below 50% (entry 3). Further lowering of the temperature to 60 °C caused for both ligands yields below 50%. Therefore, all other tested ligands were applied in reactions at 60 °C (entries 5-16).

The yields from the applications of the different box, pyrox, mepyrox and quinox ligands are in the range of 24-38% while with TMphen (**39**) 45% were achieved. Enantiomeric excesses were obtained with bidentate oxazoline ligands in a range from 1-44% ee. One remarkable exception concerning the obtained yield was found with the P,N-ligand Ph-phox (**40**), which has not been tested before as ligand in this reaction and which caused an unexpectedly high yield of 94% (entry 15). Concerning the evaluation of the achieved enantioselectivities, hardly any trend between the different groups of oxazolines was identifiable.

As depicted in scheme Scheme 7-25, it seems rather that certain oxazoline residues are responsible for activity and selectivity and the observed trends for these two factors are mainly opposite. For example, ligands with flat phenyl-residues and long and flexible *n*-butyl-residues cause medium to good yields but only low to medium enantiomeric excesses. A large benzyl-residue on a box ligand leads to comparable high enantiomeric excess but at the same time to the lowest yield of all tested ligands. The highest enantiomeric excesses were achieved by the application of the sterically demanding quinox and pybox ligands with *iso*-propyl residues (Table 7-12, entries 7 and 11). For the pybox ligand no corresponding yield was determined but the quinox ligand led to a medium yield of 33%.

Table 7-12. Ligand screening in the cyclisation of **103b**.^a

Entry	Ligand	Temp. [°C]	Yield [%] ^b	ee [%] (enantiomer) ^b
1	TMphen (39)	70	68	-
2	TMphen (39)	60	45	-
3	H-box (5i)	70	33	-
4	H-box (5i)	60	25	-
5	(<i>S</i>)-Bn-box (5h)	60	24	29 (1)
6	(<i>S</i>)- ⁱ Pr-box (5b)	60	35	<1 (1)
7	(<i>S</i>)- ⁱ Pr-quinox (20b)	60	33	44 (1)
8	(<i>S</i>)- ⁿ Bu-box (5f)	60	29	3 (1)
9	(<i>R</i>)-Ph-box (5g)	60	38	< 1 (2)
10	(<i>R</i>)-Ph-quinox (20g)	60	32	15 (2)
11	(<i>R</i>)- ⁱ Pr-pybox (36)	60	n.d.	40 (2)
12	(<i>S</i>)- ⁿ Bu-mepyrox (19f)	60	32	3 (1)
13	(<i>S</i>)- ⁿ Bu-quinox (20f)	60	32	13 (1)
14	(<i>R</i>)-Ph-mepyrox (19g)	60	39	10 (2)
15	(<i>S</i>)-Ph-phox (40)	60	94	10 (1)
16	(<i>S</i>)- ^t Bu-pyrox (10c)	60	35	26 (1)

^aReactions were carried out under argon atmosphere with 0.507 mmol of substrate **103b** in THF (1.2 mL; 4.2mol/L). ^bDetermined by GC-FID. The absolute configuration was not determined and (1) and (2) denote the opposite enantiomers.

40-44% ee	26-29% ee	10-15% ee	<1-3% ee	
ⁱ Pr-quinox	Bn-box	Ph-quinox	ⁱ Pr-box	
ⁱ Pr-pybox	^t Bu-pyrox	Ph-mepyrox	Ph-box	
		ⁿ Bu-quinox	ⁿ Bu-mepyrox	
			ⁿ Bu-box	
>90% yield	38-45% yield	32-35% yield	29% yield	24-25% yield
Ph-phox	Ph-box	Ph-quinox	ⁿ Bu-box	H-box
	Ph-mepyrox	ⁱ Pr-box		Bn-box
	TMphen	ⁱ Pr-quinox		
		^t Bu-pyrox		
		ⁿ Bu-mepyrox		
		ⁿ Bu-quinox		

Scheme 7-25. Overview of ligand groups, ordered by enantiomeric excess and yield as achieved in the kinetic resolution of **103b**.

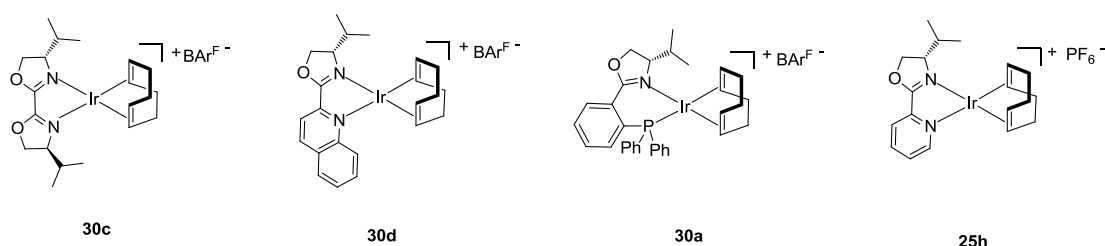
The reactions presented in this chapter bear both, potentials and drawbacks. The main challenge in the formation of the (hydrido)silyl ether is the identification of reaction conditions leading to full conversion while suppressing the formation of di-alkoxysilanes **111**. When this is accomplished, the (hydrido)silyl ethers are easily obtained in a quality suitable for the following C-H activation.

Particularly promising results were obtained from the kinetic resolution of (hydrido)silane ether **103b**. A remarkable high yield was achieved with the P,N-ligand Ph-phox (**40**), which should give reason for further investigation of these ligands in such reactions. The oxazoline ligands led to comparable yields as the usually applied TMphen ligand (**39**) and initial enantiomeric excesses up to 44% ee were obtained, which might be increased in following optimization reactions.

7.4 Hydrogenation

Asymmetric, homogeneous hydrogenation is preceded working with phox ligands, which were discovered by Pfaltz and Helmchen. These bidentate P,N-ligands are applied in $[\text{Ir}(\text{P}^{\wedge}\text{N})(\text{cod})]\text{BAR}^{\text{F}}$ complexes which serve as precatalysts (cf. chapter 4.3). Typically, homogeneous hydrogenations are performed under 5-50 bar hydrogen pressure, at room temperature and in DCM as solvent with catalyst loadings from 1-4 mol%.^[9] The BAR^{F} anion as counteranion gave the best results. Less reactive were complexes with *e.g.* PF_6^- counteranions. Consequently, BAR^{F} was chosen as counteranion for the iridium oxazoline complexes in this project (cf. chapter 4.3).

Initial experiments as well as substrate screenings were undertaken with one representative of a box and a pyrox derivative complex, respectively (Scheme 7-26). In order to check the general applicability of the method, also one phox complex **30a** was prepared. Additionally, a PF_6^- complex was tested as well in order to compare its results with these obtained by BAR^{F} complexes.

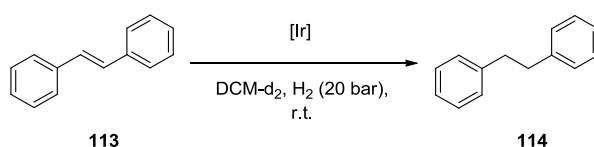


Scheme 7-26. Precatalysts for initial hydrogenation experiments. The phox complex **30a** served as control complex.

In Table 7-13 the results of the initial hydrogenation experiments of *trans*-stilbene (**113**) are collected. The yields caused by the oxazoline complexes were low to moderate under a hydrogen pressure of 20 bar. However, the results of entry 1 and 2, or 3 and 4 show that the yield increased with reaction time. A low catalyst loading of the ⁱPr-quinox complex **30d** lowered also the yield, even though a long

reaction time was applied (entry 5). A relatively high loading of the PF_6^- complex **25h** led to nearly no yield, which showed that this complex is not suitable for hydrogenation. In order to avoid the time consuming synthesis of the precatalysts **30**, an *in situ* preparation of **30d** was tried (entry 6). For this purpose, the dimeric iridium cod precursor **23**, AgBAR^{F} (**34**) and the ligand **20b** were mixed in the solvent and stirred for 10 min under exclusion of light before the substrate was added and the reaction was performed as usual. Even though a high catalyst loading for this experiment was applied, nearly no yield was detected, indicating no effective catalyst formation or negative interference of silver cations during catalysis. The quantitative yield caused by the phox complex **30a** verifies the general applicability of the reaction conditions in our labs (entry 7).

Table 7-13. Initial hydrogenation experiments using *trans*-stilbene (**113**) as substrate.^a



Entry	Complex	Cat.-loading [mol%]	Time [h]	V(solvent) [mL]	Yield ^c [%]
1	30c	5	18	0.5	9
2	30c	5	5	0.5	5
3	30d	5	18	0.5	32
4	30d	5	5	0.5	25
5	30d	1	18	0.2	7
6	30d / ^c <i>in situ</i> ^b	5	18	0.2	3
7	30a	5	5	0.5	>99
8	25h	5	5	0.5	2

^aComplexes, substrate (0.484 mmol) and solvent were mixed in a small sample vial. The vial was placed into an autoclave and left stirring under a hydrogen pressure of 20 bar. ^bSolvent, and $[\text{Ir}(\text{cod})(\text{Cl})_2]$ (**23**) (1 equiv.) were premixed with AgBAR^{F} (2equiv.) and ¹Pr-quinox (**20b**) (2 equiv.) and left stirring in the dark for 10 min before the substrate was added. ^cDetermined by ¹H-NMR spectroscopy.

After evaluating the general conditions necessary for effective catalytic hydrogenation with the oxazoline complexes **30**, it was decided to run the future reactions at elevated hydrogen pressure of 40 bar and in neat substrate, if possible. For solid substrates, a small amount of DCM-d₂ was used as solvent. In Table 7-14 the hydrogenation results for some olefins and ketones are listed. In all examples, the ¹Pr-box complex **30c** led almost always to quantitative yield while the sterically more demanding ¹Pr-quinox complex **30d** achieved yields of only 10-37%. In general, phenyl substituted olefins are more easily reduced (entry 1 and 3) while cyclooctene appeared to be a challenging substrate (entry 5 and 6). The allyl alcohol **118** was reduced quantitatively by the ¹Pr-box complex **30c** while the ¹Pr-quinox complex **30d** led to no product formation (entry 7 and 8). Ketones such as cyclohexanone **120** and 4-tert-butylcyclohexanone **121** were reduced in good to quantitative yields (entry 9-12). The prochiral latter one was reduced without any stereoselectivity. A phenylsubstituted

ketone, acetophenone **123**, was reduced with very low yield, not higher than 13% (entry 13 and 14). Since acetophenone is one of the standard substrates for hydrogenation as well as transfer hydrogenation, these yields were expected to be higher.

Table 7-14. Hydrogenation of alkenes and ketones with catalyst precursors **30c** and **30d**.

Entry	Substrate ^a	Product	Complex	Yield ^c [%]
1 ^b			30c	100
2 ^b	113	114	30d	37
3 ^b			30c	100
4 ^b	115	114	30d	24
5			30c	42
6	116	117	30d	5
7 ^b			30c	100
8 ^b	118	119	30d	0
9			30c	87
10	120	119	30d	33
11 ^b			30c	100 (syn:anti = 13:10)
12 ^b	121	122	30d	15 (syn:anti = 10:11)
13			30c	13
14	123	124	30d	10

^aReactions carried out with complexes **30**(0.0145 mmol, 3 mol%) in 0.484 mmol of neat substrate in an autoclave at 40 bar hydrogen pressure at room temperature for at least 15 h. ^bDCM-d₂ (0.1 mL) was added as solvent. ^cYields determined by ¹H-NMR spectroscopy.

The chemoselectivity of the hydrogenation was probed in the reduction of α,β -unsaturated carbonyl compounds shown in Table 7-15. With both catalysts, **30c** and **30d**, very good yields were achieved for the different unsaturated ketones and esters tested, only 2-methylcinnamaldehyde (**133**) gave practically no turnover (Entries 5 and 6). In most examples, the saturated ketone or ester arising from hydrogenation of the C-C double bond was the major product and the fully reduced alcohol was formed as a side product in small amounts, while the allylic alcohol was not observed (Entries 1, 2, 3, 4, 10 and 11). With the less reactive ⁱPr-quinox complex **30d** the preference for reduction of the olefinic double bond was more pronounced than for complex **30c**. One possible explanation for these results is the assumption that hydrogenation of the C-C double bond is generally occurring faster, while the C-O double bond is reduced only slowly. In this case, even if some allylic alcohol was formed by initial

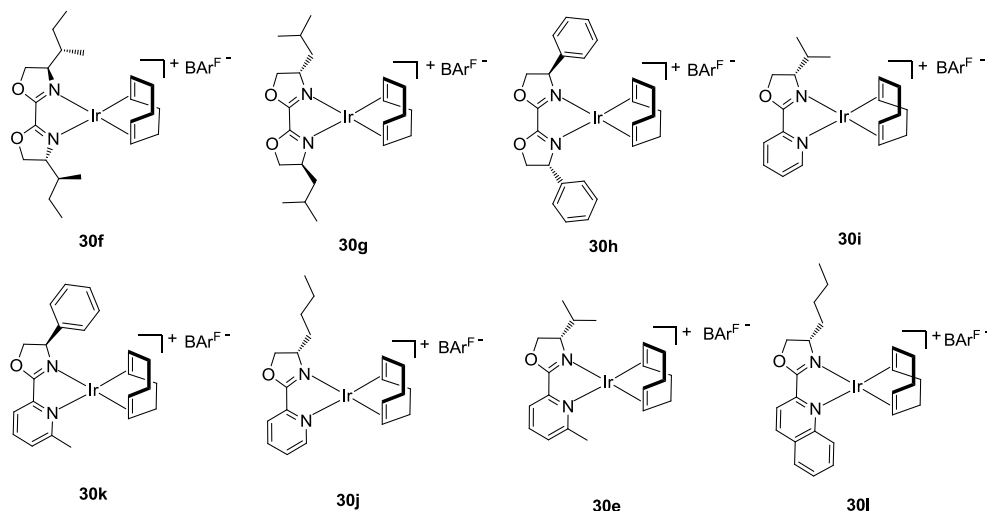
reduction of the carbonyl group, it would not accumulate and would be consumed by fast reduction to the fully reduced product. A notable exception is enone **137**, which upon hydrogenation gave significant amounts of allylic alcohol **137** and only little completely reduced **140** (Entry 7). In this case the reaction of the conjugated double bonds occurred quickly albeit with little preference for the C-C double bond, whereas the following reduction of either the carbonyl group or the isolated olefin must have been slow. For cyclohexenone (**141**) exclusively the fully reduced product **119** was obtained when complex **30c** was used (Entry 8). This result reflects the high activity of this complex towards both partially reduced intermediates, cyclohexanone **120** and cyclohexenol **118** as already described (cf. Table 7-14, entries 7-10). With the less reactive complex **30d**, the usual chemoselectivity for the reduction of the C-C double bond forming cyclohexanone **120** was observed (Entry 9). A small amount of the C-O reduced product **118** was formed, but no fully reduced product **119** was found.

Table 7-15. Hydrogenation of α,β -unsaturated system with **30c** and **30d**.^a

Entry	Substrate	Products	Complex	yield ^c [%]	Ratio
1			30c	>99	115 : 0 : 10
2			30d	97	1 : 0 : 0
3 ^[b]			30c	>99	40 : 0 : 10
4 ^[b]			30d	93	1 : 0 : 0
5			30c	traces	28 : 10 : 1
6			30d	traces	n.d.
7 ^[b]			30c	>99	17 : 10 : 18
8			30c	>99	0 : 0 : 1
9			30d	99	188 : 10 : 0
10			30c	>99	89 : 0 : 10
11			30d	96	97 : 0 : 10

^aReactions carried out with complexes **30** (0.0145 mmol, 3 mol%) in 0.484 mmol of neat substrate in an autoclave at 40 bar hydrogen pressure at room temperature for at least 15 h. ^bDCM-d₂ (0.1 mL) was added as solvent. ^cYields determined by ¹H-NMR spectroscopy or GC-FID.

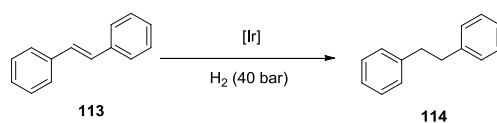
After screening different olefins, ketones and α,β -unsaturated substrates in hydrogenations with the ⁱPr-box complex **30c** and the ⁱPr-quinox complex **30d**, more complexes **30** with different oxazoline ligands were prepared (Scheme 7-27) and tested in the hydrogenation of *trans*-stilbene **113** (Table 7-16) and isophorone **142** (Table 7-17).



Scheme 7-27. Complexes applied in hydrogenation reactions as precatalysts in addition to **30c** and **30d**.

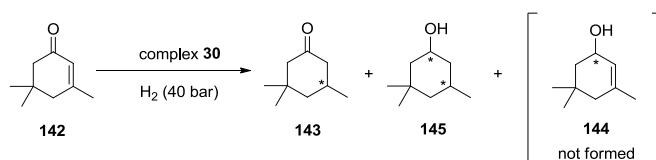
The results of the hydrogenation of *trans*-stilbene (**113**) (Table 7-16) reflect the strong dependence of catalytic activity on the steric demand of the corresponding precatalyst **30**. The box complexes led exclusively to full conversion (entries 1-4) while for the pyrox and quinox complexes the substituent played a crucial role. Complexes **30i** and **30d**, bearing an *iso*-propyl substituent, led to a yield of 37% (entries 5 and 9) while the longer, but less branched, *n*-butyl substituent of the complexes **30j** and **30l** led to quantitative yield (entries 6 and 10). The mepyrox complexes **30e** and **30k** caused no product formation, presumably due to too high steric hindrance of the 6-methyl substituent on the pyridine moiety (entries 7 and 8).

The same behavior was observed for the hydrogenation of isophorone (**142**) (Table 7-17). The mepyrox complexes **30e** and **30k** did not lead to product formation (entries 7 and 8), while the *iso*-propyl complexes **30i** and **30d** formed some product, but not quantitatively (entries 5 and 9). The remaining complexes achieved quantitative yields. The observed chemoselectivity for the preferred C-C bond reduction appeared to be very high for all complexes with ratios (C-C reduced product **143**):(fully reduced product **145**) about 10:1. In all experiments, no C-O reduced product **144** was observed. Since isophorone forms stereoisomers upon hydrogenation, an e.r. for product **143** and a d.r. for product **145** was determined, showing no stereochemical influence of the applied complexes.

Table 7-16. Hydrogenation of *trans*-stilbene (**113**) by different oxazoline complexes **30**.^a

Entry	Complex	Ligand	Yield ^b [%]
1	30c	ⁱ Pr-box	100
2	30f	ⁱ Bu-box	100
3	30g	^{sec} Bu-box	100
4	30h	Ph-box	100
5	30i	ⁱ Pr-pyrox	37
6	30j	ⁿ Bu-pyrox	100
7	30e	ⁱ Pr-mepyrox	<1
8	30k	Ph-mepyrox	<1
9	30d	ⁱ Pr-quinox	37
10	30l	ⁿ Bu-quinox	100

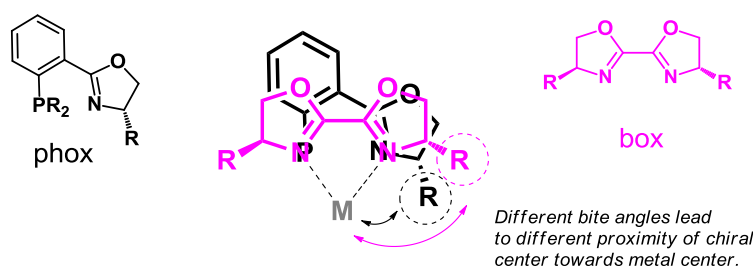
^aReactions carried out with complexes **30** (0.0145 mmol, 3 mol%) in 0.484 mmol of neat substrate in an autoclave at 40 bar hydrogen pressure at room temperature for 15 h.
^bDetermined by ¹H-NMR spectroscopy.

Table 7-17. Hydrogenation of isophorone (**142**) by different oxazoline complexes **30**.^a

Entry	Complex	Ligand	Yield ^b [%]	Product ratio ^b	e.r. 143 ^b	d.r. 145 ^b
1	30c	ⁱ Pr-box	100	89 : 10	1 : 1	1 : 1
2	30f	ⁱ Bu-box	100	83 : 10	12 : 10	11 : 10
3	30g	^{sec} Bu-box	100	118 : 10	1 : 1	10 : 11
4	30h	Ph-box	100	94 : 10	10 : 12	10 : 12
5	30i	ⁱ Pr-pyrox	28	141 : 10	11 : 10	11 : 10
6	30j	ⁿ Bu-pyrox	100	79 : 10	1 : 1	1 : 1
7	30e	ⁱ Pr-mepyrox	<1	1 : 0	n. d.	n. d.
8	30k	Ph-mepyrox	<1	1 : 0	n. d.	n. d.
9	30b	ⁱ Pr-quinox	96	97 : 10	1 : 1	11 : 10
10	30l	ⁿ Bu-quinox	100	92 : 10	1 : 1	1 : 1

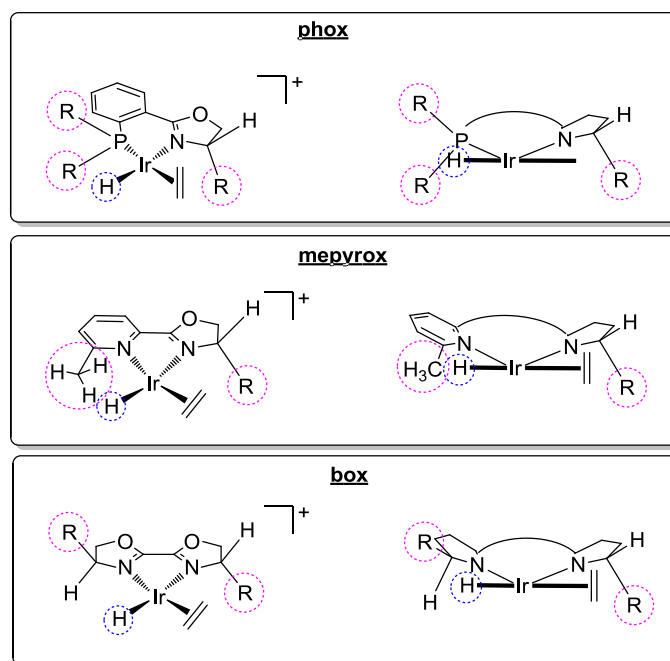
^aReactions carried out with complexes **30** (0.0145 mmol, 3 mol%) in 0.484 mmol of neat substrate in an autoclave at 40 bar hydrogen pressure at room temperature for 15 h. ^bDetermined by GC-FID.

Despite the very good chemoselectivity of the applied complexes, preferring the reduction of C-C double bonds, no stereoselectivity was observed. Also the yield caused by several complexes was very low. These results can both be explained by steric effects on the ligand. Compared to the very efficient phox ligands, one of the most prominent differences is the different bite angle found in the oxazoline ligands. Scheme 7-28 shows a graphical comparison of an arbitrary phox ligand and a box ligand. The phox ligand forms a six-membered metallacycle, while for the box ligand a five-membered one is possible. In the overlay of both ligands it becomes clear, how this smaller bite angle of the phox ligand leads to a closer proximity of the phox-stereocenter to the metal center. In comparison, the one of the box ligand is much more far away. Considering this, it seems possible that the stereocenter of the oxazoline ligands is simply too far away from the catalytic center to have any influence on the stereochemical outcome of the reaction.

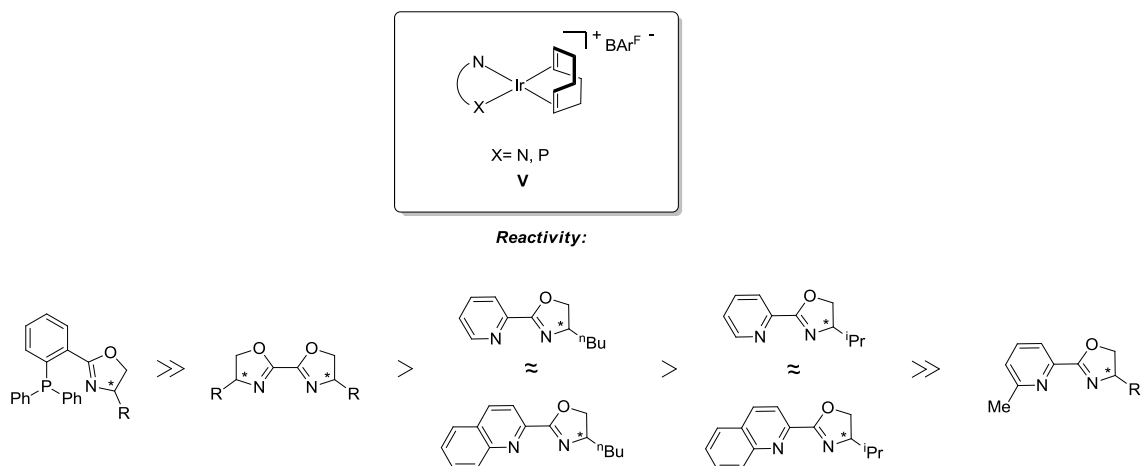


Scheme 7-28. Schematic overlay of an arbitrary phox and box ligand showing the resulting different proximity of the corresponding stereocenter towards the central metal. The stereocenter of the box ligand might be too far away to have influence on the stereochemical outcome of a catalyzed hydrogenation reaction.

In order to understand the reason for some complexes leading to no or only very low product formation, the intermediate of the catalytic cycle (cf. chapter 4.3), from which the reduction occurs, should be considered. Scheme 7-29 shows a sketch of a phox and a mepyrox complex drawn from two perspectives. The drawing shows, how the two bulky residues on the phosphorous atom point above and below the P/N-N-Ir-H plane. Therefore, these residues are not interfering with the hydrido ligand. In contrary, the methyl substituent on the mepyrox ligand cannot avoid steric interaction with the hydrido ligand because it is fixed in the same plane. Therefore, complex formation with this ligand is much more difficult, which can explain the very low product yield below 1% observed for the mepyrox complexes **30e** and **30k**. The quinoline complexes **30d** and **30l** have a little lower steric hindrance. Thus, the identity of the chiral residue on the oxazoline moiety has been given extra weight for the success of the reaction. In case of an *iso*-propyl substituent (complexes **30i** and **30d**), the total steric hindrance is too high resulting in low yields while the *n*-butyl residue (complexes **30j** and **30l**) is thin and flexible enough to make complex formation possible. In case of the box complexes **30c**, **f**, **g**, **h**, the residues obtain positions over and below the N,N,Ir,H-plane, as it was the case for the phox ligands. Therefore, these complexes are formed easily and the yields are almost always quantitative.



Scheme 7-29. Comparison of steric hindrance of phox, mepyrox and box ligands in the catalytic intermediate $[\text{Ir}(\text{ligand})(\text{alkene})(\text{H})_2\text{S}]^+$; the hydrogen and hydrido ligands besides the ligand-Ir plane are omitted for clarity. The residues of the phox ligand are not in one plane with the hydrido ligand and therefore cause less steric hindrance than the mebox ligand, which methyl group directly interferes with the hydrido ligand.



Scheme 7-30. Ligands of complex **30** applied in catalytic hydrogenation as precatalyst. The ligands are ordered in decreasing activity from left to right.

In summary, the oxazoline complexes **30** are less active than analogous phox complexes. The oxazoline complexes **30c-l** need a high hydrogen pressure of 40 bar to achieve quantitative yields while for the phox complex **30a** a hydrogen pressure of 20 bar has been enough. Despite of this, a high chemoselectivity for the oxazoline complexes was observed preferring the reduction of C-C double

bonds over C-O double bonds. All investigated complexes showed no stereoselectivity which might be attributed to the fact that the ligand stereocenters are too far away from the metal center. The complex formation might be negatively influenced by steric hindrance from the substituents, which increases from ⁿBu-quinox (**20f**) over ⁱPr-quinox (**20b**) to mepyrox (**19**) ligands. In case of the box ligands, no steric hindrance is supposed to be relevant rationalizing the much higher yields obtained with complexes containing these ligands. Based on the results discussed in this chapter, the ligands can be ordered in decreasing reactivity as depicted in Scheme 7-30.

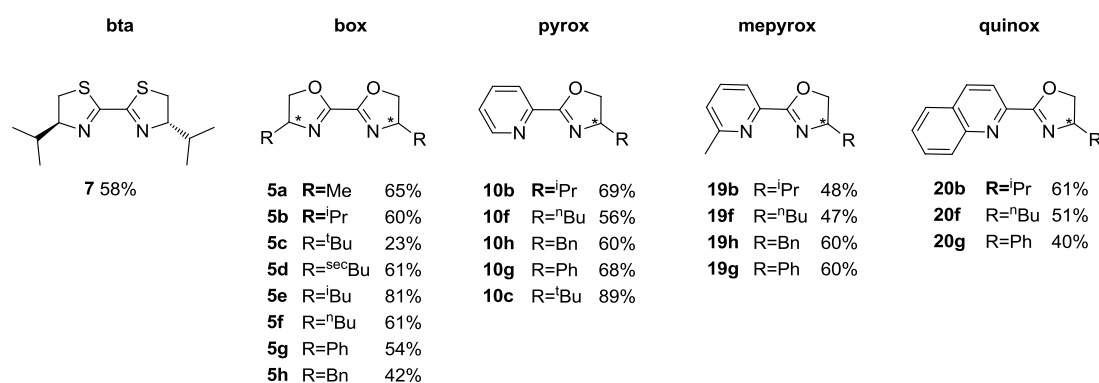
III. Summary & Conclusion

8 Summary

8.1 Synthesis of Ligands

For the preparation of box, pyrox, mepoxy and quinox ligands two synthesis routes were developed. These synthesis routes provide several advantages, for example they both start with commercially available and cheap starting materials. The first step of the pyrox synthesis, an amide coupling using standard coupling reagents, is generally transferable to many kinds of carboxylic acids. For the oxazoline ring closure itself, two different sets of reagents were optimized. The introduction of chloride as leaving group was suitable for the preparation of box compounds because the solid, chlorinated intermediates could be purified by recrystallization. The purification at this stage of the synthesis was important, because residual acid from the chlorination with thionylchloride had to be removed completely before the successful oxazoline formation. The base induced ring closure did not form any by-products, except for NaCl, which was removed by an aqueous work-up. Column chromatography was not possible because the box compounds were too polar. The procedure for the box structures was not transferable on the preparation of pyrox-type oxazolines because their oily intermediates after chloride introduction could not be purified. Therefore, a combined tosylation and base induced ring closure was developed. The pyrox-type oxazolines had to be purified after this step, which was possible by flash-chromatography over basic alox. In addition, a bithiazolin was prepared from the chlorinated box intermediates.

In total, 20 oxazoline structures were successfully prepared in good overall yields in half-gram-scale (Scheme 8-1).



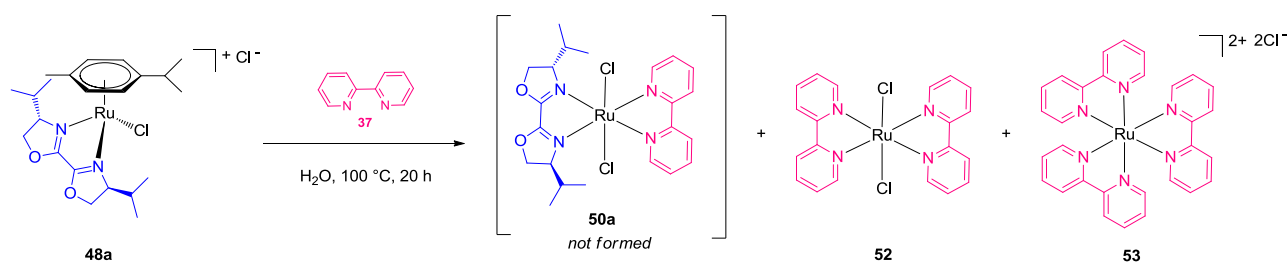
Scheme 8-1. Prepared oxazoline ligands. Total yields over two (pyrox, mepoxy and quinox) or three (box) steps, the yield of bta refers to the thiazolin ring closure step.

8.2 Synthesis of Transition Metal Complexes

Ruthenium Complexes

The preparation of heteroleptic ruthenium complexes $[\text{Ru}(\text{box})(\text{bpy})(\text{L}_2)]^{2+}$ starting with two different precursor complexes, $[\text{Ru}(p\text{-cymene})(\text{Cl})_2]$ (**46**) and $[\text{Ru}(\text{dmsO})_4\text{Cl}_2]$ (**74**), was not successful. Two major problems appeared during the synthesis of the heteroleptic ruthenium complexes:

1. The bisoxazoline ligands appeared to be much weaker ligands as bipyridine and were always substituted when introduced as first ligand (Scheme 8-2),
2. Purification of the obtained reaction mixtures was not possible in most cases. Precipitation failed because the complexes were usually oils and column chromatography was not possible because the substances decomposed.



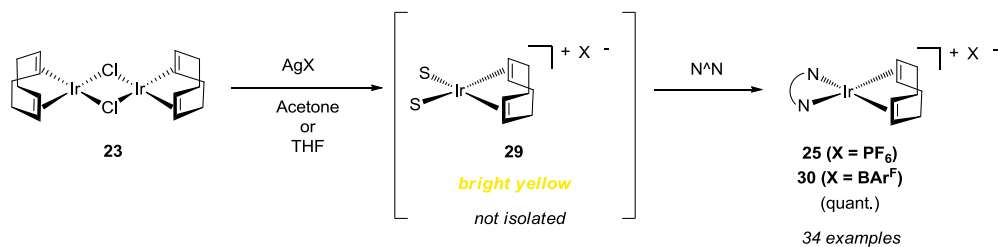
Scheme 8-2. Reaction of **48a** with bpy (**37**).

Iridium Complexes

For cod complexes of the general constitution $[\text{Ir}(\text{N}^{\wedge}\text{N})(\text{cod})]\text{Cl}$ (**24**) with Cl^- as counter anion, a strong coordination behavior of Cl^- in complexes with oxazoline ligands was observed. This is in line with a weaker coordination behavior of these box ligands in comparison with dtbpy (**32**).

For cod complexes with $\text{BAr}^{\text{F}-}$ as counter anion, the successful synthesis of cod phox complexes $[\text{Ir}(\text{t}^{\text{Pr}}\text{-phox})(\text{cod})]\text{BAr}^{\text{F}}$ (**30a**) was not transferable on the analogous structures with oxazoline ligands. The purification failed, because the oxazoline complexes were too soluble. Therefore, a new strategy was developed introducing the new counter anion using the silver salt in the first step (Scheme 8-3). This procedure did not require any work-up because the complexes $[\text{Ir}(\text{N}^{\wedge}\text{N})(\text{cod})]\text{X}$ ($\text{X} = \text{BAr}^{\text{F}}$ **30**, $\text{X} = \text{PF}_6$ **25**) were obtained as pure products. Applying this newly developed procedure, 34 cod complexes with oxazoline ligands were prepared.

The prepared cod complexes **30** were applied as pre-catalysts in homogeneous hydrogenation and the complexes **30** were further transformed into their corresponding monocarbonyl and dicarbonyl complexes **26** and **28**.



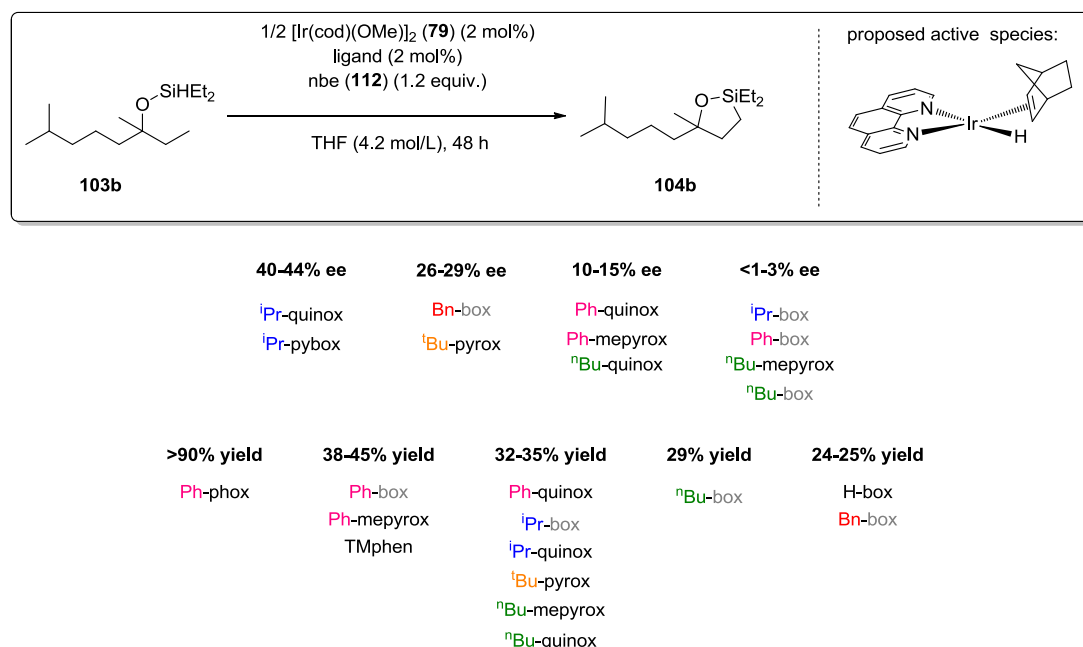
Scheme 8-3. Preparation of cod complexes **25** and **30** containing oxazoline ligands.

8.3 Catalysis

(Hydrido)Silyl Ether directed γ -C-H Activation

The oxazoline ligands were slightly less active in (hydrido)silyl ether directed γ -C-H activation on average than the commonly used, relatively electron rich, TMphen (**39**) ligand (Scheme 8-4). Among the tested oxazoline ligands, the phenyl substituted box and mepyrox ligands caused roughly the same yield of 38-45%. An unexpectedly high yield of over 90% resulted from the P,N-ligand Ph-phox (**40**). On the basis of a ligand screening with the racemic (hydrido)silyl ether **103b**, no trend between the activity of ligand groups was observed but a comparison of the residues of the ligands led to the following conclusions:

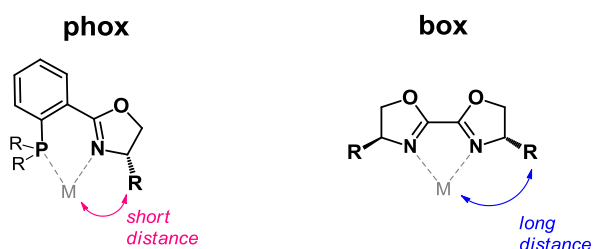
1. Flat or long residues such as phenyl or *n*-butyl cause low enantioselectivities,
2. Sterically demanding residues such as *iso*-propyl, *tert*-butyl and benzyl cause higher enantioselectivities,
3. The flexible and long *n*-butyl residue causes medium yield,
4. The phenyl residue seems to be beneficial for relatively high yield.



Scheme 8-4. Kinetic resolution of racemic (hydrido)silyl ether (**103b**) by catalytic formation of the corresponding oxasilolane (**104b**).

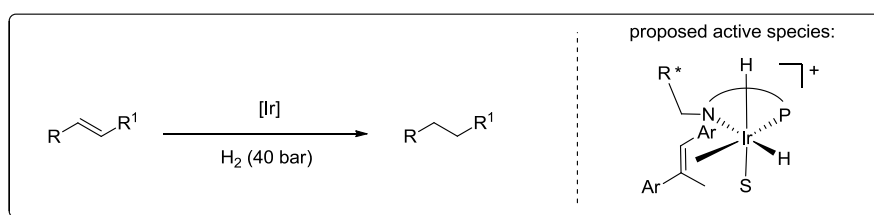
Hydrogenation

The oxazoline ligands were less effective in catalytic hydrogenation than the usually applied phox ligands. In order to achieve high yields of up to 99 %, the hydrogen pressure had to be increased to 40 bar instead of 20 bar, which was sufficient for the catalyst with a phox ligand. The chemoselectivity for C-C bonds in α,β -unsaturated ketones was very good, but when the chiral oxazolines were applied as ligands in the reduction of isophorone, no enantioselectivity was observed. A reason for this might be the smaller backbone of the oxazoline ligands in comparison with phox ligands thus leading to a too large distance between the stereogenic center and the the metal center (Scheme 8-5).

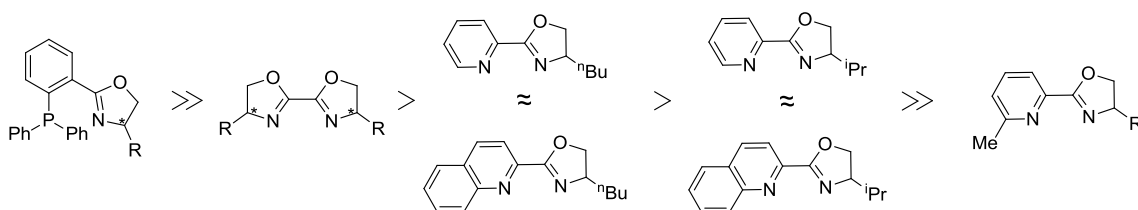


Scheme 8-5. Comparison of box and phox ligands.

Besides the lack of enantioselectivity, a clear trend for the reactivity of the oxazoline ligands was found (Scheme 8-6). This trend shows a clear correlation between activity and steric hindrance of the ligand. Following this, the flexible box ligands were most active, followed by pyrox and quinox ligand. For the latter two groups, a higher reactivity for ligands with flexible *n*-butyl residue was observed, while the yield achieved with ligands containing *iso*-propyl groups, was lower. Mepyrox ligands led to nearly no yield.



Reactivity:

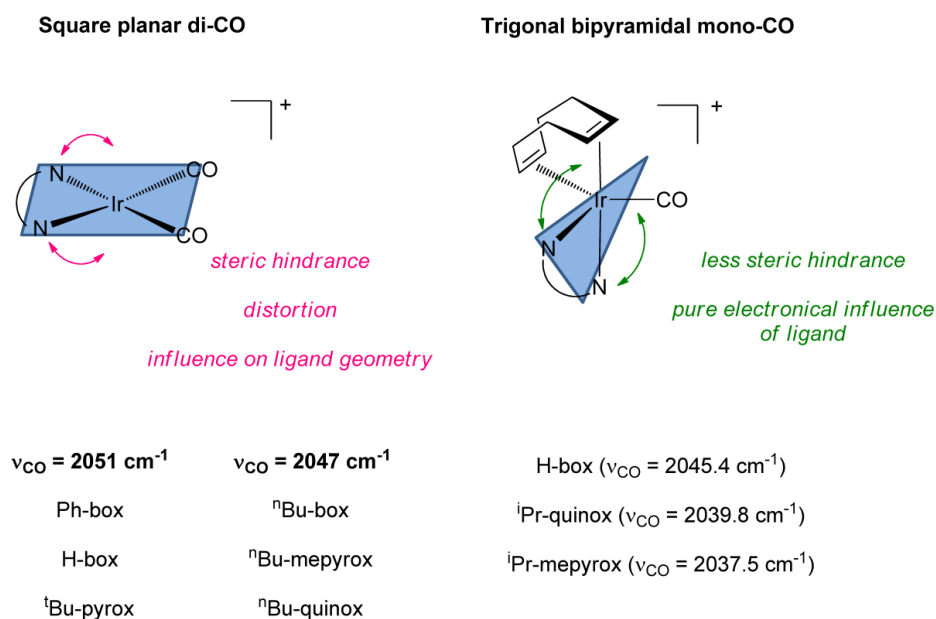


Scheme 8-6. Relative reactivity of oxazoline and phox ligands applied in homogeneous hydrogenation.

8.4 Evaluation of the Ligands in Carbonyl Complexes

In general, all groups of oxazoline ligands (**5**, **10**, **19**, **20**) and dtbpy (**32**) led to ν_{CO} absorption energies in the same range, when they were applied as ligands in square planar dicarbonyl complexes $[\text{Ir}(\text{N}^{\wedge}\text{N})(\text{CO})_2]\text{PF}_6$ (**28**). Highest ν_{CO} absorption energies of approximately 2051 cm^{-1} (average of $\nu_{\text{as, CO}}$ and $\nu_{\text{s, CO}}$) were caused by the flat Ph-box (**5g**), H-box (**5i**) and ^tBu-pyrox (**10c**) ligands (Scheme 8-7). Lowest ν_{CO} absorption energies of approximately 2047 cm^{-1} (average of $\nu_{\text{as, CO}}$ and $\nu_{\text{s, CO}}$) were obtained for complexes with flexible ⁿBu-box (**5f**), ⁿBu-mepyrox (**19f**) and ⁿBu-quinox (**20f**). For the C_2 symmetrical box ligands a high dependence on the oxazoline residue was observed, showing a trend that the most flexible residues caused the lowest ν_{CO} absorption energies. Also the sterically demanding mepyrox and quinox ligands caused relatively low ν_{CO} absorption energies, corresponding to weak C-O bonds. The weak C-O bonds could result from either a strong σ -donation of the ligand or a weak π -back bonding from the metal to the ligand. Both effects are dependent on the twisting of the ligand, caused by a highly flexible residue. The twisting either happens in the ligand backbone thus causing less conjugation of the donor atoms which results in an increased basicity or the whole ligand is twisted out of the carbonyl-iridium plane which would cause a worse overlap of the orbitals responsible for π -back donation. Consequently, in these square planar dicarbonyl complexes **28**, the ν_{CO} absorption energies were strongly influenced by the residues on the oxazoline ligands. Therefore, the dicarbonyl complexes turned out to be indicative for the steric properties of a ligand.

In trigonal bipyramidal monocarbonyl complexes $[\text{Ir}(\text{ligand})(\text{cod})\text{CO}]\text{PF}_6$ (**26**), this effect was less pronounced, showing an electronical influence of the ligands on the ν_{CO} absorption energies. Thus, it was no surprise to observe a higher electron donation by ⁱPr-mepyrox (**19b**) than for ⁱPr-quinox (**20b**), which both have caused identical ν_{CO} absorption energies in dicarbonyl complexes before.



Scheme 8-7. Dicarbonyl and monocarbonyl complexes.

The ν_{CO} absorption energies of the monocarbonyl complexes indicate similar electronical properties of dtbpy (**32**, 2042.3 cm^{-1}) and the oxazoline ligands, while the unsubstituted bpy (**37**, 2050.8 cm^{-1}) causes a much higher ν_{CO} absorption energy, corresponding to a lower electron density on iridium.

9 Conclusion

In general, the oxazoline ligands are much weaker ligands than bipyridines. The synthesis of heteroleptic ruthenium complexes showed this impressively, because the bipyridine ligands substituted the box ligands from all complexes that were tested. Also iridium complexes $[\text{Ir}(\text{N}^{\wedge}\text{N})(\text{cod})]\text{Cl}$ (**24**) were only successfully prepared with dtbpy (**32**), two pyrox ligands and with the sterically unhindered H-box ligand (**5i**). To obtain similar complexes with all oxazoline ligands, the Cl^- had to be exchanged for a non-coordinating anion such as PF_6^- and $\text{BAR}^{\text{F}-}$ before coordination of the oxazoline ligand.

The analysis of mono and dicarbonyl complexes showed similar ν_{CO} absorption energies for the oxazolines and the relatively electron rich bipyridine dtbpy (**32**). Besides this, the residues on the oxazoline moiety had a strong influence on the ν_{CO} absorption energies. Therefore, the square planar dicarbonyl complexes turned out to be an effective tool for the evaluation of steric influence in complexes with such a coordination sphere. In addition, it is also beneficial to use the same central metal for the carbonyl complexes which is applied in catalytic reactions, because the different radii of other metals could also influence the steric properties of the ligands.

In aromatic borylation and (hydrido)silyl ether directed γ -C-H activation, the oxazoline containing complexes were able to catalyze the reactions, but the achieved yields were lower than with the usually used bipyridine or phenanthroline ligands. The lower reactivity of the oxazoline complexes might be attributed to the weaker binding ability of the oxazoline ligands, which was already observed in the preparation of ruthenium and iridium complexes. The reactivity of the different oxazoline groups (box, pyrox, mepyrox and quinox) was very different in both reactions. In the aromatic borylation the C_2 -symmetric box ligands were less active than the pyrox-type ligands. This trend was not observed in the (hydrido)silyl ether directed γ -C-H activation. Here, yield and enantioselectivity seemed to be influenced mainly by the oxazoline residue and not by the ligand backbone.

Similar observations were made in homogeneous hydrogenation. The oxazoline complexes were less active than the usually applied phox complexes. Within the oxazolines a trend from box > pyrox = quinox > mepyrox in order of decreasing activity was observed. This trend indicates that an increasing steric hindrance is responsible for the decrease in activity.

In conclusion, it was shown that the prepared chiral oxazoline ligands were able to replace the non-chiral bipyridines as ligands in homogeneous catalysis. However, the oxazoline complexes showed usually a lower activity, presumably because the oxazolines are weaker ligands. If the activity of a complex can be increased by a higher basicity of the ligand, the easily prepared bithiazolines (bta, **7**) ligands could be applied instead of oxazolines, since the analysis of the carbonyl complexes showed that the change from oxygen to sulfur caused a higher electron density on the iridium. The results

obtained from the hydrogenation reactions indicated that the chiral center is too far away from the central metal, thus the application of oxazolines with a larger backbone which decreases the bite angle of the ligand, should be taken into consideration. Examples for such ligands are the methylene-bridged mebox or the cybox ligands bearing a cyclohexyl backbone (cf. chapter 2.2). Another approach for the future investigations would be to target reactions in which bipyridines were reported to deactivate the catalyst, for example the Pd(II) catalyzed alcohol oxidation.^[246] Possibly, in these reactions the weaker oxazolines might have a supporting effect on the activity of the catalyst.

All in all, it is worth seeking for conditions which lead to efficient asymmetric catalysis promoted by oxazoline complexes, since the amino acid derived ligands provide an exceptionally sustainable approach. Combinations or expansions with other naturally occurring structures such as sugars or chiral carboxylic diacids offer numerous possibilities to design chiral ligands for homogeneous catalysis.

IV. Experimental Section

10 General Methods

Chemicals were purchased from commercial suppliers and used as received unless otherwise noted. Dried solvents were taken from an *MS-Braun* solvent purification system. Reactions under inert gas conditions were performed using dried schlenk-glassware under argon as inert gas. CDCl_3 was filtered over potassium carbonate prior use. Solvents for hydrogenations were degassed by three freeze-pump-thaw cycles prior use. Ruthenium complexes were prepared under light exclusion.

Reactions were monitored by thin layer chromatography (TLC) using *Merck TLC Silica gel 60 F₂₅₄*. Products were detected using a UV/Vis lamp (254 nm). Column chromatography was performed on *Brockmann I Aluminium oxide (50-200 μm)*.

Nuclear magnetic resonance spectroscopy ($^1\text{H-NMR}$, $^{13}\text{C-NMR}$, $^{19}\text{F-NMR}$) spectra were recorded at r.t. using a *Jeol ECX 400* (1 H-NMR: 400 MHz, $^{13}\text{C-NMR}$: 101 MHz, $^{19}\text{F-NMR}$: 376 MHz), *Joel Eclipse 500* (1 H-NMR: 500 MHz, $^{13}\text{C-NMR}$: 126 MHz) or *Bruker AV 700* (1 H-NMR: 700 MHz, $^{13}\text{C-NMR}$: 176 MHz, $^{19}\text{F-NMR}$: 470 MHz). Two dimensional spectra (COSY, HMQC, HMBC) were recorded on a *Joel Eclipse 500* or *Bruker AV 700*. Data were processed with *Delta NMR Processing and Control Software* (Version: 4.3.6 [Windows_NT]), *MestreC* or *MestreNova* from MESTRELAB.

The spectra are referenced against the internal solvent.^[247] Data is reported as follows: s= singlet, d= doublet, t= triplet, q= quartet, quin= quintet and m= multiplet.

GC-MS chromatograms were recorded on a *Varian 3900 GC* with *Saturn 2100* iontrap mass spectrometer, *Varian CP-8410* autosampler

High resolution ESI-MS spectra were recorded on an *Agilent 6210 ESI-TOF*, *Agilent Technologies*. The applied charge is reported as positive (+) or negative (-). The spray charge was set to 4 kV. The defractor charge is given in Volt (V). Data is reported in mass to charge (m/z).

GC-FID chromatograms were recorded on a *Varian CP-3800* with FID-detektor, *Varian CP-8400* autosampler

ATR-IR solution measurements were performed using a *Bruker IFS66v/s* spectrometer equipped with a photoconductive MCT detector, a *Kretschmann-ATR* setup at an angle of incidence of 60° and a home-built ATR-cell with a silicon prism. Spectra were acquired in a spectral window of 4000 to 1000 cm^{-1} with a resolution of 2 cm^{-1} . ATR-IR spectra from solid compounds were recorded on a *Nicolet Avatar 320 FT-IR* in the range 4000–500 cm^{-1} on a diamant optical window. The absorption bands are given in wave numbers (cm^{-1}), intensities are reported as follows: s= strong, m= medium, w = weak.

Melting points were measured on a *BÜCHI 510 melting point* and are uncorrected.

Crystal structure analysis including measurement, structure determination and refinement was performed by Prof. Lentz or Dr. Wiecko. Structure determination by single-crystal X-ray diffraction was carried out by selecting an appropriate crystal under a stream of cold nitrogen and transferring it to the nitrogen cooled goniometer. The data set was collected with a Bruker-AXS SMART CCD at 133(2) K. The structure was solved using direct methods (SHELXS-97) and refined by full-matrix least squares procedures (SHELXL-97). Multi-scan absorption corrections were applied (SADABS). All non-hydrogen atoms were refined anisotropically, hydrogen atoms were included in the refinement at calculated positions using a riding model. The electron density of occurring solvent was addressed with the program SQUEEZE (PLATON). Molecular graphics were obtained with ORTEP and DIAMOND.

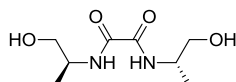
11 Ligands

11.1 Box-structures

11.1.1 Bioxalamides

11.1.1.1 *N,N'*-Bi((*S*)-1-hydroxypropan-2-yl)oxalamid (3a)

(GM 1126)



The reaction was carried out under an argon atmosphere. (*R*)-alaninol (2.00 g, 26.6 mmol) was dissolved in toluene (250 mL) and dimethyloxalate (1.57 g, 13.3 mmol) was added. The reaction mixture was heated to 80 °C (oil bath) for 2.5 h while a white solid precipitated. The mixture was filtered and the remaining solid washed with toluene. The product was obtained as colourless powder (2.10 g 10.3 mmol, 77 %).

¹H-NMR (DMSO-d₆, 500 MHz): δ = 1.06 (d, *J* = 6.5 Hz, 6H, CH₃), 3.33 (dd, *J* = 5.8, 10.9 Hz, 2H, CHH), 3.38 (dd, *J* = 5.8, 10.9 Hz, 2H, CHH), 3.76–3.85 (m, 2H, C*H), 4.80 (br. s, 2H, OH), 8.32 (d, *J* = 8.9 Hz, 2H, NH) ppm.

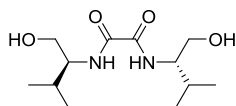
¹³C-NMR (DMSO-d₆, 125 MHz): δ = 17.2 (CH₃), 47.7 (CH₂), 64.4 (C*), 160.0 (CO) ppm.

IR (solid): $\tilde{\nu}$ = 3370 (w), 3286 (m, v NH), 2977 (w), 2937 (w), 2887 (w), 1652 (s, v CO), 1525 (s), 1474 (m), 1455 (m), 1449 (m), 1375 (w), 1365 (w), 1342 (w), 1305 (w), 1249 (m), 1215 (w), 1134 (w), 1105 (m), 1044 (s), 988 (w), 915 (w), 870 (w), 770 (s), 703 (m) cm⁻¹.

HRMS (+ESI, 200 V): *m/z* (%) = 227.1005 (100) [M+H]⁺ (calc. 227.1008).

11.1.1.2 *N,N'*-Bi((*S*)-1-hydroxy-3-methylbutan-2-yl)oxalamide (3b)

(2030)



The reaction was carried out under an argon atmosphere. (*S*)-valinol (300 mg, 2.54 mmol) and dimethyloxalate (524 mg, 5.08 mmol) were dissolved in dry toluene (70 mL) and heated to reflux for 1 hour. During the reaction, a colourless solid precipitated from the solution. The solid was separated by filtration and washed with toluene to give the product as colourless flakes (579 mg, 2.22 mmol, 87%).

¹H-NMR (CDCl₃, 400 MHz): δ = 0.93 (d, J = 6.7 Hz, 6H, CH(CH₃)₂), 0.97 (d, J = 6.7 Hz, 6H, CH(CH₃)₂), 1.88 (tt, J = 6.7, 6.7 Hz, 2H, CH(CH₃)₂), 3.60-3.76 (m, 8H, C*H-CH₂-OH), 7.66 (d, J = 9.5 Hz, 2H, NH) ppm.

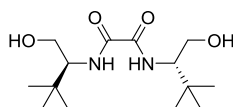
¹³C-NMR (DMSO-d₆, 100.6 MHz): δ = 19.1 (CH₃), 20.1 (CH₃), 29.0 (CH), 57.1 (CH₂), 61.3 (C*), 160.3 (C=O) ppm.

IR (solid): $\tilde{\nu}$ = 3379 (m), 3283 (s), 3068 (w), 2959 (w), 2938 (w), 2874 (w), 2650 (w), 2161 (w), 2035 (w), 1979 (w), 1645 (s), 1518 (s), 1464 (m), 1389 (m), 1369 (m), 1464 (m), 1389 (m), 1369 (m), 1336 (w), 1310 (w), 1283 (w), 1265 (w), 1227 (m), 1215 (m), 1170 (m), 1143 (m), 1067 (s), 1027 (s), 982 (w), 974 (w), 931 (w), 891 (w), 859 (w), 845 (w), 820 (w), 751 (s), 668 (m) cm⁻¹.

HRMS (+ESI, 250V): m/z (%) = 283.1625 (100) [M+Na]⁺ (calc. 283.1628).

11.1.1.3 *N,N'*-Bi((*S*)-1-hydroxy-3,3-dimethylbutan-2-yl)oxalamide (**3c**)

(GM 1004)



The reaction was carried out under an argon atmosphere. (*R*)-*tert*-leucinol (2.50 g, 21.3 mmol) and dimethyloxalat (1.26 g, 10.6 mmol) were dissolved into dry toluene (250 mL) and heated to 80°C (oil-bath) for 3 hours. During the reaction, a colourless solid precipitated from the solution. The solid was separated by filtration and washed with toluene to give the product as colourless powder (.75 g, 9.54 mmol, 89 %).

¹H-NMR (CDCl₃, 400 MHz): δ = 1.30 (s, 18H, ^tBu), 3.93 (dd, J = 2.3, 11.5 Hz, 2H, CH₂), 4.074.14 (m, 2H, C*H), 4.21 (dd, J = 8.5, 11.5 Hz, 2H, CH₂), 7.94 (d, J = 10.4 Hz, 2H, NH) ppm.

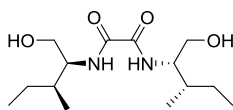
¹³C-NMR (DMSO-d₆, 100 MHz): δ = 27.4 (C-(CH₃)₃), 34.4 (C-(CH₃)₃), 59.9 (CH₂), 60.4 (C*), 160.7 (CO) ppm.

IR (solid): $\tilde{\nu}$ = 3292 (m, ν NH), 3228 (w), 2965 (w), 2864 (w), 2360 (w), 2340 (s), 2244 (w), 2211 (w), 2199 (w), 2183 (w), 1653 (m, ν CO), 1558 (w), 1522 (m), 1507 (w), 1395 (w), 1364 (w), 1338 (w), 1053 (w), 896 (w), 800 (w), 775 (w), 688 (w), 669 (m) cm⁻¹.

HRMS (+ESI, 200V): m/z (%) = 311.1914 (100) [M+Na]⁺ (calc. 311.1941).

11.1.1.4 *N,N'*-Bi((2*S*,3*S*)-1-hydroxy-3-methylpentan-2-yl)oxalamide (3d)

(GM 1022)



The reaction was carried out under an argon atmosphere. (*S,S*)-*iso*-leucinol (9c) (2.50 g, 21.3 mmol) and dimethyloxalat (1.26 g, 10.6 mmol) were dissolved in dry toluene (50 mL) and heated to 80°C (oil-bath) for 0.5 hours. During this time a colourless solid precipitated from solution. The solid was separated by filtration and washed with toluene to give the product as colourless powder (2.79 g, 10.6 mmol, 91 %):

¹H-NMR (CDCl₃/methanol-d₄ = 9/1, 500 MHz): δ = 0.750.86 (m, 12H, CH₃), 0.981.08 (m, 2H, CHH-CH₃), 1.341.43 (m, 2H, CHH-CH₃), 1.531.61 (m, 2H, C*H-CH₃), 3.483.75 (m, 8H, C*H-CH₂-OH), 7.69 (s, 2H, NH) ppm.

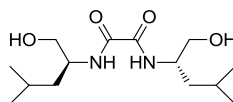
¹³C-NMR (CDCl₃/methanol-d₄ = 9/1, 125 MHz): δ = 11.1 (CH₃-CH₂), 15.2 (CH₃-C*H), 25.3 (CH₂-CH₃), 35.4 (C*H-CH₃), 56.4 (CH₂-Cl), 61.9 (C*H-NH), 160.2 (CO) ppm.

IR (solid): $\tilde{\nu}$ = 3429 (m), 3410 (m), 3279 (s, ν NH), 2962 (m), 2934 (m), 2876 (m), 1681 (w), 1644 (s, ν CO), 1522 (s), 1482 (m), 1461 (m), 1450 (m), 1424 (w), 1385 (w), 1367 (w), 1306 (w), 1287 (w), 1245 (w), 1219 (m), 1156 (w), 1142 (w), 1072 (s), 1043 (m), 1030 (m), 986 (w), 962 (w), 911 (w), 888 (w), 869 (w), 839 (w), 777 (s), 758 (s), 663 (m) cm⁻¹.

HRMS (+ESI, 200V): m/z (%) = 311.1948 (100) [M+Na]⁺ (calc. 311.1936).

11.1.1.5 *N,N'*-Bi((*S*)-1-hydroxy-4-methylpentan-2-yl)oxalamide (3e)

(2094)



The reaction was carried out under an argon atmosphere. (*S*)-leucinol (2.00 g, 18.2 mmol) and dimethyloxalat (1.01 g, 8.53 mmol) were dissolved in dry toluene (200 mL) and heated to 85°C (oil-bath) for 3 hours. During this time a colourless solid precipitated from solution. The solid was separated by filtration and washed with toluene to give the product as colourless powder (2.27 g, 7.86 mmol, 92 %).

¹H-NMR (CDCl₃/DMSO-d₆ = 10/1, 400 MHz): δ = 0.53 (d, J =6.7 Hz, 6H, CH₃), 0.97-10.13 (m, 4H, CH₂-CH(CH₃)₂), 1.18-1.28 (m, 2H, CH-(CH₃)₂), 3.11-3.20 (m, 4H, CH₂-OH), 3.55-3.64 (m, 2H, C*-H), 4.04 (s, 2H, OH), 7.46 (d, J =9.2 Hz, 2H, NH) ppm.

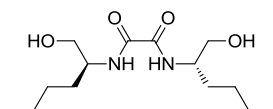
¹³C-NMR (DMSO-d₆, 100 MHz): δ = 21.4 (CH₃), 22.2 (CH₃), 23.8 (CH(CH₃)₂), 39.8 (CH₂-CH(CH₃)₂), 49.1 (C*), 63.1 (CH₂-OH), 158.9 (CO) ppm.

IR (solid): $\tilde{\nu}$ = 3365 (m), 3275 (s), 3068 (w), 2954 (m), 2872 (m), 2161 (w), 2032 (w), 1979 (w), 1650 (s), 1521 (s), 1468 (m), 1437 (m), 1385 (m), 1365 (m), 1343 (w), 1310 (w), 1293 (w), 1260 (m), 1234 (w), 1216 (m), 1170 (w), 1140 (w), 1100 (w), 1058 (m), 1046 (m), 1030 (m), 1013 (m), 966 (w), 920 (w), 885 (w), 858 (w), 811 (w), 777 (s) cm^{-1} .

HRMS (+ESI, 200 V): m/z (%) = 311.1927 (100) $[\text{M}+\text{Na}]^+$ (calc. 311.1941), 327.1667 (21) $[\text{M}+\text{K}]^+$ (calc. 327.1681), 289.2099 (9) $[\text{M}+\text{H}]^+$ (calc. 289.2122).

11.1.1.6 *N,N'*-Bi(*S*)-1-hydroxyhexan-2-yl)oxalamide (**3f**)

(2106)



The reaction was carried out under an argon atmosphere. (*R*)-2-amino-1-hexanol (1.00 g, 8.53 mmol) and dimethyloxalat (0.50 g, 4.27 mmol) were dissolved in dry toluene (10 mL) and heated to 85°C (oil-bath) for 3 hours. During this time a colourless solid precipitated from solution. The solid was separated by filtration and washed with toluene to give the product as colourless powder (1.08 g, 3.76 mmol, 88 %).

¹H-NMR ($\text{CDCl}_3/\text{DMSO-d}_6 = 10/1$, 400 MHz): δ = 0.80-0.86 (m, 3H, CH_3), 1.19-1.33 (m, 4H, CH_2), 1.42-1.62 (m, 2H, CH_2), 2.9 (s, 1H, OH), 3.53 (dd, $J=5.6, 11.4$ Hz, 1H, *CHH*-OH), 3.62 (dd, $J=3.7, 11.4$ Hz, 1H, *CHH*-OH), 3.81-3.89 (m, 1H, $\text{C}^*\text{-H}$), 7.64 (d, $J=8.3$ Hz, 1H, NH) ppm.

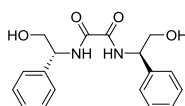
¹³C-NMR (DMSO-d_6 , 100 MHz): δ = 14.4 (CH_3), 22,5(CH_2), 28.4 (CH_2), 30.6 (CH_2), 52.0 ($\text{CH}_2\text{-OH}$), 63.4 (C^*), 160.4 ($\text{C}_{\text{carbonyl}}$) ppm.

IR (solid): $\tilde{\nu}$ = 3404 (m), 2370 (s), 3068 (w), 2952 (m), 2932 (m), 2859 (m), 2035 (w), 1979 (w), 1650 (s), 1519 (s), 1465 (m), 1442 (m), 1413 (m), 1379 (m), 1358 (w), 1325 (w), 1284 (m), 1265 (m), 1236 (m), 1227 (m), 1211 (m), 1146 (m), 1146 (w), 1124 (w), 1097 (m), 1063 (m), 1034 (s), 988 (w), 951 (w), 911 (w), 888 (w), 872 (w), 819 (w), 772 (m), 742 (m), 728 (m), 699 (m), 668 (m), 595 (m), 577 (m), 563 (m), 545 (m), 538 (m) cm^{-1} .

HRMS (+ESI, 250 V): m/z (%) = 311.1950 (100) $[\text{M}+\text{Na}]^+$ (calc. 311.1941).

11.1.1.7 *N,N'*-Bi(*S*)-2-hydroxy-1-phenylethyl)oxalamide (**3g**)

(GM 1002)



The reaction was carried out under argon atmosphere. (*R*)-phenylglycinol (2.50 g, 18.2 mmol) and dimethyloxalat (1.08 g, 9.11 mmol) were dissolved in dry toluene (250 mL) and treated at 80°C (oil-

bath) for 2 hours. During this time a colourless solid precipitated from solution. The solid was separated by filtration and washed with toluene to give the product as colourless powder (2.52 g, 7.68 mmol, 85 %).

¹H-NMR (DMSO-d₆, 400 MHz): δ = 3.603.76 (m, 4H, CH₂-OH), 4.824.90 (m, 2H, C*-H), 4.98 (s, 2H, OH), 7.197.40 (m, 10H, H_{ar}), 8.89 (d, J = 8.6, 2H, NH) ppm.

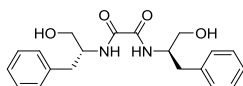
¹³C-NMR (DMSO-d₆, 100 MHz) δ = 56.3 (C*), 64.4 (CH₂), 127.4 (C_{ar}-H), 127.7 (C_{ar}-H), 128.8 (C_{ar}-H), 140.5 (C_{ar}-C), 160.3 (CO) ppm.

IR (solid): $\tilde{\nu}$ = 3290 (m, v NH), 3061 (w,), 3013 (w), 2933 (w), 2864 (w), 2359 (w), 2315 (w), 1651 (s, v CO), 1584 (w), 1514 (s), 1454 (m), 1410 (w), 1384 (w), 1273 (w), 1241 (w), 1210 (w), 1184 (w), 1071 (m), 1044 (m), 997 (w), 909 (w), 847 (m), 755 (m), 697 (s) cm⁻¹.

HRMS (+ESI, 200V): m/z (%) = 351.1351 (13) [M+Na]⁺ (calc. 351.1315).

11.1.1.8 *N,N'*-Bi((*S*)-1-hydroxy-3-phenylpropan-2-yl)oxalamide (**3h**)

(2108)



The reaction was carried out under an argon atmosphere. (*R*)-2-amino-3-phenyl-1-propanol (2.00 g, 13.2 mmol) and dimethyloxalat (0.78 g, 6.61 mmol) were dissolved into dry toluene (30 mL) and heated at 85°C (oil-bath) for 3 hours. During this time a colourless solid precipitated from solution. The solid was separated by filtration and washed with toluene to give the product as colourless powder (1.97 g, 5.51 mmol, 70 %).

¹H-NMR (DMSO-d₆, 500 MHz): δ = 2.71 (dd, J =8.5, 14.0 Hz, 1H, CHH), 2.85 (dd, J =5.5, 14.0 Hz, 1H, CHH), 3.94 (d, J =5.5 Hz, 1H, C*-H), 4.88 (s, 1H, OH), 7.13-7.25 (m, 5H, H_{ar}), 8.33 (d, J =8.9 Hz, 1H, NH) ppm.

¹³C-NMR (DMSO-d₆, 100 MHz): δ = 36.7 (CH₂), 62.8 (C*), 126.5 (C_{ar}-4), 128.7 (C_{ar}-H), 129.5 (C_{ar}-H), 139.4 (C_{ar}-C), 160.1 (C_{carbonyl}) ppm.

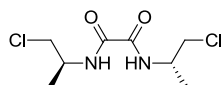
IR (solid): $\tilde{\nu}$ = 3413 (w), 3299 (m), 3082 (w), 3061 (w), 3031 (w), 3020 (w), 2912 (w), 2876 (w), 2161 (w), 2022 (w), 1933 (w), 1684 (w), 1654 (s), 1603 (w), 1584 (w), 1559 (w), 1514 (m), 1498 (m), 1464 (m), 1453 (m), 1443 (m), 1405 (w), 1383 (w), 1360 (w), 1339 (w), 1322 (w), 1296 (w), 1367 (w), 1251 (m), 1226 (w), 1208 (w), 1190 (m), 1180 (w), 1156 (w), 1102 (w), 1083 (m), 1041 (s), 1006 (m), 998 (m), 961 (m), 913 (m), 900 (m), 866 (m), 844 (w), 810 (w), 785 (m), 794 (m), 738 (s), 699 (s), 666 (m) cm⁻¹.

HRMS (+ESI, 250 V): m/z (%) = 379.1642 (100) [M+Na]⁺ (calc. 379.1628).

11.1.2 Bi- β -chlorooxalamide

11.1.2.1 *N,N'*-Bi((*S*)-1-chloropropan-2-yl)oxalamid (**4a**)

(GM 1126)



Hydroxy-diamide **3a** (1.83 g, 8.96 mmol) was dissolved in thionylchlorid (50 mL) and heated under reflux for 2 h. The solvent was removed under reduced pressure and the solid residue recrystallized from ethylacetate to yield a colourless powder (1.45 g, 6.06 mmol, 68 %).

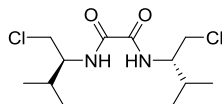
¹H-NMR (DMSO-*d*₆, 500 MHz): δ = 1.17 (d, *J* = 6.5 Hz, 6H, CH₃), 3.59 (dd, *J* = 5.4, 10.9 Hz, 2H, CHH), 3.65 (dd, *J* = 7.5, 10.9 Hz, 2H, CHH), 4.01–4.11 (m, 2H, C*H), 8.78(s, 2H, NH) ppm.

¹³C-NMR (DMSO-*d*₆, 125 MHz): δ = 18.4 (CH₃), 47.4 (CH₂), 47.9 (C*), 159.9 (CO) ppm.

IR (solid): $\tilde{\nu}$ = 3276 (m, ν NH), 3066 (w), 2979, (w), 2368 (w), 1738 (w), 1655 (s, ν CO), 1559 (w), 1529 (s), 1486 (m), 1450 (m), 1434 (m), 1377 (w), 1349 (w), 1321 (w), 1240 (m), 1191 (m), 1149 (m), 1092 (w), 1066 (w), 986 (w), 932 (w), 905 (w), 870 (w), 858 (w), 772 (s), 732 (s) cm⁻¹.

11.1.2.2 *N,N'*-Bi((*S*)-1-chloro-3-methylbutan-2-yl)oxalamide (**4b**)

(2042)



Hydroxy-diamide **3b** (4.67 g, 17.9 mmol) was dissolved in thionylchloride (25 mL) and heated under reflux for 2 h. The volatile compounds were evaporated under high vacuum and the solid residue recrystallized from ethylacetate at -22°C to give the product as colourless crystalline powder (4.24 g, 14.2 mmol, 79%).

¹H-NMR (CDCl₃, 400 MHz): δ = 0.95 (d, *J* = 6.7 Hz, 6H, CH(CH₃)₂), 0.99 (d, *J* = 6.7 Hz, 6H, CH(CH₃)₂), 2.03 (tt, *J* = 6.7, 6.7 Hz, 2H, CH(CH₃)₂), 3.63-3.73 (m, 4H, CH₂Cl), 3.87-3.94 (m, 2H, C*H), 7.56 (d, *J* = 9.5 Hz, 2H, NH) ppm.

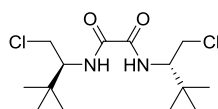
¹³C-NMR (DMSO-*d*₆, 100.6 MHz): δ = 19.1 (CH₃), 19.7 (CH₃), 32.4 (CH), 46.1 (CH₂), 57.1 (C*), 160.5 (C=O) ppm.

IR (solid): $\tilde{\nu}$ = 3273 (s), 3065 (w), 3018 (w), 2964 (w), 2941 (w), 2873 (w), 2359 (w), 2161 (w), 2029 (w), 1978 (w), 1656 (s), 1525 (s), 1472 (m), 1440 (m), 1391 (m), 1370 (m), 1343 (m), 1311 (m), 1296 (m), 1255 (m), 1231 (m), 1188 (m), 1167 (m), 1140 (m), 1124 (m), 1107 (m), 1059 (m), 1045 (m), 1025 (m), 973 (m), 960 (m), 921 (m), 8877 (m), 859 (m), 779 (m), 763 (s), 733 (s) cm⁻¹.

HRMS (+ESI, 250V): *m/z* (%) = 319.1010 (100) [M+Na]⁺ (calc. 319.0951).

11.1.2.3 *N,N'*-Bi((*S*)-1-chloro-3,3-dimethylbutan-2-yl)oxalamide (**4c**)

(GM 1008)



Hydroxy-diamide **4c** (2.75 g, 9.52 mmol) was dissolved in thionylchloride (25 mL) and heated to reflux for 2 h. The volatile components were evaporated under high vacuum and the solid residue dissolved in ethylacetate and precipitated by addition of hexane. The solid was isolated by filtration to give the product as colourless powder (2.23 g, 6.85 mmol, 72 %).

$^1\text{H-NMR}$ (CDCl_3 , 400 MHz): δ = 0.98 (s, 18H, ^tBu), 3.49 (dd, J = 2.0, 11.5 Hz, 2H, $\text{CH}_2\text{-Cl}$), 3.81 (dd, J = 3.4, 11.5 Hz, 2H, $\text{CH}_2\text{-Cl}$), 3.974.05 (m, 2H, C^*H), 7.52 (d, J = 10.5 Hz, 2H, NH) ppm.

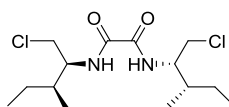
$^{13}\text{C-NMR}$ (methanol- d_4 , 100 MHz): δ = 25.6 ($\text{C-(CH}_3)_3$), 35.0 ($\text{C-(CH}_3)_3$), 43.5 (CH_2), 60.5 (C^*), 160.8 (CO) ppm.

IR (solid): $\tilde{\nu}$ = 3363 (m, v NH), 2959 (m), 2864 (w), 2361 (w), 2341 (w), 1685 (s, v CO), 1510 (s), 1473 (m), 1439 (m), 1397 (w), 1370 (m), 1330 (w), 1281 (w), 1226 (m), 1194 (w), 1177 (w), 1093 (w), 1061 (m), 1018 (w), 940 (w), 896 (w), 871 (w), 858 (w), 803 (m), 778 (w), 744 (w), (727 (s), 667 (s).

HRMS (+ESI, 250V): m/z (%) = 347.1277 (100) [M+Na] $^+$ (calc. 347.1264), 325.1454 (25) [M+H] $^+$ (calc. 325.1444), 363.1013 (14) [M+K] $^+$ (calc. 363.1003).

11.1.2.4 *N,N'*-Bi((*2S, 3S*)-1-chloro-3-methylpentan-2-yl)oxalamide (**4d**)

(GM 1026)



Hydroxy-diamide **3d** (2.68 g, 9.29 mmol) was dissolved in thionylchloride (30 mL) and heated under reflux for 2 h. The volatile components were evaporated under high vacuum and the solid residue recrystallized from ethylacetate at -20 °C to give the product as colourless powder (2.48 g, 7.64 mmol, 82 %).

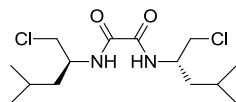
$^1\text{H-NMR}$ (CDCl_3 , 400 MHz): δ = 0.89 (t, J = 7.4 Hz, 6H, $\text{CH}_2\text{-CH}_3$), 0.95 (d, J = 6.8 Hz, 6H, $\text{C}^*\text{H-CH}_3$), 1.081.17 (m, 2H, CHH-CH_3), 1.471.55 (m, 2H, CHH-CH_3), 1.741.82 (m, 2H, $\text{C}^*\text{H-CH}_3$), 3.65-3.72 (m, 4H, $\text{CH}_2\text{-Cl}$), 3.943.99 (m, 2H, $\text{C}^*\text{H-NH}$), 7.59 (d, J = 9.2 Hz, 2H, NH) ppm.

$^{13}\text{C-NMR}$ (CDCl_3 , 100 MHz): δ = 11.1 ($\text{CH}_3\text{-CH}_2$), 15.2 ($\text{CH}_3\text{-C}^*\text{H}$), 25.1 ($\text{CH}_2\text{-CH}_3$), 35.6 ($\text{C}^*\text{H-CH}_3$), 45.8 ($\text{CH}_2\text{-Cl}$), 54.7 ($\text{C}^*\text{H-NH}$), 159.4 (CO) ppm.

IR (solid): $\tilde{\nu}$ = 3287 (m, v NH), 2966 (w), 2931 (w), 2874 (w), 1651 (s, v CO), 1503 (s), 1470 (w), 1439 (w), 1383 (w), 1333 (w), 1289 (m), 1244 (w), 1207 (m), 1165 (w), 1146 (w), 1103 (w), 1060 (w), 1041 (w), 999 (w), 905 (w), 834 (w), 811 (w), 775 (w), 737 (m), 675 (m) cm^{-1} .

11.1.2.5 *N,N'*-Bi((*S*)-2-chloro-4-methylpentan-2-yl)oxalamid (**4e**)

(2098)



Hydroxy-diamide **3e** (2.18 g, 7.56 mmol) was dissolved in thionylchloride (10 mL) and heated under reflux for 2 h. The volatile components were evaporated under high vacuum and the solid residue dissolved in ethylacetate and precipitated by addition of hexane to give the product as colourless powder which was isolated by filtration (2.28 g, 7.00 mmol, 92 %).

¹H-NMR (CDCl_3 , 400 MHz): δ = 0.83 (d, J =6.2 Hz, 12H, CH_3), 1.34-1.55 (m, 6H, $\text{CH}_2\text{-CH}(\text{CH}_3)_2$), 3.52 (dq, J = 4.6, 11.1 Hz, 4H, $\text{CH}_2\text{-Cl}$), 4.09-4.18 (m, 2H, $\text{C}^*\text{-H}$), 7.62 (d, J =9.0 Hz, 2H, NH) ppm.

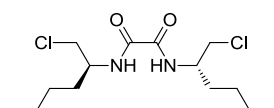
¹³C-NMR (DMSO-d_6 , 100 MHz): δ = 21.9 (CH_3), 22.7 (CH_3), 24.5 ($\text{CH}(\text{CH}_3)_2$), 40.6 ($\text{CH}_2\text{-CH}(\text{CH}_3)_2$), 47.3 (C^*), 48.6 ($\text{CH}_2\text{-Cl}$), 159.2 (CO) ppm.

IR (solid): $\tilde{\nu}$ = 3751 (m), 3066 (w), 2956 (m), 2930 (m), 2872 (w), 2360 (w), 2161 (w), 2027 (w), 1778 (w), 1733 (w), 1655 (s), 1521 (s), 1467 (m), 1438 (m), 1387 (w), 1368 (w), 1323 (w), 1297 (w), 1265 (m), 1245 (m), 1214 (m), 1185 (m), 1170 (w), 1140 (w), 1120 (w), 1095 (w), 1068 (w), 1047 (w), 1016 (w), 943 (w), 920 (w), 853 (w), 825 (m), 773 (s), 729 (s) cm^{-1} .

HRMS (+ESI, 250 V): m/z (%) = 347.1277(100) [$\text{M}+\text{K}$]⁺ (calc. 347.1264).

11.1.2.6 *N,N'*-Bi((*S*)-1-chlorohexan-2-yl)oxalamid (**4f**)

(2110)



Hydroxy-diamide **3f** (1.05 g, 3.64 mmol) was dissolved in thionylchloride (25 mL) and heated to reflux for 2 h. The volatile components were evaporated under high vacuum and the solid residue dissolved in ethylacetate and precipitated with hexane to give the product as colourless powder (0.873 g, 2.68 mmol, 73 %).

¹H-NMR (CDCl_3 , 400 MHz): δ = 0.87-0.92 (m, 3H, CH_3), 1.25-1.38 (m, 4H, CH_2), 1.57-1.75 (m, 2H, CH_2), 2.62 (dd, J = 11.4, 4.2 Hz, 1H, CHH-Cl), 3.66 (dd, J = 11.4, 4.2 Hz, 1H, CHH-Cl), 4.11-4.19 (m, 1H, $\text{C}^*\text{-H}$), 7.58 (d, J = 8.8 Hz, 1H, NH) ppm.

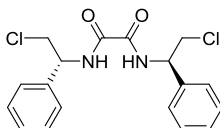
¹³C-NMR (DMSO-d_6 , 100 MHz): δ = 14.3 (CH_3), 22.2 (CH_2), 28.2 (CH_2), 31.8 (CH_2), 47.3 ($\text{CH}_2\text{-Cl}$), 51.7 (C^*), 160.5 ($\text{C}_{\text{carbonyl}}$) ppm.

IR (solid): $\tilde{\nu}$ = 3271 (m), 3060 (w), 2953 (m), 2932 (m), 2874 (w), 2858 (w), 1978 (w), 1655 (s), 1636 (m), 1522 (s), 1483 (m), 1464 (m), 1442 (m), 1377 (m), 1371 (m), 1318 (w), 1290 (m), 1261 (m), 1244 (m), 1207 (m), 1182 (m), 1140 (m), 1114 (w), 1080 (w), 1066 (m), 1013 (m), 997 (m), 969 (w), 892 (w), 870 (w), 859 (m), 788 (m), 771 (s), 736 (s), 726 (s), 697 (m), 668 (w), 578 (s).

HRMS (+ESI, 250 V): m/z (%) = 347.1258 (100) $[M+Na]^+$ (calc. 347.1264).

11.1.2.7 *N,N'*-Bi((*S*)-2-Chloro-1-phenylethyl)oxalamid (**4g**)

(GM 1010)



Hydroxy-diamide **3g** (1.98 g, 6.03 mmol) was dissolved in thionylchloride (50 mL) and treated under reflux for 2 h. The liquid compounds were evaporated under vacuum and the solid residue dissolved in ethylacetate and precipitated with hexane to give the product as colourless powder (1.63 g, 4.46 mmol, 74 %).

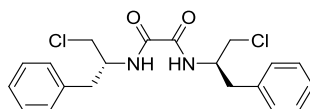
¹H-NMR (CDCl₃, 400 MHz): δ = 3.68 (dd, J = 5.1, 11.3 Hz, 2H, CH₂-Cl), 3.80 (dd, J = 7.7, 11.3 Hz, 2H, CH₂-Cl), 5.07 (dd, J = 5.1, 7.7 Hz, 2H, C*H), 7.10-7.20 (m, 10 H, H_{ar}), 8.40 (d, J = 9.04 Hz, 2H, NH) ppm.

¹³C-NMR (DMSO-d₆, 100 MHz): δ = 46.7(CH₂), 55.6(C*), 127.4(C_{ar}-H), 128.5(C_{ar}-H), 129.1(C_{ar}-H), 139.4(C_{ar}-C), 160.0 (CO) ppm.

IR (solid): $\tilde{\nu}$ = 3298 (s, v NH), 3061 (w), 3024 (w), 2960 (w), 2359 (m), 2325 (m), 1733 (w), 1653 (s, v CO), 1581 (w), 1514 (s), 1454 (m), 1429 (m), 1368 (w), 1333 (w), 1306 (w), 1248 (m), 1235 (m), 1192 (w), 1170 (w), 1075 (w), 1048 (m), 1026 (m), 1000 (w), 981 (w), 965 (w), 928 (w), 909 (w), 858 (w), 839 (w), 821 (w), 772 (m), 727 (s), 695 (s), 669 (w)cm⁻¹.

HRMS (+ESI, 200V): m/z (%) = 387.0653 (33) $[M+Na]^+$ (calc. 387.0638).

11.1.2.8 *N,N'*-Bi((*S*)-1-chloro-3-phenylpropan-2-yl)oxalamid (**4h**)



Hydroxy-diamide **3h** (1.93 g, 5.42 mmol) was dissolved in thionylchloride (50 mL) and heated under reflux for 2 h. The volatile components were evaporated under high vacuum and the solid residue dissolved in ethylacetate and precipitated with hexane to give the product as colourless powder (2.08 g, 5.30 mmol, 98 %).

¹H-NMR (CDCl₃/DMSO-d₆=10/1, 400 MHz): δ = 2.93-3.02 (m, 2H, CH₂-Ph), 3.53 (dd, J = 3.7, 11.4 Hz, 1H, CHH-O), 3.61 (dd, J = 4.2, 11.4 Hz, 1H, CHH-O), 4.36-4.44 (m, 1H, C*-H), 7.18-7.34 (m, 5H, H_{ar}), 7.67 (d, J = 8.8 Hz, 1H, NH) ppm.

¹³C-NMR (DMSO-d₆, 100 MHz): δ = 37.7 (CH₂-Ph), 46.9 (CH₂-Cl), 53.1 (C*), 126.9 (C_{ar}-H), 128.8 (C_{ar}-H), 129.5 (C_{ar}-H), 138.2 (C_{ar}-C), 159.9 (C_{carbonyl}) ppm.

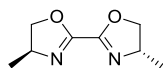
IR (solid): $\tilde{\nu}$ = 3291 (m), 3087 (w), 3082 (w), 3063 (w), 3029 (w), 2954 (w), 2954 (w), 2929 (w), 2954 (w), 2929 (w), 2858 (w), 2033 (w), 1682 (m), 1656 (s), 1635 (m), 1602 (m), 1585 (w), 1568 (w), 1557 (m), 1519 (s), 1495 (m), 1454 (m), 1442 (m), 1430 (m), 1394 (w), 1364 (m), 1355 (m), 1310 (m), 1298 (w), 1289 (w), 1242 (m), 1197 (s), 1179 (m), 1167 (m), 1127 (m), 1107 (w), 1090 (m), 1078 (m), 1044 (m), 1031 (m), 1012 (m), 981 (w), 971 (w), 944 (w), 911 (m), 873 (m), 859 (m), 844 (m), 831 (m), 792 (m), 781 (m), 770 (m), 747 (s), 753 (s), 696 (s), 655 (m) cm⁻¹.

HRMS (+ESI, 250 V): m/z (%) = 415.0961 (51) [M+Na]⁺ (calc. 415.0951).

11.1.3 Bisoxazolines

11.1.3.1 2,2'-Bi((4*S*, 4'*S*)-4,4'-dimethyl)-oxazolin (5a)

(GM 1130)



The dichloride **4a** (1.40 g, 5.84 mmol) was dissolved in boiling methanol (200 mL) and a solution of KOH (0.752 g, 13.4 mmol) in methanol (30 mL) was added. The reaction mixture was heated under reflux for 2.5 h. After cooling to room temperature, water (230 mL) was added and the methanol removed under reduced pressure. The aqueous phase was extracted with dichloromethane (4× 150 mL). The combined organic phases were dried over Na₂SO₄ and the solvent removed by rotary evaporation. The solid residue was recrystallized from ethylacetate to give the product as colourless powder (0.868 g, 5.16 mmol, 88 %).

¹H-NMR (CDCl₃, 500 MHz): δ = 1.28 (d, J = 6.8 Hz, 6H, CH₃), 3.92 (t, J = 8.2 Hz, 2H, CHH), 4.28–4.37 (m, 2H, C*H), 4.47 (dd, J = 8.2, 9.5 Hz, 2H, CHH) ppm.

¹³C-NMR (CDCl₃, 125 MHz): δ = 20.9 (CH₃), 62.5 (CH₂), 74.8 (C*), 154.7 (CO) ppm.

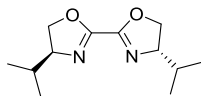
IR (solid): $\tilde{\nu}$ = 3284 (w), 2966 (w), 2926 (w), 2869 (w), 2357 (w), 2341 (w), 1656 (w), 1617 (m), 1527 (w), 1471 (w), 1448 (w), 1360 (w), 1348 (w), 1322 (w), 1282 (w), 1203 (w), 1143 (m), 1132 (m), 1092 (w), 1083 (w), 1062 (m), 948 (m), 858 (w), 835 (w), 772 (w), 735 (w), 692 (w) cm⁻¹.

HRMS(+ESI, 200 V): m/z (%) = 191.0799(100) [M+Na]⁺ (calc. 191.0796).

M.p.: 60-62 °C.

11.1.3.2 **2,2'-Bi((4*S*,4'*S*)-4,4'-diisopropyl)-oxazolin (5b)**

(2054)



Chloro-diamide **4b** (838 mg, 2.81 mmol) was dissolved in methanol (20 mL) and a solution of KOH (363 mg, 6.48 mmol) in methanol (30 mL) was added drop wise. The reaction mixture was heated under reflux for 3 h. After cooling to room temperature water (50 mL) was added and the methanol removed by rotary. The aqueous phase was extracted with dichlormethane(3× 120 mL). The combined organic layers were dried over Na₂SO₄. The solvent was evaporated under vacuum and the residue dissolved in ethylacetate. Addition of hexane (ethylacetate/hexane = 1/10) precipitated a colourless solid which was identified as the the starting material. The solution contained the pure product and yielded after evaporation of the solvent 575 mg (2.56 mmol, 91%) of a colourless solid.

¹H-NMR (CDCl₃, 400 MHz): δ = 0.81 (d, J = 6.7 Hz, 6H, CH(CH₃)₂), 0.91 (d, J = 6.7 Hz, 6H, CH(CH₃)₂), 1.74 (tt, J = 6.7 Hz, 2H, CH(CH₃)₂), 3.69-4.05 (m, 4H, CH₂Cl, C*H), 4.28-4.37 (m, 2H, CH₂Cl) ppm.

¹³C-NMR (CDCl₃, 100.6 MHz): δ = 18.3 (CH₃), 19.0 (CH₃), 32.4 (CH), 71.1 (CH₂), 73.1 (C*), 154.5 (C=N) ppm.

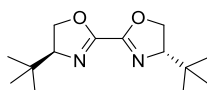
IR (solid): $\tilde{\nu}$ = 3364 (w), 3277 (w), 2986 (w), 2959 (s), 2904 (m), 2876 (s), 2360 (w), 2161 (w), 2034 (w), 1978 (w), 1695 (w), 1644 (w), 1657 (w), 1615 (s), 1524 (w), 1472 (w), 1469 (w), 1463 (w), 1449 (w), 1384 (w), 1362 (w), 1345 (w), 1316 (w), 1297 (w), 1276 (w), 1260 (w), 1176 (w), 1130 (s), 1114 (s), 1027 (m), 1010 (w), 973 (w), 946 (s), 895 (m), 871 (m), 812 (m), 790 (m), 753 (w), 730 (w), 682 (w), 666 (w), 655 (w) cm⁻¹.

HRMS (+ESI, 200V): m/z (%) = 247.1415 (100) [M+Na]⁺ (calc. 247.1417), 225.1593 (58) [M+H]⁺ (calc. 225.1598).

M.p.: 36-38 °C.

11.1.3.3 **2,2'-Bi((4*S*,4'*S*)-4,4'-di-*tert*-butyl)-oxazolin (5c)**

(GM 1012)



Chloro-diamide **4c** (1.658 g, 5.10 mmol) was dissolved in methanol (200 mL) and KOH (0.38 g, 6.73 mmol) was added dropwise as solution in methanol (30 mL). The reaction mixture was treated under reflux for 2.5 h during which a colourless solid precipitated from the solution. After cooling to room temperature the solid was separated by filtration. water (230 mL) was added to the filtrate and the methanol removed by rotary evaporation. The aqueous phase was extracted with dichlormethane (3×

120 mL). The combined organic layers were dried over Na₂SO₄. The solvent was evaporated under vacuum and the residue recrystallized from ethylacetate at -20°C to give a second fraction of colourless powder. The two powder fractions were combined (0.46 g, 1.82 mmol, 36 %).

¹H-NMR (CDCl₃, 500 MHz): δ = 0.91 (s, 18H, C(CH₃)₃), 4.06 (dd, J = 8.8, 10.2 Hz, 2H, C*H), 4.20 (dd, J = 8.8, 9.2 Hz, 2H, CHH), 4.36 (dd, J = 8.8, 10.2 Hz, 2H, CHH) ppm.

¹³C-NMR (CDCl₃, 125 MHz): δ = 25.9 (C(CH₃)₃), 33.7 (C(CH₃)₃), 69.5 (CH₂), 76.7 (C*), 154.5 (CO) ppm.

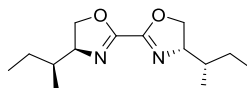
IR (solid): $\tilde{\nu}$ = 2951 (w), 2904 (w), 2869 (w), 1619 (m), 1557 (w), 1538 (w), 1485 (w), 1472 (w), 1393 (w), 1367 (w), 1359 (w), 1326 (w), 1279 (w), 1253 (w), 1213 (w), 1193 (w), 1119 (m), 1065 (w), 1020 (w), 993 (w), 943 (m), 871 (w), 858 (w), 764 (w), 697.

HRMS (+ESI, 200V): m/z (%) = 253.1941 (100) [M+H]⁺ (calc. 253.1910).

M.p.: 171-174 °C.

11.1.3.4 2,2'-Bi((4*S*, 4'*S*)-4,4'-di((*S*)-sec-butyl)-oxazolin (5d)

(GM 1030)



Chloro-diamide **4d** (2.05 g, 6.34 mmol) methanol (150 mL) and KOH (0.82 g, 14.6 mmol) was added dropwise as solution in methanol (30 mL). The reaction mixture was heated under reflux for 2.5 h. After cooling down to room temperature water (180 mL) was added and the methanol removed in vacuum. The aqueous phase was extracted three times with approximately 120 mL of dichlormethane respectively. The combined organic layers were dried over Na₂SO₄. The solvent was evaporated under vacuum to yield a colourless oil (0.97 g, 3.85 mol, 61 %).

¹H-NMR (CDCl₃, 500 MHz): δ = 0.82 (d, J = 6.8 Hz, 6H, C*H-CH₃), 0.89 (t, J = 7.4 Hz, 6H, CH₂-CH₃), 1.131.22 (m, 2H, CH₃-CHH), 1.531.69 (m, 4H, CH₃-CHH, -C*H-CH₃), 4.09 (dd, J = 8.1, 9.2 Hz, 2H, CHH-O), 4.134.19 (m, 2H, C*H-N), 4.37 (dd, J = 8.1, 9.5 Hz, 2H, CHH-O) ppm.

¹³C-NMR (CDCl₃, 125 MHz): δ = 11.3 (CH₃-CH₂), 14.5 (CH₃-C*), 38.8 (C*H-CH₃), 70.7 (CH₂-O), 71.7 (C*H-N), 154.5 (CO) ppm.

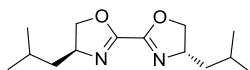
IR (oil): $\tilde{\nu}$ = 2961 (m), 2931 (m), 2876 (m), 2359 (w), 2336 (w), 1735 (w), 1693 (w), 1678 (w), 1642 (w), 1619 (s), 1557 (w), 1525 (w), 1507 (w), 1463 (w), 1378 (w), 1346 (w), 1246 (w), 1204 (w), 1120 (s), 1047 (w), 978 (w), 943 (m), 870 (w), 796 (w), 774 (w) cm⁻¹.

HRMS (+ESI, 200V): m/z (%) = 275.1738 (100) [M+Na]⁺ (calc. 275.1730), 253.1926 (35) [M+H]⁺ (calc. 253.1911).

M.p.: 31-33°C.

11.1.3.5 **2,2'-Bi((4*S*, 4'*S*)-4,4'-diisobutyl)-oxazolin (5e)**

(2098)



Chloro-diamide **4e** (1.05 g, 3.23 mmol) was dissolved in methanol (10 mL) and KOH (0.417 g, 7.43 mmol) was added dropwise as solution in methanol (5 mL). The reaction mixture was heated under reflux for 2.5 h. After cooling down to room temperature water (15 mL) was added and the methanol removed in vacuum. The aqueous phase was extracted three times with approximately 50 mL of dichloromethane respectively. The combined organic layers were dried over Na₂SO₄. The solvent was evaporated under vacuum and the residue recrystallized from ethylacetate to yield a colourless powder (3.12 g, 0.990 mmol, 96 %).

¹H-NMR (CDCl₃, 500 MHz): δ = 0.89 (d, *J*=6.8 Hz, 6H, CH₃), 0.91 (d, *J*=6.8 Hz, 6H, CH₃), 1.28-1.33 (m, 2H, CHH-CH(CH₃)₂), 1.62-1.68 (m, 2H, CHH-CH(CH₃)₂), 1.76-1.84 (m, 2H, CH(CH₃)₂), 3.95 (t, *J*=8.3 Hz, 2H, CHH-O), 4.27-4.33 (m, 2H, C*-H), 4.47 (dd, *J*=9.9, 8.7 Hz, 2H, CHH-O) ppm.

¹³C-NMR (CDCl₃, 100 MHz): δ = 22.5 (CH₃), 22.8 (CH₃), 25.2 (CH(CH₃)₂), 45.0 (CH₂-CH(CH₃)₂), 65.5 (C*), 73.9 (CH₂-O), 154.6 (CO) ppm.

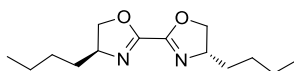
IR (solid): $\tilde{\nu}$ = 3285 (w), 2953 (s), 2928 (m), 2900 (m), 2867 (m), 2362 (w), 1656 (w), 1621 (s), 1525 (w), 1471 (m), 1461 (m), 1448 (m), 1428 (w), 1409 (w), 1380 (m), 1363 (m), 1351 (w), 1341 (w), 1320 (w), 1289 (w), 1273 (w), 1251 (w), 1235 (w), 1206 (w), 1170 (w), 1146 (w), 1133 (m), 1112 (s), 1071 (m), 1027 (w), 1013 (w), 1004 (w), 985 (w), 951 (m), 935 (s), 920 (m), 894 (w), 874 (m), 839 (w), 823 (m), 774 (w), 753 (w), 730 (m), 694 (w) cm⁻¹.

HRMS (+ESI, 250 V): *m/z* (%) = 275.1732 (100) [M+Na]⁺ (calc. 275.1730), 253.1918 (15) [M+H]⁺ (calc. 253.1911).

M.p.: 53-54 °C.

11.1.3.6 **2,2'-Bi((4*S*, 4'*S*)-4,4'-dibutyl)-oxazolin (5f)**

(2114)



Chloro-diamide **4f** (0.22 g, 0.68 mmol) was dissolved in methanol (30 mL) and KOH (0.088 g, 1.5 mmol) was added dropwise as solution in methanol (5 mL). The reaction mixture was treated under reflux for 4 h. After cooling down to room temperature water (35 mL) was added and the methanol removed in vacuum. The aqueous phase was extracted three times with approximately 30 mL of dichloromethane respectively. The combined organic layers were dried over Na₂SO₄. The solvent was

evaporated under vacuum and the residue recrystallized from ethylacetate to yield a colourless powder (0.15 g, 0.62 mmol, 90 %).

¹H-NMR (CDCl₃, 500 MHz): δ = 0.76 (t, J = 7.2 Hz, 6H, CH₃), 1.17-1.25 (m, 6H, ⁿBu-CH₂), 1.30-1.35 (m, 2H, ⁿBu-CH₂), 1.36-1.44 (m, 2H, ⁿBu-CH₂), 1.55-1.63 (m, 2H, ⁿBu-CH₂), 3.90 (t, J = 8.5 Hz, 2H, C*-CH₂), 4.10-4.17 (m, 2H, C*H), 4.36 (dd, J = 8.5, 9.5 Hz, C*-CH₂) ppm.

¹³C-NMR (CDCl₃, 100 MHz): δ = 13.9 (CH₃), 22.5 (ⁿBu-CH₂), 27.9 (ⁿBu-CH₂), 35.1 (ⁿBu-CH₂), 67.2 (C*), 73.3 (CH₂-O), 154.3 (CO) ppm.

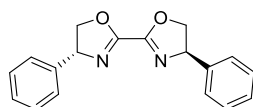
IR (solid): $\tilde{\nu}$ = 3276 (m), 2955 (m), 2929 (m), 2871 (m), 2859 (m), 1700 (w), 1675 (m), 1655 (s), 1642 (m), 1617 (s), 1523 (m), 1503 (m), 1466 (m), 1458 (m), 1444 (m), 1378 (m), 1352 (m), 1343 (m), 1304 (m), 1291 (m), 1258 (m), 1246 (m), 1215 (m), 1182 (m), 1129 (s), 1112 (s), 1080 (s), 1035 (m), 971 (m), 946 (s), 892 (m), 866 (m), 835 (w), 789 (m), 772 (m), 736 (m), 702 (w), 668 (w) cm⁻¹.

HRMS (+ESI, 250 V): m/z (%) = 275.1741 (100) [M+Na]⁺ (calc. 275.1730), 253.1917 (15) [M+H]⁺ (calc. 253.1911).

M.p.: 48-50 °C.

11.1.3.7 2,2'-Bi((4*R*, 4'*R*)-4,4'-diphenyl)-oxazolin (5g)

(GM 1010)



Chloro-diamide **4g** (1.07 g, 2.92 mmol) was dissolved in methanol (200 mL) and KOH (0.38 g, 6.73 mmol) was added dropwise as solution in methanol (20 mL). The reaction mixture was treated under reflux for 3 h. After cooling down to room temperature water (220 mL) was added and the methanol removed in vacuum. The aqueous phase was extracted three times with approximately 120 mL of dichloromethane respectively. The combined organic layers were dried over Na₂SO₄. The solvent was evaporated under vacuum and the residue dissolved in CH₂Cl₂. Precipitation with hexane yielded a colourless powder (0.74 g, 2.53 mmol, 86 %).

¹H-NMR (CDCl₃, 500 MHz): δ = 4.34 (dd, J = 8.8, 9.2 Hz, 2H, CHH), 4.85 (dd, J = 8.8, 10.2 Hz, 2H, CHH), 5.45 (dd, J = 9.2, 10.2 Hz, 2H, C*-H), 7.277.43 (m, 10H, H_{ar}) ppm.

¹³C-NMR (CDCl₃, 125 MHz): δ = 70.5 (C*), 75.3 (CH₂), 126.8 (C_{ar}-H), 128.0(C_{ar}-H), 128.9(C_{ar}-H), 140.5 (C_{ar}-C), 155.7 (CO) ppm.

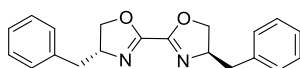
IR (solid): $\tilde{\nu}$ = 1655 (w), 1615 (m), 1583 (w), 1494 (w), 1453 (w), 1363 (w), 1303 (w), 1265 (w), 1265 (w), 1199 (w), 1178 (w), 1156 (w), 1120 (m), 1080 (w), 1055 (w), 1036 (w), 1010 (w), 999 (w), 972 (w), 956 (w), 932 (m), 919 (w), 868 (w), 850 (w), 826 (w), 807 (w), 770 (m), 755 (m), 701 (m), 670 (w)cm⁻¹.

HRMS (+ESI, 200V): m/z (%) = 315.1118 (100) $[M+Na]^+$ (calc. 315.1104), 293.1294 (59) $[M+H]^+$ (calc. 293.1285), 331.0863 (10) $[M+K]^+$ (calc. 331.0843).

M.p.: 89-92 °C.

11.1.3.8 2,2'-Bi((4*R*, 4'*R*)-4,4'-dibenzyl)-oxazolin (5h)

(2112)



Chloro-diamide **4h** (0.861 g, 2.19 mmol) was dissolved in methanol (50 mL) and KOH (0.282 g, 5.03 mmol) was added dropwise as solution in methanol (5 mL). The reaction mixture was treated under reflux for 4 h. After cooling down to room temperature water (55 mL) was added and the methanol removed in vacuum. The aqueous phase was extracted three times with approximately 50 mL of dichloromethane respectively. The combined organic layers were dried over Na_2SO_4 . The solvent was evaporated under vacuum and the residue recrystallized from ethylacetate to yield a colourless powder (0.433 g, 1.35 mmol, 61 %).

1H -NMR ($CDCl_3$, 500 MHz): δ = 2.70 (dd, $J=14.0, 9.2$ Hz, 1H, C^*H-CHH), 3.27 (dd, $J=14.0, 5.1$ Hz, 1H, C^*H-CHH), 4.16 (t, $J=8.5$ Hz, 1H, $CHH-O$), 4.37 (t, $J=9.5$ Hz, 1H, $CHH-O$), 4.57-4.64 (m, 1H, C^*H), 7.20-7.24 (m, 3H, H_{ar}), 7.29-7.32 (m, 2H, H_{ar}) ppm.

^{13}C -NMR ($CDCl_3$, 100 MHz): δ = 41.2 (C^*-CH_2), 68.2 (CH_2-O), 72.8 (C^*), 126.8 ($C_{ar}-H$), 128.7 ($C_{ar}-H$), 129.2 ($C_{ar}-H$), 137.2 ($C_{ar}-C$), 155.1 (CO) ppm.

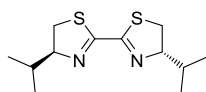
IR (solid): $\tilde{\nu}$ = 3276 (w), 3061 (w), 3026 (w), 2998 (w), 2975 (w), 2943 (w), 2927 (w), 2895 (w), 2860 (w), 2161 (w), 1979 (w), 1736 (s), 1610 (s), 1597 (m), 1581 (w), 1520 (w), 1494 (m), 1477 (m), 1454 (m), 1444 (w), 1358 (m), 1342 (m), 1308 (m), 1260 (m), 1222 (w), 1200 (w), 1180 (w), 1134 (s), 1092 (s), 1069 (s), 1043 (m), 1030 (m), 1008 (m), 978 (w), 954 (m), 941 (s), 920 (m), 78 (m), 847 (m), 814 (w), 781 (w), 760 (m), 758 (m), 709 (s), 694 (s) cm^{-1} .

HRMS (+ESI, 200 V): m/z (%) = 343.1417 (100) $[M+Na]^+$ (calc. 343.1417), 359.1169 (35) $[M+K]^+$ (calc. 359.1156), 321.1606 (25) $[M+H]^+$ (calc. 321.1598).

M.p.: 118-122 °C.

11.1.3.9 (S)-4,4'-diisopropyl-2,2'-bithiazolin (7b)

(6010, 6012)



Chloro-diamide **4b** (574 mg, 1.93 mmol) and Lawson's reagent (781 mg, 1.93 mmol) were suspended in toluene (50 mL). The reaction mixture was heated to 111 °C and stirred for 2 h, while the suspension turned into a clear solution slowly. After cooling to room temperature, triethylamine was added (10 mL, 72 mmol) and the reaction mixture was stirred for 2 h. The reaction mixture was washed with water (3×50 mL) and the organic phase was dried over Na₂SO₄. The organic solvent was evaporated in vacuum to result a colorless solid (289 mg, 1.12 mmol, 58%), which was identified as the product.

¹H-NMR (CDCl₃, 400 MHz): δ = 0.95 (d, J= 6.7 Hz, 6H, CH₃), 1.04 (d, J= 7.0 Hz, 6H, CH₃), 2.05 (sep, J= 6.7 Hz, 2H, CH(CH₃)₂), 3.06 (dd, J= 9.5, 11.1 Hz, 2H, CH₂), 3.30 (dd, J= 10.9, 11.1 Hz), 4.33-4.42 (m, 2H, C*H) ppm.

¹³C-NMR (CDCl₃, 125 MHz): δ = 19.3, 19.9, 33.1, 34.8, 83.9, 162.2 ppm.

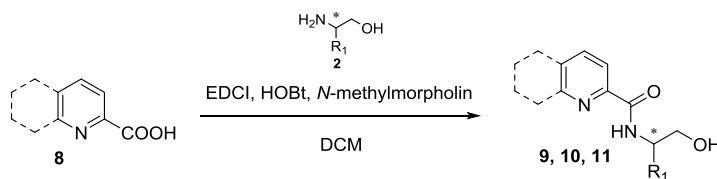
IR (solid): $\tilde{\nu}$ = 3283 (w), 3173 (w), 2975 (w), 2967 (m), 2957 (m), 2951 (m), 2936 (w), 2927 (m), 2906 (w), 2892 (w), 2885 (w), 2867 (m), 2828 (w), 1684 (w), 1685 (m), 1558 (w), 1516 (m), 1507 (m), 1490 (w), 1465 (m), 1447 (m), 1382 (w), 1362 (m), 1340 (w), 1314 (w), 1294 (w), 1284 (w), 1271 (m), 1260 (w), 1245 (w), 1228 (m), 1181 (w), 1162 (w), 1143 (w), 1124 (w), 1104 (w), 1086 (m), 1027 (m), 1018 (m), 1003 (m), 984 (w), 955 (m), 939 (m), 925 (m), 880 (m), 862 (s), 853 (s), 820 (w), 791 (m), 743 (w), 677 (w) cm⁻¹.

HRMS (+ESI, 250V): m/z (%) = 279.0972 (100) [M+Na]⁺ (calc. 279.09601), 257.1149 (20) [M+H]⁺ (calc. 257.11407).

11.2 Pyrox, mepyrox and quinox structures

11.2.1 β-Hydroxyamides

11.2.1.1 General Procedure A for β-hydroxyamides

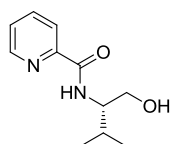


The reaction was performed under an argon atmosphere. The appropriate carboxylic acid (1.0 equiv.), picolinic acid, 6-methyl-picolinic acid or quinaldic acid, was dissolved in CH₂Cl₂ together with *N*-methylmorpholine (1.3 equiv.) and left stirring for 10 min at room temperature. The solution was

cooled down to -5°C in a brine/ice-bath and 1-ethyl-3-(3-dimethylaminopropyl)carbodiimid (1.1 equiv.) and 1-Hydroxybenzotriazol (1.2 equiv.) were added. The mixture was left stirring for 15 min at -5°C and for other 15 min at room temperature. After cooling down again to -5°C , the aminol **2** (1.2 equiv.) was added and the reaction mixture left stirring in the melting brine/ice-bath over night. During this time the reaction mixture turned orange (picolinic acid amide), orange-brown (6-methyl picolinic acid amide) or purple (quinaldic acid amide). The volume of the reaction mixture was increased by adding approximately one volume equivalent of CH_2Cl_2 and washed once with a half saturated aqueous NaHCO_3 solution. The aqueous phase was extracted twice with CH_2Cl_2 and the combined organic layers were washed again with a very small amount of a half saturated aqueous NaHCO_3 and afterwards with brine. The organic layer was dried over Na_2SO_4 and the solvent was removed by rotary evaporation to yield the crude product quantitatively as strongly coloured oil or solid (picolinic acid amide: yellow-orange, 6-methyl picolinic acid amide: brown-orange, quinaldic acid amide: blue). The crude product was used for the transformation to pyrox-type molecules **9**, **17** and **18** without any further purification.

11.2.1.2 (*S*)-*N*-(1-Hydroxy-3-methylbutan-2-yl)picolinamide (**9b**)

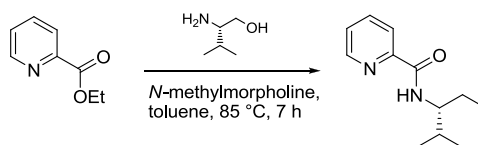
(3052)



According to general procedure A. Picolinic acid (897 mg, 7.29 mmol), (*L*)-valinol (1.025 g, 9.941 mmol), *N*-methylmorpholine (1.04 mL, 9.48 mmol), 1-Ethyl-3-(3-dimethylaminopropyl)carbodiimid (1.537 g, 8.021 mmol), Hydroxybenzotriazol (1.182 g, 8.750 mmol), CH_2Cl_2 (50 mL).

Discarded methods

(GM 1014)



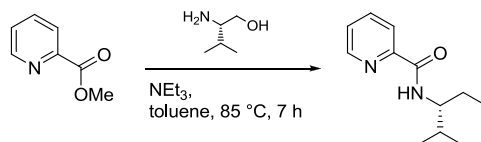
The reaction was carried out under an inert gas atmosphere. (*R*)-valinol (500 mg, 4.85 mmol) and ethylpicolinate (0.65 mL, 4.8 mmol) were separately dissolved in toluene (each in 40 mL). The solutions were combined and heated for 1.5 h under reflux. Because the TLC analysis showed no full conversion, one equivalent of *N*-methylmorpholine (0.53 mL, 4.8 mmol) was added and again one equivalent after additional 1.5 h of heating. Even though there was still no significant change on the TLC visible, the reaction was stopped after 4 h. The solvent was removed under vacuum and the crude

Experimental Section

product purified by column chromatography on silica gel (ethylacetat / hexane = 1/9, 1/4, 3/7, 4/6). The product was obtained as colorless oil in 62% yield (623 mg, 2.51 mmol)

The product was identified by $^1\text{H-NMR}$, $^{13}\text{C-NMR}$ IR and HRMS analysis.

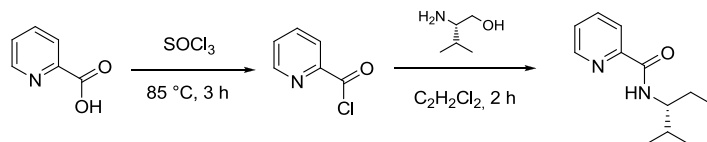
(GM 1052)



The reaction was carried out under an inert gas atmosphere. (*R*)-valinol (200 mg, 1.94 mmol) and methylpicolinate (270 mg, 1.94 mmol) were dissolved in toluene (25 mL) and heated for 2 h under reflux. Because the TLC analysis showed no full conversion, NEt_3 (0.40 mL, 2.9 mmol) was added. The addition of base was repeated after 2 h and 4 h of heating. After 7 h total reaction time the reaction was stopped and the solvent removed under vacuum and the residue redissolved in dichloromethane. The solution was washed twice with water and dried over Na_2SO_4 . The solvent was removed in vacuum to yield the crude product. Purification by column chromatography was abandoned due to the very similar retention times of the 3 different compounds in the crude product.

The product was identified by $^1\text{H-NMR}$ and HRMS analysis.

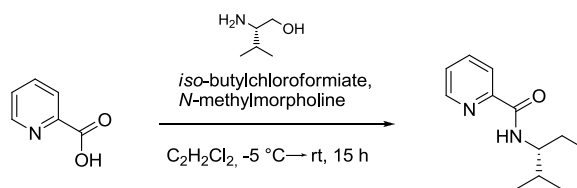
(GM 1028)



The reaction was carried out under an inert gas atmosphere. Picolinic acid (600 mg, 4.8 mmol) was dissolved in Thionylchloride (5 mL) to give a green solution. After heating to reflux for 3 h, the solvent was removed in vacuum and the green residue dried over night under high vacuum. (*R*)-valinol (500 mg, 4.85 mmol) was dissolved in dichloromethane (15 mL) and NEt_3 (0.66 mL, 4.8 mmol) was added. The valinol-solution was added to the picolinic acid chloride and the mixture was heated for 2 h under reflux while its color turned blue. After cooling down to room temperature, one volume equivalent of dichloromethane was added and the solution washed with water for four times. The organic phase was dried over Na_2SO_4 and the solvent was removed in vacuum, yielding a brown oil. Purification by column chromatography was abandoned due to the high amount of other compounds (5 fractions visible on TLC).

The product was identified by HRMS analysis. $^1\text{H-NMR}$ analysis showed a huge amount of impurities.

(GM 1032)



The reaction was carried out under an inert gas atmosphere. Picolinic acid (4.00 g, 32.5 mmol) was dissolved in dichloromethane (300 mL). *N*-methylmorpholine (5.35 mL, 37.4 mmol) and, after 15 min of stirring, *iso*-butylchloroformiate (4.91 mL, 37.4 mmol) were added and the solution stirred for 30 min at room temperature. (*R*)-valinol (3.35 g, 32.5 mmol) was dissolved in dichloromethane (15 mL) and *N*-methylmorpholine (4.11 mL, 48.7 mmol) was added. The valinol-solution was added to the ice-brine cooled picolinic acid solution. After stirring at $-5\text{ }^\circ\text{C}$ for 1 h, the reaction mixture was allowed to warm to room temperature and left stirring for 13 h while its color turned orange. The reaction mixture was washed once with diluted ammoniac chloride and twice with water. The organic phase was dried over Na_2SO_4 and the solvent was removed in vacuum, yielding an orange oil. The crude product was purified by column chromatography on silica gel (ethylacetate / hexane = 1/19, 1/9, 3/17, 1/4, 1/3, 3/7, 2/3, 1/1, 3/2, 1/0), yielding the product as colorless oil (610 mg, 3.22 mmol, 10%).

The product was identified by $^1\text{H-NMR}$ and HRMS analysis.

$^1\text{H-NMR}$ (CDCl_3 , 500 MHz): $\delta = 0.93$ (d, $J = 6.81$ Hz, 3H, CH_3), 1.02 (d, $J = 6.81$ Hz, 3H, CH_3), 2.00–2.08 (m, 1H, $\text{CH}-(\text{CH}_3)_2$), 3.74–3.83 (m, 2H, CH_2-OH), 3.89–3.95 (m, 1H, C^*H), 7.39 (t, $J = 7.4$ Hz, 1H, CH_{ar}), 7.81 (t, $J = 7.1$ Hz, 1H, CH_{ar}), 8.15 (d, $J = 7.83$, 1H, N-CH_{ar}), 8.24 (d, $J = 7.8$ Hz, 1H, OH), 8.52 (d, $J = 4.4$ Hz, 1H, NH).

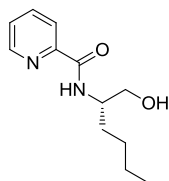
$^{13}\text{C-NMR}$ (CDCl_3 , 125 MHz): $\delta = 18.7$ (CH_3), 19.7 ($\text{CH}-(\text{CH}_3)_2$), 29.3 (CH_2-OH), 64.2 (C^*), 122.4 (C_{ar}), 126.3 (C_{ar}), 137.5 (C_{ar}), 148.2 (C_{ar}), 149.8 ($\text{C}_{\text{ar}}\text{N}$), 165.2 (CO).

IR (solid): $\tilde{\nu} = 3374$ (m), 3045 (w), 3013 (w), 2961 (m), 2928 (m), 2869 (m), 1659 (s), 1591 (w), 1569 (w), 1522 (s), 1464 (m), 1434 (m), 1388 (w), 1369 (w), 1335 (w), 1322 (w), 1291 (w), 1239 (w), 1215 (w), 1162 (w), 1138 (w), 1116 (w), 1087 (w), 1068 (w), 1042 (w), 997 (w), 967 (w), 922 (w), 904 (w), 871 (w), 818 (w), 746 (s), 691 (m), 665 (m).

HRMS (+ESI, 200 V): m/z (%) = 231.1123 (100) $[\text{M}+\text{Na}]^+$ (calc. 231.1104).

11.2.1.3 (*S*)-*N*-(1-Hydroxyhexan-2-yl)picolinamide (**9f**)

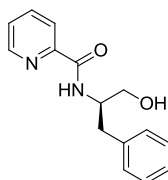
(3082)



According to general Procedure A. Picolinic acid (449 mg, 3.64 mmol), (*S*)-2-aminohexanol (512 mg, 4.37 mmol), *N*-methylmorpholine (0.5 mL, 4.74 mmol), 1-Ethyl-3-(3-dimethylaminopropyl)carbodiimid (768 mg, 4.01 mmol), Hydroxybenzotriazol (591 mg, 4.37 mmol), CH₂Cl₂ (30 mL).

11.2.1.4 (*R*)-*N*-(4-Hydroxy-1-phenylbutan-2-yl)picolinamide (**9h**)

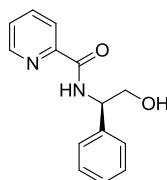
(3066)



According to general procedure A. Picolinic acid (897 mg, 7.29 mmol), (*S*)-2-amino-3-phenylpropanol (1.323 g, 8.750 mmol), *N*-methylmorpholine (1.04 mL, 9.48 mmol), 1-Ethyl-3-(3-dimethylaminopropyl)carbodiimid (1.537 g, 8.021 mmol), Hydroxybenzotriazol (1.182 g, 8.750 mmol), CH₂Cl₂ (50 mL).

11.2.1.5 (*S*)-*N*-(2-Hydroxy-1-phenylethyl)picolinamide (**9g**)

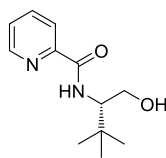
(3078)



According to general procedure A. Picolinic acid (897 mg, 7.29 mmol), (*R*)-2-Amino-2-phenylethanol (1.323 g, 8.750 mmol), *N*-methylmorpholine (1.04 mL, 9.48 mmol), 1-Ethyl-3-(3-dimethylaminopropyl)carbodiimid (1.537 g, 8.021 mmol), Hydroxybenzotriazol (1.182 g, 8.750 mmol), CH₂Cl₂ (50 mL).

11.2.1.6 (*S*)-*N*-(1-hydroxy-3,3-dimethylbutan-2-yl)picolinamide (**9c**)

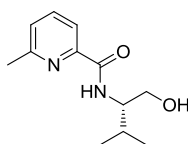
(GM 1036)



The reaction was carried out under inert gas atmosphere. Picolinic acid (2.10 g, 17.1 mmol) was dissolved in dichloromethane (150 mL) at room temperature and *N*-methylmorpholine (2.8 mL, 25 mmol) was added. After 15 min *iso*-butylchlorformiate (2.2 mL, 20 mmol) was added and the mixture stirred for 30 min. (*R*)-*tert*-leucinol (2.00 g, 17.1 mmol) was dissolved in dichloromethane (30 mL) together with *N*-methylmorpholine (2.2 mL, 20 mmol) and added to the reaction mixture dropwise under ice/brine cooling. After one hour, the ice-bath was removed and the reaction mixture left stirring for 14 h. Afterwards, The reaction mixture was washed with saturated aqueous ammoniumchloride solution (3×150 mL) and with water (3×150 mL). The organig phase was dried over Na₂SO₄ and the solvent was removed by rotary evaporation which led to a brown oil which was identified as the product by mass spectrometry. The crude product was used without any further purification.

11.2.1.7 (*S*)-*N*-(2-Hydroxy-1-phenylethyl)-6-methylpicolinamide (**17b**)

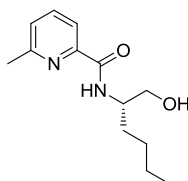
(3084)



According to general procedure A. 6-Methylpicolinic acid (1.00 g, 7.29 mmol), (*S*)-2-amino-3-phenylpropanol (1.323 g, 8.750 mmol), *N*-methylmorpholine (1.04 mL, 9.48 mmol), 1-Ethyl-3-(3-dimethylaminopropyl)carbodiimid (1.537 g, 8.021 mmol), Hydroxybenzotriazol (1.182 g, 8.750 mmol), CH₂Cl₂ (50 mL).

11.2.1.8 (*S*)-*N*-(1-Hydroxyhexan-2-yl)-6-methylpicolinamide (**17f**)

(3078)

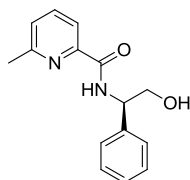


According to general procedure A. 6-Methylpicolinic acid (500 mg, 3.64 mmol), (*S*)-2-aminohexanol (512 mg, 4.37 mmol), *N*-methylmorpholine (0.5 mL, 4.74 mmol), 1-Ethyl-3-(3-

dimethylaminopropyl)carbodiimid (768 mg, 4.01 mmol), Hydroxybenzotriazol (591 mg, 4.37 mmol), CH₂Cl₂ (30 mL).

11.2.1.9 **(R)-N-(2-Hydroxy-1-phenylethyl)-6-methylpicolinamide (17h)**

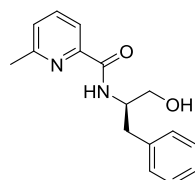
(3068)



According to general procedure A. 6-Methylpicolinic acid (1.00 g, 7.29 mmol), (*S*)-2-amino-3-phenylpropanol (1.323 g, 8.750 mmol), *N*-methylmorpholine (1.04 mL, 9.48 mmol), 1-Ethyl-3-(3-dimethylaminopropyl)carbodiimid (1.537 g, 8.021 mmol), Hydroxybenzotriazol (1.182 g, 8.750 mmol), CH₂Cl₂ (50 mL).

11.2.1.10 **(R)-N-(1-Hydroxy-3-phenylpropan-2-yl)-6-methylpicolinamide (17g)**

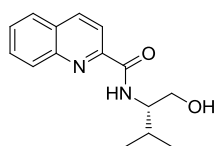
(3066)



According to general procedure A. 6-Methylpicolinic acid (1.00 g, 7.29 mmol), (*S*)-2-amino-3-phenylpropanol (1.323 g, 8.750 mmol), *N*-methylmorpholine (1.04 mL, 9.48 mmol), 1-Ethyl-3-(3-dimethylaminopropyl)carbodiimid (1.537 g, 8.021 mmol), Hydroxybenzotriazol (1.182 g, 8.750 mmol), CH₂Cl₂ (50 mL).

11.2.1.11 **(S)-N-(1-Hydroxy-3-methylbutan-2-yl)quinoline-2-carboxamide (18b)**

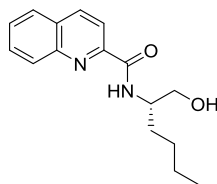
(3056)



According to general procedure A. Quinaldic acid (1.26 g, 7.29 mmol), (*S*)-2-amino-3-phenylpropanol (1.323 g, 8.750 mmol), *N*-methylmorpholine (1.04 mL, 9.48 mmol), 1-Ethyl-3-(3-dimethylaminopropyl)carbodiimid (1.537 g, 8.021 mmol), Hydroxybenzotriazol (1.182 g, 8.750 mmol), CH₂Cl₂ (50 mL).

11.2.1.12 (S)-N-(1-Hydroxyhexan-2-yl)-6-quinoline-2-carboxamide (18f)

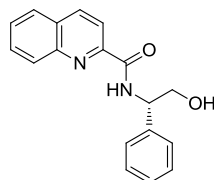
(3086)



According to general procedure A. Quinaldic acid (631 mg, 3.64 mmol), (*S*)-2-aminohexanol (512 mg, 4.37 mmol), *N*-methylmorpholine (0.5 mL, 4.74 mmol), 1-Ethyl-3-(3-dimethylaminopropyl)carbodiimid (768 mg, 4.01 mmol), Hydroxybenzotriazol (591 mg, 4.37 mmol), CH₂Cl₂ (30 mL).

11.2.1.13 (S)-N-(2-Hydroxy-1-phenylethyl)quinoline-2-carboxamide (18g)

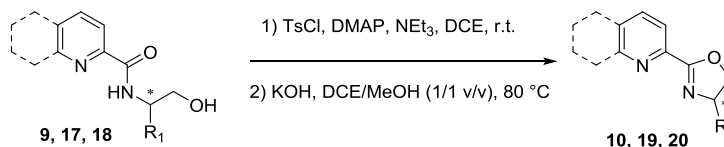
(3070)



According to general procedure A. Quinaldic acid (1.26 g, 7.29 mmol), (*S*)-2-amino-3-phenylpropanol (1.323 g, 8.750 mmol), *N*-methylmorpholine (1.04 mL, 9.48 mmol), 1-Ethyl-3-(3-dimethylaminopropyl)carbodiimid (1.537 g, 8.021 mmol), Hydroxybenzotriazol (1.182 g, 8.750 mmol), CH₂Cl₂ (50 mL).

11.2.2 Oxazolines

11.2.2.1 General Procedure B for pyridyloxazolines

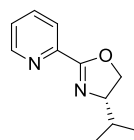


The crude amide **9**, **17** or **18** (1 equiv.) was dissolved in 1,2-dichloroethane together with triethylamine (1.5 equiv.) under an argon atmosphere and left stirring for 10 min. Tosylchloride (1.5 equiv.) and *N*-dimethyl-*p*-aminopyridin (0.1 equiv.) were added and the reaction mixture was left stirring over night at room temperature. Under normal atmosphere, a solution of KOH (1.1 equiv.) in methanol (1 volume equivalent in respect to the C₂H₄C₂-reaction mixture) was added and the reaction mixture heated under reflux for 5 h. After the reaction was finished, the reaction mixture was washed once with a half saturated aqueous NaHCO₃ solution. The aqueous phase was extracted twice with CH₂Cl₂ and the combined organic layers were washed first with a small amount of half saturated aqueous NaHCO₃

solution and second with brine. The organic layer was dried over Na₂SO₄ and the solvent removed under reduced pressure to yield the crude, strongly coloured, product as oil. The oil was purified by flash column chromatography with basic alox. The oxazoline products **10**, **19** or **20** are colourless oils or solids.

11.2.2.2 (*S*)-4-Isopropyl-2-(pyridine-2-yl)-oxazolin (**10b**)

(3060)



According to general Procedure B. Amide **9b** (7.29 mmol), triethylamine (1.52 mL, 10.9 mmol), tosylchloride (2.085 g, 0.729 mmol), *N*-dimethyl-*p*-aminopyridin (89 mg, 0.73 mmol), C₂H₄C₂ (50 mL), KOH (450 mg, 8.02 mmol), methanol (50 mL). Basic alox (3 x 10 cm; 200 mL hexane, 400 mL hexane/ethylacetate = 1/1, 200 mL ethylacetate). Produkt in fraction 1 and 2 as colourless powder (977 mg, 5.14 mmol, 69%).

¹H-NMR (CDCl₃, 500 MHz): δ = 0.91 (d, J = 6.8 Hz, 3H, CH₃), 1.02 (d, J = 6.8 Hz, 3H, CH₃), 1.81-1.89 (m, 1H, CH(CH₃)₂), 4.10-4.19 (m, 2H, CHH, C*H), 4.47 (dd, J = 8.7, 9.5 Hz, 1H, CHH), 7.34 (ddd, J = 1.0, 4.8, 7.5 Hz, 1H, H_{ar}), 7.73 (dt, J = 1.7, 7.8 Hz), 1H, H_{ar}), 8.01 (d, J = 7.8 Hz, 1H, H_{ar}), 8.66 (d, J = 4.8 Hz, 1H, H_{ar}) ppm.

¹³C-NMR (CDCl₃, 100 MHz): δ = 18.3 (CH₃), 19.1 (CH₃), 32.8 (CH(CH₃)₂), 70.8 (C*), 73.0 (CH₂), 124.0 (C_{ar}-H), 125.5 (C_{ar}-H), 136.6 (C_{ar}-H), 147.0 (C_{ar}-C), 149.8 (C_{ar}-H), 162.6 (C-O) ppm.

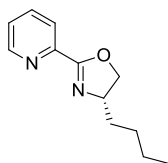
IR (solid): $\tilde{\nu}$ = 3097 (w), 3060 (w), 2992 (w), 2957 (m), 2934 (m), 2898 (m), 1869 (m), 1744 (m), 1724 (m), 1672 (m), 1640 (m), 1587 (m), 1568 (m), 1518 (m), 1466 (m), 1438 (x), 1404 (w), 1383 (m), 1353 (s), 1315 (m), 1283 (m), 1266 (m), 1244 (m), 1216 (m), 1199 (m), 1173 (m), 1146 (m), 1127 (m), 1091 (s), 1042 (s), 1027 (m), 1014 (m), 995 (m), 964 (s), 955 (s), 933 (m), 912 (m), 893 (m), 815 (m), 797 (s), 750 (s), 706 (s), 674 (s) cm⁻¹.

HRMS (+ESI, 220 V): m/z (%) = 191.1180 (100) [M+H]⁺ (calc. 191.1179), 213.0988 (60) [M+Na]⁺ (calc. 213.0998).

M.p. = 46-49° C

11.2.2.3 (*S*)-4-Butyl-2-(pyridine-2-yl)-oxazolin (10f)

(3094)



According to general procedure B. Amide **9f** (3.65 mmol), triethylamine (0.76 mL, 5.4 mmol), tosylchloride (1.043 g, 5.4 mmol), *N*-dimethyl-*p*-aminopyridin (45 mg, 0.36 mmol), C₂H₄C₂ (30 mL), KOH (250 mg, 4.01 mmol), methanol (30 mL). Basic alox (3 x 10 cm; pentane (500 mL), hexane/ethylacetate = 4/1 (500 mL), 3/2 (500 mL), ethylacetate (500 mL)). Produkt in fraction 3 as colourless oil (311 mg, 1.52 mmol, 41%).

¹H-NMR (CDCl₃, 500 MHz): δ = 0.87 (t, *J* = 7.2 Hz, 3H, CH₃), 1.28-1.37 (m, 3H, CH₂(ⁿBu)), 1.38-1.48 (m, 1H, CH₂(ⁿBu)), 1.50-1.58 (m, 1H, CH₂(ⁿBu)), 1.71-1.79 (m, 1H, CH₂(ⁿBu)), 4.07 (t, *J* = 8.2 Hz, 1H, CH₂-O), 4.26-4.33 (m, 1H, C*H), 4.23 (dd, *J* = 8.17, 9.5 Hz, 1H, CH₂-O), 7.33 (ddd, *J* = 1.0, 4.1, 7.8 Hz, 1H, H_{ar}), 7.12 (dt, *J* = 1.7, 7.8 Hz, 1H, H_{ar}), 7.98 (d, *J* = 7.8 Hz, 1H, H_{ar}), 8.65 (d, *J* = 4.8 Hz, 1H, H_{ar}) ppm.

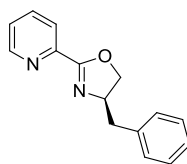
¹³C-NMR (CDCl₃, 100 MHz): δ = 14.1 (CH₃), 22.7 (CH_{2n-Bu}), 28.1 (CH_{2n-Bu}), 35.6 (CH_{2n-Bu}), 67.1 (C*), 73.2 (CH_{2ox}), 123.9 (C_{ar}-H), 125.5 (C_{ar}-H), 136.7 (C_{ar}-H), 146.9 (C_{ar}-C), 149.8 (C_{ar}-H), 162.6 (C-O) ppm.

IR (solid): $\tilde{\nu}$ = 3056 (w), 3008 (w), 2955 (m), 2928 (m), 2895 (m), 2871 (m), 2857 (m), 1640 (m), 1582 (m), 1568 (m), 1516 (w), 1467 (m), 1439 (m), 1360 (m), 1319 (m), 1304 (m), 1289 (m), 1264 (m), 1245 (m), 1214 (w), 1198 (w), 1150 (w), 1122 (m), 1095 (m), 1088 (s), 1075 (s), 1042 (s), 993 (m), 961 (s), 917 (m), 901 (m), 862 (w), 799 (s), 743 (s), 703 (s), 680 (m) cm⁻¹.

HRMS (+ESI, 240 V): *m/z* (%) = 205.1322 (100) [M+H]⁺ (calc. 205.1335), 227.1141 (32) [M+Na]⁺ (calc. 227.1155).

11.2.2.4 (*R*)-4-Benzyl-2-(pyridine-2-yl)-oxazolin (10h)

(3072)



According to general procedure B. Amide **9h** (7.29 mmol), triethylamine (1.52 mL, 10.9 mmol), tosylchloride (2.085 g, 0.729 mmol), *N*-dimethyl-*p*-aminopyridin (89 mg, 0.73 mmol), C₂H₄C₂ (50 mL), KOH (450 mg, 8.02 mmol), methanol (50 mL). Basic alox (3 x 10 cm; pentane (500 mL), pentane/diethylether = 3/7 (500 mL), diethylether (500 mL)). Produkt in fraction 3 as colourless oil (530 mg, 2.22 mmol, 28%).

¹H-NMR (CDCl₃, 500 MHz): δ = 2.75 (dd, J = 8.9, 14.0 Hz, 1H, CHH-Ph), 3.28 (d, J = 5.1, 5.1 Hz, 1H, CHH-Ph), 4.21 (t, J = 8.9 Hz, 1H, CHH_{ox}), 4.43 (t, J = 8.9 Hz, 1H, CHH_{ox}), 4.61-4.67 (m, 1H, C*H), 7.20-7.31 (m, 5H, H_{Ph}), 7.37 (ddd, J = 1.0, 4.7, 7.6 Hz, 1H, H_{py}), 7.76 (dt, J = 1.7, 7.5 Hz, 1H, H_{py}), 8.04 (d, J = 7.8 Hz, 1H, H_{py}), 8.69 (d, J = 4.8 Hz, 1H, H_{py}) ppm.

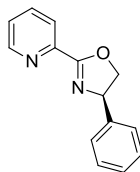
¹³C-NMR (CDCl₃, 100 MHz): δ = 41.8 (CH₂-Ph), 68.2 (CH_{2ox}), 72.6 (C*), 124.0 (C_{py}-H), 125.7 (C_{py}-H), 126.7 (C_{py}-H), 128.7 (C_{Ph}-H), 129.3 (C_{Ph}-H), 136.7 (C_{ar}-H), 137.9 (C_{ar}-C), 146.8 (C_{py}-H), 163.2 (C-O) ppm.

IR (solid): $\tilde{\nu}$ = 3083 (w), 3085 (w), 3025 (w), 3005 (w), 2961 (w), 2896 (w), 2851 (w), 1679 (m), 1638 (m), 1603 (w), 1581 (m), 1567 (m), 1512 (w), 1494 (m), 1468 (m), 1454 (m), 1438 (m), 1360 (m), 1314 (m), 1287 (m), 1260 (m), 1245 (m), 1215 (w), 1180 (w), 1150 (m), 1116 (m), 1093 (s), 1067 (m), 1042 (m), 1028 (m), 994 (m), 962 (s), 911 (m), 854 (m), 798 (s), 741 (s), 727 (s), 699 (s), 677 (s) cm⁻¹.

HRMS (+ESI, 240 V): m/z (%) = 239.1177 (100) [M+H]⁺ (calc. 239.1179), 261.0989 (55) [M+Na]⁺ (calc. 261.0998).

11.2.2.5 (*R*)-4-Phenyl-2-(pyridine-2-yl)-oxazolin (10g)

(3088)



According to general procedure B. Amide **9g** (7.29 mmol), triethylamine (1.52 mL, 10.9 mmol), tosylchloride (2.085 g, 0.729 mmol), *N*-dimethyl-*p*-aminopyridin (89 mg, 0.73 mmol), C₂H₄C₂ (50 mL), KOH (450 mg, 8.02 mmol), methanol (50 mL). Basic alox (3 x 10 cm; pentane (400 mL), hexane/ethylacetate = 4/1 (500 mL), 1/1 (500 mL), ethylacetate (500 mL)). Produkt in fraction 2, 3 and 4 as colourless oil (1.127 g, 5.023 mmol, 68%).

¹H-NMR (CDCl₃, 500 MHz): δ = 4.24 (t, J = 8.5 Hz, 1H, C*-H), 4.75 (dd, J = 8.5, 10.2 Hz, 1H, O-CHH-C*), 5.33 (dd, J = 8.5, 10.2 Hz, 1H, O-CHH-C*), 7.13-7.27 (m, 6H, H_{py}, H_{Ph}), 7.63 (dt, J = 1.7, 7.8 Hz, 1H, H_{py}), 8.03 (d, J = 8.2 Hz, 1H, H_{py}), 8.60 (d, J = 4.8 Hz, 1H, H_{py}) ppm.

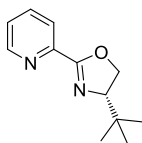
¹³C-NMR (CDCl₃, 100 MHz): δ = 70.2 (CH₂), 75.3 (C*), 124.3 (C_{ar}-H), 125.8 (C_{ar}-H), 126.8 (C_{ar}-H), 127.7 (C_{ar}-H), 128.8 (C_{ar}-H), 136.7 (C_{py}-H), 141.8 (C_{ar}-C), 146.6 (C_{ar}-C), 149.7 (C_{py}-H), 163.8 (C-O) ppm.

IR (solid): $\tilde{\nu}$ = 3084 (w), 3057 (w), 3028 (w), 3005 (w), 2965 (w), 2897 (w), 1637 (m), 1602 (w), 1580 (m), 1567 (m), 1494 (m), 1468 (m), 1454 (m), 1439 (m), 1359 (m), 1317 (m), 1289 (m), 1274 (m), 1246 (m), 1205 (w), 1178 (w), 1152 (w), 1114 (m), 1096 (s), 1078 (m), 1040 (m), 993 (m), 970 (m), 950 (m), 899 (s), 844 (w), 799 (m), 759 (m), 742 (s), 698 (s), 675 (s) cm⁻¹.

HRMS (+ESI, 250 V): m/z (%) = 247.0842 (100) [M+Na]⁺ (calc. 247.0842).

11.2.2.6 (*S*)-4-(*tert*-butyl)-2-(pyridine-2-yl)-oxazolin (**10c**)

(4138)



According to general procedure B. Amide **9b** (6.25 mmol), triethylamine (1.30 mL, 9.37 mmol), tosylchloride (1.79 g, 9.37 mmol), *N*-dimethyl-*p*-aminopyridin (76 mg, 0.62 mmol), C₂H₄C₂ (50 mL), KOH (455 mg, 8.12 mmol), methanol (50 mL). Basic alox (3 x 10 cm; hexane (300 mL), hexane/ethylacetate = 95/5 '(300 mL), 90/10 '(300 mL), 80/20 '(400 mL)). Produkt in fraction 1 and 2 as colourless powder (1.145 g, 5.608 mmol, 89%).

The analytical data are in agreement with the literature.^[248]

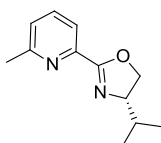
¹H-NMR (CDCl₃, 400 MHz): δ = 0.96 (s, 9H, C (CH₃)₃), 4.12 (t, *J* = 8.6 Hz, 1H, CH₂), 4.30 (t, *J* = 8.6 Hz, 1H, CH₂), 4.43 (dd, *J* = 8.8, 10.2 Hz, 1H, C*H), 7.34-7.39 (m, 1H, H_{ar}), 7.75 (dt, *J* = 1.6, 8.1 Hz, 1H, H_{ar}), 8.07 (d, *J* = 7.4, 1H, H_{ar}), 8.69 (s, 1H, H_{ar}) ppm.

¹³C-NMR (CDCl₃, 100 MHz): δ = 25.9, 34.0, 69.4, 124.1, 125.5, 136.7, 147.0, 149.8, 162.7 ppm.

IR (solid): $\tilde{\nu}$ = 3375 (w), 3057 (w), 3009 (w), 2954 (m), 2904 (w), 2869 (w), 1717 (w), 1699 (w), 1683 (w), 1658 (w), 1645 (m), 1616 (w), 1586 (w), 1582 (w), 1569 (w), 1559 (w), 1539 (w), 1520 (m), 1506 (w), 1471 (m), 1466 (m), 1440 (m), 1430 (w), 1417 (w), 1394 (w), 1359 (m), 1342 (w), 1311 (w), 1290 (w), 1264 (w), 1246 (w), 1209 (w), 1194 (w), 1149 (w), 1116 (w), 1100 (m), 1084 (w), 1061 (w), 1042 (w), 1028 (w), 994 (w), 964 (m), 931 (w), 908 (w), 860 (w), 844 (w), 801 (w), 778 (w), 745 (m), 710 (w), 667 (w) cm⁻¹.

11.2.2.7 (*S*)-4-Isopropyl-2-(6-methylpyridin-2-yl)-oxazolin (**19b**)

(3062)



According to general procedure B. Amide **17b** (7.29 mmol), triethylamine (1.52 mL, 10.9 mmol), tosylchloride (2.085 g, 0.729 mmol), *N*-dimethyl-*p*-aminopyridin (89 mg, 0.73 mmol), C₂H₄C₂ (50 mL), KOH (450 mg, 8.02 mmol), methanol (50 mL). Basic alox (3 x 10 cm; hexane (500 mL), hexane/ethylacetate = 1/1 '(400 mL), ethylacetate (400 mL)). Produkt in fraction 1 and 2 as colourless powder (726 mg, 3.22 mmol, 48%).

¹H-NMR (CDCl₃, 500 MHz): δ = 0.90 (d, *J* = 6.8 Hz, 3H, CH(CH₃)₂), 1.02 (d, *J* = 6.8 Hz, 3H, CH(CH₃)₂), 1.82-1.92 (m, 1H, CH(CH₃)₂), 2.60 (s, 3H, C_{ar}-CH₃), 4.09-4.14 (m, 1H, C*H), 4.18 (t,

$J = 8.5$ Hz, 1H, *CHH*), 4.67 (dd, $J = 8.2, 9.5$ Hz, 1H, *CHH*), 7.21 (d, $J = 7.5$ Hz, 1H, H_{ar}), 7.61 (t, $J = 7.8$ Hz, 1H, H_{ar}), 7.86 (d, $J = 7.5$ Hz, 1H, H_{ar}) ppm.

$^{13}\text{C-NMR}$ (CDCl_3 , 100 MHz): $\delta = 18.2$ ($\text{CH}(\text{CH}_3)_2$), 19.2 ($\text{CH}(\text{CH}_3)_2$), 24.8 ($\text{CH}(\text{CH}_3)_2$), 32.8 ($\text{C}_{ar}\text{-CH}_3$), 70.8 (CH_2), 72.9 (C^*), 121.2 ($\text{C}_{ar}\text{-H}$), 125.3 ($\text{C}_{ar}\text{-H}$), 136.8 ($\text{C}_{ar}\text{-H}$) 146.8 ($\text{C}_{ar}\text{-C}$), 158.8 ($\text{C}_{ar}\text{-C}$), 126.8 (CO) ppm.

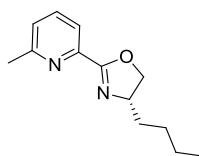
IR (solid): $\tilde{\nu} = 3056$ (w), 2977 (w), 2958 (m), 2932 (w), 2926 (w), 2905 (w), 2884 (w), 2868 (w), 1683 (w), 1634 (s), 1589 (m), 1571 (m), 1520 (w), 1497 (w), 1461 (s), 1406 (w), 1385 (w), 1372 (m), 1356 (m), 1327 (m), 1215 (m), 1273 (m), 1254 (m), 1230 (m), 1215 (w), 1179 (w), 1185 (m), 1129 (w), 1109 (s), 1079 (s), 1040 (m), 1023 (m), 1000 (m), 987 (m), 963 (s), 932 (m), 915 (m), 895 (m), 842 (w), 827 (w), 811 (s), 747 (s), 710 (m), 678 (w), 669 (m) cm^{-1} .

HRMS (+ESI, 200 V): m/z (%) = 205.1316 (100) $[\text{M}+\text{H}]^+$ (calc.205.1335), 227.1133 (37) $[\text{M}+\text{Na}]^+$ (calc. 227.1154).

M.p. = 38-40 °C

11.2.2.8 (*S*)-4-Butyl-2-(6-methylpyridin-2-yl)-oxazolin (**19f**)

(3096)



According to general procedure B. Amide **17f** (3.65 mmol), triethylamine (0.72 mL, 5.4 mmol), tosylchloride (1.043 g, 5.4 mmol), *N*-dimethyl-*p*-aminopyridin (45 mg, 0.36 mmol), $\text{C}_2\text{H}_4\text{C}_2$ (30 mL), KOH (250 mg, 4.01 mmol), methanol (30 mL). Basic alox (3 x 10 cm; pentane (500 mL), hexane/ethylacetate = 9/1 (500 mL), 7/3 (500 mL), ethylacetate (500 mL)). Produkt in fraction 3 as colourless oil (303 mg, 1.71 mmol, 47%).

$^1\text{H-NMR}$ (CDCl_3 , 500 MHz): $\delta = 0.89$ (t, $J = 6.1$ Hz, 3H, $\text{CH}_3(^n\text{Bu})$), 1.29-1.57 (m, 5H, $\text{CH}_2(^n\text{Bu})$), 1.74-1.81 (m, 1H, $\text{CH}_2(^n\text{Bu})$), 2.60 (s, 3H, $\text{CH}_3(\text{Py})$), 4.08 (t, $J = 8.2$ Hz, 1H, *CHH*-O), 4.25-4.32 (m, 1H, C^*H), 4.53 (t, $J = 8.8$ Hz, *CHH*-O), 7.21 (t, $J = 7.8$ Hz, 1H, H_{ar}), 7.61 (t, $J = 7.8$ Hz, 1H, H_{ar}), 7.82 (d, $J = 7.8$ Hz, 1H, H_{ar}) ppm.

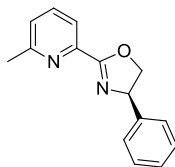
$^{13}\text{C-NMR}$ (CDCl_3 , 100 MHz): $\delta = 14.1$ ($\text{CH}_3(^n\text{Bu})$), 22.7 ($\text{CH}_2(^n\text{Bu})$), 24.7 ($\text{CH}_3(\text{Py})$), 28.2 ($\text{CH}_2(^n\text{Bu})$), 35.6 ($\text{CH}_2(^n\text{Bu})$), 67.1 (C^*), 73.2 ($\text{CH}_2\text{-O}$), 121.2 ($\text{C}_{ar}\text{-H}$), 125.4 ($\text{C}_{ar}\text{-H}$), 136.8 ($\text{C}_{ar}\text{-H}$)146.4 ($\text{C}_{ar}\text{-C}$), 158.8 ($\text{C}_{ar}\text{-C}$), 162.8 (C-O) ppm.

IR (solid): $\tilde{\nu} = 3063$ (w), 2955 (m), 2927 (m), 2894 (m), 2870 (m), 2857 (m), 1716 (w), 1678 (w), 1639 (s), 1589 (m), 1574 (m), 1515 (w), 1477 (m), 1459 (s), 1407 (w), 1375 (m), 1362 (s), 1318 (m), 1291 (w), 1267 (m), 1255 (m), 1234 (m), 1199 (w), 1162 (m), 1138 (m), 1125 (m), 1111 (s), 1078 (s), 1036 (m) 999 (m), 989 (m), 963 (s), 930 (m), 909 (m), 892 (w), 864 (w), 833 (w), 808 (s), 744 (s), 730 (s), 697 (s), 668 (m) cm^{-1} .

HRMS (+ESI, 200 V): m/z (%) = 219.1470 (100) $[M+H]^+$ (calc. 219.1492), 241.1286 (42) $[M+Na]^+$ (calc.214.1311).

11.2.2.9 (*R*)-2-(6-Methylpyridin-2-yl)-oxazolin (**19g**)

(3090)



According to general procedure B. Amide **17g** (7.29 mmol), triethylamine (1.52 mL, 10.9 mmol), tosylchloride (2.085 g, 0.729 mmol), *N*-dimethyl-*p*-aminopyridin (89 mg, 0.73 mmol), $C_2H_4C_2$ (50 mL), KOH (450 mg, 8.02 mmol), methanol (50 mL). Basic alox (3 x 10 cm; pentane (400 mL), hexane (500 mL), hexane/ethylacetate = 9/1 (500 mL), 7/3 (500 mL), ethylacetate (500 mL)). Produkt in fraction and 3 as colourless oil (1.058 g, 4.440 mmol, 60%).

1H -NMR ($CDCl_3$, 500 MHz): δ = 2.63 (s, 3H, CH_3), 4.36 (t, J = 8.5 Hz, 1H, CHH), 4.86 (dd, J = 8.5, 10.2 Hz, 1H, CHH), 5.41 (dd, J = 8.5, 10.2 Hz, 1H, C^*-H), 7.24-7.35 (m, 6H, H_{ar}), 7.65 (t, J = 7.8 Hz, 1H, H_{py}), 7.97 (d, J = 7.8 Hz) ppm.

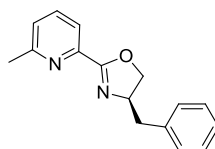
^{13}C -NMR ($CDCl_3$, 100 MHz): δ = 24.8 (CH_3), 70.4 (C^*), 75.5 (CH_2), 125.7 (C_{py-H}), 126.9 (C_{ar-H}), 127.8 (C_{ar-H}), 136.9 (C_{py-H}), 142.0 (C_{ar}), 146.2 (C_{ar}), 158.9 (C_{ar}), 164.1 (CO) ppm.

IR (solid): $\tilde{\nu}$ = 3105 (w), 3083 (w), 3061 (w), 3028 (w), 3003 (w), 2946 (w), 2921 (w), 2897 (w), 1637 (m), 1589 (m), 1573 (m), 1541 (w), 1516 (w), 1493 (w), 1473 (w), 1453 (s), 1407 (w), 1378 (w), 1361 (m), 1317 (w), 1294 (w), 1278 (w), 1253 (m), 1234 (m), 1207 (w), 1177 (w), 1158 (s), 1114 (m), 1081 (s), 1028 (w), 998 (m), 989 (m), 971 (m), 955 (m), 917 (m), 911 (m), 838 (w), 807 (m), 757 (s), 744 (s), 728 (s), 698 (s), 670 (s) cm^{-1} .

HRMS (+ESI, 250 V): m/z (%) = 239.1174 (100) $[M+H]^+$ (calc. 239.1178), 261.0982 (22) $[M+Na]^+$ (calc. 261.0998).

11.2.2.10 (*R*)-4-Benzyl-2-(6-methylpyridin-2-yl)-oxazolin (**19h**)

(3074)



According to general procedure B. Amide **17h** (7.29 mmol), triethylamine (1.52 mL, 10.9 mmol), tosylchloride (2.085 g, 0.729 mmol), *N*-dimethyl-*p*-aminopyridin (89 mg, 0.73 mmol), $C_2H_4C_2$ (50 mL), KOH (450 mg, 8.02 mmol), methanol (50 mL). Basic alox (3 x 10 cm; pentane (500 mL), pentane/diethylether = 7/3 (500 mL), diethylether (500 mL)). Produkt in fraction 1, 2 and 3 as colourless oil (1.134 g, 4.500 mmol, 60%).

¹H-NMR (CDCl₃, 500 MHz): δ = 2.62 (s, 3H, CH₃), 2.73 (dd, J = 9.2, 13.7 Hz, 1H, Ph-CHH), 3.30 (dd, J = 4.8, 13.7 Hz, 1H, Ph-CHH), 4.21 (t, J = 7.8 Hz, 1H, O-CHH), 4.42 (t, J = 9.5 Hz, 1H, O-CHH), 4.60-4.65 (m, 1H, C*H), 7.19-7.31 (m, 6H, HPh, HPy), 7.64 (t, J = 7.8 Hz, HPy), 7.86 (t, J = 7.8 Hz) ppm.

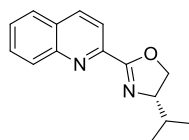
¹³C-NMR (CDCl₃, 100 MHz): δ = 24.8 (CH₃), 41.8 (CH₂-Ph), 68.2 (C*), 72.6 (CH₂-O), 121.3 (C_{Py}-H), 125.5 (C_{ar}-H), 126.7 (C_{ar}-H), 129.5 (C_{ar}-H), 137.5 (C_{Py}-H), 137.9 (C_{ar}-C), 146.2 (C_{ar}-C), 158.9 (C_{ar}-C), 163.4 (C-O) ppm.

IR (solid): $\tilde{\nu}$ = 3083 (w), 3061 (w), 3026 (w), 3000 (w), 2959 (w), 2959 (w), 2921 (w), 2898 (w), 2853 (w), 1723 (w), 1674 (m), 1638 (m), 1590 (m), 1573 (m), 1512 (m), 1496 (m), 1473 (m), 1453 (s), 1408 (w), 1377 (m), 1363 (m), 1316 (m), 1291 (m), 1257 (m), 1234 (m), 1158 (m), 1116 (m), 1083 (s), 1067 (m), 1028 (m), 1012 (m), 999 (m), 965 (m), 932 (m), 864 (w), 840 (w), 806 (s), 745 (s), 699 (s), 669 (m) cm⁻¹.

HRMS (+ESI, 250 V): m/z (%) = 275.1129 (100) [M+Na]⁺ (calc.275.1154), 253.1309 (88) [M+H]⁺ (calc.253.135).

11.2.2.11 (S)-4-Isopropyl-2-(quinolin-2-yl)-oxazolin (20b)

(3064)



According to general procedure B. Amide **18b** (7.29 mmol), triethylamine (1.52 mL, 10.9 mmol), tosylchloride (2.085 g, 0.729 mmol), *N*-dimethyl-*p*-aminopyridin (89 mg, 0.73 mmol), C₂H₄C₂ (50 mL), KOH (450 mg, 8.02 mmol), methanol (50 mL). Basic alox (3 x 10 cm); pentane (300 mL), hexane (500 mL), hexane/ethylacetate = 9/1 (500 mL), ethylacetate (500 mL)). Produkt in fraction 1, 2, and 3 as colourless powder (1.076 g, 4.476 mmol, 61%).

¹H-NMR (CDCl₃, 500 MHz): δ = 0.95 (d, J = 6.8 Hz, 3H, CH(CH₃)₂), 1.06 (d, J = 6.8 Hz, 3H, CH(CH₃)₂), 1.88-2.00 (m, 1H, CH(CH₃)₂), 4.18-4.23 (m, 1H, C*-H), 4.29 (t, J = 8.2 Hz, 1H, CHH-O), 4.57 (dd, J = 8.2, 9.9 Hz, Hz, 1H, CHH-O), 7.56 (t, J = 7.5 Hz, 1H, H_{ar}), 7.72 (t, J = 7.8 Hz, 1H, H_{ar}), 7.81 (d, J = 8.2 Hz, 1H, H_{ar}), 8.19 (s, 2H, H_{ar}), 8.25 (d, J = 9.0 Hz, 1H, H_{ar}) ppm.

¹³C-NMR (CDCl₃, 100 MHz): δ = 18.3 (CH(CH₃)₂), 19.2 (CH(CH₃)₂), 32.9 (CH(CH₃)₂), 71.1 (CH₂), 73.1 (C*), 121.0 (C_{ar}-H), 127.6 (C_{ar}-H), 127.9 (C_{ar}-H), 128.8 (C_{ar}-C), 130.1 (C_{ar}-H), 130.5 (C_{ar}-H), 136.7 (C_{ar}-H), 147.1 (C_{ar}-C), 147.7 (C_{ar}-C), 162.9 (C-O) ppm.

IR (solid): $\tilde{\nu}$ = 3060 (w), 2986 (m), 2970 (m), 2957 (m), 2922 (m), 2907 (m), 2892 (m), 2868 (m), 1717 (w), 1666 (w), 1653 (w), 1634 (s), 1593 (m), 1558 (m), 1539 (m), 1502 (m), 1475 (m), 1462 (m), 1444 (m), 1428 (m), 1368 (s), 1357 (s), 1339 (m), 1331 (m), 1319 (m), 1300 (m), 1269 (m), 1243 (m),

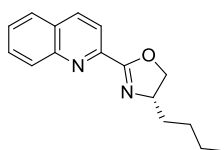
1207 (m), 1178 (m), 1141 (m), 1118 (s), 1084 (s), 1036 (m), 1012 (m), 970 (s), 950 (m), 919 (m), 892 (m), 883 (m), 838 (s), 823 (m), 795 (m), 778 (m), 760 (s), 726 (m), 698 (m), 669 (m) cm^{-1} .

HRMS (+ESI, 250 V): m/z (%) = 241.1341 (100) $[\text{M}+\text{H}]^+$ (calc. 241.1335), 263.1163 (95) $[\text{M}+\text{Na}]^+$ (calc. 263.1155).

M.p. = 60-63 °C

11.2.2.12 (S)-4-Butyl-2-(quinolin-2-yl)-oxazolin (20f)

(3098)



According to general procedure B. Amide **18f** (3.65 mmol), triethylamine (0.72 mL, 5.4 mmol), tosylchloride (1.043 g, 5.4 mmol), *N*-dimethyl-*p*-aminopyridin (45 mg, 0.36 mmol), $\text{C}_2\text{H}_4\text{C}_2$ (30 mL), KOH (250 mg, 4.01 mmol), methanol (30 mL). Basic alox (3 x 10 cm; pentane (500 mL), hexane (500 mL), hexane/ethylacetate = 4/1 (500 mL), hexane/ethylacetate = 3/2 (500 mL), ethylacetate (500 mL)). Produkt in fraction 3 and 4 as colourless oil (1.523 g, 1.523 mmol, 5%).

$^1\text{H-NMR}$ (CDCl_3 , 500 MHz): δ = 0.68 (t, $J=6.6$ Hz, 3H, CH_3), 1.00-1.18 (m, 5H, $\text{CH}_2(^n\text{Bu})$), 1.22-1.30 (m, 1H, $\text{CH}_2(^n\text{Bu})$), 1.33-1.40 (m, 1H, $\text{CH}_2(^n\text{Bu})$), 1.54-1.62 (m, 1H, $\text{CH}_2(^n\text{Bu})$), 3.93 (t, $J=8.2$ Hz, 1H, C^*-CH_2), 4.10-4.16 (m, 1H, C^*-H), 4.38 (t, $J=8.2$ Hz, 1H, C^*-CH_2), 7.28 (t, $J=7.6$ Hz, 1H, H_{ar}), 7.47 (t, $J=7.6$ Hz, 1H, H_{ar}), 7.51 (d, $J=8.3$ Hz, 1H, H_{ar}), 7.90-7.94 (m, 2H, H_{ar}), 8.05 (d, $J=8.5$ Hz, 1H, H_{ar}) ppm.

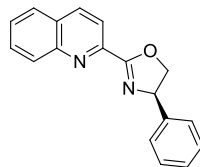
$^{13}\text{C-NMR}$ (CDCl_3 , 100 MHz): δ = 13.9 (CH_3), 22.5 ($\text{CH}_2(^n\text{Bu})$), 27.9 ($\text{CH}_2(^n\text{Bu})$), 35.4 ($\text{CH}_2(^n\text{Bu})$), 66.9 (C^*), 73.2 (C^*-CH_2), 120.5 ($\text{C}_{\text{ar}}-\text{H}$), 127.3 ($\text{C}_{\text{ar}}-\text{H}$), 127.6 ($\text{C}_{\text{ar}}-\text{H}$), 128.4 ($\text{C}_{\text{ar}}-\text{C}$), 129.8 ($\text{C}_{\text{ar}}-\text{H}$), 130.1 ($\text{C}_{\text{ar}}-\text{H}$), 136.4 ($\text{C}_{\text{ar}}-\text{H}$), 146.4 ($\text{C}_{\text{ar}}-\text{C}$), 147.3 ($\text{C}_{\text{ar}}-\text{C}$), 162.5 ($\text{C}-\text{O}$) ppm.

IR (solid): $\tilde{\nu}$ = 3085 (w), 3021 (w), 2957 (m), 2927 (m), 2893 (m), 2867 (w), 2857 (m), 1731 (w), 1671 (w), 1537 (s), 1592 (m), 1558 (m), 1526 (w), 1505 (m), 1473 (m), 1462 (m), 1428 (w), 1364 (s), 1342 (m), 1217 (m), 1296 (m), 1261 (m), 1240 (m), 1211 (m), 1183 (m), 1156 (m), 1143 (m), 1125 (s), 1079 (s), 1072 (s), 1019 (m), 998 (m), 982 (m), 961 (s), 945 (m), 916 (m), 873 (w), 858 (w), 844 (s), 802 (m), 767 (s), 783 (s), 715 (m), 698 (m), 671 (m) cm^{-1} .

HRMS (+ESI, 250 V): m/z (%) = 255.1503 (100) $[\text{M}+\text{H}]^+$ (calc. 255.1492), 277.1315 (38) $[\text{M}+\text{Na}]^+$ (calc. 277.1311).

11.2.2.13 (R)-4-Phenyl-2-(quinolin-2-yl)-oxazolin (20g)

(3076)



According to general procedure B. Amide **18g** (7.29 mmol), triethylamine (1.52 mL, 10.9 mmol), tosylchloride (2.085 g, 0.729 mmol), *N*-dimethyl-*p*-aminopyridin (89 mg, 0.73 mmol), C₂H₄Cl₂ (50 mL), KOH (450 mg, 8.02 mmol), methanol (50 mL). Basic alox (3 x 10 cm; pentane (750 mL), pentane/Et₂O = 1/1 (500 mL), Et₂O (500 mL)). Produkt was found in fraction 3 and 4 as Mixture with starting material (660 mg). The product was recrystallized with toluene from fraction 3 and obtained as colourless crystalline powder (0.115 g, 0.418 mmol, 5%).

¹H-NMR (CDCl₃, 400 MHz): δ = 4.47 (dt, J =1.0, 8.6 Hz, 1H, CH₂), 4.94-5.00 (m, 1H, C*-H), 5.50 (t, J =9.5 Hz, 1H, CH₂), 7.25-7.39 (m, 5H, H_{ar}), 7.60 (dd, J =7.0, 7.9 Hz, 1H, H_{ar}), 7.76 (dd, J =6.0, 8.3 Hz, 1H, H_{ar}), 7.85 (d, J =8.1 Hz, 1H, H_{ar}), 8.22-8.30 (m, 3H, H_{ar}) ppm.

¹³C-NMR (CDCl₃, 100 MHz): δ = 70.6 (C*), 75.7 (CH₂), 121.1 (C_{Ph}-H), 127.0 (C_{quin}-H), 127.7 (C_{quin}-H), 127.9 (C_{quin}-H), 128.2 (C_{Ph}-H), 128.9 (C_{quin}-C), 130.2 (C_{quin}-C), 130.5 (C_{quin}-H), 136.8 (C_{quin}-H), 141.8 (C_{Ph}-C), 146.8 (C_{quin}-C), 147.7 (C_{quin}-C), 164.2 (C-O) ppm.

IR (solid): $\tilde{\nu}$ = 3080 (w), 3052 (w), 3027 (w), 3008 (w), 3003 (w), 2957 (w), 2936 (w), 2925 (w), 2897 (w), 1633 (s), 1593 (m), 1558 (m), 1506 (m), 1490 (m), 1473 (m), 1460 (m), 1451 (m), 1429 (w), 1365 (m), 1350 (m), 1340 (m), 1319 (m), 1297 (w), 1275 (m), 1253 (w), 1243 (m), 1208 (m), 1196 (m), 1176 (w), 1154 (w), 1142 (w), 1125 (s), 1089 (s), 1080 (s), 1036 (m), 1027 (m), 1018 (w), 1000 (m), 980 (m), 970 (s), 943 (m), 916 (m), 879 (m), 838 (s), 802 (m), 794 (s), 759 (s), 735 (m), 696 (s), 675 (m) cm⁻¹.

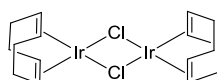
HRMS (+ESI, 250 V): m/z (%) = 297.1002 (100) [M+Na]⁺ (calc. 297.0998), 275.1180 (29) [M+H]⁺ (calc. 275.1180). **M.p.** = 129-130 °C

12 Complexes

12.1 Starting Materials

12.1.1 *bis*-(1,5-Cyclooctadien)-di-iridium(I)chloride, [Ir(cod)Cl]₂ (23)

(5060, GM 1098)



The reaction was carried out under an argon atmosphere. Iridiumtrichlorid (1.00 g, 3.34 mmol) was dissolved in an ethanol (17.5 mL) / water (8.75 mL) mixture to give a violet homogeneous solution. The solution was degassed by leading an argon stream for 30 min through it. The argon inlet was not removed but the stream of argon reduced to a minimum and 1,5-Cyclooctadien (3.00 mL, 24.4 mmol) was added. The reaction mixture was heated to reflux for approximately 10 h while its color turned to orange. After cooling down to -5 °C (brine/ice), the red precipitated solid was separated by filtration and washed with 2x2 mL cold methanol and 10 mL hexane. The solid was dried in high vacuum to yield the product as red-orange powder (0.85 g, 1.26mmol, 75 %)

¹H-NMR (CDCl₃, 500 MHz): δ = 1.46–1.59 (m, 8H, CHH), 2.20–2.31 (m, 8H, CHH), 4.18–4.29 (m, 8H, CH) ppm.

¹³C-NMR (CDCl₃, 125 MHz): δ = 31.9 (CH₂), 62.3 (CH) ppm.

IR (solid): $\tilde{\nu}$ = 3482 (w), 3258 (m), 2940 (m), 2913 (m), 2834 (m), 2360 (w), 2330 (w), 2288 (w), 2181 (w), 2032 (w), 1930 (w), 1682 (m), 1554 (w), 1538 (w), 1472 (m), 1448 (m), 1433 (m), 1338 (w), 1324 (m), 1390 (w), 1298 (w), 1263 (w), 1236 (w), 1207 (w), 1183 (w), 1168 (w), 1154 (w), 1135 (w), 1114 (w), 1074 (w), 1002 (m), 978 (m), 953 (m), 908 (m), 871 (m), 835 (m), 804 (w), 784 (w), 738 (w), 708 (m), 675 (w) cm⁻¹.

12.1.2 Silver (*tetrakis*-3,5-bis(trifluoromethyl)phenyl)borate; AgBAR^F (34)

(3128, 4030, 5024)

AgBAR^F was prepared following an optimized procedure of Buschmann and Miller.^[241]

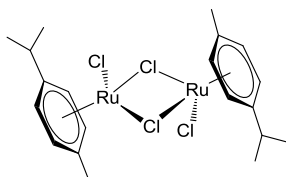
It is important to care for light absence during the whole process! Inert gas is not necessary.

NaBAR^F (33) (1.000 g, 1.129 mmol) and AgNO₃ (35) were separately dissolved in MeCN (5-10 mL each), to make sure that both salts are dissolved completely. The two solutions were mixed at room temperature and left stirring for 30 min. The precipitated solid was removed by filtration and flushed with DCM. The combined organic phases (MeCN and DCM solution) were reduced to dryness under high vacuum (rotary evaporation is not recommended due to the elevated temperatures necessary for

this method). The slimy residue was dissolved again in DCM and the DMC was removed under high vacuum. This step was repeated as often as necessary until the residue was a solid. This off-white solid was dissolved in a few milliliters of DCM and overlaid by hexane. At $-20\text{ }^{\circ}\text{C}$ the product formed colorless crystals over a period of some days. The crystals were removed by filtration and washed with hexane. From the reduced filtrate more crystals could be obtained at $-20\text{ }^{\circ}\text{C}$. The product was obtained quantitatively. The IR spectral analysis was in accordance with the reported data.

12.1.3 $[\text{RuCl}_2(\eta^6\text{-}p\text{-cymol})]_2$, Di- μ -chloro-bis- $[(\eta^6\text{-}p\text{-cymol})\text{-chloro-ruthenium(II)}]$ (**46**)

(1040)



$[\text{Ru}(\text{cymol})\text{Cl}]_2$ was prepared following a procedure from Bennett and Smith.^[249]

Rutheniumtrichlorid (**17**) (6.27 g, 24.0 mmol) and α -Phellandren (**18**) (racemat, 38.9 mL, 240 mmol) were dissolved in ethanol (350 mL) and heated under reflux for 5 h. While cooling down to room temperature, a red solid precipitates. The solid was removed by filtration and washed with ethanol. The product is a red powder (5.53 g, 9.0 mmol, 75%).

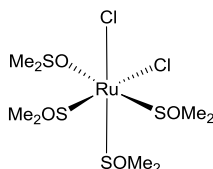
The $^1\text{H-NMR}$ and IR spectrum are in accordance with the data reported in literature.

$^1\text{H-NMR}$ (CD_2Cl_2 , 500 MHz): $\delta = 1.24$ (d, $J = 6.9$ Hz, 6H, $\text{CH}(\text{CH}_3)_2$), 2.12 (s, 3H, Ph-CH_3), 2.88 (sep, $J = 6.9$ Hz, 1H, $\text{CH}(\text{CH}_3)_2$), 5.30 (d, $J = 6.0$ Hz, 2H, H_{ar}), 5.44 (d, $J = 6.0$ Hz, 2H, H_{ar}).

IR (solid): $\tilde{\nu} = 3048$ (m), 3029 (m), 2960 (m), 2923 (m), 2868 (m), 2534 (w), 2161 (w), 2038 (w), 1978 (w), 1531 (w), 1495 (m), 1470 (s), 1460 (s), 1447 (s), 1408 (m), 1388 (s), 1378 (s), 1362 (s), 1325 (m), 1280 (m), 1217 (m), 1200 (m), 1160 (m), 1145 (m), 1113 (m), 1093 (m), 1055 (s), 1033 (s), 1004 (m), 960 (m), 943 (w), 927 (w), 902 (w), 876 (s), 804 (m), 689 (w), 670 (m) cm^{-1} .

12.1.4 Dichlorotetrakis(dimethyl-sulfoxid)ruthenium(II); $[\text{Ru}(\text{DMSO})_4\text{Cl}_2]$ (**47**)

(CG 2066)



The synthesis was performed on the basis of a procedure of the Toyama group.^[134]

The reaction was performed under an argon atmosphere. $\text{RuCl}_3 \times 3 \text{H}_2\text{O}$ (5.00 g, 23.0 mmol) was dissolved in dry DMSO (5 mL) and heated at $190\text{ }^{\circ}\text{C}$ oil-bath temperature for 5 min. After cooling down to room temperature, the volume of the reaction mixture was reduced in high vacuum to a resulting

mixture volume of approx. 2.5 mL. A yellow solid was precipitated from the reaction mixture by addition of acetone (40 mL). The solid was separated by filtration and washed with acetone and diethylether. After drying the solid in high vacuum, a yellow powder was obtained as product (7.54 g, 15.5 mmol, 67%).

The $^1\text{H-NMR}$ analysis is in accordance with the data reported in literature.

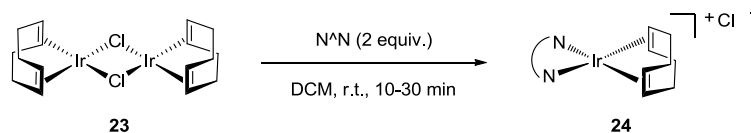
$^1\text{H-NMR}$ (CDCl_3 , 400 MHz): δ = 3.52 (s, 6H, CH_3), 3.49 (s, 6H, CH_3), 3.43 (s, 12H, CH_3), 3.32 (s, 6H, CH_3), 2.72 (s, 6H, CH_3), 2.61 (s, 6H, CH_3) ppm.

HRMS (+ESI, 150 V): m/z (%) = 506.8887 (50) $[\text{M}+\text{Na}]^+$ (calc. 506.8876), 448.9261 (25) $[\text{M}-\text{Cl}]^+$ (calc. 448.9289).

IR (solid): $\tilde{\nu}$ = 3021 (w), 3006 (w), 2921 (w), 1420 (w), 1398 (w), 1306 (w), 1289 (w), 1111 (s), 1093 (w), 1084 (s), 1036 (w), 1019 (s), 991 (s), 959 (m), 930 (s), 715 (s), 675 (s) cm^{-1} .

12.2 Iridium(I)-cod Cl^- Complexes

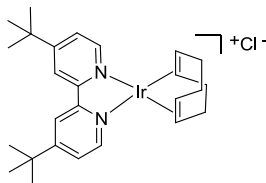
12.2.1 General Procedure C for $[\text{Ir}(\text{N}^{\wedge}\text{N})(\text{cod})]\text{Cl}$ Complexes **24**



$[\text{Ir}(\text{cod})\text{Cl}]_2$ (**23**) (50.0 mg, 1.00 \AA q, 0.0744 mmol, 1 equiv.) was dissolved in DCM (4 mL) resulting in an orange solution. The $\text{N}^{\wedge}\text{N}$ ligand (0.149 mmol, 2 equiv.) was dissolved in DCM (2 mL) to make sure that it was completely in solution. Both solutions were combined resulting in a spontaneous color change to red or violet. The reaction mixture was stirred for 10-30 min. Subsequently the solvent was completely removed in high vacuum to result the remaining solid as product **24** in quantitatively.

12.2.2 1,5-Cyclooctadiene[(4,4'-di-tert-butyl-2,2'-bipyridine)]iridium(I) chlorid, [Ir(dtbpy)(cod)]Cl (24a)

(GM 1106, 1120, 1132, 1140)



Following general procedure C.

Ligand: dtbpy (**32**) (39.9 mg, 0.149 mmol)

Reaction time: 10 min

Product: violet solid

¹H-NMR (CD₂Cl₂, 500 MHz): δ = 1.43 (s, 18H, (CH₃)₃), 1.69–1.76 (m, 4H, C_{cod}HH), 2.28–2.37 (m, 4H, C_{cod}HH), 3.66–3.71 (m, 4H, C_{cod}H), 7.53 (dd, J = 2.0, 5.8 Hz, 2H, H_{ar}), 8.17–8.22 (m, 4H, H_{ar}) ppm.

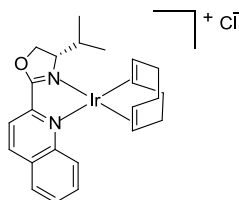
¹³C-NMR (CD₂Cl₂, 125 MHz): δ = 30.0 (CH₃), 31.9 (C_{cod}H₂), 35.6 (C(CH₃)₃), 60.0 (C_{cod}H), 119.8 (C_{ar}), 124.2 (C_{ar}), 147.0 (C_{ar}), 156.1 (C_{ar}), 161.6 (C_{ar}) ppm.

IR (solid): $\tilde{\nu}$ = 3664 (w), 3391 (w), 3194 (w), 3109 (w), 3034 (w), 2960 (m, ν CH_{ar}), 2909 (w, ν CH_{ar}), 2871 (m, ν CH_{ar}), 2829 (w, ν CH_{ar}), 1614 (m), 1544 (w), 1481 (m), 1442 (w), 1411 (m), 1366 (m), 1321 (w), 1295 (w), 1254 (w), 1203 (w), 1157 (w), 1133 (w), 1076 (w), 1020 (w), 972 (w), 955 (w), 924 (w), 900 (w), 837 (w), 804 (w), 744 (w), 707 (w), 670 (w) cm⁻¹.

(Anion exchange experiments: GM1102, 1002, 1110, 1116, 1114.)

12.2.3 1,5-Cyclooctadiene[((S)-4-Isopropyl-2-(quinolin-2-yl)-oxazolin)]iridium(I) chlorid, [Ir(ⁱPr-quinox)(cod)]Cl (24b)

(GM 1108)



Following general procedure C.

Ligand: ⁱPr-quinox (**20b**) (35.7 mg, 0.149 mmol)

Reaction time: 30 min

Product: dark red solid

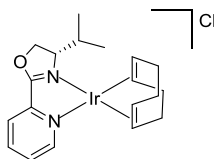
¹H-NMR (CD₂Cl₂, 500 MHz): δ = 1.18 (d, J = 6.9 Hz, 3H, CH₃), 1.25 (d, J = 6.9 Hz, 3H, CH₃), 1.27–1.34 (m, 2H, C_{cod}H), 1.38–1.45 (m, 2H, C_{cod}H), 2.20–2.35 (m, 4H, C_{cod}HH), 2.61–2.75 (m, 1H, CH), 3.28–3.46 (m, 4H, C_{cod}HH), 4.67 (quartett, J = 6.9 Hz, 1H, CHH), 4.70–4.75 (m, 1H, C*H), 4.80 (dd, 1H, J = 7.2, 9.3 Hz CHH), 7.76 (t, J = 7.6 Hz, 1H, CH_{ar}), 7.91 (d, J = 7.9 Hz, 1H, CH_{ar}), 7.95 (d, J = 7.6 Hz, 1H, CH_{ar}), 8.01 (ddd, J = 1.4, 7.6, 7.9 Hz, 1H, CH_{ar}), 8.38 (d, J = 8.6 Hz, 1H, CH_{ar}), 9.72 (d, J = 8.6 Hz, 1H, CH_{ar}) ppm.

¹³C-NMR (CD₂Cl₂, 125 MHz): δ = 16.7(CH₃), 19.2 (CH₂), 31.5 (C_{cod}H₂), 33.5 (CH(CH₃)₂), 71.1 (C_{cod}H), 72.6 (C*), 120.1 (C_{ar}), 127.9 (C_{ar}), 129.5 (C_{ar}), 129.9 (C_{ar}), 131.2 (C_{ar}), 132.1 (C_{ar}), 136.5 (C_{ar}), 138.4 (C_{ar}), 146.7 (C_{ar}), 169.3 (CO) ppm.

IR (solid): $\tilde{\nu}$ = 3420 (w), 3057 (m, ν CH_{ar}), 2922 (m, ν CH_{ar}), 2872 (m, ν CH_{ar}), 2834 (w ν CH_{ar}), 1733 (w), 1719 (w), 1650 (m), 1615 (w), 1592 (m), 1561 (w), 1509 (w), 1480 (m), 1487 (m), 1433 (w), 1398 (m), 1388 (m), 1302 (m), 1367 (m), 1339 (w), 1303 (w), 1284 (w), 1251 (w), 1214 (w), 1165 (m), 1148 (w), 1114 (m), 1085 (w), 1006 (w), 967 (m), 953 (m), 922 (w), 895 (w), 875 (w), 838 (m), 785 (m), 709 (m), 675 (w) cm⁻¹.

12.2.4 1,5-Cyclooctadien[(S)-4-isopropyl-2-(pyridin-yl)-oxazolin]iridium(I) chlorid, [Ir(ⁱPr-pyrox)(cod)]Cl (**24c**)

(GM 1134)



Following general procedure C.

Ligand: ⁱPr-pyrox (**10b**) (28.32 mg, 0.149 mmol)

Reaction time: 30 min

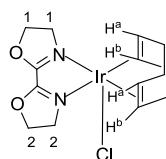
Product: violet solid

¹H-NMR (CD₂Cl₂, 500 MHz): δ = 0.94(d, J = 6.8 Hz, 3H, CH₃), 1.00 (d, J = 6.8 Hz, 3H, CH₃), 1.18–1.29 (m, 1H, CH), 1.42–1.52 (m, 2H, H_{cod}), 1.64–1.75 (m, 2H, H_{cod}), 2.04–2.13 (m, 2H, H_{cod}), 2.16–2.24 (m, 2H, H_{cod}), 2.26–2.35 (m, 2H, H_{cod}), 3.69–3.75 (m, 1H, C*H), 3.81–3.86 (m, 1H, CHH), 3.89–3.93 (m, 1H, CHH), 4.62–4.96 (m, 2H, H_{cod}), 7.57–8.16 (m, 4H, H_{ar}) ppm.

IR (solid): $\tilde{\nu}$ = 3387 (w), 3066 (w), 2957 (w ν CH_{ar}), 2871 (w ν CH_{ar}), 2837 (w ν CH_{ar}), 2294 (w), 2197 (w), 2005 (w), 1652 (w), 1618 (w), 1590 (m), 1567 (w), 1494 (w), 1464 (w), 1437 (w), 1409 (m), 1390 (m), 1372 (w), 1332 (w), 1249 (w), 1254 (w), 1204 (w), 1160 (w), 1114 (w), 1091 (w), 1053 (w), 1000 (w), 953 (m), 927 (m), 891 (w), 871 (w), 797 (w), 754 (m), 107 (m), 668 (m) cm⁻¹.

12.2.5 1,5-Cyclooctadien[2,2'-bioxazolin]iridium(I) chlorid, [Ir(H-box)(cod)]Cl (**24d**)

(GM 1118, 1124)



Following general procedure C.

Ligand: H-box (**5i**) (26.1 mg, 0.149 mmol)

Reaction time: 20 min

Product: red solid

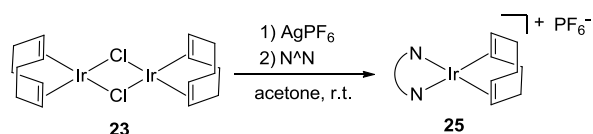
¹H-NMR (CD₂Cl₂, 500 MHz): δ = 1.58–1.69 (m, 4H, C_{cod}HH), 2.15–2.28 (m, 4H, C_{cod}HH), 3.30 (t, J = 7.5 Hz, 2H, NC¹H₂), 3.52 (t, J = 7.5 Hz, 2H, OC¹H₂), 3.58–3.63 (m, 2H, C_{cod}H^a), 3.74 (t, J = 9.9 Hz, 2H, NC²H₂), 3.84–3.88 (m, 2H, C_{cod}H^b), 4.72 (t, J = 9.9 Hz, 2H, OC²H₂) ppm.

¹³C-NMR (CD₂Cl₂, 125 MHz): δ = 31.5 (C_{cod}H₂), 31.7 (C_{cod}H₂), 41.9 (NC¹), 46.3 (NC²), 48.6 (OC¹), 60.5 (OC²), 66.6 (C_{cod}H), 72.0 (C_{cod}H), 164.1 (OC¹N), 172.7 (OC²N) ppm.

IR (solid): $\tilde{\nu}$ = 3407 (w), 2933 (w), 2880 (w), 2821 (w), 2293 (w), 2202 (w), 1624 (s), 1533 (w), 1500 (m), 1474 (w), 1453 (w), 1431 (w), 1363 (w), 1325 (w), 1312 (w), 1259 (m), 1192 (w), 1156 (w), 1040 (m), 996 (m), 953 (m), 917 (m), 870 (w), 818 (w), 780 (w), 735 (w), 707 (m), 675 (w) cm⁻¹.

12.3 Iridium(I)-cod PF₆⁻ Complexes **25**

12.3.1 General procedure D for the formation of [Ir(N^N)(cod)]PF₆ complexes **25**

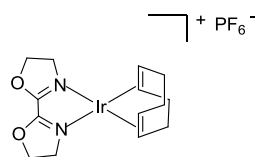


[Ir(cod)(Cl)]₂ (**23**) (140 mg, 0.208 mmol, 1 equiv.) was given into a schlenk-tube and the air exchanged for argon. Degassed acetone (42 mL) was added and the mixture stirred until the solid was nearly completely dissolved to give an orange solution. In an argon stream AgPF₆ (107.8 mg, 0.4165 mmol, 2 equiv.) was added and the clear orange solution turned into a bright yellow suspension immediately. The reaction mixture was stirred for 30 min at room temperature and then left standing for 60 min without stirring. The yellow solution was dekantated under argon from the colorless solid and carefully filterdered to remove residual solid completely, because previous experiments showed that this was

crucial for obtaining reproducible result. The obtained filtrated was divided into 6 portions of 6 mL, containing an equivalent of 20 mg/0.0298 mmol $[\text{Ir}(\text{cod})(\text{Cl})_2]$ (**23**). Each portion was filled under argon into a Schlenk-tube and the ligand (0.0595 mmol) was added. Complexation was observed by an immediate color change to dark red, brown or green (depending on the ligand). The complexes **25** were quantitatively obtained as pure compounds, as verified by NMR-spectroscopy, HRMS and IR.

12.3.2 1,5-Cyclooctadiene[(2,2'-bioxazole)]iridium(I) hexafluorophosphate, $[\text{Ir}(\text{H-box})(\text{cod})]\text{PF}_6$ (**25a**)

(6116A, 6132B, GM 1160)



The synthesis was carried out following general procedure D with H-box (**5i**) (8.4 mg). The product was obtained as dark blue-red solid.

$^1\text{H-NMR}$ (Acetone- d_6 , 400 MHz): δ = 1.75 (q, J = 8.1 Hz, 4H, cod), 2.18-2.30 (m, 4H, cod), 4.09 (t, J = 10.2 Hz, 4H, box- CH_2), 4.27-4.34 (m, 4H, cod), 5.20 (t, J = 10.0 Hz, 4H, box- CH_2) ppm.

$^{13}\text{C-NMR}$ (Acetone- d_6 , 100 MHz): δ = 31.5, 49.6, 67, 5, 76.2, 167, 9 ppm.

$^{19}\text{F-NMR}$ (Acetone- d_6 , 470 MHz): δ = -72.4 (d, $J^{19\text{F}-31\text{P}}$ = 707 Hz) ppm.

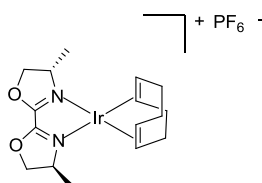
$^{31}\text{P-NMR}$ (Acetone- d_6 , 161 MHz): δ = -145.8 (sep, $J^{31\text{P}-19\text{F}}$ = 707 Hz) ppm.

IR (solid): $\tilde{\nu}$ = 2975 (w), 2946 (w), 2916 (w), 2885 (w), 2837 (w), 1727 (w), 1695 (m), 1652 (w), 1626 (w), 1609 (w), 1541 (w), 1515 (m), 1468 (w), 1431 (w), 1375 (w), 1325 (w), 1282 (m), 1248 (m), 1212 (w), 1195 (w), 1171 (w), 1157 (w), 1138 (w), 1081 (w), 1030 (w), 1011 (m), 985 (w), 970 (w), 918 (w), 901 (w), 868 (m), 826 (s), 780 (m), 740 (m), 697 (w), 668 (w) cm^{-1} .

HRMS (+ESI, 250 V): m/z (%) = 457.1190 (100) $[\text{Ir}(\text{H-box})(\text{cod})(\text{O})]^+$ (calc. 457.10977), 441.1132 (90) $[\text{Ir}(\text{H-box})(\text{cod})]^+$ (calc. 441.11485), 473.1179 (5) $[\text{Ir}(\text{H-box})(\text{cod})(\text{O}_2)]^+$ (calc. 473.1182).

12.3.3 1,5-Cyclooctadiene[(2,2'-Bis((4S, 4'S)-4,4'-dimethyl)-oxazolin)]iridium(I) hexafluorophosphate, [Ir(Me-box)(cod)]PF₆ (**25b**)

(6116B, 6146C)



The synthesis was carried out following general procedure D with Me-box (**5a**) (10.0 mg). The product was obtained as dark dark red solid.

¹H-NMR (Acetone-d₆, 400 MHz): δ = 1.35 (d, J = 6.5 Hz, 6H, box-CH₃), 2.07-2.16 (m, 4H, cod), 2.32-2.43 (m, 2H, cod), 4.43-4.53 (m, 2H, cod), 4.68-4.74 (m, 2H, box-C*H), 5.16 (t, J = 8.8 Hz, 4H, box-CH₂, box-C*H) ppm.

¹³C-NMR (Acetone-d₆, 100 MHz): δ = 19.8, 33.0, 59.6, 65.3, 65.6, 67.1, 81.3, 167.3 ppm.

¹⁹F-NMR (Acetone-d₆, 470 MHz): δ = -72.4 (d, $J^{19F-31P}$ = 707 Hz) ppm.

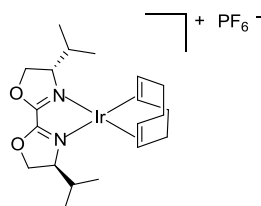
³¹P-NMR (Acetone-d₆, 161 MHz): δ = -145.8 (sep, $J^{31P-19F}$ = 707 Hz) ppm.

IR (solid): $\tilde{\nu}$ = 2976 (w), 2937 (w), 2877 (w), 2837 (w), 1694 (w), 1652 (w), 1626 (w), 1538 (w), 1508 (m), 1463 (m), 1447 (w), 1383 (w), 1373 (w), 1321 (w), 1289 (w), 1264 (m), 1249 (m), 1208 (w), 1171 (w), 1138 (w), 1075 (w), 1031 (w), 1002 (m), 965 (w), 920 (m), 875 (m), 828 (s), 77 (m), 740 (m), 667 (m) cm⁻¹.

HRMS (+ESI, 200 V): m/z (%) = 485.1509 (100) [Ir(Me-box)(cod)(O)]⁺ (calc. 485.14107), 469.1533 (48) [Ir(Me-box)(cod)]⁺ (calc. 469.14615), 501.1455 (4) [Ir(Me-box)(cod)(O₂)]⁺ (calc. 501.13598).

12.3.4 1,5-Cyclooctadiene[(2,2'-Bis((4S,4'S)-4,4'-diisopropyl)-oxazolin)]iridium(I) hexafluorophosphate, [Ir(ⁱPr-box)(cod)]PF₆ (**25c**)

(6116C, 6132A)



The synthesis was carried out following general procedure D with ⁱPr-box (**5b**) (13.3 mg). The product was obtained as dark dark red solid.

¹H-NMR (Acetone-d₆, 400 MHz): δ = 0.90 (d, J = 6.7 Hz, 6H, box-CH₃), 0.94 (d, J = 6.9 Hz, 6H, box-CH₃), 1.23-1.33 (m, 2H, cod), 1.96-2.02 (m, 2H, box-CH(CH₃)₂), 2.07-2.15 (m, 4H, cod), 2.36-2.44 (m, 2H, cod), 4.44-4.51 (m, 4H, cod), 4.64 (dq, J = 7.9, 3.5 Hz, 2H, box-CH₂), 5.01 (s, 2H, box-C*H), 5.00-5.05 (m, 4H, box-CH₂, box-CH₂) ppm.

$^{13}\text{C-NMR}$ (Acetone- d_6 , 100 MHz): $\delta = 13.4, 17.8, 33.1, 66.0, 66.7, 68.6, 74.8, 167.0$ ppm.

$^{19}\text{F-NMR}$ (Acetone- d_6 , 470 MHz): $\delta = -72.4$ (d, $J^{19\text{F}-31\text{P}} = 707$ Hz) ppm.

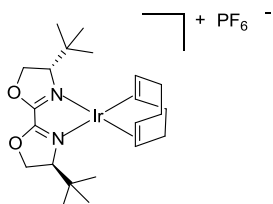
$^{31}\text{P-NMR}$ (Acetone- d_6 , 161 MHz): $\delta = -145.9$ (sep, $J^{31\text{P}-19\text{F}} = 709$ Hz) ppm.

IR (solid): $\tilde{\nu} = 2963$ (w), 2934 (w), 2875 (w), 2838 (w), 1699 (w), 1634 (w), 1559 (w), 1506 (m), 1480 (w), 1457 (w), 1395 (w), 1373 (w), 1354 (w), 1337 (w), 1295 (w), 1248 (m), 1208 (w), 1179 (w), 1135 (w), 1116 (w), 1036 (w), 1021 (w), 1004 (w), 966 (w), 922 (m), 898 (w), 873 (m), 830 (s), 775 (m), 740 (m), 666 (w).

HRMS (+ESI, 250 V): m/z (%) = 541.2075 (100) [$\text{Ir}(\text{Pr-box})(\text{cod})(\text{O})$] $^+$ (calc. 541.20367), 525.2122 (52) [$\text{Ir}(\text{Pr-box})(\text{cod})$] $^+$ (calc. 525.20875).

12.3.5 1,5-Cyclooctadiene[(2,2'-Bis((4*S*,4'*S*)-4,4'-di-*tert*-butyl)-oxazolin)]iridium(I) hexafluorophosphate, [$\text{Ir}(\text{tBu-box})(\text{cod})$] PF_6 (**25d**)

(6116D, 6142A, 6146A)



The synthesis was carried out following general procedure D with tBu-box (**5c**) (15.0 mg). The product was obtained as red-orange solid.

$^1\text{H-NMR}$ (Acetone- d_6 , 400 MHz): $\delta = 1.49$ (s, 18H, box- $\text{C}(\text{CH}_3)_3$), 1.76-1.85 (m, 4H, cod), 2.31-2.40 (m, 4H, cod), 3.64-3.74 (m, 2H, cod), 4.46-4.56 (m, 4H, cod, box- CH_2), 4.89 (t, $J = 10.0$ Hz, 2H, box- C^*H), 5.11 (dd, $J = 9.5, 6.0$ Hz, 2H, box- CH_2) ppm.

$^{13}\text{C-NMR}$ (Acetone- d_6 , 100 MHz): $\delta = 26.2, 34.5, 53.6, 58.8, 67.0, 71.6, 75.9, 157.2$ ppm.

$^{19}\text{F-NMR}$ (Acetone- d_6 , 470 MHz): $\delta = -72.4$ (d, $J^{19\text{F}-31\text{P}} = 707$ Hz) ppm.

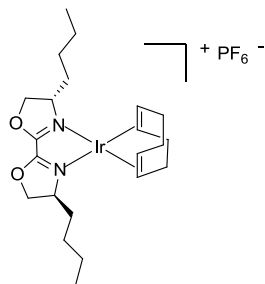
$^{31}\text{P-NMR}$ (Acetone- d_6 , 161 MHz): $\delta = -145.8$ (sep, $J^{31\text{P}-19\text{F}} = 707$ Hz) ppm.

IR (solid): $\tilde{\nu} = 2959$ (w), 2912 (w), 2877 (w), 2837 (w), 1772 (w), 1756 (w), 1726 (w), 1695 (m), 1658 (m), 1620 (m), 1562 (w), 1540 (w), 1496 (w), 1478 (m), 1452 (w), 1422 (w), 1402 (w), 1370 (w), 1321 (w), 1294 (w), 1248 (m), 1211 (w), 1192 (w), 1170 (w), 1139 (w), 1085 (w), 1045 (w), 1022 (m), 1003 (w), 984 (w), 963 (w), 929 (w), 873 (m), 829 (s), 778 (m), 739 (m), 692 (w), 662 (w) cm^{-1} .

HRMS (+ESI, 250 V): m/z (%) = 569.2434 (77) [$\text{Ir}(\text{tBu-box})(\text{cod})(\text{O})$] $^+$ (calc. 569.23497), 553.2456 (30) [$\text{Ir}(\text{tBu-box})(\text{cod})$] $^+$ (calc. 553.24005). The signal of the free ligand appears in the measured spectrum with an intensity of 100%: 275.1760 (100) [$\text{tBu-box}(\text{Na})$] $^+$ (calc. 275.17300).

12.3.6 1,5-Cyclooctadiene[(2,2'-Bis((4*S*, 4'*S*)-4,4'-dibutyl)-oxazolin)]iridium(I) hexafluorophosphate, [Ir(ⁿBu-box)(cod)]PF₆ (**25e**)

(6116E, 6146F)



The synthesis was carried out following general procedure D with ⁿBu-box (**5f**) (15.0 mg). The product was obtained as dark red solid.

¹H-NMR (Acetone-d₆, 400 MHz): δ = 0.88 (t, J = 6.7 Hz, 6H, box-CH₃), 1.27-1.42 (m, 11H, box-ⁿBu-CH₂), 1.57-1.74 (3H, box-ⁿBu-CH₂, cod), 2.07-2.16 (m, 4H, cod), 2.33-2.44 (m, 4H, cod), 4.42-4.50 (m, 4H, cod), 4.54-4.62 (m, 2H, box-C*H), 4.88 (m, 2H, box-CH₂), 5.09-5.16 (m, 2H, box-CH₂) ppm.

¹³C-NMR (Acetone-d₆, 100 MHz): δ = 13.3, 22.2, 25.9, 32.9, 33.1, 63.8, 65.5, 67.2, 79.2, 167.2 ppm.

¹⁹F-NMR (Acetone-d₆, 470 MHz): δ = -72.4 (d, $J^{19\text{F}-31\text{P}}$ = 707 Hz) ppm.

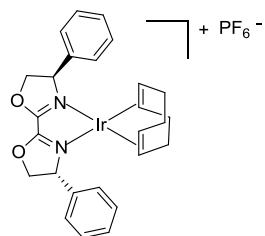
³¹P-NMR (Acetone-d₆, 161 MHz): δ = -145.8 (sep, $J^{31\text{P}-19\text{F}}$ = 707 Hz) ppm.

IR (solid): $\tilde{\nu}$ = 2956 (w), 2931 (w), 2872 (w), 2861 (w), 2838 (w), 1695 (w), 1651 (w), 1627 (w), 1507 (m), 1464 (w), 1375 (w), 1339 (w), 1325 (w), 1295 (w), 1268 (w), 1246 (m), 1222 (w), 1212 (w), 1137 (w), 1118 (w), 1086 (w), 1025 (w), 1001 (w), 987 (w), 963 (w), 935 (w), 915 (w), 896 (w), 875 (m), 829 (s), 776 (m), 739 (m), 662 (w) cm⁻¹.

HRMS (+ESI, 250 V): m/z (%) = 553.2404 (100) [Ir(ⁿBu-box)(cod)]⁺ (calc. 553.24005), 569.2324 (62) [Ir(ⁿBu-box)(cod)(O)]⁺ (calc. 569.23497), 585.2372 (4) [Ir(ⁿBu-box)(cod)(O₂)]⁺ (calc. 585.22988).

12.3.7 1,5-Cyclooctadiene[(2,2'-Bis((4*R*, 4'*R*)-4,4'-diphenyl)-oxazolin)]iridium(I) hexafluorophosphate, [Ir(Ph-box)(cod)]PF₆ (**25f**)

(6116F)



The synthesis was carried out following general procedure D with Ph-box (**5g**) (17.4 mg). The product was obtained as dark brown-red solid.

¹H-NMR (Acetone-d₆, 400 MHz): δ = 0.96-1.07 (m, 2H, cod), 1.51—61 (m, 2H, cod), 1.65-1.74 (m, 2H, cod), 2.07-2.13 (m, 2H, cod), 3.03-3.10 (m, 2H, cod), 4.18-4.23 (m, 2H, cod), 4.96 (dd, J = 9.3,

7.4 Hz, 2H, box-C*H), 5.57 (dd, $J = 11.1, 8.8$ Hz, 2H, box-CH₂), 5.66 (dd, $J = 10.7, 7.4$ Hz, 2H, box-CH₂), 7.45-7.53 (m, 10H, box-H_{ar}) ppm.

¹³C-NMR (Acetone-d₆, 100 MHz): $\delta = 32.1, 65.9, 66.7, 66.9, 82.7, 127.8, 129.3, 129.6, 138.0, 167.9$ ppm.

¹⁹F-NMR (Acetone-d₆, 470 MHz): $\delta = -72.4$ (d, $J^{19\text{F}-31\text{P}} = 707$ Hz) ppm.

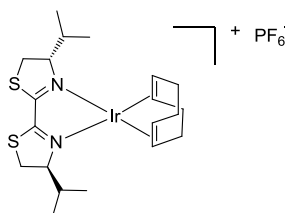
³¹P-NMR (Acetone-d₆, 161 MHz): $\delta = -145.8$ (sep, $J^{31\text{P}-19\text{F}} = 707$ Hz) ppm.

IR (solid): $\tilde{\nu} = 2961$ (w), 2939 (w), 2913 (w), 2885 (w), 2839 (w), 1695 (m), 1627 (w), 1509 (m), 1495 (m), 1455 (m), 1432 (w), 1371 (w), 1329 (w), 1399 (w), 1246 (m), 1308 (w), 1184 (w), 1159 (w), 1136 (w), 1084 (w), 1050 (w), 1028 (w), 1007 (w), 997 (m), 915 (w), 901 (w), 876 (m), 831 (s), 792 (m), 778 (m), 761 (m), 740 (m), 725 (m), 698 (m), 663 (m) cm⁻¹.

HRMS (+ESI, 150 V): m/z (%) = 609.17344 (51) [Ir(Ph-box)(cod)(O)]⁺ (calc. 609.17237), 593.1790 (24) [Ir(Ph-box)(cod)]⁺ (calc. 593.17745). The signal of the free ligand appears in the measured spectrum with an intensity of 100%: 293.1296 (100) [(Ph-box)(H)]⁺ (calc. 293.12845).

12.3.8 1,5-Cyclooctadiene[((4*S*,4'*S*)-4,4'-diisopropyl-2,2'-bithiazolin)]iridium(I) hexafluorophosphate, [Ir(ⁱPr-bta)(cod)]PF₆ (25g)

(6128D)



Synthesis was carried out following general procedure D with ⁱPr-bta (7) (9.9 mg). The product was obtained as dark brown solid.

¹H-NMR (Acetone-d₆, 400 MHz): $\delta = 0.98$ (d, $J = 7.0$ Hz, 6H, bta-ⁱPr-CH₃), 1.07 (d, $J = 7.2$ Hz, 6H, bta-ⁱPr-CH₃), 1.27-1.41 (m, 2H, bta-ⁱPr-CH), 2.07-2.13 (m, 2H, cod), 2.15-2.25 (m, 4H), 2.33-2.43 (m, 2H, cod), 3.97 (dd, $J = 3.0, 12.3$ Hz, bta-CH₂), 4.09 (dd, $J = 10.0, 12.3$ Hz, 2H, bta-CH₂), 4.35-4.42 (m, 2H, cod), 4.70 (t, $J = 6.7$ Hz, 2H, cod), 4.78 (td, $J = 3.0, 10.0$ Hz, 2H, bta-C*H) ppm.

¹³C-NMR (Acetone-d₆, 100 MHz): $\delta = 14.8, 18.5, 30.6, 32.6, 33.6, 33.9, 35.1, 66.5, 71.7, 77.0$ ppm.

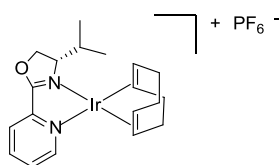
¹⁹F-NMR (Acetone-d₆, 470 MHz): $\delta = -72.4$ (d, $J^{19\text{F}-31\text{P}} = 707$ Hz) ppm.

³¹P-NMR (Acetone-d₆, 161 MHz): $\delta = -145.8$ (sep, $J^{31\text{P}-19\text{F}} = 709$ Hz) ppm.

IR (solid): $\tilde{\nu} = 3282$ (w), 2963 (w), 2934 (w), 2877 (w), 2840 (w), 1729 (w), 1694 (m), 1652 (w), 1621 (w), 1539 (w), 1506 (w), 1470 (w), 1436 (w), 1394 (w), 1374 (w), 1335 (w), 1289 (w), 1250 (m), 1189 (w), 1172 (w), 1139 (w), 1088 (w), 1029 (w), 998 (w), 961 (w), 919 (w), 875 (m), 834 (s), 777 (w), 739 (w), 696 (w), 668 (w) cm⁻¹.

12.3.9 1,5-Cyclooctadiene[(S)-4-isopropyl-2-(pyridin-yl)-oxazolin]iridium(I) hexafluorophosphate, [Ir(ⁱPr-pyrox)(cod)]PF₆ (25h)

(6120A1, 6132D, GM 1158)



The synthesis was carried out following general procedure D with ⁱPr-pyrox (**10b**) (11.3 mg). The product was obtained as dark red solid.

¹H-NMR (Acetone-d₆, 500 MHz): δ = 0.92 (d, J = 6.7 Hz, 3H, pyrox-CH₃), 1.01 (d, J = 7.0 Hz, 3H, pyrox-CH₃), 1.61-1.71 (m, 2H, cod), 2.03-2.10 (m, 2H, cod), 2.13-2.19 (m, 1H, pyrox-CH(CH₃)₂), 2.21-2.30 (m, 2H, cod), 2.36-2.47 (m, 2H, cod), 4.38-4.45 (m, 2H, cod), 4.51-4.57 (m, 2H, cod), 4.61-4.66 (m, 1H, pyrox-C*H), 5.05 (t, J = 9.7 Hz, 1H, pyrox-CH₂), 5.13 (dd, J = 6.6, 9.5 Hz, 1H, pyrox-CH₂), 8.09 (dq, J = 1.4, 5.6 Hz, 1H, pyrox-H_{ar}), 8.17 (d, J = 7.7 Hz, pyrox-H_{ar}), 8.48-8.54 (m, 2H, pyrox-H_{ar}) ppm.

¹³C-NMR (Acetone-d₆, 125 MHz): δ = 13.3, 17.6, 30.2, 32.2, 66.8, 68.2, 74.1, 126.4, 131.5, 145.8, 145.3, 142.8, 131.5, 142.8, 145.3, 150.6, 177.9 ppm.

ppm.

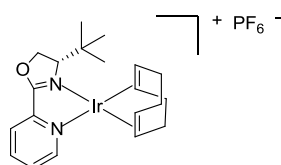
³¹P-NMR (Acetone-d₆, 161 MHz): δ = -145.8 (sep, $J^{31\text{P}-19\text{F}}$ = 707 Hz) ppm.

IR (solid): $\tilde{\nu}$ = 2962 (w), 2936 (w), 2876 (w), 2849 (w), 1700 (w), 1652 (w), 1646 (w), 1593 (w), 1569 (w), 1559 (w), 1505 (w), 1501 (w), 1479 (w), 1466 (w), 1455 (w), 1422 (m), 1394 (w), 1374 (w), 1363 (w), 1338 (w), 1314 (w), 1299 (w), 1258 (w), 1224 (w), 1202 (w), 1168 (w), 1139 (w), 1117 (w), 1094 (w), 1054 (w), 1038 (w), 1013 (w), 928 (w), 872 (w), 833 (s), 795 (m), 775 (w), 754 (w), 740 (w), 709 (w), 665 (w) cm⁻¹.

HRMS (+ESI, 250 V): m/z (%) = 507.1606 (100) [Ir(ⁱPr-pyrox)(cod)(O)]⁺ (calc. 507.16235), 491.1652 (53) [Ir(ⁱPr-pyrox)(cod)]⁺ (calc. 491.16744).

12.3.10 1,5-Cyclooctadiene[(S)-4-(tert-butyl)-2-(pyridine-2-yl)-oxazolin]iridium(I) hexafluorophosphate, [Ir(^tBu-pyrox)(cod)]PF₆ (25i)

(6120B1, 6132C, 6154, GM 1158)



The synthesis was carried out following general procedure D with ^tBu-pyrox (**10c**) (12.2 mg). The product was obtained as dark red solid.

¹H-NMR (Acetone-d₆, 500 MHz): δ = 1.05 (s, 9H, pyrox-CH₃), 1.54-1.65 (m, 2H, cod), 2.10-2.22 (m, 2H, cod), 2.39-2.50 (m, 2H, cod), 4.13-4.21 (m, 3H, cod, pyrox-C*H), 4.63 (t, J = 7.4 Hz, 2H, cod), 4.99 (dd, J = 8.6, 9.7 Hz, 1H, pyrox-CH₂), 5.41 (dd, J = 2.5, 9.8 Hz, 1H, pyrox-CH₂), 8.06-8.11 (m, 1H, pyrox-H_{ar}), 8.20-8.23 (m, 1H, pyrox-H_{ar}), 8.48-8.55 (m, 2H, pyrox-H_{ar}) ppm.

¹³C-NMR (Acetone-d₆, 125 MHz): δ = 25.0, 33.0, 34.9, 70.5, 71.4, 76.1, 126.3, 131.4, 142.6, 145.6, 150.5, 176.2 ppm.

¹⁹F-NMR (Acetone-d₆, 470 MHz): δ = -72.3 (d, $J^{19F-31P}$ = 707 Hz) ppm.

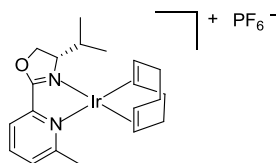
³¹P-NMR (Acetone-d₆, 161 MHz): δ = -145.8 (sep, $J^{31P-19F}$ = 707 Hz) ppm.

IR (solid): $\tilde{\nu}$ = 3098 (w), 2960 (w), 2915 (w), 2876 (w), 2848 (w), 1727 (w), 1695 (m), 1627 (w), 1586 (m), 1569 (w), 1538 (w), 1501 (w), 1479 (w), 1421 (m), 1402 (w), 1373 (w), 1340 (w), 1300 (w), 1285 (w), 1251 (m), 1213 (w), 1195 (w), 1168 (w), 1138 (w), 1123 (w), 1096 (w), 1063 (w), 1029 (w), 1015 (w), 963 (w), 926 (w), 873 (m), 831 (s), 793 (m), 755 (m), 739 (w), 708 (w), 693 (w), 664 (w) cm⁻¹.

HRMS (+ESI, 250 V): m/z (%) = 505.1862 (100) [Ir(^tBu-pyrox)(cod)]⁺ (calc. 505.18309), 521.1792 (11) [Ir(^tBu-pyrox)(cod)(O)]⁺ (calc. 521.17800).

12.3.111,5-Cyclooctadiene[*((S)-4-Isopropyl-2-(6-methylpyridin-2-yl)-oxazolin)*iridium(I) hexafluorophosphate, [Ir(ⁱPr-mepyrox)(cod)]PF₆ (**25j**)

(6120F1, 6132F)



The synthesis was carried out following general procedure D with ⁱPr-mepyrox (**19b**) (12.2 mg). The product was obtained as red solid.

¹H-NMR (Acetone-d₆, 400 MHz): δ = 0.86 (d, J = 6.7 Hz, 3H, mepyrox-ⁱPr-CH₃), 1.04 (d, J = 7.0 Hz, 3H, mepyrox-ⁱPr-CH₃), 1.46-1.54 (m, 2H, cod), 1.94-2.01 (m, 2H, cod), 2.15-2.26 (m, 3H, cod, mepyrox-ⁱPr-CH), 2.32-2.41 (2H, cod), 2.71 (s, mepyrox-CH₃), 4.31-4.36 (m, 1H, mepyrox-C*H), 4.48 (dd, J = 2.6, 7.2 Hz, 2H, cod), 4.67-4.72 (m, 2H, cod), 4.95 (mepyrox-CH₂), 5.16 (dd, J = 4.4, 9.5 Hz, 1H, mepyrox-CH₂), 7.95 (dd, J = 1.2, 8.1 Hz, 1H, mepyrox-H_{ar}), 8.01 (dd, J = 1.2, 7.7 Hz, 1H, mepyrox-H_{ar}), 8.32 (t, J = 7.9 Hz, 1H, mepyrox-H_{ar}) ppm.

¹³C-NMR (Acetone-d₆, 100 MHz): δ = 13.9, 17.9, 23.0, 31.6, 32.6, 65.4, 66.2, 68.2, 73.7, 90.7, 124.5, 133.0, 141.9, 133.0, 141.9, 145.0, 166.8, 175.4 ppm.

¹⁹F-NMR (Acetone-d₆, 470 MHz): δ = -72.4 (d, $J^{19F-31P}$ = 707 Hz) ppm.

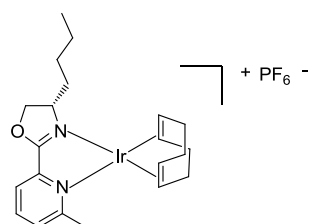
³¹P-NMR (Acetone-d₆, 161 MHz): δ = -145.8 (sep, $J^{31P-19F}$ = 709 Hz) ppm.

IR (solid): $\tilde{\nu}$ = 3089 (w), 2961 (w), 2934 (w), 2914 (w), 2876 (w), 2847 (w), 1729 (w), 1698 (m), 1648 (w), 1595 (m), 1573 (w), 1490 (w), 1462 (w), 1449 (w), 1434 (m), 1390 (w), 1377 (w), 1360 (w), 1339 (w), 1316 (w), 1297 (w), 1262 (m), 1248 (m), 1208 (w), 1191 (w), 1160 (w), 1138 (w), 1119 (w), 1101 (w), 1033 (w), 1006 (w), 951 (w), 928 (w), 876 (w), 833 (s), 807 (m), 775 (w), 749 (w), 740 (w), 687 (w), 658 (w) cm^{-1} .

HRMS (+ESI, 150 V): m/z (%) = 521.1874 (100) $[\text{Ir}(\text{Pr-mepyrox})(\text{cod})(\text{O})]^+$ (calc. 521.17800), 505.1855 (95) $[\text{Ir}(\text{Pr-mepyrox})(\text{cod})]^+$ (calc. 505.18309).

12.3.121,5-Cyclooctadiene[*((S)*-4-butyl-2-(6-methylpyridin-2-yl)-oxazolin)]iridium(I) hexafluorophosphate, $[\text{Ir}(\text{Bu-mepyrox})(\text{cod})]\text{PF}_6$ (**25k**)

(6124B, 6142C, 6146B)



The synthesis was carried out following general procedure D with Bu-mepyrox (**19f**) (12.9 mg). The product was obtained as orange-red solid.

$^1\text{H-NMR}$ (Acetone- d_6 , 400 MHz): δ = 0.93-1.00 (m, 3H, mepyrox- Bu-CH_3), 1.43-1.558 (m, 6H, mepyrox- Bu-CH_2 , cod), 1.76-1.89 (m, 4H, mepyrox- Bu-CH_2 , cod), 2.17 (s, 3H, mepyrox- CH_3), 2.26-2.44 (m, 2H, cod), 2.48-2.62 (m, 2H, cod), 4.86 (t, J = 9.3 Hz, pyrox- C^*H), 5.51 (t, J = 7.9 Hz, 1H, mepyrox- CH_2), 5.22-5.28 and 5.26 (m and dd, J = 8.8, 10.0 Hz, 3H, pyrox- CH_2 , cod), 5.35 (dt, J = 4.2, 8.3 Hz, 2H, cod), 7.66 (t, J = 6.7 Hz, 1H, mepyrox- H_{ar}), 7.89 (dd, J = 1.2, 8.1 Hz, 1H, mepyrox- H_{ar}), 8.01 (dd, J = 1.0, 7.7 Hz, 1H, mepyrox- H_{ar}), 8.27 (t, J = 7.9 Hz, 1H, mepyrox- H_{ar}) ppm.

$^{13}\text{C-NMR}$ (Acetone- d_6 , 100 MHz): δ = 8.6, 13.5, 22.2, 28.1, 35.7, 67.6, 76.9, 81.1, 87.9, 103.2, 124.6, 132.6, 133.1, 140.3, 142.9, 164.1, 173.4 ppm.

$^{19}\text{F-NMR}$ (Acetone- d_6 , 470 MHz): δ = -72.4 (d, $J^{19\text{F}-31\text{P}}$ = 707 Hz) ppm.

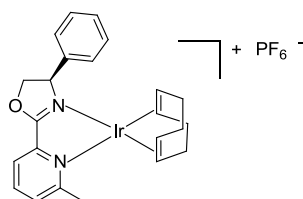
$^{31}\text{P-NMR}$ (Acetone- d_6 , 161 MHz): δ = -143.9 (sep, $J^{31\text{P}-19\text{F}}$ = 709 Hz) ppm.

IR (solid): $\tilde{\nu}$ = 3092 (w), 3041 (w), 2957 (w), 2931 (w), 2872 (w), 287 (w), 1699 (w), 1652 (w), 1645 (w), 1593 (m), 1558 (w), 1539 (w), 1506 (w), 1489 (w), 1454 (w), 1437 (m), 1393 (w), 1362 (w), 1318 (w), 1287 (w), 1266 (w), 1250 (w), 1222 (w), 1192 (w), 1156 (w), 1136 (w), 1123 (w), 1100 (w), 1034 (w), 1005 (w), 956 (w), 915 (w), 873 (m), 835 (s), 807 (m), 781 (w), 751 (w), 740 (w), 692 (w), 677 (w), 663 (w) cm^{-1} .

HRMS (+ESI, 150 V): m/z (%) = 535.1913 (100) $[\text{Ir}(\text{Bu-mepyrox})(\text{cod})(\text{O})]^+$ (calc. 535.19310).

12.3.131,5-Cyclooctadiene[*(R)*-2-(6-methylpyridin-2-yl)-4-phenyl-oxazolin]iridium(I) hexafluorophosphate, [Ir(Ph-mepyrox)(cod)]PF₆ (25l)

(6124C, 6142D, 6146E)



The synthesis was carried out following general procedure D with Ph-mepyrox (**19g**) (14.2 mg). The product was obtained as brown-red solid.

¹H-NMR (Acetone-d₆, 400 MHz): δ = 1.28-1.47 (m, 2H, cod), 1.67-1.86 (m, 2h, cod), 2.07-2.16 (m, 2H, cod), 2.71 (s, 3H, mepyrox-CH₃), 4.24-4.31 (m, 1H, cod), 4.61-4.67 (m, 1H, cod), 4.83-4.90 (m, 1H, mepyrox-C*H), 5.45-5.56 (m, 2H, cod, mepyrox-CH₂), 5.63-5.68 (m, 1H, mepyrox-CH₂), 5.69-5.77 (m, 1H, cod), 7.45-7.50 (m, 3H, mepyrox-H_{ar}), 7.51-7.56 (m, 1H, mepyrox-H_{ar}), 7.60-7.63 (m, 1H, mepyrox-H_{ar}), 7.65-7.68 (m, 1H, mepyrox-H_{ar}), 7.71-7.775 (m, 1H, mepyrox-H_{ar}), 7.92-7.96 (1H, mepyrox-H_{ar}), 7.97-8.01 (m, 1H, mepyrox-H_{ar}) ppm. The spectrum showed 5% free ligand as assigned by the mepyrox-CH₃ singlet at 2.72 ppm.

¹⁹F-NMR (Acetone-d₆, 470 MHz): δ = -72.4 (d, $J^{19F-31P}$ = 707 Hz) ppm.

³¹P-NMR (Acetone-d₆, 161 MHz): δ = -145.8 (sep, $J^{31P-19F}$ = 707 Hz) ppm.

IR (solid): $\tilde{\nu}$ = 3090 (w), 3032 (w), 2956 (w), 2916 (w), 2891 (w), 2866v, 2848 (w), 1733 (w), 1705 (m), 1684 (w), 1653 (w), 1641 (w), 1592 (m), 1558 (w), 1539 (w), 1521 (w), 1506 (w), 1487 (w), 1457 (m), 1433 (m), 1391 (w), 1362 (w), 1336 (w), 1315 (w), 1288 (w), 1275 (w), 1244 (w), 1223 (w), 1191 (w), 1159 (w), 1137 (w), 1122 (w), 1100 (w), 1084 (w), 1058 (w), 1038 (w), 1000 (w), 955 (w), 933 (w), 914 (w), 874 (w), 836 (s), 810 (m), 764 (w), 752 (w), 740 (w), 703 (m), 678 (w), 661 (w) cm⁻¹.

HRMS (+ESI, 150 V): m/z (%) = 555.1648 (100) [Ir(**Ph-box**)(cod)(O)]⁺ (calc. 555.16180).

¹H-NMR (Acetonitrile-d₃, 400 MHz): δ = 1.30-1.53 (m, 2H, cod), 2.02-2.12 (m, 2H, cod), 2.24-2.33 (m, 2H, cod), 3.09-3.17 (m, 2H, cod), 3.25 (s, 3H, py-CH₃), 5.00 (t, J = 9.5 Hz, 1H, ox-H), 5.30 (t, J = 10.0 Hz, 1H, ox-H), 5.80 (dd, J = 8.1, 10.4 Hz, 1H, ox-H), 7.40-7.51 (m, 3H, H_{ar}), 7.58-7.61 (m, 2H, H_{ar}), 7.79 (d, J = 7.9 Hz, 1H, H_{ar}), 7.86 (d, J = 7.7 Hz, 1H, H_{ar}), 8.03 (t, J = 7.2 Hz, 1H, H_{ar}) ppm.

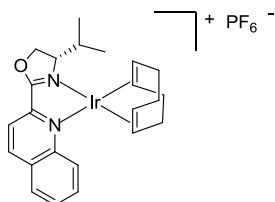
¹³C-NMR (Acetonitrile-d₃, 100 MHz): δ = 27.4, 31.7, 55.2, 56.3, 68.7, 78.2, 122.7, 128.7, 128.8, 128.9, 129.0, 139.4, 143.7, 161.8 ppm.

¹⁹F-NMR (Acetonitrile-d₃, 470 MHz): δ = -72.8 (d, $J^{19F-31P}$ = 703 Hz) ppm.

³¹P-NMR (Acetonitrile-d₃, 161 MHz): δ = -146.2 (sep, $J^{31P-19F}$ = 700 Hz) ppm.

12.3.141,5-Cyclooctadiene[*((S)*-4-isopropyl-2-(quinolin-2-yl)-oxazole)]iridium(I) hexafluorophosphate, [Ir(ⁱPr-quinox)(cod)]PF₆ (**25m**)

(6120E1, 6132E, GM 1156)



The synthesis was carried out following general procedure D with ⁱPr-quinox (**20b**) (14.3 mg). The product was obtained as dark brown solid.

¹H-NMR (Acetone-d₆, 400 MHz): δ = 0.92 (d, J = 7.0 Hz, 3H, quinox-ⁱPr-CH₃), 1.08 (d, J = 7.0 Hz, 3H, quinox-ⁱPr-CH₃), 1.16-1.20 (m, 1H, quinox-ⁱPr-CH), 1.45-1.54 (m, 2H, cod), 2.03-2.09 (m, 2H, cod), 2.18-2.28 (m, 2H, cod), 2.30-2.41 (m, 2H, cod), 4.35-4.42 (m, 3H, cod, quinox-C*H), 4.81-4.87 (m, 2H, cod), 5.03 (t, J = 9.5 Hz, 1H, quinox-CH₂), 5.23-5.28 (m, 1H, quinox-CH₂), 7.89 (d, J = 8.8 Hz, 1H, quinox-H_{ar}), 7.95 (t, J = 7.4 Hz, 1H, quinox-H_{ar}), 8.07-8.16 (m, 2H, quinox-H_{ar}), 8.22 (d, J = 8.3 Hz, 1H, quinox-H_{ar}), 8.33 (dd, J = 1.2, 8.3 Hz, 1H, quinox-H_{ar}), 9.11 (d, J = 8.3 Hz, 1H, quinox-H_{ar}) ppm.

¹³C-NMR (Acetone-d₆, 125 MHz): δ = 14.4, 18.0, 29.9, 31.3, 32.6, 65.0, 66.5, 68.6, 74.0, 120.9, 125.1, 130.1, 130.6, 132.0, 134.5, 144.5, 147.2, 148.6, 175.1 ppm.

¹⁹F-NMR (Acetone-d₆, 470 MHz): δ = -72.4 (d, $J^{19F-31P}$ = 707 Hz) ppm.

³¹P-NMR (Acetone-d₆, 161 MHz): δ = -145.9 (sep, $J^{31P-19F}$ = 709 Hz) ppm.

IR (solid): $\tilde{\nu}$ = 3070 (w), 2961 (w), 2934 (w), 2906 (w), 2874 (w), 2837 (w), 1727 (w), 1698 (w), 1642 (w), 1633 (w), 1615 (w), 1487 (w), 1474 (w), 1451 (w), 1436 (w), 1420 (w), 1394 (w), 1375 (w), 1359 (w), 1341 (w), 1296 (w), 1285 (w), 1260 (w), 1250 (w), 1219 (w), 1184 (w), 1158 (w), 1138 (w), 1123 (w), 1105 (w), 1041 (w), 973 (w), 941 (w), 875 (w), 833 (s), 812 (w), 796 (w), 775 (w), 739 (w), 117 (w), 658 (w) cm⁻¹.

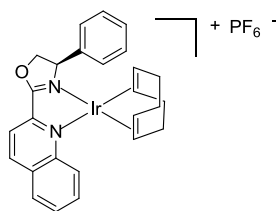
HRMS (+ESI, 250 V): m/z (%) = 591.1643 (94) [Ir(ⁱPr-quinox)(cod)(O)]⁺ (calc. 591.16235), 575.1678 (23) [Ir(ⁱPr-quinox)(cod)]⁺ (calc. 575.16744). The signal of the free ligand appears in the measured spectrum with an intensity of 100%: 297.1008 (100) [(ⁱPr-quinox)(K)]⁺ (calc. 279.08942)

¹H-NMR (CD₃CN, 400 MHz): δ = 1.04 (d, J = 6.3 Hz, 3H, quinox-CH₃), 1.16 (d, J = 6.0 Hz, 3H, quinox-CH₃), 1.46-1.62 (m, 2H, cod), 2.06 (s, 6H, cod), 2.25-2.46 (m, 2H, cod), 3.36 (dt, J = 2.6, 7.7 Hz, 2H, cod), 3.48 (dt, J = 3.3, 7.9 Hz, 2H, cod), 4.76-4.93 (m, 3H, quinox-C*H-CH₂), 7.89 (m, 2H, quinox-H_{ar}), 8.11-8.19 (m, 2H, quinox-H_{ar}), 8.69 (d, J = 8.8 Hz, 1H, quinox-H_{ar}), 9.62 (d, J = 8.3 Hz, 1H, quinox-H_{ar}).

¹³C-NMR (CD₂Cl₂, 100 MHz): δ = 15.8, 18.1, 30.1, 31.0, 31.2, 33.0, 55.8, 57.3, 70.2, 73.3, 120.6, 128.1, 128.2, 128.8, 129.6, 130.2, 130.6, 131.1, 132.3, 137.4, 140.6, 144.9, 146.8, 149.6.

12.3.151,5-Cyclooctadiene[*(R)*-4-Phenyl-2-(quinolin-2-yl)-oxazolin]iridium(I) hexafluorophosphate, [Ir(Ph-quinox)(cod)]PF₆ (25o**)**

(6120C1)



The synthesis was carried out following general procedure D with Ph-quinox (**20g**) (16.3 mg). The product was obtained as dark black-brown solid.

¹H-NMR (Acetone-d₆, 400 MHz): δ = 1.43-1.51 (m, 2H, cod), 1.84-1.92 (m, 2H, cod), 2.07-2.21 (m, 4H, cod), 4.29-4.35 (m, 2H, cod), 4.82-4.89 (m, 2H, cod), 4.99 (dd, J = 6.7, 8.6 Hz, 1H, quinox-C*H), 5.56 (t, J = 10.0 Hz, 1H, quinox-CH₂), 5.73 (dd, J = 6.7, 10.2 Hz, 1H, quinox-CH₂), 7.47-7.52 (m, 2H, quinox-H_{ar}), 7.56-7.60 (m, quinox-H_{ar}), 7.79-7.85 (m, 1H, quinox-H_{ar}), 7.99 (t, J = 7.7 Hz, 1H, quinox-H_{ar}), 8.12-8.18 (m, 1H, quinox-H_{ar}), 8.32-8.40 (m, 2H, quinox-H_{ar}), 9.18 (d, J = 8.3 Hz, 1H, quinox-H_{ar}) ppm.

¹³C-NMR (Acetone-d₆, 100 MHz): δ = 32.3, 65.5, 65.6, 67.5, 81.0, 121.7, 124.8, 127.1, 129.2, 129.4, 129.6, 130.3, 130.5, 132.4, 134.8, 139.3, 144.6, 147.2, 147.9, 148.5, 178.0 ppm.

¹⁹F-NMR (Acetone-d₆, 470 MHz): δ = -72.4 (d, $J^{19\text{F}-31\text{P}}$ = 707 Hz) ppm.

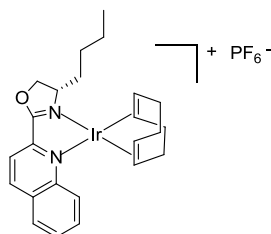
³¹P-NMR (Acetone-d₆, 161 MHz): δ = -145.8 (sep, $J^{31\text{P}-19\text{F}}$ = 709 Hz) ppm.

IR (solid): $\tilde{\nu}$ = 3063 (w), 3032 (w), 2948 (w), 2917 (w), 2892 (w), 2850 (w), 1704 (m), 1653 (w), 1629 (w), 1611 (w), 1590 (w), 1558 (w), 1538 (w), 1516 (w), 1504 (w), 1480 (m), 1467 (w), 1457 (w), 1436 (w), 1415 (m), 1467 (w), 1457 (w), 1436 (w), 1415 (m), 1386 (w), 1362 (w), 1207 (w), 1294 (w), 1283 (w), 1257 (w), 1248 (w), 1220 (m), 1180 (m), 1159 (w), 1139 (w), 1123 (m), 1087 (w), 1055 (w), 1038 (w), 1004 (w), 975 (w), 949 (w), 937 (w), 873 (m), 829 (s), 795 (m), 781 (m), 764 (s), 740 (m), 720 (m), 703 (m), 660 (w) cm⁻¹.

HRMS (+ESI, 150 V): m/z (%) = 571.1973 (100) [Ir(**Ph-quinox**)(cod)(O)]⁺ (calc. 571.19365).

12.3.161,5-Cyclooctadiene[*(S)*-4-Butyl-2-(quinolin-2-yl)-oxazolin]iridium(I) hexafluorophosphate, [Ir(ⁿBu-quinox)(cod)]PF₆ (25n**)**

(6120D1)



The synthesis was carried out following general procedure D with ⁿBu-quinox (**20f**) (15.1 mg). The product was obtained as dark yellow-brown solid.

¹H-NMR (Acetone-d₆, 400 MHz): δ = 0.93 (*t*, *J* = 7.2 Hz, 3H, quinox-CH₃), 1.38-1.59 (*m*, 6H, quinox-ⁿBu-CH₂, cod), 1.80-1.89 (*m*, 2H, cod), 1.95-2.01 (*m*, 2H, quinox-ⁿBu-CH₂), 2.20-2.30 (*m*, 2H, cod), 2.3-2.45 (*m*, 2H, cod), 4.40-4.48 (*m*, 3H, cod, quinox-C*H), 4.81-4.87 (*m*, 2H, cod), 5.11-5.15 (*m*, 2H, quinox-CH₂), 7.92 (*d*, *J* = 8.8 Hz, 1H, quinox-H_{ar}), 7.97 (*t*, *J* = 7.4 Hz, 1H, quinox-H_{ar}), 8.08-8.16 (*m*, 1H, quinox-H_{ar}), 8.23 (*d*, *J* = 8.3 Hz, 1H, quinox-H_{ar}), 8.35 (*d*, *J* = 8.3 Hz, 1H, quinox-H_{ar}), 9.12 (*d*, *J* = 8.2 Hz, 1H, quinox-H_{ar}) ppm.

¹³C-NMR (Acetone-d₆, 100 MHz): δ = 13.4, 22.5, 32.5, 34.9, 61.7, 64.7, 78.2, 78.2, 87.9, 120.7, 121.8, 125.1, 129.4, 130.5, 132.2, 134.8, 144.2, 146.8, 147.4 ppm.

¹⁹F-NMR (Acetone-d₆, 470 MHz): δ = -72.4 (*d*, *J*^{19F-31P} = 707 Hz) ppm.

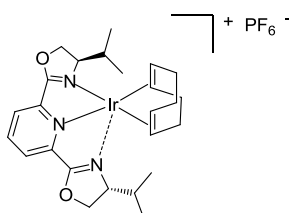
³¹P-NMR (Acetone-d₆, 161 MHz): δ = -145.9 (*sep*, *J*^{31P-19F} = 709 Hz) ppm.

IR (solid): $\tilde{\nu}$ = 3071 (*w*), 3030 (*w*), 2956 (*w*), 2932 (*w*), 2872 (*w*), 2858 (*w*), 1695 (*w*), 1684 (*w*), 1653 (*w*), 1632 (*w*), 1615 (*w*), 1590 (*w*), 1558 (*w*), 1516 (*w*), 1506 (*w*), 1485 (*m*), 1471 (*w*), 1456 (*w*), 1436 (*w*), 1422 (*m*), 1374 (*w*), 1346 (*w*), 1294 (*w*), 1261 (*m*), 1249 (*m*), 1418 (*w*), 1183 (*w*), 1157 (*w*), 1141 (*w*), 1124 (*w*), 1038 (*w*), 977 (*w*), 955 (*w*), 937 (*w*), 914 (*w*), 875 (*m*), 830 (*s*), 797 (*m*), 779 (*m*), 768 (*m*), 739 (*m*), 727 (*w*), 689 (*w*), 658 (*w*) cm⁻¹.

HRMS (+ESI, 150 V): *m/z* (%) = 557.1808 (100) [Ir(ⁿBu-quinox)(cod)(O)]⁺ (calc. 557.17800).

12.3.171,5-Cyclooctadiene[(2,6-bis(*R*)-4-*iso*-propyl-oxazolin)pyridine]iridium(I) hexafluorophosphate, [Ir(ⁱPr-pybox)(cod)]PF₆ (25p**)**

(6128A)



The synthesis was carried out following general procedure D with ⁱPr-pybox (**36**) (17.9 mg). The product was obtained as red-brown solid.

¹H-NMR (Acetone-d₆, 400 MHz): δ = No assignement of signals possible. The complex possibly exists as undefined mixture of *bis* and *tris*-coordinating ligand, which leads to too many overlapping signals.

¹⁹F-NMR (Acetone-d₆, 470 MHz): δ = -72.4 (d, $J^{19\text{F}-31\text{P}} = 707$ Hz) ppm.

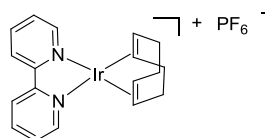
³¹P-NMR (Acetone-d₆, 161 MHz): δ = -145.8 (sep, $J^{31\text{P}-19\text{F}} = 709$ Hz) ppm.

IR (solid): $\tilde{\nu}$ = 3091 (w), 2962 (w), 2912 (w), 2876 (w), 2836 (w), 1725 (w), 1698 (m), 1658 (w), 1637 (w), 1617 (w), 1588 (w), 1569 (w), 1505 (w), 1484 (w), 1465 (w), 1448 (w), 1418 (w), 1394 (w), 1367 (w), 1333 (w), 1307 (w), 1289 (w), 1247 (m), 1210 (w), 1179 (w), 1156 (w), 1139 (w), 1117 (w), 1090 (w), 1033 (w), 967 (m), 956 (m), 907 (w), 874 (m), 830 (s), 787 (m), 775 (m), 740 (m), 667 (w) cm⁻¹.

HRMS (+ESI, 150 V): m/z (%) = 618.2401 (100) [Ir(ⁱPr-pybox)(cod)(O)]⁺ (calc.618.23022).

12.3.181,5-Cyclooctadiene[(2,2'-bipyridine)]iridium(I) hexafluorophosphate, [Ir(bpy)(cod)]PF₆ (25q)

(6136A, 6150A)



The synthesis was carried out following general procedure D with bpy (**37**) (9.3 mg). The product was obtained as dark red solid.

¹H-NMR (acetonitrile-d₃, 400 MHz): δ = 1.992.05 (m, 4H, cod), 2.36-2.44 (m, 4H, cod), 4.39-4.45 (m, 4H, cod), 7.74 (ddd, $J = 1.4, 5.8, 7.2$ Hz, 2H, bpy-H_{ar}), 8.21 (d, $J = 5.1$ Hz, 2H, bpy-H_{ar}), 8.29 (dt, $J = 1.4, 6.7$ Hz, 2H, bpy-H_{ar}), 8.34-8.38 (m, 2H, bpy-H_{ar}) ppm.

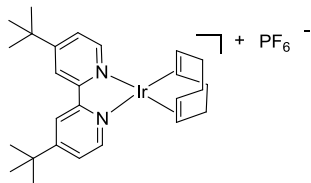
¹³C-NMR (acetonitrile-d₃, 100 MHz): δ = 29.2, 30.7, 36.1, 70.1, 121.2, 125.1, 149.1, 157.8, 167.4 ppm.

¹⁹F-NMR (acetonitrile-d₃, 470 MHz): δ = -72.8 (d, $J^{19\text{F}-31\text{P}} = 7$ Hz) ppm.

³¹P-NMR (acetonitrile-d₃, 161 MHz): δ = -145.8 (sep, $J^{31\text{P}-19\text{F}} = 702$ Hz) ppm.

12.3.191,5-Cyclooctadiene[(4,4'-di-tert-butyl-2,2'-bipyridine)]iridium(I) hexafluorophosphate, [Ir(dtbpy)(cod)]PF₆ (**25r**)

(6124D, 6136B, 6160, GM 1152)



The synthesis was carried out following general procedure D with dtbpy (**32**) (16.0 mg). The product was obtained as dark orange-brown solid.

¹H-NMR (acetonitrile-d₃, 400 MHz): δ = 1.44 (s, 18H, dtbpy-CH₃), 1.97-2.04 (m, 4H, cod), 2.34-2.41 (m, 4H, cod), 4.35-4.38 (m, 4H, cod), 7.70 (dd, J = 2.2, 6.0 Hz, 2H, dbpy-H_{ar}), 8.09 (d, J = 6.0 Hz, 2H, dtbpy-H_{ar}), 8.32 (d, J = 2.1 Hz, 2H, dtbpy-H_{ar}) ppm.

¹³C-NMR (acetonitrile-d₃, 100 MHz): δ = 29.2, 30.7, 36.1, 70.1, 121.2, 125.1, 149.1, 157.8, 167.4 ppm.

¹⁹F-NMR (acetonitrile-d₃, 470 MHz): δ = -72.3 (d, $J^{19F-31P}$ = 707 Hz) ppm.

³¹P-NMR (acetonitrile-d₃, 161 MHz): δ = -144.0 (sep, $J^{31P-19F}$ = 706 Hz) ppm.

IR (solid): $\tilde{\nu}$ = 2962 (w), 2911 (w), 2872 (w), 2834 (w), 1792 (w), 1771 (w), 1733 (w), 1700 (w), 1684 (w), 1669 (w), 1653 (w), 1646 (w), 1617 (m), 1576 (w), 1569 (w), 1558 (w), 1539 (w), 1521 (w), 1506 (w), 1485 (w), 1457 (w), 1415 (m), 1399 (w), 1367 (w), 1301 (w), 1269 (w), 1252 (w), 1220 (w), 1204 (w), 1157 (w), 1129 (w), 1077 (w), 1025 (w), 929 (w), 902 (w), 873 (m), 834 (s), 804 (w), 748 (w), 739 (w), 668 (w) cm⁻¹.

HRMS (+ESI, 150 V): m/z (%) = 585.2487 (100) [Ir(dtbpy)(cod)(O)]⁺ (calc. 585.24514), 569.2527 (30) [Ir(dtbpy)(cod)]⁺ (calc. 569.25022), 601.2476 (5) [Ir(dtbpy)(cod)(O₂)]⁺ (calc. 601.24005)

¹H-NMR (CD₂Cl₂, 500 MHz): δ = 1.46 (s, 18H, (CH₃)₃), 2.00–2.06 (m, 4H, C_{cod}HH), 2.36–2.46 (m, 4H, C_{cod}HH), 4.32–4.38 (m, 4H, C_{cod}H), 7.70 (dd, J = 1.7, 5.8 Hz, 2H, H_{ar}), 8.03 (d, J = 5.8 Hz, 2H, H_{ar}), 8.23 (d, J = 1.7 Hz, 2H, H_{ar}) ppm.

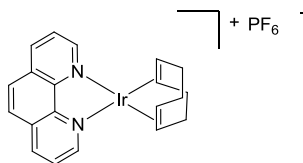
¹³C-NMR (CD₂Cl₂, 125 MHz): δ = 29.8 (CH₃), 31.0 (C_{cod}H₂), 36.3 (C(CH₃)₃), 70.7 (C_{cod}H), 120.3 (C_{ar}), 125.4 (C_{ar}), 148.5 (C_{ar}), 157.8 (C_{ar}), 167.7 (C_{ar}) ppm.

¹⁹F-NMR (CD₂Cl₂, 470 MHz): δ = -73.4 (d, $J^{19F-31P}$ = 712 Hz).

³¹P-NMR (CD₂Cl₂, 161 MHz): δ = -144.1 (sep, $J^{31P-19F}$ = 700 Hz)

12.3.201,5-Cyclooctadiene[(1,10-phenanthroline)iridium(I) hexafluorophosphate, [Ir(phen)(cod)]PF₆ (25s)

(6124E, 6136C)



The synthesis was carried out following general procedure D with phen (**38**) (10.7 mg). The product was obtained as blue-green solid.

¹H-NMR (acetonitrile-d₃, 400 MHz): δ = 2.04-2.11 (m, 4H, cod), 2.40-2.47 (m, 4H, cod), 4.61-4.67 (m, 4H, cod), 8.04 (dd, J = 5.3, 8.3 Hz, 2H, phen-Har), 8.17 (s, 2H, phen-Har), 8.62 (dd, J = 1.4, 5.1 Hz, 2H, phen-Har), 8.86 (dd, J = 1.4, 8.1 Hz, 2H, phen-Har) ppm.

¹³C-NMR (acetonitrile-d₃, 100 MHz): δ = 14.9, 30.6, 69.5, 116.4, 124.3, 135.4, 150.4 ppm.

¹⁹F-NMR (acetonitrile-d₃, 470 MHz): δ = -69.0 (d, $J^{19\text{F}-31\text{P}}$ = 712 Hz) ppm.

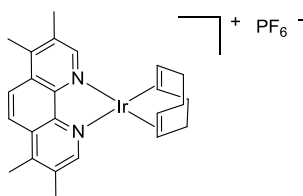
³¹P-NMR (acetonitrile-d₃, 161 MHz): δ = -143.1 (sep, $J^{31\text{P}-19\text{F}}$ = 722 Hz) ppm.

IR (solid): $\tilde{\nu}$ = 3096 (w), 2998 (w), 2943 (w), 2911 (w), 2869 (w), 2851 (w), 2840 (w), 1724 (w), 1691 (m), 1657 (w), 1633 (w), 1605 (w), 1582 (w), 1558 (w), 1544 (w), 1516 (w), 1495 (w), 1472 (w), 1430 (m), 1414 (w), 1343 (w), 1285 (w), 1251 (m), 1226 (w), 1199 (w), 1147 (w), 1110 (w), 1095 (w), 1082 (w), 1052 (w), 1036 (w), 1029 (w), 1003 (w), 984 (w), 961 (w), 926 (w), 915 (w), 876 (m), 835 (s), 777 (w), 740 (w), 722 (m), 668 (w) cm⁻¹.

HRMS (+ESI, 150 V): m/z (%) = 497.1160 (100) [Ir(phen)(cod)(O)]⁺ (calc. 497.11994), 481.1201 (15) [Ir(Ph-box)(cod)]⁺ (calc. 481.12502), 513.1123 (2) [Ir(phen)(cod)(O₂)]⁺ (calc. 513.11485).

12.3.211,5-Cyclooctadiene[(3,4,7,8-tetramethyl-1,10-phenanthroline)iridium(I) hexafluorophosphate, [Ir(TMphen)(cod)]PF₆ (25t)

(6124F, 6136D)



The synthesis was carried out following general procedure D with TMphen (**39**) (14.1 mg). The product was obtained as bright red solid.

¹H-NMR (acetonitrile-d₃, 400 MHz): δ = 2.02-2.08 (m, 4H, cod), 2.14 (s, 6H, phen-CH₃), 2.39-2.44 (m, 4H, cod), 2.56 (s, 3H, phen-CH₃), 2.79 (s, 3H, phen-CH₃), 4.58-4.63 (m, 4H, cod), 8.26-8.29 (m, 4H, phen-H_{ar}) ppm.

¹³C-NMR (acetonitrile-d₃, 100 MHz): δ = 15.1, 17.1, 30.6, 69.3, 116.5, 124.1, 135.3, 150.4 ppm.

¹⁹F-NMR (acetonitrile-d₃, 470 MHz): δ = -69.7 (d, $J^{19\text{F}-31\text{P}} = 707$ Hz) ppm.

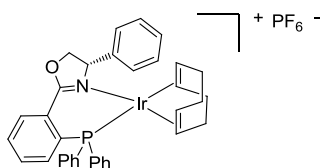
³¹P-NMR (acetonitrile-d₃, 161 MHz): δ = -144.2 (sep, $J^{31\text{P}-19\text{F}} = 702$ Hz) ppm.

IR (solid): $\tilde{\nu}$ = 2930 (w), 2871 (w), 1696 (w), 1624 (w), 1598 (w), 1578 (w), 1536 (w), 1528 (w), 1471 (w), 1446 (w), 1430 (w), 1390 (w), 1360 (w), 1334 (w), 1304 (w), 1261 (w), 1248 (w), 1221 (w), 1203 (w), 1192 (w), 1176 (w), 1138 (w), 1121 (w), 1092 (w), 1036 (w), 1022 (w), 962 (w), 950 (w), 926 (w), 871 (w), 840 (s), 811 (w), 784 (w), 773 (w), 759 (w), 740 (w), 722 (w), 694 (w), 667 (w) cm⁻¹.

HRMS (+ESI, 150 V): m/z (%) = 553.1796 (100) [Ir(TMphen)(cod)(O)]⁺ (calc. 553.18254).

12.3.221,5-Cyclooctadiene[*(S)*-2-(2-(diphenylphosphanyl)phenyl)-4-phenyl-oxazolin]iridium(I) hexafluorophosphate, [Ir(Ph-phox)(cod)]PF₆ (**25u**)

(6128B)



The synthesis was carried out following general procedure D with Ph-phox (**40**) (24.2 mg). The product was obtained as bright red solid.

¹H-NMR (Acetone-d₆, 400 MHz): δ = 1.46-1.56 (m, 1H, cod), 1.63-1.72 (m, 1H, cod), 1.76-1.84 (m, 1H, cod), 1.94-2.04 (m, 1H, cod), 2.20-2.28 (m, 2H, cod), 2.42-2.55 (m, 2H, cod), 2.99-3.06 (m, 2H, cod), 3.24-3.31 (m, 1H, cod), 4.53 (q, $J = 4.9$ Hz, 1H, phox-C*H), 5.19 and 4.22 (dd, $J = 9.3, 10.0$ Hz and quin, $J = 7.2$ Hz, 2H, phox-CH₂, cod), 5.59-5.65 (m, 1H, cod), 5.86 (dd, $J = 4.9, 10.2$ Hz, 1H, phox-CH₂), 6.91-6.95 (m, 2H, phox-H_{ar}), 7.18-7.27 (m, 4H, phox-H_{ar}), 7.36 (t, $J = 7.4$ Hz, 1H, phox-H_{ar}), 7.53-7.66 (m, 8H, phox-H_{ar}), 7.786-7.80 (m, 1H, phox-H_{ar}), 7.88 (tt, $J = 1.0, 7.2$ Hz, 1H, phox-H_{ar}), 7.94 (tt, $J = 1.4, 7.9$ Hz, 1H, phox-H_{ar}), 8.44 (dq, $J = 1.4, 4.2$ Hz, 1H, phox-H_{ar}) ppm.

¹³C-NMR (Acetone-d₆, 100 MHz): δ = 26.4, 32.1, 35.1, 62.3, 63.4, 69.6, 76.9, 94.4, 97.6, 132.3, 123.9, 126.2, 128.6, 128.8, 128.9, 129.4, 129.4, 130.0 (d, $J^{13\text{C}-31\text{P}} = 10$ Hz), 131.9, 132.6, 132.7, 133 (d, $J^{13\text{C}-31\text{P}} = 10$ Hz), 134.0, 134.5, 134.8, 135.1 (d, $J^{13\text{C}-31\text{P}} = 12$ Hz), 140.2, 165.4 ppm.

¹⁹F-NMR (Acetone-d₆, 470 MHz): δ = -72.5 (d, $J^{19\text{F}-31\text{P}} = 707$ Hz) ppm.

³¹P-NMR (Acetone-d₆, 161 MHz): δ = -145.8 (sep, $J^{31\text{P}-19\text{F}} = 709$ Hz), 16.0 (Ph-phox) ppm.

IR (solid): $\tilde{\nu}$ = 3059 (w), 3033 (w), 3005 (w), 2961 (w), 2946 (w), 2921 (w), 2885 (w), 2835 (w), 1725 (w), 1698 (m), 1594 (m), 1580 (w), 1563 (m), 1495 (w), 1482 (w), 1455 (m), 1436 (m), 1379 (m),

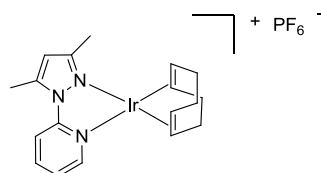
1333 (w), 1307 (w), 1280 (w), 1248 (m), 1218 (w), 1186 (w), 1145 (w), 1124 (m), 1096 (m), 1083 (w), 1065 (w), 1029 (w), 998 (w), 955 (w), 932 (w), 875 (w), 830 (s), 783 (w), 751 (m), 793 (m), 731 (m), 698 (s), 687 (m), 654 cm^{-1} .

HRMS (+ESI, 150 V): m/z (%) = 708.2033 (100) $[\text{Ir}(\text{Ph-phox})(\text{cod})]^+$ (calc. 708.20018), 724.1943 (32) $[\text{Ir}(\text{Ph-phox})(\text{cod})(\text{O})]^+$ (calc. 742.19509).

HRMS (+ESI, 150 V): m/z (%) = 573.1546 (100) $[\text{Ir}(\text{Pr-bta})(\text{cod})(\text{O})]^+$ (calc. 573.15798), 557.1621 (63) $[\text{Ir}(\text{Pr-bta cod})]^+$ (calc. 557.16307).

12.3.231,5-Cyclooctadiene[(2-(3,5-dimethyl-1H-pyrazol-1-yl)pyridine)]iridium(I) hexafluorophosphate, $[\text{Ir}(\text{pypyraz})(\text{cod})]\text{PF}_6$ (25v)

(6124A)



The synthesis was carried out following general procedure D with pyrim (**41**) (10.3 mg). The product was obtained as bright orange solid.

$^1\text{H-NMR}$ (Acetone- d_6 , 400 MHz): δ = 1.96 (q, J = 8.1 Hz, 4H, cod), 2.34-2.40 (m, 4H, cod), 2.43 (s, 3H, pypyraz- CH_3), 2.94 (s, 3H, pypyraz- CH_3), 4.63 (s, 4H, cod), 6.68 (s, 1H, pypyraz-CH), 7.68-7.72 (m, 1H, pypyraz- H_{ar}), 8.24-8.26 (m, 1H, pypyraz- H_{ar}), 8.34-8.36 (m, 1H, pypyraz- H_{ar}), 8.44-8.49 (m, 1H, pypyraz- H_{ar}) ppm.

$^{13}\text{C-NMR}$ (Acetone- d_6 , 100 MHz): δ = 12.1, 14.6, 30.9, 68.9, 113.8, 116.0, 123.8, 143.6, 146+4, 147.4, 152.0, 158.8 ppm.

$^{19}\text{F-NMR}$ (Acetone- d_6 , 470 MHz): δ = -72.5 (d, $J^{19\text{F}-31\text{P}} = 707$ Hz) ppm.

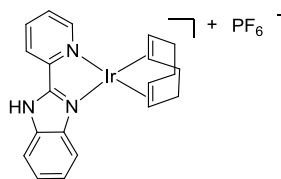
$^{31}\text{P-NMR}$ (Acetone- d_6 , 161 MHz): δ = -143.6 (sep, $J^{31\text{P}-19\text{F}} = 707$ Hz) ppm.

IR (solid): $\tilde{\nu}$ = 3151 (w), 3108 (w), 2950 (w), 2927 (w), 2892 (w), 2881 (w), 2843 (w), 1699 (w), 1609 (w), 1578 (w), 1561 (w), 1484 (m), 1476 (m), 1454 (m), 1439 (w), 1416 (w), 1388 (w), 1383 (w), 1374 (w), 1322 (w), 1305 (w), 1273 (w), 1255 (w), 1234 (w), 1221 (w), 1190 (w), 1172 (w), 1133 (w), 1106 (w), 1082 (w), 1073 (w), 1067 (w), 1040 (w), 1030 (w), 1005 (w), 1000 (w), 977 (w), 899 (w), 877 (m), 834 (s), 815 (m), 780 (w), 763 (m), 741 (w), 701 (w) cm^{-1} .

HRMS (+ESI, 300 V): m/z (%) = 474.1617 (100) $[\text{Ir}(\text{pyrim})(\text{cod})(\text{O})]^+$ (calc. 474.15157), 490.1509m (20) $[\text{Ir}(\text{pyrim})(\text{cod})]^+$ (calc. 490.14649).

12.3.241,5-Cyclooctadiene[2-(pyridine-2-yl)-1H-benzo[d]imidazole]iridium(I) hexafluorophosphate, [Ir(pybenzim)(cod)]PF₆ (**25w**)

(6136E)



The synthesis was carried out following general procedure D with (**42**) (11.6 mg). The product was obtained as solid.

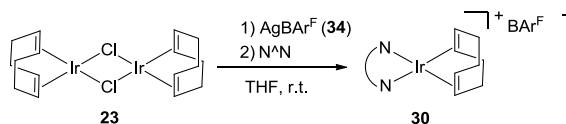
¹H-NMR (acetonitrile-d₃, 400 MHz): δ = 1.84-1.91 (m, 4H, cod), 2.28-2.41 (m, 4H, cod), 4.61-4.73 (m, 4H, cod), 7.36-7.43 (m, 3H, H_{ar}), 7.60-7.64 (m, 1H, H_{ar}), 7.69-7.74 (m, 1H, H_{ar}), 8.14-8.18 (m, 2H, H_{ar}), 8.23-8.29 (m, 1H, H_{ar}) ppm.

¹⁹F-NMR (acetonitrile-d₃, 470 MHz): δ = -72.8 (d, $J^{19F-31P}$ = 712 Hz) ppm.

³¹P-NMR (acetonitrile-d₃, 161 MHz): δ = -144.1 (sep, $J^{31P-19F}$ = 723 Hz) ppm.

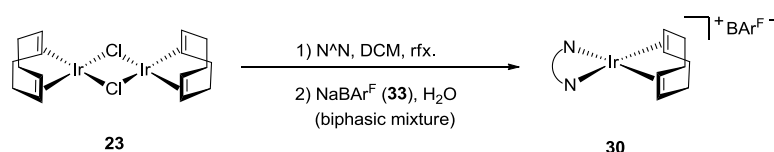
12.4 Iridium(I)-cod BAr^{F-} complexes **30**

12.4.1 General Procedure E for [Ir(N^N)(cod)]BAr^F complexes **30**



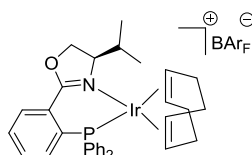
In a Schlenk tube under argon atmosphere [Ir(cod)(Cl)]₂ (**23**) (20.0 mg, 0.030 mmol) was dissolved in tetrahydrofuran (1.5 mL). Addition of AgBAr^F (57.9 mg, 0.060 mmol) caused immediately a color change from red to yellow and a colorless solid precipitated. The suspension was left without stirring for 5 hours and the solution was removed by careful decantation under argon into another Schlenk tube. The ligand (0.060 mmol) was added to the clear yellow solution. A fast color change to dark red-brown indicated successful complexation. The solution was stirred for 15 min at room temperature and the solvent was evaporated under reduced pressure to obtain complex **30** quantitatively.

12.4.2 General Procedure F for $[\text{Ir}(\text{N}^{\wedge}\text{N})(\text{cod})]\text{BAR}^{\text{F}}$ complexes **30**



In a Schlenk tube under argon atmosphere $[\text{Ir}(\text{cod})(\text{Cl})_2]$ (**23**) (50.0 mg, 0.074 mmol) was dissolved in DCM (10 mL) and the ligand (0.149 mmol) was added. The reaction mixture was stirred under reflux for 1 h – 2 h. After cooling down to room temperature, NaBAR^{F} (**33**) (198 mg, 0.223 mmol) as solution in water (10 mL) was added and the mixture stirred for 30 min. The phases were separated and the aqueous phase was extracted with DCM (2×5 mL). The combined organic phases were evaporated to dryness under high vacuum.

12.4.3 1,5-cyclooctadiene[(4S)-2-(diphenylphosphino-P)phenyl)-oxazolin]iridium(I) tetrakis-[3,5-bis(trifluoromethyl)phenyl]borate (**30a**)

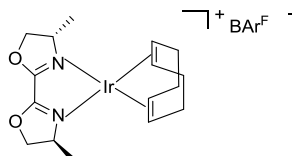


The synthesis was carried out following general procedure F (PK3100) and literature reference.^[99]

The product was purified by slow precipitation with water from an ethanolic solution (10 mL) and isolated by filtration as red crystals (94 mg, 0.061 mmol, 82%). The $^1\text{H-NMR}$ spectrum matches the one reported in literature.

$^1\text{H-NMR}$ (CDCl_3 , 400MHz): $\delta = 8.11$ (s, 1H, H_{Ar}), 7.71 (s, 8H, $\text{BCHCF}_{\text{BAR}^{\text{F}}}$), 7.65 – 7.36 (m, 14H, $\text{CFCHCF}_{\text{BAR}^{\text{F}}}$, H_{Ar}), 7.13 – 7.04 (m, 3H, H_{Ar}), 5.00 (s, 1H, OCHH), 4.91 (s, 1H, OCHH), 4.48 – 4.38 (m, 2H, $\text{C}_{\text{cod}}\text{H}$), 4.33 (t, $J = 9.4$ Hz, 1H, NCH), 4.15 – 4.05 (s, 2H, $\text{C}_{\text{cod}}\text{H}$), 2.18 - 1.90 (m, 5H, $\text{C}_{\text{cod}}\text{H}_2$), $\text{CH}(\text{CH}_3)_2$, 1.73 - 1.38 (m, 4H, $\text{C}_{\text{cod}}\text{H}_2$), 0.84 (s, 3H, $\text{C}(\text{CH}_3)_2$), 0.82 (s, 3H, $\text{C}(\text{CH}_3)_2$) ppm.

12.4.4 1,5-Cyclooctadiene[(2,2'-Bis((4S,4'S)-4,4'-methyl)-oxazolin)]iridium(I) tetrakis[3,5-bis(trifluoromethyl)phenyl]borate (**30b**)



The synthesis was carried out following general procedure F (PK 3110).

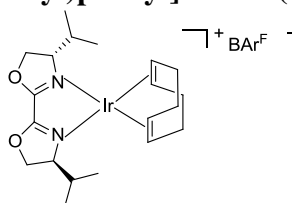
The product is a brown solid. In the proton NMR spectrum the signals for the $\text{BAr}^{\text{F}-}$ anion integrates two times too high.

$^1\text{H-NMR}$ (CD_2Cl_2 , 500MHz): $\delta = 7.76 - 7.72$ (m, $2 \times 8\text{H}$, $\text{BCHCF}_{\text{BAr}^{\text{F}}}$), 7.59 (s, $2 \times 4\text{H}$, $\text{CFCHCF}_{\text{BAr}^{\text{F}}}$), 5.00 (t, $J = 9.5$ Hz, 2H , OCHH), $4.55 - 4.46$ (m, 4H , OCHH , NCH), $4.42 - 4.34$ (m, 4H , $\text{C}_{\text{cod}}\text{H}$), $2.43 - 2.32$ (m, 2H , $\text{C}_{\text{cod}}\text{H}_2$), $2.17 - 2.07$ (m, 2H , $\text{C}_{\text{cod}}\text{H}_2$), $1.33 - 1.30$ (m, 8H , CH_3 , $\text{C}_{\text{cod}}\text{H}_2$), $1.30 - 1.26$ (m, 2H , $\text{C}_{\text{cod}}\text{H}_2$) ppm.

$^{13}\text{C-NMR}$ (CD_2Cl_2 , 126MHz): $\delta = 166.76$, 162.98 , 162.59 , 162.19 , 161.79 , 135.45 ($\text{BCHCF}_{\text{BAr}^{\text{F}}}$), 129.65 , 129.39 , 128.50 , 126.33 , 124.17 , 122.00 , 117.57 ($\text{CFCHCF}_{\text{BAr}^{\text{F}}}$), 81.08 (OCH_2), 69.55 ($\text{C}_{\text{cod}}\text{H}$), 68.54 ($\text{C}_{\text{cod}}\text{H}$), 60.98 (NCH), 33.61 ($\text{C}_{\text{cod}}\text{H}_2$), 30.33 ($\text{C}_{\text{cod}}\text{H}_2$), 29.87 ($\text{C}_{\text{cod}}\text{H}_2$), 20.86 (CH_3) ppm.

IR (solid): $\tilde{\nu} = 2922$ (m, νCH_{Ar}), 2852 (w, νCH_{Ar}), 1629 (w), 1610 (w), 1510 (w), 1464 (w), 1354 (m), 1275 (s), 1116 (s), 932 (w), 887 (m), 838 (m), 800 (m), 744 (w), 712 (m), 681 (m), 670 (m) cm^{-1} .

12.4.5 1,5-Cyclooctadiene[(2,2'-Bis((4S,4'S)-4,4'-diisopropyl)-oxazolin)]iridium(I) tetrakis[3,5-bis(trifluoromethyl)phenyl]borate (30c)



The synthesis was carried out following general procedure E (4038, 4172, 5028).

The product is a blue-red solid.

$^1\text{H-NMR}$ (CD_2Cl_2 , 400 MHz): $\delta = 0.84$ (d, $J = 7.0$ Hz, 6H , $\text{box-CH}(\text{CH}_3)_2$), 0.87 (d, $J = 7.0$ Hz, 6H , $\text{box-CH}(\text{CH}_3)_2$), $1.22-1.31$ (m, 2H , cod-CH_2), $1.88-1.95$ (m, 2H , $\text{box-CH}(\text{CH}_3)_2$), $2.03-2.16$ (m, 4H , cod-CH_2), $2.32-2.43$ (m, 2H , cod-CH_2), $4.30-4.37$ (m, 4H , cod-HC=CH , $\text{box-C}^*\text{H}$), $4.34-4.46$ (m, 2H , cod-HC=CH), 4.72 (dd, $J = 7.4$, 10.0 Hz, 2H , box-CH_2), 4.82 (t, $J = 10.4$ Hz, 2H , box-CH_2), 7.55 (s, 4H , $\text{BAr}^{\text{F}}\text{-H}_{\text{ar}}$), 7.71 (s, 8H , BAr^{F}) ppm. Using HMQC and COSY.

$^{13}\text{C-NMR}$ (CD_2Cl_2 , 100 MHz): $\delta = 13.7$ ($\text{box-CH}(\text{CH}_3)_2$), 18.3 ($\text{box-CH}(\text{CH}_3)_2$), 29.4 (cod-CH_2), 29.6 ($\text{box-CH}(\text{CH}_3)_2$), 33.1 (cod-CH_2), 68.1 (cod-C=C), 68.5 (box-C^*), 69.1 (cod-C=C), 74.6 (box-CH_2), 117.5 ($\text{BAr}^{\text{F}}\text{-C}_{\text{ar}}\text{H}$), 120.6 , 123.3 , 125.0 , 128.9 (q, $J^{\text{C-F}} = 29\text{Hz}$, $\text{BAr}^{\text{F}}\text{-CF}_3$), 134.9 ($\text{BAr}^{\text{F}}\text{-C}_{\text{ar}}\text{H}$), 161.3 (q, $J^{\text{C-11B}} = 48$ Hz, $\text{BAr}^{\text{F}}\text{-BC}_{\text{ar}}$), 165.8 (CO ppm). Using HMQC.

$^{11}\text{B-NMR}$ (CD_2Cl_2 , 128 MHz): $\delta = -7.4$.

$^{19}\text{F-NMR}$ (CD_2Cl_2 , 470 MHz): $\delta = -63.2$.

IR (solid): $\tilde{\nu} = 2972$ (w), 2936 (w), 2913 (w), 2881 (w), 2843 (w), 1644 (w), 1634 (w), 1611 (w), 1559 (w), 1512 (w), 1478 (w), 1461 (w), 1397 (w), 1375 (w), 1352 (s), 1316 (w), 1270 (s), 1248 (m),

1160 (s), 1114 (s), 1094 (s), 1059 (m), 1036 (m), 1022 (m), 1004 (m), 967 (w), 926 (m), 897 (m), 885 (m), 838 (m), 815 (w), 806 (w), 763 (w), 744 (w), 712 (s), 681 (s), 668 (s) cm^{-1} .

HRMS (+ESI, 250 V): m/z (%) = 541.2040 (100) $[\text{Ir}(\mathbf{5b})(\text{cod})(\text{O})]^+$ (calc. 541.20422), 557.1980 (15) $[\text{Ir}(\mathbf{5b})(\text{cod})(\text{O}_2)]^+$ (calc. 557,19913).

The synthesis was carried out following general procedure F (PK 3114).

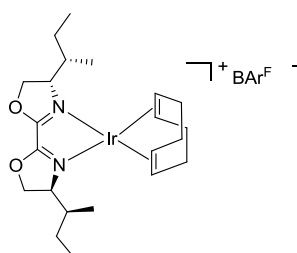
The product is a brown-black solid. In the proton NMR spectrum the signals for the $\text{BAr}^{\text{F}-}$ anion appear two times too high.

$^1\text{H-NMR}$ (CD_2Cl_2 , 500MHz): δ = 7.80 – 7.68 (m, $2 \times 8\text{H}$, $\text{BCHCF}_{\text{BArF}}$), 7.58 (s, $2 \times 4\text{H}$, $\text{CFCHCF}_{\text{BArF}}$), 4.84 (dd, $J = 10.4, 9.9$ Hz, 2H , OCHH), 4.74 (dd, $J = 9.8, 7.6$ Hz, 2H , OCHH), 4.45 (dd, $J = 13.1, 7.5$ Hz, 2H , NCH), 4.39 – 4.33 (m, 4H , C_{codH}), 2.43 – 2.34 (m, 2H , C_{codH_2}), 2.17 – 2.06 (m, 4H , C_{codH_2} , $\text{CH}(\text{CH}_3)_2$), 1.98 – 1.91 (m, 2H , C_{codH_2}), 1.39 – 1.19 (m, 2H , C_{codH_2}), 0.88 (d, $J = 7.0$ Hz, 6H , $\text{C}(\text{CH}_3)_2$), 0.86 (d, $J = 6.9$ Hz, 6H , $\text{C}(\text{CH}_3)_2$) ppm.

$^{13}\text{C-NMR}$ (CD_2Cl_2 , 126MHz): δ = 166.47, 163.01, 162.61, 162.21, 161.82, 135.48 ($\text{BCHCF}_{\text{BArF}}$), 129.67, 129.42, 126.35, 124.19, 122.02, 118.13 ($\text{CFCHCF}_{\text{BArF}}$), 75.23 (OCH_2), 69.78 (C_{codH}), 69.10 (C_{codH}), 68.78 (NCH), 33.71 (C_{codH_2}), 30.33, 30.25 (C_{codH_2} , CH), 29.97 (C_{codH_2}), 18.88 ($\text{C}(\text{CH}_3)_2$), 14.25 ($\text{C}(\text{CH}_3)_2$) ppm.

IR (solid): $\tilde{\nu}$ = 2922 (w, νCH_{Ar}), 1610 (w), 1510 (w), 1462 (w), 1354 (m), 1273 (s), 1114 (s), 927 (w), 886 (m), 838 (m), 806 (m), 744 (w), 712 (m), 681 (m), 669 (m) cm^{-1} .

12.4.6 1,5-Cyclooctadiene[(2,2'-Bis((4S, 4'S)-4,4'-di((S)-sec-butyl)-oxazolin)]iridium(I) tetrakis[3,5-bis(trifluoromethyl)phenyl]borate (**30f**)



The synthesis was carried out following general procedure E (5002, 5026A).

The product is a blue-red solid.

$^1\text{H-NMR}$ (CD_2Cl_2 , 500 MHz): δ = 0.83 (d, $J = 6.7$ Hz, 6H , $\text{box-CH}_2\text{-CH}_3$), 0.90 (t, $J = 7.2$ Hz, 6H , box-CH-CH_3), 1.13-1.23 (m, 4H , $\text{box-CH}_2\text{-CH}_3$), 1.24-1.31 (m, 2H , cod-CH_2), 1.60-1.68 (m, 2H , CH-CH_3), 2.03-2.18 (m, 4H , cod-CH_2), 2.31-2.44 (m, 2H , cod-CH_2), 4.08-4.23 (m, 2H), 4.28-4.35 (m, 2H , cod-CH), 4.40-4.47 (m, 2H , cod-CH), 4.64-4.86 (m, 4H), 7.56 (s, 4H , $\text{BAr}^{\text{F}-}\text{-H}_{\text{ar}}$), 7.72 (s, 8H , $\text{BAr}^{\text{F}-}\text{-H}_{\text{ar}}$) ppm. Using COSY and HMQC.

^{13}C -NMR (CD_2Cl_2 , 100 MHz): δ = 11.4 (box- C^* - CH_3), 11.6 (box- C^* - CH_2 - CH_3), 26.2 (cod- CH_2), 33.1 (cod- CH_2), 36.3 (box- C^* - CH_3), 68.2 (box- C^* - CH_2 -O), 68.4 (cod- $\text{C}=\text{C}$), 74.7 (box- C^* - CH_2 -O), 117.5 (BAr^{F} - $\text{C}_{\text{ar}}\text{H}$), 120.6, 123.3, 126.0, 128.9 (q, $J^{\text{C-F}}$ = 32 Hz, BAr^{F} - CF_3), 134.8 (BAr^{F} - $\text{C}_{\text{ar}}\text{H}$), 161.8 (q, $J^{\text{C-}^{11}\text{B}}$ = 53 Hz, BAr^{F} - BC_{ar}), 165.9 (CO)ppm. Using HMQC.

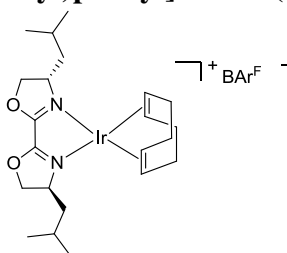
^{11}B -NMR (CD_2Cl_2 , 128 MHz): δ = -7.6ppm.

^{19}F -NMR (CD_2Cl_2 , 470 MHz): δ = -63.2ppm.

IR (solid): $\tilde{\nu}$ = 3075 (w), 2968 (w), 2935 (w), 2881 (w), 2862 (w), 1771 (w), 1675 (w), 1623 (w), 1610 (w), 1509 (m), 1476 (w), 1462 (w), 1425 (w), 1386 (w), 1353 (s), 1273 (s), 1248 (m), 1178 (m), 1159 (s), 1114 (s), 1091 (s), 1057 (m), 1028 (m), 1000 (m), 953 (s), 924 (m), 896 (m), 886 (s), 837 (s), 804 (m), 772 (m), 744 (m), 710 (s), 678 (s), 667v cm^{-1} .

HRMS (+ESI, 250 V): m/z (%) = 569.2347 (100) [$\text{Ir}(\mathbf{5d})(\text{cod})(\text{O})$] $^+$ (calc. 569.23497), 557.1980 (15) [$\text{Ir}(\mathbf{5d})(\text{cod})(\text{O}_2)$] $^+$ (calc. 585.23043), 553.2237 (3) [$\text{Ir}(\mathbf{5d})(\text{cod})$] $^+$ (calc. 553.24060).

12.4.7 1,5-Cyclooctadiene[(2,2'-Bis((4S, 4'S) -4,4'-diisobutyl)-oxazolin)]iridium(I) tetrakis[3,5-bis(trifluoromethyl)phenyl]borate (30g)



The synthesis was carried out following general procedure E (5004, 5026B, 5052A).

The product is a blue-red solid.

^1H -NMR (CD_2Cl_2 , 400 MHz): δ = 0.89 (d, J = 6.3 Hz, 4H, box- CH_3), 0.93 (d, J = 6.5 Hz, 4H, box- CH_3), 1.25-1.35 (m, 2H, cod- CH_2), 1.40-1.57 (m, 6H, box- CH_2 - $\text{CH}(\text{CH}_3)_2$), 2.08-2.17 (m, 2H, cod- CH_2), 4.21-4.29 (m, 2H, box- C^*H), 4.33 (t, J = 7.0 Hz, 2H, cod- $\text{HC}=\text{CH}$), 4.47 (q, J = 6.7 Hz, 2H, cod- $\text{HC}=\text{CH}$), 4.63 (dd, J = 7.0, 9.5 Hz, box- CH_2 -O), 4.93 (t, J = 9.1 Hz, box- CH_2 -O), 7.56 (s, 4H, BAr^{F} , H_{ar}), 7.72 (s, 8H, BAr^{F} - H_{ar})ppm. Using COSY and HMQC.

^{13}C -NMR (CD_2Cl_2 , 100 MHz): δ = 20.7 (box- CH_3), 23.2 (box- CH_3), 25.2 (box- CH_2 - $\text{CH}(\text{CH}_3)_2$), 29.6 (cod- CH_2), 33.2 (cod- CH_2), 43.1 (box- CH_2 - $\text{CH}(\text{CH}_3)_2$), 63.4 (box- C^*), 67.8 (cod- $\text{C}=\text{C}$), 69.0 (cod- $\text{C}=\text{C}$), 79.7 (box- CH_2 -O), 177.4 (BAr^{F} - C_{ar}), 120.6, 123.3, 125.9, 128.9 (q, $J^{\text{C-F}}$ = 3 Hz, BAr^{F} - CF_3), 134.8 (BAr^{F} - C_{ar}), 134.8 (BAr^{F} - $\text{C}_{\text{ar}}\text{H}$), 161.8 (q $J^{\text{C-}^{11}\text{B}}$ = 49 Hz, BAr^{F} - BC_{ar}), 166.1 (CO)ppm. Using HMQC.

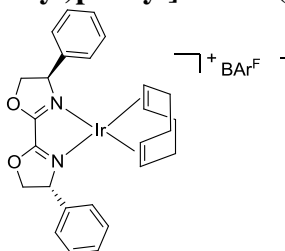
^{11}B -NMR (CD_2Cl_2 , 128 MHz): δ = -7.4ppm.

^{19}F -NMR (CD_2Cl_2 , 470 MHz): δ = -62.5ppm.

IR (solid): $\tilde{\nu}$ = 2963, 2935 (w), 2904 (w), 2876 (w), 2855 (w), 1610 (w), 1558 (w), 1507 (m), 1467 (w), 1428 (w), 1418 (w), 1391 (w), 1352 (s), 1319 (w), 1272 (s), 1159 (s), 1113 (s), 1094 (s), 1030 (m), 987 (m), 931 (m), 885 (s), 837 (s), 804 (m), 744 (m), 711 (s), 680 (s), 669 (s) cm^{-1} .

HRMS (+ESI, 250 V): m/z (%) = 569.2349 (100) $[\text{Ir}(\mathbf{5e})(\text{cod})(\text{O})]^+$ (calc.569.23497), 585.2300 (14) $[\text{Ir}(\mathbf{5e})(\text{cod})(\text{O}_2)]^+$ (calc.569.585.23043).

12.4.8 1,5-Cyclooctadiene[(2,2'-Bis((4*R*, 4'*R*)-4,4'-diphenyl)-oxazolin)]iridium(I) tetrakis[3,5-bis(trifluoromethyl)phenyl]borate (**30h**)



The synthesis was carried out following general procedure E (5006, 5026C).

The product is a blue-red solid.

¹H-NMR (CD_2Cl_2 , 500 MHz): δ = 1.00-1.08 (m, 2H, cod- CH_2), 1.58-1.67 (m, 2H, cod- CH_2), 1.73-1.80 (m, 2H, cod- CH_2), 2.05-2.14 (m, 2H, cod- CH_2), 3.12 (q, J = 6.8 Hz, 2H, cod- $\text{HC}=\text{CH}$), 4.13 (dt, J = 2.4, 6.8 Hz, 2H, cod- $\text{HC}=\text{CH}$), 4.85 (dd, J = 8.2, 9.2 Hz, 2H, box- CH_2), 5.28-5.32 (m, 2H, box- C^*-H), 5.37 (dd, J = 10.9, 9.2 Hz, box- CH_2), 7.25-7.28 (m, 6H, box- H_{ar}), 7.43-7.49 (m, 6H, box- H_{ar}), 7.59 (s, 4H, $\text{BARF}^{\text{F}}-\text{H}_{\text{ar}}$), 7.75 (s, 8H, $\text{BARF}^{\text{F}}-\text{H}_{\text{ar}}$)ppm. Using COSY and HMQC.

¹³C-NMR (CD_2Cl_2 , 100 MHz): δ = 29, 9 (cod- CH_2), 37.3 (cod- CH_2), 67.6 (box- C^*), 68.8 (cod- $\text{C}=\text{C}$), 69.2 (box- CH_2), 117.6 ($\text{BARF}^{\text{F}}-\text{C}_{\text{ar}}\text{H}$), 120.6, 123.3, 126.0, 127.1 (box- $\text{C}_{\text{ar}}\text{H}$), 128.8 (q, $J^{\text{C-F}}$ = 30 Hz, $\text{BARF}^{\text{F}}-\text{CF}_3$), 129.9 (box- $\text{C}_{\text{ar}}\text{H}$), 130.4 (box- $\text{C}_{\text{ar}}-\text{H}$), 134.9 ($\text{BARF}^{\text{F}}-\text{C}_{\text{ar}}\text{H}$), 135.7, 161.8 (q, $J^{\text{C-11B}}$ = 48 Hz, $\text{BARF}^{\text{F}}-\text{BC}_{\text{ar}}$), 166.3 (CO)ppm. Using HMQC.

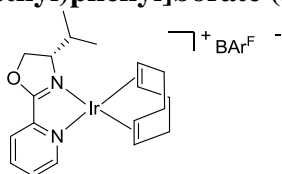
¹¹B-NMR (CD_2Cl_2 , 128 MHz): δ = -7.8 ppm.

¹⁹F-NMR (CD_2Cl_2 , 470 MHz): δ = -62.7ppm.

IR (solid): $\tilde{\nu}$ = 3071 (w), 3039 (w), 2963 (w), 2911 (w), 2878 (w), 1610 (m), 1558 (m), 1507 (m), 1471 (m), 1457 (m), 1417 (w), 1352 (s), 1215 (w), 1271 (s), 1241 (s), 1160 (s), 1115 (s), 1090 (s), 1030 (m), 996 (m), 924 (m), 885 (m), 837 (s), 803 (m), 758 (m), 744 (m), 711 (s), 699 (s), 680 (s), 669 (s) cm^{-1} .

HRMS (+ESI, 250 V): m/z (%) = 609.1719 (100) $[\text{Ir}(\mathbf{5g})(\text{cod})(\text{O})]^+$ (calc. 609.17292), 625.1673 (5) $[\text{Ir}(\mathbf{5g})(\text{cod})(\text{O}_2)]^+$ (calc. 625.16783), 593.1723 (3) $[\text{Ir}(\mathbf{5g})(\text{cod})]^+$ (calc. 593.17800)

12.4.9 1,5-Cyclooctadiene[*(S)*-4-Isopropyl-2-(pyridine-2-yl)-oxazolin]iridium(I) tetrakis[3,5-bis(trifluoromethyl)phenyl]borate (30i)



The synthesis was carried out following general procedure E (5026D, 5052B).

The product is a brown-red solid.

¹H-NMR (CD₂Cl₂, 400 MHz): δ = 0.84 (d, J = 7.0 Hz, 3H, pyrox-CH₃), 0.92 (d, J = 7.0 Hz, 3H, pyrox-CH₃), 1.53-1.72 (m, 2H, cod-CH₂), 2.03-2.08 (m, 1H, pyrox-CH(CH₃)₂), 2.09-2.22 (m, 4H, cod-CH₂), 2.25-2.47 (m, 4H, cod-CH₂), 4.05-4.24 (m, 2H, cod-CH), 4.27-4.32 (m, 1H, pyrox-C*H), 4.52-4.59 (m, 2H, cod-CH), 4.74-4.83 (m, 2H, pyrox-CH₂), 7.55 (s, 4H, BAr^F-H_{ar}), 7.72 (s, 8H, BAr^F-H_{ar}), 7.76 (ddd, J = 1.4, 5.3, 7.9 Hz, 1H, pyrox-H_{ar}), 7.85 (d, J = 7.9 Hz, 1H, pyrox-H_{ar}), 8.08 (d, J = 5.3 Hz, 1H, pyrox-H_{ar}), 8.15 (dt, J = 1.6, 7.9 Hz, 1H, pyrox-H_{ar}) ppm. Using COSY and HMQC.

¹³C-NMR (CD₂Cl₂, 100 MHz): δ = 13.7 (pyrox-CH₃), 18.4 (pyrox-CH₃), 30.0 (pyrox-CH(CH₃)₂), 31.1 (cod-CH₂), 31.5 (cod-CH₂), 67.3 (cod-CH), 68.4 (pyrox-C*), 68.7 (cod-CH), 69.4, 72.9, 73.4 (pyrox-CH₂), 117.6 (BAr^F-C_{ar}H), 120.4, 123.3, 126.0, 126.4, 127.9, 128.9 (q, J^{C-11B} = 30 Hz, BAr^F-CF₃), 131.2 (pyrox-C_{ar}H), 134.8 (BAr^F-C_{ar}H), 142.1 (pyrox-C_{ar}H), 145.1, 149.5 (pyrox-C_{ar}H), 161.8 (q, J^{C-F} = 50 Hz, BAr^F-B-C_{ar}) ppm. Using HMQC.

¹¹B-NMR (CD₂Cl₂, 128 MHz): δ = -7.3 ppm.

¹⁹F-NMR (CD₂Cl₂, 470 MHz): δ = -62.5 ppm.

IR (solid): $\tilde{\nu}$ = 2958 (w), 2938 (w), 2925 (w), 2880 (w), 2854 (w), 1772 (w), 1750 (w), 1732 (w), 1716 (w), 1698 (w), 1683 (w), 1669 (w), 1651 (w), 1644 (w), 1636 (w), 1609 (w), 1592 (m), 1574 (w), 1569 (w), 1558 (w), 1540 (w), 1532 (w), 1520 (w), 1506 (w), 1499 (w), 1488 (w), 1471 (w), 1456 (w), 1449 (w), 1422 (m), 1396 (w), 1352 (s), 1319 (w), 1272 (s), 1272 (s), 1161 (s), 1113 (s), 1092 (s), 1035 (m), 1012 (m), 993 (m), 942 (m), 928 (m), 898 (m), 885 (s), 861 (m), 837 (s), 807 (m), 797 (m), 753 (m), 744 (m), 711 (s), 693 (m), 680 (s), 669 (s) cm⁻¹.

HRMS (+ESI, 250 V): m/z (%) = 507.1651 (100) [Ir(**10b**)(cod)(O)]⁺ (calc. 507.16235), 523.1550 (5) [Ir(**10b**)(cod)(O₂)]⁺ (calc. 523.15727)

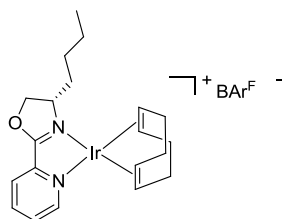
The synthesis was carried out following general procedure F (PK 3126).

The product is a black solid. In the proton NMR spectrum the signals for the BAr^F- anion integrates two times too high.

¹H-NMR (CD₂Cl₂, 500MHz): δ = 8.15 (td, J = 7.8, 1.5 Hz, 1H, H_{Ar}), 8.12 – 8.09 (m, 1H, H_{Ar}), 7.86 (ddd, J = 7.7, 1.4, 0.7 Hz, 1H, H_{Ar}), 7.81 – 7.77 (m, 1H, H_{Ar}), 7.78 – 7.73 (m, 2 × 8H, BCHCF_{BArF}), 7.58 (s, 2 × 4H, CFCHCF_{BArF}), 4.81 (ddd, J = 22.7, 14.5, 8.2 Hz, 2H, OCH₂), 4.64 – 4.53 (m, 2H, C_{cod}H), 4.32 (ddd, J = 10.2, 6.7, 3.7 Hz, 1H, NCH), 4.23 (t, J = 6.1 Hz, 1H, C_{cod}H), 4.09 (dd, J = 11.7,

7.4 Hz, 1H, C_{cod}H), 2.49 – 2.28 (m, 4H, C_{cod}H₂), 2.22 – 2.01 (m, 5H, C_{cod}H₂, CH(CH₃)₂), 0.94 (d, *J* = 7.0 Hz, 3H, C(CH₃)₂), 0.86 (d, *J* = 6.9 Hz, 3HC(CH₃)₂) ppm. ¹³C-NMR (CD₂Cl₂, 126MHz): δ = 177.53, 163.04, 162.65, 162.24, 161.85, 150.04 (C_{Ar}), 145.92, 142.63 (C_{Ar}), 135.49 (BCHCF_{BARF}), 131.71, 129.72, 129.47, 128.52, 126.99, 126.36 (C_{Ar}), 124.19, 122.02, 118.15 (CFCHCF_{BARF}), 74.06 (OCH₂), 73.52, 70.10, 69.33, 69.01 (NCH), 67.96, 33.60, 32.10, 31.82, 30.65, 30.36, 29.81, 18.91 (C(CH₃)₂), 14.21 (C(CH₃)₂) ppm.

12.4.101,5-Cyclooctadiene[*((S)*-4-Butyl-2-(pyridine-2-yl)-oxazolin)]iridium(I) tetrakis[3,5-bis(trifluoromethyl)phenyl]borate (30j)



The synthesis was carried out following general procedure E (5010, 5026E, 5052C).

The product is a brown-red solid.

¹H-NMR (tetrahydrofuran-d₈, 400 MHz): δ = 0.93-1.14 (m, 5H, pyrox-nBu-CH₃, cod-CH₂), 1.27-1.44 (m, 1H, pyrox-ⁿBu-CH₂), 1.67-1.73 (m, 2H, cod-CH₂), 1.80-1.85 (m, 2H, cod), 1.91-1.99 (m, 2H, pyrox-ⁿBu-CH₂), 2.03-2.12 (m, 1H, pyrox-ⁿBu-CH₂), 2.03-2.12 (m, 1H, pyrox-ⁿBu-CH₂), 2.19-2.40 (m, 4H, pyrox-ⁿBu-CH₂, cod-CH₂), 3.71-3.79 (m, 2H, pyrox-C*-CH₂-O), 3.99-4.05 (m, 1H, pyrox-C*H), 7.59 (s, 4H, BARF^F-H_{ar}), 7.80 (s, 8H, BARF^F-H_{ar}), 7.90-7.797 (m, 1H, pyrox-H_{ar}), 8.29-8.43 (m, 1H, pyrox-H_{ar}), 8.29-8.43 (m, 2H, pyrox-H_{ar}), 8.49-8.55 (m, 1H, pyrox-H_{ar}). Using COSY.

¹³C-NMR (CD₂Cl₂, 100 MHz): δ = 18.2 (pyrox-ⁿBu), 19.5 (pyrox-ⁿBu), 25.6 (cod), 26.6 (cod), 29.4 (pyrox), 57.8 (pyrox), 64.2 (pyrox), 67.0 (cod), 70.6 (cod), 117.5 (BARF^F), 120.5 (pyrox), 122.1, 123.3, 126.0 (pyrox), 126.7, 128.9 (q, *J*^{C-11B} = 28 Hz, BARF^F-B-C_{ar}), 134.9 (BARF^F), 137.7 (pyrox), 148.4 (pyrox), 161.7 (q, *J*^{C-F} = 46 Hz, 165.6) ppm. Using HMQC.

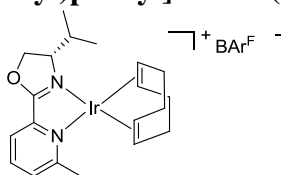
¹¹B-NMR (CD₂Cl₂, 128 MHz): δ = -7.4 ppm.

¹⁹F-NMR (CD₂Cl₂, 470 MHz): δ = -62.5 ppm.

IR (solid): $\tilde{\nu}$ = 2963 (w), 2938 (w), 2908 (w), 2878 (w), 2862 (w), 1650 (w), 1609 (m), 1597 (m), 1569 (w), 1500 (w), 1467 (w), 1450 (w), 1418 (m), 1352 (s), 1315 (w), 1271 (s), 1184 (m), 1158 (s), 1110 (s), 1092 (s), 1033 (m), 1000 (m), 948 (m), 390 (m), 885 (s), 837 (s), 814 (m), 792 (m), 754 (m), 744 (m), 711 (s), 680 (s), 669 (s) cm⁻¹.

HRMS (+ESI, 250 V): *m/z* (%) = 521.1768 (100) [Ir(**10f**)(cod)(O)]⁺ (calc. 521.17800), 537.1714 (43) [Ir(**10f**)(cod)(O₂)]⁺ (calc. 537.17292), 505.1814 (36) [Ir(**10f**)(cod)]⁺ (calc. 505.18309)

12.4.111,5-Cyclooctadiene[*((S)*-4-Isopropyl-2-(6-methylpyridin-2-yl)-oxazolin)]iridium(I) tetrakis[3,5-bis(trifluoromethyl)phenyl]borate (30e)



The synthesis was carried out following general procedure E (4192, 5026F, 5022D).

The product is a blue-red solid.

¹H-NMR (tetrahydrofurane-d₈, 500 MHz): δ = 1.00-1.04 (m, 3H, mepyrox ⁱPr-CH₃), 1-10-1.15 (m, 3H, mepyrox ⁱPr-CH₃), 1.44-1.51 (m, 2H, cod), 1.63-1.70 (m, 2H, cod), 2.21-2.40 (m, 4H, cod), 3.18 (s, 3H, mepyrox-CH₃), 3.53-3.63 (m, 4H, cod), 4.59-4.89 (m, 3H, mepyrox), 7.59 (s, 4H, BARF^F), 7.80 (s, 8H, BARF^F), 7.83-8.06 (m, 3H, mepyrox-H_{ar}) ppm. Using COSY.

¹³C-NMR (CD₂Cl₂, 100 MHz): δ = 18.3, 25.4, 26.3, 30.5, 32.2, 64.7, 66.5, 67.8, 70.4, 117.5 (BARF^F), 120.6 (mepyrox), 123.2 (mepyrox), 126.0 (mepyrox), 128.8 (q, J^{C-11B} = 30 Hz, BARF^F), 134.8 (BARF^F), 144.6, 161.8 (q, J^{C-F} = 48 Hz, BARF^F) ppm.

¹¹B-NMR (CD₂Cl₂, 128 MHz): δ = -7.6 ppm.

¹⁹F-NMR (CD₂Cl₂, 470 MHz): δ = -63.2 ppm.

IR (solid): $\tilde{\nu}$ = 3019 (w), 2964 (w), 2936 (w), 224 (w), 2880 (w), 2856 (w), 1699 (w), 1681 (w), 1648 (w), 1607, 1595, 1595, 1572 (w), 1558 (w), 1490 (w), 1461 (w), 1451 (w), 1436 (m), 1390 (w), 1377 (w), 1352 (s), 1315 (w), 1271 (s), 1183 (m), 1159 (w), 1110 (w), 1095 (w), 1039 (m), 1006 (m), 949 (m), 936 (m), 885 (s), 868 (m), 837 (m), 808 (m), 764 (m), 745 (m), 711 (s), 680 (s), 669 (s) cm⁻¹.

HRMS (+ESI, 250 V): m/z (%) = 521.1777(100) [Ir(**19b**)(cod)(O)]⁺ (calc. 521.17800), 537.1719 (60) [Ir(**19b**)(cod)(O)]⁺ (calc. 537.17292).

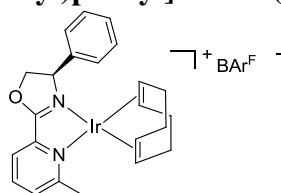
The synthesis was carried out following general procedure F (PK 3092).

The product is a red-brown solid. In the proton NMR spectrum the signals for the BARF^{F-} anion integrates two times too high.

¹H-NMR (CD₂Cl₂, 400MHz): δ = 7.94 (t, J = 7.8 Hz, 1H, H_{Ar}), 7.73 (s, 2 × 8H, BCHCF_{BARF}, H_{Ar}), 7.62 (dd, J = 8.0, 1.2 Hz, 1H, H_{Ar}), 7.56 (s, 2 × 4H, CFCHCF_{BARF}), 4.80 (dd, J = 9.5, 5.6 Hz, 1H, OCHH), 4.71 (t, J = 9.5 Hz, 1H, OCHH), 4.22 – 4.14 (m, 3H, NCH, C_{cod}H), 4.06 (td, J = 7.4, 2.5 Hz, 2H, C_{cod}H), 2.79 (s, 3H, CH₃), 2.39 – 2.30 (m, 2H, C_{cod}H₂), 2.28 – 2.17 (m, 3H, C_{cod}H₂, CH(CH₃)₂), 1.88 (ddd, J = 14.8, 7.4, 3.2 Hz, 2H, C_{cod}H₂), 1.47 (ddd, J = 13.2, 7.8, 4.1 Hz, 2H, C_{cod}H₂), 1.02 (d, J = 7.0 Hz, 3H, C(CH₃)₂), 0.86 (d, J = 6.8 Hz, 3H, C(CH₃)₂) ppm.

IR (solid): $\tilde{\nu}$ = 2962 (w, ν CH_{Ar}), 1651 (w), 1607 (w), 1491 (w), 1437 (w), 1391 (w), 1352 (m), 1273 (s), 1260 (s), 1092 (s), 1015 (s), 937 (w), 885 (m), 838 (m), 795 (s), 745 (w), 712 (m), 682 (m), 669 (m) cm⁻¹.

12.4.121,5-Cyclooctadiene[*(R)*-4-phenyl-2-(6-Methylpyridin-2-yl)-oxazolin]iridium(I) tetrakis[3,5-bis(trifluoromethyl)phenyl]borate (30k)



The synthesis was carried out following general procedure E (5026G).

The product is a red-orange solid.

¹H-NMR (CD₂Cl₂, 400 MHz): δ = 1.34-1.42 (m, 2H, cod-CH₂), 1.75-1.80 (m, 2H, cod-CH₂), 2.03-2.19 (m, 4H, cod-CH₂), 2.64 (s, 3H, pyrox-CH₃), 4.09-4.15 (m, 2H, cod-CH=CH), 4.32-4.37 (m, 2H, cod-CH=CH), 4.78 (dd, J = 6.7, 9.0 Hz, 1H, pyrox-CH₂), 5.17 (dd, J = 9.3, 10.2 Hz, 1H, pyrox-CH₂), 5.27-5.30 (m, 1H, C*-H), 7.25-7.28 (m, 2H, pyrox-Ph-H), 7.43-7.47 (m, 3H, pyrox-Ph-H), 7.57 (s, 4H, BAr^F), 7.64 (dd, J = 1.4, 1.8 Hz, 1H, pyrox-H_{ar}), 7.74 (s, 8H, BAr^F), 7.84 (dd, J = 1.4, 7.7 Hz, 1H, pyrox-H_{ar}), 8.00 (t, J = 7.9 Hz, 1H, pyrox-H_{ar}) ppm. Using HMQC and COSY.

¹³C-NMR (CD₂Cl₂, 100 MHz): δ = 24.1 (pyrox-CH₃), 30.2 (cod-CH₂), 32.5 (cod-CH₂), 65.9 (pyrox-C*), 66.8 (cod-C=C), 67.4 (cod-C=C), 80.1 (pyrox-CH₂), 117.6 (BAr^F-C_{ar}-H), 120.5, 123.3 (pyrox-C_{ar}-H), 124.5, 126.0, 126.4, 128.9 (q, J^{C-F} = 31Hz, BAr^F-CF₃), 129.7 (pyrox-C_{ar}-H), 133.4 (pyrox-C_{ar}-H), 134.8 (BAr^F-C_{ar}-H), 161.8 (q, J^{C-11B} = 50Hz, BAr^F-C_{ar}), 166.0, 176.6 ppm. Using HMQC.

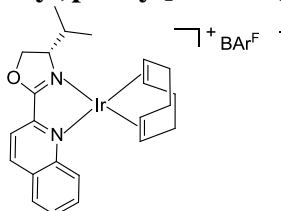
¹¹B-NMR (CD₂Cl₂, 128 MHz): δ = -7.6 ppm.

¹⁹F-NMR (CD₂Cl₂, 470 MHz): δ = -62.7 ppm.

IR (solid): $\tilde{\nu}$ = 3039 (w), 2962 (m), 2938 (w), 2905 (w), 2876 (w), 1641 (w), 1609 (w), 1592 (m), 1571 (w), 1496 (w), 1486 (w), 1458 (w), 1447 (w), 1434 (w), 1412 (w), 1392 (w), 1352 (s), 1314 (w), 1270 (s), 1259 (s), 1184 (m), 1159 (m), 1107 (s), 1092 (s), 1015 (s), 954 (m), 933 (m), 896 (m), 885 (m), 864 (m), 837 (m), 795 (s), 761 (m), 745 (m), 711 (s), 700 (m), 680 (s), 668 (s) cm⁻¹.

HRMS (+ESI, 200 V): m/z (%) = 555.1665 (100) [Ir(**19h**)(cod)(O)]⁺ (calc. 555.16235).

12.4.131,5-Cyclooctadiene[*(S)*-4-Isopropyl-2-(quinolin-2-yl)-oxazolin]iridium(I) tetrakis[3,5-bis(trifluoromethyl)phenyl]borate (30d)



The synthesis was carried out following general procedure E (4040, 4174, 4194, 5030).

The product is a red-orange solid.

¹H-NMR (tetrahydrofuran-*d*₈, 500 MHz): δ = . 1.11 (d, *J* = 6.8 Hz, 3H, quinox-CH₃), 1.22 (d, *J* = 7.2 Hz, 3H, quinox-CH₃), 1.57-1.68 (m, 4H, cod-CH₂), 2.29-2.36 (m, 2H, cod-CH₂), 2.41-2.50 (m, 2H, cod-CH₂), 2.57-2.62 (m, 1H, quinox-CH(CH₃)₂), 3.56-3.65 (m, 4H, cod-CH), 4.80- 4.86 (m, 1H, quinox-C*H), 4.88-5.02 (m, 2H, quinox-CH₂), 7.60 (s, 4H, BAr^F-H_{ar}), 7.80 (s, 8H, BAr^F-H_{ar}), 7.94 (t, *J* = 7.2 Hz, 1H, quinox-H_{ar}), 8.10 (d, *J* = 8.5 Hz, 1H, quinox-H_{ar}), 8.16-8.23 (m, 2H, quinox-H_{ar}), 8.80 (d, *J* = 9.2 Hz, 1H, quinox-H_{ar}), 9.53 (d, *J* = 8.9 Hz, 1H, quinox-H_{ar}). Using COSY and HMQC.

¹³C-NMR (tetrahydrofuran-*d*₈, 500 MHz): δ = 15.5 (quinox-CH₃), 18.0 (quinox-CH₃), 31.3 (cod-CH₂), 31.5 (quinox-CH(CH₃)₂), 32.5 (cod-CH₂), 57.2 (cod-CH), 58.7 (cod-CH), 69.9 (quinox-C*), 73.3 (quinox-CH₂), 117.0 (BAr^F-C_{ar}H), 120.5 (quinox-C_{ar}H), 123.5, 125.7, 126.9, 129.2 (q, *J*^{C-11B} = 32 Hz, BAr^F-BC_{ar}), contains also two signals for quinox-C_{ar}H), 130.2 (quinox-C_{ar}H), 130.4 (quinox-C_{ar}H), 132.6, 134.7 (BAr^F-C_{ar}H), 141.0 (quinox-C_{ar}H), 162.0 (q, *J*^{C-F} = 50 Hz, BAr^F-CF₃) ppm. Using HMQC.

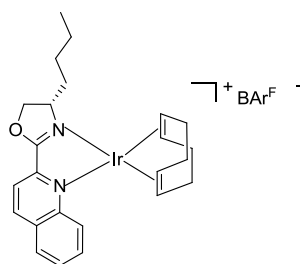
¹¹B-NMR (CD₂Cl₂, 128 MHz): δ = -7.3 ppm.

¹⁹F-NMR (CD₂Cl₂, 470 MHz): δ = -63.2 ppm.

IR (solid): $\tilde{\nu}$ = 3077 (w), 3043 (w), 2965 (w), 2934 (w), 2915 (w), 2878 (w), 2858 (w), 2842 (w), 1610 (w), 1590 (w), 1517 (w), 1487 (w), 1420 (w), 1395 (w), 1351 (s), 1316 (w), 1272 (s), 1217 (w), 1179 (m), 1159 (s), 1113 (s), 1093 (s), 1036 (m), 1016 (m), 997 (m), 971 (m), 953 (s), 926 (m), 897 (m), 886 (s), 863 (m), 837 (s), 827 (m), 808 (w), 795 (w), 778 (m), 766 (m), 744 (m), 710 (s), 680 (s), 669 (s) cm⁻¹.

HRMS (+ESI, 250 V): *m/z* (%) = 557.1788 (100) [Ir(**20b**)(cod)(O)]⁺ (calc. 557.17800), 587.1712 (20) [Ir(**20b**)(cod)(O₂)]⁺ (calc. 573.17292)

12.4.141,5-Cyclooctadiene[*(S)*-4-Butyl-2-(quinolin-2-yl)-oxazolin]iridium(I) tetrakis[3,5-bis(trifluoromethyl)phenyl]borate (**30l**)



The synthesis was carried out following general procedure E (5016, 5026H).

The product is a red-orange solid.

¹H-NMR (CD₂Cl₂, 500 MHz): δ = 0.96-1.01 (m, 3H, ⁿBu-CH₂), 1.40-1.52 (m, 6H, ⁿBu-CH₂, cod-CH₂), 1.73-1.84 (m, 6H, ⁿBu-CH₂, cod-CH₂), 1.90-2.09 (m, 2H, ⁿBu-CH₂), 2.40-2.47 (m, 2H, ⁿBu-CH₂), 4.28-4.37 (m, 1H, quinox-C*H), 4.56-4.67 (m, 2H, cod-CH=CH), 4.71 (t, *J* = 9.5 Hz, 1H, quinox-CH₂), 4.95-5.06 (m, 2H, cod-CH=CH), 5.12 (t, *J* = 9.5 Hz, 1H, quinox-CH₂), 6.76 (t, *J* = 7.5 Hz, 1H, quinox-H_{ar}), 7.18 (t, *J* = 7.5 Hz, 1H, quinox-H_{ar}), 7.56 (s, 4H, BAr^F-H_{ar}), 7.73 (s, 4H, BAr^F-H_{ar}), 7.77 (d, *J* =

8.9 Hz, 1H, quinox-H_{ar}), 7.84 (d, $J = 8.5$ Hz, 1H, quinox-H_{ar}), 8.10 (d, $J = 8.2$ Hz, 1H, quinox-H_{ar}) ppm. Using HMQC and COSY.

¹³C-NMR (CD₂Cl₂, 100 MHz): $\delta = 13.5$ (ⁿBu-CH₃), 20.6 (ⁿBu-CH₂), 22.2 (cod-CH₂), 24.2 (ⁿBu-CH₂), 25.5 (cod-CH₂), 26.9 (ⁿBu-CH₂), 67.8 (quinox-C*), 77.1 (quinox-CH₂), 83.2 (cod-C=C), 88.5 (cod-C=C), 117.5 (BAr^F-C_{ar}H), 121.1 (quinox-C_{ar}H), 121.4 (C_{ar}), 123.6 (C_{ar}), 123.8 (quinox-C_{ar}H), 125.7 (C_{ar}), 127.9 (C_{ar}), 128.9 (q, $J^{C-F} = 33$ Hz, BAr^F-CF₃), 129.4 (quinox-C_{ar}H), 129.7 (quinox-C_{ar}H), 130.2 (quinox-C_{ar}H), 134.8 (BAr^F-C_{ar}H), 141.4 (quinox-C_{ar}H), 161.6 (q, $J^{C-11B} = 51$ Hz, BAr^F-C_{ar}), 163.5 (CO) ppm. Using HMQC.

¹¹B-NMR (CD₂Cl₂, 128 MHz): $\delta = -7.7$ ppm.

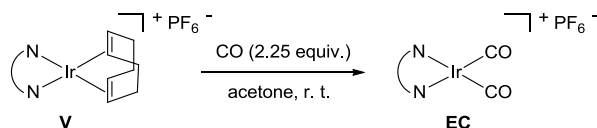
¹⁹F-NMR (CD₂Cl₂, 470 MHz): $\delta = -62.7$ ppm.

IR (solid): $\tilde{\nu} = 2962$ (m), 2938 (w), 2925 (w), 2905 (w), 2874 (w), 2856 (w), 1736 (w), 1635 (w), 1610 (w), 1590 (w), 1515 (w), 1507 (w), 1485 (w), 1470 (w), 1436 (w), 1420 (w), 1397 (w), 1352 (s), 1316 (w), 1272 (s), 1259 (s), 1216 (w), 1180 (m), 1159 (s), 1110 (s), 1093 (s), 1025 (s), 1018 (s), 975 (m), 953 (m), 936 (m), 900 (m), 885 (s), 862 (m), 837 (s), 818 (s), 796 (s), 765 (s), 744 (m), 711 (s), 680 (s), 669 (s) cm⁻¹.

HRMS (+ESI, 250 V): m/z (%) = 571.1979 (100) [Ir(**20f**)(cod)(O)]⁺ (calc. 571.19365), 587.1924 (20) [Ir(**20f**)(cod)(O₂)]⁺ (calc. 587.18857).

12.5 Carbonyl complexes

12.5.1 General procedure G for the formation of $[\text{Ir}(\text{N}^{\wedge}\text{N})(\text{CO})_2]\text{PF}_6$ complexes **28**



The solution of complex **25** (0.0595 mmol in 1-2 mL acetone), as it was obtained from its preparation (cf. general procedure F), was given into a Schlenk tube. The tube was closed with a rubber septum and the air was exchanged for argon. CO gas was added *via* a syringe (3.0 mL, 0.134 mmol, 2.25equiv.) and the solution was shaken for approx. 10 sec, while its color changed from dark brown or red to bright yellow. The solution was left standing for 10 min while its color turned dark orange, brown, green or red (depending on the ligand). The complexes were usually used without any work-up for solid-IR measurements by giving a drop of the complex solution on the ATR-diamond. After the solvent was evaporated, the IR was measured from the remaining solid. $^1\text{H-NMR}$ measurements were performed from the crude reaction mixture as well.

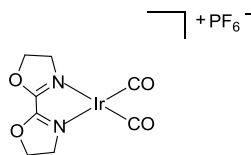
For IR measurements in solution, the solvent was evaporated in a stream of argon. The remaining solid was dissolved in THF (1 mL) and the solution was placed onto ATR-silicon prism within a home-built ATR-cell of the group of Prof. Hildebrandt. For each spectrum a total of 2000 scans of the dissolved dicarbonyl complex and 2000 scans of pure THF, as a background spectrum, were accumulated. While measuring the spectra the ATR-cell was closed with a Teflon cover to prevent the THF from evaporation.

Some complexes were purified by precipitation with hexane (6 mL) and decantation of the resulting solid compound from the solution. This procedure was repeated two times. Subsequently, the solid compound was dried in high vacuum for 30 min.

For the preparation of the carbonyl complexes, alternatively THF, MeCN or DCM can be used as solvent.

12.5.2 Bi-carbonyl[(2,2'-bioxazole)]iridium(i) hexafluorophosphate, [Ir(H-box)(CO)₂]⁺PF₆⁻ (28a)

(5170, 6118A, 6134B)



The synthesis was carried out following general procedure G. The product was obtained as brown solid which gave a yellow-orange solution in acetone.

¹H-NMR (CD₃CN, 400 MHz): δ = 4.16 (t, *J* = 10.0 Hz, 4H), 5.08 (t, *J* = 10.0 Hz, 4H) ppm.

¹³C-NMR (CD₂Cl₂, 100 MHz): δ = 53.8, 77.7, 170.1 ppm.

¹⁹F-NMR (CD₂Cl₂, 470 MHz): δ = -72.8 (d, *J*^{19F-31P} = 707 Hz) ppm.

³¹P-NMR (CD₂Cl₂, 161 MHz): δ = -146.2 (sep, *J*^{31P-19F} = 698 Hz) ppm

HRMS (+ESI, 250 V): *m/z* (%) = 389.0186 (100) [Ir(H-box)(CO)₂]⁺ (calc. 389.01078).

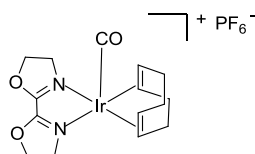
IR (solid): $\tilde{\nu}$ = 3055 (w), 2962 (w), 2925 (w), 2904 (w), 2855 (w), **2093.8 (s, ν_{CO})**, **2022.5 (s, ν_{CO})**, 1760 (w), 1733 (w), 1688 (w), 1683 (w), 1654 (w), 1644 (w), 1537(m), 1515 (w), 1470 (w), 1459 (w), 1453 (w), 1412 (w), 1382 (w), 1351 (w), 1299 (w), 1279 (m), 1257 (s), 1187 (w), 1088 (m), 1043 (s), 1015 (s), 957 (w), 916 (w), 834 (s), 815 (s), 793 (s), 741 (m), 701 (m), 661 (w) cm⁻¹.

¹H-NMR (Acetone-d₆, 400 MHz): δ = 4.46 (t, *J* = 10.0 Hz, 2H), 5.34 (t, *J* = 10 Hz, 2H) ppm. The signals at 2.33 and 5.53 ppm were assigned to free cod

IR (solution in THF): $\tilde{\nu}$ = 2085.9, 2017.2 cm⁻¹.

12.5.3 Carbonyl(1,5-cyclooctadiene)(2,2'-bioxazole)iridium(i) hexafluorophosphate, [Ir(H-box)(cod)(CO)]⁺PF₆⁻ (26a)

(3178)

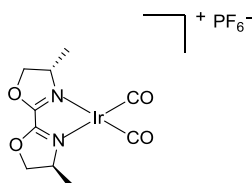


The reaction was carried out following general procedure G, and stopped by precipitation of the complex with hexane when the color of the reaction mixture turned yellow. The solid was separated from the solution by decantation and dried for 30 min in high vacuum.

IR (solution in THF): $\tilde{\nu}$ = 2045.4 cm⁻¹.

12.5.4 Bi-carbonyl[(2,2'-Bis((4S, 4'S)-4,4'-dimethyl)-oxazolin)]iridium(I) hexafluorophosphate, [Ir(Me-box)(CO)₂]⁺PF₆⁻ (28b)

(6118B, 6148C)



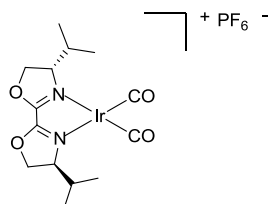
The synthesis was carried out following general procedure G. The product was obtained as brown solid which gave an orange solution in acetone.

IR (solid): $\tilde{\nu}$ = 2982 (w), 2939 (w), 2883 (w), 2846 (w), **2084.7** (s, ν_{CO}), **2013.8** (s, ν_{CO}), 1706 (w), 1676 (w), 1652 (w), 1635 (w), 1535 (m), 1509 (w), 1463 (w), 1452 (w), 1390 (w), 1380 (w), 1371 (w), 1322 (w), 1271 (w), 1261 (w), 1243 (w), 1226 (w), 1136 (w), 1077 (w), 1026 (w), 1008 (w), 958 (w), 915 (w), 874 (w), 834 (s), 740 (w), 715 (w), 656 (w) cm^{-1} .

IR (solution in THF): $\tilde{\nu}$ = 2083.7, 2015.3 cm^{-1} .

12.5.5 Bi-carbonyl [(2,2'-Bis((4S,4'S)-4,4'-diisopropyl)-oxazolin)]iridium(I) hexafluorophosphate, [Ir(ⁱPr-box)(CO)₂]⁺PF₆⁻ (28c)

(6118C, 6134A)



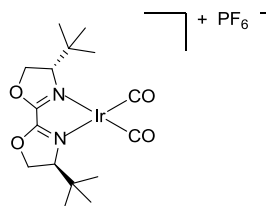
The synthesis was carried out following general procedure G. The product was obtained as brown solid which gave an orange solution in acetone.

IR (solid): $\tilde{\nu}$ = 3004 (w), 2966 (w), 2931 (w), 2905 (w), 2878 (w), 2855 (w), 2827 (w), **2077.4** (s, ν_{CO}), **2008.5** (s, ν_{CO}), 1724 (w), 1699 (w), 1685 (w), 1653 (w), 1635 (w), 1525 (m), 1509 (w), 1480 (w), 1457 (w), 1429 (w), 1399 (w), 1375 (w), 1333 (w), 1293 (w), 1259 (m), 1248 (m), 1202 (w), 1182 (w), 1138 (w), 1117 (w), 1086 (w), 1048 (w), 1032 (w), 1019 (w), 1009 (w), 966 (w), 934 (w), 921 (m), 895 (w), 872 (m), 831 (s), 799 (m), 776 (m), 751 (w), 740 (w), 725 (w), 653 (w) cm^{-1} .

IR (solution in THF): $\tilde{\nu}$ = 2082.8, 2015.3 cm^{-1} .

12.5.6 Bi-carbonyl [(2,2'-Bis((4*S*,4'*S*)-4,4'-di-*tert*-butyl)-oxazolin)]iridium(I) hexafluorophosphate, [Ir(^tBu-box)(CO)₂]⁺PF₆⁻ (28d)

(6118D, 6134C, 6148A)



The synthesis was carried out following general procedure G. The product was obtained as brown solid which gave a brown solution in acetone.

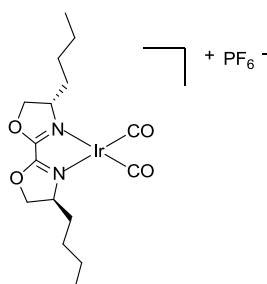
¹H-NMR (Acetonitrile-d₃, 400 MHz): δ = 1.07 (s, 18H, C(CH₃)₃), 4.30 (d, J=10.0 Hz, 2H, C*H), 4.93 (t, J= 10.0 Hz, 1H, CH₂), 5.17 (d, J= 10.0 Hz, 2H, CH₂) ppm. The signals at 2.34 and 5.54 ppm were assigned to free cod.

IR (solid): $\tilde{\nu}$ = 3123 (s), 3010 (s), 2960 (s), 2920 (s), 2878 (s), **2083.2** (s, ν_{CO}), **2014.3** (s, ν_{CO}), 1728 (s), 1698 (m), 1640 (s), 1623 (s), 1590 (m), 1558 (s), 1513 (s), 1480 (s), 1457 (s), 1428 (m), 1402 (s), 1373 (s), 1339 (s), 1312 (s), 1297 (s), 1265 (m), 1249 (m), 1211 (s), 1197 (s), 1169 (s), 1138 (s), 1101 (s), 1087 (s), 1065 (s), 1045 (s), 1030 (s), 1007 (s), 984 (s), 963 (s), 913 (s), 875 (s), 826 (s), 792 (s), 752 (s), 740 (s), 726 (s), 710 (s), 669 (s) cm⁻¹.

IR (solution in THF): $\tilde{\nu}$ = 2086.6, 2015.1 cm⁻¹.

12.5.7 Bi-carbonyl [(2,2'-Bis((4*S*, 4'*S*)-4,4'-dibutyl)-oxazolin)]iridium(I) hexafluorophosphate, [Ir(ⁿBu-box)(CO)₂]⁺PF₆⁻ (28e)

(6118E, 6148F)



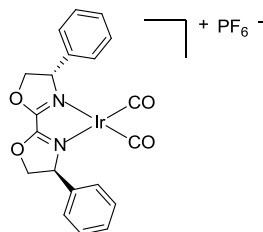
The synthesis was carried out following general procedure G. The product was obtained as orange-brown solid which gave an orange solution in acetone.

IR (solid): $\tilde{\nu}$ = 2960 (w), 2934 (w), 2873 (w), 2861 (w), **2079.9** (s, ν_{CO}), **2009.0** (s, ν_{CO}), 1650 (w), 1635 (w), 1533 (m), 1467 (w), 1458 (w), 1383 (w), 1297 (w), 1262 (w), 1244 (w), 1136 (w), 1117 (w), 1088 (w), 1034 (w), 1015 (w), 993 (w), 938 (w), 911 (w), 876 (w), 835 (s), 797 (w), 740 (w), 659 (w) cm⁻¹.

IR (solution in THF): $\tilde{\nu} = 2082.5, 2012.6 \text{ cm}^{-1}$.

12.5.8 Bi-carbonyl [(2,2'-Bis((4*R*, 4'*R*)-4,4'-diphenyl)-oxazolin)]iridium(I) hexafluorophosphate, [Ir(Ph-box)(CO)₂]⁺PF₆⁻ (28f)

(6118F, 6148D)



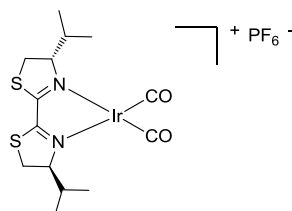
The synthesis was carried out following general procedure G. The product was obtained as brown solid which gave an orange solution in acetone.

IR (solid): $\tilde{\nu} = 3062 \text{ (w)}, 2961 \text{ (w)}, 2927 \text{ (w)}, 2895 \text{ (w)}, 2849 \text{ (w)}, 2082.3 \text{ (s, } \nu_{\text{CO}}), 2014.3 \text{ (s, } \nu_{\text{CO}}), 1699 \text{ (w)}, 1631 \text{ (w)}, 1532 \text{ (m)}, 1496 \text{ (w)}, 1456 \text{ (w)}, 1379 \text{ (w)}, 1361 \text{ (w)}, 1335 \text{ (w)}, 1257 \text{ (w)}, 1225 \text{ (w)}, 1207 \text{ (w)}, 1137 \text{ (w)}, 1086 \text{ (w)}, 1027 \text{ (w)}, 933 \text{ (w)}, 917 \text{ (w)}, 875 \text{ (w)}, 834 \text{ (s)}, 764 \text{ (w)}, 740 \text{ (w)}, 701 \text{ (w)}, 664 \text{ (w)} \text{ cm}^{-1}$.

IR (solution in THF): $\tilde{\nu} = 2085.3, 2017.8 \text{ cm}^{-1}$.

12.5.9 1,5-Cyclooctadiene[((4*S*,4'*S*)-4,4'-diisopropyl-2,2'-bithiazolin)]iridium(I) hexafluorophosphate, [Ir(ⁱPr-bta)(CO)₂]⁺PF₆⁻ (28g)

(6130D)



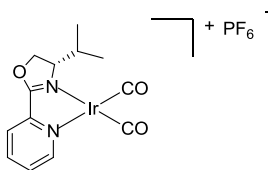
The synthesis was carried out following general procedure G. The product was obtained as dark red-brown solid which gave a dark brown solution in acetone.

IR (solid): $\tilde{\nu} = 2963 \text{ (w)}, 2931 \text{ (w)}, 2898 \text{ (w)}, 2878 \text{ (w)}, 2849 \text{ (w)}, 2065.4 \text{ (s, } \nu_{\text{CO}}), 2016.2 \text{ (s, } \nu_{\text{CO}}), 1705 \text{ (w)}, 1653 \text{ (w)}, 1558 \text{ (w)}, 1506 \text{ (w)}, 1471 \text{ (w)}, 1418 \text{ (w)}, 1394 \text{ (w)}, 1374 \text{ (w)}, 1333 \text{ (w)}, 1288 \text{ (w)}, 1253 \text{ (w)}, 1235 \text{ (w)}, 1226 \text{ (w)}, 1186 \text{ (w)}, 1139 \text{ (w)}, 1090 \text{ (w)}, 1036 \text{ (w)}, 1023 \text{ (w)}, 994 \text{ (w)}, 874 \text{ (w)}, 837 \text{ (w)}, 787 \text{ (w)}, 739 \text{ (w)}, 655 \text{ (w)} \text{ cm}^{-1}$.

IR (solution in THF): $\tilde{\nu} = 2079.8, 2013.7 \text{ cm}^{-1}$.

12.5.10 Bi-carbonyl [(S)-4-isopropyl-2-(pyridin-yl)-oxazolin]iridium(I) hexafluorophosphate, [Ir(ⁱPr-pyrox)(CO)₂]PF₆ (28h)

(6122A1, 6134D, GM 1158)



The synthesis was carried out following general procedure G. The product was obtained as dark brown solid which gave a brown solution in acetone.

¹H-NMR (CD₂Cl₂, 400 MHz): δ = 0.77 (d, *J* = 6.9 Hz, 3H, CH₃), 0.89 (d, *J* = 6.9 Hz, 3H, CH₃), 4.49–4.56 (m, 1H, CH), 4.74–4.80 (m, 1H, C*H), 4.92 (t, *J* = 9.7 Hz, 2H, CH₂), 7.82–7.88 (m, 1H, H_{ar}), 7.94 (d, *J* = 7.9 Hz, 1H, H_{ar}), 8.27 (dt, *J* = 1.2, 7.9 Hz, 1H, H_{ar}), 8.83 (d, *J* = 5.6 Hz, 1H, H_{ar}) ppm.

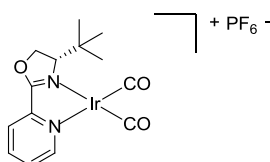
¹H-NMR (Acetone-d₆, 400 MHz): δ = 1.02 (d, *J* = 7.2 Hz, 3H, iPr-CH₃), 1.12 (d, *J* = 7.7 Hz, 3H, iPr-CH₃), 2.32–2.39 (m, 1H, iPr-CH), 4.82 (dt, *J* = 3.9, 8.3 Hz, 1H, C*H), 5.27 (d, *J* = 8.3 Hz, 2H, CH₂), 8.24 (ddd, *J* = 1.4, 5.3, 7.9 Hz, 1H, H_{ar}), 8.35 (d, *J* = 7.9 Hz, 1H, H_{ar}), 8.67 (dt, *J* = 1.4, 7.9 Hz, 1H, H_{ar}), 9.22 (d, *J* = 5.3 Hz, 1H, H_{ar}) ppm. The signals at 2.42 and 5.75 ppm were assigned to free cod.

IR (solid): $\tilde{\nu}$ = 3120 (w), 3095 (w), 3010 (w), 2964 (w), 2936 (w), 2880 (w), 2838 (w), **2084.2** (s, ν_{CO}), **2017.7** (s, ν_{CO}), 1725 (w), 1698 (w), 1647 (w), 1594 (m), 1513 (w), 1479 (w), 1465 (w), 1447 (w), 1428 (m), 1395 (w), 1376 (w), 1338 (w), 1299 (w), 1251 (w), 1209 (w), 1169 (w), 1140 (w), 1118 (w), 1100 (w), 1054 (w), 1030 (w), 1009 (w), 963 (w), 920 (w), 876 (w), 834 (s), 796 (m), 754 (w), 740 (w), 668 (w) cm⁻¹.

IR (solution in THF): $\tilde{\nu}$ = 2084.6, 2016.4 cm⁻¹.

12.5.11 Bi-carbonyl [(S)-4-(tert-butyl)-2-(pyridine-2-yl)-oxazolin]iridium(I) hexafluorophosphate, [Ir(^tBu-pyrox)(CO)₂]PF₆ (28i)

(6122B1, 6134C, 6156, GM 1158)



The synthesis was carried out following general procedure G. The product was obtained as brown solid which gave a brown solution in acetone.

¹H-NMR (Acetone-d₆, 400 MHz): δ = 1.16 (s, 9H, C(CH₃)₃), 4.60 (dd, J =3.5, 9.5 Hz, 1H, C*H), 5.10 (t, J = 9.5 Hz, 1H, CH₂), 5.50 (dd, J = 3.5, 10.0 Hz, 1H, CH₂), 8.24 (ddd, J = 16, 5.6, 8.1 Hz, 1H, H_{ar}), 8.34 (d, J = 7.9 Hz, 1H, H_{ar}), 8.66 (dt, J =1.4, 7.2 Hz, 1H, H_{ar}), 9.22 (d, J = 5.6 Hz, 1H, H_{ar}) ppm. The signals at 2.39 and 5.76 ppm were assigned to free cod

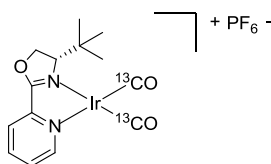
¹³C-NMR (Acetone-d₆, 100 MHz): δ = 25.1, 28.5, 32.5, 35.1, 47.1, 77.2, 125.4, 127.6, 128.2, 128.9, 132.9, 140.8, 142.9, 144.1, 156.2 ppm. The signals at 27.8 and 128.5 were assigned to free cod.

IR (solid): $\tilde{\nu}$ = 3118 (w), 3095 (w), 2962 (w), 2938 (w), 2916 (w), 2875 (w), 2853 (w), **2084.7 (s, ν_{CO})**, **2016.2 (s, ν_{CO})**, 1729 (w), 1698 (w), 1644 (w), 1624 (w), 1590 (m), 1558 (w), 1539 (w), 1514 (w), 1480 (w), 1428 (m), 1402 (w), 1373 (w), 1339 (w), 1310 (w), 1262 (m), 1250 (m), 1212 (w), 1197 (w), 1170 (w), 1139 (w), 1101 (w), 1065 (w), 1031 (w), 974 (w), 964 (w), 915 (w), 875 (m), 834 (s), 791 (m), 754 (m), 740 (m), 710 (w), 668 (w) cm⁻¹.

IR (solution in THF): $\tilde{\nu}$ = 2085.7, 2017.2 cm⁻¹.

12.5.12 Bis-(¹³C-carbonyl)[((*S*)-4-(*tert*-butyl)-2-(pyridine-2-yl)-oxazolin)]iridium(I) hexafluorophosphate, [Ir(^tBu-pyrox)(¹³CO)₂]₂PF₆ (¹³C-28i)

(6160)



Generation of ¹³CO: Under argon atmosphere 9-methyl-9H-fluorene-9-carbonyl-¹³C chloride (115.5 mg, 242.7 mmol), [Pd(dibenzylideneacetone)₂] (13.7 mg, 0.0238 mmol) and tri-*tert*-butylphosphine (5.0 mg, 0.024 mmol) were given into a Schlenk tube, which was equipped with a stirring bar. The tube was closed with a rubber septum and a rubber balloon was connected to the tube via a syringe. The atmosphere was exchanged three times. Dry toluene (4 mL) and di-*iso*-propyl ethyl amine (0.12 mL, 0.71 mmol) were added *via* syringes. The reaction mixture was heated to 85 °C (oil-bath temperature) and stirred for 30 min while gas evolution from the reaction mixture was visible. When no gas evolution was visible any more, the reaction mixture was removed from the oil-bath.

Preparation of the ¹³CO-complex: The precursor complex **25i** (0.119 mmol) was given into a Schlenk tube as solution in acetone-d₆. The tube was closed with a rubber septum and the air was exchanged three times for argon. With a syringe, 12 mL of the gas volume were removed from the tube via syringe and immediately replaced by gas which was obtained from the ¹³CO generation. The reaction mixture was shaken for approx. 10 sec, while the color turned from dark red to bright yellow and left standing for 10 min while the color changed to brown-red. The obtained dicarbonyl complex was used for IR and NMR analysis without further purification. For IR measurements from solution, the solvent was evaporated in a stream of argon and the resulting brown solid was dissolved in THF.

¹H-NMR (Acetone-d₆, 500 MHz): δ = 1.16 (s, 9H, C(CH₃)₃), 4.61 (dd, J=3.4, 9.5 Hz, 1H, C*H), 5.20 (t, J= 9.9 Hz, 1H, CH₂), 5.51 (dd, J=3.8, 9.5 Hz, 1H, CH₂), 8.25 (ddd, j= 1.4, 5.5, 7.8 Hz, 1H, Har), 8.37 (d, J= 7.5 Hz, 1H, Har), 8.68 (dt, J=1.4, 7.8 Hz, 1H, Har), 9.23 (dd, J= 0.7, 5.8 Hz, 1H, Har) ppm. The signals at 2.35 and 5.59 were assigned to free cod.

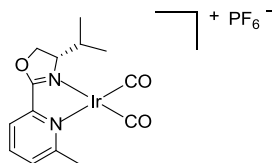
¹³C-NMR (Acetone-d₆, 100 MHz): δ = 25.9 (C(CH₃)₃), 35.9 (C(CH₃)₃), 74.9 (C*), 77.9 (CH₂), 125.8, 128.5 (C_{ar}H), 133.7 (C_{ar}H), 144.9 (C_{ar}H), 156.9 (C_{ar}H), 167.9, 169.7, 171.0 (s, 1C, ¹³CO), 172.3(s, 1C, ¹³CO), 179.0 (ox-CO) ppm. The signals at 28.6 and 129.1 were assigned to free cod.

IR (solid): $\tilde{\nu}$ = 3115 (w), 3095 (w), 2962 (w), 2917 (w), 2877 (w), 2851 (w), **2035.0** (s, ν_{CO}), **1969.5** (s, ν_{CO}), 1729 (w), 1698 (w), 1640 (w), 1626 (w), 1590 (m), 1570 (w), 1559 (w), 1539 (w), 1514 (w), 1481 (w), 1481 (w), 1469 (w), 1428 (m), 1402 (w), 1374 (w), 1340 (w), 1310 (w), 1295 (w), 1264 (w), 1250 (m), 1212 (w), 1198 (w), 1170 (w), 1138 (w), 1101 (w), 1065 (w), 1046 (w), 1030 (w), 981 (w), 964 (w), 938 (w), 913 (w), 875 (w), 834 (s), 791 (w), 754 (w), 740 (w), 669 (w) cm⁻¹.

IR (solution in THF): $\tilde{\nu}$ = 2035.62, 1970.05 cm⁻¹.

12.5.13 Bi-carbonyl [(*S*)-4-Isopropyl-2-(6-methylpyridin-2-yl)-oxazolin]iridium(I) hexafluorophosphate, [Ir(ⁱPr-mepyrox)(CO)₂]⁺PF₆⁻ (**28j**)

(6122F1, 6134F)



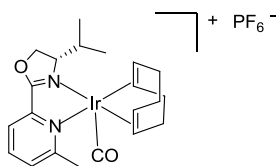
The synthesis was carried out following general procedure G. The product was obtained as green solid which gave a green solution in acetone.

IR (solid): $\tilde{\nu}$ = 3094 (w), 2964 (w), 2936 (w), 2919 (w), 2839 (w), **2080.8** (s, ν_{CO}), **2009.5** (s, ν_{CO}), 1727 (w), 1698 (w), 1652 (w), 1603 (m), 1574 (w), 1495 (w), 1464 (w), 1448 (m), 1436 (w), 1389 (m), 1376 (w), 1362 (w), 1339 (w), 1315 (w), 1298 (w), 1264 (m), 1250 (m), 1208 (w), 1193 (w), 1163 (w), 1138 (w), 1118 (w), 1104 (w), 1044 (w), 1026 (w), 1007 (w), 952 (w), 927 (m), 875 (m), 833 (s), 810 (m), 776 (m), 740 (m), 680 (w), 659 (w) cm⁻¹.

IR (solution in THF): $\tilde{\nu}$ = 2083.3, 2013.9 cm⁻¹.

12.5.14 Carbonyl(1,5-cyclooctadiene) [((*S*)-4-Isopropyl-2-(6-methylpyridin-2-yl)-oxazolin)]iridium(I) hexafluorophosphate, [Ir(ⁱPr-mepyrox)(cod)(CO)]PF₆ (26j)

(3152)

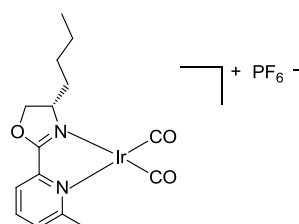


The reaction was carried out following general procedure G, and stopped by precipitation of the complex with hexane when the color of the reaction mixture turned yellow. The solid was separated from the solution by decantation and dried for 30 min in high vacuum.

IR (solution in THF): $\tilde{\nu} = 2037.5 \text{ cm}^{-1}$.

12.5.15 Bi-carbonyl[((*S*)-4-butyl-2-(6-methylpyridin-2-yl)-oxazolin)]iridium(I) hexafluorophosphate, [Ir(ⁿBu-mepyrox)(CO)₂]PF₆ (28k)

(6126B, 6144C)



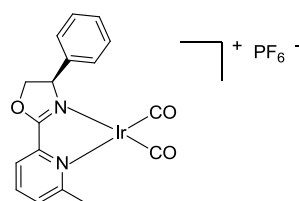
The synthesis was carried out following general procedure G. The product was obtained as yellow-orange solid which gave a yellow solution in acetone.

IR (solid): $\tilde{\nu} = 3094 \text{ (w)}, 2956 \text{ (w)}, 2932 \text{ (w)}, 2872 \text{ (w)}, 2864 \text{ (w)}, 2079.4 \text{ (s, } \nu_{\text{CO}}), 2008.5 \text{ (s, } \nu_{\text{CO}}), 1653 \text{ (w)}, 1603 \text{ (m)}, 1573 \text{ (w)}, 1498 \text{ (w)}, 1467 \text{ (w)}, 1450 \text{ (m)}, 1389 \text{ (w)}, 1321 \text{ (w)}, 1302 \text{ (w)}, 1267 \text{ (w)}, 1188 \text{ (w)}, 1158 \text{ (w)}, 1136 \text{ (w)}, 1105 \text{ (w)}, 1039 \text{ (w)}, 1013 \text{ (w)}, 938 \text{ (w)}, 876 \text{ (w)}, 835 \text{ (s)}, 811 \text{ (w)}, 777 \text{ (w)}, 751 \text{ (w)}, 688 \text{ (w)} \text{ cm}^{-1}$.

IR (solution in THF): $\tilde{\nu} = 2082.8, 2012.8 \text{ cm}^{-1}$.

12.5.16 Bi-carbonyl [((*R*)-2-(6-methylpyridin-2-yl)-4-phenyl-oxazolin)]iridium(I) hexafluorophosphate, [Ir(Ph-mepyrox)(CO)₂]PF₆ (28l)

(6124C, 6144D, 6148E)



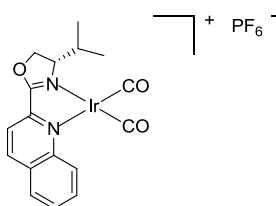
The synthesis was carried out following general procedure G. The product was obtained as dark red which gave an orange solution in acetone.

¹H-NMR (Acetone-d₆, 400 MHz): δ = 2.99 (s, 3H, CH₃), 4.86 (t, J =9.0 Hz, 1H, C*H), 5.47 (dd, J = 9.5, 10.7 Hz, 1H, CH₂), 5.66 (dd, J = 8.8, 10.4 Hz, 1H, CH₂), 7.50 (s, 5H, Har), 7.99 (dq, J = 1.4, 7.4 Hz, 2H, Har), 8.28 (t, J = 7.9 Hz, 1H, Har) ppm. The signals at 2.98 and 5.54 ppm were assigned to free cod. **IR** (solid): $\tilde{\nu}$ = 3094 (w), 3033 (w), 2961 (w), 2918 (w), 2893 (w), 2844 (w), **2081.8** (s, ν_{CO}), **2011.9** (s, ν_{CO}), 1708 (w), 1653 (w), 1603 (w), 1594 (w), 1573 (w), 1496 (w), 1469 (w), 1456 (w), 1444 (w), 1436 (w), 1390 (w), 1363 (w), 1335 (w), 1262 (w), 1224 (w), 1191 (w), 1158 (w), 1134 (w), 1101 (w), 1087 (w), 1005 (w), 954 (w), 934 (w), 874 (w), 835 (w), 811 (w), 765 (w), 752 (w), 740 (w), 702 (w), 667 (w) cm⁻¹.

IR (solution in THF): $\tilde{\nu}$ = 2084.3, 2013.4 cm⁻¹.

12.5.17 Bi-carbonyl [((S)-4-isopropyl-2-(quinolin-2-yl)-oxazole)]iridium(I) hexafluorophosphate, [Ir(ⁱPr-quinox)(CO)₂]⁺PF₆⁻ (**28m**)

(6122E1, 6134D, GM 1156)



The synthesis was carried out following general procedure G. The product was obtained as orange-brown solid which gave an orange solution in acetone.

¹H-NMR (CD₂Cl₂, 400 MHz): δ = 0.83 (d, J = 6.9 Hz, 3H, CH₃), 0.92 (d, J = 6.9 Hz, 3H, CH₃), 4.41–4.49 (m, 1H, CH), 4.76–4.83 (m, 1H, C*H), 4.94 (t, J = 9.7 Hz, 2H, CH₂), 7.77 (t, J = 8.1 Hz, 1H, CH_{ar}), 7.91–8.03 (m, 3H, CH_{ar}), 8.34 (d, J = 8.7 Hz, 1H, CH_{ar}), 8.71 (d, J = 8.1 Hz, 1H, CH_{ar}) ppm.

IR (solid): $\tilde{\nu}$ = 3069 (w), 3010 (w), 2962 (w), 2922 (w), 2874 (w), 2359 (w), 2330 (w), **2083.2** (s, ν_{CO}), **2012.8** (s, ν_{CO}), 1646 (w), 1615 (w), 1589 (w), 1557 (w), 1519 (w), 1487 (w), 1424 (w), 1423 (w), 1391 (w), 1376 (w), 1333 (w), 1294 (w), 1257 (w), 1219 (w), 1186 (w), 1148 (w), 1132 (w), 1119 (w), 1047 (w), 1012 (w), 970 (w), 926 (w), 876 (w), 829 (s), 766 (s), 740 (w), 714 (w), 668 (w) cm⁻¹.

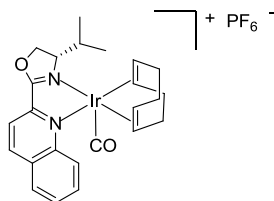
HRMS (+ESI, 300 V): m/z (%) = 539.1754 (100) [M-CO+Na]²⁺ (calc. 540.1134).

IR (solid): $\tilde{\nu}$ = 3093 (w), 3072 (w), 2963 (w), 2935 (w), 2878 (w), **2082.7** (s, ν_{CO}), **2012.4** (s, ν_{CO}), 1699 (w), 1634 (w), 1616 (w), 1590 (w), 1560 (w), 1516 (w), 1488 (m), 1474 (w), 1437 (w), 1422 (w), 1395 (w), 1376 (w), 1351 (w), 1338 (w), 1318 (w), 1295 (w), 1258 (w), 1251 (w), 1220 (w), 1185 (w), 1158 (w), 1148 (w), 1133 (w), 1123 (w), 1090 (w), 1046 (w), 975 (w), 927 (w), 876 (m), 835 (s), 796 (w), 769 (m), 740 (w), 661 (w) cm⁻¹.

IR (solution in THF): $\tilde{\nu} = 2082.7, 2013.9 \text{ cm}^{-1}$.

12.5.18 Carbonyl(1,5-cyclooctadiene[*((S)*-4-isopropyl-2-(quinolin-2-yl)-oxazole)]iridium(i) hexafluorophosphate, [Ir(*i*Pr-quinox)(cod)(CO)]PF₆ (26m)

(3154, 3144, 3142)

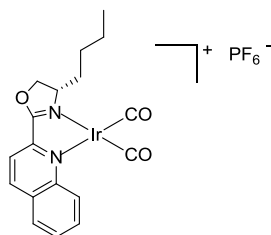


The reaction was carried out following general procedure G in DCM as solvent. The carbonylation was stopped on the stage of monocarbonylation by precipitating the yellow complex with hexane. Single crystals were obtained by vapor diffusion of hexane into a DCM/acetone solution of the complex. The crystals were orange needles.

IR (solution in THF): $\tilde{\nu} = 2039.8 \text{ cm}^{-1}$.

12.5.19 Bi-carbonyl [((*S*)-4-Butyl-2-(quinolin-2-yl)-oxazolin)]iridium(i) hexafluorophosphate, [Ir(ⁿBu-quinox)(CO)₂]PF₆ (28n)

(6122D1, 6144B)



The synthesis was carried out following general procedure G. The product was obtained as yellow-green solid which gave a yellow solution in acetone.

¹H-NMR (Acetonitrile-d₃, 400 MHz): $\delta = 0.93\text{-}0.98$ (m, 3H, ⁿBu-CH₃), 1.38-1.48 (m, 5H, ⁿBu-CH₂), 1.80-1.88 (m, 1H, ⁿBu-CH₂), 4.63-4.70 (m, 1H, C*H), 4.93 (dd, J=7.0, 9.6 Hz, 1H, CH₂), 5.18 (t, J=9.0 Hz, 1H, CH₂), 7.99 (ddd, J=1.0, 7.2, 7.9 Hz, 1H, H_{ar}), 8.10 (d, J=8.1 Hz, 1H, H_{ar}), 8.21 (ddd, J=1.6, 7.0, 8.6 Hz, 1H, H_{ar}), 8.27 (dd, J=1.4, 8.3 Hz, 1H, H_{ar}), 9.03 (d, J=6.7 Hz, 1H, H_{ar}) ppm. The signals at 5.54 and 2.33 ppm were assigned to free cod.

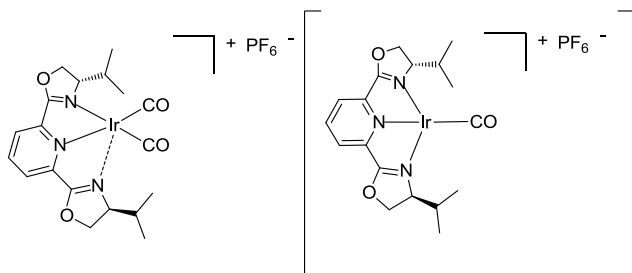
IR (solid): $\tilde{\nu} = 3089$ (w), 2958 (w), 2932 (w), 2958 (w), 2932 (w), 2872 (w), 2861 (w), **2081.3** (s, ν_{CO}), **2012.4** (s, ν_{CO}), 1725 (w), 1698 (m), 1643 (w), 1615 (m), 1590 (m), 1562 (w), 1516 (w), 1486 (m),

1469 (w), 1437 (w), 1423 (m), 1379 (w), 1347 (w), 1313 (w), 1293 (w), 1260 (m), 1351 (m), 1219 (m), 1184 (m), 1155 (w), 1133 (w), 1125 (m), 1087 (w), 1033 (w), 978 (w), 925 (w), 936 (w), 876 (s), 834 (m), 767 (m), 739 (w), 660 (w) cm^{-1} .

IR (solution in THF): $\tilde{\nu} = 2082.4, 2012.7 \text{ cm}^{-1}$.

12.5.20 Bi-carbonyl [(2,6-bis((S)-4-iso-propyl-oxazolin)pyridine)]iridium(I) hexafluorophosphate, [Ir(ⁱPr-pybox)(CO)₂PF₆ (28o)

(6130A)



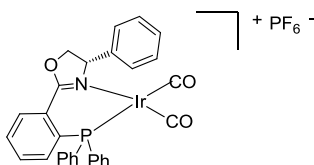
The synthesis was carried out following general procedure G. The product was obtained as orange-brown solid which gave a brown solution in acetone.

IR (solid): $\tilde{\nu} = 2962 \text{ (w)}, 2932 \text{ (w)}, 2908 \text{ (w)}, 2877 \text{ (w)}, 2847 \text{ (w)}, 2051.9 \text{ (s, } \nu_{\text{CO}}), 1983.0 \text{ (s, } \nu_{\text{CO}}), 1726 \text{ (w)}, 1698 \text{ (m)}, 1652 \text{ (w)}, 1590 \text{ (w)}, 1568 \text{ (w)}, 1487 \text{ (w)}, 1465 \text{ (w)}, 1446 \text{ (w)}, 1413 \text{ (w)}, 1446 \text{ (w)}, 1413 \text{ (w)}, 1393 \text{ (w)}, 1369 \text{ (w)}, 1334 \text{ (w)}, 1308 \text{ (w)}, 1287 \text{ (w)}, 1248 \text{ (m)}, 1209 \text{ (w)}, 1180 \text{ (w)}, 1157 \text{ (w)}, 1138 \text{ (w)}, 1117 \text{ (w)}, 1089 \text{ (w)}, 1035 \text{ (w)}, 1013 \text{ (w)}, 991 \text{ (w)}, 960 \text{ (w)}, 928 \text{ (w)}, 907 \text{ (w)}, 875 \text{ (w)}, 829 \text{ (s)}, 776 \text{ (w)}, 740 \text{ (w)}, 669 \text{ (w)} \text{ cm}^{-1}$.

IR (solution in THF): $\tilde{\nu} = 2063.4, 1984.4 \text{ cm}^{-1}$.

12.5.21 Bi-carbonyl [((S)-2-(2-(diphenylphosphanyl)phenyl)-4-phenyl-oxazolin)]iridium(I) hexafluorophosphate, [Ir(Ph-phox)(CO)₂PF₆ (28u)

(6130B)



The synthesis was carried out following general procedure G. The product was obtained as yellow-orange solid which gave an orange solution in acetone.

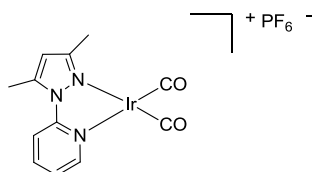
IR (solid): $\tilde{\nu} = 3145 \text{ (w)}, 3061 \text{ (w)}, 3033 \text{ (w)}, 3009 \text{ (w)}, 2926 \text{ (w)}, 2891 \text{ (w)}, 2853 \text{ (w)}, 2083.2 \text{ (s, } \nu_{\text{CO}}), 2016.7 \text{ (s, } \nu_{\text{CO}}), 1725 \text{ (w)}, 1698 \text{ (m)}, 1605 \text{ (m)}, 1582 \text{ (w)}, 1566 \text{ (w)}, 1495 \text{ (w)}, 1482 \text{ (w)}, 1456 \text{ (w)},$

1437 (m), 1386 (m), 1319 (w), 1308 (w), 1280 (w), 1247 (m), 1212 (w), 1189 (w), 1148 (w), 1129 (m), 1212 (w), 1098 (m), 1065 (w), 1028 (w), 998 (w), 955 (w), 932 (w), 875 (m), 829 (s), 783 (m), 749 (m), 731 (m), 694 (m), 655 (w) cm^{-1} .

IR (solution in THF): $\tilde{\nu} = 2068.9, 1990.1 \text{ cm}^{-1}$.

12.5.22Bi-carbonyl [(2-(3,5-dimethyl-1H-pyrazol-1-yl)pyridine)iridium(I) hexafluorophosphate, [Ir(pypyraz)(CO)₂]PF₆ (28v)

(6126A)



The synthesis was carried out following general procedure G. The product was obtained as green-black solid which gave an orange solution in acetone.

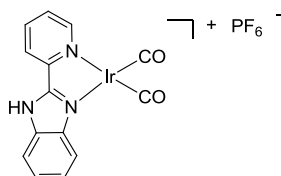
¹H-NMR (Acetone-d₆, 400 MHz): $\delta = 2.74$ (s, 3H, CH₃), 2.99 (s, 3H, CH₃), 6.83 (1H, CH), 7.81 (ddd, $J=1.0, 5.8, 7.2$ Hz, H_{ar}), 8.43 (d, $J=8.6$ Hz, 1H, H_{ar}), 8.61 (ddd, $J= 1.6, 7.7, 8.8$ Hz, 1H, H_{ar}), 9.06 (dd, $J= 1.6, 5.6$ Hz, 1H, H_{ar}) ppm. The singlets at 2.33 and 5.62 ppm were assigned to free cod.

IR (solid): $\tilde{\nu} = 3111$ (w), 2999 (w), 2955 (w), 2924 (w), 2884 (w), 2850 (w), 2831 (w), **2091.4** (s, ν_{CO}), **2077.0** (s, ν_{CO}), **2033.1** (s, ν_{CO}), **2022.0** (s, ν_{CO}), 1726 (w), 1699 (w), 1611 (w), 1578 (w), 1561 (w), 1491 (w), 1481 (m), 1455 (w), 1445 (w), 1397 (w), 1378 (w), 1328 (w), 1299 (w), 1275 (w), 1249 (w), 1172 (w), 1144 (w), 1125 (w), 1084 (w), 1070 (w), 1045 (w), 1030 (w), 1000 (w), 877 (w), 835 (s), 807 (m), 790 (w), 768 (m), 741 (w), 704 (w), 651 (w) cm^{-1} .

IR (solution in THF): $\tilde{\nu} = 2084.4, 2018.5 \text{ cm}^{-1}$.

12.5.23Bi-carbonyl[2-(pyridine-2-yl)-1H-benzo[d]imidazole]iridium(I) hexafluorophosphate, [Ir(TMphen)(CO)₂]PF₆ (28w)

(6138E)



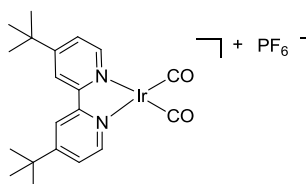
The synthesis was carried out following general procedure G. The product was obtained as orange-brown solid which gave an orange solution in acetone.

IR (solid): $\tilde{\nu}$ = 3647 (w), 3357 (w), 3080 (w), 2923 (w), **2071.2 (s, v CO)**, **2017.7 (s, v CO)**, 1609 (w), 1559 (w), 1521 (w), 1485 (w), 1460 (w), 1447 (w), 1399 (w), 1375 (w), 1325 (w), 1307 (w), 1289 (w), 1262 (w), 1232 (w), 1159 (w), 1139 (w), 1100 (w), 1059 (w), 1032 (w), 1011 (w), 991 (w), 906 (w), 871 (m), 830 (s), 788 (w), 753 (m), 737 (m), 693 (w), 658 (w) cm^{-1} .

IR (solution in THF): $\tilde{\nu}$ = 2080.7, 2010.4 cm^{-1} .

12.5.24 Bi-carbonyl [(4,4'-di-tert-butyl-2,2'-bipyridine)]iridium(I) hexafluorophosphate, **[Ir(dtbpy)(CO)₂]⁺PF₆⁻ (28r)**

(3170, 6126D, 6138B, GM 1152)



The synthesis was carried out following general procedure G in acetonitrile as solvent. The product was obtained as blue-green solid which gave a yellow solution in acetone.

¹H-NMR (CD₃CN, 500 MHz): δ = 1.45 (s, 18H, CH₃), 7.78 (dd, J = 2.0, 6.1 Hz, 2H, H_{ar}), 8.41–8.43 (m, 2H, H_{ar}), 8.79 (d, J = 6.1 Hz, 2H, H_{ar}) ppm.

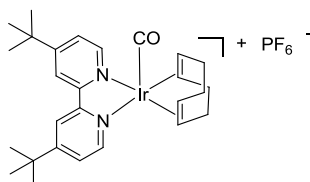
IR (solid): $\tilde{\nu}$ = 2965 (w, vCH_{ar}), 2912 (w, vCH_{ar}), 2869 (w, vCH_{ar}), 2362(w), 2325 (w), **2073 (s, v CO)**, **2024 (s, v CO)**, 1614 (m), 1543 (w), 1486 (w), 1466 (w), 1421 (w), 1399 (w), 1372 (w), 1317 (w), 1300 (w), 1257 (w), 1207 (w), 1159 (w), 1135 (w), 1076 (w), 1046 (w), 1036 (w), 956 (w), 903 (w), 835 (s), 816 (s), 738 (w), 719 (w), 712 (w), 676 (w) cm^{-1} .

HRMS (+ESI, 300 V): m/z (%) = 517.1403 (100) [M-CO]⁺ (calc. 517.1600).

IR (solution in THF): $\tilde{\nu}$ = 2074.3, 2024.6 cm^{-1} .

12.5.25 Carbonyl(1,5-cyclooctadiene)[(4,4'-di-tert-butyl-2,2'-bipyridine)] iridium(I) hexafluorophosphate, **[Ir(dtbpy)(cod)(CO)]⁺PF₆⁻ (26r)**

(6126D)

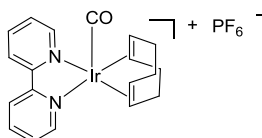


The reaction was carried out following general procedure G, and stopped by precipitation of the complex with hexane when the color of the reaction mixture turned yellow. The solid was separated from the solution by decantation and dried for 30 min in high vacuum.

IR (solution in THF): $\tilde{\nu} = 2042.3 \text{ cm}^{-1}$.

12.5.26 Carbonyl(1,5-cyclooctadiene)(2,2'-bipyridine) iridium(I) hexafluorophosphate, [Ir(bpy)(cod)(CO)]PF₆ (26q)

(6138A, 6152A)



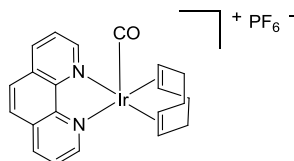
The synthesis was carried out following general procedure G in acetonitrile as solvent.

IR (solid): $\tilde{\nu} = 3208 \text{ (w)}, 3125 \text{ (w)}, 3080 \text{ (w)}, 2935 \text{ (w)}, 2872 \text{ (w)}, 2852 \text{ (w)}, 2073.6 \text{ (s, } \nu_{\text{CO}}), 2034.0 \text{ (s, } \nu_{\text{CO}}), 1992.6 \text{ (s, } \nu_{\text{CO}}), 1635 \text{ (w)}, 1605 \text{ (m)}, 1506 \text{ (w)}, 1487 \text{ (m)}, 1473 \text{ (m)}, 1449 \text{ (m)}, 1428 \text{ (w)}, 1374 \text{ (w)}, 1318 \text{ (w)}, 1300 \text{ (w)}, 1274 \text{ (w)}, 1264 \text{ (w)}, 1178 \text{ (w)}, 1164 \text{ (w)}, 1138 \text{ (w)}, 1113 \text{ (w)}, 1071 \text{ (w)}, 1035 \text{ (w)}, 967 \text{ (w)}, 899 \text{ (w)}, 876 \text{ (m)}, 836 \text{ (s)}, 798 \text{ (w)}, 761 \text{ (s)}, 741 \text{ (w)}, 720 \text{ (w)}, 669 \text{ (w)} \text{ cm}^{-1}$.

IR (solution in THF): $\tilde{\nu} = 2050.8 \text{ cm}^{-1}$.

12.5.27 Carbonyl(1,5-cyclooctadiene)(1,10-phenanthroline) iridium(I) hexafluorophosphate, [Ir^(phen)(cod)(CO)]PF₆ (26s)

(6126E, 6138C)



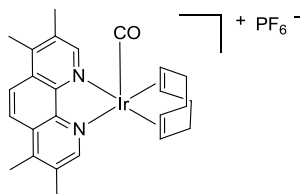
The synthesis was carried out following general procedure G in acetonitrile as solvent.

IR (solid): $\tilde{\nu} = 3094 \text{ (w)}, 2956 \text{ (w)}, 2932 \text{ (w)}, 2872 \text{ (w)}, 2864 \text{ (w)}, 2056.2 \text{ (s, } \nu_{\text{CO}}), 2026.3 \text{ (s, } \nu_{\text{CO}}), 1634 \text{ (w)}, 1520 \text{ (w)}, 1431 \text{ (w)}, 1301 \text{ (w)}, 1149 \text{ (w)}, 840 \text{ (w)}, 775 \text{ (w)}, 721 \text{ (w)}, 655 \text{ (w)} \text{ cm}^{-1}$.

IR (solution in THF): $\tilde{\nu} = 2050.1 \text{ cm}^{-1}$.

12.5.28 Carbonyl(1,5-cyclooctadiene)(3,4,7,8-tetramethyl-1,10-phenanthroline) iridium(I) hexafluorophosphate, [Ir(TMphen)(cod)(CO)]PF₆ (26t)

(6126F, 6138D)



The synthesis was carried out following general procedure G in acetonitrile as solvent.

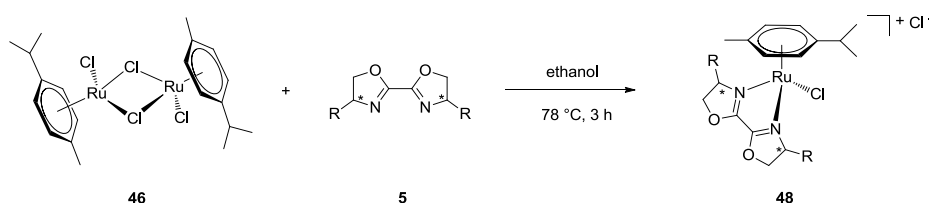
IR (solid): $\tilde{\nu}$ = 3086 (w), 2920 (w), 2852 (w), 2107 (w), 2087 (w), 2059 (w), **2107.8 (s, v CO)**, **2089.0 (s, v CO)**, **2062.5 (s, v CO)**, 1683 (w), 1653 (w), 1605 (w), 1489 (w), 1475 (m), 1450 (w), 1321 (w), 1279 (w), 1252 (w), 1169 (w), 1134 (w), 1073 (w), 1026 (w), 971 (w), 894 (w), 834 (s), 803 (m), 760 (s), 742 (s), 722 (s), 704 (m), 669 (m) cm^{-1} .

IR (solution in THF): $\tilde{\nu}$ = 2040.7 cm^{-1} .

12.6 Ruthenium Complexes

12.6.1 Reactions based on $[\text{Ru}(\text{cymene})\text{Cl}_2]_2$

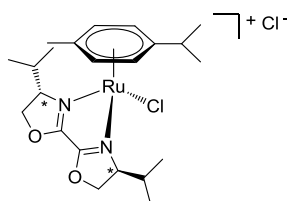
12.6.1.1 General procedure H for complexation of box ligands **5** with $[\text{Ru}(\text{cymene})\text{Cl}_2]_2$ (**46**)



The reaction was carried out under argon atmosphere. Light was excluded by wrapping the reaction flask in aluminum foil. $[\text{Ru}(\text{cymene})\text{Cl}_2]_2$ (**46**) (30.6 mg, 0.050 mmol) and the box ligand **5** (0.100 mmol) were dissolved in degassed ethanol and heated at 80 °C for 3 h. After cooling down to room temperature, the solvent was removed in vacuum and the solid residue was dried under high vacuum over night. The product was obtained as orange solid.

12.6.1.2 [chloro-[(2,2'-Bis((4*S*,4'*S*)-4,4'-diisopropyl)-oxazolin)]-(η^6 -*p*-cymol)-ruthenium(II)] chloride; [Ru(^{*i*}Pr-box)(cymene)Cl]Cl (**48a**)

(CG 2026, 2032)



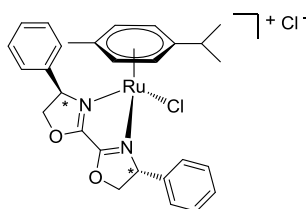
The reaction was carried out following general procedure H using ^{*i*}Pr-box (**5b**) (22.4 mg). The product was obtained quantitatively as orange solid.

¹H-NMR (CDCl₃, 700 MHz): δ = 6.13 (1H, d, J = 6.1 Hz, cymol-CH_{ar}), 6.02 (1H, d, J = 6.1 Hz, cymol-CH_{ar}), 5.89 (1H, d, J = 6.1 Hz, cymol-CH_{ar}), 5.75 (1H, d, J = 6.1 Hz, cymol-CH_{ar}), 5.03 (1H, m, box-CH₂), 5.01 (1H, m, box-CH₂), 4.98 (1H, m, box-CH₂), 4.89 (1H, m, box-CH), 4.86 (1H, m, box-CH), 4.38 (1H, m, box-CH), 2.91 (1H, m, cymol-CH), 2.65 (1H, m, ^{*i*}Pr-CH), 2.31 (1H, m, ^{*i*}Pr-CH), 2.28 (3H, s, cymol-CH₃), 1.31 (3H, d, J = 6.9 Hz, ^{*i*}Pr-CH₃), 1.28 (3H, d, J = 7.2 Hz, ^{*i*}Pr-CH₃), 1.11 (3H, d, J = 6.9 Hz, ^{*i*}Pr-CH₃), 1.09 (6H, q, J = 5.6, 7.2 Hz, cymol-CH₃), 0.87 (3H, d, J = 6.9 Hz, ^{*i*}Pr-CH₃) ppm.

HRMS (+ESI, 250V): m/z (%) = 495.1344 (100) [Ru(cymene)(^{*i*}Pr-box)Cl]⁺ (calc. 495.1352)

12.6.1.3 [chloro-[(2,2'-Bis((4*R*,4'*R*)-4,4'-diphenyl)-oxazolin)]-(η^6 -*p*-cymol)-ruthenium(II)]chloride; [Ru(Ph-box)(cymene)Cl]Cl (**48b**)

(CG 2030, 2044)



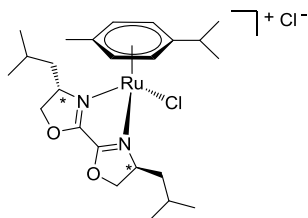
The reaction was carried out following general procedure H using Ph-box (**5g**) (29.2 mg). The product was obtained quantitatively as orange solid.

¹H-NMR (CDCl₃, 700 MHz): δ = 7.74-7.50 (10H, m, Ph-CH_{ar}), 6.09 (1H, t, J = 10.8 Hz, box-CH₂), 5.61 (1H, q, J = 9.4, 10.4 Hz, box-CH), 5.44 (1H, m, box-CH₂), 5.40 (1H, m, box-CH₂), 5.39 (1H, d, J = 7.2 Hz, cymen-CH_{ar}), 5.32 (1H, d, J = 6.1 Hz, cymen-CH_{ar}), 5.08 (1H, t, J = 9.4 Hz, box-CH₂), 4.81 (1H, q, J = 9.4, 10.9 Hz, box-CH), 4.62 (1H, d, J = 6.1 Hz, cymen-CH_{ar}), 4.42 (1H, d, J = 6.1 Hz, cymen-CH_{ar}), 2.29 (1H, m, cymen-CH), 1.91 (3H, s, cymen-CH₃), 1.10 (3H, d, J = 6.9 Hz, cymen-CH₃), 0.87 (3H, d, J = 6.9 Hz, cymen-CH₃) ppm.

HRMS (+ESI, 400V): m/z (%) = 563.1052 (10) [Ru(cymene)(Ph-box)Cl]⁺ (calc. 563.1039)

12.6.1.4 [chloro-[2,2'-Bis((4*S*,4'*S*)-4,4'-diisobutyl)-oxazolin]-(η^6 -*p*-cymol)-ruthenium(II)]chloride; [Ru(^{*i*}Bu-box)(cymene)Cl]Cl (**48c**)

(CG 2052)

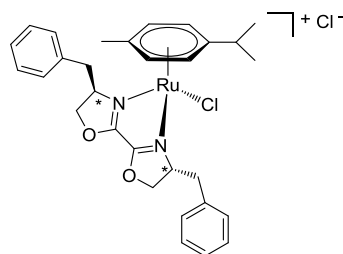


The reaction was carried out following general procedure H using ^{*i*}Bu-box (**5e**) (25.2 mg). The product was obtained as orange solid. The complex **48c** was identified by HRMS but not by ¹H-NMR spectroscopy because the spectrum showed too many signals.

HRMS (+ESI, 350V): m/z (%) = 523.1657 (100) [Ru(cymene)(^{*i*}Bu-box)Cl]⁺(calc. 523.1660)

12.6.1.5 [chloro-[2,2'-Bis((4*R*,4'*R*)-4,4'-dibenzyl)-oxazolin]-(η^6 -*p*-cymol)-ruthenium(II)]chloride; [Ru(Bn-box)(cymene)Cl]Cl (**48d**)

(CG 2050)

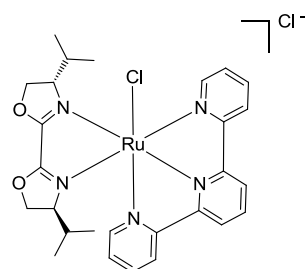


The reaction was carried out following general procedure H using Bn-box (**5h**) (32.0 mg). The product was obtained as orange solid. The complex **48d** was identified by HRMS, ¹H-NMR analysis failed due to too many overlapping signals in the spectrum.

HRMS (+ESI, 350V): m/z (%) = 591.1357 (100) [Ru(cymene)(Bn-box)Cl]⁺(calc. 591.1347)

12.6.1.6 [dichloro-[(2,2'-Bis((4S,4'S)-4,4'-diisopropyl)-oxazolin)]-[2,2':6',2''-Terpyridin]-ruthenium(II)]; [Ru(ⁱPr-box)(tpy)Cl₂] (54a)

(CG 2040, 2042)



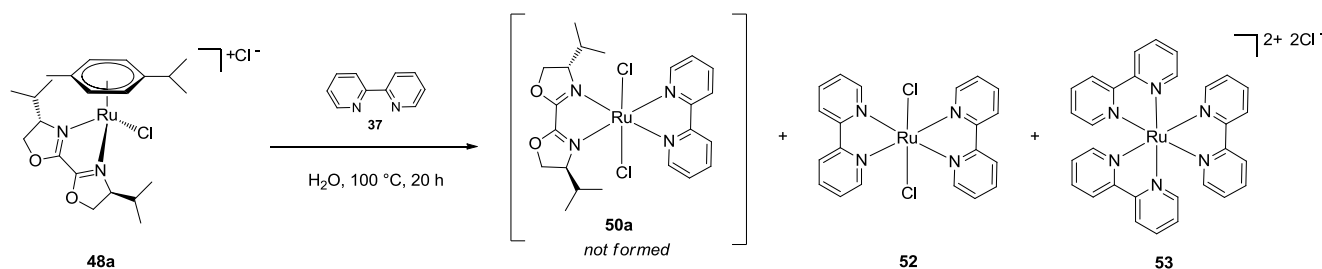
[Ru(ⁱPr-box)(dms_o)₂(Cl)₂] (**49a**) (10.0 mg, 0.020 mmol) and terpyridine **51** (4.71 mg, 0.020 mmol) were dissolved in degassed water (2.0 mL) and heated at 100 °C for 20 h. After 20 h, the water was removed under high vacuum obtaining a black solid. Purification attempts by crystallization failed because the total amount of prepared substance was too small.

¹H-NMR analysis failed due to too many overlapping signals in the spectrum.

HRMS (+ESI, 250V): *m/z* (%) = 594.1224 (25) [Ru(ⁱPr-box)(tpy)Cl]⁺ (calc. 594.1210)

 12.6.1.7 Reaction of [Ru(ⁱPr-box)(cymene)Cl]Cl (**48a**) with bipyridine **37**

(CG 2056)



[Ru(ⁱPr-box)(tpy)Cl₂] (**48a**) (10.0 mg, 0.020 mmol) and terpyridine **37** (3.15 mg, 0.020 mmol) were dissolved in degassed water (2.0 mL) and heated at 100 °C for 20 h. After 20 h, the water was removed under high vacuum obtaining a black solid.

The ¹H-NMR signals could not be assigned because of too many overlapping signals. The absence of the typical doublets of the iso-propyl groups of the oxazolin ligands indicated that no oxazolin ligand was left in the reaction mixture.

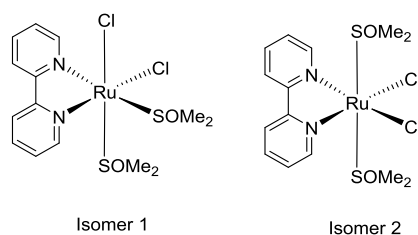
The complexes **52** and **53** were identified by HRMS.

HRMS (+ESI, 350V): m/z (%) = 449.0136 (50) $[\text{Ru}(\text{bpy})_2\text{Cl}]^+$ (calc. 449.010015), 285.0568 (43) $[\text{Ru}(\text{bpy})_3]^{2+}$ (calc. 285.0548).

12.6.2 Reactions based on $[\text{Ru}(\text{dmsso})_4\text{Cl}_2]$

12.6.2.1 Dichloro(2,2'-bipyridyl)-bis-((s)-dimethylsulfoxid)ruthenium(II); $[\text{Ru}(\text{bpy})(\text{dmsso})_2\text{Cl}_2]$ (**56**)

(CG 2068)



$[\text{Ru}(\text{dmsso})_4\text{Cl}_2]$ (**47**) (1.21 g, 2.50 mmol) and 2,2'-bipyridine (**37**) (0.390 g, 2.50 mmol) were dissolved in ethanol (30 mL) and DMSO (2.5 mL) was added. The reaction mixture was heated at 90°C oil bath temperature for 1.5 h. During this, the color changed from yellow to orange. After cooling down to room temperature, the reaction volume was reduced to half of its original volume under vacuum. During this procedure, an orange solid precipitated. The solid was removed by filtration and washed with cold ethanol. After drying under high vacuum, an orange powder (0.950 g, 1.96 mmol, 78%) was obtained as product.

Isomer 1:

$^1\text{H-NMR}$ (CDCl_3 , 400 MHz): δ = 9.87 (d, J = 5.3 Hz, 2H, CH_{ar}), 9.71 (d, J = 5.8 Hz, 1H, CH_{ar}), 8.17 (d, J = 7.8 Hz, 1H, CH_{ar}), 8.12 (d, J = 7.6 Hz, 1H, CH_{ar}), 8.01 (m, 1H, CH_{ar}), 7.90 (1H, m, CH_{ar}), 7.60 (t, J = 6.2 Hz, 1H, CH_{ar}), 7.45 (t, J = 6.7 Hz, 1H, CH_{ar}), 3.55 (s, 3H, DMSO-CH_3), 3.52 (s, 3H, DMSO-CH_3), 3.21 (s, 3H, DMSO-CH_3), 2.64 (s, 3H, DMSO-CH_3) ppm.

Isomer 2:

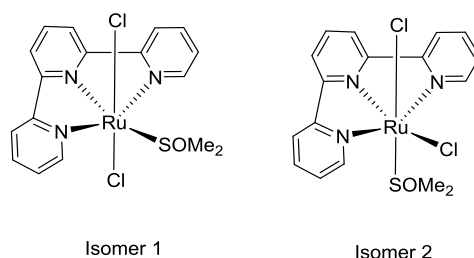
$^1\text{H-NMR}$ (CDCl_3 , 400 MHz): δ = 9.71 (d, J = 5.8 Hz, 2H, CH_{ar}), 8.01 (m, 2H, CH_{ar}), 7.90 (m, 2H, CH_{ar}), 7.50 (t, J = 6.3 Hz, 2H, CH_{ar}), 3.08 (s, 12H, DMSO-CH_3) ppm.

HRMS (+ESI, 150 V): m/z (%) = 506.9318 (75) $[\text{Ru}(\text{tpy})(\text{dmsso})_2(\text{Cl})_2\text{Na}]^+$ (calc. 506.9284), 448.9628 (25) $[\text{M-Cl}]^+$ (calc. 448.9698).

IR (solid): $\tilde{\nu}$ = 3110 (w), 3020 (w), 3007 (w), 2923 (w), 1603 (w), 1473 (w), 1446 (m), 1422 (w), 1412 (w), 1312 (w), 1240 (w), 1173 (w), 1164 (w), 1083 (s), 1061 (w), 1008 (s), 970 (m), 936 (w), 802 (w), 768 (s), 729 (m), 716 (m), 680 (m) cm^{-1} .

12.6.2.2 Dichloro(2,2':6',2''-terpyridyl)((s)-dimethylsulfoxid)ruthenium(II); [Ru(tpy)(dmsO)Cl₂] (57)

(CG 2094, 2126, 2150)



[Ru(dmsO)₄Cl₂] (**47**) (121 mg, 0.250 mmol) and 2,2':6,2''-terpyridine (**51**) (58.3 mg, 0.250 mmol) were dissolved in ethanol (5 mL) and DMSO (0.2 mL) was added. The reaction mixture was heated to 90°C (oil bath temperature) and stirred for 1.5 h. During this, the color changed from yellow to brown. After cooling down to room temperature, the reaction mixture was reduced to half of its original volume under vacuum. During this procedure, a dark brown solid precipitated. The solid was removed by filtration and washed with cold ethanol. After drying under high vacuum, a black powder (104 mg, 0.216 mmol, 86%) was obtained as product.

Isomer 1 (trans-complex):

¹H-NMR (DMSO-d₆, 500 MHz): δ = 9.35 (d, *J* = 5.8 Hz, 2H, CH_{ar}), 8.66 (d, *J* = 8.2 Hz, 2H, CH_{ar}), 8.58 (t, *J* = 7.3 Hz, 2H, CH_{ar}), 8.19 (t, *J* = 8.0 Hz, 1H, CH_{ar}), 7.99 (dt, *J* = 7.8 Hz, 1.4 Hz, 2H, CH_{ar}), 7.53 (m, 2H, CH_{ar}), 3.58 (s, 5H, DMSO-CH₃) ppm. The dmsO-signals were only partially visible.

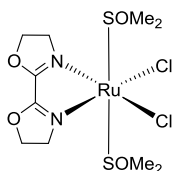
Isomer 2 (cis-complex):

¹H-NMR (DMSO-d₆, 500 MHz): δ = 9.02 (d, *J* = 5.5 Hz, 2H, CH_{ar}), 8.58 (t, *J* = 7.3 Hz, 2H, CH_{ar}), 8.53 (d, *J* = 8.2 Hz, 2H, CH_{ar}), 8.15 (dt, *J* = 7.8 Hz, 1.7 Hz, 2H, CH_{ar}), 8.02 (t, *J* = 8.0 Hz, 1H, CH_{ar}), 7.78 (m, 2H, CH_{ar}), 3.58 (s, 5H, DMSO-CH₃) ppm. The dmsO-signals were only partially visible.

HRMS (+ESI, 150 V): *m/z* (%) = 447.9829 (100) [Ru(tpy)(dmsO)Cl]⁺ (calc. 447.9824), 505.9413 (25) [M+Na]⁺ (calc. 505.9411).

12.6.2.3 Dichloro(2,2'-bis[oxazolin-2-yl])bis(dimethylsulfoxid)ruthenium(II); [Ru(H-box)(dmsO)₂Cl₂] (49a)

(CG 2112, 2122, 2128)



[Ru(dms_o)₄Cl₂] (**47**) (48.4 mg, 0.100 mmol) and H-box (**5i**) (15.4 mg, 0.110 mmol) were dissolved in ethanol (2 mL) and DMSO (0.1 mL) was added. The reaction mixture was heated to 90°C oil bath temperature for 1 h. During this, the color changed from yellow to orange. After cooling down to room temperature, the reaction mixture was reduced to half of its original volume under vacuum. During this procedure, an orange solid precipitated. The solid was removed by filtration and washed with cold ethanol. After drying under high vacuum, an orange powder (27.1 mg, 0.057 mmol, 57%) was obtained as product.

Purification attempts: Vapor diffusion of diethylether into a concentrated MeCN solution of the product yielded orange crystals. The crystals were no single crystals and therefore not suitable for crystal structure analysis.

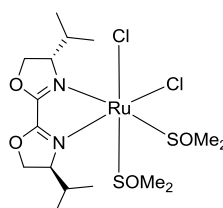
¹H-NMR (CDCl₃, 500 MHz): δ = 4.90 (4H, t, *J* = 9.9 Hz, box-CH), 4.37 (4H, t, *J* = 9.9Hz, box-CH), 3.41 (12H, s, CH₃) ppm.

HRMS (+ESI, 150 V): *m/z* (%) = 490.9157 (100) [Ru(H-box)(dms_o)₂(Cl)₂Na]⁺(calc. 490.9183).

IR (Feststoff): $\tilde{\nu}$ = 3027 (w), 3004 (w), 2921 (w), 1651 (w) 1629 (w), 1604 (w), 1505 (m), 1473 (m), 1420 (w), 1401 (w), 1371 (w), 1300 (w), 1277 (s), 1222 (s), 1191 (w), 1086 (s), 1010 (s), 997 (s), 958 (m), 911 (s), 869 (m), 717 (m), 681 (s) cm⁻¹.

12.6.2.4 Dichloro(4,4'-diisopropyl-2,2'-bis[oxazolin-2-yl])bis((s)-dimethylsulfoxid)ruthenium(II); [Ru(ⁱPr-box)(dms_o)₂Cl₂] (**49b**)

(CG 2124, 2130)



[Ru(dms_o)₄Cl₂] (**47**) (24.2 mg, 0.050 mmol) and ⁱPr-box (**5b**) (7.70 mg, 0.055 mmol) were dissolved in ethanol (1 mL) and DMSO (0.05 mL) was added. The reaction mixture was heated to 90°C oil bath temperature for 1 h. During this, the color changed from yellow to orange. After cooling down to room temperature, the reaction volume was reduced to half of its original volume under vacuum. During this procedure, an orange solid precipitated. The solid was removed by filtration and washed with cold ethanol. After drying under high vacuum, an orange powder was obtained and identified as raw product.

The raw product was dissolved in ethanol or chloroform and precipitation with diethylether or hexane respectively, tried. These attempts were not successful. A preparative TLC analysis on silica gel with

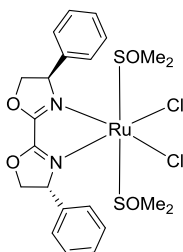
an eluent mixture of MeCN/water (=9/1) containing KNO₃, failed as well. After the separation of different visible fractions, no product was present any more as analyzed by ¹H-NMR spectroscopy.

HRMS (+ESI, 150 V): m/z (%) = 517.0567 (25) [Ru(Pr-box)(dms_o)₂Cl]⁺(calc. 517.0536), 575.0154 (10) [M+Na]⁺(calc. 575.0122).

IR (solid): $\tilde{\nu}$ = 3387 (w), 3276 (w), 3010 (w), 2960 (m), 2923 (m), 2871 (w), 1739 (w), 1666 (m), 1620 (w), 1500 (s), 1459 (m), 1391 (m), 1366 (m), 1311 (w), 1294 (w), 1257 (m), 1230 (m), 1086 (s), 1014 (s), 960 (w), 924 (m), 871 (w), 797 (m), 718 (w), 680 (m) cm⁻¹.

12.6.2.5 Dichloro(4,4'-diphenyl-2,2'-bis[oxazolin-2-yl])bis(dimethylsulfoxid)ruthenium(II); [Ru(Ph-box)(dms_o)₂Cl₂] (49c)

(CG 2146)



[Ru(dms_o)₄Cl₂] (**47**) (24.2 mg, 0.050 mmol) and Ph-box (**5g**) (16.1 mg, 0.055 mmol) were dissolved in ethanol (1 mL) and DMSO (0.05 mL) was added. The reaction mixture was heated at 90°C oil bath temperature for 1 h. During this, the color changed from yellow to orange. After cooling down to room temperature, the reaction volume was reduced to half of its original volume under vacuum. During this procedure, an orange solid precipitated. The solid was removed by filtration and washed with cold ethanol. After drying under high vacuum, an orange powder was obtained as raw product.

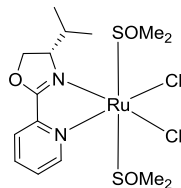
¹H-NMR (CDCl₃, 500 MHz): δ = 7.28-7.40 (m, 10H, Ph-CH_{ar}), 5.84 (dd, J = 10.6, 5.5 Hz, 1H, box-CH₂), 5.41 (dd, J = 10.6, 4.9 Hz, 1H, box-CH₂), 5.35 (dd, J = 10.6, 9.2 Hz, 1H, box-CH₂), 5.21 (dd, J = 9.2, 5.5 Hz, 1H, box-CH₂), 5.19 (dd, J = 10.6, 8.9 Hz, 1H, box-CH), 4.69 (dd, J = 8.9, 4.9 Hz, 1H, box-CH), 3.11 (s, 3H, DMSO-CH₃), 3.03 (s, 3H, DMSO-CH₃), 2.26 (s, 3H, DMSO-CH₃), 2.22 (s, 3H, DMSO-CH₃) ppm.

HRMS (+ESI, 200 V): m/z (%) = 585.0222 (100) [Ru(Ph-box)(dms_o)₂Cl]⁺(calc. 585.0223), 642.9814 (25) [M+Na]⁺(calc. 642.9809).

IR (solid): $\tilde{\nu}$ = 3406 (w), 3027 (w), 3007 (w), 2921 (w), 1990 (w), 1746 (w), 1705 (m), 1672 (m), 1634 (w), 1616 (w), 1496 (s), 1455 (m), 1412 (w), 1361 (m), 1331 (w), 1310 (w), 1290 (w), 1226 (s), 1082 (s), 1015 (s), 921 (s), 876 (w), 798 (w), 759 (m), 699 (s), 680 (w) cm⁻¹.

12.6.2.6 Dichloro(2-[4'-isopropyl-oxazolin-2-yl]pyridyl)bis((s)-dimethylsulfoxid)ruthenium(II); [Ru(ⁱPr-pyrox)(dms_o)₂Cl₂] (49d)

(CG 2148)



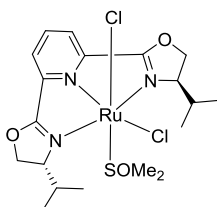
[Ru(dms_o)₄Cl₂] (**47**) (24.2 mg, 0.050 mmol) and ⁱPr-pyrox (**10b**) (10.5 mg, 0.055 mmol) were dissolved in ethanol (1 mL) and DMSO (0.05 mL) was added. The reaction mixture was heated at 90°C oil bath temperature for 1 h. During this, the color changed from yellow to orange. After cooling down to room temperature, the reaction volume was reduced to half of its original volume under vacuum. During this procedure, an orange solid precipitated. The solid was removed by filtration and washed with cold ethanol. After drying under high vacuum, an orange powder was obtained as raw product. An identification by ¹H-NMR spectroscopy failed due to too many overlapping signals. In the HRMS spectrum, also a signal for the related cationic complex [Ru(ⁱPr-pyrox)(dms_o)₃Cl]Cl (**57d**) was detected.

HRMS (+ESI, 200 V): *m/z* (%) = 483.0129 (100) [Ru(ⁱPr-pyrox)(dms_o)₂Cl]⁺(calc. 483.0117), 540.9761 (15) [M+Na]⁺(calc. 540.9703).

IR(solid): $\tilde{\nu}$ = 3463 (w), 3067 (w), 3005 (w), 2962 (w), 2923 (w), 2871 (w), 1969 (w), 1707 (s), 1651 (m), 1636 (m), 1590 (m), 1496 (m), 1464 (w), 1411 (s), 1389 (w), 1362 (m), 1309 (w), 1296 (w), 1251 (m), 1223 (m), 1163 (w), 1088 (s), 1051 (w), 1012 (s), 970 (w), 916 (s), 796 (m), 754 (m), 714 (w) 674 (m) cm⁻¹.

12.6.2.7 Dichloro(2,6-bis[4'-isopropyl-oxazolin-2-yl]pyridyl)((s)-dimethylsulfoxid)ruthenium(II), [Ru(ⁱPr-pybox)(dms_o)Cl₂] (58)

(CG 2116, 2144)



[Ru(dms_o)₄Cl₂] (**47**) (24.2 mg, 0.050 mmol) and ⁱPr-pybox (**36**) (16.5 mg, 0.055 mmol) were dissolved in ethanol (1 mL) and DMSO (0.05 mL) was added. The reaction mixture was heated at 90°C oil bath

temperature for 1 h. During this, the color changed from yellow to orange. After cooling down to room temperature, the reaction volume was reduced to half of its original volume under vacuum. During this procedure, an orange solid precipitated. The solid was removed by filtration and washed with cold ethanol. After drying under high vacuum, an orange powder was obtained as raw product.

An identification by $^1\text{H-NMR}$ spectroscopy failed due to too many overlapping signals. In the HRMS spectrum, also a signal for the related cationic complex $[\text{Ru}(\text{Pr-pybox})(\text{dmsO})_3\text{Cl}]\text{Cl}$ (**64**) was detected.

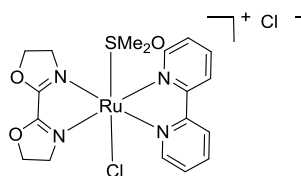
HRMS (+ESI, 150 V): m/z (%) = 516.0648(70) $[\text{Ru}(\text{Pr-pybox})(\text{dmsO})\text{Cl}]^+$ (calc. 516.0662), 574.0209 (25) $[\text{M}+\text{Na}]^+$ (calc. 574.0248).

IR (solid): $\tilde{\nu}$ = 3445 (m), 3062 (w), 2959 (m), 2925 (m), 2871 (w), 1708 (w), 1659 (w), 1591 (m), 1567 (m), 1534 (w), 1489 (m), 1464 (w), 1438 (w), 1399 (s), 1387 (s), 1334 (w), 1314 (w), 1282 (m), 1249 (m), 1207 (w), 1177 (w), 1145 (w), 1078 (s), 1014 (s), 956 (s), 926 (m), 818 (w), 771 (w), 754 (m), 717 (w), 676 (m), 656 (w) cm^{-1} .

12.6.2.8 [chloro(2,2'-bis[oxazolin-2-yl])(2,2'-bipyridyl)(dimethyl-sulfoxid)ruthenium(II)] chlorid; $[\text{Ru}(\text{H-box})(\text{bpy})((\text{s-dmsO})\text{Cl})^+\text{Cl}^-$ (**61**)

(method 1 CG 2074, 2090, 2104, 2138)

(method 2 CG 2088, 2134, 2142)



Method 1:

$[\text{Ru}(\text{bpy})(\text{dmsO})_2\text{Cl}_2]$ (**57**) (96.8 mg, 0.200 mmol) and H-box (**5i**) (28.0 mg, 0.200 mmol) were dissolved in degassed ethanol (50 mL). The reaction mixture was heated to 80 °C for 1.5 h. After cooling down to room temperature, the solvent was removed in vacuum and the resulting oily mixture was purified by column chromatography (SiO_2 , eluent: acetonitrile/water = 95/5, 9/1, 85/15 containing 10 drops of concentrated aqueous KNO_3 solution per 10 mL eluent-mixture). The product was obtained as orange powder (55.0 mg, 0.096 mmol, 48%).

Method 2:

$[\text{Ru}(\text{H-box})(\text{dmsO})_2\text{Cl}_2]$ (**49a**) (23.4 mg, 0.050 mmol) was dissolved in degassed ethanol (2 ml) and 2,2'-bipyridin (**37**) (7.81 mg, 0.050 mmol) was added. The reaction mixture was heated to 80 °C for 1.5 h. After cooling down to room temperature the solvent was removed in vacuum. The product was obtained with strong impurities.

Isomer 1:

¹H-NMR (D₂O, 700 MHz): δ = 9.46 (m, 1H, bpy-CH_{ar}), 8.59 (d, J = 7.0 Hz, 1H, bpy-CH_{ar}), 8.52 (d, J = 7.0 Hz, 1H, bpy-CH_{ar}), 8.47 (m, 1H, bpy-CH_{ar}), 8.34 (dt, J = 7.7 Hz, 1.5 Hz, 1H, bpy-CH_{ar}), 8.23 (dt, J = 7.7 Hz, 1.5 Hz, 1H, bpy-CH_{ar}), 7.89 (m, 1H, bpy-CH_{ar}), 7.68 (m, 1H, bpy-CH_{ar}), 5.26 (m, 2H, box-CH₂), 5.01 (m, 1H, box-CH₂), 4.85 (m, 1H, box-CH₂), 4.65 (m, 1H, box-CH₂), 4.42 (m, 1H, box-CH₂), 3.69 (m, 1H, box-CH₂), 3.36 (m, 1H, box-CH₂), 3.32 (s, 3H, DMSO-CH₃), 2.61 (s, 3H, DMSO-CH₃) ppm.

Isomer 2:

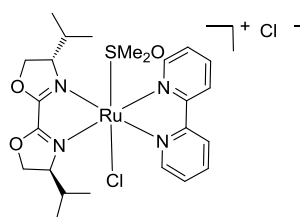
¹H-NMR (D₂O, 700 MHz): δ = 9.01 (m, 1H, bpy-CH_{ar}), 8.64 (d, J = 7.0 Hz, 1H, bpy-CH_{ar}), 8.52 (d, J = 7.0 Hz, 1H, bpy-CH_{ar}), 8.40 (m, 2H, bpy-CH_{ar}), 8.23 (m, 1H, bpy-CH_{ar}), 7.96 (m, 1H, bpy-CH_{ar}), 7.68 (m, 1H, bpy-CH_{ar}), 5.34 (m, 1H, box-CH₂), 5.26 (m, 1H, box-CH₂), 5.01 (m, 1H, box-CH₂), 4.91 (m, 1H, box-CH₂), 4.71 (m, 1H, box-CH₂), 4.53 (m, 1H, box-CH₂), 3.73 (m, 1H, box-CH₂), 3.36 (m, 1H, box-CH₂), 3.28 (s, 3H, DMSO-CH₃), 2.66 (s, 3H, DMSO-CH₃) ppm.

HRMS (+ESI, 150 V): m/z (%) = 511.0146 (100) [Ru(H-box)(bpy)(dmsO)Cl]⁺(calc. 511.0145).

IR (solid): $\tilde{\nu}$ = 3424 (w), 2955 (m), 2924 (s), 2853 (m), 1887 (w), 1604 (m), 1506 (s), 1465 (w), 1446 (w), 1417 (w), 1334 (s), 1280 (m), 1230 (m), 1159 (w), 1084 (m), 1038 (w), 1017 (m), 999 (m), 958 (w), 918 (m), 870 (m), 825 (w), 801 (w), 771 (m), 731 (w), 687 (w), 667 (w) cm⁻¹.

12.6.2.9 [chloro(4,4'-diisopropyl-2,2'-bis[oxazolin-2-yl])(2,2'-bipyridyl)((s)-dimethylsulfoxid)ruthenium(II)] chlorid; [Ru(ⁱPr-box)(bpy)(dmsO)Cl]⁺Cl⁻ (61b**)**

(CG 2102, 2106, 2118, 2160)

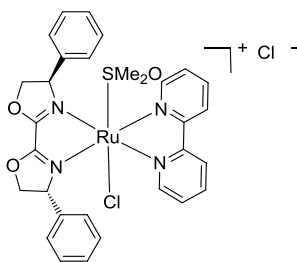


[Ru(bpy)(dmsO)₂Cl₂] (**57**) (48.4 mg, 0.100 mmol) was dissolved in degassed ethanol (25 mL) and *i*Pr-box (**5b**) (22.4 mg, 0.100 mmol) was added. The reaction mixture was heated to 80 °C for 1.5 h. After cooling down to room temperature the solvent was removed in vacuum. The product was obtained as orange powder quantitatively. The analysis of the ¹H-NMR spectrum failed due to too many overlapping signals.

HRMS (+ESI, 150 V): m/z (%) = 595.1050 (100) [Ru(ⁱPr-box)(bpy)(dmsO)Cl]⁺(calc. 595.1084).

IR (solid): $\tilde{\nu}$ = 3387 (w), 3288 (w), 2963 (m), 2929 (w), 2872 (m), 1661 (s), 1604 (w), 1502 (s), 1463 (m), 1420 (w), 1390 (w), 1370 (m), 1339 (w), 1311 (w), 1258 (m), 1232 (m), 1093 (s), 1018 (m), 1003 (m), 961 (w), 924 (m), 873 (w), 800 (m), 773 (m), 732 (w), 682 (w), 664 (w) cm^{-1} .

12.6.2.10 **[chloro(4,4'-diphenyl-2,2'-bis[oxazolin-2-yl])(2,2'-bipyridyl)(dimethylsulfoxid)ruthenium(II)] chlorid; [Ru(Ph-box)(bpy)(dmsO)Cl]⁺Cl⁻ (61c)**
(CG 2152)



[Ru(bpy)(dmsO)₂Cl₂] (**57**) (10.0 mg, 0.021 mmol) was dissolved in degassed ethanol (5 mL) and ⁱPr-box (**5b**) (6.03 mg, 0.0212 mmol) was added. The reaction mixture was heated to 80 °C for 1.5 h. After cooling down to room temperature the solvent was removed in vacuum. The product was obtained as orange crystalline powder quantitatively. The analysis of the ¹H-NMR spectrum was not possible due to too many overlapping signals.

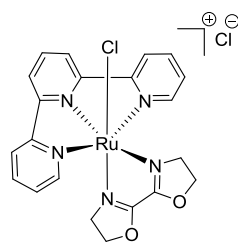
HRMS (+ESI, 200 V): m/z (%) = 663.0844 (100) [Ru(Ph-box)(tpy)(dmsO)Cl]⁺(calc. 663.0771).

IR (solid): $\tilde{\nu}$ = 3412 (w), 2969 (w), 2867 (m), 1707 (w), 1672 (w), 1638 (w), 1604 (w), 1498 (m), 1455 (m), 1419 (w), 1371 (m), 1310 (w), 1259 (m), 1229 (m), 1094 (s), 1015 (w), 924 (m), 875 (w), 797 (m), 765 (m), 730 (w), 700 (m) cm^{-1} .

12.6.2.11 **[chloro(2,2'-bis[oxazolin-2-yl])(2,2':6',2''-terpyridyl)ruthenium(II)] chlorid; [Ru(H-box)(tpy)Cl]⁺Cl⁻ (54b)**

(Method 1: 2098, 2132, 2154)

(Method 2: 2164)



Method 1:

[Ru(tpy)(dmsO)Cl₂] (**57**) (50.0 mg, 0.103 mmol) was dissolved in degassed ethanol (25 mL) and H-box (**5i**) (15.9 mg, 0.113 mmol) was added. The reaction mixture was heated to 80 °C for 1.5 h. After cooling down to room temperature, the solvent was removed in vacuum. The product was obtained as brown-black solid. The analysis of the ¹H-NMR spectrum failed due to too many overlapping signals.

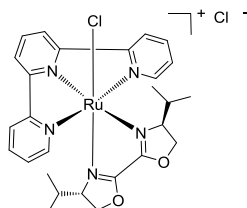
Method 2:

[Ru(H-box)(dmsO)₂Cl₂] (**49a**) (11.7 mg, 0.025 mmol) was dissolved in degassed ethanol (6 ml) and 2,2':6',2''-terpyridin (**51**) (5.83 mg, 0.025 mmol) was added. The reaction mixture was heated to 80 °C for 6 h. After cooling down to room temperature the solvent was removed in vacuum. The product was obtained as brown-red solid quantitatively. The analysis of the ¹H-NMR spectrum failed due to too many overlapping signals.

HRMS (+ESI, 150 V): *m/z* (%) = 510.0407 (100) [Ru(H-box)(tpy)Cl]⁺(calc. 510.0271).

IR (solid): $\tilde{\nu}$ = 3359 (m), 3064 (w), 2961 (w), 2924 (w), 2854 (w), 1963 (w), 1741 (w), 1662 (m), 1598 (s), 1505 (s), 1466 (w), 1445 (m), 1384 (w), 1363 (w), 1281 (m), 1259 (m), 1227 (m), 1160 (w), 1080 (s), 1051 (w), 1014 (s), 992 (w), 956 (m), 919 (m), 866 (m), 773 (s), 733 (w), 726 (w), 685 (w), 673 (w) cm⁻¹.

12.6.2.12 [chloro(4,4'-diisopropyl-2,2'-bis[oxazolin-2-yl])(2,2':6',2''-terpyridyl)ruthenium(II)] chlorid; [Ru(ⁱPr-box)(tpy)Cl]⁺Cl⁻ (**54a**)
(CG 2158)



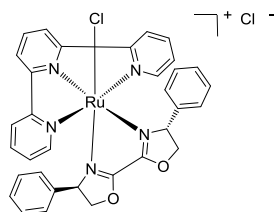
[Ru(tpy)(dmsO)Cl₂] (**57**) (12.1 mg, 0.025 mmol) was dissolved in degassed ethanol (6 mL) and ⁱPr-box (**5b**) (6.17 mg, 0.027 mmol) was added. The reaction mixture was heated to 80 °C for 1.5 h. After cooling down to room temperature, the solvent was removed in vacuum. The product was obtained as red-brown solid. The analysis of the ¹H-NMR spectrum failed due to too many overlapping signals.

HRMS (+ESI, 200 V): *m/z* (%) = 594.1221 (100) [Ru(ⁱPr-box)(tpy)Cl]⁺(calc. 594.1210).

IR (solid): $\tilde{\nu}$ = 3387 (w), 3061 (w), 2961 (m), 2930 (w), 2904 (w), 2872 (m), 1673 (m), 1643 (w), 1620 (s), 1504 (s), 1466 (m), 1448 (w), 1386 (m), 1370 (m), 1340 (w), 1299 (w), 1279 (w), 1259 (m), 1231 (w), 1118 (s), 1036 (w), 1000 (w), 947 (m), 894 (w), 870 (w), 796 (m), 774 (m), 735 (w), 686 (w), 674 (w) cm⁻¹.

12.6.2.13 [chloro(4,4'-diphenyl-2,2'-bis[oxazolin-2-yl])(2,2':6,2''-terpyridyl)ruthenium(II)] chlorid; [Ru(Ph-box)(tpy)Cl]⁺Cl⁻ (**54c**)

(CG 2156)



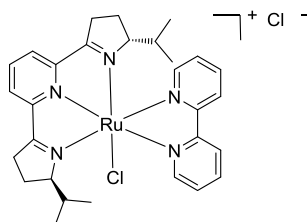
[Ru(tpy)(dmsO)Cl₂] (**57**) (10.0 mg, 0.021 mmol) was dissolved in degassed ethanol (6 mL) and Ph-box (**5h**) (6.65 mg, 0.023 mmol) was added. The reaction mixture was heated to 80 °C for 1.5 h. After cooling down to room temperature, the solvent was removed in vacuum. The product was obtained as red-brown solid. The analysis of the ¹H-NMR spectrum failed due to too many overlapping signals.

HRMS (+ESI, 200 V): *m/z* (%) = 662.0965 (100) [Ru(Ph-box)(tpy)Cl]⁺(calc. 662.0965).

IR (solid): $\tilde{\nu}$ = 3384 (m), 3061 (w), 3030 (w), 2968 (w), 2901 (w), 2869 (w), 1742 (w), 1673 (w), 1616 (m), 1602 (w), 1499 (s), 1449 (s), 1386 (w), 1358 (w), 1334 (w), 1281 (w), 1233 (m), 1123 (s), 1099 (s), 1085 (s), 1048 (w), 1011 (w), 982 (w), 957 (w), 930 (m), 871 (w), 767 (s), 701 (s), 670 (w) cm⁻¹.

12.6.2.14 [chloro(2,6-bis[(*S*)-4'-isopropyl-oxazolin-2-yl]pyridyl) (2,2'-bipyridyl)-ruthenium(II)] chlorid; [Ru(ⁱPr-pybox)(bpy)Cl]⁺Cl⁻ (**64**)

(CG 2166)



[Ru(ⁱPr-pybox)(dmsO)Cl₂] (**58**) (20.0 mg, 0.036 mmol) was dissolved in degassed ethanol (10 mL) and 2,2'-bipyridine (**37**) (5.67 mg, 0.036 mmol) was added. The reaction mixture was heated to 80 °C for 3 h. After cooling down to room temperature, the solvent was removed in vacuum. The product was obtained as red-brown solid. The analysis of the ¹H-NMR spectrum failed due to too many overlapping signals.

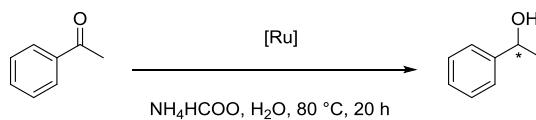
HRMS (+ESI, 200 V): *m/z* (%) = 594.1228 (100) [Ru(ⁱPr-pybox)(bpy)Cl]⁺(calc. 594.1210).

IR (solid): $\tilde{\nu}$ = 3852 (w), 3733 (w), 3627 (w), 2961 (m), 2924 (w), 2854 (w), 2359 (w), 1685 (w), 1540 (w), 1507 (w), 1456 (w), 1259 (s), 1090 (m), 1020 (s), 864 (w), 798 (s), 682 (w), 669 (w) cm⁻¹.

12.6.2.15 **Transferhydrogenation**

(CG 2162, 2168)

(further transferhydrogenation test reactions: CG 2136, 2140)



Acetophenone (**66**) (38.4 mg, 0.320 mmol) was dissolved in water (5 mL) and the precatalyst and HCOONH₄ (9.60 mmol) were added. The pH-value was adjusted to 4 by addition of aqueous HCOOH (1M) or KOH (1M). The reaction mixture was heated to 80 °C for 20 h. The reaction was stopped by cooling the mixture down to 8 °C by putting the reaction vial into the fridge. The reaction mixture was extracted with diethylether and the ether phase was analyzed by GC-MS.

Qualitative results:[Ru(bpy)(H-box)(DMSO)Cl]NO₃ (**65**) (0.5 mol%) – product formation[Ru(bpy)(H-box)(DMSO)Cl]NO₃ (**65**) (3.0 mol%) – product formation[Ru(ⁱPr-pybox)(bpy)Cl]Cl (**64**) (2.5 mol%) – product formation

13 Catalysis

13.1 Aromatic Borylation

13.1.1 Independent Preparation of Borylation products

General procedure I for Miyaura coupling

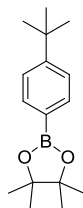
The procedure was performed on basis of a procedure from the Miyaura group.^[245] Bis(pinacolato)diboron (**66**) (610 mg, 2.40 mmol), potassium hydroxide (**71**) (590 mg, 6.00 mmol), [1,1'-Bis(diphenylphosphino)-ferrocene]dichloro palladium(II) (**70**) (44.0 mg, 0.05 mmol) and the corresponding aryl halide **69** or **72** (2.00 mmol) were filled into a Schlenk-flask and set under an argon-atmosphere. Dry dimethylsulfoxide (5 mL) was added and the reaction mixture was heated up to 90°C (oil bath) and stirred over night. After cooling to room temperature three volume equivalents of water were added and the aqueous phase was extracted three times with 60 mL diethylether respectively. The combined organic layers were dried over Na₂SO₄ and evaporation of the solvent under vacuum yielded the crude product. The product was isolated by column chromatography. During chromatography, only the starting material and homocoupling product was visible on TLC (Cer staining reagent). The product was isolated between these two fractions and identified by GC-MS.

GC method: Carrier gas: Helium
Temperature (column): 80°C (hold 2.5 min), 80→280°C (rate 20°C/min)
Temperature (injection): 300°C
Column Flow: 1.0 mL/min
Split Ratio: 10% (initial), 100% (0.01 min→1.00 min), 40% (1.00→end)

Column: Capillary Column (VF-5ms, 5% phenyl, 95% dimethylpolysiloxane, 30 x 0.25 mm, D_f = 0.25 μm, CP-8944)

13.1.1.1 2-(4-(*tert*-butyl)phenyl)-4,4,5,5-tetramethyl-1,3,2-dioxaborolane (68a)

(CCT 1063)



The reaction was carried out following general procedure I.

Purification by column chromatography (SiO₂, hexane/diethylether = 1/0→19/1), colorless crystalline powder (333 mg, 1.28 mmol, 64%).

The ¹H-NMR and ¹³C-NMR data are in accordance with these reported in literature.^[250]

¹H-NMR (CDCl₃, 500 MHz): δ = 1.33 (s, 9H, C(CH₃)₃), 1.34 (s, 12H, CH₃(Bpin)), 7.41 (d, J =8.5 Hz, 2H, H_{ar}-2, H_{ar}-6), 7.77 (d, J =8.5 Hz, 2H, H_{ar}-3, H_{ar}-5) ppm.

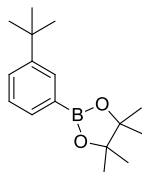
¹³C-NMR (CDCl₃, 100 MHz): δ = 24.9 (CH₃ (Bpin)), 31.3 (C-CH₃), 34.9 (C-CH₃), 83.7 (C-O), 124.8 (C_{ar}), 134.8 (C_{ar}), 154.6 (C_{ar}-4) ppm.

¹¹B-NMR (CDCl₃, 500MHz)): δ = 30.2 ppm.

GC-MS retention time = 9.5 min

13.1.1.2 2-(3-(*tert*-butyl)phenyl)-4,4,5,5-tetramethyl-1,3,2-dioxaborolane (67a)

(CCT 1062)



The reaction was carried out following general procedure I.

Purification by column chromatography (SiO₂, hexane/diethylether = 1/0→19/1), colorless crystalline powder (224 mg, 0.86 mmol, 43%).

¹H-NMR (CDCl₃, 500 MHz): δ = 1.40 (s, 12H, CH₃ (Bpin)), 1.41 (s, 9H, C(CH₃)₃), 7.38 (t, J =7.5 Hz, 1H, H_{ar}-5), 7.57 (d, J =7.8 Hz, 1H, H_{ar}-4), 7.71 (d, J =7.2 Hz, 1H, H_{ar}-6), 7.91 (s, 1H, H_{ar}-2) ppm.

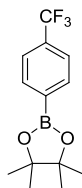
¹³C-NMR (CDCl₃, 100 MHz): δ = 25.0 (CH₃ (Bpin)), 31.6 (C(CH₃)₃), 34.8 (C(CH₃)), 83.8 (C-O), 127.6 (C_{ar}), 128.5 (C_{ar}), 131.5 (C_{ar}), 132.2 (C_{ar}), 150.3 (C_{ar}-3) ppm.

¹¹B-NMR (CDCl₃, 500MHz)): δ = 31.2 ppm.

GC-MS retention time = 9.1 min

13.1.1.3 **4,4,5,5-tetramethyl-2-(4-(trifluoromethyl)phenyl)-1,3,2-dioxaborolane (68b)**

(CCT 1064)



The reaction was carried out following general procedure I.

Purification by column chromatography (SiO₂, hexane/diethylether = 1/0→9/1→19/1→9/1), colorless crystalline powder (153 mg, 0.564 mmol, 28%).

The ¹H-NMR data is in accordance with these reported in literature.^[162]

¹H-NMR (CDCl₃, 500 MHz): δ = 1.36 (s, 12H, CH₃), 7.62 (d, *J*=7.8 Hz, 2H, H_{ar}-3, H_{ar}-5), 7.92 (d, *J*=7.8 Hz, 2H, H_{ar}-2, H_{ar}-6) ppm.

¹³C-NMR (CDCl₃, 100 MHz): δ = 24.9 (CH₃ (Bpin)), 84.3 (C-O), 124.2 (q, *J*^{CF}=273 Hz, CF₃), 124.4 (q, *J*^{CF}=4 Hz, C_{ar}-3, C_{ar}-5), 132.8 (q, *J*^{CF}=33 Hz, C_{ar}-4), 135.1 (C_{ar}) ppm.

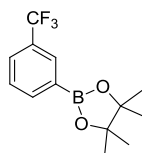
¹¹B-NMR (CDCl₃, 500MHz): δ = 29.9 ppm.

¹⁹F-NMR (CDCl₃, 500MHz): δ = -63.1 ppm.

GC-MS retention time = 7.2 min

13.1.1.4 **4,4,5,5-tetramethyl-2-(3-(trifluoromethyl)phenyl)-1,3,2-dioxaborolane (67b)**

(CCT 1065)



The reaction was carried out following general procedure I.

Purification by column chromatography (SiO₂, hexane/diethylether = 1/0→9/1→19/1), colorless oil (95 mg, 0.350 mmol, 17%).

The ¹H-NMR data is in accordance with these reported in literature.^[162]

¹H-NMR (CDCl₃, 500 MHz): δ = 1.36 (s, 12H, CH₃), 7.49 (t, *J*=7.8 Hz, 1H, H_{ar}-5), 7.70 (d, *J*=7.8 Hz, 1H, H_{ar}-4), 7.99 (d, *J*=7.5 Hz, 1H, H_{ar}-6), 8.08 (s, 1H, H_{ar}-2) ppm.

¹³C-NMR (CDCl₃, 100 MHz): δ = 24.9 (CH₃ (Bpin)), 84.3 (C-O), 124.8 (q, *J*^{CF}=270 Hz, CF₃), 127.8 (q, *J*^{CF}=3 Hz, C_{ar}-2, C_{ar}-4), 130.1 (q, *J*^{CF}=33 Hz, C_{ar}-3), 131.4 (C_{ar}), 138.1 (C_{ar}) ppm.

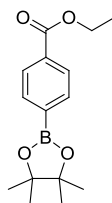
¹¹B-NMR (CDCl₃, 500MHz): δ = 29.3 ppm.

¹⁹F-NMR (CDCl₃, 500MHz): δ = -62.7 ppm.

GC-MS retention time = 7.2 min

13.1.1.5 ethyl 4-(4,4,5,5-tetramethyl-1,3,2-dioxaborolan-2-yl)benzoate (68c)

(CCT 1066)



The reaction was carried out following general procedure I.

Purification by column chromatography (SiO₂, hexane/dieethylether = 1/0→19/1→10/1), colorless oil (265 mg, 0.962 mmol, 48%).

The ¹H-NMR data is in accordance with these reported in literature.^[162]

¹H-NMR (CDCl₃, 500 MHz): δ = 1.29 (s, 12H, CH₃ (Bpin)), 1.34 (t, *J*=7.2 Hz, 3H, CH₂-CH₃), 4.32 (q, *J*=7.2 Hz, 2H, CH₂-CH₃), 7.83 (d, *J*=8.2 Hz, 2H, H_{ar}-2, H_{ar}-6), 7.98 (d, *J*=8.2 Hz, 2H, H_{ar}-3, H_{ar}-5) ppm.

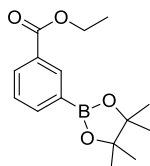
¹³C-NMR (CDCl₃, 100 MHz): δ = 14.4 (CH₂-CH₃), 24.9 (CH₃ (Bpin)), 61.0 (CH₂-CH₃), 84.1 (C-O (Bpin)), 128.6 (C_{ar}), 132.7 (C_{ar}-4), 134.9 (C_{ar}), 166.6 (CO) ppm.

¹¹B-NMR (CDCl₃, 500MHz)): δ = 29.3 ppm.

GC-MS retention time = 10.4 min

13.1.1.6 ethyl 3-(4,4,5,5-tetramethyl-1,3,2-dioxaborolan-2-yl)benzoate (67c)

(2144)



The reaction was carried out following general procedure I.

Purification by column chromatography (SiO₂, hexane/dieethylether = 1/0→49/1→19/1→10/1), colorless oil (56 mg, 0.20 mmol, 10%).

The ¹H-NMR data is in accordance with these reported in literature.^[162]

¹H-NMR (CDCl₃, 500 MHz): δ = 1.35 (s, 12H, CH₃ (Bpin)), 1.41 (t, *J*=7.2 Hz, 3H, CH₂-CH₃), 4.38 (q, *J*=7.2 Hz, 2H, CH₂-CH₃), 7.44 (t, *J*=7.8 Hz, 1H, H_{ar}-5), 7.98 (d, *J*=7.5 Hz, 1H, H_{ar}-6), 8.13 (d, *J*=7.8 Hz, 1H, H_{ar}-2), 8.46 (s, 1H, H_{ar}-2) ppm.

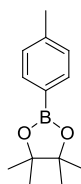
¹³C-NMR (CDCl₃, 100 MHz): δ = 14.5 (CH₂-CH₃), 24.9 (CH₃ (Bpin)), 61.1 (C-O (Bpin)), 127.8 (C_{ar}), 130.0 (C_{ar}-3), 132.1 (C_{ar}), 135.8 (C_{ar}), 139.2 (C_{ar}), 166.8 (CO) ppm.

¹¹B-NMR (CDCl₃, 500MHz)): δ = 30.6 ppm.

GC-MS retention time = 10.4 min

13.1.1.7 **4,4,5,5-tetramethyl-2-(p-tolyl)-1,3,2-dioxaborolane (68d)**

(2136)



The reaction was carried out following general procedure I.

The $^1\text{H-NMR}$ data is in accordance with these reported in literature.^[162]

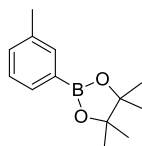
$^1\text{H-NMR}$ (CDCl_3 , 500 MHz): $\delta = 1.38$ (s, 12H, CH_3 (Bpin)), 2.41 (s, 3H, CH_3 (tol)), 7.24 (d, $J=7.8$ Hz, 2H, $\text{H}_{\text{ar-2}}$, $\text{H}_{\text{ar-6}}$), 7.78 (d, $J=7.8$ Hz, 2H, $\text{H}_{\text{ar-3}}$, $\text{H}_{\text{ar-5}}$) ppm.

$^{13}\text{C-NMR}$ (CDCl_3 , 100 MHz): $\delta = 21.9$ (CH_3 (tol)), 25.0 (CH_3 (Bpin)), 83.7 (C-O), 128.7 (C_{ar}), 134.9 (C_{ar}), 141.5 ($\text{C}_{\text{ar-4}}$) ppm.

$^{11}\text{B-NMR}$ (CDCl_3 , 500MHz): $\delta = 30.4$ ppm.

GC-MS retention time = 8.1 min

13.1.1.8 **4,4,5,5-tetramethyl-2-(m-tolyl)-1,3,2-dioxaborolane (67d)**



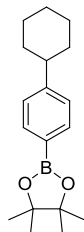
The reaction was carried out following general procedure I.

The $^1\text{H-NMR}$ data is in accordance with these reported in literature.^[162]

$^1\text{H-NMR}$ (CDCl_3 , 400 MHz): $\delta = 1.35$ (s, 12H, CH_3 (Bpin)), 2.36 (s, 3H, CH_3 (tol)), 7.26-7.29 (m, 2H, $\text{H}_{\text{ar-2}}$, $\text{H}_{\text{ar-6}}$), 7.61-7.65 (m, 2H, $\text{H}_{\text{ar-4}}$, $\text{H}_{\text{ar-5}}$) ppm.

13.1.1.9 **2-(4-cyclohexylphenyl)-4,4,5,5-tetramethyl-1,3,2-dioxaborolane (68e)**

(2138)



The reaction was carried out following general procedure I.

Purification by column chromatography (SiO_2 , hexane/diethylether = 1/0 \rightarrow 24/1), colorless powder (296 mg, 1.03 mmol, 52%).

¹H-NMR (CDCl₃, 500 MHz): δ = 1.40 (s, 12H, CH₃), 1.42-1.53 (m, 5H, CH₂), 1.80-1.95 (m, 5H, CH₂), 2.56-2.61 (m, 1H, CH), 7.31 (d, J =7.8 Hz, 2H, H_{ar}-3, H_{ar}-5), 7.85 (d, J =7.8 Hz, 2H, H_{ar}-2, H_{ar}-6) ppm.

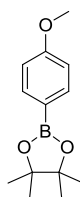
¹³C-NMR (CDCl₃, 100 MHz): δ = 25.0 (CH₃), 26.4 (C-4'), 27.0 (C-3', C-5'), 34.5 (C-2', C'-6'), 45.0 (CH), 83.7 (C-O), 126.5 (C_{ar}-3, C_{ar}-5), 135.1 (C_{ar}-2, C_{ar}-6), 151.6 (C_{ar}-4) ppm.

¹¹B-NMR (CDCl₃, 500MHz): δ = 29.8 ppm.

GC-MS retention time = 11.5 min

13.1.1.10 2-(4-methoxyphenyl)-4,4,5,5-tetramethyl-1,3,2-dioxaborolane (68f)

(2146)



The reaction was carried out following general procedure I.

Purification by column chromatography (SiO₂, hexane/dieethylether = 1/0→49/1→19/1→10/1), colorless oil (302 mg, 1.29 mmol, 65%).

The ¹H-NMR data is in accordance with these reported in literature.^[162]

¹H-NMR (CDCl₃, 500 MHz): δ = 1.34 (s, 12H, CH₃(Bpin)), 3.80 (s, 3H, OCH₃), 6.91 (d, J =8.9 Hz, H_{ar}-2, H_{ar}-6), 7.80 (d, J =8.9 Hz, H_{ar}-3, H_{ar}-5) ppm.

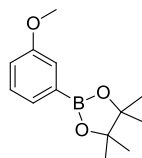
¹³C-NMR (CDCl₃, 100 MHz): δ = 25.0 (CH₃(Bpin)), 55.0 (O-CH₃), 83.6 (C-O), 113.4 (C_{ar}), 136.7 (C_{ar}), 162.3 (C_{ar}-4) ppm.

¹¹B-NMR (CDCl₃, 500MHz): δ = 29.3 ppm.

GC-MS retention time = 9.1 min

13.1.1.11 2-(3-methoxyphenyl)-4,4,5,5-tetramethyl-1,3,2-dioxaborolane (67f)

(2142)



The reaction was carried out following general procedure I.

Purification by column chromatography (SiO₂, hexane/dieethylether = 1/0→49/1→19/1→10/1), colorless oil (179 mg, 0.76 mmol, 38%).

The ¹H-NMR data is in accordance with these reported in literature.^[162]

¹H-NMR (CDCl₃, 500 MHz): δ = 1.36 (s, 12H, CH₃(Bpin)), 3.84 (s, 3H, OCH₃), 7.02 (dd, J =8.2, 2.7 Hz, 1H, H_{ar}), 7.33 (t, J =7.5 Hz, 1H, H_{ar}), 7.37 (d, J =2.4 Hz, 1H, H_{ar}), 7.44 (d, J =7.2 Hz, H_{ar}) ppm.

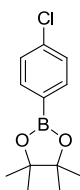
¹³C-NMR (CDCl₃, 100 MHz): δ = 25.1 (CH₃ (Bpin)), 55.3 (OCH₃), 83.9 (C-O), 117.96 (C_{ar}), 118.9 (C_{ar}), 127.3 (C_{ar}), 129.1 (C_{ar}), 159.2 (C_{ar}-3) ppm.

¹¹B-NMR (CDCl₃, 500MHz): δ = 30.4 ppm.

GC-MS retention time = 8.9 min

13.1.2 2-(4-chlorophenyl)-4,4,5,5-tetramethyl-1,3,2-dioxaborolane (68g)

(2150)



The reaction was carried out following general procedure I.

Purification by column chromatography (SiO₂, hexane/diethylether = 1/0→99/1→97/3→19/1), colorless crystalline powder (180 mg, 0.54 mmol, 27%).

The ¹H-NMR data is in accordance with these reported in literature.^[251]

¹H-NMR (CDCl₃, 500 MHz): δ = 1.33 (s, 12H, CH₃), 7.34 (d, J =8.2 Hz, 2H, H_{ar}-2, H_{ar}-6), 7.74 (d, J =8.2 Hz, 2H, H_{ar}-3, H_{ar}-5) ppm.

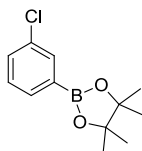
¹³C-NMR (CDCl₃, 100 MHz): δ = 24.9 (CH₃), 84.1 (C-O), 128.1 (C_{ar}), 136.3 (C_{ar}), 137.6 (C_{ar}-4) ppm.

¹¹B-NMR (CDCl₃, 500MHz): δ = 30.5 ppm.

GC-MS retention time = 8.6 min

13.1.2.1 2-(3-chlorophenyl)-4,4,5,5-tetramethyl-1,3,2-dioxaborolane (67g)

(2150)



The reaction was carried out following general procedure I.

Purification by column chromatography (SiO₂, hexane/diethylether = 1/0→99/1→97/3→19/1), colorless oil (60 mg, 0.18 mmol, 9%).

The ¹H-NMR data is in accordance with these reported in literature.^[252]

$^1\text{H-NMR}$ (CDCl_3 , 500 MHz): $\delta = 1.35$ (s, 12H, CH_3), 7.31 (t, $J=7.8$ Hz, 1H, H_{ar}), 7.42 (d, $J=7.8$ Hz, 1H, H_{ar}), 7.67 (d, $J=7.5$ Hz, 1H, H_{ar}), 7.79 (s, 1H, H_{ar}) ppm.

$^{13}\text{C-NMR}$ (CDCl_3 , 100 MHz): $\delta = 24.9$ (CH_3), 84.2 (C-O), 129.2 (C_{ar}), 131.3 (C_{ar}), 132.7 (C_{ar}), 134.1 ($\text{C}_{\text{ar}}-3$), 134.6 (C_{ar}) ppm.

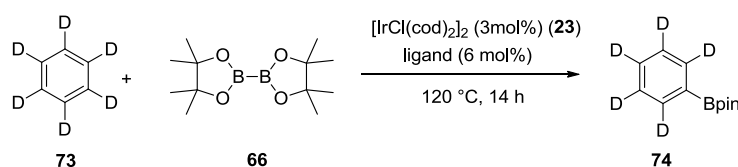
$^{11}\text{B-NMR}$ (CDCl_3 , 500MHz): $\delta = 30.8$ ppm.

GC-MS retention time = 8.6 min

13.1.3 Borylation Experiments

13.1.3.1 Borylation of C_6D_6

(2056)



In an argon filled glovebox a NMR-tube was charged with bispinacolatodiboron (**66**) (30 mg, 0.11 mmol), $[\text{IrCl}(\text{cod})_2]_2$ (**23**) (2.3 mg, 0.003 mmol, 0.03 equiv.) and the ligand (0.006 mmol, 0.06 equiv.); 4,4'-di-*tert*-butyl-2,2'-bipyridine (**32**) (1.8 mg) or (4*S*,4'*S*)-4,4'-diisopropyl-4,4',5,5'-tetrahydro-2,2'-bioxazole (**5g**) (1.5 mg). The components were dissolved in C_6D_6 (1 mL, 11.2 mmol). The reaction was carried out in the sealed NMR tube at 120°C for 14 h. After cooling down to room temperature, $^{11}\text{B-NMR}$ and $^1\text{H-NMR}$ spectra were measured from the sealed tube. After these measurements the NMR tube was opened and a small amount of the crude reaction mixture was taken for GC analysis.

GC method: Carrier gas: Helium
 Temperature (column): 80°C (hold 2.5 min), $80 \rightarrow 280^\circ\text{C}$ (rate $20^\circ\text{C}/\text{min}$)
 Temperature (injection): 300°C
 Column Flow: 1.0 mL/min
 Split Ratio: 10% (initial), 100% (0.01 min \rightarrow 1.00 min), 40% (1.00 \rightarrow end)
 Column: Capillary Column (VF-5ms, 5% phenyl, 95% dimethylpoysiloxane, 30 x 0.25 mm, $D_f = 0.25 \mu\text{m}$, CP-8944)

Analytical data for $\text{B}_{2\text{pin}}_2$

$^1\text{H-NMR}$ (C_6D_6 , 400 MHz): $\delta = 1.01$

$^{11}\text{B-NMR}$ (C_6D_6 , 400MHz): $\delta = 30.4$

GC: retention time = 8.7 min

Analytical data for 4-(pinacolatoboron)-benzene-d₅¹H-NMR (C₆D₆, 400 MHz): δ = 1.11¹¹B-NMR (C₆D₆, 400MHz): δ = 30.2

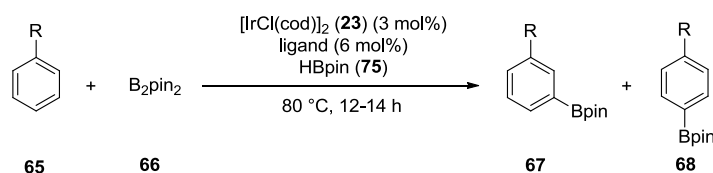
GC: retention time = 7.4 min

Results:

In both reactions almost full conversion of B₂pin₂ (**66**) to PhBpin (**74**) was observed by ¹H-NMR. The identity of the product was confirmed by ¹¹B-NMR and GC-MS.

13.1.3.2 Borylation of Monosubstituted Arenes Using [Ir(cod)Cl] (23**) as Iridium Source**

(GM 1058, 1060, 1064)



In an argon filled glove-box B₂pin₂ (**66**) (50 mg, 19.7 mmol), HBpin (**75**) (1.51 mg, 6 mol%), [IrCl(cod)]₂ (**23**) (3.97 mg, 3 mol%) and the ligand (6 mol%) were weighed/added into a NMR tube and the liquid substrate was added (1 mL). Outside the glove box, the tube was flame-sealed and heated to 80 °C (oil bath) for 12-14 h. After cooling to room temperature an ¹¹B-NMR spectrum was measured from the sealed tube. Afterwards the tube was opened and the volatile compounds of the reaction mixture were removed in high vacuum over night. The solid residue was dissolved in CDCl₃ and filtered over a small amount of celite (fixed by cotton wool in a pipette). Subsequently, ¹H-NMR analysis of the filtrate was undertaken.

It was not possible to identify residual B₂pin₂ in the ¹¹B-NMR spectra, because its signal at 29.0 ppm had approximately the same shift as these from the borylation product **67** and **68**.

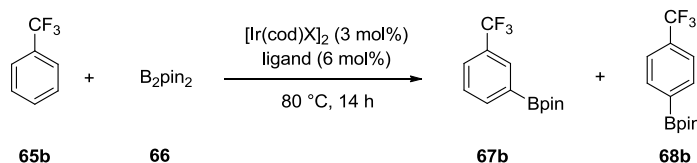
HBpin (**75**) was in the ¹¹B-NMR spectrum identified at 25.9 ppm.

Results:

Entry	R	¹ H-NMR signals used for analysis [ppm]	Ligand	m(ligand) [mg]	m:p - ratio	HBpin
1	Me	7.61-7.64 (m, 2H, <i>meta</i> -H _{ar})	dtbpy (32)	3.17	2.0:1.0	×
2	Me	7.71 (d, 2H, <i>para</i> -H _{ar})	ⁱ Pr-box (5b)	2.65	2.0:1.0	×
3	Me		^t Bu-box (5c)	2.98	2.0:1.0	×
4	Me		^{sec} Bu-box (5d)	2.98	2.0:1.0	×
5	Me		Ph-box (5g)	2.76	2.0:1.0	×
6	Cl	7.66 (d, 2H, <i>para</i> -H _{ar})	dtbpy(32)	3.17	3.3:1.0	×
7	Cl	7.72 (d, 1H, <i>meta</i> -H _{ar})	ⁱ Pr-box (5b)	2.65	3.3:1.0	×
8	Cl		^t Bu-box (5c)	2.98	3.6:1.0	×
9	Cl		^{sec} Bu-box (5d)	2.98	3.6:1.0	×
10	Cl		Ph-box (5g)	2.76	3.0:1.0	×
11	CF ₃	7.90 (d, 2H, <i>para</i> -H _{ar})	dtbpy(32)	3.17	2.6: 1.0	×
12	CF ₃	7.97 (d, 1H, <i>meta</i> -H _{ar})	ⁱ Pr-box (5b)	2.65	2.6: 1.0	×
13	CF ₃		^t Bu-box (5c)	2.98	2.7: 1.0	×
14	CF ₃		^{sec} Bu-box (5d)	2.98	3.4: 1.0	×
15	CF ₃		Ph-box (5g)	2.76	2.2: 1.0	×

13.1.3.3 Optimization of the Catalytic System

(3124, 3134)



In an argon filled glove-box B₂pin₂ (**66**) (50.0 mg, 0.197 mmol), the iridium precursor (0.0059 mmol), the ligand (0.0118 mmol) were added/weighed into a NMR tube. The solvent/substrate mixture was added and the tube was flame-sealed. The tubes were heated to 80 °C for 14 h. After cooling to room temperature, the tubes were opened and the content quantitatively transferred into a small flask and 1,2,3-trimethoxybenzene (**80**) (4.03 mg, 0.0234 mmol). The volatile compounds were removed under high vacuum over night and the solid residue dissolved in CDCl₃. The solution was used for ¹H-NMR analysis.

Applied Amounts:

[Ir]	Ligand	Amount [mg]
[Ir(cod)Cl] ₂ (23)		3.69
[Ir(cod)OMe] ₂ (79)		2.77
	dtbpy (32)	3.17
	H-box (5i)	1.65
	ⁿ Bu-box (5g)	2.98

As solvent either 1.5 mL neat substrate (**65**) or 1.5 mL of a 1:2 mixture substrate (**65**):cyclohexane (**78**) (v/v) was applied.

¹H-NMR signals used for yield calculation:

Substance	Relevant Chemical Shift [pm]
1,2,3-trimethoxybenzene (80)	6.09 (s, 3H, H _{ar})
<i>m</i> -CF ₃ -Ph-Bpin (67b)	7.97 (d, 1H, H _{ar})
<i>p</i> -CF ₃ -Ph-Bpin (68b)	7.90 (d, 2H, H _{ar})

Entry	Ligand	X	Solvent	Yield [%]	meta [%]	para [%]	m:p - ratio
1	dtbpy (32)	Cl	-	78	60	18	3.2:1.0
2	dtbpy (32)	Cl	CHex (78)	91	69	22	3.2:1.0
3	dtbpy (32)	OMe	-	76	57	19	3.2:1.0
4	dtbpy (32)	OMe	CHex (78)	47	36	11	3.3:1.0
5	H-box (5i)	Cl	CHex (78)	14	10	4	2.5:1.0
6	H-box (5i)	OMe	-	72	51	21	2.5:1.0
7	H-box (5i)	OMe	CHex (78)	49	35	14	2.4:1.0
8	ⁿ Bu-box (5f)	Cl	CHex (78)	30	24	6	4.0:1.0
9	ⁿ Bu-box (5f)	OMe	-	34	26	8	3.3:1.0
10	ⁿ Bu-box (5f)	OMe	CHex (78)	34	26	8	3.3:1.0

13.1.3.4 Borylation of PhCF₃ (65b**) at 80 °C**

(4058, 4060, 4062, 4064, 4066, 4068, 4090)



In an argon filled glove box, [Ir(cod)(OMe)]₂ (**79**) (2.77 mg, 0.0059 mmol, 3 mol% or 0.46 mg, 0.00069 mmol, 0.35 mol%), B₂pin₂ (**66**) (50.0 mg, 0.197 mmol), and the ligand were into a NMR tube and trifluorotoluene (**65b**) (1.0 mL) was added. Outside the box, the tube was flame-sealed and heated to 80 °C (oil bath) for 12-14 h. After cooling to room temperature, an ¹¹B-NMR spectrum of the sealed tube was measured. The tube was opened and quantitatively transferred into a small vial. The standard *n*-dodecane was added, the mixture well mixed and subsequently filtered over celite (a small amount of celite was fixed by cotton wool in a pipette) and a volume of 0.1 mL of the filtrate was used for GC measurements (diluted with 0.9 mL hexane). The rest of the filtrate was transferred into a small flask and the volatile compounds were removed under high vacuum over night. The resulting solid was dissolved in CDCl₃ and a ¹H-NMR spectrum was measured.

Results for box, pyrox, mepyrox and quinox ligands (4058, 4060, 4062, 4064, 4090):

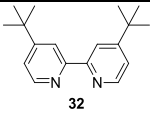
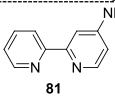
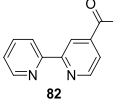
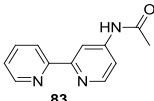
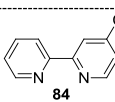
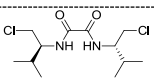
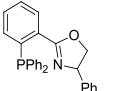
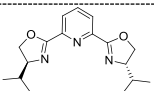
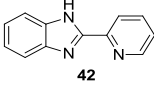
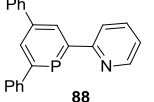
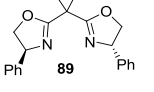
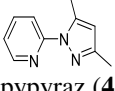


Entry	Ligand	M (ligand) [mg]	Cat.-loading [mol%]	<i>m:p</i> -ratio	Conv. [%]	HBpin
1	ⁱ Pr-pyrox (10b)	2.25	3	3.0 : 1	100	-
2	Ph-pyrox (10g)	2.65	3	3.0 : 1 ^d	100	-
3	ⁿ Bu-pyrox (10f)	2.98	3	3.8 : 1	100	-
4	Bn-pyrox (10h)	3.78	3	4.0 : 1	100	-
5	ⁱ Pr-mepyrox (19b)	2.41	3	2.7 : 1	100	-
6	Ph-mepyrox (19g)	2.82	3	2.8 : 1	100	-
7	ⁿ Bu-pyrox (19f)	2.58	3	3.8 : 1	100	-
8	Bn-pyrox (19h)	2.98	3	3.3 : 1	100	-
9	ⁱ Pr-quinox (20b)	2.84	3	4.3 : 1	100	-
11	ⁱ Pr-quinox (20b)	0.47	0.35	3.6 : 1 ^b	100	-
12	Ph-quinox (20g)	3.24	3	2.6 : 1	100	-
13	ⁿ Bu-quinox (20h)	3.00	3	3.3 : 1	100	-
14	ⁱ Pr-box (5b)	2.65	3	3.7 : 1	100	-
15	ⁱ Pr-box (5b)	0.44	0.35	3.8 : 1	87	×
16	Ph-box (5g)	3.45	3	2.1 : 1	100	×
17	^t Bu-box (5c)	2.98	3	3.1 : 1	94	×
18	ⁱ Bu-box (5e)	2.98	3	3.5 : 1	100	-
19	ⁿ Bu-box (5f)	2.98	3	3.0 : 1	100	×
20	Bn-box (5h)	3.78	3	3.2 : 1	100	-
21	H-box (5i)	1.65	3	2.9 : 1	100	-
22	Me-box (5a)	1.98	3	3.4 : 1	100	×
23	^{sec} Bu-box (5d)	2.98	3	3.3 : 1	99	-

^aLow signal intensity. ^b¹H-NMR shows impurities in the aromatic region.

Experimental Section

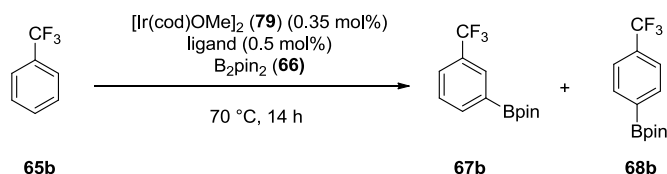
Results for further ligands (4066, 4068, 4090)(Cat.-loading was always 3 mol%):

Entry	Ligand	m(ligand) [mg]	m:p - ratio	Conv. [%]	HBpin
1	 32 dtbpy	3.16	3.0 : 1 ^b	100	-
2	 81	2.02	3.3 : 1 ^b	100	-
3	 82	2.53	2.5 : 1	100	-
4	 83	2.52	3.2 : 1	100	-
5	 84	2.14	2.7 : 1 ^b	100	-
6	 <i>i</i> Pr-dichloride (85)	-	-	52	×
7	Ph-dichloride (86)	-	2.3 : 1 ^a	59	×
8	ⁿ Bu-dichloride (87)	-	2.3 : 1 ^a	54	×
9	 Ph-phox (40)	-	2.0 : 1 ^a	76	×
10	 <i>i</i> Pr-pybox (36)	-	3.1 : 1	100	-
11	 42	-	2.7 : 1	100	-
12	 88	-	2.7 : 1 ^c	32	×
13	 89	-	2.4 : 1	90	×
14	 pypyraz (41)	-	3.2 : 1	100	-
15	-	-	-	17	-

^aLow signal intensity. ^{b1}H.NMR shows impurities in the aromatic region.

13.1.3.5 Borylation of PhCF₃ (**65b**) at 70 °C

(4106)



In an argon filled glove box, [Ir(cod)(OMe)]₂ (**79**) (0.46 mg, 0.00069 mmol), B₂pin₂ (**66**) (50.0 mg, 0.197 mmol), and the ligand (0.0099 mmol) were into a NMR tube and trifluorotoluene (**65b**) (0.8 mL) was added. Outside the box, the tube was flame-sealed and heated to 70 °C (oil bath) for 14 h. After cooling, an ¹¹B-NMR spectrum of the sealed tube was measured. The tube was opened and quantitatively transferred into a small vial. The standard *n*-dodecane was added, the mixture well mixed and subsequently filtered over celite (a small amount of celite was fixed by cotton wool in a pipette) and a volume of 0.1 mL of the filtrate was used for GC measurements (diluted with 0.9 mL hexane). The rest of the filtrate was transferred into a small flask and the volatile compounds were removed under high vacuum over night. The resulting solid was dissolved in CDCl₃ and a ¹H-NMR spectrum was measured.

GC-FID

GC-FID method: Carrier gas: Nitrogen
 Temperature (detector): 300 °C
 Temperature (column): 100 °C (hold 20 min)
 Temperature (injection): 270 °C
 Column Flow: 1.0 mL/min
 Split Ratio: 50%

Column: Capillary Column Agilent J&W (CP-Sil 5 CB 30 m x 0.25 mm)

Retention times: 4.4 min (standard); 9.4 min (*p*-CF₃-Ph); 9.6 min (*m*-CF₃-Ph),
 12.6 min (B₂pin₂)

Calibration (5051): product[%]=61.2 × [(Int. product)/(Int. standard)]
 Calibration (4070): starting material[%]=70.85 × [(Int. starting material)/(Int. standard)]

¹H-NMR (peaks used for determination of *m*:*p* – ratio)

7.97 (d, 1H, H_{ar}) / *m*-CF₃-Ph-Bpin (**67b**)

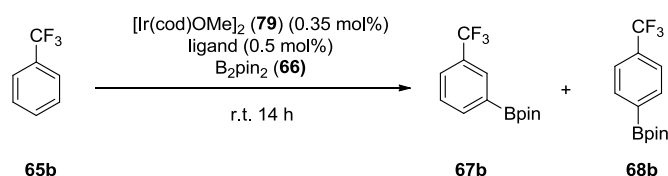
7.90 (d, 2H, H_{ar}) / *p*-CF₃-Ph-Bpin (**68b**)

¹¹B-NMRHBpin (**75**): 25.9 ppm.**Results and used amount of ligands:**

Entry	Ligand	M(ligand) [mg]	meta:para-ratio ^b	Conv. [%] ^c	Yield [%] ^c	HBpin ^d
1	ⁿ Bu-pyrox (10f)	0.36	3.3 : 1.0	100	87	-
2	ⁿ Bu-mepyrox (19f)	0.43	2.8 : 1.0	100	87	-
3	ⁿ Bu-quiniox (20f)	0.43	2.8 : 1.0	99	80	×
4	ⁿ Bu-box (5f)	0.50	2.6 : 1.0	84	28	×
5	ⁱ Pr-box (5b)	0.44	2.7 : 1.0	79	34	×
6	ⁱ Pr-quiniox (20b)	0.47	2.7 : 1.0	100	86	-
7	Ph-box (5g)	0.58	2.0 : 1.0	90	42	×
8	^{sec} Bu-box (5d)	0.43	2.9 : 1.0	96	52	×
9	H-box (5i)	0.28	2.5 : 1.0	100	33	×
10	ⁱ Pr-pyrox (10b)	0.38	3.0 : 1.0	100	84	-
11	ⁱ Pr-mepyrox (19b)	0.40	3.0 : 1.0	100	81	-
12	ⁱ Pr-pybox (36)	0.59	2.3 : 1.0	100	79	×

13.1.3.6 Borylation of PhCF₃ (**65b**) at Room Temperature

(4118)



In an argon filled glove box, [Ir(cod)(OMe)₂] (**79**) (0.46 mg, 0.00069 mmol), B₂pin₂ (**66**) (50.0 mg, 0.197 mmol), and the ligand (0.0099 mmol) were into a small reaction vial and trifluorotoluene (**65b**) (0.8 mL) was added. The reaction mixture was left stirring at room temperature for 14 h. Afterwards, the standard *n*-dodecane was added, the mixture well mixed and transferred into a NMR tube without loss of substance. An ¹¹B-NMR was measured and subsequently the mixture was filtered over celite (a small amount of celite was fixed by cotton wool in a pipette) and a volume of 0.1 mL of the filtrate was used for GC measurements (diluted with 0.9 mL hexane). The rest of the filtrate was transferred into a small flask and the volatile compounds were removed under high vacuum over night. The resulting solid was dissolved in CDCl₃ and a ¹H-NMR spectrum was measured.

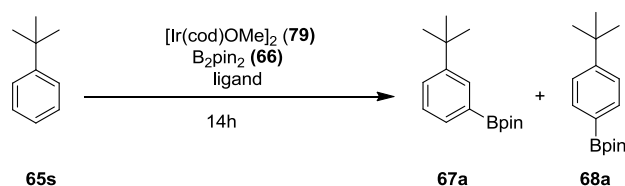
Analysis (see 13.1.3.5)

Results and used amount of ligands:

Entry	Ligand	M(ligand) [mg]	meta:para-ratio ^b	Conv. [%] ^c	Yield [%] ^c	HBpin ^d
1	ⁿ Bu-pyrox(10f)	0.36	3.5 : 1.0	90	31	-
2	ⁱ Pr-pyrox (10b)	0.38	3.5 : 1.0	99	45	-

13.1.3.7 Borylation of *tert*-butyl-benzene (65a**)**

(4116, SP 1002, 1004, 1010, 1012, 1022, 1024)



In an argon filled glove box, $[\text{Ir}(\text{cod})(\text{OMe})_2]$ (**79**), B_2pin_2 (**66**) (50.0 mg, 0.197 mmol), and the ligand were into a NMR tube and trifluorotoluene (**65a**) (0.8 mL) was added. Outside the box, the tube was flame-sealed and heated to 70 °C (oil bath) for 14 h. After cooling, an ^{11}B -NMR spectrum of the sealed tube was measured. The tube was opened and quantitatively transferred into a small vial. The standard *n*-dodecane was added, the mixture well mixed and subsequently filtered over celite (a small amount of celite was fixed by cotton wool in a pipette) and a volume of 0.1 mL of the filtrate was used for GC measurements (diluted with 0.9 mL hexane). The rest of the filtrate was transferred into a small flask and the volatile compounds were removed under high vacuum over night. The resulting solid was dissolved in CDCl_3 and a ^1H -NMR spectrum was measured.

Applied Amounts:

[Ir]	Ligand	m [mg]	n [mmol]
$[\text{Ir}(\text{cod})\text{OMe}]_2$ (79)		A 2.77	0.00407 (2.1 mol%)
		B 0.46	0.00069 (0.35 mol%)
	dtbpy (32)	A 2.21	0.00820
		B 0.53	0.00200
	ⁿ Bu-pyrox (10f)	A 1.70	0.00820
		B 0.40	0.00200
	ⁿ Bu-mepyrox (19f)	A 1.79	0.00820
		B 0.44	0.00200
	ⁿ Bu-quinox (Rf)	A 2.10	0.00820
		B 0.51	0.00200
	ⁿ Bu-box (5f)	A 2.06	0.00820

Experimental Section

	B 0.49	0.00200
¹ Pr-box (5b)	A 1.84	0.00820
	B 0.44	0.00200
¹ Pr-quinox (20b)	A 1.98	0.00820
	B 0.47	0.00200
Ph-box (5g)	A 2.42	0.00820
	B 0.60	0.00200
H-box (5i)	A 2.33	0.00820
	B 0.28	0.00200
^{sec} Bu-box (5d)	A 0.49	0.00820
	B	0.00200
¹ Pr-pyrox (10b)	A 1.17	0.00820
	B 0.36	0.00200
¹ Pr-mepyrox (19b)	A 1.58	0.00820
	B 0.40	0.00200
¹ Pr-pybox (36)	A 1.58	0.00820
	B 0.60	0.00200

GC-FID

GC-FID method:

Carrier gas: Nitrogen

Temperature (detector): 300 °C

Temperature (column): 100 °C (hold 20 min)

Temperature (injection): 270 °C

Column Flow: 1.0 mL/min

Split Ratio: 50%

Column:

Capillary Column Agilent J&W (CP-Sil 5 CB 30 m x 0.25 mm)

Retention times:

4.4 min (standard);

12.6 min (B₂pin₂)

Calibration (4070):

starting material[%]=70.85 × [(Int. starting material)/(Int. standard)]

¹H-NMR (peaks used for determination of *m:p* – ratio)

7.91 (d, 1H, H_{ar}) / *m*-Ph-Bpin (**37a**)

7.76 (d, 2H, H_{ar}) / *p*-*tert*-butyl-Ph-Bpin (**38a**)

¹¹B-NMRHBpin (**75**): 25.9 ppm.**Results for Catalysis at 70 °C and 2.1 mol% [Ir] (Amounts A).****HBpin was not detected.:**

Entry	Ligand	M:p - ratio	Conv. [%]
1	ⁿ Bu-pyrox (10f)	1.7:1.0	100
2	ⁿ Bu-mepyrox (19f)	0.6:1.0	55
3	ⁿ Bu-quiniox (20f)	1.7:1.0	78
4	ⁿ Bu-box (5f)	1.2:1.0	49
5	ⁱ Pr-box (5b)	1.0:1.0	47
6	ⁱ Pr-quiniox (20b)	2.0:1.0	83
7	Ph-box (5g)	0.1:1.0	64
8	^{sec} Bu-box (5d)	-	98
9	H-box (5i)	0.5:1.0	40
10	ⁱ Pr-pyrox (10b)	1.5:1.0	100
11	ⁱ Pr-mepyrox (19b)	0.1:1.0	63
12	ⁱ Pr-pybox (36)	0.3:1.0	55
13	dtbpy (32)	1.4:1.0	100

Results for Catalysis at 60 °C and 2.1 mol% [Ir] (Amounts A).**HBpin was not detected.:**

Entry	Ligand	m:p - ratio	conv. [%]
1	ⁿ Bu-pyrox (10f)	1.3:1.0	100
2	ⁿ Bu-mepyrox (19f)	2.0:1.0	100
3	ⁿ Bu-quiniox (20f)	0.3:1.0	65
4	ⁿ Bu-box (5f)	0.7:1.0	85
5	ⁱ Pr-box (5b)	0.7:1.0	43
6	ⁱ Pr-quiniox (20b)	0.5:1.0	51
7	Ph-box (5g)	0.8:1.0	80
8	^{sec} Bu-box (5d)	1.6:1.0	40
9	H-box (5i)	0.8:1.0	47

Experimental Section

10	<i>i</i> Pr-pyrox (10b)	0.4:1.0	37
11	<i>i</i> Pr-mepyrox (19b)	0.8:1.0	62
12	<i>i</i> Pr-pybox (36)	1.6:1.0	100
13	dtbpy (32)	1.0:1.0	33

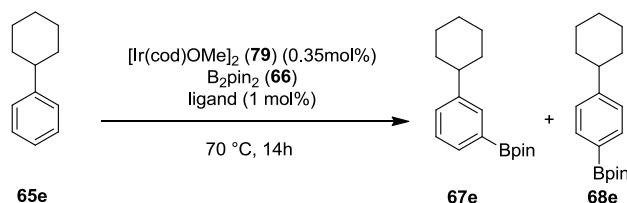
Results for Catalysis at 60 °C and 0.35 mol% [Ir] (Amounts B).

HBpin was dot detected.:

Entry	Ligand	m:p - ratio	Conv. [%]
1	dtbpy (32)	1.3:1.0	100
2	ⁿ Bu-pyrox (10f)	2.0:1.0	100
3	ⁿ Bu-mepyrox (Qf)	0.3:1.0	65
4	ⁿ Bu-quinox (Rf)	0.7:1.0	85
5	ⁿ Bu-box (Ef)	0.7:1.0	43
6	<i>i</i> Pr-box (5b)	0.5:1.0	51
7	<i>i</i> Pr-quinox (20b)	0.8:1.0	80
8	Ph-box (5g)	1.6:1.0	40
9	^{sec} Bu-box (5d)	0.8:1.0	47
10	H-box (5i)	0.4:1.0	37
11	<i>i</i> Pr-pyrox (10b)	0.8:1.0	62
12	<i>i</i> Pr-pyrox (10b)	1.6:1.0	100
13	<i>i</i> Pr-pybox (36)	1.0:1.0	33

13.1.3.8 Borylation of cyclohexylbenzene (**65e**)

(SP 1006, 1008, 1022)



In an argon filled glove box, $[\text{Ir}(\text{cod})(\text{OMe})_2]_2$ (**79**), B_2pin_2 (**66**) (50.0 mg, 0.197 mmol), and the ligand were into a NMR tube and trifluorotoluene (**65e**) (0.8 mL) was added. Outside the box, the tube was flame-sealed and heated to 70 °C (oil bath) for 14 h. After cooling, an ^{11}B -NMR spectrum of the sealed tube was measured. The tube was opened and quantitatively transferred into a small vial. The standard *n*-dodecane was added, the mixture well mixed and subsequently filtered over celite (a small amount of celite was fixed by cotton wool in a pipette) and a volume of 0.1 mL of the filtrate was used for GC measurements (diluted with 0.9 mL hexane). The rest of the filtrate was transferred into a small flask and the volatile compounds were removed under high vacuum over night. The resulting solid was dissolved in CDCl_3 and a ^1H -NMR spectrum was measured.

GC-FID

GC-FID method: Carrier gas: Nitrogen
 Temperature (detector): 300 °C
 Temperature (column): 100 °C (hold 20 min)
 Temperature (injection): 270 °C
 Column Flow: 1.0 mL/min
 Split Ratio: 50%

Column: Capillary Column Agilent J&W (CP-Sil 5 CB 30 m x 0.25 mm)

Retention times: 4.4 min (standard);
 12.6 min (B_2pin_2)

Calibration (4070): starting material[%]=70.85 × [(Int. starting material)/(Int. standard)]

^1H -NMR (peaks used for determination of *m:p* – ratio)

7.66 (d, 1H, H_{ar}) / *m*- -Cy-Bpin (**67e**)

7.74 (d, 2H, H_{ar}) / *p* -Cy-Ph-Bpin (**68e**)

¹¹B-NMR

 HBpin (**75**): 25.9 ppm.

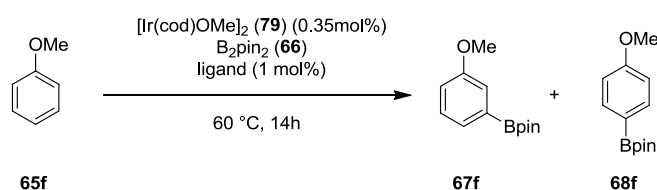
Results for Catalysis at 70 °C and 0.35 mol% [Ir] (Amounts B, see Fehler! Verweisquelle konnte nicht gefunden werden.).

HBpin was dot detected.:

Entry	Ligand	¹¹ B-NMR[ppm]	m/p - ratio	Gonv. [%]
1	ⁿ Bu-pyrox (10f)	27.7, 21.1	15:10	100
2	ⁿ Bu-mepyrox (19f)	27.6, 20.9	-	36
3	ⁿ Bu-quiniox (20f)	27.8, 21.0	-	65
4	ⁿ Bu-box (5f)	27.7, 20.9	14:10	32
5	ⁱ Pr-box (5b)	21.0	-	51
6	ⁱ Pr-quiniox (20b)	27.8, 21.1	8:10	45
7	Ph-box (5g)	21.1	-	76
8	^{sec} Bu-box (5d)	21.1	-	89
9	H-box (5i)	27.7	18:10	46
10	ⁱ Pr-pyrox (10b)	27.6, 21.1	18:10	100
11	ⁱ Pr-mepyrox (19b)	21.1	-	24
12	ⁱ Pr-pybox (36)	27.8, 21.8, 21.1	-	27
13	dtbpy (32)	27.7	14:10	21

 13.1.3.9 Borylation of anisol (**65f**) at Room Temperature

(SP 1028)



In an argon filled glove box, [Ir(cod)(OMe)]₂ (**79**), B₂pin₂ (**66**) (50.0 mg, 0.197 mmol), and the ligand were into a NMR tube and anisol (**65f**) (0.8 mL) was added. Outside the box, the tube was flame-sealed and heated to 70 °C (oil bath) for 14 h. After cooling, an ¹¹B-NMR spectrum of the sealed tube was measured. The tube was opened and quantitatively transferred into a small vial. The standard *n*-dodecane was added, the mixture well mixed and subsequently filtered over celite (a small amount of celite was fixed by cotton wool in a pipette) and a volume of 0.1 mL of the filtrate was used for GC

measurements (diluted with 0.9 mL hexane). The rest of the filtrate was transferred into a small flask and the volatile compounds were removed under high vacuum over night. The resulting solid was dissolved in CDCl_3 and a $^1\text{H-NMR}$ spectrum was measured.

GC-FID:

Method: carrier gas: N_2
 temperature (detektor): 300 °C
 temperature (column): 80 - 280 °C
 temperature (injection): 270 °C
 Column Flow: 1.0 mL/min
 Split Ratio: 0–7 min → 40%, 7–15 min → aus

Column: Capillary Column Agilent J&W (CP-Sil 8 CB 30 m x 0.25 mm)

Retention times: 3.28 min (starting material **65f**); 4.86 min (standard dodecane);
 7.46 min (*m*-product **67f**); 7.61 min (*p*-product **68f**).

Calibration (SP 1044): $\text{product}[\%]=6.51 \times [(\text{Int. product})/(\text{Int. standard})]$

$^1\text{H-NMR}$ (peaks used for determination of *m:p* – ratio)

7.40 (d, 1H, H_{ar}) / *m*-OMe-Bpin (**67f**)

7.76 (d, 2H, H_{ar}) / *p*-OMe-Ph-Bpin (**68f**)

$^{11}\text{B-NMR}$

HBpin (**75**): 25.9 ppm.

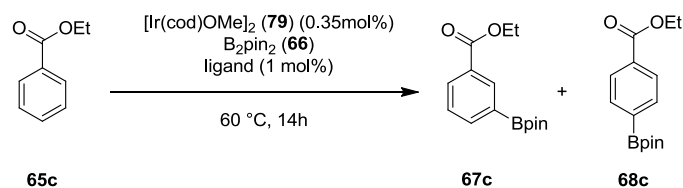
Results for Catalysis at 60 °C and 0.35 mol% [Ir] (Amounts B, see Fehler! Verweisquelle konnte nicht gefunden werden.).

HBpin was dot detected.:

Entry	Ligand	m:p-ratio ($^1\text{H-NMR}$)	m:p – ratio (GC-FID)	Conv. [%]	Yield [%]
1	ⁿ Bu-pyrox (10f)	40:10	41:10	100	15
2	ⁿ Bu-mepyrox (19f)	35:10	39:10	93	8
3	ⁿ Bu-quiniox (20f)	37:10	40:10	56	5
4	ⁱ Pr-quiniox (20b)	40:10	43:10	100	11
5	H-box (5i)	40:10	40:10	77	5
6	dtbpy (32)	32:10	37:10	81	10

13.1.3.10 Borylation of ethylbenzoate (**65c**) at Room Temperature

(1030)



In an argon filled glove box, $[\text{Ir}(\text{cod})(\text{OMe})]_2$ (**79**), B_2pin_2 (**66**) (50.0 mg, 0.197 mmol), and the ligand were into a NMR tube and ethyl benzoate (**65c**) (0.8 mL) was added. Outside the box, the tube was flame-sealed and heated to 70 °C (oil bath) for 14 h. After cooling, an ^{11}B -NMR spectrum of the sealed tube was measured. The tube was opened and quantitatively transferred into a small vial. The standard *n*-dodecane was added, the mixture well mixed and subsequently filtered over celite (a small amount of celite was fixed by cotton wool in a pipette) and a volume of 0.1 mL of the filtrate was used for GC measurements (diluted with 0.9 mL hexane). The rest of the filtrate was transferred into a small flask and the volatile compounds were removed under high vacuum over night. The resulting solid was dissolved in CDCl_3 and a ^1H -NMR spectrum was measured.

GC-FID:

Method:

carrier gas: N_2

temperature (detektor): 300 °C

temperature (column): 80 - 280 °C

temperature (injection): 270 °C

Column Flow: 1.0 mL/min

Split Ratio: 0–7 min → 40%, 7–15 min → aus

Column:

Capillary Column Agilent J&W (CP-Sil 8 CB 30 m x 0.25 mm)

Retention times:

4.78 min (starting material **65c**); 4.86 min (standard dodecane);8.84 min (*m*-product **67c**); 8.97 min (*p*-product **68c**).Calibration (SP 1046): $\text{product}[\%]=6.99 \times [(\text{Int. product})/(\text{Int. standard})]$ ^1H -NMR (peaks used for determination of *m*:*p* – ratio)8.44 (s, 1H, H_{ar}) / *m*-COOEt-Bpin (**67c**)7.85 (d, 2H, H_{ar}) / *p*-COOEt-Ph-Bpin (**68c**) ^{11}B -NMRHBpin (**75**): 25.9 ppm.

Results for Catalysis at 60 °C and 0.35 mol% [Ir] (Amounts B, see Fehler! Verweisquelle konnte nicht gefunden werden.).

HBpin was dot detected.:

Entry	Ligand	m:p-ratio (¹ H-NMR)	m:p – ratio (GC-FID)	Conv. [%]	Yield [%]
1	ⁿ Bu-pyrox (10f)	14:10	14:10	100	11
2	ⁿ Bu-mepyrox (19f)	13:10	14:10	83	8
3	ⁿ Bu-quiniox (20f)	12:10	13:10	100	6
4	ⁱ Pr-quiniox (20b)	16:10	17:10	100	7
5	H-box (5i)	13:10	13:10	100	6
6	dtbpy (32)	13:10	13:10	100	10

13.2 Aliphatic Borylation

13.2.1 Borylation of *n*-Octane (**98**)

GC-MS

GC-MS method: Carrier gas: Helium
 Temperature (column): 80°C (hold 2.5 min), 80→280°C (rate 20°C/min)
 Temperature (injection): 300°C
 Column Flow: 1.0 mL/min
 Split Ratio: 10% (initial), 100% (0.01 min→1.00 min), 40% (1.00→end)

Coloumn: Capillary Column (VF-5ms, 5% phenyl, 95% dimethylpolysiloxane, 30 x 0.25 mm, D_f = 0.25 μm, CP-8944)

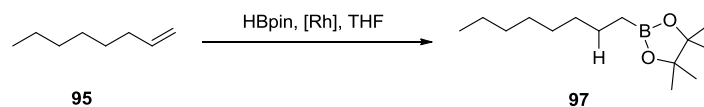
GC-FID

GC-MS method: Carrier gas: Nitrogen
 Temperature (detector): 300 °C
 Temperature (column): 80 - 280 °C
 Temperature (injection): 270 °C
 Column Flow: 1.0 mL/min
 Split Ratio: 0–7 min → 40%, 7–15 min → off

Coloumn: Capillary Column Agilent J&W (CP-Sil 8 CB 30 m x 0.25 mm)

13.2.1.1 Preparation of Reference Compound *n*-Octyl picanolato borane (**97**)

(2134)



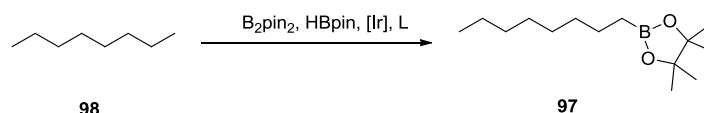
In a glove box a vial was equipped with 1-octene (**95**) (30 mg, 0.26 mmol), pinacolborane (**75**) (30 mg, 0.24 mmol) and [Rh(Cl)(PPh₃)₃] (**96**) (5 mg, 0.005 mmol). The reaction mixture was stirred for 3 hours at room temperature.

A GC-MS sample of 0.1 mL was taken from the crude reaction mixture and diluted in 0.9 mL hexane.

GC-MS retention time: 7.98 min ($m/z = 225$ [$M - (\text{CH}_3)^\cdot$]⁺)

13.2.1.2 Borylation of *n*-Octane

(GM 1068)



In a glove-box bispinacolatodiborane (**66**) (50 mg, 0.20 mmol), [Ir(Cl)cod]₂ (**23**) (3.9 mg, 0.059 mmol) and 0.012 mmol of the ligand were suspended in 1.0 mL of a solution of pinacolborane (x75) in dry *n*-octane (0.12M). The suspension was given into an NMR-tube which was flame-sealed outside the glove box. The mixture was heated up to 130 °C (oil-bath temperature) over night.

GC-MS analysis

0.1 mL of the filtered reaction mixture (over Silica gel) diluted in approx. 0.9 mL of hexane.

At $t_R = 7.98-7.99$ min two substances were detected:

Substance		
	97	99
Detected as		
m/z	225	255

NMR Analysis

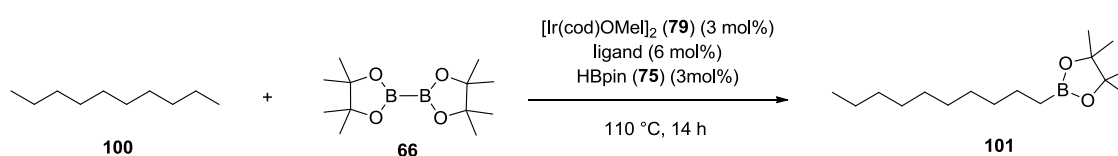
¹¹B-NMR spectra were taken from the sealed reaction tube after the reaction was finished.

Results

Ligand	97	99	# Further Signals	¹¹ B-NMR signals [ppm]
Phen (38)	(x)	x	10	33.6, 20.5
ⁱ Pr-box (5b)	(x)	x	10	33.2, 20.5
Ph-box (5g)	(x)	x	6	33.6, 29.0, 22.0
Bn-box (5h)	x	x	3	33.6, 30.2, 20.5
^{sec} Bu-box (5d)	(x)	x	2	33.4, 20.5
ⁱ Bu-box (5e)	(x)	x	10	33.0, 21.6
^t Bu-box (5c)	x	x	2	33.0, 21.4
ⁿ Bu-box (5f)	x	x	8	33.0, 30.0, 21.4

13.2.1.3 Borylation of *n*-Decane (100**)**

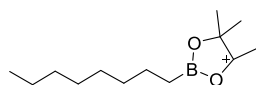
(SP 1026)



Under an argon atmosphere $[\text{Ir}(\text{cod})\text{OMe}]_2$ (**79**) (3.0 mg, 4.07 μmol), B_2pin_2 **2** (50 mg, 0.19 mmol) and the corresponding ligand (8.26 μmol) were into a NMR tube. The substrate *n*-decane (**100**) (0.8 mL), which served as solvent at the same time, was added and the tube was flame sealed. The reaction mixture was heated to 110 °C (oil bath temperature) for 14 h. After cooling to room temperature the tube was opened and the standard *n*-dodecane (50 μL) was added. The reaction mixture was filtered over a small amount celite (fixed in a pipette with cotton wool) without flushing the celite with solvent. An amount of 0.1 mL was taken and diluted with 0.9 mL of *n*-hexane. This mixture was used for GC-analysis. The residue of the filtrate was transferred into a small flask and the volatile compounds were removed under high vacuum overnight. The resulting solid was stored at -20 °C for further analysis.

GC-MS analysis

Detected compound:

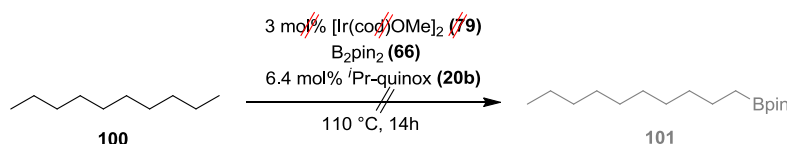
 $t_R = 13.05$ min $m/z = 253$

GC-FID analysis
 $t_R(\mathbf{101}) = 7.75 \text{ min}$

 calibration (SP 1038): $\text{product \%} = 52.922 \times (\text{Integral-product})/(\text{integral-standard})$
Results

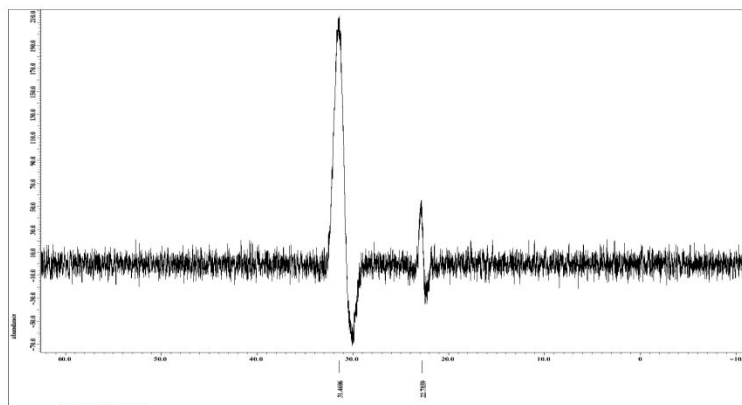
Entry	Ligand	mg (Ligand)	GC-MS ($t_R=13.05 \text{ min}$)	Conv. (GC-FID) [%]	Yield (CG-FID) [%]
1	ⁱ Pr-box (5b)	2.83	×	87	>1
2	ⁱ Pr-quinox (20b)	3.02	×	92	>1
3	ⁱ Pr-pyrox (10b)	2.40	×	99	>1
4	ⁱ Pr-mepyrox (19b)	2.54	×	99	>1
5	ⁱ Pr-pybox (36)	3.80	×	77	>1
6	TMphen (39)	2.98	×	84	3

(SP1048)

13.2.1.4 Control experiments for the borylation of *n*-decane (100**)**
Reaction without iridium


Under an argon atmosphere B_2pin_2 (**66**) ($50 \pm 0.2 \text{ mg}$, 0.19 mmol) and the ligand ⁱPr-quinox (**20b**) ($1.96 \text{ } \mu\text{mol}$) were given into a NMR tube. *n*-Decane (**100**) (0.8 mL , 4.10 mmol) was added and the tube was flame sealed. The reaction mixture was heated to $110 \text{ }^\circ\text{C}$ (oil bath temperature) for 14 h. After cooling to room temperature the tube was opened and the standard *n*-dodecane ($50 \text{ } \mu\text{L}$) was added. The reaction mixture was filtered over a small amount celite (fixed in a pipette with cotton wool) without flushing the celite with solvent. An amount of 0.1 mL was taken and diluted with 0.9 mL of *n*-hexane. This mixture was used for GC-analysis. The residue of the filtrate was transferred into a small flask and the volatile compounds were removed under high vacuum over night. The resulting solid was dissolved in CDCl_3 and used for proton-NMR-analysis. $^1\text{H-NMR}$ analysis failed due to too many overlapping signals.

^{11}B (160 MHz): $\delta=31.5$ (B_2pin_2), 22.8 ppm.

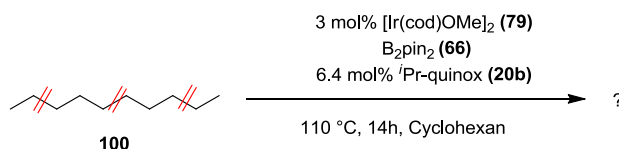


GC-MS: no product

$t_{\text{R}} = 11.09$ min; $m/z = 239$ ($(\text{B}_2\text{pin}_2)^-\cdot\text{CH}_3^+$)

HRMS (+ESI): m/z (%) = 293.1509 (100) [$(\text{B}_2\text{pin}_2)+\text{K}$] $^+$ (calc. 293.1492).

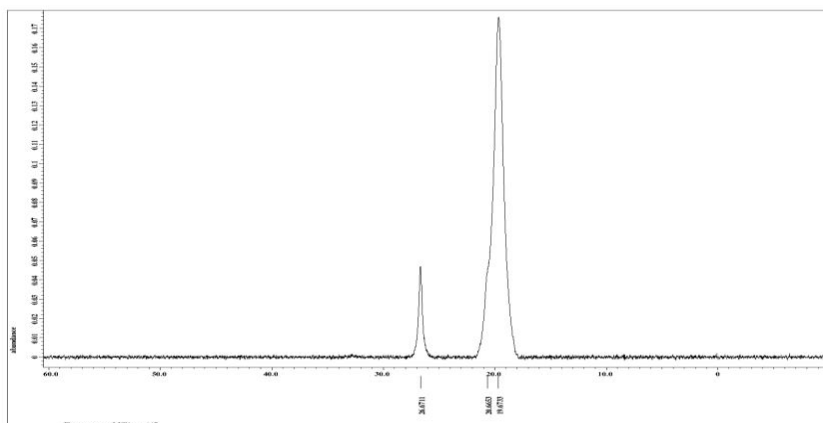
Reaction without *n*-decane



Under an argon atmosphere B_2pin_2 (**66**) (50 ± 0.2 mg, 0.19 mmol) and the ligand $i\text{Pr}$ -quinox (**20b**) ($1.96\text{ }\mu\text{mol}$) were added to a NMR tube. The solvent cyclohexane (0.8 mL) was added and the tube was flame sealed. The reaction mixture was heated to $110\text{ }^\circ\text{C}$ (oil bath temperature) for 14 h. After cooling to room temperature the tube was opened and the standard *n*-dodecane ($50\text{ }\mu\text{L}$) was added. The reaction mixture was filtered over a small amount celite (fixed in a pipette with cotton wool) without flushing the celite with solvent. An amount of 0.1 mL was taken and diluted with 0.9 mL of *n*-hexane. This mixture was used for GC-analysis. The residue of the filtrate was transferred in a small flask and the volatile compounds were removed under high vacuum over night. The resulting solid was dissolved in CDCl_3 and used for proton-NMR-analysis. ^1H -NMR analysis failed due to too many overlapping signals.

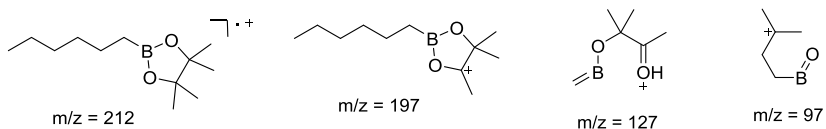
Experimental Section

NMR: ^{11}B (160 MHz): $\delta=26.7$ (HBpin), 20.7, 19.7 ppm.

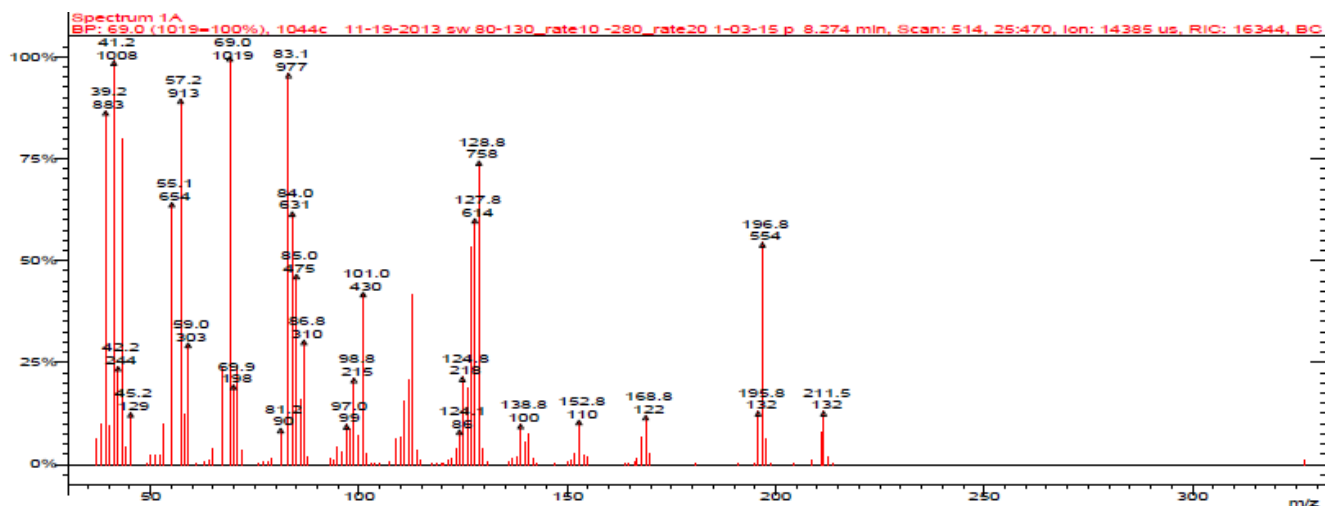


GC-MS:

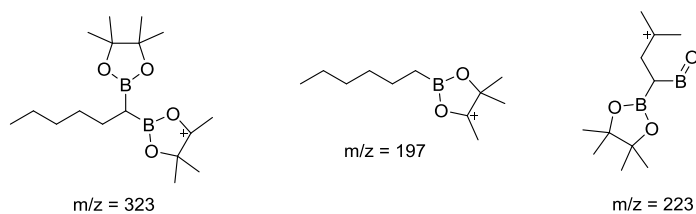
t_R : 8.27 min



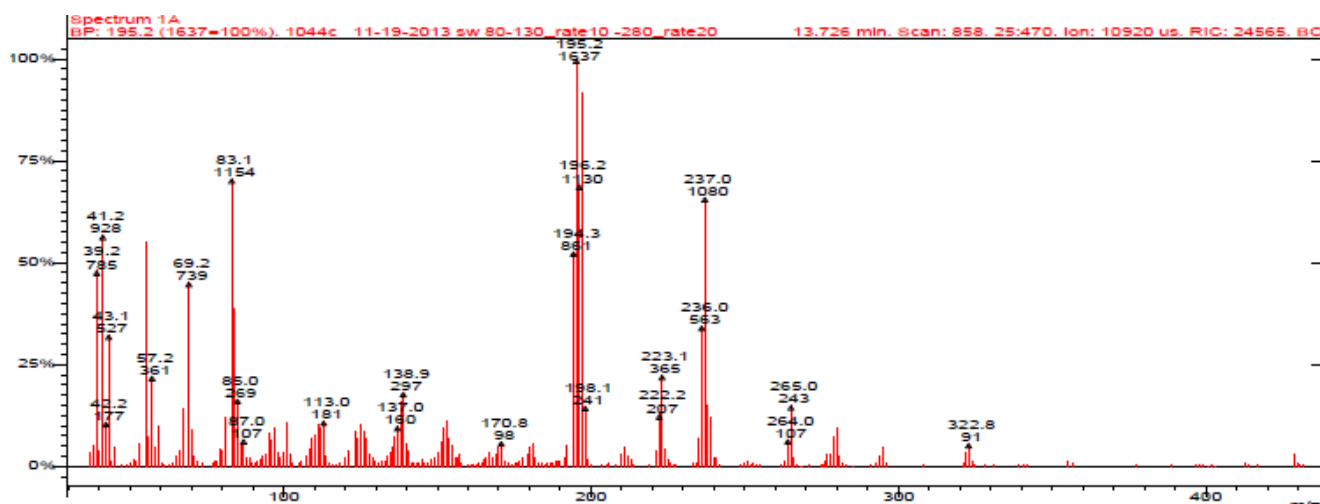
Alkyl fragments $m/z = 43$ (C_3H_7), 57 (C_4H_{10}), 85 (C_6H_{14})



t_R : 13.73 min



Alkyl fragments $m/z = 43$ (C_3H_7), 57 (C_4H_{10}), 85 (C_6H_{14})

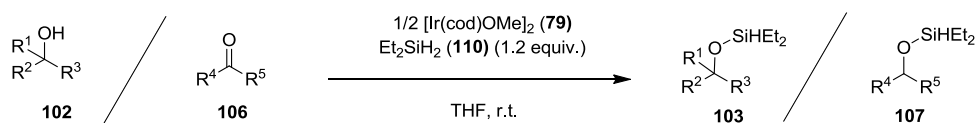


HRMS (+ESI): m/z (%) = 361.2693 (90) $[(C_6H_{12})(Bpin)_2+Na]^+$ calc. 361.2697, 487.3554
(100) $[(C_6H_{11})(Bpin)_3+Na]^+$ calc. 487.3550.

13.3 (Hydrido)silyl Ether Directed γ -C-H Activation

13.3.1 (Hydrido)silyl ethers

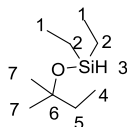
13.3.1.1 General procedure J for the formation of (hydrido)silyl ethers **103** and **107** from ketones **102** or alcohols **106**



Inside an argon filled glove-box, the substrate was dissolved in THF. Another solution of $[Ir(cod)(OMe)_2]$ (**79**) in THF was prepared and both solutions were combined in a small reaction vial. Diethylsilane (**110**) was added. The vial was equipped with a Teflon coated stirring bar and the reaction was stirred at room temperature. In case of the alcohol substrate pressure release from time to time was very important due to the formed hydrogen gas. The reaction progress was monitored by GC-MS. After the reaction had finished, the volatile components were evaporated in vacuum for 2-4 h. Reaction mixtures of very low molecular weight substrates were cooled down to -78°C (dry ice/ethanol) before the volatiles were removed.

13.3.1.2 diethyl(*tert*-pentyloxy)silane (**103c**)

(SP 1050, 1064)



The reaction was carried out following general procedure J.

tert-amyl alcohol (**102c**) 0.54 mL, 5.0 mmol

Et₂SiH₂ (**110**) (0.77 mL, 6.0 mmol)

[Ir(cod)(OMe)]₂ (**79**) (1.33 mg, 0.002 mmol)

THF (5.0 mL)

Time: 89 h

Product: Colourless oil (350 mg, 2.01 mmol, 97%) (cooled down for purification)

NMR: ¹H (500 MHz, CD₂Cl₂): δ = 4.53 (quin, 0.8H, H₃, *J* = 2.38 Hz), 1.50 (q, 2H, H₅, *J* = 7.83 Hz), 1.21 (s, 6H, H₇), 0.97 (t, 6H, H₁, *J* = 7.83 Hz), 0.89 (t, 3H, H₄, *J* = 7.83 Hz), 0.61 (dq, 4H, H₂, *J* = 7.83, 2.38 Hz) ppm. Using COSY and HMQC.

¹³C (126 MHz, CD₂Cl₂): δ = 74.5 (C₆), 37.2 (C₅), 28.9 (C₇), 8.9 (C₄), 7.2 (C₁), 7.0 (C₂) ppm.

GC-MS

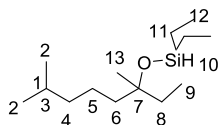
Column: Capillary Column (VF-5ms, 5% phenyl, 95% dimethylpoysiloxane, 30 x 0.25 mm, D_f = 0.25 μm, CP-8944).

Method: carrier gas: N₂ / temperature (detektor): 300 °C / temperature (column): 80 - 280 °C / temperature (injection): 300 °C / Column Flow: 1.0 mL/min / split ratio: 10 - initial, 0.01 - 100, 1.00 - 40

t_R = 4.13 min [m/z (%) = 174 [M]⁺ (0.1), 159 [M-CH₃]⁺ (20), 145 [M-C₂H₆]⁺ (100), 103 [M-C₃H₁₁]⁺ (35), 71 [M-OSiEt₂H]⁺ (30)].

13.3.1.3 ((3,7-dimethyloctan-3-yl)oxy)diethylsilane (**103b**)

(SP 1056, 1066, AE 1072, 1076, 1116)



The reaction was carried out following general procedure J.

tetrahydrolanilool (**102b**) (2010 mg, 12.68 mmol)

Et₂SiH₂ (**110**) 1340 mg, 15.2 mmol

[Ir(cod)(OMe)]₂ (**79**) 84 mg, 0.127 mmol

THF (0.4 mL)

Time: 12 h

Product: Colourless oil as mixture with THF (3.10 g/10.1 mL, 88.1% product as determined by $^1\text{H-NMR} \rightarrow 100\%$ yield)

NMR: ^1H (500 MHz, CD_2Cl_2): $\delta = 4.57$ (quin, 1H, H_{10} , $J = 2.38$ Hz), 1.61 - 1.50 (m, 3H, $\text{H}_8 + \text{H}_3$, $J = 7.83$, 6.81 Hz), 1.47 - 1.43 (m, 2H, H_6), 1.36 - 1.29 (m, 2H, H_5), 1.20 - 1.15 (m, 5H, $\text{H}_4 + \text{H}_{13}$), 0.98 (t, 6H, H_{12} , $J = 7.83$ Hz), 0.91 - 0.86 (m, 9H, $\text{H}_1 + \text{H}_9$, $J = 7.83$, 6.81 Hz), 0.63 (dq, 4H, H_{11} , $J = 7.83$, 2.38 Hz) ppm. Using COSY and HMQC.

^{13}C (126 MHz, CD_2Cl_2): $\delta = 76.8$ (C_6), 42.2 (C_5), 40.3 (C_3), 34.9 (C_7), 28.9 (C_2), 26.7 (C_9), 23.0 (C_1), 22.4 (C_4), 8.9 (C_8), 7.5 (C_{12}), 7.2 (C_{11}) ppm.

GC-MS

Column: Capillary Column (VF-5ms, 5% phenyl, 95% dimethylpoysiloxane, 30 x 0.25 mm, $D_f = 0.25$ μm , CP-8944).

Method: carrier gas: N_2 / temperature (detektor): 300 $^\circ\text{C}$ / temperature (column): 80 - 280 $^\circ\text{C}$ / temperature (injection): 300 $^\circ\text{C}$ / Column Flow: 1.0 mL/min / split ratio: 10 - initial, 0.01 - 100, 1.00 - 40

$t_R = 10.52$ min [m/z (%) = 243 [M-H] $^+$ (10), 215 [$\text{M-C}_2\text{H}_5$] $^+$ (92), 159 [$\text{M-C}_6\text{H}_{13}$] $^+$ (100)].

GC-FID

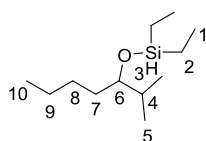
Column: Capillary Column Agilent J&W (CP-Sil 8 CB 30 m x 0.25 mm)

Method: carrier gas: N_2 / temperature (detektor): 300 $^\circ\text{C}$ / temperature (column): 80 - 280 $^\circ\text{C}$ / temperature (injection): 270 $^\circ\text{C}$ / Column Flow: 1.0 mL/min / Split Ratio: 0-7 min \rightarrow 40%, 7-15 min \rightarrow off.

$t_R = 5.99$ min.

13.3.1.4 diethyl((2-methylheptan-3-yl)oxy)silane (**103b**)

(SP 1060, 1068, AE 1078, 1138, 1158, 1160)



The reaction was carried out following general procedure J.

2-methylheptan-3-on(**102b**) (326 mg, 2.55 mmol)

Et_2SiH_2 (**110**) (269 mg, 3.05 mmol)

$[\text{Ir}(\text{cod})(\text{OMe})_2]$ (**79**) (1.69 mg, 0.0025 mmol)

THF (5 mL)

Time: 12 h

Product: Colourless oil as mixture with THF (80% yield; determined by $^1\text{H-NMR}$)

NMR: ^1H (500 MHz, CD_2Cl_2): δ = 4.42 (quin, 0.8H, H_3 , J = 2.38 Hz), 3.43 (dt, 1H, H_6 , J = 6.81, 4.77 Hz), 2.57 (hept, 4H, $\text{H}_4+\text{H}_{\text{Ed}}$, J = 6.81 Hz), 2.41 (t, 10H, $\text{H}_7+\text{H}_{\text{Ed}}$, J = 7.49 Hz), 1.72 (dsex, 1H, J = 4.42, 2.28 Hz), 1.50 (quin, 10H, $\text{H}_8+\text{H}_{\text{Ed}}$, J = 7.49 Hz), 1.43 -1.36 (m, 2H, H_7), 1.28 (sext, 10H, $\text{H}_9+\text{H}_{\text{Ed}}$, J = 7.49 Hz), 1.04 (d, 30H, $\text{H}_5+\text{H}_{\text{Ed}}$, J = 6.81 Hz), 0.97 (t, 6H, H_1 , J = 7.81 Hz), 0.91 - 0.84 (t,dd, 21H, $\text{H}_{10}+\text{H}_{\text{Ed}}+\text{H}_7$, J = 10.9, 7.49, 6.81 Hz), 0.67 - 0.62 (m, 4H, H_2) ppm.

^{13}C (126 MHz, CD_2Cl_2): δ = 214.7 (C_{Ed}), 79.4 (C_6), 41.1 (C_4), 40.4 (C_7), 33.7 (C_7), 33.5 (C_7), 28.4 (C_7), 26.3 (C_{Ed}), 23.4 (C_9), 22.9 (C_{Ed}), 18.8 (C_7), 18.5 (C_{Ed}), 17.7 (C_7), 14.3 (C_7), 14.1 (C_{Ed}), 7.0 (C_1), 6.9 (C_{Ed}), 6.1 (C_2), 6.0 (C_{Ed}) ppm.

MS (GC):

Column: Capillary Column (VF-5ms, 5% phenyl, 95% dimethylpoysiloxane, 30 x 0.25 mm, D_f = 0.25 μm , CP-8944).

Method: carrier gas: N_2 / temperature (detektor): 300 $^\circ\text{C}$ / temperature (column): 80 - 280 $^\circ\text{C}$ / temperature (injection): 300 $^\circ\text{C}$ / Column Flow: 1.0 mL/min / split ratio: 10 - initial, 0.01 - 100, 1.00 - 40

t_R = 8.20 min [m/z (%) = 215 [$\text{M}-\text{H}$] $^+$ (10), 173 [$\text{M}-\text{C}_2\text{H}_5$] $^+$ (100), 159 [$\text{M}-\text{C}_4\text{H}_9$] $^+$ (10)].

FID (GC):

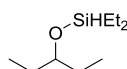
Column: Capillary Column Agilent J&W (CP-Sil 8 CB 30 m x 0.25 mm)

Method: carrier gas: N_2 / temperature (detektor): 300 $^\circ\text{C}$ / temperature (column): 80 - 280 $^\circ\text{C}$ / temperature (injection): 270 $^\circ\text{C}$ / Column Flow: 1.0 mL/min / Split Ratio: 0–7 min \rightarrow 40%, 7–15 min \rightarrow off.

t_R = 5.02 min.

13.3.1.5 diethyl(pentan-3-yloxy)silane (107b)

(AE 1122, 1136)



The reaction was carried out following general procedure J.

Pentane-3-one (**106b**) (1.50 g, 17.41 mmol)

Et_2SiH_2 (**110**) (1.85 g, 20.90 mmol)

$[\text{Ir}(\text{cod})(\text{OMe})_2]$ (**79**) (57.8 mg, 87.07 μmol)

THF (2 ml)

Time: 12 h

Product: The product was identified by ^1H -NMR spectroscopy. It was obtained as mixture with the corresponding di-alkoxysilane.

NMR: ^1H (500 MHz, CD_2Cl_2): δ = 0.62-0.71 (m, 4H, Si-ethyl- CH_2), 0.85-0.93 (m, 6H, Si-ethyl- CH_3), 0.97-1.05 (m, ethyl- CH_3), 1.25-1.48 (m, 4H, ethyl- CH_2), 3.44-3.49 (1H, SiH), 4.47-4.51 (m, 1H, CH) ppm.

Side product:

GC-MS:

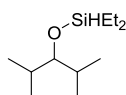
Column: Capillary Column (VF-5ms, 5% phenyl, 95% dimethylpolysiloxane, 30 x 0.25 mm, Df = 0.25 μm , CP-8944).

Method: carrier gas: N_2 / temperature (detektor): 300 $^\circ\text{C}$ / temperature (column): 80 - 280 $^\circ\text{C}$ / temperature (injection): 300 $^\circ\text{C}$ / Column Flow: 1.0 mL/min / split ratio: 10 - initial, 0.01 - 100, 1.00 - 40

$t_{\text{R}} = 4.66$ min [m/z (%) = 245 [$\text{M}-\text{CH}_3$] $^+$ (16), 173 [$\text{M}-\text{C}_3\text{H}_7\text{O}$] $^+$ (7), 145 [$\text{M}-\text{C}_7\text{H}_{16}\text{O}$] $^+$ (100), 117 [$\text{M}-\text{C}_9\text{H}_{21}\text{O}$] $^+$ (19)] $^+$.

13.3.1.6 ((2,4-dimethylpentan-3-yl)oxy)diethylsilane (107d)

(AE 1098)



The reaction was carried out following general procedure J.

2,4-dimethyl-pentane-3-one (**106d**) (1.80 g, 15.76 mmol)

Et_2SiH_2 (**110**) (1.56 g, 17.62 mmol)

$[\text{Ir}(\text{cod})(\text{OMe})_2]$ (**79**) (42.7 mg, 62.42 μmol)

THF (1 ml)

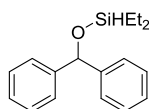
Time: 12 h

Product: Colorless solution in THF. The concentration was determined by ^1H -NMR spectroscopy (6.59 g solution, $c = 106.27$ g/mol; $n_{\text{product}} = 15.8$ mmol, 98%)

NMR: ^1H (500 MHz, THF- d_8): δ = 0.66-0.73 (m, 4H, ethyl- CH_2), 0.89 (dd, $J = 5.2, 6.4$ Hz, $^i\text{Pr}-\text{CH}_3$), 0.97-1.04 (m, 8H, $^i\text{Pr}-\text{CH}$, ethyl- CH_3), 3.14 (t, $J = 5.5$ Hz, SiH), 4.52-4.54 (m, 1H, CHOSi) ppm.

13.3.1.7 (benzhydryloxy)diethylsilane (107e)

(AE 1120)



The reaction was carried out following general procedure J.

Benzophenone (**106e**) (2.20 g, 12.07 mmol)

Et₂SiH₂ (**110**) (1.29 g, 14.67 mmol)

[Ir(cod)(OMe)]₂ (**79**) (80.6 mg, 121.59 μmol)

Ligand

THF (1 ml)

Time: 12 h

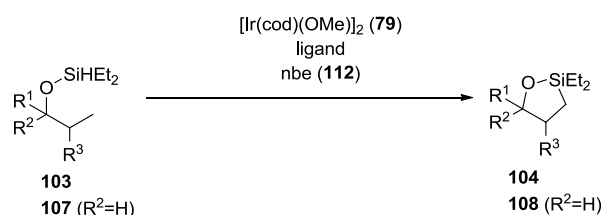
Product: Colorless solution in THF. The concentration was determined by ¹H-NMR spectroscopy (5.089 g solution; n_{product}=38.7 mmol, 96%)

NMR: ¹H (500 MHz, THF-d₈): δ = 0.61-0.72 (m, 4H, ethyl-CH₂), 0.92-0.99 (m, 6H, ethyl-CH₃), 4.54-4.57 (m, 1H, SiH), 5.85-5.88 (m, 1H, CH), 7.16-7.22 (m, 2H, Har), 7.25-7.30 (m, 4H, Har), 7.37-7.42 (m, 4H, Har) ppm.

13.3.2 Oxasilolanes

GC-MS:

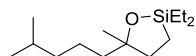
13.3.2.1 General procedure K for the formation of oxasilolanes **104** and **108**



In an argon filled glove-box, the substrate (1.0 equiv.), norbornene (**112**), [Ir(cod)(OMe)]₂ (**79**) and the ligand were given into a small reaction vial and dissolved into THF. The vial was equipped with a teflon coated stirring bar and closed with a Teflon sealed screwing cap. The reaction mixture was stirred at room temperature for 4 h and subsequently heated in an aluminum block. After the reaction had finished, *n*-dodecane (50 μL) was added as GC standard and a small amount of the original reaction mixture was used for GC analysis. Alternatively the crude mixture was worked up under normal air. Therefore the volume of the reaction mixture was first reduced under high vacuum to remove nbe (**112**) and THF. Subsequently, a kugelrohrdistillation was performed to obtain the pure product.

13.3.2.2 2,2-diethyl-5-methyl-5-(4-methylpentyl)-1,2-oxasilolane (**104b**)

(SP 1058)



The reaction was carried out following general procedure K.

Conditions A

((3,7-dimethyloctan-3-yl)oxy)diethylsilane (**103b**) (172 mg, 1.00 mmol)

norbornene (**112**) (113 mg, 1.20 mmol)

[Ir(dod)(OMe)₂] (**79**) (3.3 mg, 0.0050 mmol)

ligand (0.00125 mmol)

Conditions B

((3,7-dimethyloctan-3-yl)oxy)diethylsilane (**103b**) (0.306 g, 1.25 mmol)

norbornene (**112**) (113 mg, 1.20 mmol)

[Ir(cod)(OMe)₂] (**79**) (50.04 mg, 76.03 μmol)

ligand (156.57 μmol)

Time: 48 h

Temperature: 80 °C

Work-up: Kugelrohrdistillation

Product: Colorless oil

Results

Entry	Ligand	Conditions	m(Ligand) [mg]	Yield [%]
1	TM-phen (39)	B	37.0	95
2	H-box (5i)	A	1.75	29
3	ⁱ Pr-pyrox (10b)	A	2.38	14

GC-MS:

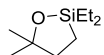
Column: Capillary Column (VF-5ms, 5% phenyl, 95% dimethylpoysiloxane, 30 x 0.25 mm, Df = 0.25 μm, CP-8944).

Method: carrier gas: N₂ / temperature (detector): 300 °C / temperature (column): 80-130 °C (10 °/min), 130-280 °C (20 °/min) / temperature (injection): 300 °C / Column Flow: 1.0 mL/min / split ratio: 10 - initial, 0.01 - 100, 1.00 - 40

t_R = 11.28 min [m/z (%) = 227 [M-CH₃]⁺ (6), 185 [M-C₄H₁₀]⁺ (4) 157 [M-C₆H₁₃O]⁺ (100)]

13.3.2.3 2,2-diethyl-5,5-dimethyl-1,2-oxasilolane (**104c**)

(SP 1054)



The reaction was carried out following general procedure K.

((3,7-dimethyloctan-3-yl)oxy)diethylsilane (**103c**) (172 mg, 1.00 mmol)

norbornene (**112**) (113 mg, 1.20 mmol)

[Ir(cod)(OMe)]₂ (**79**) (3.3 mg, 0.0050 mmol)

Ligand (0.00125 mmol)

THF (1.6 mL)

Time: 48 h

Temperature: 80 °C

Work-up: Kugelrohrdistillation

Product: Colorless oil

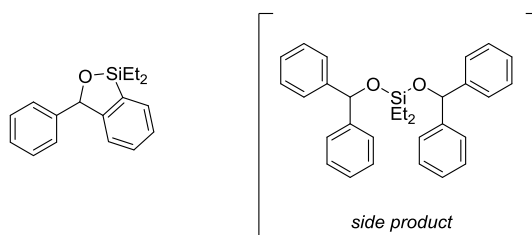
Results

Entry	Ligand	m(Ligand) [mg]	Yield [%]
1	TMphen (39)	2.95	12
2	H-box (5i)	1.75	25

(No analytical data available)

13.3.2.4 1,1-diethyl-3-phenyl-1,3-dihydrobenzo[*c*][1,2]oxasilole (**108e**)

(AE 1140, 1150)



The reaction was carried out following general procedure K.

(benzhydryloxy)diethylsilane (**107e**) (314 mg, 1.16 mmol)

norbornene (**112**) (131 mg, 1.39 mmol)

[Ir(cod)(OMe)]₂ (**79**) (7.69 mg, 0.0116 mmol)

TMphen (**39**) (6.03 mg, 0.0255 mmol)

THF (0.2 mL)

Time: 48 h

Temperature: 80 °C

Work-up: Kugelrohrdistillation (hv, 280 °C, two receiving flasks cooled with ice (fraction 1) and dry ice (fraction 2), product was found in fraction 2)

Product: Colorless solid in colorless oil, 131.8 mg mixture of product and side product (GC-MS). The ¹H-NMR spectrum shows the product and some minor, unidentified impurities. It was not possible to identify a signal set for the side product.

¹H-NMR (500 MHz, CDCl₃): δ = 0.84-0.96 (m, 3H, SiCH₂CH₃), 0.96-1.02 (m, 4H, SiCH₂), 1.08-1.10 (t, *J* = 7.8 Hz, 3H, SiCH₂CH₃), 6.16 (s, 1H, SiH), 7.02 (d, *J* = 6.8 Hz, 1H, H_{ar}), 7.27-7.35 (m, 7H, H_{ar}), 7.62 (d, *J* = 5.8 Hz, 1H, H_{ar}).

GC-MS:

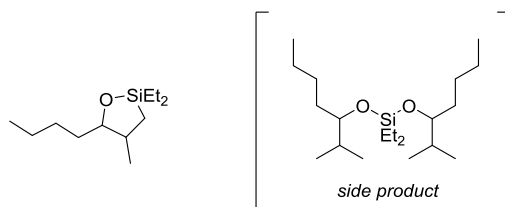
Column: Capillary Column (VF-5ms, 5% phenyl, 95% dimethylpoysiloxane, 30 x 0.25 mm, Df = 0.25 μm, CP-8944).

Method: carrier gas: N₂ / temperature (detector): 300 °C / temperature (column): 80-130 °C (10 °/min), 130-280 °C (20 °/min) / temperature (injection): 300 °C / Column Flow: 1.0 mL/min / split ratio: 10 - initial, 0.01 - 100, 1.00 - 40

t_R = 14.56 min (product **107e**) [m/z: 165, 211, 239], 14.73 min (side product **111e**) [m/z: 167, 269]

13.3.2.5 5-butyl-2,2-diethyl-4-methyl-1,2-oxasilolane (**108c**)

(AE, 1126, 1114, 1094)



The reaction was carried out following general procedure K.

diethyl((2-methylheptan-3-yl)oxy)silane (**107c**) (212 mg, 0.981 mmol),

norbornene (**112**) (130 mg, 1.38 mmol)

[Ir(cod)(OMe)]₂ (**79**) (8.00 mg, 0.0120 mmol)

TMphen (**39**) (5.70 mg, 0.0240 mmol)

THF (0.2 mL)

Time: 48 h

Temperature: 80 °C

Work-up: Kugelrohrdistillation (hv, 280 °C, two receiving flasks cooled with ice (fraction 1) and dry ice (fraction 2), the product was found in fraction 2)

Product: Colorless solid in colorless oil, 180 mg mixture of product and side product (GC-MS).

GC-MS:

Column: Capillary Column (VF-5ms, 5% phenyl, 95% dimethylpoysiloxane, 30 x 0.25 mm, Df = 0.25 μ m, CP-8944).

Method: carrier gas: N₂ / temperature (detector): 300 °C / temperature (column): 80-130 °C (10 °/min), 130-280 °C (20 °/min) / temperature (injection): 300 °C / Column Flow: 1.0 mL/min / split ratio: 10 - initial, 0.01 - 100, 1.00 - 40

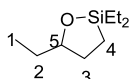
t_R = 8.22 min (starting material **106c**) [m/z (%) = 187 [M-C₂H₅]⁺ (9), 173 [M-C₃H₇]⁺ (100) 159 [M-C₄H₉]⁺ (7), 103 [M-C₈H₁₇]⁺ (11), 75 [103-C₂H₅]⁺ (14)]

t_R = 9.27 min (product **107c**) [m/z (%) = 185 [M-C₂H₅]⁺ (95), 157 [M-C₄H₉]⁺ (100)]

t_R = 10.49 min (side product **111c**) [m/z (%) = 215 [M-C₈H₁₇O]⁺ (100), 201 [M-C₉H₂₀O]⁺ (38), 173 [M-C₁₁H₂₄O]⁺ (25), 103 [M-C₁₆H₃₄O]⁺ (25)]

13.3.2.6 2,2,5-triethyl-1,2-oxasilolane (108c)

(AE 1122, 1134, 1152)



The reaction was carried out following general procedure K. The reactants were cooled down by an ice-brine mixture upon addition to the reaction vial to avoid an exothermic reaction.

diethyl(pentan-3-yloxy)silane (**107c**) 297 1.70

norbornene (**112**) (94.2 mg, 2.04 mmol)

[Ir(cod)(OMe)]₂ (**79**) (11.3 mg, 0.0170 mmol)

TMphen (**39**) (8.86 mg, 0.0375 mmol)

THF (2.5 mL)

Time: 48 h

Temperature: 80 °C

Work-up: Kugelrohrdistillation (hv, 220 °C, two receiving flasks cooled with ice (fraction 1) and dry ice (fraction 2), product was found in fraction 2)

Product: Colorless solid in colorless oil, 160.8 mg mixture of product and side product (GC-MS). The ¹H-NMR spectrum shows the product and hardly any unidentified impurities.

¹HNMR (500 MHz, CDCl₃): δ = 0.58 (q, J = 7.8 Hz, 4H, SiCH₂), 0.86 (t, J = 7.8 Hz, 3H, SiCH₂CH₃), 0.94-0.99 (m, 4H, H-4, H-1), 1.39-1.52 (m, 4H, H-3, H-2), 3.64 (quin, J = 5.8 Hz, 1H, H-5) ppm.

GC-MS:

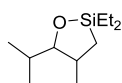
Column: Capillary Column (VF-5ms, 5% phenyl, 95% dimethylpoysiloxane, 30 x 0.25 mm, Df = 0.25 μ m, CP-8944).

Method: carrier gas: N₂ / temperature (detector): 300 °C / temperature (column): 80-130 °C (10 °/min), 130-280 °C (20 °/min) / temperature (injection): 300 °C / Column Flow: 1.0 mL/min / split ratio: 10 - initial, 0.01 - 100, 1.00 -

t_R = 5-15 min (product) m/z = 143 [M-C₂H₅]⁺

13.3.2.7 2,2-diethyl-5-isopropyl-4-methyl-1,2-oxasilolane (108d)

(AE1104, 1128, 1130, 1132, 1144, 1146)



The reaction was carried out following general procedure K.

((2,4-dimethylpentan-3-yl)oxy)diethylsilane (**107d**) (319 mg, 1.58 mmol)

norbornene (**112**) (182.7 mg, 1.94 mmol)

[Ir(cod)(OMe)]₂ (**79**) (63.5 mg, 0.096 mmol)

TMphen (**39**) (45.3 mg, 0.192 mmol)

THF (1.5 mL)

Time: 48 h

Temperature: 80 °C

Work-up: Kugelrohrdistillation (hv, 220 °C, two receiving flasks cooled with ice (fraction 1) and dry ice (fraction 2), product was found in fraction 2)

Product: Colorless oil (180 mg, 0.90 mmol, 57%).

GC-MS

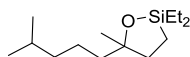
Column: Capillary Column (VF-5ms, 5% phenyl, 95% dimethylpoysiloxane, 30 x 0.25 mm, Df = 0.25 μ m, CP-8944).

Method: carrier gas: N₂ / temperature (detector): 300 °C / temperature (column): 80-130 °C (10 °/min), 130-280 °C (20 °/min) / temperature (injection): 300 °C / Column Flow: 1.0 mL/min / split ratio: 10 - initial, 0.01 - 100, 1.00 - 40

t_R = 8.22 (7.36)min [m/z (%) = 171 [M-C₂H₅]⁺ (11), 157 [M-C₃H₇]⁺ (100), 129 [M-C₅H₁₂]⁺ (8)]

2,2-diethyl-5-methyl-5-(4-methylpentyl)-1,2-oxasilolane (104b)

(AE 1092, 1106, 1110, 1112, 1124, 1142, 1154, 1156)



Preparation of reference substance for calibration (1092, 1106):

The reaction was carried out following general procedure K.

((3,7-dimethyloctan-3-yl)oxy)diethylsilane (**103b**) (153 mg, 0.625 mmol)

norbornene (**112**) (73.5 mg, 0.780 mmol)

[Ir(cod)(OMe)]₂ (**79**) (8.60 mg, 0.0129 mmol)

TMphen (**39**) (6.10 mg, 25.8 mmol)

THF (4.5 mL)

Time: 48 h

Temperature: 80 °C

Work-up: Kugelrohrdistillation (hv, 220 °C, two receiving flasks cooled with ice (fraction 1) and dry ice (fraction 2), product was found in fraction 2)

Product: Colorless oil (85.8 mg, 0.35 mmol, 55%)

GC-MS:

Column: Capillary Column (VF-5ms, 5% phenyl, 95% dimethylpoysiloxane, 30 x 0.25 mm, Df = 0.25 μm, CP-8944).

Method: carrier gas: N₂ / temperature (detector): 300 °C / temperature (column): 80 - 280 °C / temperature (injection): 300 °C / Column Flow: 1.0 mL/min / split ratio: 10 - initial, 0.01 - 100, 1.00 - 40

t_R = 14.56 min (product 104b) [m/z: 239[M-C₂H₅]⁺ (80), 211 [M-C₄H₁₀]⁺ (48), 163 [M-C₈H₁₀]⁺ (23)]

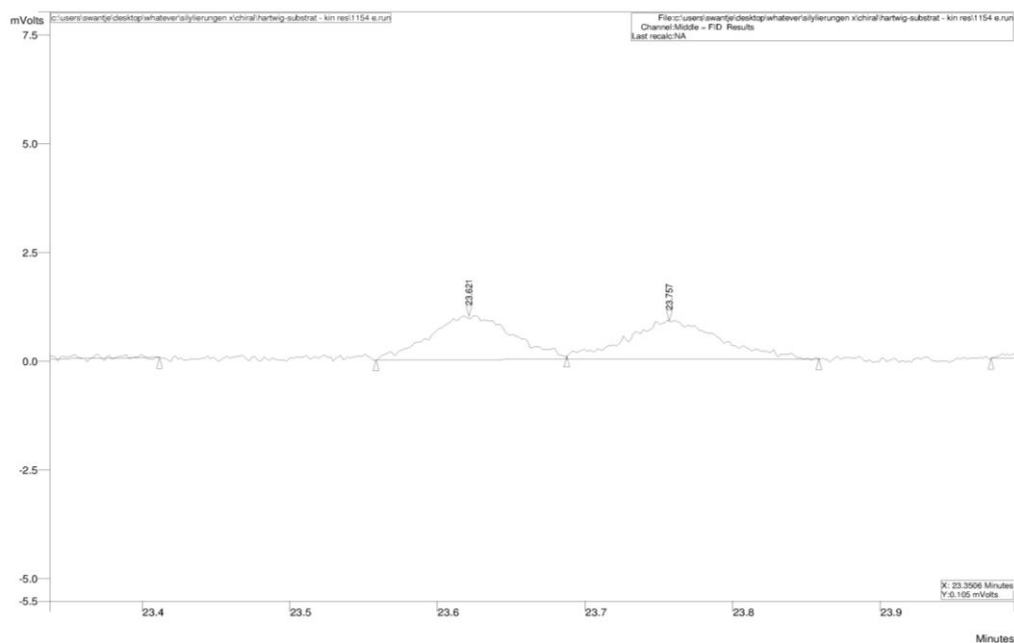
t_R = 14.73 min (side product) [m/z: 269 [M-C₁₃H₁₁O]⁺ (100), 167 [M-C₂₆H₂₂O]⁺ (42)]

GC-FID:

Column: Chrompack CP-Chirasil-Dex CB, 25 m x 0.25 mm, 0.25 μm

Method: split injector (1:80), T = 225 °C (injector), T = 275 °C (FID detector), carrier gas: N₂, 5 bar; 40 °C (hold 5 min), 40-120 °C, 5 °/min, 120 °C (hold 10 min)

t_R = 23.62 min (enantiomer 1), 23.75 min (enantiomer 2).



Calibration (AE 1102): $p[\%] = 0.022 \times [(\text{Int. product})/(\text{Int. standard})]$

Ligand screening(1154, 1156):

The reaction was carried out following general procedure K.

((3,7-dimethyloctan-3-yl)oxy)diethylsilane (**104b**) (124 mg, 0.507 mmol)

norbornene (**112**) (57.3 mg, 0.608 mmol)

$[\text{Ir}(\text{cod})(\text{OMe})_2]$ (**79**) (3.37 mg, 0.005 mmol)

Ligand (0.0112 mmol)

THF (1.2 mL)

Time: 48 h

Temperature: 80 °C

Analysis: Quantification by GC-FID

Results

Entry	Ligand	m(Ligand) [mg]	Yield [%]	ee [%] (enantiomer)	Config. (ligand)
1	Bn-box (5h)	3.48	24	29 (1)	<i>S</i>
2	ⁱ Pr-box (5b)	2.44	35	<1 (1)	<i>S</i>
3	ⁱ Pr-quinox (20b)	2.61	33	44 (1)	<i>S</i>
4	ⁿ Bu-box (5f)	2.74	29	3 (1)	<i>S</i>
5	Ph-box (5g)	3.18	38	< 1 (2)	<i>R</i>
6	Ph-quinox (20g)	2.98	32	15 (2)	<i>R</i>
7	ⁱ Pr-pybox (36)	3.28	n.d.	40 (2)	<i>R</i>
8	ⁿ Bu-mepyrox (19f)	2.37	32	3 (1)	<i>S</i>
9	ⁿ Bu-quinox (20f)	2.77	32	13 (1)	<i>S</i>
10	Ph-mepyrox (x9g)	2.59	39	10 (2)	<i>R</i>
11	Ph-phox (40)	4.43	94	10 (1)	<i>S</i>
12	^t Bu-pyrox (10c)	2.22	35	26 (1)	<i>S</i>

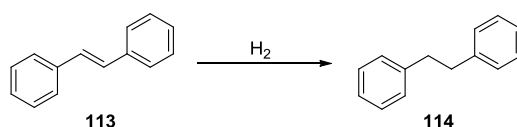
13.4 Hydrogenation

13.4.1 General Procedure La and Lb for Hydrogenations.

Substrate (0.484 mmol) and catalyst (0.0145mmol, 3 mol%) were added to a 2 mL glass vial which was equipped with a teflon coated magnetic stirring bar and a cap with small holes. The reaction was performed in neat substrate (**La**) or in CD₂Cl₂ (0.1 mL) as solvent (**Lb**). The glass vial was placed in an autoclave, which was sealed. The air present in the autoclave was replaced by argon before applying a hydrogen pressure of approximately 5 bar. The hydrogen was released carefully and the procedure repeated for three times. Afterwards, the autoclave was pressurized to 40 bar. The reaction mixture was stirred at room temperature for at least 15 hours. The reaction mixtures were analyzed by ¹H-NMR spectroscopy or GC-FID.

13.4.2 (E)-1,2-Diphenylethene (113)

(4048, 4088, 4124, 4186, 5018)



According to general procedure La with **113** (87.1 mg, 0.484 mmol) and varying catalyst loadings (see table for results below). The reaction mixture was analyzed without any purification. ¹H-NMR (CDCl₃, 400 MHz): δ = 2.97 (s, 4H, **114**-CH₂), 7.21-7.34 (m, 10H, **114** -H_{ar}), 7.14 (s, 2H, **113**-HC=CH), 7.26 (t, J = 17.7 Hz, 2H, **113** -H_{ar}), 7.36 (t, J =7.9 Hz, 4H, **113** -H_{ar}), 7.53 (d, J =7.2 Hz, 4H, **113** -H_{ar}) ppm. The signals at δ = 2.97 ppm (4H, **114**) and 7.14 ppm (2H, **113**) were used for quantification.

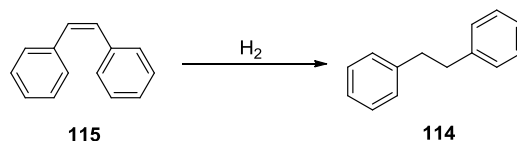
Results:

Catalyst	Cat-loading	Reaction time	Yield 114
30c	5 mol%	16 h	100%
30c	5 mol%	16 h	85%
30c	3 mol%	15 h	100%
30c	3 mol%	15 h	37%
30c	1 mol%	15 h	45%
30c	1 mol%	15 h	15%
30f	3 mol%	15 h	100%
30g	3 mol%	15 h	100%
30h	3 mol%	15 h	100%
30i	3 mol%	15 h	37%
30j	3 mol%	15 h	100%
30h	3 mol%	15 h	<1%
30k	3 mol%	15 h	<1%
30l	3 mol%	15 h	100%
[Ir(ⁱ Pr-pyrox)(cod)]PF ₆	5 mol%	24 h	2%
[Ir(cod)Cl] ₂ , ⁱ Pr-box (5b), AgBAR ^{F a}	1 mol%	15 h	<1%
[Ir(cod)Cl] ₂ , ⁱ Pr-quinox (5b), AgBAR ^{F a}	1 mol%	15 h	<1%

^a [Ir(cod)Cl]₂ (**23**) (0.00242 mmol) was mixed with AgBAR^F (**34**) (0.00484 mmol) in CD₂Cl₂ (0.1 mL) and stirred under exclusion of light for 20 min. The ligand (0.005 mmol) was added and the mixture stirred under exclusion of light for another 10 min. The substrate (0.484 mmol) was added and the hydrogenation started in the autoclave as described in general procedure Ea and Eb.

13.4.3 (Z)-1,2-Diphenylethene (115)

(5034)



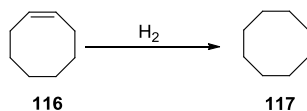
According to general procedure Lb with **115** (0.086 mL, 0.484 mmol) and a reaction time of 15 h. The reaction mixture was analyzed without any purification.

¹H-NMR (CD₂Cl₂, 400 MHz): δ = 3.01 (s, 4H, CH₂), 7.26-7.30 (m, 6H, H_{ar}), 7.33-7.38 (m, 4H, H_{ar}) ppm. No starting material present.

Result for catalyst **30c**: 100% **114**; catalyst **30d**: 24% **114**.

13.4.4 Cyclooctene (116)

(4184)



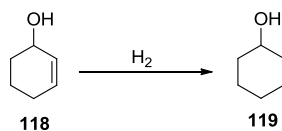
According to general procedure La with **116** (0.63 mL, 0.484 mmol) and a reaction time of 15 h. The reaction mixture was analyzed without any purification.

¹H-NMR (CDCl₃, 400 MHz): δ = 1.52 (s, 16H, **117**-CH₂). Starting material **116** ¹H-NMR (CDCl₃, 400 MHz): δ = 1.48-1.53 (m, 8H, **116** -CH₂), 2.10-2.16 (m, 4H, **116** -CH₂), 5.57-5.64 (m, 2H, **116** -HC=CH), Since the signal of **117** is completely incorporated in the multiplett of **116** at 1.48-1.53 ppm, the amount of **117** was calculated by comparing the integral of this area with the integral of the signal at 5.57-5.64 ppm which belongs to 2H of **116**.

Result for catalyst **30c**: 42% **117**, result for catalyst **30d**: 5% **117**

13.4.5 Cyclohex-2-enol (118)

(5042)



According to general procedure Lb with **118** (0.047 mL) and a reaction time of 15 h. The reaction mixture was analyzed without any purification.

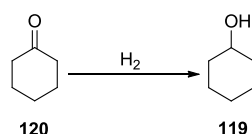
¹H-NMR (CD₂Cl₂, 400 MHz): δ = 1.09-1.30 (m, 5H, **119**-CH₂), 1.47-1.54 (m, 1H, **119** -CH₂), 1.63-1.74 (m, 2H, **119** -CH₂), 1.78-1.87 (m, 2H, **119** -CH₂), 3.49-3.56 (m, 1H, **119** -CH) ppm. Starting material **118** ¹H-NMR (CD₂Cl₂, 400 MHz): δ = 1.49-2.05 (m, 6H, CH₂), 4.12, (s, 1H, CH-OH),

5.66-5.71 (m, 1H, HC=CH), 5.75-5.80 (m, 1H, HC=CH)ppm. The absence of the signals at $\delta = 4.12$ (1H, **118**), 5.66-5.71 (1H, **118**) and 5.75-5.80 (1H, **118**) indicated full conversion of starting material.

Results for catalyst **30c**: 100% **119**. No conversion was observed when catalyst **30d** was applied.

13.4.6 Cyclohexanone (**120**)

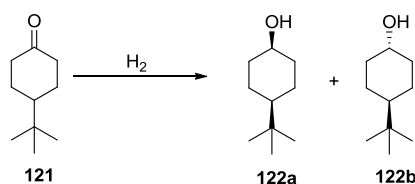
(4130)



According to general procedure La with **120** (0.05 mL, 0.484 mmol) and a reaction time of 16.5 h. The reaction mixture was analyzed without any purification. ¹H-NMR (CDCl₃, 400 MHz): $\delta = 1.09$ -1.31 (m, 4H, **119**), 1.47-1.55 (m, 1h, **119**), 1.64-1.73 (m, 2H, **119**), 1.80-1.89 (m, 2H, **119**), 2.11 (s, 1H, **119**), 3.51-3.59 (m, 1H, **119** -CH), 1.62-1.69 (m, 2H, **120**) ppm. Starting material **120** ¹H-NMR (CDCl₃, 400 MHz): $\delta = 1.76$ -1.83 (m, 4H), 2.27 (t, $J = 6.5$ Hz, 4H). The signals at $\delta = 2.27$ (4H, **120**) and 3.51-3.59 (1H, **119**) ppm were used for quantification. Result for catalyst **30c**: 87% **119**, result for catalyst **30d**: 33% **119**.

13.4.7 4-(*tert*-Butyl)cyclohexanone (**121**)

(5046)



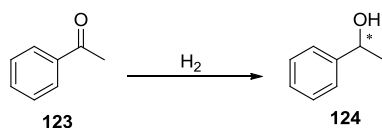
According to general procedure Lb with **121** (74.65 mg, 0.484) and a reaction time of 15 h. The reaction mixture was analyzed without any purification.

¹H-NMR (CD₂Cl₂, 400 MHz): $\delta = 0.82$ (s, 9H, **122b**-C(CH₃)₃), 0.84 (s, 9H, **122a**-C(CH₃)₃), 0.90-1.52 (m, **122a**, **122b**), 1.72-1.80 (m, **122a**, **122b**), 1.91-1.97 (m, **122a**, **122b**), 3.44 (tt, $J = 4.4, 10.9$ Hz, 1H, **122b** -C*H-OH), 3.96 (distorted t, $J = 2.6$ Hz, 1H, **122a** -C*H-OH). Starting material **121** ¹H-NMR (CD₂Cl₂, 400 MHz): $\delta = 0.89$ (s, 9H, C(CH₃)₃), 1.34-1.51 (m, 3H), 2.01-2.08 (m, 2H), 2.25-2.32 (m, 4H), The assignment of the signals for diastereomers is consistent with data reported in the literature.^[253] The signals at $\delta = 2.25$ -2.32 (4H, **121**), 3.44 (1H, **122b**) and 3.96 (1H, **122a**) were used for quantification.

Results for **30c**: 57% **122a**, 43% **122b**, results for **30d**: 7% **122a**, 8% **122b**.

13.4.8 Acetophenone (**123**)

(4170, 4188)



According to general procedure L with **123** (0.056 mL, 0.484 mmol) and a reaction time of 22 h and varying catalyst loadings (see table below). The reaction mixture was analyzed without any purification.

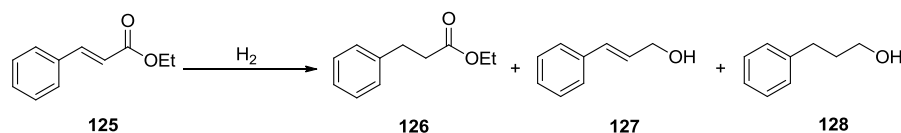
¹H-NMR (CDCl₃, 400 MHz): δ = 1.49 (d, J = 6.5 Hz, 3H, **124**-CH₃), 2.05 (s, 1H, **124** -OH), 4.88 (q, J = 6.5 Hz, 1H, **124** -C*H), 3.25-7.31 (m, 1H, **124** -H_{ar}), 7.32-7.39 (m, 4H, **124**-H_{ar}) ppm. Starting material **123** ¹H-NMR (CDCl₃, 400 MHz): δ = 2.57 (s, 3H, CH₃), 7.43 (t, J = 7.0 Hz, 2H, H_{ar}), 7.53 (dt, J = 1.4, 7.4 Hz, 1H, H_{ar}), 7.93 (d, J = 7.2 Hz, 2H, H_{ar}) ppm. The signals at 1.49 (3H, **124**) and 2.57 (3H, **123**) ppm were used for quantification.

Results:

Catalyst	Cat-loading	Procedure	Yield 124
30c	3 mol%	Ea	13%
30d	3 mol%	Ea	10%
30c	3 mol%	Eb	5%
30d	3 mol%	Eb	<1%
30c	1 mol%	Eb	1%
30d	1 mol%	Eb	<1%

13.4.9 Ethyl cinnamate (**125**)

(5036)



According to general procedure La with **125** (0.081 mL, 0.484 mmol) and a reaction time of 15 h. The reaction mixture was analyzed without any purification.

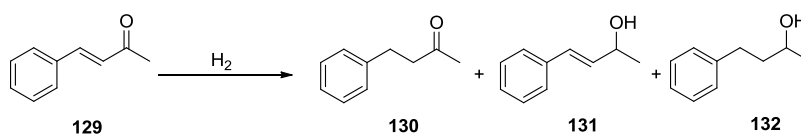
¹H-NMR (CDCl₃, 400 MHz): δ = 1.23 (t, J = 7.2 Hz, 3H, **126**-CH₃), 2.63 (t, J = 7.4 Hz, 2H, **126**-CH₂), 2.96 (t, J = 8.1 Hz, 2H, **126**-CH₂), 4.13 (q, J = 7.2 Hz, 2H, **126**-CH₂), 7.19-7.24 (m, 3H, **126**-H_{ar}), 7.27-7.32 (m, 2H, **126** -H_{ar}), , 2.31 (t, J = 8.1 Hz, **128**-CH) ppm. Starting material **125** ¹H-NMR

(CDCl₃, 400 MHz): δ = 1.33 (t, J = 7.0 Hz, 3H, CH₃), 4.25 (q, J = 7.2 Hz, 2H, CH₂), 6.44 (d, J = 16 Hz, 1H, CH), 7.35-7.54 (m, 3H, H_{ar}), 7.50-7.54 (m, 2H, H_{ar}), 7.68 (d, J = 16 Hz, 1H, CH) ppm. The signals at δ = 2.96 (2H, **126**), 2.31 (2H, **128**) and 6.44 (1H, **125**) ppm were used for quantification.

Results for catalyst **30c**: 92% **126**, 0% **22b**, 8% **128**, results for catalyst **30d**: 97% **126**, 0% **127**, 0% **128**.

13.4.10(*E*)-4-Phenylbut-3-en-2-one (**129**)

(5040)



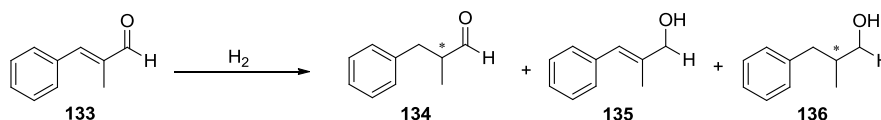
According to general procedure Lb with **129** (70.8 mg, 0.484 mmol) and a reaction time of 15 h. The reaction mixture was analyzed without any purification.

¹H-NMR (CD₂Cl₂, 400 MHz): δ = 2.13 (s, 3H, **130**-CH₃), 2.75 (t, J = 7.2 Hz, 2H, **130**-CH₂), 2.89 (t, J = 7.7 Hz, 2H, **130**-CH₂), 7.16-7.22 (m, 3H, **130**-H_{ar}), 7.25-7.30 (m, 2H, **130**-H_{ar}), 1.54 (s, 3H, **132**-CH₃), 2.60-2.73 (m, 4H, **132**-CH₂), 3.72-3.79 (m, 1H, **132**-C*H), 7.25-7.32 (m, 3H, **132**-H_{ar}), 7.25-7.32 (m, 2H, **132**-H_{ar}) ppm. Starting material **129** ¹H-NMR (CD₂Cl₂, 400 MHz): δ = 3.33 (s, 3H, CH₃), 6.69 (d, J = 16.5 Hz, 1H, CH), 7.37-7.41 (m, 3H, H_{ar}), 7.48 (d, J = 16.2 Hz, 1H, CH), 7.54-7.57 (m, 2H, H_{ar}) ppm. The signals at δ = 2.13 (3H, **130**), 1.54 (3H, **132**), 2.89 (2H, **130**) and 6.69 (1H, **129**) ppm were used for quantification.

Results for catalyst **30c**: 80% **130**, 0% **131**, 20% **132**, results for catalyst **30d**: 93% **130**, 0% **131**, 0% **132**.

13.4.11(*E*)-2-Methyl-3-phenylacrylaldehyde (**133**)

(4178)



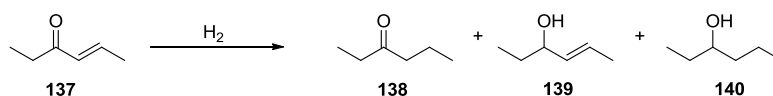
According to general procedure La with **133** (0.067 mL, 0.484 mmol) and a reaction time of 25 h. The reaction mixture was analyzed without any purification.

GC-FID (Agilent CP-Sil 8 CB, 30 m × 0.25 mm, 0.25 μm; split injector (1:50), T = 270 °C, FID detector, carrier gas: N₂, 5 bar; 100-250 °C, 15 °/min): t_R = 8.5 min (**135**), 9.4 min (**136**), 9.9 min (**133**), 10.3 min (**134**).

Results for catalyst **30c**: 17% (**134**), 6% (**135**), 6% (**136**), results for catalyst **30d**: traces **134**, no **135**, **136**.

13.4.12(*E*)-Hex-4-en-3-one (**137**)

(5032)



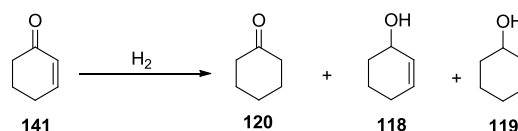
According to general procedure Lb with **137** (0.055 mL, 0.484 mmol) and a reaction time of 15 h. The reaction mixture was analyzed without any purification.

¹H-NMR (CD₂Cl₂, 400 MHz): δ = 0.87 (t, J = 7.5 Hz, 3H, **138**-CH₃), 0.98 (t, J = 7.2 Hz, 3H, **138**-CH₃), 1.50-1.58 (m, 2H, **138**-CH₂), 2.32-2.40 (m, 4H, **138**-CH₂), 3.44-3.50 (m, **140**-CH), 3.66 (distorted t, J = 6.6 Hz, **139**-CH) ppm. No starting material present. The signals at δ = 2.32-2.40 (4H, **138**), 3.44-3.50 (1H, **140**) and 3.66 (1H, **25b**) ppm were used for quantification.

Result for catalyst **30c**: 86% **138**, 5% **139** and 9% **140**.

13.4.13Cyclohex-2-enone (**141**)

(5044)



According to general procedure La with **141** (0.046 mL, 0.484 mmol) and a reaction time of 15 h. The reaction mixture was analyzed without any purification.

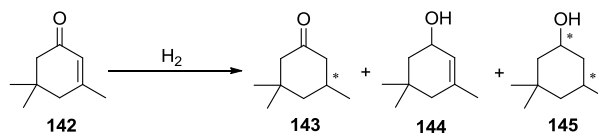
¹H-NMR (CDCl₃, 400 MHz): δ = 1.63-1.70 (m, 2H, **120**), 1.76-1.83 (m, 4H, **120**), 2.25 (t, J = 6.5 Hz, 4H, **120**), 1.08-1.30 (m, 5H, **119**-CH₂), 1.47-1.54 (m, 1H, **119**-CH₂), 1.65-1.73 (m, 2H, **119**-CH₂), 1.79-1.87 (m, 2H, **119**-CH₂), 2.57 (s, 1H, **119**-OH), 3.49-3.56 (m, 1H, **119**-CH-OH) ppm. Starting material **141** **¹H NMR** (CDCl₃, 400 MHz): δ = 1.96 (quin, J = 6.0 Hz, 2H, CH₂), 2.27-2.33 (m, 2H, CH₂), 2.37 (t, J = 7.0 Hz, 2H, CH₂), 5.95 (dt, J = 1.9, 10.2, 1H, CH), 6.95 (dt, J = 4.2, 10.2, 1H, CH) ppm. The absence of the signals at 5.95 (1H, **141**) and 6.95 (1H, **141**) ppm, indicates full conversion of starting material when catalysts **30c** or **30d** were used.

GC-FID (Agilent CP-Sil 8 CB, 30 m \times 0.25 mm, 0.25 μ m; split injector (1:50), T=270 °C, FID detector, carrier gas: N₂, 5 bar; 100-250 °C, 15 °/min): t_R = 4.7 min (**119**), 4.9 min (**120**), 5.4 min (**141**).

Results for catalyst **30c**: 100% **119**, results for catalyst **30d**: 5% **118**, 94% **120**.

13.4.143,5,5-Trimethylcyclohex-2-enone (142)

(4176, 5020)



According to procedure L with **142** (0.076 mL, 0.484 mmol). The reaction mixture was analyzed without any purification. GC-FID (Agilent CP-Sil 8 CB, 30 m × 0.25 mm, 0.25 μm; split injector (1:50), T=270 °C, FID detector, carrier gas: N₂, 5 bar; 100-250 °C, 15 °/min): t_R = 5.9 min (**134**), 6.1 min (**145**), 7.3 min (**142**). Chiral GC-FID (Chrompack CP-Chirasil-Dex CB, 25 m × 0.25 mm, 0.25 μm; split injector (1:80), T= 225 °C; FID detector, carrier gas: N₂, 5 bar; 40-120, 8 °/min, 120 °C 3 min): t_R = 9.8 min (**134**-enantiomer 1), 10.0 min (**134**-enantiomer 2), 11.2 min (**145**-diastereomer 1), 11.5 min (**145**-diastereomer 2), 11.9 min (**142**).

Catalyst	Reaction time	Procedure	conversion	Ratio 134: 144: 145	e.r. 134	d.r. 145
30c	23 h	Ea	100%	89 : 0 : 10	1 : 1	1 : 1
30c	23 h	Ea	94%	97 : 0 : 10	12 : 10	11 : 10
30f	15 h	Eb	100%	83 : 0 : 10	1 : 1	10 : 11
30g	15 h	Eb	100%	118 : 0 : 10	10 : 12	10 : 12
30h	15 h	Eb	100%	94 : 0 : 10	11 : 10	10 : 11
30i	15 h	Eb	72%	141 : 0 : 10	1 : 1	1 : 1
30j	15 h	Eb	100%	79 : 0 : 10	-	-
30h	15 h	Eb	<1%	1 : 0 : 0	-	-
30k	15 h	Eb	<1%	1 : 0 : 0	1 : 1	11 : 10
30l	15 h	Eb	100%	92 : 0 : 10	1 : 1	1 : 1

Bibliography

- [1] T. Ishiyama, J. Takagi, K. Ishida, N. Miyaura, N. R. Anastasi, J. F. Hartwig, *J. Am. Chem. Soc.* **2001**, *124*, 390–391.
- [2] T. Ishiyama, J. Takagi, J. F. Hartwig, N. Miyaura, *Angew. Chem. Int. Ed.* **2002**, *41*, 3056–3058.
- [3] J. P. Wolfe, S. L. Buchwald, *J. Am. Chem. Soc.* **1997**, *119*, 6054–6058.
- [4] J. J. Concepcion, J. W. Jurss, J. L. Templeton, T. J. Meyer, *J. Am. Chem. Soc.* **2008**, *130*, 16462–16463.
- [5] C. A. Tolman, *Chem. Rev.* **1977**, *77*, 313–348.
- [6] C. A. Tolman, *J. Am. Chem. Soc.* **1970**, *92*, 2953–2956.
- [7] G. Mestroni, A. Camus, *Inorg. Nucl. Chem. Letters* **1973**, *9*, 261–263.
- [8] G. Mestroni, A. Camus, G. Zassinovich, *J. Organomet. Chem.* **1974**, *73*, 119–127.
- [9] S. J. Roseblade, A. Pfaltz, *Acc. Chem. Res.* **2007**, *40*, 1402–1411.
- [10] E. M. Simmons, J. F. Hartwig, *Nature* **2012**, *483*, 70–73.
- [11] H. Brunner, U. Obermann, *Chem. Ber.* **1989**, *122*, 499–507.
- [12] J. Chen, X. Lu, W. Lou, Y. Ye, H. Jiang, W. Zeng, *J. Org. Chem.* **2012**, *77*, 8541–8548.
- [13] J. C. Anderson, G. P. Howell, R. M. Lawrence, C. S. Wilson, *J. Org. Chem.* **2005**, *70*, 5665–5670.
- [14] K. Yamaguchi, J. Yamaguchi, A. Studer, K. Itami, *Chemical Science* **2012**, *3*, 2165–2169.
- [15] J. M. Takacs, E. C. Lawson, J. Michael Reno, M. A. Youngman, D. A. Quinicy, *Tetrahedron: Asymmetry* **1997**, *8*, 3073–3078.
- [16] D. L. Davies, J. Fawcett, S. A. Garratt, D. R. Russell, *J. Organomet. Chem.* **2002**, *662*, 43–50.
- [17] N. K. Shee, S. Nag, M. G. B. Drew, D. Datta, *Inorg. Chim. Acta* **2013**, *405*, 111–115.
- [18] G. Desimoni, G. Faita, K. A. Jørgensen, *Chem. Rev.* **2011**, *111*, PR284–PR437.
- [19] H. Nishiyama, S. Yamaguchi, S.-B. Park, K. Itoh, *Tetrahedron: Asymmetry* **1993**, *4*, 143–150.
- [20] D. Müller, G. Umbricht, B. Weber, A. Pfaltz, *Helv. Chim. Acta* **1991**, *74*, 232–240.
- [21] I. Butula, G. Karlović, *Liebigs Ann. Chem.* **1976**, *1976*, 1455–1464.
- [22] R. I. McDonald, P. B. White, A. B. Weinstein, C. P. Tam, S. S. Stahl, *Org. Lett.* **2011**, *13*, 2830–2833.
- [23] F. Menges, M. Neuburger, A. Pfaltz, *Org. Lett.* **2002**, *4*, 4713–4716.
- [24] G. Chelucci, S. Medici, A. Saba, *Tetrahedron: Asymmetry* **1997**, *8*, 3183–3184.
- [25] A. Scheurer, P. Mosset, W. Bauer, Rolf W. Saalfrank, *Eur. J. Org. Chem.* **2001**, *2001*, 3067–3074.
- [26] U. Bremberg, F. Rahm, C. Moberg, *Tetrahedron: Asymmetry* **1998**, *9*, 3437–3443.
- [27] C. G. Frost, J. M. J. Williams, *Tetrahedron Lett.* **1993**, *34*, 2015–2018.
- [28] H. Witte, W. Seeliger, *Angew. Chem. Int. Ed.* **1972**, *11*, 287–288.
- [29] C. Bolm, K. Weickhardt, M. Zehnder, T. Ranff, *Chem. Ber.* **1991**, *124*, 1173–1180.
- [30] B. W. Michel, L. D. Steffens, M. S. Sigman, *J. Am. Chem. Soc.* **2011**, *133*, 8317–8325.
- [31] H. A. McManus, P. J. Guiry, *J. Org. Chem.* **2002**, *67*, 8566–8573.
- [32] H. Vorbrüggen, K. Krolkiewicz, *Tetrahedron* **1993**, *49*, 9353–9372.
- [33] M. Peer, J. C. de Jong, M. Kiefer, T. Langer, H. Rieck, H. Schell, P. Sennhenn, J. Sprinz, H. Steinhagen, B. Wiese, G. Helmchen, *Tetrahedron* **1996**, *52*, 7547–7583.
- [34] D. Sirbu, G. Consiglio, B. Milani, P. G. A. Kumar, P. S. Pregosin, S. Gischig, *J. Organomet. Chem.* **2005**, *690*, 2254–2262.
- [35] S. E. Denmark, N. Nakajima, O. J. C. Nicaise, A.-M. Faucher, J. P. Edwards, *J. Org. Chem.* **1995**, *60*, 4884–4892.
- [36] A. J. Phillips, Y. Uto, P. Wipf, M. J. Reno, D. R. Williams, *Org. Lett.* **2000**, *2*, 1165–1168.
- [37] H. A. McManus, S. M. Barry, P. G. Andersson, P. J. Guiry, *Tetrahedron* **2004**, *60*, 3405–3416.
- [38] M. Z. Gao, B. Wang, D. Kong, R. A. Zingaro, A. Clearfield, Z. L. Xu, *Synth. Commun.* **2005**, *35*, 2665–2673.
- [39] H. Bao, U. K. Tambar, *J. Am. Chem. Soc.* **2012**, *134*, 18495–18498.
- [40] L. Mei, Z. J. Hai, S. Jie, Z. S. Ming, Y. Hao, H. K. Liang, *ACS Comb. Sci.* **2009**, *11*, 220–227.
- [41] M. Gomez, S. Jansat, G. Muller, M. A. Maestro, J. M. Saavedra, M. Font-Bardia, X. Solans, *J. Chem. Soc., Dalton Trans.* **2001**, 1432–1439.

- [42] S. Hanessian, E. Jnoff, N. Bernstein, M. Simard, *Can. J. Chem.* **2004**, *82*, 306–313.
- [43] S.-g. Lee, C. W. Lim, C. E. Song, I. O. Kim, C.-H. Jun, *Tetrahedron: Asymmetry* **1997**, *8*, 2927–2932.
- [44] D. H. Woodmansee, A. Pfaltz, *Chem. Commun.* **2011**, *47*, 7912–7916.
- [45] T.-S. Mei, E. W. Werner, A. J. Burckle, M. S. Sigman, *J. Am. Chem. Soc.* **2013**, *135*, 6830–6833.
- [46] J. J. Miller, S. Rajaram, C. Pfaffenroth, M. S. Sigman, *Tetrahedron* **2009**, *65*, 3110–3119.
- [47] S. Rajaram, M. S. Sigman, *Org. Lett.* **2005**, *7*, 5473–5475.
- [48] P. Västilä, I. M. Pastor, H. Adolfsson, *J. Org. Chem.* **2005**, *70*, 2921–2929.
- [49] Y. Kodama, M. Ori, T. Nishio, *Helv. Chim. Acta* **2005**, *88*, 187–193.
- [50] B. Hoppe, J. Martens, *Chemie in unserer Zeit* **1984**, *18*, 73–86.
- [51] L. Krieg, Düsseldorf, **2002**, pp. 4–9.
- [52] Y. J. Mast, W. Wohlleben, E. Schinko, *Journal of Biotechnology* **2011**, *155*, 63–67.
- [53] A. S. Bommarius, M. Schwarm, K. Stingl, M. Kottenhahn, K. Huthmacher, K. Drauz, *Tetrahedron: Asymmetry* **1995**, *6*, 2851–2888.
- [54] S. M. Podhajsky, Y. Iwai, A. Cook-Sneathen, M. S. Sigman, *Tetrahedron* **2011**, *67*, 4435–4441.
- [55] S.-g. Lee, C. W. Lim, C. E. Song, I. O. Kim, *Tetrahedron: Asymmetry* **1997**, *8*, 4027–4031.
- [56] Y. Himeda, N. Onozawa-Komatsuzaki, H. Sugihara, H. Arakawa, K. Kasuga, *J. Mol. Catal. A: Chem.* **2003**, *195*, 95–100.
- [57] R. Boulch, A. Scheurer, P. Mosset, R. W. Saalfrank *, *Tetrahedron Lett.* **2000**, *41*, 1023–1026.
- [58] G. Chelucci, M. G. Sanna, S. Gladiali, *Tetrahedron* **2000**, *56*, 2889–2893.
- [59] G. Chelucci, S. Medici, A. Saba, *Tetrahedron: Asymmetry* **1999**, *10*, 543–550.
- [60] G. Chelucci, S. P. Deriu, A. Saba, R. Valenti, *Tetrahedron: Asymmetry* **1999**, *10*, 1457–1464.
- [61] G. Chelucci, S. Deriu, G. A. Pinna, A. Saba, R. Valenti, *Tetrahedron: Asymmetry* **1999**, *10*, 3803–3809.
- [62] M. Austeri, D. Linder, J. Lacour, *Chem. Eur. J.* **2008**, *14*, 5737–5741.
- [63] K. H. Jensen, T. P. Pathak, Y. Zhang, M. S. Sigman, *J. Am. Chem. Soc.* **2009**, *131*, 17074–17075.
- [64] K. H. Jensen, J. D. Webb, M. S. Sigman, *J. Am. Chem. Soc.* **2010**, *132*, 17471–17482.
- [65] R. Jana, T. P. Pathak, K. H. Jensen, M. S. Sigman, *Org. Lett.* **2012**, *14*, 4074–4077.
- [66] K. S. Yoo, C. P. Park, C. H. Yoon, S. Sakaguchi, J. O'Neil, K. W. Jung, *Org. Lett.* **2007**, *9*, 3933–3935.
- [67] C. C. Oliveira, R. A. Angnes, C. R. D. Correia, *J. Org. Chem.* **2013**, *78*, 4373–4385.
- [68] G. Yang, C. Shen, W. Zhang, *Angew. Chem. Int. Ed.* **2012**, *51*, 9141–9145.
- [69] F. Jiang, Z. Wu, W. Zhang, *Tetrahedron Lett.* **2010**, *51*, 5124–5126.
- [70] X. Ye, P. B. White, S. S. Stahl, *J. Org. Chem.* **2013**, *78*, 2083–2090.
- [71] A. B. Weinstein, S. S. Stahl, *Angew. Chem. Int. Ed.* **2012**, *51*, 11505–11509.
- [72] R. H. Crabtree, *The Organometallic Chemistry of the Transition Metals*, 5th ed., Wiley & Sons, Hoboken, New Jersey, USA, **2009**.
- [73] C. Elschenbroich, *Organometallic Chemie*, 6th ed., B. G. Teubner Verlag, Wiesbaden, Germany, **2008**.
- [74] A. Behr, *Angewandte Homogene Katalyse*, 1st ed., Wiley-VCH Verlag GmbH Co. KGaA, Weinheim, Germany, **2008**.
- [75] B. C. G. S. Louis S. Hegedus, *Transition Metals in the Synthesis of Complex Molecules*, 3rd ed., University Science Books Sausalito, California, USA, **2010**.
- [76] E. W. Abel, F. G. A. Stone, *Quarterly Reviews, Chemical Society* **1969**, *23*, 325–371.
- [77] D. G. Gusev, *Organometallics* **2009**, *28*, 763–770.
- [78] W. Strohmeier, F.-J. Müller, *Chem. Ber.* **1967**, *100*, 2812–2821.
- [79] W. Strohmeier, F. J. Müller, *Z. Naturforsch.* **1967**, *22b*, 451–452.
- [80] R. Dorta, E. D. Stevens, N. M. Scott, C. Costabile, L. Cavallo, C. D. Hoff, S. P. Nolan, *J. Am. Chem. Soc.* **2005**, *127*, 2485–2495.
- [81] D. G. Gusev, *Organometallics* **2009**, *28*, 6458–6461.
- [82] S. C. van der Slot, J. Duran, J. Luten, P. C. J. Kamer, P. W. N. M. van Leeuwen, *Organometallics* **2002**, *21*, 3873–3883.
- [83] A. Fürstner, M. Alcarazo, H. Krause, C. W. Lehmann, *J. Am. Chem. Soc.* **2007**, *129*, 12676–12677.
- [84] W. A. Herrmann, J. Schütz, G. D. Frey, E. Herdtweck, *Organometallics* **2006**, *25*, 2437–2448.

- [85] G. Altenhoff, R. Goddard, C. W. Lehmann, F. Glorius, *J. Am. Chem. Soc.* **2004**, *126*, 15195–15201.
- [86] A. R. Chianese, X. Li, M. C. Janzen, J. W. Faller, R. H. Crabtree, *Organometallics* **2003**, *22*, 1663–1667.
- [87] T. A. Schmedake, M. Haaf, B. J. Paradise, A. J. Millevolte, D. R. Powell, R. West, *J. Organomet. Chem.* **2001**, *636*, 17–25.
- [88] C. Cocevar, G. Mestroni, A. Camus, *J. Organomet. Chem.* **1972**, *35*, 389–395.
- [89] G. Mestroni, A. Camus, G. Zassinovich, *J. Organomet. Chem.* **1974**, *65*, 119–129.
- [90] G. Clauti, G. Zassinovich, G. Mestroni, *Inorg. Chim. Acta* **1986**, *112*, 103–106.
- [91] P. Haddad, A. Mauro, V. Nogueira, S. Klein, *Transition Metal Chemistry* **2003**, *28*, 899–904.
- [92] L. Kromer, B. Spingler, R. Alberto, *Dalton Trans.* **2008**, 5800–5806.
- [93] B. Li, T. Liu, C. V. Popescu, A. Bilko, M. Y. Darensbourg, *Inorg. Chem.* **2009**, *48*, 11283–11289.
- [94] W.-F. Liaw, J.-H. Lee, H.-B. Gau, C.-H. Chen, G.-H. Lee, *Inorg. Chim. Acta* **2001**, *322*, 99–105.
- [95] A. G. W. Hodson, S. J. Coles, M. B. Hursthouse, *Polyhedron* **2007**, *26*, 1285–1291.
- [96] P. Frediani, M. Bianchi, A. Salvini, R. Guarducci, L. C. Carluccio, F. Piacenti, *J. Organomet. Chem.* **1994**, *476*, 7–11.
- [97] G. Song, Y. Zhang, Y. Su, W. Deng, K. Han, X. Li, *Organometallics* **2008**, *27*, 6193–6201.
- [98] R. Trebbe, R. Goddard, A. Ruffinska, K. Seevogel, K.-R. Pörschke, *Organometallics* **1999**, *18*, 2466–2472.
- [99] A. Lightfoot, P. Schnider, A. Pfaltz, *Angew. Chem. Int. Ed.* **1998**, *37*, 2897–2899.
- [100] G. K. N. Reddy, C. H. Susheelamma, *J. Chem. Soc. D: Chem. Comm.* **1970**, 54–54.
- [101] J. V. Kingston, G. R. Scollary, *J. Chem. Soc. D: Chem. Comm.* **1970**, 670–670.
- [102] B. C. Hui, B. R. James, *Inorg. Nucl. Chem. Letters* **1970**, *6*, 367–370.
- [103] B. P. Sullivan, D. J. Salmon, T. J. Meyer, *Inorg. Chem.* **1978**, *17*, 3334–3341.
- [104] L. Spiccia, G. B. Deacon, C. M. Kepert, *Coord. Chem. Rev.* **2004**, *248*, 1329–1341.
- [105] D. Heseck, Y. Inoue, S. R. L. Everitt, H. Ishida, M. Kunieda, M. G. B. Drew, *Inorg. Chem.* **2000**, *39*, 308–316.
- [106] R. P. Thummel, F. Lefoulon, S. Chirayil, *Inorg. Chem.* **1987**, *26*, 3072–3074.
- [107] G. C. Vougioukalakis, T. Stergiopoulos, G. Kantonis, A. G. Kontos, K. Papadopoulos, A. Stublla, P. G. Potvin, P. Falaras, *J. Photochem Photobio. A: Chem.* **2010**, *214*, 22–32.
- [108] S. H. Wadman, J. M. Kroon, K. Bakker, R. W. A. Havenith, G. P. M. van Klink, G. van Koten, *Organometallics* **2010**, *29*, 1569–1579.
- [109] N. C. Thomas, G. B. Deacon, A. Llobet, T. J. Meyer, in *Inorg. Synth.*, John Wiley & Sons, Inc., **2007**, pp. 107–110.
- [110] P. A. Anderson, G. B. Deacon, K. H. Haarmann, F. R. Keene, T. J. Meyer, D. A. Reitsma, B. W. Skelton, G. F. Strouse, N. C. Thomas, *Inorg. Chem.* **1995**, *34*, 6145–6157.
- [111] G. B. Deacon, C. M. Kepert, N. Sahely, B. W. Skelton, L. Spiccia, N. C. Thomas, A. H. White, *J. Chem. Soc., Dalton Trans.* **1999**, 275–278.
- [112] M. Haukka, J. Kiviaho, M. Ahlgren, T. A. Pakkanen, *Organometallics* **1995**, *14*, 825–833.
- [113] P. Homanen, M. Haukka, T. A. Pakkanen, J. Pursiainen, R. H. Laitinen, *Organometallics* **1996**, *15*, 4081–4084.
- [114] P. Homanen, M. Haukka, S. Luukkanen, M. Ahlgren, T. A. Pakkanen, *Eur. J. Inorg. Chem.* **1999**, *1999*, 101–106.
- [115] M. Haukka, P. Hirva, S. Luukkanen, M. Kallinen, M. Ahlgren, T. A. Pakkanen, *Inorg. Chem.* **1999**, *38*, 3182–3189.
- [116] E. Eskelinen, S. Luukkanen, M. Haukka, M. Ahlgren, T. A. Pakkanen, *J. Chem. Soc., Dalton Trans.* **2000**, 2745–2752.
- [117] D. Black, G. Deacon, N. Thomas, *Aust. J. Chem.* **1982**, *35*, 2445–2453.
- [118] N. C. Fletcher, F. Richard Keene, *J. Chem. Soc., Dalton Trans.* **1998**, 2293–2302.
- [119] L. Ruiz-Ramirez, T. A. Stephenson, *J. Chem. Soc., Dalton Trans.* **1974**, 1640–1650.
- [120] J. A. Treadway, T. J. Meyer, *Inorg. Chem.* **1999**, *38*, 2267–2278.
- [121] C. M. Kepert, G. B. Deacon, N. Sahely, L. Spiccia, G. D. Fallon, B. W. Skelton, A. H. White, *Inorg. Chem.* **2004**, *43*, 2818–2827.
- [122] D. A. Freedman, J. K. Evju, M. K. Pomije, K. R. Mann, *Inorg. Chem.* **2001**, *40*, 5711–5715.
- [123] D. R. Robertson, I. W. Robertson, T. A. Stephenson, *J. Organomet. Chem.* **1980**, *202*, 309–318.
- [124] S. Günnaz, N. Özdemir, S. Dayan, O. Dayan, B. Çetinkaya, *Organometallics* **2011**, *30*, 4165–4173.

- [125] M. H. V. Huynh, J. Smyth, M. Wetzler, B. Mort, P. K. Gong, L. M. Witham, D. L. Jameson, D. K. Geiger, J. M. Lasker, M. Charepoo, M. Gornikiewicz, J. M. Cintron, G. Imahori, R. R. Sanchez, A. C. Marschilok, L. M. Krajkowski, D. G. Churchill, M. R. Churchill, K. J. Takeuchi, *Angew. Chem. Int. Ed.* **2001**, *40*, 4469–4473.
- [126] X. Hua, M. Shang, A. G. Lappin, *Inorg. Chem.* **1997**, *36*, 3735–3740.
- [127] I. P. Evans, A. Spencer, G. Wilkinson, *J. Chem. Soc., Dalton Trans.* **1973**, 204–209.
- [128] O. Johansson, M. Borgström, R. Lomoth, M. Palmblad, J. Bergquist, L. Hammarström, L. Sun, B. Åkermark, *Inorg. Chem.* **2003**, *42*, 2908–2918.
- [129] S. M. Zakeeruddin, M. K. Nazeeruddin, R. Humphry-Baker, P. Péchy, P. Quagliotto, C. Barolo, G. Viscardi, M. Grätzel, *Langmuir* **2002**, *18*, 952–954.
- [130] K. A. Maxwell, M. Sykora, J. M. DeSimone, T. J. Meyer, *Inorg. Chem.* **1999**, *39*, 71–75.
- [131] R. Ziessel, V. Grosshenny, M. Hissler, C. Stroh, *Inorg. Chem.* **2004**, *43*, 4262–4271.
- [132] V. Grosshenny, R. Ziessel, *J. Organomet. Chem.* **1993**, *453*, C19–C22.
- [133] S. M. Zakeeruddin, M. K. Nazeeruddin, R. Humphry-Baker, M. Grätzel, V. Shklover, *Inorg. Chem.* **1998**, *37*, 5251–5259.
- [134] M. Toyama, K.-i. Inoue, S. Iwamatsu, N. Nagao, *Bull. Chem. Soc. Jpn.* **2006**, *79*, 1525–1534.
- [135] F. Geneste, C. Moinet, G. Jezequel, *New J. Chem.* **2002**, *26*, 1539–1541.
- [136] T. Lazarides, H. Adams, D. Sykes, S. Faulkner, G. Calogero, M. D. Ward, *Dalton Trans.* **2008**, 691–698.
- [137] E. Alessio, G. Mestroni, G. Nardin, W. M. Attia, M. Calligaris, G. Sava, S. Zorzet, *Inorg. Chem.* **1988**, *27*, 4099–4106.
- [138] I. Serrano, X. Sala, E. Plantalech, M. Rodríguez, I. Romero, S. Jansat, M. Gómez, T. Parella, H. Stoeckli-Evans, X. Solans, M. Font-Bardia, B. Vidjayacoumar, A. Llobet, *Inorg. Chem.* **2007**, *46*, 5381–5389.
- [139] S. P. Mulcahy, K. Grundler, C. Frias, L. Wagner, A. Prokop, E. Meggers, *Dalton Trans.* **2010**, *39*, 8177–8182.
- [140] Z. Chen, J. J. Concepcion, J. W. Jurss, T. J. Meyer, *J. Am. Chem. Soc.* **2009**, *131*, 15580–15581.
- [141] Z. Chen, J. J. Concepcion, H. Luo, J. F. Hull, A. Paul, T. J. Meyer, *J. Am. Chem. Soc.* **2010**, *132*, 17670–17673.
- [142] A. K. Vannucci, J. F. Hull, Z. Chen, R. A. Binstead, J. J. Concepcion, T. J. Meyer, *J. Am. Chem. Soc.* **2012**, *134*, 3972–3975.
- [143] A. K. Vannucci, L. Alibabaei, M. D. Losego, J. J. Concepcion, B. Kalanyan, G. N. Parsons, T. J. Meyer, *Proceedings of the National Academy of Sciences* **2013**, *110*, 20918–20922.
- [144] W. Chen, F. N. Rein, R. C. Rocha, *Angew. Chem. Int. Ed.* **2009**, *48*, 9672–9675.
- [145] T. Kojima, K. Nakayama, M. Sakaguchi, T. Ogura, K. Ohkubo, S. Fukuzumi, *J. Am. Chem. Soc.* **2011**, *133*, 17901–17911.
- [146] J. Clayden, N. Greeves, S. Warren, P. Wothers, *Organic Chemistry*, 1st ed., Oxford University Press, Oxford New York, USA, **2007**.
- [147] M. Nishida, T. Tagata, *Journal of Synthetic Organic Chemistry, Japan* **2011**, *69*, 1212–1220.
- [148] T. Kinzel, Y. Zhang, S. L. Buchwald, *J. Am. Chem. Soc.* **2010**, *132*, 14073–14075.
- [149] A. D. Finke, J. S. Moore, *Org. Lett.* **2008**, *10*, 4851–4854.
- [150] D. W. Robbins, J. F. Hartwig, *Org. Lett.* **2012**, *14*, 4266–4269.
- [151] A. G. Crawford, Z. Liu, I. A. I. Mkhaliid, M.-H. Thibault, N. Schwarz, G. Alcaraz, A. Steffen, J. C. Collings, A. S. Batsanov, J. A. K. Howard, T. B. Marder, *Chem. Eur. J.* **2012**, *18*, 5022–5035.
- [152] T. Teraoka, S. Hiroto, H. Shinokubo, *Org. Lett.* **2011**, *13*, 2532–2535.
- [153] J.-H. Cheng, C.-L. Yi, T.-J. Liu, C.-F. Lee, *Chem. Comm.* **2012**, *48*, 8440–8442.
- [154] J. F. Hartwig, *Chem. Soc. Rev.* **2011**, *40*, 1992–2002.
- [155] N. D. Litvinas, P. S. Fier, J. F. Hartwig, *Angew. Chem. Int. Ed.* **2012**, *51*, 536–539.
- [156] T. Liu, X. Shao, Y. Wu, Q. Shen, *Angew. Chem. Int. Ed.* **2012**, *51*, 540–543.
- [157] J. M. Murphy, C. C. Tzschucke, J. F. Hartwig, *Org. Lett.* **2007**, *9*, 757–760.
- [158] S. Manna, S. Maity, S. Rana, S. Agasti, D. Maiti, *Org. Lett.* **2012**, *14*, 1736–1739.
- [159] C. C. Tzschucke, J. M. Murphy, J. F. Hartwig, *Org. Lett.* **2007**, *9*, 761–764.
- [160] H. Tajuddin, L. Shukla, A. C. Maxwell, T. B. Marder, P. G. Steel, *Org. Lett.* **2010**, *12*, 5700–5703.
- [161] C. N. Iverson, M. R. Smith, *J. Am. Chem. Soc.* **1999**, *121*, 7696–7697.
- [162] J.-Y. Cho, C. N. Iverson, M. R. Smith, *J. Am. Chem. Soc.* **2000**, *122*, 12868–12869.
- [163] M. K. Tse, J.-Y. Cho, M. R. Smith, *Org. Lett.* **2001**, *3*, 2831–2833.

- [164] J.-Y. Cho, M. K. Tse, D. Holmes, R. E. Maleczka, M. R. Smith, *Science* **2002**, *295*, 305–308.
- [165] T. Ishiyama, Y. Nobuta, J. F. Hartwig, N. Miyaura, *Chem. Comm.* **2003**, 2924–2925.
- [166] C. W. Liskey, C. S. Wei, D. R. Pahls, J. F. Hartwig, *Chem. Comm.* **2009**, 5603–5605.
- [167] I. I. B. A. Vanchura, S. M. Preshlock, P. C. Roosen, V. A. Kallepalli, R. J. Staples, J. R. E. Maleczka, D. A. Singleton, I. I. I. M. R. Smith, *Chem. Comm.* **2010**, *46*, 7724–7726.
- [168] H. Tamura, H. Yamazaki, H. Sato, S. Sakaki, *J. Am. Chem. Soc.* **2003**, *125*, 16114–16126.
- [169] G. A. Chotana, I. I. B. A. Vanchura, M. K. Tse, R. J. Staples, J. R. E. Maleczka, I. I. I. M. R. Smith, *Chem. Comm.* **2009**, 5731–5733.
- [170] T. M. Boller, J. M. Murphy, M. Hapke, T. Ishiyama, N. Miyaura, J. F. Hartwig, *J. Am. Chem. Soc.* **2005**, *127*, 14263–14278.
- [171] P. C. Roosen, V. A. Kallepalli, B. Chattopadhyay, D. A. Singleton, R. E. Maleczka, M. R. Smith, *J. Am. Chem. Soc.* **2012**, *134*, 11350–11353.
- [172] M. A. Larsen, J. F. Hartwig, *J. Am. Chem. Soc.* **2014**, *136*, 4287–4299.
- [173] T. Ishiyama, J. Takagi, Y. Yonekawa, J. F. Hartwig, N. Miyaura, *Adv. Synth. Catal.* **2003**, *345*, 1103–1106.
- [174] J. Takagi, K. Sato, J. F. Hartwig, T. Ishiyama, N. Miyaura, *Tetrahedron Lett.* **2002**, *43*, 5649–5651.
- [175] H. Tajuddin, P. Harrisson, B. Bitterlich, J. C. Collings, N. Sim, A. S. Batsanov, M. S. Cheung, S. Kawamorita, A. C. Maxwell, L. Shukla, J. Morris, Z. Lin, T. B. Marder, P. G. Steel, *Chemical Science* **2012**, *3*, 3505–3515.
- [176] A. G. Green, P. Liu, C. A. Merlic, K. N. Houk, *J. Am. Chem. Soc.* **2014**, *136*, 4575–4583.
- [177] A. J. Roering, L. V. A. Hale, P. A. Squier, M. A. Ringgold, E. R. Wiederspan, T. B. Clark, *Org. Lett.* **2012**, *14*, 3558–3561.
- [178] T. Ishiyama, H. Isou, T. Kikuchi, N. Miyaura, *Chem. Comm.* **2010**, *46*, 159–161.
- [179] S. H. Cho, J. F. Hartwig, *J. Am. Chem. Soc.* **2013**, *135*, 8157–8160.
- [180] T. E. Hurst, T. K. Macklin, M. Becker, E. Hartmann, W. Kügel, J.-C. Parisienne-La Salle, A. S. Batsanov, T. B. Marder, V. Snieckus, *Chem. Eur. J.* **2010**, *16*, 8155–8161.
- [181] T. Mita, Y. Ikeda, K. Michigami, Y. Sato, *Chem. Comm.* **2013**, *49*, 5601–5603.
- [182] A. Ros, B. Estepa, R. López-Rodríguez, E. Álvarez, R. Fernández, J. M. Lassaletta, *Angew. Chem. Int. Ed.* **2011**, *50*, 11724–11728.
- [183] T. Ohmura, T. Torigoe, M. Sugimoto, *Organometallics* **2013**, *32*, 6170–6173.
- [184] T. Ohmura, T. Torigoe, M. Sugimoto, *J. Am. Chem. Soc.* **2012**, *134*, 17416–17419.
- [185] Q. Li, C. W. Liskey, J. F. Hartwig, *J. Am. Chem. Soc.* **2014**, *136*, 8755–8765.
- [186] C. W. Liskey, J. F. Hartwig, *J. Am. Chem. Soc.* **2012**, *134*, 12422–12425.
- [187] H. Chen, J. F. Hartwig, *Angew. Chem. Int. Ed.* **1999**, *38*, 3391–3393.
- [188] C. E. Webster, Y. Fan, M. B. Hall, D. Kunz, J. F. Hartwig, *J. Am. Chem. Soc.* **2003**, *125*, 858–859.
- [189] K. Kawamura, J. F. Hartwig, *J. Am. Chem. Soc.* **2001**, *123*, 8422–8423.
- [190] J. M. Murphy, J. D. Lawrence, K. Kawamura, C. Incarvito, J. F. Hartwig, *J. Am. Chem. Soc.* **2006**, *128*, 13684–13685.
- [191] H. Chen, S. Schlecht, T. C. Semple, J. F. Hartwig, *Science* **2000**, *287*, 1995–1997.
- [192] J. F. Hartwig, *Acc. Chem. Res.* **2011**, *45*, 864–873.
- [193] N. Tsukada, J. F. Hartwig, *J. Am. Chem. Soc.* **2005**, *127*, 5022–5023.
- [194] E. M. Simmons, J. F. Hartwig, *J. Am. Chem. Soc.* **2010**, *132*, 17092–17095.
- [195] B. Li, M. Driess, J. F. Hartwig, *J. Am. Chem. Soc.* **2014**, *136*, 6586–6589.
- [196] S. M. Bachrach, *J. Org. Chem.* **2008**, *73*, 2466–2468.
- [197] A. Fürstner, K. Langemann, *J. Org. Chem.* **1996**, *61*, 8746–8749.
- [198] R. M. Beesley, C. K. Ingold, J. F. Thorpe, *Journal of the Chemical Society, Transactions* **1915**, *107*, 1080–1106.
- [199] Y. Kuninobu, T. Nakahara, H. Takeshima, K. Takai, *Org. Lett.* **2013**, *15*, 426–428.
- [200] A. Parija, R. B. Sunoj, *Org. Lett.* **2013**, *15*, 4066–4069.
- [201] H. Nishiyama, H. Sakaguchi, T. Nakamura, M. Horihata, M. Kondo, K. Itoh, *Organometallics* **1989**, *8*, 846–848.
- [202] W.-L. Duan, M. Shi, G.-B. Rong, *Chem. Comm.* **2003**, 2916–2917.
- [203] V. César, S. Bellemin-Laponnaz, H. Wadepohl, L. H. Gade, *Chem. Eur. J.* **2005**, *11*, 2862–2873.
- [204] C. Reyes, A. Prock, W. P. Giering, *J. Organomet. Chem.* **2003**, *671*, 13–26.
- [205] R. Kuwano, T. Uemura, M. Saitoh, Y. Ito, *Tetrahedron: Asymmetry* **2004**, *15*, 2263–2271.
- [206] A. Albright, R. E. Gawley, *J. Am. Chem. Soc.* **2011**, *133*, 19680–19683.

- [207] J. F. Hartwig, *Organotransition Metal Chemistry*, 1st ed., University Science Books, **2010**.
- [208] H. Takaya, T. Ohta, N. Sayo, H. Kumobayashi, S. Akutagawa, S. Inoue, I. Kasahara, R. Noyori, *J. Am. Chem. Soc.* **1987**, *109*, 1596–1597.
- [209] G. Helmchen, A. Pfaltz, *Acc. Chem. Res.* **2000**, *33*, 336–345.
- [210] A. Pfaltz, J. Blankenstein, R. Hilgraf, E. Hörmann, S. McIntyre, F. Menges, M. Schönleber, S. P. Smidt, B. Wüstenberg, N. Zimmermann, *Adv. Synth. Catal.* **2003**, *345*, 33–43.
- [211] K. Källström, I. Munslow, P. G. Andersson, *Chem. Eur. J.* **2006**, *12*, 3194–3200.
- [212] A. Bartoszewicz, N. Ahlsten, B. Martín-Matute, *Chem. Eur. J.* **2013**, *19*, 7274–7302.
- [213] J. J. Verendel, O. Pàmies, M. Diéguez, P. G. Andersson, *Chem. Rev.* **2013**, *114*, 2130–2169.
- [214] D. G. Blackmond, A. Lightfoot, A. Pfaltz, T. Rosner, P. Schnider, N. Zimmermann, *Chirality* **2000**, *12*, 442–449.
- [215] R. H. Crabtree, H. Felkin, T. Fillebeen-Khan, G. E. Morris, *J. Organomet. Chem.* **1979**, *168*, 183–195.
- [216] R. Crabtree, *Acc. Chem. Res.* **1979**, *12*, 331–337.
- [217] P. Brandt, C. Hedberg, P. G. Andersson, *Chem. Eur. J.* **2003**, *9*, 339–347.
- [218] J. Mazuela, P.-O. Norrby, P. G. Andersson, O. Pàmies, M. Diéguez, *J. Am. Chem. Soc.* **2011**, *133*, 13634–13645.
- [219] Y. Fan, X. Cui, K. Burgess, M. B. Hall, *J. Am. Chem. Soc.* **2004**, *126*, 16688–16689.
- [220] R. Dietiker, P. Chen, *Angew. Chem. Int. Ed.* **2004**, *43*, 5513–5516.
- [221] S. Gruber, A. Pfaltz, *Angew. Chem. Int. Ed.* **2014**, *53*, 1896–1900.
- [222] K. H. Hopmann, L. Frediani, A. Bayer, *Organometallics* **2014**, *33*, 2790–2797.
- [223] M. Sparta, C. Riplinger, F. Neese, *Journal of Chemical Theory and Computation* **2014**, *10*, 1099–1108.
- [224] S. Gruber, M. Neuburger, A. Pfaltz, *Organometallics* **2013**, *32*, 4702–4711.
- [225] S. P. Smidt, A. Pfaltz, E. Martínez-Viviente, P. S. Pregosin, A. Albinati, *Organometallics* **2003**, *22*, 1000–1009.
- [226] S. P. Smidt, N. Zimmermann, M. Studer, A. Pfaltz, *Chem. Eur. J.* **2004**, *10*, 4685–4693.
- [227] S. Bell, B. Wüstenberg, S. Kaiser, F. Menges, T. Netscher, A. Pfaltz, *Science* **2006**, *311*, 642–644.
- [228] Pier G. Cozzi, N. Zimmermann, R. Hilgraf, S. Schaffner, A. Pfaltz, *Adv. Synth. Catal.* **2001**, *343*, 450–454.
- [229] D. Ragueot, A. Pfaltz, *Helv. Chim. Acta* **2012**, *95*, 2176–2193.
- [230] A. Schumacher, M. Bernasconi, A. Pfaltz, *Angew. Chem. Int. Ed.* **2013**, *52*, 7422–7425.
- [231] J. Shang, Z. Han, Y. Li, Z. Wang, K. Ding, *Chem. Commun.* **2012**, *48*, 5172–5174.
- [232] M.-A. Müller, A. Pfaltz, *Angew. Chem. Int. Ed.* **2014**, *53*, 8668–8671.
- [233] J.-Q. Li, X. Quan, P. G. Andersson, *Chem. Eur. J.* **2012**, *18*, 10609–10616.
- [234] G. Helmchen, A. Krotz, K.-T. Ganz, D. Hansen, *Synlett* **1991**, *1991*, 257–259.
- [235] R. Alan Aitken, D. P. Armstrong, R. H. B. Galt, S. T. E. Mesher, *J. Chem. Soc., Perkin Trans. 1* **1997**, 935–944.
- [236] J. P. Perdew, *Physical Review B* **1986**, *33*, 8822–8824.
- [237] A. D. Becke, *Physical Review A* **1988**, *38*, 3098–3100.
- [238] M. J. Cowley, R. W. Adams, K. D. Atkinson, M. C. R. Cockett, S. B. Duckett, G. G. R. Green, J. A. B. Lohman, R. Kerssebaum, D. Kilgour, R. E. Mewis, *J. Am. Chem. Soc.* **2011**, *133*, 6134–6137.
- [239] C. R. Baiz, P. L. McRobbie, J. M. Anna, E. Geva, K. J. Kubarych, *Acc. Chem. Res.* **2009**, *42*, 1395–1404.
- [240] J. R. Webb, T. M. Figg, B. M. Otten, T. R. Cundari, T. B. Gunnoe, M. Sabat, *Eur. J. Inorg. Chem.* **2013**, *2013*, 4515–4525.
- [241] W. E. Buschmann, J. S. Miller, *Chem. Eur. J.* **1998**, *4*, 1731–1737.
- [242] F.-W. Grevels, K. Kerpen, W. E. Klotzbücher, R. E. D. McClung, G. Russell, M. Viotte, K. Schaffner, *J. Am. Chem. Soc.* **1998**, *120*, 10423–10433.
- [243] D. F. Shriver, P. W. Atkins, C. H. Langford, *Anorganische Chemie*, WILEY-VCH GmbH, Weinheim, **2004**.
- [244] S. Wiebalck, Master Thesis thesis, Freie Universität Berlin (Berlin), **2010**.
- [245] T. Ishiyama, M. Murata, N. Miyaura, *J. Org. Chem.* **1995**, *60*, 7508–7510.
- [246] T. Nishimura, T. Onoue, K. Ohe, S. Uemura, *J. Org. Chem.* **1999**, *64*, 6750–6755.
- [247] G. R. Fulmer, A. J. M. Miller, N. H. Sherden, H. E. Gottlieb, A. Nudelman, B. M. Stoltz, J. E. Bercaw, K. I. Goldberg, *Organometallics* **2010**, *29*, 2176–2179.

- [248] H. Shimizu, J. C. Holder, B. M. Stoltz, *Beilstein. J. Org. Chem.* **2013**, *9*, 1637–1642.
- [249] M. A. Bennett, A. K. Smith, *J. Chem. Soc., Dalton Trans.* **1974**, 233–241.
- [250] W. K. Chow, C. M. So, C. P. Lau, F. Y. Kwong, *Chem. Eur. J.* **2011**, *17*, 6913–6917.
- [251] M. Murata, T. Oyama, S. Watanabe, Y. Masuda, *J. Org. Chem.* **1999**, *65*, 164–168.
- [252] T. A. Boebel, J. F. Hartwig, *Organometallics* **2008**, *27*, 6013–6019.
- [253] R. J. Abraham, J. J. Byrne, L. Griffiths, M. Perez, *Magn. Reson. Chem.* **2006**, *44*, 491–509.

Curriculum Vitae

(Entfällt aus Datenschutzgründen in der elektronischen Version)

Scientific Contributions

PUBLICATIONS RELATED TO THIS WORK

S. Wiebalck, J. Kozuch, S. Plachetta, P. Kuhrt, G. Meissner, D. Lentz, P. Hildebrandt, C. C. Tzschucke, Synthesis and Analysis of Square Planar Ir(I) Carbonyl Complexes Containing Bidentate Oxazoline Ligands, *in preparation*.

S. Wiebalck, G. Meissner, C. C. Tzschucke, Optimized Synthesis of Bisoxazolines and Pyridyloxazolines, *in preparation*.

FURTHER PUBLICATIONS

S. Wiebalck, J. Kozuch, C. C. Tzschucke, P. Hildebrandt, A Novel Artificial Membrane System Tailored for the Infrared Spectroscopic Investigation of Membrane Proteins, *in preparation*.

E. Oehlke, S. Kong, P. Arciszewski, **S. Wiebalck**, U. Abram, Aryl and NHC Compounds of Technetium and Rhenium, *J. Am. Chem. Soc.*, **2012**, 134, 9118-9121.

ORAL PRESENTATIONS

31/05/2013 **BIG-NSE/UniCat Mid-Term Symposium**, Berlin

11/05/2012 **BIG-NSE/UniCat Mid-Term Symposium**, Berlin

07/01/2011 **BIG-NSE/UniCat PhD Proposal Workshop**, Berlin

POSTER PRESENTATIONS

13-18/07/2014 **BOSS XIV**: Belgium organic synthesis symposium (Louvain-la-Neuve/Belgium)

30/06-04/07/2013 **ICIQ-UniCat Summer School** (Tarragona/Spain)

6-19/03/2013 **JCF** (*Jung Chemiker Forum*): Symposium of young Chemists from GDCh (Berlin/Germany)

24-26/09/2012 **ORCHEM**: Organic chemistry symposium of the GDCh (Weimar/Germany)

28/06/2012 **TDC** (*Tag der Chemie*): Day of chemistry, organized by university and industry (Berlin/Germany)

20-23/02/2011 **Activation of Small Molecules**: Joint International Symposium of UniCat and CRC546, Erkner (Berlin/Germany)



*Why do we fall, sir?
So that we can learn to pick ourselves up.*

(Alfred in „Batman Begins“)

V. Appendix

Appendix A: Crystallographic Data

Appendix B: NMR Spectra

Appendix C: IR Spectra of Carbonyl Complexes

Appendix A: Crystallographic Data

Crystal structure analysis of complex $[\text{Ir}(\text{PR-box})(\text{CO})_2]\text{BF}_4$ (**43**) including measurement, structure determination and refinement was performed by Prof. Dieter Lentz. Crystal data was provided by Prof. Dieter Lentz as well.

Table 1. Crystal data and structure refinement for pk3106a.

Identification code	pk3106a
Empirical formula	C ₁₄ H ₂₀ B F ₄ Ir N ₂ O ₄
Formula weight	559.33
Temperature	100(2) K
Wavelength	0.71073 Å
Crystal system	Trigonal
Space group	P3(1)21
Unit cell dimensions	a = 9.184(3) Å $\angle = 90^\circ$. b = 9.184(3) Å $\angle = 90^\circ$. c = 19.117(10) Å $\angle = 120^\circ$.
Volume	1396.4(9) Å ³
Z	3
Density (calculated)	1.995 Mg/m ³
Absorption coefficient	7.231 mm ⁻¹
F(000)	804
Crystal size	0.49 x 0.08 x 0.07 mm ³
Theta range for data collection	2.56 to 30.90°.
Index ranges	-13 ≤ h ≤ 11, -12 ≤ k ≤ 13, -27 ≤ l ≤ 26
Reflections collected	22344
Independent reflections	2932 [R(int) = 0.0407]
Completeness to theta = 30.90°	99.7 %
Absorption correction	Semi-empirical from equivalents
Max. and min. transmission	0.746 and 0.435
Refinement method	Full-matrix least-squares on F ²
Data / restraints / parameters	2932 / 0 / 119
Goodness-of-fit on F ²	1.169
Final R indices [I > 2σ(I)]	R1 = 0.0242, wR2 = 0.0396
R indices (all data)	R1 = 0.0295, wR2 = 0.0412

Absolute structure parameter	0.011(10)
Largest diff. peak and hole	2.186 and -1.792 e.Å ⁻³

Table 2. Atomic coordinates ($\times 10^4$) and equivalent isotropic displacement parameters ($\text{\AA}^2 \times 10^3$) for pk3106a. $U(\text{eq})$ is defined as one third of the trace of the orthogonalized U^{ij} tensor.

	x	y	z	U(eq)
Ir(1)	0	-3424(1)	1667	11(1)
B(1)	6664(7)	6664(7)	0	22(1)
C(1)	1639(5)	-4066(4)	1524(2)	14(1)
C(2)	914(4)	103(4)	1571(2)	12(1)
C(3)	3598(4)	2108(5)	1368(2)	16(1)
C(4)	3410(4)	316(4)	1282(2)	13(1)
C(5)	3737(4)	-128(4)	535(2)	15(1)
C(6)	2637(5)	73(5)	-31(2)	20(1)
C(7)	5645(5)	938(5)	357(2)	20(1)
F(1)	7058(4)	8075(3)	420(1)	45(1)
F(2)	6317(4)	5302(3)	439(2)	52(1)
N(1)	1607(4)	-817(4)	1498(2)	14(1)
O(1)	2664(3)	-4424(3)	1437(2)	22(1)
O(2)	1821(3)	1762(3)	1486(1)	17(1)

Table 3. Bond lengths [\AA] and angles [$^\circ$] for pk3106a.

Ir(1)-C(1)#1	1.891(4)
Ir(1)-C(1)	1.891(4)
Ir(1)-N(1)#1	2.117(3)
Ir(1)-N(1)	2.117(3)
B(1)-F(2)	1.404(4)
B(1)-F(2)#2	1.404(4)
B(1)-F(1)	1.409(4)
B(1)-F(1)#2	1.409(4)
C(1)-O(1)	1.154(4)
C(2)-N(1)	1.295(4)
C(2)-O(2)	1.331(4)
C(2)-C(2)#1	1.498(6)
C(3)-O(2)	1.515(4)

C(3)-C(4)	1.575(5)
C(3)-H(3A)	0.9900
C(3)-H(3B)	0.9900
C(4)-N(1)	1.508(5)
C(4)-C(5)	1.555(5)
C(4)-H(4)	1.0000
C(5)-C(6)	1.553(5)
C(5)-C(7)	1.559(5)
C(5)-H(5)	1.0000
C(6)-H(6A)	0.9800
C(6)-H(6B)	0.9800
C(6)-H(6C)	0.9800
C(7)-H(7A)	0.9800
C(7)-H(7B)	0.9800
C(7)-H(7C)	0.9800
C(1)#1-Ir(1)-C(1)	89.6(2)
C(1)#1-Ir(1)-N(1)#1	96.74(11)
C(1)-Ir(1)-N(1)#1	173.53(17)
C(1)#1-Ir(1)-N(1)	173.53(17)
C(1)-Ir(1)-N(1)	96.74(11)
N(1)#1-Ir(1)-N(1)	77.01(18)
F(2)-B(1)-F(2)#2	112.0(5)
F(2)-B(1)-F(1)	108.57(16)
F(2)#2-B(1)-F(1)	109.81(18)
F(2)-B(1)-F(1)#2	109.81(18)
F(2)#2-B(1)-F(1)#2	108.57(16)
F(1)-B(1)-F(1)#2	108.0(5)
O(1)-C(1)-Ir(1)	178.7(3)
N(1)-C(2)-O(2)	120.2(3)
N(1)-C(2)-C(2)#1	116.1(2)
O(2)-C(2)-C(2)#1	123.76(17)
O(2)-C(3)-C(4)	104.6(3)
O(2)-C(3)-H(3A)	110.8
C(4)-C(3)-H(3A)	110.8
O(2)-C(3)-H(3B)	110.8
C(4)-C(3)-H(3B)	110.8
H(3A)-C(3)-H(3B)	108.9

N(1)-C(4)-C(5)	111.1(3)
N(1)-C(4)-C(3)	101.6(3)
C(5)-C(4)-C(3)	115.8(3)
N(1)-C(4)-H(4)	109.3
C(5)-C(4)-H(4)	109.3
C(3)-C(4)-H(4)	109.3
C(6)-C(5)-C(4)	112.7(3)
C(6)-C(5)-C(7)	111.5(3)
C(4)-C(5)-C(7)	109.9(3)
C(6)-C(5)-H(5)	107.5
C(4)-C(5)-H(5)	107.5
C(7)-C(5)-H(5)	107.5
C(5)-C(6)-H(6A)	109.5
C(5)-C(6)-H(6B)	109.5
H(6A)-C(6)-H(6B)	109.5
C(5)-C(6)-H(6C)	109.5
H(6A)-C(6)-H(6C)	109.5
H(6B)-C(6)-H(6C)	109.5
C(5)-C(7)-H(7A)	109.5
C(5)-C(7)-H(7B)	109.5
H(7A)-C(7)-H(7B)	109.5
C(5)-C(7)-H(7C)	109.5
H(7A)-C(7)-H(7C)	109.5
H(7B)-C(7)-H(7C)	109.5
C(2)-N(1)-C(4)	107.9(3)
C(2)-N(1)-Ir(1)	115.4(2)
C(4)-N(1)-Ir(1)	136.6(2)
C(2)-O(2)-C(3)	104.5(3)

Symmetry transformations used to generate equivalent atoms:

#1 -x,-x+y,-z+1/3 #2 y,x,-z

Table 4. Anisotropic displacement parameters ($\text{\AA}^2 \times 10^3$) for pk3106a. The anisotropic displacement factor exponent takes the form: $-2\pi^2 [h^2 a^{*2} U^{11} + \dots + 2 h k a^* b^* U^{12}]$

	U ¹¹	U ²²	U ³³	U ²³	U ¹³	U ¹²
Ir(1)	10(1)	10(1)	12(1)	0(1)	1(1)	5(1)
B(1)	17(2)	17(2)	26(4)	-4(1)	4(1)	4(2)
C(1)	11(2)	9(1)	21(2)	1(1)	0(2)	3(1)
C(2)	14(2)	10(1)	11(2)	0(1)	-1(1)	5(1)
C(3)	11(2)	10(2)	24(2)	-2(1)	2(1)	2(1)
C(4)	8(1)	10(1)	18(2)	0(1)	-1(1)	2(1)
C(5)	13(2)	11(2)	21(2)	-1(1)	-1(1)	5(1)
C(6)	21(2)	19(2)	19(2)	-1(2)	-1(1)	9(2)
C(7)	15(2)	22(2)	22(2)	-1(2)	3(2)	9(1)
F(1)	75(2)	37(2)	34(2)	-12(1)	-17(2)	36(2)
F(2)	74(2)	23(1)	42(2)	8(1)	12(2)	12(1)
N(1)	13(2)	14(1)	13(2)	0(1)	0(1)	6(1)
O(1)	15(1)	19(1)	35(2)	0(1)	1(1)	10(1)
O(2)	14(1)	11(1)	26(2)	1(1)	1(1)	6(1)

Crystal structure analysis of complex $[\text{Ir}(\text{iPr-box})(\text{CO})_2]\text{PF}_6$ (**28c**) including measurement, structure determination and refinement was performed by Prof. Dieter Lentz. Crystal data was provided by Prof. Dieter Lentz as well.

Table 1. Crystal data and structure refinement for sw3148a.

Identification code	sw3148a	
Empirical formula	C ₁₄ H ₂₀ F ₆ Ir N ₂ O ₄ P	
Formula weight	617.49	
Temperature	100(2) K	
Wavelength	0.71073 Å	
Crystal system	Trigonal	
Space group	P3(1)21	
Unit cell dimensions	a = 9.1168(10) Å	a = 90°.
	b = 9.1168(10) Å	b = 90°.
	c = 19.565(4) Å	g = 120°.
Volume	1408.3(4) Å ³	
Z	3	
Density (calculated)	2.184 Mg/m ³	
Absorption coefficient	7.277 mm ⁻¹	
F(000)	888	
Crystal size	0.24 x 0.22 x 0.07 mm ³	
Theta range for data collection	2.58 to 30.57°.	
Index ranges	-12 ≤ h ≤ 13, -13 ≤ k ≤ 13, -27 ≤ l ≤ 26	
Reflections collected	22810	
Independent reflections	2859 [R(int) = 0.0377]	
Completeness to theta = 30.57°	99.6 %	
Absorption correction	Semi-empirical from equivalents	
Max. and min. transmission	0.746 and 0.477	
Refinement method	Full-matrix least-squares on F ²	
Data / restraints / parameters	2859 / 0 / 130	
Goodness-of-fit on F ²	1.136	
Final R indices [I > 2σ(I)]	R1 = 0.0199, wR2 = 0.0468	
R indices (all data)	R1 = 0.0205, wR2 = 0.0470	
Absolute structure parameter	-0.015(8)	
Largest diff. peak and hole	2.025 and -0.897 e.Å ⁻³	

Table 2. Atomic coordinates ($\times 10^4$) and equivalent isotropic displacement parameters ($\text{\AA}^2 \times 10^3$) for sw3148a. $U(\text{eq})$ is defined as one third of the trace of the orthogonalized U^{ij} tensor.

	x	y	z	U(eq)
Ir(1)	3527(1)	3527(1)	0	11(1)
N(1)	2539(4)	945(3)	170(1)	12(1)
C(1)	5782(5)	4161(5)	75(2)	16(1)
C(2)	925(4)	23(4)	97(2)	15(1)
C(3)	1605(4)	-1936(5)	332(2)	18(1)
C(4)	3192(4)	-157(4)	412(2)	14(1)
C(5)	3909(4)	334(4)	1140(2)	16(1)
C(6)	4760(4)	-688(5)	1344(2)	21(1)
C(7)	2571(5)	127(5)	1664(2)	23(1)
F(1)	5431(5)	867(5)	7899(2)	104(2)
F(2)	4580(3)	1556(3)	8859(1)	29(1)
F(3)	2127(5)	-871(5)	8772(2)	98(2)
O(1)	7185(3)	4548(4)	95(2)	28(1)
O(2)	187(3)	-1608(3)	200(1)	18(1)
P(1)	3786(1)	0	8333	16(1)

Table 3. Bond lengths [\AA] and angles [$^\circ$] for sw3148a.

Ir(1)-C(1)	1.842(4)
Ir(1)-C(1)#1	1.842(4)
Ir(1)-N(1)	2.085(3)
Ir(1)-N(1)#1	2.085(3)
N(1)-C(2)	1.287(4)
N(1)-C(4)	1.478(4)
C(1)-O(1)	1.145(4)
C(2)-O(2)	1.305(4)
C(2)-C(2)#1	1.474(7)
C(3)-O(2)	1.489(4)
C(3)-C(4)	1.550(5)
C(3)-H(3A)	0.9900
C(3)-H(3B)	0.9900
C(4)-C(5)	1.537(5)

C(4)-H(4)	1.0000
C(5)-C(7)	1.532(5)
C(5)-C(6)	1.534(5)
C(5)-H(5)	1.0000
C(6)-H(6A)	0.9800
C(6)-H(6B)	0.9800
C(6)-H(6C)	0.9800
C(7)-H(7A)	0.9800
C(7)-H(7B)	0.9800
C(7)-H(7C)	0.9800
F(1)-P(1)	1.553(3)
F(2)-P(1)	1.602(2)
F(3)-P(1)	1.566(3)
P(1)-F(1)#2	1.553(3)
P(1)-F(3)#2	1.566(3)
P(1)-F(2)#2	1.602(2)
C(1)-Ir(1)-C(1)#1	88.7(2)
C(1)-Ir(1)-N(1)	97.23(13)
C(1)#1-Ir(1)-N(1)	172.09(16)
C(1)-Ir(1)-N(1)#1	172.09(16)
C(1)#1-Ir(1)-N(1)#1	97.23(13)
N(1)-Ir(1)-N(1)#1	77.33(16)
C(2)-N(1)-C(4)	108.0(3)
C(2)-N(1)-Ir(1)	115.3(2)
C(4)-N(1)-Ir(1)	136.5(2)
O(1)-C(1)-Ir(1)	177.3(3)
N(1)-C(2)-O(2)	119.8(3)
N(1)-C(2)-C(2)#1	116.06(19)
O(2)-C(2)-C(2)#1	124.17(18)
O(2)-C(3)-C(4)	104.9(3)
O(2)-C(3)-H(3A)	110.8
C(4)-C(3)-H(3A)	110.8
O(2)-C(3)-H(3B)	110.8
C(4)-C(3)-H(3B)	110.8
H(3A)-C(3)-H(3B)	108.8
N(1)-C(4)-C(5)	110.9(3)
N(1)-C(4)-C(3)	101.3(3)

C(5)-C(4)-C(3)	115.9(3)
N(1)-C(4)-H(4)	109.5
C(5)-C(4)-H(4)	109.5
C(3)-C(4)-H(4)	109.5
C(7)-C(5)-C(6)	111.4(3)
C(7)-C(5)-C(4)	112.8(3)
C(6)-C(5)-C(4)	109.6(3)
C(7)-C(5)-H(5)	107.6
C(6)-C(5)-H(5)	107.6
C(4)-C(5)-H(5)	107.6
C(5)-C(6)-H(6A)	109.5
C(5)-C(6)-H(6B)	109.5
H(6A)-C(6)-H(6B)	109.5
C(5)-C(6)-H(6C)	109.5
H(6A)-C(6)-H(6C)	109.5
H(6B)-C(6)-H(6C)	109.5
C(5)-C(7)-H(7A)	109.5
C(5)-C(7)-H(7B)	109.5
H(7A)-C(7)-H(7B)	109.5
C(5)-C(7)-H(7C)	109.5
H(7A)-C(7)-H(7C)	109.5
H(7B)-C(7)-H(7C)	109.5
C(2)-O(2)-C(3)	104.5(3)
F(1)-P(1)-F(1)#2	89.4(4)
F(1)-P(1)-F(3)#2	90.7(3)
F(1)#2-P(1)-F(3)#2	179.9(4)
F(1)-P(1)-F(3)	179.9(3)
F(1)#2-P(1)-F(3)	90.7(3)
F(3)#2-P(1)-F(3)	89.2(4)
F(1)-P(1)-F(2)#2	88.86(15)
F(1)#2-P(1)-F(2)#2	90.43(15)
F(3)#2-P(1)-F(2)#2	89.51(15)
F(3)-P(1)-F(2)#2	91.21(16)
F(1)-P(1)-F(2)	90.43(16)
F(1)#2-P(1)-F(2)	88.86(15)
F(3)#2-P(1)-F(2)	91.21(16)
F(3)-P(1)-F(2)	89.51(16)
F(2)#2-P(1)-F(2)	179.00(19)

Symmetry transformations used to generate equivalent atoms:

#1 y,x,-z #2 x-y,-y,-z+5/3

Table 4. Anisotropic displacement parameters ($\text{\AA}^2 \times 10^3$) for sw3148a. The anisotropic displacement factor exponent takes the form: $-2\pi^2 [h^2 a^{*2} U^{11} + \dots + 2 h k a^* b^* U^{12}]$

	U ¹¹	U ²²	U ³³	U ²³	U ¹³	U ¹²
Ir(1)	10(1)	10(1)	12(1)	0(1)	0(1)	6(1)
N(1)	12(1)	14(1)	13(1)	1(1)	0(1)	7(1)
C(1)	17(2)	12(1)	18(2)	1(1)	1(1)	8(1)
C(2)	16(2)	13(2)	16(2)	0(1)	-2(1)	7(1)
C(3)	19(2)	11(2)	23(2)	0(1)	-5(1)	7(1)
C(4)	14(2)	13(2)	17(2)	1(1)	-1(1)	9(1)
C(5)	16(2)	12(1)	19(2)	2(1)	-1(1)	7(1)
C(6)	22(2)	22(2)	22(2)	4(1)	-4(1)	13(2)
C(7)	29(2)	24(2)	17(2)	0(1)	2(1)	14(2)
F(1)	59(2)	71(3)	106(3)	-59(2)	57(2)	-26(2)
F(2)	31(1)	24(1)	27(1)	-11(1)	2(1)	10(1)
F(3)	47(2)	95(3)	63(2)	-46(2)	31(2)	-33(2)
O(1)	12(1)	25(2)	47(2)	2(1)	0(1)	9(1)
O(2)	14(1)	12(1)	26(1)	2(1)	-2(1)	4(1)
P(1)	17(1)	17(1)	15(1)	-1(1)	-1(1)	8(1)

Crystal structure analysis of complex $[\text{Ir}^{\text{I}}\text{Pr-quinox})(\text{cod})(\text{CO})_2]\text{PF}_6$ (**26m**) including measurement, structure determination and refinement was performed by Dr. Jelena Wiecko. Crystal data was provided by Dr. Jelena Wiecko as well.

Identification code	sw3154	
Empirical formula	C ₂₄ H ₂₈ Ir N ₂ O ₂ , F ₆ P	
Formula weight	713.65	
Temperature	200(2) K	
Wavelength	0.71073 Å	
Crystal system	orthorhombic	
Space group	P 21 21 2	
Unit cell dimensions	a = 11.3150(10) Å	a = 90°.
	b = 12.8807(8) Å	b = 90°.
	c = 17.3441(11) Å	g = 90.00
Volume	2527.8(3)	
Z	4	
Density (calculated)	1.875 Mg/m ³	
Absorption coefficient	5.414 mm ⁻¹	
F(000)888		
Crystal size	0.50 x 0.20 x 0.05 mm ³	
Theta range for data collection	3.36 to 29.28°.	
Index ranges	-15 ≤ h ≤ 15, -17 ≤ k ≤ 14, -23 ≤ l ≤ 22	
Reflections collected	18764	
Independent reflections	4108 [R(int) = 0.0386]	
Completeness to theta = 29.28°	98.7 %	
Absorption correction	Semi-empirical from equivalents	
Max. and min. transmission	0.746 and 0.477	
Refinement method	Full-matrix least-squares on F ²	
Data / restraints / parameters	6812 / 0 / 325	
Goodness-of-fit on F ²	0.761	
Final R indices [I > 2σ(I)]	R1 = 0.0796 wR2 = 0.0556	
R indices (all data)	R1 = 0.0386, wR2 = 0.0631	
Absolute structure parameter	-0.018(10)	
Largest diff. peak and hole	1.418 and -3.351 e.Å ⁻³	

Table 2. Atomic coordinates ($\times 10^4$) and equivalent isotropic displacement parameters ($\text{\AA}^2 \times 10^3$) for sw3154. $U(\text{eq})$ is defined as one third of the trace of the orthogonalized U^{ij} tensor.

x	y	z	U(eq)	
C(1)	6686(6)	6920(8)	1322(5)	45(2)
H(1)	6249	6898	1810	54
C(2)	6058(6)	6229(11)	726(6)	66(4)
H(2)	5434	5831	969	79
H(2)	5715	0.6649	319	79
C(3)	7899(7)	5670(7)	903(5)	32(2)
C(4)	8981(6)	5096(6)	755(5)	306(19)
C(5)	9095(8)	4371(7)	163(5)	46(3)
H(5)	0.8440	4181	-128	55
C(6)	10155(8)	3949(7)	16(5)	47(3)
H(6)	10240	3466	-379	57
C(7)	11150(7)	4246(7)	468(5)	40(2)
C(8)	12278(9)	3846(9)	317(6)	63(3)
H(8)	12397	3389	-91	76
C(9)	13184(9)	4132(8)	769(6)	54(3)
H(9)	13925	3845	679	65
C(10)	13053(7)	4858(8)	1381(6)	49(3)
H(10)	13702	5050	1678	59
C(11)	11948(7)	5276(7)	1530(5)	37(2)
H(11)	11843	5752	1927	44
C(12)	10978(7)	4964(7)	1064(5)	31(2)
C(13)	6896(9)	8043(8)	1096(6)	61(3)
H(13)	7369	8368	1503	73
C(14)	7606(8)	8106(8)	337(5)	61(3)
H(14A)	8346	7751	399	91
H(14B)	7751	8821	211	91
H(14C)	7163	7787	-71	91
C(15)	5722(10)	8633(12)	1039(7)	115(5)
H(15)	5873	9343	0902	172
H(15)	5323	8609	1528	172
H(15)	5233	8317	0652	172
C(16)	10318(7)	7443(7)	1663(4)	32(2)
C(17)	9694(7)	7292(6)	3210(4)	34(2)

H(17)	10087	7962	3133	41
C(18)	8478(7)	7280(6)	2993(5)	36(2)
H(18)	8169	7947	2811	44
C(19)	7568(7)	6581(8)	3382(5)	44(3)
H(19)	6831	6630	3098	53
H(19)	7423	6842	3898	53
C(20)	7921(8)	5432(8)	3438(6)	42(3)
H(20)	8278	5303	3938	50
H(20)	7219	5003	3398	50
C(21)	08785(6)	5131(6)	2809(6)	283(18)
H(21)	08536	4530	2503	34
C(22)	10045(7)	5202(7)	2921(6)	34(2)
H(22)	10489	4650	2663	41
C(23)	10641(10)	5605(7)	3634(4)	45(2)
H(23)	11482	5668	3534	55
H(23)	10539	5103	4046	55
C(24)	10169(7)	6661(7)	3907(5)	44(3)
H(24A)	10798	7045	4159	53
H(24B)	9540	6555	4279	53
N(1)	7826(4)	6336(7)	1411(3)	320(14)
N(2)	9887(6)	5376(6)	1233(4)	264(18)
O(1)	6982(5)	5525(5)	407(3)	517(18)
O(2)	10897(5)	8038(5)	1327(3)	499(18)
P(1)	13663(2)	7983(3)	31725(17)	537(8)
F(1)	13863(5)	9177(5)	3025(5)	90(2)
F(2)	12328(4)	8245(7)	3390(5)	132(4)
F(3)	13431(6)	6793(5)	3362(5)	101(3)
F(4)	14988(4)	7762(6)	2988(6)	122(3)
F(5)	14007(6)	8153(6)	4062(4)	100(2)
F(6)	13293(7)	7844(7)	2333(4)	126(3)
Ir(1)	94162(2)	63984(3)	214134(17)	2577(6)

Table 3. Bond lengths [Å] and angles [°] for sw3154

C(1)-N(1)	1.502(9)
C(1)-C(13)	1.517(13)
C(1)-C(2)	1.538(13)
C(1)-H(1)	0.9800
C(2)-O(1)	1.490(12)
C(2)-H(2A)	0.9700
C(2)-H(2B)	0.9700
C(3)-N(1)	1.232(11)
C(3)-O(1)	1.360(9)
C(3)-C(4)	1.453(11)
C(4)-N(2)	1.366(9)
C(4)-C(5)	1.394(11)
C(5)-C(6)	1.341(11)
C(5)-H(5)	0.9300
C(6)-C(7)	1.424(11)
C(6)-H(6)	0.9300
C(7)-C(12)	1.401(12)
C(7)-C(8)	1.401(11)
C(8)-C(9)	1.343(13)
C(8)-H(8)	0.9300
C(9)-C(10)	1.423(13)
C(9)-H(9)	0.9300 .
C(10)-C(11)	1.386(11)
C(10)-H(10)	0.9300
C(11)-C(12)	1.421(11)
C(11)-H(11)	0.9300
C(12)-N(2)	1.375(9)
C(13)-C(15)	1.534(13)
C(13)-C(14)	1.545(12)
C(13)-H(13)	0.9800
C(14)-H(14A)	0.9600
C(14)-H(14B)	0.9600
C(14)-H(14C)	0.9600
C(15)-H(15A)	0.9600
C(15)-H(15B)	0.9600
C(15)-H(15C)	0.9600
C(16)-O(2)	1.165(9)
C(16)-Ir(1)	1.881(9)

C(17)-C(18)	1.427(11)
C(17)-C(24)	1.554(11)
C(17)-Ir(1)	2.204(7)
C(17)-H(17)	0.9800
C(18)-C(19)	1.525(11)
C(18)-Ir(1)	2.144(8)
C(18)-H(18)	0.9800
C(19)-C(20)	1.537(13)
C(19)-H(19A)	0.9700
C(19)-H(19B)	0.9700
C(20)-C(21)	1.516(12)
C(20)-H(20A)	0.9700
C(20)-H(20B)	0.9700
C(21)-C(22)	1.443(8)
C(21)-Ir(1)	2.126(8)
C(21)-H(21)	0.9800
C(22)-C(23)	1.501(13)
C(22)-Ir(1)	2.170(9)
C(22)-H(22)	0.9800
C(23)-C(24)	1.536(12)
C(23)-H(23A)	0.9700
C(23)-H(23B)	0.9700
C(24)-H(24A)	0.9700
C(24)-H(24B)	0.9700
N(1)-Ir(1)	2.202(5)
N(2)-Ir(1)	2.121(7)
P(1)-F(6)	1.526(7)
P(1)-F(4)	1.559(5)
P(1)-F(1)	1.575(6)
P(1)-F(3)	1.589(8)
P(1)-F(2)	1.593(6)
P(1)-F(5)	1.606(7)
N(1)-C(1)-C(13)	111.7(7)
N(1)-C(1)-C(2)	100.1(7)
C(13)-C(1)-C(2)	116.8(8)
N(1)-C(1)-H(1)	109.3
C(13)-C(1)-H(1)	109.3
C(2)-C(1)-H(1)	109.3
O(1) C(2)-C(1)	106.1(6)
O(1) C(2)-H(2A)	110.5

C(1)-C(2)-H(2A)	110.5
O(1)-C(2)-H(2B)	110.5
C(1)-C(2)-H(2B)	110.5
H(2A)-C(2)-H(2B)	108.7
N(1)-C(3)-O(1)	119.7(8)
N(1)-C(3)-C(4)	122.4(7)
O(1)-C(3)-C(4)	117.5(8)
N(2)-C(4)-C(5)	123.7(7)
N(2)-C(4)-C(3)	113.0(7)
C(5)-C(4)-C(3)	123.3(7)
C(6)-C(5)-C(4)	119.6(8)
C(6)-C(5)-H(5)	120.2
C(4)-C(5)-H(5)	120.2
C(5)-C(6)-C(7)	119.5(8)
C(5)-C(6)-H(6)	120.2
C(7)-C(6)-H(6)	120.2
C(12)-C(7)-C(8)	120.5(9)
C(12)-C(7)-C(6)	118.3(7)
C(8)-C(7)-C(6)	121.2(9)
C(9)-C(8)-C(7)	119.0(10)
C(9)-C(8)-H(8)	120.5
C(7)-C(8)-H(8)	120.5
C(8)-C(9)-C(10)	122.5(9)
C(8)-C(9)-H(9)	118.8
C(10)-C(9)-H(9)	118.8
C(11)-C(10)-C(9)	119.2(9)
C(11)-C(10)-H(10)	120.4
C(9)-C(10)-H(10)	120.4
C(10)-C(11)-C(12)	118.8(8)
C(10)-C(11)-H(11)	120.6
C(12)-C(11)-H(11)	120.6
N(2)-C(12)-C(7)	122.5(7)
N(2)-C(12)-C(11)	117.6(8)
C(7)-C(12)-C(11)	119.9(7)
C(1)-C(13)-C(15)	110.7(9)
C(1)-C(13)-C(14)	110.6(8)
C(15)-C(13)-C(14)	111.7(8)
C(1)-C(13)-H(13)	107.9
C(15)-C(13)-H(13)	107.9
C(14)-C(13)-H(13)	107.9

C(13)-C(14)-H(14A)	109.5
C(13)-C(14)-H(14B)	109.5
H(14A)-C(14)-H(14B)	109.5
C(13)-C(14)-H(14C)	109.5
H(14A)-C(14)-H(14C)	109.5
H(14B)-C(14)-H(14C)	109.5
C(13)-C(15)-H(15A)	109.5
C(13)-C(15)-H(15B)	109.5
H(15A)-C(15)-H(15B)	109.5
C(13)-C(15)-H(15C)	109.5
H(15A)-C(15)-H(15C)	109.5
H(15B)-C(15)-H(15C)	109.5
O(2)-C(16)-Ir(1)	175.1(7)
C(18)-C(17)-C(24)	122.3(7)
C(18)-C(17)-Ir(1)	68.6(5)
C(24)-C(17)-Ir(1)	115.5(5)
C(18)-C(17)-H(17)	114.2
C(24)-C(17)-H(17)	114.2
Ir(1)-C(17)-H(17)	114.2
C(17)-C(18)-C(19)	122.7(8)
C(17)-C(18)-Ir(1)	73.1(5)
C(19)-C(18)-Ir(1)	109.1(6)
C(17)-C(18)-H(18)	114.8
C(19)-C(18)-H(18)	114.8
Ir(1)-C(18)-H(18)	114.8
C(18)-C(19)-C(20)	114.9(7)
C(18)-C(19)-H(19A)	108.5
C(20)-C(19)-H(19A)	108.5
C(18)-C(19)-H(19B)	108.5
C(20)-C(19)-H(19B)	108.5
H(19A)-C(19)-H(19B)	107.5
C(21)-C(20)-C(19)	111.6(7)
C(21)-C(20)-H(20A)	109.3
C(19)-C(20)-H(20A)	109.3
C(21)-C(20)-H(20B)	109.3
C(19)-C(20)-H(20B)	109.3
H(20A)-C(20)-H(20B)	108.0
C(22)-C(21)-C(20)	121.6(9)
C(22)-C(21)-Ir(1)	72.1(5)
C(20)-C(21)-Ir(1)	114.4(6)

C(22)-C(21)-H(21)	114.1
C(20)-C(21)-H(21)	114.1
Ir(1)-C(21)-H(21)	114.1
C(21)-C(22)-C(23)	125.3(10)
C(21)-C(22)-Ir(1)	68.7(5)
C(23)-C(22)-Ir(1)	114.5(6)
C(21)-C(22)-H(22)	113.5
C(23)-C(22)-H(22)	113.5
Ir(1)-C(22)-H(22)	113.5
C(22)-C(23)-C(24)	113.8(8)
C(22)-C(23)-H(23A)	108.8
C(24)-C(23)-H(23A)	108.8
C(22)-C(23)-H(23B)	108.8
C(24)-C(23)-H(23B)	108.8
H(23A)-C(23)-H(23B)	107.7
C(23)-C(24)-C(17)	110.1(7)
C(23)-C(24)-H(24A)	109.6
C(17)-C(24)-H(24A)	109.6
C(23)-C(24)-H(24B)	109.6
C(17)-C(24)-H(24B)	109.6
H(24A)-C(24)-H(24B)	108.2
C(3)-N(1)-C(1)	109.5(6)
C(3)-N(1)-Ir(1)	112.5(5)
C(1)-N(1)-Ir(1)	137.9(6)
C(4)-N(2)-C(12)	116.2(7)
C(4)-N(2)-Ir(1)	115.2(5)
C(12)-N(2)-Ir(1)	128.5(6)
F(6)-P(1)-F(4)	92.7(5)
F(6)-P(1)-F(1)	89.9(5)
F(4)-P(1)-F(1)	90.4(4)
F(6)-P(1)-F(3)	92.2(5)
F(4)-P(1)-F(3)	91.5(4)
F(1)-P(1)-F(3)	177.1(5)
F(6)-P(1)-F(2)	89.4(4)
F(4)-P(1)-F(2)	177.4(6)
F(1)-P(1)-F(2)	88.2(4)
F(3)-P(1)-F(2)	89.9(4)
F(6)-P(1)-F(5)	177.8(5)
F(4)-P(1)-F(5)	89.4(5)
F(1)-P(1)-F(5)	89.3(5)

F(3)-P(1)-F(5)	88.5(4)
F(2)-P(1)-F(5)	88.5(4)
C(16)-Ir(1)-N(2)	88.9(3)
C(16)-Ir(1)-C(21)	166.4(3)
N(2)-Ir(1)-C(21)	90.7(3)
C(16)-Ir(1)-C(18)	101.1(3)
N(2)-Ir(1)-C(18)	164.7(3)
C(21)-Ir(1)-C(18)	82.3(3)
C(16)-Ir(1)-C(22)	127.2(3)
N(2)-Ir(1)-C(22)	86.6(3)
C(21)-Ir(1)-C(22)	39.2(2)
C(18)-Ir(1)-C(22)	96.3(4)
C(16)-Ir(1)-N(1)	102.5(3)
N(2)-Ir(1)-N(1)	75.8(3)
C(21)-Ir(1)-N(1)	90.6(3)
C(18)-Ir(1)-N(1)	90.6(3)
C(22)-Ir(1)-N(1)	126.9(3)
C(16)-Ir(1)-C(17)	85.4(3)
N(2)-Ir(1)-C(17)	155.9(3)
C(21)-Ir(1)-C(17)	89.5(3)
C(18)-Ir(1)-C(17)	38.3(3)
C(22)-Ir(1)-C(17)	78.4(3)
N(1)-Ir(1)-C(17)	128.3(3)

Symmetry transformations used to generate equivalent atoms:

#1 y,x,-z #2 x-y,-y,-z+5/3

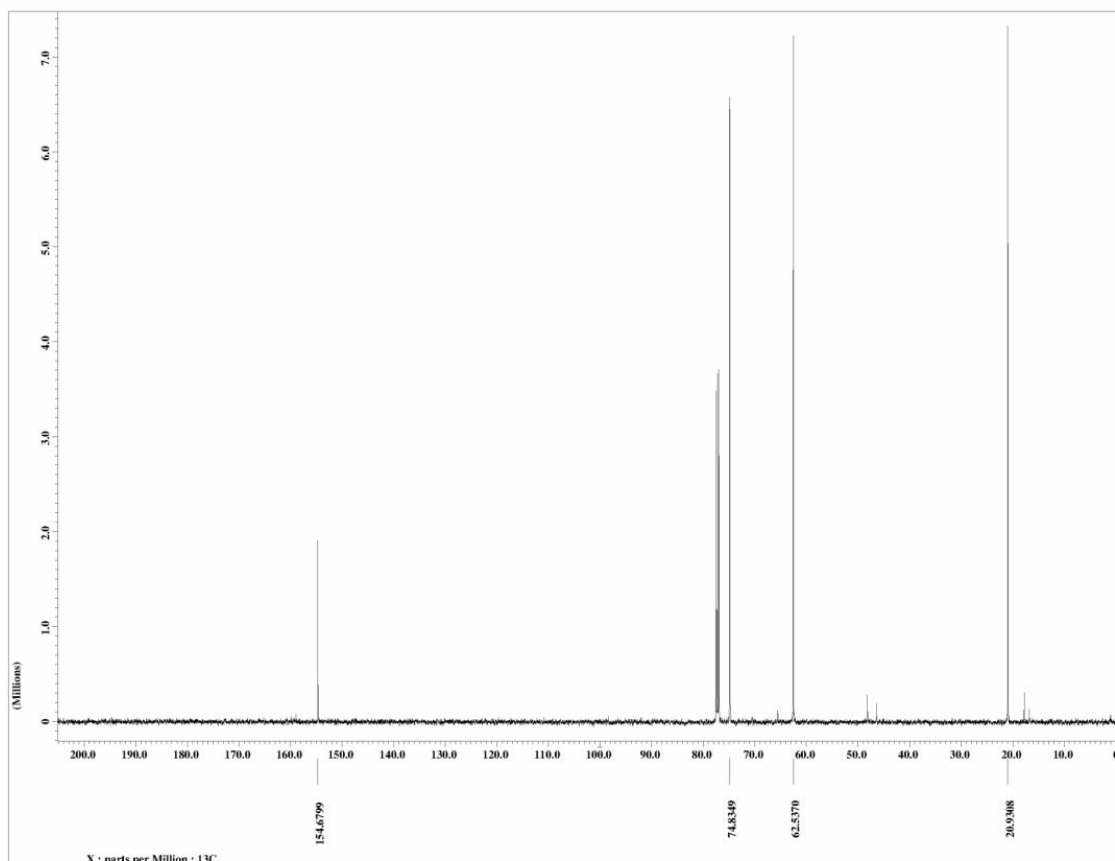
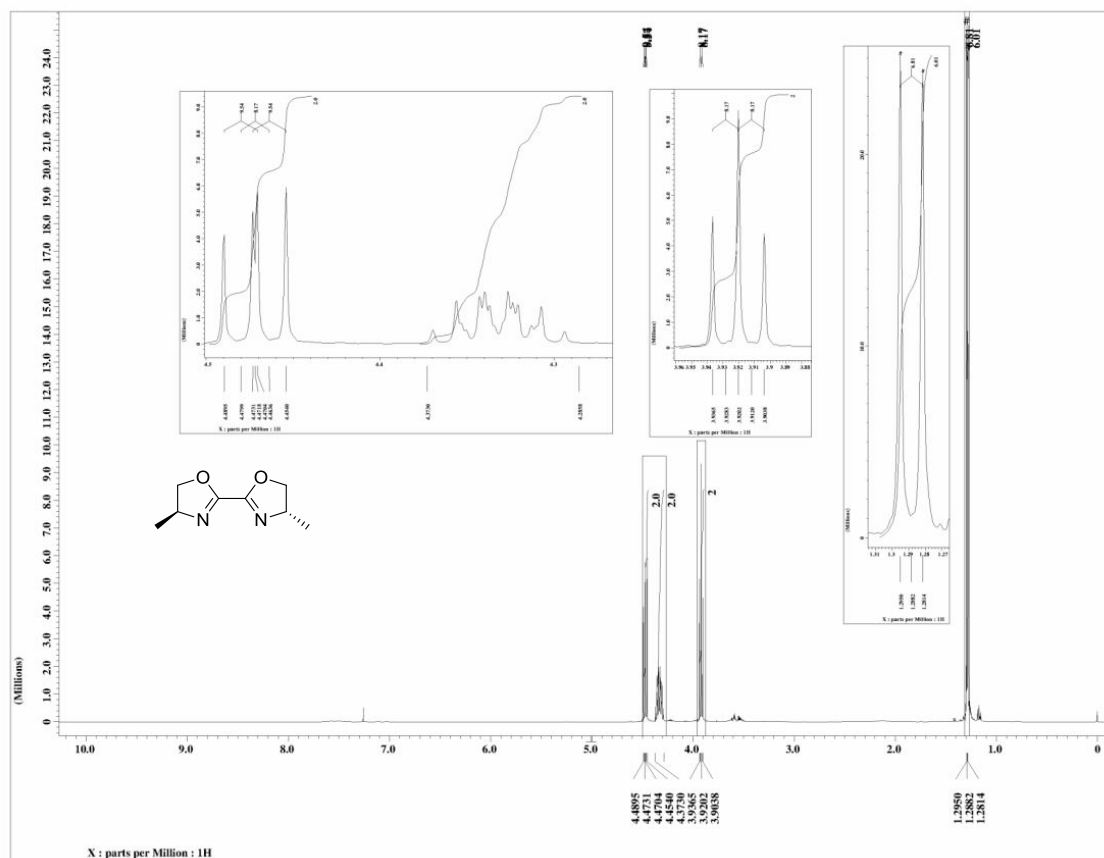
Table 4. Anisotropic displacement parameters ($\text{\AA}^2 \times 10^3$) for sw3154. The anisotropic displacement factor exponent takes the form: $-2\pi^2 [h^2 a^{*2} U^{11} + \dots + 2 h k a^* b^* U^{12}]$

	U^{11}	U^{22}	U^{33}	U^{23}	U^{13}	U^{12}	
C(1)	0.029(4)		65(7)	43(5)	16(5)	5(4)	14(4)
C(2)	0.031(4)		103(11)	65(7)	18(8)	0(4)	3(6)
C(3)	0.034(4)		32(5)	29(5)	3(4)	-7(4)	-10(4)
C(4)	0.039(4)		25(5)	27(4)	-4(4)	-8(3)	-5(3)
C(5)	0.073(8)		38(6)	26(5)	-3(4)	-6(4)	-7(5)

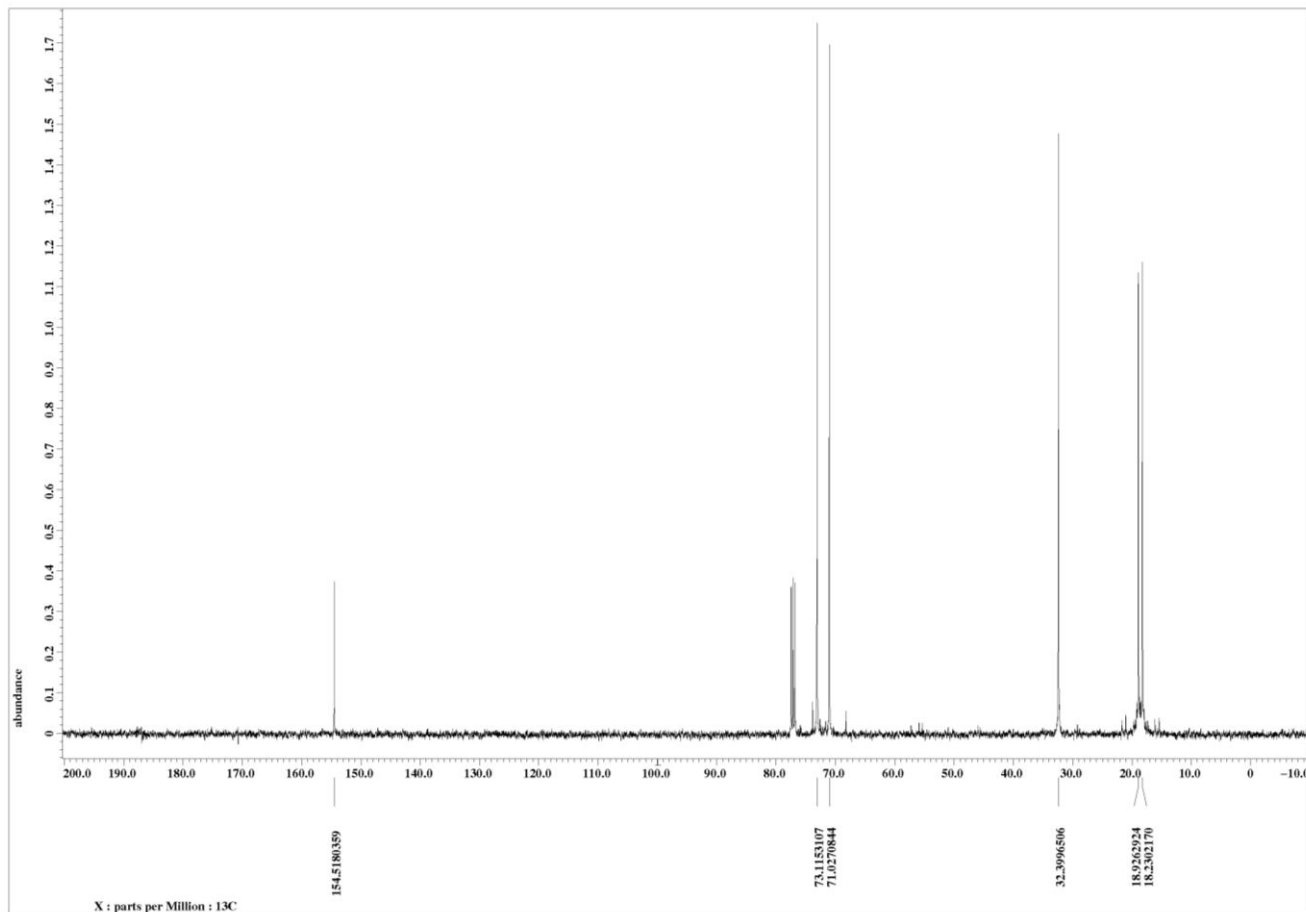
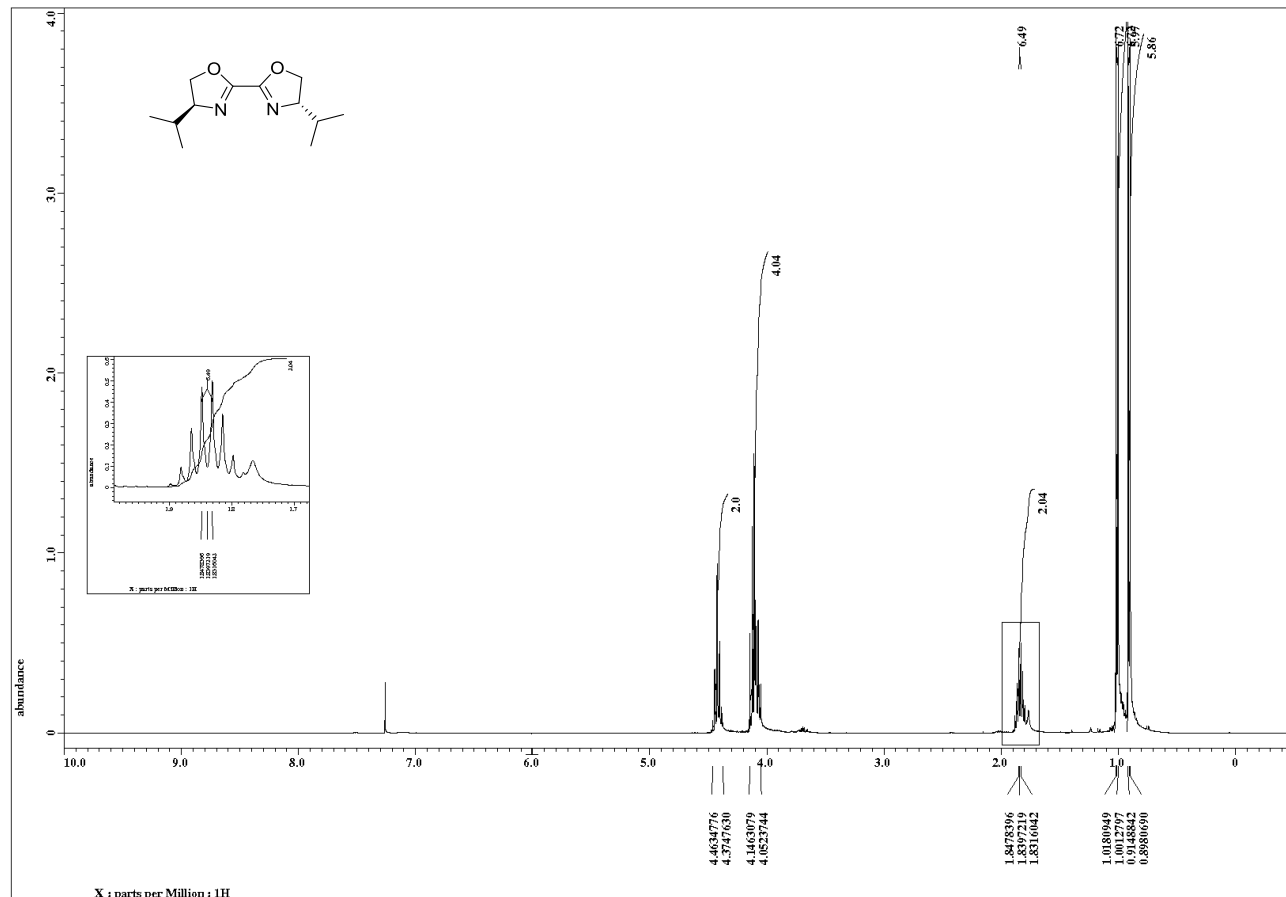
C(6)	0.083(7)	35(6)	24(5)	-6(4)	5(4)	3(4)
C(7)	0.054(5)	29(5)	36(5)	12(4)	22(4)	13(4)
C(8)	0.078(7)	59(9)	52(6)	7(6)	18(5)	33(6)
C(9)	0.053(6)	52(7)	59(7)	21(6)	28(5)	29(5)
C(10)	0.033(5)	58(7)	56(6)	16(6)	13(4)	-4(4)
C(11)	0.037(5)	33(5)	41(5)	8(4)	17(4)	05(4)
C(12)	0.034(4)	28(5)	30(5)	2(4)	11(3)	4(3)
C(13)	0.070(6)	54(7)	58(7)	13(6)	-6(5)	24(5)
C(14)	0.073(6)	60(7)	49(6)	21(5)	-12(5)	-10(5)
C(15)	0.102(8)	111(10)	132(11)	78(10)	35(9)	57(11)
C(16)	0.042(5)	36(5)	18(4)	-11(4)	-1(3)	10(4)
C(17)	0.067(6)	19(4)	17(4)	-2(3)	2(4)	-3(4)
C(18)	0.046(5)	32(5)	31(6)	1(4)	0(4)	8(4)
C(19)	0.041(4)	52(8)	39(5)	10(5)	17(4)	10(5)
C(20)	0.043(5)	46(7)	37(6)	9(5)	15(4)	-1(4)
C(21)	0.043(4)	23(4)	19(4)	-1(5)	2(4)	-3(3)
C(22)	0.054(5)	27(5)	21(5)	-4(5)	-2(5)	7(4)
C(23)	0.057(5)	49(6)	30(4)	3(4)	-13(5)	-12(6)
C(24)	0.061(6)	45(8)	26(5)	-5(4)	-9(4)	-4(4)
N(1)	0.030(3)	46(4)	20(3)	6(4)	-1(2)	4(4)
N(2)	0.037(4)	22(4)	20(4)	-4(3)	6(3)	2(3)
O(1)	0.036(3)	75(5)	44(4)	8(4)	-14(3)	-10(3)
O(2)	0.067(5)	45(4)	38(4)	1(3)	18(3)	-23(3)
P(1)	0.0394(14)	64(2)	574(18)	148(15)	-94(12)	45(13)
F(1)	0.095(4)	61(4)	116(7)	38(5)	5(4)	-5(3)
F(2)	0.045(3)	171(10)	179(8)	83(7)	24(4)	10(4)
F(3)	0.120(5)	58(5)	126(6)	12(4)	-24(5)	-11(4)
F(4)	0.050(3)	147(7)	168(8)	-25(7)	8(4)	44(3)
F(5)	0.137(6)	91(6)	71(4)	17(4)	-25(4)	4(4)
F(6)	0.154(6)	148(8)	75(6)	10(5)	-54(5)	-23(5)
Ir(1)	0.02908(10)	2530(11)	2293(10)	14(19)	-0.19(16)	-0000.3(17)

Appendix B: NMR Spectra

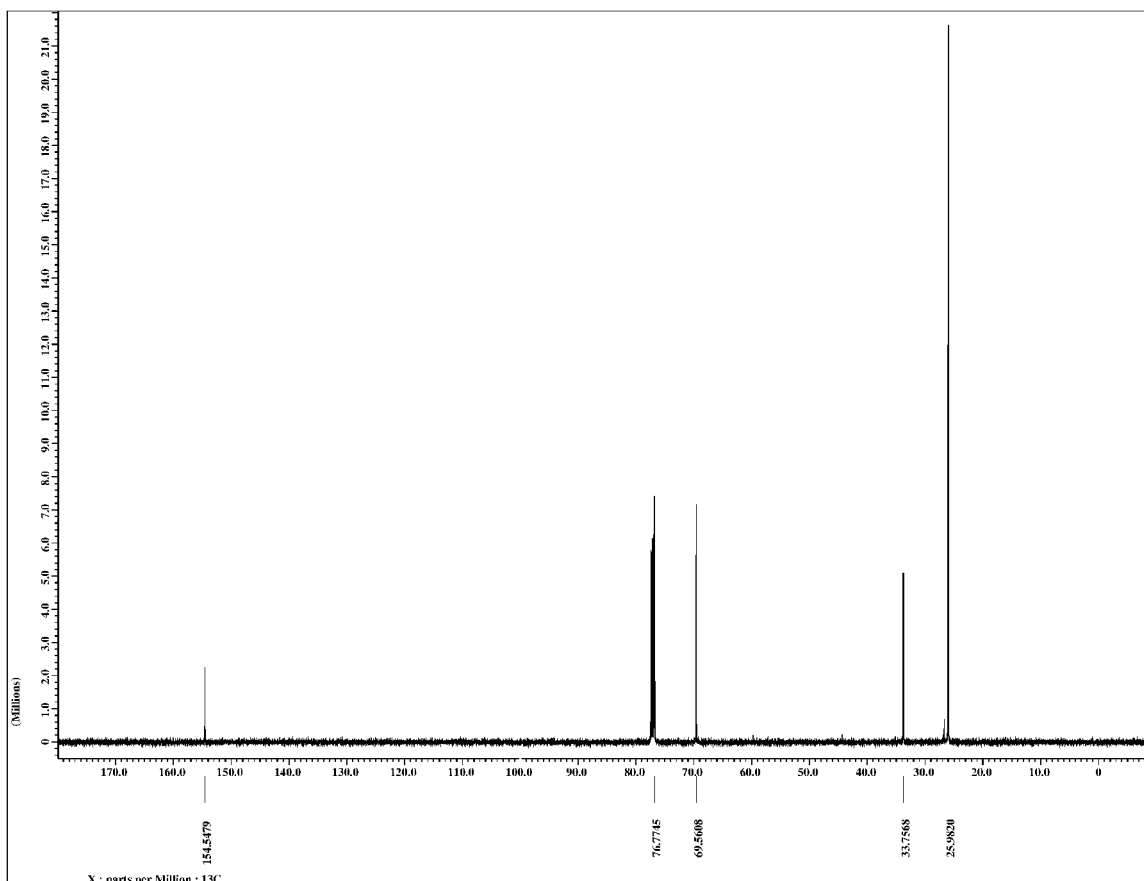
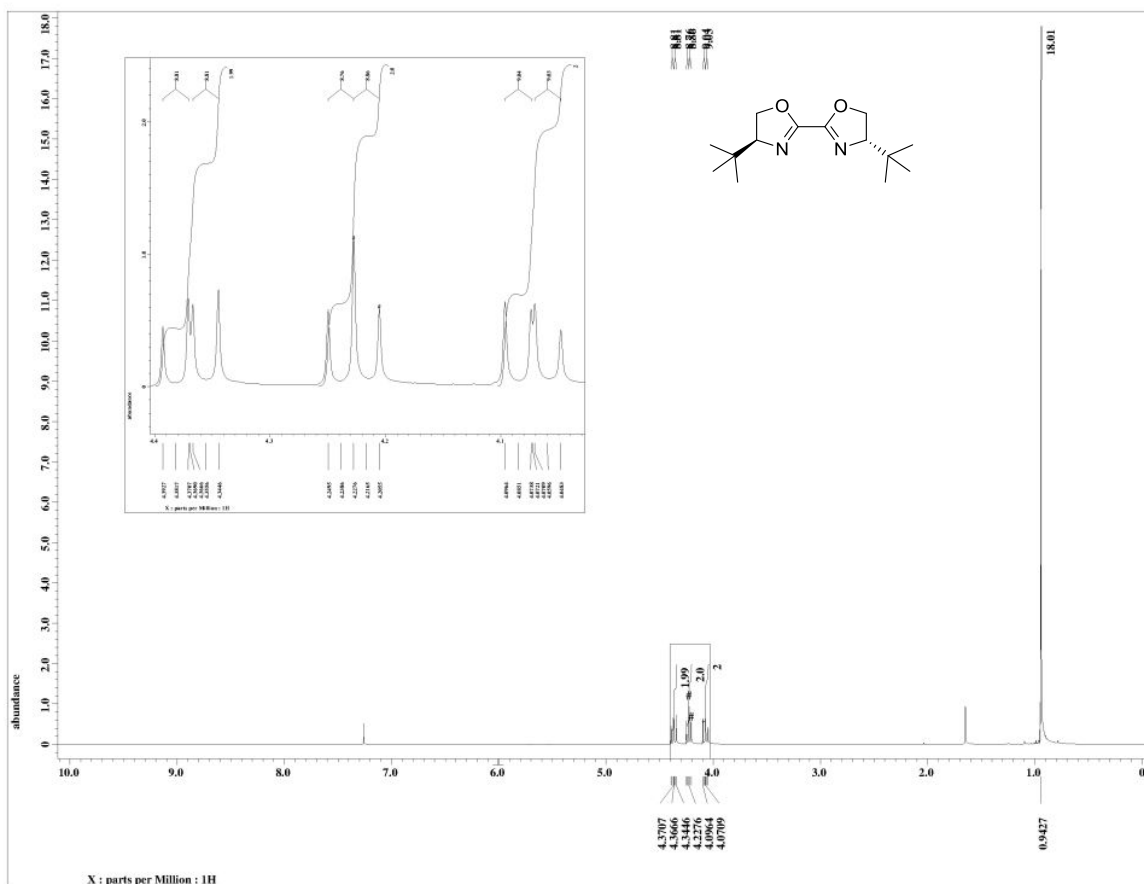
2,2'-Bi((4*S*, 4'*S*)-4,4'-dimethyl)-oxazolin (5a)



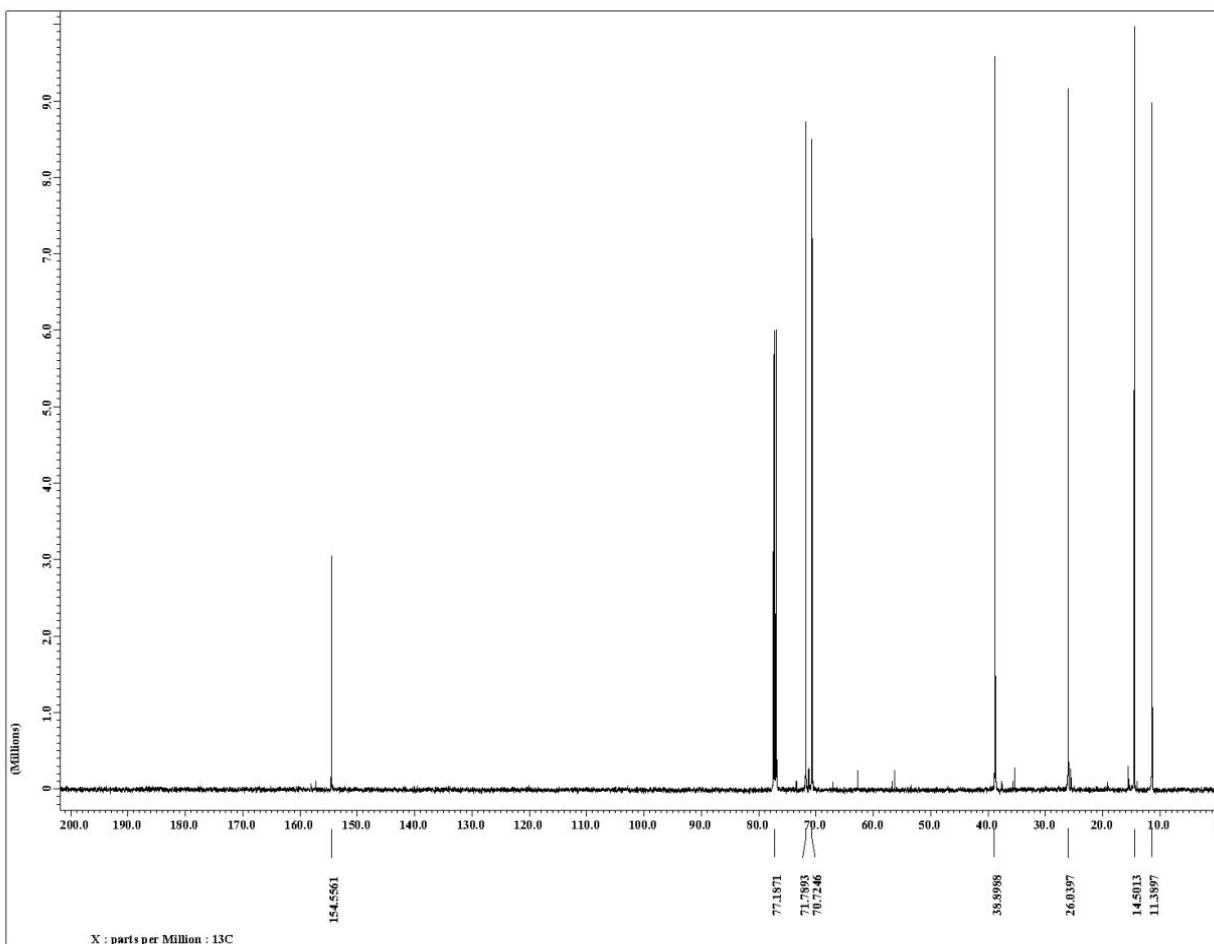
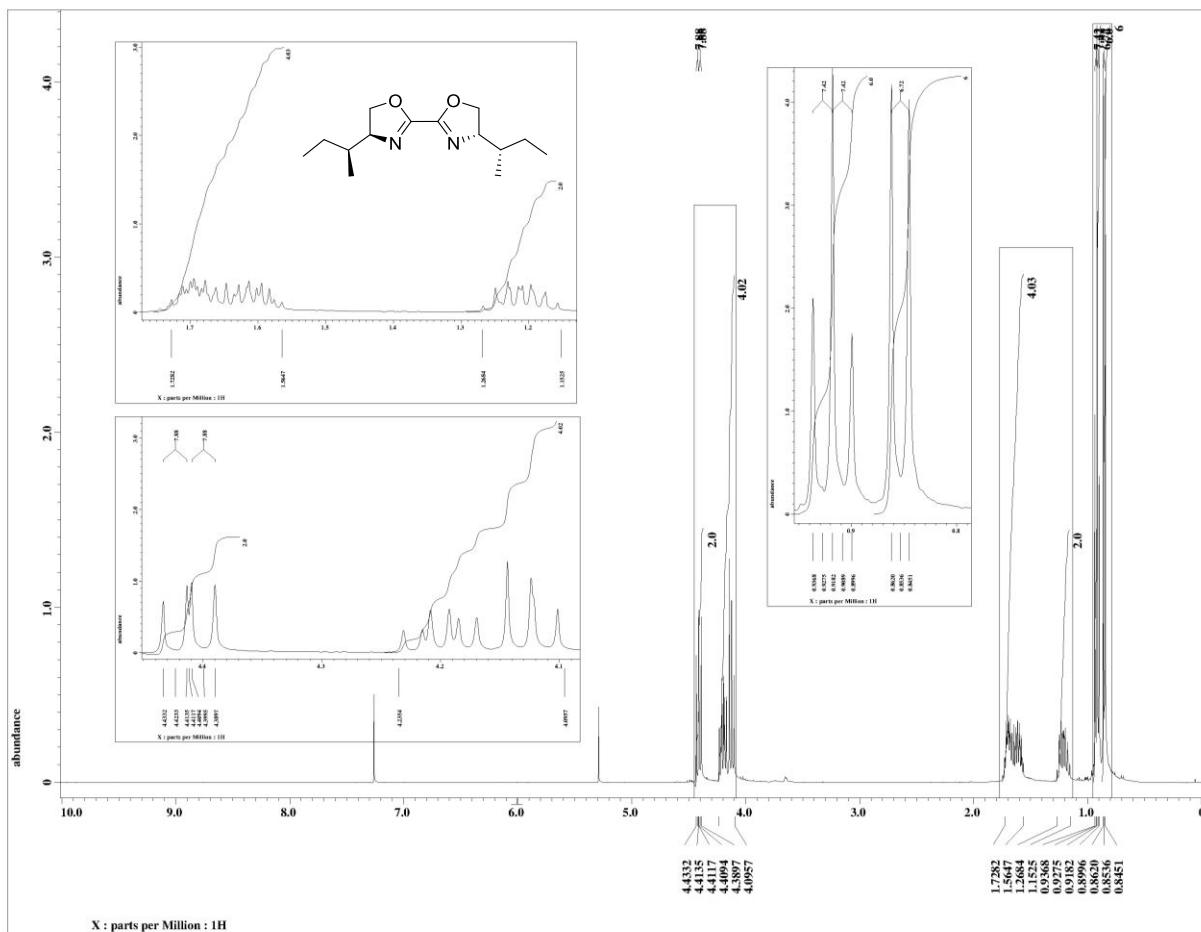
2,2'-Bi((4*S*,4'*S*)-4,4'-diisopropyl)-oxazolin (5b)



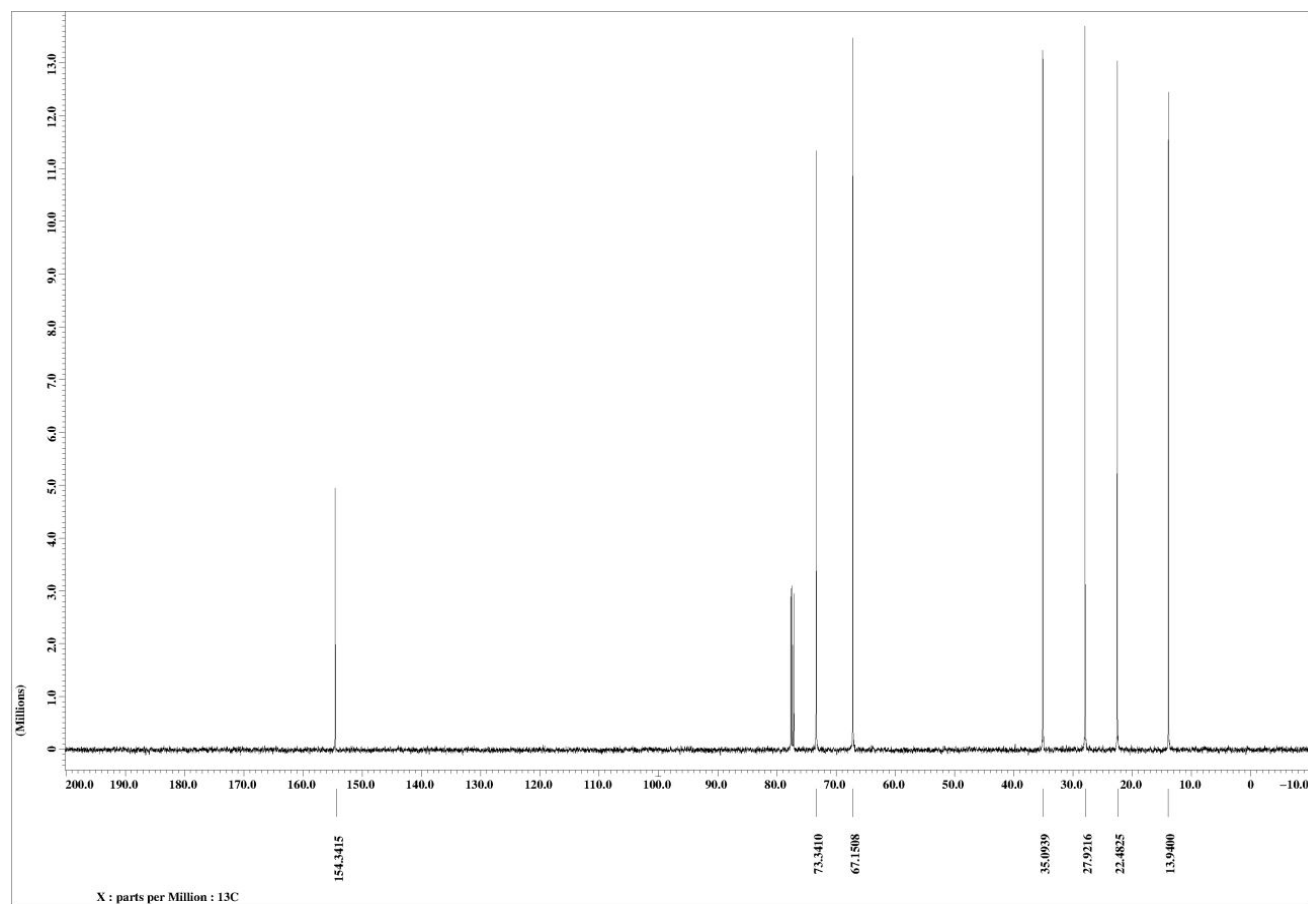
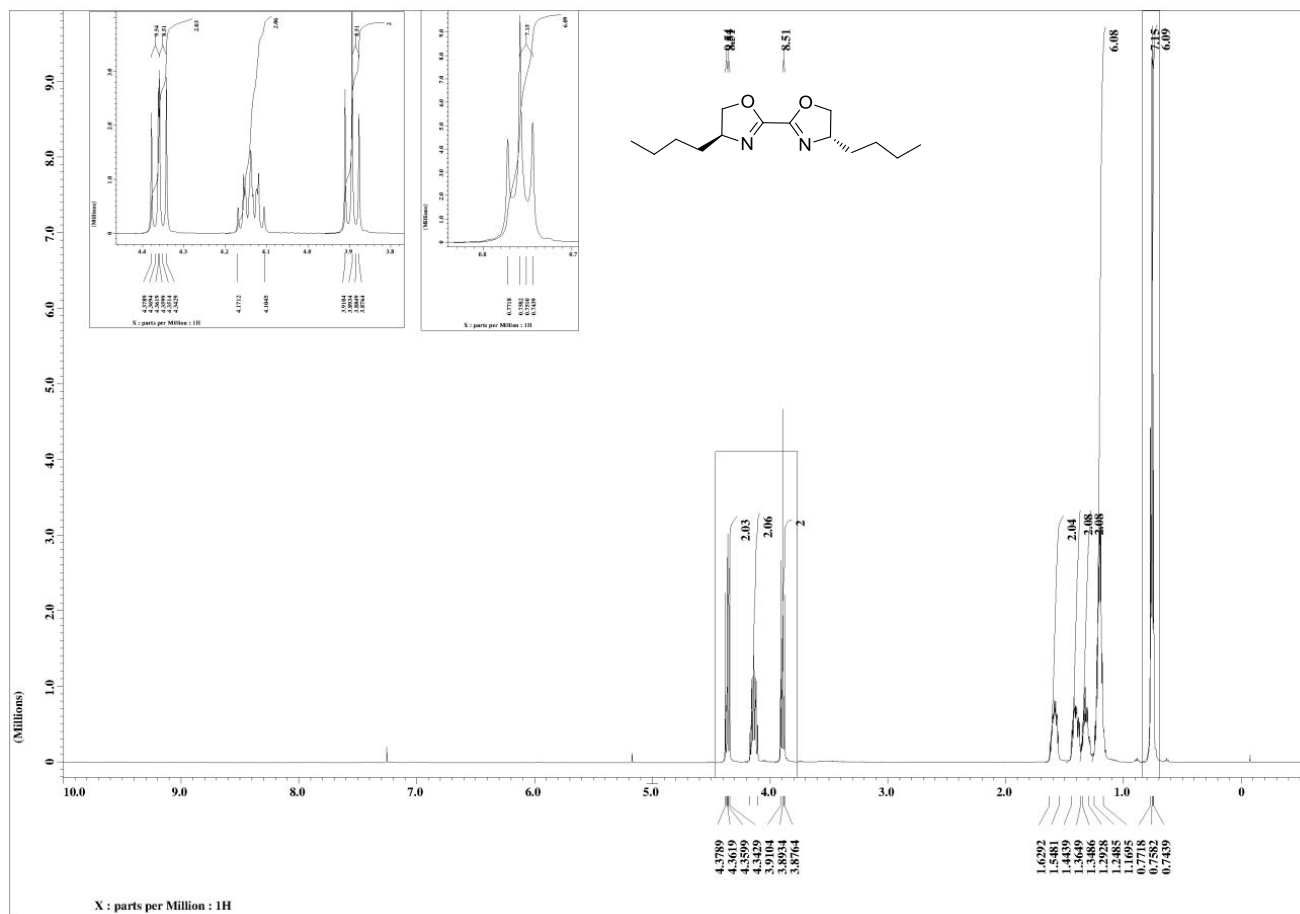
2,2'-Bi((4*S*,4'*S*)-4,4'-di-*tert*-butyl)-oxazolin (5c)



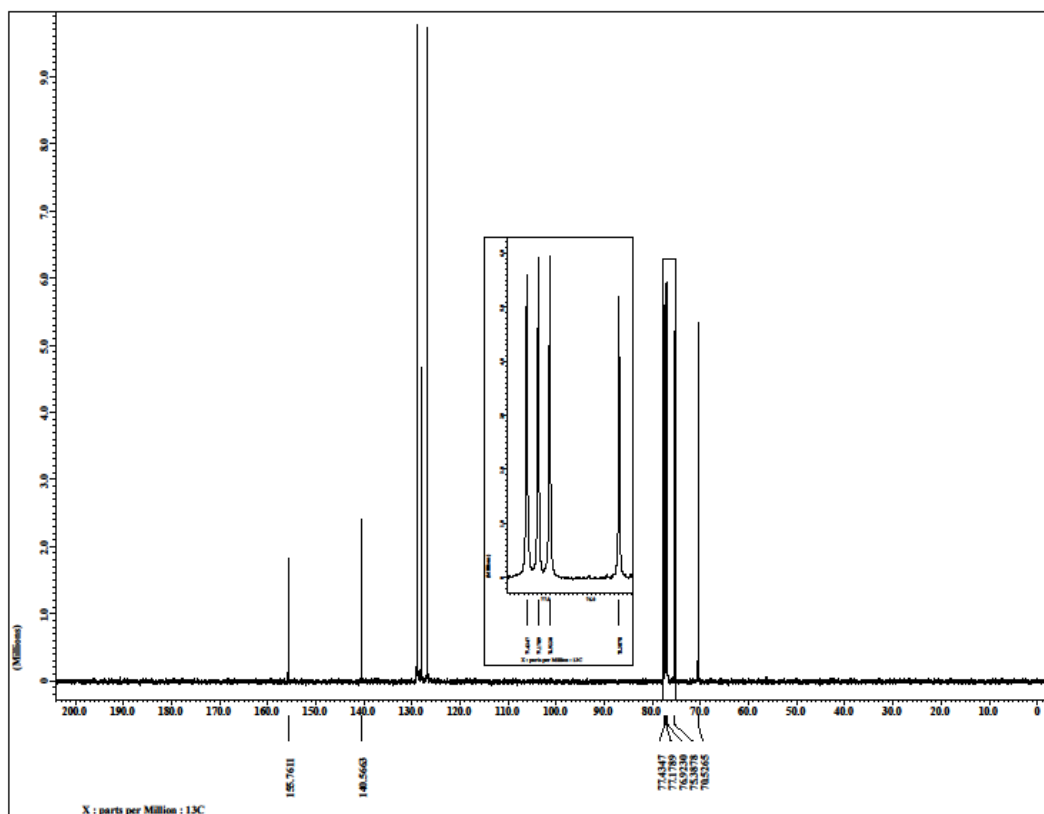
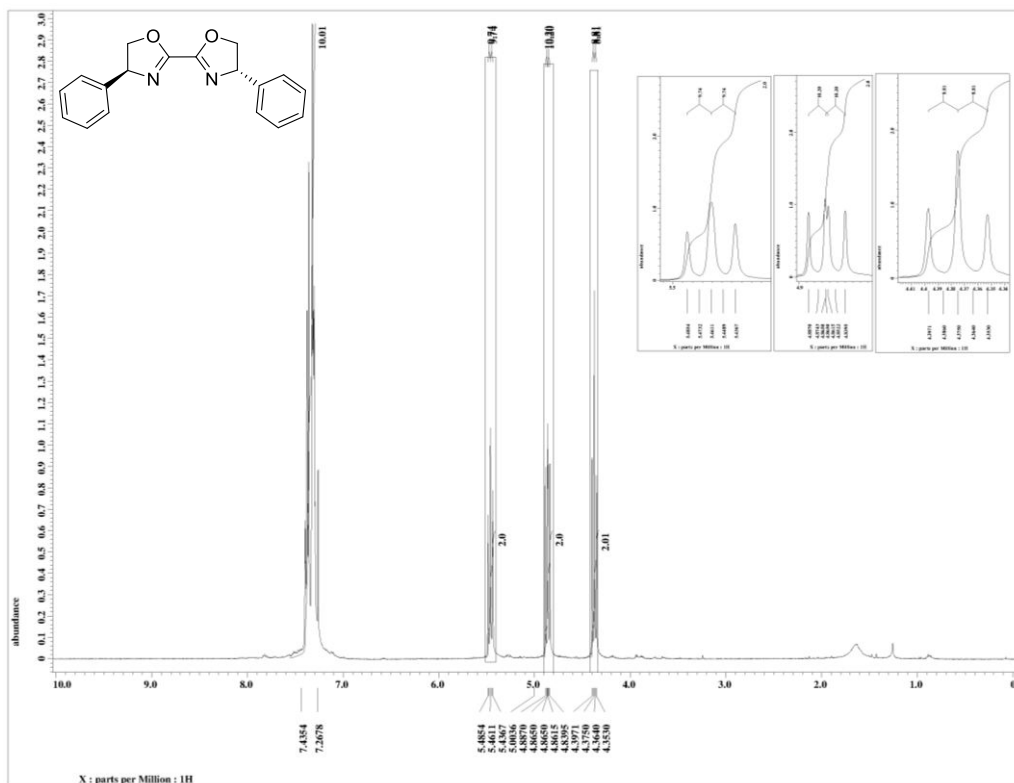
2,2'-Bi((4*S*, 4'*S*)-4,4'-di((*S*)-sec-butyl)-oxazolin (5d)



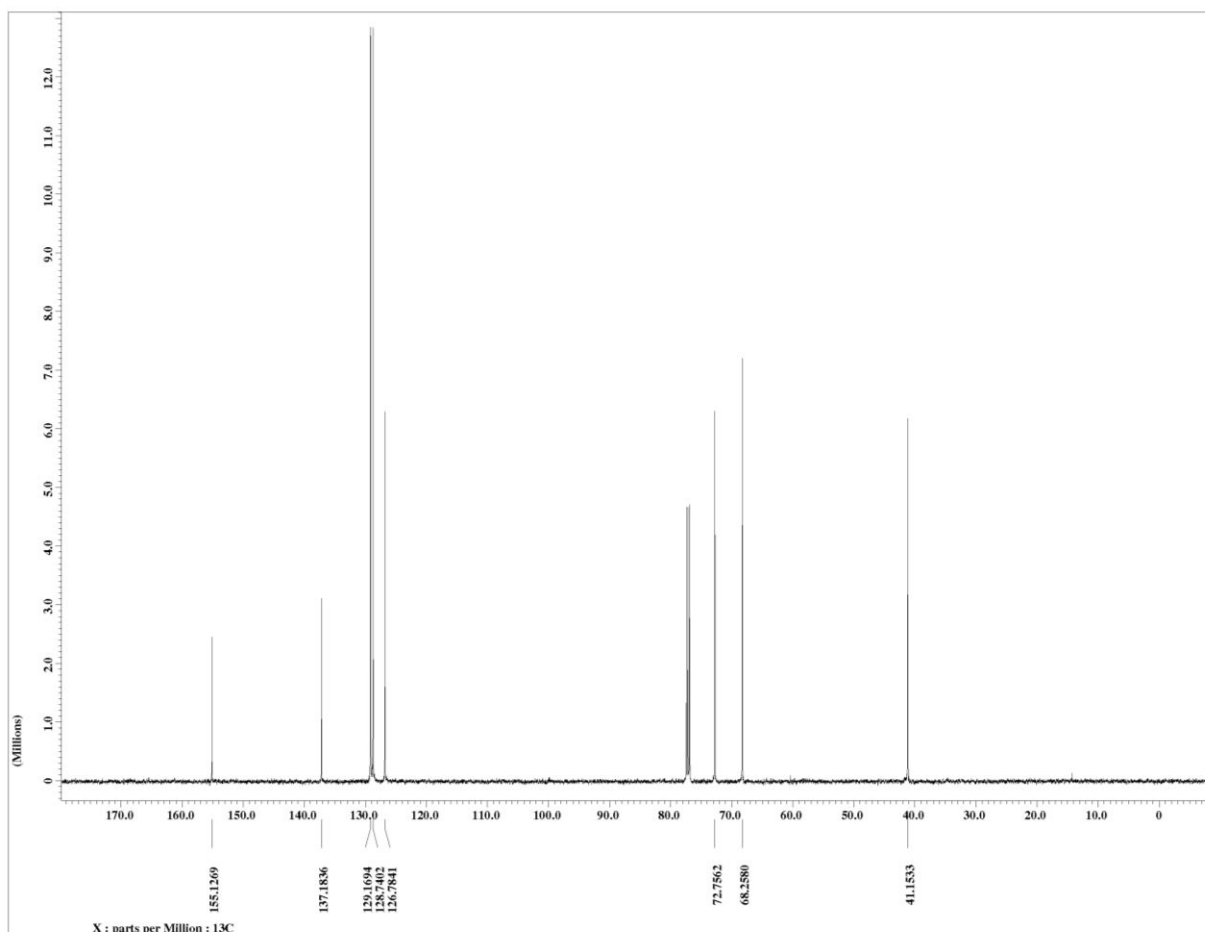
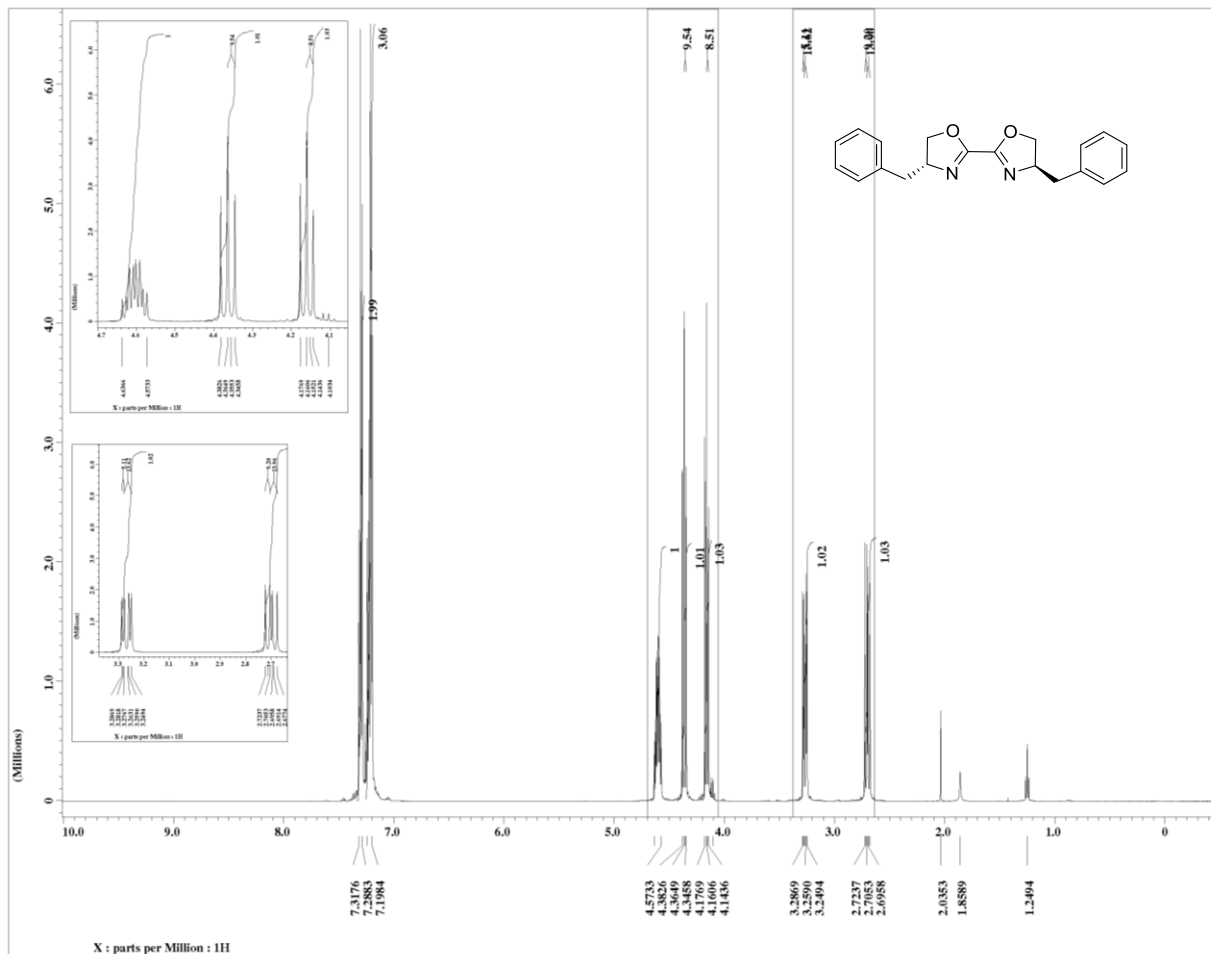
2,2'-Bi((4*S*, 4'*S*)-4,4'-dibutyl)-oxazolin (5f)



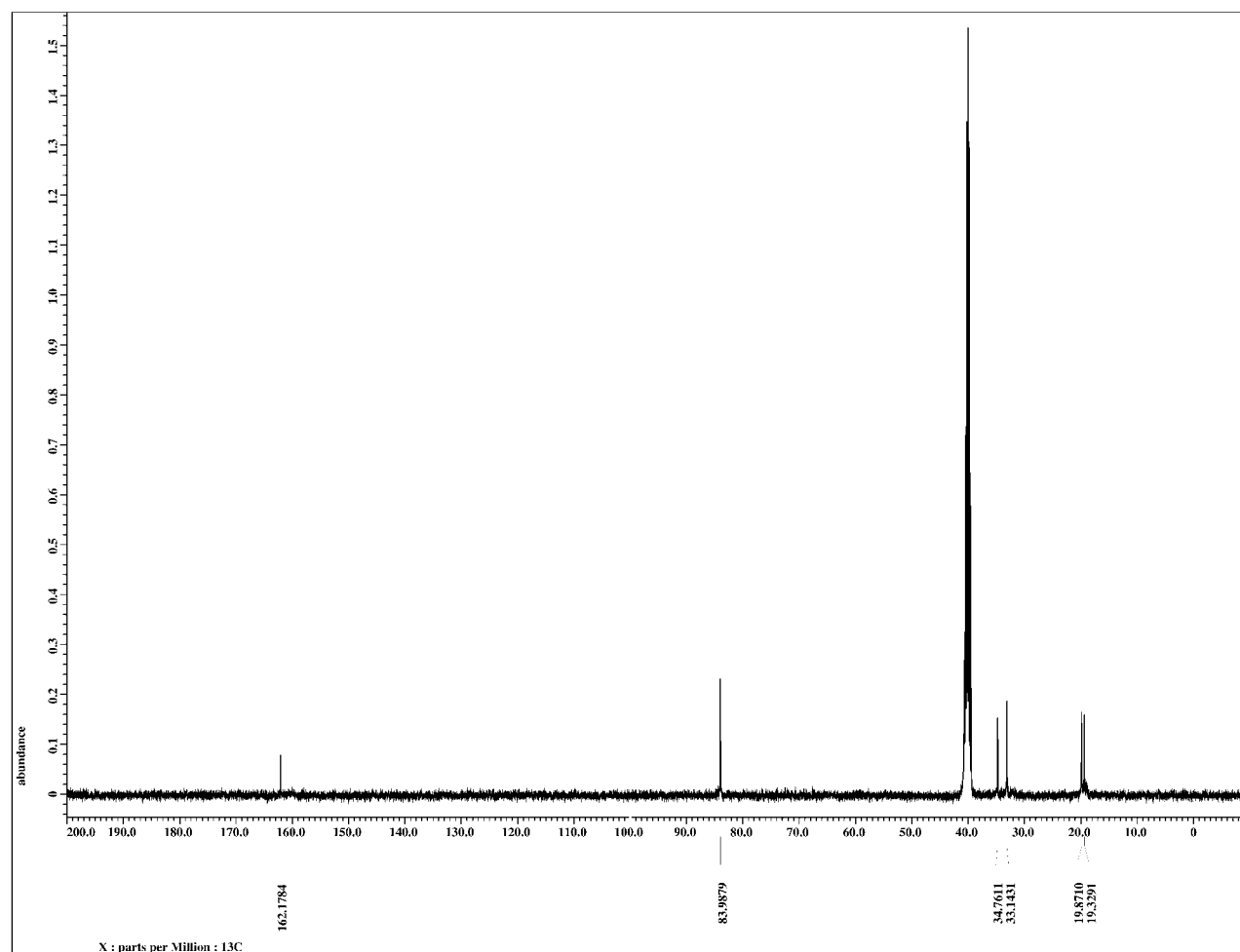
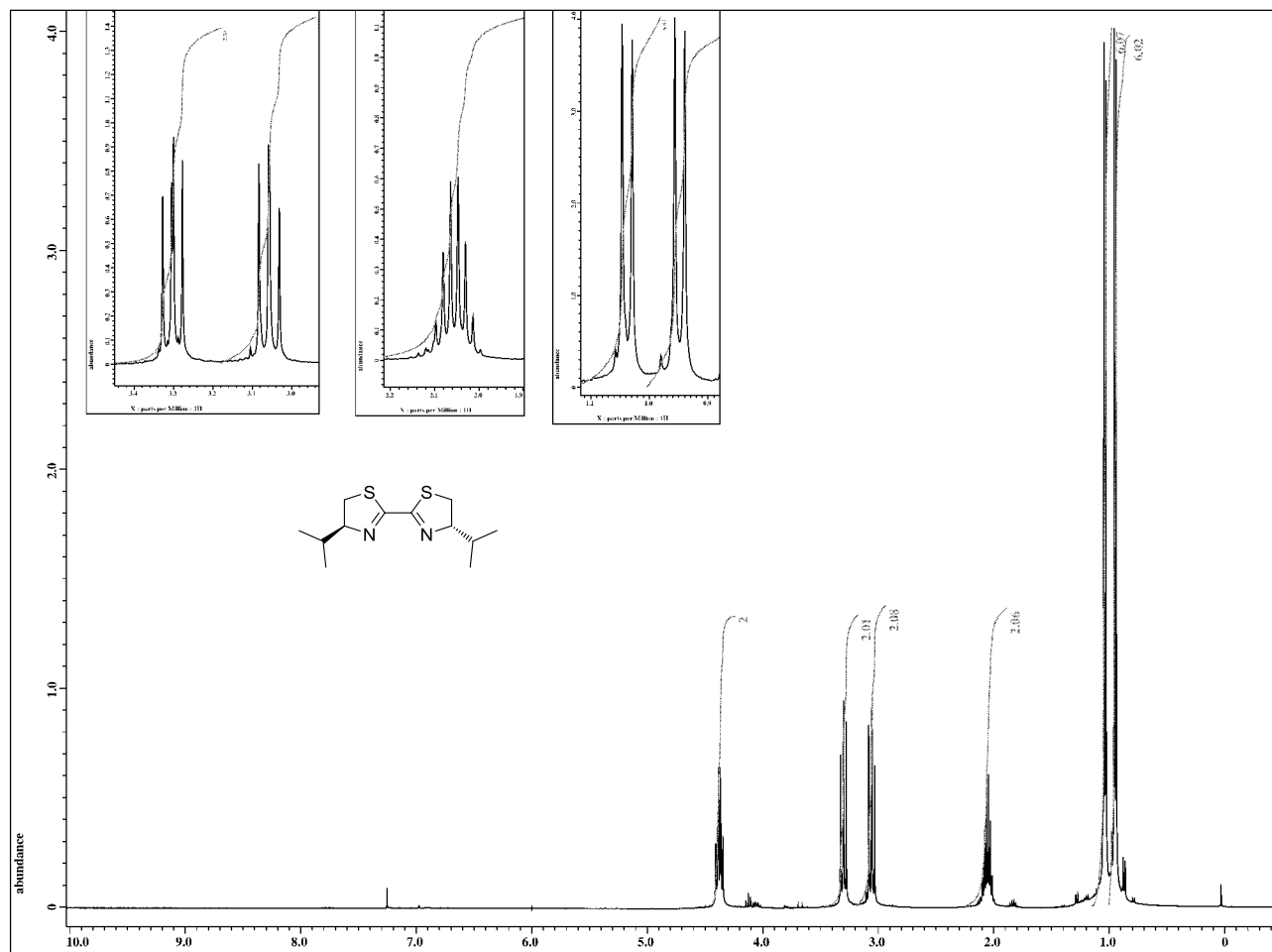
2,2'-Bi((4*R*, 4'*R*)-4,4'-diphenyl)-oxazolin (5g)



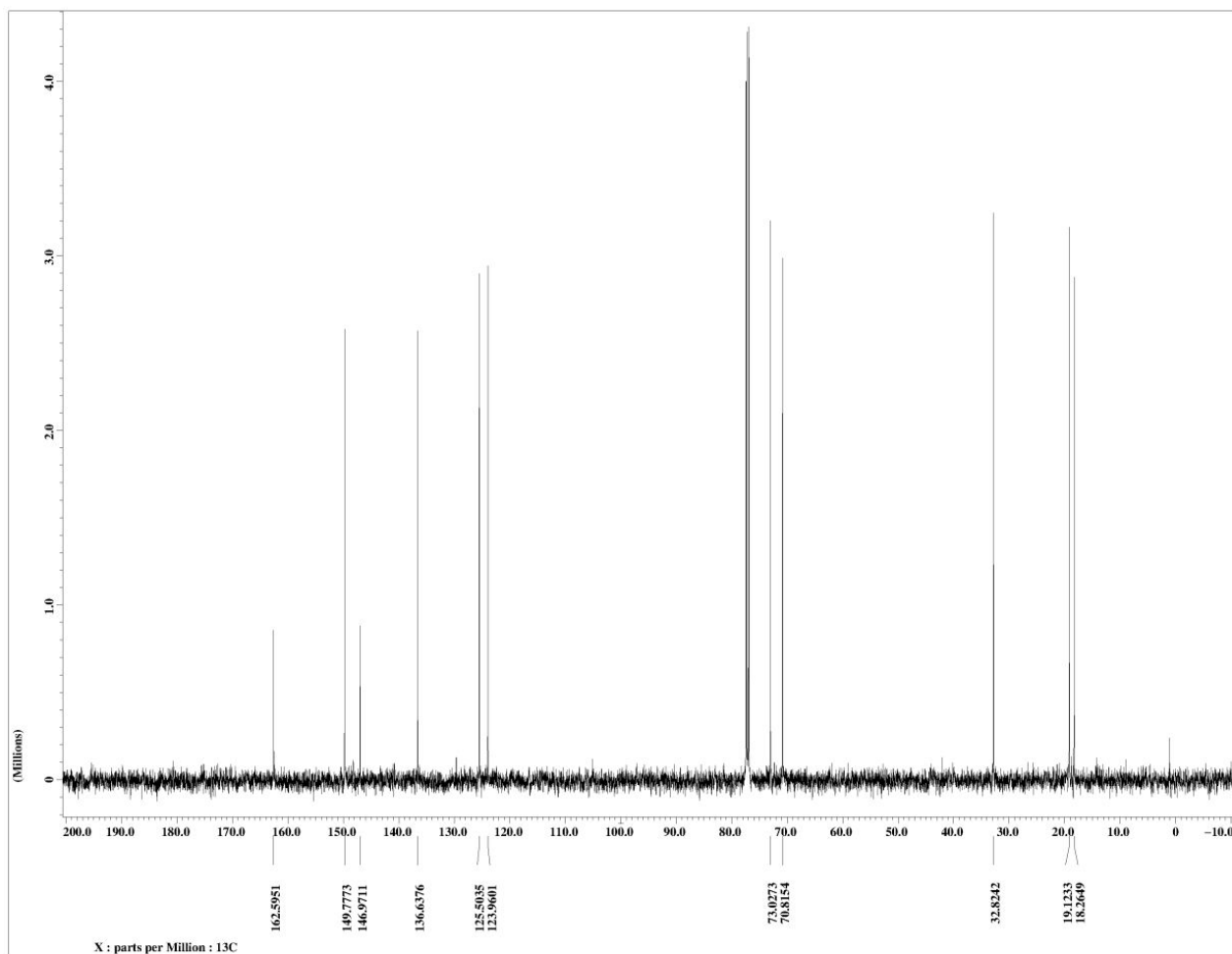
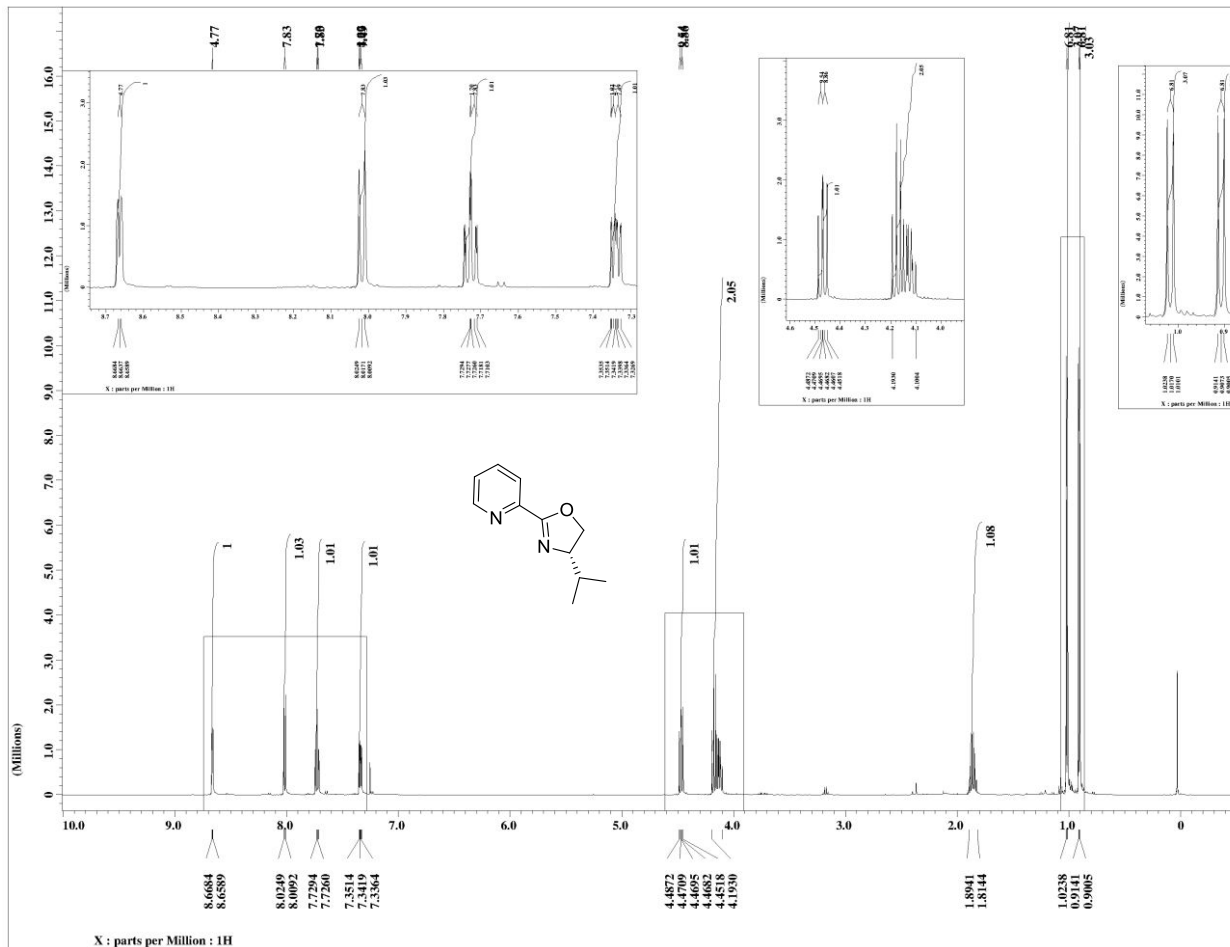
2,2'-Bi((4*R*, 4'*R*)-4,4'-dibenzyl)-oxazolin (5h)



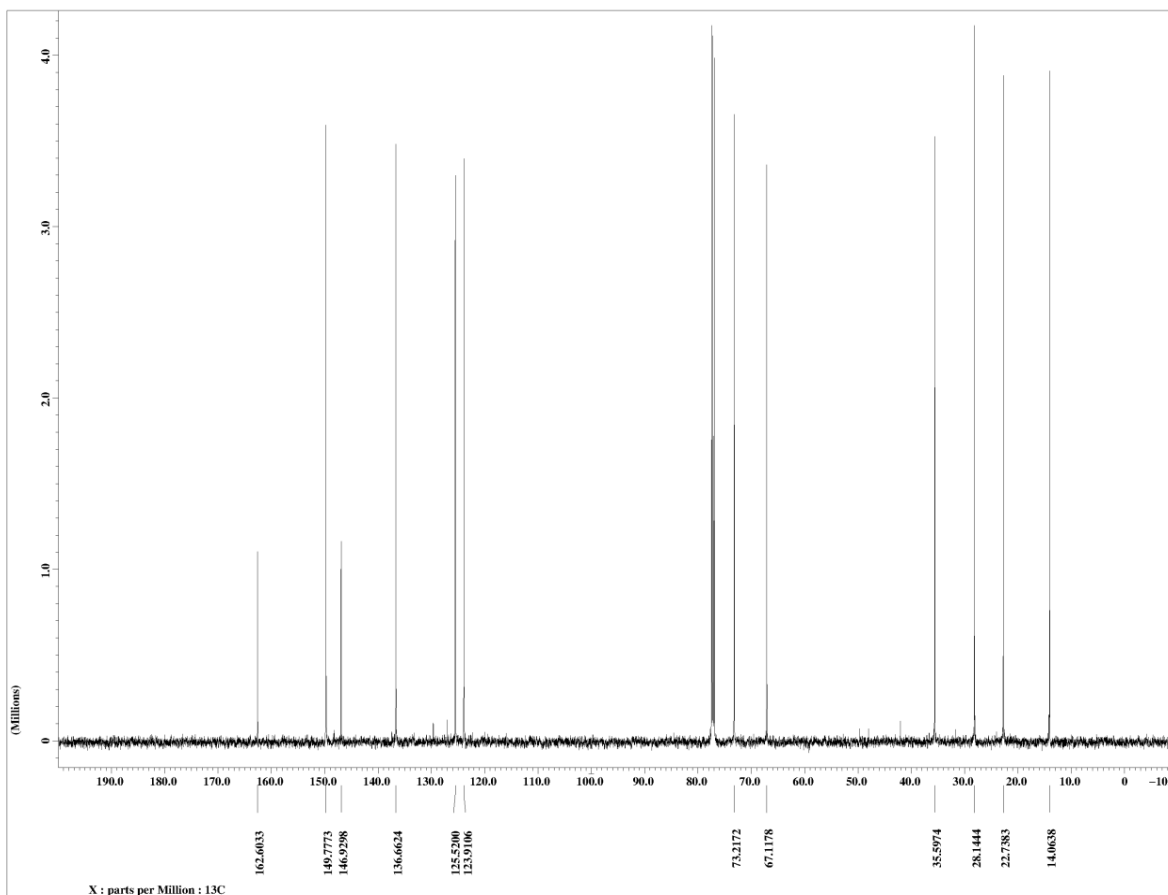
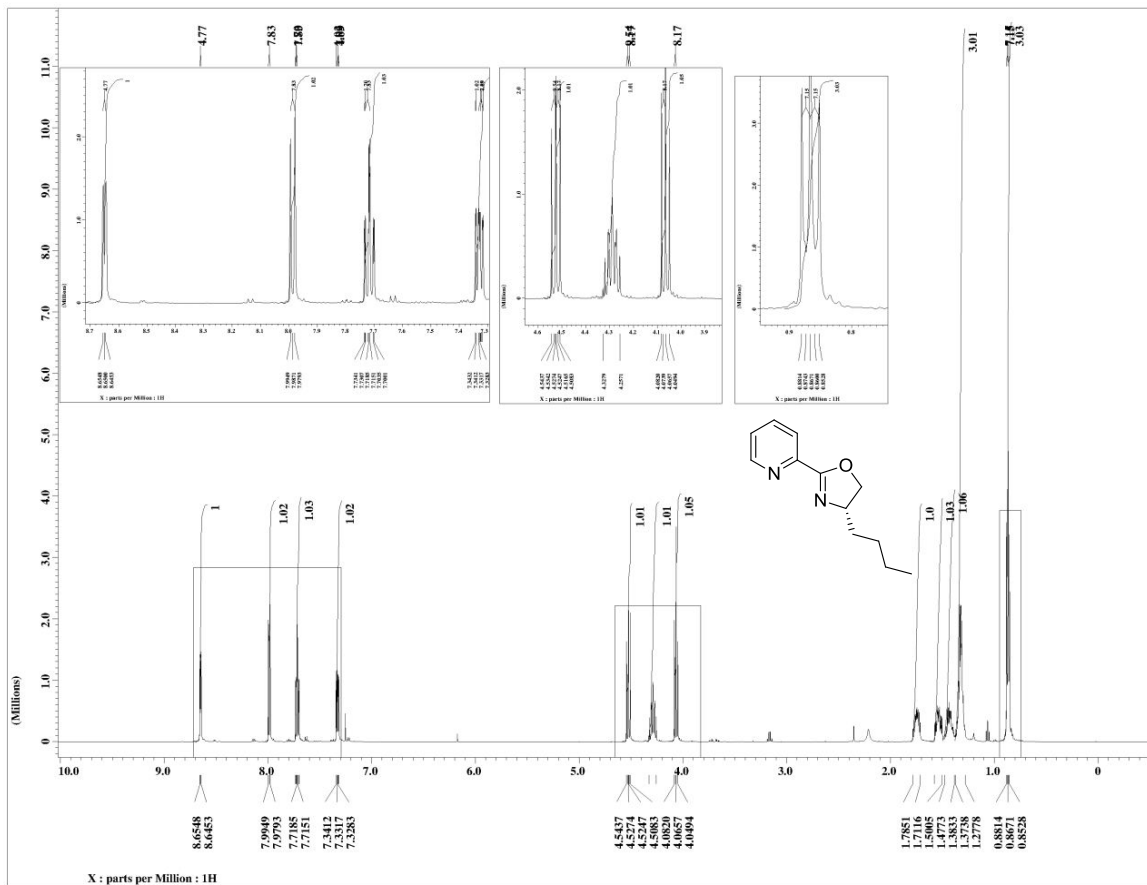
2,2'-Bi ((4*R*, 4'*R*)-4,4'-dibenzyl)-oxazolin (5h) (*S*)-4,4'-diisopropyl-thiazolin (7b)



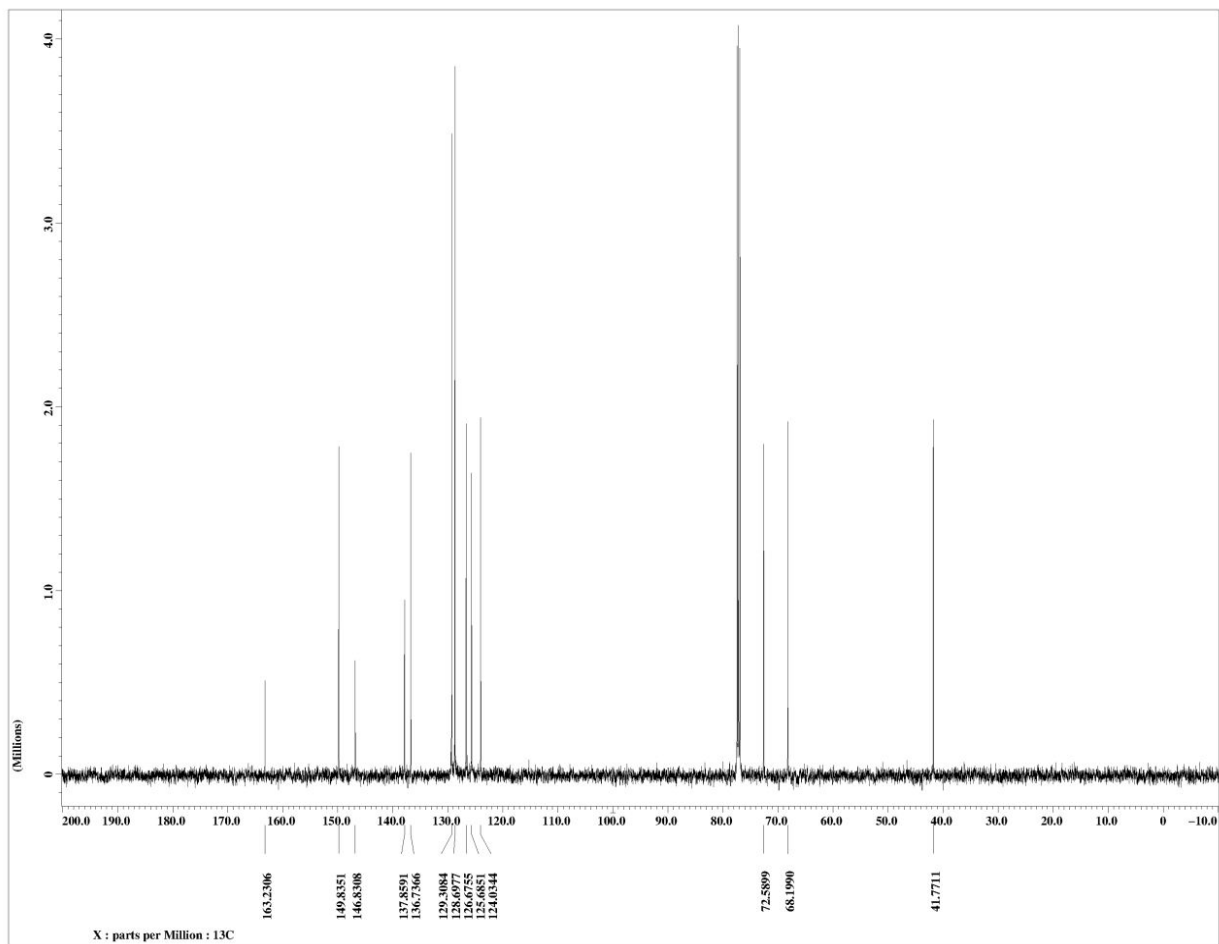
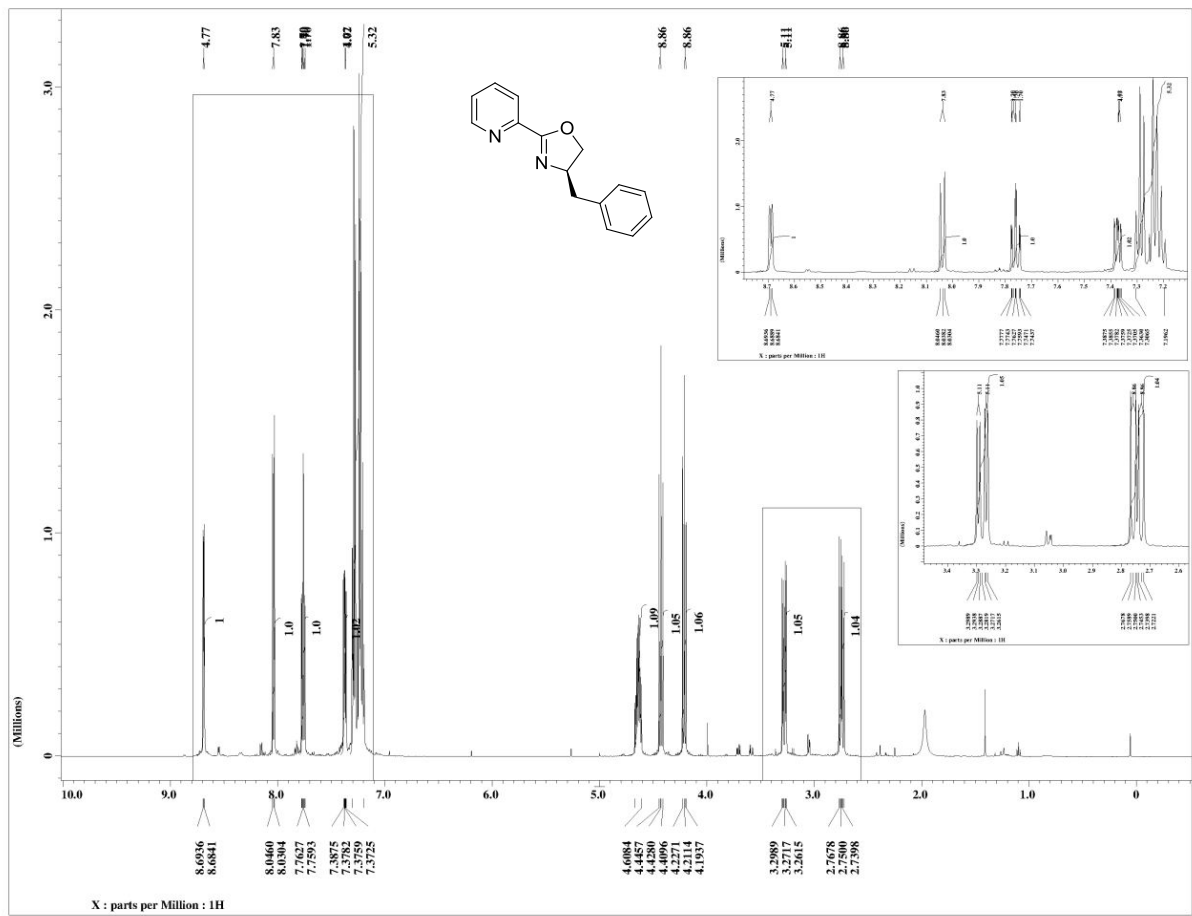
(S)-4-Isopropyl-2-(pyridine-2-yl)-oxazolin (10a)



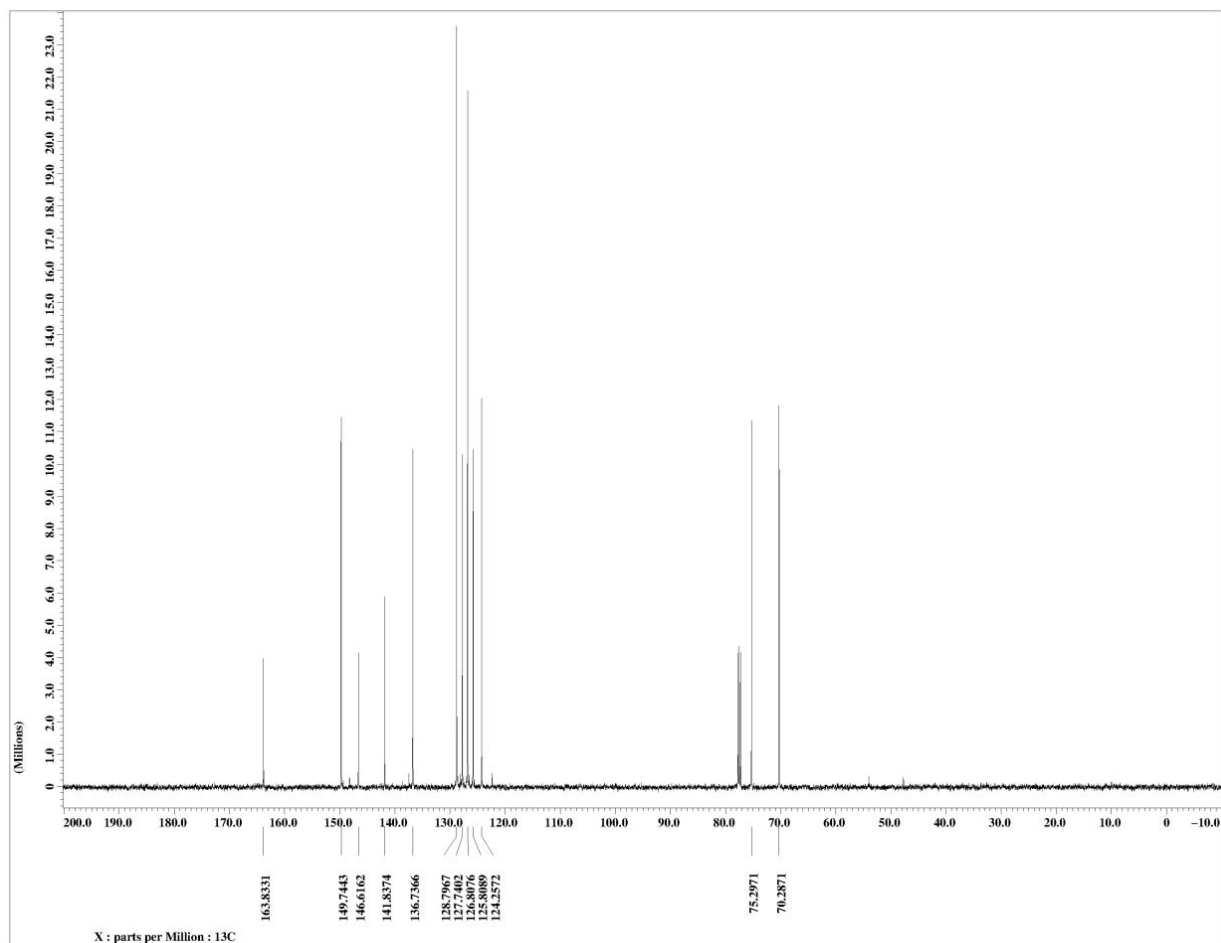
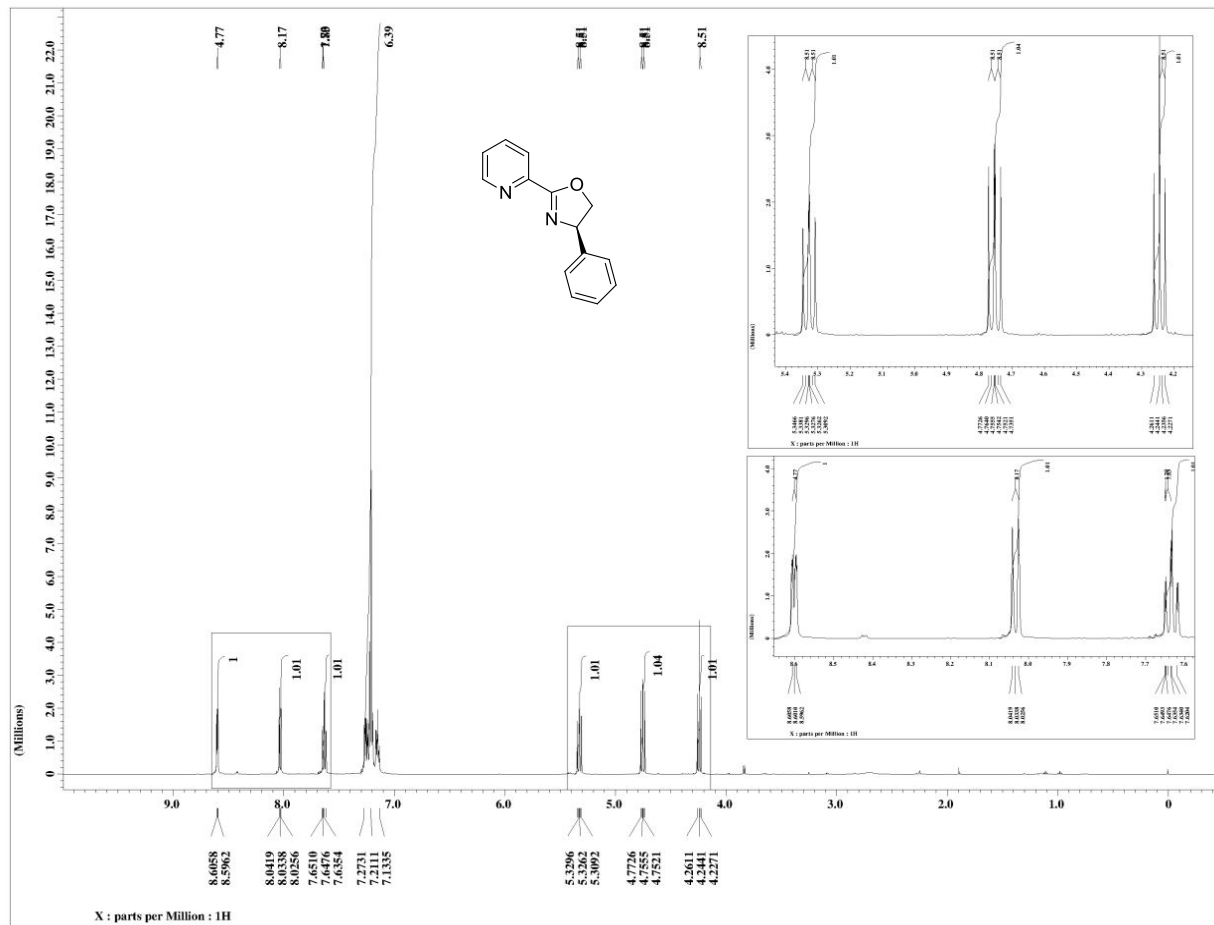
(S)-4-Butyl-2-(pyridine-2-yl)-oxazolin (10b)



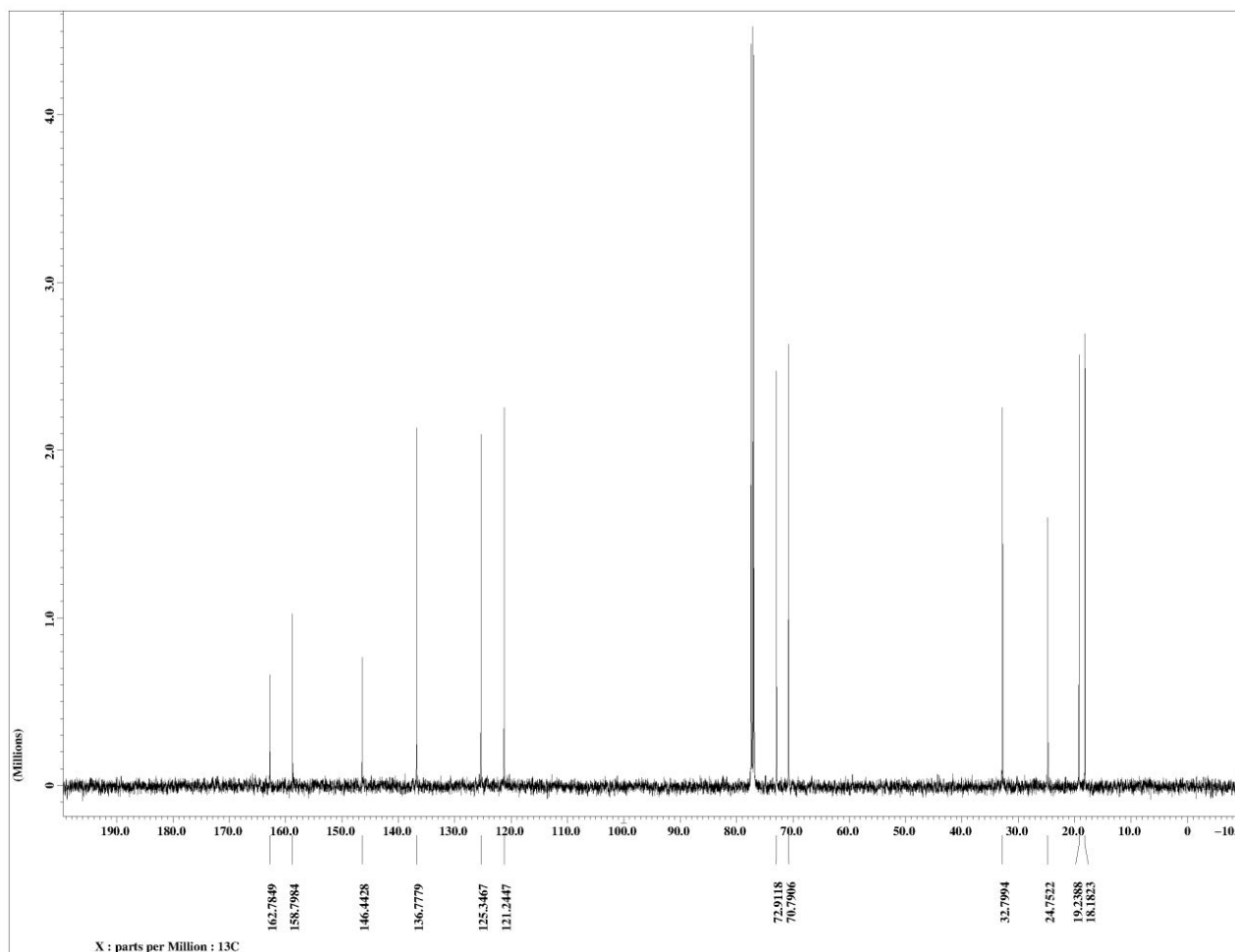
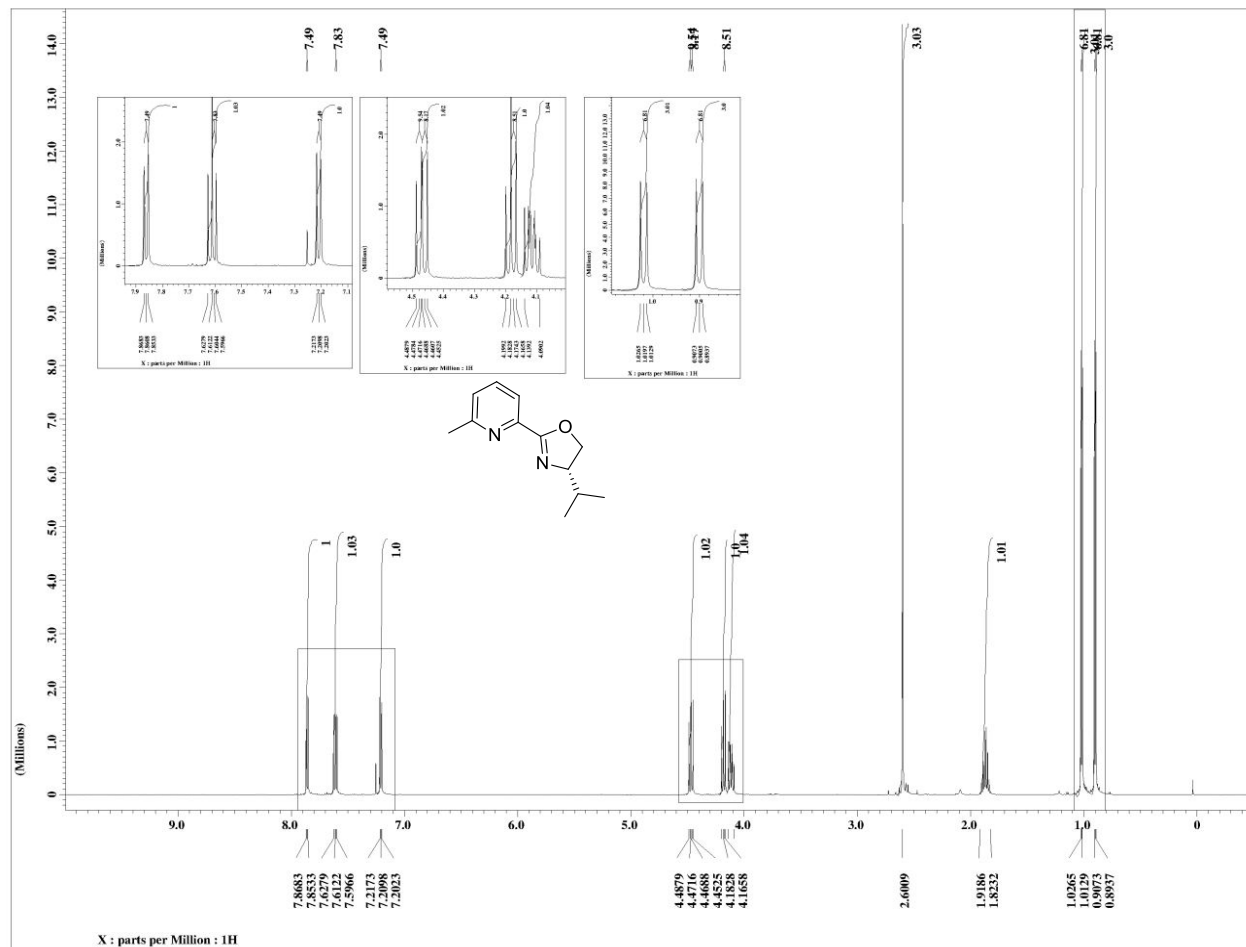
(R)-4-Benzyl-2-(pyridine-2-yl)-oxazolin (10c)



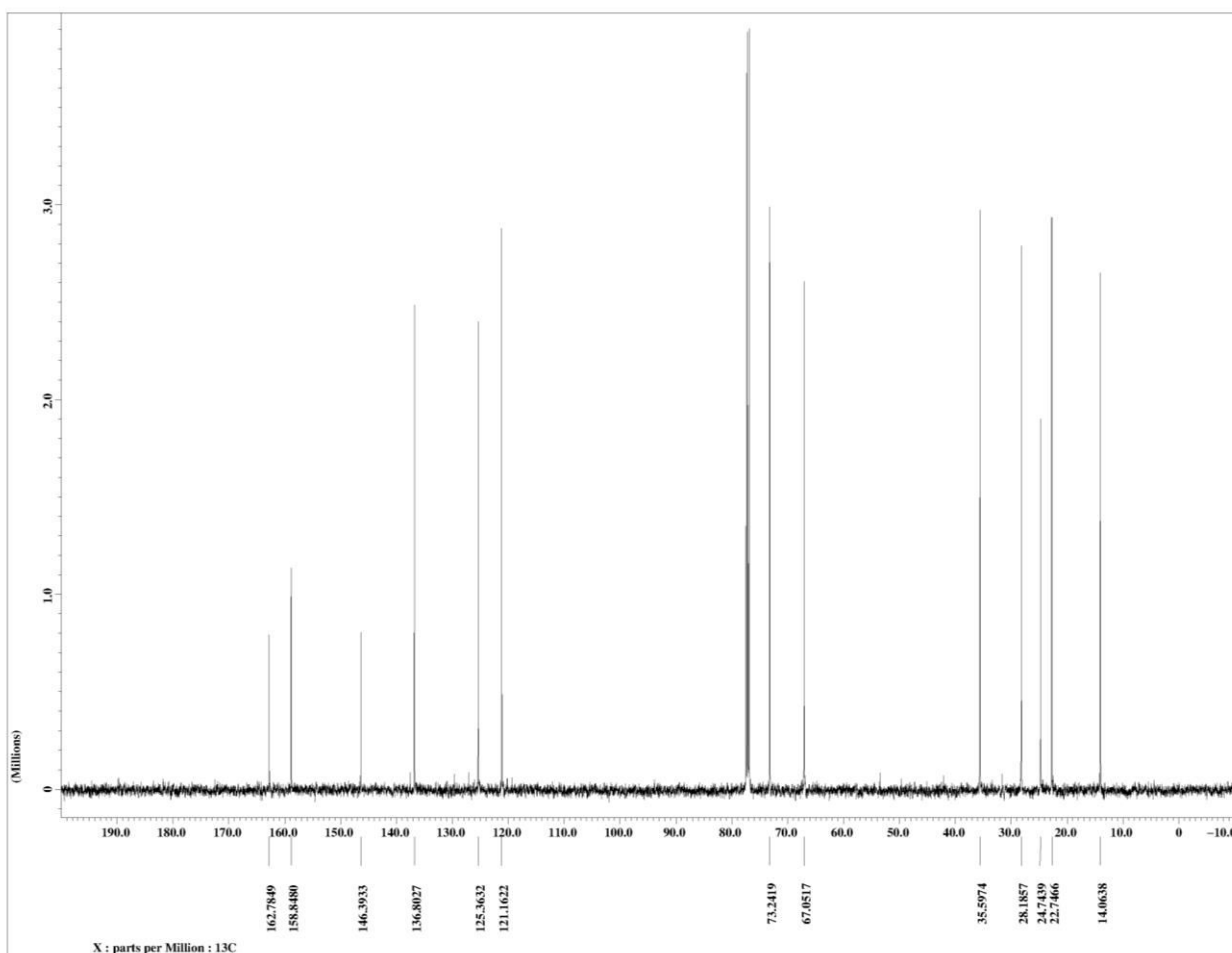
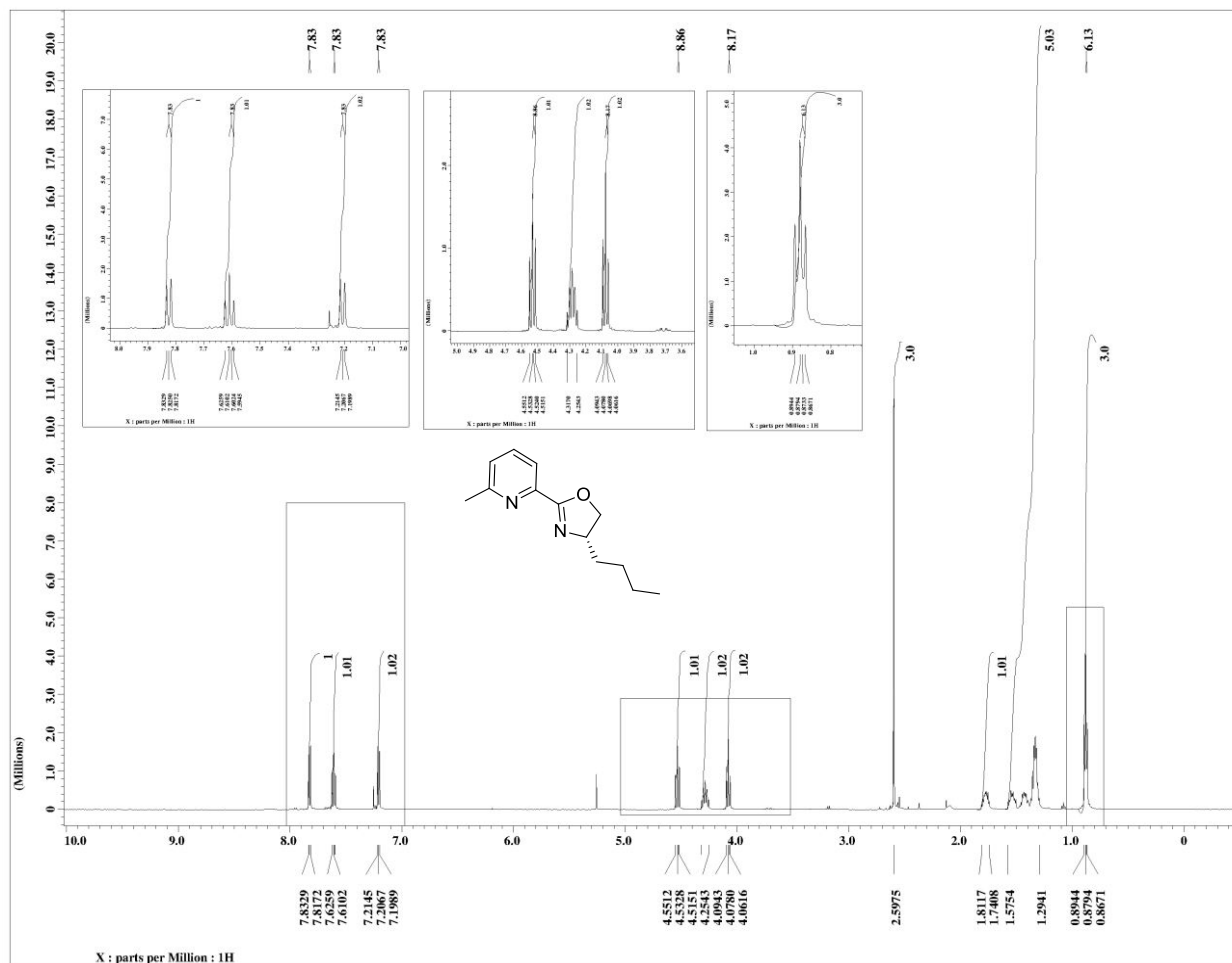
(R)-4-Phenyl-2-(pyridine-2-yl)-oxazolin (10d)



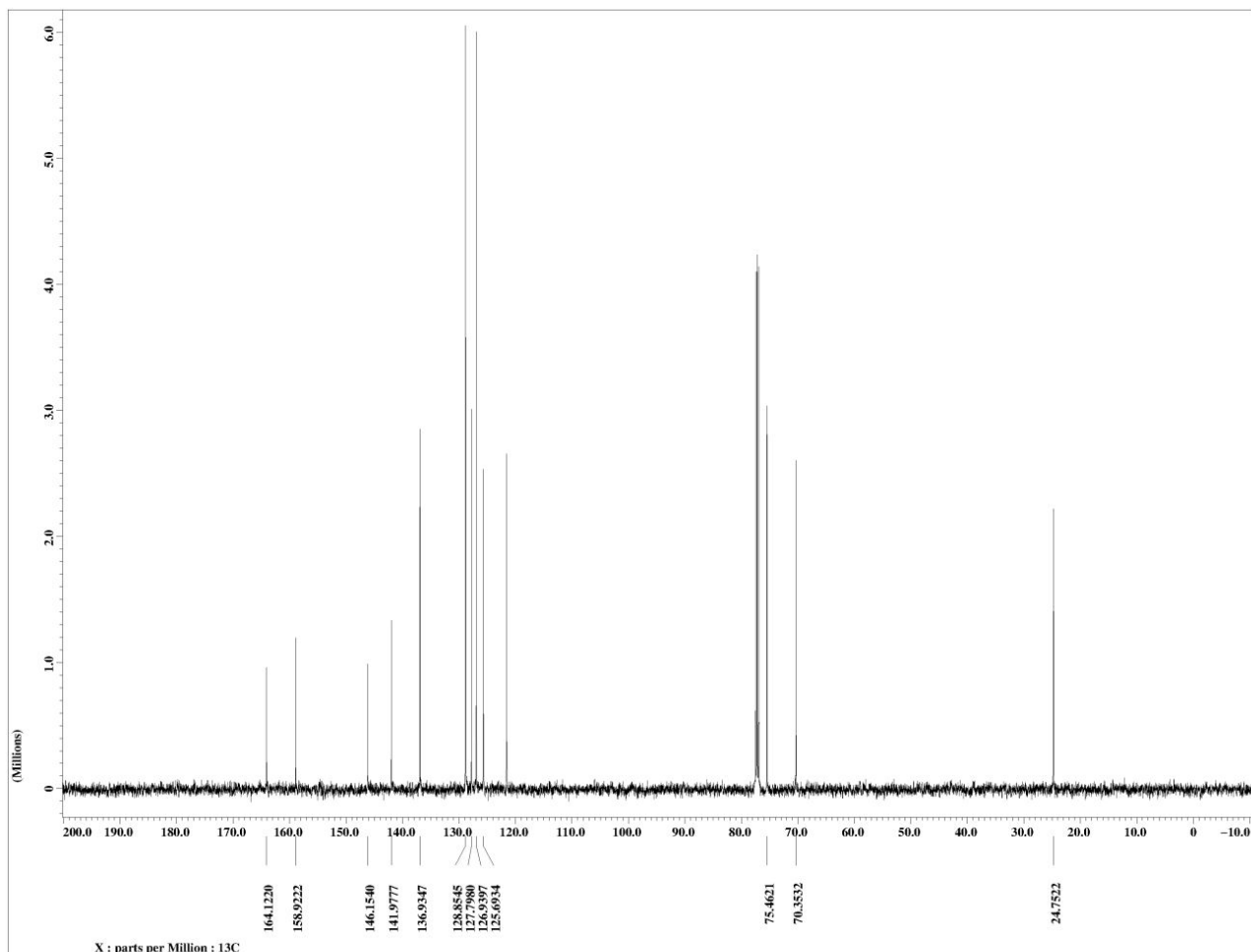
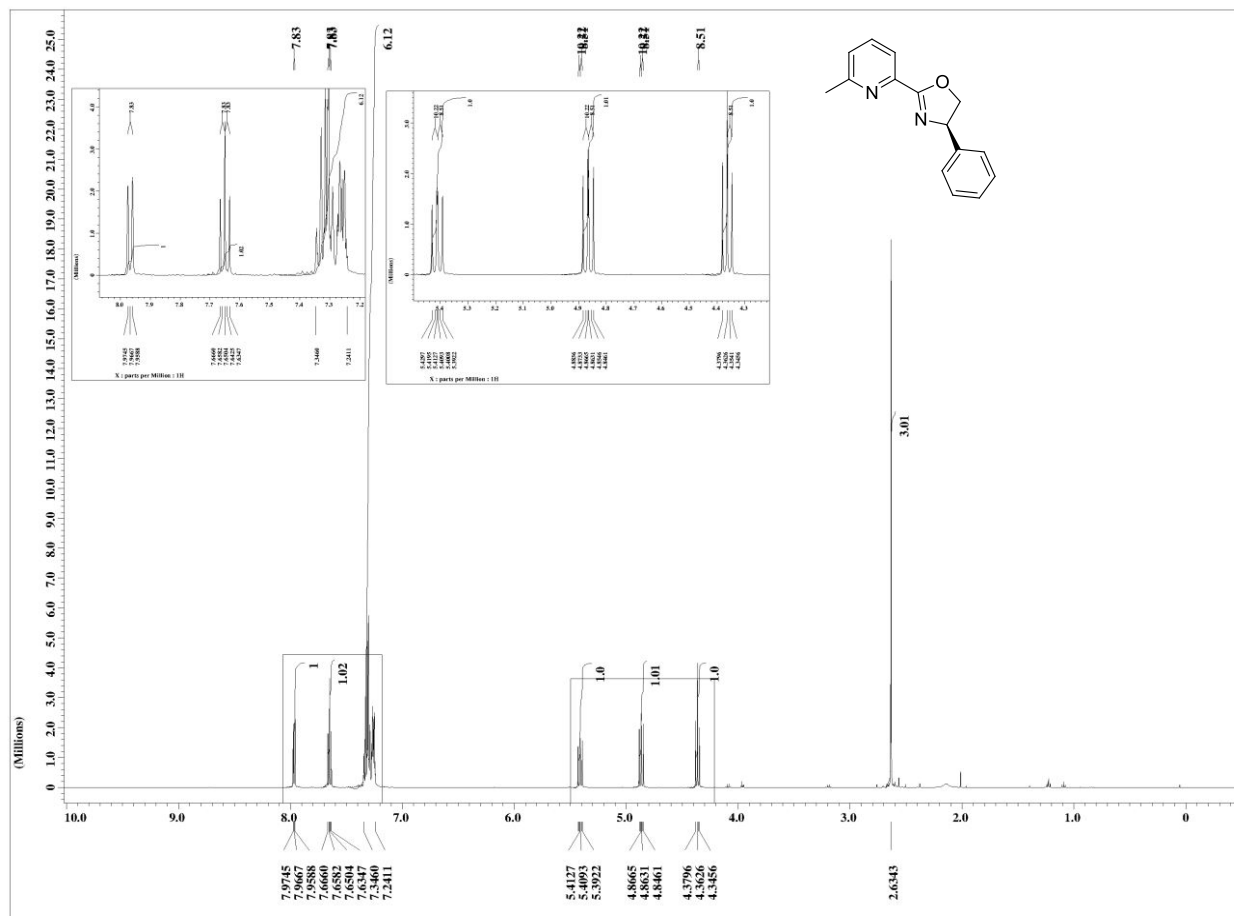
(S)-4-Isopropyl-2-(6-methylpyridin-2-yl)-oxazolin (19e)



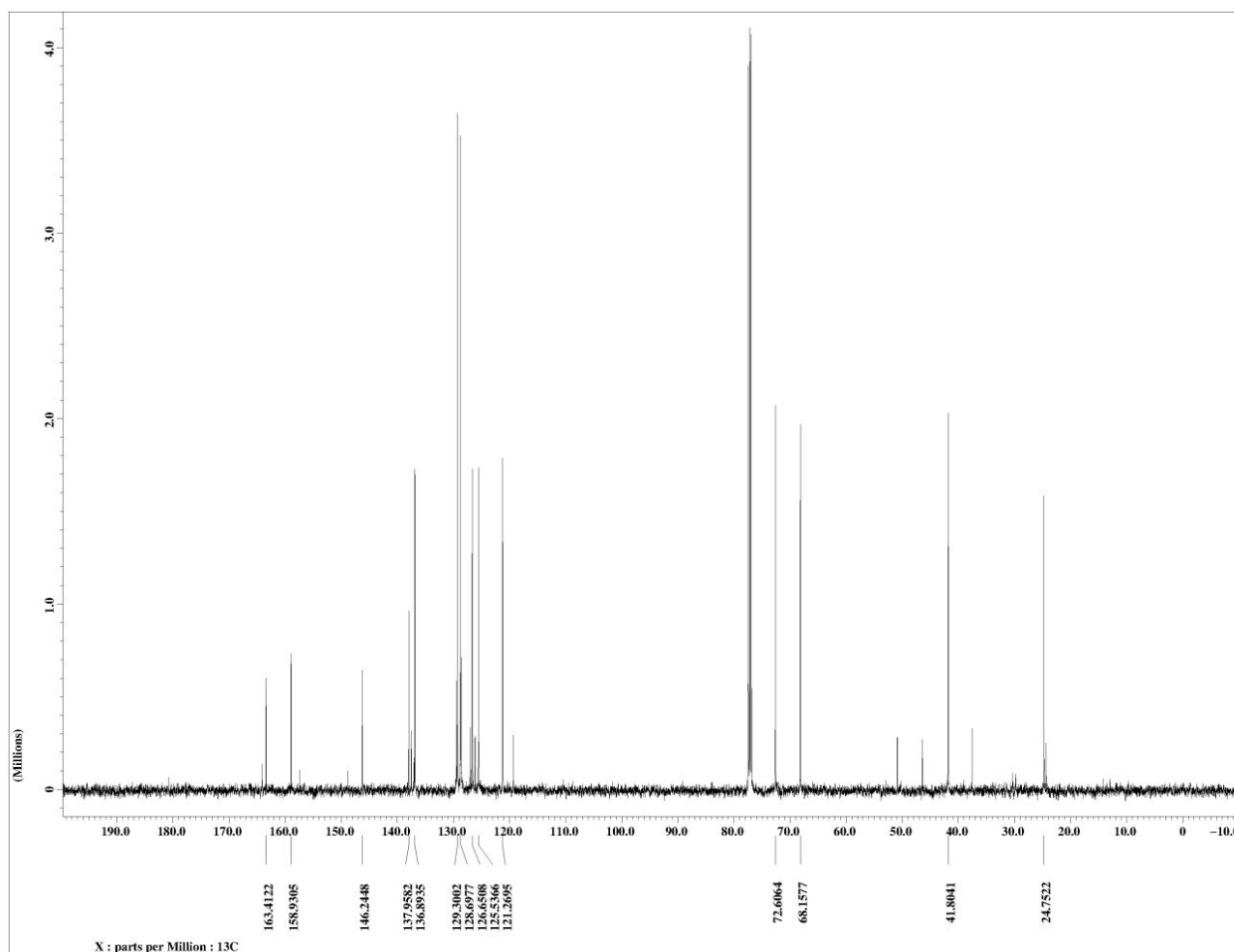
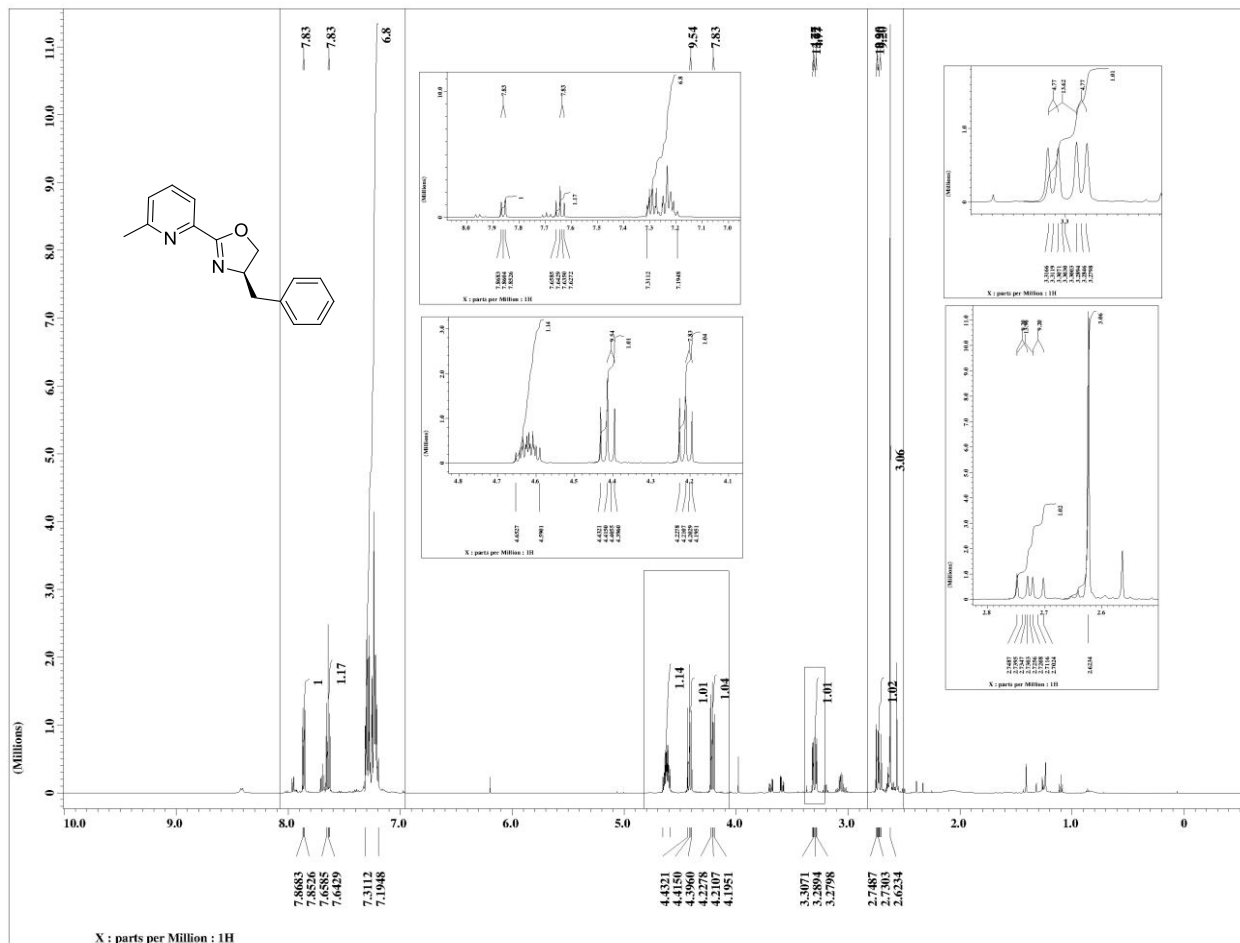
(S)-4-Butyl-2-(6-methylpyridin-2-yl)-oxazolin (19f)



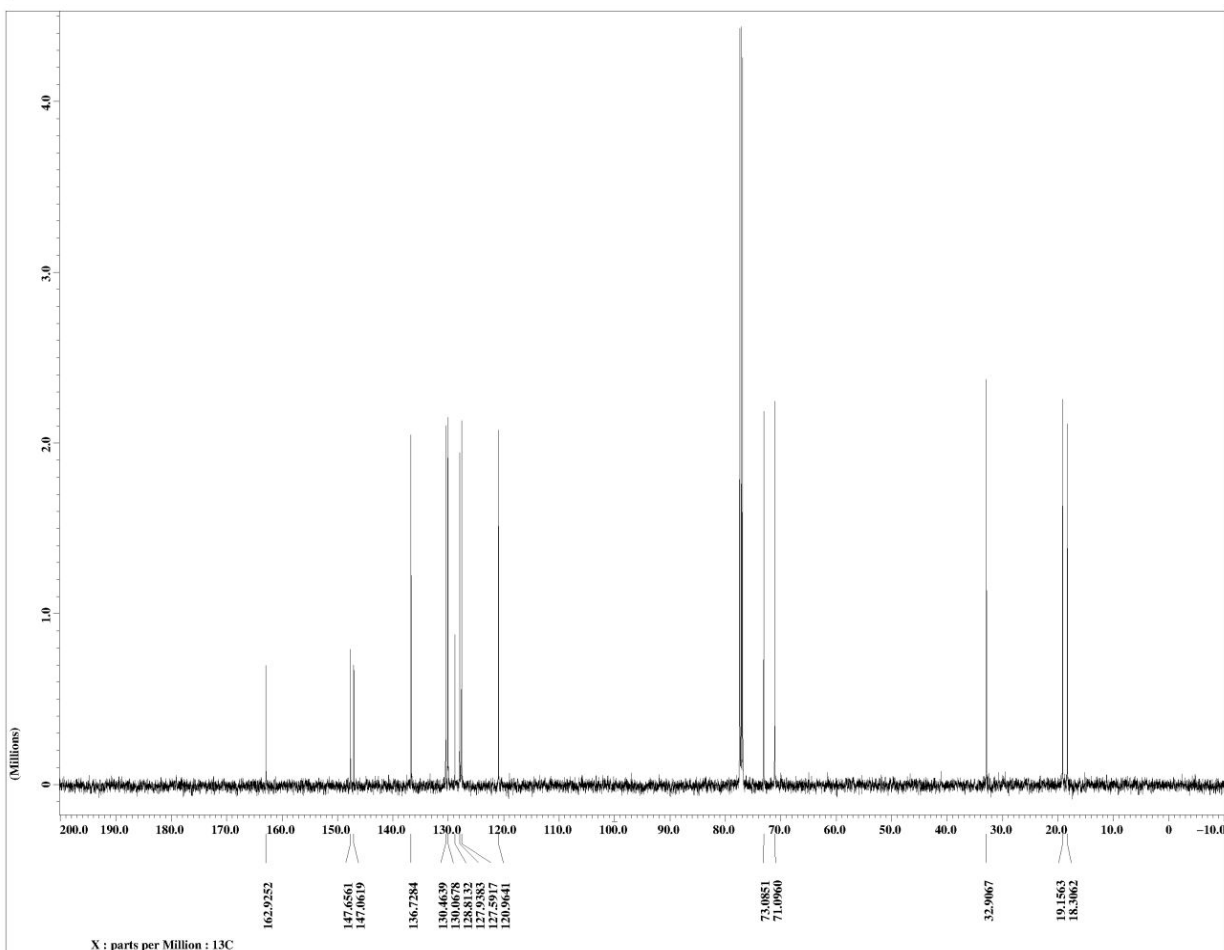
(R)-2-(6-Methylpyridin-2-yl)-oxazolin (19g)



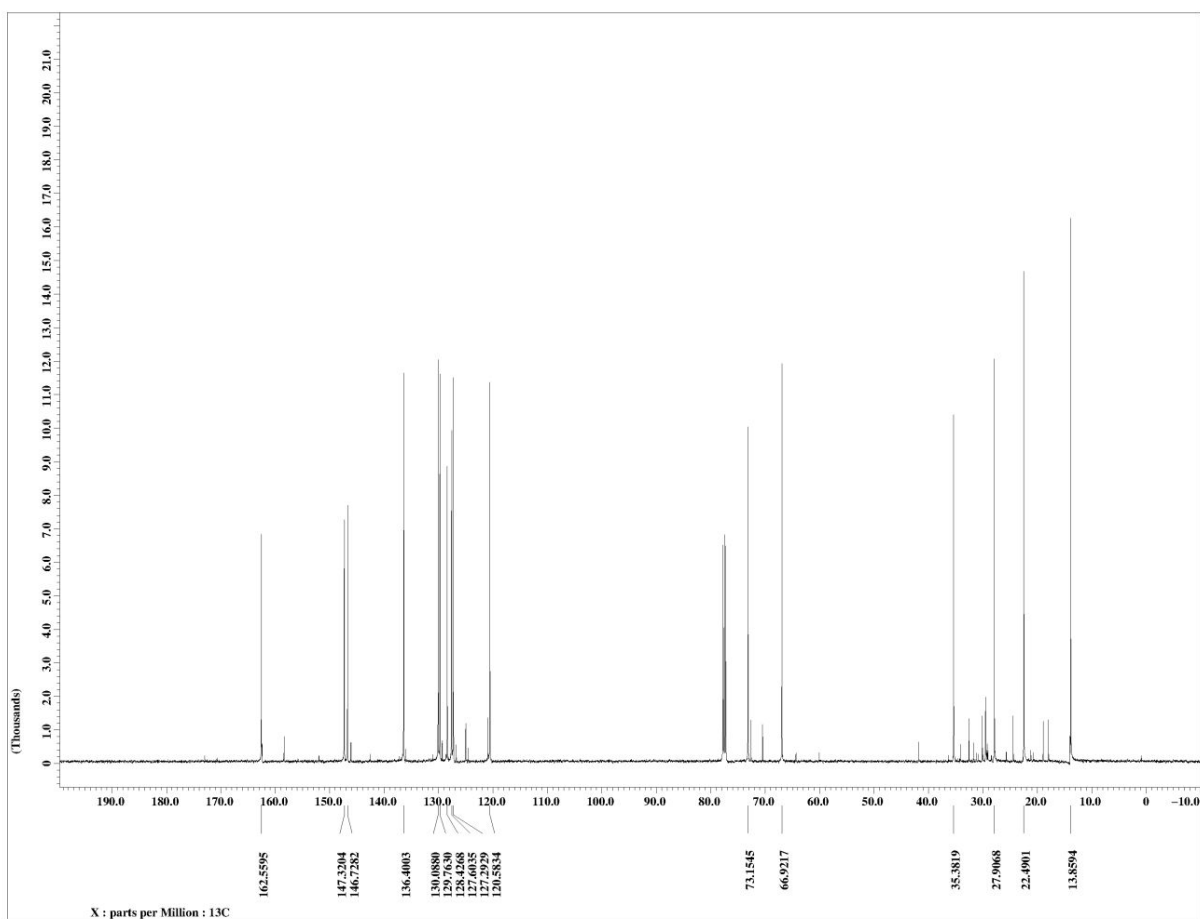
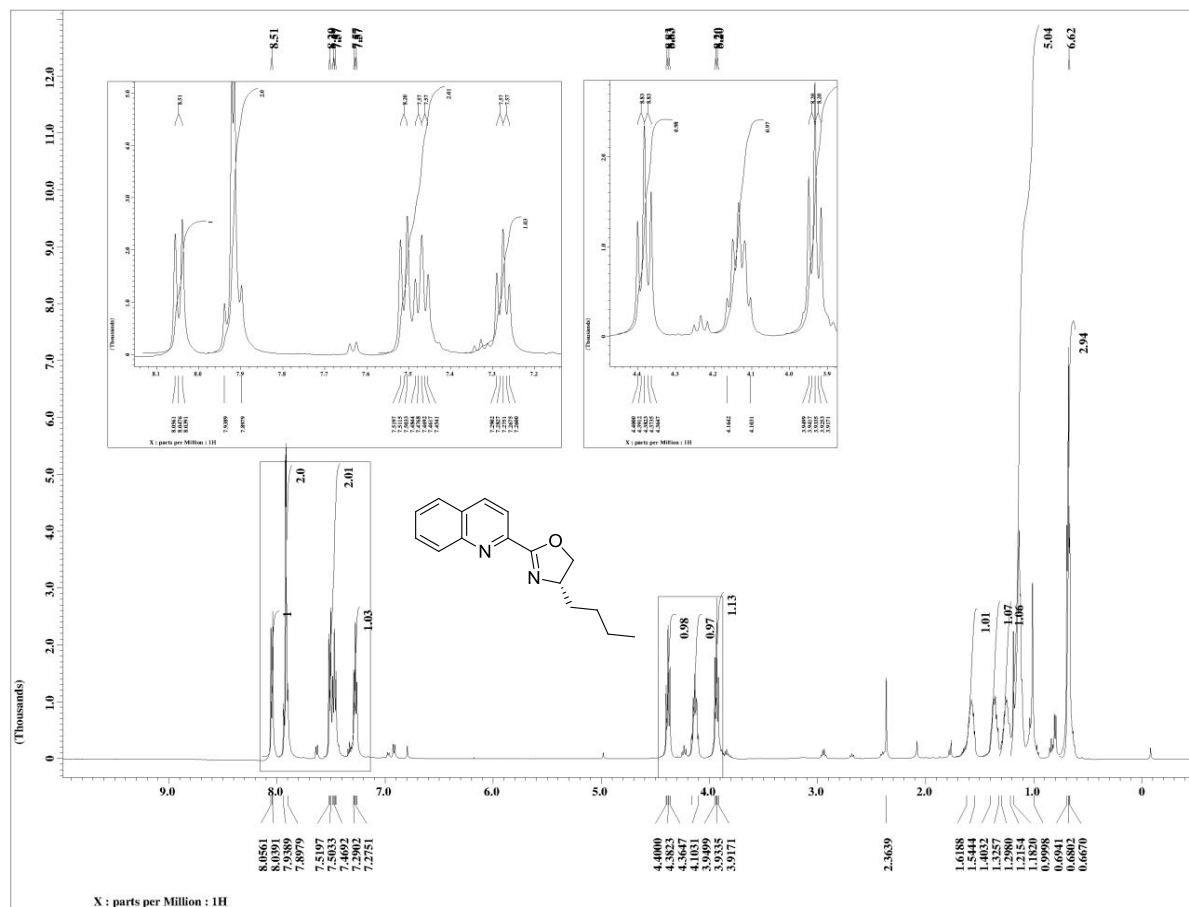
(R)-4-Benzyl-2-(6-methylpyridin-2-yl)-oxazolin (19h)



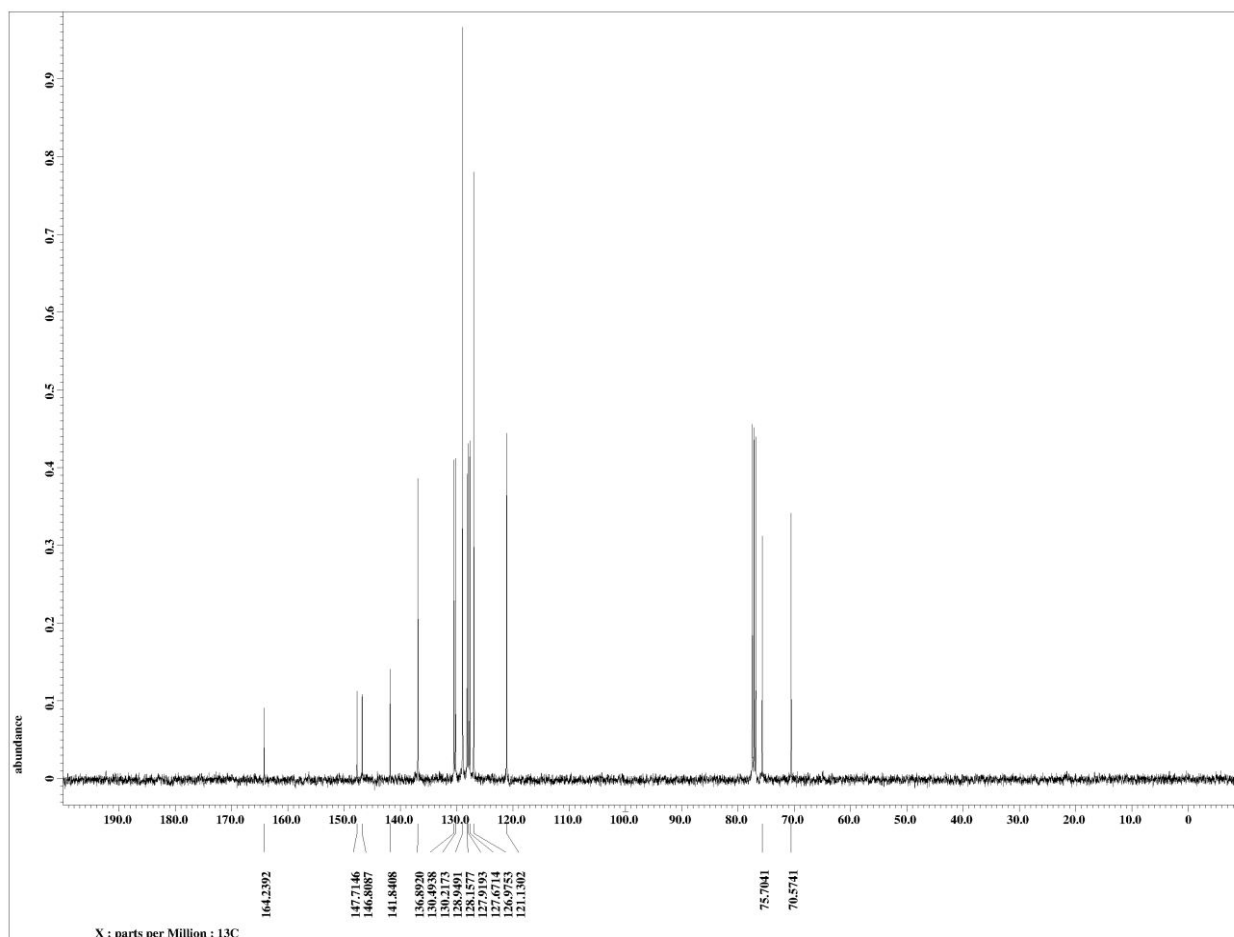
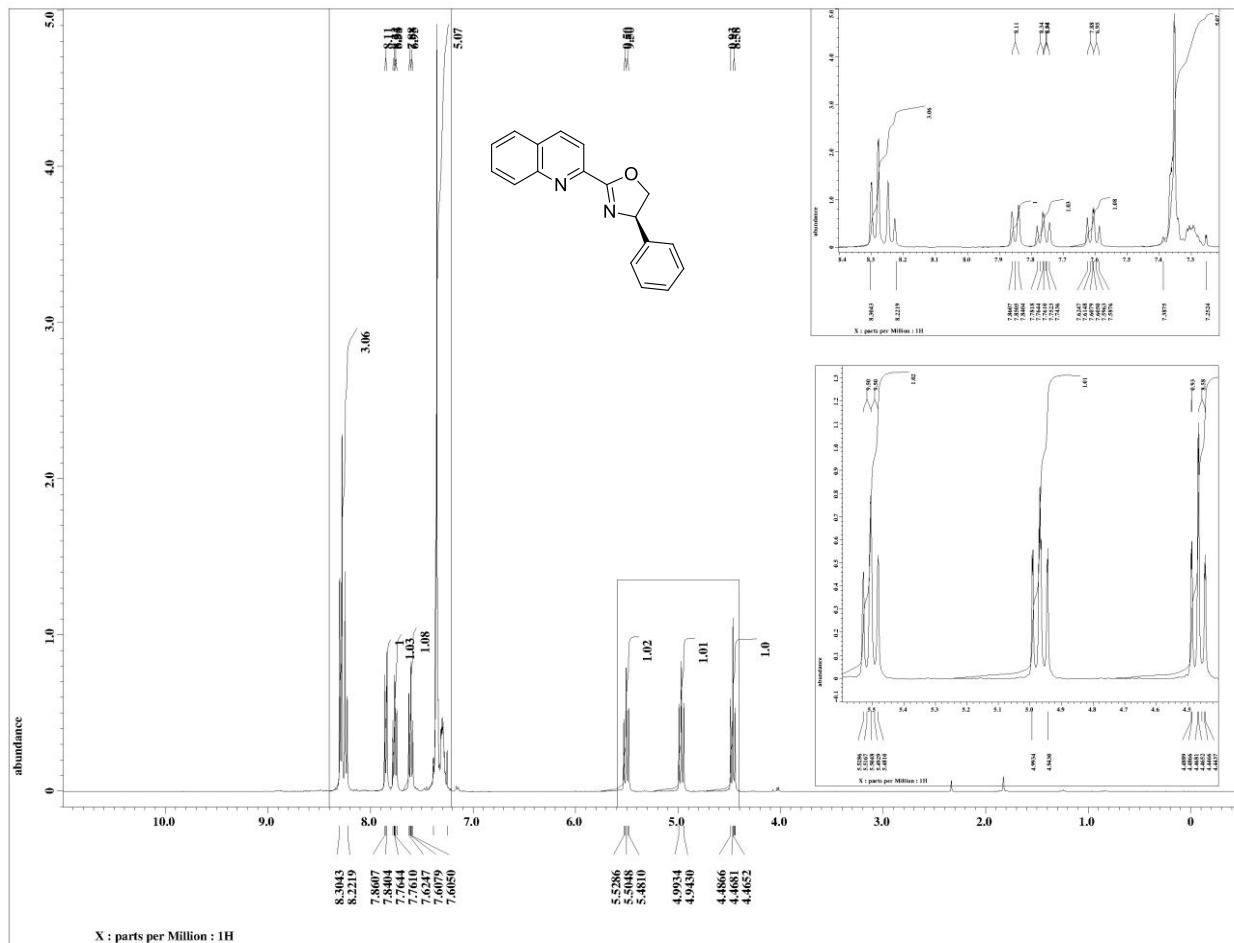
(S)-4-Isopropyl-2-(quinolin-2-yl)-oxazolin (20i)



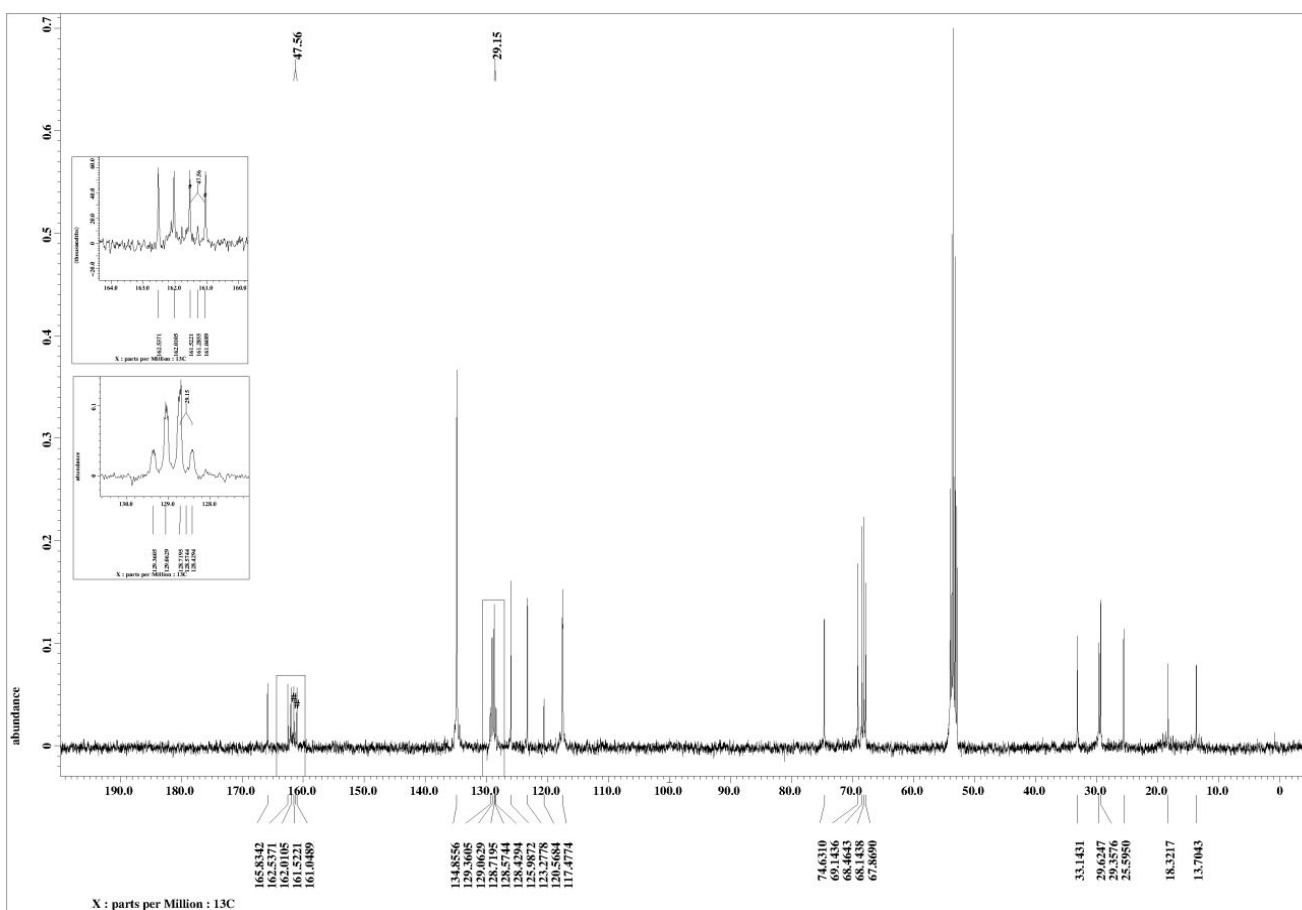
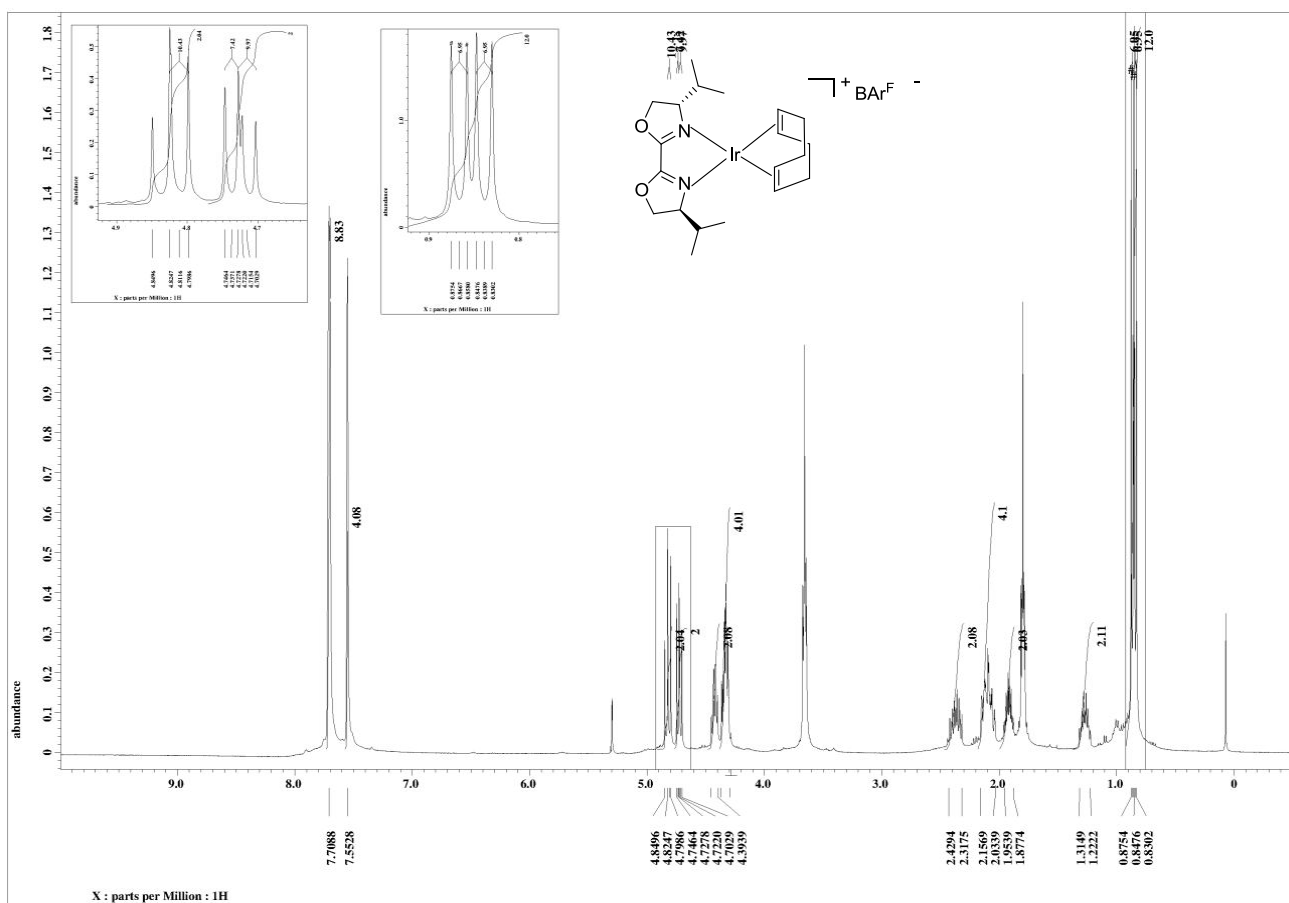
(S)-4-Butyl-2-(quinolin-2-yl)-oxazolin (20j)



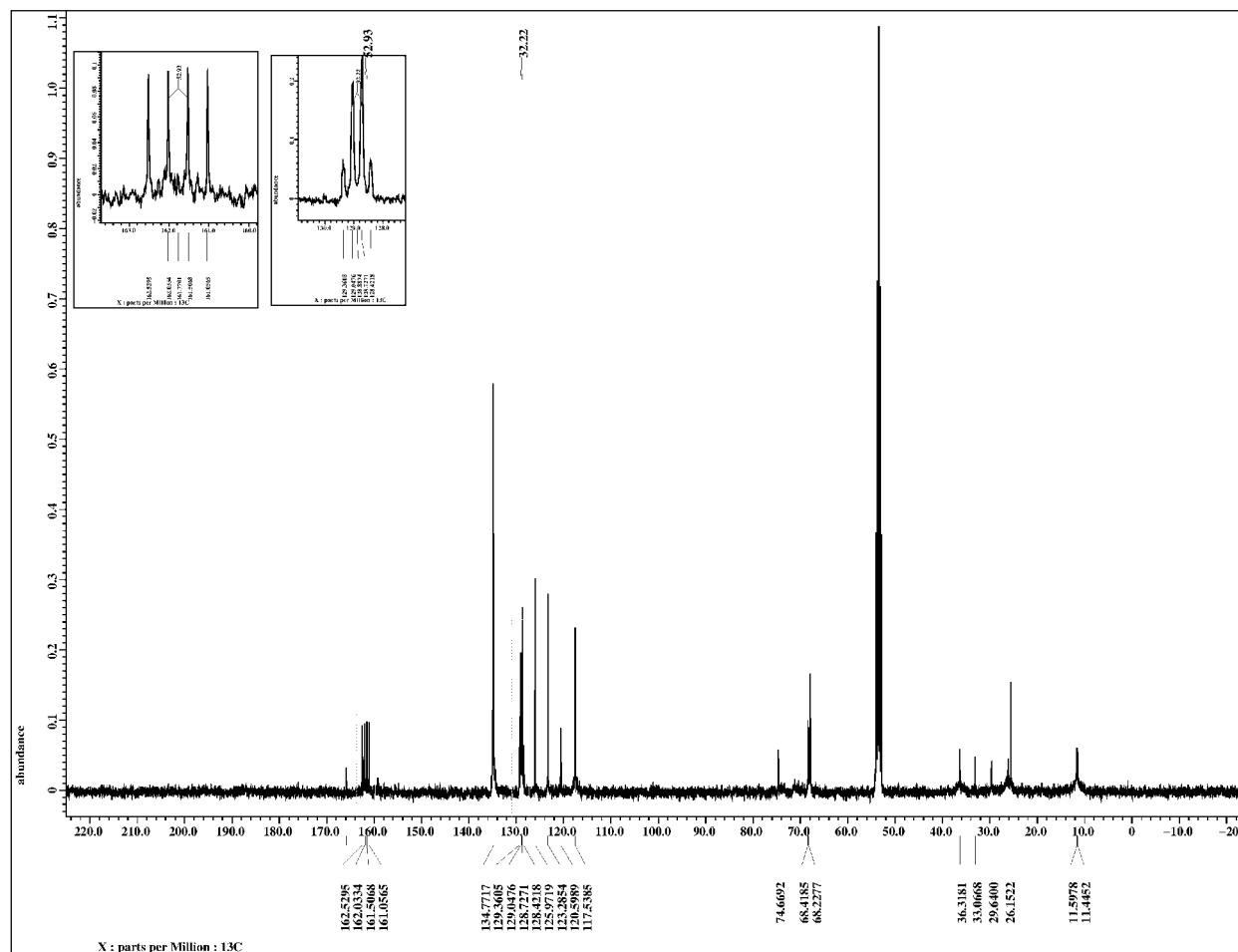
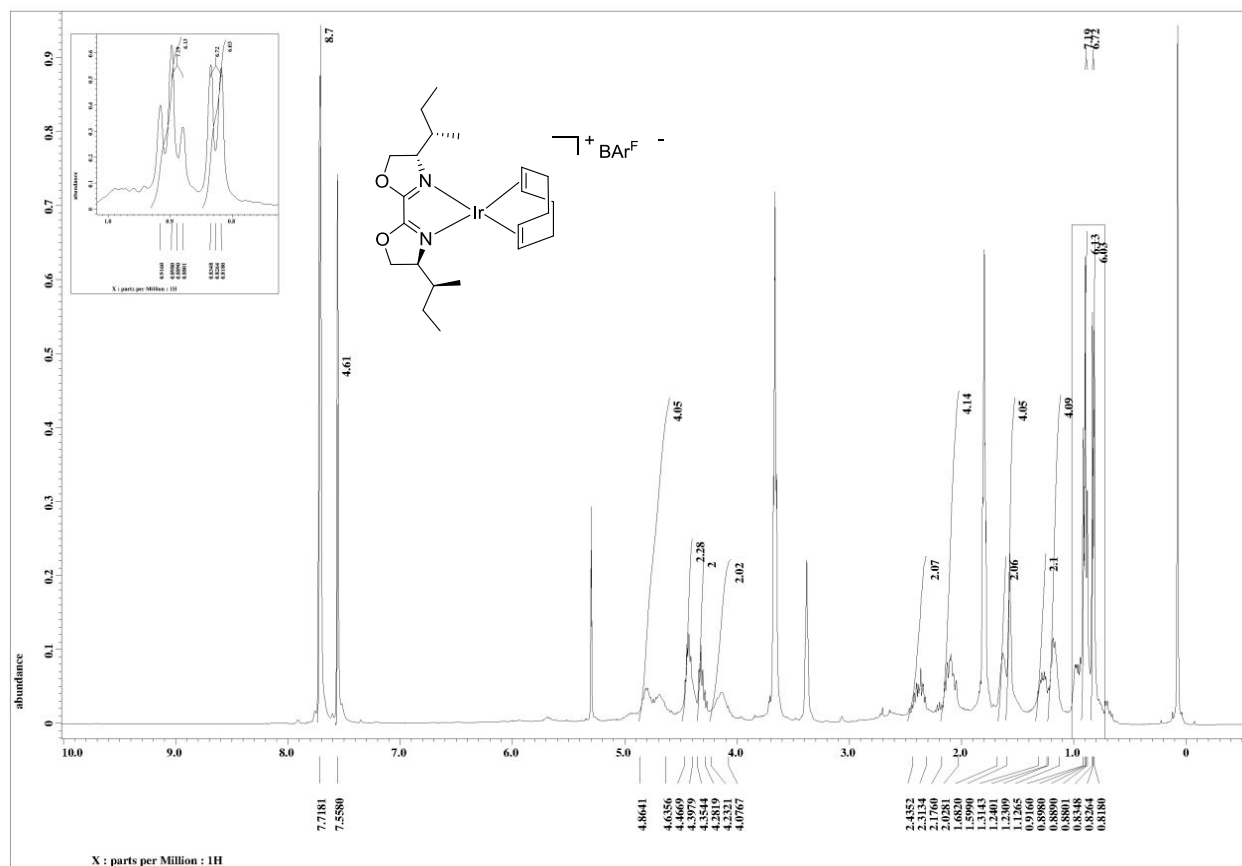
(R)-4-Phenyl-2-(quinolin-2-yl)-oxazolin (20k)



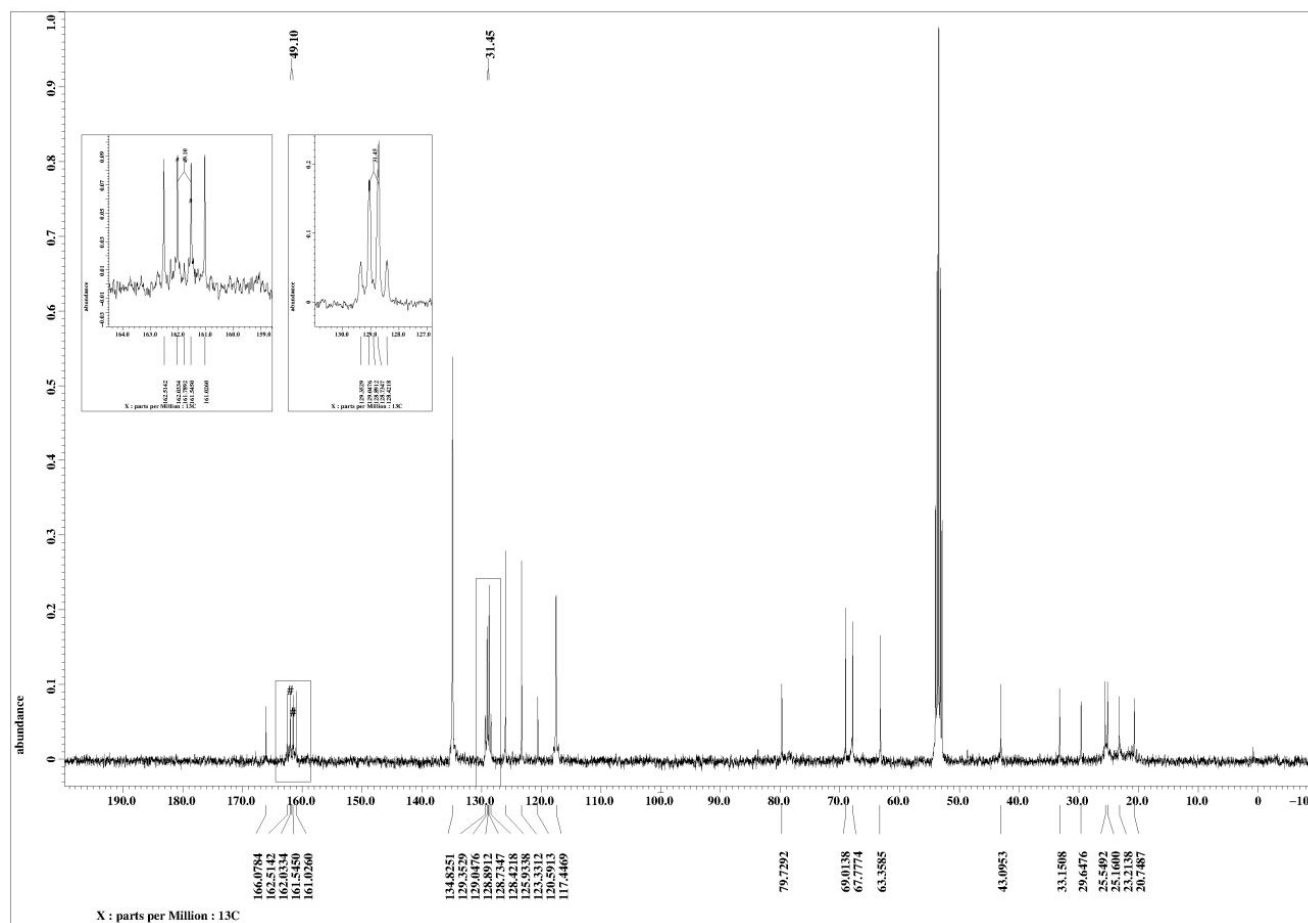
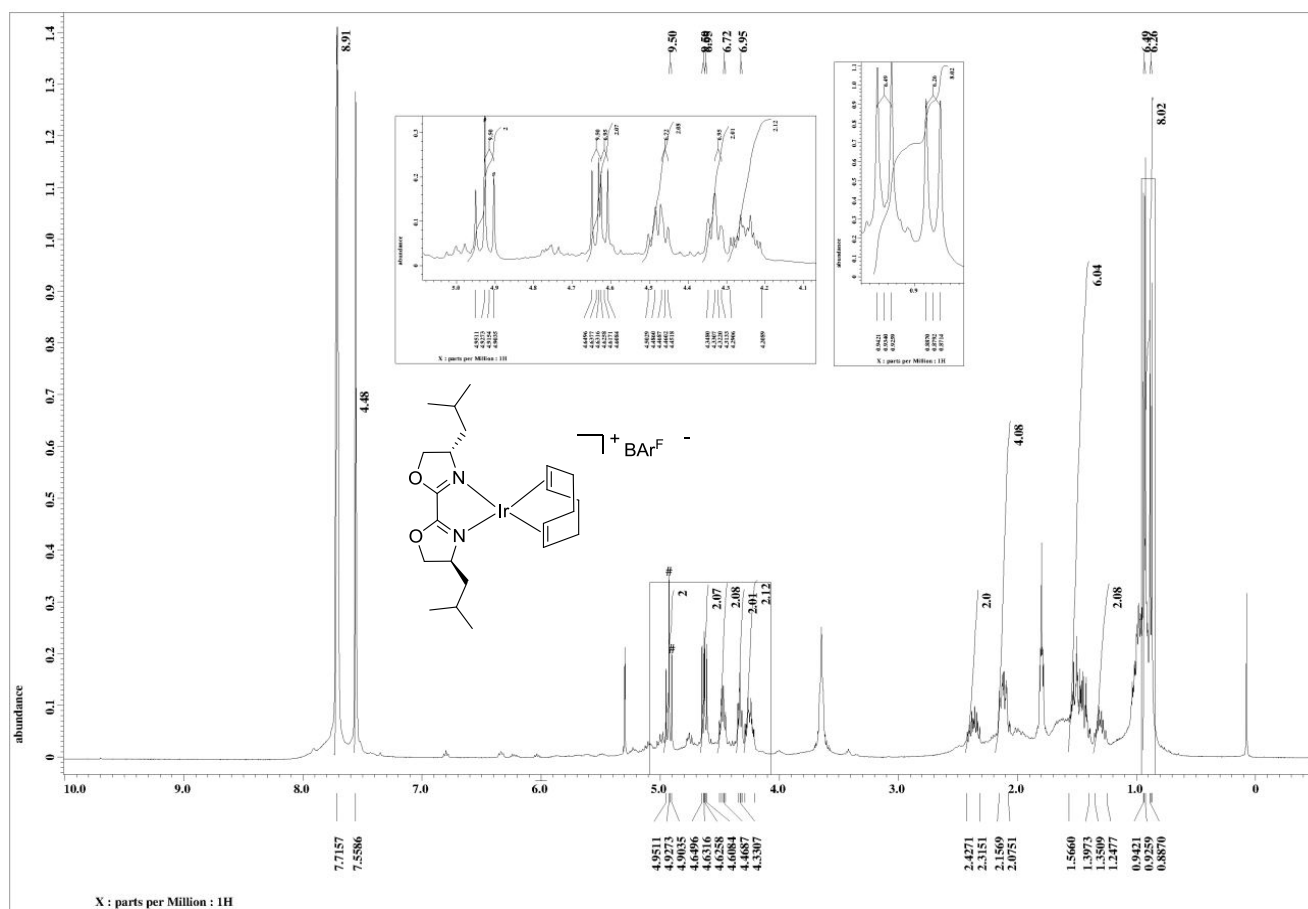
1,5-Cyclooctadiene[(2,2'-Bis((4*S*,4'*S*)-4,4'-diisopropyl)-oxazolin)]iridium(I) tetrakis[3,5-bis(trifluoromethyl)phenyl]borate (30b)



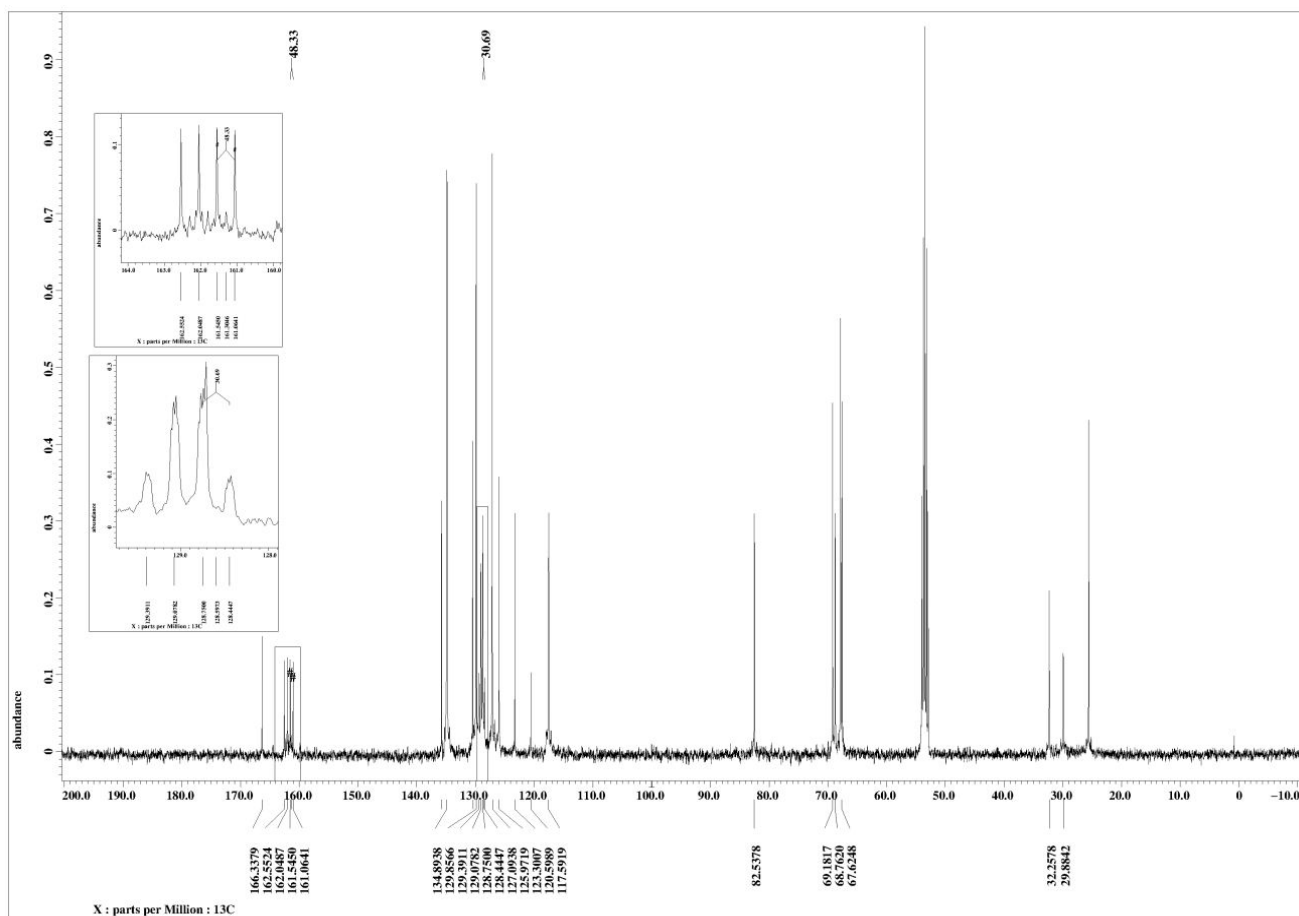
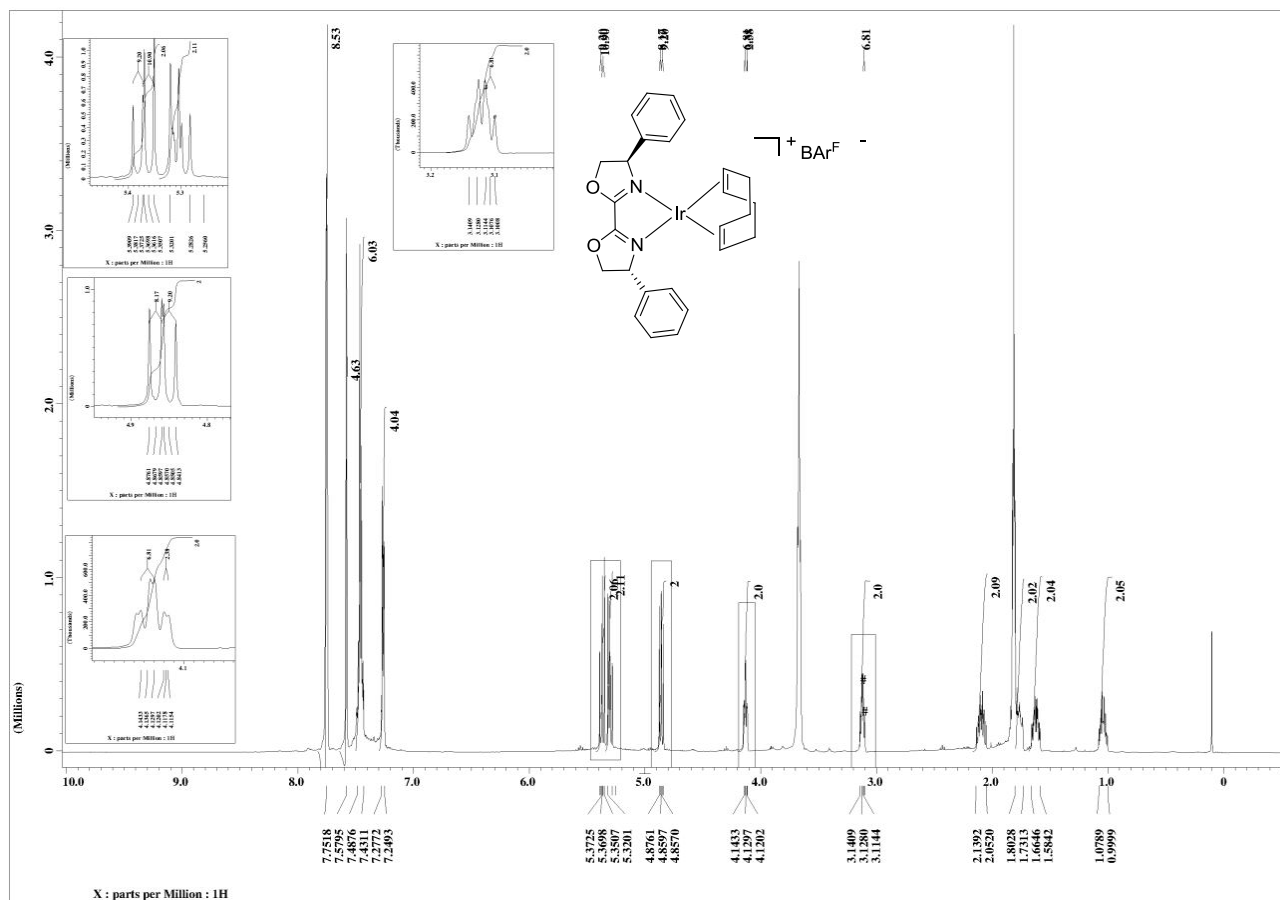
1,5-Cyclooctadiene[(2,2'-Bis((4*S*, 4'*S*)-4,4'-di((*S*)-sec-butyl)-oxazolin)]iridium(I) tetrakis[3,5-bis(trifluoromethyl)phenyl]borate(30f)



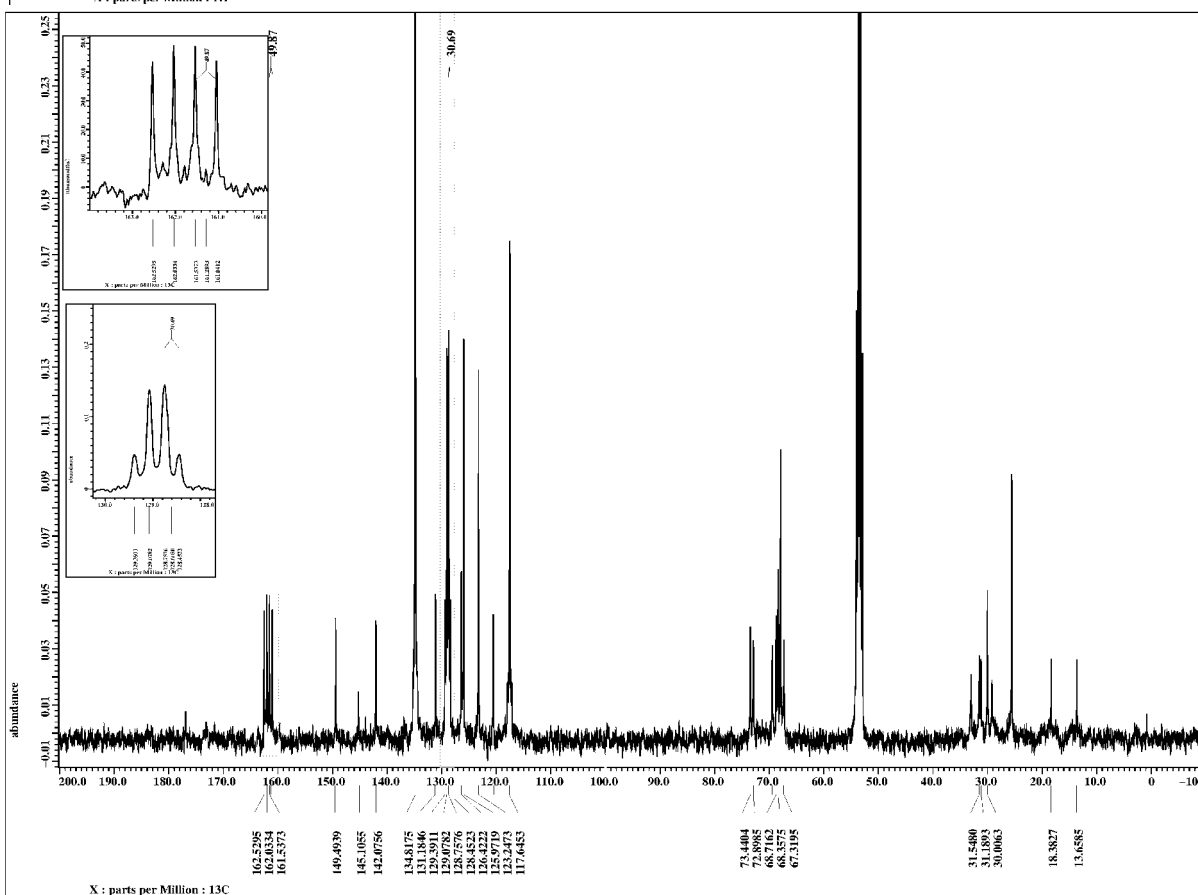
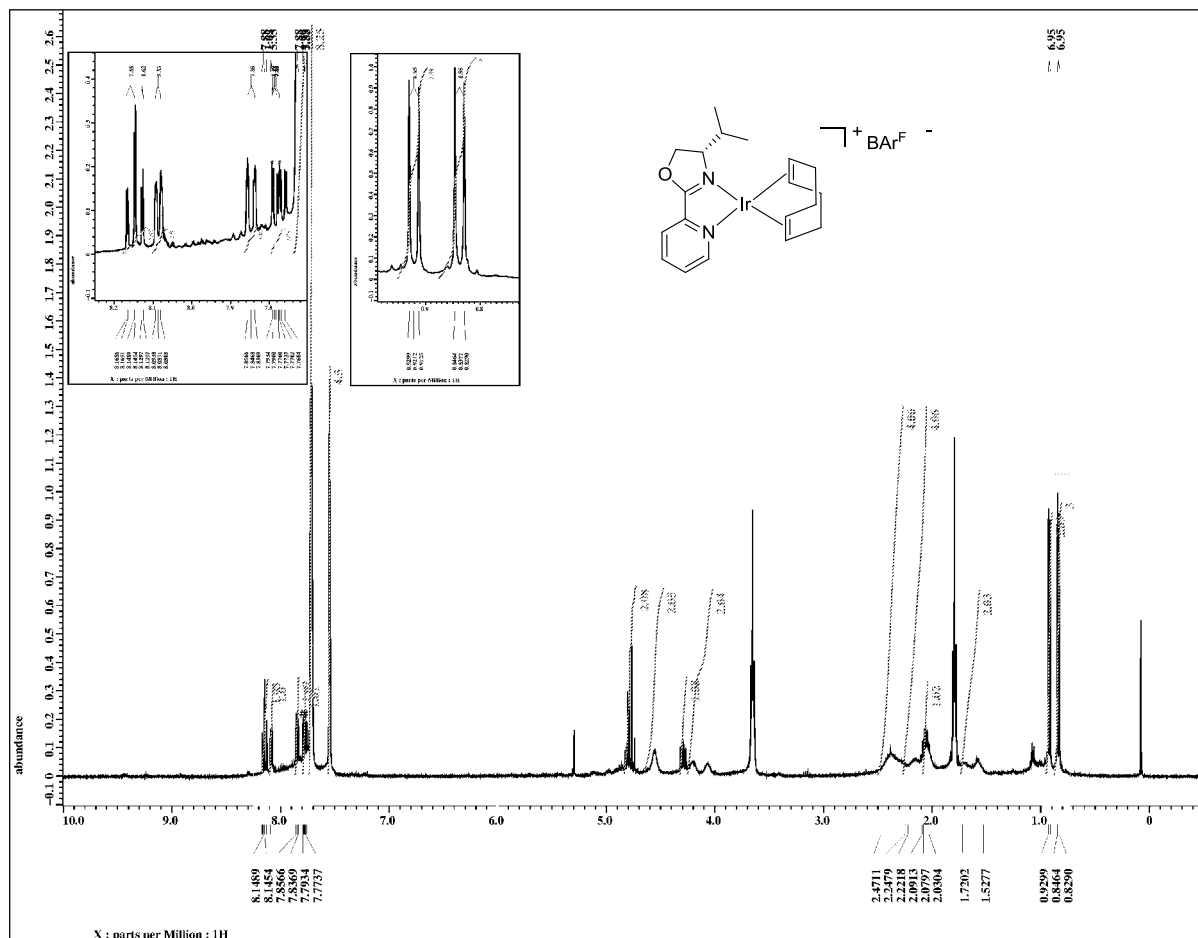
1,5-Cyclooctadiene[(2,2'-Bis((4*S*, 4'*S*)-4,4'-diisobutyl)-oxazolin)]iridium(I) tetrakis[3,5-bis(trifluoromethyl)phenyl]borate (2)



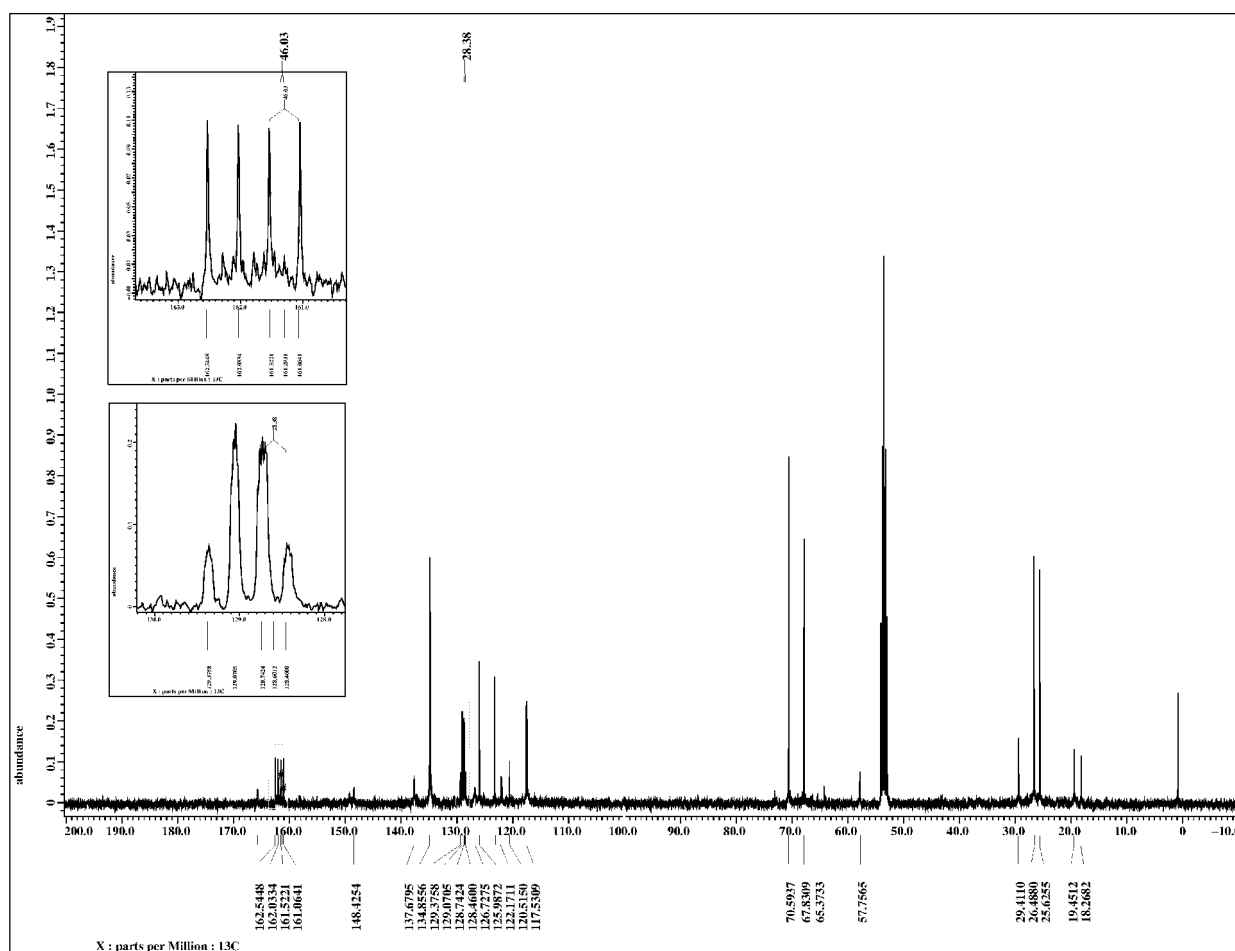
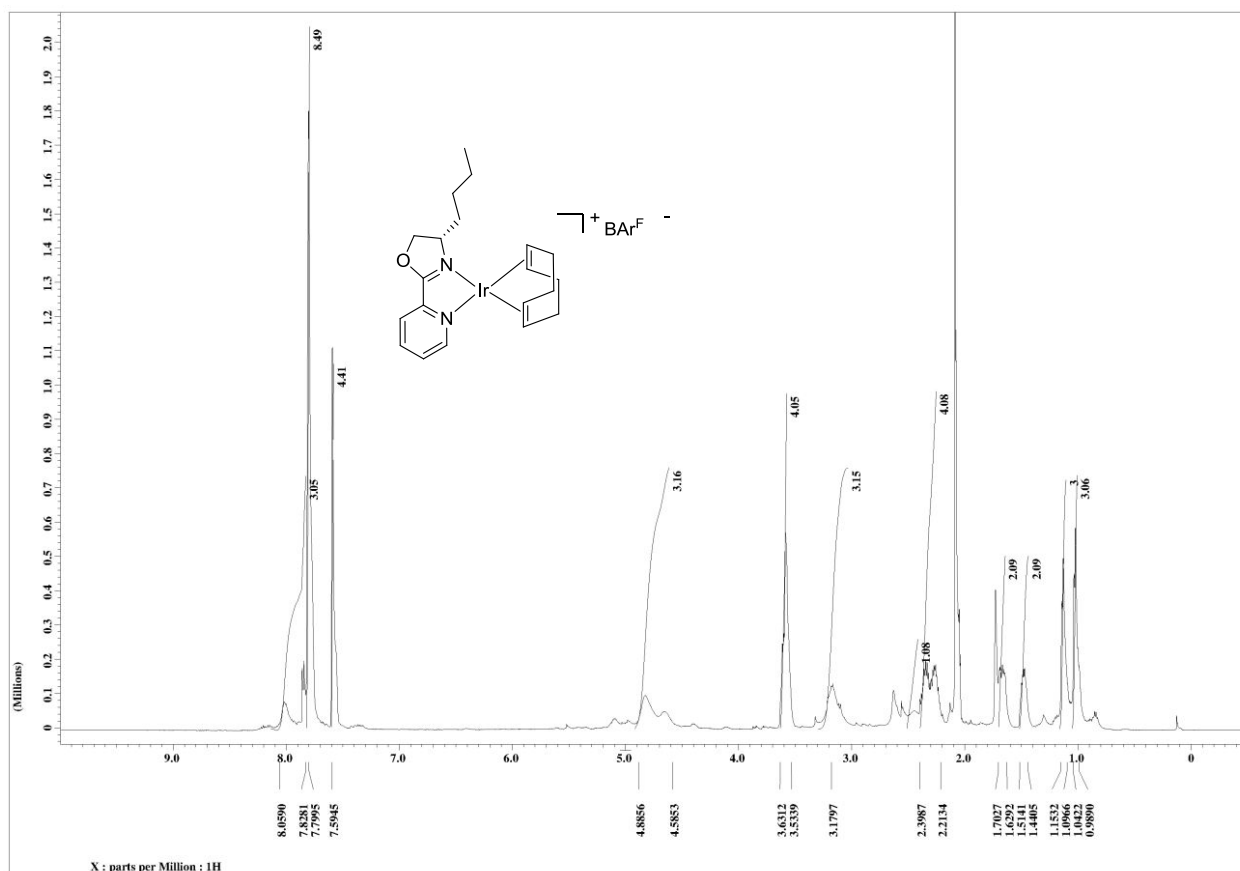
1,5-Cyclooctadiene[(2,2'-Bis((4*R*, 4'*R*)-4,4'-diphenyl)-oxazolin)]iridium(I) tetrakis[3,5-bis(trifluoromethyl)phenyl]borate (xx)



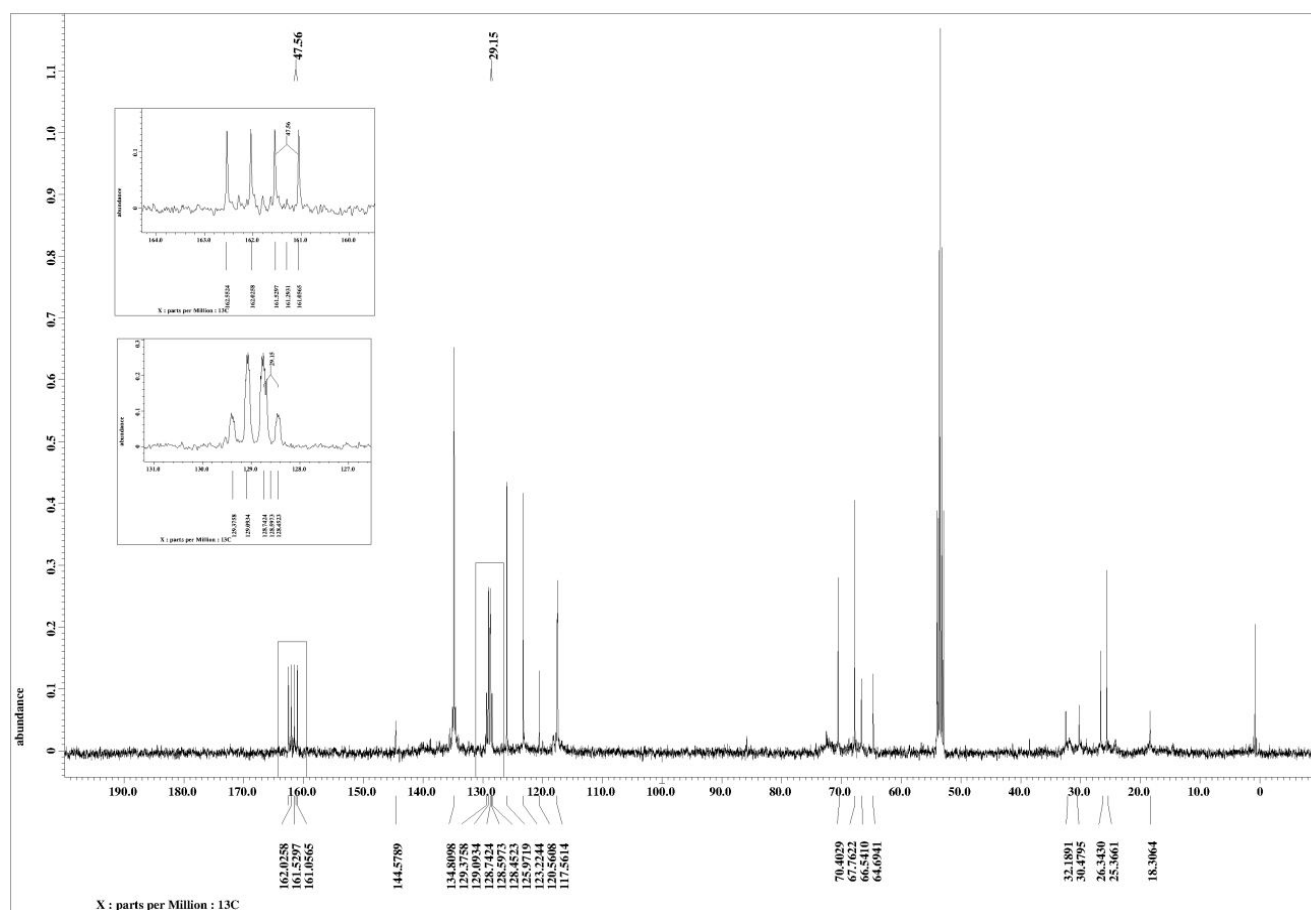
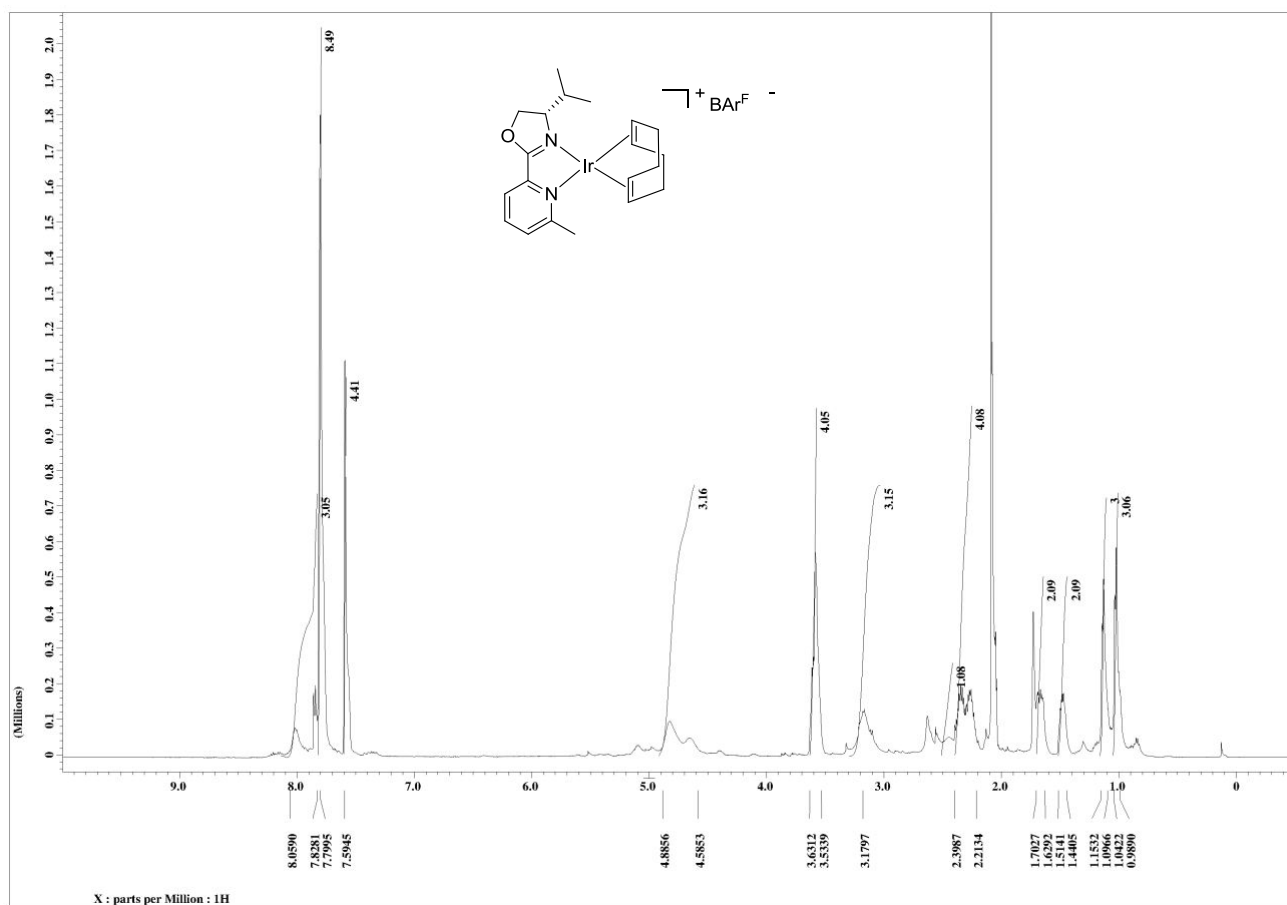
1,5-Cyclooctadiene[*((S)*-4-Isopropyl-2-(pyridine-2-yl)-oxazolin)]iridium(I) tetrakis[3,5-bis(trifluoromethyl)phenyl]borate (30i)



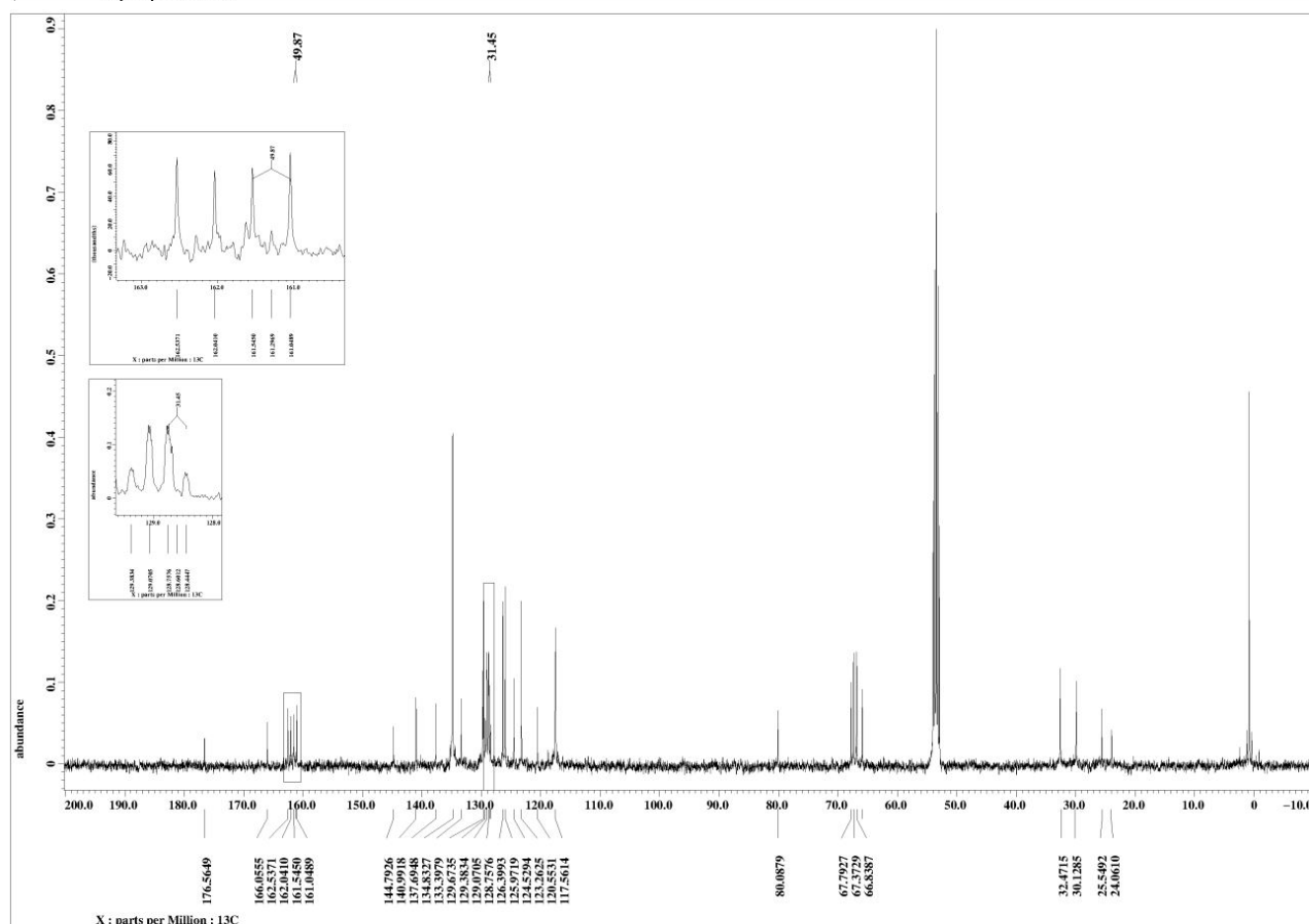
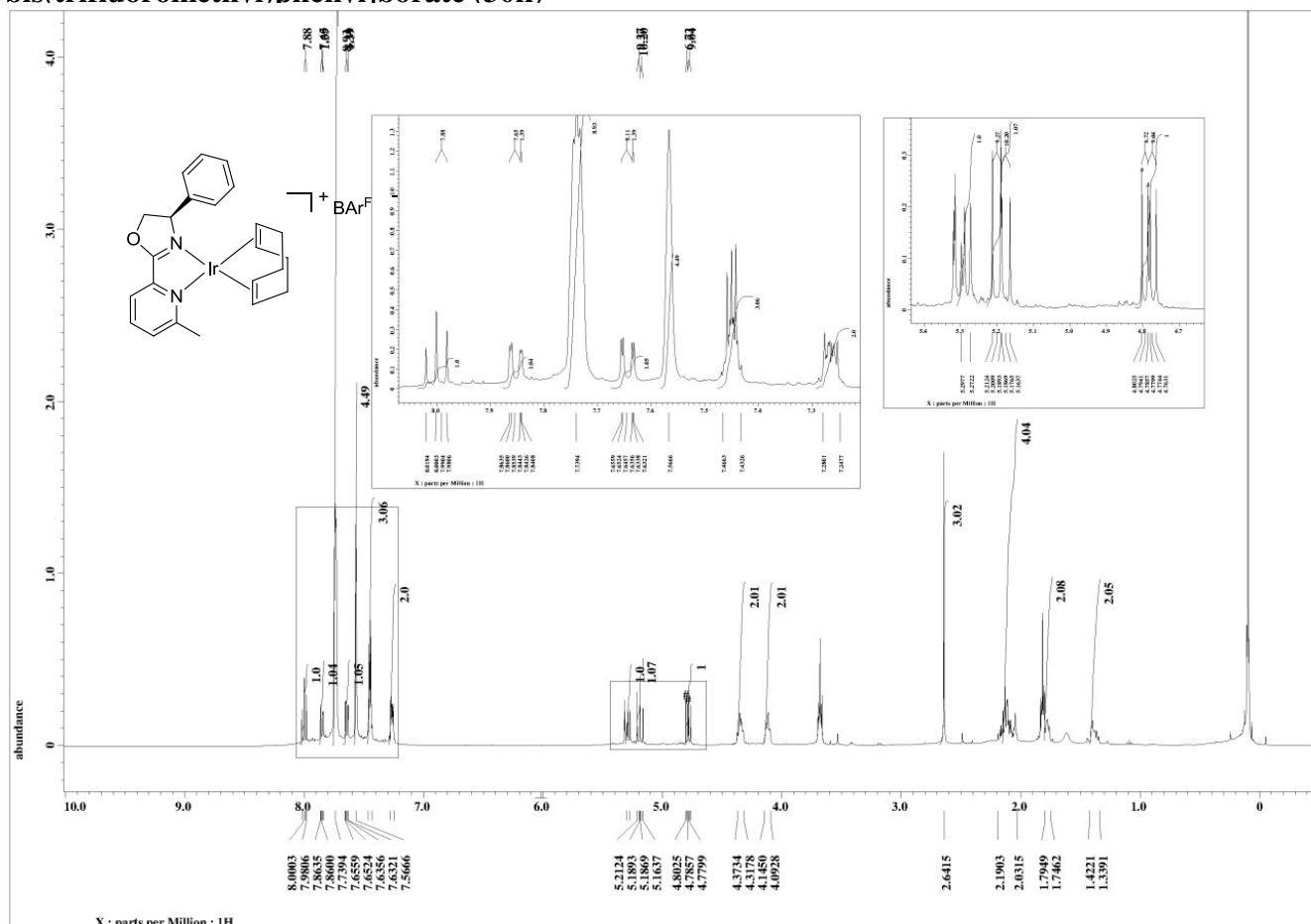
1,5-Cyclooctadiene[[(S)-4-Butyl-2-(pyridine-2-yl)-oxazolin]iridium(I) tetrakis[3,5-bis(trifluoromethyl)phenyl]borate (30j)



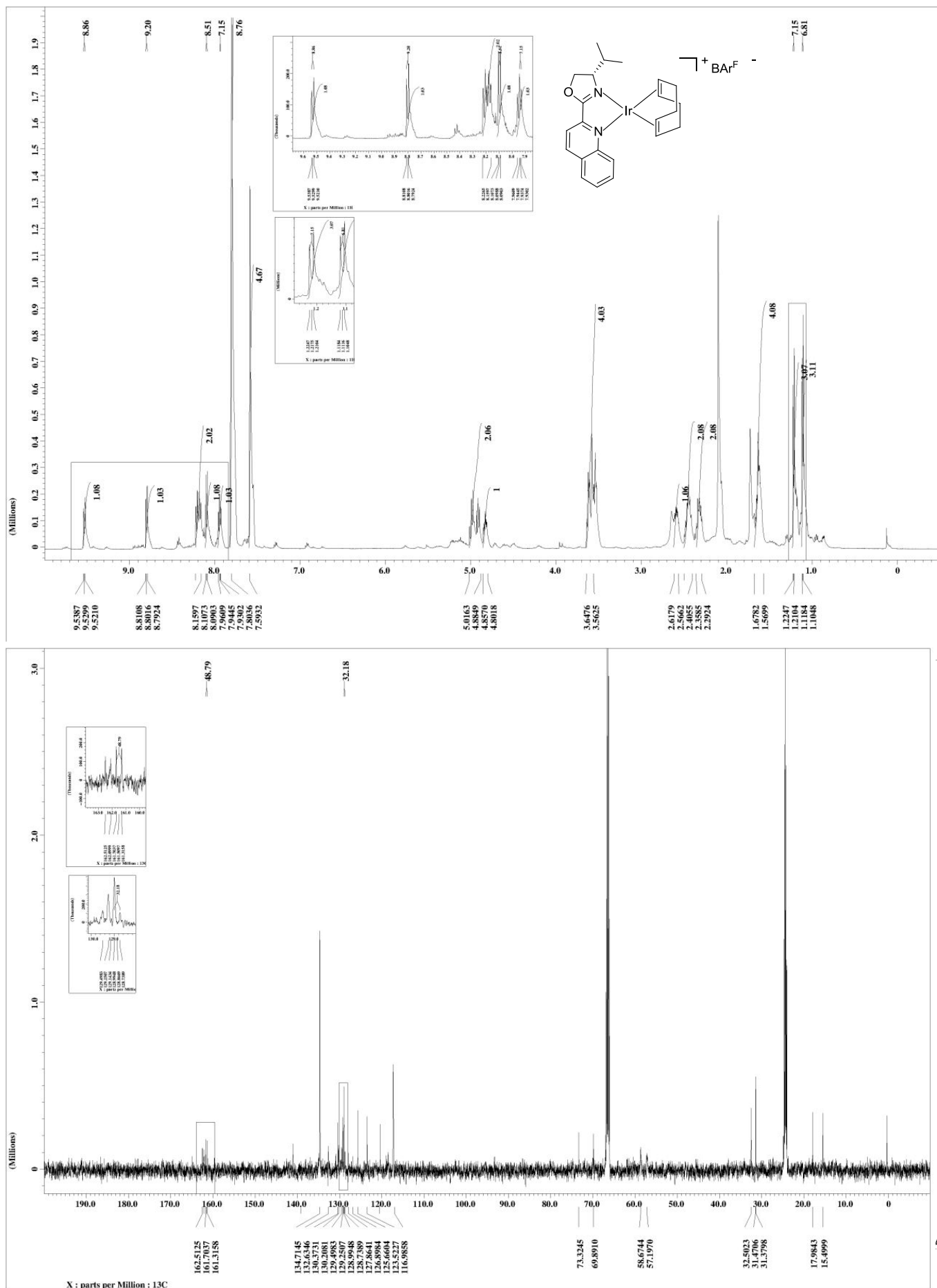
1,5-Cyclooctadiene[(*S*)-4-Isopropyl-2-(6-methylpyridin-2-yl)-oxazolin]iridium(I) tetrakis[3,5-bis(trifluoromethyl)phenyl]borate (30e)



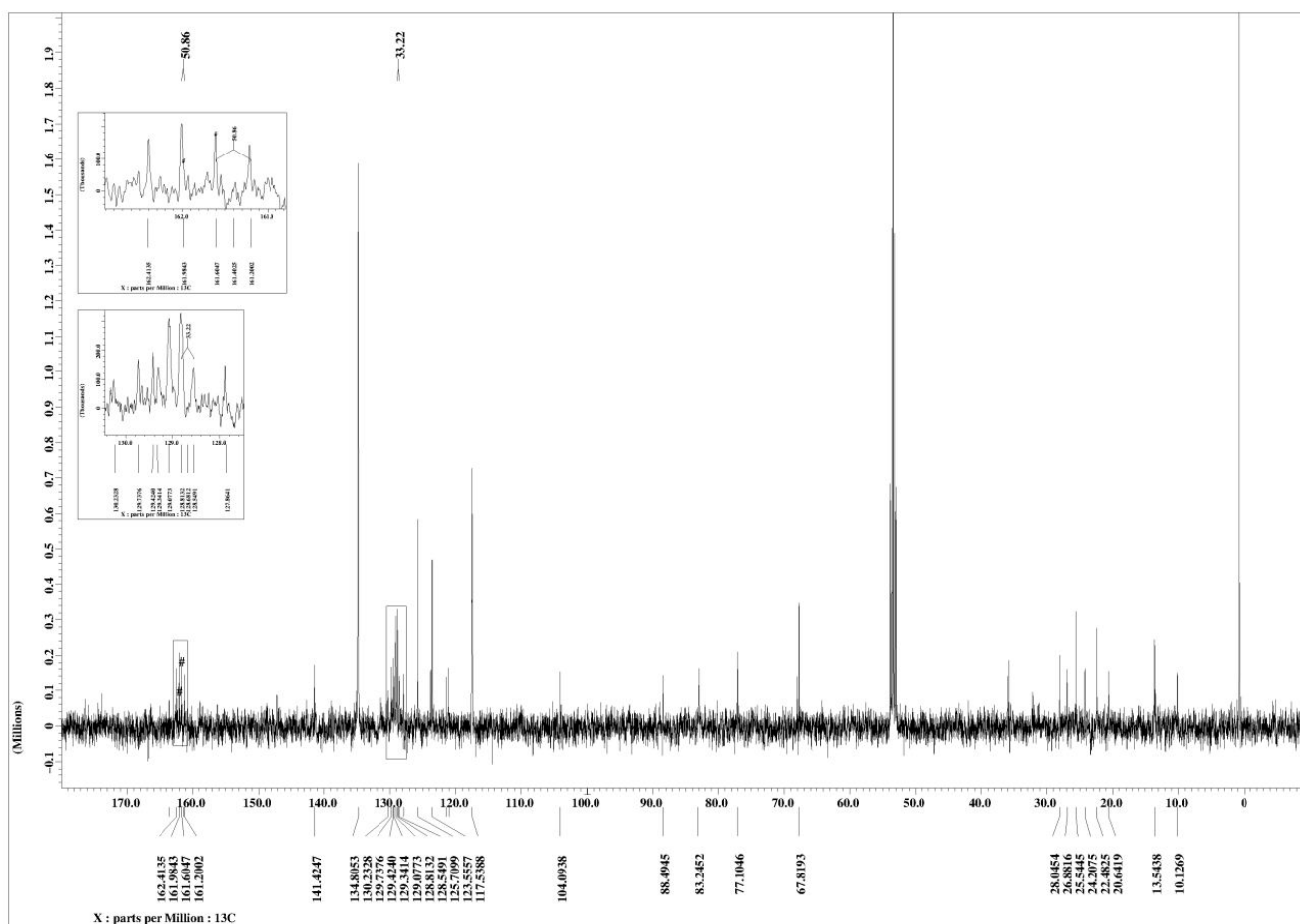
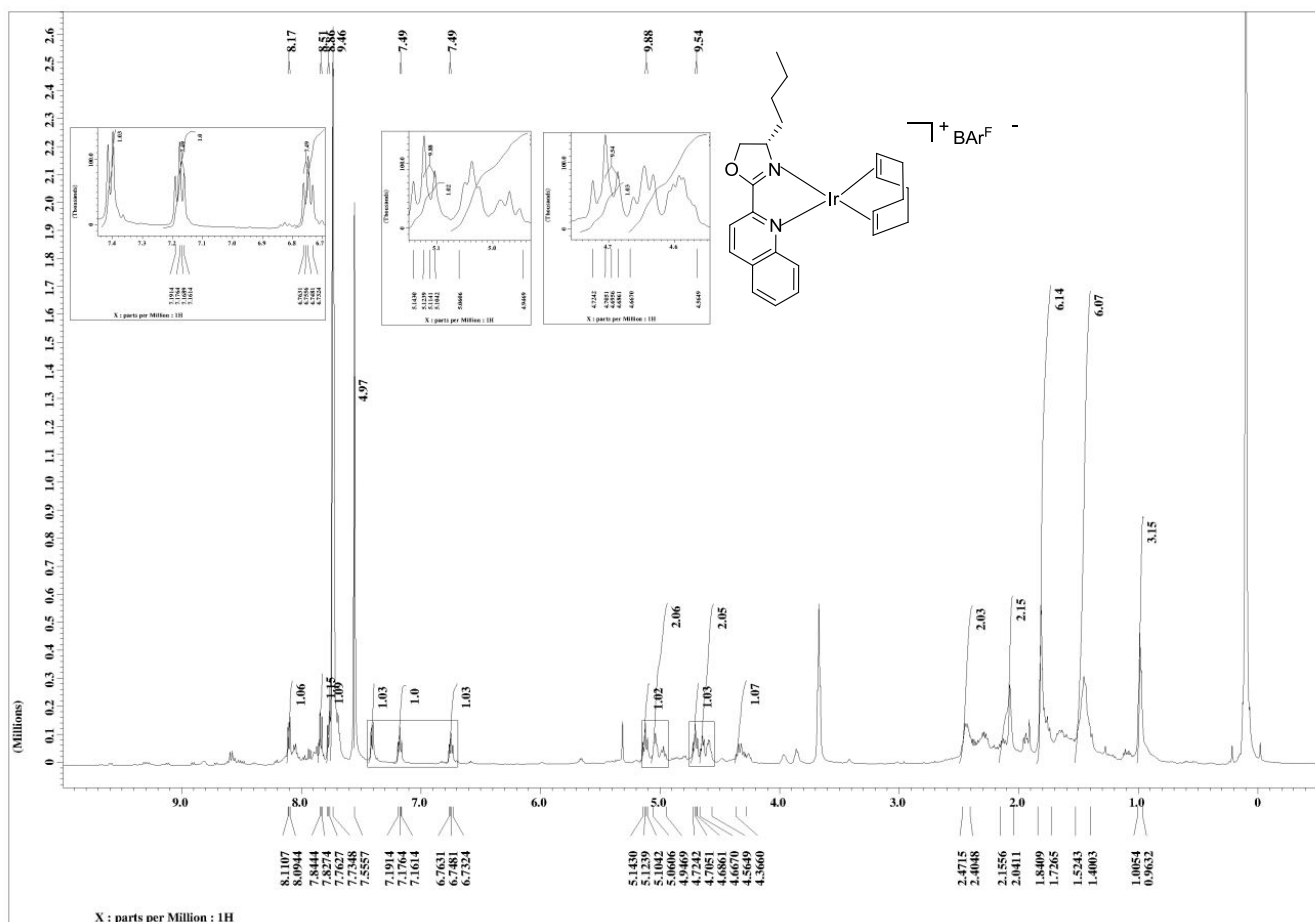
1,5-Cyclooctadiene[*(R)*-2-(6-Methylpyridin-2-yl)-oxazolin]iridium(I) tetrakis[3,5-bis(trifluoromethyl)phenyl]borate (30k)



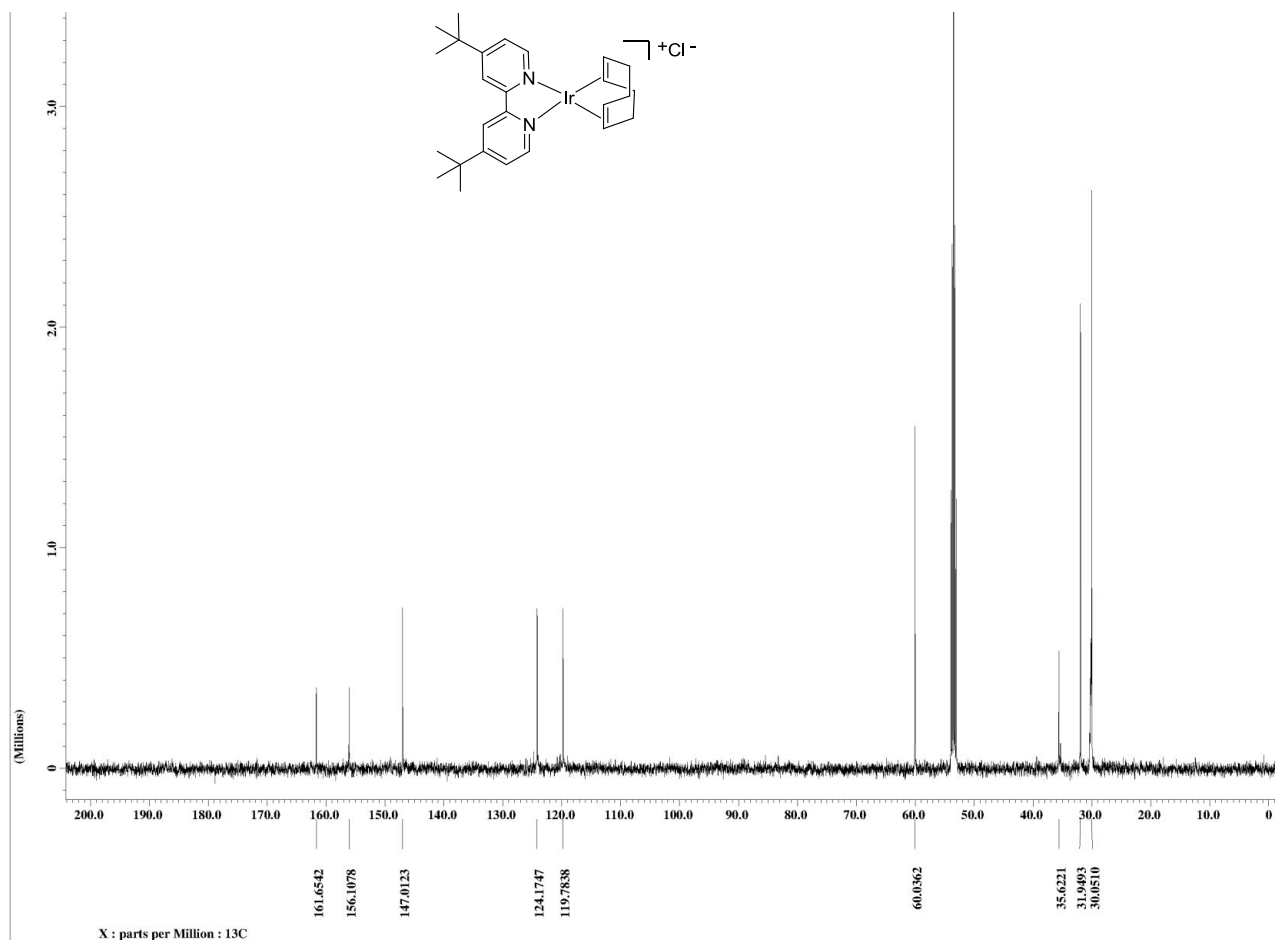
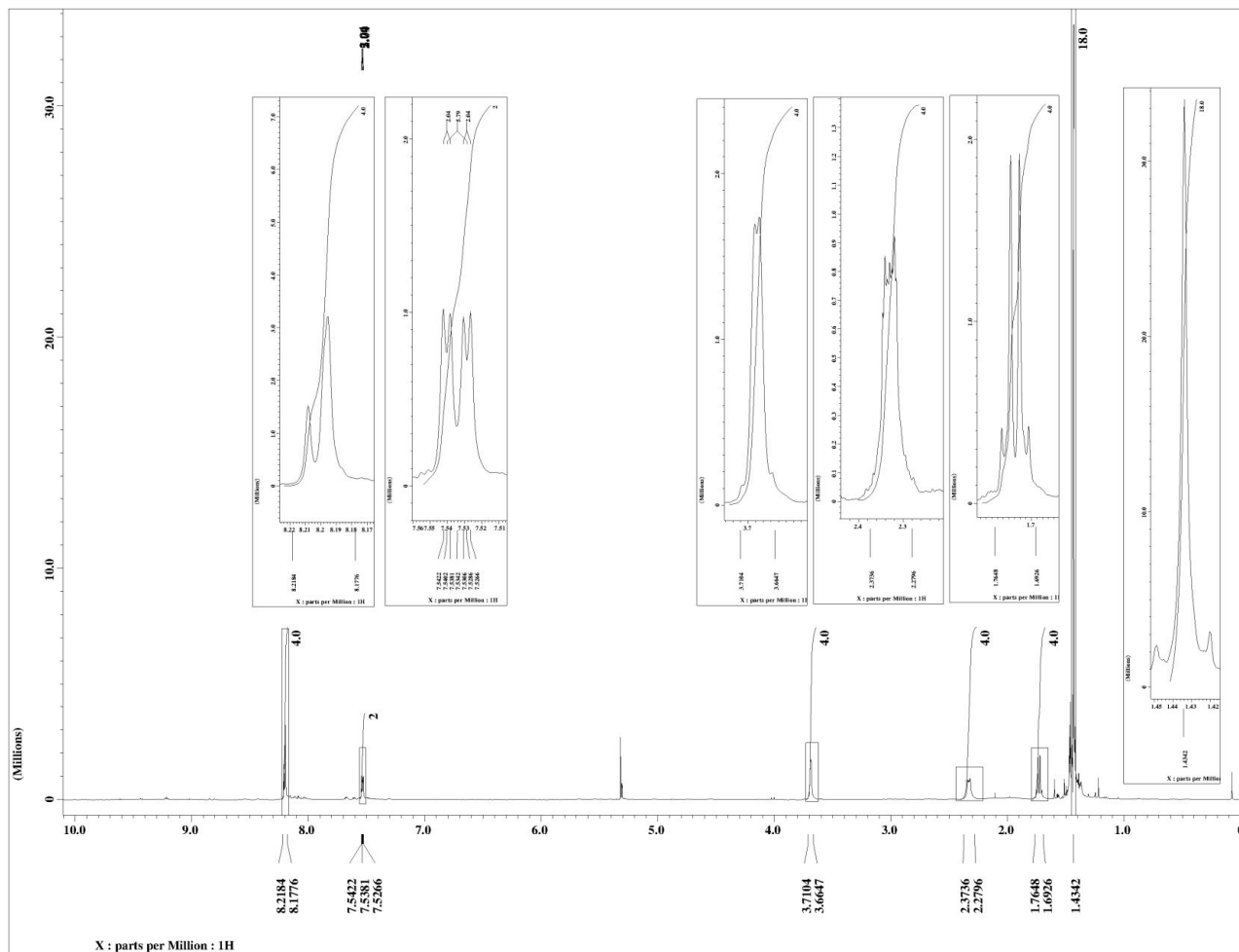
1,5-Cyclooctadiene[(*S*)-4-Isopropyl-2-(quinolin-2-yl)-oxazolin]iridium(I) tetrakis[3,5-bis(trifluoromethyl)phenyl]borate (30d)



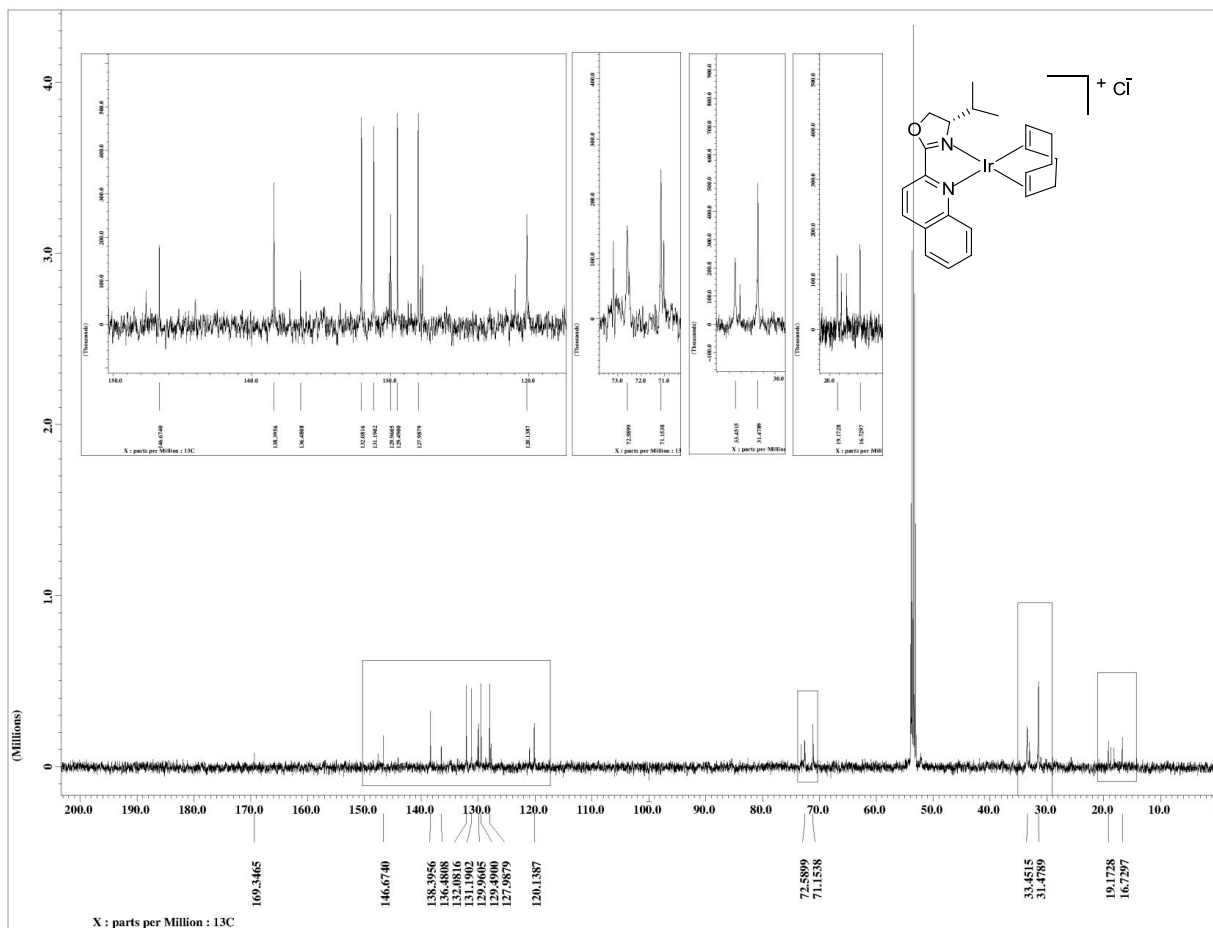
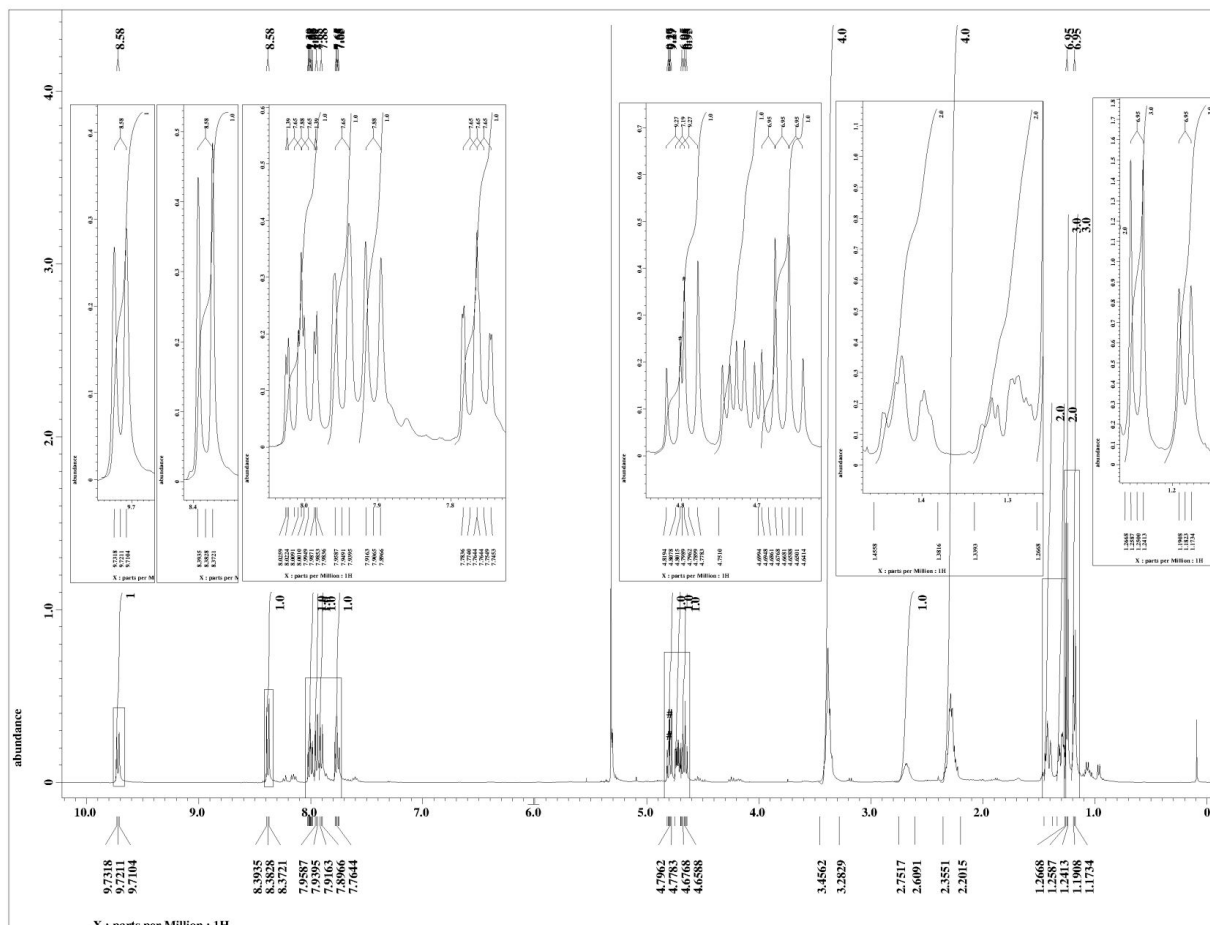
1,5-Cyclooctadiene[[(S)-4-Butyl-2-(quinolin-2-yl)-oxazolin]iridium(I) tetrakis[3,5-bis(trifluoromethyl)phenyl]borate (30)



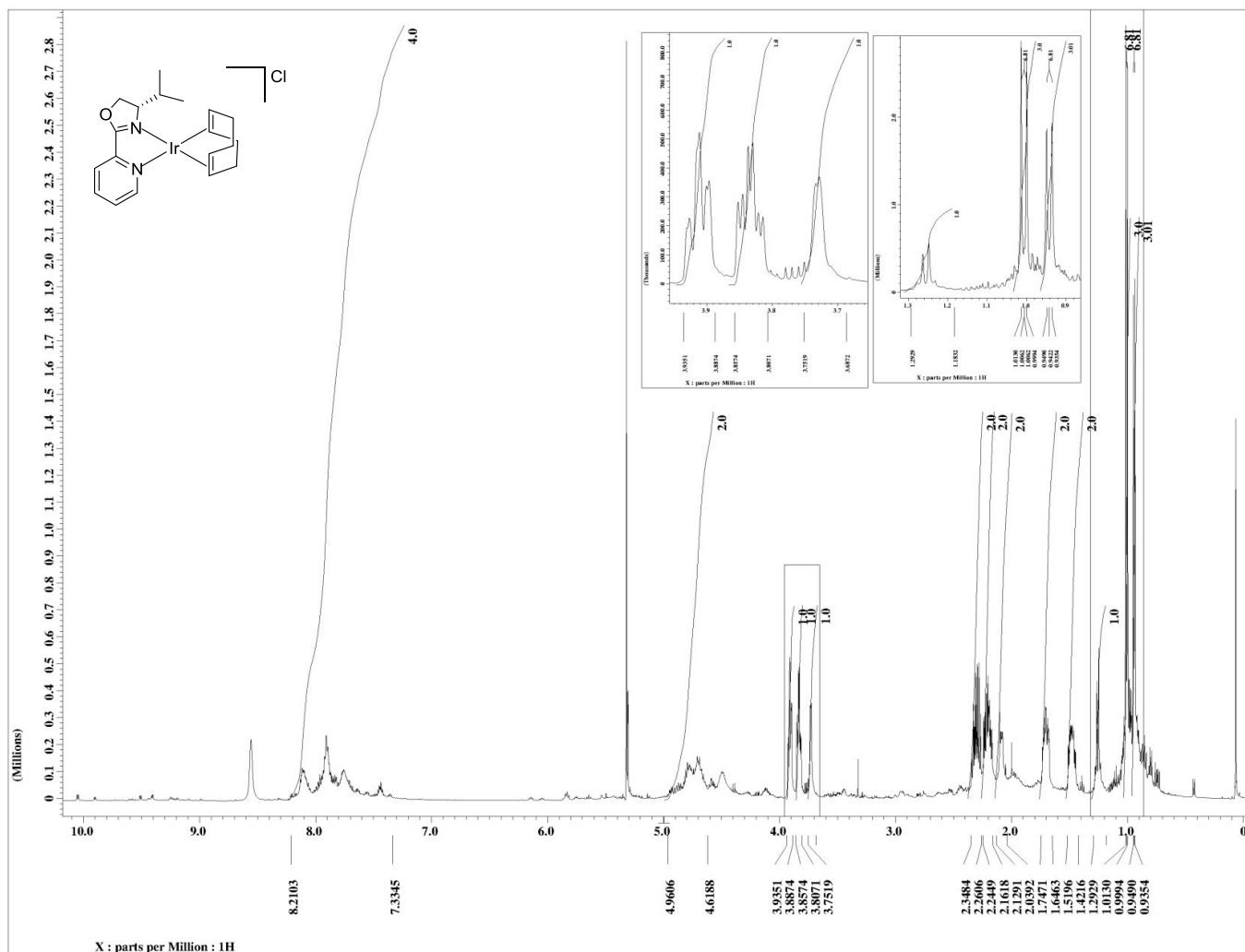
1,5-Cyclooctadiene[(4,4'-di-tert-butyl-2,2'-bipyridine)]iridium(I) chlorid, [Ir(dtbp)(cod)]Cl (24a)



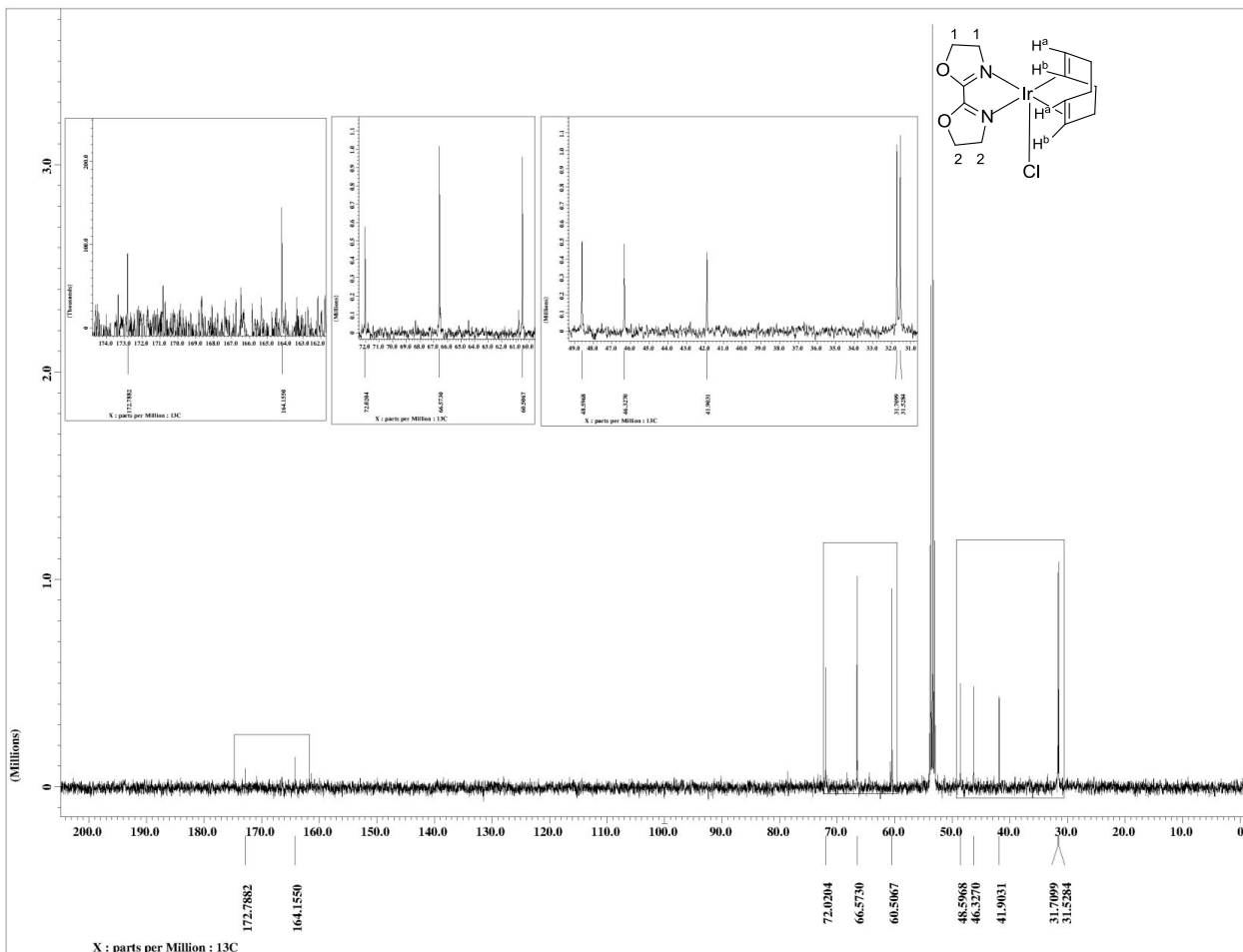
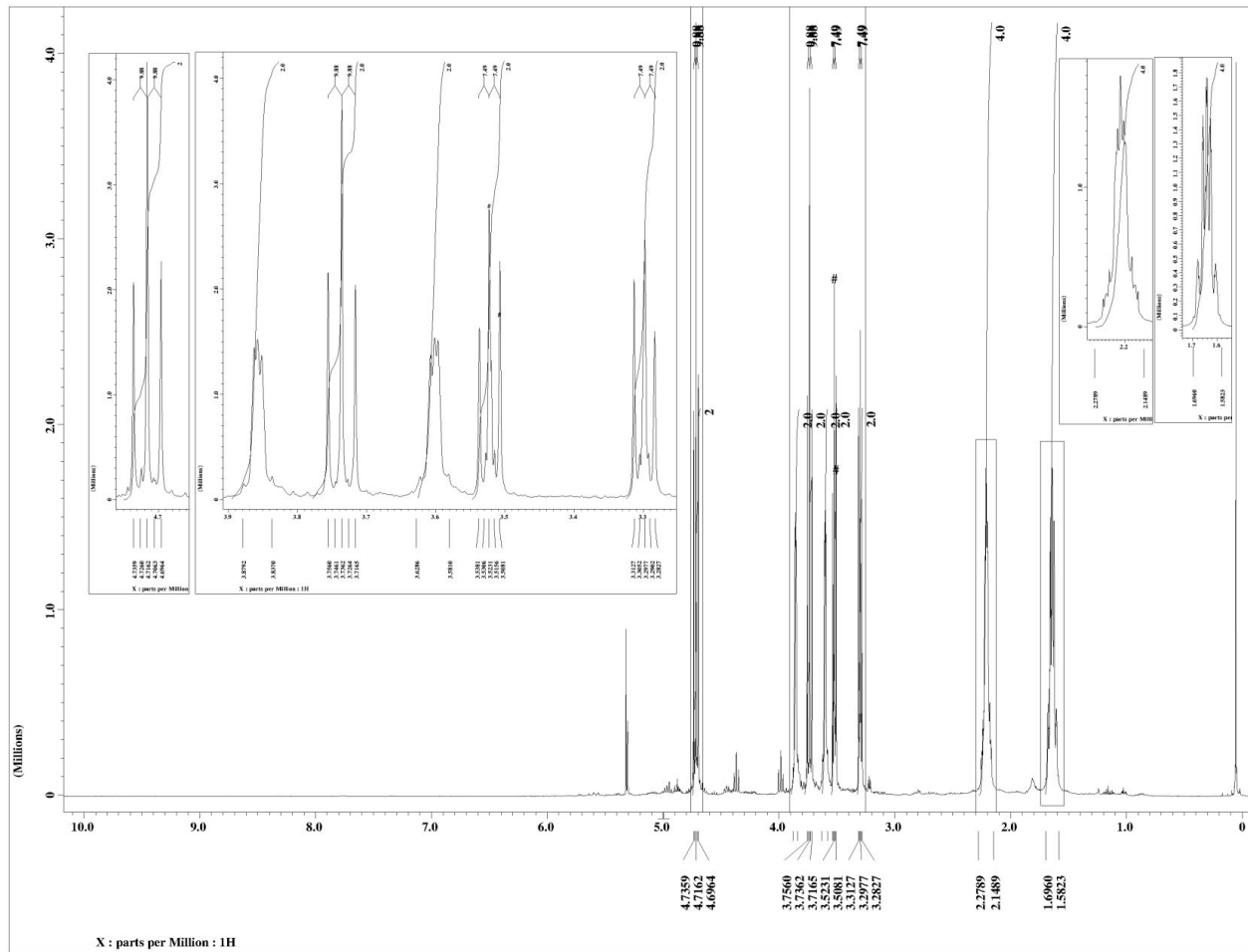
1,5-Cyclooctadiene[(*S*)-4-Isopropyl-2-(quinolin-2-yl)-oxazolin]iridium(I) chlorid, [Ir(^{*i*}Pr-quinox)(cod)]Cl (24b)



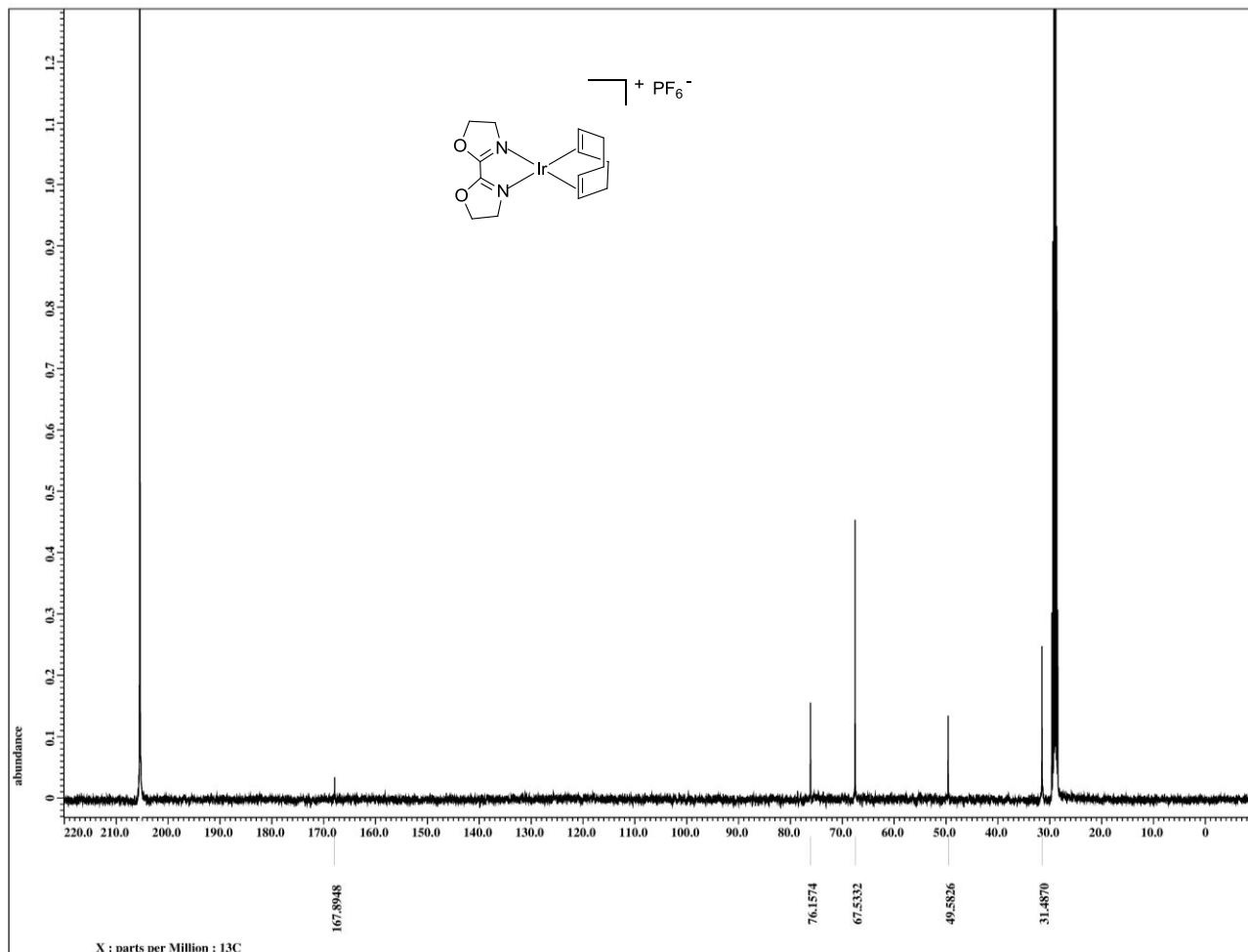
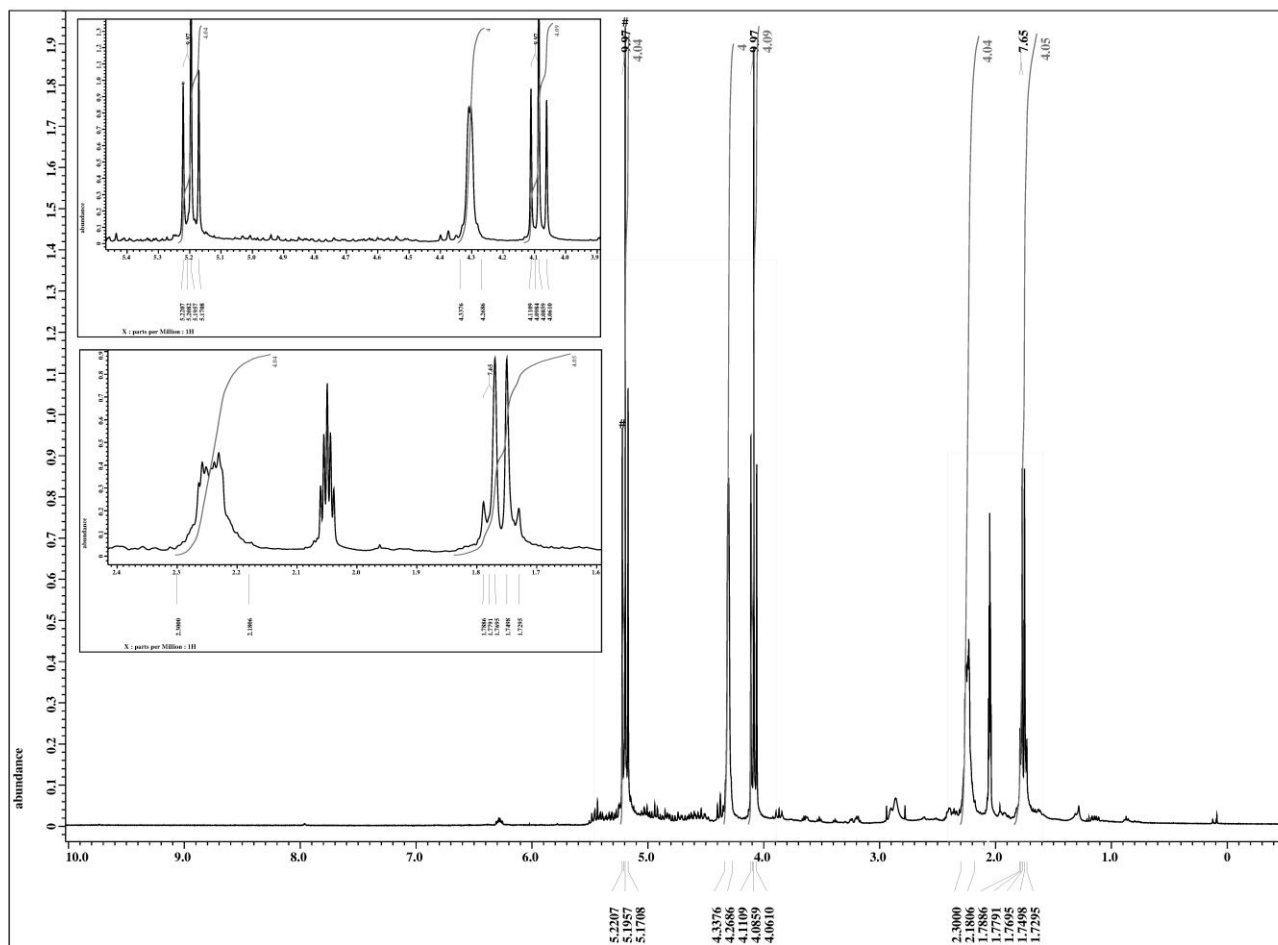
1,5-Cyclooctadien[(S)-4-isopropyl-2-(pyridin-yl)-oxazolin]iridium(I) chlorid, [Ir(iPr-pyrox)(cod)]Cl (24c)



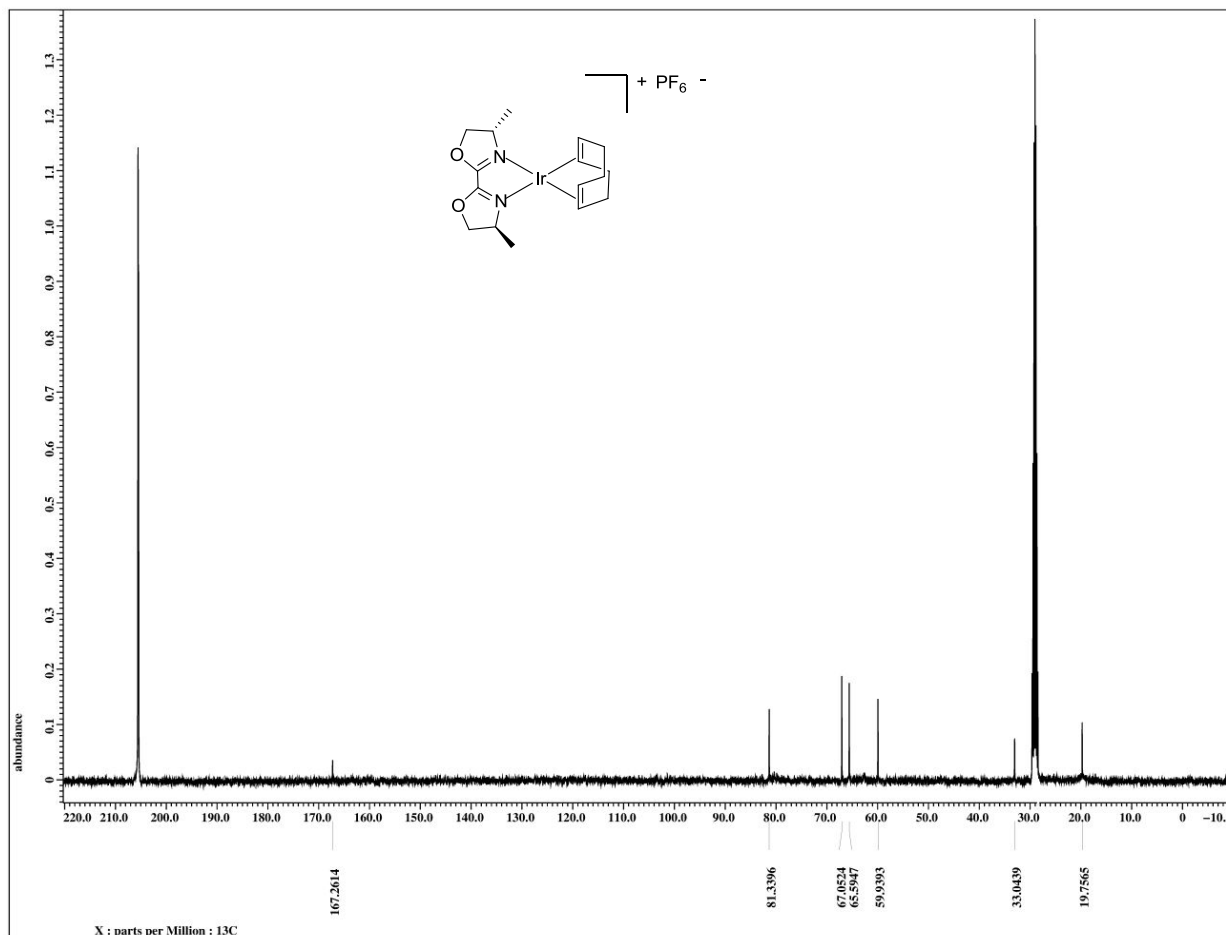
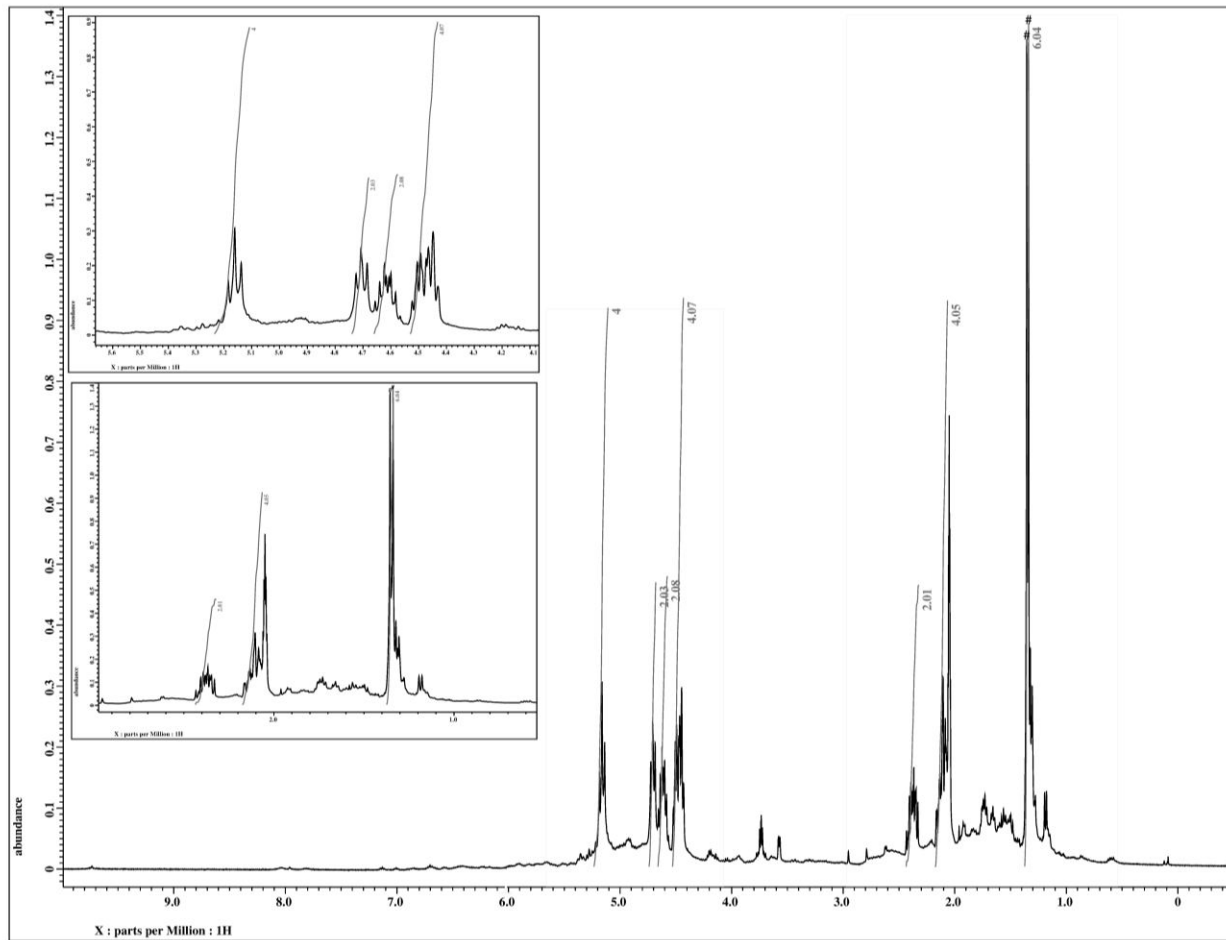
Cyclooctadien[2,2'-bioxazolin]iridium(I) chlorid, [Ir(H-box)(cod)]Cl (42d)



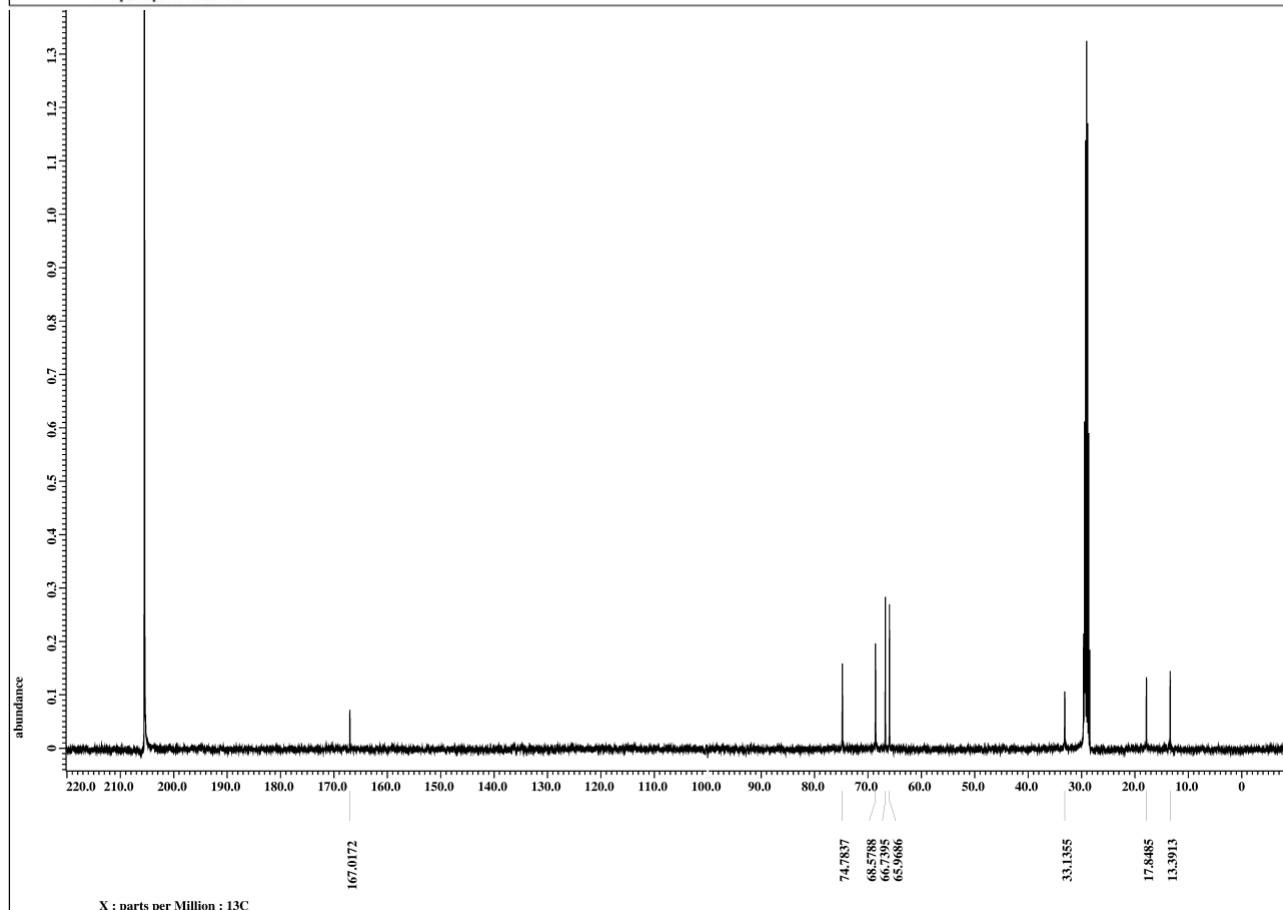
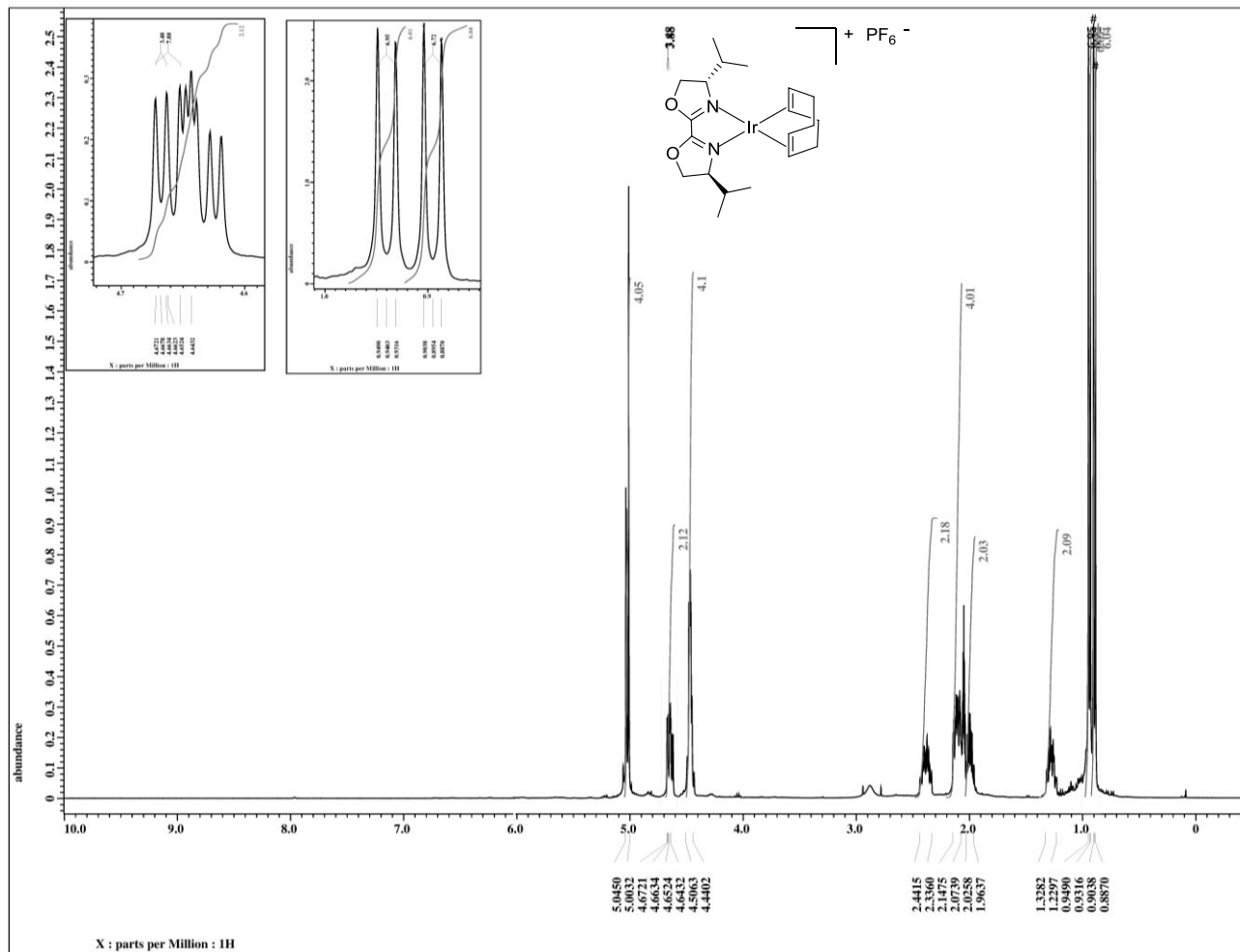
1,5-Cyclooctadiene[(2,2'-bioxazole)]iridium(I) hexafluorophosphate, [Ir(H-box)(cod)]PF₆ (25a)



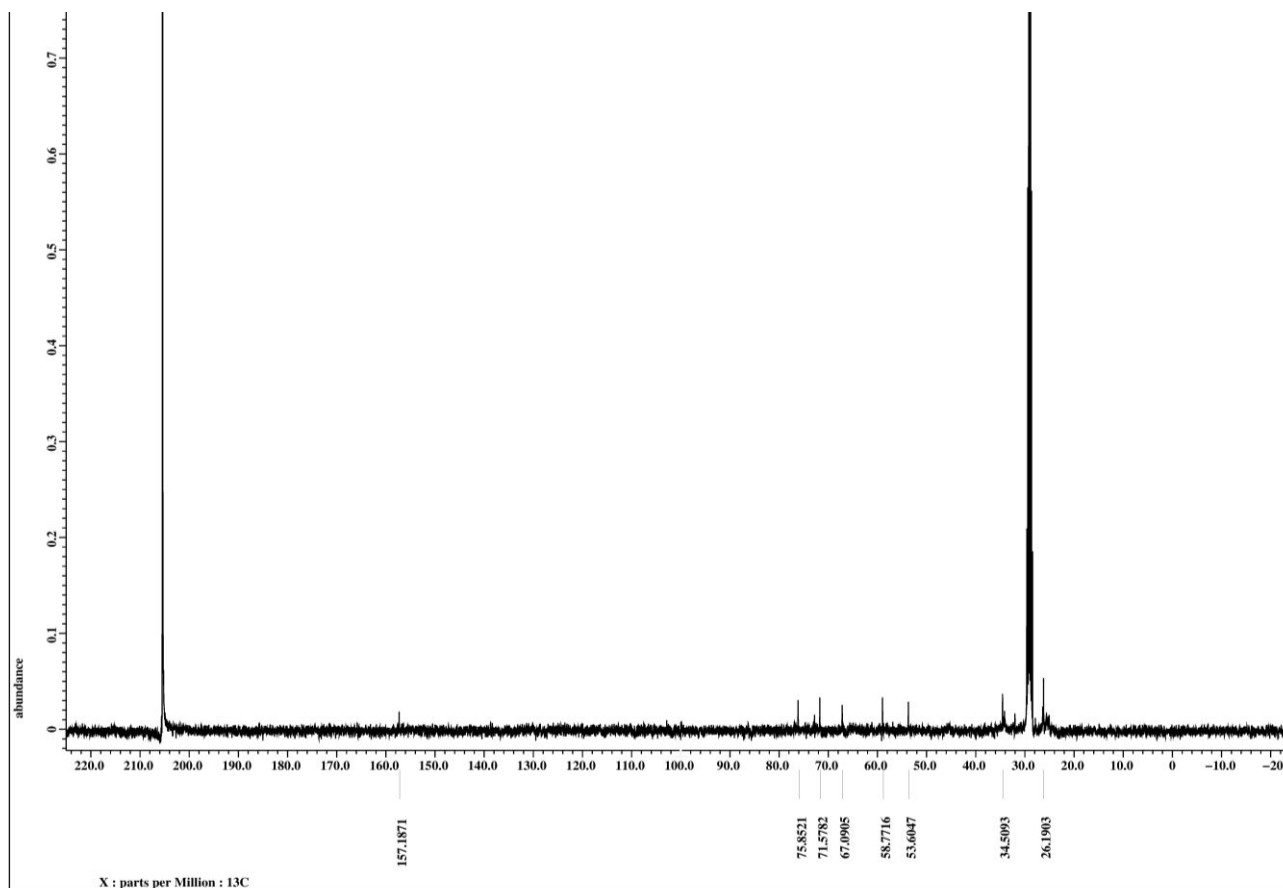
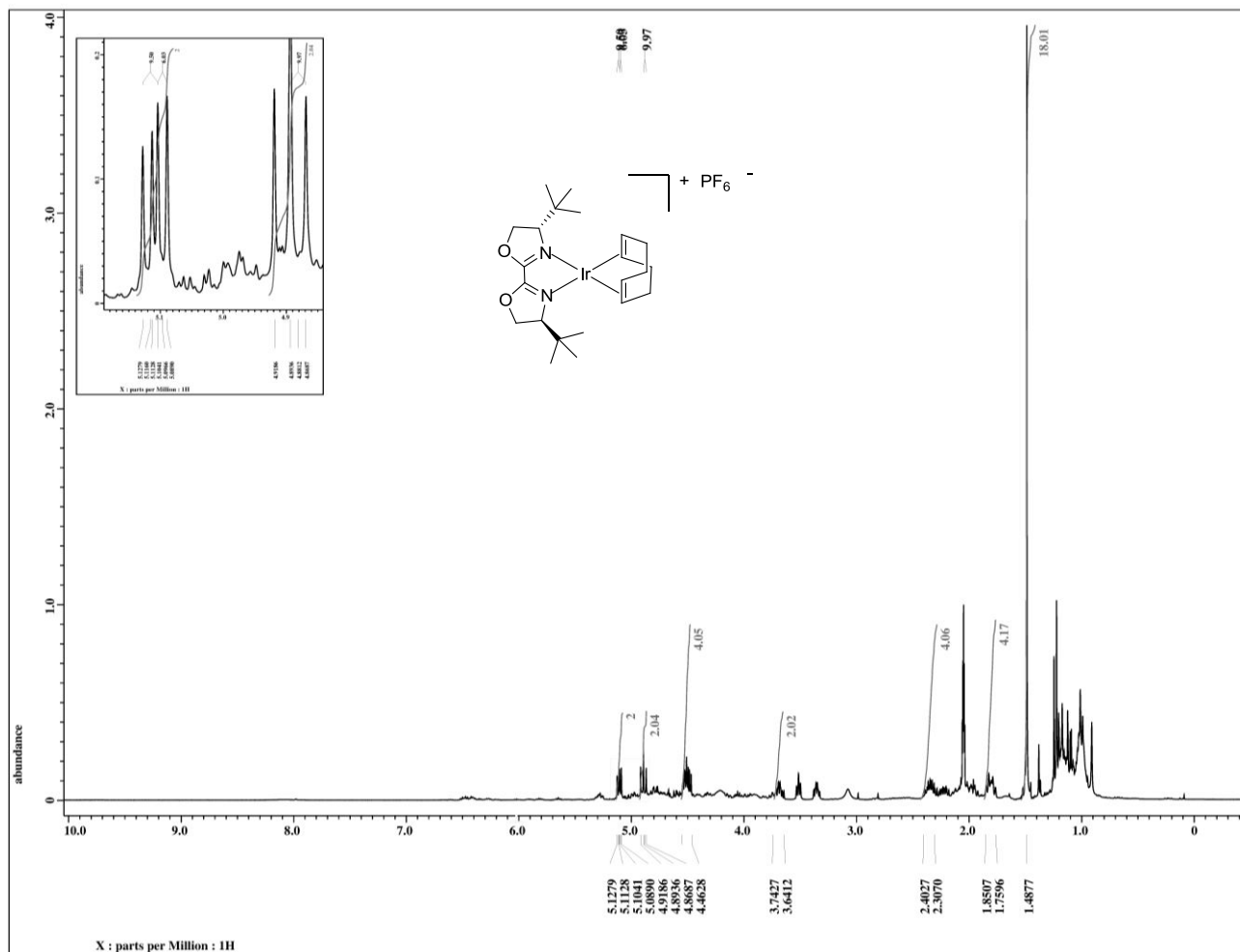
1,5-Cyclooctadiene[(2,2'-Bis((4*S*, 4'*S*)-4,4'-dimethyl)-oxazolin)]iridium(I) hexafluorophosphate, [Ir(Me-box)(cod)]PF₆ (25b)



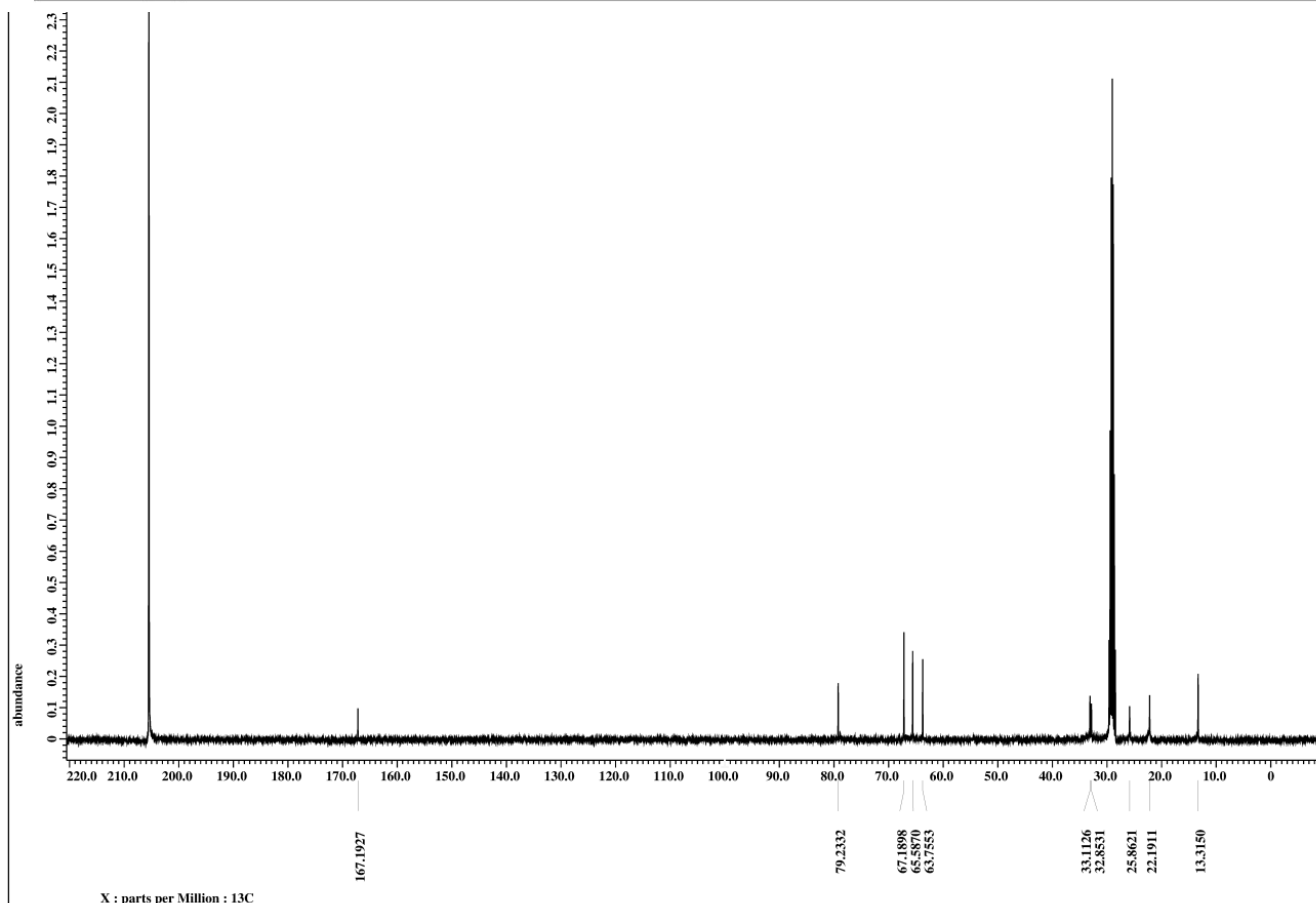
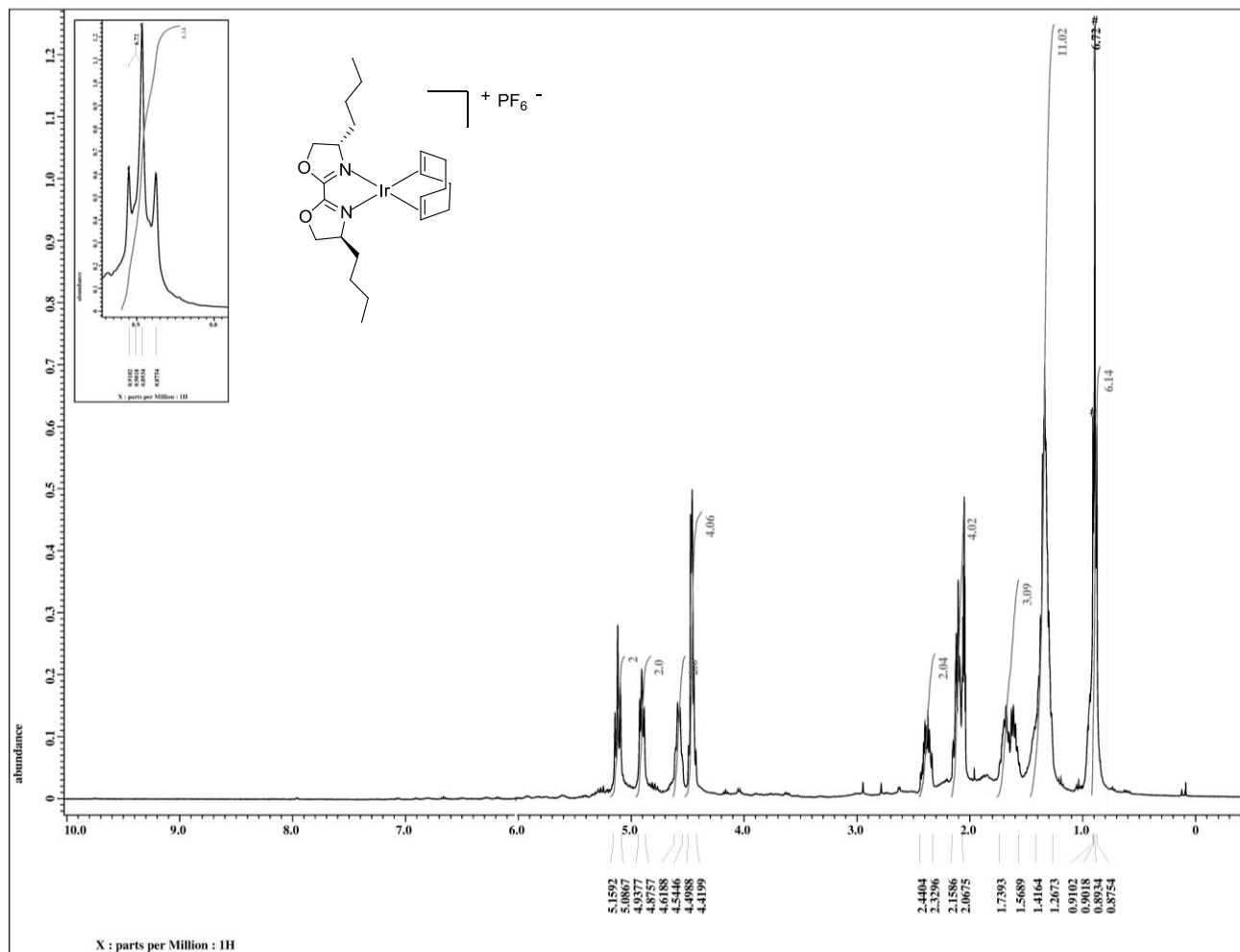
1,5-Cyclooctadiene[(2,2'-Bis((4*S*,4'*S*)-4,4'-diisopropyl)-oxazolin)]iridium(I) hexafluorophosphate, [Ir(ⁱPr-box)(cod)]PF₆ (25c**)**



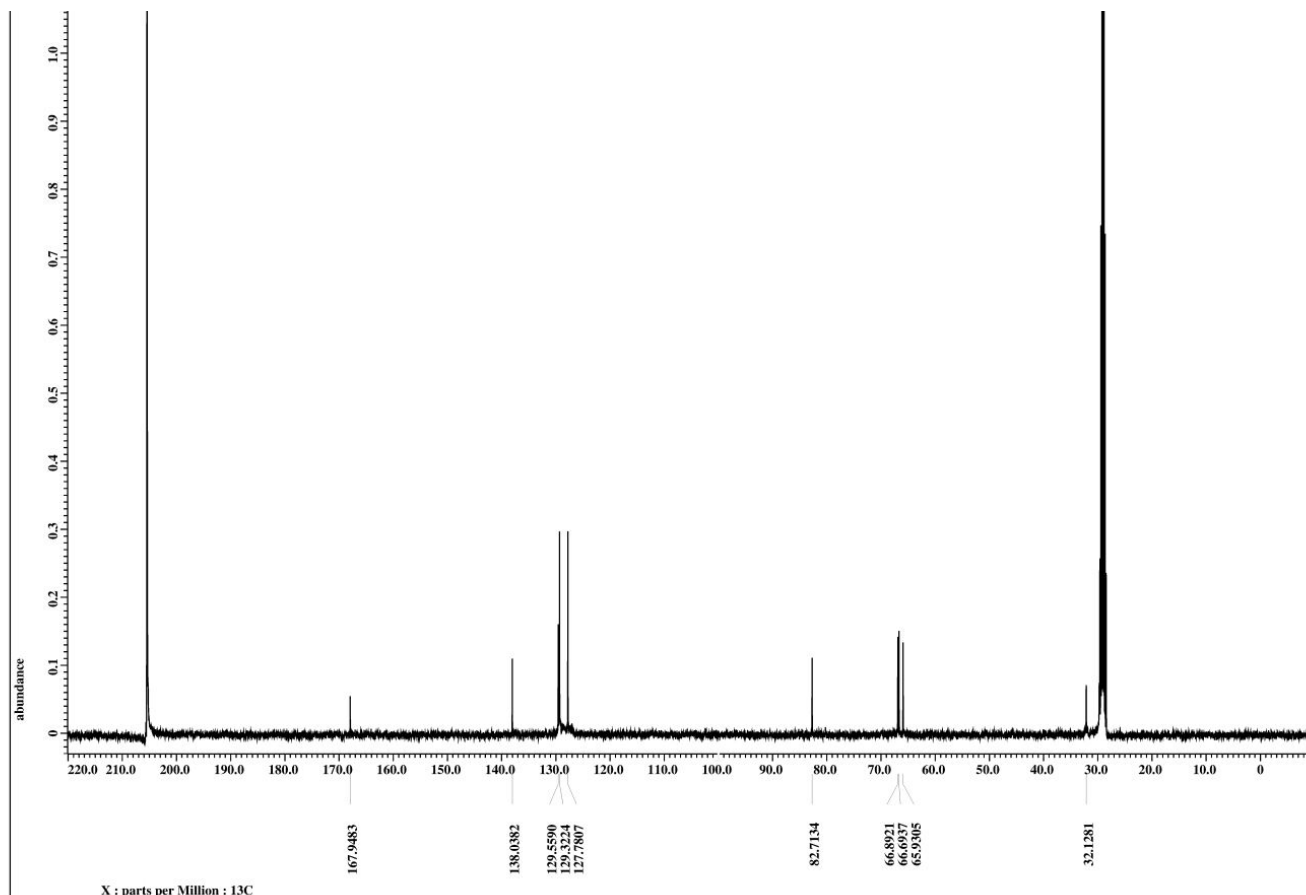
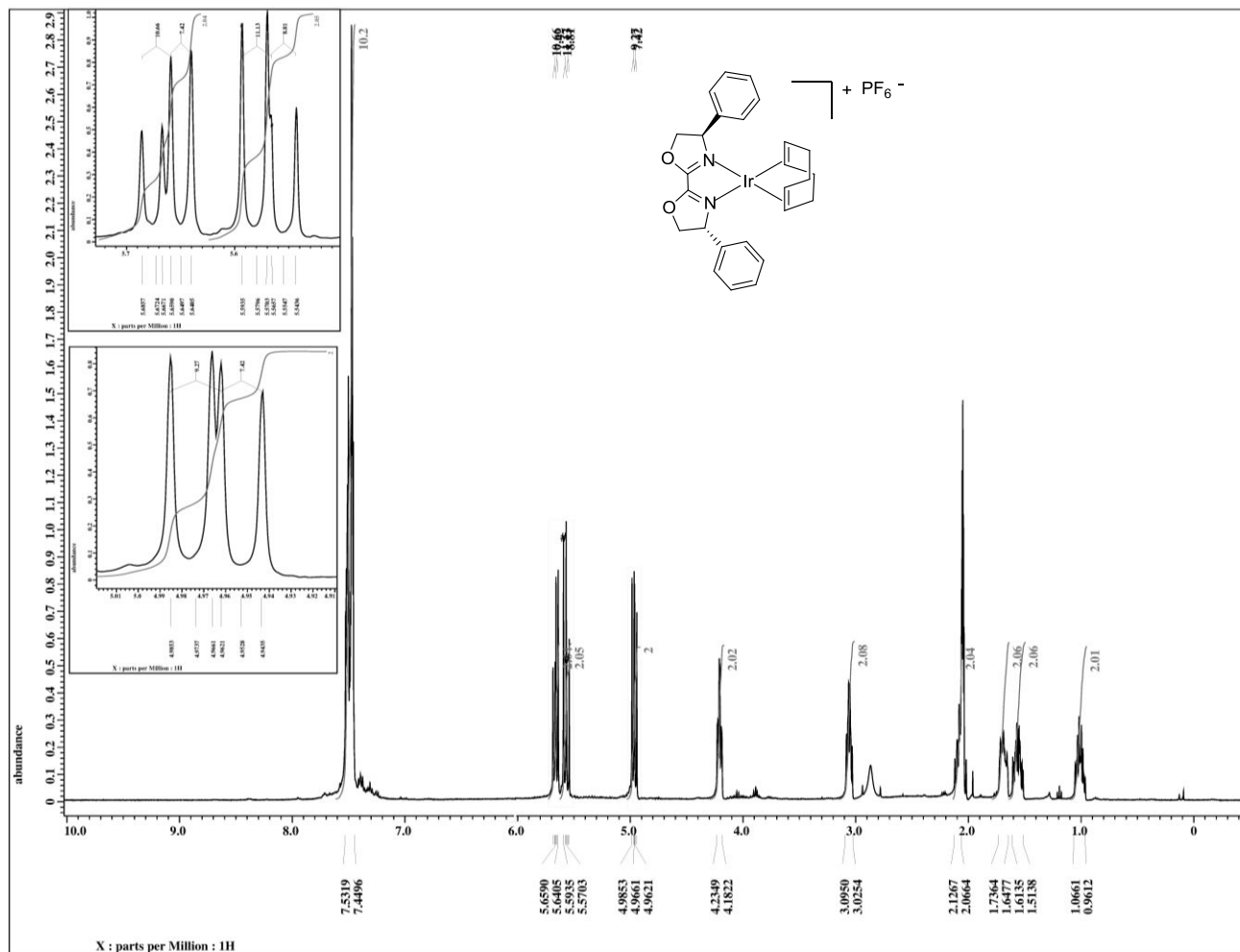
1,5-Cyclooctadiene[(2,2'-Bis((4*S*,4'*S*)-4,4'-di-*tert*-butyl)-oxazolin)]iridium(I) hexafluorophosphate, [Ir(H-box)(cod)]PF₆ (25d)



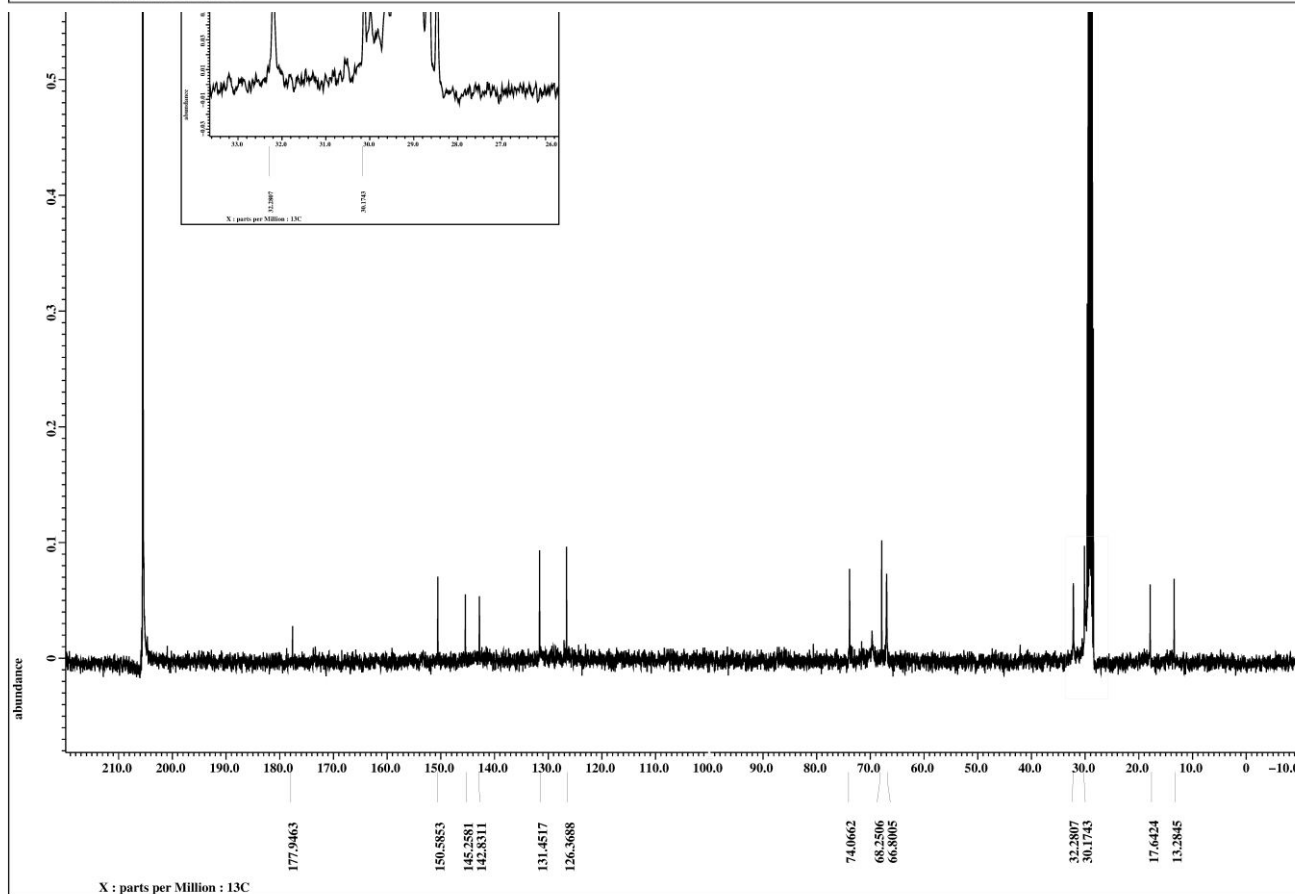
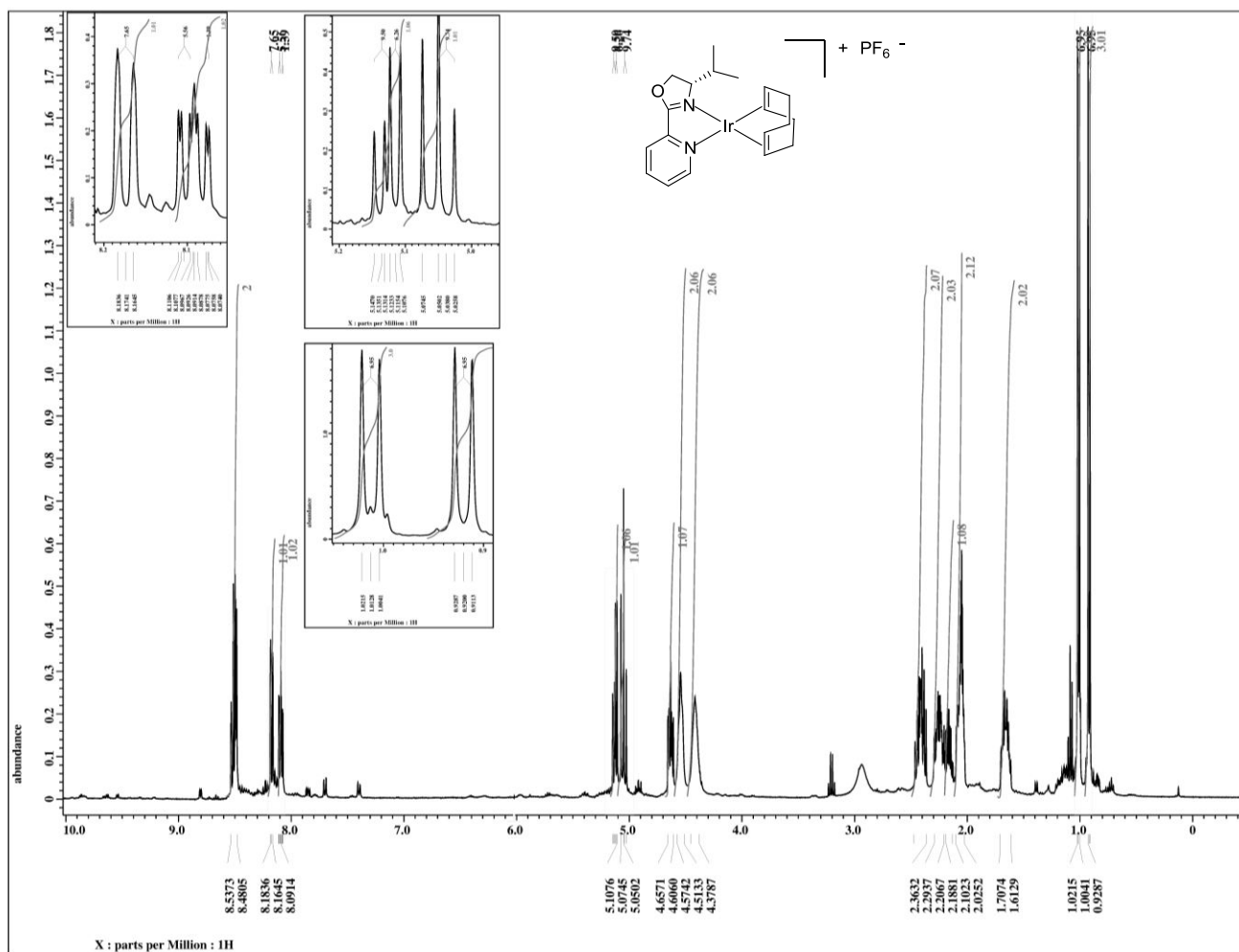
1,5-Cyclooctadiene[(2,2'-Bis((4*S*, 4'*S*)-4,4'-dibutyl)-oxazolin)]iridium(I) hexafluorophosphate, [Ir^(I)Bu-box)(cod)]PF₆ (25e**)**



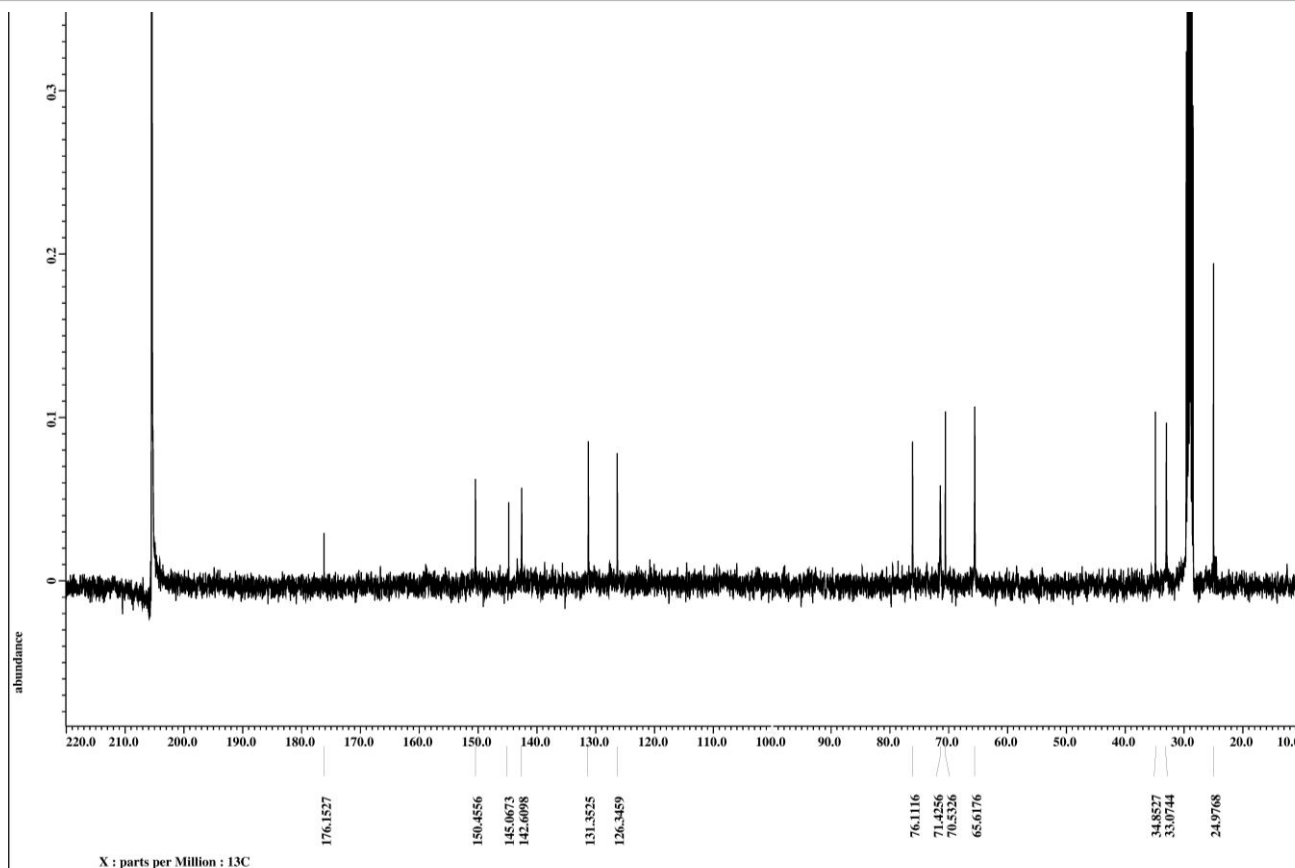
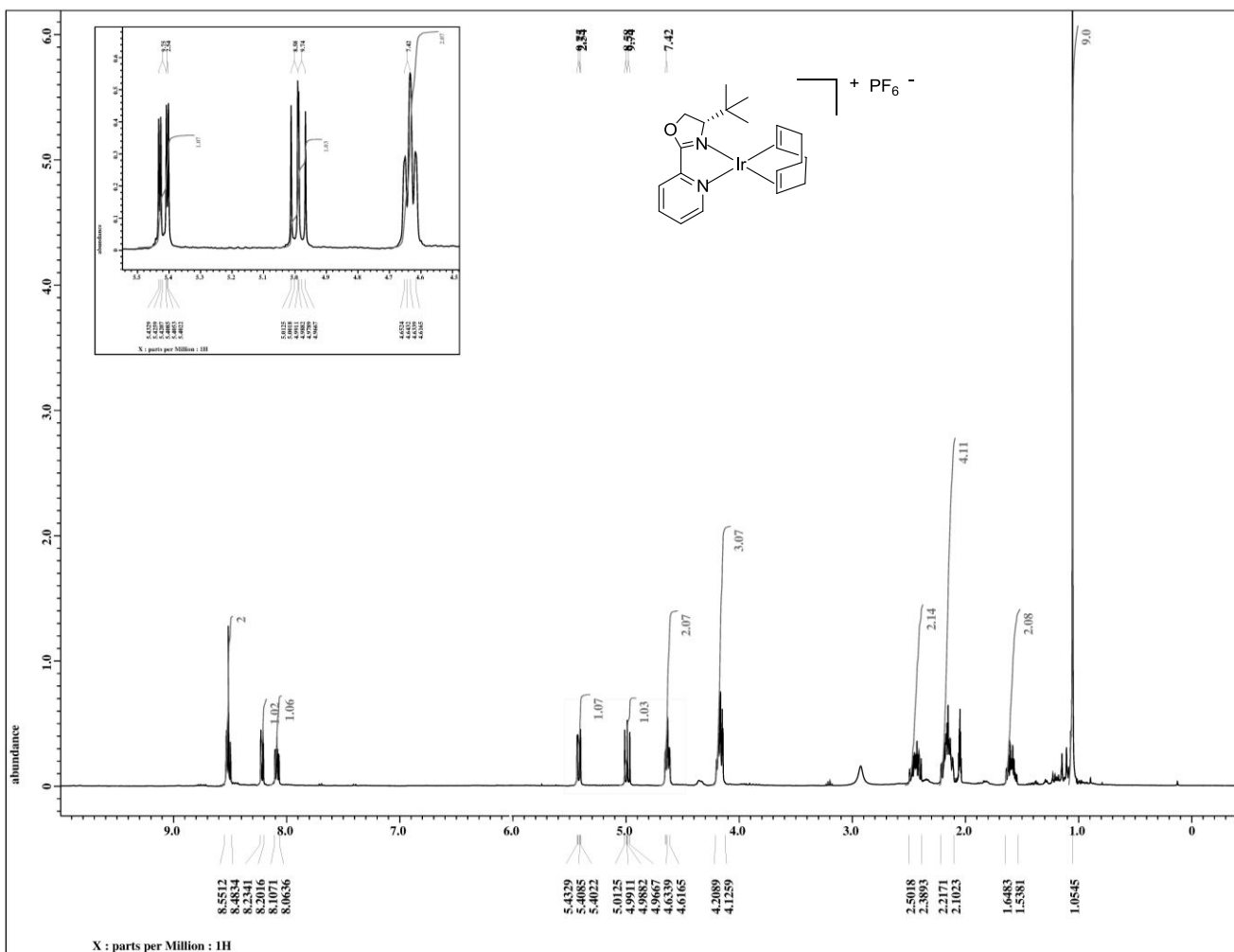
1,5-Cyclooctadiene[(2,2'-Bis((4*R*, 4'*R*)-4,4'-diphenyl)-oxazolin)]iridium(I) hexafluorophosphate, [Ir(Ph-box)(cod)]PF₆ (25f)



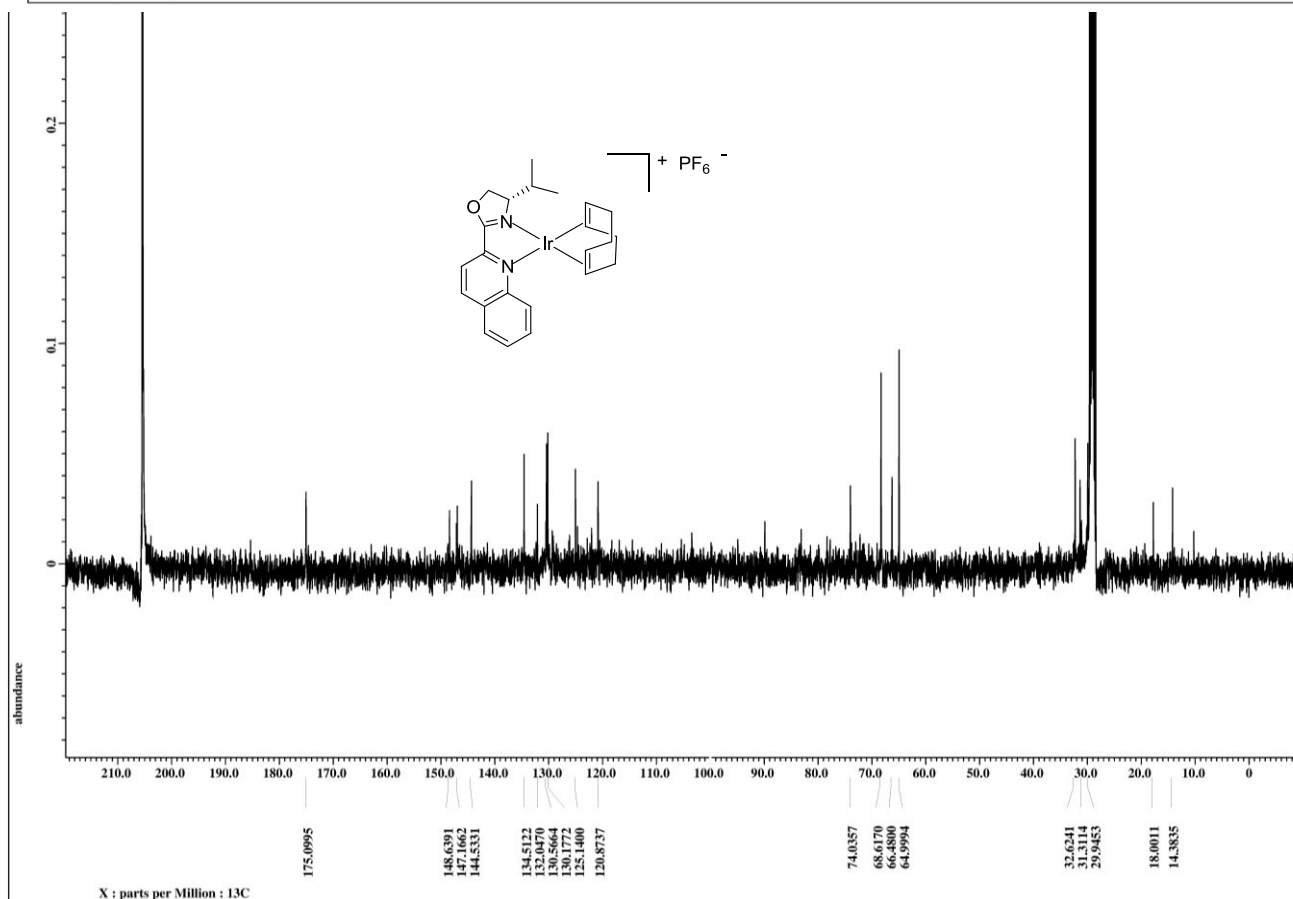
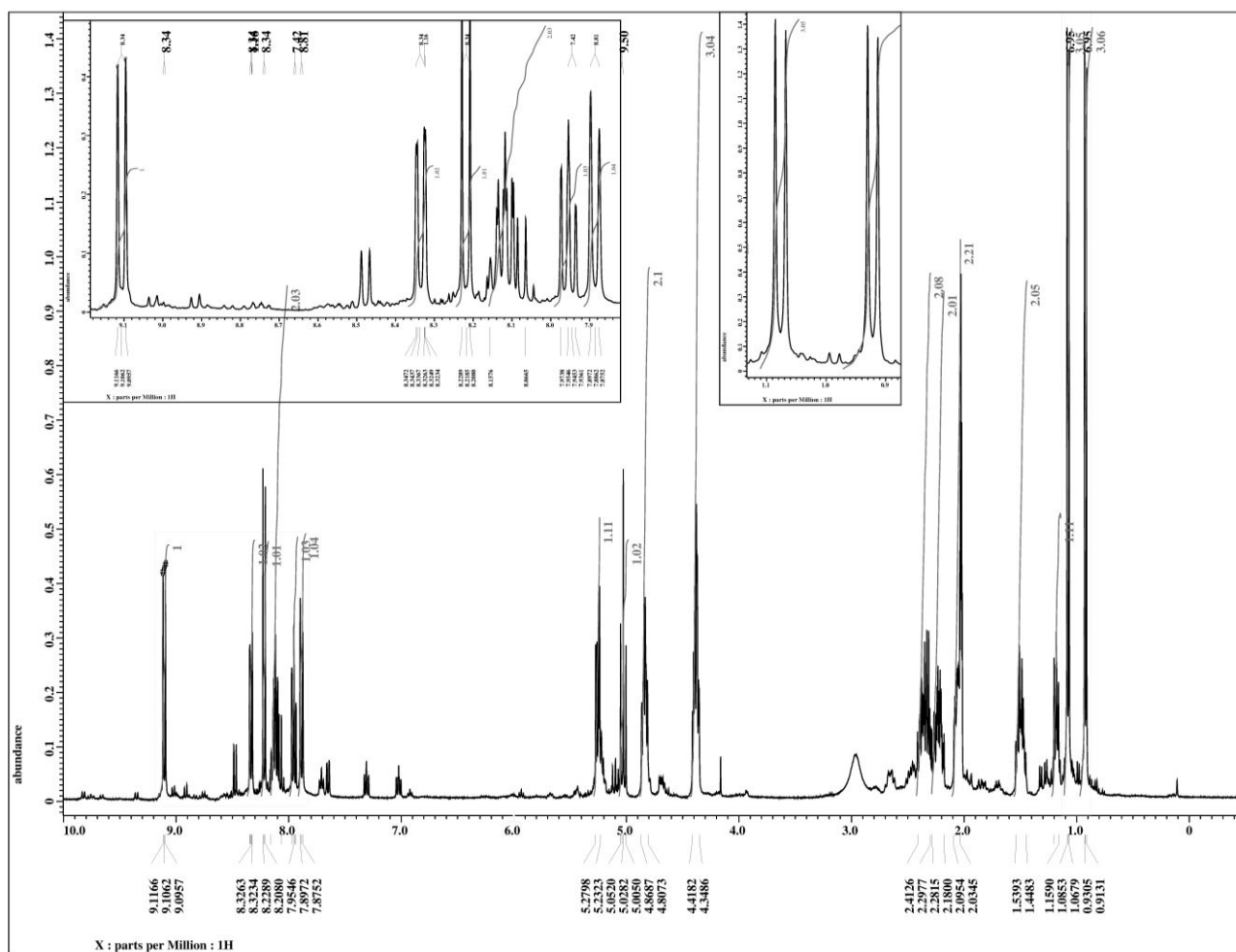
1,5-Cyclooctadiene[(2,2'-bis((4*S*,4'*S*)-4,4'-diisopropyl)-oxazolin)]iridium(I) hexafluorophosphate, [Ir(ⁱPr-pyrox)(cod)]PF₆ (25h)



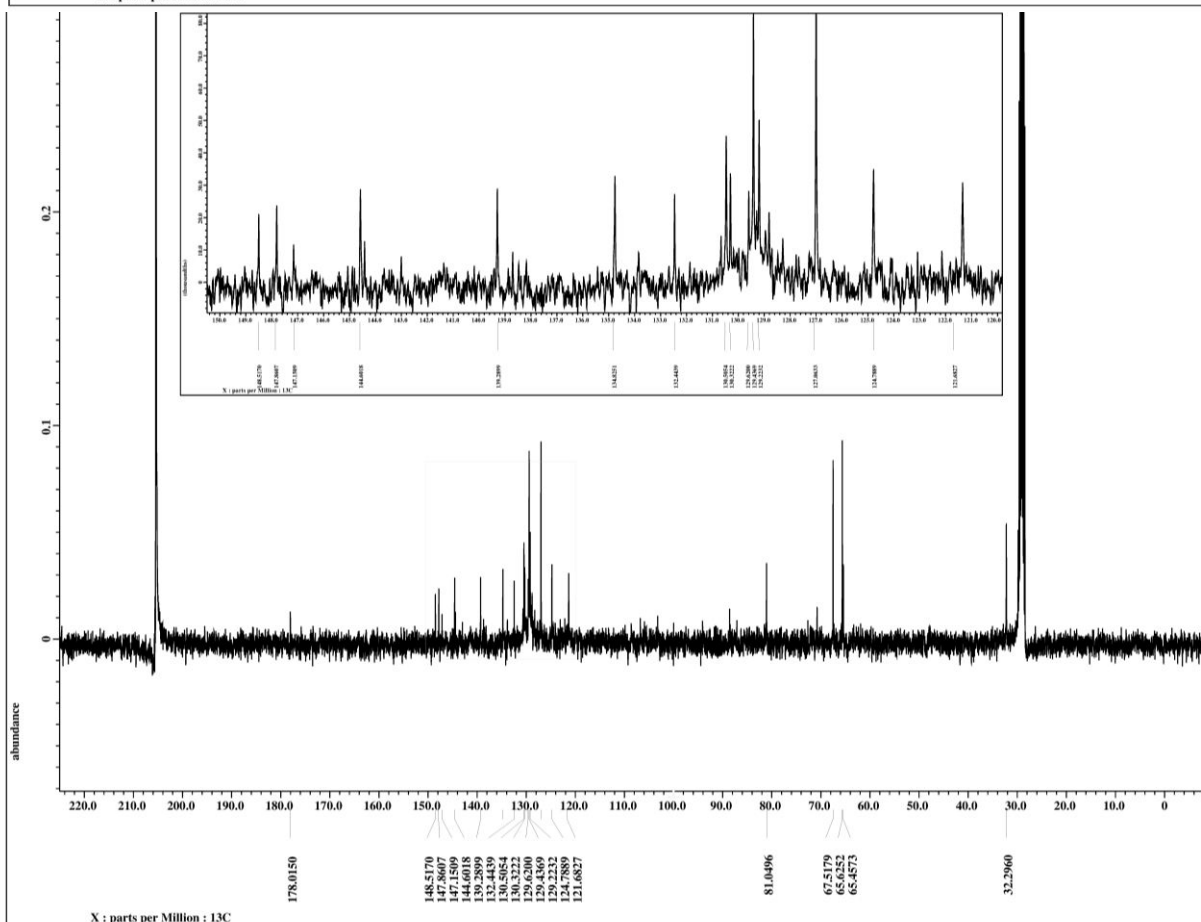
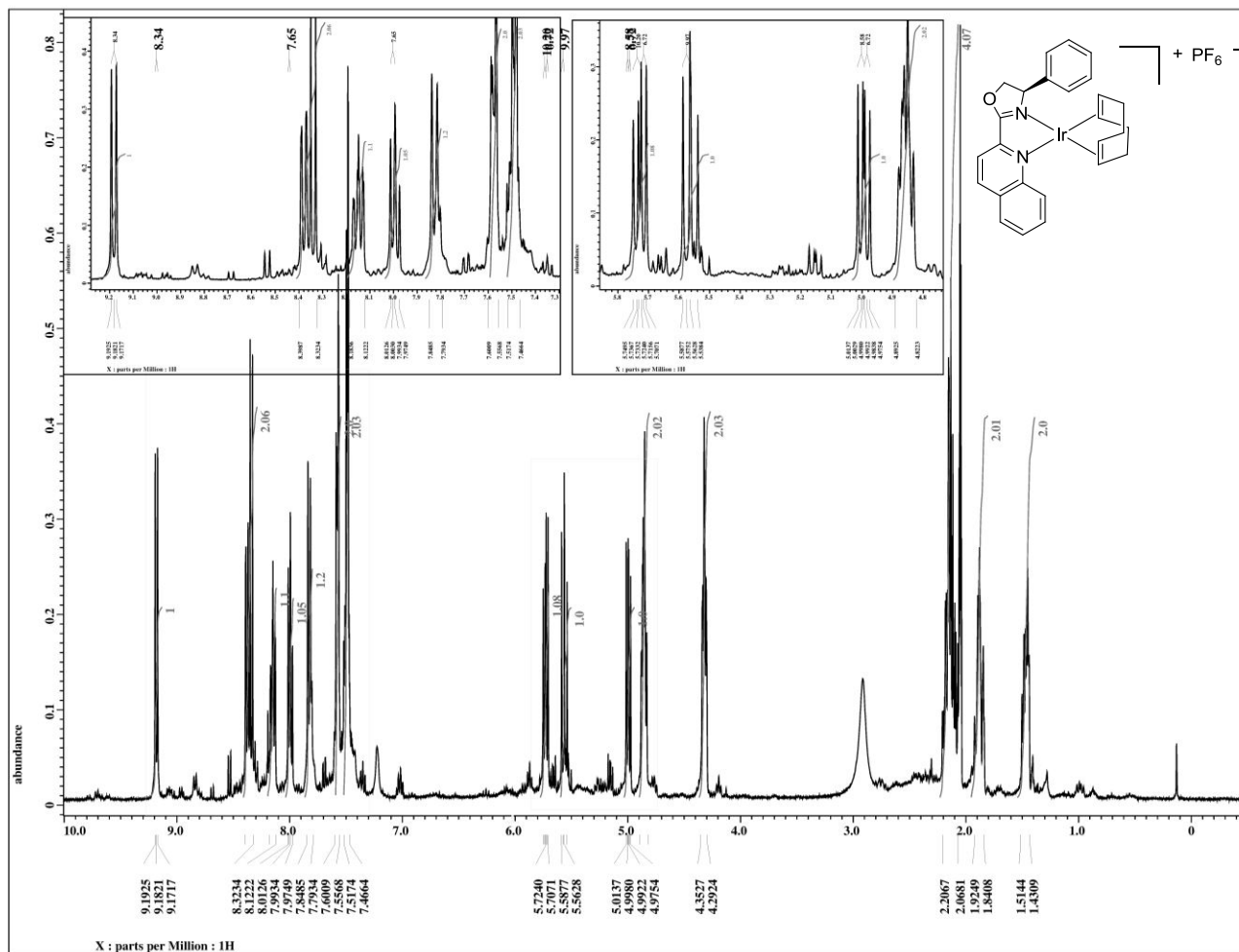
1,5-Cyclooctadiene[*((S)*-4-(*tert*-butyl)-2-(pyridine-2-yl)-oxazolin)]iridium(I) hexafluorophosphate, [Ir(*t*Bu-pyrox)(cod)]PF₆ (25i)



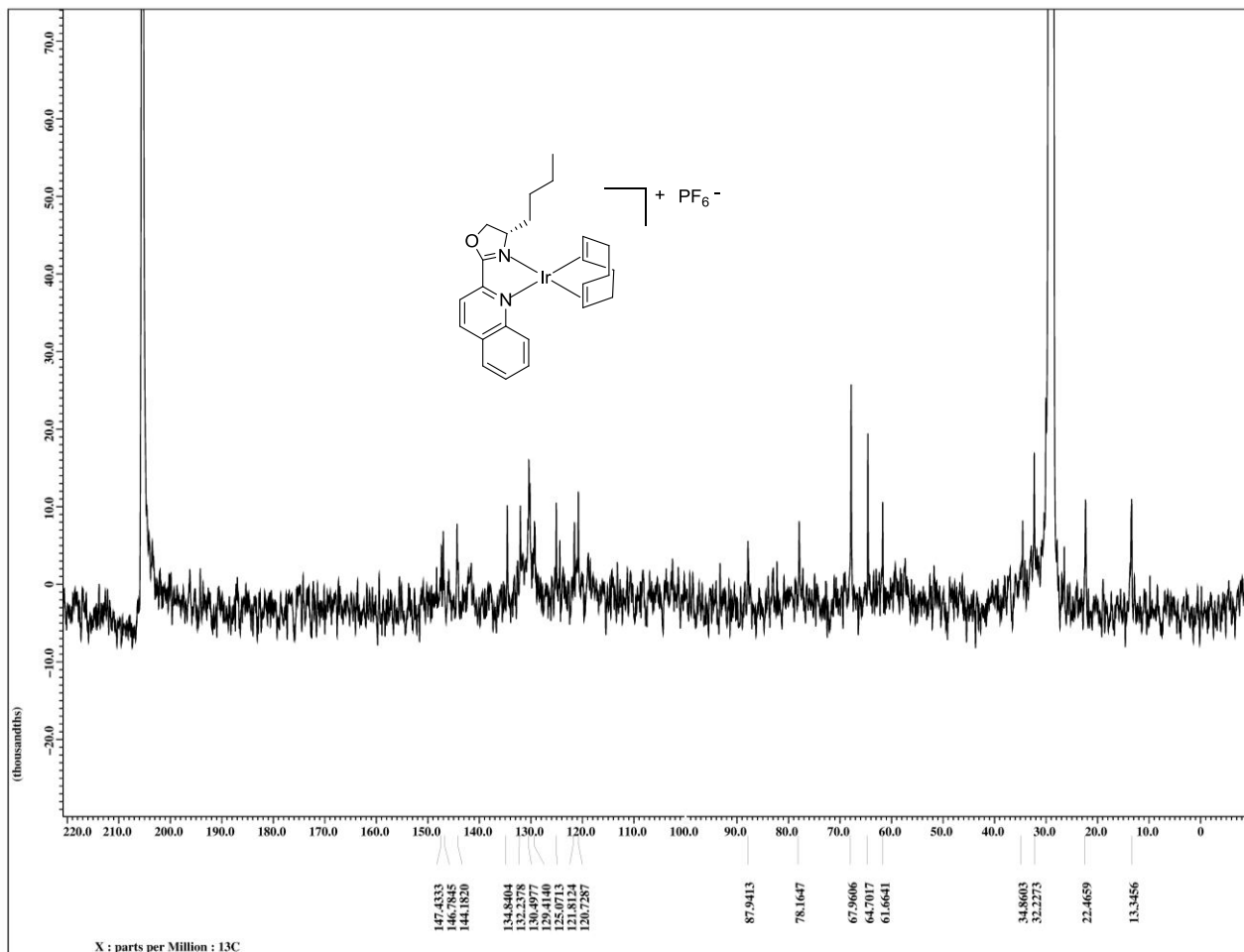
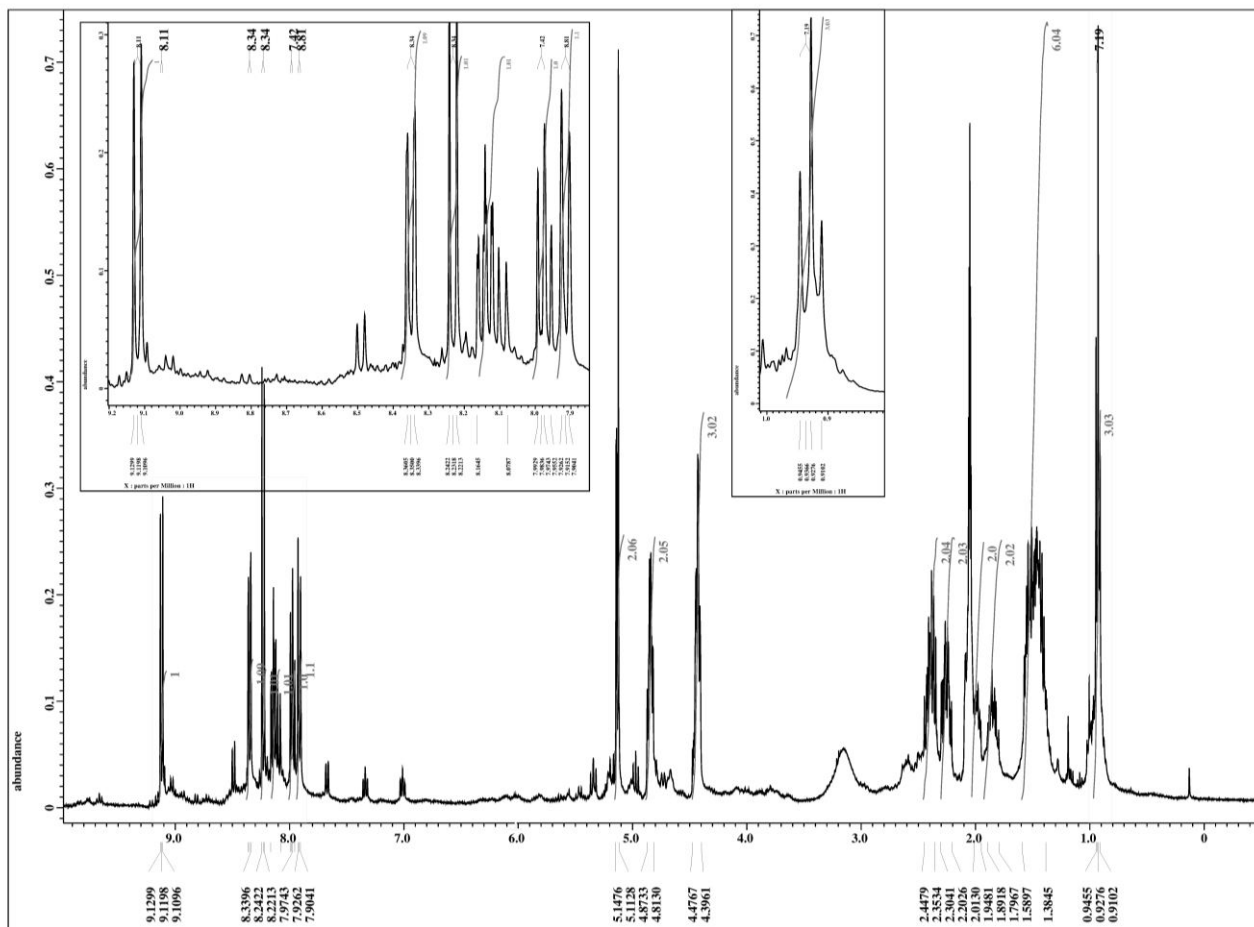
1,5-Cyclooctadiene[(*S*)-4-isopropyl-2-(quinolin-2-yl)-oxazole]iridium(I) hexafluorophosphate, [Ir(ⁱPr-quinox)(cod)]PF₆ (25m)



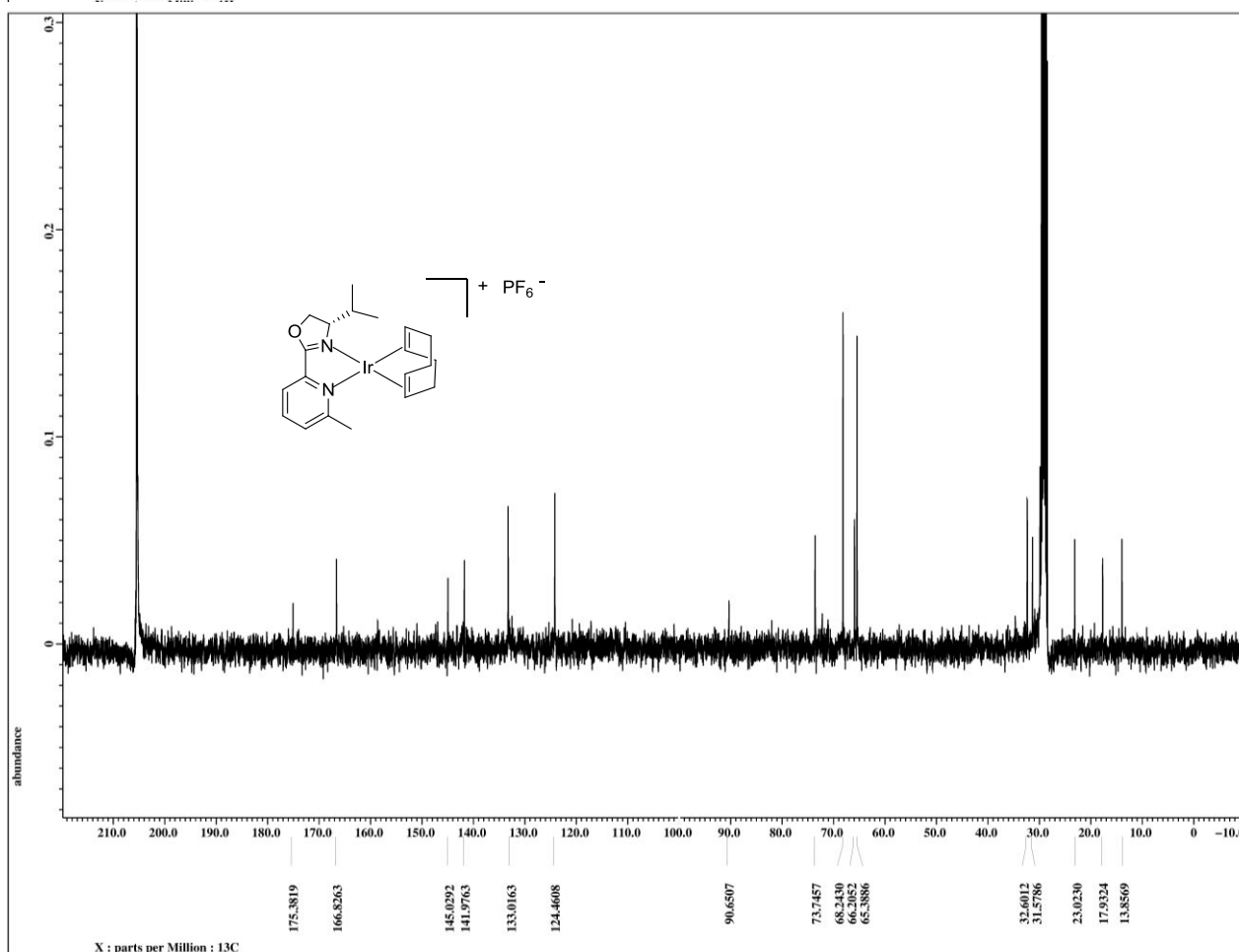
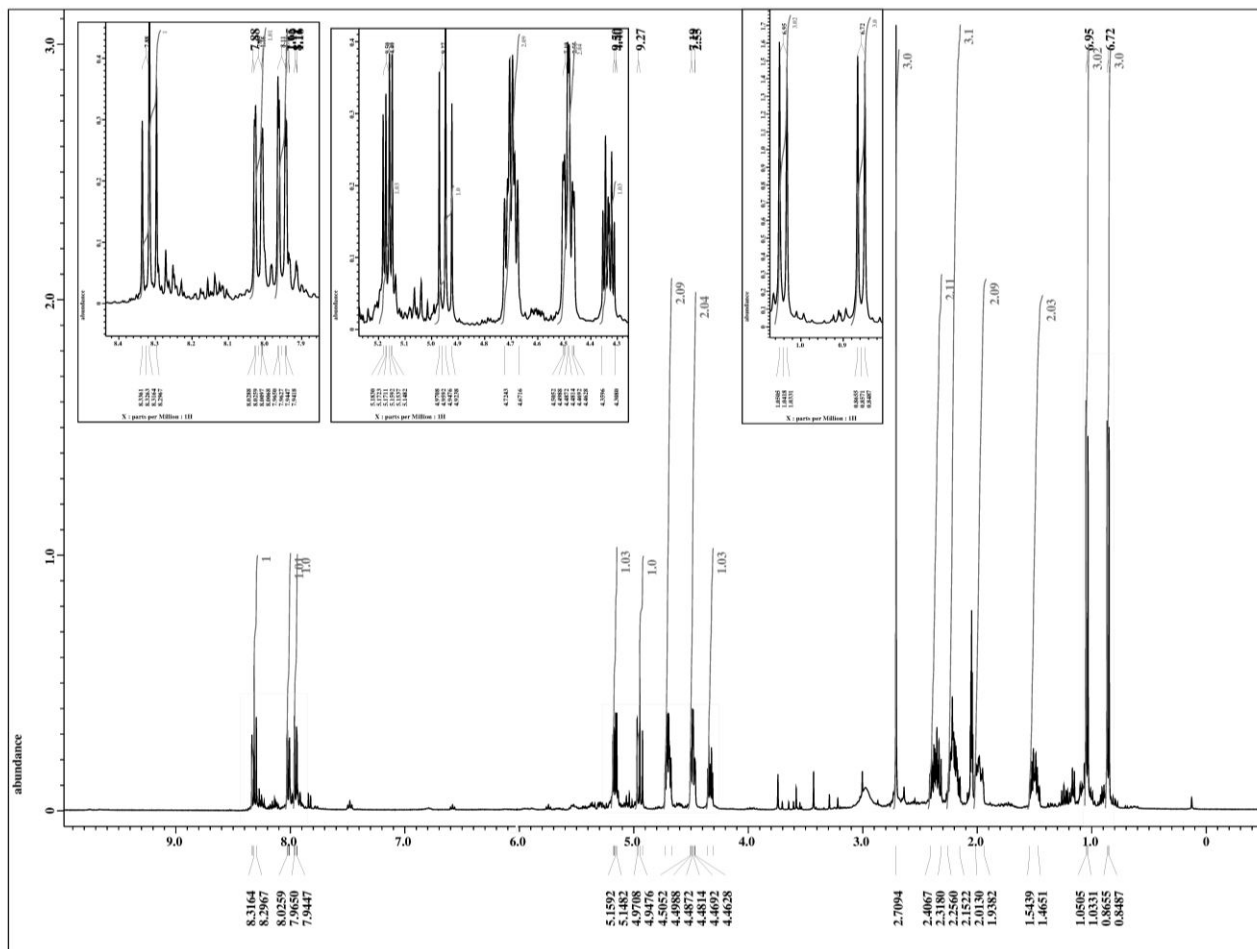
1,5-Cyclooctadiene[*(R)*-4-Phenyl-2-(quinolin-2-yl)-oxazolin]iridium(I) hexafluorophosphate, [Ir(Ph-quinox)(cod)]PF₆ (25o)



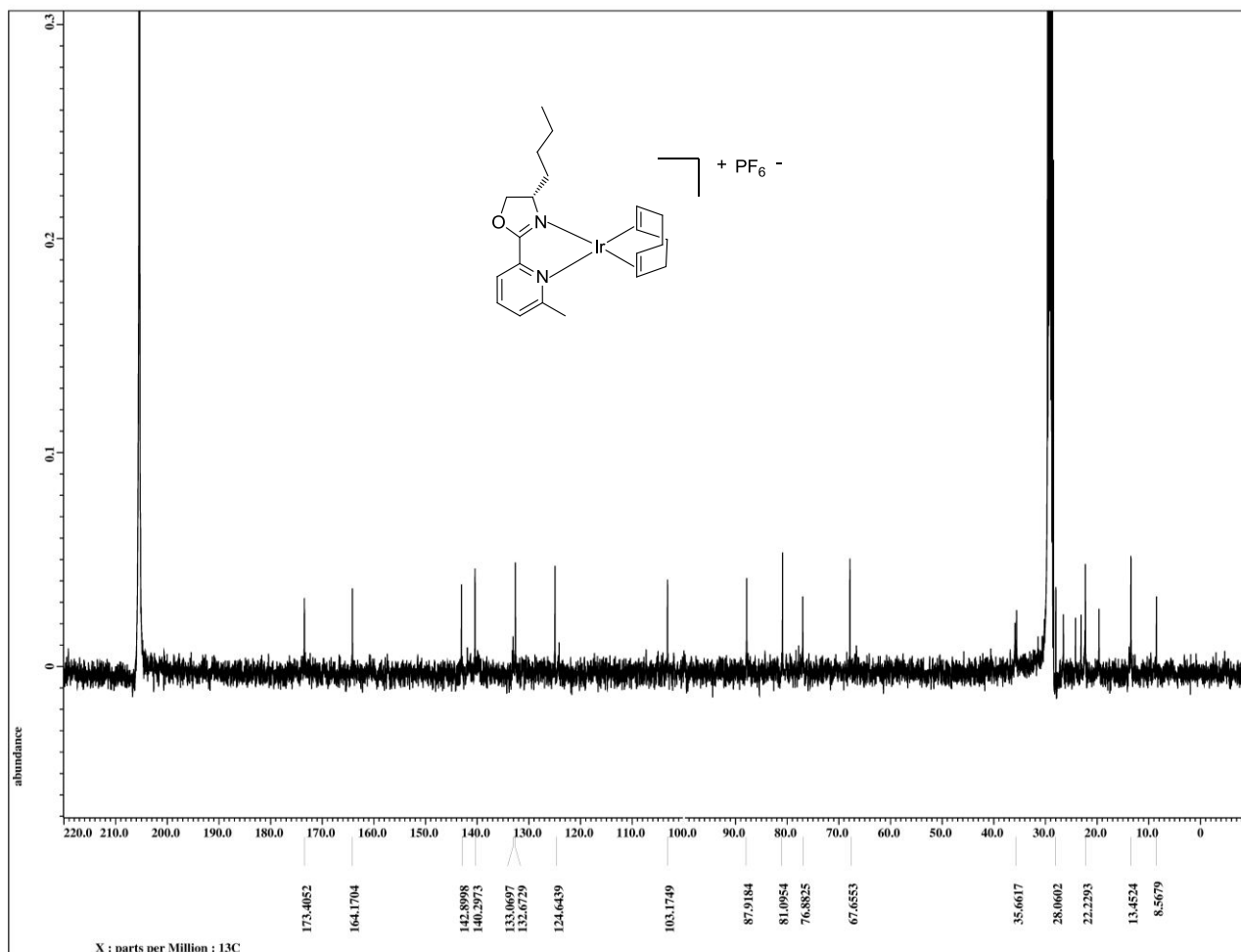
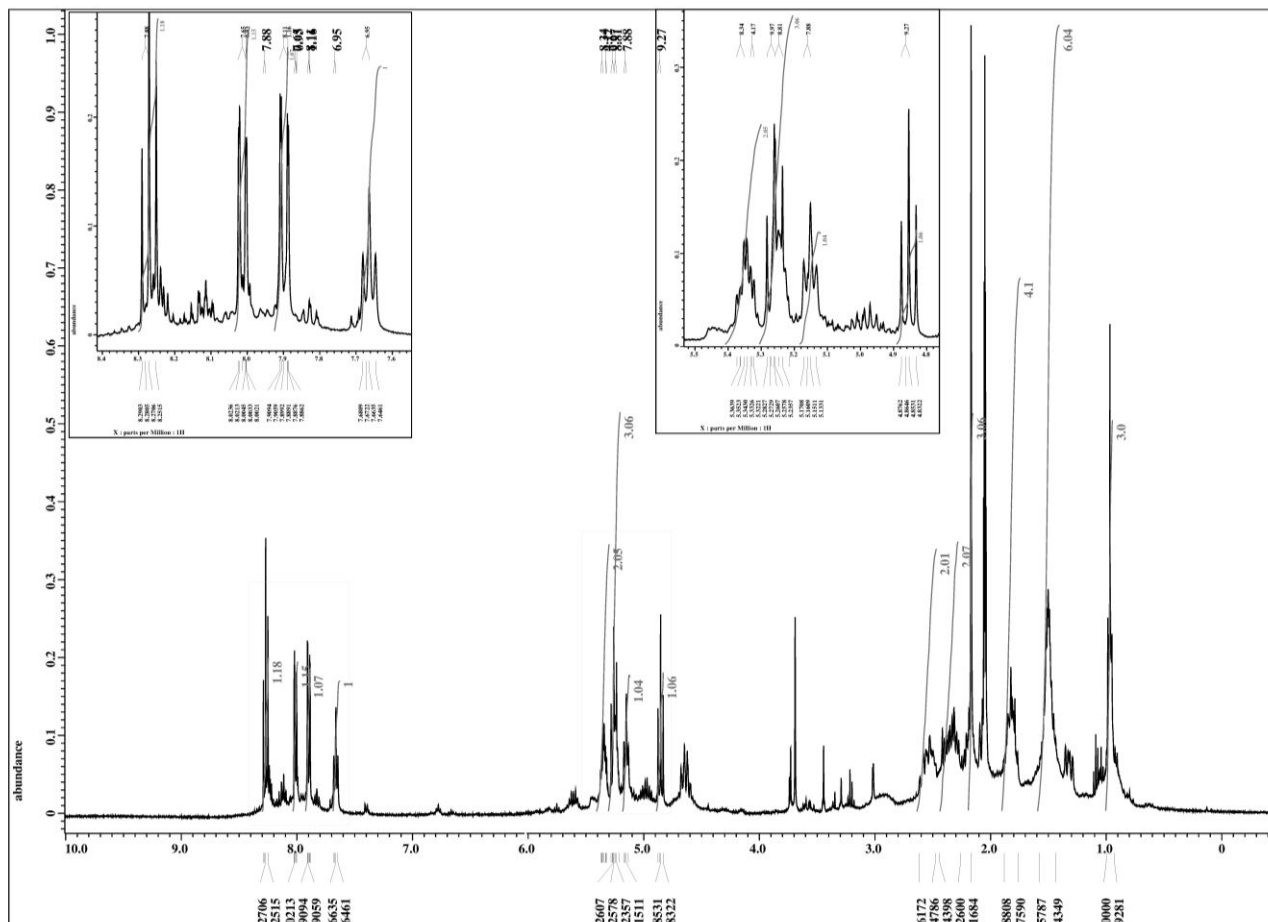
1,5-Cyclooctadiene[(*S*)-4-Butyl-2-(quinolin-2-yl)-oxazolin]iridium(I) hexafluorophosphate, [Ir(^{*i*}Pr-quinox)(cod)]PF₆ (25n)



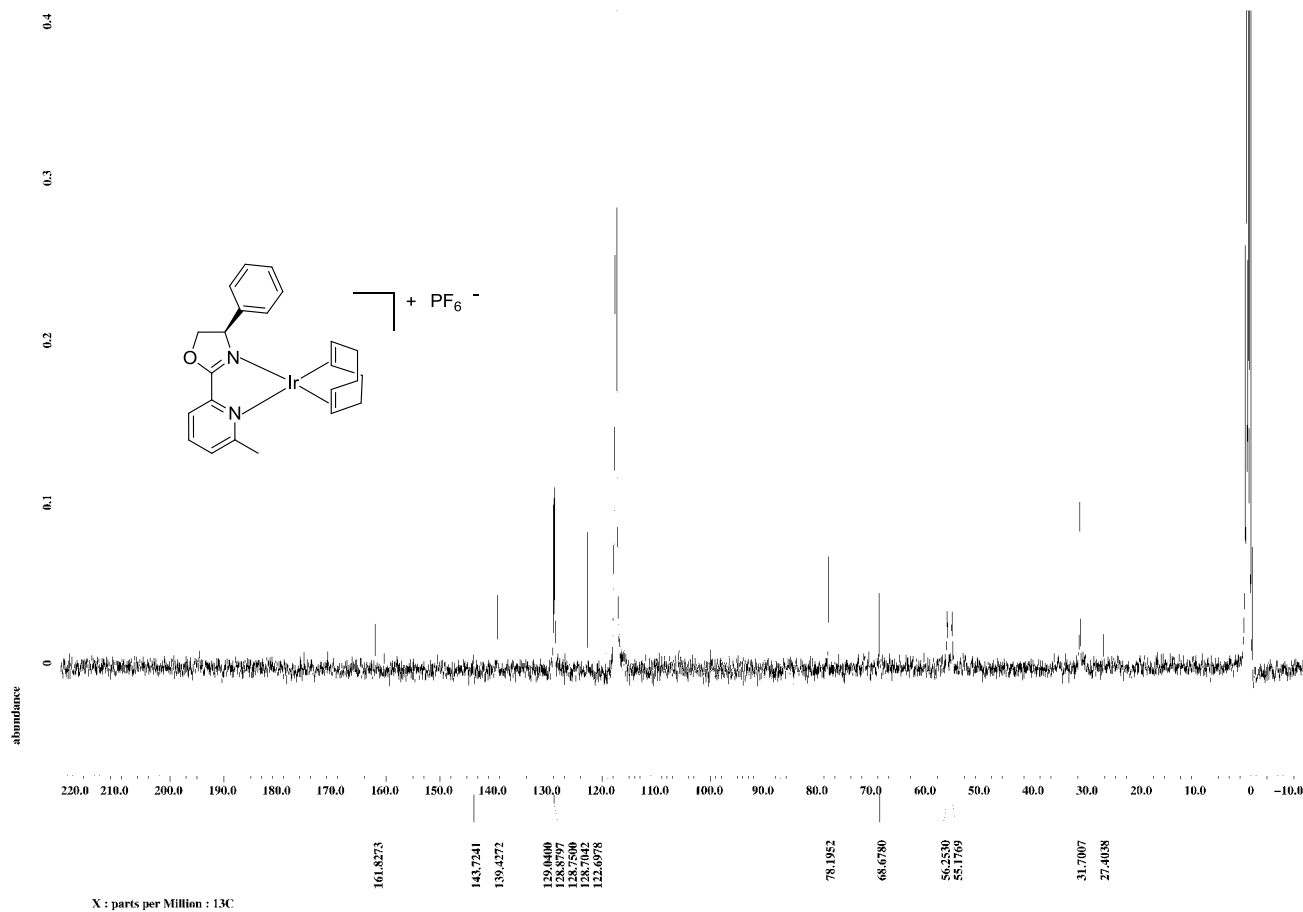
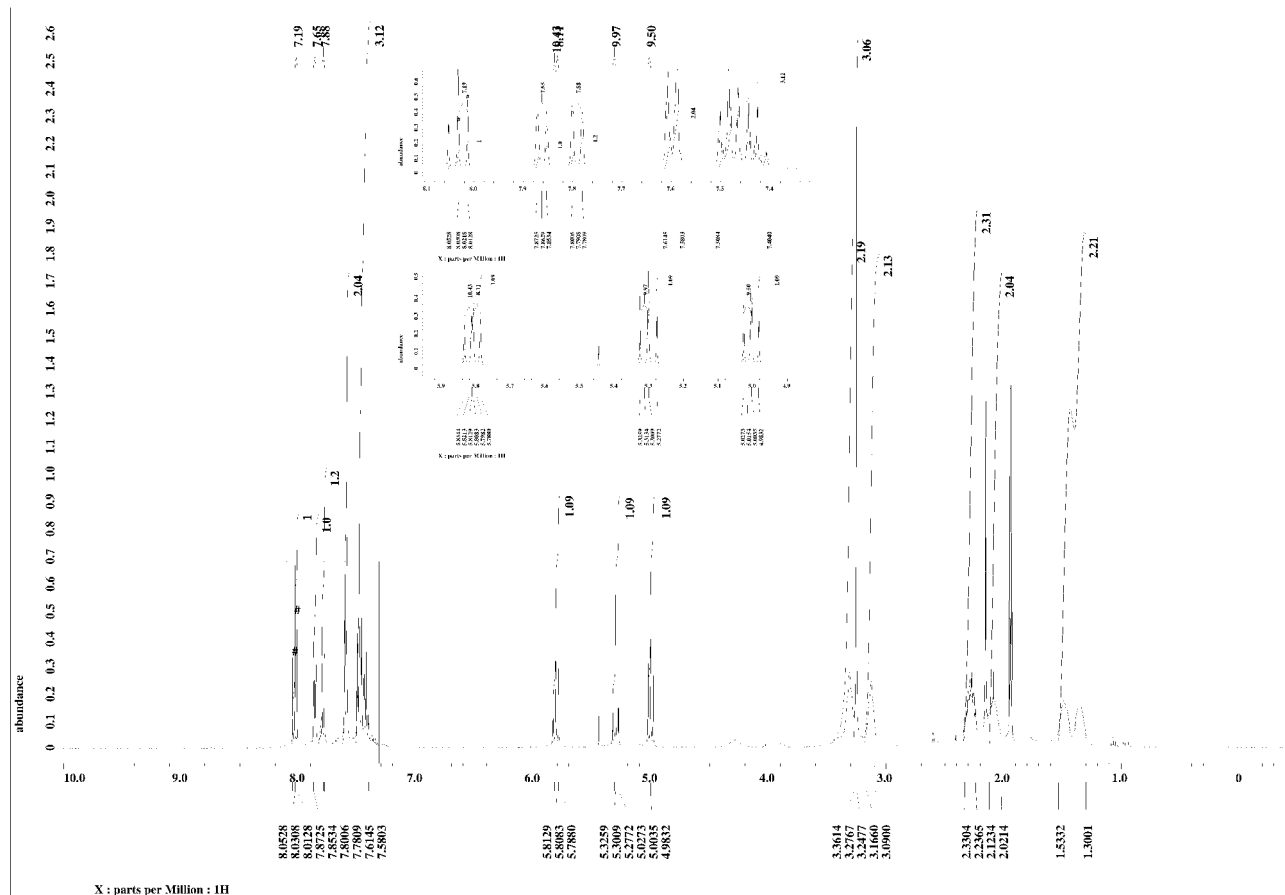
1,5-Cyclooctadiene[(*S*)-4-Isopropyl-2-(6-methylpyridin-2-yl)-oxazolin]iridium(I) hexafluorophosphate, [Ir(iPr-mepyx)(cod)]PF₆ (25j)



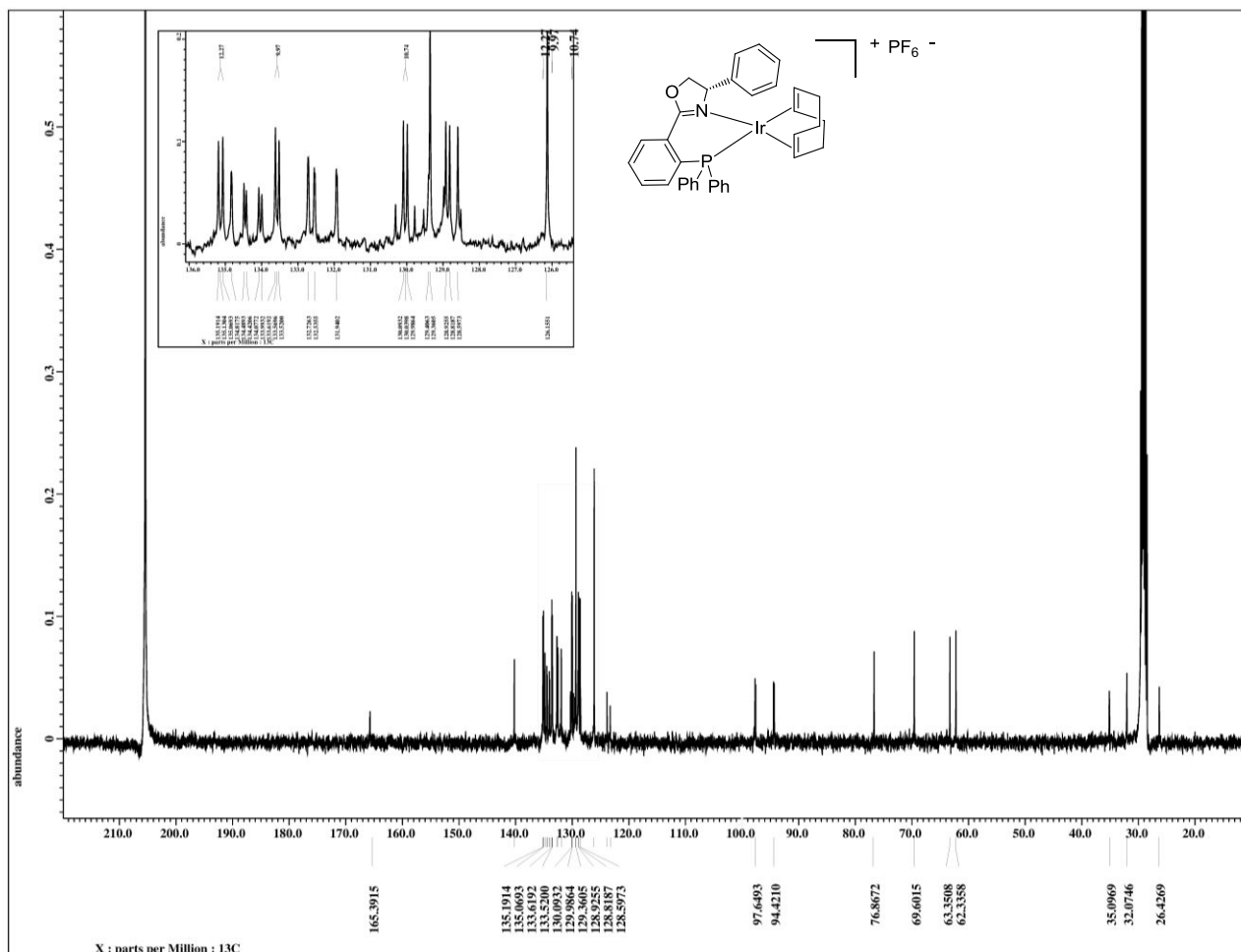
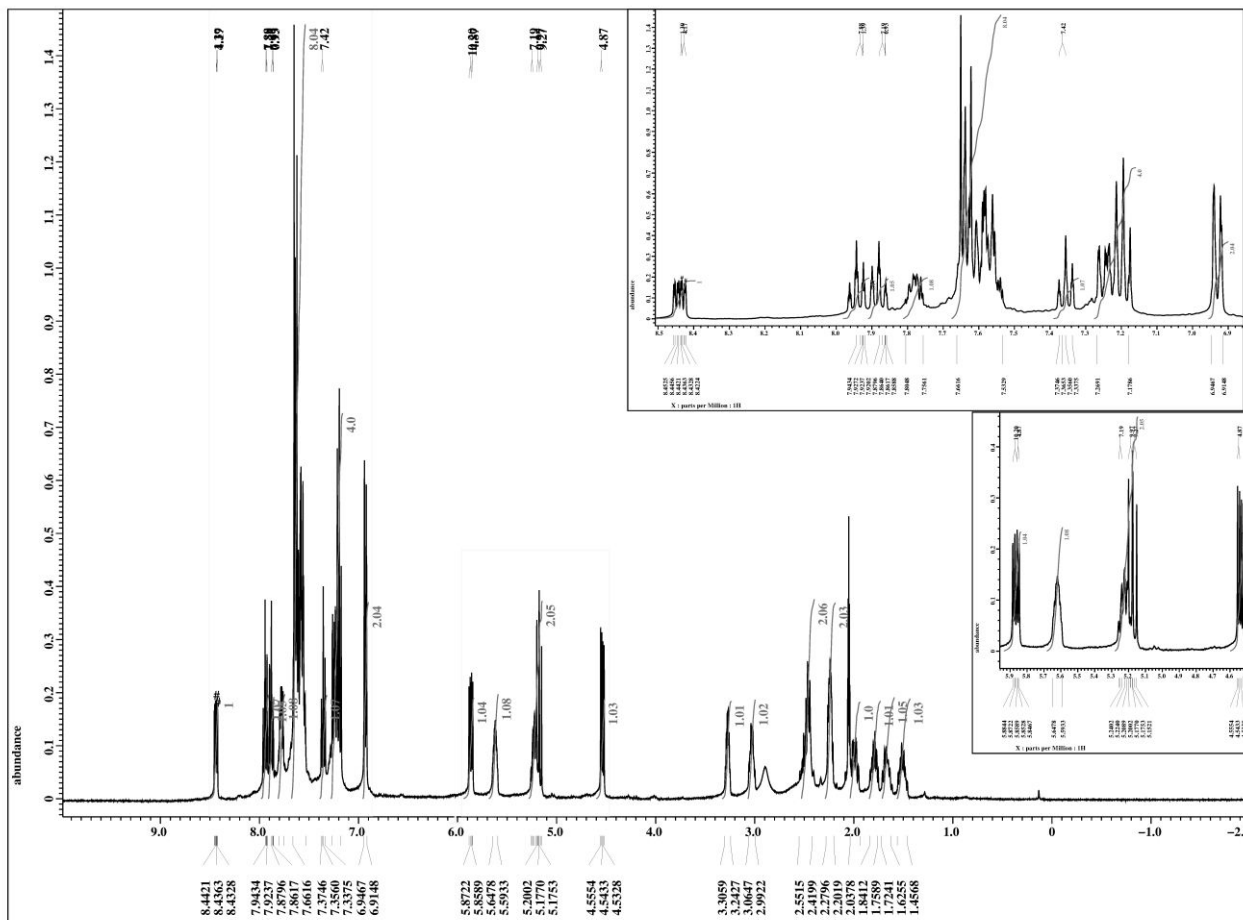
1,5-Cyclooctadiene[[*(S)*-4-butyl-2-(6-methylpyridin-2-yl)-oxazolin]iridium(I) hexafluorophosphate, [Ir(ⁿBu-mepyrox)(cod)]PF₆ (25k)



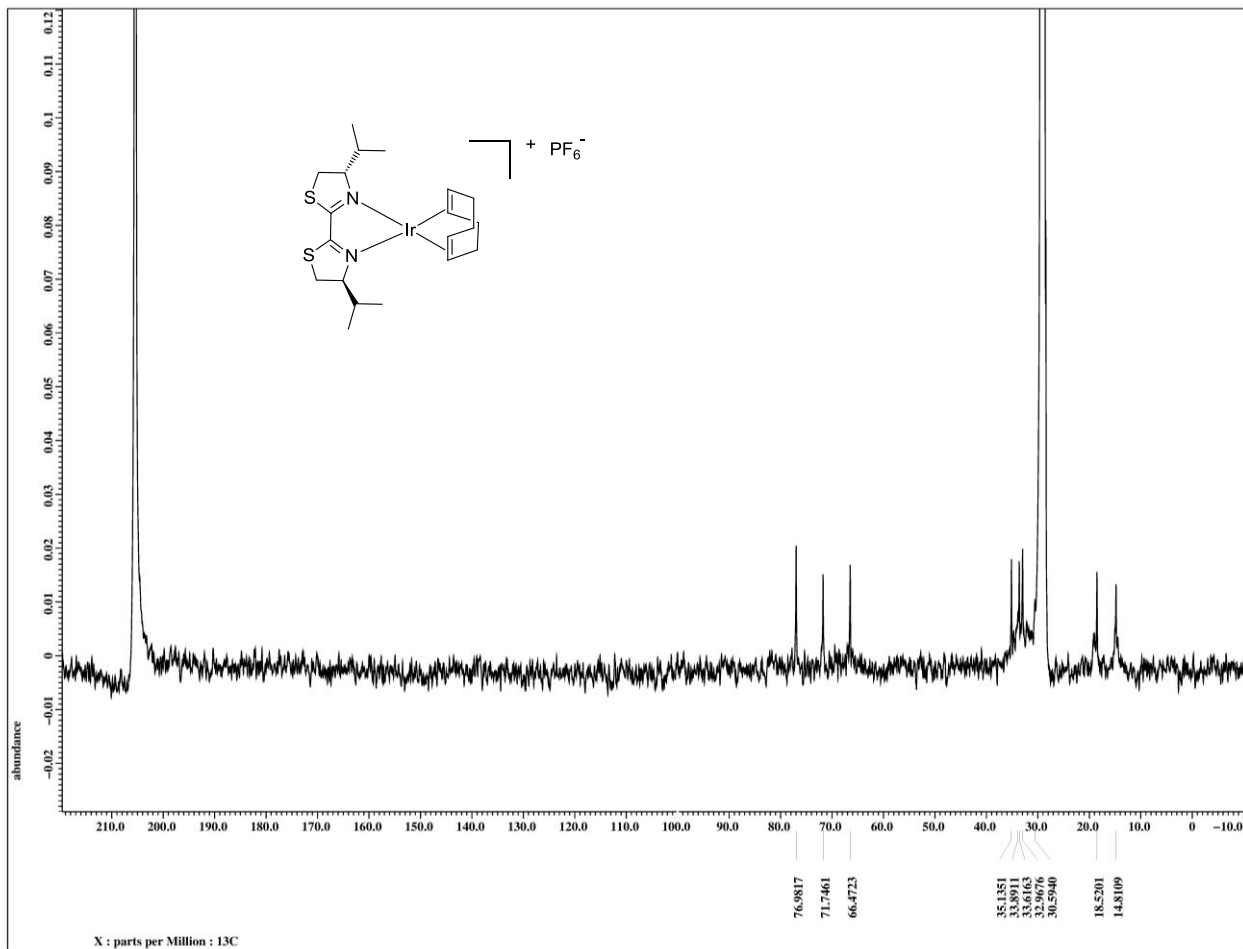
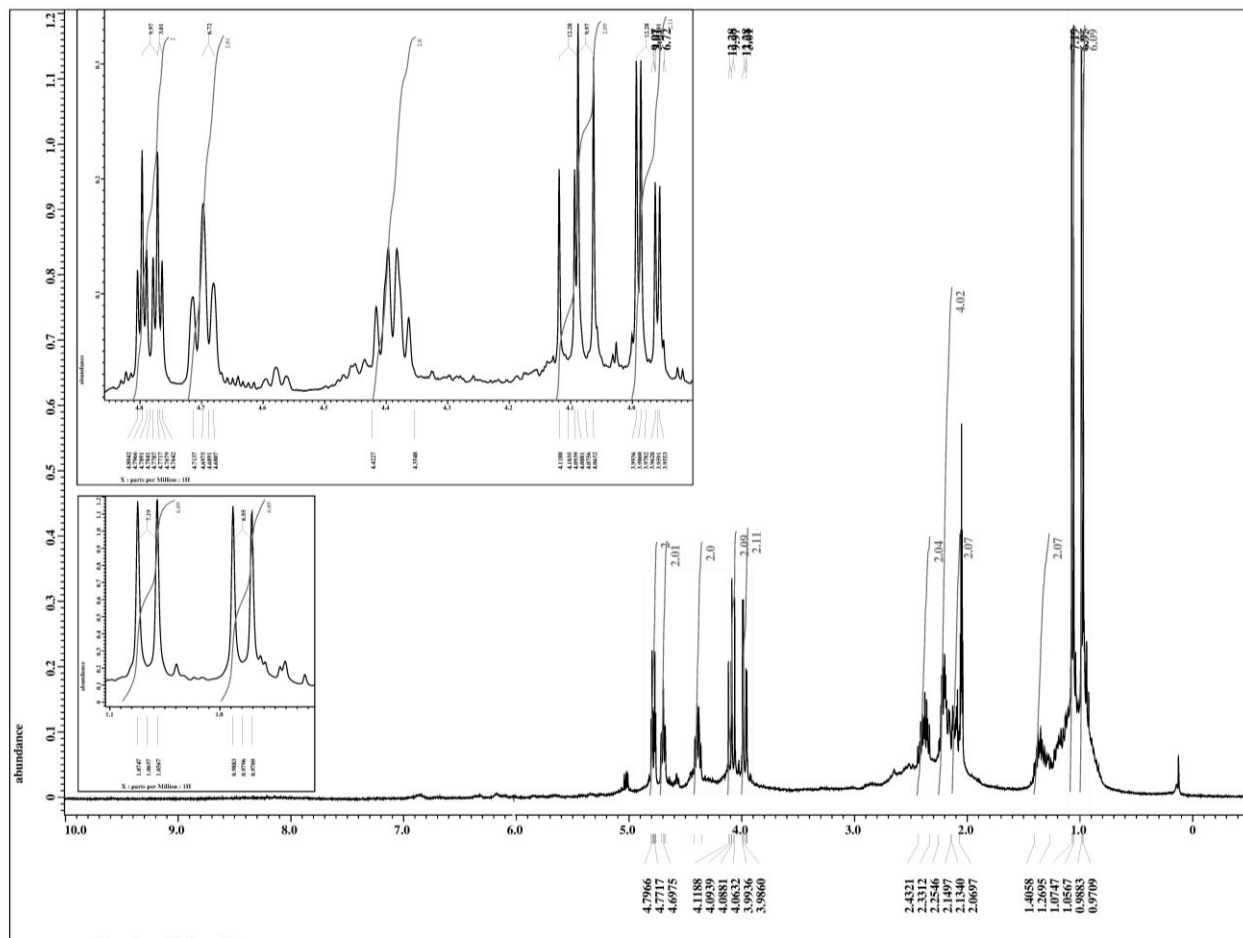
1,5-Cyclooctadiene[[*(R)*-2-(6-methylpyridin-2-yl)-4-phenyl-oxazolin]iridium(I) hexafluorophosphate, [Ir(Ph-mepyrox)(cod)]PF₆ (251)



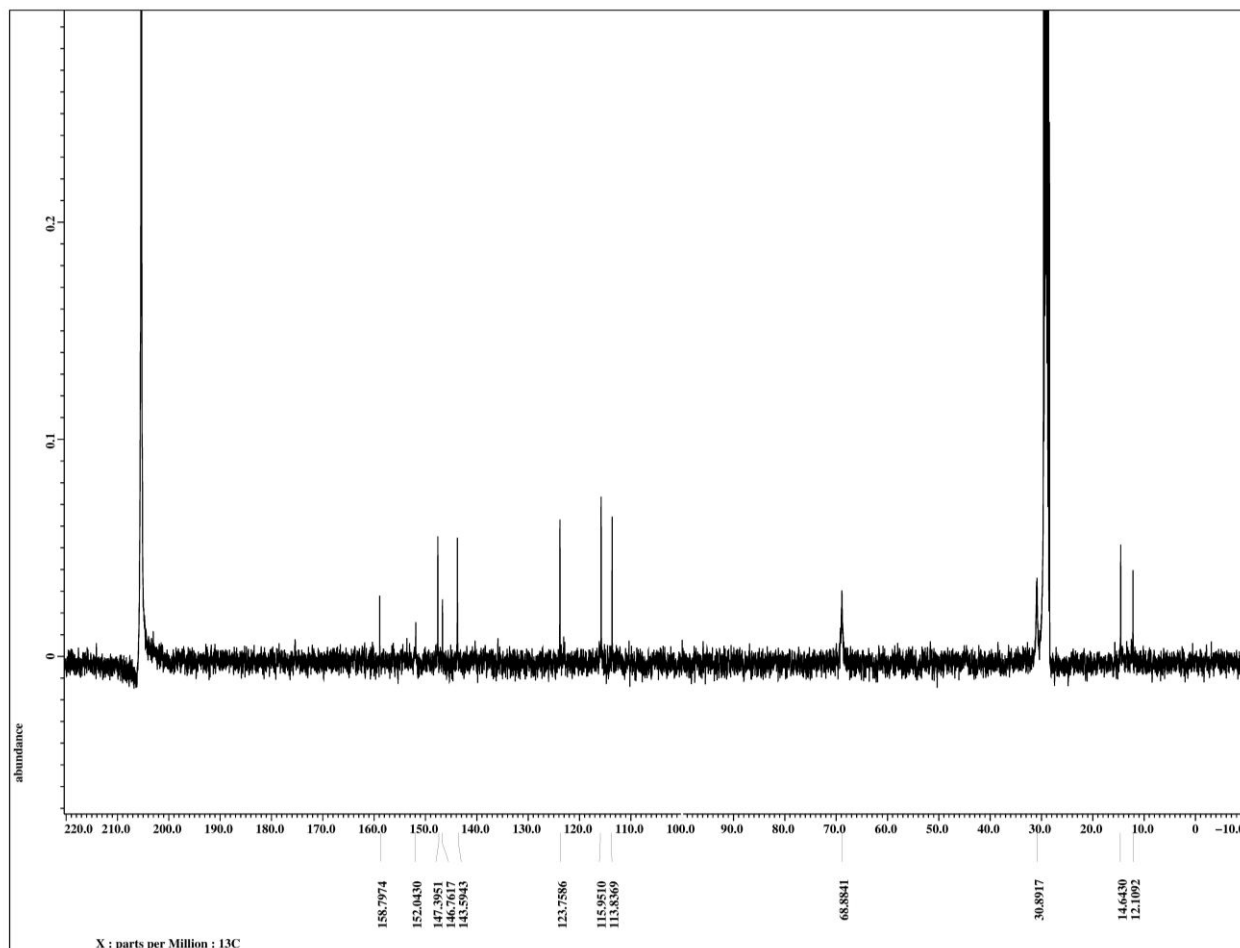
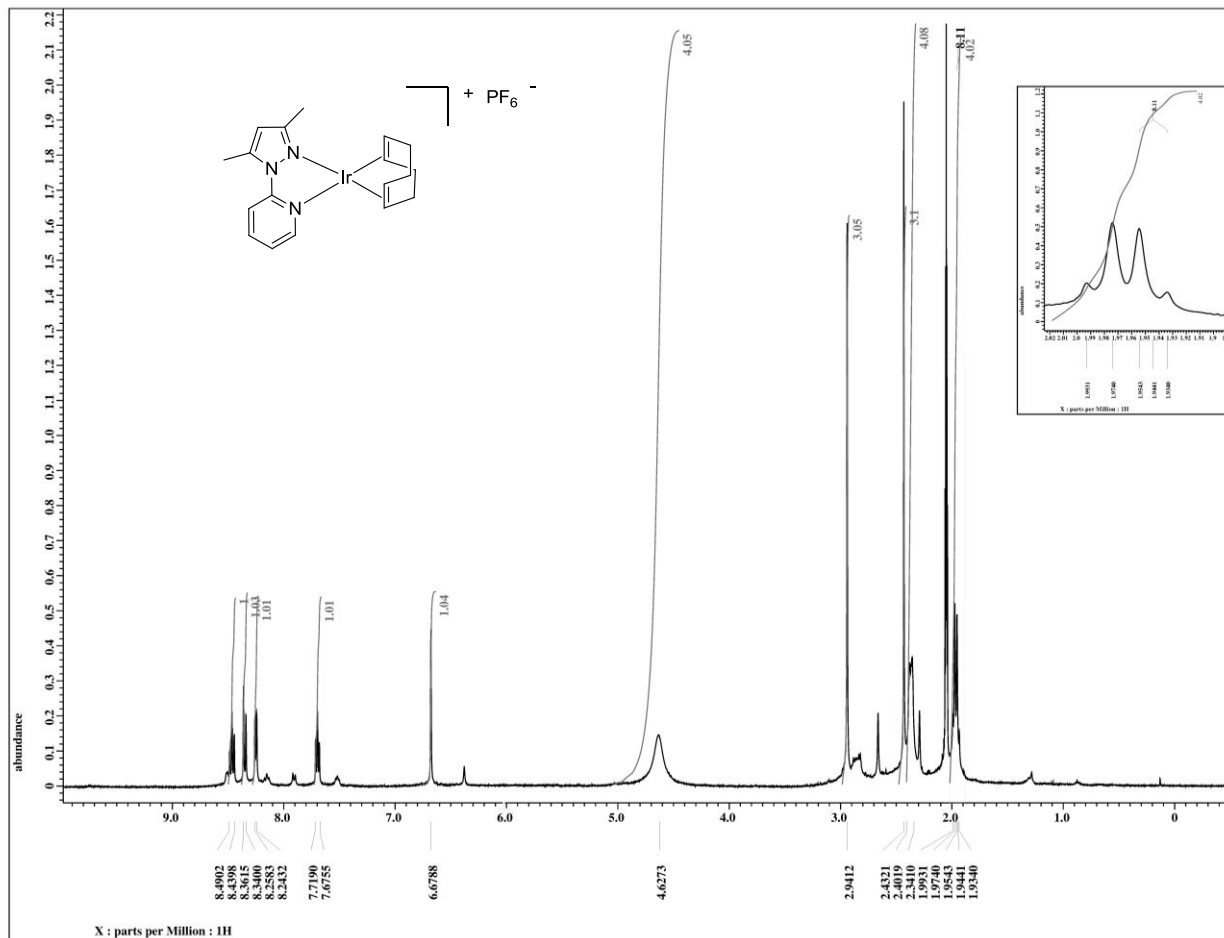
1,5-Cyclooctadiene[[*(S)*-2-(2-(diphenylphosphanyl)phenyl)-4-phenyl-oxazolin]iridium(I) hexafluorophosphate, [Ir(Ph-phox)(cod)]PF₆ (25u)



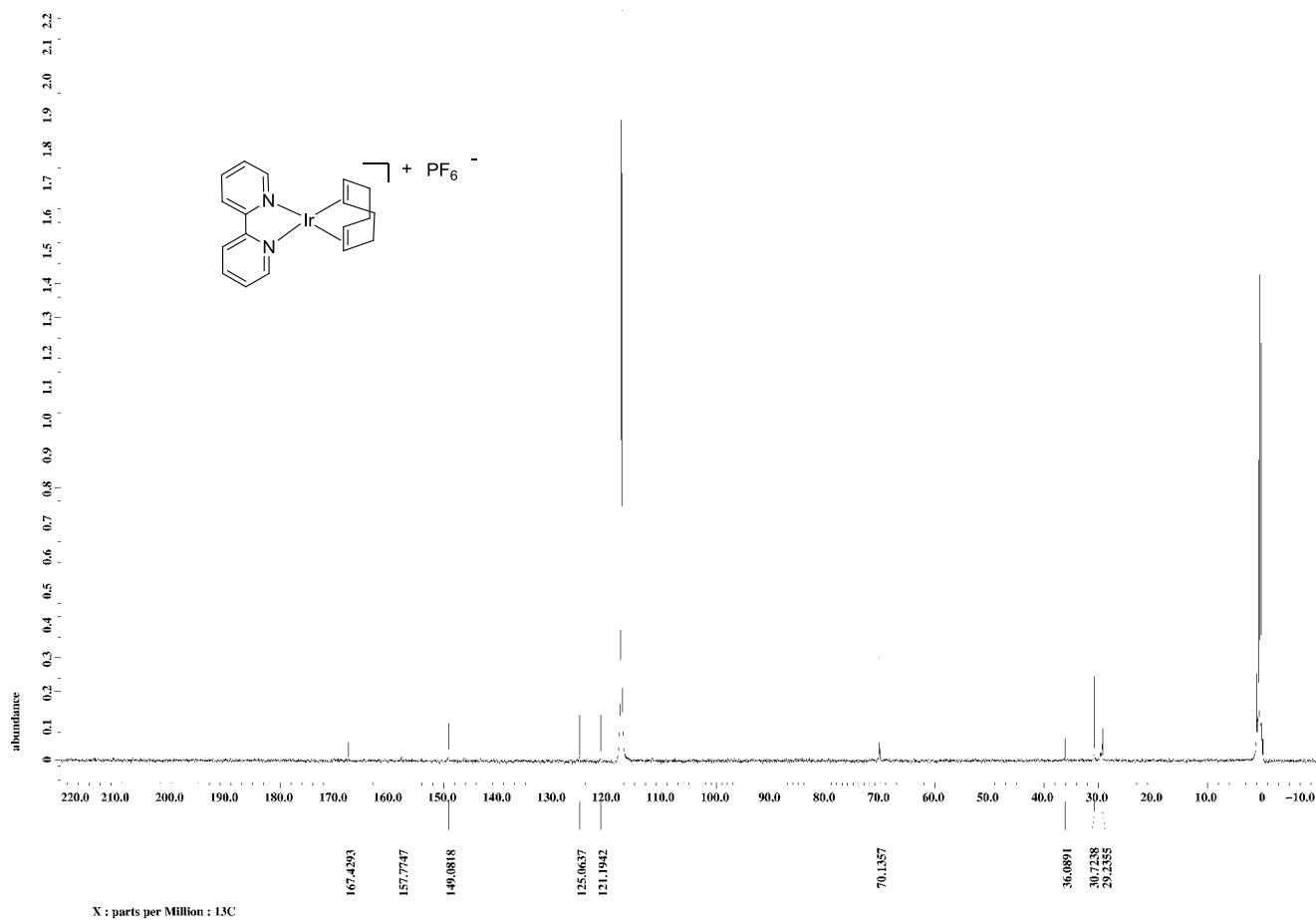
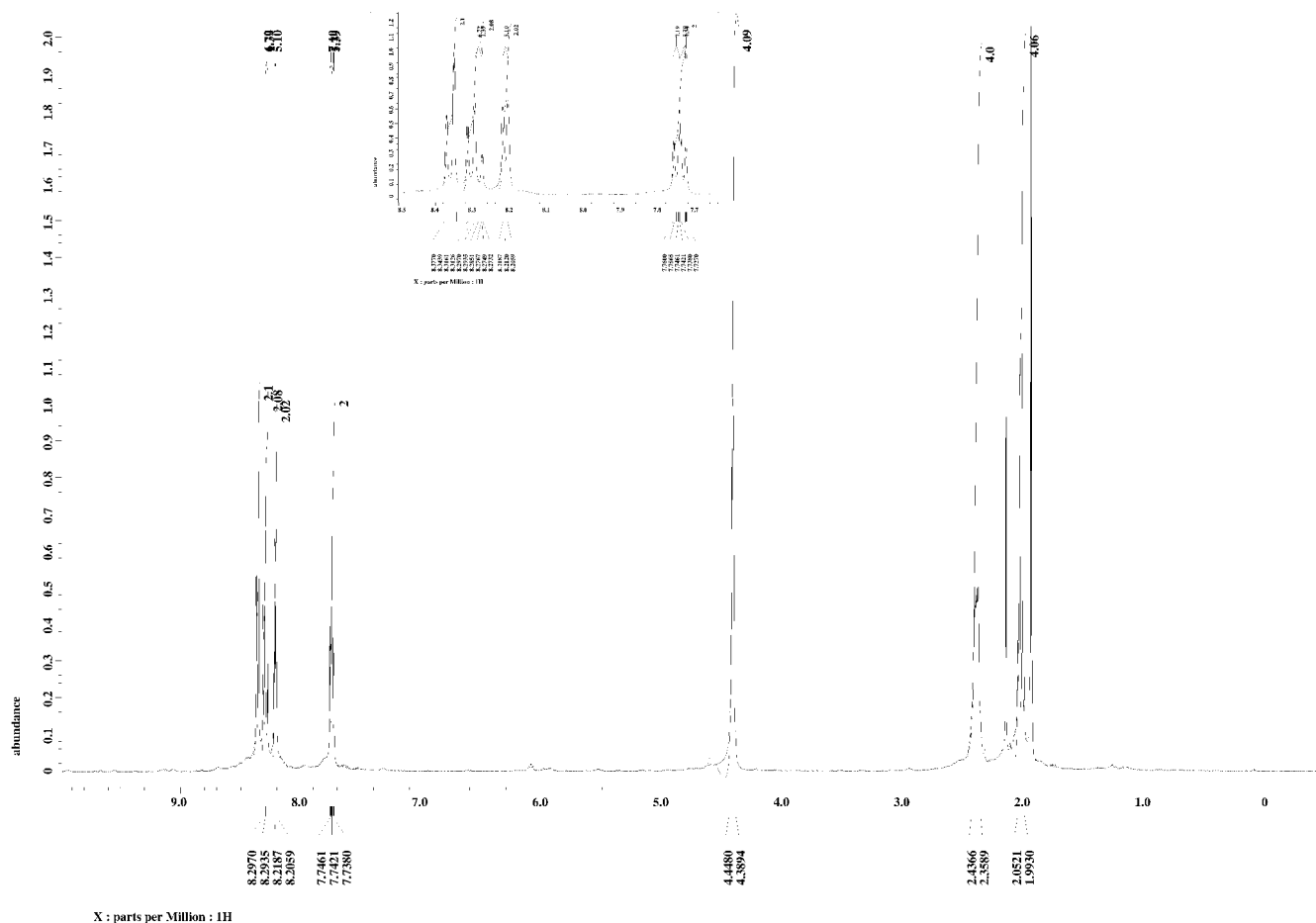
1,5-Cyclooctadiene[*((4S,4'S)*-4,4'-diisopropyl-2,2'-bithiazolin)]iridium(I) hexafluorophosphate, [Ir(ⁱPr-bta)(cod)]PF₆ (25g)



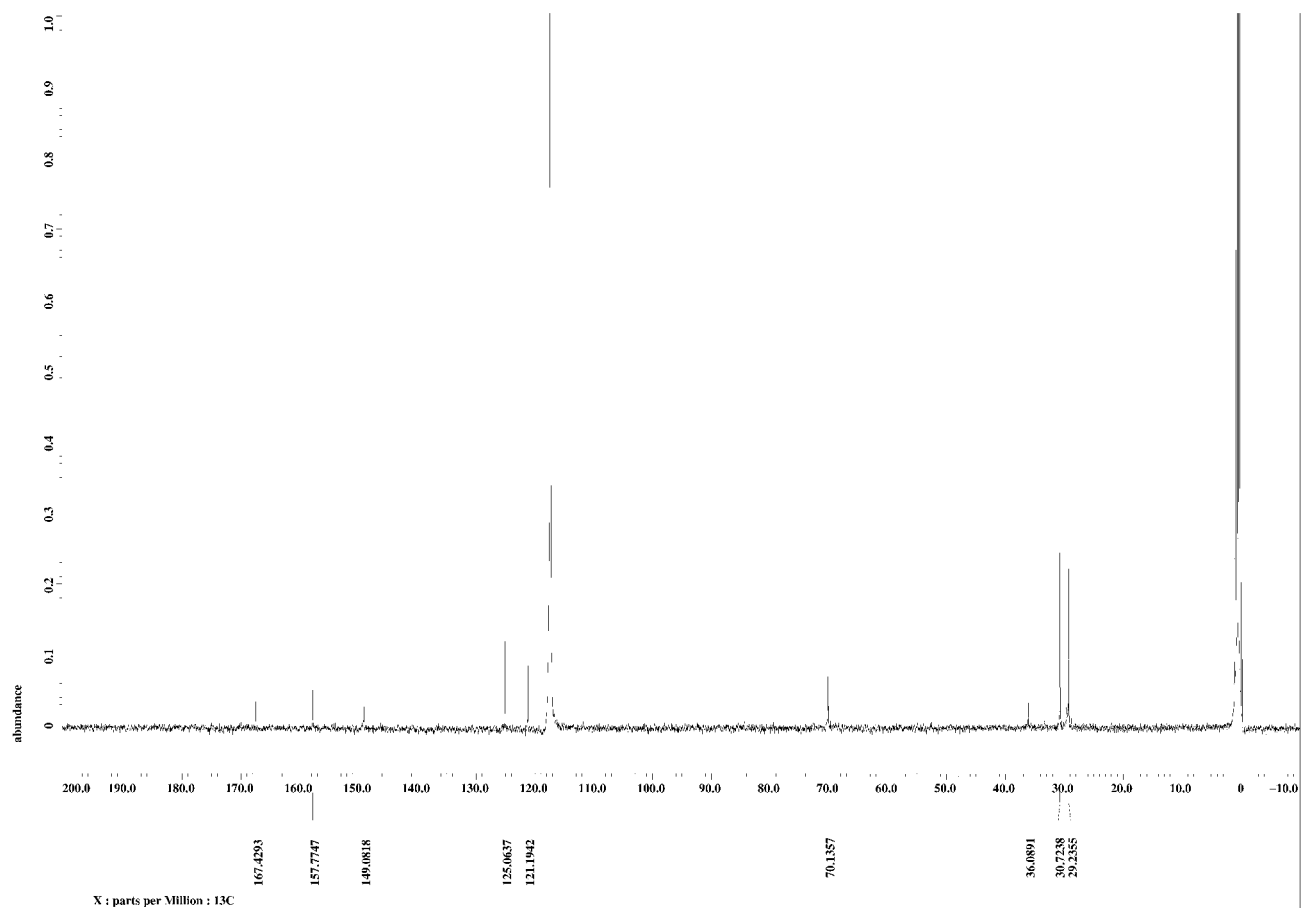
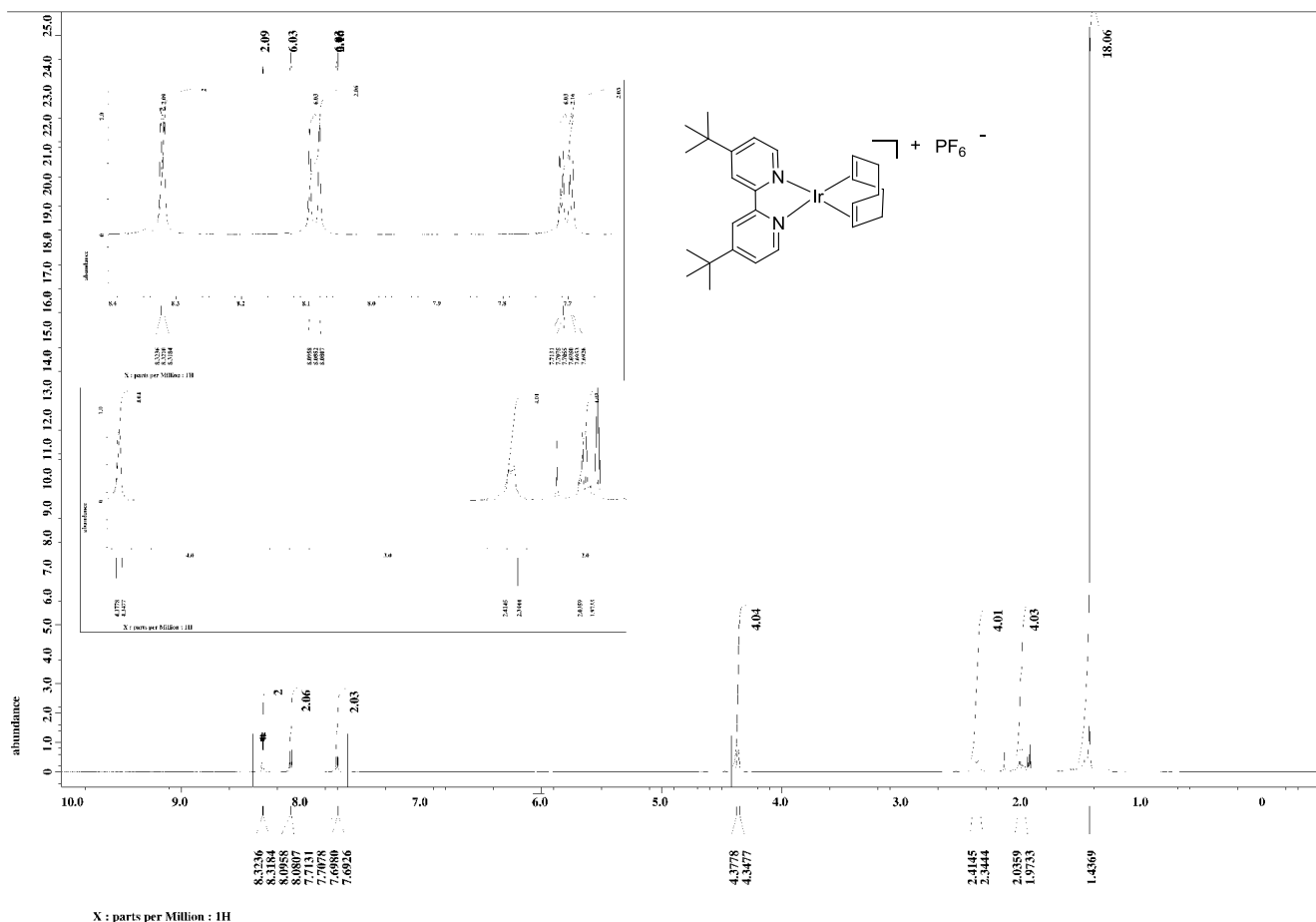
1,5-Cyclooctadiene[(2-(3,5-dimethyl-1*H*-pyrazol-1-yl)pyridine)]iridium(I) hexafluorophosphate, [Ir(pypyraz)(cod)]PF₆ (25v)



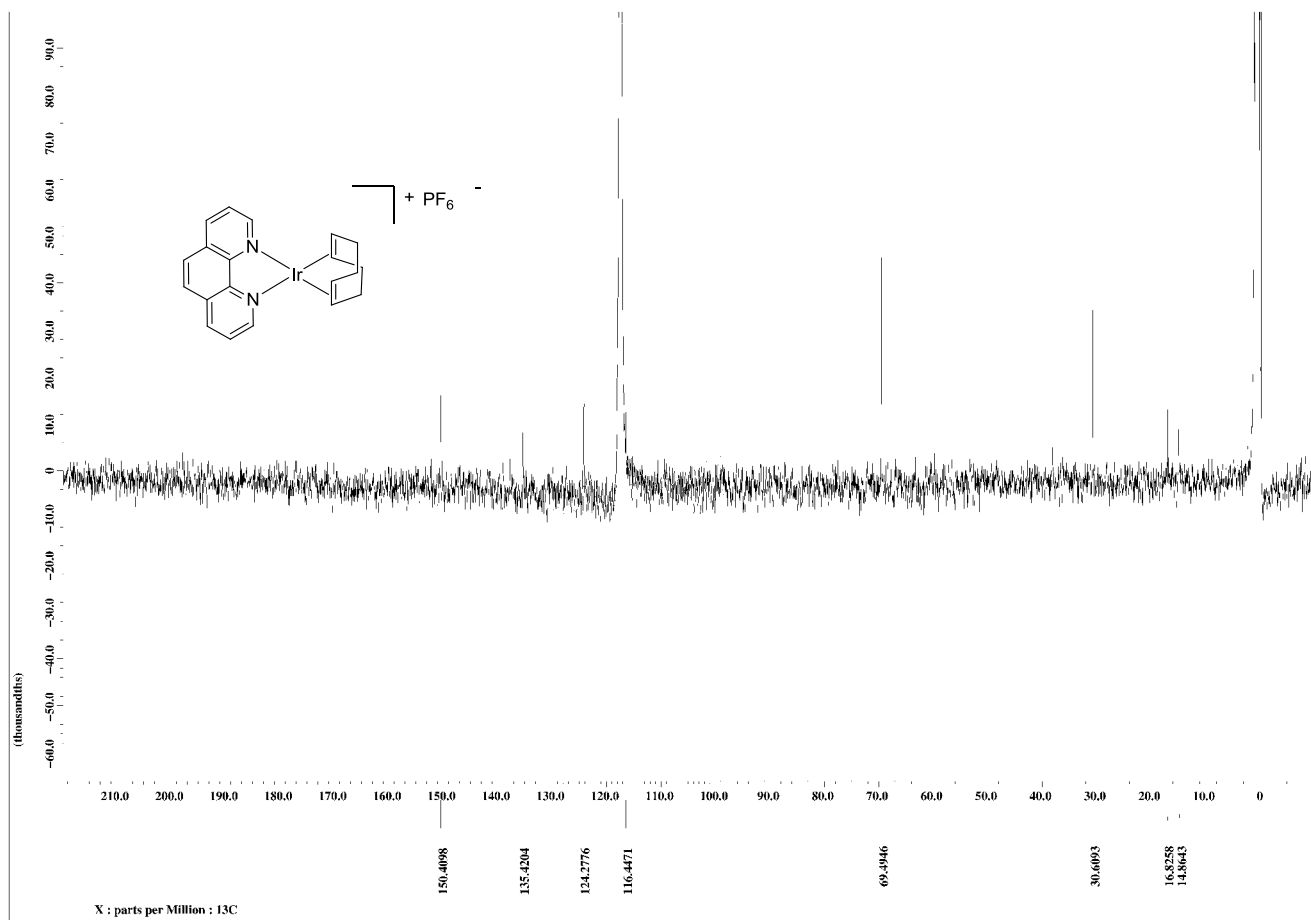
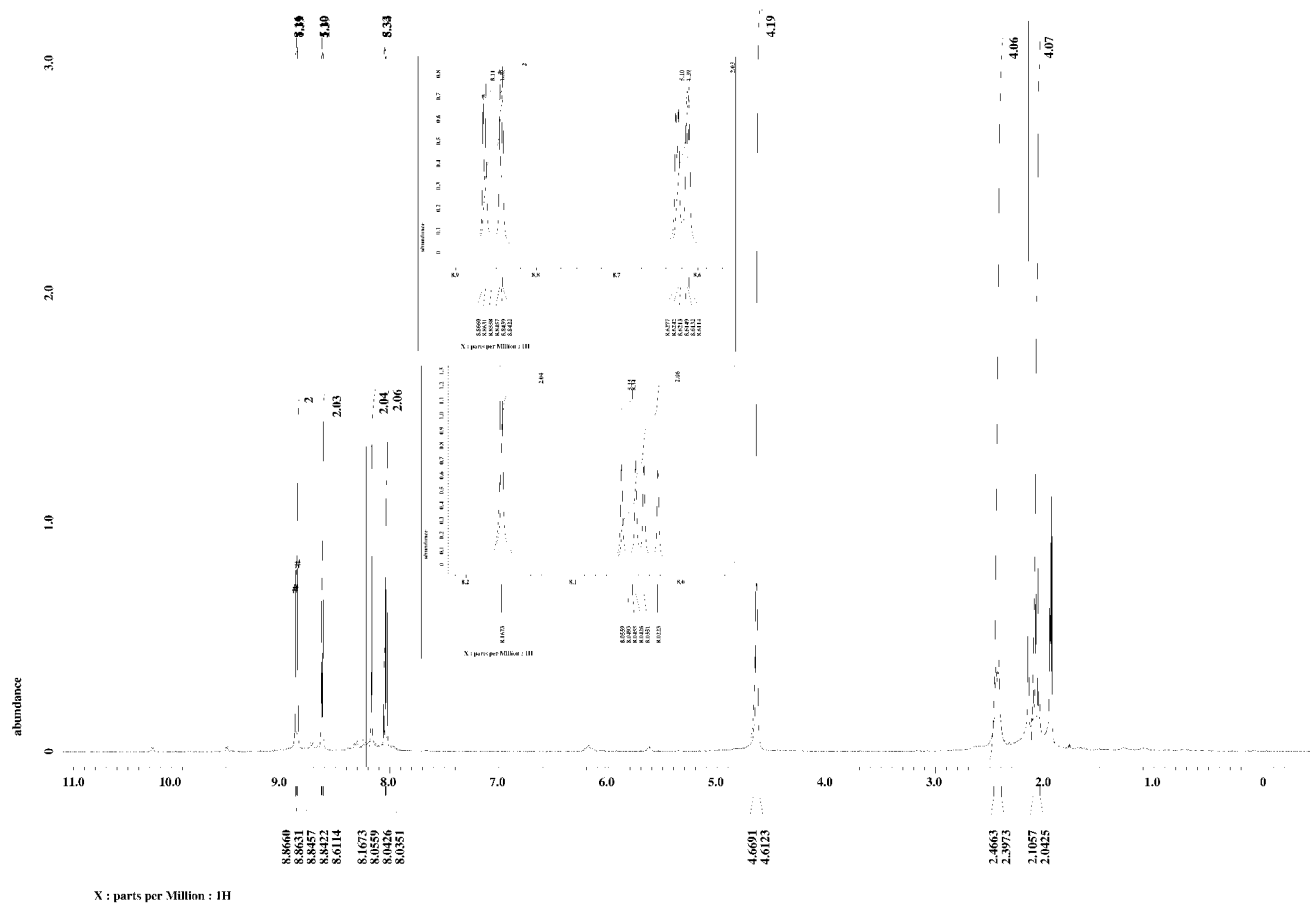
1,5-Cyclooctadiene[(2,2'-bipyridine)]iridium(I) hexafluorophosphate, [Ir(dtbpv)(cod)]PF₆ (25q)



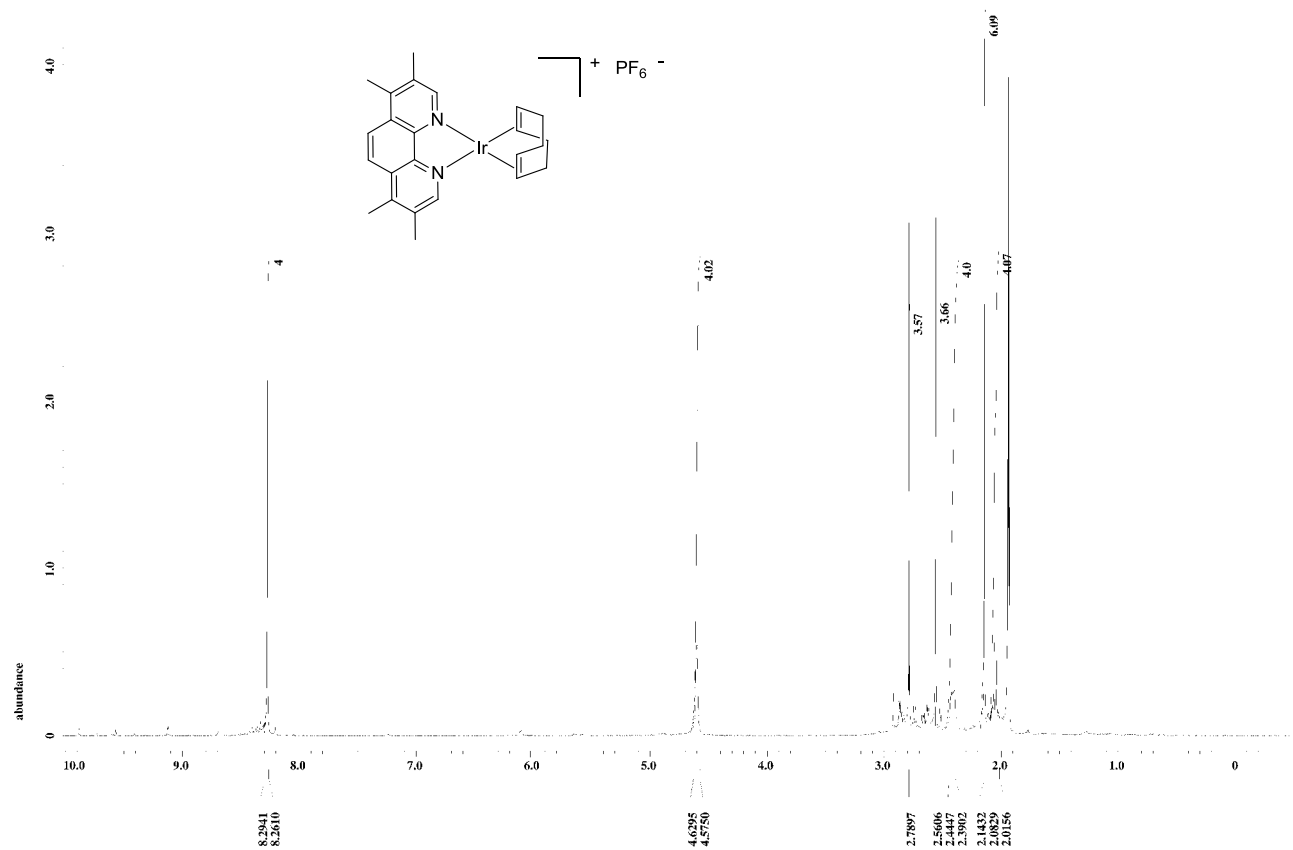
1,5-Cyclooctadiene[(4,4'-di-tert-butyl-2,2'-bipyridine)]iridium(I) hexafluorophosphate, [Ir(dtbpv)(cod)]PF₆ (25r)



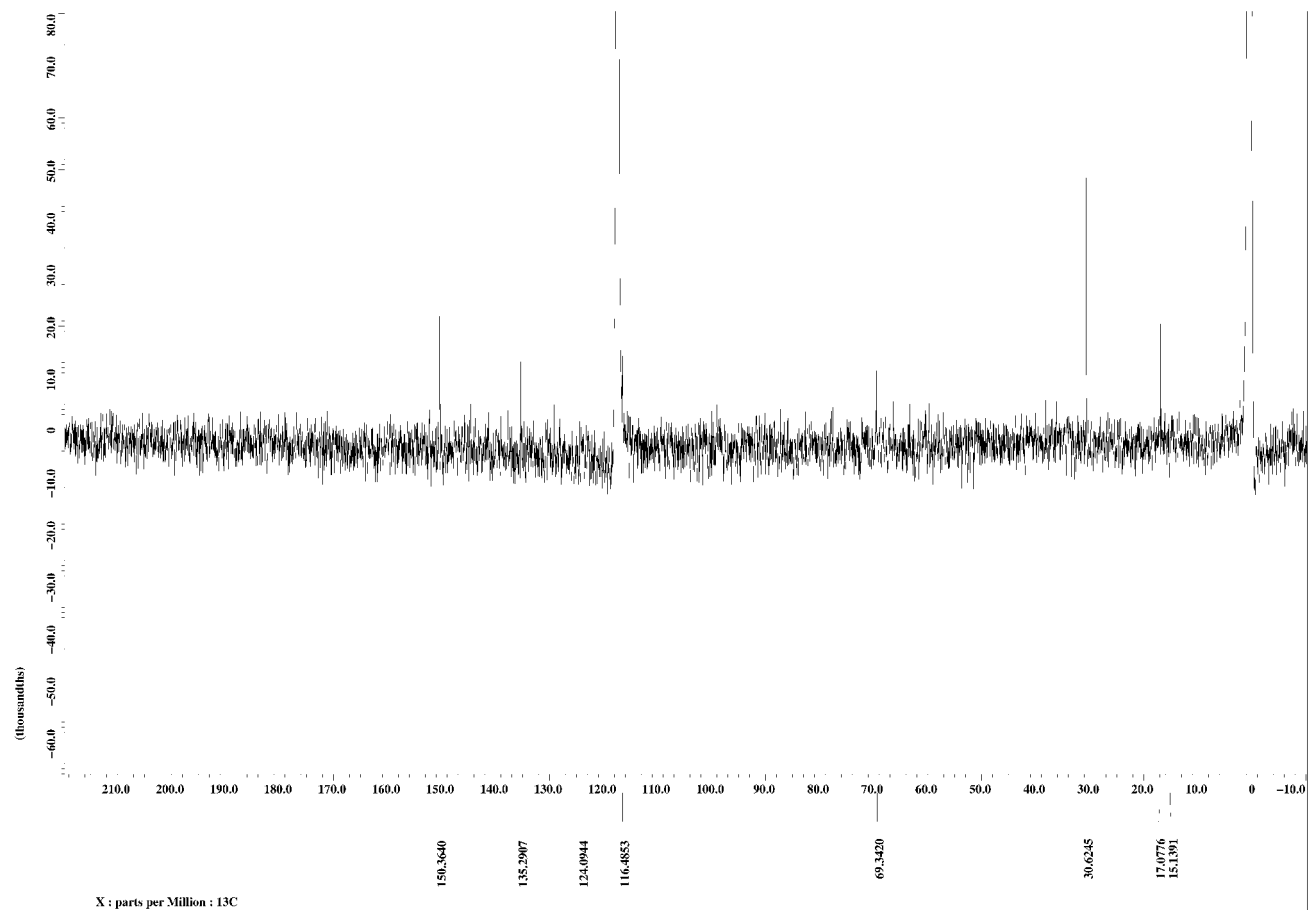
1,5-Cyclooctadiene[(1,10-phenanthroline)]iridium(I) hexafluorophosphate, [Ir(phen)(cod)]PF₆ (25s)



1,5-Cyclooctadiene[(3,4,7,8-tetramethyl-1,10-phenanthroline)iridium(I) hexafluorophosphate, [Ir(TMphen)(cod)]PF₆ (25t)

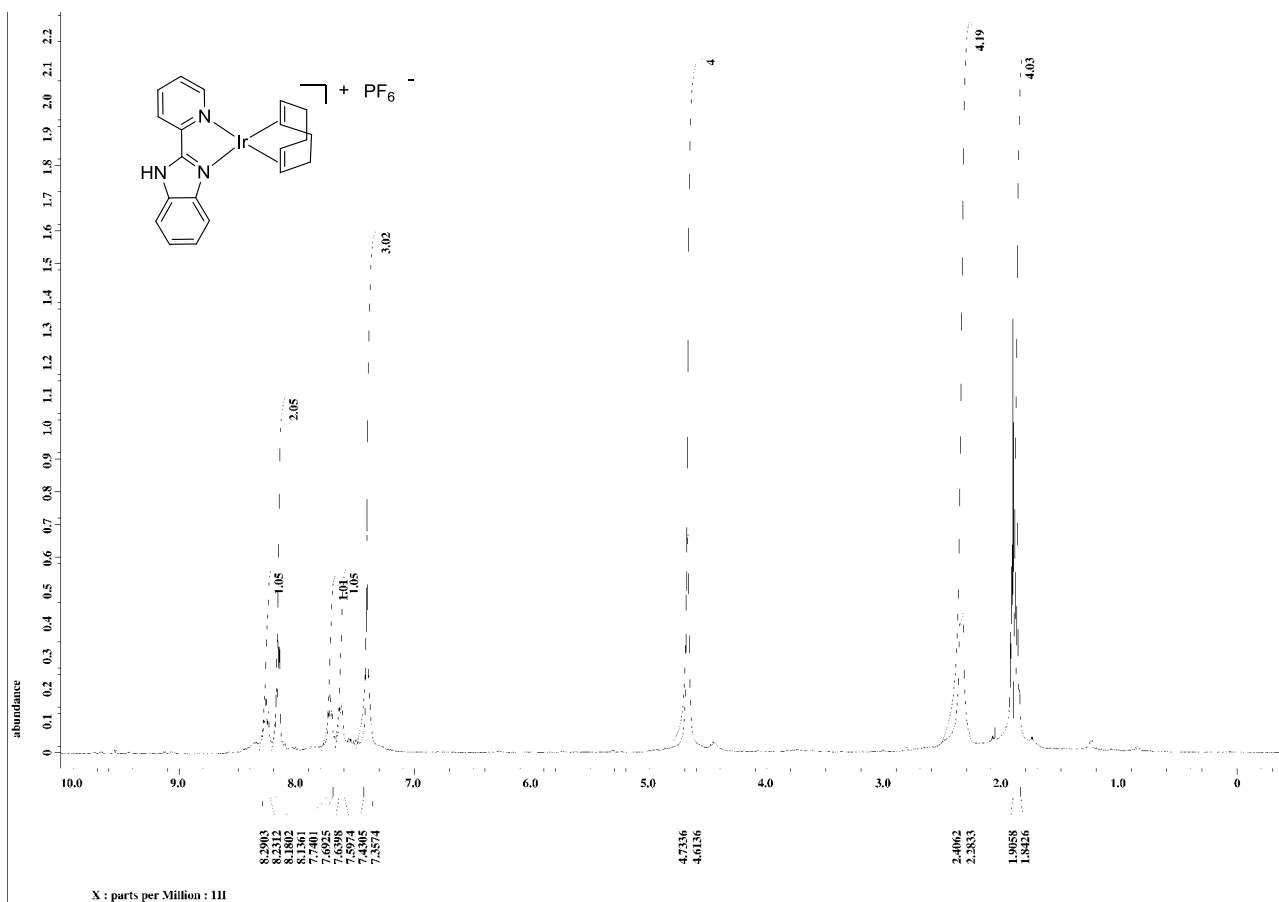


X : parts per Million : 1H

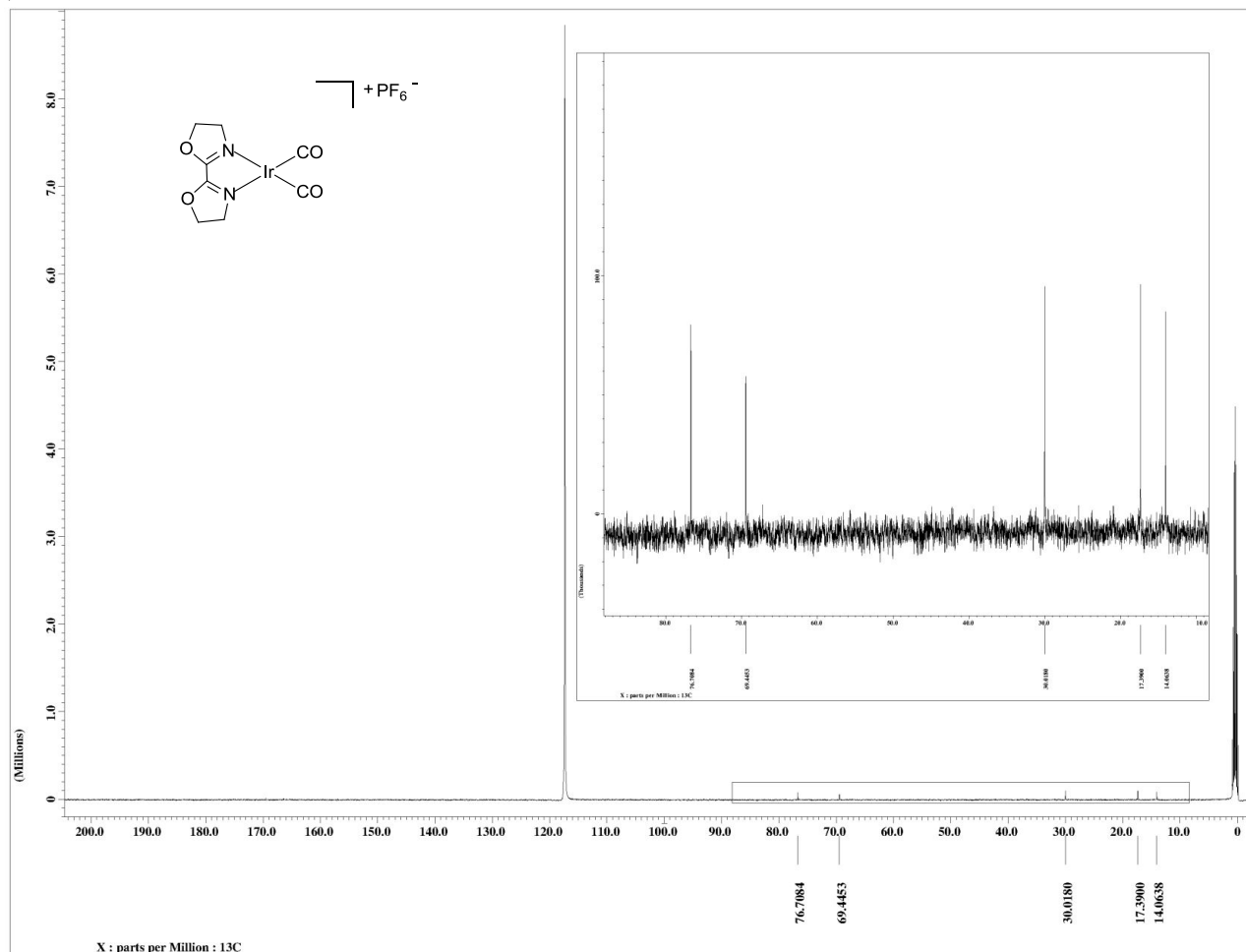
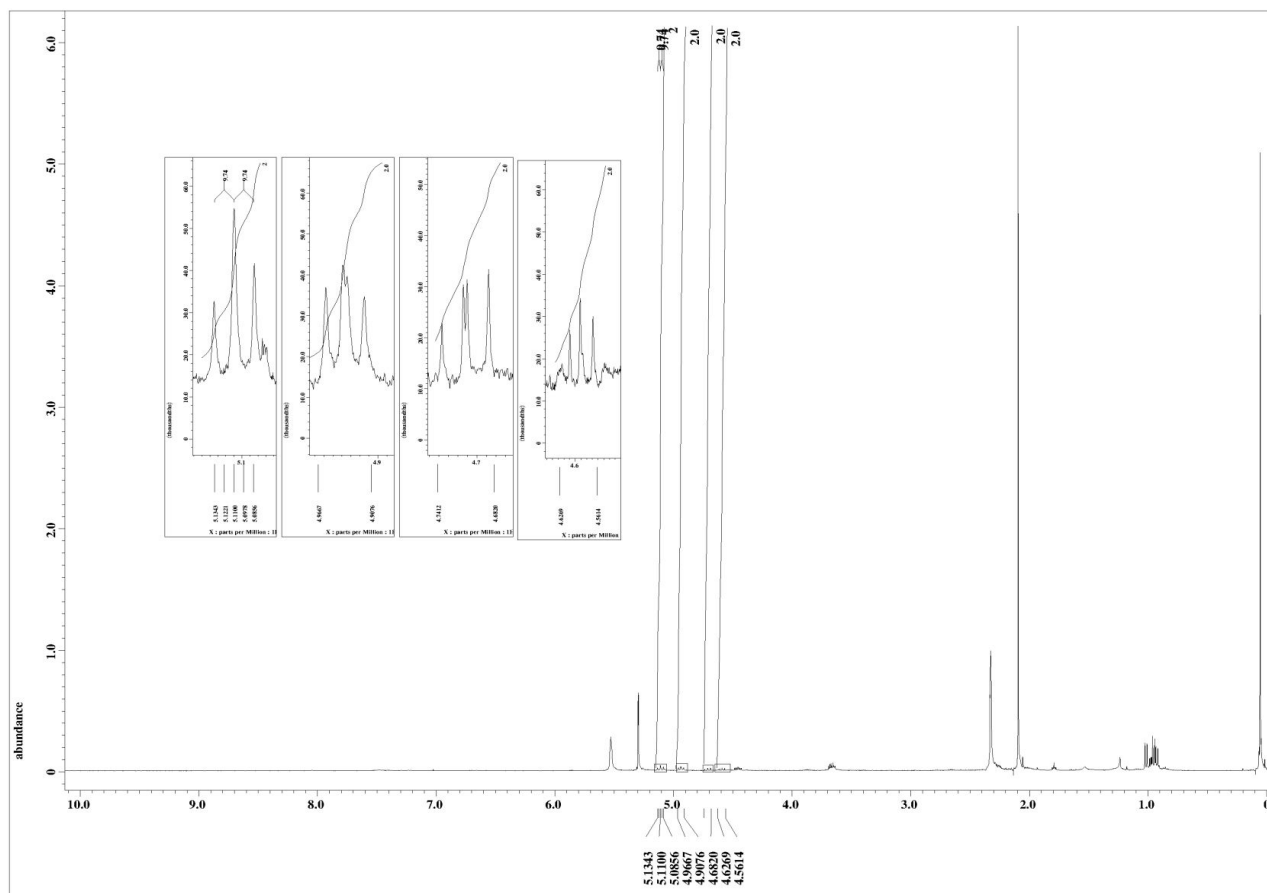


X : parts per Million : 13C

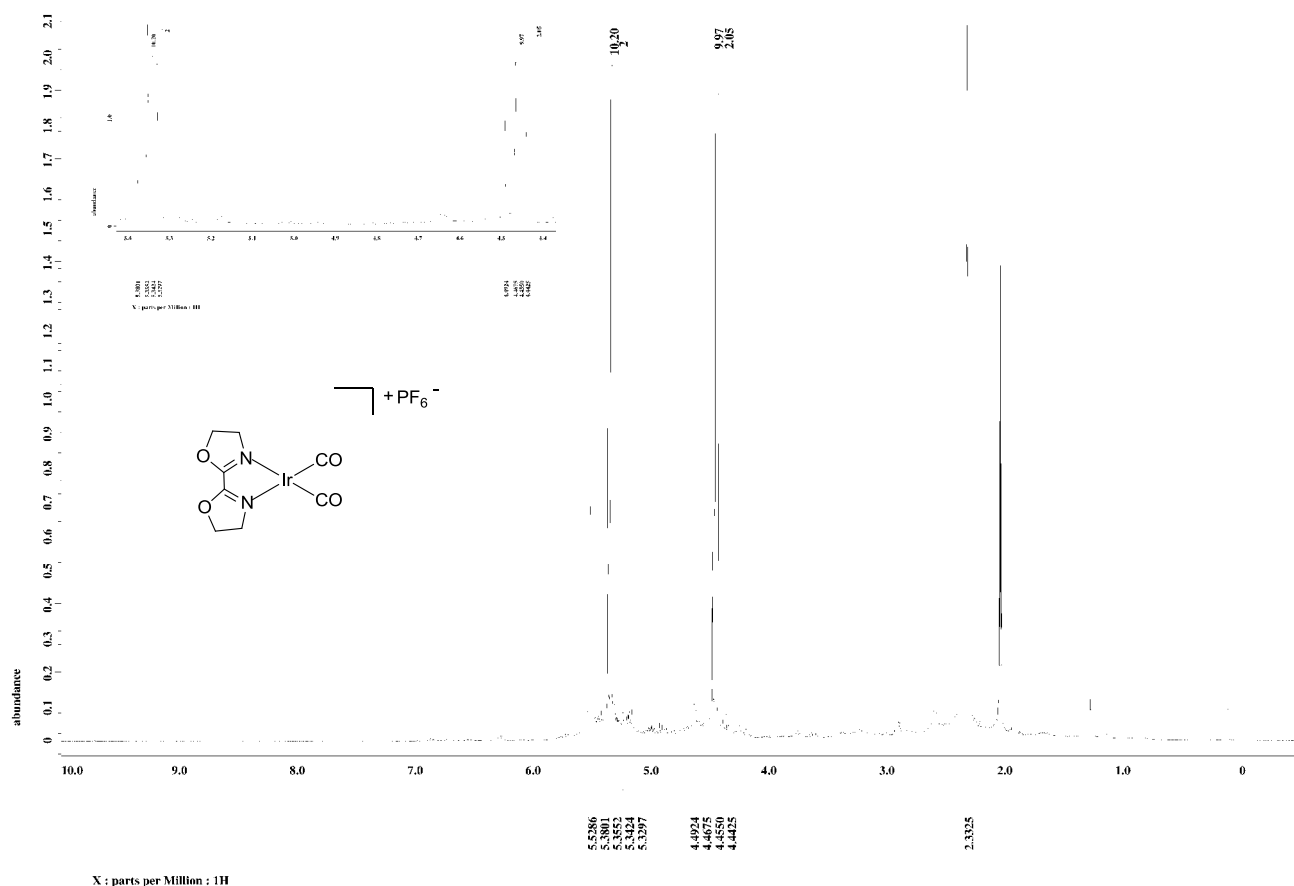
1,5-Cyclooctadiene[2-(pyridine-2-yl)-1H-benzo[d]imidazole]iridium(I) hexafluorophosphate, [Ir(TMphen)(cod)]PF₆ (25v)



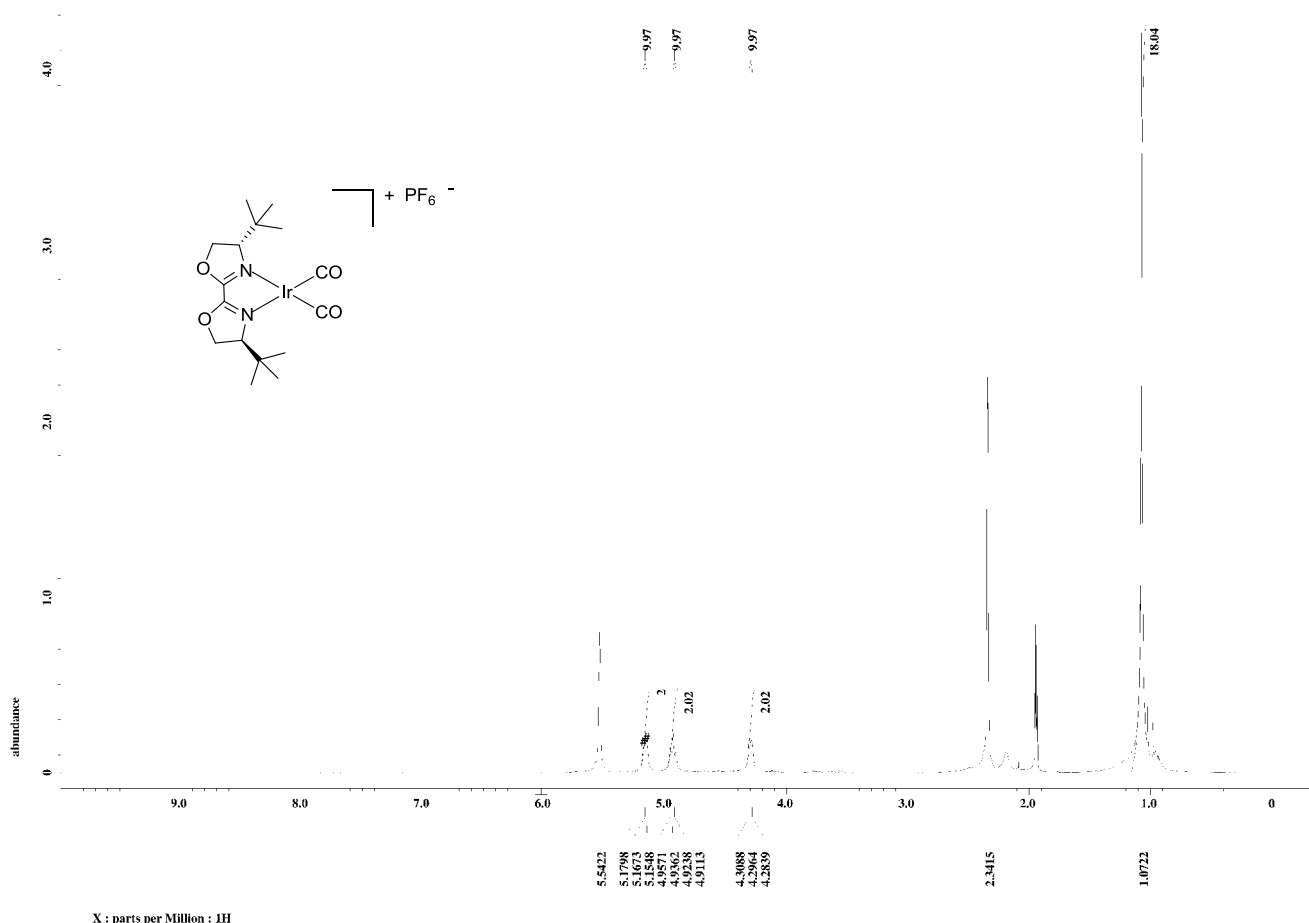
Bis-carbonyl[(2,2'-bioxazole)]iridium(I) hexafluorophosphate, [Ir(H-box)(CO)₂]PF₆ (28a) (spectrum in CD₂Cl₂)



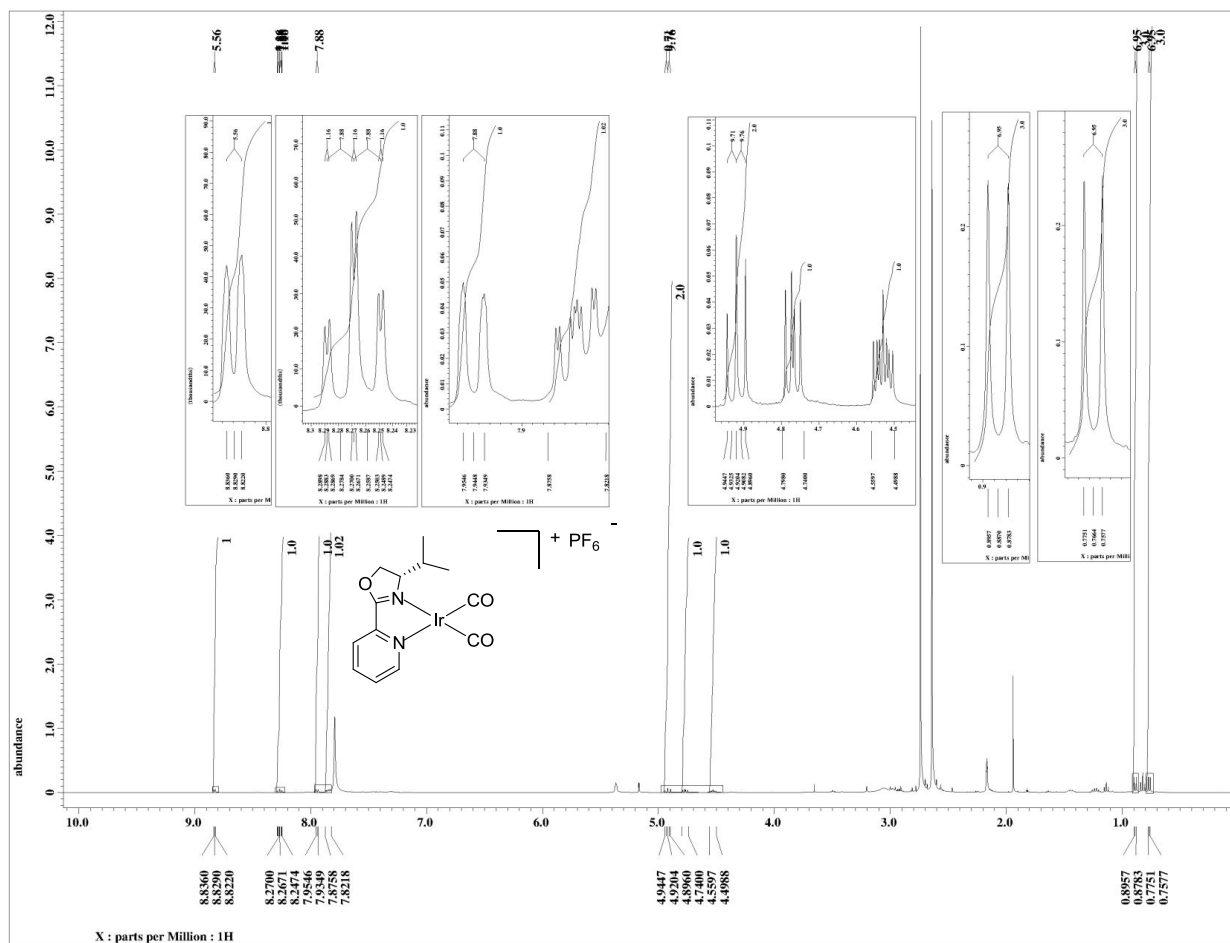
Bis-carbonyl[(2,2'-bioxazole)]iridium(I) hexafluorophosphate, [Ir(H-box)(CO)₂]PF₆ (28a) (spectrum in Acetone-d₆, from crude reaction mixture)



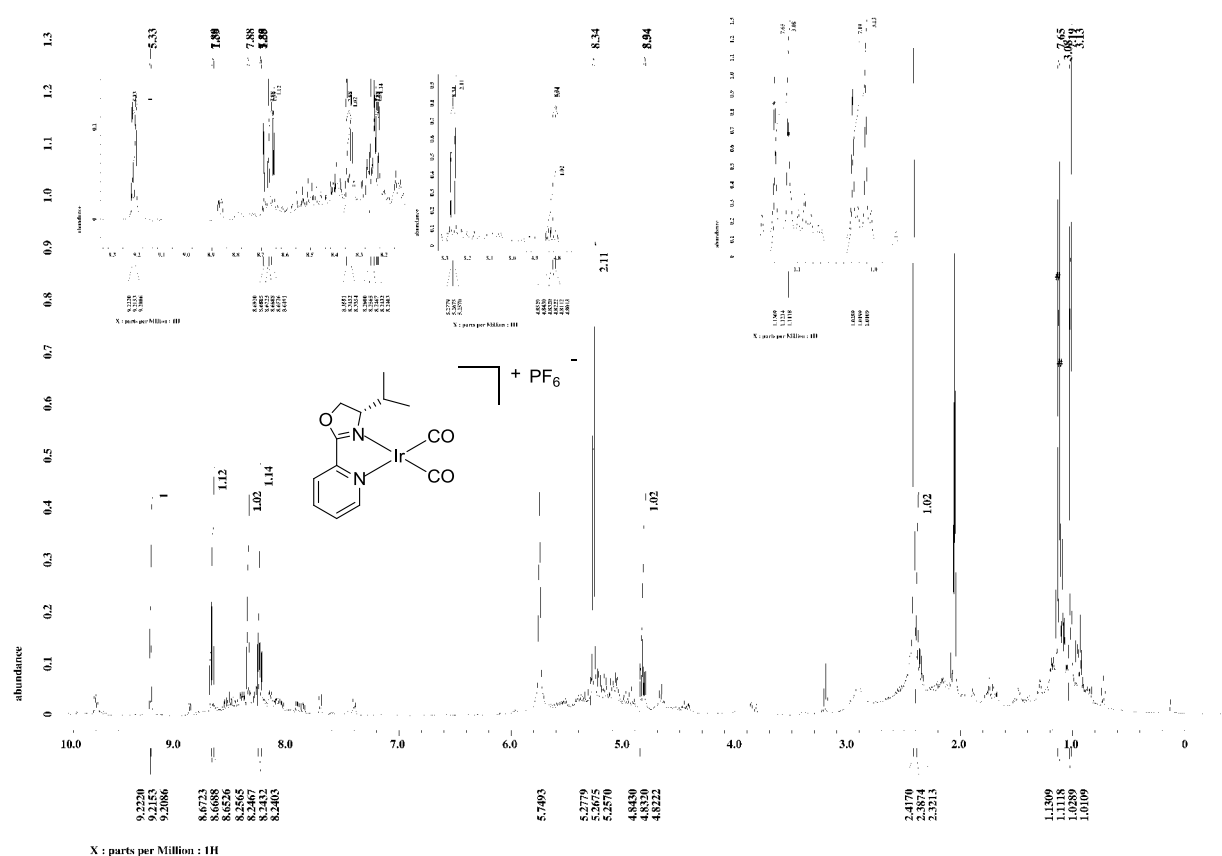
Bis-carbonyl [(2,2'-Bis((4S,4'S)-4,4'-di-tert-butyl-oxazolin)]iridium(I) hexafluorophosphate, [Ir(^tBu-box)(cod)]PF₆ (28d) (spectrum in Acetonitrile-d₃, from crude reaction mixture)



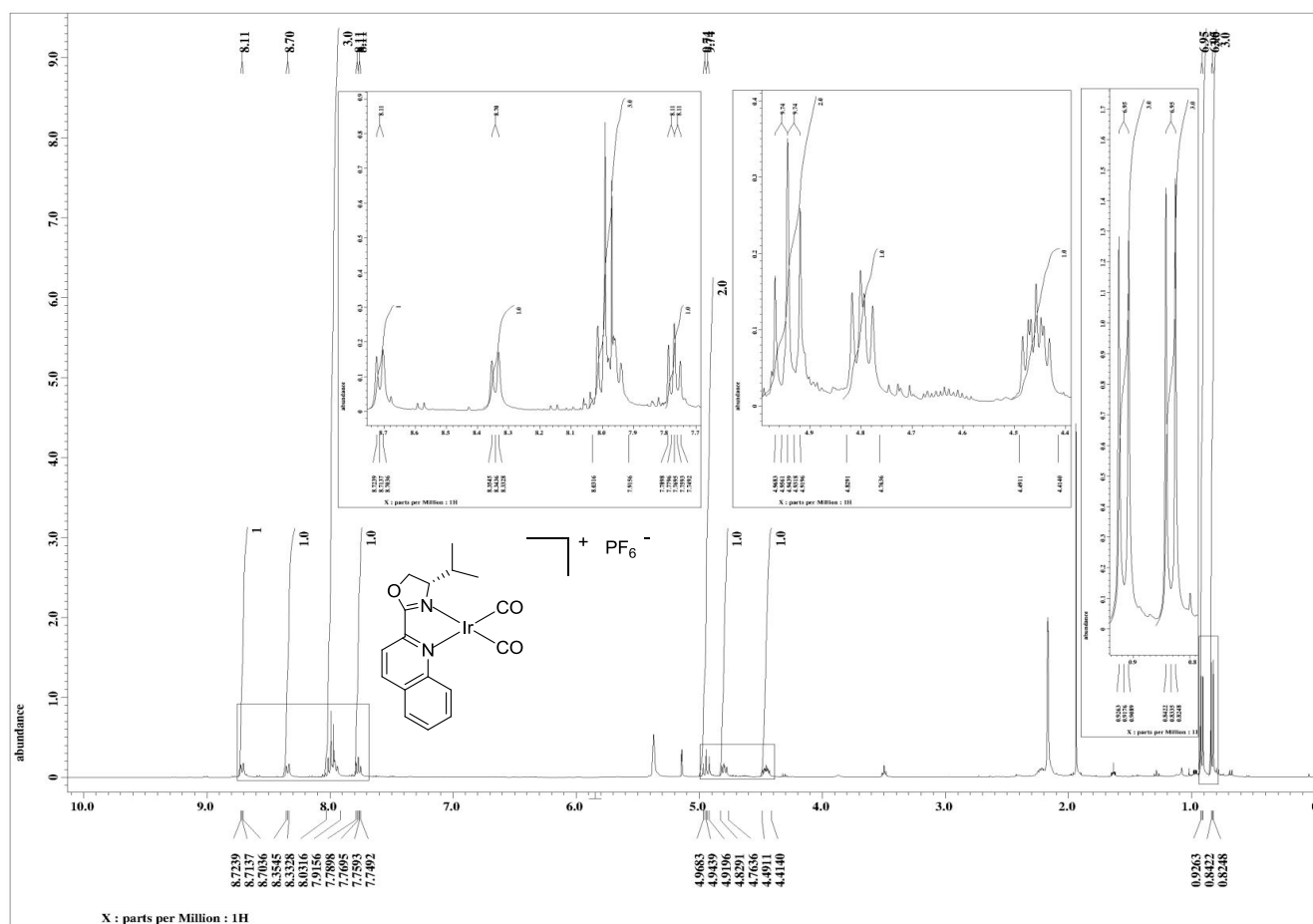
Bis-carbonyl [(S)-4-isopropyl-2-(pyridin-yl)-oxazolin]iridium(I) hexafluorophosphate, [Irⁱ(Pr-pyrox)(cod)]PF₆ (28b) (spectrum in CD₂Cl₂)



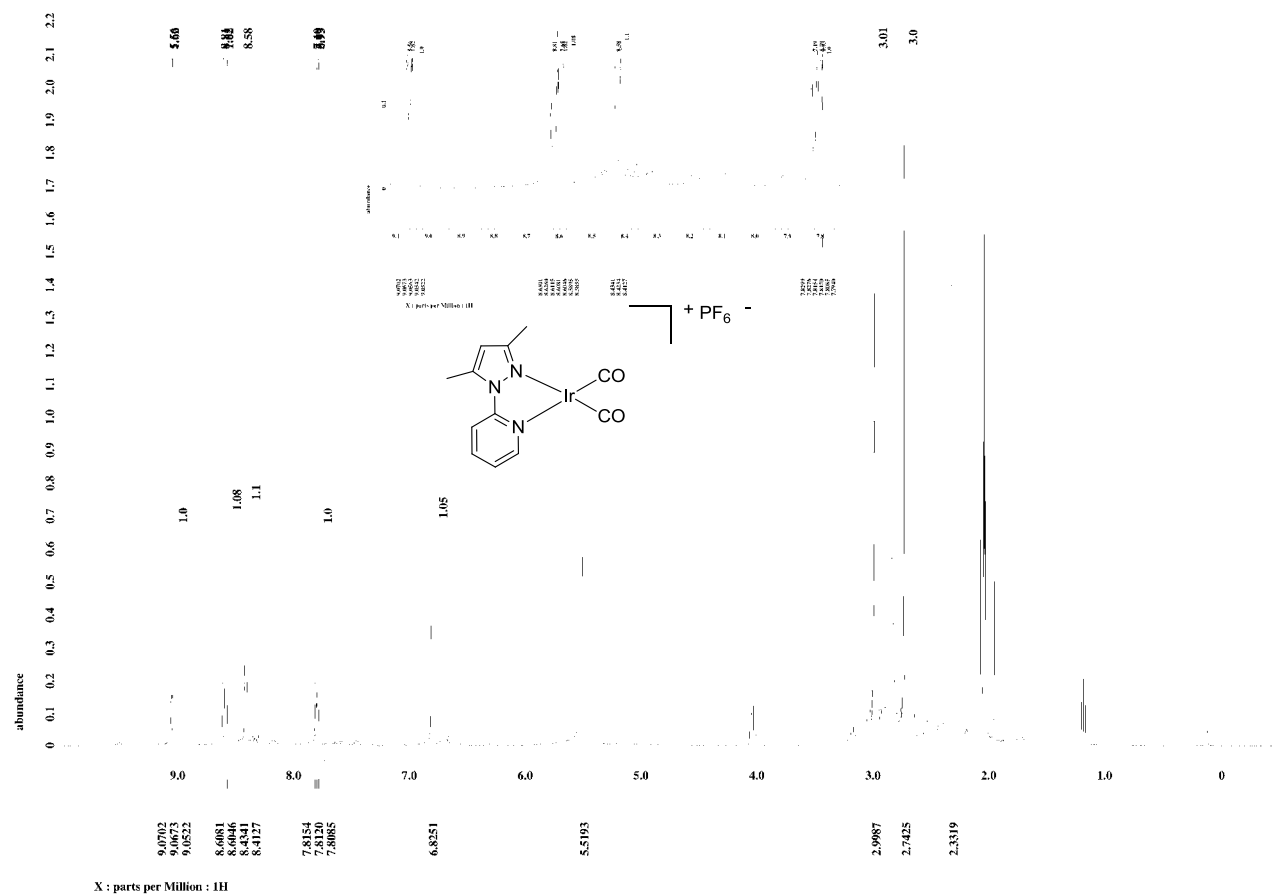
Bis-carbonyl [(S)-4-isopropyl-2-(pyridin-yl)-oxazolin]iridium(I) hexafluorophosphate, [Irⁱ(Pr-pyrox)(cod)]PF₆ (28b) (spectrum in Acetone-d₆, from crude reaction mixture)



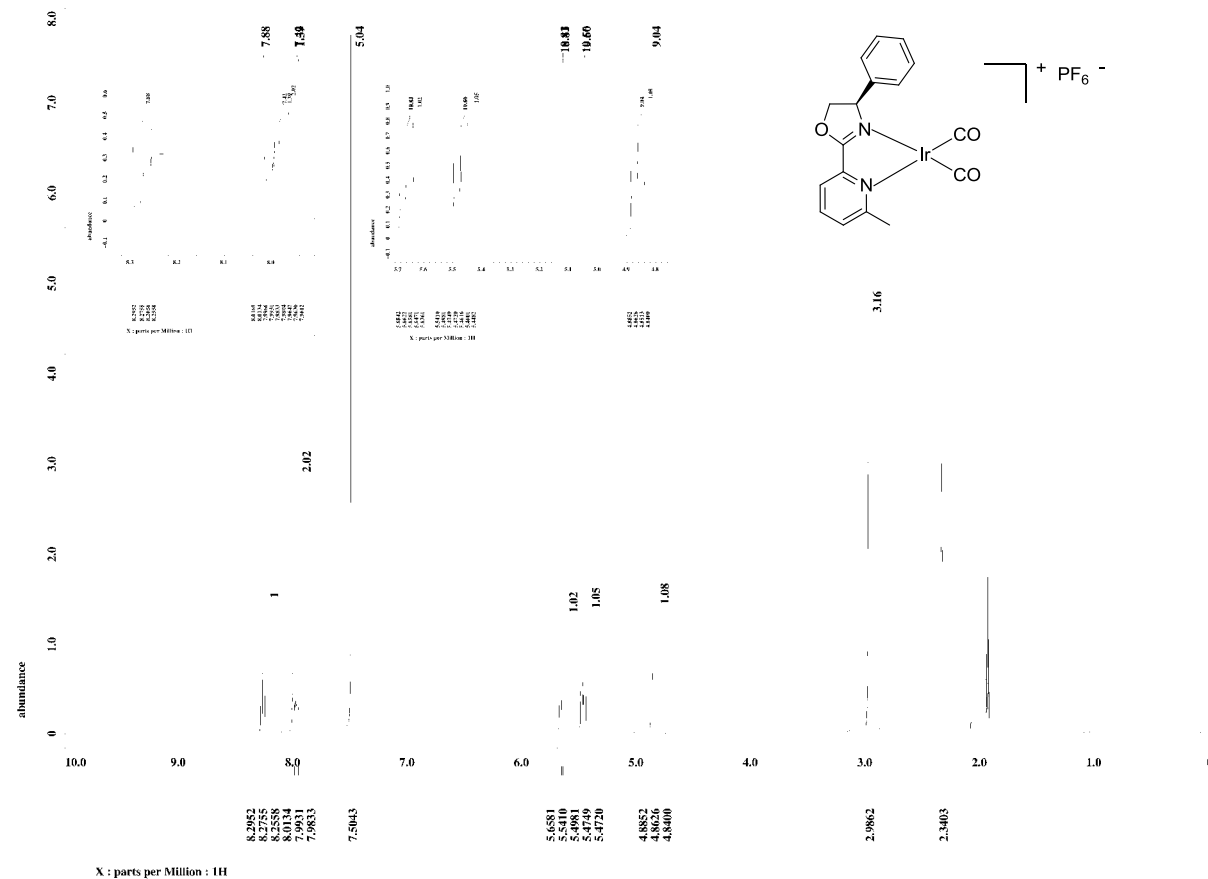
Bis-carbonyl [((S)-4-isopropyl-2-(quinolin-2-yl)-oxazole)]iridium(I) hexafluorophosphate, [IrⁱPr-quinox)(cod)]PF₆ (28m) (spectrum in CD₂Cl₂)



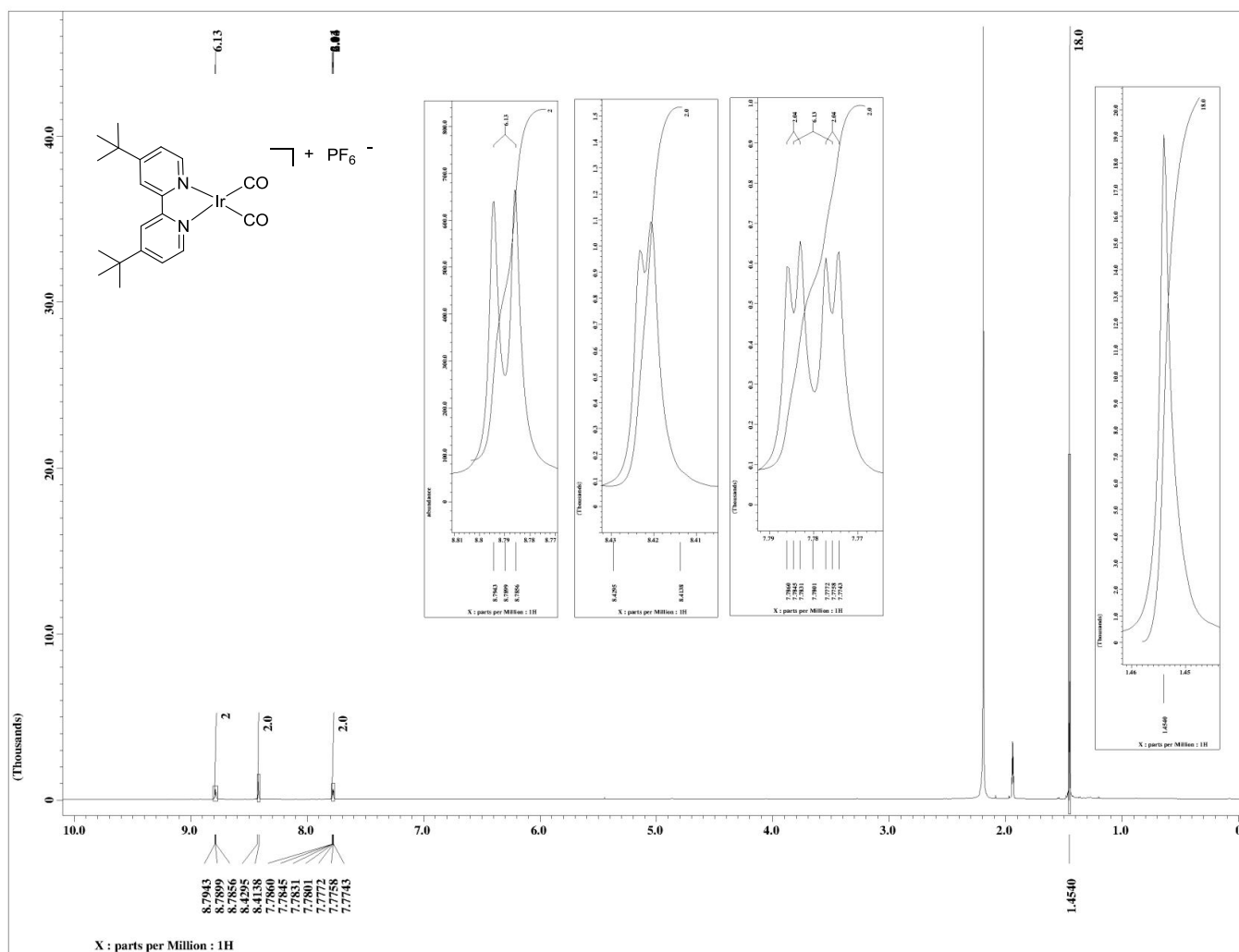
Bis-carbonyl [(2-(3,5-dimethyl-1H-pyrazol-1-yl)pyridine)]iridium(I) hexafluorophosphate, [Ir(pypyraz)(cod)]PF₆ (28v) (spectrum in Acetone-d₆, from crude reaction mixture)



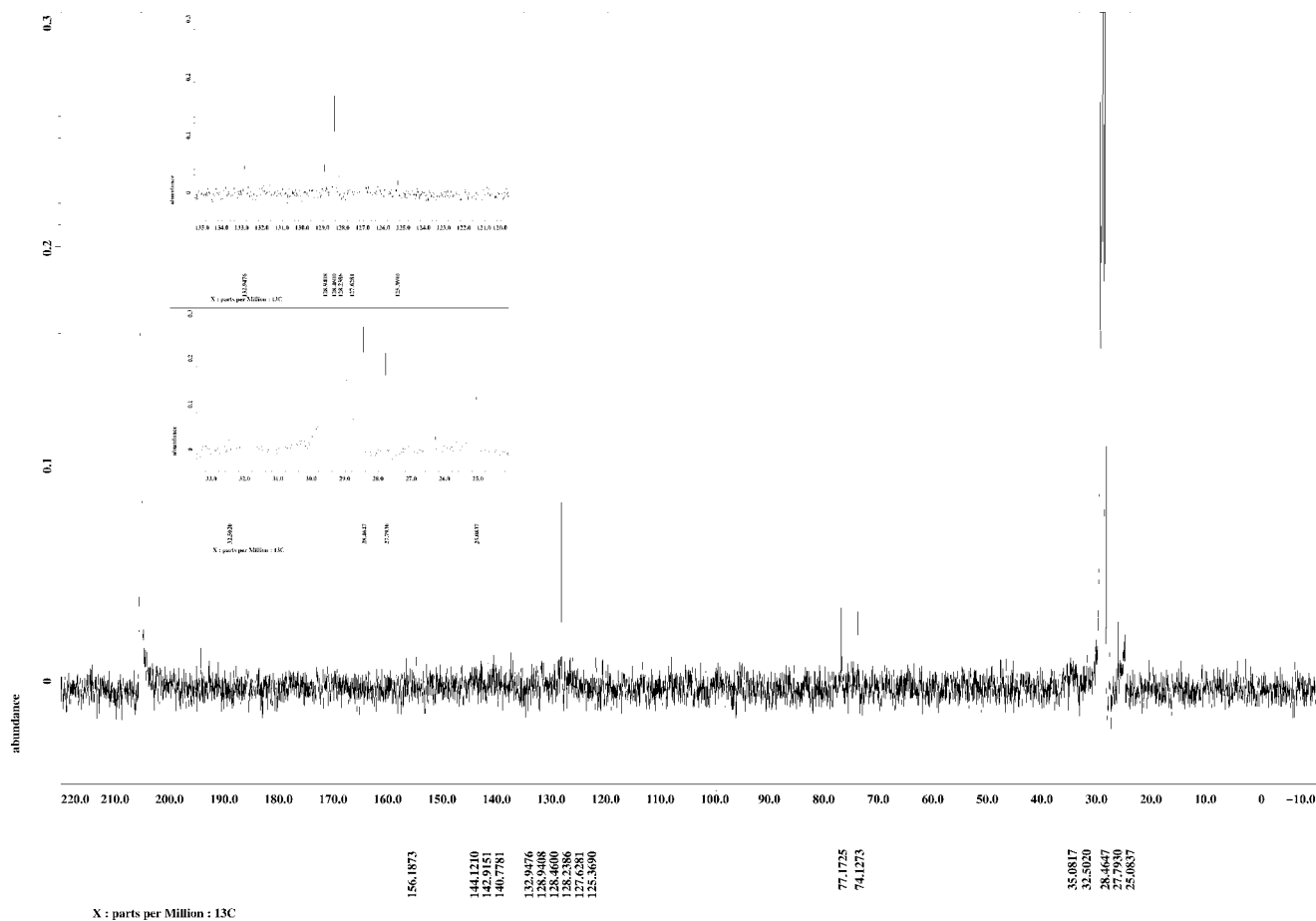
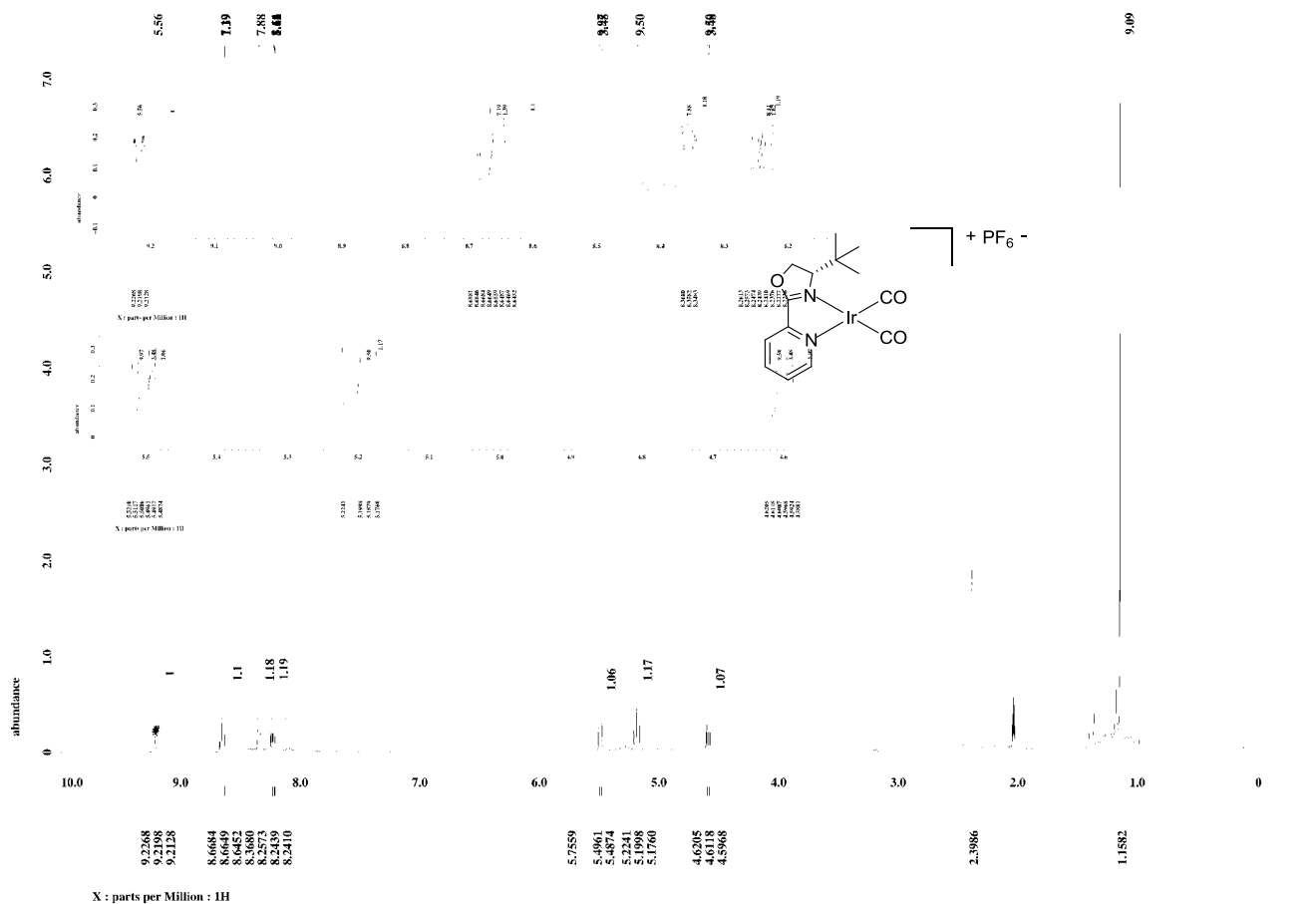
Bis-carbonyl [((R)-2-(6-methylpyridin-2-yl)-4-phenyl-oxazolin)]iridium(I) hexafluorophosphate, [Ir(Ph-mepyrox)(cod)]PF₆ (28l) (spectrum in Acetone-d₆, from crude reaction mixture)



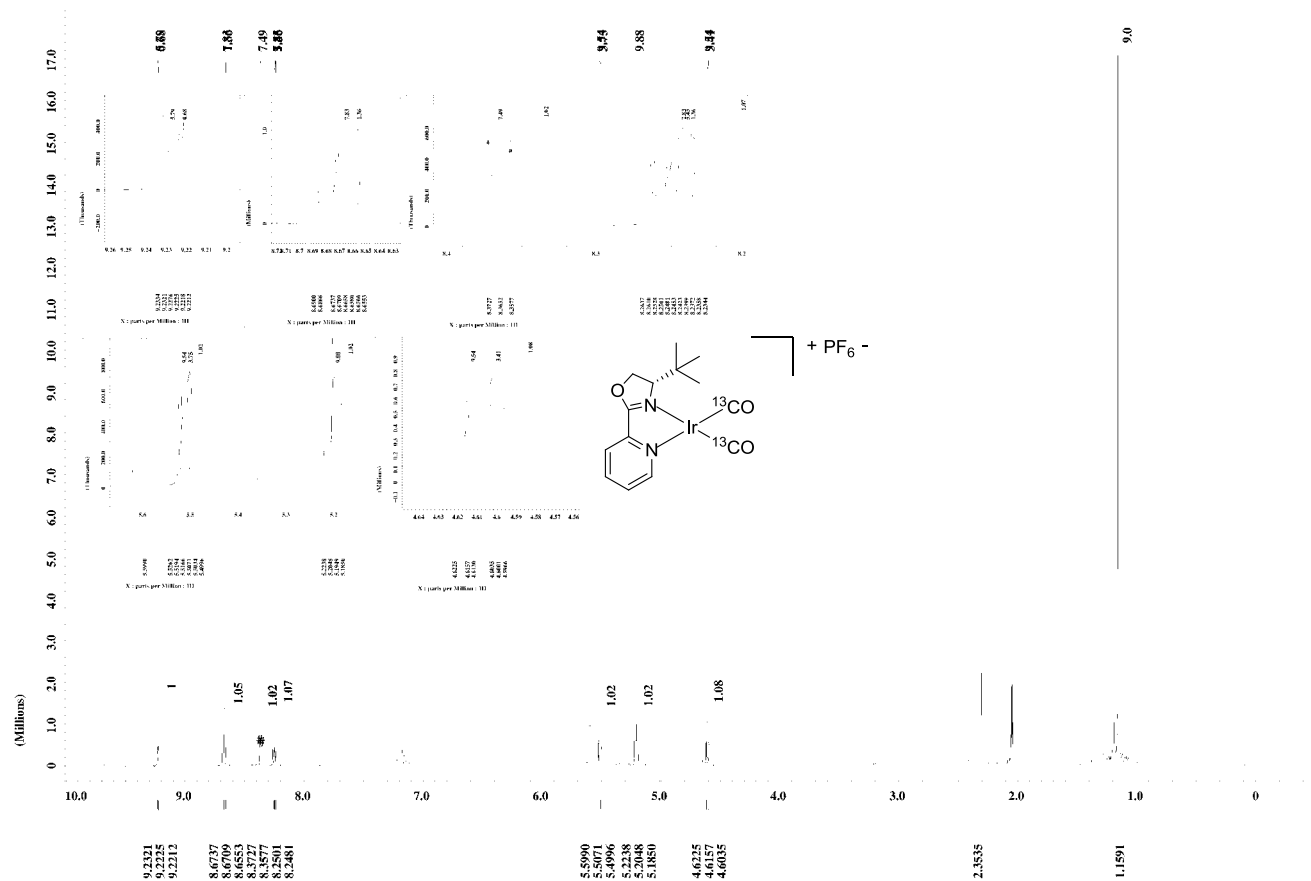
Bis-carbonyl [(4,4'-di-tert-butyl-2,2'-bipyridine)]iridium(I) hexafluorophosphate, [Ir(dt bpy)(cod)]PF₆ (28r) (spectrum in CD₂Cl₂)



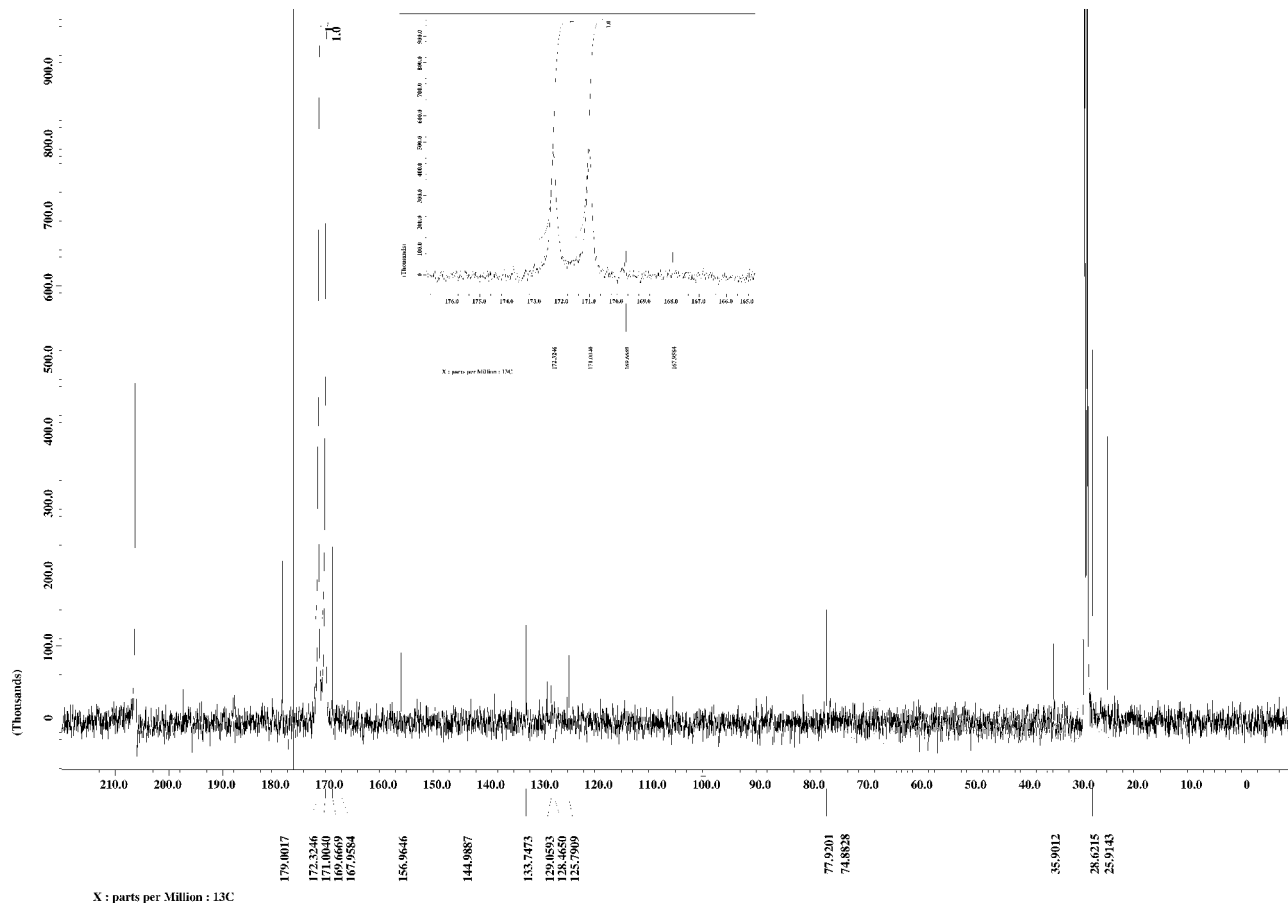
Bis-carbonyl [((S)-4-(tert-butyl)-2-(pyridine-2-yl)-oxazolin)]iridium(I) hexafluorophosphate, [Ir(^tBu-pyrox)(cod)]PF₆ (28i) (spectrum in Acetone-d₆, from crude reaction mixture)



Bis-(¹³C-carbonyl)[((S)-4-(tert-butyl)-2-(pyridine-2-yl)-oxazolin)]iridium(I) hexafluorophosphate, [Ir(^tBu-pyrox)(cod)]PF₆ (¹³C-28i) (spectrum in Acetone-d₆, from crude reaction mixture)

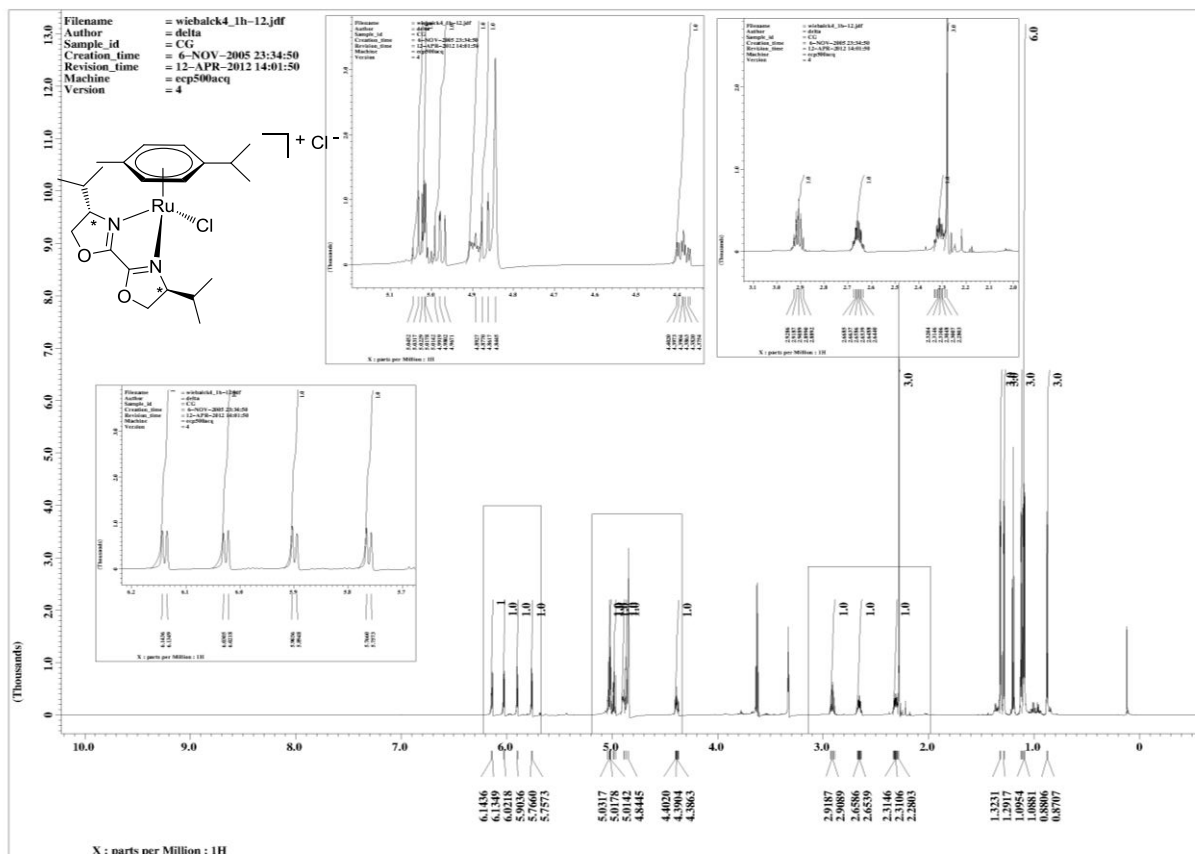


X : parts per Million : 1H

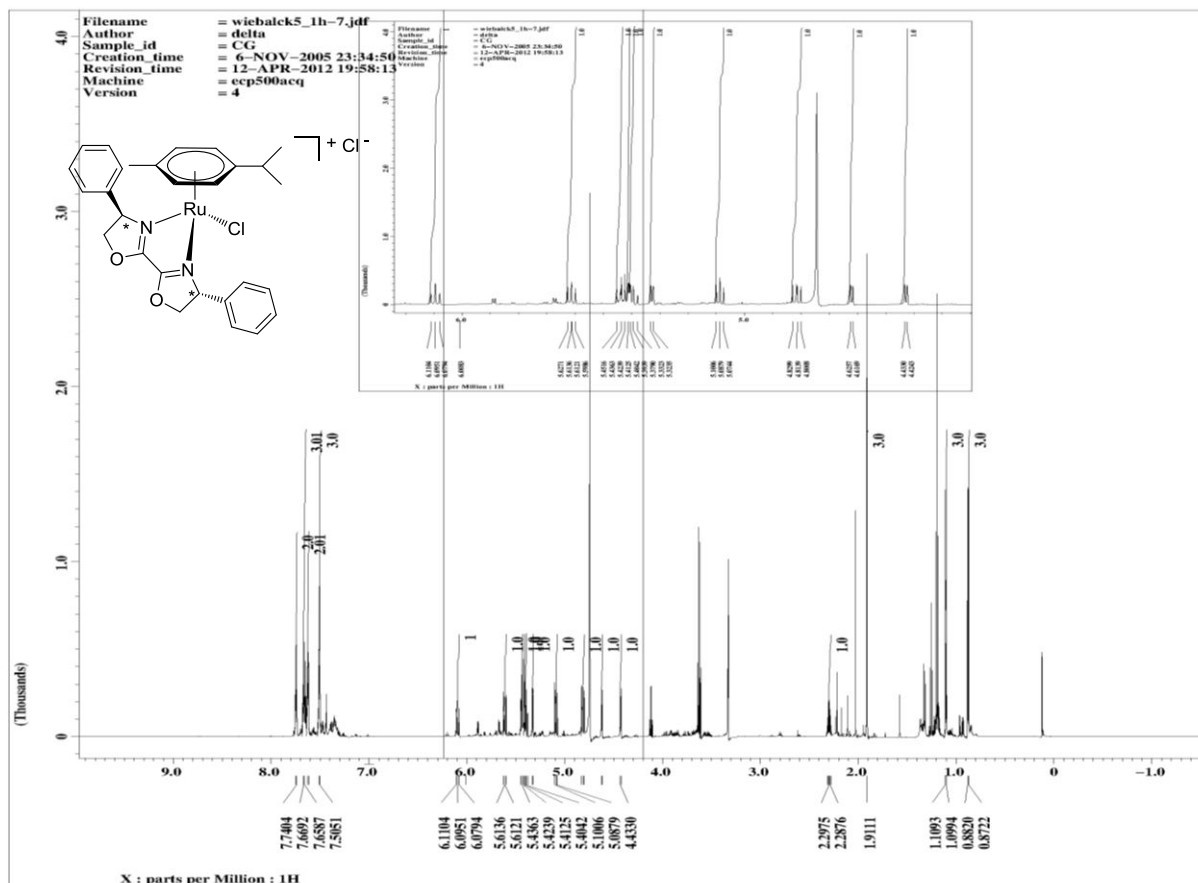


X : parts per Million : 13C

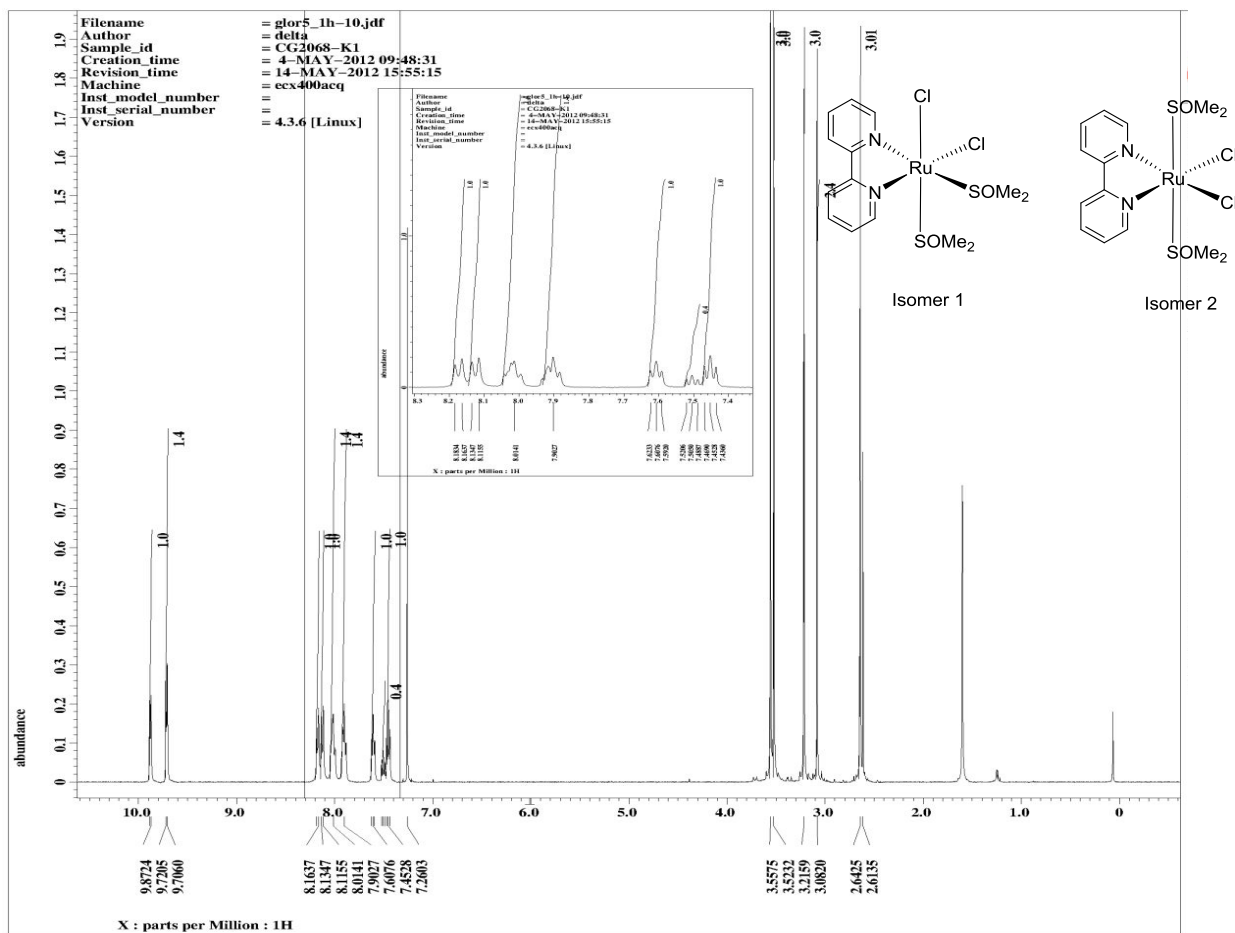
[[2,2'-Bis((4*S*,4'*S*)-4,4'-diisopropyl)-oxazolin)]-chloro-(η^6 -*p*-cymol)-ruthenium(II)]chloride; [Ru(Pr-box)(cymene)Cl]Cl (48a)



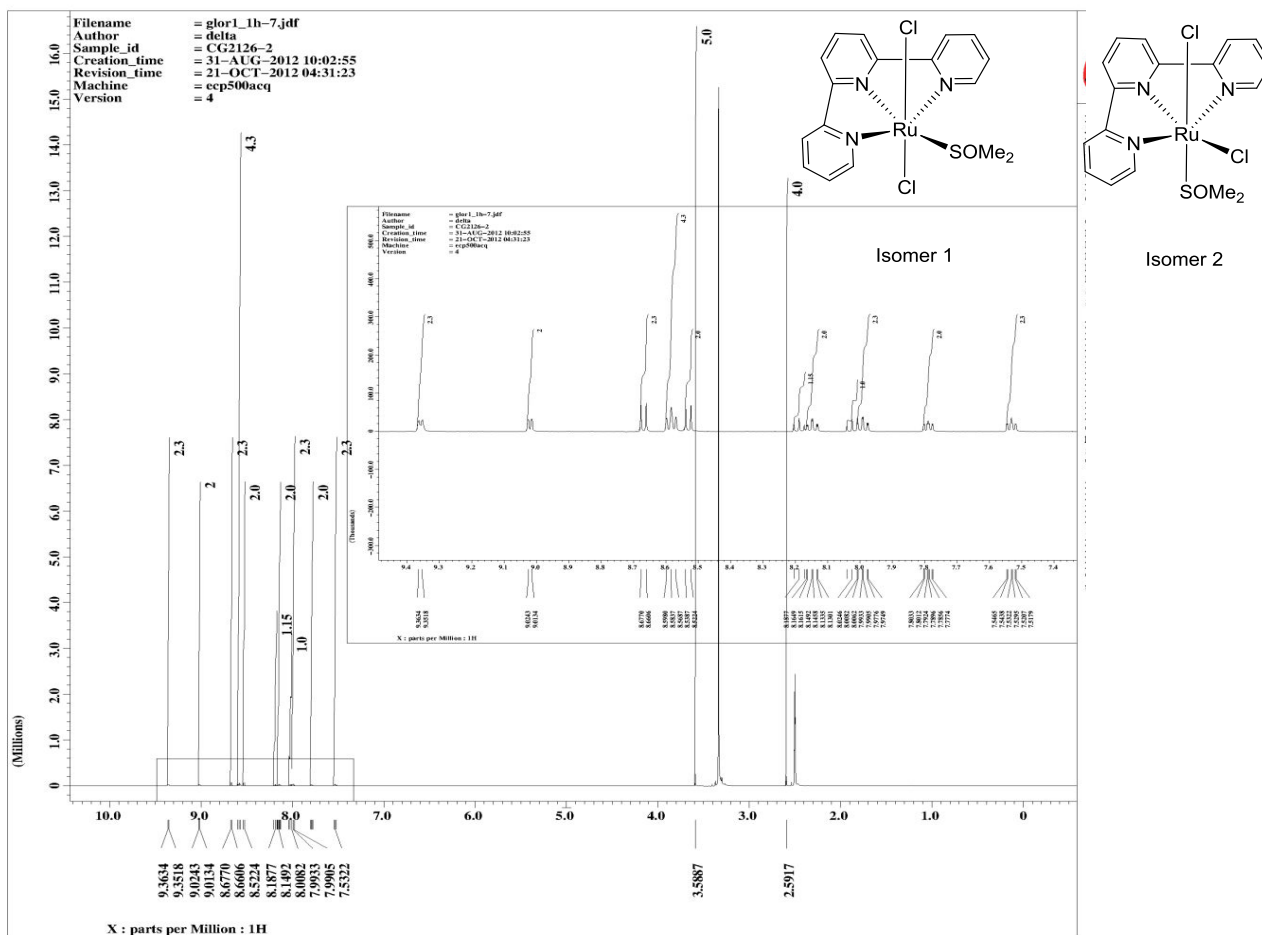
[[2,2'-Bis((4*R*,4'*R*)-4,4'-diphenyl)-oxazolin)]-chloro-(η^6 -*p*-cymol)-ruthenium(II)]chloride; [Ru(Ph-box)(cymene)Cl]Cl (48b)



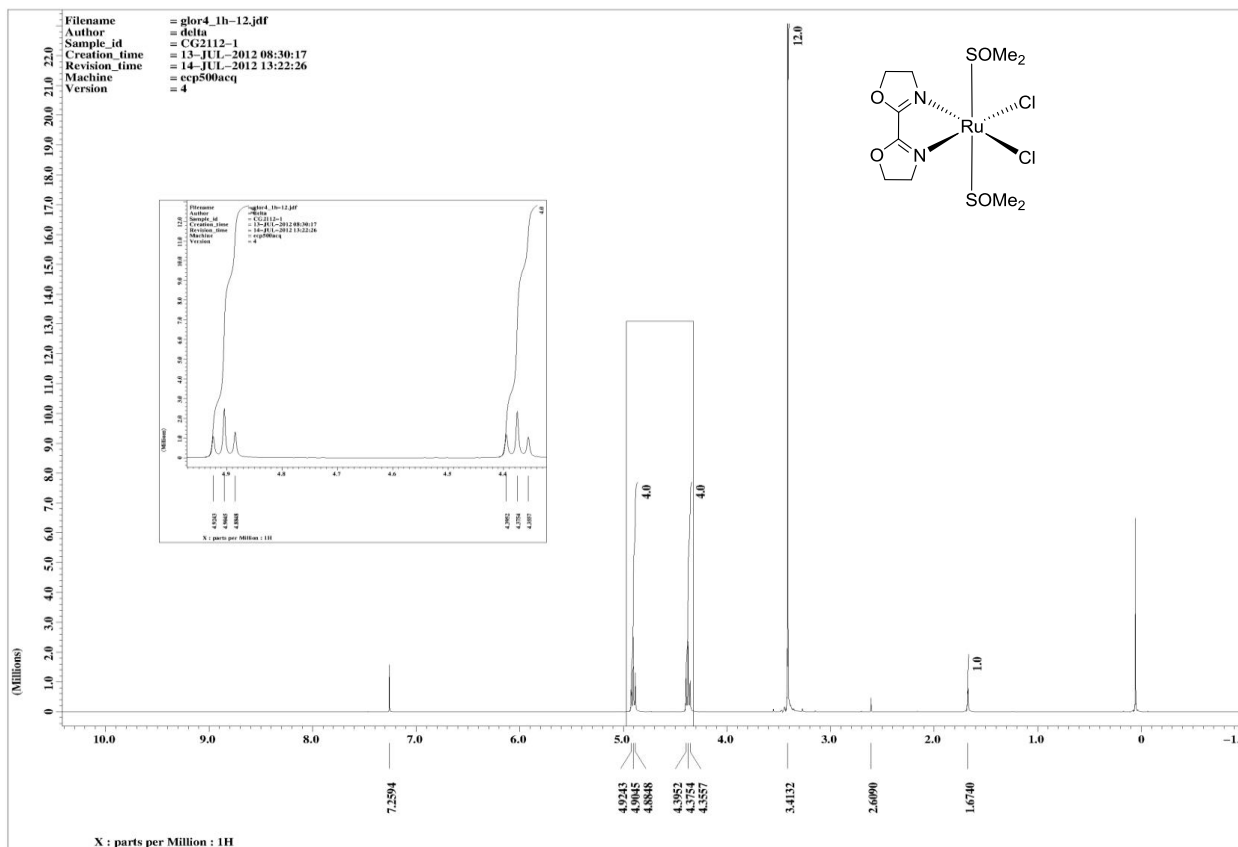
Dichloro(2,2'-bipyridyl)bis((s)-dimethyl-sulfoxid)ruthenium(II);[Ru(bpy)(dmsO)₂Cl₂] (56)



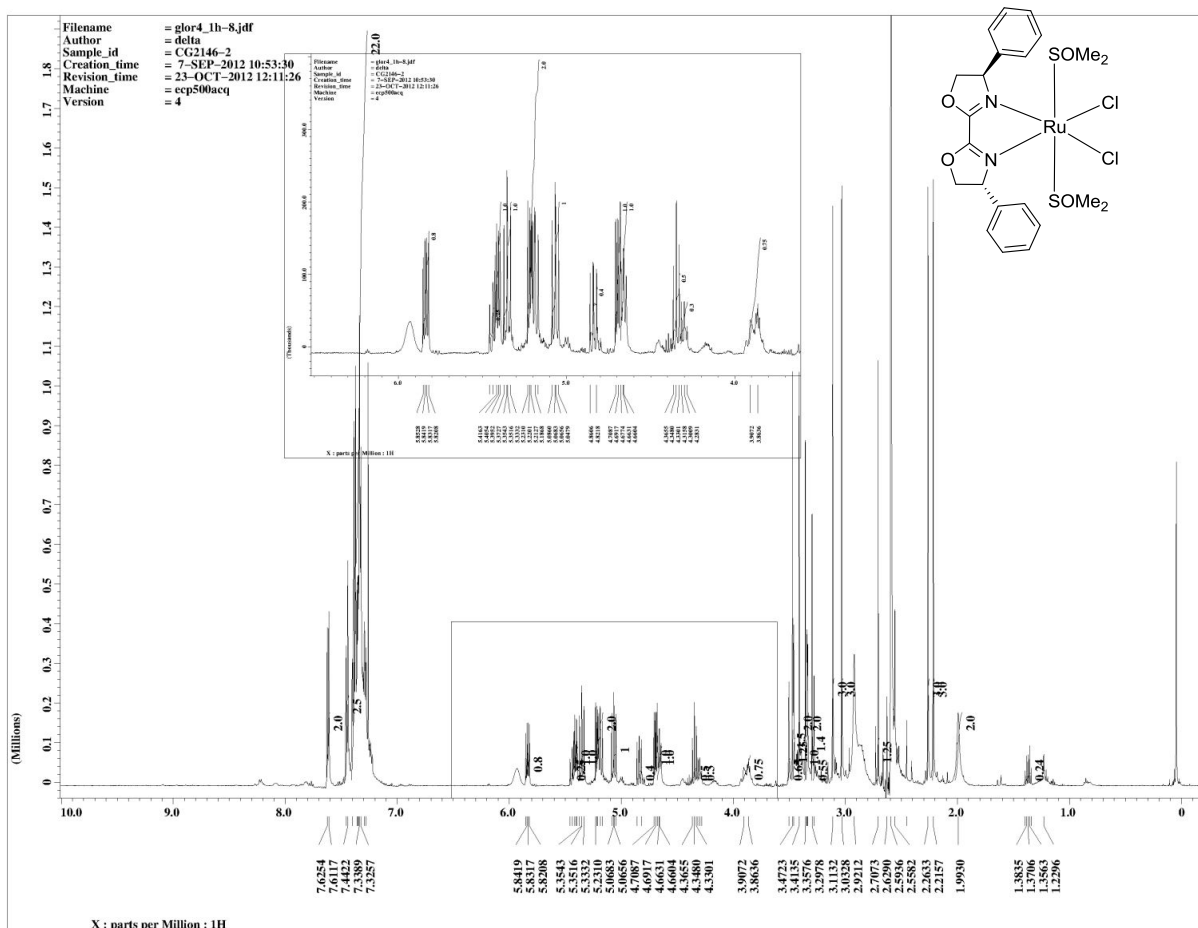
Dichloro(2,2':6',2''-terpyridyl)((s)-dimethyl-sulfoxid)ruthenium(II);[Ru(tpy)(dmsO)₂Cl₂] (57)



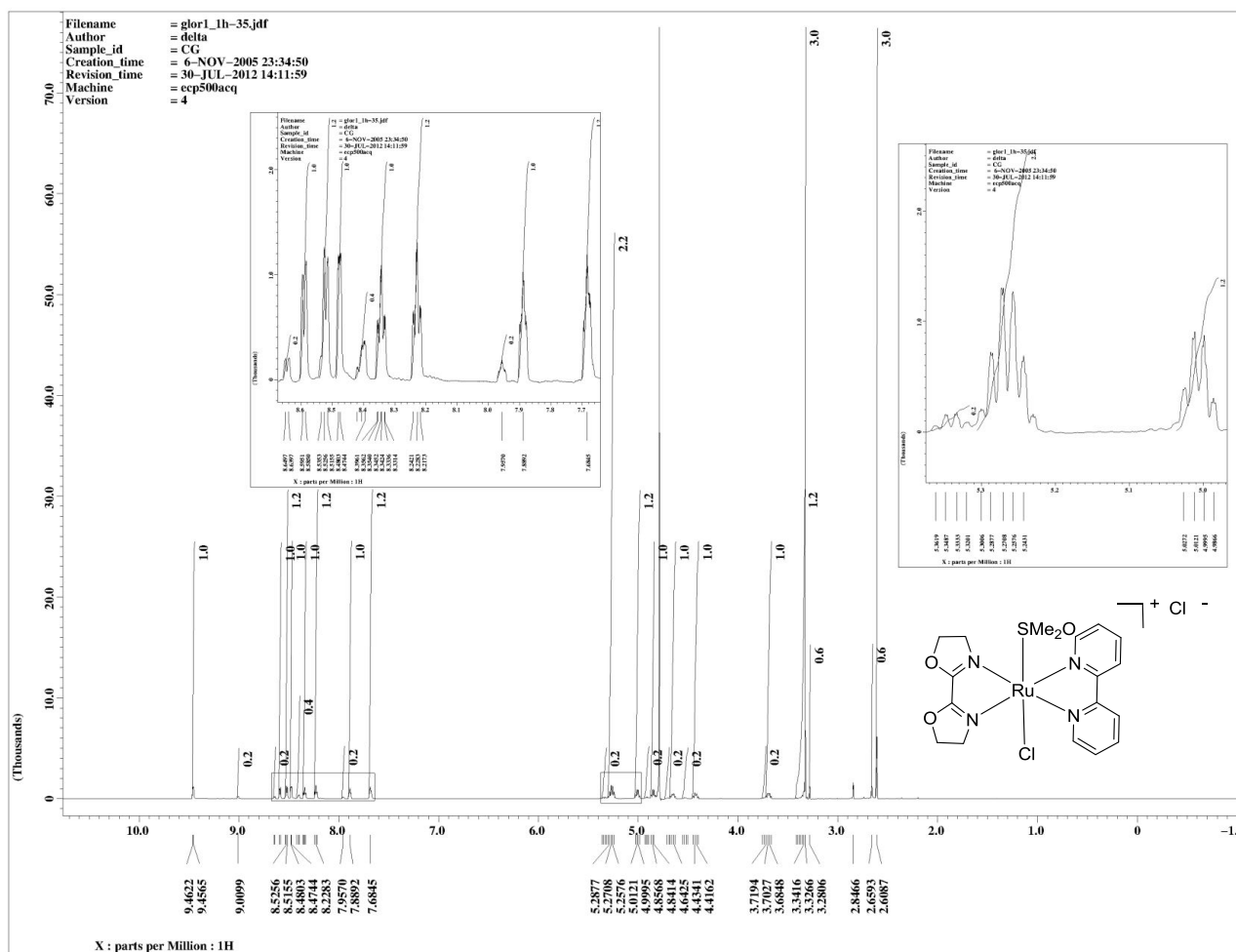
Dichloro(2,2'-bis[oxazolin-2-yl])bis(dimethyl-sulfoxid)ruthenium(II);[Ru(H-box)(dms_o)₂Cl₂] (49a)



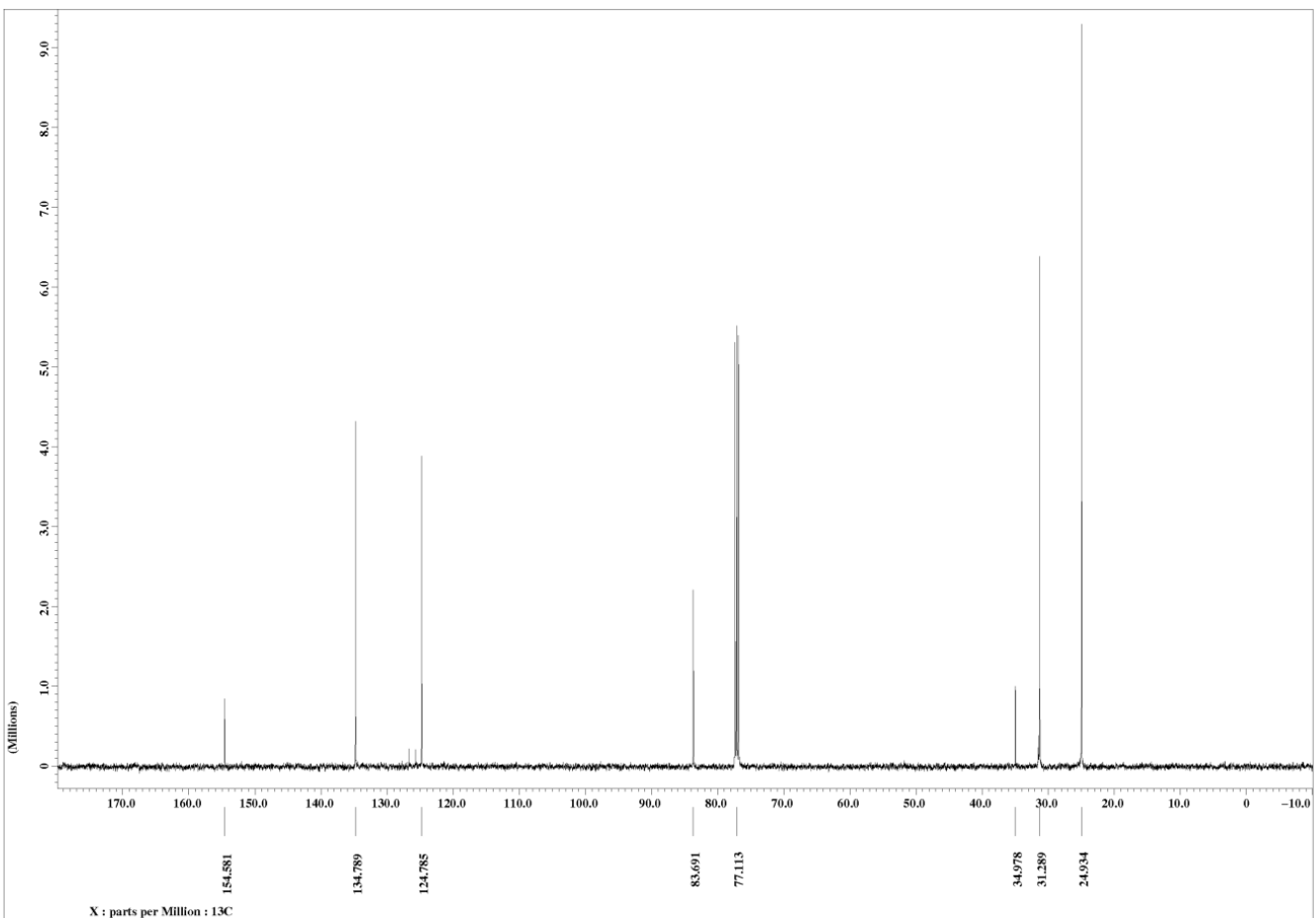
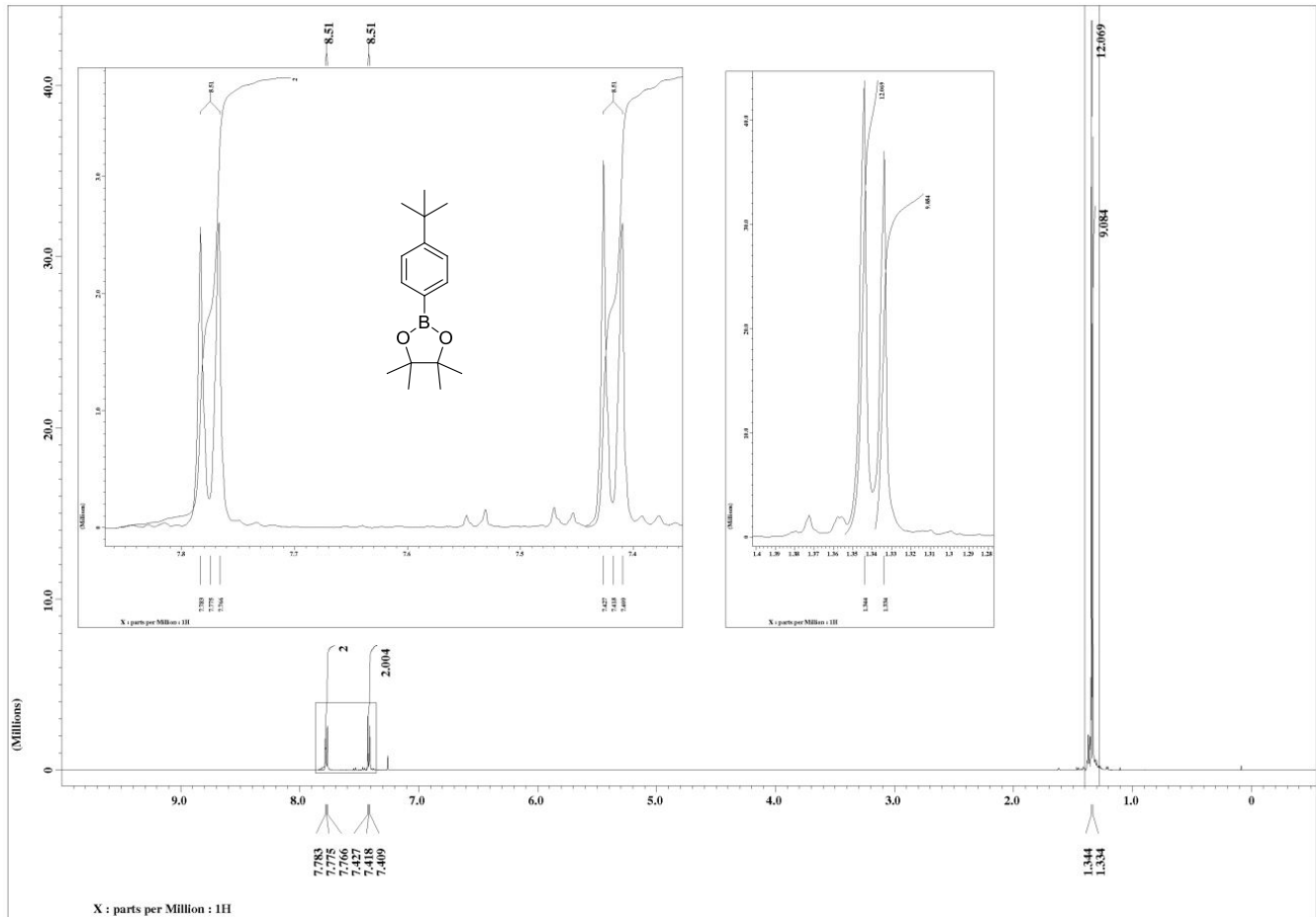
Dichloro(4,4'-diphenyl-2,2'-bis[oxazolin-2-yl])bis(dimethyl-sulfoxid)ruthenium(II);[Ru(Ph-box)(dms_o)₂Cl₂] (49c)



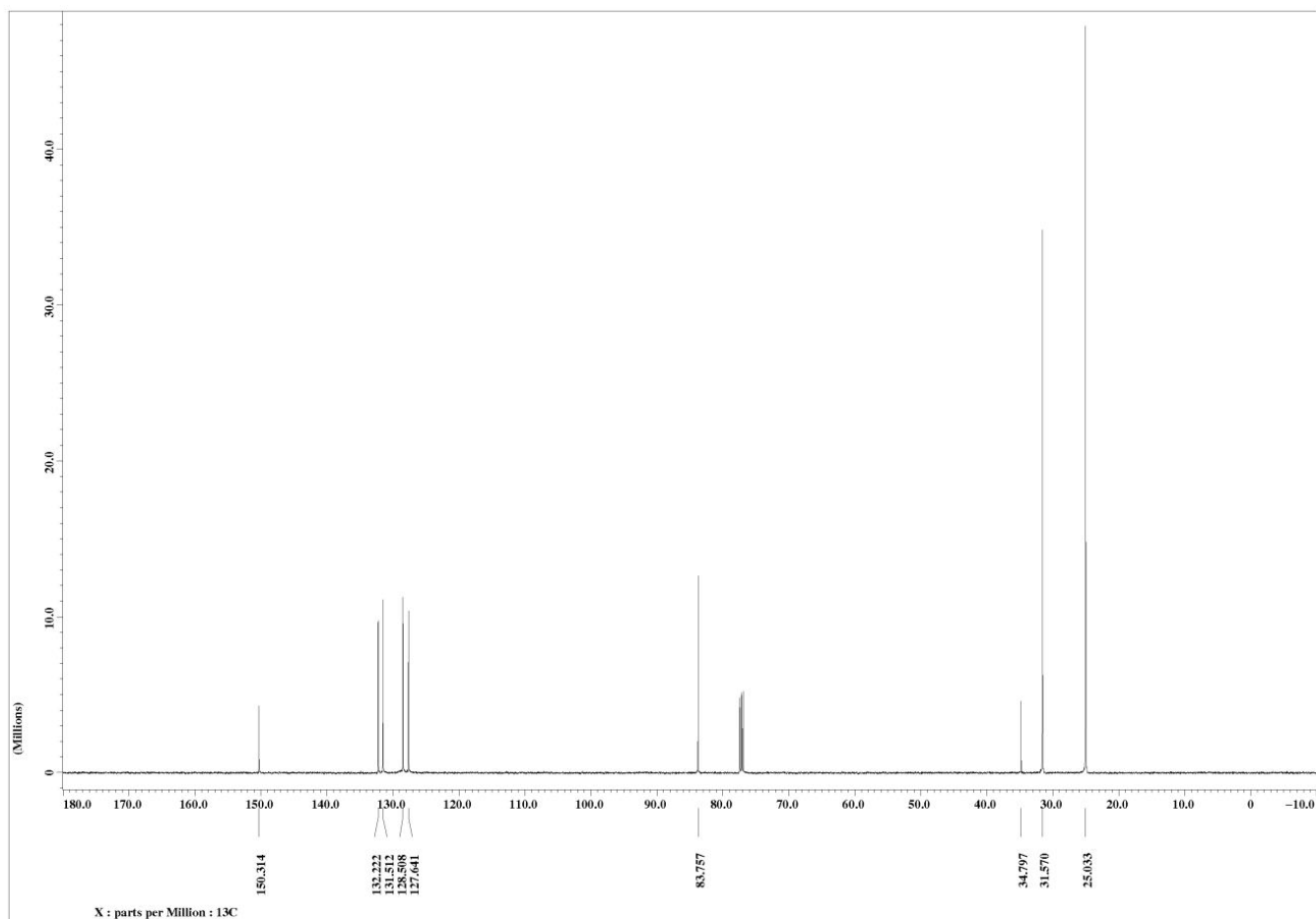
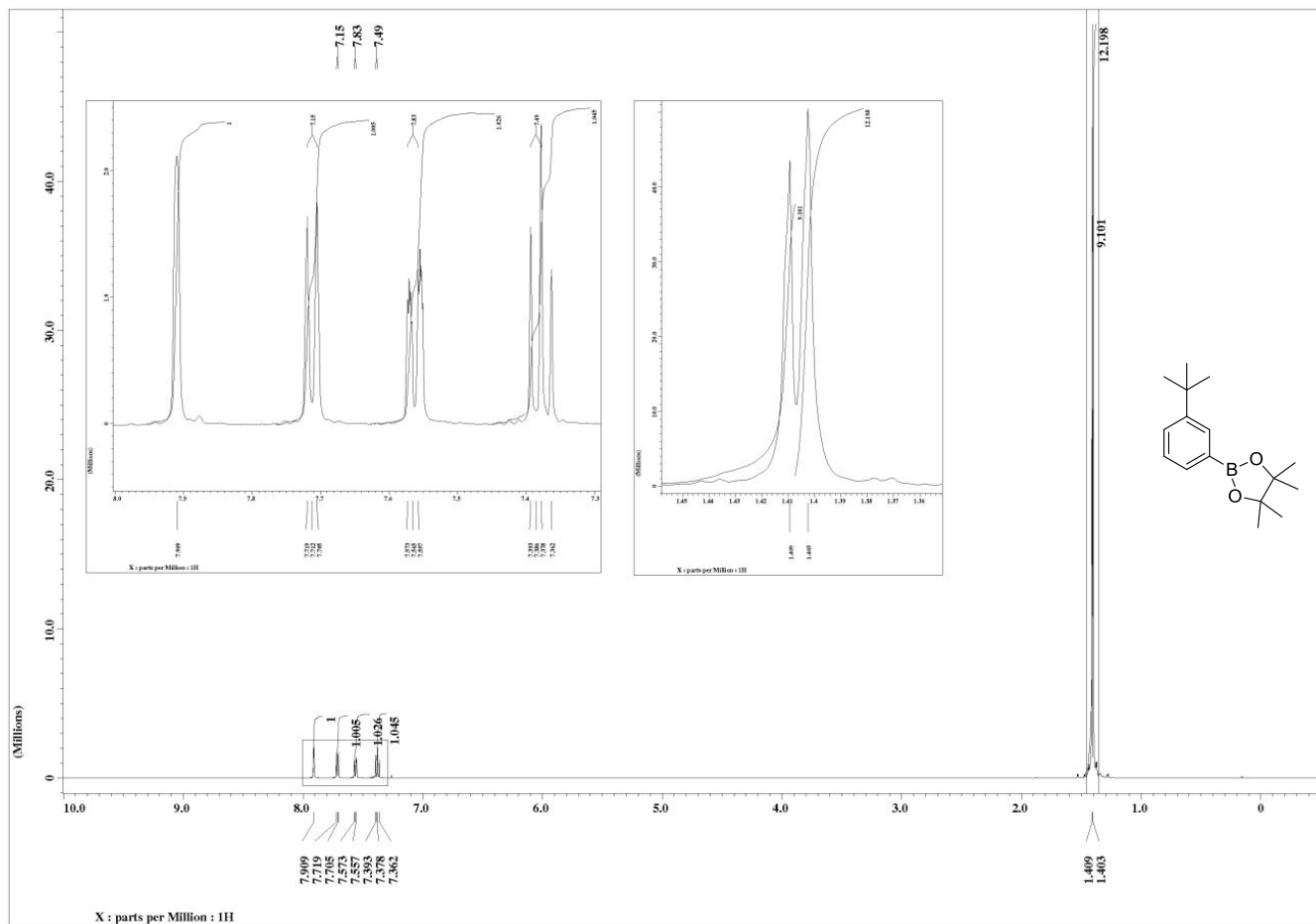
Chloro(2,2'-bis[oxazolin-2-yl])(2,2'-bipyridyl)(dimethyl-sulfoxid)ruthenium(II)-chlorid; [Ru(H-box)(bpy)((s-dms)Cl)]⁺Cl⁻ (61)



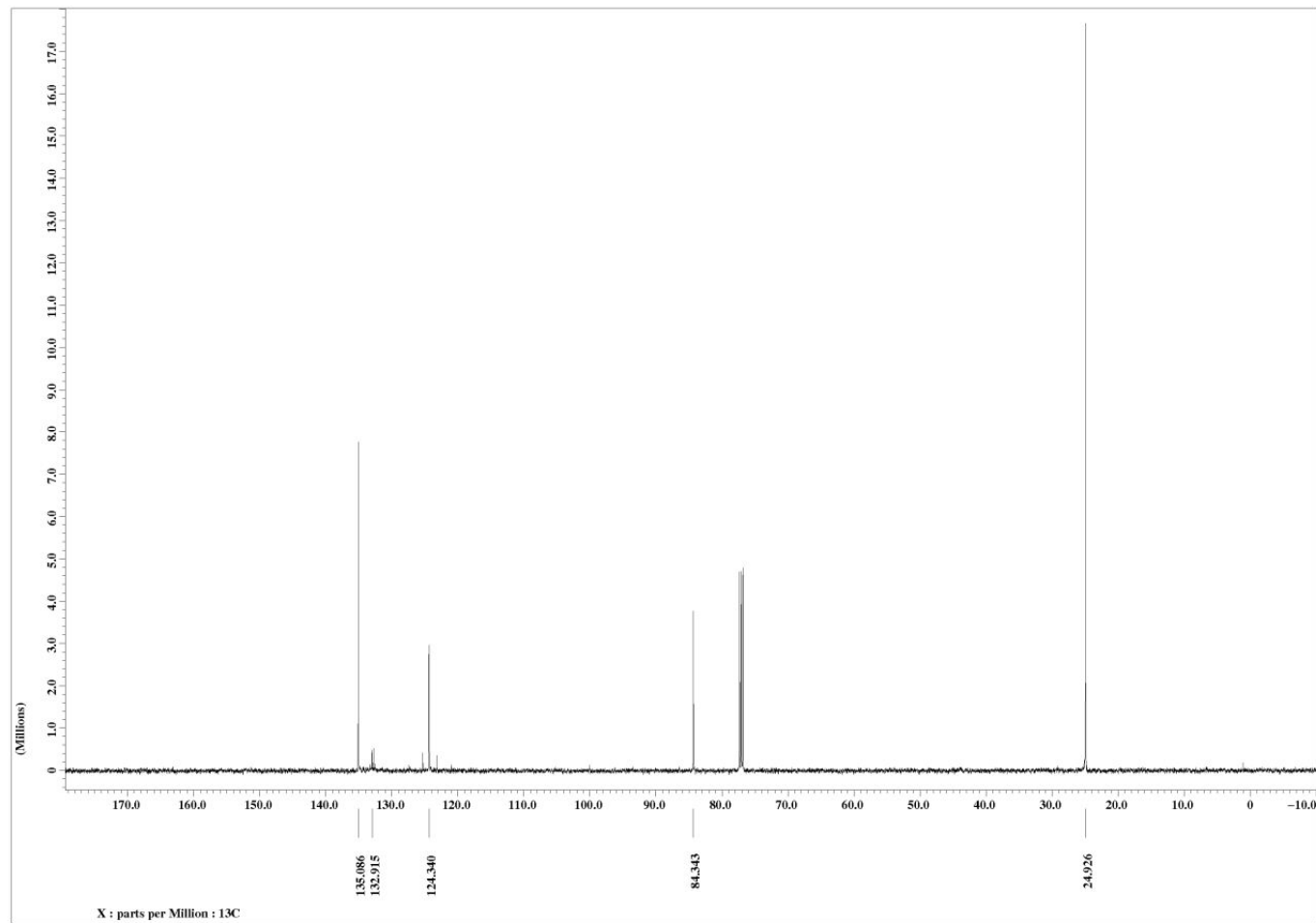
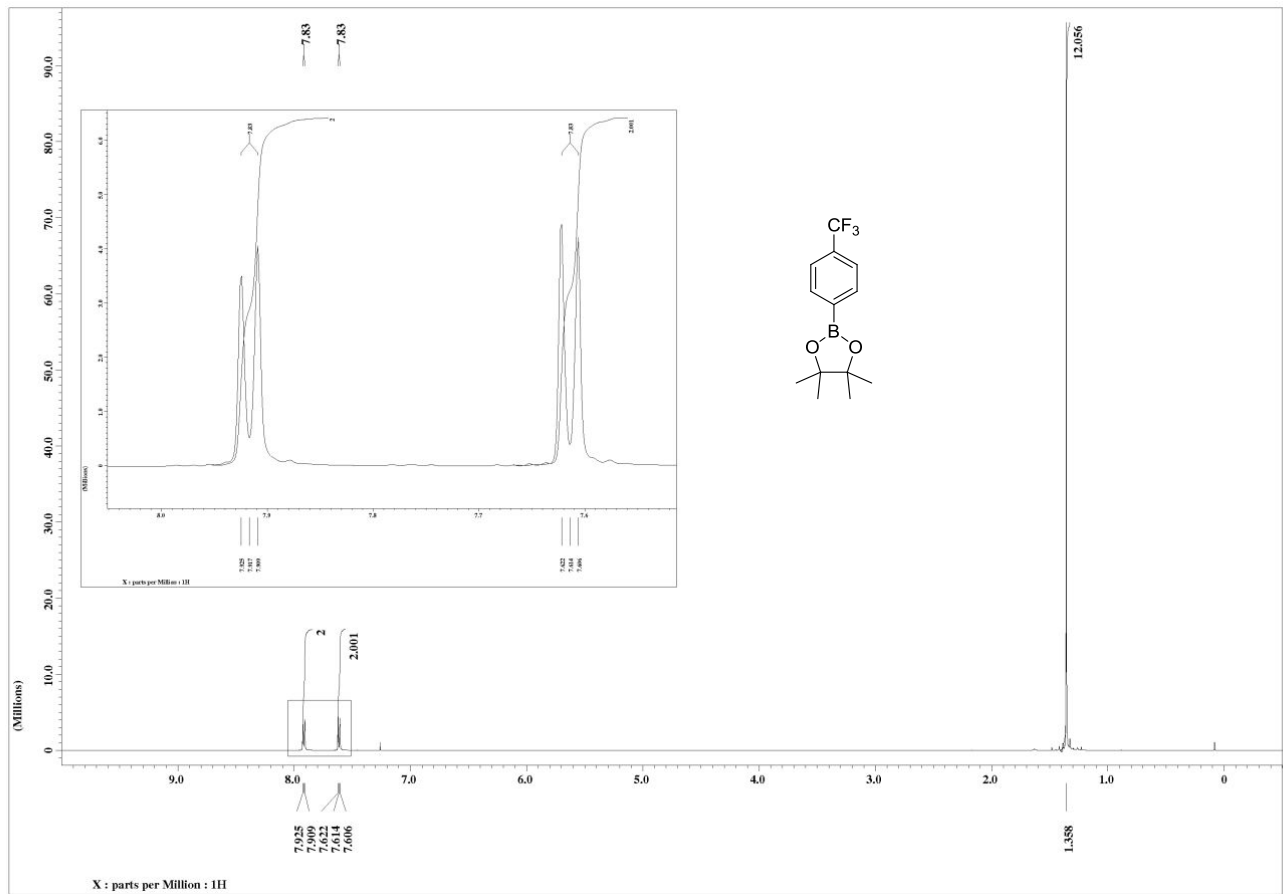
2-(4-(*tert*-butyl)phenyl)-4,4,5,5-tetramethyl-1,3,2-dioxaborolane (68a)



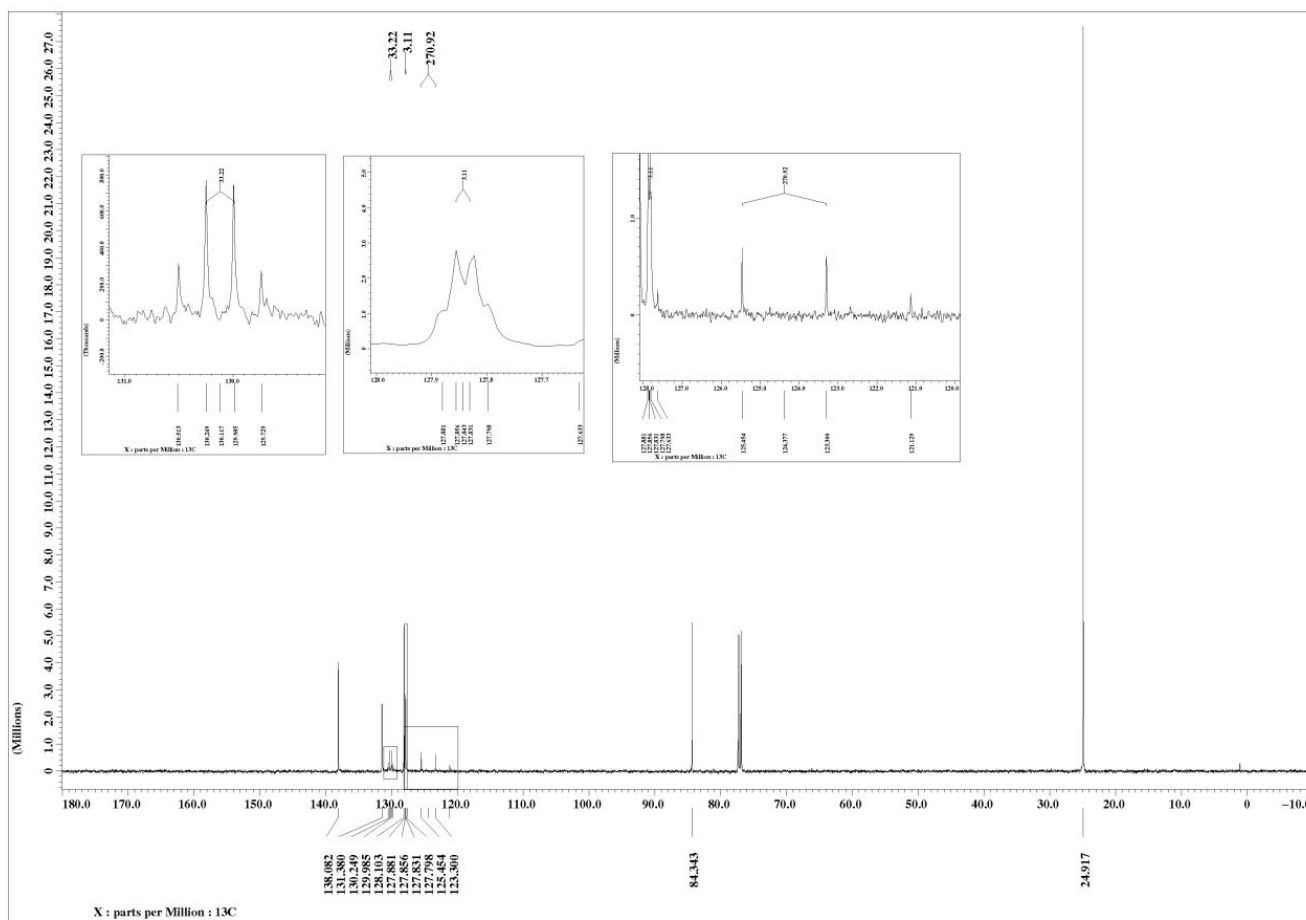
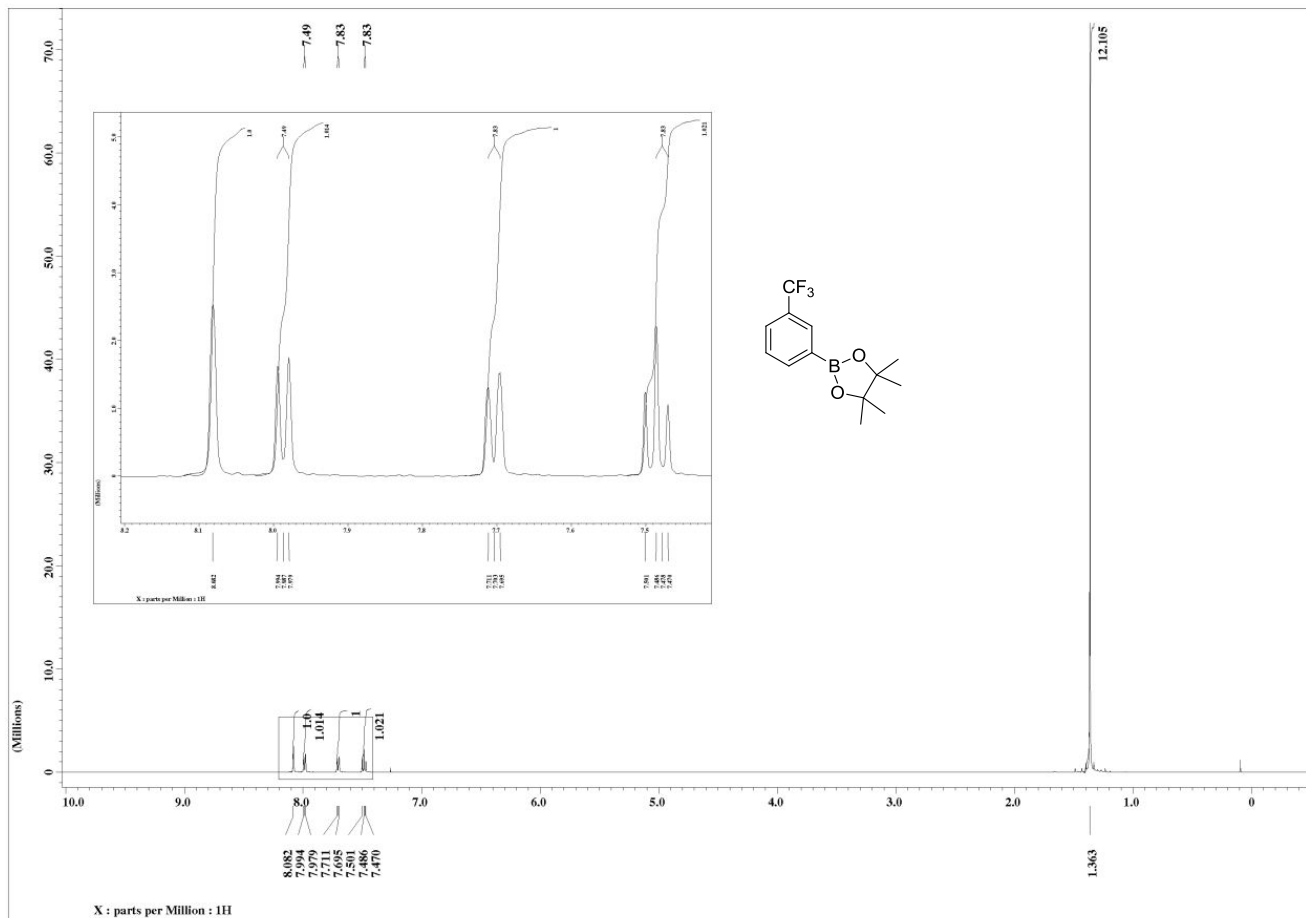
2-(3-(*tert*-butyl)phenyl)-4,4,5,5-tetramethyl-1,3,2-dioxaborolane (67a)



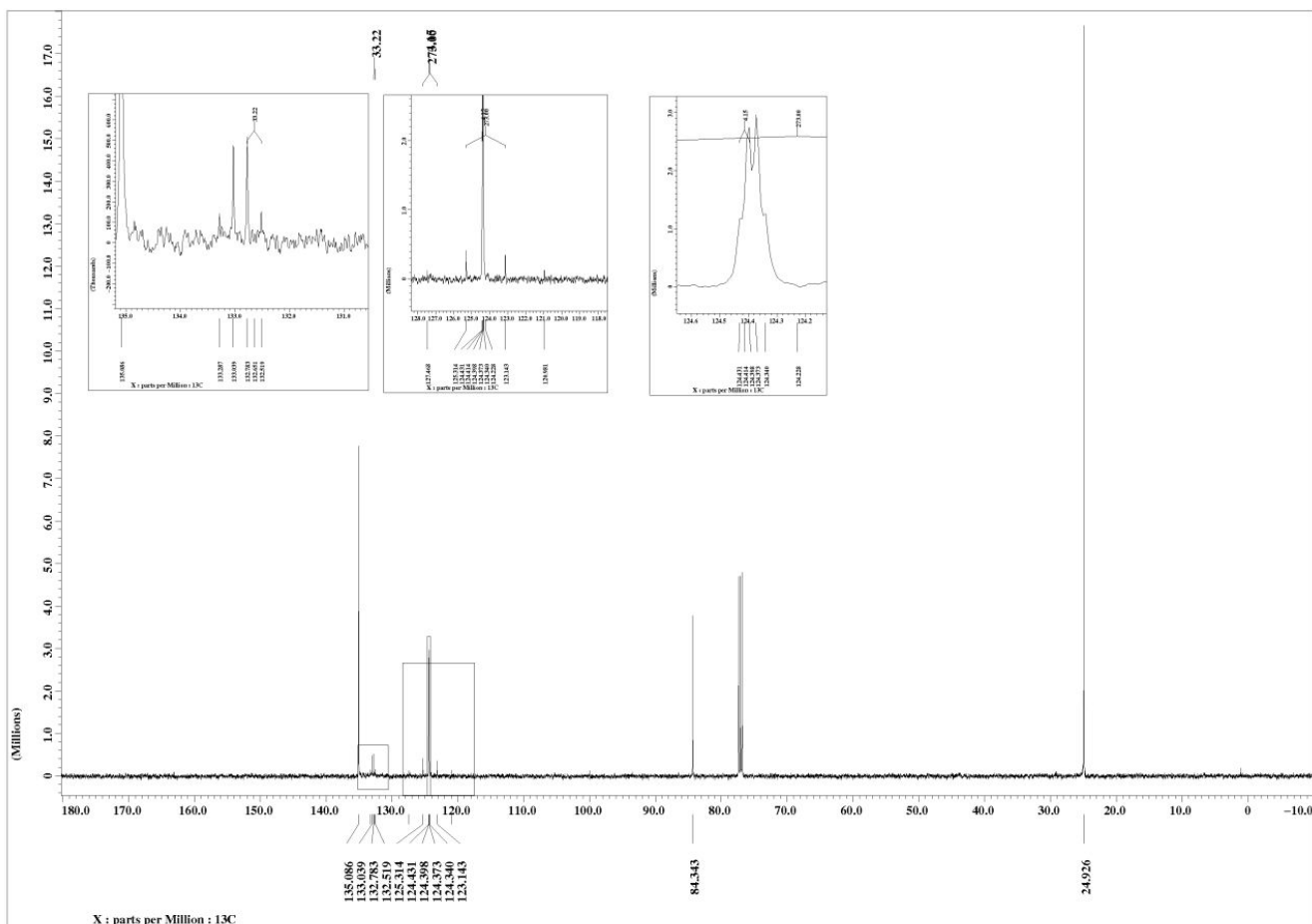
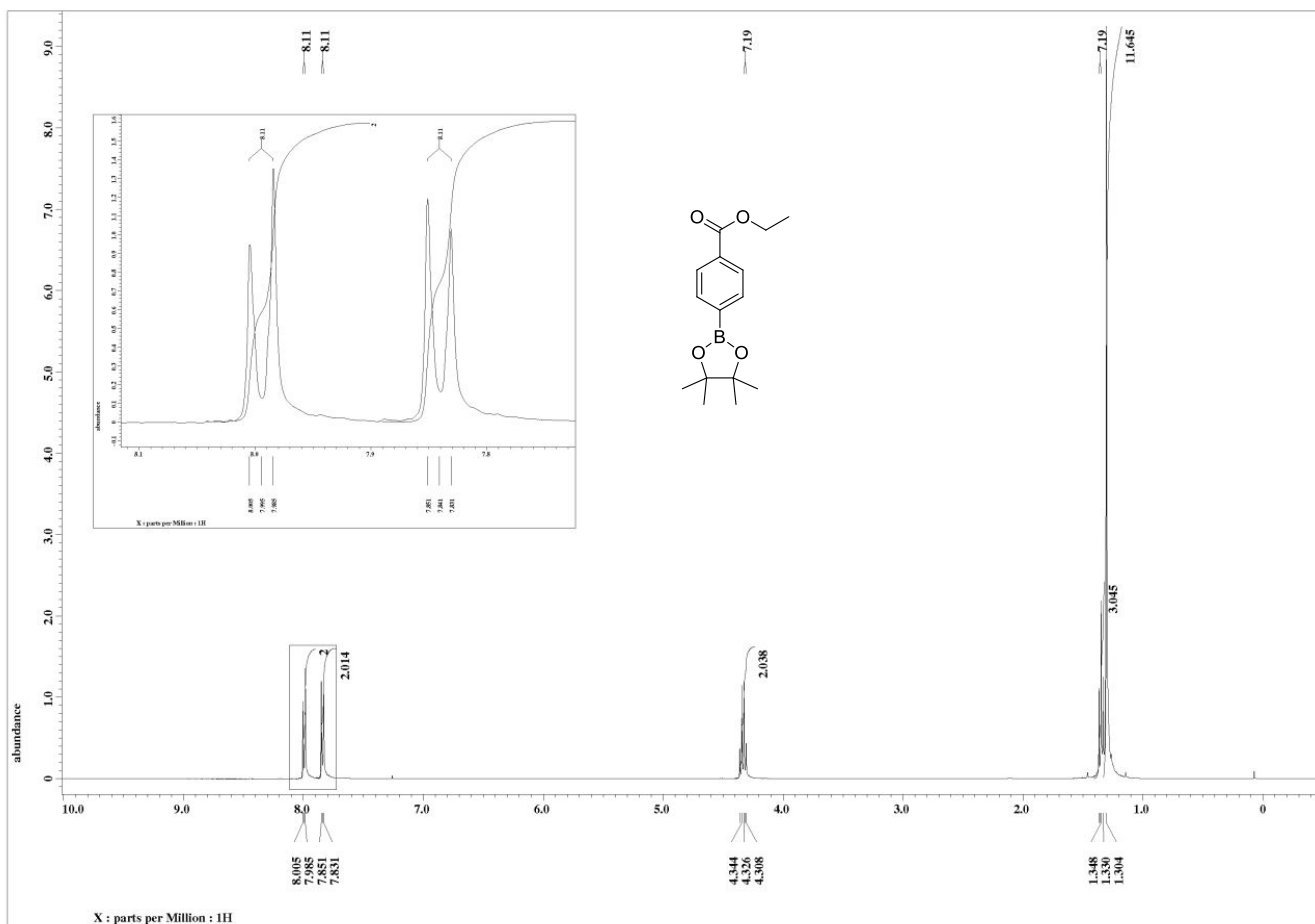
4,4,5,5-tetramethyl-2-(4-(trifluoromethyl)phenyl)-1,3,2-dioxaborolane (68b)



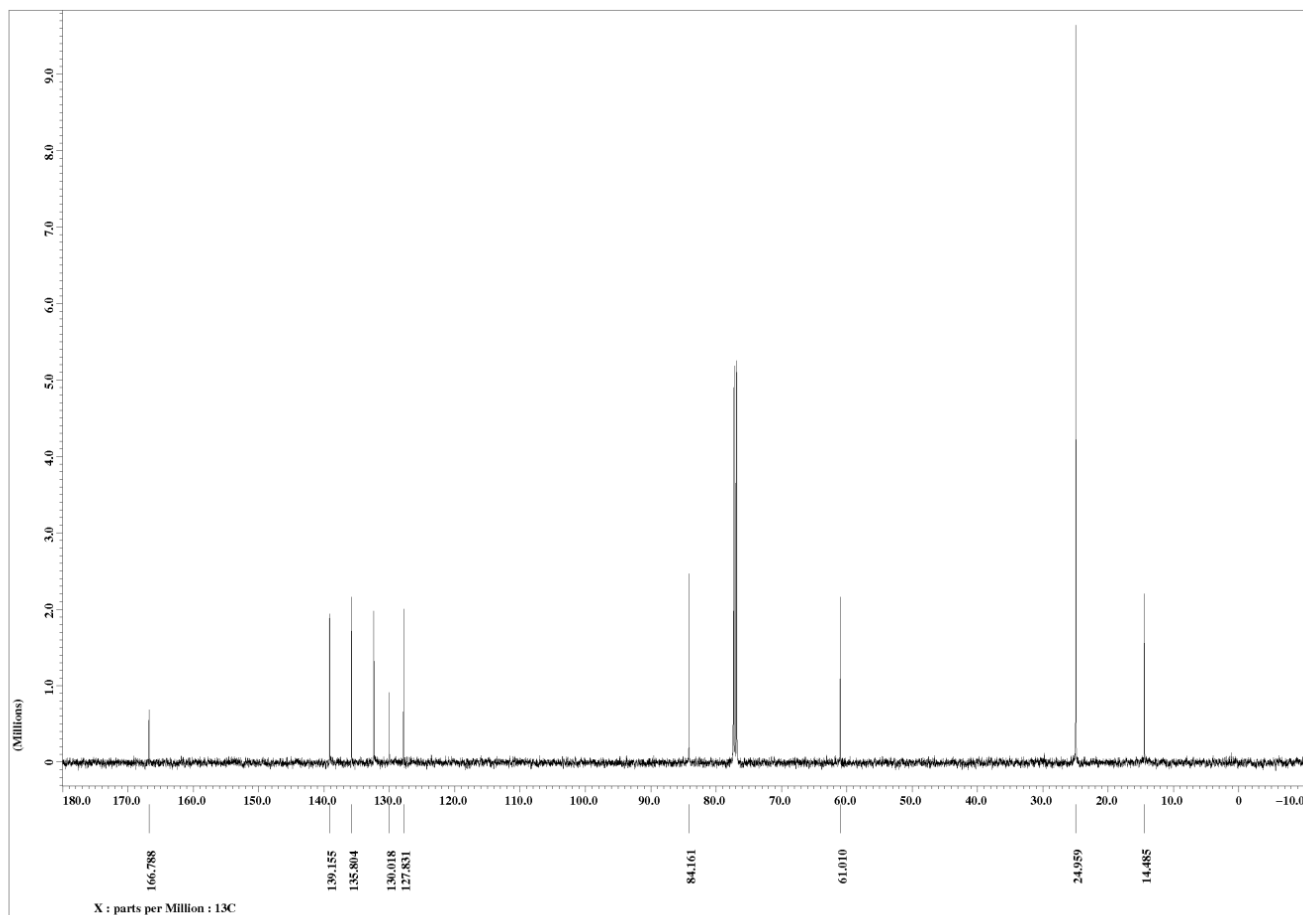
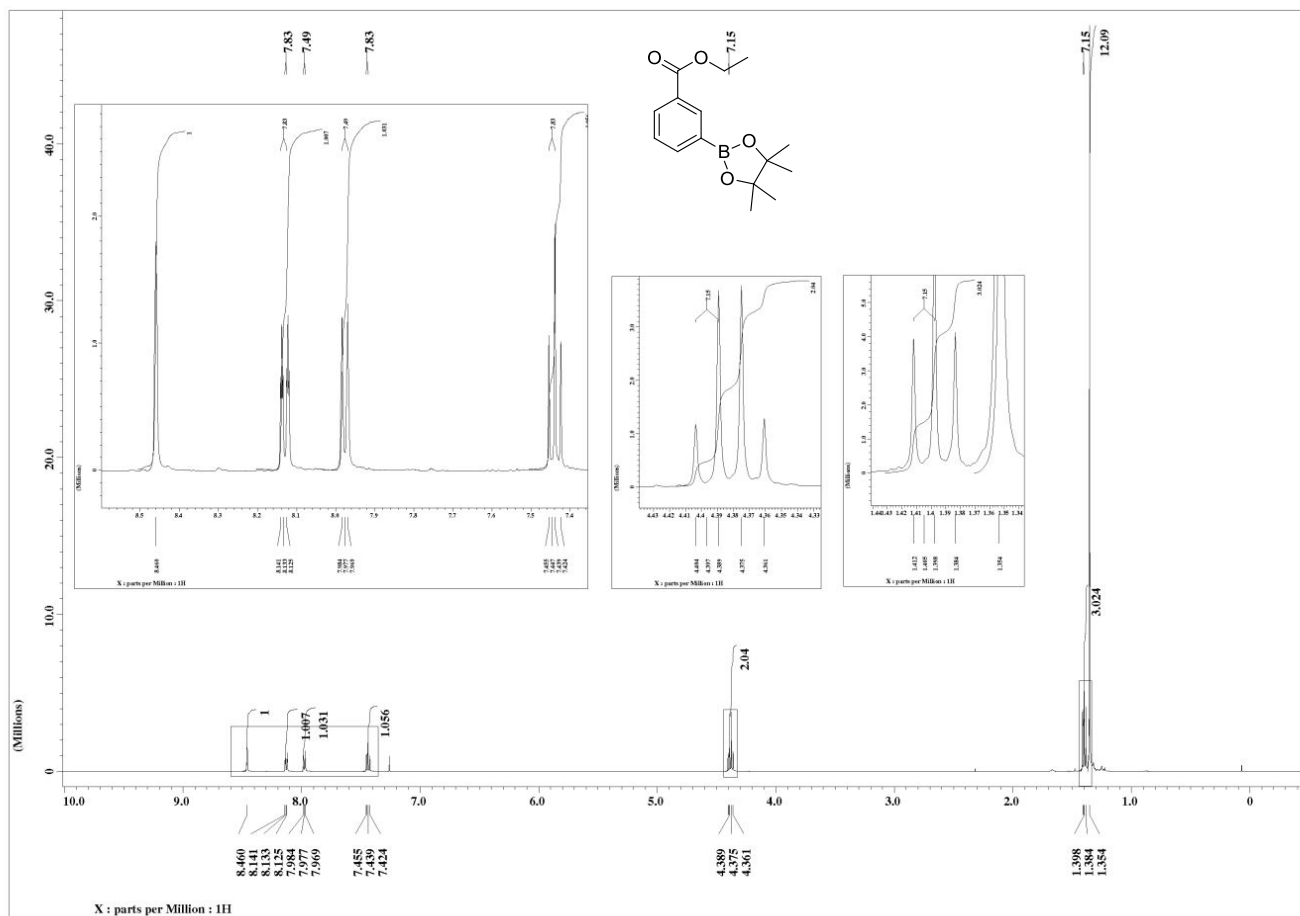
4,4,5,5-tetramethyl-2-(3-(trifluoromethyl)phenyl)-1,3,2-dioxaborolane (67b)



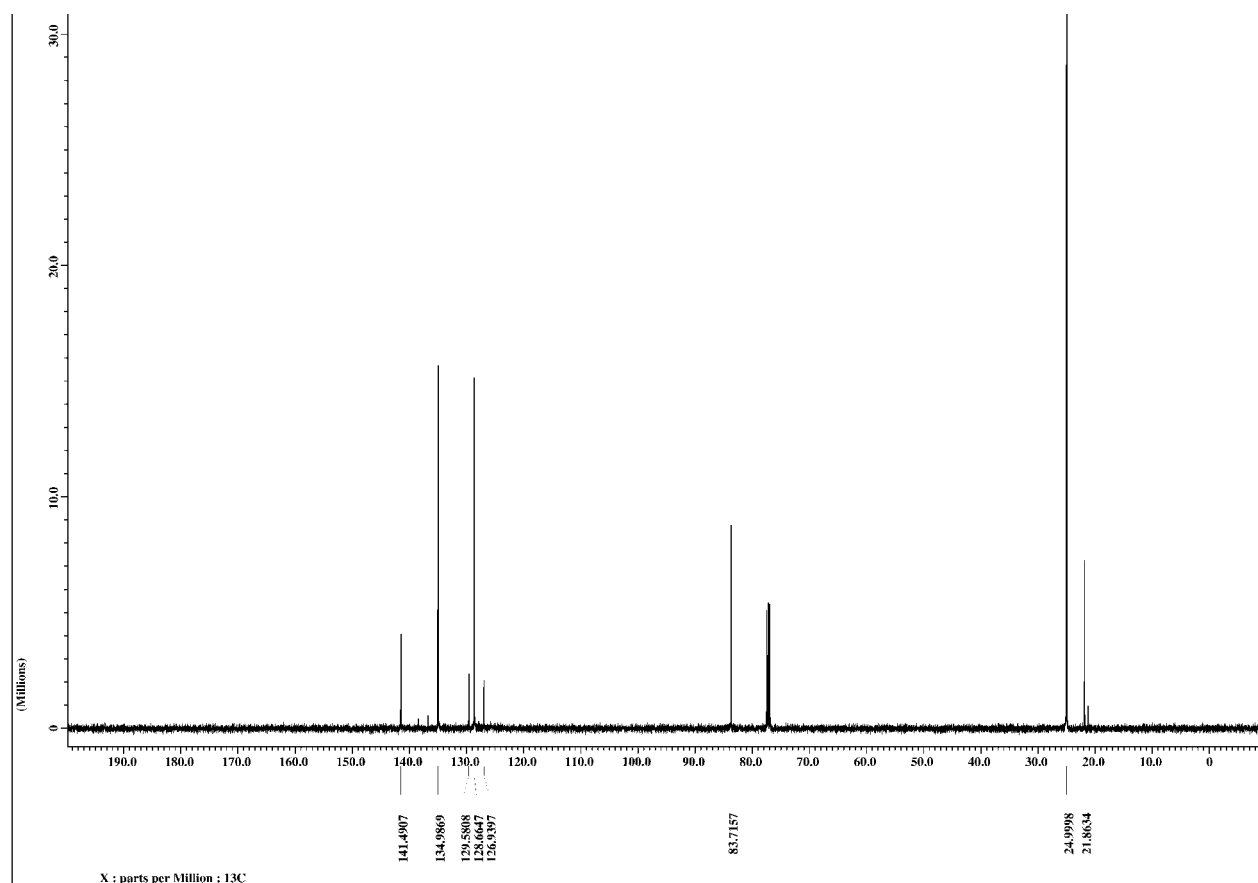
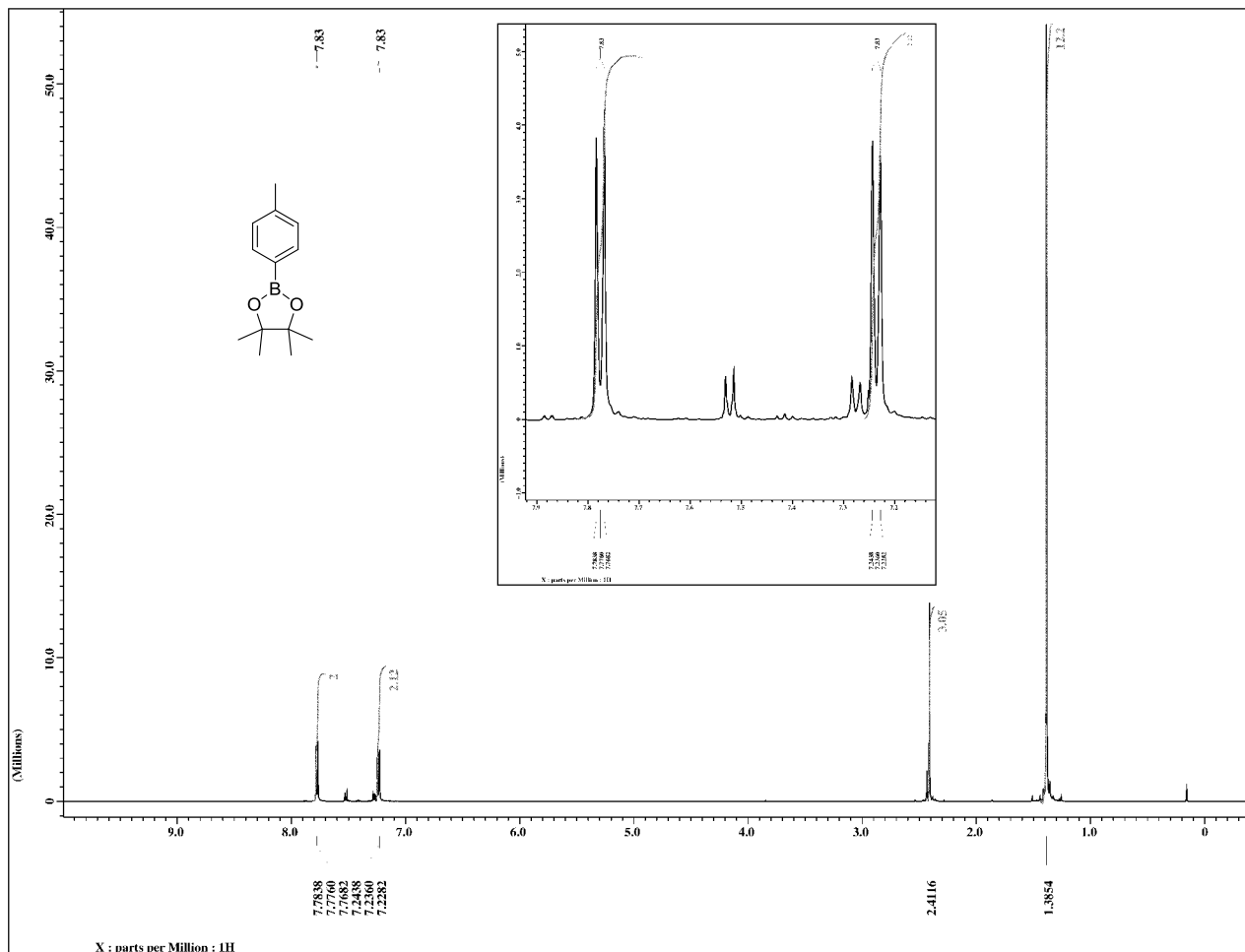
ethyl 4-(4,4,5,5-tetramethyl-1,3,2-dioxaborolan-2-yl)benzoate (68c)



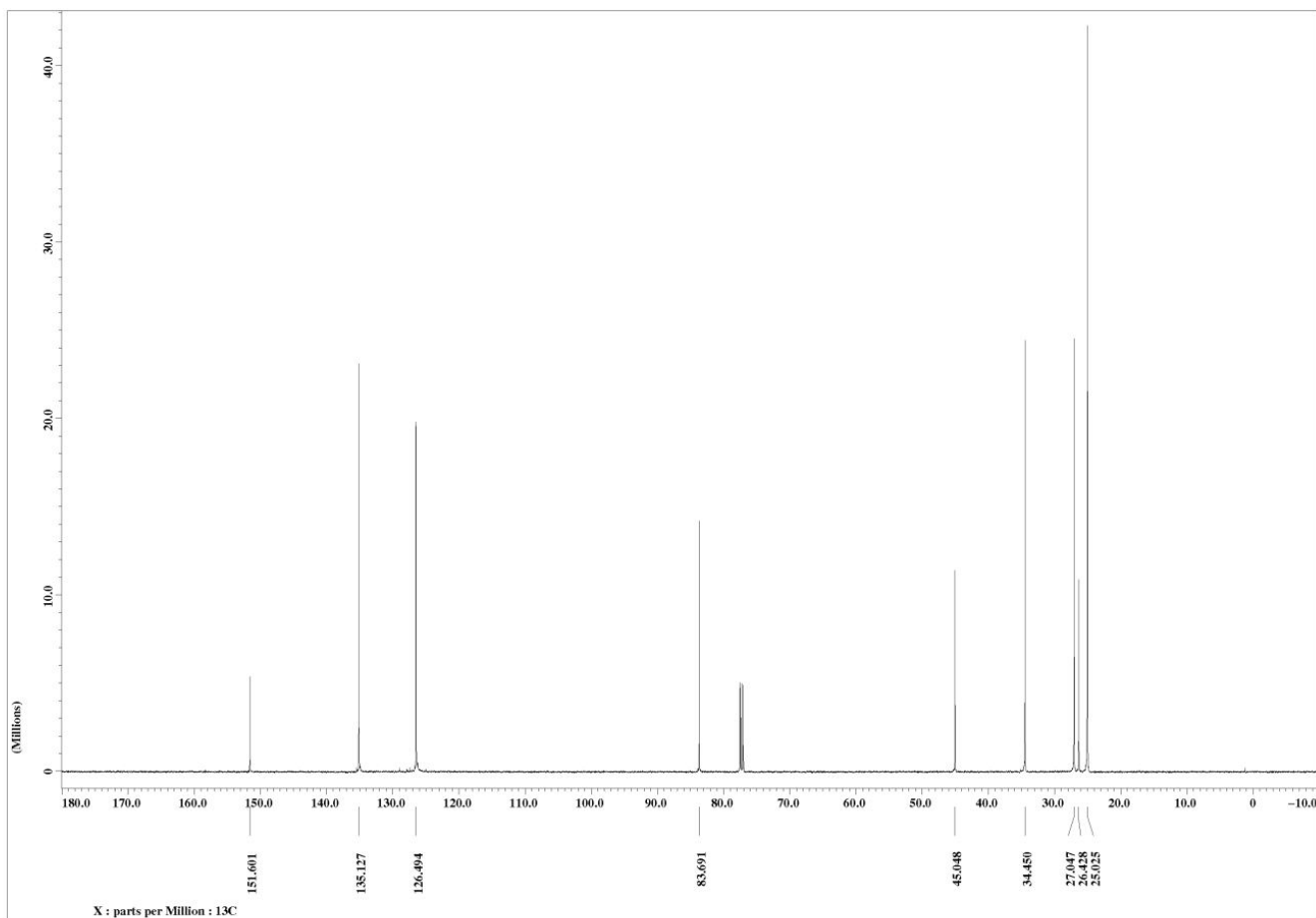
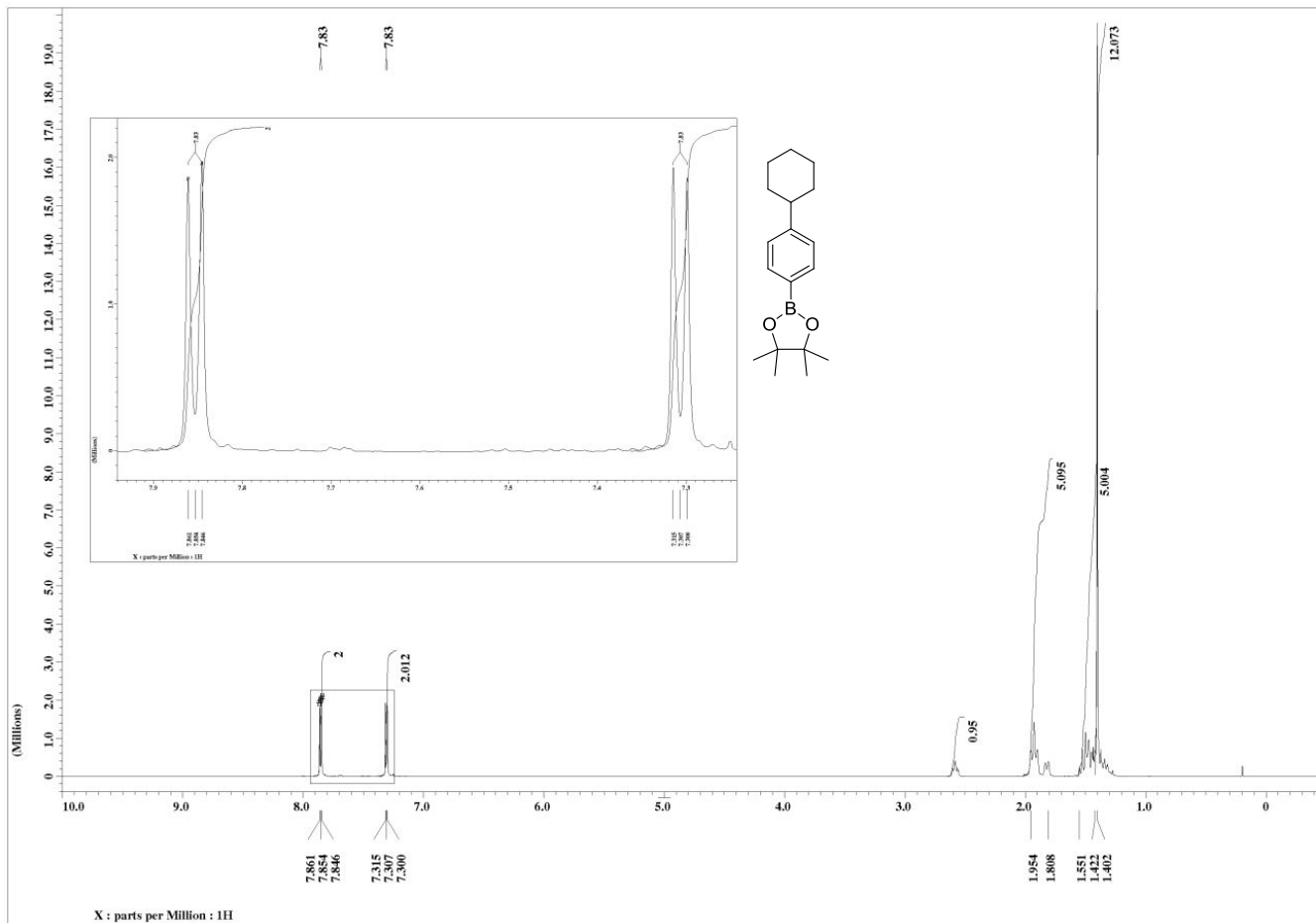
ethyl 3-(4,4,5,5-tetramethyl-1,3,2-dioxaborolan-2-yl)benzoate (67b)



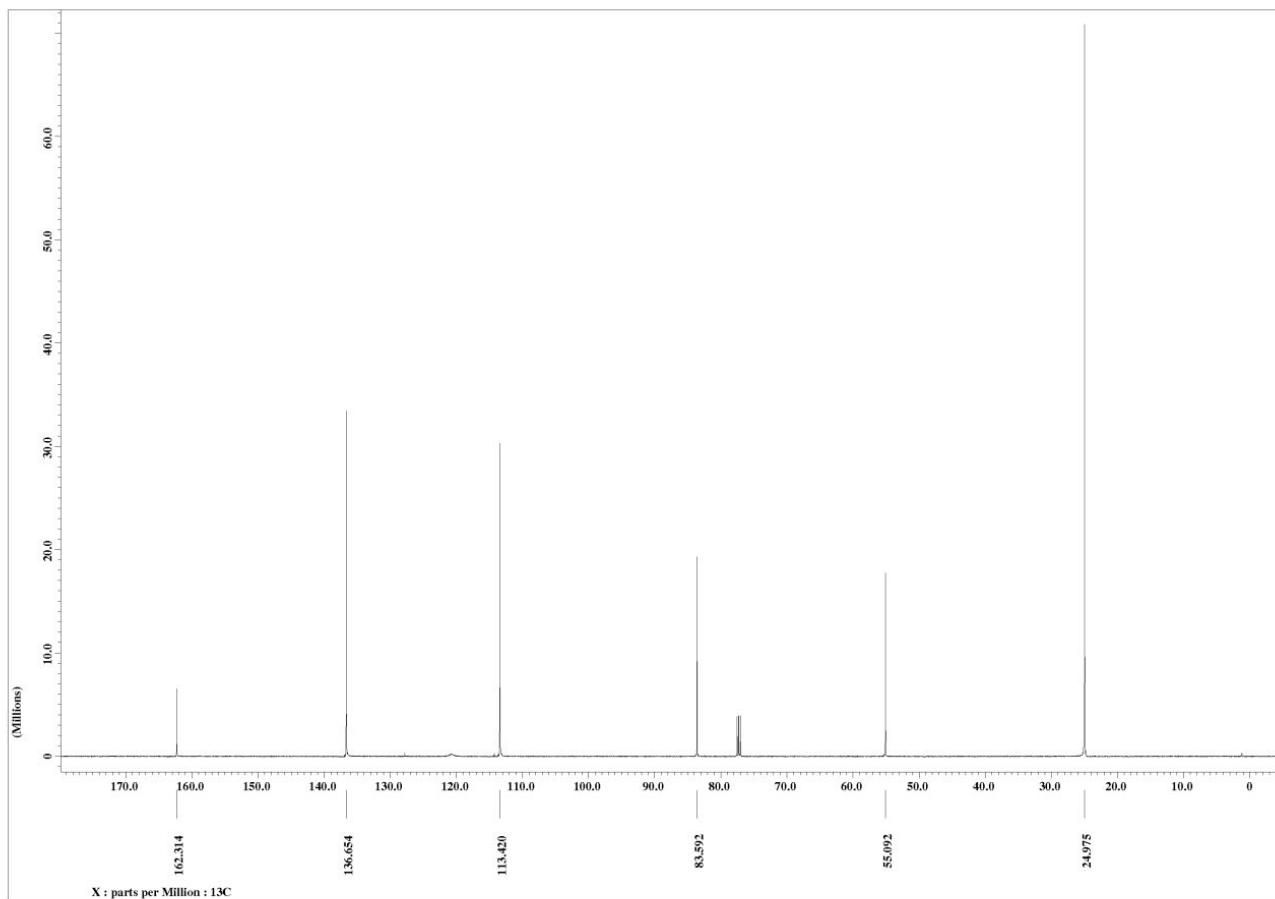
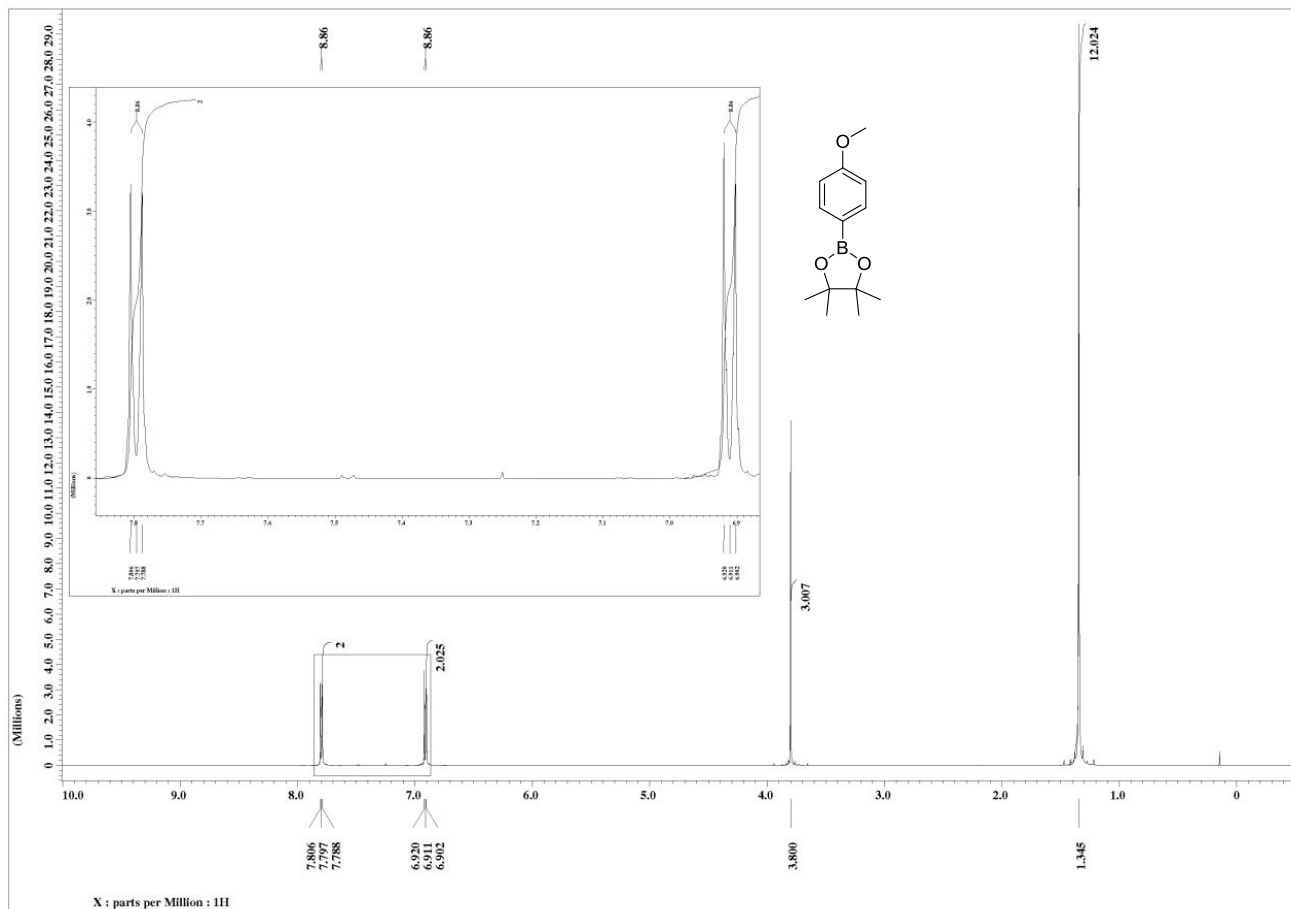
4,4,5,5-tetramethyl-2-(p-tolyl)-1,3,2-dioxaborolane (68d)



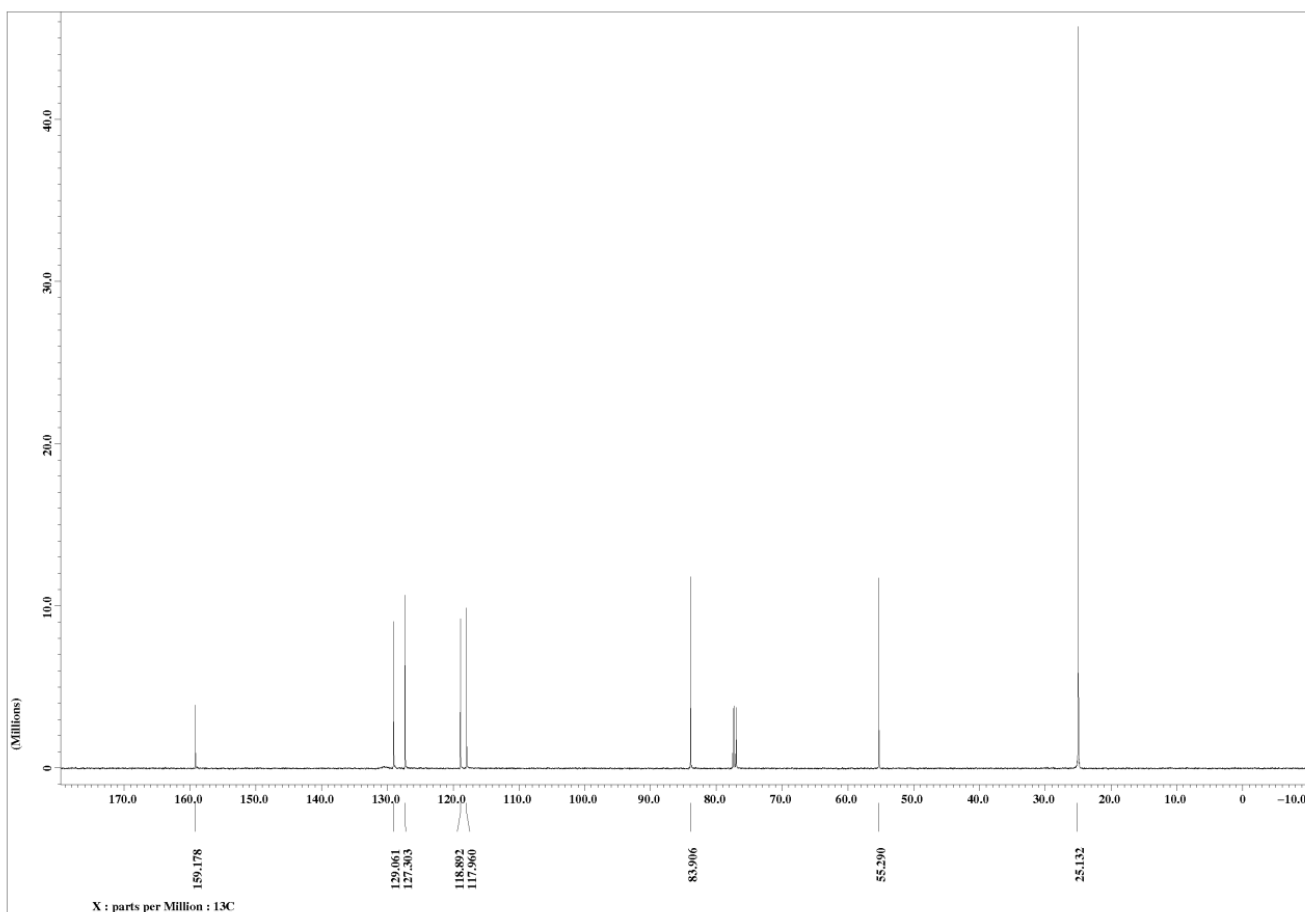
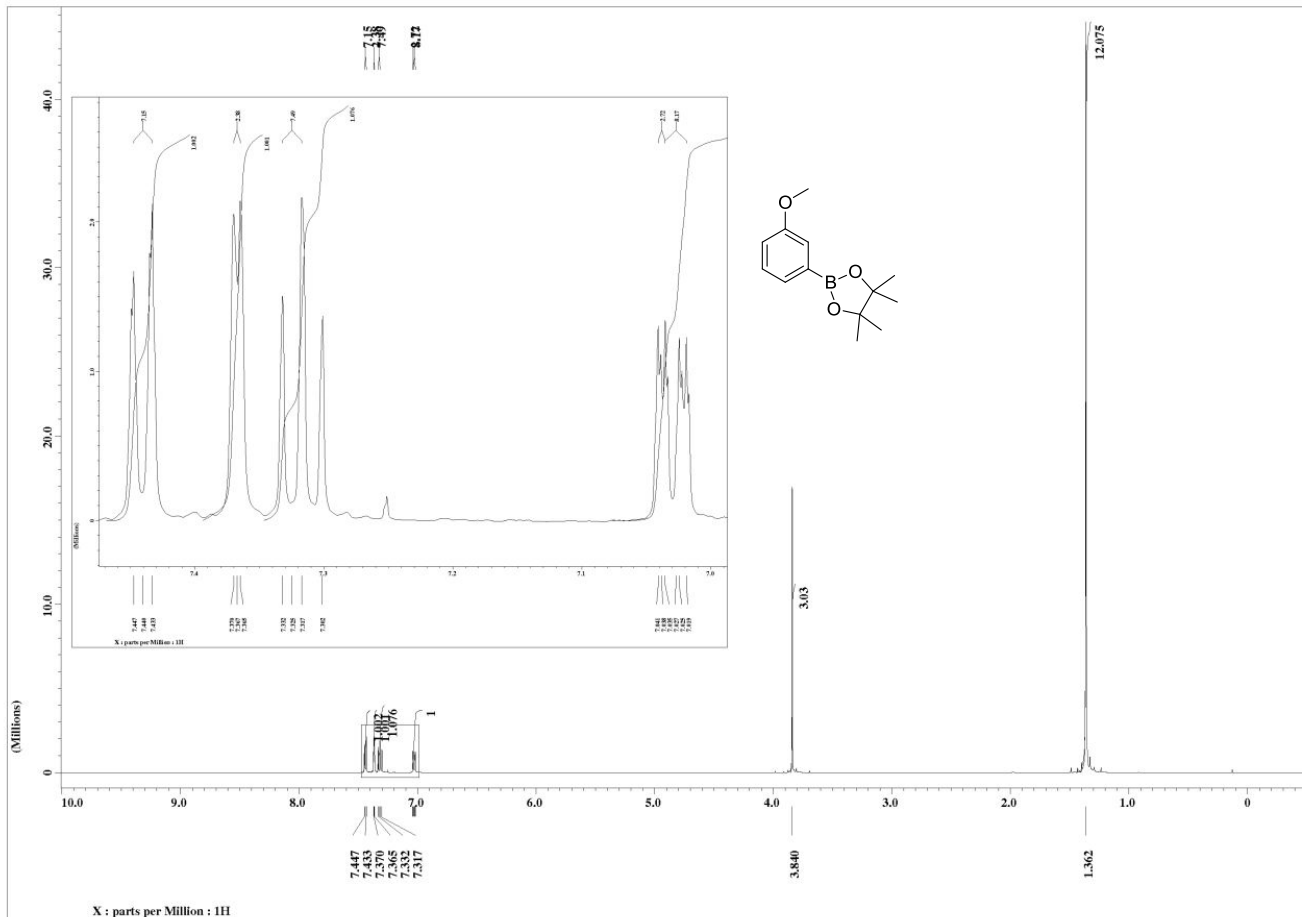
2-(4-cyclohexylphenyl)-4,4,5,5-tetramethyl-1,3,2-dioxaborolane (67d)



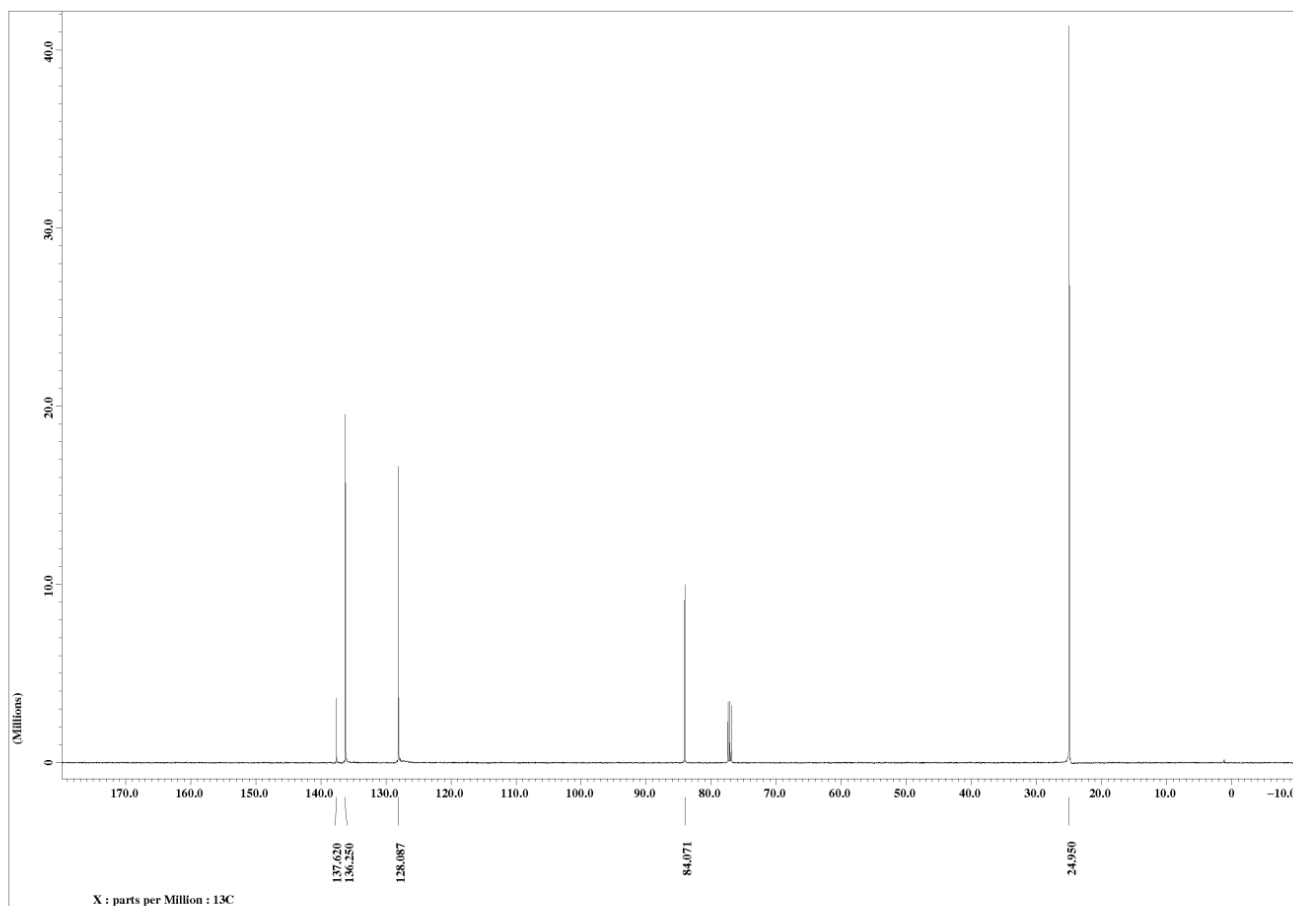
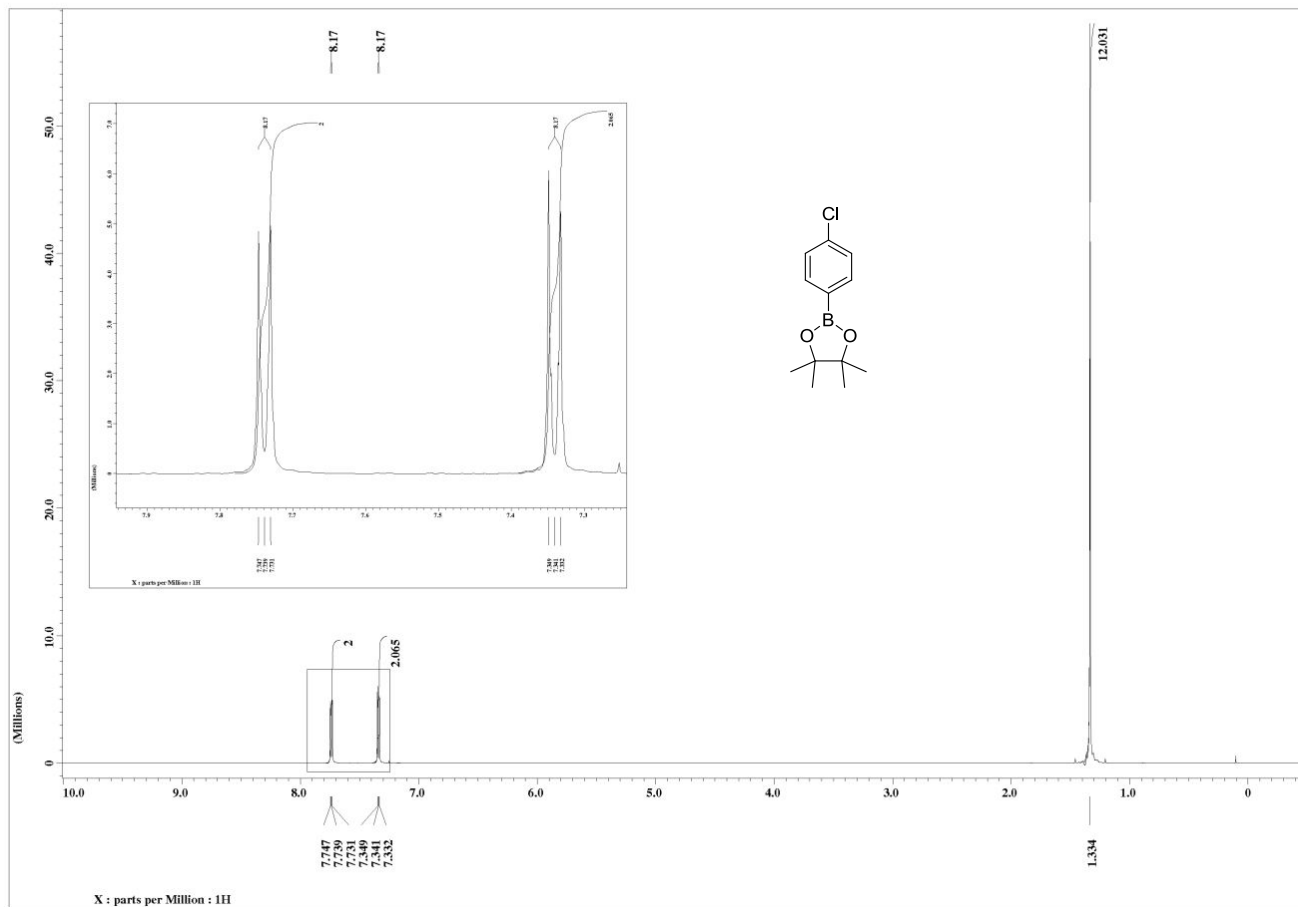
2-(4-methoxyphenyl)-4,4,5,5-tetramethyl-1,3,2-dioxaborolane (68f)



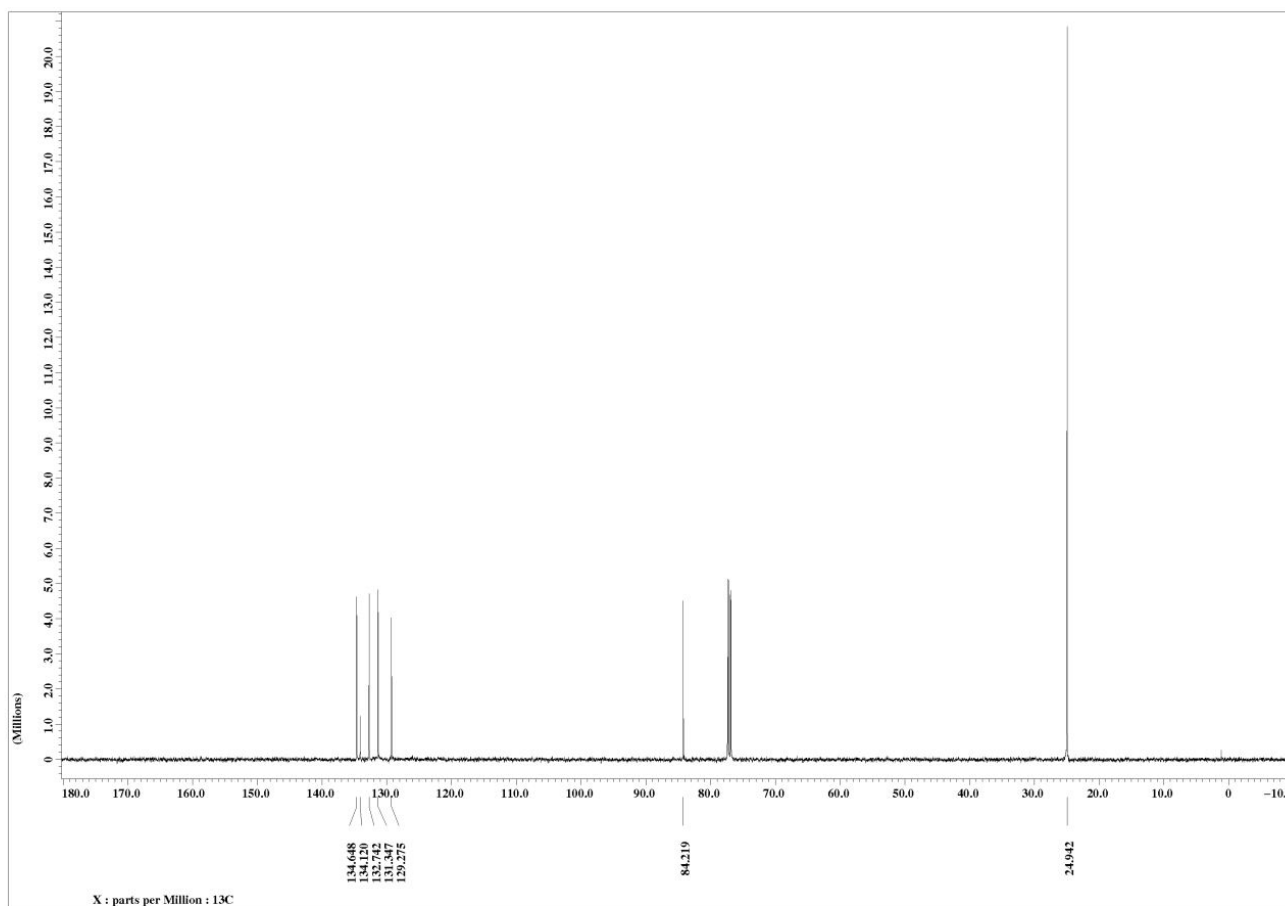
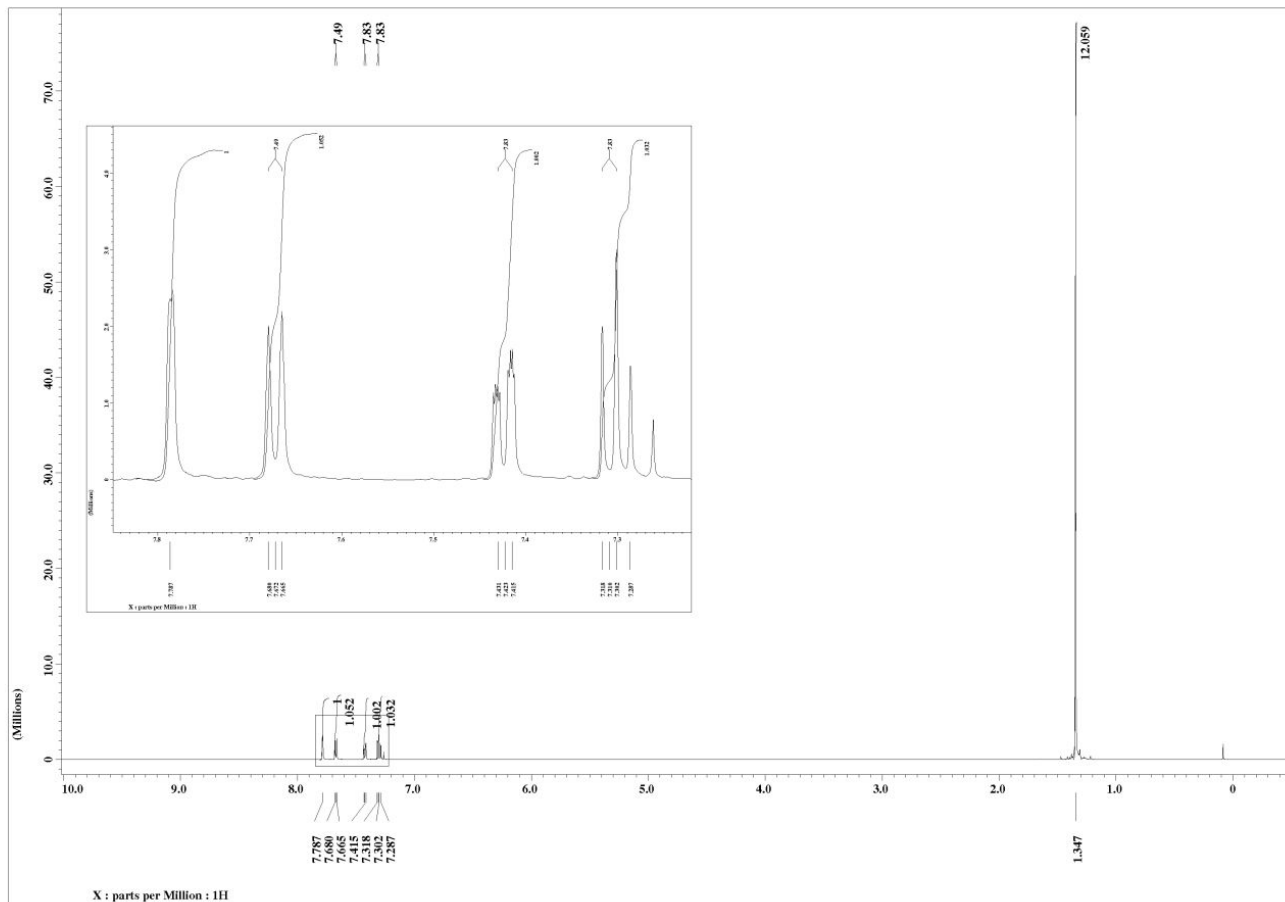
2-(3-methoxyphenyl)-4,4,5,5-tetramethyl-1,3,2-dioxaborolane (67f)



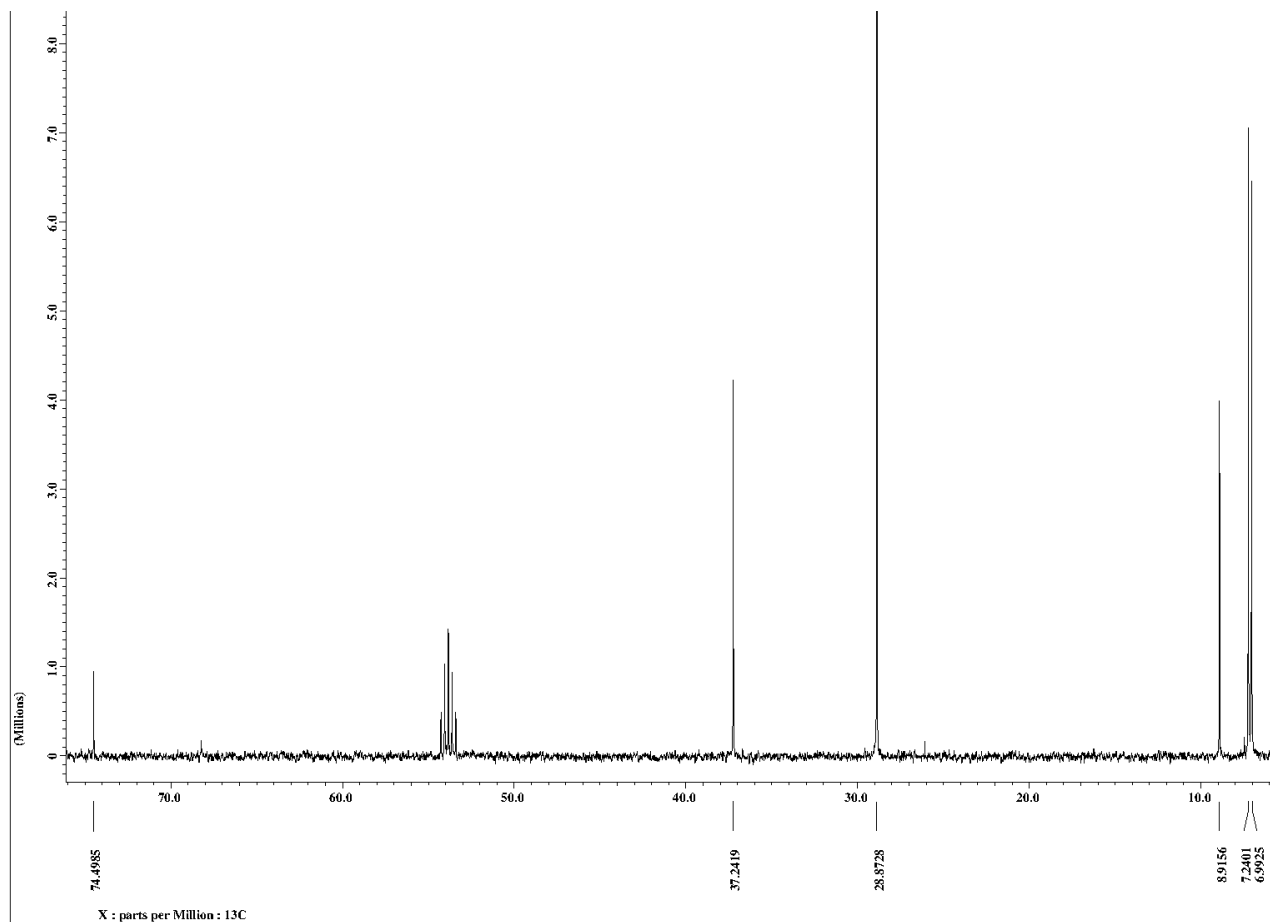
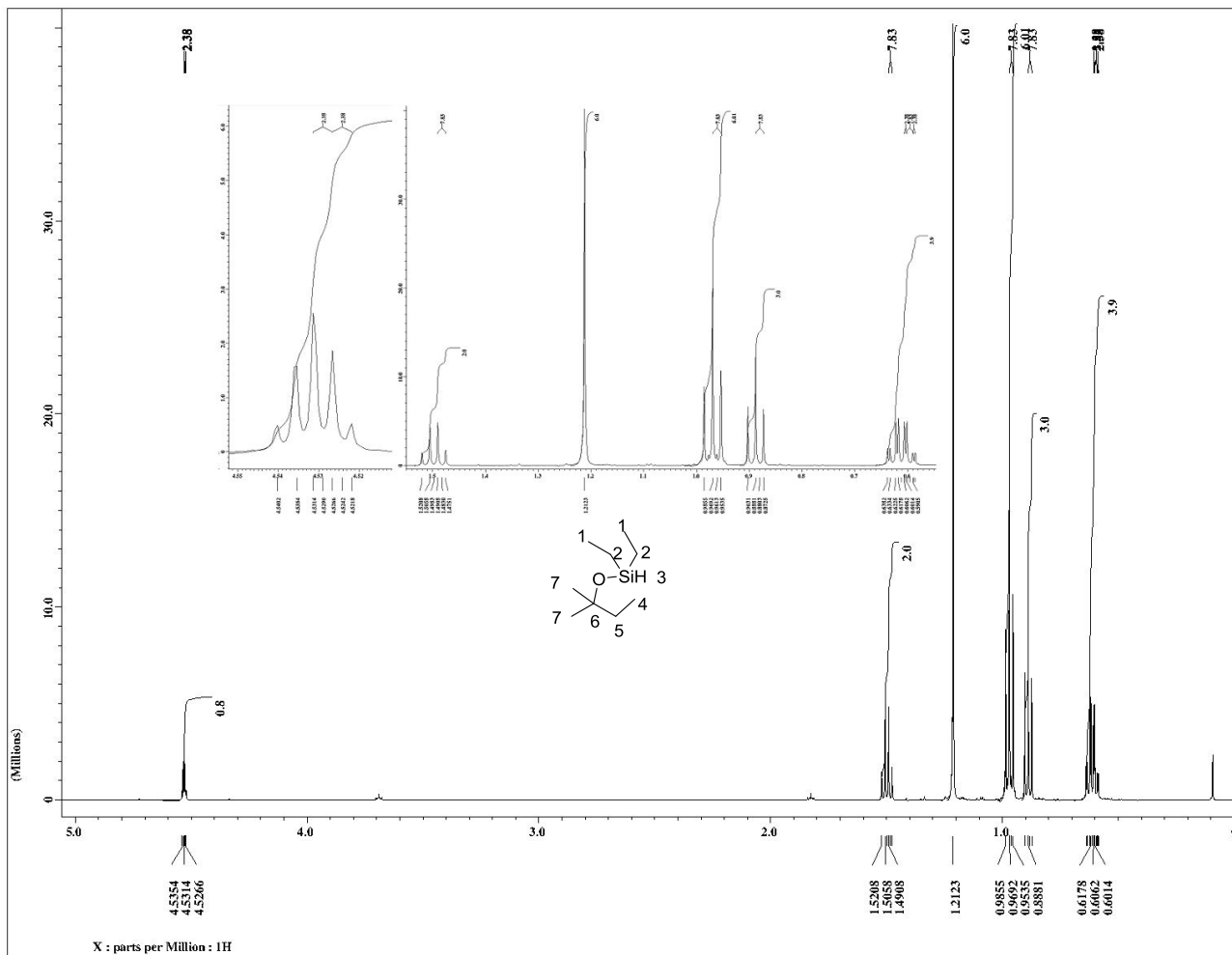
2-(4-chlorophenyl)-4,4,5,5-tetramethyl-1,3,2-dioxaborolane (68g)



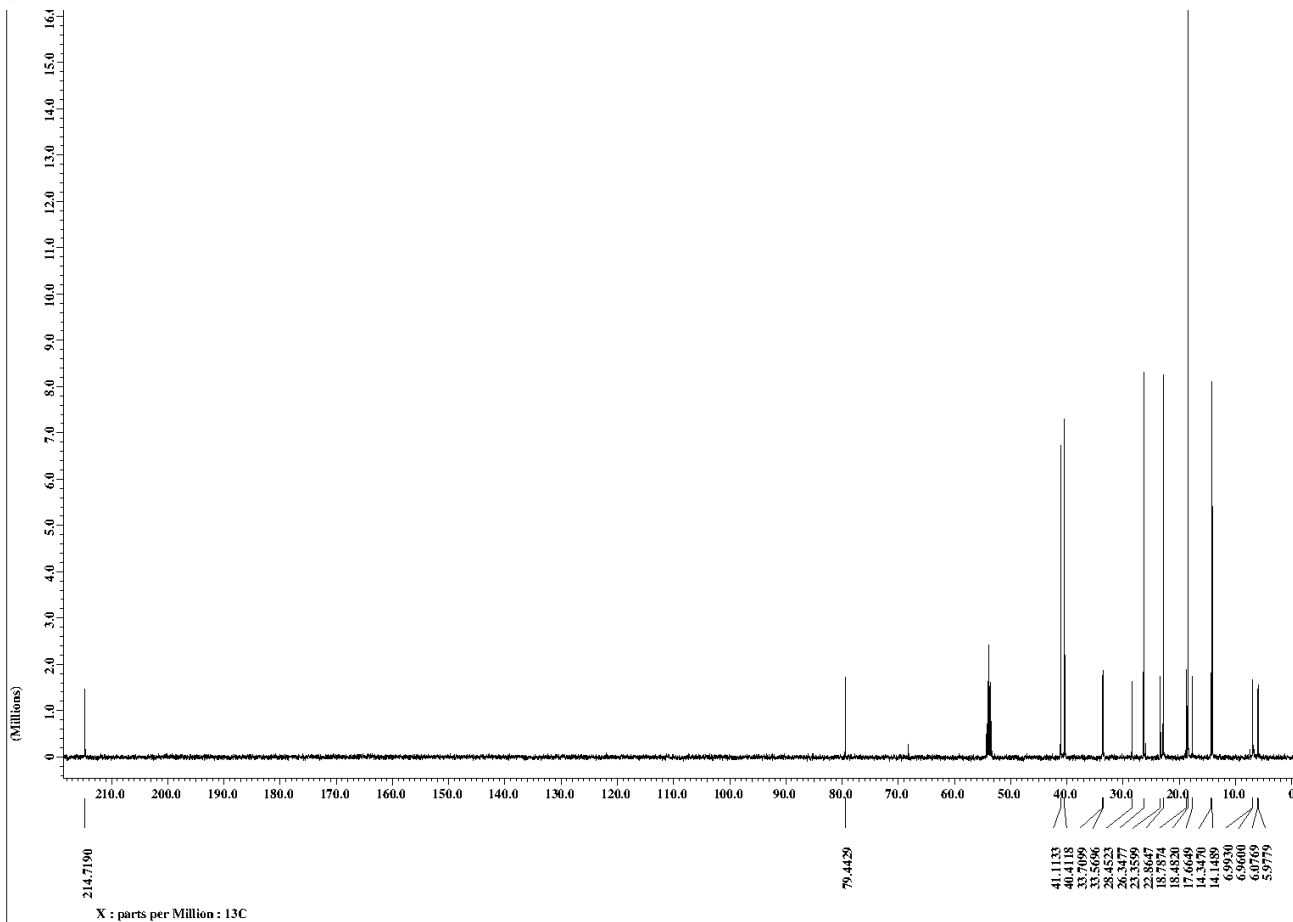
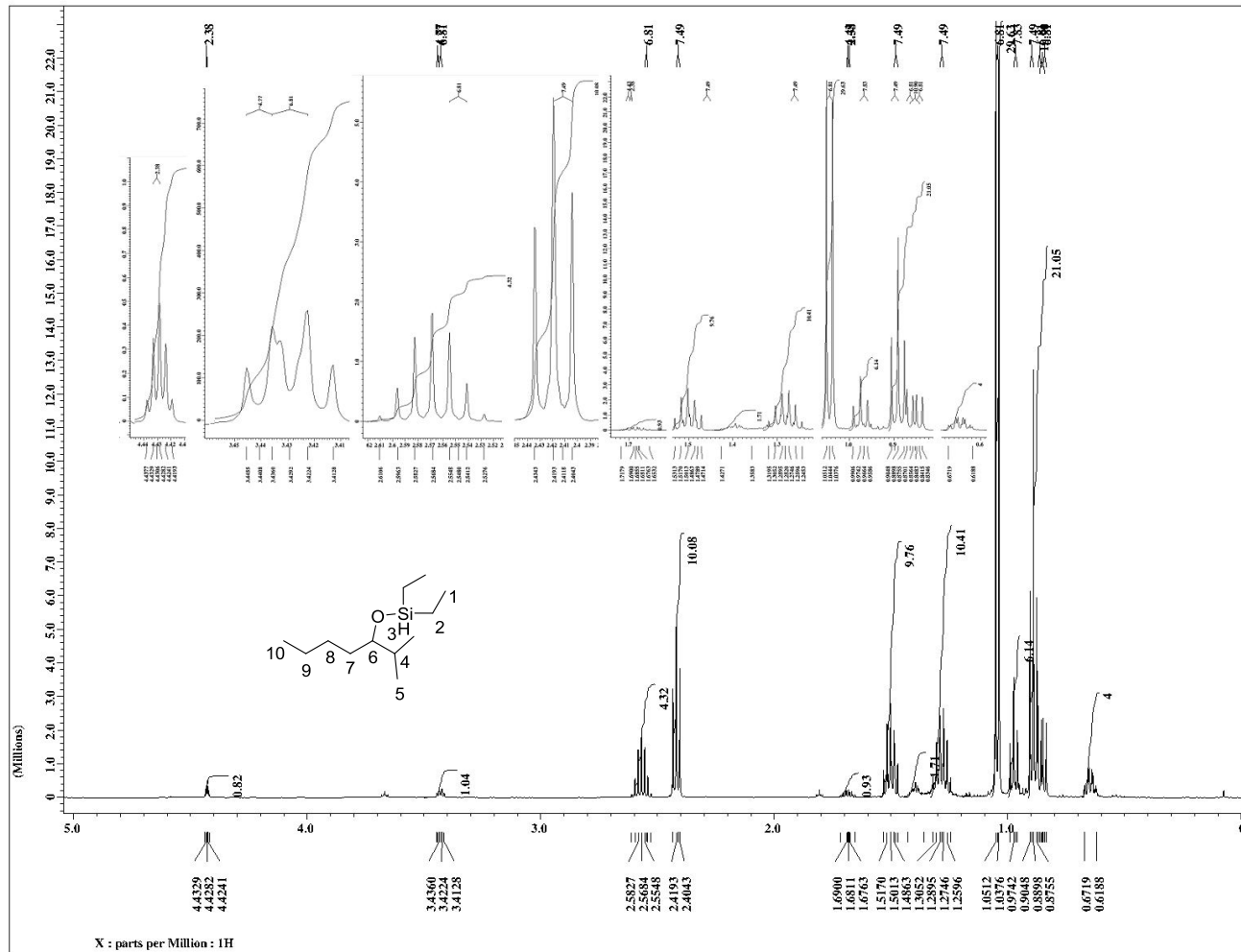
2-(3-chlorophenyl)-4,4,5,5-tetramethyl-1,3,2-dioxaborolane (67g)



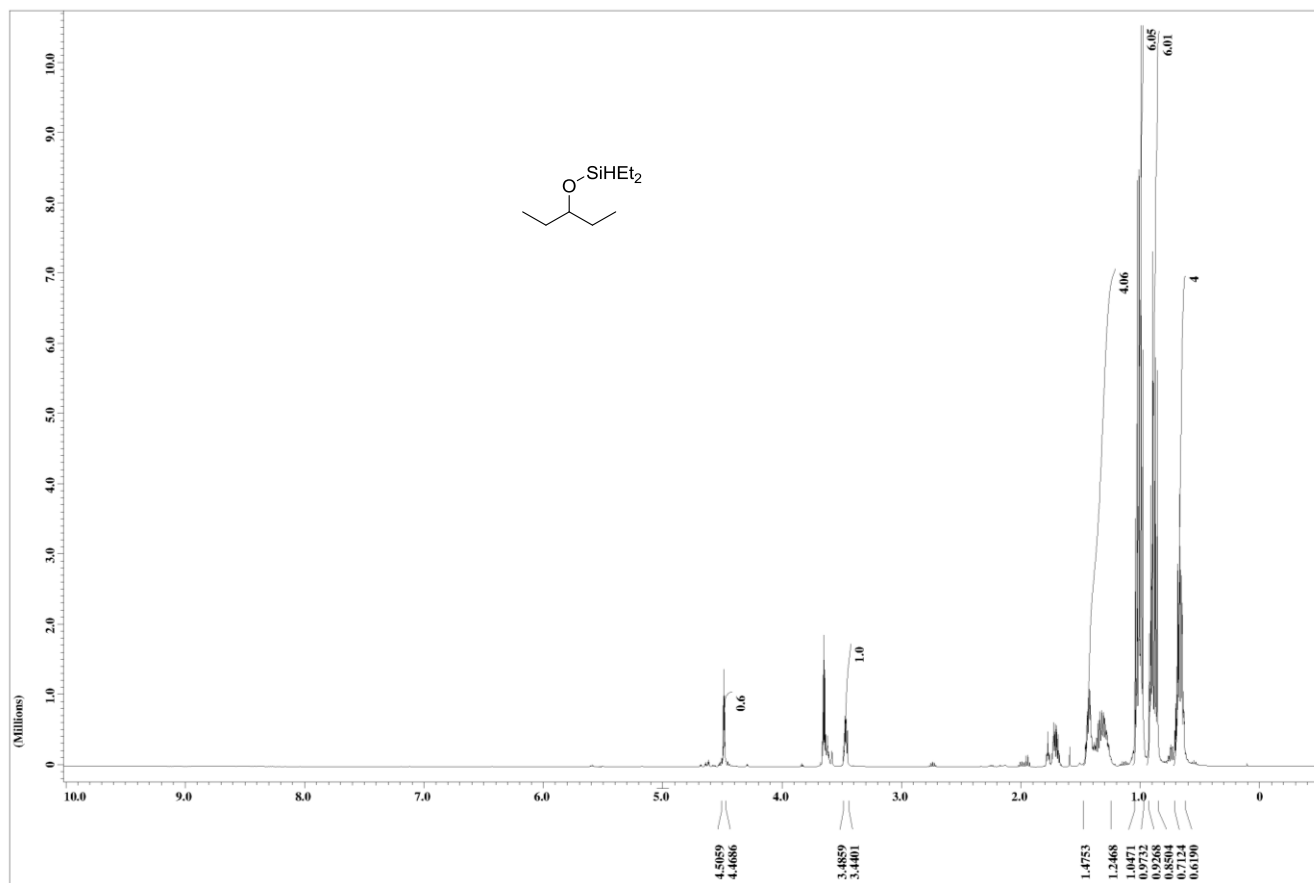
diethyl(tert-pentyloxy)silane (103c)



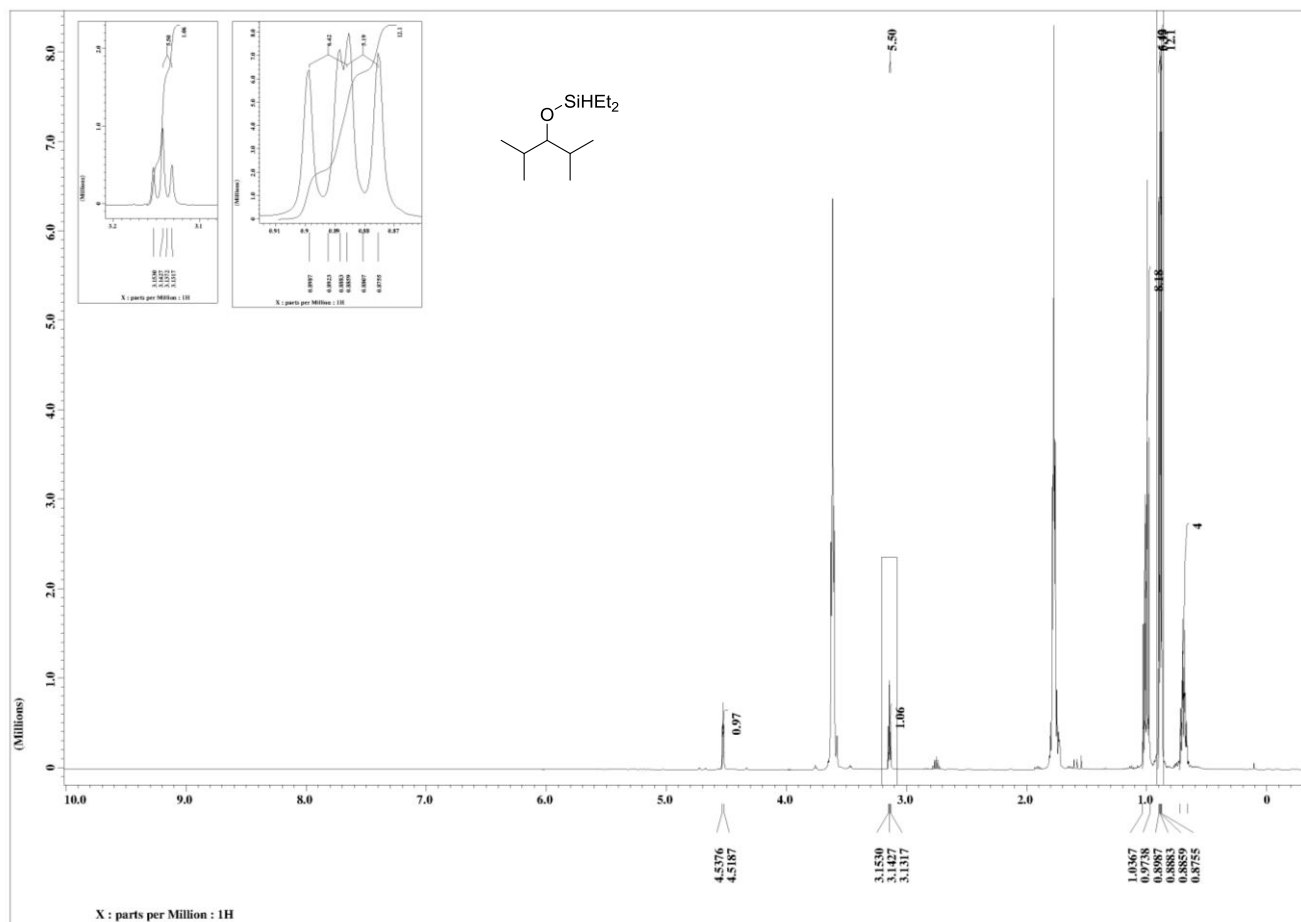
diethyl((2-methylheptan-3-yl)oxy)silane (103b)



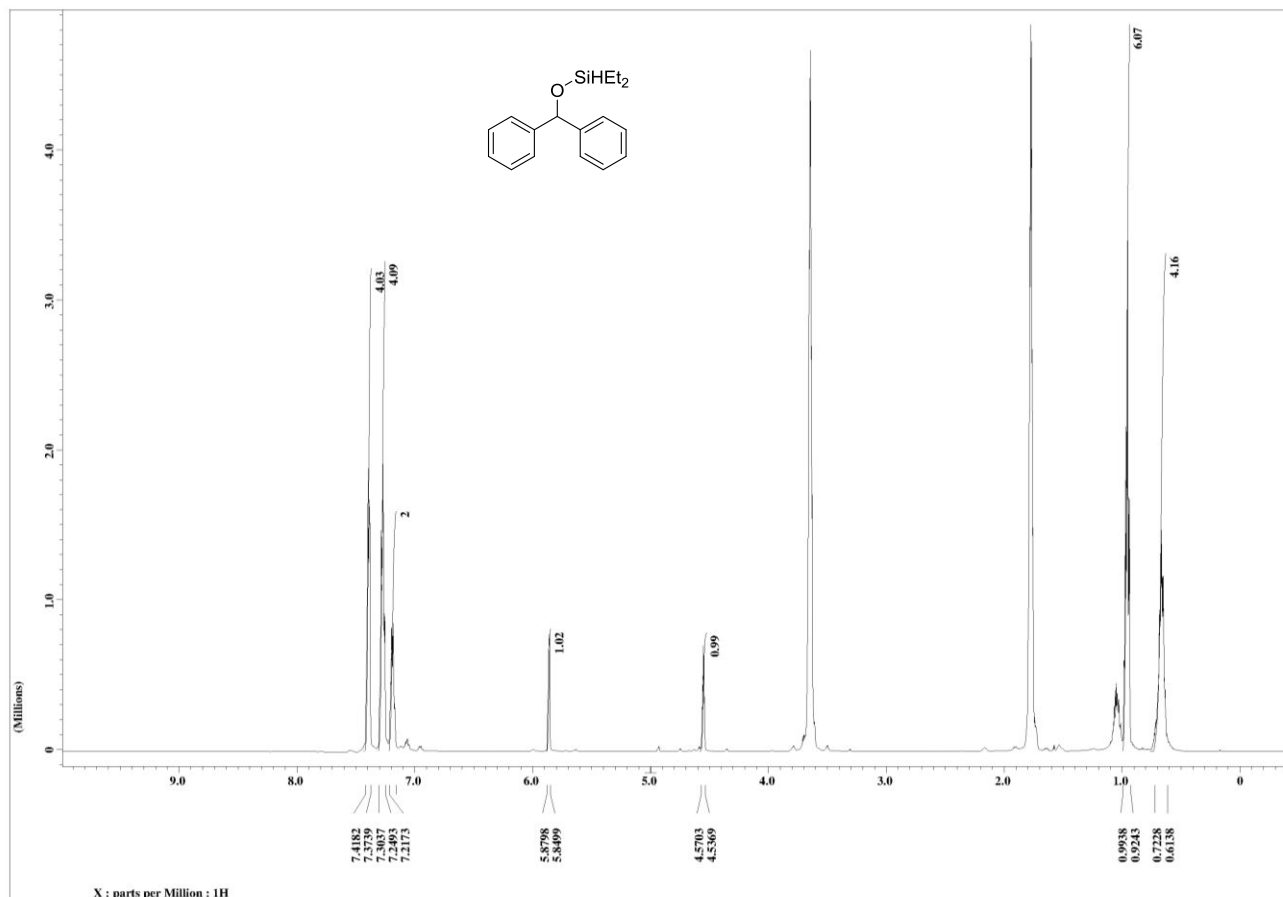
diethyl(pentan-3-yloxy)silane (107b)



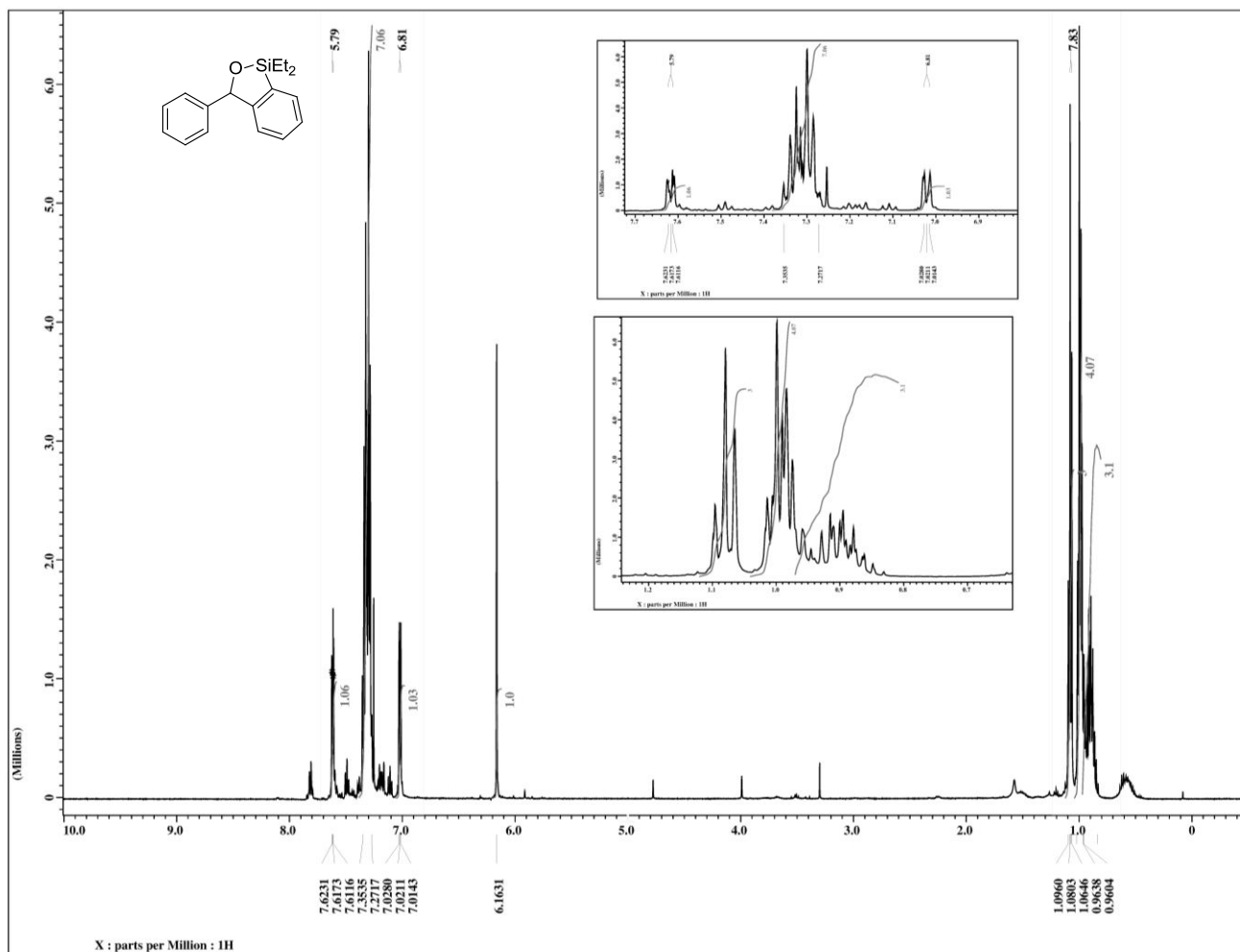
((2,4-dimethylpentan-3-yl)oxy)diethylsilane (107d)



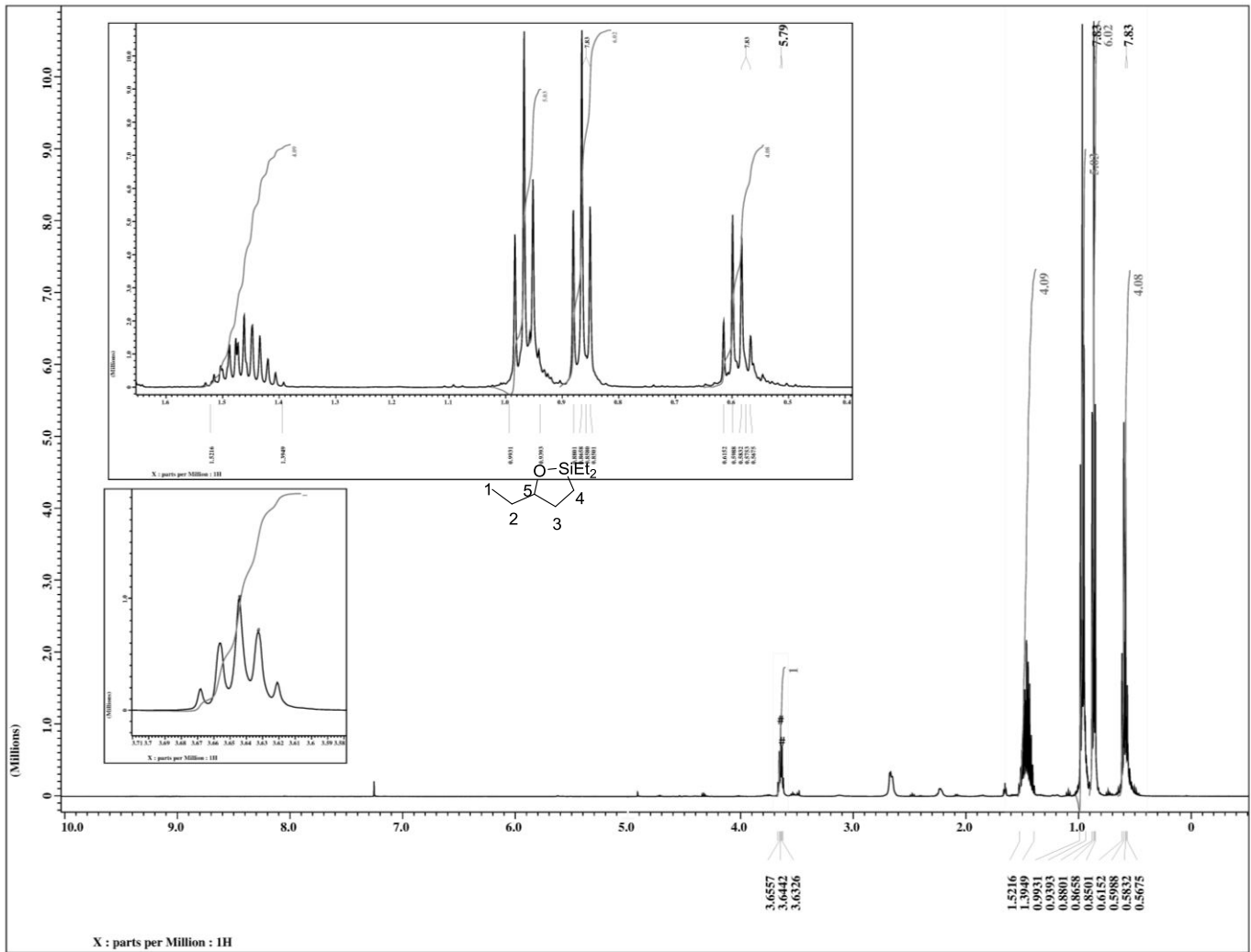
(benzhydryloxy)diethylsilane (107e)



1,1-diethyl-3-phenyl-1,3-dihydrobenzo[c][1,2]oxasilole (108e)

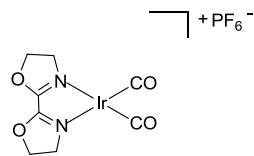
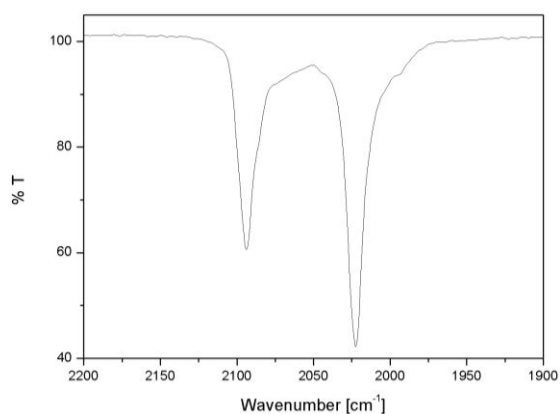


2,2,5-triethyl-1,2-oxasilolane (108c)

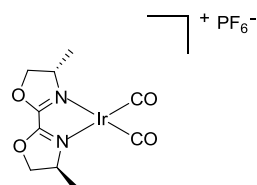
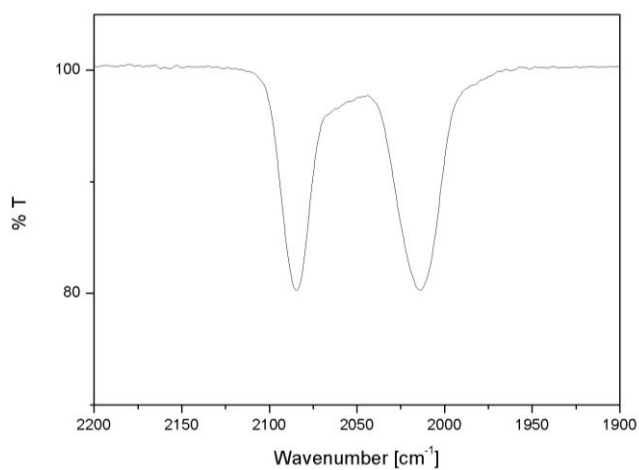


Appendix C: IR Spectra of Carbonyl Complexes

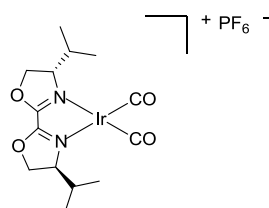
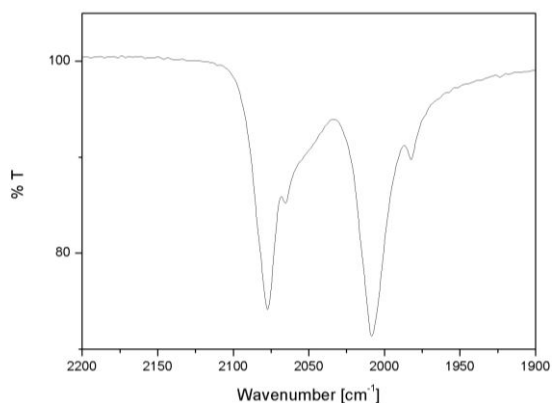
[Ir(H-box)(CO)₂PF₆ (28a) – solid IR



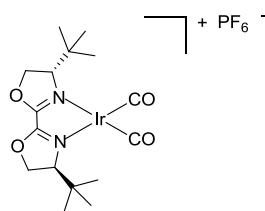
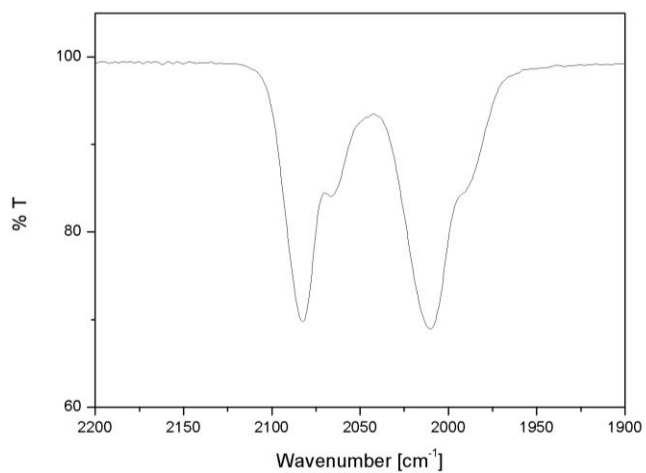
[Ir(Me-box)(CO)₂PF₆ (28b) – solid IR



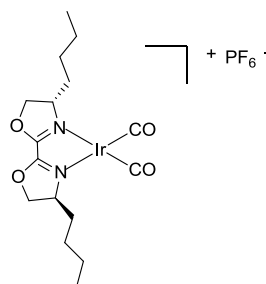
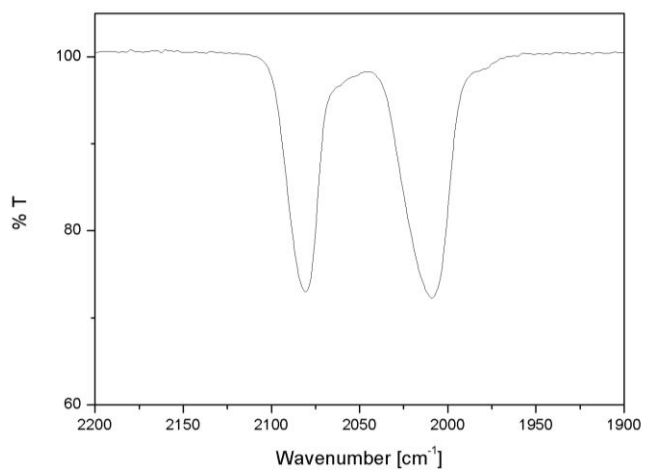
[Ir(ⁱPr-box)(CO)₂PF₆ (28c) – solid IR



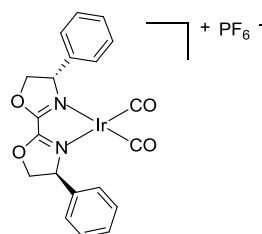
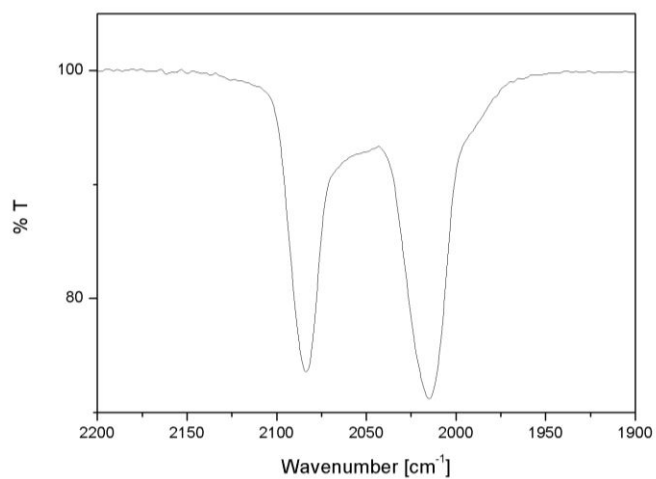
[Ir(^tBu-box)(CO)₂PF₆ (28d) – solid IR



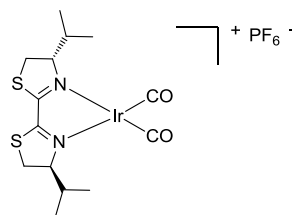
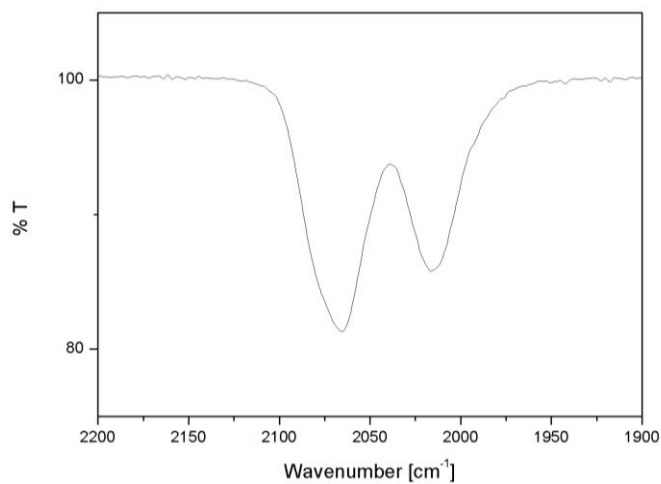
[Ir(ⁿBu-box)(CO)₂PF₆ (28e) – solid IR



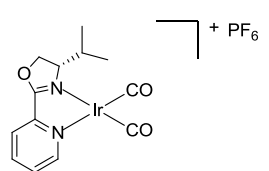
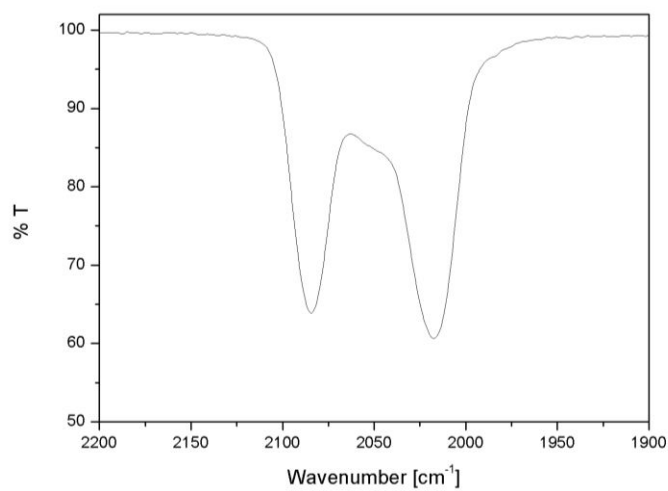
[Ir(Ph-box)(CO)₂PF₆ (28f) – solid IR



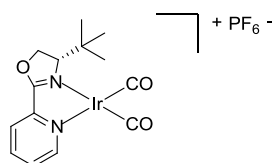
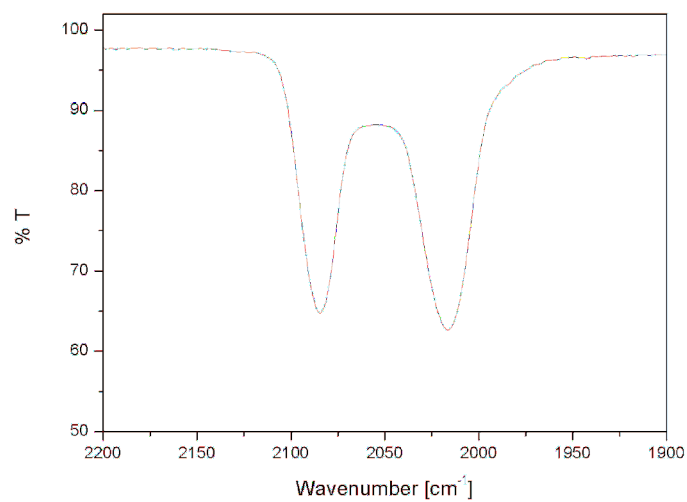
[Ir(ⁱPr-bta)(CO)₂PF₆ (28g) – solid IR



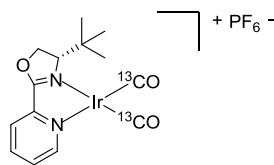
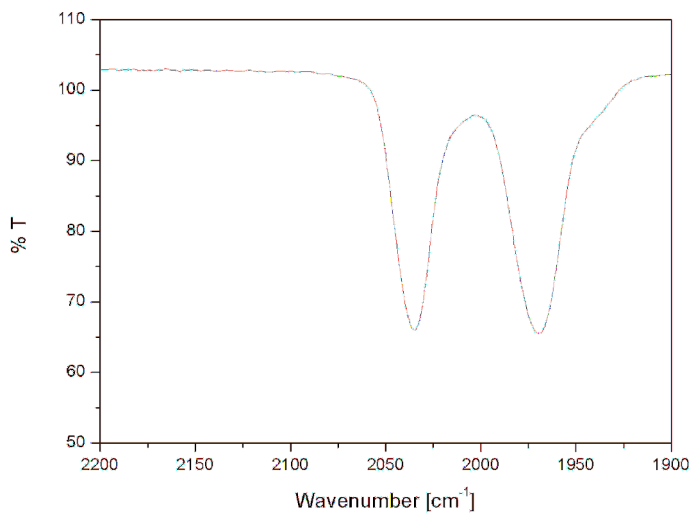
[Ir(ⁱPr-pyrox)(CO)₂PF₆ (28h) – solid IR



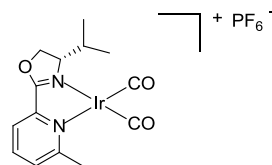
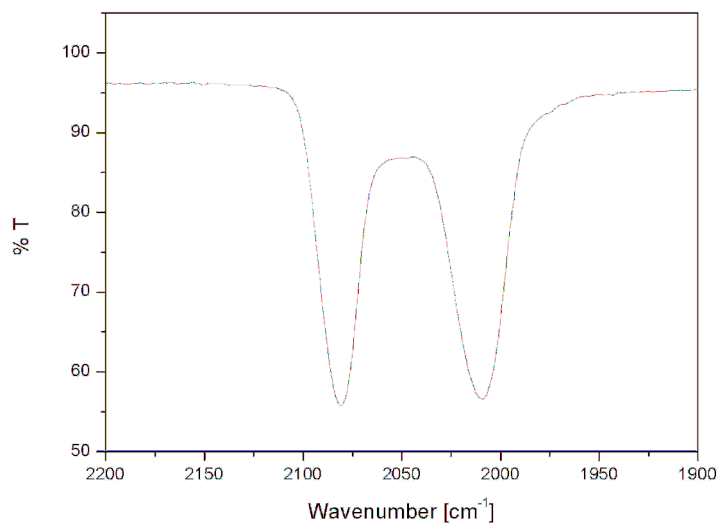
[Ir(^tBu-pyrox)(CO)₂PF₆ (28i) – solid IR



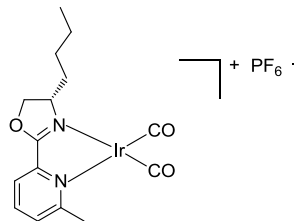
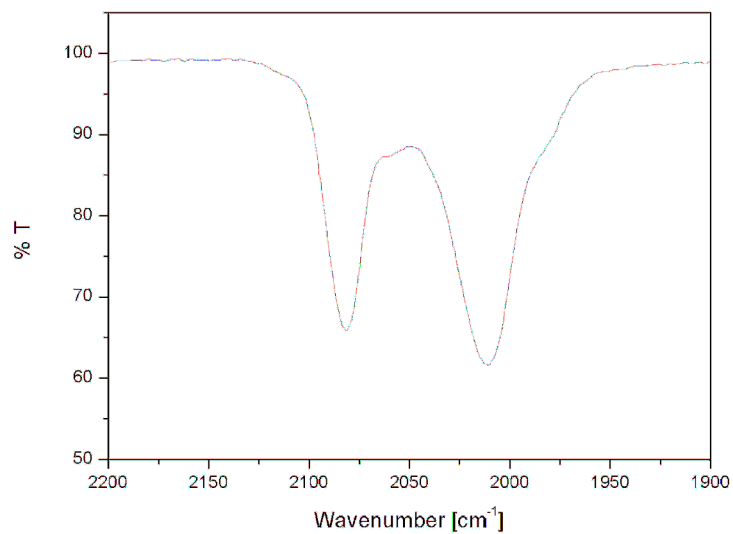
[Ir(^tBu-pyrox)(¹³CO)₂]PF₆ (¹³C-28i) – solid IR



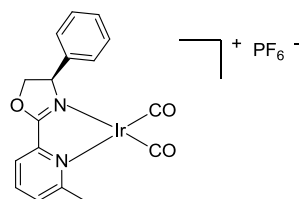
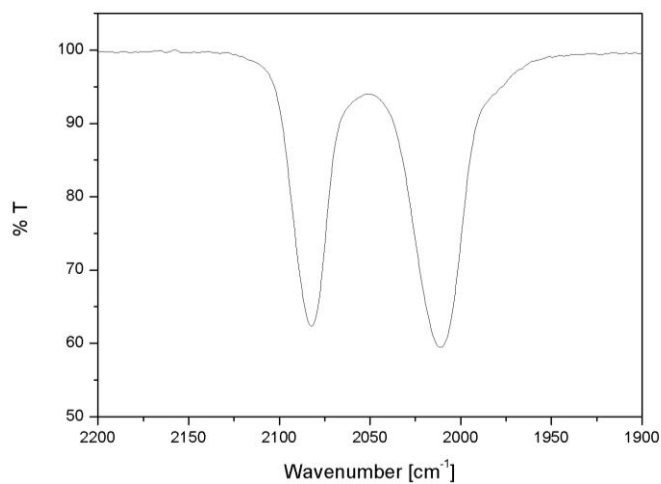
[Ir(ⁱPr-mepyrox)(CO)₂]PF₆ (28j) – solid IR



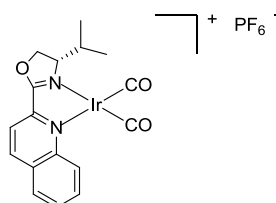
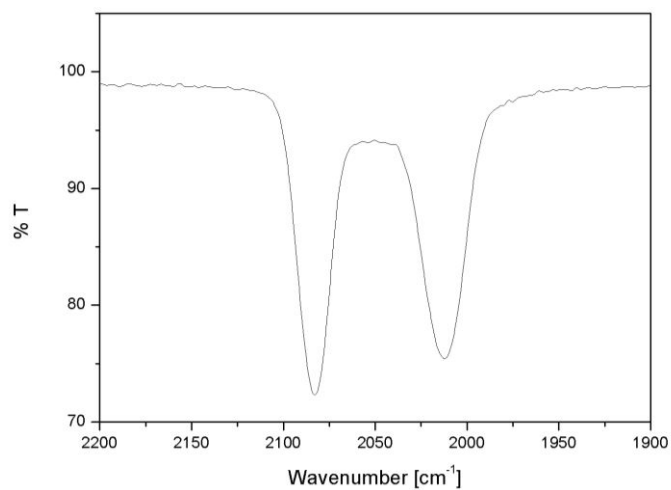
[Ir(ⁿBu-mepyrox)(CO)₂]PF₆ (28k) – solid IR



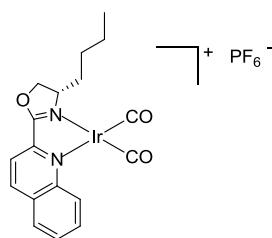
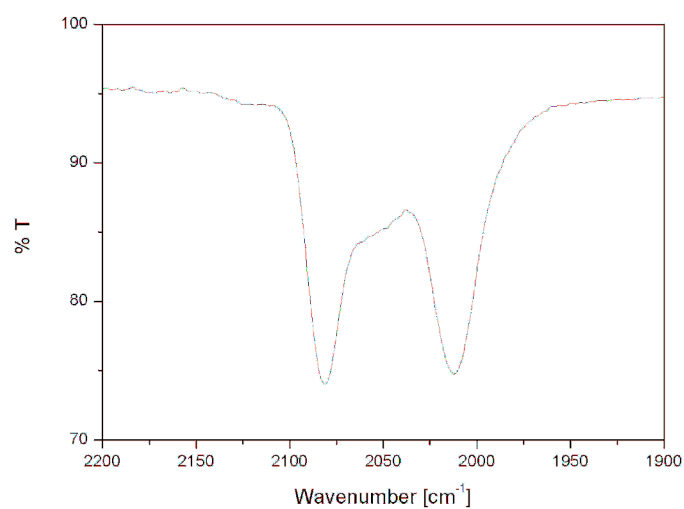
[Ir(Ph-mepyrox)(CO)₂PF₆ (28l) – solid IR



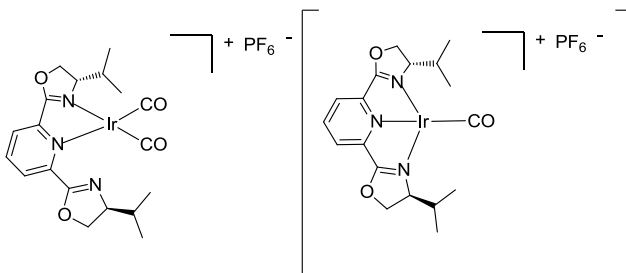
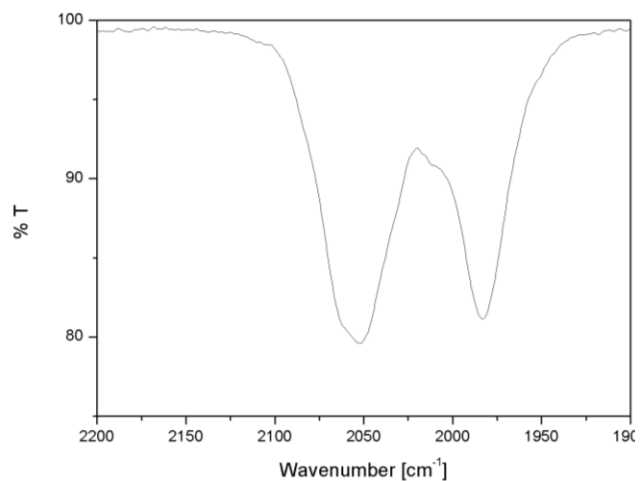
[Ir(ⁱPr-quinox)(CO)₂PF₆ (28m) – solid IR



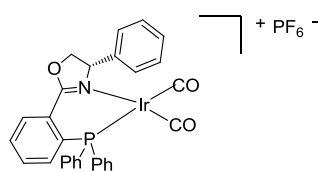
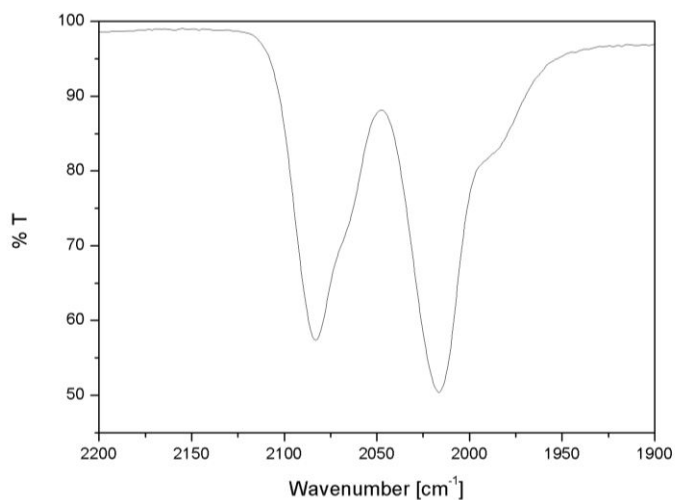
[Ir(ⁿBu-quinox)(CO)₂PF₆ (28n) – solid IR



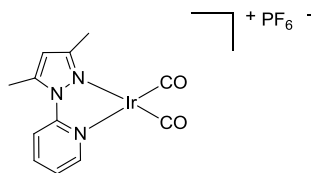
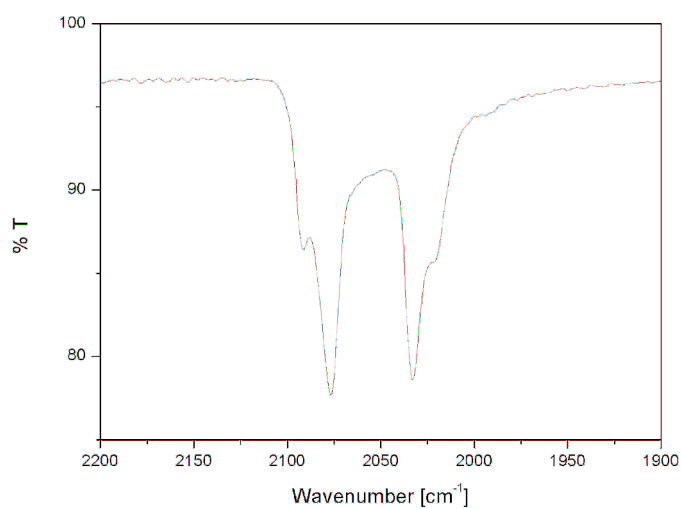
[Ir(ⁱPr-pybox)(CO)₂PF₆ (28p) – solid IR



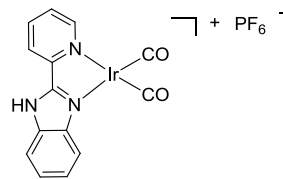
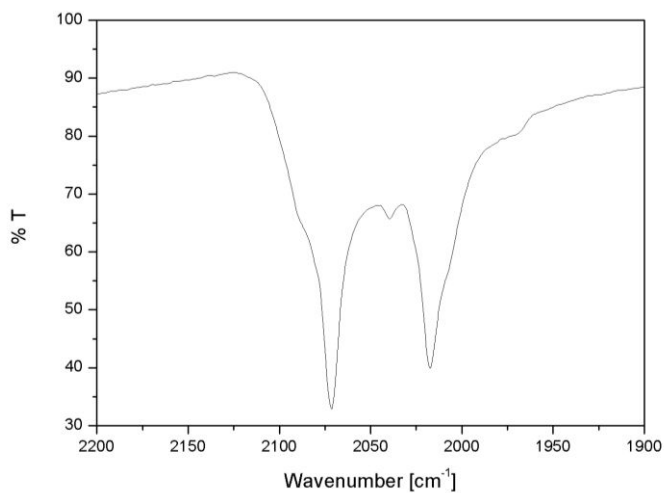
[Ir(Ph-phox)(CO)₂PF₆ (28u) – solid IR



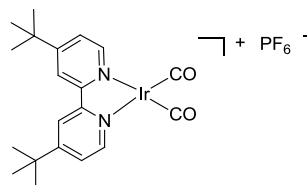
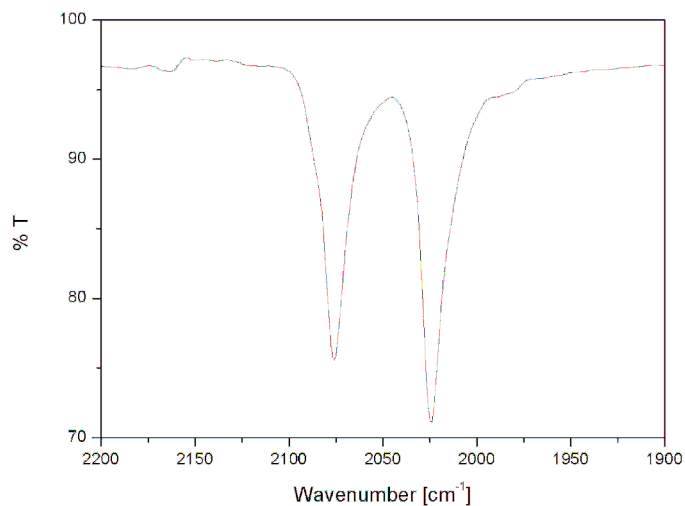
[Ir(pypyraz)(CO)₂PF₆ (28v) – solid IR



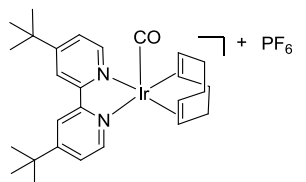
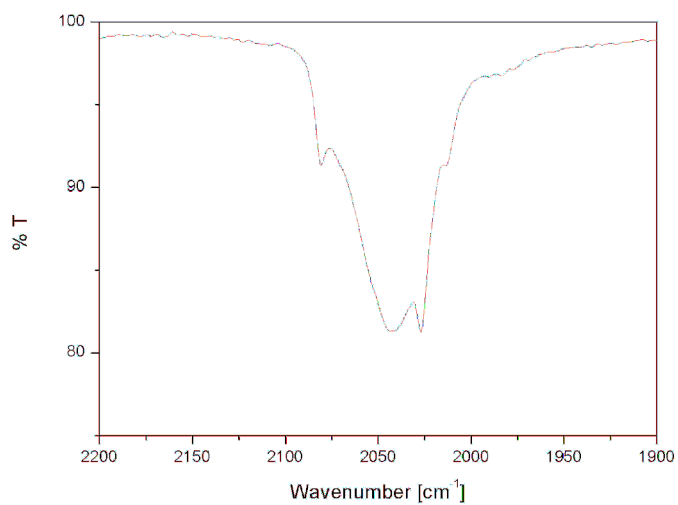
[Ir(TMphen)(CO)₂PF₆ (28w) – solid IR



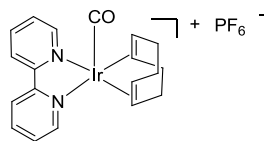
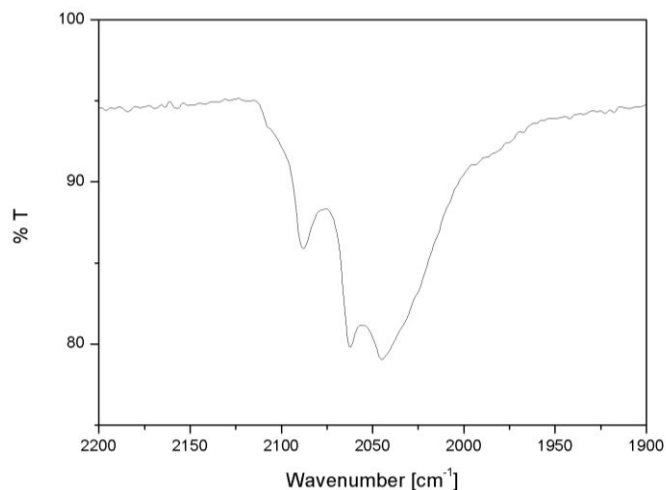
[Ir(dtbpv)(CO)₂PF₆ (28r) – solid IR



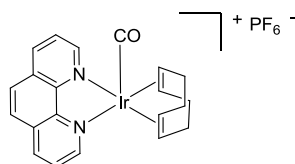
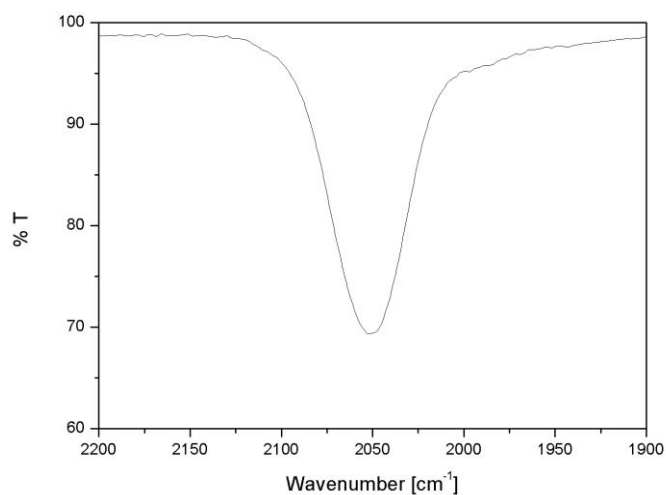
[Ir(dtbpv)(cod)(CO)PF₆ (26r) – solid IR



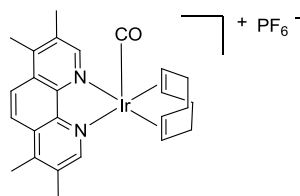
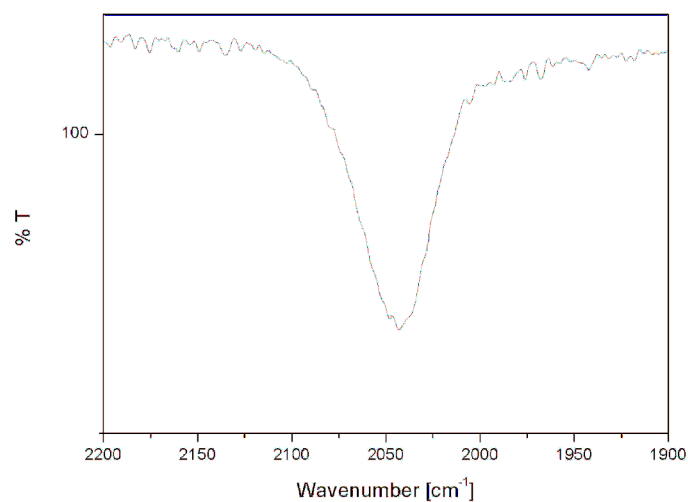
[Ir(bpy)(cod)(CO)]PF₆ (26q) – solid IR



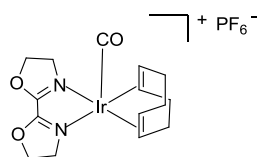
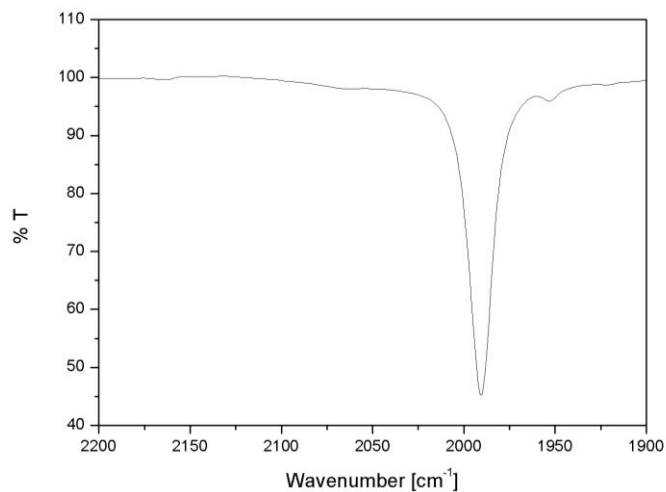
[Ir(phen)(cod)(CO)]PF₆ (26s) – solid IR



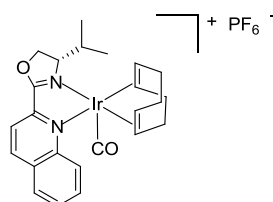
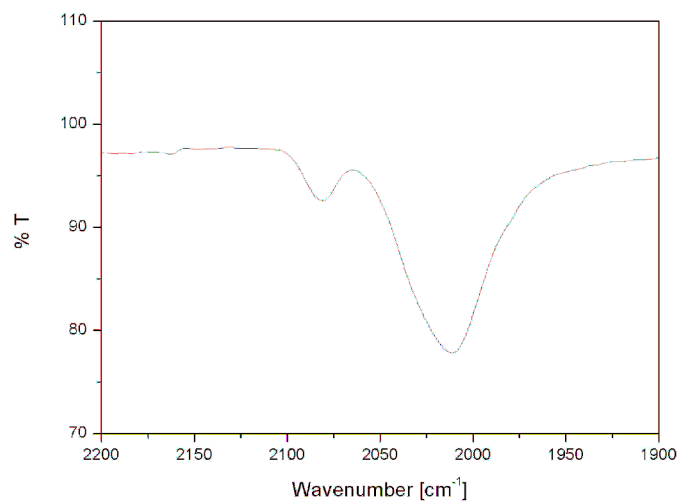
[Ir(TMphen)(cod)(CO)]PF₆ (26t) – solid IR



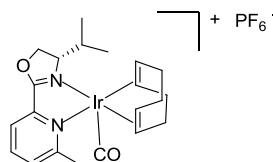
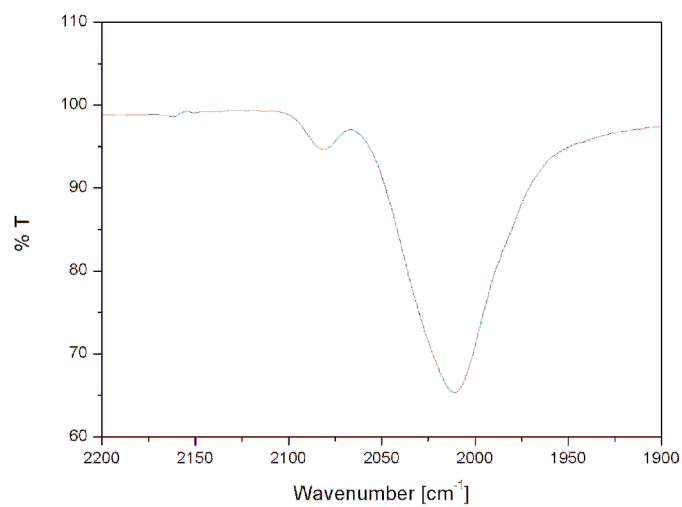
[Ir(H-box)(cod)(CO)]PF₆ (26a) – solid IR



[Ir(ⁱPr-quinox)(cod)(CO)]PF₆ (26m) – solid IR

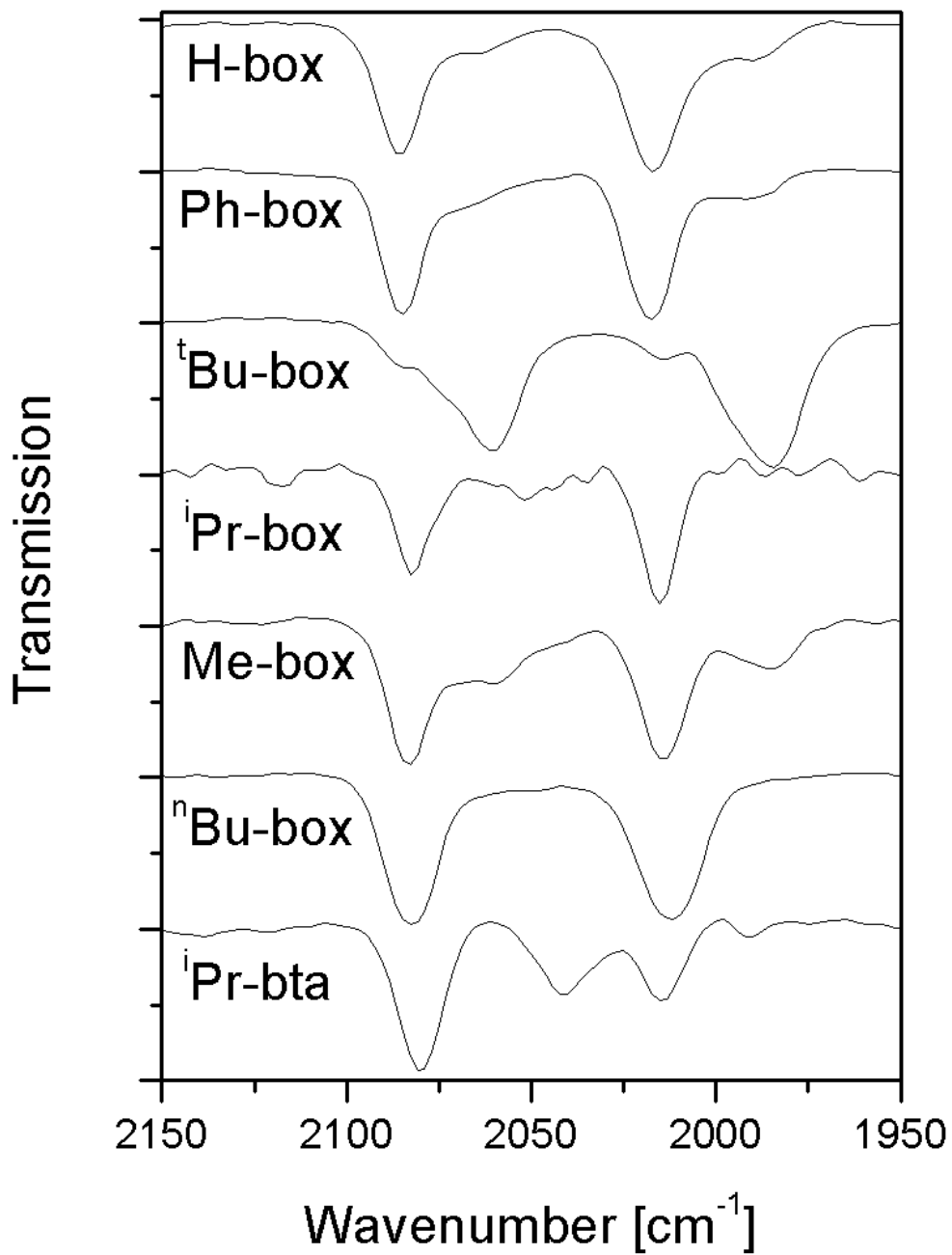


[Ir(ⁱPr-mepyrox)(cod)(CO)]PF₆ (26j) – solid IR



ATR-IR of [Ir(box)(CO)₂]PF₆ in THF solution

box = H-box (**28a**), Ph-box (**28f**), ^tBu-box (**28d**), ⁱPr-box (**28c**), Me-box (**28b**), ⁿBu-box (**28e**), ⁱPr-bta (**28g**)

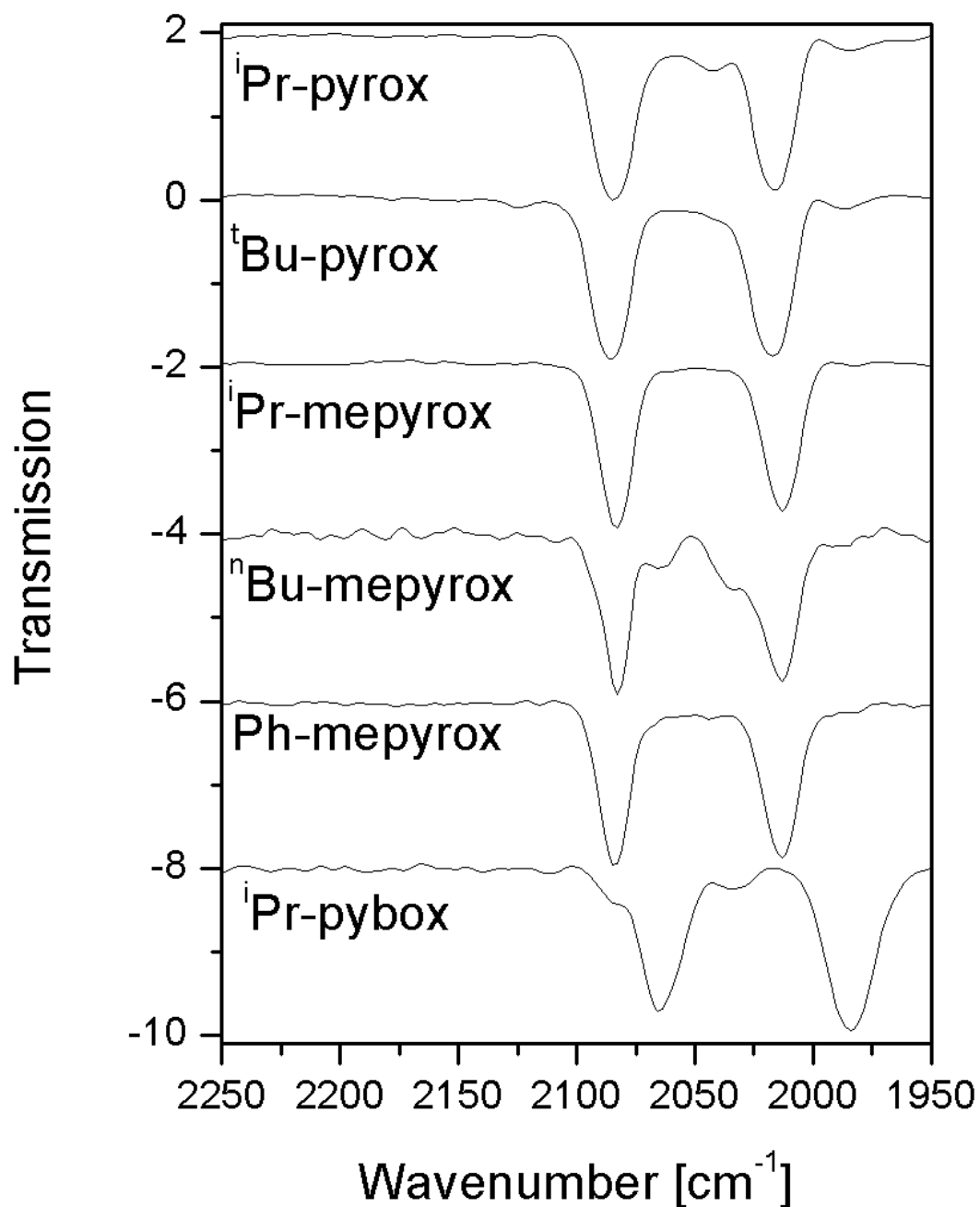


ATR-IR of [Ir(pyrox)(CO)₂]PF₆, [Ir(mepyrox)(CO)₂]PF₆ and [Ir(pybox)(CO)₂]PF₆ in THF solution

pyrox = ⁱPr-pyrox (**28h**), ^tBu-pyrox (**28i**)

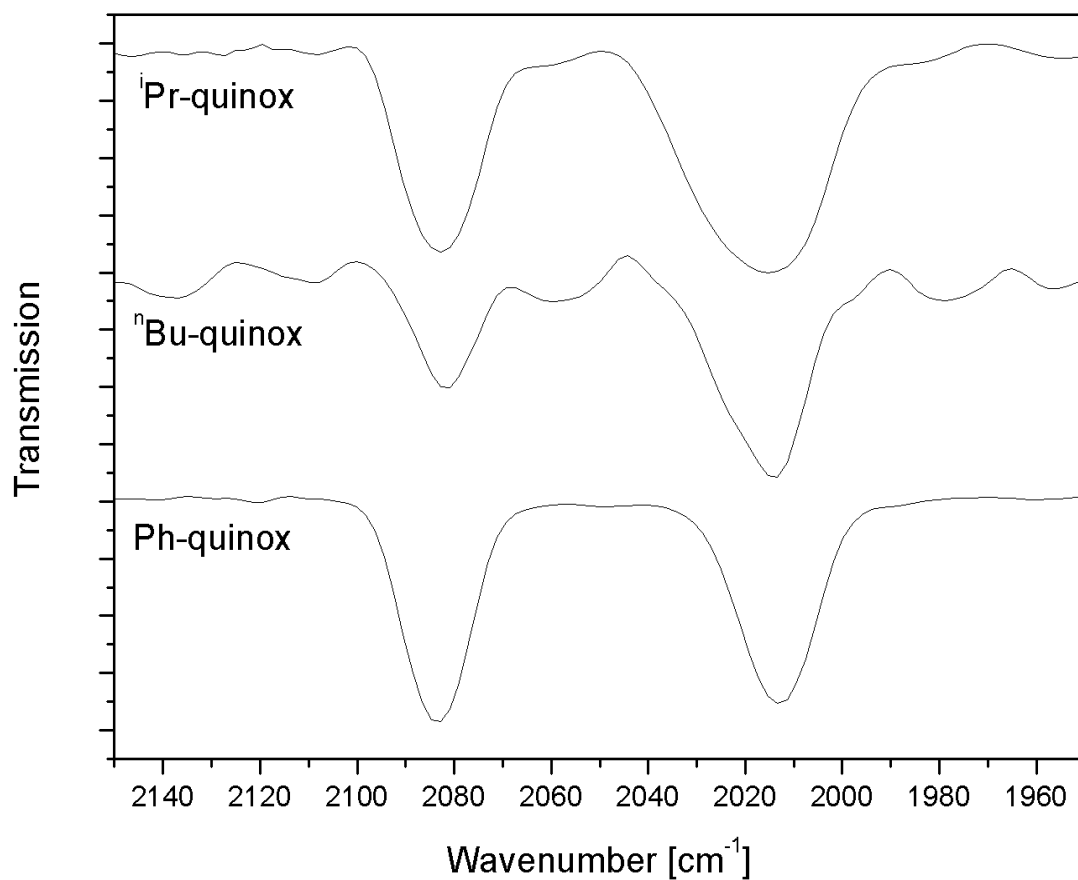
mepyrox = ⁱPr-mepyrox (**25j**), ⁿBu-mepyrox (**28k**), Ph-mepyrox (**28l**)

pybox = ⁱPr-pybox (**28p**)

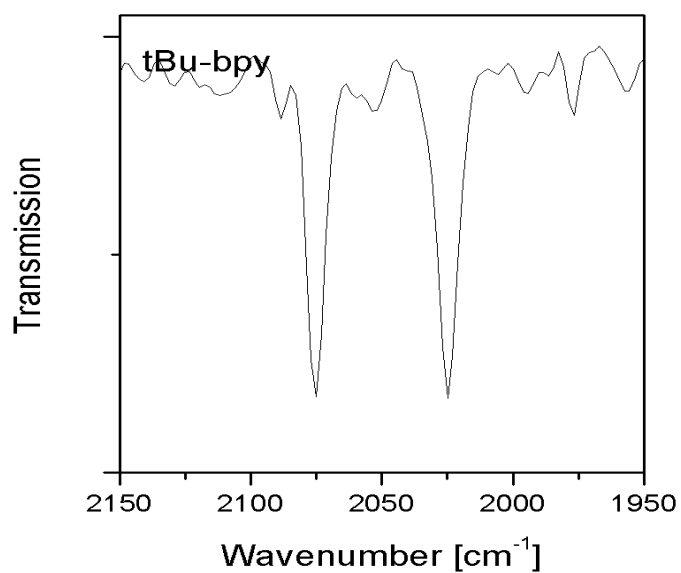


ATR-IR of $[\text{Ir}(\text{quinox})(\text{CO})_2]\text{PF}_6$ in THF solution

quinox = ⁱPr-quinox (**28m**), ⁿBu-quinox (**28n**), Ph-quinox (**28o**)



ATR-IR of $[\text{Ir}(\text{bpy})(\text{CO})_2]\text{PF}_6$ (**28r**) in THF solution



ATR-IR of [Ir(ligand)(cod)(CO)]PF₆ in THF solution

ligand = bpy (26q), phen (26s), H-box (26a), dtbpy (26r), TMphen (26t), ⁱPr-quinox (26m),
ⁱPr-mepyrox (26j)

